International Journal of
Molecular Sciences

Topical Collection Reprint

Feature Papers in Bioactives and Nutraceuticals

Volume II

Edited by
Maurizio Battino

mdpi.com/journal/ijms/topical_collections

MDPI

Feature Papers in Bioactives and Nutraceuticals-Volume II

Feature Papers in Bioactives and Nutraceuticals-Volume II

Editor

Maurizio Battino

MDPI

Basel • Beijing • Wuhan • Barcelona • Belgrade • Novi Sad • Cluj • Manchester

Editor
Maurizio Battino
Università Politecnica delle Marche
Ancona
Italy

Editorial Office
MDPI
St. Alban-Anlage 66
4052 Basel, Switzerland

This is a reprint of articles from the Topical Collection published online in the open access journal *International Journal of Molecular Sciences* (ISSN 1422-0067) (available at: https://www.mdpi.com/journal/ijms/topical_collections/featurepapers_bioactives).

For citation purposes, cite each article independently as indicated on the article page online and as indicated below:

Lastname, A.A.; Lastname, B.B. Article Title. *Journal Name* **Year**, *Volume Number*, Page Range.

Volume II
ISBN 978-3-7258-1001-7 (Hbk)
ISBN 978-3-7258-1002-4 (PDF)
doi.org/10.3390/books978-3-7258-1002-4

Set
ISBN 978-3-7258-0997-4 (Hbk)
ISBN 978-3-7258-0998-1 (PDF)

Contents

About the Editor

Maurizio Battino

Maurizio Battino is a Professor of Nutrition in the Faculty of Medicine at Università Politecnica delle Marche, Ancona, Italy. He obtained his B.Sc. from the University of Bologna, Italy, in 1984, a Ph.D. from the Italian Minister of Science in 1991, and an M.D. (Hon) from the Faculty of Medicine and Pharmacy, Carol Davila, Bucharest, Romania, in 2008. He also obtained an M.S. in ITC and Telemedicine from the Faculty of Medicine, Università Politecnica delle Marche, Ancona, Italy, in 2010. Currently, he hold the positions of Full Professor at the Faculty of Medicine and Director of various Research Centers in Spain (University of Vigo, Vigo, and Universidad Europea del Atlantico, Santander) and China (Jiangsu University). Battino's current and previous research interests include bioenergetics, nutritional biochemistry, membranes, and periodontology. He have published approximately 500 papers with an h-index of 80 (Scopus) and 72 (WoS). Battino has also been a member of SFRBM, PSE, and other international societies and a highly cited researcher, according to Clarivate-Web of Science, during the last 9 consecutive years.

International Journal of
Molecular Sciences

MDPI

Review

Biologically Active Diterpenoids in the *Clerodendrum* Genus—A Review

Łukasz Kuźma * and Jan Gomulski

Department of Biology and Pharmaceutical Botany, Medical University of Lodz, Muszyńskiego 1, 90-151 Lodz, Poland
* Correspondence: lukasz.kuzma@umed.lodz.pl

Abstract: One of the key areas of interest in pharmacognosy is that of the diterpenoids; many studies have been performed to identify new sources, their optimal isolation and biological properties. An important source of abietane-, pimarane-, clerodane-type diterpenoids and their derivatives are the members of the genus *Clerodendrum*, of the *Lamiaceae*. Due to their diverse chemical nature, and the type of plant material, a range of extraction techniques are needed with various temperatures, solvent types and extraction times, as well as the use of an ultrasound bath. The diterpenoids isolated from *Clerodendrum* demonstrate a range of cytotoxic, anti-proliferative, antibacterial, anti-parasitic and anti-inflammatory activities. This review describes the various biological activities of the diterpenoids isolated so far from species of *Clerodendrum* with the indication of the most active ones, as well as those from other plant sources, taking into account their structure in terms of their activity, and summarises the methods for their extraction.

Keywords: antibacterial; anti-parasitic; *Clerodendrum* spp.; cytotoxic; diterpenoids; insecticidal

Citation: Kuźma, Ł.; Gomulski, J. Biologically Active Diterpenoids in the *Clerodendrum* Genus—A Review. *Int. J. Mol. Sci.* **2022**, *23*, 11001. https://doi.org/10.3390/ijms231911001

Academic Editor: David Arráez-Román

Received: 3 April 2022
Accepted: 9 September 2022
Published: 20 September 2022

1. Introduction

The name *Clerodendrum* is derived from two Greek words: *kleros* (destiny or chance) and *dendron* (tree) [1]. It probably has a dual meaning: in ancient times, some plants were believed to have healing properties, while others were poisonous [1].

The genus *Clerodendrum* was first described by Linneus in 1753, and this was followed by the species *C. infortunatum* [2]. This unusual genus was originally classified into the *Verbenaceae* family by Liang [3] and Munir [4], among others, but is now included in the *Lamiaceae* family [2]. It currently includes about 500 species [5] growing in warm temperate and tropical regions of Africa, southern and eastern Asia, as well as America and northern Australia [6]. The genus includes a range of deciduous or evergreen shrubs, small trees, perennial herbs and woody vines [7]; in addition, some species are subshrubs or herbs. Young branchlets are usually four-angled with simple leaves, which are opposite or, rarely, whorled. Inflorescences are loosely cymose or capitate, arranged in terminal or, rarely, axillary paniculate thyrses. The calyx is campanulate or cup shaped. The corolla has a slender tube, five spreading lobes and four stamens. The style has two acute stigmatic lobes. A fruiting calyx is partly inflated. The fruit is a type of drupe and has four one-seeded pyrenes [3].

The members of the *Clerodendrum* genus are grown as ornamental plants [1], and some demonstrate pesticidal or insecticidal properties [7]. Furthermore, many others have been recommended for use in treating pyrexia, asthma, common cold, hypertension, furunculosis, dysentery, rheumatism, mammitis, anorexia, leucoderma, leprosy, arthrophlogosis and toothache [8–11]. Due to these numerous therapeutic properties, many *Clerodendrum* species have been the subject of phytochemical investigations over the past 40 years, resulting in the extraction, isolation, purification and identification of a range of phytocompounds, including various mono- and sesquiterpene diterpenoids, triterpenoids, flavonoids and their glycosylated forms; in addition, various phenylethanoid glycosides, steroids and their

glycoside derivatives, cyclohexylethanoids, anthraquinones and cyanogenic glycosides have been noted [12–21].

Diterpenes are natural plant-derived secondary metabolites with the general formula $C_{20}H_{32}$. They constitute a chemically diverse group of secondary metabolites which are biosynthesised in the flowering shoots, roots or rhizomes. Such plant diterpenoids most commonly occur in a cyclic form [22]. The diterpenoids are classified into abietane, caurane, caurene, clerodane and labdane types according to their main skeleton [23].

As a result of this structural variation, they also demonstrate a range of pharmacological and biological activities, including antitumor (paclitaxel) [24], positive inotropic (forskolin) [25], vasodilatory, and hypotensive (manool) properties [26], as well as antiplatelet potential (forskolin) [27]. Some diterpenoids also demonstrate antibacterial properties. For example, salvipisone and aethiopinone, isolated from *Salvia sclarea* roots, exhibit bactericidal activity against Gram-positive bacteria [28]. Taxodione and its unique derivative 7-2′-oxohexyl-taxodione, both isolated from *Salvia austriaca* roots, exhibit strong cytotoxic activities against various tumour cell lines [29]. Furthermore, taxodione inhibits acethylcholine- and butyrylcholine-esterase (ACE and BCE) [30].

The diterpenes are believed to exert cytotoxic activities through a range of possible mechanisms. Fronza et al. (2012) suggest that they exert their cytotoxic activity by targetting the biological membrane, with its lipophilic character [31]. Other abietane diterpenes could exert their cytotoxicity effects by their alkylating [31] and protonophoric properties [32]. In addition, sphaeropsidin A, a pimarane diterpene isolated from a fungal pathogen, was found to significantly affect cellular homeostasis by modulating the ion-transporter activity of the Na-K-2Cl electrochemical cotransporter or the Cl^{-}/HCO^{3-} anion exchanger, thus increasing cellular volume [33].

Due to their diverse and often strong biological activities, diterpenoids make an interesting class of natural compounds. There are also attempts to identify new plant sources. A range of reports indicate that the roots and aerial parts of the *Clerodendrum* genus are rich in abietane-, pimarane- and clerodane-type diterpenoids and their derivatives, including their glycoside forms (Figure 1).

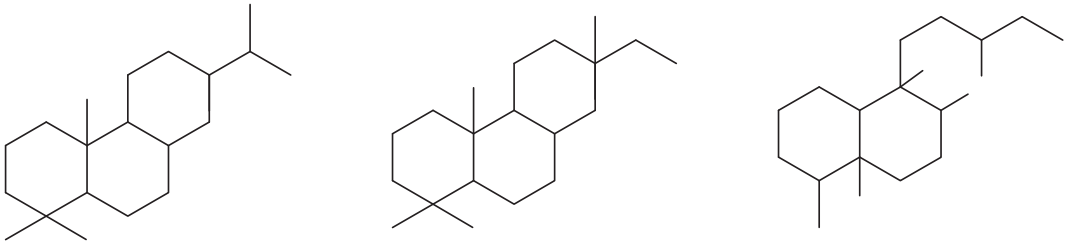

(**A**) (**B**) (**C**)

Figure 1. The structure of abietane (**A**), pimarane (**B**) and clerodane (**C**) diterpenoids.

Therefore, this review examines the members of the genus *Clerodendrum* and their diterpenoid presence, highlighting their biological potential in the area of the most often studied activities, such as cytotoxic, antibacterial, antifungal and others. The chemical structures of the constituents are shown in Figure 2. The present review encompasses the literature data describing the diterpenes present in *Clerodendrum* from 1981 to 2022. The main sources of literature data were Google Scholar, Google, PUBS ACS, ScienceDirect, Springer, Ebsco and others.

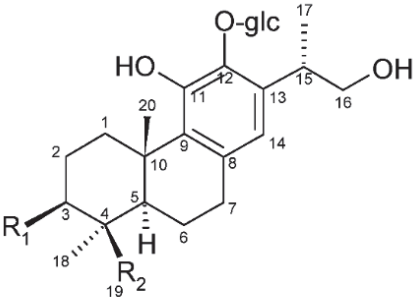

(3): R_1 = OH, R_2 = CH_3,
(4): R_1 = O-glc, R_2 = CH_3,
(5): R_1 = H, R_2 = COO-glc,
(8): R_1 = H, R_2 = CH_2O-glc,

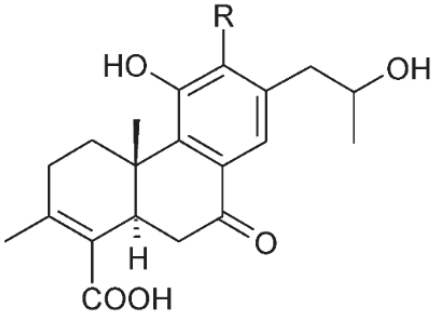

(6)

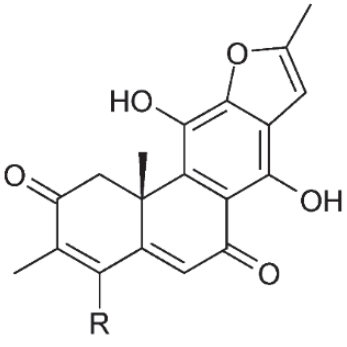

(7): R = CH_2OH
(10): R = CH_3

Figure 2. *Cont.*

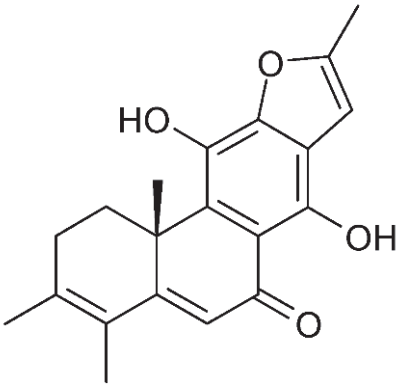

(9)

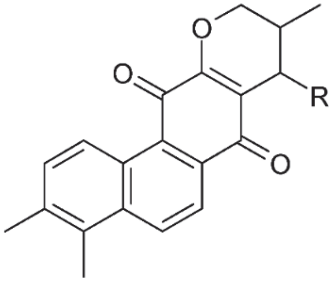

(1): R = H
(2): R = CH_2OH

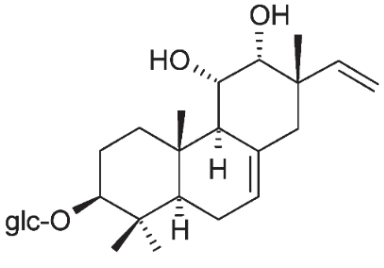

(11)

Figure 2. *Cont.*

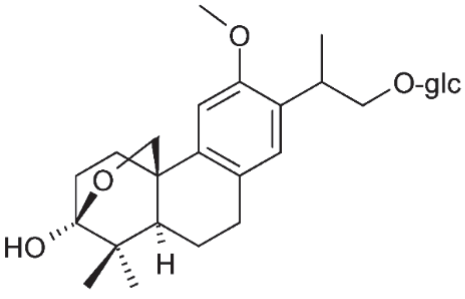

(12)

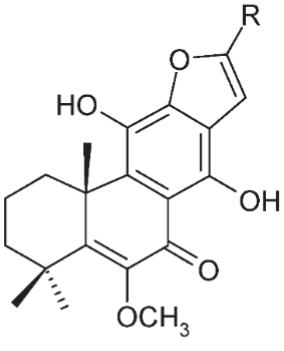

(13): R = COO-CH_3
(15): R = CH_3
(16): R = CH_2OH

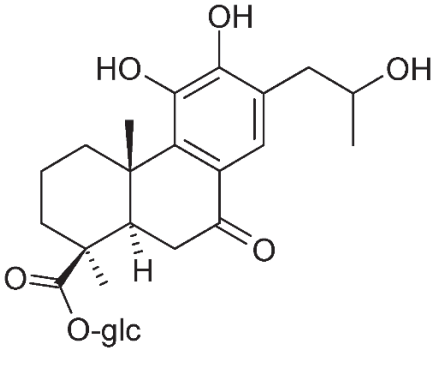

(14)

Figure 2. *Cont.*

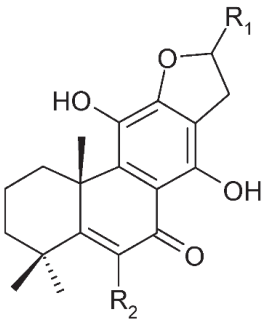

(17): $R_1 = CH_3$, $R_2 = OCH_3$
(85): $R_1 = CH_2OH$, $R_2 = OH$

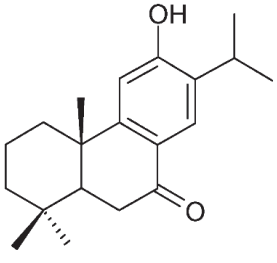

(18)

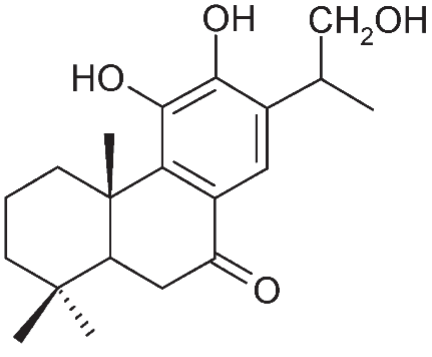

(21)

Figure 2. *Cont.*

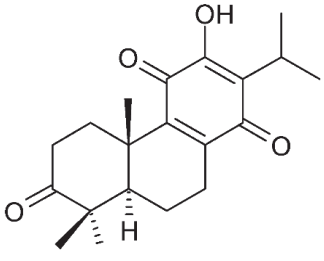

(22)

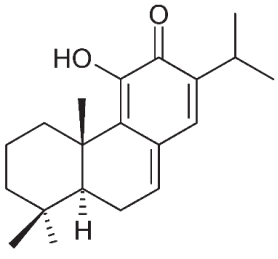

(25)

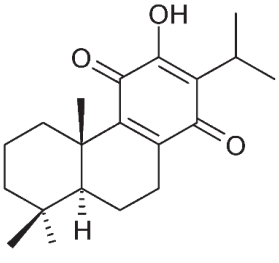

(23)

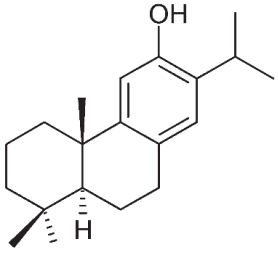

(26)

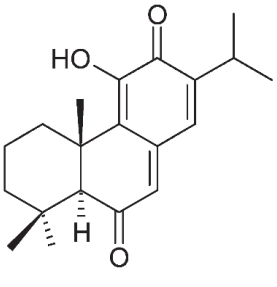

(24)

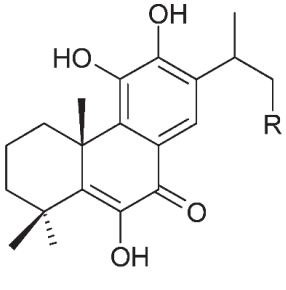

(27): R = H
(28): R = OH

Figure 2. *Cont.*

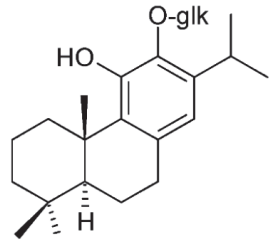

(29)

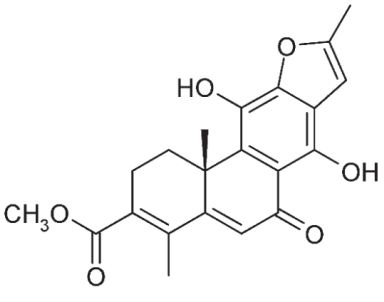

(30)

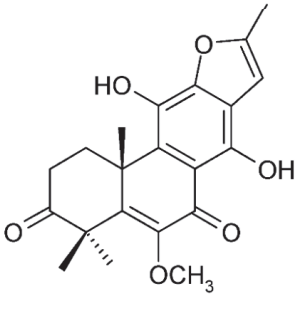

(31)

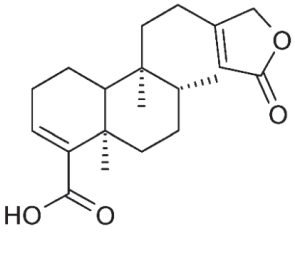

(38)

Figure 2. *Cont.*

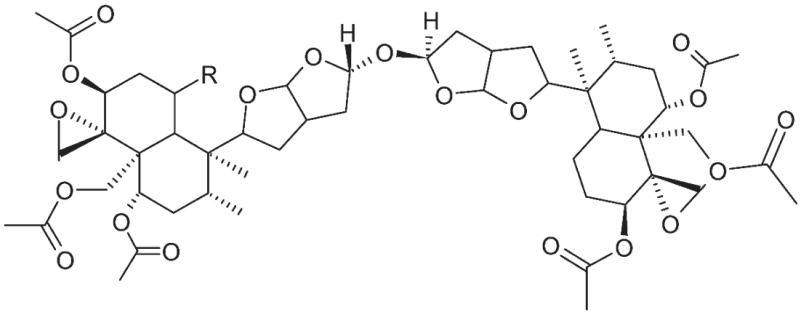

(39): R = H
(40): R = OCH_3

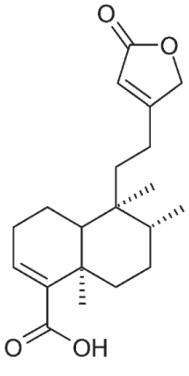

(32)

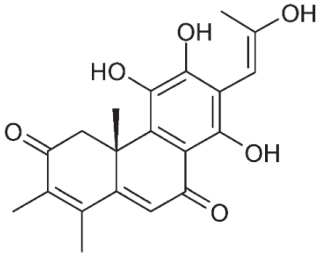

(42)

Figure 2. *Cont.*

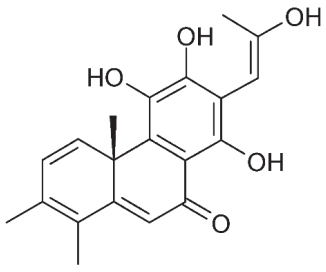

(43)

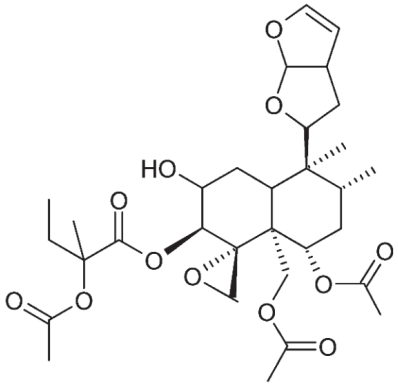

(33)

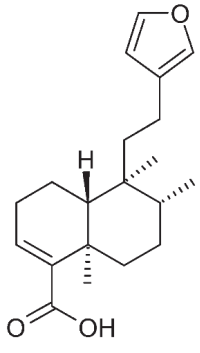

(44)

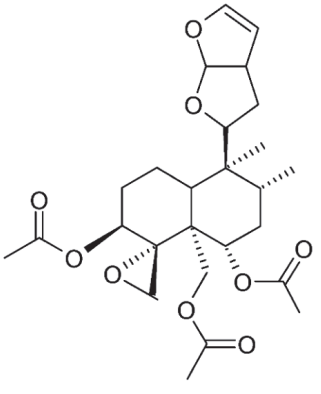

(34)

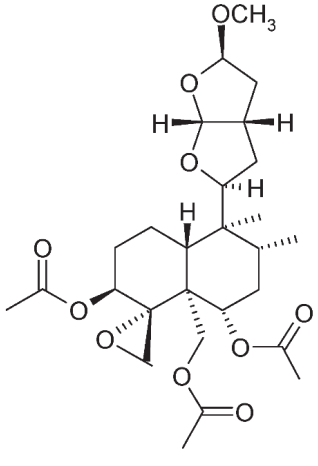

(41)

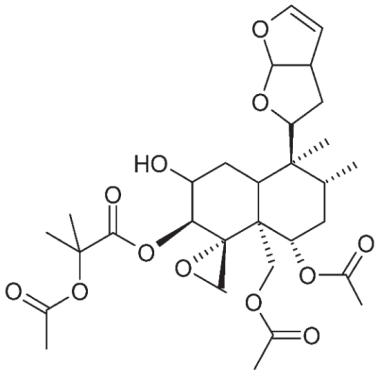

(35)

Figure 2. *Cont.*

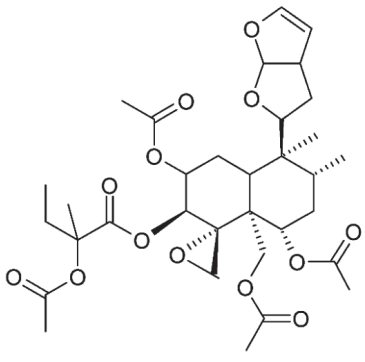

(36)

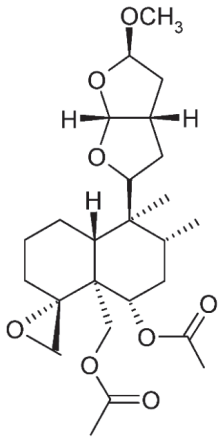

(46)

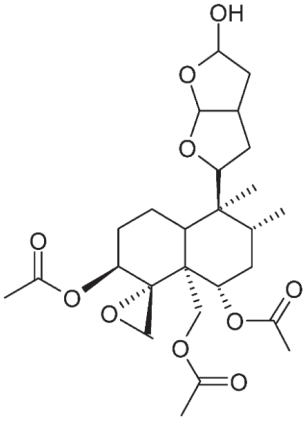

(37)

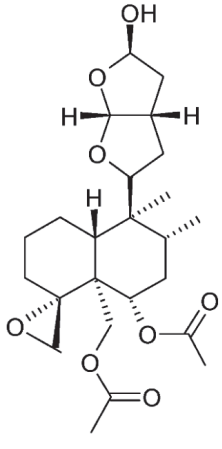

(47)

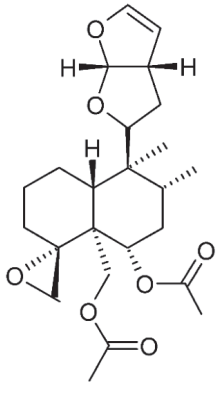

(45)

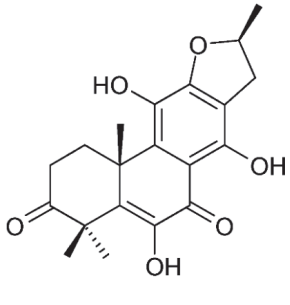

(48)

Figure 2. *Cont.*

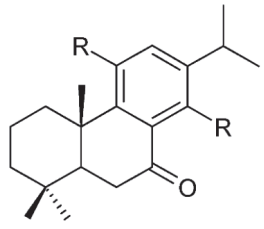

(49): R = OH
(50): R = H

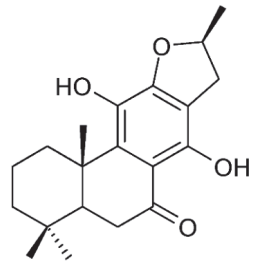

(53)

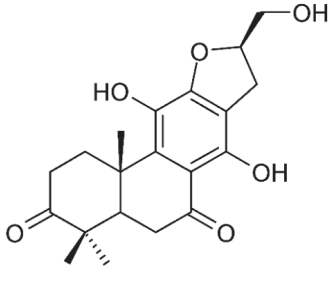

(51)

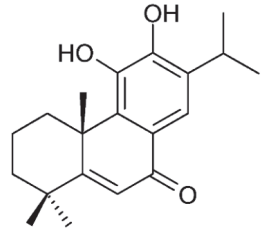

(54)

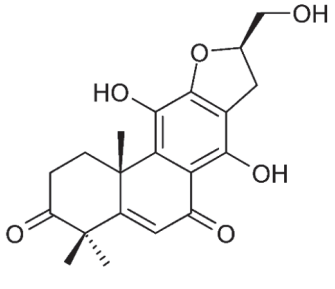

(52)

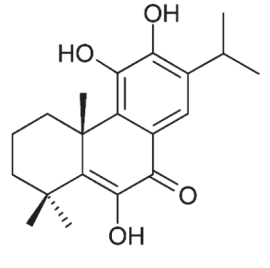

(55)

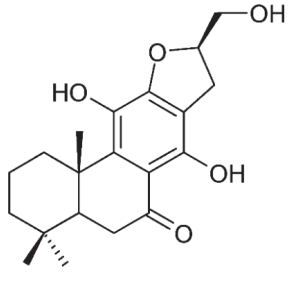

(58)

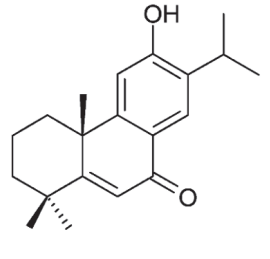

(56)

Figure 2. *Cont.*

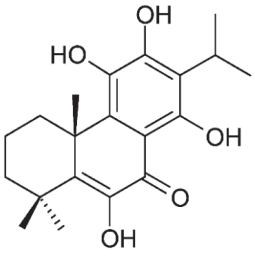

(57)

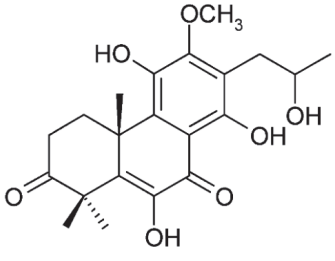

(59)

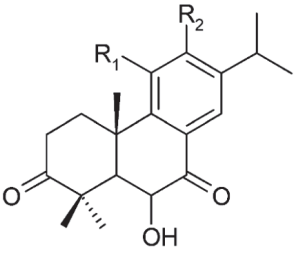

(60): R_1 = H, R_2 = OH
(61): R_1 = OH, R_2 = OCH_3

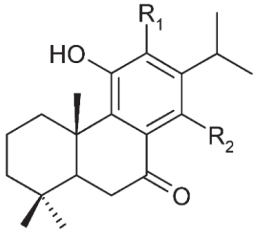

(62): R_1 = OH, R_2 = H
(63): R_1 = OCH_3, R_2 = H
(64): R_1 = H, R_2 = OH

Figure 2. *Cont.*

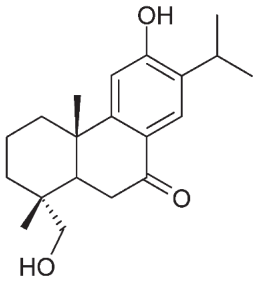

(65)

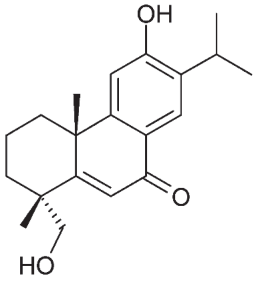

(66)

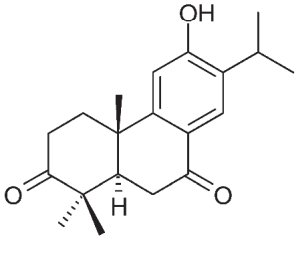

(60)

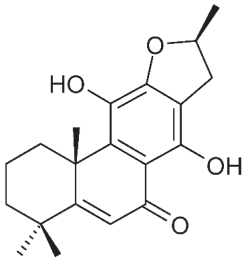

(67)

Figure 2. *Cont.*

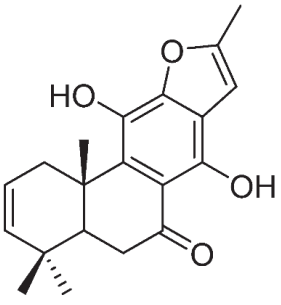

(68)

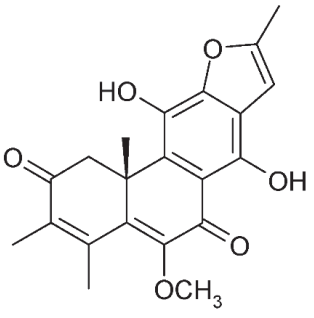

(72)

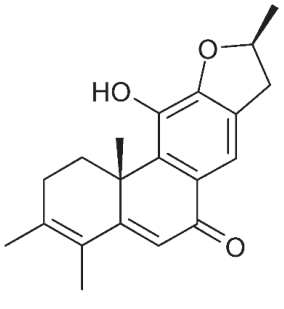

(69)

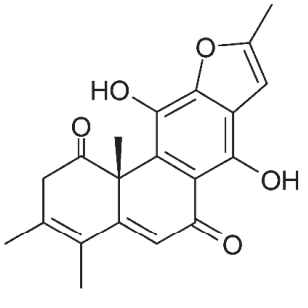

(73)

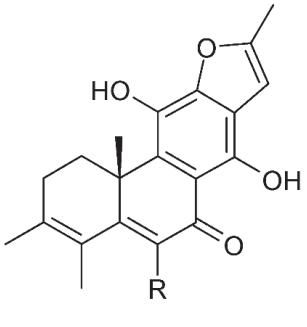

(70): R = H
(71): R = OH

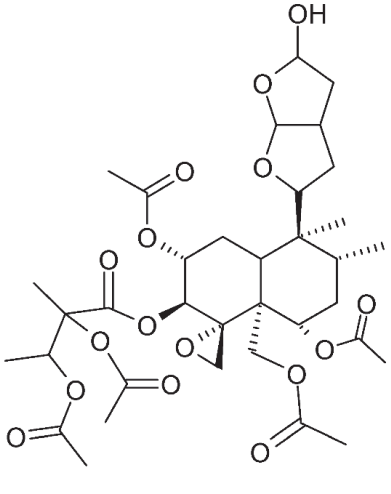

(74)

Figure 2. *Cont.*

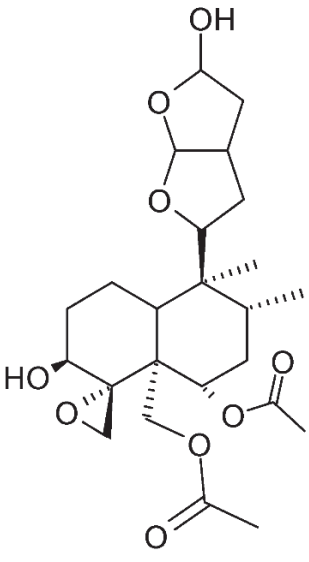

(75)

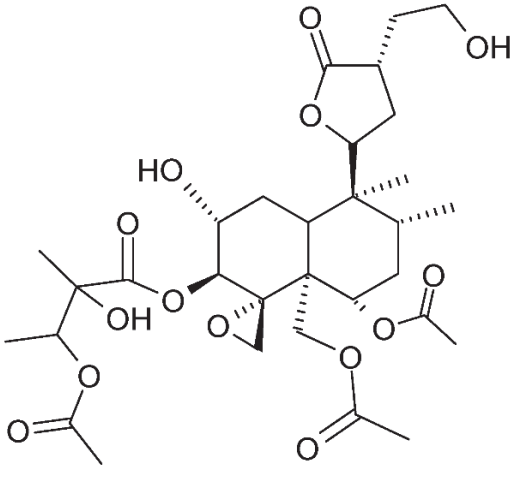

(76)

Figure 2. *Cont.*

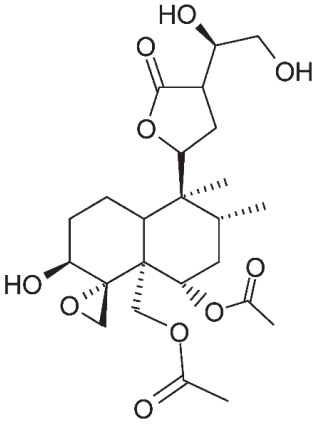

(77)

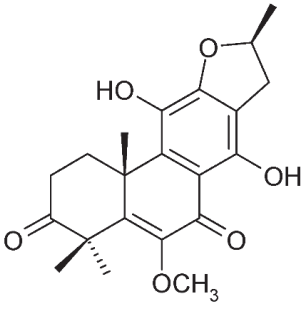

(81)

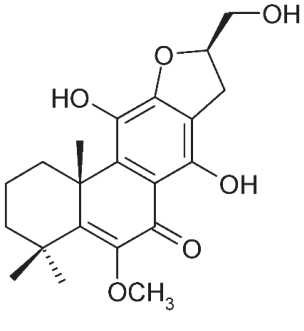

(79)

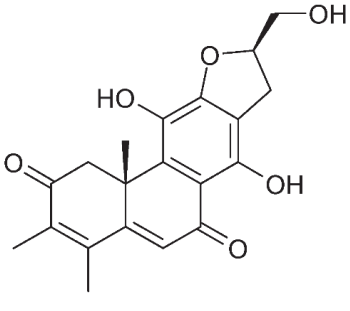

(83)

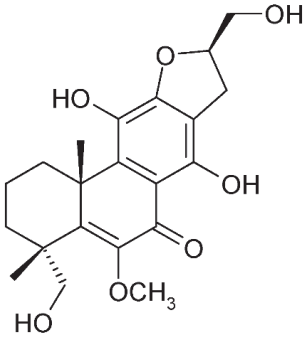

(80)

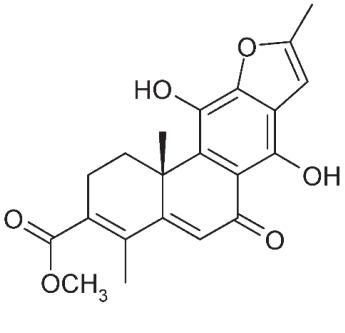

(30)

Figure 2. *Cont.*

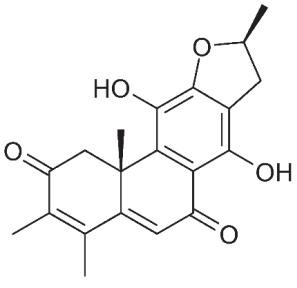

(86)

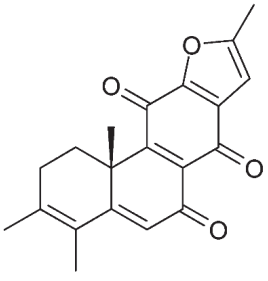

(87)

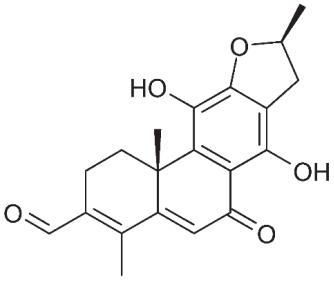

(82)

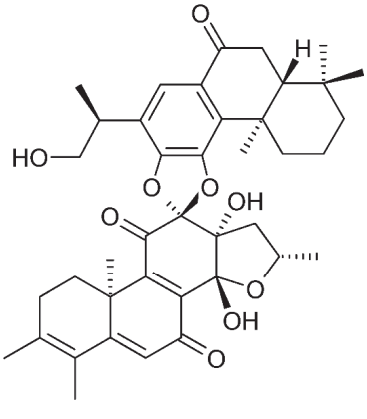

(78)

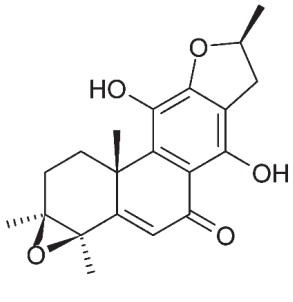

(84)

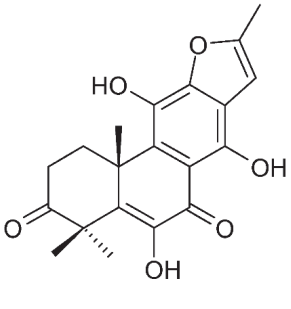

(88)

Figure 2. *Cont.*

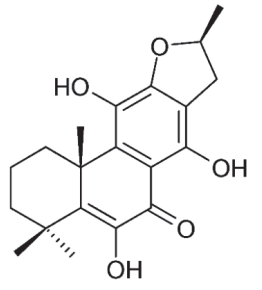

(89)

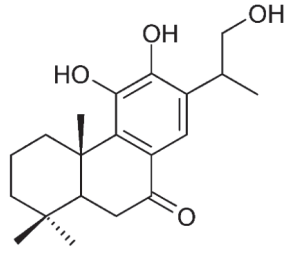

(21)

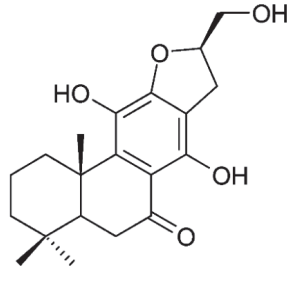

(90)

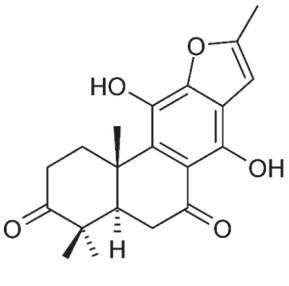

(91)

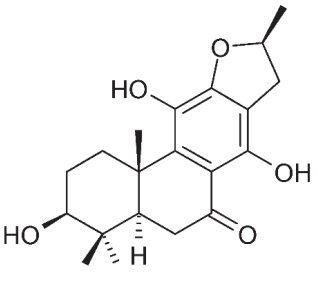

(92)

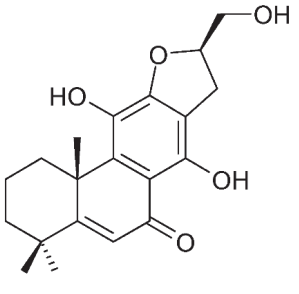

(93)

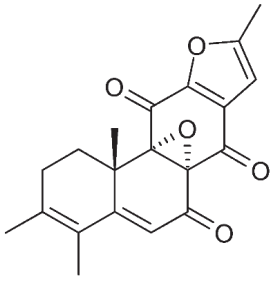

(94)

Figure 2. *Cont.*

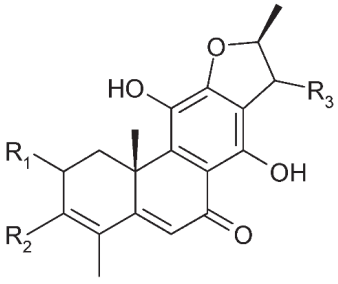

(95): R_1 = H, R_2 = $COOCH_3$, R_3 = H
(97): R_1 = OH, R_2 = CH_3, R_3 = H
(98): R_1 = H, R_2 = CH_3, R_3 = OH

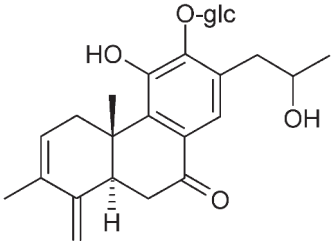

(101)

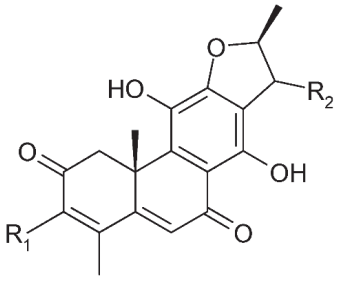

(96): R_1 = CH_2OH, R_2 = H
(99): R_1 = CH_3, R_2 = OH

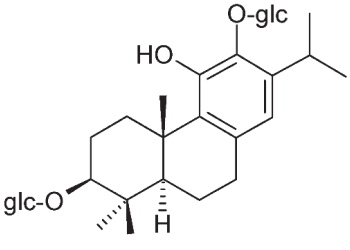

(102)

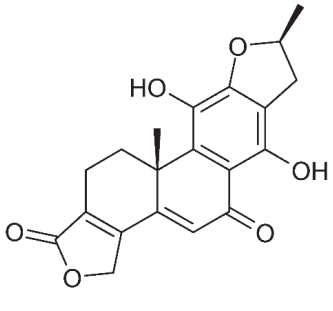

(100)

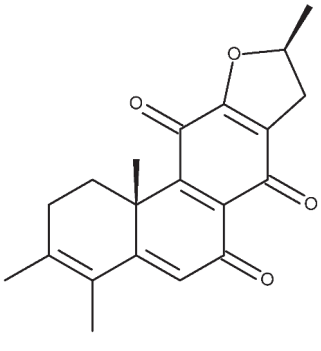

(103)

Figure 2. *Cont.*

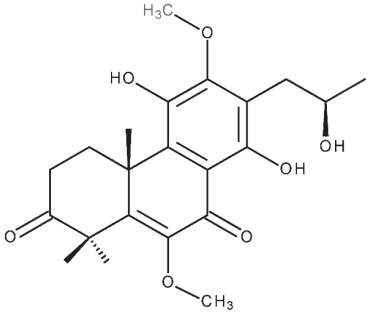

(104)

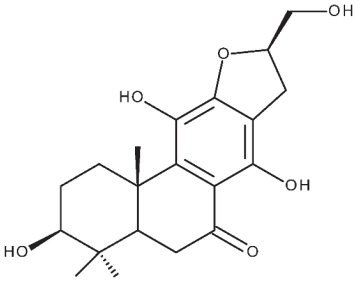

(107)

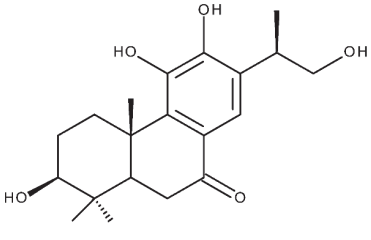

(105)

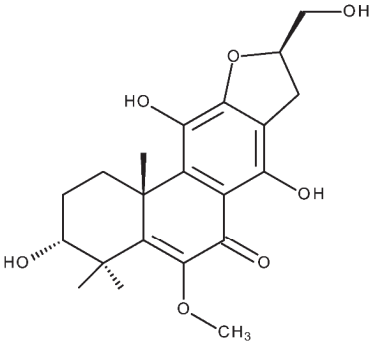

(108)

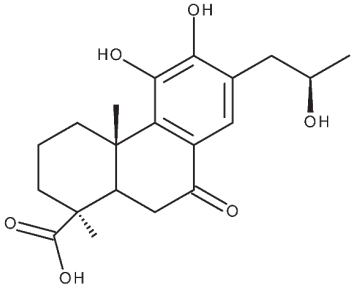

(106)

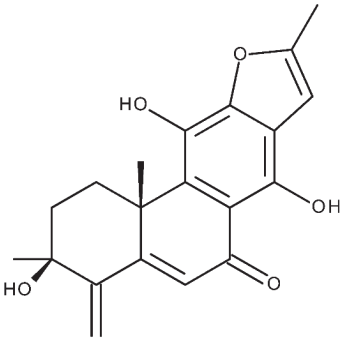

(109)

Figure 2. *Cont.*

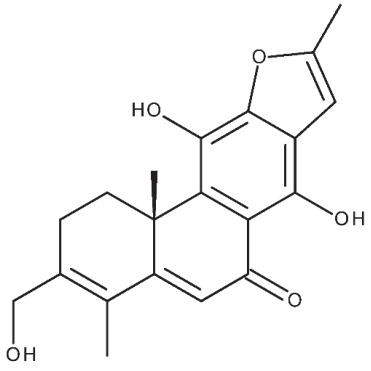

(110)

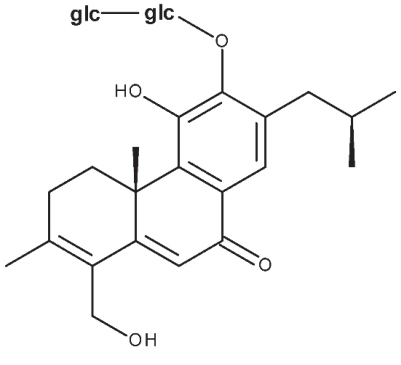

(111)

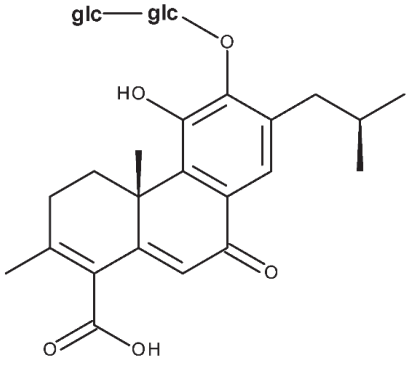

(112)

Figure 2. The chemical structure of the compounds isolated from *Clerodendrum* genus.

2. A Review of Diterpenoid Compounds Isolated from *Clerodendrum* Genus

Diterpenoids demonstrate various chemical properties, with a variety of polarities, affinity for the organic phase and solubility. Therefore, the solvent and extraction method must be chosen carefully to optimise the extraction process. The selection of solvent not only depends on the plant species, but also on the organ (overground, underground), and the amount of contaminants, including the presence of chlorophyll. The various solvents and methods used for diterpenoid extraction from *Clerodendrum* are given in Tables 1–13, together with the parts of the plants used for isolation.

2.1. Clerodendrum bungei

In Chinese folk medicine, *C. bungei* (eng. name: rose glory bower, Chinese name: Chou mu dan) is a plant raw material whose roots and leaves are used to treat boils, haemorrhoids, hypertension, lung cancer and eczema [34]. This species is known to be rich in diterpenoids, some of which exhibit potential biological activities [34–36]. The parts of the plant and the extraction methods used for the phytochemical analyses for this plant species are shown in Table 1.

Table 1. The diterpenoid extraction methods and *C. bungei* plant material for diterpenoid isolation.

Species	Material	Solvent and Extraction Method	Isolated Diterpenoids	References
C. bungei	Roots	70% aqueous acetone. Dried roots extracted in room temperature. Solvent removed in vacuo.	12-O-D-glucopyranosyl-3,11,16-trihydroxyabieta-8,11,13-triene **(3)** 3,12-O-D-diglucopyranosyl-11,16-dihydroxyabieta-8,11,13-triene **(4)** 19-O-D-carboxyglucopyranosyl-12-O-D-glucopyranosyl-11,16-dihydroxyabieta-8,11,13-triene **(5)** 11,16-dihydroxy-12-O-D-glucopyranosyl-17(15f16),18(4f3)-abeo-4-carboxy-3,8,11,13-abietatetraen-7-one **(6)** 19-hydroxyteuvincenone F **(7)** ajugaside A **(8)** uncinatone **(9)**	[36]
C. bungei	Stem	**EtOH**. Dried and pulverised stems were extracted three times with hot solvent. The solvent was removed in vacuo.	bungone A **(1)** bungone B **(2)** sugiol **(18)** uncinatone **(9)** teuvincenone F **(10)**	[35]
C. bungei	Roots	**95% EtOH.** Air-dried powdered root parts were extracted three times at room temperature. The solvent was removed in vacuo. The crude EtOH extract was suspended in hot water and then partitioned with EtOAc four times.	3β-(β-D-glucopyranosyl)isopimara-7,15-diene-11α,12a-diol **(11)** 16-O-β-D-glucopyranosyl-3β-20-epoxy-3-hydroxyabieta-8,11,13-triene **(12)**	[34]
C. bungei	Roots	**70% aqueous acetone.** Air-dried roots were extracted at room temperature. The extract was filtered through a Buchner funnel using Whatman No. 1 filter paper. The solvent was removed in vacuo.	12-O-β-D-glucopyranosyl-3,11,16-trihydroxyabieta-8,11,13-triene **(3)** 3,12-O-β-D-diglucopyranosyl-11,16-dihydroxyabieta-8,11,13-triene **(4)** ajugaside A **(8)** uncinatone **(9)** 19-hydroxyteuvincenone F **(7)**	[37]

Table 1. *Cont.*

Species	Material	Solvent and Extraction Method	Isolated Diterpenoids	References
C. bungei	Roots	**EtOH.** Dried roots were extracted three times under conditions of reflux (every 2 h). Organic extracts were combined. The solvent was removed under reduced pressure. **EtOH.** Dried roots were extracted three times at room temperature for three times. The residue was re-suspended in L water and partitioned successively with EtOAc and *n*-BuOH.	bungnate A **(13)** bungnate B **(14)** 15-dehydrocyrtophyllone A **(15)** 15-dehydro-17-hydroxycyrtophyllone A **(16)** 12,16-epoxy-11,14,17-trihydroxy-6-methoxy-17(15→16)-abeo-abieta-5,8,11,13-tetraene-7-one **(16)** cyrtophyllone A **(17)** villosin C **(85)** teuvincenone F **(10)** 19-hydroxyteuvincenone F **(7)** mandarone E **(70)** 12-O-β-D-glucopyranosyl-3,11,16-trihydroxyabieta-8,11,13-triene **(3)** uncinatone **(9)** crolerodendrum B **(42)** crolerodendrum A **(43)**	[38] [39]

This plant species was first investigated for diterpenoid content by Fan et al. in 1999 [35]. The authors isolated two new royleanone-type compounds from *C. bungei* roots: 9,10-dihydro-3,4,9-trimethyl phenanthro [3,2-b]pyran (7H)-7, 12(8H)-dione (bungone A **(1)**) and 9,10-dihydro-8-hydroxymethyl-3,4,9-trimethylphenanthro [3,2-β]pyran(2H)-7,12-dione (bungone B **(2)**). While these abietane diterpenoids are structurally similar to the royleanones, with both possessing an 11,14-para benzoquinone group, the C-12 has an oxygen enclosed by an additional aliphatic ring instead of a hydroxyl group, which is typical for roylanones. Due to their cytotoxic activities, these compounds are very interesting for further research; like other diterpenes, including horminone or acetyl-horminone, royleanone is able to damage DNA and inhibit topoisomerase I and II [31,40,41].

Liu et al. (2008) [36] isolated other abietane-type diterpenoids from the roots of *Clerodendrum bungei*. Five were new structures: 12-*O*-*β*-D-glucopyranosyl-3,11,16-trihydroxyabieta-8,11,13-triene **(3)**, 3,12-*O*-*β*-D-diglucopyranosyl-11,16-dihydroxyabieta-8,11,13-triene **(4)**, 19-*O*-*β*-D-carboxyglucopyranosyl-12-*O*-*β*-D-glucopyranosyl-11,16-dihydroxyabieta-8,11,13-triene **(5)**, 11,16-dihydroxy-12-*O*-*β*-D-glucopyranosyl-17(15→16),18(4→3)-*abeo*-4-carboxy-3,8,11,13-abietate traen-7-one **(6)** and 19-hydroxyteuvincenone F **(7)**. All are glycosides, apart from compound **(7)**, and all contain aglycone, either as an abietatriene or abietatetraene.

In addition, the diterpenoids ajugaside A **(8)**, uncinatone **(9)** and teuvincenone F **(10)**, first isolated from other plant materials, were also isolated, purified and identified from the aqueous acetone crude extract of *C. bungei* roots. The identified compounds were tested for their potential cytotoxic activity against three cell lines: B16 murine melanoma, HGC-27 human gastric, and HEK-293 human epithelial kidney. Of the tested compounds, only uncinatone **(9)**, a rearranged abietane derivative containing a 17(15→16), 18(4→3)-*diabeo*-abietane framework, was found to demonstrate moderate cytotoxicity against tested cell lines: the IC_{50} value ranged from 1.2 to 6.4 μM depending on the treated cell line, as indicated by MTT, i.e., 3-(4,5-dimethylythiazol-2-yl)-2,5-diphenyl-2*H*-tetrazolium bromide. This diterpenoid also inhibited cell proliferation and induced cell-cycle G2/M phase arrest [36].

In addition, 12-*O*-*β*-D-glucopyranosyl-3,11,16-trihydroxyabieta-8,11,13-triene **(3)**, 3,12-*O*-*β*-D-diglucopyranosyl-11,16-dihydroxyabieta- 8,11,13-triene **(4)**, ajugaside A **(8)**, uncinatone **(9)** and 19-hydroxyteuvincenone F **(7)** demonstrated significant anti-complement activity on the classical pathway complement system, as expressed by total hemolytic activity [37]. The inhibitory activity of these compounds against the complement system recorded an IC_{50} range from 24 μM to 232 μM. The most active compound was found to be 12-*O*-*β*-D-glucopyranosyl-3,11,16-trihydroxyabieta-8,11,13-triene **(3)** [37]. Kim et al. (2010) postulate that the hydroxyl group in position 3 of this compound may play an important role in its high anti-complement activity. Other diterpenes with glucose, methyl, or hydrogen moieties at position 3 demonstrated significantly lower anti-complement activ-

ities [37]. In addition, another two new diterpenoids were isolated from *C. bungei*: 3*β*-(*β*-D-glucopyranosyl)isopimara-7,15-diene-11α,12α-diol **(11)** and 16-*O*-*β*-D- D-glucopyranosyl-3 *β*-20-epoxy-3-hydroxyabieta-8,11,13-triene **(12)** together with other known compounds, such as 12-*O*-*β*-D-glucopyranosyl-3,11,16-trihydroxyabieta-8,11,13-triene **(3)** and 3,12-*O*-*β*-D-diglucopyranosyl-11,16-dihydroxy-abieta-8,11,13-triene **(4)** [34]. All isolated, purified and identified secondary metabolites were evaluated for cytotoxicity against the following tumour cell lines: B16 murine melanoma, HGC-27 human gastric and BEL-7402 human hepatocellular carcinoma. Sun et al. (2014) report that only 16-*O*-*β*-D-glucopyranosyl-3*β*-20-epoxy-3-hydroxyabieta-8,11,13-triene **(12)** appeared to be active among all tested compounds; it demonstrated moderate cytotoxicity against B16, HGC-27, and BEL-7402 cells, manifested with IC_{50} values of 8.8, 9.8, and 7.1 μM, respectively [34]. The authors emphasise the structural similarities between this diterpenoid and bioactive compounds isolated from the same plant material [34,35,37]. It is worth adding, that this metabolite has a hydroxyl group at the third carbon, which is believed to be responsible for the biological activities of compounds isolated from *C. bungei* roots [37].

Further studies on *C. bundei* resulted in the isolation and identification of the following diterpenoids: bungnate A **(13)** (12,16-epoxy-6-methoxy-11,14-dihydroxy-17(15→16)-abeo-5,8,11,13,15-abietapentaen-7-one-17-carboxylate), bungnate B **(14)** (19-O-β-D-carboxyglucop yranosyl-11,12,16-trihydroxy-abieta-8,11,13-triene-7-one), 15-dehydrocyrtophyllone A **(15)** (12,16-epoxy-6-methoxy-11,14-dihydroxy-17(15→16)-abeo-5,8,11,13,15-abietapentaen-7-one) 15-dehydro-17-hydroxycyrtophyllone A **(16)** (12,16-epoxy-6-methoxy-11,14,17-trihydroxy-17(15→16)-abeo-5,8,11,13,15-abietapentaen-7-one), and cyrtophyllone A **(17)** [38]. Of these, 15-dehydrocyrtophyllone A **(15)** demonstrated ACE (Angiotensin Converting Enzyme) inhibition activity, with an IC_{50} value of 42.7 μM. Among the tested diterpenoids, none inhibited α-glucosidase [38].

2.2. Clerodendrum cyrtophyllum

This genus, known in Chinese medicine as "Da quing", is recommended for treating infectious diseases, common cold and malaria [42]. Many relevant compounds have been extracted from the plant, including the diterpenoids teuvincenone F **(10)**, uncinatone **(9)** and sugiol **(18)**, the triterpenoids friedelin **(19)** and clerodolone **(20)** and the phytosteroids stigmasta-5,22,25-trien-3*β*-ol and clerosterol. In addition, two new abietane derivatives, cyrtophyllone A **(17)** (16(*S*)-12,16-epoxy-11,13-dihydroxy-6-methoxy-17(15-16)-*abeo*-abieta-5,8,11,13-tetraen-7-one) and cyrtophyllone B **(21)** ((+)-11,12,16-trihydroxy-abieta-8,11,13-trien-7-one) have been isolated from ethanolic extract of the entire *C. cyrtophyllum* plant following cleaning by water and chloroform mix [42]. The former has a 17(15-16)-*abeo*-abietane framework.

The diterpenes sugiol **(18)**, uncinatone **(9)** and cyrtophyllone B **(21)**, also isolated from *C. cyrtophyllum*, have also been identified in *Aegiphila lhotzkyan* roots. These phytocompounds were tested for antiproliferative activity against leukaemia (CEM and HL-60), breast (MCF-7), colon (HCT-8) and skin (B-16) cancer cell lines in three independent experiments [43]. Of these, only cyrtophyllone B **(21)** is able to inhibit the proliferation of all tested tumour cell lines; however, it did not demonstrate strong inhibition (IC_{50} values above 1 μg mL^{-1}) [43]. In addition, diterpenoids isolated from *Caryopteris mongolica* roots were found to inhibit acethyl- and butyrylcholineesterase (AChE and BChE) [44]. The extraction method used for the phytochemical analyses of this plant species is shown in Table 2.

2.3. Clerodendrum eriophyllum

This unusual plant was previously used in malaria treatment in Kenya [45]. An alcoholic *C. eriophyllum* root bark extract demonstrated significant chemosuppressive properties against *Plasmodium berghei* in infected experimental mice [46]. The first phytochemical study of *Clerodendrum eriophyllum* was recorded by Machumi et. al. in 2010 [47]. The extraction methods used for the phytochemical analyses of this plant species are shown in

Table 3. The dichloromethane-methanolic root extract was found to contain ten abietane diterpenoids, with one being a new discovery: 12-hydroxy-8,12-abietadiene-3,11,14-trione **(22)**. The remaining nine diterpenes had previously been isolated from other plant materials: royleanone **(23)**, taxodione **(24)**, 6-deoxy-taxodione **(25)** (11-hydroxy-7,9(11),13-abietatrien-12-one), sugiol **(18)**, ferruginol **(26)**, 6-hydroxysalvinolone **(27)**, 6,11,12,16-tetrahydroxy-5,8,11,13-abietatetra-en-7-one **(28)**, uncinatone **(9)** and 11-hydroxy-8,11,13-abietatriene-12-O-β-xylopyranoside **(29)** [47].

Table 2. The diterpenoid extraction method and *C. cyrtophyllum* plant material for diterpenoid isolation.

Species	Material	Solvent and Extraction Method	Isolated Diterpenoids	References
C. cyrtophyllum	Stem	EtOH. The whole plant was dried and pulverised. It was extracted three times with hot solvent. The solvent was recovered in vacuo.	Cyrtophyllone A **(17)** Cyrtophyllone B **(21)** Teuvincenone F **(10)** Uncinatone **(9)** Sugiol **(18)**	[42]

One of the abietane diterpenoids, royleanone **(23)**, was first isolated from *Inula royleana* roots [48]. However, its presence has also been confirmed in other plant species, e.g., in transformed *Salvia austriaca* roots [49] and non-transformed *Salvia officinalis* roots [32]. Royleanone **(23)**, the diterpenoid characterised by the presence of a *p*-quinone grouping in the C ring, is also well known for its various biological activities. It has been found to demonstrate cytotoxicity against the cancer cell lines HeLa and Hep-2, particularly against Hep-2, with an IC_{50} value of 34 μg mL^{-1} [50]. It has also been found to demonstrate some antibacterial activity, but with weaker activity against methycyllin- and vancomycin-resistant *S. aureus* strains (MRSA and VRE) compared to other diterpenoids from outside the *Clerodendrum* genus (MIC = 32 and above 64 μg mL^{-1}, respectively) [51].

Table 3. The diterpenoid extraction method and *C. eriophyllum* plant material for diterpenoid isolation.

Species	Material	Solvent and Extraction Method	Isolated Diterpenoids	References
C. eriophyllum	Roots	1:1 MeOH/CH_2Cl_2; MeOH. Roots were dried and pulverised. They were extracted by cold percolation at room temperature using three portions of 1:1 MeOH/CH_2Cl_2 and then extracted with 100% MeOH once.	12-hydroxy-8,12-abietadiene-3,11,14-trione **(22)** Royleanone **(23)** Taxodione **(24)** 6-deoxy-taxodione **(25)** Sugiol **(18)** Ferruginol **(26)** 6-hydroxysalvinolone **(27)** 6,11,12,16-tetrahydroxy-5,8,11,13-abietatetra-en-7-one **(28)** Uncinatone **(9)** 11-hydroxy-8,11,13-abietatriene-12-O-β-xylopyranoside **(29)**	[47]

Taxodione **(24)** is a very well-known abietane-type diterpenoid with a metide-quinone moiety, which was first isolated from entire *Taxodium distichum* plant [52]. This compound has been found to demonstrate in vivo cytotoxic activity against Walker intramuscular carcinosarcoma 256 in rats and in vitro activity against human nosopharynx carcinoma cells KB [52]. Its high cytotoxicity was confirmed in further studies on Hep-2 and HeLa [50] and A549 [30]. This compound also demonstrates weak AChE and BChE inhibition. Computer modelling found the phytocompound to demonstrate low cardio- and genotoxicity and good permeability of the blood–brain barrier [30]. It has also been found to demonstrate strong antibacterial activity, particularly against MRSA and VRE strains (MIC = 4–10 μg mL^{-1}) [51].

6-deoxy-taxodione **(25)**, isolated from *C. eriophyllum* roots, is also detected in various parts of other plant species, e.g., in winter cones of *Taxodium distichum* and fruits of *Cupressus sempervirens* [52–54]. Like taxodione **(24)**, both isolated from *Cupressus sempervirens* cones, this compound demonstrates potent anti-leishmanial activity, with IC_{50} values of

0.077 μg mL^{-1} for 6-deoxy-taxodione **(25)** and 0.025 μg mL^{-1} for taxodione **(24)**. The two diterpenoids demonstrated much stronger activity against *Leishmania donovani* and its promastigotes than the anti-leishmanial drugs used as controls: pentamidine (IC_{50} 1.62 μg mL^{-1}) and amphotericin B (IC_{50} 0.11 μg mL^{-1}) [53]. In addition, 6-deoxy-taxodione **(25)** was found to demonstrate potent antibacterial activities against methicillin-resistant *Staphylococcus aureus* (MRSA), with IC_{50} values being 0.80 μg mL^{-1} for **(25)** and 0.85 μg mL^{-1} for **(26)** [53].

Another abietane-type diterpenoid is sugiol **(18)**, isolated from *Clerodendrum eriophyllum* roots. This compound has an oxygen atom connected to the B ring and an aromatic C ring. This unusual aromatic diterpene demonstrates various antioxidant, antibacterial, antiviral, anticancer, anti-tumour and anti-inflammatory activities [55]. Its antioxidant activity is similar to those of α-tocopherol and ascorbic acid based on DPPH (2,2-diphenyl-1-picrylhydrazyl) radical scavenging assay (84% and 82%, respectively) [56]. Sugiol **(18)** also demonstrates a concentration-dependent inhibitory effect (72.4%) against NO (nitric oxide), at a concentration of 100 μg mL^{-1}; it also demonstrated similar superoxide radical scavenging activity at a concentration of 250 μg mL^{-1}, to ascorbic acid and α-tocopherol activities (73% for sugiol compared to 73% and 74.5%, respectively) [56]. Sugiol **(18)** is also active against various foodborne pathogenic bacteria but neutralises Gram-positive bacteria more effectively than Gram-negative bacteria. When isolated from *Metasequoia glyptostroboides* cones, the compound was also found to demonstrate stronger antibacterial action against Gram-positive bacteria than the streptomycin used as a control [57]. Sugiol **(18)** has also been found to exhibit antiviral activity against the H1N1 virus in infected Madin-Darby canine kidney (MDCK) cells: no cytopathic changes were observed following 72 h of exposure following treatment with 500 μg mL^{-1} sugiol **(18)**. Hence, sugiol **(18)** could be a potential antiviral compound that can prevent H1N1-mediated cytopathy in MDCK cells [58].

The diterpenoid sugiol **(18)** also demonstrated cytotoxic activity against tumour cell lines, inhibiting the growth of three prostate tumour cell lines (LNCap, PC3 and DU145) and a non-tumorigenic cell line (MCF10A) [55]. Similarly, sugiol **(18)** treatment was found to reduce tumour weight and volume by as much as 75% in mice subcutaneously injected with DU145 cells in comparison with the control group. However, sugiol **(18)** did not affect the body weight of the mouse [55].

The abietane diterpenoid ferruginol **(26)** was first isolated in 1939 from the *Podocarpus ferruginea* tree. Structurally, ferruginol is similar to sugiol **(18)**, although it lacks an oxygen in the B ring. The biologically active ferruginol has been recorded in many plants including those of the Podocarpaceae, Cupressaceae, Lamiaceae and Verbenaceae [59]. This diterpenoid exhibits antibacterial and antifungal activities [60]. It has been found to inhibit the growth of *Bacillus brevis*, *B. subtilis* and *Staphylococcus aureus*, with inhibition zone diameters of 18, 10 and 9 mm, respectively. Ferruginol **(26)** demonstrated fungicidal activity against the pathogenic *Paecilomyces variotii*, with an inhibition zone of 10 mm [60], and Ferruginol **(26)** isolated from *Chamaecyparis lawsoniana* cones also demonstrated antibacterial activity against *S. aureus*, with MIC values ranging from 4 to 16 μg mL^{-1} depending on the strain [61]. It has demonstrated potent antimalarial activity [59], with EC_{50} values against *Plasmodium falciparum* ranging from 2.47 to 19.57 μM, depending on the strain [59]. In addition, ferruginol **(26)** has displayed moderate cytotoxic activity against NALM-6 human leukaemia lymphoblastic cells (IC_{50} 27.2 μg mL^{-1}) and promyelocytic HL-60 cells (IC_{50} 33.6 μg mL^{-1}) [62].

The abietane diterpenoid 6-hydroxysalvinolone **(27),** containing oxygen and hydroxyl groups in the B ring, demonstrates strong cytotoxicity against carcinoma cell lines. Following isolation from *Salvia chorassanica* roots, the compound exhibited strong cytotoxic activity against HL-60 and K562 cell lines with IC_{50} values of 36.3 and 33.3 μM, respectively. It appeared to demonstrate a substantially less cytotoxic effect on non-cancerous human cell lines. When administered at concentrations of 2.5 and 5.0 μM for 48 h, it also enhanced the expression of the proapoptotic protein Bax, and cleaved caspase-3 and PARP [63]. It also was found to exhibit

moderate cytotoxic activity against monkey kidney fibroblasts (VERO) with an IC_{50} level of 4.5 μg mL^{-1} [47]. Similarly to taxodione **(24)**, 6-hydroxysalvinolone **(27)** also demonstrated antifungal activity, especially against *Candida neoformans* with an IC_{50} value of 0.96 μg mL^{-1}. In the same assay, the IC_{50} of taxodione **(24)** was found to be 0.58 μg mL^{-1}, which is comparable with that of standard amphotericin B (IC_{50} = 0.44 μg mL^{-1}) [47].

Another abietane-type diterpenoid is 6,11,12,16-tetrahydroxy-5,8,11,13-abietatetra-en-7-one **(28)**, isolated from *Avicennia marina* twigs; it differs from 6-hydroxysalvinolone **(27)** by the presence of a hydroxyl group in the isopropyl moiety. It demonstrated moderate antiproliferative properties against L-929 (mouse fibroblasts) and K562 (human chronic myeloid leukaemia), and cytotoxic activities against the HeLa (human cervix carcinoma) cell line [64]. In biological tests, 6,11,12,16-tetrahydroxy-5,8,11,13-abietatetra-en-7-one **(28)** demonstrated GI_{50} (concentration causing 50% cell growth inhibition) values of 9.6 and 8.9 μg mL^{-1}, against L-929 (DSM ACC 2, mouse fibroblasts) and K562 cell lines (DSM ACC 10, human chronic myeloid leukaemia), and a CC_{50} (concentration that reduced the cell viability by 50%) of 18 μg mL^{-1} against the HeLa cell line [64]. The compound also demonstrated antibacterial activity against Gram-positive and Gram-negative bacteria and antifungal potential. A study of its antibacterial activity against *Bacillus subtilis* ATTC 6 633 (IMET) NA, *Bacillus subtilis* ATTC 6 633 (IMET) AS, *Escherichia coli* SG 458, *Pseudomonas aeruginosa* K 799/61, *Mycobacterium vaccae* IMET 10 670, *Sporobolomyces salmonicolor* SBUG 549, *Candida albicans* BMSY 212 and *Penicillium notatum* JP [64] found zone inhibition to range from 12 mm (for *C. albicans*) to 25 mm (for *B. subtilis* ATTC 6 633 (IMET) AS) [64].

Uncinatone **(9)**, a diterpenoid known for its biological activity, also exhibits potent antileishmanial activity. The IC_{50} value for *L. donovani* is 0.2 μg mL^{-1} [47].

2.4. C. formicarum

The *abeo*-abietane diterpenoid formidiol **(30)** was first obtained by methanolic extraction of *Clerodendrum formicarum* leaves and chromatographic separation of its triterpenoid constituents [65]. It was accompanied by the diterpenoid 12,16-epoxy-11,14-dihydroxy-6-methoxy-17(15→16)-abeo-abieta-5,8,11,13,15-pentanene-3,7-dione **(31)**, which had been previously isolated from a hexane extract of *Aegiphila lhotzkiana* roots. It was found to demonstrate antiproliferative activity against the leukaemia cell lines HL-60 (IC_{50} 4.4 μM) and CEM (IC_{50} 8.4 μM) [43]. Due to its structural similarity to formidiol **(30)**, compound **(31)** should be included in future studies of anti-proliferative activity. The extraction method used for the phytochemical analyses of this plant species is shown in Table 4.

Table 4. The diterpenoid extraction method and *C. formicarum* plant material for diterpenoid isolation.

Species	Material	Solvent and Extraction Method	Isolated Diterpenoids	References
C. formicarum	Leaves	EtOH. Leaves were dried under shade for a week. Powdered material was soaked in ethanol for six days. The resulting extract was concentrated by evaporation under vacuum distillation.	formidiol **(30)** 12,16-epoxy-11,14-dihydroxy-6-methoxy-17(15→16)-abeo-abieta-5,8,11,13,15-pentanene-3,7-dione **(31)**	[65]

2.5. Clerodendrum inerme

Studies on the aerial parts of *Clerodendrum inerme* resulted in the isolation of cleroinermin **(32)** a *neo*-clerodane diterpenoid [66] consisting of a bicyclic ring decalin moiety and a six-carbon side chain including a furane skeleton. The compound, first isolated from *Heteroplexis micocephala*, showed neuroprotective activity against MPP+ induced PC12-syn cell damage, with a relative cell proliferation rate of 104.32% [67]. Elsewhere, the *neo*-clerodane diterpenoids clerodendrin B **(33)**, 3-epicaryoptin **(34)**, clerodendrin C **(35)**, 2-acetoxyclerodendrin B **(36)** and 15-hydroxyepicaryoptin **(37)** have since been isolated [68]. The extraction methods used for the phytochemical analyses of this plant species are given in Table 5. These compounds have been found to be effective antifeedants against *Earias*

vitella at 10 μg cm^{-3} of diet (30 μg g^{-1}) and against *Spodoptera litura* at 10 μg cm^{-2} of leaf mass [68].

Table 5. The diterpenoid extraction methods and *C. inerme* plant materials for diterpenoid isolation.

Species	Material	Solvent and Extraction Method	Isolated Diterpenoids	References
C. inerme	Leaves	Hexane–EtOAc. Dried and finely powdered aerial parts of the plant were extracted with hexane—EtOAc (40:60)—fraction 1; and hexane—EtOAc (25:75)—fraction 2.	Inermes A **(39)** Inermes B **(40)** 14,15-dihydro-15β-methoxy-3-epicaryoptin **(41)**	[69]
	Aerial parts	MeOH. Dried and powdered aerial parts were extracted in a Soxhlet apparatus for 15 h. The extract was concentrated under red. pres., dil. with H_2O and the liberated solid was exhaustively extracted with Et_2O.	Cleroinermin **(32)**	[66]
	Leaves	MeOH. Air-dried and powdered roots were extracted three times by sonication for 30 min., concentrated under reduced pressure. They were suspended in water and successively partitioned with dichloromethane three times.	Crolerodendrum B **(42)** Crolerodendrum A **(43)** Uncinatone **(9)** Harwickiic acid **(44)** 14,15-dihydro-15β-methoxy-3-epicaryoptin **(41)**	[70]
	Aerial parts	The shade-dried, crushed aerial parts were percolated with *n*-hexane (three times) for 24 h. The resulting extract was then concentrated under vacuum to obtain a residue	clerodendrin B **(33)** 3-epicaryoptin **(34)** Clerodendrin C **(35)** 2-acetoxyclerodendrin B **(36)** 15-hydroxyepicaryoptin **(37)**	[68]

C. inerme has become an interesting subject of research for diterpenoid isolation. The aerial parts are a source of the neo-clerodane-type diterpenoids: clerodermic acid **(38)**, inermes A **(39)** and B **(40)**, as well as 14,15-dihydro-15β-methoxy-3-epicaryoptin **(41)** [69,71]. Among these compounds, clerodermic acid **(38)** deserves special attention due to its strong biological activity. The compound, isolated from the dichloromethane extract of the aerial part of *Salvia nemorosa*, was found to reduce the viability of A549 cells in a concentration-dependent manner, with an IC_{50} of 35 μg mL^{-1} at 48 h, based on the MTT assay [72]. Furthermore, clerodermic acid treatment resulted in various morphological changes, including diminished cell density, membrane blebbing and an increased number of floating cells, all of them being a manifestation of cell death **(38)**. DNA ladder, DAPI staining, cell cycle analysis, and annexin V/PI testing indicated that clerodermic acid demonstrates strong geno- and cytotoxicity and is able to induce apoptosis in A549 cells, as evidenced also by DNA fragmentation and chromatin condensation [72].

C. inerme aerial parts have also been found to include a newly rearranged abietane diterpenoid, crolerodendrum B **(42)**, as well as other known diterpenoids, such as crolerodendrum A **(43)**, uncinatone **(9)** and harwickiic acid **(44)** [70]. Harwickiic acid **(44)** was first isolated from *Sindora sumatrana* MIQ fruits [73]. This clerodane-type diterpenoid, obtained from the stem bark of *Croton sylvaticus*, was found to demonstrate significant antileishmanial activity against *L. donovani* promastigotes with an IC_{50} of 31.57 μM, as well as cytotoxic activity against RAW 264.7 (CC_{50} = 247.83 μM) [74]. Harwickiic acid **(44)**, isolated from *C. inerme* aerial parts, together with crolerodendrum B **(42)** and uncinatone **(9)** also demonstrates strong antioxidant activity measured as DPPH radical-scavenging activity; these compounds have been found to have respective ED_{50} values of 11.3 μM **(44)**, 17.6 μM **(42)** and 10.1 μM **(9)** [70].

2.6. Clerodendrum infortunatum

Crystallization and chromatographic separation of the leaf extract resulted in the isolation and identification of the clerodane diterpenoids clerodin **(45)**, 15-methoxy-14,15-dihydroclerodin **(46)** and 15-hydroxy-14,15-dihyroclerodin **(47)** [75]. The extraction methods used for the phytochemical analyses of this plant species are shown in Table 6. The isolated compounds were tested against *Helicoverpa armigera*. Studies on the growth inhibition potential of these diterpenoids found topical application of clerodin **(45)**, 15-methoxy-14,15-dihydroclerodin **(46)** and 15-hydroxy-14,15-dihyroclerodin **(47)** to yield GI_{50} values of 13, 21 and 11 ppm, respectively; in contrast, azadirachtin was found to have a GI_{50} value of 15 ppm [75].

Table 6. The diterpenoid extraction methods and *C. infortunatum* plant materials for diterpenoid isolation.

Species	Material	Solvent and Extraction Method	Isolated Diterpenoids	References
C. infortunatum	Aerial parts Leaves	The shade was dried, the crushed aerial parts were exhaustively extracted with *n*-hexane (3×). The extract was then concentrated in vacuo to ∼250 mL The leaves were extracted with **acetone**. The extract was concentrated in vacuo. The residue was solvated in a solution of water: methanol and partitioned with ethyl acetate and *n*-butanol, respectively.	Clerodin **(45)** (5*R*,10*S*,16*R*)-11,16,19-trihydroxy-12-O-β-D-glucopyranosyl-(1→2)-β-D-glucopyranosyl-17(15→16),18(4→3)-*diabeo*-3,8,11,13-abietatetraene-7-one (5*R*,10*S*,16*R*)-11,16-dihydroxy-12-O-β-D-glucopyranosyl-(1→2)-β-D-glucopyranosyl-17(15→16),18(4→3)-*diabeo*-4-carboxy-3,8,11,13-abietatetraene-7-one	[68] [76]
	Leaves	*n*-hexane/MeOH. The leaves were dried in the shade at room temperature and then ground in an electric grinder. The leaf powder was soaked in *n*-hexane for 72 h, shaken occasionally. The extract was filtered, concentrated in a rotary vacuum evaporator, then partitioned into hexane and methanol. After filtration, the leaf powder residue was further extracted with methanol and concentrated. This extract was further partitioned with hexane, ethyl acetate, and butanol.	clerodin **(45)** 15-methoxy-14,5- dihydroclerodin **(46)** 15-hydroxy-14,15-dihyroclerodin **(47)**	[75]

The purified diterpenoids, together with their extracts and fractions, also demonstrated insecticidal activity against the highly polyphagous cotton bollworm (*Helicoverpa armigera*) [77]. The antifeedant activity of the isolated diterpenoids was tested using choice and no-choice tests with 24- and 48-h observation intervals. In the no-choice test conditions, clerodin **(45)** and 15-methoxy-14,15-dihydroclerodin **(46)** demonstrated significantly higher antifeedant activity compared to high concentration azadirachtin, the key ingredient in many commercial pesticides [77], with the second diterpenoid demonstrating similar antifeedant activity to that of azadirachtin. In the choice test conditions, all isolated and identified compounds, as well as azadirachtin, demonstrated 100% antifeedant activity at the highest concentration. Furthermore, clerodin **(45)** has also been found to demonstrate antifeedant activity against *Earias vitella* and *Spodoptera litura* [68]. The antifeedant index (AI_{50}) values for clerodin **(45)**, 15-methoxy-14,15-dihydroclerodin **(46)** and 15-hydroxy-14,15-dihyroclerodin **(47)** were found to be 6, 6, and 8 ppm in the choice tests, and 8, 9, and 11 ppm in the no-choice tests, respectively.

The antifeedant activity of clerodanes has been attributed to the presence of a perhydrofuranofuran moiety and the degree of its unsaturation; a significant role may also be played by the presence of a trans-decalin ring system bearing an epoxide, together with ac-

etate groups [78,79]. These results suggest that the diterpenoids isolated from *Clerodendrum infortunatum* leaf extract offer promise as biopesticides and require further studies [77].

2.7. Clerodendrum kaichianum

Clerodendrum kaichianum P. S. Hsu is known to be the source of two new abietane-type compounds, *viz*. 17-hydroxyteuvincenone G **(51)** and 17-hydroxyteuvincen-5(6)-enone G **(52)**, as well as four known diterpenoids: teuvincenone A **(48)**, 11,14-dihydroxyabieta-8,11,13-trien-7-one **(49)**, dehydroabietan-7-one **(50)** and sugiol **(18)** [80]. These new secondary metabolites demonstrated relatively strong cytotoxic activities against HL-60 and A-549 cell lines in vitro based on the MTT assay. This action was compared to *cis*-platin, which was used as a control compound. In addition, 17-hydroxyteuvincenone G **(51)** yielded IC_{50} scores of 5.95 and 9.37 μM for HL-60 and A-549 cells, respectively; this activity was slightly higher than that of 17-hydroxyteuvincen-5(6)-enone G **(52)** (IC_{50} of 15.91 and 10.35 μM against the same cell lines) [80].

Further chromatographic separation from *C. kaichianum* stem extract resulted in the isolation of a newly rearranged abietane diterpenoid with five known compounds: villosin A **(53)**, salvinolone **(54)**, 14-deoxyloleon U **(55)**, 5,6-dehydrosugiol **(56)**, and coleon U **(57)**. This new diterpenoid was identified as (16R)-12,16-epoxy-11,14,17-trihydroxy-17(15→16)-abeo-8,11,13-abietatrien-7-one **(58)** [81]. Villosin A **(53)**, salvinolone **(54)** and 5,6-dehydrosugiol **(56)** were noted in the *Clerodendrum* genus for the first time. All extraction methods used for the phytochemical analyses of this plant species are shown in Table 7. All isolated constituents were tested for their cytotoxic activities against the viable HL-60 tumour cell line based on the MTT assay. The highest cytotoxic activity was demonstrated by (16R)-12,16-epoxy-11,14,17-trihydroxy-17(15→16)-abeo-8,11,13-abietatrien-7-one **(58)** with an IC_{50} value of 18.5 μM, with villosin A **(53)** and coleon U **(57)** demonstrating IC_{50} values of 20.1 and 24.1 μM, respectively. Salvinolone **(54)**, 14-deoxyloleon U **(55)** and 5,6-dehydrosugiol **(56)** demonstrated more than two-fold weaker cytotoxic activity, with IC_{50} values over 40 μM [81].

Table 7. The diterpenoid extraction method and *C. kaichianum* plant material for diterpenoid isolation.

Species	Material	Solvent and Extraction Method	Isolated Diterpenoids	References
C. kaichianum	Stem	**EtOH.** The air-dried and powdered stems was extracted with 75% aq. EtOH three times each at 75 °C for 4 h. The EtOH extracts were combined and evaporated.	17-hydroxyteuvincenone G **(51)** 17-hydroxyteuvincen-5(6)-enone G **(52)** Teuvincenone A **(48)** 11,14-dihydroxyabieta-8,11,13-trien-7-one **(49)** Dehydroabietan-7-one **(50)** Sugiol **(18)**	[80]
			(16R)-12,16-epoxy-11,14,17-trihydroxy-17(15→16)-abeo-8,11,13-abietatrien-7-one **(58)** Villosin A **(53)** Salvinolone **(54)** 14-deoxycoleon U **(55)** 5,6-dehydrosugiol **(56)** Coleon U **(57)**	[81]

2.8. Clerodendrum kiangsiense and C. mandarinorum

A phytochemical study on the aerial parts of *C. kiangsiense* resulted in the isolation of eight diterpenoids, one of which was a novel *abeo*-abietane diterpenoid. Spectroscopic analyses resulted in its identification as 12-methoxy-6,11,14,16-tetrahydroxy-17(15→16)-abeo-5,8,11,13-abietatetraen-3,7-dione **(59)** [82]. The remaining secondary metabolites were identified as mandarone A **(60)** ((5*R*,10*S*)-12-hydroxy-8,11,13-abietatriene-37-dione), taxusabietane A **(61)**, 12-O-demethylcryptojaponol **(62)**, cryptojaponol **(63)**, 11,14-dihydroxy-

8,11,13-abietatrien-7-one **(64)**, fortunin E **(65)** and fortunin F **(66)** [82]. Mandarone A **(60)** had previously been isolated from *Clerodendrum mandarinorum* stem [83] and *Euonymus lutchuensis* roots [84].

Various other mandarones have also been isolated from *C. mandarinorum* stem, including mandarone B **(67)** ((16 *S*)-12,16-epoxy-11,14-dihydroxy-17(15→16)-abeo-abieta-5,8,11,13-tetraene-7-one), mandarone C **(68)** (12,16-epoxy-11,14-dihydroxy-17(15→16)-abeo-abieta-2,5,8,11,13,15-hexaene-7-one) [84], mandarone D **(69)** (16*S*)-12,16-epoxy-l1-hydroxy-17(15→16),18(4→3)-diabeo-abieta-3,5.8,11,13-pentaene-7-one, mandarone E **(70)** (12.l6-epoxy-l1,14-dihydroxy-17(15→16),18(4→3)-diabeo-abieta-3,5,8,11,13,15-hexaene-7-one), mandarone F **(71)** (12,16-epoxy-6,11,14-trihydroxy-17(15→16),18(4→3)-diabeo-abieta-3,5,8, 11,13,15-hexaene-7-one), mandarone G **(72)** (12,16-epoxp-11,14-dihydroxy-6-methoxy-17 (15→16),18(4→3)-diabeo-abieta-3,5,8,11,13,15-hexaene-2,7-dione) and mandarone H **(73)** (12,16-epoxy-11,14-dihydroxy-17(15→16),18(4→3)-diabeo-abieta-3,5,8,11,13,15-hexaene-1,7-dione) [85]. The extraction methods used for the phytochemical analyses of these plant species are shown in Tables 8 and 9.

Table 8. The diterpenoid extraction method and *C. kiangsiense* plant material for diterpenoid isolation.

Species	Material	Solvent and Extraction Method	Isolated Diterpenoids	References
C. kiangsiense	Stem	EtOH. The air-dried and powdered stems extracted by 90% ethanol three times at 65 °C. The solvents were combined and evaporated to dryness under vacuum.	12-methoxy-6,11,14,16-tetrahydroxy-17(15→16)-abeo-5,8,11,13-abietatetraen-3,7-dione **(59)** Mandarone A **(60)** Taxusabietane A **(61)** 12-O-demethyl-cryptojaponol **(62)** Cryptojaponol **(63)** 11,14-dihydroxy-8,11,13-abietatrien-7-one **(64)** Fortunin E **(65)** Fortunin F **(66)**	[82]

Table 9. The diterpenoid extraction method and *C. mandarinorum* plant material for diterpenoid isolation.

Species	Material	Solvent and Extraction Method	Isolated Diterpenoids	References
C. mandarinorum	Stem	EtOH. The naturally dried and pulverised stems were extracted with hot EtOH three times. The solvent was removed in vacuo.	Mandarone D **(69)** Mandarone E **(70)** Mandarone F **(71)** Mandarone G **(72)** Mandarone H **(73)**	[85]
			Mandarone A **(60)** Mandarone B **(67)** Mandarone C **(68)**	[83]

Taxusabietane A **(61)**, isolated from bark extract of *Taxus wallichiana* Zucc. (in addition to taxusabietane C and taxamairin F), was found to demonstrate considerable lipoxygenase (LOX) inhibitory activity at an IC_{50} of 57 μM compared to controls (baicalein IC_{50} 22.1 μM) based on in vitro lipooxygenase inhibition assay and in vivo carrageenan-induced paw oedema model [86]. Cryptojaponol **(63)**, isolated from extracted *Taxodium distichum* bark, demonstrated moderate cytotoxic activity against human pancreatic carcinoma (PANC-1) [87] with an EC_{50} of about 38 μM and selective index (SI) of 7.9 [87].

In addition, 11,14-dihydroxy-8,11,13-abietatrien-7-one **(64)**, an abietane diterpenoid found in *Clerodendrum kiangsiense* aerial parts, exhibits some interesting biological activities. Costa-Lotufo et al. (2004) found it to demonstrate moderate cytotoxic activity against tumour cell lines, together with as well as carnasol, isolated from *Hyptis martiusii* roots [88]. Zadali et al. (2020) also reported it to be present in the aerial parts and roots of *Zhumeria majdae* and to show promising antiprotozoal activity; the IC_{50} value was found to be 8.65 μM,

with a selectivity index (SI) of 4.6 [89]. Additionally, it has also been found to demonstrate greater binding affinity at the active site of AChE in comparison to donepezil [90].

2.9. Clerodendrum splendens

Scientific research on this species allowed to isolate and identify four new clerodane diterpenoids, namely 2α-acetoxy-3β-(2′,3′-diacetoxy-2′-methyl)-butanoyloxy-14-hydro-15-hydroxyclerodin **(74)**, 3β,15-dihydroxy-14-hydro-clerodin **(75)**, 2α,15-dihydroxy-3β-(2′-hydroxy-2′-methyl-3′-acetoxy)-butanoyloxy-6α,18-diacetoxy-4α,17-epoxy-clerodan-11,16-lactone **(76)** and 3β,14S,15-trihydroxy-6α,18-diacetoxy-4α,17-epoxy-clerodan-11,16-lactone **(77)** [91]. The extraction method used for the phytochemical analyses of this plant species is shown in Table 10. Faiella et al. (2013) tested these compounds for their potential antiproliferative activity against HeLa cells. Briefly, the HeLa cells were incubated for 24 h with the diterpenoids at a concentration of 50 μM, and the results were compared with 15 μM phenethylisothiocyanate (PEITC) as a control. The results indicate that 2α-acetoxy-3β-(2′,3′-diacetoxy-2′-methyl)-butanoyloxy-14-hydro-15-hydroxyclerodin **(74)** and 2α,15-dihydroxy-3β-(2′-hydroxy-2′-methyl-3′-acetoxy)-butanoyloxy-6α,18-diacetoxy-4α,17-epoxy-clerodan-11,16-lactone **(76)** exhibit cell growth inhibition activity. In addition, the IC_{50} values for the two compounds, viz., **(76)** and **(74)**, were found to be 101 μM and 98 μM, respectively, after 72 h incubation [91].

Table 10. The diterpenoid extraction method and *C. splendens* plant material for diterpenoid isolation.

Species	Material	Solvent and Extraction Method	Isolated Diterpenoids	References
C. splendens	Aerial parts	Dried powdered aerial parts of C. splendens were successively and separately extracted for 48 h with *n*-hexane, $CHCl_3$, $CHCl_3$–MeOH (9:1), and MeOH, by exhaustive maceration	2α-acetoxy-3β-(2′,3′-diacetoxy-2′-methyl)-butanoyloxy-14-hydro-15-hydroxyclerodin **(74)** 3β,15-dihydroxy-14-hydro-clerodin **(75)** 2α,15-dihydroxy-3β-(2′-hydroxy-2′-methyl-3′-acetoxy)-butanoyloxy-6α,18-diacetoxy-4α,17-epoxy-clerodan-11,16-lactone **(76)** 3β,14S,15-trihydroxy-6α,18-diacetoxy-4α,17-epoxy-clerodan-11,16-lactone **(77)**	[91]

2.10. Clerodendrum trichotomum

Trichotomone **(78)** was first isolated from *Clerodendrum trichotomum* roots by careful semi-preparative chromatographical analysis. This diterpenoid is a rare phenolic ketal of a regular abietane derivative, cyrtophyllone B **(21)**, and a rearranged abietane derivative related to uncinatone **(9)** [89]. Trichotomone **(78)** demonstrates moderate cytotoxic activity against some tumour cell lines (A549, Jurkat, BGC-823 and 293T WT) with IC_{50} values ranging between 7.51 and 19.38 μM [92].

Wang et al. (2013) report the isolation of various other diterpenoid compounds from the species, including 17(15→16)-*abeo*-abietane (6-methoxyvillosin C **(79)** (=(10*R*,16*R*)-12,16-epoxy-11,14,17-trihydroxy-6-methoxy-17(15→16)-abeoabieta-5,8,11,13-tetraene-7-one), 18-hydroxy-6-methoxyvillosin C **(80)** (=(10*R*,16*R*)-12,16-epoxy-6-methoxy-11,14,17,18-tetrahydroxy-17(15→16)-abeo-abieta-5,8,11,13-tetraene-7-one) and (10*R*,16*S*)-12,16-epoxy-11,14-dihydroxy-6-methoxy-17(15→16)-abeo-abieta-5,8,11,13-tetraene-3,7-dione **(81)** and 17(15→16),18(4→3)-*diabeo*-abietane diterpenoids (trichotomone D **(82)** (=10*R*,16*S*)-12,16-epoxy-11,14-dihydroxy-18-oxo-17(15→16),18(4→3)-diabeo-abieta-3,5,8,11,13-pentaene-7-one, (10*R*,16*R*)-12,16-epoxy-11,14,17-trihydroxy-17(15→16),18(4→3)-diabeo-abieta-3,5,8,11,13-pentaene-2,7-dione **(83)** and trichotomone F **(84)** =(3*S*,4*R*,10*R*,16*S*)-3,4:12,16-diepoxy-11,14-dihydroxy-17(15→16),18(4→3)-*diabeo*-abieta-5,8,11,13-tetraene-7-one) [93]. In addition, the following known diterpenoids were also isolated: villosin C **(85)**, 12,16-epoxy-11,14-dihydroxy-6-methoxy-17(15→16)-abeo-abieta-5,8,11,13,15-pentanene-3,7-dione **(31)**, uncinatone **(9)**, mandarone E **(70)**, formidiol **(30)**, teuvincenone E **(86)**, teuvincenone

F **(10)** and Trichotomone H **(87)** (=12,16-epoxy-17(15→16),18(4→3)-*diabeo*-abieta-3,5,8,12,15-pentaene-7,11,14-trione) [93].

Of the 14 isolated compounds, (10*R*,16*S*)-12,16-epoxy-11,14-dihydroxy-6-methoxy-17(15→16)-abeo-abieta-5,8,11,13-tetraene-3,7-dione **(81)** is a newly discovered naturally occurring compound. All the extraction methods used for the phytochemical analyses of this plant species are shown in Table 11. The cytotoxic activities of these diterpenoids were studied against tumour cell lines BGC-823, Huh-7, KB, KE-97, and Jurkat based on CellTiter Glo™ Luminescent cell viability assay. Of all the tested compounds, trichotomone D **(82)**, F **(84)** and H **(87)**, teuvincenone E and H **(88)**, uncinatone **(9)** and mandarone E **(70)** showed cytotoxic activity. IC_{50} values ranged from 0.83 to 50.99 μM. The most active diterpenoid was found to be Teuvincenone E **(86)**, with IC_{50} values of 3.95, 5.37, 1.18, 1.27, and 0.83 μM against the BGC-823, Huh-7, KB, KE-97, and Jurkat lines, respectively. The authors attribute the high cytotoxic activity of this compound to its rearranged A ring and intact 2-methyl-3-dihydro-furan fragment [93].

In further phytochemical studies, air-dried stems of *Clerodendrum trichotomum* were extracted and chromatographically separated. Eleven compounds were identified, including seven abietane diterpenes: sugiol **(18)**, teuvincenone A **(48)**, teuvincenone B **(89)**, teuvincenone F **(10)**, teuvincenone H **(88)**, uncinatone **(9)** and cyrtophyllone B **(21)** [94]. In further studies on *C. trichotomum* stems, the same authors also identified the diterpenoids villosin B **(90)** and villosin C **(85)**; these demonstrate remarkable cytotoxic activities against tumour cell lines A549, HepG-2, MCF-7 and 4T1 with IC_{50} values ranging from 14.93 to 29.74 μM [95].

Hu et al. (2018) isolated twelve new abietane diterpenoids from *C. trichotomum* roots: 15,16-dehydroteuvincenone G **(91)**, 3-dihydroteuvincenone G **(92)**, 17-hydroxymandarone B **(93)**, trichotomin A **(94)**, 15,16-dihydroformidiol **(95)**, 18-hydroxyteuvincenone E **(96)**, 2α-hydrocaryopincaolide F **(97)**, 15α-hydroxyuncinatone **(98)**, 15α-hydroxyteuvincenone E **(99)**, trichotomin B **(100)**, trichotomside A **(101)** and B **(102)** [96]. As earlier studies indicate that *C. trichotomum* roots possess anti-inflammatory properties [17], all the secondary metabolites isolated by Hu et al. (2018) were tested for their ability to inhibit NO production in LPS-stimulated RAW 264.7 cells, a marker of inflammation [96]. Of the tested substances, 15,16-dehydroteuvincenone G, trichotomin A, 2α-hydrocaryopincaolide F, as well as other isolated compounds, such as villosin C **(85)**, 15-dehydro-17-hydroxycyrtophyllone A **(16)**, demethylcryptojaponol, 6β-hydroxydemethylcryptojaponol and trichotomone **(78)**, exhibited IC_{50} values ranging from 6.0 to 16.1 μM, with 15,16-dehydroteuvincenone G being the most active diterpenoid (IC_{50} value 6.0 μM). It is worth adding that all these active compounds acted at non-cytotoxic concentrations and demonstrated stronger activity than aminoguanidine hydrochloride (IC_{50} 26.2 μM) [96].

Table 11. The diterpenoid extraction methods and *C. trichotomum* plant materials for diterpenoid isolation.

Species	Material	Solvent and Extraction Method	Isolated Diterpenoids	References
C. trichotomum	Roots	The dried roots were first extracted with petroleum ether/EtOAc (1:1) three times at room temperature, assisted by ultrasonication. After filtration, the filtrate was concentrated at reduced pressure to give a dark brown residue	6-methoxyvillosin C **(79)** 18-hydroxy-6-methoxyvillosin C **(80)** (10*R*,16*S*)-12,16-epoxy-11,14-dihydroxy-6-methoxy-17(15→16)-abeo-abieta-5,8,11,13-tetraene-3,7-dione **(81)** Trichotomone D **(82)** (10*R*,16*R*)-12,16-epoxy-11,14,17-trihydroxy-17(15→16),18(4→3)-diabeo-abieta-3,5,8,11,13-pentaene-2,7-dione **(83)** Trichotomone F **(84)** 12,16-epoxy-11,14-dihydroxy-6-methoxy-17(15→16)-abeo-abieta-5,8,11,13,15-pentanene-3,7-dione **(31)** Uncinatone **(9)** Mandarone E **(70)** Formidiol **(30)** Teuvincenone E **(86)** Teuvincenone F **(10)** Trichotomone H **(87)** Villosin C **(85)**	[93]

Table 11. *Cont.*

Species	Material	Solvent and Extraction Method	Isolated Diterpenoids	References
C. trichotomum	Roots	Dried roots of *C. trichotomum* were exhaustively extracted with petroleum ether/EtOAc (1:1) at room temperature, yielding a semi-dry residua	Trichotomone **(78)**	[92]
C. trichotomum	Stems	The air-dried stems were cut into small pieces and extracted with 85% EtOH under reflux three times. The combined extracts were filtered and the solvent was removed under reduced pressure with a rotary evaporator at 60 °C to obtain a brown crude extract.	Sugiol **(18)** Teuvincenone F **(10)** Teuvincenone A **(48)** Teuvincenone H **(88)** Uncinatone **(9)** Teuvincenone B **(89)** Cyrtophyllone B **(21)**	[88]
C. trichotomum	Stems	The air-dried stems were cut into small pieces and extracted with 85% EtOH under reflux three times. The combined extracts were filtered and the solvent was removed under vacum to obtain a crude extract.	Villosin B **(90)** Villosin C **(85)** Cyrtophyllone B **(21)** Uncinatone **(9)** Teuvincenone B **(89)** Sugiol **(18)** Teuvincenone F **(10)** Teuvincenone A **(48)** Teuvincenone H **(88)**	[95]
C. trichotomum	Roots	Cut and air-dried roots were extracted under reflux with 95% EtOH Extract was filtered and organic solvents evaporated to receive the crude residue	15,16-dehydroteuvincenone G **(91)** 3-dihydroteuvincenone G **(92)** 17-hydroxymandarone B **(93)** Trichotomin A **(94)** 15,16-dihydroformidiol **(95)** 18-hydroxyteuvincenone E **(96)** 2α-hydrocaryopincaolide F **(97)** 15α-hydroxyuncinatone **(98)** 15α-hydroxyteuvincenone E **(99)** Trichotomin B **(100)** Trichotomside A **(101)** Trichotomside B **(102)**	[96]

3. The Latest Data

Woody branches and healthy stems of *Clerodendrum bracteatum* were the plant materials used for the extraction, isolation and purification to identify two new abietane diterpenes compounds, which are defined as: (10*S*,16*S*)-12,16-epoxy-17(15→16)-*abeo*-3,5,8,12-abietatetraen-7,11,14-trione (**103**) and 11,14,16-trihydroxy-6,12-dimethoxy-17(15→16)-abeo-5,8,11,13- abietatetraen-3,7-dione (**104**) [97]. The extraction method used for the phytochemical analyses of this plant species is shown in Table 12. Both phytochemicals have an *abeo*-abietane structure, the first of which has *p*-quinone and *p*-benzoquinone moieties. In compound **104,** four methyls, two ketones at C-3 and C-7, as well as the presence of a methine group at C-16 were detected. According to Li et al. (2021), two newly isolated structures (**103** and **104**) have the strongest antioxidant and cytotoxic activities against HL-60 and A-549 tumour cell lines among seven isolated diterpenes [97].

Table 12. The diterpenoid extraction methods and *Clerodendrum bracteatum* plant materials for diterpenoid isolation.

Species	Material	Solvent and Extraction Method	Isolated Diterpenoids	References
C. bracteatum	Stems	EtOH. Cut and air-dried stems were extracted under reflux with 90% Ethanol and evaporated to to afford a gummy residue. The crude extract was suspended in water and fractionated with EtOAc and *n*-BuOH.	(10*S*,16*S*)-12,16-epoxy-17(15→16)-*abeo*-3,5,8,12-abietatetraen-7,11,14-trione (**103**) 11,14,16-trihydroxy-6,12-dimethoxy-17(15→16)-abeo-5,8,11,13- abietatetraen-3,7-dione (**104**)	[97]

Interesting new data on diterpenes were published in the work of Qi et al. in 2021 [98]. The authors successfully undertook the extraction of *Clerodendrum chinense* roots, which resulted in the isolation and identification of 6 new diterpenes: Clerodenoids A–F (**105–110**) (Table 13). All of these compounds have an aromatised C ring. It is worth noting that

structures **106–108** are the rearranged abietane diterpenoids sharing a 17(15→16)-abeo-abietane skeleton, while compounds **109–110** are 17(15→16),18(4→3)-diabeo-abietane moieties. Furthermore, compound **110** has a persubstituted Δ3 double bond and methylhydroxyl function in the A ring. All six newly isolated diterpenes were examined towards antiproliferative activities against HL-60 and A-549 human tumour cell lines [98]. The most active diterpene was compound **110** demonstrating IC_{50} values at 1.36 and 1.00 μM against HL-60 and A-549 cell lines, respectively [98].

Table 13. The diterpenoid extraction methods and *Clerodendrum chinense* plant materials for diterpenoid isolation.

Species	Material	Solvent and Extraction Method	Isolated Diterpenoids	References
C. chinense	Roots	EtOH. The dried roots were soaked with 95% EtOH (20 L × 3) and the residue was suspended in water followed by extraction with EtOAc to afford an EtOAc extract	Clerodenoid A Clerodenoid B Clerodenoid C Clerodenoid D Clerodenoid E Clerodenoid F	[98]

Clerodendrum infortunatum aerial parts were used for extraction and isolation of terpenoid compounds [76]. Among various known compounds, two previously unknown diterpenes were isolated and identified as (5*R*,10*S*,16*R*)-11,16,19-trihydroxy-12-O-β-D-glucopyranosyl-(1→2)-β-D-glucopyranosyl-17(15→16),18(4→3)-*diabeo*-3,8,11,13-abietatetraene-7-one (**111**) and (5*R*,10*S*,16*R*)-11,16-dihydroxy-12-O-β-D-glucopyranosyl-(1→2)-β-D-glucopyranosyl-17(15→16),18(4→3)-*diabeo*-4-carboxy-3,8,11,13-abietatetraene-7-one (**112**) [76]. The extraction method used for the phytochemicals analyses of this plant species is shown in Table 6. Inhibition of converting carbohydrates into monosaccharides is considered to be an adjunct to the treatment of type 2 diabetes. Therefore, it was justified by the authors to investigate this activity among isolated compounds. The isolated secondary metabolites were tested for their ability to inhibit α-amylase and α-glucosidase. Compound **111** ((5*R*,10*S*,16*R*)-11,16,19-trihydroxy-12-O-β-D-glucopyranosyl-(1→2)-β-D-glucopyranosyl-17(15→16),18(4→3)-*diabeo*-3,8,11,13-abietatetraene-7-one) inhibited these enzymes activity with an IC_{50} value of 18.5 and 24.6 μM, respectively. (5R,10S,16R)-11,16-dihydroxy-12-O-β-D-glucopyranosyl-(1→2)-β-D-glucopyranosyl-17(15→16),18(4→3)-*diabeo*-4-carboxy-3,8,11,13-abietatetraene-7-one demonstrated weaker activity (IC_{50} = 64.6 and 78.3 μM) [76]. Additionally, the studied compounds were tested for acethyl- and buthyrylcholinesterase (AChE and BChE) inhibition, showing weak activity against AChE with an IC_{50} of 191 and 139 μM, respectively [76].

The diterpenes present in *C. inerme* [69] were isolated from the dried roots of *Clerodendrum bungei* crolerodendrum A (**43**) and B (**42**) for the first time in this species [20,22].

Compound **42** is known for its antioxidant properties [70] and exhibits significant inhibition against the α-glucosidase enzyme with an IC_{50} value of 17 μM [39].

The biological activities of the diterpenoids isolated from the *Clerodendrum* genus are summarised in Table 14.

Table 14. The biological activities of diterpenoids isolated from *Clerodendrum* genus.

Compound Name	Occurence in *Clerodendrum* Species	Biological Activity	References of the Active Compounds
uncinatone	*C. bungei* (roots), *C. eriophyllum* (roots), *C. inerme* (aerial parts) *C. trichotomum* (roots)	Cytotoxic; inhibition the cell proliferation and induction cell-cycle G2/M phase arrest; anti-complement activity on the classical pathway complement system, antileishmanial, antioxidant;	[36,41,70]

Table 14. *Cont.*

Compound Name	Occurence in *Clerodendrum* Species	Biological Activity	References of the Active Compounds
12-O-β-D-glucopyranosyl-3,11,16-trihydroxyabieta-8,11,13-triene; 3,12-O-β-D-diglucopyranosyl-11,16-dihydroxyabieta- 8,11,13-triene; 19-hydroxyteuvincenone F	*C. bungei* (roots)	anti-complement activity on the classical pathway complement system;	[37]
16-O-β-D-D-glucopyranosyl-3β-20-epoxy-3-hydroxyabieta-8,11,13-triene	*C. bungei* (roots)	Cytotoxic	[34]
15-Dehydrocyrtophyllone A	*C. bungei* (roots)	ACE (angiotensin-converting enzyme) inhibition;	[38]
cyrtophyllone B	*C. cyrtophyllum* (whole plant)	cytotoxic; acethyl- and butyrylcholineesterase inhibition;	[43]
royleanone; taxodione; 6-deoxy-taxodione; sugiol; ferruginol; 6-hydroxysalvinolone; 6,11,12,16-tetrahydroxy-5,8,11,13-abietatetra-en-7-one;	*C. eriophyllum* (roots)	Cytotoxic, weak antibacterial; cytotoxic, antibacterial, acethyl- and butyrylcholineesterase inhibition; antibacterial and antileishmanial antioxidant, antibacterial, antiviral, anticancer, anti-tumor and anti-inflammatory, antiviral, cytotoxic; antibacterial, antifungal, antimalarial, cytotoxic; apoptose induction, antifungal, cytotoxic; antibacterial, antifungal, cytostatic, cytotoxic;	[50,51] [30,50–52] [53] [55–58] [59–62] [47,63] [64]
12,16-epoxy-11,14-dihydroxy-6-methoxy-17(15→16)-abeo-abieta-5,8,11,13,15-pentanene-3,7-dione	*C. formicarum* (leaves)	antiproliferative	[43]
cleroinermin; clerodendrin B; 3-epicaryoptin; clerodendrin C; 2-acetoxyclerodendrin B; 15-hydroxyepicaryoptin; clerodermic acid harwickiic acid crolerodendrum B	*Clerodendrum inerme* (aerial parts) *Clerodendrum inerme* and *C. bungei* (aerial parts)	Neuroprotective, insecticidal, antiproliferative and apoptose induction antileishmanial, cytotoxic, antioxidant, antioxidant, α-glucosidase inhibition	[67] [68] [72] [74] [70] [39]
clerodin; 15-methoxy-14,15-dihydroclerodin; 15-hydroxy-14,15-dihyroclerodin	*C. infortunatum* (leaves)	insecticidal	[68,75,77]
(5*R*,10*S*,16*R*)-11,16,19-trihydroxy-12-O-β-D-glucopyranosyl-(1→2)-β-D-glucopyranosyl-17(15→16),18(4→3)-*diabeo*-3,8,11,13-abietatetraene-7-one (5R,10S,16R)-11,16-dihydroxy-12-O-β-D-glucopyranosyl-(1→2)-β-D-glucopyranosyl-17(15→16),18(4→3)-*diabeo*-4-carboxy-3,8,11,13-abietatetraene-7-one 17-hydroxyteuvincenone G; 17-hydroxyteuvincen-5(6)-enone G; villosin A; salvinolone; 14-deoxyloleon U; 5,6-dehydrosugiol; coleon U; (16R)-12,16-epoxy-11,14,17-trihydroxy-17(15→16)-abeo-8,11,13-abietatrien-7-one	*C. infortunatum* (leaves) *C. kaichianum* (steams)	Acethyl- and buthyrylcholinesterase (AChE and BChE) inhibition, α-amylase and α-glucosidase inhibition cytotoxic	[76] [80,81]
taxusabietane A; cryptojaponol; 11,14-dihydroxy-8,11,13-abietatrien-7-one	*C. kiangsiense* (aerial parts)	Anti-inflammatory Cytotoxic Cytotoxic, antiprotozoal	[86] [87] [88,89]
2α-acetoxy-3β-(2′,3′-diacetoxy-2′-methyl)-butanoyloxy-14-hydro-15-hydroxyclerodin; 2α,15-dihydroxy-3β-(2′-hydroxy-2′-methyl-3′-acetoxy)-butanoyloxy-6α,18-diacetoxy-4α,17-epoxy-clerodan-11,16-lactone	*C. splendens*	Antiproliferative	[91]

Table 14. *Cont.*

Compound Name	Occurence in *Clerodendrum* Species	Biological Activity	References of the Active Compounds
trichotomone D, F and H; teuvincenone E and H, uncinatone; mandarone E	*C. trichotomum* (roots)	Cytotoxic Cytotoxic	[92,93] [95]
villosin B and C	(steams)	Anti-inflammatory	[96]
15,16-dehydroteuvincenone G; trichotomin A; 2α-hydrocaryopincaolide F; villosin C; 15-dehydro-17-hydroxycyrtophyllone A; demethylcryptojaponol; 6β-hydroxydemethylcryptojaponol; trichotomone	(roots) *Clerodendrum bracteatum* (stems) *Clerodendrum chinense* (roots)	Antioxidant, cytotoxic Cytotoxic	[97] [98]
(10*S*,16*S*)-12,16-epoxy-17(15→16)-*abeo*-3,5,8,12-abietatetraen-7,11,14-trione			
11,14,16-trihydroxy-6,12-dimethoxy-17(15→16)-abeo-5,8,11,13-abietatetraen-3,7-dione			
Clerodenoid A			
Clerodenoid D			
Clerodenoid E			
Clerodenoid F			

4. Concluding Remarks

The members of the genus *Clerodendrum*, of the family *Lamiaceae*, are rich in diterpenoid secondary metabolites, both in the aerial parts and the roots. Due to their moderate, and in some cases strong, biological activities, these diterpenoids are interesting experimental objects. This is particularly true for in vivo pharmacological evaluation. Some of the diterpenes isolated from *Clerodendrum* spp. are structurally similar to the more highly active phytocompounds; however, they have not been tested for their potential biological activities. This is an important area for further study, as both infectious and civilization diseases, such as cancer, require the search for new therapeutically active structures. The new metabolites obtained from *Clerodendrum* spp. demonstrate high pharmacological potential, and could be an interesting object of further studies, particularly plant in vitro culture aimed at optimizing the cultivation conditions to increase biomass and secondary metabolite production, especially diterpenes. These biotechnological investigations should determine the effect of culture type (callus, shoot, modified root) and growth conditions such as basal medium and light wavelength, regardless of climatic conditions, season and environmental pollution.

Another interesting area of research concerning the diterpenes from *Clerodendrum* could be the chemical modification of the isolated phytocompounds. These would include the production of semisynthetic analogues with enhanced biological activities, and improved bioavailability or safety [99,100].

Another equally interesting area of research into these diterpenes is biotransformation [101]. Biotransformation is a very useful tool for the structural modification of natural products with complex chemical structures. Research into the biotransformation of metabolic pathways is essential to understand the potential toxicity and efficacy of new drug candidates and should be a mandatory part of preclinical studies [102].

Author Contributions: Conceptualization, Ł.K. and J.G.; writing—original draft preparation, Ł.K.; writing—review and editing, Ł.K. and J.G.; data curation, J.G.; visualization, J.G. All authors have read and agreed to the published version of the manuscript.

Funding: This work was supprted by Medical University of Łódź, a Grant No. 503/3-012-01/503-90-000 and 503/3-012-01/503-31-001-19-00.

Institutional Review Board Statement: Not applicable.

Informed Consent Statement: Not applicable.

Data Availability Statement: Not applicable.

Acknowledgments: Not applicable.

Conflicts of Interest: The authors declare no conflict of interest.

References

1. Rueda, R.M. The Genus Clerodendrum (Verbenaceae) in Mesoamerica. *Ann. Mo. Bot. Gard.* **1993**, *80*, 870–890. [CrossRef]
2. Leeratiwong, C.; Chantaranothai, P.; Paton, A.J. A synopsis of the genus *Clerodendrum* L. (Lamiaceae) in Thailand. *Trop. Nat. Hist.* **2011**, *11*, 177–211.
3. Shou-liang, C.; Gilbert, M.G. Verbenaceae. In *Flora of China*; Missouri Botanical Garden: St. Louis, MI, USA; Science Press: Beijing, China, 1994; pp. 1–49.
4. Munir, A.M. A Taxonomic Revision of the Genus *Clerodendrum* L. (Verbenaceae) in Australia. *J. Adelaide Bot. Gard.* **1989**, *11*, 101–173.
5. Harley, R.M.; Atkins, S.; Budantsev, A.L.; Cantino, P.D.; Conn, B.J.; Grayer, R.; Harley, M.M.; Kok, R.; Krestovskaja, T.; Morales, R.; et al. *The Family and Genera of Vascular Plants*; Springer: Berlin/Heidelberg, Germany, 2004; pp. 167–275.
6. Mabberley, D.J. *A Portable Dictionary of Plants, Their Classification and Uses*, 3rd ed.; Cambridge University Press: Cambridge, UK, 2008.
7. Muthu, C.; Baskar, K.; Ignacimuthu, S.; Ai-Khaliel, A.S. Ovicidal and oviposition deterrent activities of the flavonoid pectolinaringenin from *Clerodendrum phlomidis* against *Earias vittella*. *Phytoparasitica* **2013**, *41*, 365–372. [CrossRef]
8. Shrivastava, N.; Patel, T. *Clerodendrum* and healthcare: An overview. *Med. Aromat. Plant Sci. Biot.* **2007**, *1*, 209–223.
9. Chethana, G.S.; Hari, V.K.R.; Gopinath, S.M. Review on *Clerodendrum inerme*. *J. Pharm. Sci. Innov.* **2013**, *2*, 38–40.
10. Baker, J.T.; Borris, R.P.; Carté, B.; Geoffrey, A.; Soejarto, C.D.D.; Cragg, G.M.; Gupta, M.P.; Iwu, M.M.; Madulid, D.R.; Tyler, V.E. Natural product drug discovery and development; new perspective on international collaboration. *J. Nat. Prod.* **1995**, *58*, 1325–1357. [CrossRef]
11. Hazekamp, A.; Verpoorte, R.; Panthong, A.; Hazekamp, A.; Verpoorte, R.; Panthong, A. Isolation of a bronchodilator flavonoid from the Thai medicinal plant *Clerodendrum petasites*. *J. Ethnopharmacol.* **2001**, *78*, 45–49. [CrossRef]
12. Nishida, R.; Kawai, K.; Amano, T.; Kuwahara, Y. Pharnacophagous feeding stimulate activity of neoclerodane diterpenoids for the turnip sawfly, Athalia rosae ruficornis. *Biochem. Syst. Ecol.* **2004**, *32*, 15–25. [CrossRef]
13. Ganapaty, S.; Rao, D.V. Triterpenoids of the stem bark of *Cleodendrum morifolium*. *Indian J. Pharm. Sci.* **1985**, *47*, 167–168.
14. Achari, B.; Chaudhuri, C.; Saha, C.R.; Dutta, P.K.; Pakrashi, S.C. A clerodane diterpene and other constituents of *Clerodendrum inerme*. *Phytochemistry.* **1990**, *29*, 3671–3673. [CrossRef]
15. Sinha, N.K.; Seth, K.K.; Pandey, V.B.; Dasgupta, B.; Shah, A.H. Flavonoids from the flowers of *Clerodendron infortunatum*. *Planta Med.* **1981**, *42*, 296–298. [CrossRef] [PubMed]
16. Chae, S.; Kang, K.A.; Ju, S.K.; Jin, W.H.; Kang, S.S. Trichotomoside: A new antioxidative phenylpropanoid glycoside from *Clerodendron trichotomum*. *Chem. Biodivers.* **2006**, *3*, 41–48. [CrossRef]
17. Kim, K.H.; Kim, S.; Min, Y.J.; Ham, I.H.; Wan, K.W. Anti-inflammatory phenylpropanoid glycosides from *Clerodendron trichotomum* leaves. *Arch. Pharm. Res.* **2009**, *32*, 7–13. [CrossRef] [PubMed]
18. Akihisa, T.; Ghosh, P.; Thakur, S.; Nagata, H.; Tamura, T.; Matsumoto, T. 24, 24-dimethyl-25-dehydrolophenol, a 4α-methylsterol from *Clerodendrum inerme*. *Phytochemistry* **1990**, *29*, 1639–1641. [CrossRef]
19. Xu, R.L.; Wang, R.; Wei, H.; Shi, Y.P. New cyclohexylethanoids from the leaves of *Clerodendrum trichotomum*. *Phytochem. Lett.* **2014**, *7*, 111–113. [CrossRef]
20. Jadeja, R.; Thounaojam, M.; Ansarullah; Ramchandran, A.V.; Devkar, R. Phytochemical constituents and free radical scavenging activity of *Clerodendrum glandulosum* Coleb methanolic extract. *J. Complement. Integr. Med.* **2009**, *6*, 1–23. [CrossRef]
21. Adsersen, A.; Adsersen, H.; Brimer, L. Cyanogenic constituents in plants from the Galapagos Islands. *Biochem. Syst. Ecol.* **1988**, *16*, 65–77. [CrossRef]
22. Kuźma, Ł. Plant Cell and Tissue Differentiation and Secondary Metabolites. In *Reference Series in Phytochemistry*; Springer: Cham, Swizherland, 2020; pp. 561–584.
23. Hu, Z.; Liu, X.; Tian, M.; Ma, Y.; Jin, B.; Gao, W.; Cui, G.; Guo, J.; Huang, L. Recent progress and new perspectives for diterpenoid biosynthesis in medicinal plants. *Med. Res. Rev.* **2021**, *41*, 2971–2997. [CrossRef]
24. Kingston, D.G.I. Taxol: The chemistry and structure-activity relationships of a novel anticancer agent. *Trends Biotechnol.* **1994**, *12*, 222–227. [CrossRef]
25. Lindner, E.; Dohadwalla, A.N.; Bhattacharya, B.K. Positive inotropic and blood pressure lowering activity of a diterpene derivative isolated from *Coleus forskohli*: Forskolin. *Arzneimittel-Forschung* **1978**, *28*, 284–289. [PubMed]
26. Monteiro, A.S.N.; Campos, D.R.; Albuquerque, A.A.S.; Evora, P.R.B.; Ferreira, L.G.; Celotto, A.C. Effect of diterpene manool on the arterial blood pressure and vascular reactivity in normotensive and hypertensive rats. *Arq. Bras. Cardiol.* **2020**, *115*, 669–677. [CrossRef] [PubMed]
27. Laurenza, A.; Sutkowski, E.M.; Seamon, K.B. Forskolin: A specific stimulator of adenylyl cyclase or a diterpene with multiple sites of action? *Trends Pharmacol. Sci.* **1989**, *10*, 442–447. [CrossRef]
28. Kuźma, Ł.; Różalski, M.; Walencka, E.; Różalska, B.; Wysokińska, H. Antimicrobial activity of diterpenoids from hairy roots of *Salvia sclarea* L.: Salvipisone as a potential anti-biofilm agent active against antibiotic resistant staphylococci. *Phytomedicine* **2007**, *14*, 31–35. [CrossRef] [PubMed]
29. Kuźma, Ł.; Wysokińska, H.; Różalski, M.; Krajewska, U.; Kisiel, W. An unusual taxodione derivative from hairy roots of *Salvia austriaca*. *Fitoterapia* **2012**, *83*, 770–773. [CrossRef] [PubMed]

30. Kuźma, Ł.; Wysokińska, H.; Sikora, J.; Olszewska, P.; Mikiciuk-Olasik, E.; Szymański, P. Taxodione and Extracts from *Salvia austriaca* roots as human cholinesterase inhibitors. *Phytother. Res.* **2016**, *30*, 234–242. [CrossRef]
31. Fronza, M.; Lamy, E.; Günther, S.; Heinzmann, B.; Laufer, S.; Merfort, I. Abietane diterpenes induce cytotoxic effects in human pancreatic cancer cell line MIA PaCa-2 through different modes of action. *Phytochemistry* **2012**, *78*, 107–119. [CrossRef]
32. Spiridonov, N.A.; Arkhipov, V.V.; Foigel, A.G.; Shipulina, L.D.; Fomkina, M.G. Protonophoric and uncoupling activity of royleanones from Salvia officinalis and euvimals from Eucalyptus viminalis. *Phytother. Res.* **2003**, *17*, 1228–1230. [CrossRef]
33. Reveglia, P.; Cimmino, A.; Masi, M.; Nocera, P.; Berova, N.; Ellestad, G.; Evidente, A. Pimarane diterpenes: Natural source, stereochemical configuration, and biological activity. *Chirality* **2018**, *30*, 1115–1134. [CrossRef]
34. Sun, L.; Wang, Z.; Ding, G.; Bi, Y.; Meng, Z.; Xiao, W. Isolation and structure characterization of two new diterpenoids from *Clerodendrum bungei*. *Phytochem. Lett.* **2014**, *7*, 221–224. [CrossRef]
35. Fan, T.; Min, Z.; Iinuma, M. Two novel diterpenoids from *Clerodendrum bungei*. *Chem. Pharm. Bull.* **1999**, *12*, 1797–1798. [CrossRef]
36. Liu, S.; Zhu, H.; Zhang, S.; Zhang, X.; Yu, Q.; Xuan, L. Abietane Diterpenoids from *Clerodendrum bungei*. *J. Nat. Prod.* **2008**, *71*, 755–759. [CrossRef] [PubMed]
37. Kim, S.-K.; Cho, S.-B.; Moon, H.-I. Anti-complement activity of isolated compounds from the roots of *Clerodendrum bungei* Steud. *Phytother. Res.* **2010**, *24*, 1720–1723. [CrossRef] [PubMed]
38. Liu, Q.; Hu, H.-J.; Li, P.-F.; Yang, Y.-B.; Wub, L.-H.; Chou, G.-X.; Wanga, Z.-T. Diterpenoids and phenylethanoid glycosides from the roots of *Clerodendrum bungei* and their inhibitory effects against angiotensin converting enzyme and α-glucosidase. *Phytochemistry* **2014**, *103*, 196–202. [CrossRef] [PubMed]
39. Wu, D.X.; Yu, J.H.; Song, X.Q.; Ma, Y.Z.; Shan, P.; Zhang, H. Diterpenoids from the Roots of *Clerodendrum bungei*. *Rec. Nat. Prod.* **2022**, *16*, 27–33.
40. Slamenová, D.; Masterová, I.; Lábaj, J.; Horváthová, E.; Kubala, P.; Jakubíková, J.; Wsólová, L. Cytotoxic and DNA-damaging effects of diterpenoid quinones from the roots of *Salvia officinalis* L. on colonic and hepatic human cells cultured in vitro. *Basic Clin. Pharmacol. Toxicol.* **2004**, *94*, 282–290. [CrossRef]
41. Han, H.-J.; Tan, N.-H.; Zeng, G.-Z.; Fan, J.-T.; Huang, H.-Q.; Ji, C.-J.; Jia, R.-R.; Zhao, Q.-S.; Zhang, Y.-J.; Hao, X.-J.; et al. Natural inhibitors of DNA topoisomerase I with cytotoxicities. *Chem. Biodivers.* **2008**, *5*, 1364–1368. [CrossRef]
42. Tian, X.-D.; Min, Z.-D.; Xie, N.; Lei, Y.; Tian, Z.-Y.; Zheng, Q.-T.; Xu, R.-N.; Tanaka, T.; Iinuma, M.; Mizuno, M. Abietane diterpenes from *Clerodendron cyrtophyllum*. *Chem. Pharm. Bull.* **1993**, *42*, 1415–1417. [CrossRef]
43. Costa-Lotufo, L.V.; Silveira, E.R.; Barros, M.C.; Lima, M.A.; De Moraes, M.E.; De Moraes, M.O.; Pessoa, C. Antiproliferative effects of abietane diterpenes from *Aegiphila lhotzkyana*. *Planta Med.* **2004**, *70*, 180–182.
44. Murata, T.; Ishikawa, Y.; Saruu, E.; Selenge, E.; Sasaki, K.; Umehara, K.; Yoshizaki, F.; Batkhuu, J. Abietane-type diterpenoids from the roots of *Caryopteris mongolica* and their cholinesterase inhibitory activities. *Phytochemistry* **2016**, *130*, 152–158. [CrossRef]
45. Beentje, H.J. *Kenya Trees, Shrubs and Lianas*; National Museums of Kenya: Nairobi, Kenya, 1994; p. 613.
46. Muthaura, C.N.; Rukunga, G.M.; Chhabra, S.C.; Omar, S.A.; Guantai, A.N.; Gathirwa, J.W.; Tolo, F.M.; Mwitari, P.G.; Keter, L.K.; Kirira, P.G.; et al. Antimalarial activity of aome plants traditionally used in Meru district of Kenya. *Phytother. Res.* **2007**, *21*, 860–867. [CrossRef] [PubMed]
47. Machumi, F.; Samoylenko, V.; Yenesewa, A.; Deresea, S.; Midiwoa, J.O.; Wiggers, F.T.; Jacob, M.R.; Tekwani, B.L.; Khan, S.I.; Walker, L.A.; et al. Antimicrobial and antiparasitic abietane diterpenoids from the roots of *Clerodendrum eriophyllum*. *Nat. Prod. Commun.* **2010**, *5*, 853–858. [CrossRef] [PubMed]
48. Edwards, O.E.; Feniak, G.; Los, M. Diterpenoid quinones of *Inula royleana* D. C. *Can. J. Chem.* **1962**, *40*, 1540–1546. [CrossRef]
49. Kuźma, Ł.; Kisiel, W.; Królicka, A.; Wysokińska, H. Genetic transformation of *Salvia austriaca* by *Agrobacterium rhizogenes* and diterpenoid isolation. *Pharmazie* **2011**, *66*, 904–907.
50. Moujir, L.; Gutiérrez-Navarro, A.M.; Andrés, L.S.; Luis, J.G. Bioactive diterpenoids isolated from *Salvia mellifera*. *Phytother. Res.* **1996**, *10*, 172–174. [CrossRef]
51. Yang, Z.; Kitano, Y.; Chiba, K.; Shibata, N.; Kurokawa, H.; Doi, Y.; Arakawa, Y.; Tada, M. Synthesis of variously oxidized abietane diterpenes and their antibacterial activities against MRSA and VRE. *Bioorg. Med. Chem.* **2001**, *9*, 347–356. [CrossRef]
52. Kupchan, S.M.; Karim, A.; Marcks, C. Tumor inhibitors. XXXIV. Taxodione and taxodone, two novel diterpenoid quinone methide tumor inhibitors from *Taxodium distichum*. *J. Am. Chem. Soc.* **1968**, *90*, 5923–5924. [CrossRef]
53. Zhang, J.; Rahman, A.A.; Jain, S.; Jacob, M.R.; Khan, S.I.; Tekwani, B.L.; Ilias, M. Antimicrobial and antiparasitic abietane diterpenoids from *Cupressus sempervirens*. *Res. Rep. Med. Chem.* **2012**, *2*, 1–6.
54. Đapić, N.M.; Ristić, M.S. Chemical profile of *Taxodium distichum* winter cones. *Acta Period. Technol.* **2017**, *48*, 77–83. [CrossRef]
55. Bajpai, V.K.; Sonwal, S.; Hwang, S.-K.; Shukla, S.; Khan, I.; Dey, D.K.; Chen, L.; Simal-Gandara, J.; Xiao, J.; Huh, Y.S.; et al. Sugiol, a diterpenoid: Therapeutic actions and molecular pathways involved. *Pharmacol. Res.* **2021**, *163*, 105313. [CrossRef]
56. Bajpai, V.K.; Sharma, A.; Kang, S.C.; Baek, K.-H. Antioxidant, lipid peroxidation inhibition and free radical scavenging efficacy of a diterpenoid compound sugiol isolated from *Metasequoia glyptostroboides*. *Asian Pac. J. Trop. Med.* **2014**, *7*, 9–15. [CrossRef]
57. Juvik, O.J.; Nguyen, X.H.T.; Andersen, H.L.; Fossen, T. Growing with dinosaurs: Natural products from the Cretaceous relict *Metasequoia glyptostroboides* Hu & Cheng—a molecular reservoir from the ancient world with potential in modern medicine. *Phytochem. Rev.* **2016**, *15*, 161–195. [PubMed]
58. Bajpai, V.K.; Kim, N.-H.; Kim, K.; Kang, S.C. Antiviral potential of a diterpenoid compound sugiol from *Metasequoia glyptostroboides*. *Pak. J. Pharm. Sci.* **2016**, *29*, 1077–1080. [PubMed]

59. González, M.A.; Clark, J.; Connelly, M.; Rivas, F. Antimalarial activity of abietane ferruginol analogues possessing a phthalimide group. *Bioorg. Med. Chem. Lett.* **2014**, *24*, 5234–5237. [CrossRef]
60. Becerra, J.; Flores, C.; Mena, J.; Aqueveque, P.; Alarcón, J.; Bittner, M.; Hernández, V.; Hoeneisen, M.; Ruiz, E.; Silva, M. Antifungal and antibacterial activity of diterpenes isolated from wood extractables of chilean Podocarpaceae. *J. Chil. Chem. Soc.* **2002**, *47*, 151–157. [CrossRef]
61. Smith, E.C.J.; Williamson, E.M.; Wareham, N.; Kaatz, G.W.; Gibbons, S. Antibacterials and modulators of bacterial resistance from the immature cones of *Chamaecyparis lawsoniana*. *Phytochemistry* **2007**, *68*, 210–217. [CrossRef]
62. Różalski, M.; Kuźma, Ł.; Krajewska, U.; Wysokińska, H. Cytotoxic and proapoptotic activity of diterpenoids from in vitro cultivated *Salvia sclarea* roots. Studies on the leukemia cell lines. *Z. Naturforsch.* **2006**, *61*, 483–488. [CrossRef] [PubMed]
63. Tayarani-Najaran, Z.; Mousavi, S.H.; Tajfard, F.; Asili, J.; Soltani, S.; Hatamipour, M.; Emamid, S.A. Cytotoxic and apoptogenic properties of three isolated diterpenoids from *Salvia chorassanica* through bioassay-guided fractionation. *Food Chem. Toxicol.* **2013**, *57*, 346–351. [CrossRef]
64. Han, L.; Huang, X.; Dahse, H.-M.; Moellmann, U.; Grabley, S.; Lin, W.; Sattler, I. New abietane diterpenoids from the mangrove *Avicennia marina*. *Planta Med.* **2008**, *74*, 432–437. [CrossRef] [PubMed]
65. Ali, A.S.; Ahmed, Z.; Ngoupayo, J.; Ali, M.I. Terpenoids from *Clerodendrum formicarum* Gürke (Lamiaceae) of Cameroon. *Z. Naturforsch.* **2010**, *65*, 521–524. [CrossRef]
66. Raha, P.; Das, A.K.; Adityachaudhuri, N.; Majumder, P.L. Cleroinermin, a *neo*-clerodane diterpenoid from *Clerodendron inermi*. *Phytochemistry* **1991**, *30*, 3812–3814. [CrossRef]
67. Fan, X.; Lin, S.; Zhu, C.; Hu, J.; Liu, Y.; Chen, X.; Chen, N.; Wang, W.; Shi, J. Terpenoids of *Heteroplexis micocephala* and their bioactivities. *Zhongguo Zhong Yao Za Zhi.* **2010**, *35*, 315–322. [PubMed]
68. Kumari, G.N.K.; Balachandran, J.; Aravind, S.; Ganesh, M.R. Antifeedant and growth inhibitory effects of some *neo*-clerodane diterpenoids isolated from *Clerodendron Species* (Verbenaceae) on *Earias vitella* and *Spodoptera litura*. *J. Agric. Food Chem.* **2003**, *51*, 1555–1559. [CrossRef] [PubMed]
69. Pandey, R.; Verma, R.K.; Gupta, M.M. *Neo*-clerodane diterpenoids from *Clerodendrum inerme*. *Phytochemistry* **2005**, *66*, 643–648. [CrossRef]
70. Vinh, L.B.; Minh, N.T.N.; Yang, S.Y.; Kim, J.H.; Vien, L.T.; Huong, P.T.T.; Thanh, N.V.; Cuong, N.X.; Nam, N.H.; Minh, C.V.; et al. A new rearranged abietane diterpene from *Clerodendrum inerme* with antioxidant and cytotoxic activities. *Nat. Prod. Res.* **2018**, *32*, 2001–2007. [CrossRef]
71. Pandey, R.; Verma, R.K.; Singh, S.C.; Gupta, M.M. 4α-Methyl-24β-ethyl-5α-cholesta-14,25-dien-3 β -ol and 24 β -ethylcholesta-5, 9(11), 22E-trien-3 β -ol, sterols. *Phytochemistry* **2003**, *63*, 415–420. [CrossRef]
72. Bahadori, M.B.; Eskandani, M.; De Mieri, M.; Hamburger, M.; Nazemiyeh, H. Anti-proliferative activity-guided isolation of clerodermic acid from *Salvia nemorosa* L.: Geno/cytotoxicity and hypoxia-mediated mechanism of action. *Food Chem. Toxicol.* **2018**, *120*, 155–163. [CrossRef]
73. Heymann, H.; Tezuka, Y.; Kikuchi, T.; Supriyatna, S. Constituents of *Sindora sumatrana* MIQ. III.New *trans*-clerodane diterpenoids from the dried pods. *Chem. Pharm. Bull.* **1994**, *42*, 1202–1207. [CrossRef]
74. Crentsil, J.A.; Yamthe, L.R.T.; Anibea, B.Z.; Broni, E.; Kwofie, S.K.; Tetteh, J.K.A.; Osei-Safo, D. Leishmanicidal Potential of Hardwickiic Acid Isolated From *Croton sylvaticus*. *Front. Pharmacol.* **2020**, *11*, 753. [CrossRef]
75. Abbaszadeh, G.; Srivastava, C.; Walia, S. Insect growth inhibitory activity of clerodane diterpenoids isolated from *Clerodendron infortunatum* L. on the cotton bollworm, *Helicoverpa armigera* (Hubner). *Natl. Acad. Sci. Lett.* **2012**, *35*, 457–464. [CrossRef]
76. Uddin, J.; Russo, D.; Haque, A.; Çiçek, S.Z.; Sönnichsen, F.D.; Milella, L.; Zidorn, C. Bioactive Abietane-Type Diterpenoid Glycosides from Leaves of *Clerodendrum infortunatum* (Lamiaceae). *Molecules* **2021**, *26*, 4121. [CrossRef] [PubMed]
77. Abbaszadeh, G.; Srivastava, C.; Walia, S. Insecticidal and antifeedant activities of clerodane diterpenoids isolated from the Indian bhant tree, *Clerodendron infortunatum*, against the cotton bollworm, *Helicoverpa armigera*. *J. Insect Sci.* **2014**, *14*, 29. [CrossRef] [PubMed]
78. Bremner, P.D.; Simmonds, M.S.J.; Blaney, W.M.; Veitch, N.C. *Neo*-clerodane diterpenoid insect antifeedants from *Ajuga reptans* cv Catlins Giant. *Phytochemistry* **1998**, *47*, 1227–1232. [CrossRef]
79. Rongtao, L.; Morris-Natschkeb, S.L.; Kuo-Hsiung, L. Clerodane diterpenes: Sources, structures, and biological activities. *Nat. Prod. Rep.* **2016**, *33*, 1166–1226.
80. Xu, M.; Shen, L.; Wang, K.; Du, Q. Two New Abietane diterpenoids from the stems of *Clerodendrum kaichianum* P. S. Hsu. *Helv. Chim. Acta* **2011**, *94*, 539–544. [CrossRef]
81. Xu, M.; Shen, L.; Wang, K.; Du, Q.; Wang, N. Bioactive diterpenes from *Clerodendrum kaichianum*. *Nat. Prod. Commun.* **2011**, *6*, 3–5. [CrossRef]
82. Xu, M.; Wang, S.; Jia, O.; Zhu, Q.; Shi, L. Bioactive diterpenoids from *Clerodendrum kiangsiense*. *Molecules* **2016**, *21*, 86. [CrossRef]
83. Fan, T.; Min, Z.; Songc, G.; Iinumac, M.; Tanaka, T. Abietane diterpenoids from *Clerodendrum mandarinorum*. *Phytochemistry* **1999**, *51*, 1005–1008. [CrossRef]
84. Inaba, Y.; Hasuda, T.; Hitotsuyanagi, Y.; Aoyagi, Y.; Fujikawa, N.; Onozaki, A.; Watanabe, A.; Kinoshita, T.; Takeya, K. Abietane diterpenoids and a sesquiterpene pyridine alkaloid from *Euonymus lutchuensis*. *J. Nat. Prod.* **2013**, *76*, 1085–1090. [CrossRef]
85. Fan, T.-P.; Min, Z.-D.; Iinuma, M.; Tanaka, T. Rearranged abietane diterpenoids from *Clerodendrum mandarinorum*. *J. Asian Nat. Prod. Res.* **2000**, *2*, 237–243. [CrossRef]

86. Khan, I.; Nisar, M.; Shah, M.R.; Shah, H.; Gilani, S.N.; Gul, F.; Abdullah, S.M.; Ismail, M.; Khan, N.; Kaleem, W.A.; et al. Anti-inflammatory activities of taxusabietane A isolated from *Taxus wallichiana* Zucc. *Fitoterapia* **2011**, *82*, 1003–1007. [CrossRef] [PubMed]
87. Zaher, A.M.; Lin, J.; Arai, M. Cytotoxic activity of abietane-type diterpenes isolated from *Taxodium distichum* against cancer cells adapted to nutrient-starved conditions. *Nat. Prod. Commun.* **2020**, *15*, 1934578X20915298. [CrossRef]
88. Costa-Lotufo, L.V.; Araújo, E.C.C.; Lima, M.A.S.; Moraes, M.E.A.; Pessoa, C.; Silviera, E.R.; Moraes, M.O. Antiproliferative effects of abietane diterpenoids isolated from *Hyptis martiusii* Benth (Labiatae). *Pharmazie* **2004**, *59*, 78–79.
89. Zadali, R.; Ebrahimi, S.N.; Tofighi, Z.; Es-Haghi, A.; Hamburger, M.; Kaiser, M.; D'Ambola, M.; De Tommasi, N.; Hadjiakhoondi, A. Antiprotozoal activity of diterpenoids isolated from *Zhumeria majdae*- absolute configuration by circular dichroism. *DARU J. Pharm. Sci.* **2020**, *28*, 455–462. [CrossRef] [PubMed]
90. Musayeib, N.M.A.; Amina, M.; Al-Hamoud, G.A.; Mohamed, G.A.; Ibrahim, S.R.M.; Shabana, S. Plectrabarbene, a new abietane diterpene from *Plectranthus barbatus* aerial parts. *Molecules* **2020**, *25*, 2365. [CrossRef] [PubMed]
91. Faiella, L.; Temraz, A.; Cotugno, R.; De Tommasi, N.; Braca, A. Diterpenes and phenylpropanoids from *Clerodendrum splendens*. *Planta Med.* **2013**, *79*, 1341–1347. [CrossRef]
92. Wang, W.-X.; Zhu, J.-J.; Zou, Y.; Hong, Z.-L.; Liu, S.-T.; Li, M.; Huang, Y.; Xiong, J.; Zhao, Y.; Yang, G.-X.; et al. Trichotomone, a new cytotoxic dimeric abietane-derived diterpene from *Clerodendrum trichotomum*. *Tetrahedron. Lett.* **2013**, *54*, 2549–2552. [CrossRef]
93. Wang, W.-X.; Xiong, J.; Tang, Y.; Zhu, J.-J.; Li, M.; Zhao, Y.; Yang, G.-X.; Xia, G.; Hu, J.-F. Rearranged abietane diterpenoids from the roots of *Clerodendrum trichotomum* and their cytotoxicities against human tumor cells. *Phytochemistry* **2013**, *89*, 89–95. [CrossRef]
94. Li, L.-Z.; Wang, M.-H.; Sun, J.-B.; Liang, J.-Y. Abietane diterpenoids and other constituents from *Clerodendrum trichotomum*. *Biochem. Syst. Ecol.* **2014**, *56*, 218–220. [CrossRef]
95. Li, L.; Wu, L.; Wang, M.; Sun, J.; Liang, J. Abietane diterpenoids from *Clerodendrum trichotomum* and correction of NMR data of villosin C and B. *Nat. Prod. Commun.* **2014**, *9*, 907–910. [CrossRef]
96. Hu, H.-J.; Zhou, Y.; Han, Z.-Z.; Shi, Y.-H.; Zhang, S.-S.; Wang, Z.-T.; Wang, Z.T.; Yang, L. Abietane diterpenoids from the roots of *Clerodendrum trichotomum* and their nitric oxide inhibitory activities. *J. Nat. Prod.* **2018**, *81*, 1508–1516. [CrossRef] [PubMed]
97. Li, P.; Li, L.; Zhu, Q.; Xu, M. Abietane Diterpenoids Isolated from *Clerodendrum bracteatum* and Their Antioxidant and Cytotoxic Activities. *Molecules* **2021**, *26*, 4870. [CrossRef] [PubMed]
98. Qi, J.; Zhang, Y.; Liu, Q.; Liu, H.C.; Fan, Y.; Yue, J. Clerodenoids A–F: C-ring aromatized and/or rearranged abietane diterpenoids from *Clerodendrum chinense* var. *simplex*. *Chin. J. Chem.* **2021**, *39*, 1891–1897. [CrossRef]
99. Lozama, A.; Prisinzano, T.E. Chemical methods for the synthesis and modification of neoclerodane diterpenes. *Bioorg. Med. Chem. Lett.* **2009**, *19*, 5490–5495. [CrossRef] [PubMed]
100. Quaglio, D.; Mangoni, M.L.; Stefanelli, R.; Corradi, S.; Casciaro, B.; Vergine, V.; Lucantoni, F.; Cavinato, L.; Cammarone, S.; Loffredo, M.R.; et al. *ent*-Beyerane Diterpenes as a Key Platform for the Development of ArnT-Mediated Colistin Resistance Inhibitors. *J. Org. Chem.* **2020**, *85*, 10891–10901. [CrossRef]
101. Rico-Martínez, M.; Medina, F.G.; Marrero, J.G.; Osegueda-Robles, S. Biotransformation of diterpenes. *RSC Adv.* **2014**, *4*, 10627–10647. [CrossRef]
102. de Sousa, I.P.; Teixeira, M.V.S.; Furtado, N.A.J.C. An overview of biotransformation and toxicity of diterpenes. *Molecules* **2018**, *23*, 1387. [CrossRef]

International Journal of
Molecular Sciences

MDPI

Article

Anti-Inflammatory and Analgesic Effects of Curcumin Nanoparticles Associated with Diclofenac Sodium in Experimental Acute Inflammation

Ioana Boarescu [1,†], Raluca Maria Pop [2,†], Paul-Mihai Boarescu [2,*], Ioana Corina Bocșan [2], Dan Gheban [3], Ruxandra-Mioara Râjnoveanu [4], Armand Râjnoveanu [5], Adriana Elena Bulboacă [6], Anca Dana Buzoianu [2] and Sorana D. Bolboacă [1]

[1] Department of Medical Informatics and Biostatistics, Iuliu Haţieganu University of Medicine and Pharmacy Cluj-Napoca, Louis Pasteur Street, No. 6, 400349 Cluj-Napoca, Romania
[2] Department of Pharmacology, Toxicology and Clinical Pharmacology, Iuliu Haţieganu University of Medicine and Pharmacy Cluj-Napoca, Gheorghe Marinescu Street, No. 23, 400337 Cluj-Napoca, Romania
[3] Department of Pathological Anatomy, Iuliu Haţieganu University of Medicine and Pharmacy Cluj-Napoca, Clinicilor Street, No. 3-5, 400006 Cluj-Napoca, Romania
[4] Department of Palliative Medicine, Iuliu Haţieganu University of Medicine and Pharmacy Cluj-Napoca, B.P. Hașdeu Street, No. 6, 400371 Cluj-Napoca, Romania
[5] Department of Occupational Medicine, Iuliu Haţieganu University of Medicine and Pharmacy Cluj-Napoca, Clinicilor Street, No. 3-5, 400006 Cluj-Napoca, Romania
[6] Department of Pathophysiology, Iuliu Haţieganu University of Medicine and Pharmacy Cluj-Napoca, Victor Babeş Street, No. 2-4, 400012 Cluj-Napoca, Romania
* Correspondence: boarescu.paul@umfcluj.ro; Tel.: +40-752-921-725
† These authors contributed equally to this work.

Citation: Boarescu, I.; Pop, R.M.; Boarescu, P.-M.; Bocșan, I.C.; Gheban, D.; Râjnoveanu, R.-M.; Râjnoveanu, A.; Bulboacă, A.E.; Buzoianu, A.D.; Bolboacă, S.D. Anti-Inflammatory and Analgesic Effects of Curcumin Nanoparticles Associated with Diclofenac Sodium in Experimental Acute Inflammation. *Int. J. Mol. Sci.* **2022**, *23*, 11737. https://doi.org/10.3390/ijms231911737

Academic Editor: Luká Kubala

Received: 27 August 2022
Accepted: 29 September 2022
Published: 3 October 2022

Abstract: The present study evaluated the anti-inflammatory and analgesic effects of conventional curcumin (cC) and curcumin nanoparticles (nC) associated with diclofenac sodium (D) in experimental acute inflammation (AI) induced by carrageenan administration. Seven groups of eight randomly selected Wistar-Bratislava white rats were evaluated. One group was the control (C), and AI was induced in the other six groups. The AI group was treated with saline solution, the AID group was treated with D, the AIcC200 and AInC200 groups were treated with cC and nC, respectively, while AIcC200D and AInC200D were treated with cC and nC, respectively, both associated with D. Conventional curcumin, nC, and D were administered in a single dose of 200 mg/kg b.w. for cC and nC and 5 mg/kg b.w. for D. Association of cC or nC to D resulted in significant antinociceptive activity, and improved mechanical pressure stimulation and heat thresholds at 3, 5, 7 and 24 h ($p < 0.03$). The association of cC and nC with D (AIcC200D and AInC200D groups) showed significantly lower plasma and tissue levels of tumor necrosis factor-α (TNF-α), interleukin-6 (IL-6), and interleukin-1β (IL-1β) up to 2.5 times, with the best results in the group who received nC. Moreover, AInC200D presented the least severe histopathological changes with a reduced level of inflammation in the dermis and hypodermis. The combination of nC to D showed efficiency in reducing pain, inflammatory cytokines, and histological changes in acute inflammation.

Keywords: curcumin; nanoparticles; diclofenac sodium; carrageenan; inflammation; cytokines

1. Introduction

Inflammation is a broad and ancient medical term referring to a set of classic signs and symptoms, including pain, edema, hyperemia, warmth, and loss of function [1]. It is characterized by a group of complex changing responses to tissue injury primarily caused by harmful stimuli, such as pathogens, physical agents, chemical compounds, or damaged cells [2].

Carrageenan is a pro-inflammatory polysaccharide used to induce local inflammation (paw edema) [2,3]. The release of bradykinin, serotonin, histamine, and prostaglandins

under cyclooxygenase enzymes (COX) occurs in the early phase of inflammation. In the late phase, prostaglandin generation is continued together with neutrophil infiltration and release of pro-inflammatory cytokines such as tumor necrosis factor (TNF-α) and interleukin-1 β (IL-1β) [4]. The overproduction of neutrophil-derived free radicals and nitric oxide (NO) is also involved in the delayed phase of carrageenan-induced acute inflammation [5]. It was suggested that drugs targeting the COX enzyme, pro-inflammatory expression (e.g., inducible nitric oxide synthase; iNOS), and free radical formation might better control the inflammation process [6].

Non-Steroidal Anti-Inflammatory Drugs (NSAIDs) are one of the most commonly prescribed medications for acute and chronic inflammation. Their major therapeutic actions are related to their ability to block certain prostaglandins (PGs) synthesis through cyclooxygenase enzymes (COX-1 and COX-2) inhibition [7]. Cyclooxygenase enzyme 1 (COX-1) is expressed in normal cells and produces PGs and thromboxane A2, which control renal homeostasis, platelet aggregation, and mucosal barrier in the gastrointestinal tract and possess other physiological functions. Cyclooxygenase enzyme 2 (COX-2) is induced in inflammatory cells and produces PGs related to inflammation, pain, and fever. The inhibition of COX-2 most likely represents the desired effect of NSAIDs by providing anti-inflammatory, analgesic, and antipyretic responses; inhibition of the COX-1 enzyme plays a major role in the undesired side effects such as injury to the gastrointestinal mucosa [8]. Therefore, in some circumstances, NSAID administration may cause acute renal failure, gastrointestinal ulcers, hypertension, or serious cardiovascular events (such as stroke or acute myocardial infarction). These adverse effects may be prevented first by limiting NSAID dosage and duration of administration and also by performing risk assessments for each patient depending on the associated pathology [9].

Diclofenac (D) is a nonselective NSAID widely used as an anti-inflammatory, antipyretic, and analgesic drug but it has a reduced bioavailability due to hepatic first-pass metabolism and associates many adverse effects on gastrointestinal, hepatic, renal, and cardiovascular systems [10,11].

Curcumin is a major bioactive phytochemical in the rhizome of turmeric (*Curcuma longa* L.). It has advantageous pharmacological properties, including antioxidant, anti-inflammatory, anticancer, and anti-infective properties but its utility in clinical practice is limited due to its low aqueous solubility, poor absorption, and metabolic instability, which lead to poor oral bioavailability [12].

We previously demonstrated that conventional curcumin (cC) and curcumin nanoparticles (nC) potentiate the antiedematous effects and antioxidant activity of diclofenac in carrageenan-induced paw edema, with better results for nC [13]. The present study aimed to evaluate the anti-inflammatory and analgesic effects of conventional curcumin and curcumin nanoparticles associated with diclofenac sodium in experimental acute inflammation induced by carrageenan administration.

2. Results

2.1. Motility Test

Rats from the C group exhibited, without any exception, scores of 2 to all determinations (Figure 1, Table S1). Rats from the AI group presented the lowest motility score starting from the first hour after carrageenan administration up to 24 h (Figure 1). Conventional curcumin and curcumin nanoparticles improved the motility score, with a better motility score for nC, which was similar to D (Figure 1, Table S1). Better walking abilities of the rats in the AIcC200D and AInC200D groups were observed than in the D group, with the highest motility score in the AInC200D group (Figure 1).

Figure 1. Effects of diclofenac sodium (D), conventional curcumin (cC), and curcumin nanoparticles (nC) on motility score (MS). Interpretation: MS = 2 indicates no motility problems; MS = 1 indicates some motility problems (walk with difficulty but with the toe of the inflamed paw touching the floor), and MS = 0 indicates motility problems (walk with difficulties and avoided touching the right hind paw to the floor). C—control (n = 8); AI—Acute inflammation (n = 8); D—Diclofenac sodium (n = 8); cC—conventional curcumin solution (200 mg/kg b.w.; n = 8); nC—curcumin nanoparticles solution (200 mg/kg b.w.; n = 8).

2.2. *Paw Pressure Test*

The AI group's rat presented a statistically reduced threshold in the paw pressure test compared to the control group at 3, 5, 7, and 24 h ($p < 0.0001$, Figure 2). The nociceptive thresholds presented a progressive decrease, reaching the minimum values 5 h after AI induction. Diclofenac administration improved nociceptive thresholds but no statistical significance was found compared to the AI group, at any follow-up measurements ($p > 0.0753$, Figure 2). Rats treated with cC and nC had a better but not statistically significant ($p > 0.8711$, Figure 2) analgesic response compared to the AI group, which was less efficient than diclofenac alone (Figure 2). Moreover, rat responses from the above-mentioned

groups were significantly reduced compared to the C group ($p \leq 0.0190$, Figure 2), starting with the first hour after AI induction. When cC and nC were associated with D, rats had a significantly better nociceptive response at 3, 5, 7, and 24 h, with thresholds significantly higher than in the AI group ($p \leq 0.0285$, Figure 2). However, they were not significantly different than the C group ($p \geq 0.6693$, Figure 2), with the best results observed when D was associated with nC (AInC200D group, Figure 2).

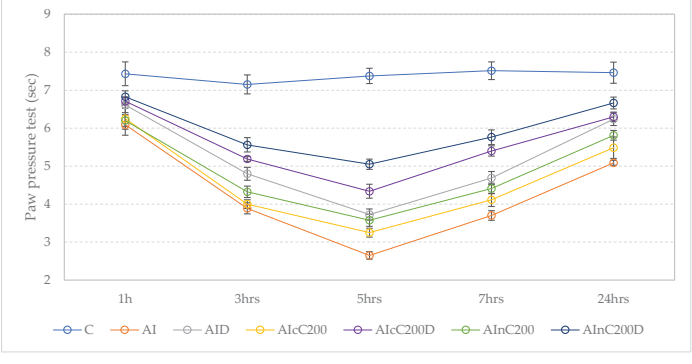

Figure 2. Effects of diclofenac sodium (D), conventional curcumin (cC) and curcumin nanoparticles (nC) on nociceptive thresholds. Circles represent the mean value of each group; whiskers represent the value of the SEM (standard error of the mean). C—control (n = 8); AI—Acute inflammation (n = 8); D—Diclofenac sodium (n = 8) ; cC—conventional curcumin solution (200 mg/kg b.w.; n = 8); nC—curcumin nanoparticles solution (200 mg/kg b.w.; n = 8).

The mean and standard deviations for each group on paw pressure test are presented in Table S2, while the p-values for comparisons between groups are presented in Table S3.

2.3. Hot Plate Test

Carrageenan administration led to a reduction in reaction time to the heat, starting from the first hour. In the AI group, this reduction was progressive and statically significant compared to the C group ($p \leq 0.0002$, Figure 3), with the minimum values at 5 h (Figure 3).

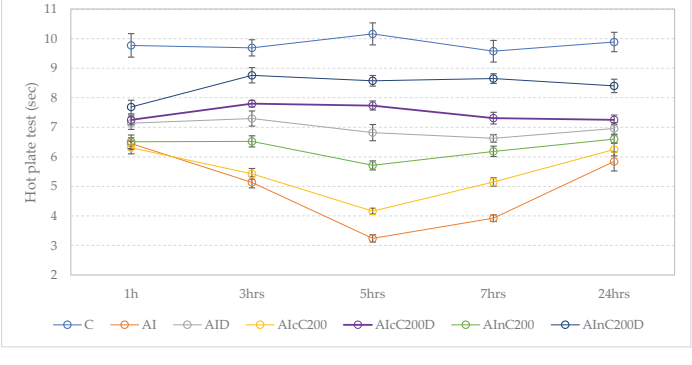

Figure 3. Effects of diclofenac sodium (D), conventional curcumin (cC), and curcumin nanoparticles (nC) on reactions time to the heat. Circles represent the mean value of each group; whiskers represent the value of the SEM (standard error of the mean). C—control (n = 8); AI—Acute inflammation (n = 8); D—Diclofenac sodium (n = 8) ; cC—conventional curcumin solution (200 mg/kg b.w.; n = 8); nC—curcumin nanoparticles solution (200 mg/kg b.w.; n = 8).

Diclofenac improved the time response in all measurements but the improvement was not statistically significant compared to the AI group ($p \geq 0.0545$, Figure 3). Conventional curcumin and curcumin nanoparticles showed an elevation in pain threshold compared to the AI group but without statistical significance ($p \geq 0.3832$, Figure 3). Compared to the C group, both cC and nC groups had significantly reduced thresholds ($p \leq 0.0052$, Figure 3). Association of cC or nC to D resulted in significant antinociceptive activity and improved thresholds to the heat at 3, 5, and 7 h for both groups, and at 24 h for AInC200D, when compared to the AI group ($p < 0.0175$, Figure 3). A similar reaction time to the heat was observed in the AInC200D group and C group ($p > 0.9999$, Figure 3).

The mean and standard deviation for each group on the hot plate test responses are presented in Table S4. The results of comparisons between groups are expressed as *p*-values shown in Table S5.

2.4. Inflammatory Cytokines

Administration of carrageenan led to increased plasma and tissue levels of all evaluated pro-inflammatory cytokines, namely tumor necrosis factor (TNF-α), interleukin 6 (IL-6), and interleukin 1β (IL-1β). All these cytokines were significantly increased in the AI group compared to the C group ($p < 0.0001$, Figures 4–6). Diclofenac sodium administration significantly reduced the plasma levels of TNF-α ($p = 0.0170$, Figure 4). Tissue levels of TNF-α and both plasma and tissue levels of IL-6 and IL-1β were also reduced by D administration compared to the AI group but statistical significances were not reached ($p \geq 0.14$, Figures 4B, 5 and 6).

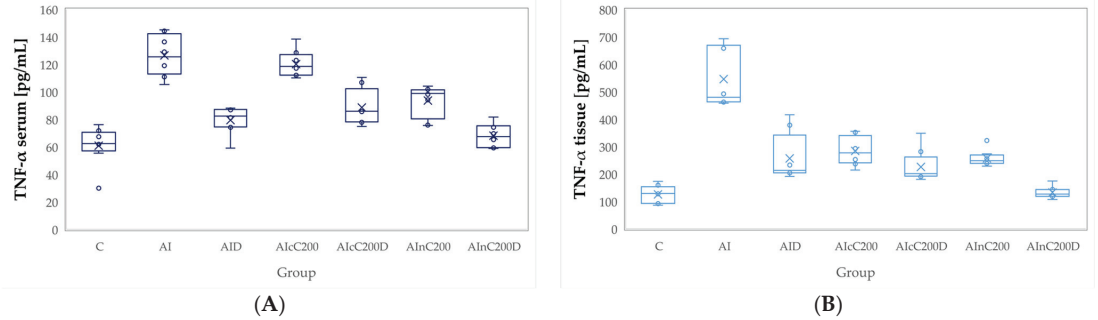

(**A**) (**B**)

Figure 4. Variation by groups of TNF-α (Tumor necrosis factor α): (**A**) in the plasma (**B**) in the tissue. C—control; AI—Acute inflammation; D—Diclofenac; cC—conventional curcumin solution (200 mg/kg b.w.); nC—curcumin nanoparticles solution (200 mg/kg b.w).

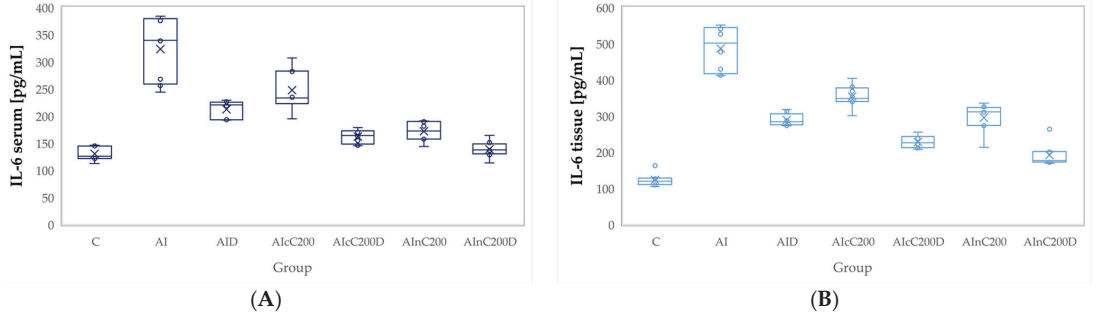

(**A**) (**B**)

Figure 5. Variation by groups of IL-6 (Interleukin 6): (**A**) in the plasma (**B**) in the tissue. C—control; AI—Acute inflammation; D—Diclofenac; cC—conventional curcumin solution (200 mg/kg b.w.); nC—curcumin nanoparticles solution (200 mg/kg b.w.).

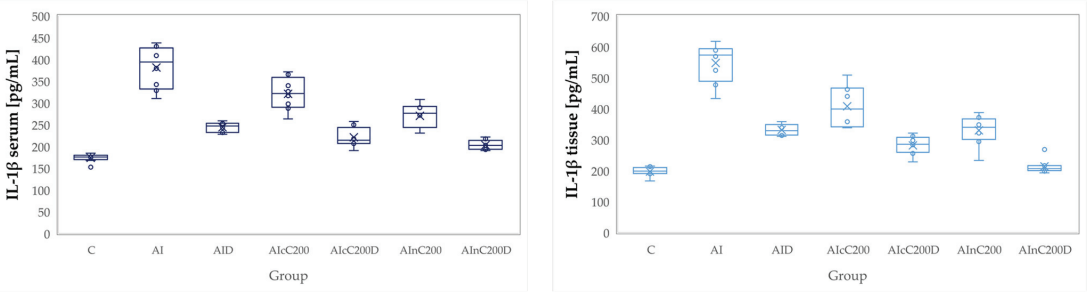

(**A**) (**B**)

Figure 6. Variation by groups of IL-1β (Interleukin 1β): (**A**) in the plasma (**B**) in the tissue. C—control; AI—Acute inflammation; D—Diclofenac; cC—conventional curcumin solution (200 mg/kg b.w.); nC—curcumin nanoparticles solution (200 mg/kg b.w.).

The cC alone group offered a slightly reduced anti-inflammatory effect, proved by the reduction of the plasma and tissue levels of all three cytokines, insignificantly compared to the AI group ($p > 0.9999$, Figures 4–6). Rats from the AIcC200 group had statistically higher levels of all evaluated cytokines compared to the control group ($p \leq 0.0044$, Figures 4–6). Similar results but with lower levels than the AIcC200 group of the evaluated pro-inflammatory cytokines were observed when nC was administered alone (Figures 4–6).

Tissue levels of TNF-α and both plasma and tissue levels of IL-6 and IL-1β were reduced when cC was added to D and then D alone (Figures 4B, 5 and 6) without reaching statistical significance ($p > 0.05$). When the AIcC200D group was compared to the AI group, statistical significance was reached for the above-mentioned parameters ($p \leq 0.0212$). The combination of nC and D improved plasma and tissue levels of all three cytokines compared to the AI group ($p \leq 0.0002$, Figures 4–6). Moreover, the cytokine levels in the AInC200D group were similar to those of the control group ($p \geq 0.9999$, Figures 4–6).

The summary statistics of pro-inflammatory cytokines by each group are presented in Table S6, with the results of the comparison between groups presented in Table S7.

Excepting the plasma levels of IL-1β where the difference had only a tendency to statistical significance ($p < 0.10$), nC enhances the therapeutic effect of diclofenac on all evaluated markers, both in plasma and tissue significantly better than cC (Figure 7).

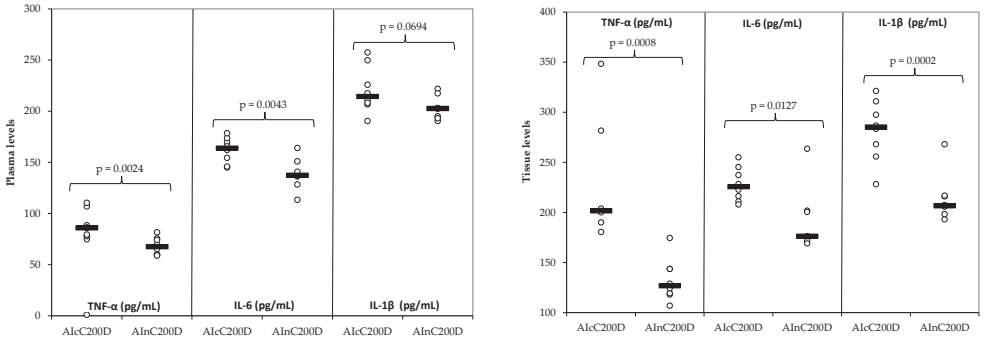

(**A**) (**B**)

Figure 7. The increase in the therapeutic effect of diclofenac D when combined with conventional curcumin (cC) and curcumin nanoparticles (nC): (**A**) in the plasma (**B**) in the tissue. C—control; AI—Acute inflammation; D—Diclofenac; cC—conventional curcumin solution (200 mg/kg b.w.); nC—curcumin nanoparticles solution (200 mg/kg b.w.). The dots are the primary data and the line indicates the median value.

2.5. Quantification of Plasma Curcumin

Curcumin levels before hydrolyzation were 1.4-fold higher in rats treated with nC than cC, while plasma levels of its metabolites were 1.3-fold higher after nC administration compared to cC, with only a tendency to statistical significance for curcumin metabolites (Figure 8).

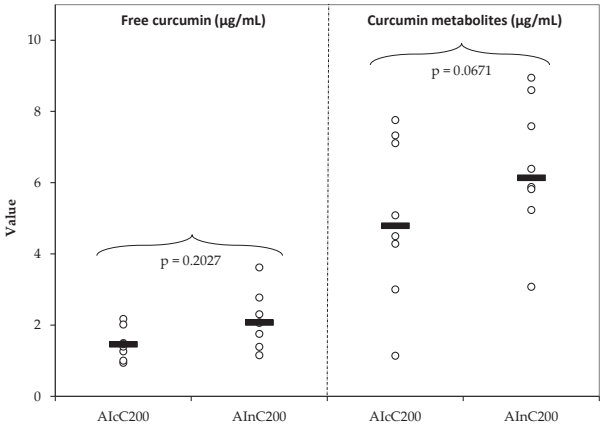

Figure 8. Variation of cC and nC: free curcumin before hydrolyzation and curcumin's metabolites after hydrolyzation. AI—Acute inflammation; cC—conventional curcumin solution (200 mg/kg b.w.); nC—curcumin nanoparticles solution (200 mg/kg b.w.). The dots are the primary data and the line indicates the median value.

2.6. Histopathological Examination

Histopathological examination of the hind paw of the control group showed normal structure and architecture without signs of inflammation in the dermis and hypodermis (Figure 9A). In the AI group, severe inflammation was observed after carrageenan administration, characterized by acute purulent inflammation in the dermis and hypodermis, extending to the underlying muscular tissue (Figure 9B). In the D group, 24 h after the AI induction, the histological examination revealed signs of acute purulent inflammation in the dermis and hypodermis with microabscess formation and micro-thrombi in several vascular lumens (Figure 9C). Conventional curcumin and nC administrated alone did not influence the histopathological aspects of the hind paw, highlighted by the same histopathological changes observed in the AI group: acute purulent inflammation in the dermis and hypodermis, with extension to the underlying muscular tissue (AIcC200 group in Figure 9D and AInC200 in Figure 9F). Conventional curcumin associated with diclofenac (AIcC200D group) led to inflammation focalized only in the hypodermis but associated with microabscess formation (Figure 9E). Less severe histopathological changes were observed in groups treated with nC and D (AInC200D group) as rats presented reduced inflammation of the dermis and hypodermis (Figure 9G).

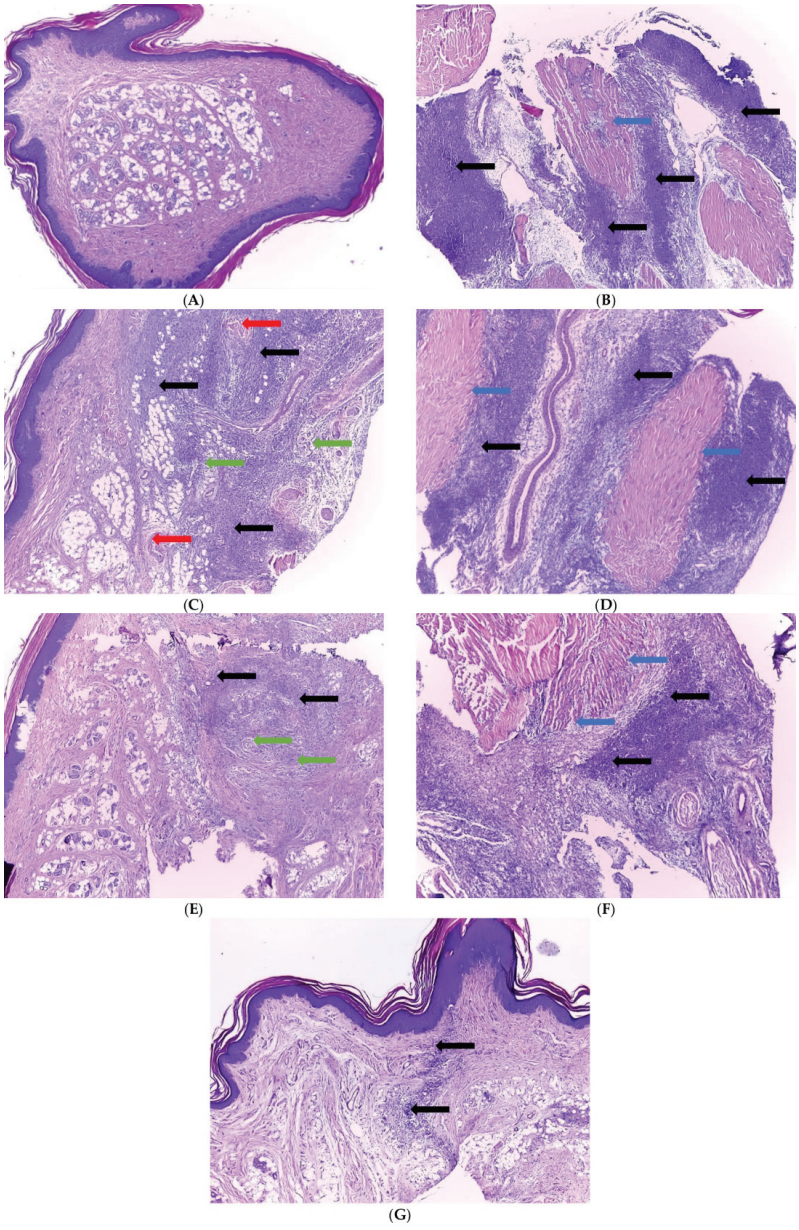

Figure 9. Histopathological examinations of the fragments from right-hind paw: (**A**) C-normal architecture of dermis and hypodermis of the plantar surface of the foot; (**B**) AI-acute purulent inflammation in the dermis, hypodermis (**black arrow**), with an extension on the underlying muscular tissue (**blue arrow**); (**C**) AID-dermis and hypodermis with signs of acute purulent inflammation (**black arrow**), micro-abscess formation (**green arrow**), and micro-thrombi (**red arrow**) in several vascular lumens; (**D**) AIcC200-acute purulent inflammation in the dermis, hypodermis (**black arrow**), with the extension on the underlying muscular tissue (**blue arrow**); (**E**) AIcC200D-inflammation focalized in the hypodermis (**black arrow**) associated with microabscess formation (**green arrow**); (**F**) AInC200-acute purulent inflammation in the dermis, hypodermis (**black arrow**), with an extension on the underlying muscular tissue (**blue arrow**); (**G**) AInC200D-reduced level of inflammation on dermis and hypodermis (**black arrow**).

3. Discussion

The results of our study demonstrated that the association of conventional curcumin and curcumin nanoparticles to diclofenac sodium could potentiate the analgesic and anti-inflammatory effects of diclofenac sodium in reduced doses, with the best results obtained for curcumin nanoparticles.

Curcumin (both cC and nC) potentiates the anti-edematogenic activity of diclofenac [13], leading to the improvement of the motility score regardless of its form as cC or nC (Figure 1).

The paw pressure test helps to assess nociceptive thresholds to mechanical pressure stimulation, as a measure of mechanical hyperalgesia [14]. Diclofenac has already proved to have an analgesic effect and to increase the withdrawal threshold in the paw pressure test [15]. Higher doses of diclofenac sodium (e.g., 20 mg/kg b.w.) provided higher tolerance of mechanical hyperalgesia compared to the control group [16,17]. In our study, the dose of diclofenac sodium (5 mg/kg b.w.) was observed to have a limited effect on response thresholds to mechanical pressure stimulation (Figure 2), most probably explained by the reduced dose of the active substance. Curcumin administration (cC and nC) also had an analgesic effect (Figure 2). Its analgesic effect could be explained by the stimulation of protein expression of β-endorphin and encephalin, which are endogenous opioid peptides [18]. We observed that the association of cC and nC to D has better analgesic effects (Figure 2), most probably because the combination acts on two mechanisms to reduce the pain threshold.

The hot plate test assesses the central activity since the response reflex is mediated by supraspinal centers. Even more, it was stated that any agent that causes a prolongation of the hot plate latency using this test must act centrally [19]. Diclofenac, like other NSAIDs, has an analgesic effect characterized by elevation of time to paw withdrawal to thermal stimuli (Figure 3), which is attributed to inhibition of the COX-mediated biosynthesis of PGs, with peripheral and central sites of action [20]. As regards curcumin administration, it was previously reported as having a good analgesic effect on thermal injury pain, an effect that could be mediated through suppression of inflammatory protein-induced pain perception (peripheral action) [21], but since it prolonged the response to the hot plate test, it may also have a central activity.

Tumor necrosis factor α (TNF-α) is an inflammatory cytokine produced by macrophages/monocytes during acute inflammation [22]. It participates in leukocyte adhesion to the epithelium by expressing adhesion molecules, vasodilatation, and edema formation [23]. In carrageenan-induced mouse paw edema, TNF-α promoted collateral cytotoxicity by acting as a stimulator of prostaglandin synthesis, an activator of the NF-κB signal transduction pathway, as NO formation inducer, and a stimulator of neutrophil migration [24].

Interleukin-6 (IL-6) is a pro-inflammatory cytokine produced by many types of cells, expressed during states of cellular stress, such as cancer, infection, wound sites, and inflammation [25]. In the inflammation process, IL-6 is produced at the site of inflammation in the initial stage and moves to the liver through the bloodstream. It leads to the rapid synthesis of an extensive range of acute phase proteins such as C-reactive protein (CRP), fibrinogen, haptoglobin, serum amyloid A, and α1-antichymotrypsin [26]. In carrageenan-induced paw edema, increased levels of IL-6 at the site of inflammation facilitate leukocyte recruitment and mediate edema formation and inflammatory pain hypersensitivity [27].

Interleukin-1 α and β are prototypic pro-inflammatory cytokines that play key roles in acute and chronic inflammatory, autoimmune disorders, or other pathologies, as they have pleiotropic effects on various cells [28,29]. Interleukin-1β is a potent mechanical and thermal hyperalgesic agent when injected into peripheral tissues [30]. Intraplantar injection of an inflammatory agent, such as carrageenan, produces mechanical or thermal hyperalgesia associated with an upregulation of IL-1β and other inflammatory cytokines in the inflamed tissue and the dorsal root ganglia [31]. It was also suggested that IL-1β inhibition could represent a broad-acting and efficacious method for managing pain and inflammation across various conditions such as gout, rheumatoid arthritis, or neuropathic pain [28].

Diclofenac, as an NSAID drug, may reduce the levels of pro-inflammatory cytokines (Figures 4–6) through COX enzyme inhibition. Consequently, it may also reduce the production of prostaglandins and thromboxanes, which participate in the inflammatory response [32]. Moreover, it was observed that NSAIDs might interact with transcriptional factors and affect the production of cytokines by inhibiting the levels of TNF-α and IL-6 [33]. The reduced dose of diclofenac sodium might explain the limited reduction of all three studied pro-inflammatory cytokines (Figures 4–6).

Curcumin administration was observed to prevent the elevation of interleukin IL-1β, IL-6, and TNF-α (Figures 4–6) since curcumin can reduce inflammatory responses by interfering with NF-κB activation, a critical pathway in the regulation of transcription of pro-inflammatory related genes [34]. The increased anti-inflammatory effect of nC can be explained by its increased tissue distribution [35–37] compared to cC.

The beneficial effects of curcumin are limited due to its hydrophobic characteristics, as curcumin is not soluble in water, is poorly absorbed in the small intestine, and it has an extensive reductive and conjugative metabolism in the liver [38]. The use of biocompatible water-based polymers offers enhanced solubility, stability, pharmacological activity, and bioavailability, and avoids physical and chemical degradation of curcumin [39].

Following oral administration, curcumin is rapidly converted into glucuronide and sulfate metabolites. On intravenous or intraperitoneal injection, curcumin is also reduced to dihydrocurcumin (DHC), tetrahydrocurcumin (THC), and hexahydrocurcumin (HHC), of which THC is the predominant species. Other metabolites of curcumin are curcumin glucuronide-sulfate and glucuronide conjugates of THC and HHC [40]. Higher levels of plasma-free curcumin and its metabolites (curcumin glucuronide and curcumin sulfate) quantified after nC administration (Figure 8) are the results of higher bioavailability. This is attributed to the increased absorption of curcumin nanoparticles through the gastrointestinal tract offered by the encapsulation of the active compound in nano-carriers [41]. As a result, the therapeutical effect of D is significantly increased when nC is added as compared to the addition of cC (Figure 7).

In the present study, no significant differences were found between the AI group and the groups pretreated with cC or nC regarding the histopathological changes, as all the rats presented purulent inflammation in the dermis and hypodermis, with an extension on the underlying muscular tissue (Figure 9B,D,F). Diclofenac sodium slightly reduced the inflammatory process. Limited effects of diclofenac sodium on the histopathological changes in the carrageenan-induced rat paw edema model were also reported by Abdelhameed et al. [42]. Even if they used a higher dose of diclofenac sodium (30 mg/kg b.w.), Abdelhameed et al. reported that the oral or topical administration of diclofenac did not have a curative effect [42]. The presence of the micro-thrombi in some vascular lumens observed in the AID group might be due to the prothrombotic effects of diclofenac [43]. The association of cC with D reduced the inflammation level as it was focalized in the hypodermis associated with microabscess formation (Figure 9E), most probably because curcumin can enhance the anti-inflammatory effect of diclofenac sodium through inhibition of prostaglandin synthesis via the cyclooxygenase pathway [44]. Curcumin nanoparticles were already demonstrated to provide superior anti-inflammatory effects in an animal model of acute and chronic inflammations when given orally [45]. It is suggested that by reducing curcumin's particle size to the nanoscale, the bioavailability is improved by enhancing the solubility [45]. Therefore, much of the active compound reaches the tissue and potentiates the diclofenac's anti-inflammatory effects. It could explain the best histological results obtained when nC was associated with D, with reduced inflammation of the dermis and hypodermis (Figure 9G).

In an experimental study performed by Nurullahoglu et al. [46], curcumin suspension in a dose of 400 mg/kg b.w. prepared in 5% ethanol solution, proved more potent than diclofenac alone in the early phase of pain on formalin test. Jain et al. [47] observed that curcumin–diclofenac conjugate enhanced the bioavailability of curcumin more than five-fold and alleviated the symptoms of arthritis as compared to both diclofenac and curcumin

in a streptococcal cell wall-induced arthritis model. Moreover, one study performed by De Paz-Campos revealed that the diclofenac–curcumin combination might have therapeutic advantages for the clinical treatment of inflammatory pain [48]. Another experimental study concluded that curcumin nanoparticles present better anti-inflammatory effects of carrageenan-induced inflammation than conventional curcumin [45].

To our knowledge, no evaluation of the additional anti-inflammatory and analgesic effects of cC or nC to diclofenac sodium in experimental acute inflammation induced by carrageenan had been previously published. Moreover, in this study, we also reported an HPLC-UV method for quantifying cC and nC before and after hydrolyzation of its major metabolites, curcumin glucuronide and curcumin sulfate, in rat plasma.

4. Materials and Methods

4.1. Chemicals and Drugs

Conventional curcumin (cC) and carrageenan (a high-molecular-weight sulfated pro-inflammatory polysaccharide) were purchased from Sigma-Aldrich (St. Louis, MO, USA), and curcumin nanoparticles (nC) were bought from CVI Pharma (Hanoi, Vietnam), while diclofenac sodium (D) and saline solution were purchased from a local pharmacy. For the curcumin nanoparticles, the active compound is encapsulated in biocompatible water-based polymers with a size between 30 and 100 nm. Standard curcumin, β-glucuronidase from Helix Pomatia, sulfatase from Helix pomatia, HPLC grade acetonitrile and methanol, ammonium acetate, dibasic potassium phosphate (K_2HPO_4), dimethylsulfoxide (DMSO) and Phosphate buffered saline (PBS) tablets were purchased from Merk (Darmstadt, Germany).

4.2. Animals and Experimental Design

Fifty-six (56) ten-week-old white male Wistar-Bratislava rats (300 ± 10 g) were randomly divided into eight groups of seven animals each, following the flowchart from Figure 10, explained in detail in our previous research [13].

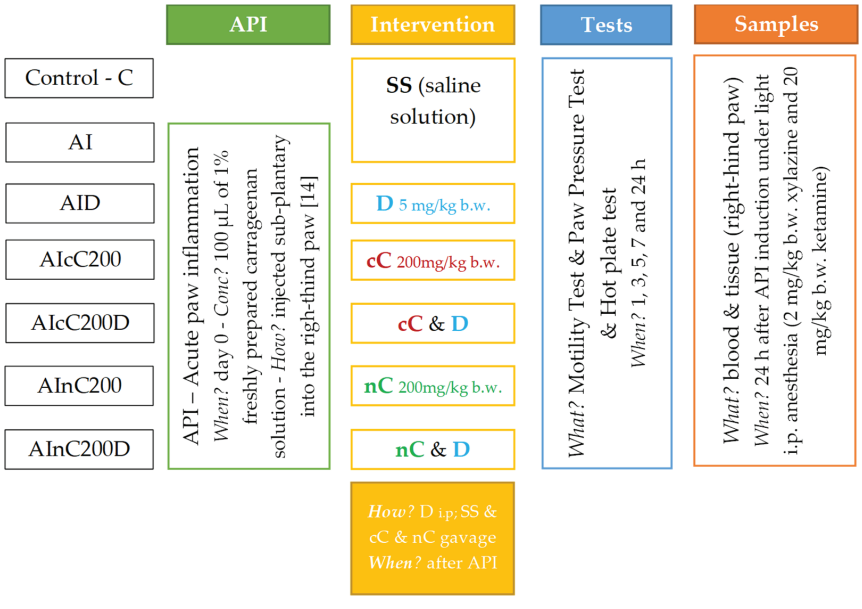

Figure 10. Flowchart demonstrating the study groups and interventions.

4.3. Time Point Measurements

The motility test, the paw pressure test and the hot plate test were performed at 1, 3, 5, 7, and 24 h after carrageenan injection.

4.3.1. Motility Test

The motility pattern of the rats from all groups was noted for 5 min. Each rat was scored with 2 if the rat walked easily; 1 if the rat walked with little difficulty but with the toe of the inflamed paw touching the floor; and 0 if the rat had difficulties in walking and avoided touching the right hind paw to the floor [49].

4.3.2. Paw Pressure Test

An analgesia meter (Ugo Basile, Milan, Italy) was used for the mechanical nociceptive response measurement. For this test, plantar mechanical pressure was applied linearly by increasing the mechanical force to the rat's right-hind paw. The value of 500 g was set as cut-off pressure and the retraction of the paw of the rat's squeak was recorded as the latency response [50].

4.3.3. Hot Plate Test

The hot plate test is a therm analgesic method that measures the threshold response to pain. This thermal test was selected because it is sensitive to strong analgesics and limits tissue damage because of a cut-off point that is usually applied to reduce the time the rats spend on the hot plate [19]. The heat sensitivity of the paw was assessed using an Ugo Basile hot plate (Milan, Italy) heated to 55 °C. During the whole test, the plate was kept at a constant temperature of 55 ± 0.1 °C. Rats from all groups were placed on the hot plate, and their reactions were observed. Time of latency was defined as the time between the zero moment when the rat was placed on the hot plate surface and the moment when the rat licked its hind paw or jumped off to avoid thermal pain. Thirty seconds was the cut-off time chosen to minimize tissue damage [51].

4.4. Blood Samples

Under light anesthesia with ketamine (20 mg/kg b.w., i.p.) and xylazine (2 mg/kg b.w., i.p.), the blood samples were collected in heparinized tubes (Startstedt AG and Co., Nümbrecht, Germany) from the retro-orbital plexuses of each rat, at 24 h after AI induction. Plasma samples were obtained by centrifugation at 4 °C for 20 min at 1620 (×g). The obtained plasma was further transferred in Eppendorf tubes and kept at −80 °C until further analysis. All rats were sacrificed by an overdose of anesthetics at the end of the experiment.

4.5. Tissue Homogenate

Tissue samples were taken from the right-hind paw of rats from all groups immediately after scarification. The tissue samples were weighed and homogenized using an automated Witeg Homogenizer (HG-15D, Wertheim, Germany) in four volumes of phosphate-buffered saline solution, centrifuged at 1500 (×g) for 15 min at °C and the resulting clear supernatant was stored used for further biochemical analysis.

4.6. Biochemical Assays

The plasma and tissue levels of the inflammatory cytokines (TNF-α, IL-6, and IL-1β) were measured using the enzyme-linked immunosorbent assay (ELISA) technique (Stat Fax 303 Plus Microstrip Reader, Minneapolis, MN, USA), with commercially available kits (rat TNF-α, IL-6, and IL-1β ABTS ELISA Development kits, PeproTech EC, Ltd., London, UK).

4.7. Quantification of Plasma Curcumin

4.7.1. Preparation of Stock Solutions and Calibration Standards

Standard curcumin 5 mg was accurately weighed and transferred to a 5 mL amber-colored volumetric flask. The volume was made with DMSO obtaining a concentration

of 1 mg/mL. This solution was diluted with DMSO to obtain a final concentration range between 0.05 and 5 μg/mL. The dilutions were also prepared in amber-colored HPLC vials and stored at −20 °C not longer than one month after preparation. Standard solutions were freshly prepared each day using the stock solution for intraday and interday analysis. Before injecting into the HPLC system, the solutions were filtered using 0.45 μm nylon filters.

4.7.2. Sample Extraction Procedure

An aliquot of 125 μL of each rat plasma sample (hydrolyzed or unhydrolyzed) was loaded into a Strata™ XA 33 mm polymeric strong anion (30 mg/1 mL) tubes (Phenomenex) and fixed on a complete LiChrolut extraction unit (Merck, Darmstadt, Germany). The cartridge was prior conditioned with 3 mL of acetonitrile and equilibrated with 3 mL of water. Afterward, samples were loaded and washed with 3 mL of methanol: water (30/70, *v*/*v*). Before elution, a 10 min drying step under full vacuum conditions was applied to improve the extraction efficiency. Curcumin was then eluted using 1 mL of formic acid: acetonitrile solution (5:95, *v*/*v*). After elution, the solution was evaporated to dryness using a Techne Sample Concentrator FSC (Scientific Laboratory Supplies, England and Wales) under a stream of nitrogen gas at 45 °C. The dried samples were reconstituted in a 150 μL mobile phase, vortexed for 30 s, and 10 μL was further injected into the chromatograph.

4.7.3. Sample Hydrolyzation

Samples were hydrolyzed to quantify major curcumin metabolites formed after curcumin ingestion (curcumin glucuronide and curcumin sulfate). β-glucuronidase and sulfatase, both from Helix pomatia, were used for curcumin metabolites conversion to their parent curcuminoid. Enzymes were dissolved in 0.1 M phosphate buffer (pH 6.8) to obtain 1800 units of β-glucuronidase and 160 units of sulfatase in 100 μL as described in Mahale et al. [52]. The hydrolysis was performed at 37 °C for 3.5 h by mixing 100 μL β-glucuronidase/sulfatase solution with 100 μL of rat plasma. Before incubation, samples were vortexed for 2 min. The curcumin extraction procedure was performed as previously described.

4.7.4. Identification and Quantification of Curcumin by HPLC-UV

Curcumin from hydrolyzed and unhydrolyzed plasma samples was quantified using the method described by Mahale et al. [52]. Accordingly, an HPLC-UV Waters Alliance 2695 system equipped with a quaternary gradient proportioning valve, autosampler, and degasser, was used. The HPLC system was coupled with a 2489 Waters UV/Visible detector. Separations were performed using a reverse phase-HPLC column (Atlantis® dC18; 4.6 mm × 150 mm, 3 μm particle size, Waters, Hertfordshire, UK) at 25 °C. The chromatographic separation was performed using a mixture of two mobile phases. Mobile phase (A) was 10 mM ammonium acetate (pH 4.5), while mobile phase (B) was acetonitrile. The elution program started from 90% A. The percent of A was further decreased as follows: 90–60% (0–15 min), 60–15% (15–25 min), and 15–0% (25–30 min). After 30 min, the initial conditions were achieved by increasing the percentage of mobile phase A by 90% in 1 min, followed by a 3 min equilibration. The absorbance was recorded at 426 nm. The flow rate was set at 1 mL/min, the injection volume at 10 μL, and the autosampler temperature at 4 °C. Data acquisition and analysis were carried out using the Empower software. The identification of curcumin was carried out using the UV–visible spectra, retention time, co-chromatography with standard, and literature data. The quantity was expressed as μg/mL curcumin equivalents.

4.8. Histopathological Examination

Fragments from right-hind paws were taken and fixed in 10% formalin after rats were sacrificed by an overdose of anesthetics. After being embedded in paraffin, fragments were sectioned, stained with hematoxylin and eosin, and examined under a light microscope by a pathologist blinded to the study groups.

4.9. Statistical Analysis

Statistica program (v. 13.5, TIBCO Software Inc, Palo Alto, CA, USA) was used for statistical analysis. Multiple comparisons Kruskal–Wallis test was used to assess the differences between groups, followed by posthoc analysis whenever $p < 0.05$. Student *t*-test for independent sample was used to compare the free curcumin and curcumin metabolites between AIcC200 and AInC200 as well as the additional therapeutical effect of cC and nC to D. In the box and whisker plots, the upper line connected with a perpendicular line with the box is the maximum value, the bottom line that is connected with the box represents the minimum value, the upper box edge corresponds to the third quartile, the lower box edge corresponds to the first quartile, line through the center is the median, and × indicates the mean.

5. Conclusions

In monotherapy at 200 mg/kg b.w., both conventional curcumin and curcumin nanoparticles have limited analgesic and anti-inflammatory effects in carrageenan-induced paw edema. Curcumin and curcumin nanoparticles associated with diclofenac potentiate its therapeutical effects, with the best results obtained for curcumin nanoparticles. The association of curcumin nanoparticles to a low dose of diclofenac could be an appropriate combination to decrease NSAID doses used to reduce pain, inflammatory cytokines, and histological changes in acute inflammation. Still, additional evaluations are needed to achieve clinical evaluation.

Supplementary Materials: The following supporting information can be downloaded at: https://www.mdpi.com/article/10.3390/ijms231911737/s1.

Author Contributions: Conceptualization, I.B. and I.C.B.; methodology, I.B. and P.-M.B.; software, D.G. and S.D.B.; validation, I.C.B., R.-M.R. and S.D.B.; formal analysis, R.M.P. and D.G.; investigation, I.B. and P.-M.B.; resources, R.M.P. and R.-M.R.; data curation, R.M.P. and A.E.B.; writing—original draft preparation, I.B. and P.-M.B.; writing—review and editing, A.D.B. and S.D.B.; visualization, A.R. and S.D.B.; supervision, A.E.B. and A.D.B.; project administration, R.M.P. and P.-M.B.; funding acquisition, I.B. and A.R. All authors have read and agreed to the published version of the manuscript.

Funding: This research was funded by the Iuliu Haţieganu University of Medicine and Pharmacy Cluj-Napoca grant number PCD 1032/16/ 13 January 2021.

Institutional Review Board Statement: The study was conducted according to the guidelines of the Declaration of Helsinki, and approved by the Ethics Committee of the Iuliu Haţieganu University of Medicine and Pharmacy (UMFIH) Cluj-Napoca (approval number 25/3 February 2021). It was also approved by the Sanitary-Veterinary and Food Safety Directorate from Cluj-Napoca (approval number 252/17 March 2021).

Informed Consent Statement: Not applicable.

Data Availability Statement: The presented data will not be publicly available until the associated Ph.D. thesis is publicly defended. Raw data can be obtained upon reasonable request when addressed to Ioana Boarescu (e-mail: ioana.chirila.boarescu@elearn.umfcluj.ro).

Acknowledgments: The authors would like to thank Molnar Mirel for helping handle the rats during the experiment.

Conflicts of Interest: The authors declare no conflict of interest.

References

1. Punchard, N.A.; Whelan, C.J.; Adcock, I. The journal of inflammation. *J. Inflamm.* **2004**, *1*, 1. [CrossRef] [PubMed]
2. Corsini, E.; Di Paola, R.; Viviani, B.; Genovese, T.; Mazzon, E.; Lucchi, L.; Cuzzocrea, S. Increased carrageenan-induced acute lung inflammation in old rats. *Immunology* **2005**, *115*, 253–261. [CrossRef] [PubMed]
3. Winter, C.A.; Risely, E.A.; Nuss, G.W. Carrageenan induced edema in hind paw of the rat as an assay for anti-inflammatory. *Proc. Soc. Exp. Biol. Med.* **1962**, *111*, 544–547. [CrossRef] [PubMed]
4. Mansouri, M.T.; Hemmati, A.A.; Naghizadeh, B.; Mard, S.A.; Rezaie, A.; Ghorbanzadeh, B. A study of the mechanisms underlying the anti-inflammatory effect of ellagic acid in carrageenan-induced paw edema in rats. *Indian J. Pharmacol.* **2015**, *47*, 292–298. [CrossRef] [PubMed]

5. Halici, Z.; Dengiz, G.O.; Odabasoglu, F.; Suleyman, H.; Cadirci, E.; Halici, M. Amiodarone has anti-inflammatory and anti-oxidative properties: An experimental study in rats with carrageenan-induced paw edema. *J. Pharmacol.* **2007**, *566*, 215–221. [CrossRef]
6. Ronchetti, D.; Borghi, V.; Gaitan, G.; Herrero, J.F.; Impagnatiello, F. NCX 2057, a novel NO-releasing derivative of ferulic acid, suppresses inflammatory and nociceptive responses in in vitro and in vivo models. *Br. J. Pharmacol.* **2009**, *158*, 569–579. [CrossRef]
7. Atkinson, T.J.; Fudin, J. Nonsteroidal antiinflammatory drugs for acute and chronic pain. *Phys. Med. Rehabil. Clin. N. Am.* **2020**, *31*, 219–231. [CrossRef]
8. Wongrakpanich, S.; Wongrakpanich, A.; Melhado, K.; Rangaswami, J. A comprehensive review of non-steroidal anti-inflammatory drug use in the elderly. *Aging Dis.* **2018**, *9*, 143–150. [CrossRef]
9. Vonkeman, H.E.; van de Laar, M.A. Nonsteroidal anti-inflammatory drugs: Adverse effects and their prevention. *Semin. Arthritis Rheum.* **2010**, *39*, 294–312. [CrossRef]
10. Kołodziejska, J.; Kołodziejczyk, M. Diclofenac in the treatment of pain in patients with rheumatic diseases. *Reumatologia* **2018**, *56*, 174–183. [CrossRef]
11. Yarishkin, O.V.; Hwang, E.M.; Kim, D.; Yoo, J.C.; Kang, S.S.; Kim, D.R.; Shin, J.-H.; Chung, H.-J.; Jeong, H.-S.; Kang, D.; et al. Diclofenac, a non-steroidal anti-inflammatory drug, inhibits L-type Ca2+ channels in neonatal rat ventricular cardiomyocytes. *Korean J. Physiol. Pharmacol.* **2009**, *13*, 437–442. [CrossRef] [PubMed]
12. Phumsuay, R.; Muangnoi, C.; Dasuni Wasana, P.W.; Vajragupta, O.; Rojsitthisak, P.; Towiwat, P. Molecular insight into the anti-inflammatory effects of the curcumin ester prodrug curcumin diglutaric acid in vitro and in vivo. *Int. J. Mol. Sci.* **2020**, *21*, 5700. [CrossRef] [PubMed]
13. Boarescu, I.; Boarescu, P.-M.; Pop, R.M.; Bocșan, I.C.; Gheban, D.; Râjnoveanu, R.-M.; Râjnoveanu, A.; Bulboacă, A.E.; Buzoianu, A.D.; Bolboacă, S.D. Curcumin Nanoparticles Enhance Antioxidant Efficacy of Diclofenac Sodium in Experimental Acute Inflammation. *Biomedicines* **2022**, *10*, 61. [CrossRef] [PubMed]
14. Deuis, J.R.; Dvorakova, L.S.; Vetter, I. Methods used to evaluate pain behaviors in rodents. *Front. Mol. Neurosci.* **2017**, *10*, 284. [CrossRef] [PubMed]
15. Pop, R.M.; Sabin, O.; Suciu, Ș.; Vesa, S.C.; Socaci, S.A.; Chedea, V.S.; Bocsan, I.C.; Buzoianu, A.D. Nigella Sativa's Anti-Inflammatory and Antioxidative Effects in Experimental Inflammation. *Antoxidants* **2020**, *9*, 921. [CrossRef]
16. Goh, J.Z.; Tang, S.N.; Chiong, H.S.; Yong, Y.K.; Zuraini, A.; Hakim, M.N. Evaluation of antinociceptive activity of nanoliposome-encapsulated and free-form diclofenac in rats and mice. *Int. J. Nanomed.* **2014**, *10*, 297–303. [CrossRef]
17. Gupta, A.K.; Parasar, D.; Sagar, A.; Choudhary, V.; Chopra, B.S.; Garg, R.; Khatri, N. Analgesic and anti-inflammatory properties of gelsolin in acetic acid induced writhing, tail immersion and carrageenan induced paw edema in mice. *PLoS ONE* **2015**, *10*, e0135558. [CrossRef]
18. Zhao, G.; Shi, Y.; Gong, C.; Liu, T.; Nan, W.; Ma, L.; Wu, Z.; Da, C.; Zhou, K.; Zhang, H. Curcumin Exerts Antinociceptive Effects in Cancer-Induced Bone Pain via an Endogenous Opioid Mechanism. *Front. Neurosci.* **2021**, *15*, 696861. [CrossRef]
19. Ibironke, G.F.; Ajiboye, K.I. Studies on the anti-inflammatory and analgesic properties of Chenopodium ambrosioides leaf extract in rats. *Int. J. Pharmacol.* **2007**, *3*, 111–115. [CrossRef]
20. Burian, M.; Tegeder, I.; Seegel, M.; Geisslinger, G. Peripheral and central antihyperalgesic effects of diclofenac in a model of human inflammatory pain. *Clin. Pharmacol. Ther.* **2003**, *74*, 113–120. [CrossRef]
21. Babu, A.; Prasanth, K.G.; Balaji, B. Effect of curcumin in mice model of vincristine-induced neuropathy. *Pharm. Biol.* **2015**, *53*, 838–848. [CrossRef] [PubMed]
22. Idriss, H.T.; Naismith, J.H. TNFα and the TNF receptor superfamily: Structure-function relationship (s). *Microsc. Res. Tech.* **2000**, *50*, 184–195. [CrossRef]
23. Page, M.J.; Bester, J.; Pretorius, E. The inflammatory effects of TNF-α and complement component 3 on coagulation. *Sci. Rep.* **2018**, *8*, 1812. [CrossRef] [PubMed]
24. Calimag, K.P.D.; Arbis, C.C.H.; Collantes, T.M.A.; Bariuan, J.V.; Ang, M.J.C.; Cervancia, C.A.; Desamero, M.J.M.; Estacio, M.A.C. Attenuation of carrageenan-induced hind paw edema and plasma TNF-α level by Philippine stingless bee (*Tetragonula biroi* Friese) propolis. *Exp. Anim.* **2021**, *70*, 185–193. [CrossRef]
25. Choy, E.; Rose-John, S. Interleukin-6 as a multifunctional regulator: Inflammation, immune response, and fibrosis. *J. Scleroderma Relat. Disord.* **2017**, *2*, S1–S5. [CrossRef]
26. Tanaka, T.; Narazaki, M.; Kishimoto, T. IL-6 in inflammation, immunity, and disease. *Cold Spring Harb. Perspect. Biol.* **2014**, *6*, a016295. [CrossRef]
27. Annamalai, P.; Thangam, E.B. Local and systemic profiles of inflammatory cytokines in carrageenan-induced paw inflammation in rats. *Immunol. Investig.* **2017**, *46*, 274–283. [CrossRef]
28. Ren, K.; Torres, R. Role of interleukin-1β during pain and inflammation. *Brain Res. Rev.* **2009**, *60*, 57–64. [CrossRef]
29. Boarescu, P.-M.; Boarescu, I.; Pop, R.M.; Roşian, Ș.H.; Bocșan, I.C.; Rus, V.; Mada, R.O.; Popa, I.D.; Neagu, N.; Bulboacă, A.E.; et al. Evaluation of Oxidative Stress Biomarkers, Pro-Inflammatory Cytokines, and Histological Changes in Experimental Hypertension, Dyslipidemia, and Type 1 Diabetes Mellitus. *Int. J. Mol. Sci.* **2022**, *23*, 1438. [CrossRef]
30. Curto-Reyes, V.; Kirschmann, G.; Pertin, M.; Drexler, S.K.; Decosterd, I.; Suter, M.R. Neuropathic pain phenotype does not involve the NLRP3 inflammasome and its end product interleukin-1β in the mice spared nerve injury model. *PLoS ONE* **2015**, *10*, e0133707. [CrossRef]

31. Safieh-Garabedian, B.; Poole, S.; Allchorne, A.; Winter, J.; Woolf, C.J. Contribution of interleukin-1β to the inflammation-induced increase in nerve growth factor levels and inflammatory hyperalgesia. *Br. J. Pharmacol.* **1995**, *115*, 1265–1275. [CrossRef] [PubMed]
32. Atzeni, F.; Masala, I.F.; Sarzi-Puttini, P. A review of chronic musculoskeletal pain: Central and peripheral effects of diclofenac. *Pain Ther.* **2018**, *7*, 163–177. [CrossRef] [PubMed]
33. Lisboa, F.A.; Bradley, M.J.; Hueman, M.T.; Schobel, S.A.; Gaucher, B.J.; Styrmisdottir, E.L.; Potter, B.K.; Forsberg, J.A.; Elster, E.A. Nonsteroidal anti-inflammatory drugs may affect cytokine response and benefit healing of combat-related extremity wounds. *Surgery* **2017**, *161*, 1164–1173. [CrossRef] [PubMed]
34. Kim, Y.S.; Park, H.J.; Joo, S.Y.; Hong, M.H.; Kim, K.H.; Hong, Y.J.; Kim, J.H.; Park, H.W.; Jeong, M.H.; Cho, J.G.; et al. The protective effect of curcumin on myocardial ischemia–reperfusion injury. *Korean Circ. J.* **2008**, *38*, 353–359. [CrossRef]
35. Matabudul, D.; Pucaj, K.; Bolger, G.; Vcelar, B.; Majeed, M.; Helson, L. Tissue distribution of (Lipocurc™) liposomal curcumin and tetrahydrocurcumin following two-and eight-hour infusions in beagle dogs. *Anticancer Res.* **2012**, *32*, 4359–4364.
36. Boarescu, P.-M.; Boarescu, I.; Bulboacă, A.E.; Bocșan, I.C.; Pop, R.M.; Gheban, D.; Râjnoveanu, R.-M.; Râjnoveanu, A.; Roşian, Ş.H.; Buzoianu, A.D.; et al. Multi-Organ Protective Effects of Curcumin Nanoparticles on Drug-Induced Acute Myocardial Infarction in Rats with Type 1 Diabetes Mellitus. *Appl. Sci.* **2021**, *11*, 5497. [CrossRef]
37. Dogaru, G.; Bulboaca, A.E.; Gheban, D.; Boarescu, P.M.; Rus, V.; Festila, D.; Sitar-Taut, A.V.; Stanescu, I. Effect of liposomal Curcumin on acetaminophen hepatotoxicity by down-regulation of oxidative stress and matrix metalloproteinases. *Vivo* **2020**, *34*, 569–582. [CrossRef]
38. Dei Cas, M.; Ghidoni, R. Dietary Curcumin: Correlation between Bioavailability and Health Potential. *Nutrients* **2019**, *11*, 2147. [CrossRef]
39. Hettiarachchi, S.S.; Dunuweera, S.P.; Dunuweera, A.N.; Rajapakse, R.G. Synthesis of curcumin nanoparticles from raw turmeric rhizome. *ACS Omega* **2021**, *6*, 8246–8252. [CrossRef]
40. Anand, P.; Thomas, S.G.; Kunnumakkara, A.B.; Sundaram, C.; Harikumar, K.B.; Sung, B.; Tharakan, S.T.; Misra, K.; Priyadarsini, I.K.; Rajasekharan, K.N.; et al. Biological activities of curcumin and its analogues (Congeners) made by man and Mother Nature. *Biochem. Pharmacol.* **2008**, *76*, 1590–1611. [CrossRef]
41. Ravichandran, R. Pharmacokinetic study of nanoparticulate curcumin, oral formulation for enhanced bioavailability. *J. Biomater. Nanobiotechnol.* **2013**, *4*, 291–299. [CrossRef]
42. Abdelhameed, M.F.; Asaad, G.F.; Ragab, T.I.M.; Ahmed, R.F.; El Gendy, A.E.-N.G.; Abd El-Rahman, S.S.; Elgamal, A.M.; Elshamy, A.I. Oral and Topical Anti-Inflammatory and Antipyretic Potentialities of Araucaria bidiwillii Shoot Essential Oil and Its Nanoemulsion in Relation to Chemical Composition. *Molecules* **2021**, *26*, 5833. [CrossRef] [PubMed]
43. Struthmann, L.; Hellwig, N.; Pircher, J.; SOHN, H.Y.; Buerkle, M.A.; Klauss, V.; Mannell, H.; Pohl, U.; Krötz, F. Prothrombotic effects of diclofenac on arteriolar platelet activation and thrombosis in vivo. *J. Thromb. Haemost.* **2009**, *7*, 1727–1735. [CrossRef] [PubMed]
44. Buadonpri, W.; Wichitnithad, W.; Rojsitthisak, P.; Towiwat, P. Synthetic curcumin inhibits carrageenan-induced paw edema in rats. *J. Health Res.* **2009**, *23*, 11–16.
45. Rachmawati, H.; Safitri, D.; Pradana, A.T.; Adnyana, I.K. TPGS-Stabilized Curcumin Nanoparticles Exhibit Superior Effect on Carrageenan-Induced Inflammation in Wistar Rat. *Pharmaceutics* **2016**, *8*, 24. [CrossRef]
46. Nurullahoglu, K.E.; Okudan, N.; Belviranli, M.; Oz, M. The comparison of preemptive analgesic effects of curcumin and diclofenac. *Bratisl. Lek. Listy* **2014**, *115*, 757–760. [CrossRef]
47. Jain, S.K.; Gill, M.S.; Pawar, H.S.; Suresh, S. Novel curcumin diclofenac conjugate enhanced curcumin bioavailability and efficacy in streptococcal cell wall-induced arthritis. *Indian J. Pharm. Sci.* **2014**, *76*, 415–422.
48. De Paz-Campos, M.A.; Ortiz, M.I.; Piña, A.E.C.; Zazueta-Beltrán, L.; Castañeda-Hernández, G. Synergistic effect of the interaction between curcumin and diclofenac on the formalin test in rats. *Phytomedicine* **2014**, *21*, 1543–1548. [CrossRef]
49. Amdekar, S.; Roy, P.; Singh, V.; Kumar, A.; Singh, R.; Sharma, P. Anti-inflammatory activity of lactobacillus on carrageenan-induced paw edema in male wistar rats. *Int. J. Inflam.* **2012**, *2012*, 752015. [CrossRef]
50. Szabo, A.; Bocsan, I.; Suciu, S.; Buzoianu, A. Comparative animal study of the antinociceptive efficacy of lamotrigine and gabapentin for the management of pain. *Acta Physiol. Hung.* **2015**, *102*, 363–371. [CrossRef]
51. Rus, N.N.; Bocşan, C.; Vesa, Ş.C.; Coadă, C.A.; Buzoianu, A.D. Topiramate in nociceptive pain-experimental analgesia study. *HVM Bioflux* **2013**, *5*, 70–76.
52. Mahale, J.; Howells, L.M.; Singh, R.; Britton, R.G.; Cai, H.; Brown, K. An HPLC-UV method for the simultaneous quantification of curcumin and its metabolites in plasma and lung tissue: Potential for preclinical applications. *Biomed. Chromatogr.* **2018**, *32*, e4280. [CrossRef] [PubMed]

International Journal of
Molecular Sciences

MDPI

Article

Nontoxic and Naturally Occurring Active Compounds as Potential Inhibitors of Biological Targets in *Liriomyza trifolii*

Israa M. Shamkh [1,2,*], Mohammed Al-Majidi [3], Ahmed Hassen Shntaif [3], Peter Tan Deng Kai [4], Ngoc Nh-Pham [5], Ishrat Rahman [6], Dalia Hamza [7], Mohammad Shahbaz Khan [8], Maii S. Elsharayidi [9], Eman T. Salah [10], Abdullah Haikal [11], Modupe Akintomiwa Omoniyi [12], Mahmoud A. Abdalrahman [13] and Tomasz M. Karpinski [14,*]

1 Botany and Microbiology Department, Faculty of Science, Cairo University, Cairo 12613, Egypt
2 Chemo and Bioinformatics Lab, Bio Search Research Institution, BSRI, Giza 12613, Egypt
3 Department of Chemistry, College of Science for Women, University of Babylon, Alhilla 51002, Iraq
4 Victoria Junior College, Crimson Research Institute, Singapore 449035, Singapore
5 Department of Biotechnology, Faculty of Biology and Biotechnology, VNU-HCM University of Science, Ho Chi Minh City 700000, Vietnam
6 Department of Basic Dental Sciences, College of Dentistry, Princess Nourah bint Abdulrahman University, Riyadh 11564, Saudi Arabia
7 Zoonoses Department, Faculty of Veterinary Medicine, Cairo University, Giza 11221, Egypt
8 Children's National Hospital, Washington, DC 20010, USA
9 Central Public Health Laboratories, Egyptian Ministry of Health, Cairo 11511, Egypt
10 Biochemistry Department, Faculty of Science, Ain Shams University, Ain Shams 11591, Egypt
11 Department of Pharmacognosy, Faculty of Pharmacy, Mansoura University, Mansoura 35516, Egypt
12 Department of Chemistry, Faculty of Science, University of Lagos, Lagos 101017, Nigeria
13 Science Department—Chemistry, Milton Academy, Crimson Research Institute, Milton, MA 02186, USA
14 Chair and Department of Medical Microbiology, Poznań University of Medical Sciences, Wieniawskiego 3, 61-712 Poznań, Poland
* Correspondence: israamshamkh@gmail.com (I.M.S.); tkarpin@ump.edu.pl (T.M.K.)

Citation: Shamkh, I.M.; Al-Majidi, M.; Shntaif, A.H.; Deng Kai, P.T.; Nh-Pham, N.; Rahman, I.; Hamza, D.; Khan, M.S.; Elsharayidi, M.S.; Salah, E.T.; et al. Nontoxic and Naturally Occurring Active Compounds as Potential Inhibitors of Biological Targets in *Liriomyza trifolii*. *Int. J. Mol. Sci.* **2022**, *23*, 12791. https://doi.org/10.3390/ijms232112791

Academic Editor: Wolfgang Sippl

Received: 19 August 2022
Accepted: 17 October 2022
Published: 24 October 2022

Abstract: In recent years, novel strategies to control insects have been based on protease inhibitors (PIs). In this regard, molecular docking and molecular dynamics simulations have been extensively used to investigate insect gut proteases and the interactions of PIs for the development of resistance against insects. We, herein, report an in silico study of (disodium 5′-inosinate and petunidin 3-glucoside), (calcium 5′-guanylate and chlorogenic acid), chlorogenic acid alone, (kaempferol-3,7-di-O-glucoside with hyperoside and delphinidin 3-glucoside), and (myricetin 3′-glucoside and hyperoside) as potential inhibitors of acetylcholinesterase receptors, actin, α-tubulin, arginine kinase, and histone receptor III subtypes, respectively. The study demonstrated that the inhibitors are capable of forming stable complexes with the corresponding proteins while also showing great potential for inhibitory activity in the proposed protein-inhibitor combinations.

Keywords: protein inhibitors; *Liriomyza trifolii*; molecular docking; inhibitory activity; protein-ligand interactions; yeast extraction; bean-leaf extraction

1. Introduction

A concerning problem that threatens food security around the world is the emergence of insects capable of developing resistance to insecticides [1]. Excessive use of many of these insecticides is associated with various health and environmental issues [2–4]. *Liriomyza trifolii* is a highly polyphagous pest in crop fields and greenhouses that has detrimental economic impacts [5]. Both larvae and adults selectively eat only the layers with the least amount of plant cellulose [6]. Stippling is one example of the damage in crop plants caused by the sap-sucking female fly; internal mining caused by larvae is another such example. These various types of damage allow pathogenic fungi to enter the leaves through feeding holes. These types of damage also facilitate the mechanical

transmission of some plant viruses [7,8]. Both leaf mining and leaf spotting can greatly reduce the level of photosynthesis in a plant [9], resulting in lower crop quality and yield. In this work, the study of the interactions between proteins and ligand inhibitors is proposed as for potential defense for increased resistance in crop plants [10]. The biological role of PIs is based on the inhibition of the proteins present in the guts of insects, which in turn reduces the availability of amino acids necessary for their growth and development [11]. The harmful effects of synthetic insecticides on the environment and on human health have drawn the attention of researchers to develop safer alternatives. In recent years, many studies investigated the chemical composition of plants and the possibility of using their extracts as bioinsecticides. In particular, these studies focused on probing the possibility of inhibiting the action of a number of enzymes that are found in common pests. Our work is complementary to the experimental results obtained by Mashamaite et al. [12], which showed that some chemicals extracted from natural materials such as plants can be effective compounds as biopesticides. Their work also suggested that compounds such as the (disodium 5′-inosinate and petunidin 3-glucoside), (calcium 5′-guanylate and chlorogenic acid), chlorogenic acid alone, (kaempferol-3,7-di-O-glucoside with hyperoside and delphinidin 3-glucoside), and (myricetin 3′-glucoside and hyperoside), can be used for the development of multitarget bioinsecticides. To confirm and reproduce the results obtained by the work of Mostafa et al. [13], it is necessary to perform structural modeling, binding site interaction prediction, molecular docking free energy calculations, binding pose analysis, dynamic stability and conformational perturbation analyses, radius of gyration analysis, hydrogen bond analysis, and molecular mechanics PBSA free energy calculations. The goal is to confirm, computationally, that these compounds could exert their bioactivities by altering the activities of acetylcholinesterase receptors, actin, α-tubulin, arginine kinase, and histone receptor III subtypes. Reproducing these results would also confirm the importance and versatility of the computational methods employed in this work in studying protein-ligand interactions.

We herein report the results of our structural modeling, binding site interaction prediction, molecular docking free energy calculations, binding pose analysis, dynamic stability and conformational perturbation analyses, radius of gyration analysis, hydrogen bond analysis, and molecular mechanics PBSA free energy calculations.

2. Results and Discussion

2.1. Database Search, Structural Modeling, and Model Validation

The homology modeling search of the query proteins sequences with the target *Liriomyza trifolii* proteins, namely acetylcholinesterase, α-tubulin, actin, arginine kinase, histone subunit III, Hsp90, and elongation factor 1-alpha, was performed using Blast on the NCBI server. The query coverage of proteins sequences showed (96%, 100%, 100%, 98%, 100%, 31% and 97%) with (54%, 61%, 60%, 58%, 59%, 56% and 55%) identity with the template proteins (1dx4.1.A, 5kx5.1.C, 4cbu.1.A, 4bg4.1.A, 4zux.1.A, 4cwr.1.A., and 5o8w.1.A), respectively. These were used as template proteins for the homology modeling of our target proteins. The Swissmodel server (https://Swissmodel.expasy.org/, accessed on 10 August 2022) generated (25, 35, 56, 58, 30, and 31) predictive models for *Liriomyza trifolii* proteins (acetylcholinesterase, *α-tubulin*, actin, arginine kinase, histone subunit III Hsp90, and elongation factor 1-alpha) with identity and Qualitative Model Energy Analysis (QMEAN) score values [14]. The models with low values of QMEAN scores were selected as the final models for in silico characterization and docking studies.

2.2. Structural Modeling, In Silico Characterization, and Model Validation

The selected models were verified for their stereochemical quality assessment. Furthermore, in each case of qualitative assessment, a comparative study was done with experimentally solved crystal structures to check the quality, reliability, accuracy, stability, and compatibility of the computationally predicted protein through a Ramachandran plot, the ERRAT score which is a so-called "overall quality factor" for nonbonded atomic

interactions, with higher scores indicating higher quality [15], and the QMEAN score. The Ramachandran plot obtained through the PROCHECK module of the PDBSum server justified the stereochemical suitability of the predicted proteins. Acetylcholinesterase, α-tubulin, actin, arginine kinase, histone subunit III Hsp90, and elongation factor 1-alpha had 92.3 %, 94.3%, 94.6%, 94.2%, 96.4%, 93.5%, and 94.0% residues, respectively, accommodating in the most favored regions (A, B, and L). They also only had 7.7 %, 5.5%, 5.4%, 5.0%, 0.3%, 0.6%, and 5.2% residues occupied in the additionally allowed regions (a, b, l, and p), respectively (Table 1, Figure S1). Residues in generously allowed regions (a, b, l, and p) are (0.0%, 0.3%, 0.0%, 0.8%, 0.0%, 0.0%, and 0.4%) and residues in disallowed regions are (0.0%, 0.0%, 0.0%, 0.0%, 0.0%, 0.5% and 0.4%), respectively. The ERRAT scores for the modeled structure were found to be (100%, 89.3519%, 95.9596%, 93.1298%, 100%, 96.4824%, 92.5373%, and 81.7204%), respectively. The QMEAN score values of the models were (−0.11, −1.00, 0.13, 0.43, 0.25, 0.28, and 0.66), respectively. The three parameters suggested that the predicted model had satisfactory stereochemical quality and was close to the template structure.

Table 1. Ramachandran plot values obtained through PROCHECK. Structurally and energetically favored regions are classified into allowed, generously allowed, and disallowed categories.

Protein	Ramachandran Plot Values			
	Core %	Allowed %	Generously %	Disallowed %
Acetylcholinesterase	92.3	7.7	0.0	0.0
α-tubulin	94.3	5.5	0.3	0.0
Actin	94.6	5.4	0.0	0.0
Arginine kinase	94.2	5.0	0.8	0.0
Histone subunit 3	96.4	0.3	0.0	0.0
Hsp90	93.5	0.6	0.0	0.5
Elongation factor	94.0	5.2	0.4	0.4
Carbamoyl phosphate synthase	85.6	13.2	0.0	1.1

2.3. Binding Site Prediction and Protein-Ligand Interaction

The putative ligand binding sites (both major and minor) for the predicted proteins were identified through Discovery studio software and were visualized (Figure 1). All target proteins (acetylcholinesterase, α-tubulin, actin, arginine kinase, histone subunit III, Hsp90, elongation factor 1-alpha, and carbomoylphosphate synthase) were docked with the ligands, most of which were phytochemicals derived from the leaves of *Phaseolus vulgaris* [16,17] and the yeast extract. We evaluated the protein-ligand interaction through SAMSON software [18]. It was found that the tool has discrepancies in results for accurate pose prediction among the various putative docking poses.

2.4. Molecular Docking and Binding Free Energy Calculation

The prepared protein structures of (acetylcholinesterase, *α-tubulin*, actin, arginine kinase, histone subunit III, Hsp90, elongation factor 1-alpha, and carbamoyl phosphate synthase) were docked using SAMSON software with phytochemical compounds and yeast extracted compounds listed in the supplementary data. The results of the docking studies were provided in Table 2, and it was revealed that the phytochemical compounds were superior to the yeast extract compounds based on the docking score. All docking results were monitored by scoring functions that predict how well the ligand binds in a particular docked pose. This scoring function gives the ranking of the ligands. In the present study, the docking score was taken into consideration for the selection of the best ligands. This allowed us to explain the mechanisms of insect death. A mathematical empirical scoring function was used to approximately predict the binding affinity between two molecules after they have been docked by approximating the ligand's binding free energy [20]. It includes various force field interactions such as electrostatic and van der Waals contributions, which influence ligand binding. Subsequently, the docked structures were queried for binding free energy calculation. The results of binding free energy

calculation were provided in Table 2. It was found that binding energy values supported the docking result well. Hesperidin, Naringin, and Rosmarinic acid have higher binding energies than other compounds. All of the other values contribute to the ΔG values which reflect the binding energy of the protein-ligand complex.

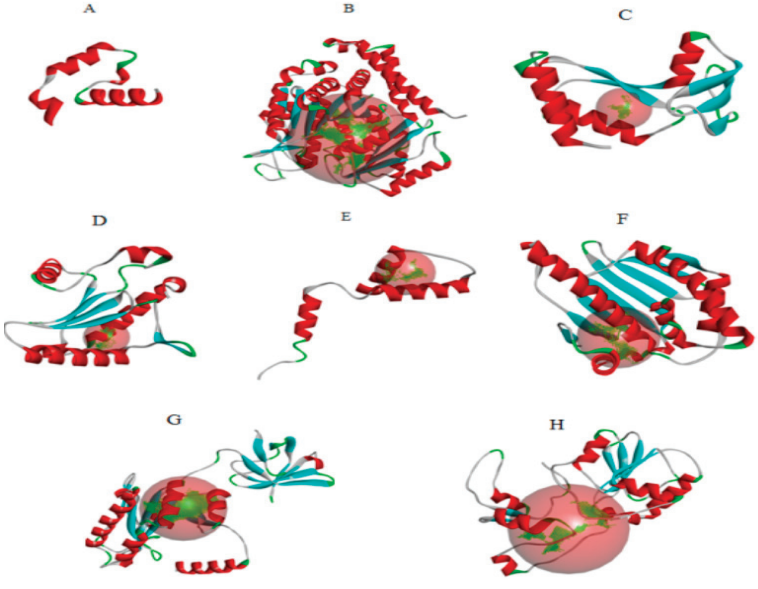

Figure 1. (**A**) acetylcholinesterase, (**B**) α-tubulin, (**C**) actin, (**D**) arginine kinase, (**E**) histone subunit III (**F**) Hsp90, (**G**) elongation factor 1-alpha, and (**H**) carbamoyl phosphate synthase of the *Liriomyza trifolii* modeled proteins through homology modeling using the Swissmodel server and visualized through the Discovery Studio 3.0 visualization tool [19]. The large red sphere represents the cavities surrounding the active sites and was visualized using the visualization module of Discovery Studio 3.0 visualization.

Table 2. Protein Genbank sequences and modeling parameters for building with template ID, sequences identities, the coverage of the protein, and quality mean estimation for validation of the protein in quality.

Protein	Genbank:	Template	Seq Identity	Coverage	QMEAN
Acetylcholinesterase	CAI30732.1	1dx4.1.A	54%	96%	−0.11
α-tubulin	ARQ84036.1	5kx5.1.C	61%	100%	−1.00
Actin	ARQ84030.1	4cbu.1.A	60%	100%	0.13
Argenin Kinase	ARQ84038.1	4bg4.1.A	58%	98%	0.43
Histone Subunit3	ARQ84034.1	4zux.1.A	59%	100%	0.25
Hsp90	AGI19327.1	4cwr.1.A	56%	31%	0.28
Elongation Factor	ARQ84032.1	5o8w.1.A	55%	97%	0.66

2.5. Binding Pose Analysis

The binding mode of the compounds with proteins (acetylcholinesterase, α-tubulin, actin, arginine kinase, histone subunit III, Hsp90, elongation factor 1-alpha, and carbamoyl phosphate synthase) showed the different interactions between the proteins and ligands showed in Table 3. The interactions between the inhibitors and their target proteins, as well as their binding modes and orientations, are shown in Figures 2–9.

Table 3. Docking scores and molecular properties of bioactive phytochemical components from the HPLC of *Phaseolus vulgaris* leaves (ref) and the yeast extract compounds. The molecular docking table shows the protein target, the interactive ligands with the highest binding energy, the type of bound of the highest score ligands, and the X, Y and Z geometry values of the protein.

Target	Ligands	Binding Energy of Direct Kcal/mole	Binding Energy of Indirect Kcal/mole	Binging Site	Type of Bond	X, Y and Z Value
Acetylcolenestras	Disodium 5′-inosinate	−6.5	0	SER36, CYS33, SER29, ASN22, ASN19, CYS18		center_x = 15.4462 center_y = 85.5487 center_z = −1.2087
	Petunidin 3-glucoside	0	−6.9	ASN17, CYS18 ASN19, ASN22 SER29, VAL30 GLN32, CYS33, SER36VAL37, ASP38	Alkyl Conventional H-bond carbon H-bond Amide -pi stacked pi-Alkyl Van der waals pi-Alkyl pi-Anion Halogen (Fluorine) Pi-Sulfur	
α-tubulin	Chlorogenic acid ID	0	−10.3	GLN11, ALA12 ASP69, ALA100 GLY144, ILE171 TYR224, ASN228	Conventional H-bond pi-Alkyl Amide-pi stacked Pi-Pi Stacked Pi-Sigma Unfavourable Donor–Donor Unfavourable Acceptor–Acceptor	center_x = 12.8911 center_y = 28.1478 center_z = −3.7346
Actin	Calcium 5′-guanylate D	−7.6	0	THR30, ALA32 LEU34, ASN39, GLN61, ARG101	Conventional H-bond cabon H-bond Unfavourable Donor–Donor Pi-Sigma	center_x = 16.2688 center_y = 30.1281 center_z = 30.8989
	Chlorogenic acid ID	0	−7.4	GLU31, LEU34 ASN35, TYR57 ALA59, ILE60 VAL63	Cabon H-bond Pi-Sigma pi-Alkyl Conventional H-bond Unfavourable Acceptor–Acceptor	
Arginine kinase	Kaempferol-3,7-di-O-glucoside I	0	−9.9	PHE135, SER128 PRO126, ILE98 HIS95	cabon H-bond Conventional H-bond Unfavourable Donor–Donor Pi-Pi Stacked	center_x = 21.1887 center_y = −3.9607 center_z = 13.2428
	Hyperoside D	−9	0	ASN142, LEU136, PHE135, SER128, PHE127, VAL118, ILE98	Van der waals Conventional H-bond Unfavourable Acceptor–Acceptor pi-Alkyl Pi-Pi Stacked Pi-Pi T–shaped	
	Delphinidin 3-glucoside ID	−9	−9	ASN142, PHE135, PHE127, VAL118, LEU96	Van der waals Conventional H-bond Unfavourable Acceptor–Acceptor pi-Alkyl Pi-Pi Stacked Pi-Pi T–shaped	
Hsp90	Cyanidin 3-glucoside ID –1	0	−10.9	ASN40 GLY86 LEU96 PHE127 TYR128 TRP151 THR173	cabon H-bond Conventional H-bond Unfavourable Donor–Donor Pi-Pi Stacked Pi-Pi T–shaped Pi-Sigma	center_x = 0.6349 center_y = 14.4620 center_z = 20.6177

Table 3. *Cont.*

Target	Ligands	Binding Energy of Direct Kcal/mole	Binding Energy of Indirect Kcal/mole	Binging Site	Type of Bond	X, Y and Z Value
Hsp90	Delphinidin 3-glucoside D/ID	−10	12	ASN40, ASP82 GLY86, LEU96, GLY126 PHE127, TRP151 THR173	Cabon H-bond Conventional H-bond Pi-Sigma Pi-Pi T–shaped Pi-Pi Stacked	center_x = 0.6349 center_y = 14.4620 center_z = 20.6177
	Hyperoside D	−9	0	ASN40 ASP82 GLY86 LEU96 GLY126 PHE127 TRP151 THR173	Conventional H-bond Pi-Sigma Pi-Pi T–shaped Pi-Pi Stacked	
Histone subunit3	Myricetin 3′-glucoside ID	0	−8.5	LEU66 GLN69 ARG70 ARG73 LEU83	Cabon H-bond Conventional H-bond Unfavourable Donor–Donor pi-Alkyl	center_x = 74.957 center_y = 39.323 center_z = −20.6626
	Hyperoside D	−6		TYR55 SER58 THR59 GLU60		
Elongation factor	kaempferol3-O-xylosylglucoside,	0	−9.8	HIS85, ALA58 GLN57, MET51 ALA41, ASP40, THR37	Van der waals Conventional H-bond pi-Alkyl Pi-Pi T–shaped Pi-Sigma Pi-Sigma	center_x = 22.1139 center_y = 30.3465 center_z = 31.8549
	Delphinidin 3-glucoside ID/D	−9.5	−9.5	HIS85, VAL62 CYS60, ALA58 GLN57, MET51 ALA41, THR37	Cabon H-bond Conventional H-bond Pi-Sigma Pi-Pi T–shaped pi-Alkyl Pi-Sulfur	
	hyperoside D	−9.9	0	HIS85, CYS60, ALA58, MET51, ALA41, THR37	Cabon H-bond Conventional H-bond Pi-Sigma Pi-Pi T–shaped pi-Alkyl Pi-Sulfur	
Carbamoyl phosphate synthase	disodium 5′-guanylate	−8.1	0	LYS196, MET195, LYS194, GLN182, CYS178, ASN152, GLY151, GLY149, PRO81, SER60	Cabon H-bond Conventional H-bond pi-Alkyl Pi-Cation	
	Petunidin 3-glucoside	0	−6.8	TRP34, LEU31, GLU29, LYS28, ARG26, LEU13, ILE10, ILE8, PHE2	Cabon H-bond Conventional H-bond Pi-Sigma pi-Alkyl Unfavourable Donor–Donor Halogen (Fluorine)	center_x = 21.3610 center_y = 59.0995 center_z = 103.8306

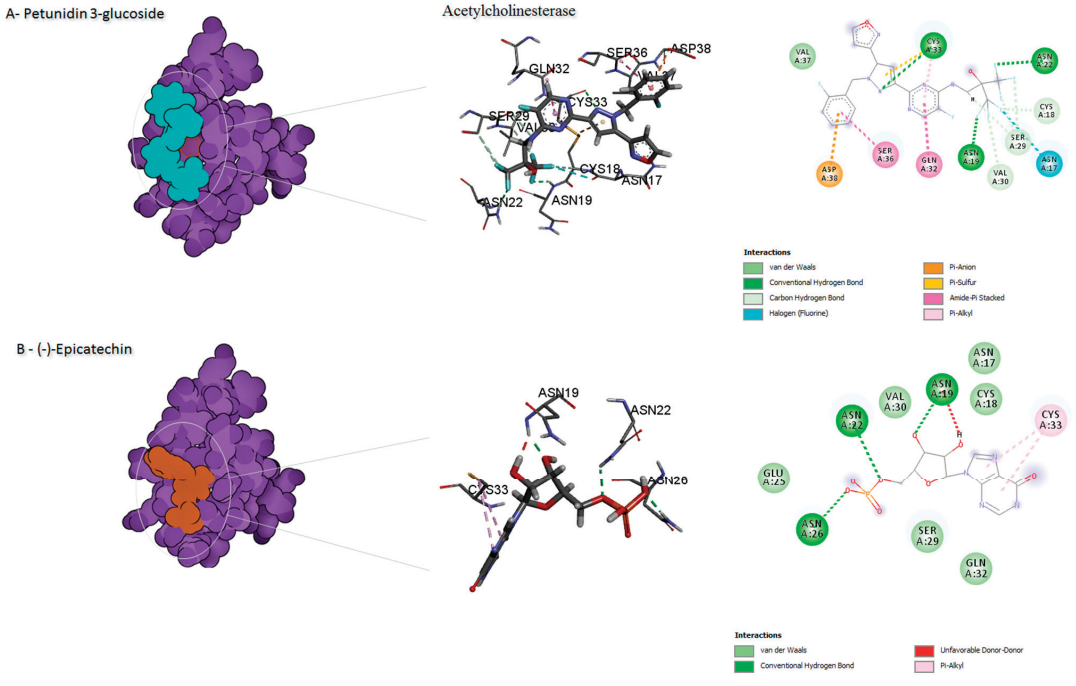

Figure 2. Predicted binding mode for acetylcholinesterase with petunidin 3-glucoside and disodium 5′-inosinate.

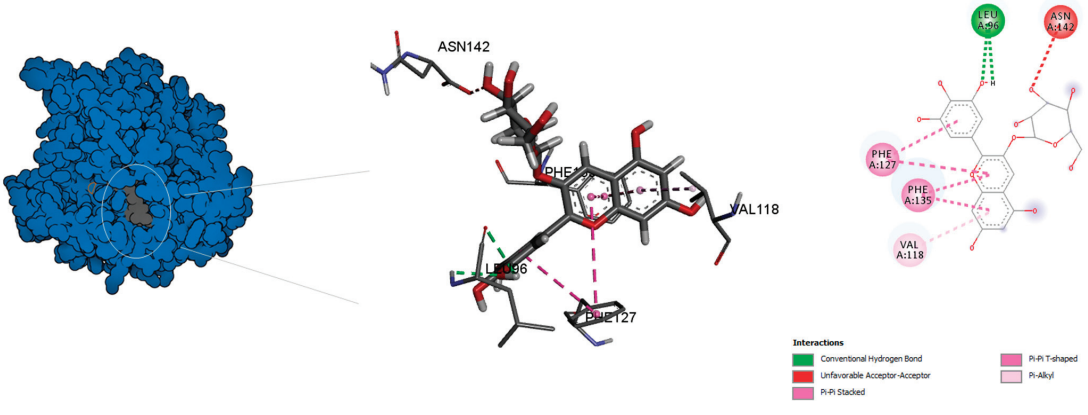

Figure 3. Predicted binding mode for α-tubulin with chlorogenic acid.

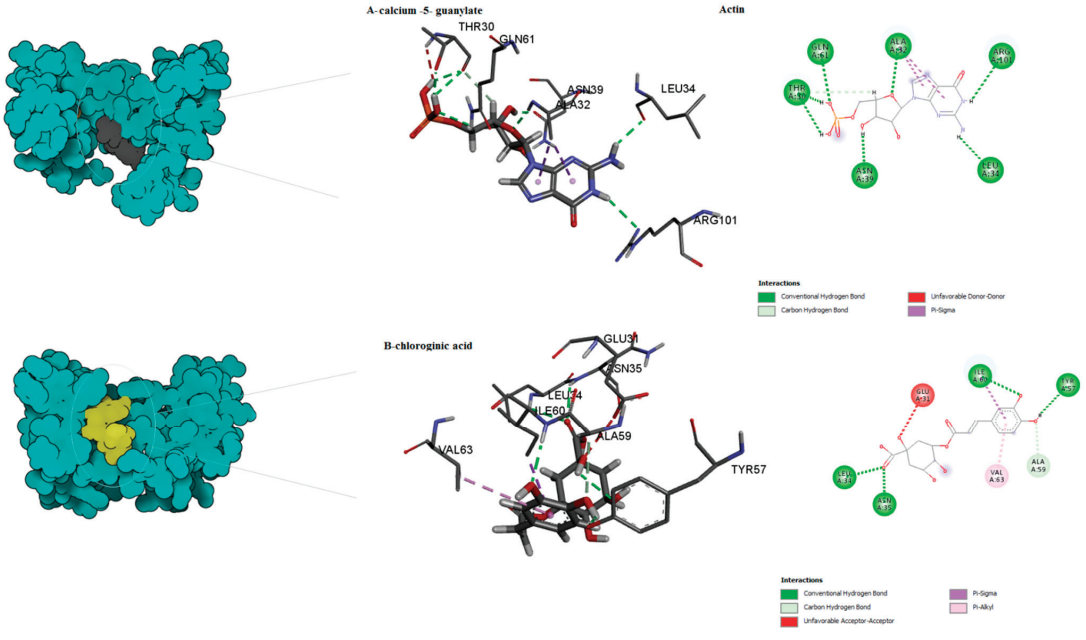

Figure 4. Predicted binding mode for actin with calcium 5- guanylate and chlorogenic acid.

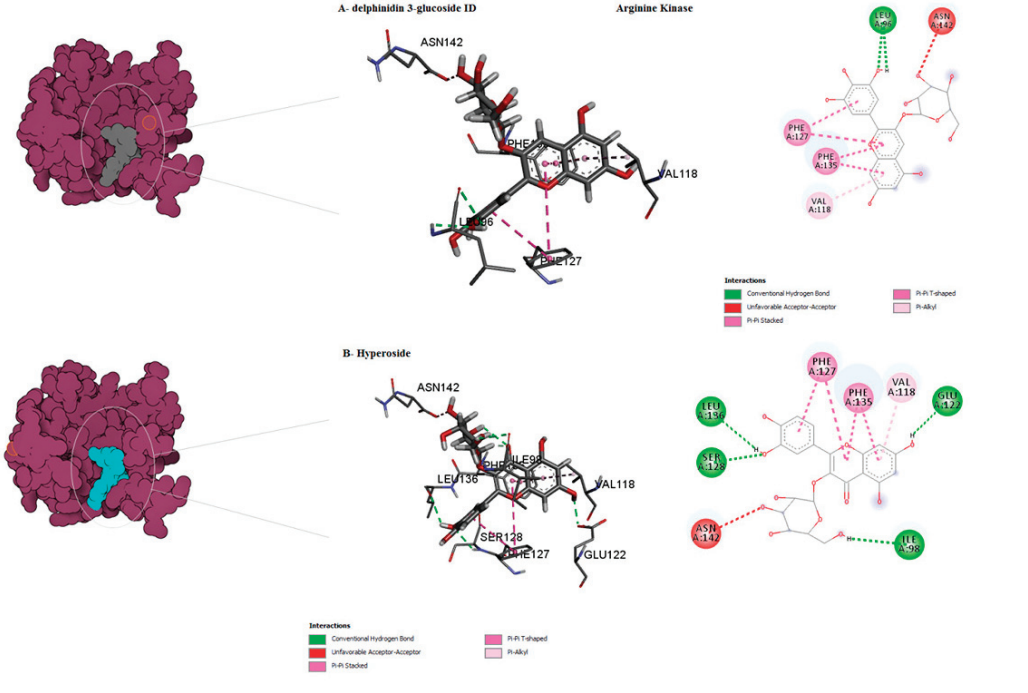

Figure 5. Predicted binding mode for arginine kinase with hyperoside and delphinidin 3-glucoside ID.

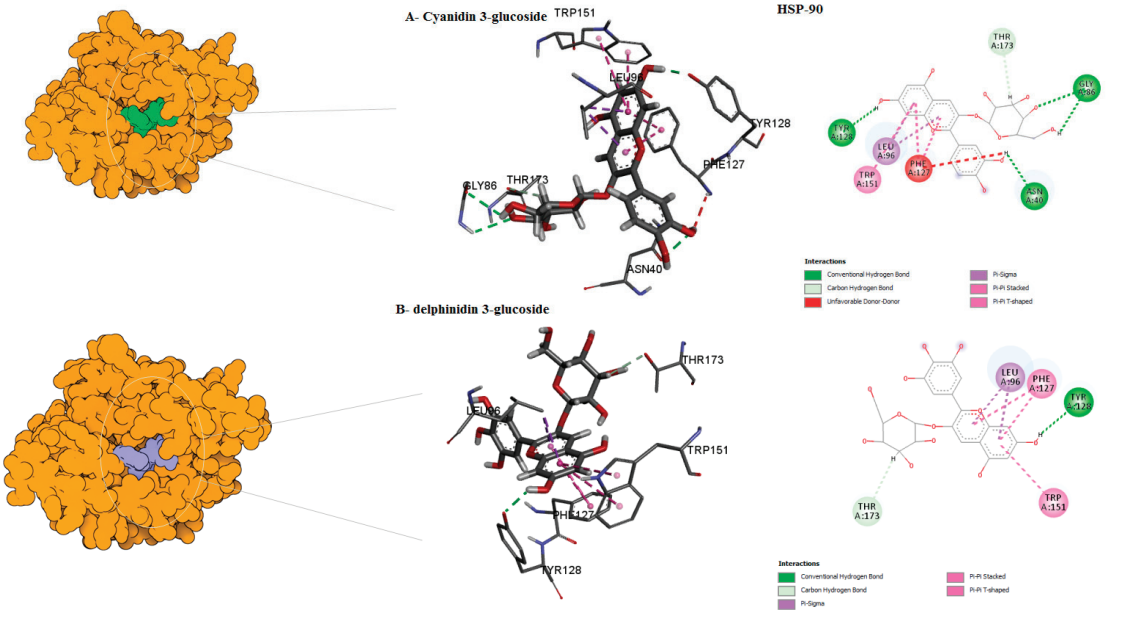

Figure 6. Predicted binding mode for Hsp90 with cyanidin 3-glucoside ID–1 and delphinidin 3-glucoside D/ID.

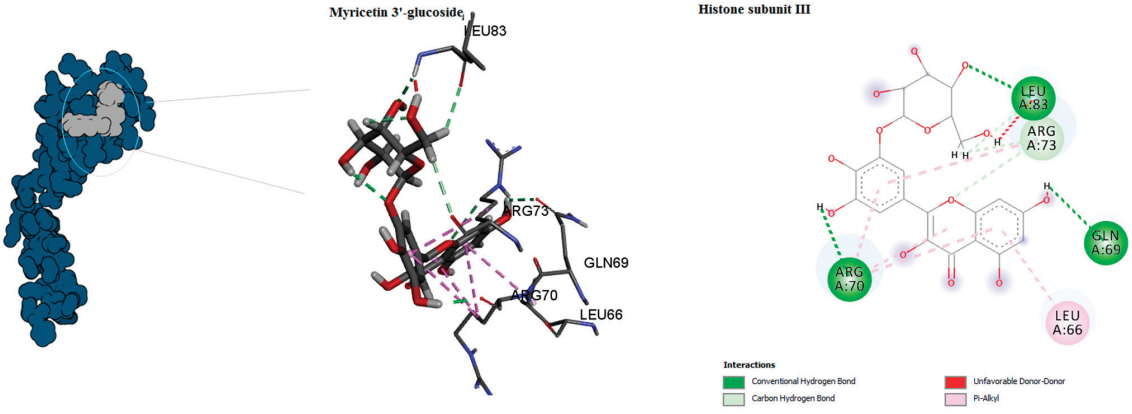

Figure 7. Predicted binding mode for histone subunit III with myricetin 3′-glucoside ID.

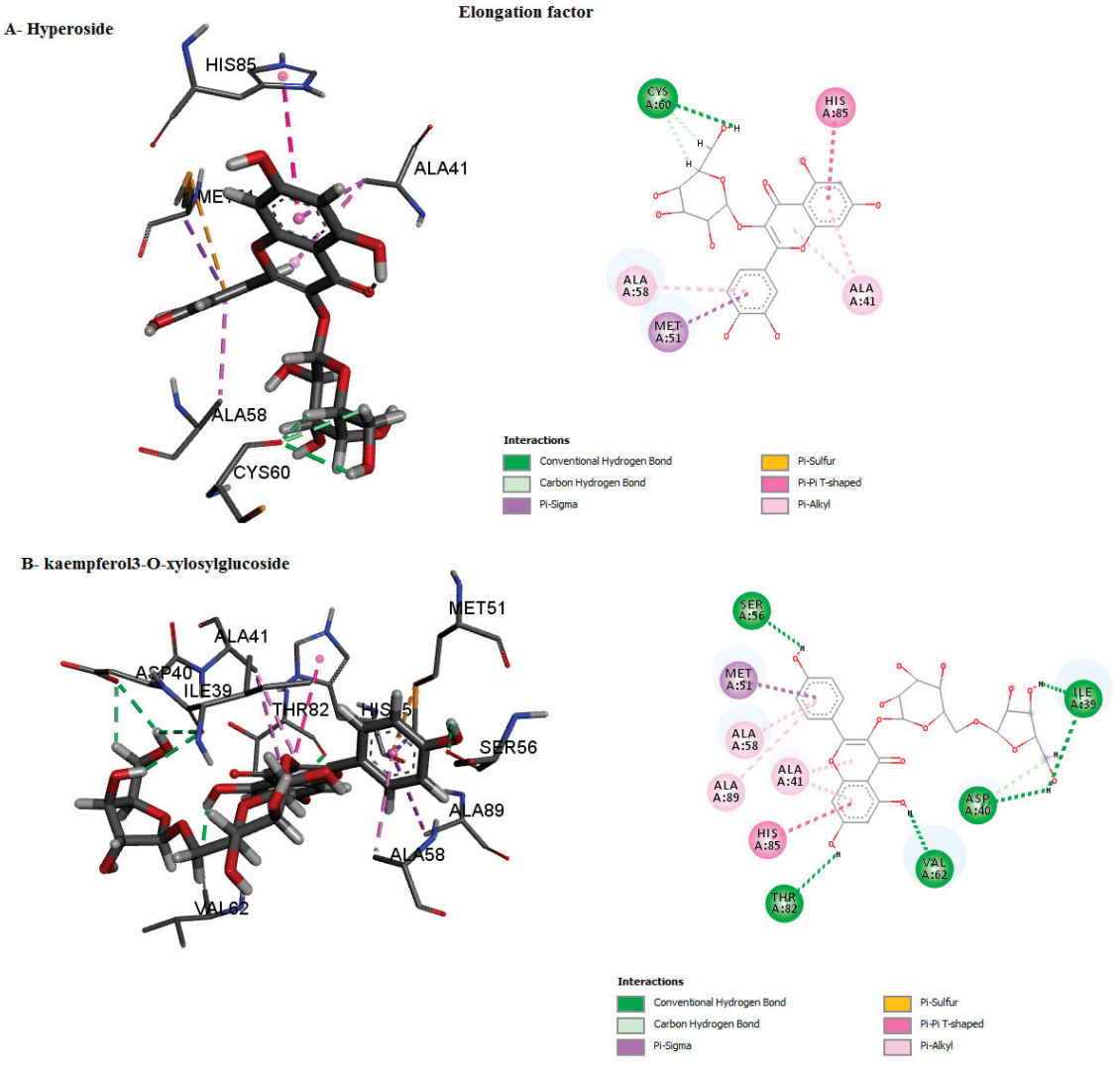

Figure 8. Predicted binding mode for elongation factor with kaempferol3-O-xylosylglucoside and hyperoside D.

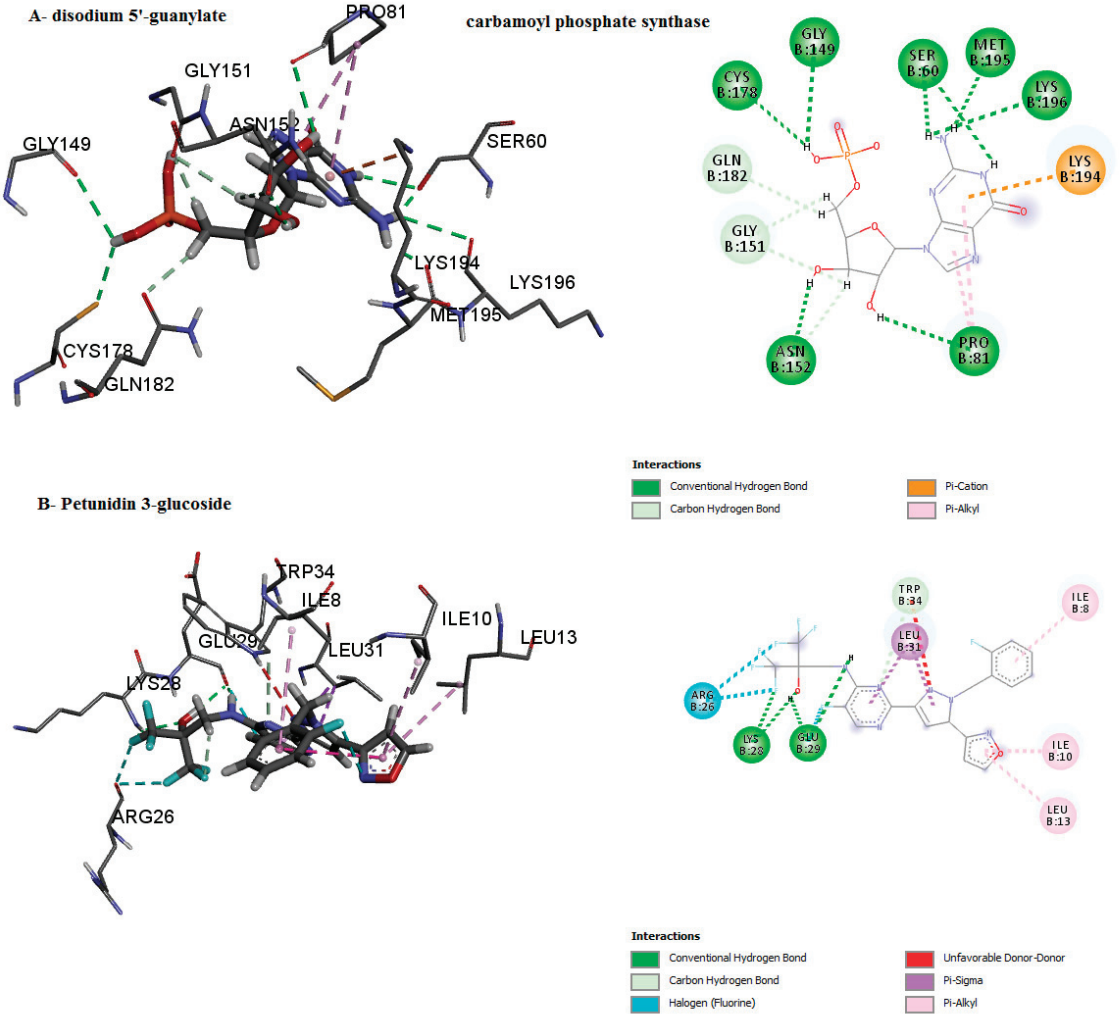

Figure 9. Predicted binding mode for carbamoyl phosphate synthase with disodium 5′-guanylate and petunidin 3-glucoside.

2.5.1. Root Mean Square Deviation (RMSD) Analysis

Calculations of the RMSD for the ligand-enzymes complex were used to determine the dynamic stability and conformational perturbation, which occur in each of the simulated systems during the simulation time scale. The RMSD values were calculated for the following protein-inhibitors combinations: acetylcholinesterase with disodium 5′-inosinate and petunidin 3-glucoside; actin with calcium 5′-guanylate D and chlorogenic acid; α-tubulin with chlorogenic acid alone; arginine kinase with kaempferol-3,7-di-O-glucoside I, hyperoside D, delphinidin 3-glucoside ID, and histone subunit III complexes with myricetin 3′-glucoside ID and hyperoside D. All the trajectories reached equilibrium state after 20 ns, as shown in Figure 10. The RMSD values for all complexes are observed to be stable during the 50 ns simulation.

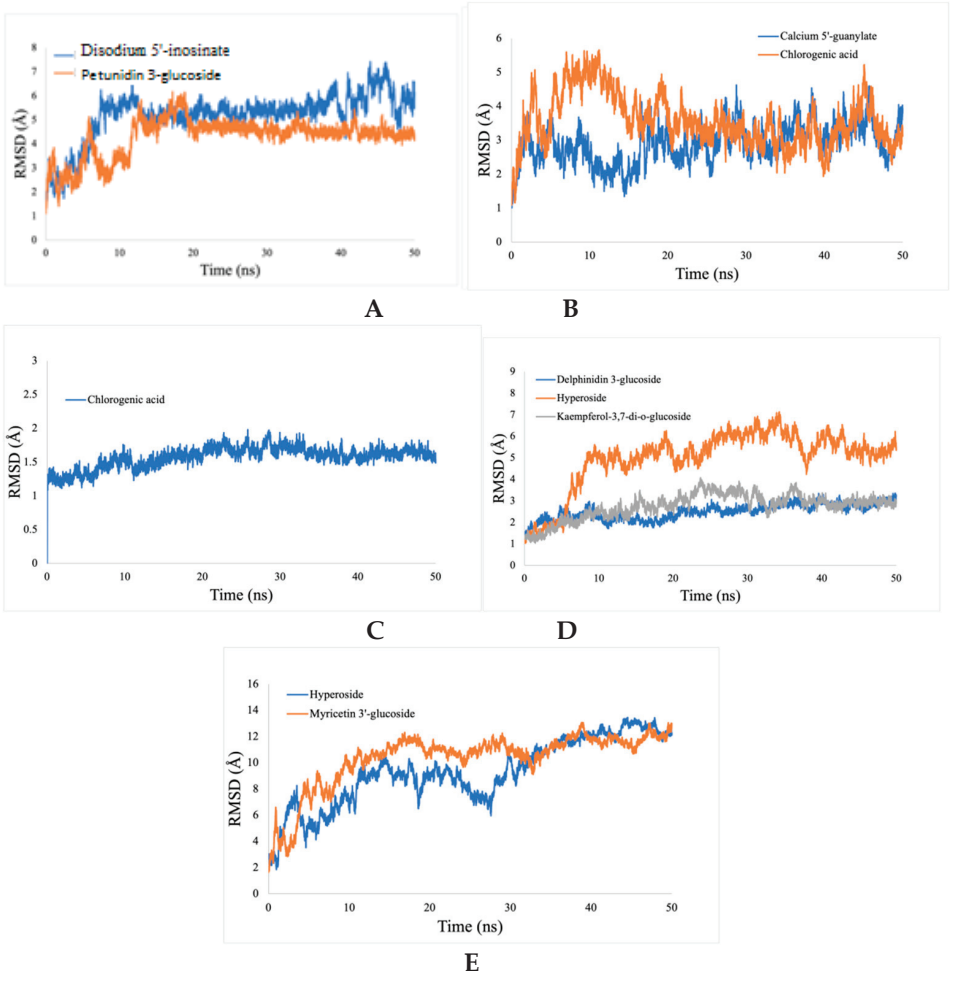

Figure 10. RMSD analyses of protein-ligand complexes. (**A**) acetylcholine esterase, (**B**) actin, (**C**) α-tubulin, (**D**) arginine kinase, and (**E**) histone subunit III with inhibitors (disodium 5′-inosinate and petunidin 3-glucoside), (calcium 5′-guanylate D and chlorogenic acid), chlorogenic acid, (kaempferol-3,7-di-O-glucoside I, hyperoside D, delphinidin 3-glucoside ID) and (myricetin 3′-glucoside ID, hyperoside D), respectively.

2.5.2. Radius of Gyration (Rg) Analysis

The Rg factor is best described for the stability of receptor-ligand complexes during the molecular dynamics simulations. The results demonstrate that the Rg values during different time points for the acetylcholine esterase, actin, α-tubulin, arginine kinase, and histone subunit III complexes to their respective ligands are constant during 50 ns simulation, which indicates the compactness of all of the proteins (Figure 11).

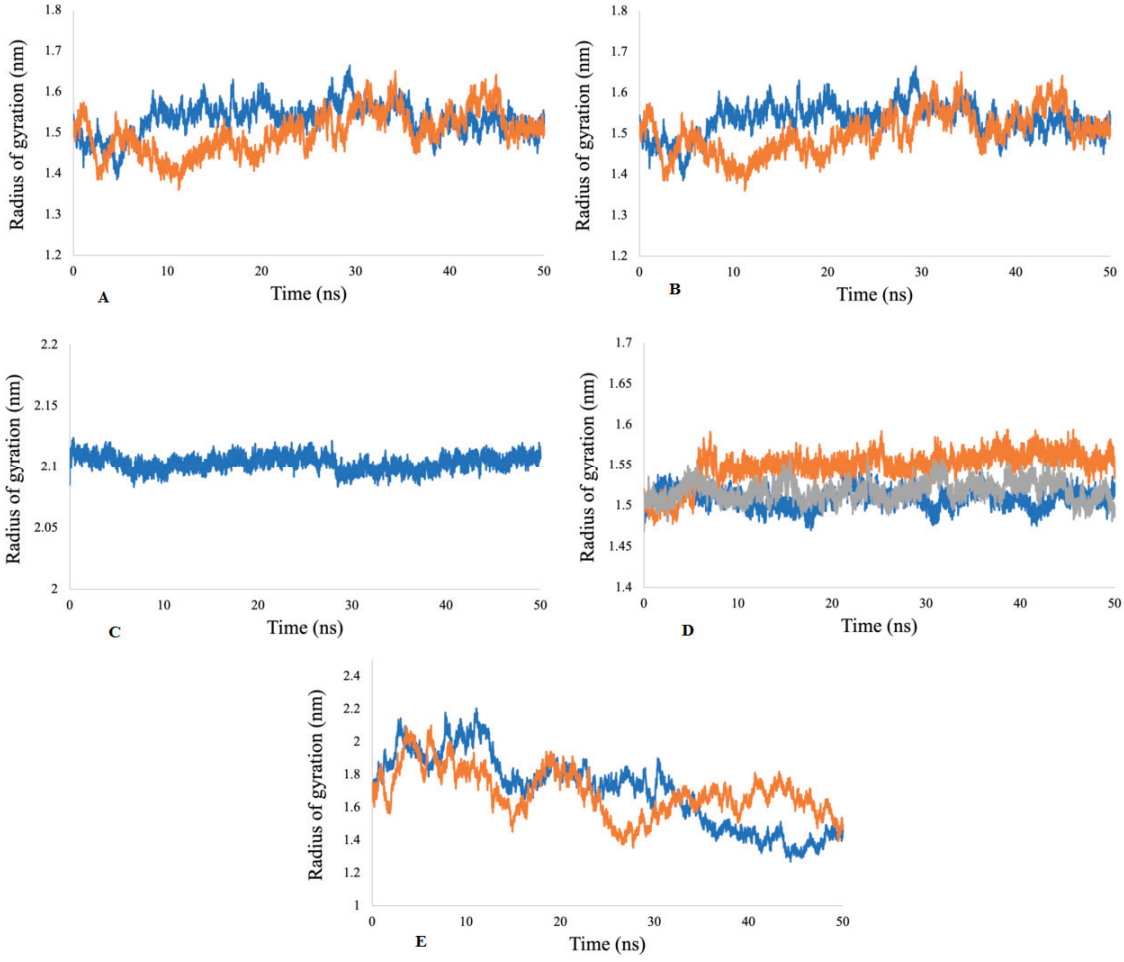

Figure 11. Radii of gyration for (**A**) acetylcholine esterase, (**B**) actin, (**C**) α-tubulin, (**D**) arginine kinase, and (**E**) histone subunit III with inhibitors (disodium 5′-inosinate and petunidin 3-glucoside), (calcium 5′-guanylate D and chlorogenic acid), chlorogenic acid, (kaempferol-3,7-di-O-glucoside I, hyperoside D, delphinidin 3-glucoside ID), and (myricetin 3′-glucoside ID, hyperoside D) complexes.

2.5.3. Hydrogen Bond Analysis

The number of hydrogen bonds for the ligand-enzymes complexes are plotted over a 50-ns MD simulation interval (Figure 12). Since hydrogen bonds constitute a transient connection that provides stability to the receptor-ligand complex, they constitute an important factor to consider when discussing receptor-ligand stability. These bonds determine the specificity of the binding mode. In this study, we have calculated all of the hydrogen bonds for all of the complexes. The numbers of hydrogen bonds at different time points have been calculated, as shown in Figure 12. The average number of hydrogen bonds calculated for inhibitors (disodium 5′-inosinate and petunidin 3-glucoside), (calcium 5′-guanylate D and chlorogenic acid), chlorogenic acid, (kaempferol-3,7-di-O-glucoside I, hyperoside D, delphinidin 3-glucoside ID) and (myricetin 3′-glucoside ID, hyperoside D) are (0–6, 0–5), (0–7, 0–9), 0–9, (0–8, 0–9, 0–10), respectively. All of the predicated ligands have shown continuous hydrogen bonding during the 50 ns simulation, which demonstrates the stabil-

ity of the complexes. The only exception was chlorogenic acid, which only shows stable hydrogen bonding in the span of 35 ns.

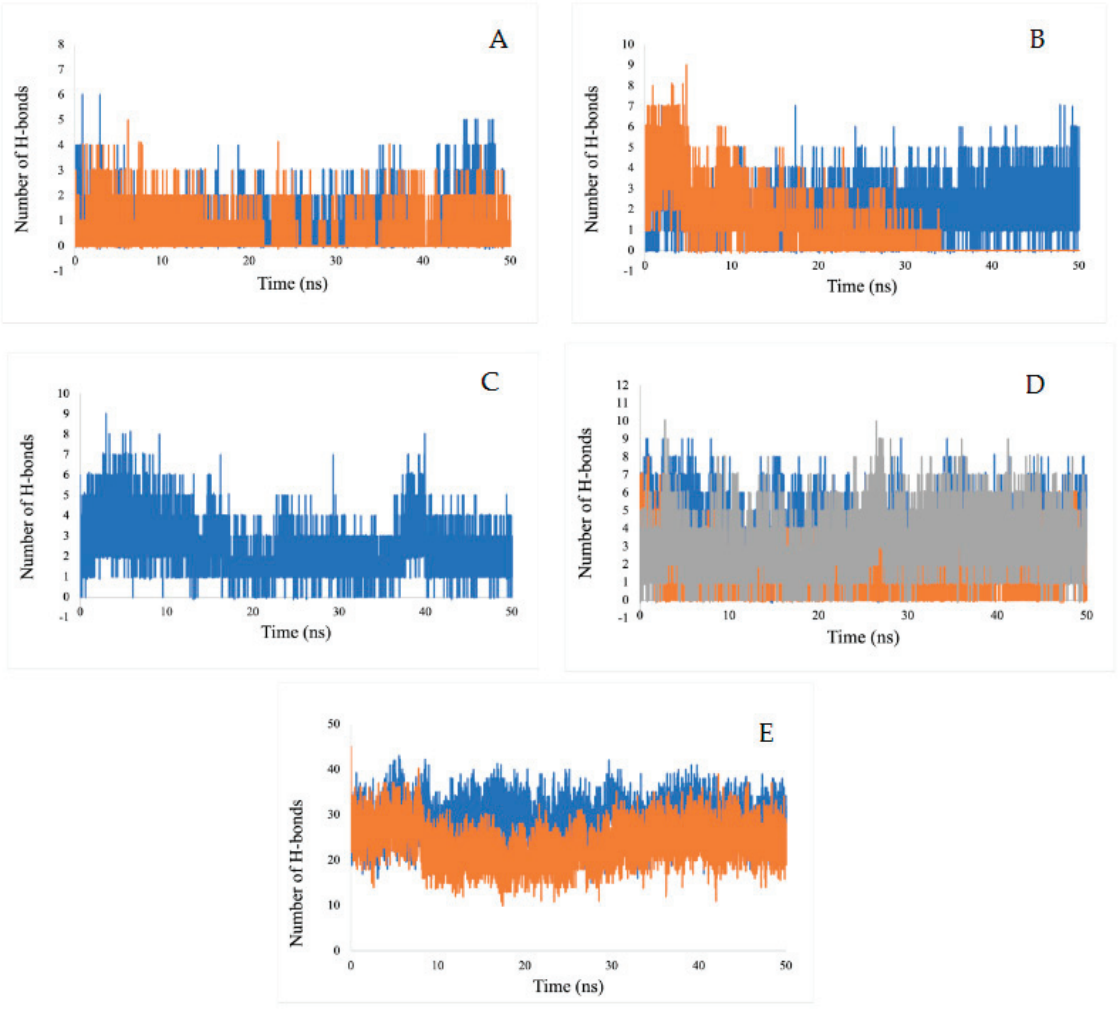

Figure 12. Estimation of the hydrogen bond number during a 50 ns MD simulation of for (**A**) actylcholine esterase, (**B**) actin, (**C**) α-tubulin, (**D**) arginine kinase, and (**E**) histone subunit III with inhibitors (disodium 5′-inosinate and petunidin 3-glucoside), (calcium 5′-guanylate D and chlgenic acid), chlorogenic acid, (kaempferol-3,7-di-O-glucoside I, hyperoside D, delphinidin 3-glucoside ID), and (myricetin 3′-glucoside ID, hyperoside D) complexes.

2.5.4. Root Mean Square Fluctuation Analysis (RMSF)

The RMSF value refers to the flexibility and mobility of structure—a higher value of RMSF indicates a loosely bonded structure with twists, curves, and coils, while a lower value of RMSF indicates a stable secondary structure, including α-helix and beta-sheets. Our RMSF analysis demonstrates that all of the ligands showed less conformational variations during binding and can act as stable complexes (Figure 13).

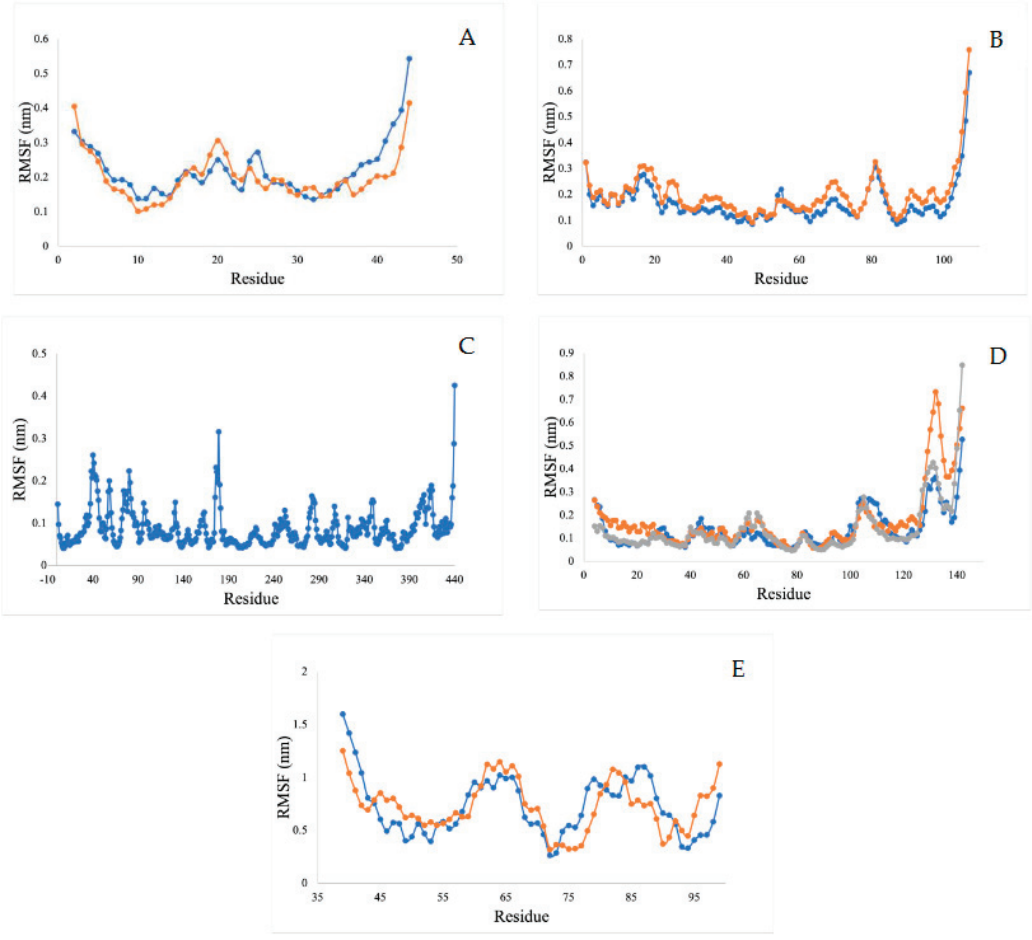

Figure 13. RMSF analysis for (**A**) acetylcholine esterase, (**B**) actin, (**C**) A-tubulin, (**D**) arginine kinase, and (**E**) histone subunit III with inhibitors (disodium 5′-inosinate and petunidin 3-glucoside), (calcium 5′-guanylate D and chlorogenic acid), chlorogenic acid, (kaempferol-3,7-di-o-glucoside I, hyperoside D, delphinidin 3-glucoside ID), and (myricetin 3′-glucoside ID, hyperoside D) complexes.

2.5.5. Molecular Mechanics Poisson-Boltzmann Surface Area Free Energy Calculations

The binding capacity of the ligand towards the receptor is quantitatively estimated by binding free energy analysis. Binding free energy is the summation of all non-bonded interaction energies. The binding free energy of the interactions between acetylcholine esterase, actin, α-tubulin, arginine kinase, and histone subunit III and the docked ligands has been estimated using the molecular mechanics Poisson-Boltzmann surface area tool (G_MMPBSA) [21]. This useful tool allows for efficient and reliable free energy simulation to model protein-ligand interactions. Our binding energy analysis spanning 50 ns MD simulation trajectories show that all ligands have a binding affinity towards enzyme inhibition and form stable complexes. Other different kinds of interaction energies, such as van der Waals energy, electrostatic energy, polar solvation energy, and solvent accessible surface area (SASA) energy, have been also calculated for all the Tools Shapes complexes (Figure 14). Results indicate that van der Waals, electrostatic, and SASA energy negatively contribute to the total interaction energy, while only polar solvation energy positively contributes to the total free binding energy. In particular, the contribution of van der Waals

interactions is much greater than that of the electrostatic interactions in all cases except the complexes arginine kinase-delphinidin 3-glucoside and histone subunit-myricetin 3′-glucoside. Furthermore, the contribution of SASA energy is relatively small when compared to the total binding energy. The negative value of van der Waals energy also points to the significant hydrophobic interaction between the ligands and the enzymes [22].

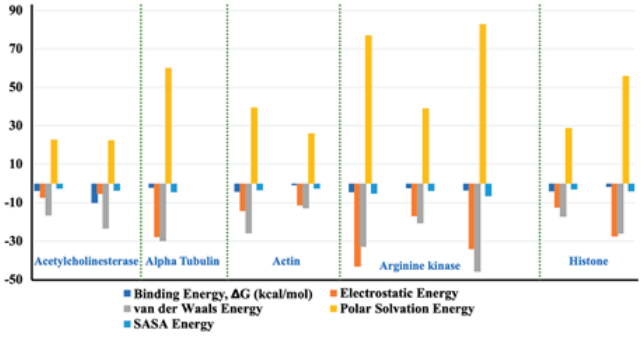

Figure 14. Representation of the van der Waals, electrostatic, polar solvation, SASA, and binding energy for docked compounds into: Acetylcholine esterase, Actin, A-tubulin, Arginine kinase and histone subunit III with inhibitors (disodium 5′-inosinate and petunidin 3-glucoside), (calcium 5′-guanylate D and chlorogenic acid), chlorogenic acid, (kaempferol-3,7-di-o-glucoside I, hyperoside D, delphinidin 3-glucoside ID), and (myricetin 3′-glucoside ID, hyperoside D) complexes.

2.5.6. Principal Component Analysis (PCA)

Principal component analysis is a method that utilizes linear combinations of measured variables, which allows for the reduction of the dimensionality of data and helps identify the principal sources of variation. In molecular dynamics simulations, PCA is a popular method to account for the essential dynamics of the system on a low-dimensional free energy landscape [23]. To analyze the collective motion of all complexes, PCA analysis based on C-a atoms has been performed. It was observed that the first few eigenvectors of the principal components (PCs) of the structures play an important role and describe the overall motions of the entire system. These data suggest that kaempferol-3,7-di-O-glucoside ID has formed very stable complexes with arginine kinase and myricetin 3′-glucoside ID with histone subunit III, which can be considered as a lead compound (Figure 15).

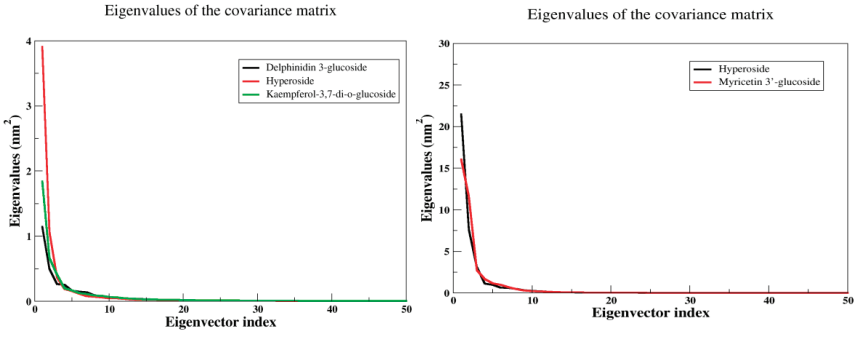

Figure 15. The PCA analysis, the plot of eigenvalues vs. eigenvectors have been considered.

Since it was previously found that the first five eigenvectors constitute the majority portion of the total dynamics of the whole system, we plotted only the first two eigenvectors against each other, where each dot represents correlated motions (Figure 16). The well-

stable clustered dots signify the more stable structure, and low-clustered dots represent the weaker stable structure.

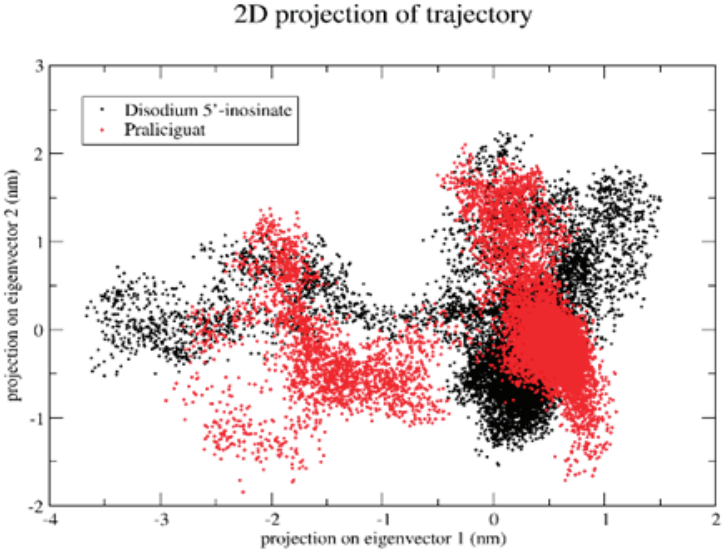

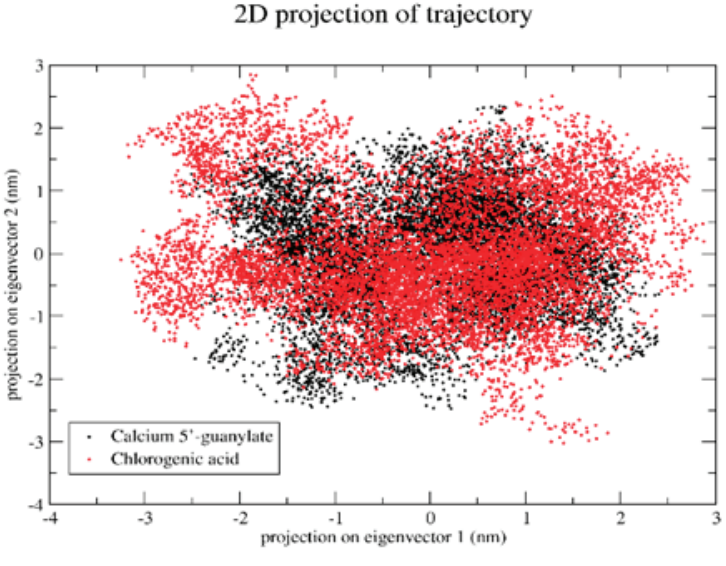

Figure 16. *Cont.*

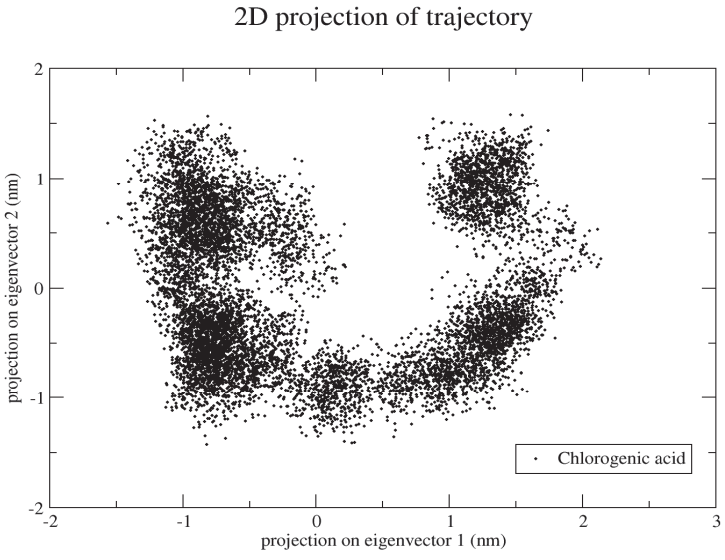

Figure 16. Projection of the motion of a protein in phase along the principal components (PC1 and PC2).

3. Materials and Methods

3.1. Database Search, Structural Modeling, and Model Validation

All protein sequences were obtained from NCBI (https://www.ncbi.nlm.nih.gov/, accessed on 10 August 2022) in FASTA format and are mentioned by their Gen Bank accession number in Table 2. The *Liriomyza trifolii* NCBI taxonomy (tax ID: 32264) proteins were selected by searching all of the sequential homolog and orthologs using NCBI Blast server [24] with the default values, and against the nonredundant protein sequences. The sequences were retrieved in the FASTA format as an amino-acid sequence. The initial atomic structures of the proteins, based on homology modeling, were built using the Swissmodel server (https://Swissmodel.expasy.org/, accessed on 10 August 2022). In this study, a sequence of Blast-P similarities for recognition of closely related structural homologs in *Liriomyza trifolii* was queried against a PDB database [18]. The first hit on the annotation Blast-p was obtained to identify the templates based on PDB template ID. The Protein Data Bank collected the PDB file of the templates and was aligned using BLAST. The Swissmodel server used the target sequence file, the alignment file, the PDB file for the prototype, and all the template proteins to build the homology model. Homology models with a score of <-4 were chosen. The optimized models (acetylcholinesterase, α-tubulin, actin, arginine kinase, histone subunit III, heat shock protein 90 (Hsp90), and elongation factor 1-alpha) were found to be suitable based on several qualitative background checks, including the PROCHECK (PDBSum) and Swissmodel server (https://saves.mbi.ucla.edu/, accessed on 10 August 2022). The Ramachandran plot evaluated that the predicted models were closer to the template with (99.1%, 92.6%, 86.7%, 84.4%, 88.6%, 88.4%) residues lying in the favored regions. The ERRAT score values of 99.1304, 89.7527, 96.4539, 82.0707, 96.5217, 90.9774, and QMEAN score indicated that the predicted models were reliable and satisfactory, as they are higher than the ideal values of the QMEAN score <-4, and ERRAT around 95% for a model with a satisfactory resolution [24].

3.2. Preparation of Proteins and Ligands

The sequences of the *Liriomyza trifolii* proteins (acetylcholinesterase, actin, α-tubulin, arginine kinase, elongation factor 1-alpha, Hsp90, and histone subunit III) with GenBank accession no. number (CAI30732.1, ARQ84036.1, ARQ84030.1, ARQ84038.1, ARQ84034.1,

AGI19327.1, ARQ84032.1, ABL07756.1, respectively) were obtained from NCBI. The protein sequences were retrieved in the FASTA format. The 3-D structures of proteins were built using the Swissmodel server (https://Swissmodel.expasy.org/, accessed on 10 August 2022). Here, proteins were selected as target receptor proteins and were imported to the 3-D refine server to perform energy minimization for the six proteins (http://sysbio.rnet.missouri.edu/3Drefine/, accessed on 10 August 2022). During docking studies, all water molecules and ligands were removed, and hydrogen atoms were added to the target proteins. The docking system was built using SAMSON software 2020 (https://www.samson-connect.net/, accessed on 10 August 2022). The structures were prepared using the protein preparation wizard of the Autodock Vina extension of SAMSON 2020 software. The X, Y, and Z dimensions of the receptor grid, used for the blind docking of ligands to proteins, are reported in Table 3. The ligands were retrieved from the PubChem database in SDF format. Subsequently, each ligand was converted into MOL2 format using OpenBabel software (http://openbabel.org/wiki/Main_Page, accessed on 10 August 2022), followed by an energy minimization at pH 7.0 $\pm$ 2.0 in SAMSON software.

3.3. Binding Site Prediction and Protein-Ligand Docking

Discovery studio software and SAMSON software were used for binding site prediction. SAMSON software uses Autodock Vina as an extension to maximize the accuracy of these predictions while minimizing computer run-time [25]. It uses the interaction energy between the protein and a simple van der Waals probe to locate energetically favorable binding sites. The program is based on quantum mechanics, and it predicts the potential affinity, molecular structure, geometry optimization of the structure, vibration frequencies of coordinates of atoms, bond length, and bond angle. Following an exhaustive search, 100 poses were analyzed, and the best scoring poses were used to calculate the binding affinity of the ligands. The ligands that tightly bind to a target protein with high scores were selected in Table 3. The proteins were docked against a variety of bioactive compounds that are phytochemical components from the HPLC of leaves of *Phaseolus vulgaris* (ref) and yeast extract using SAMSON software [21]. The 2-D interaction was carried out to find favorable binding geometries of the ligand with the proteins using Discovery Studio software. Thus, the 2-D interaction images of the docked protein-ligand complexes with high scores to the predicted active sites were obtained.

3.4. Protein Ligand Interaction Using SAMSON and Discovery Studio Software

The ligands were docked with the target proteins (acetylcholinesterase, actin, α-tubulin, arginine kinase, elongation factor 1-alpha, Hsp90, and histone subunit III), and the best docking poses were identified. Figures 1 and 2 show the 2-D and 3-D structures of the binding poses of the compounds, respectively.

3.5. Protein–Protein Interaction Network

The *Liriomyza trifolii* proteins were submitted to the server for functional interaction associated network between partners for the STRING (Research Online of Interacting Genes/Proteins Data Basis version 10.0)13 [24]. The interactions were examined at medium and high confidences.

3.6. Molecular Dynamics Simulation

The molecular dynamic approach is widely used to assess atoms' behavior and structural stability, and to study the conformational changes at an atomic level. Understanding the stability of protein upon ligand binding is significantly improved by molecular dynamics simulation studies. Gromacs 4.6.2 [26] with GROMOS96 54a7 force field [27] was used for MD simulation studies of two systems, at 50 ns each. The ProdrG2 Server was used to generate the topology of the analysis of enzyme-ligand complexes. Each system was placed in the center of the cubic box, with a distance of 1.0 nm between the enzyme and the edge of the simulation box. Each system was solvated with explicit water molecules.

Before proceeding towards energy minimization, all systems were neutralized by adding Na^+ and Cl^- ions, accordingly. The steepest descent method was used for the energy minimization of each system. MD simulations with NVT (isochoric-isothermal) and NPT (isobaric-isothermal) ensembles (N$\frac{1}{4}$ constant particle number, V$\frac{1}{4}$Volume, P$\frac{1}{4}$Pressure, T$\frac{1}{4}$Temperature) were performed for 1 ns, each, to equilibrate the enzyme-ligand system for constant volume, pressure (1 atm), and temperature (300 K). To calculate electrostatic interaction, the Particle Mesh Ewald (PME) algorithm [25] was used with a grid spacing of 1.6 Å and a cutoff of 10 Å, and the LINCS method was used to restrain the bond length. Finally, the trajectories were saved at every 2-fs time step and the production MD simulation of the enzyme-ligand complex was performed for 50 ns [28].

4. Conclusions

This study presented an array of naturally occurring, nontoxic, easily extractable, low-cost ligands that show great potential as inhibitors of a variety of proteins found in the gut of the polyphagous pest *L. trifolii* that is known to attack a myriad of crops. The target proteins are acetylcholinesterase, actin, α-tubulin, arginine kinase, and histone receptor III subtypes. The proposed inhibitors or inhibitor combinations are (disodium 5′-inosinate and praliciguat), (calcium 5′-guanylate and chlorogenic acid), chlorogenic acid alone, (kaempferol-3,7-di-O-glucoside with hyperoside and delphinidin 3-glucoside), and (myricetin 3′-glucoside and hyperoside), respectively. In lieu of an experimentally available structure of the target proteins, the initial models of the protein of *L. trifolii* origin were constructed using homology modeling. The analyses used in this investigation included structural modeling, binding site interaction prediction, molecular docking free energy calculations, binding pose analysis, dynamic stability and conformational perturbation analysis, radius of gyration analysis, hydrogen bond analysis, and molecular mechanics PBSA free energy calculations. The results demonstrated that the proposed inhibitors formed stable complexes with their target proteins while also having great potentials for inhibitory activity. All five ligand-protein complexes have favorable parameter values in RMSD, RMSF, RoG, intermolecular hydrogen bonding, and binding free energy for 50 ns. Trajectories analysis showed that the studied complexes displayed structural stability during the MD runs.

The are many various methods of predicting protein 3-D structures, for example, I-Tasser to obtain their 'starting' structures or AlphaFold server and Swissmodel server. Though the principle is the same for all of the homology modeling software, it is based on the template structure that the final model is built. Different software uses different templates to model, but we can conclude that the most exact commonly used online tool is Swissmodel; it is easy and the most widely feasible, and not too expensive to be used for predicting protein 3-D structures. Moreover, all of the various methods of predicting protein 3-D structures "yield the same predicted protein structures".

The development of computer systems in biological studies has had a great impact on developing and understanding the effects of protein inhibitors. This allows the opportunity for optimizing and utilizing computational methods, such as the ones used in this study, as low-cost, efficient, and effective means of predicting protein-ligand interactions.

Supplementary Materials: The supporting information can be downloaded at: https://www.mdpi.com/article/10.3390/ijms232112791/s1.

Author Contributions: Conceptualization, I.M.S. and A.H.; Data curation, I.M.S.; Formal analysis, I.M.S. and N.N.-P.; Funding acquisition, I.M.S., I.R., E.T.S., M.A.O., M.A.A. and T.M.K.; Methodology, I.M.S., M.A.-M., A.H.S., P.T.D.K., M.S.K., M.A.A. and T.M.K.; Project administration, I.M.S.; Resources, Dalia Hamza; Software, I.M.S.; Supervision, I.M.S.; Validation, M.A.-M.; Visualization, I.M.S., A.H.S. and M.A.A.; Writing – original draft, I.M.S., M.A.-M., A.H.S. and M.A.A.; Writing – review & editing, I.M.S., M.A.-M., A.H.S., N.N.-P., I.R., D.H., M.S.E., M.A.A. and T.M.K. All authors have read and agreed to the published version of the manuscript.

Funding: This research received no external funding.

Acknowledgments: We acknowledge Chemo and Bioinformatics Lab, Bio Search gate Research Institution, BSRI, Giza, Egypt, for supporting project number (22880). Thanks to Princess Nourah bint Abdulrahman University Researchers Supporting Project number (PNURSP2022R179), Princess Nourah bint Abdulrahman University, Riyadh, Saudi Arabia. We thank Israa M Shamkh for the computational chemistry and biology support. All of the authors are thankful to their respective institutions for their support.

Conflicts of Interest: The authors declare no conflict of interest.

References

1. Berlinge, R.G. *Pest Resistance to Pesticides*; Department of Entomology, Clemson University: Clemson, SC, USA, 1996.
2. Van der Werf, H.M.G. Assessing the impact of pesticides on the environment. *Agric. Ecosyst. Environ.* **1996**, *60*, 81–96. [CrossRef]
3. Maroni, M.; Fanetti, A.C.; Metruccio, F. Risk assessment and management of occupational exposure to pesticides in agriculture. *Med. Lav.* **2006**, *97*, 430–437. [PubMed]
4. Ibrahim, Y.A. Health and environmental impacts of pesticides: A responsibility principle and two novel systems for hazard classification and external cost determination. *J. Toxicol. Health* **2016**, *3*, 2056–3779. [CrossRef]
5. Spencer, K.A. *Agromyzidae (Diptera) of Economic Importance*; 9 Series Entomologica; The Hague Publishers: Bath, UK, 1973; pp. 19–28.
6. Fürstenberg-Hägg, J.; Zagrobelny, M.; Bak, S. Plant Defense against Insect Herbivores. *Int. J. Mol. Sci.* **2013**, *14*, 10242–10297. [CrossRef] [PubMed]
7. Dietzgen, R.G.; Mann, K.S.; Johnson, K.N. Plant Virus-Insect Vector Interactions: Current and Potential Future Research Directions. *Viruses* **2016**, *8*, 303. [CrossRef]
8. Polston Jane, E.; Capobianco, H. Transmitting plant viruses using whiteflies. *J. Vis. Exp. JoVE* **2013**, *81*, e4332. [CrossRef]
9. Chen, J.; Shen, Z.; Lu, W.; Liu, X.; Wu, F.; Gao, G.; Liu, Y.; Wu, C.; Yan, C.; Fan, H.; et al. Leaf miner-induced morphological, physiological and molecular changes in mangrove plant *Avicennia marina* (Forsk.) Vierh. *Tree Physiol.* **2017**, *37*, 82–97. [CrossRef]
10. Clemente, M.; Corigliano, M.G.; Pariani, S.A.; Sánchez-López, E.F.; Sander, V.A.; Ramos-Duarte, V.A. Plant Serine Protease Inhibitors: Biotechnology Application in Agriculture and Molecular Farming. *Int. J. Mol. Sci.* **2019**, *20*, 1345. [CrossRef]
11. De Leo, F.; Volpicella, M.; Licciulli, F.; Liuni, S.; Gallerani, R.; Ceci, L.R. PLANT-PIs: A database for plant protease inhibitors and their genes. *Nucleic Acids Res.* **2002**, *30*, 347–348. [CrossRef]
12. Mashamaite, C.V.; Ngcobo, B.L.; Manyevere, A.; Bertling, I.; Fawole, O.A. Assessing the Usefulness of *Moringa oleifera* Leaf Extract as a Biostimulant to Supplement Synthetic Fertilizers: A Review. *Plants* **2022**, *11*, 2214. [CrossRef]
13. Mostafa, A.A.; El-Rahman, S.N.A.; Shehata, S.; Abdallah, N.A.; Omar, H.S. Assessing the Effects of a Novel Biostimulant to Enhance Leafminer Resistance and Plant Growth on Common Bean. *Sci. Rep.* **2021**, *11*, 20020. [CrossRef] [PubMed]
14. Studer, G.; Biasini, M.; Schwede, T. Assessing the local structural quality of transmembrane protein models using statistical potentials (QMEANBrane). *Bioinformatics* **2014**, *30*, i505–i511. [CrossRef] [PubMed]
15. Messaoudi, A.; Belguith, H.; Ben Hamida, J. Homology modeling and virtual screening approaches to identify potent inhibitors of VEB-1 β-lactamase. *Theor. Biol. Med. Model.* **2013**, *10*, 22. [CrossRef] [PubMed]
16. Lin, Y.; Yoo, S.; Sanchez, R. SiteComp: A server for ligand binding site analysis in protein structures. *Bioinformatics* **2012**, *28*, 1172–1173. [CrossRef]
17. Yang, Q.Q.; Gan, R.Y.; Ge, Y.Y.; Zhang, D.; Corke, H. Polyphenols in Common Beans (*Phaseolus vulgaris* L.): Chemistry, Analysis, and Factors Affecting Composition. *Compr. Rev. Food Sci. Food Saf.* **2018**, *17*, 1518–1539. [CrossRef] [PubMed]
18. Berman, R.M.; Cappiello, A.; Anand, A.; Oren, D.A.; Heninger, G.R.; Charney, D.S.; Krystal, J.H. Antidepressant effects of ketamine in depressed patients. *Biol. Psychiatry* **2000**, *47*, 351–354. [CrossRef]
19. BIOVIA DS. *Discovery Studio Modeling Environment*; Dassault Systemes: San Diego, CA, USA, 2015.
20. OneAngstrom. SAMSON. 2020. Available online: https://www.samson-connect.net/ (accessed on 10 August 2022).
21. Jain, A.N. Scoring functions for protein-ligand docking. *Curr. Protein Pept. Sci.* **2006**, *7*, 407–420. [CrossRef]
22. Gelpi, J.; Hospital, A.; Goñi, R.; Orozco, M. Molecular dynamics simulations: Advances and applications. *Adv. Appl. Bioinform. Chem.* **2015**, *8*, 37–47. [CrossRef]
23. Kumari, S.; Krishnan, V.; Sachdev, A. Impact of soaking and germination durations on antioxidants and anti-nutrients of black and yellow soybean (*Glycine max*. L) varieties. *J. Plant Biochem. Biotechnol.* **2015**, *24*, 355–358. [CrossRef]
24. Maisuradze, G.G.; Liwo, A.; Scheraga, H.A. Principal Component Analysis for Protein Folding Dynamics. *J. Mol. Biol.* **2009**, *385*, 312–329. [CrossRef]
25. Szklarczyk, D.; Morris, J.H.; Cook, H.; Kuhn, M.; Wyder, S.; Simonovic, M.; Santos, A.; Doncheva, N.T.; Roth, A.; Bork, P.; et al. The STRING database in 2017: Quality-controlled protein-protein association networks, made broadly accessible. *Nucleic Acids Res.* **2017**, *45*, D362–D368. [CrossRef] [PubMed]
26. Altschul, S.F.; Madden, T.L.; Schäffer, A.A.; Zhang, J.; Zhang, Z.; Miller, W.; Lipman, D.J. Gapped BLAST and PSI-BLAST: A new generation of protein database search programs. *Nucleic Acids Res.* **1997**, *25*, 3389–3402. [CrossRef] [PubMed]

27. Trott, O.; Olson, A.J. AutoDock Vina: Improving the speed and accuracy of docking with a new scoring function, efficient optimization, and multithreading. *J. Comput. Chem.* **2010**, *31*, 455–461. [CrossRef] [PubMed]
28. Hess, B.; Kutzner, C.; van der Spoel, D.; Lindahl, E. GROMACS 4: Algorithms for Highly Efficient, Load-Balanced, and Scalable Molecular Simulation. *J. Chem. Theory Comput.* **2008**, *4*, 435–447. [CrossRef] [PubMed]

International Journal of
Molecular Sciences

MDPI

Article

DPP-IV Inhibitory Peptides GPF, IGL, and GGGW Obtained from Chicken Blood Hydrolysates

Gisela Carrera-Alvarado, Fidel Toldrá and Leticia Mora *

Instituto de Agroquímica y Tecnología de Alimentos (CSIC), Avenue Agustín Escardino 7, 46980 Paterna, Spain
* Correspondence: lemoso@iata.csic.es; Tel.: +34-960-308222 (ext. 435217); Fax: +34-963-636-301

Abstract: Blood is a meat by-product rich in proteins with properties that can be improved after hydrolysis, making it a sustainable alternative for use in the generation of bioactive peptides. The objective of this study was to identify dipeptidyl peptidase IV (DPP-IV) inhibitory peptides obtained from different chicken blood hydrolysates prepared using combinations of four different enzymes. Best results were observed for AP (2% Alcalase + 5% Protana Prime) and APP (2% Alcalase + 5% Protana Prime + 3% Protana UBoost) hydrolysates obtaining inhibition values of 60.55 and 53.61%, respectively, assayed at a concentration of 10 mg/mL. Free amino acids were determined to establish the impact of exopeptidase activity in the samples. A total of 79 and 12 sequences of peptides were identified by liquid chromatography and mass spectrometry in tandem (LC-MS/MS) in AP and APP samples, respectively. Nine of the identified peptides were established as potential DPP-IV inhibitory using in silico approaches and later synthesized for confirmation. Thus, peptides GPF, IGL, and GGGW showed good DPP-IV inhibitory activity with IC_{50} values of 0.94, 2.22, and 2.73 mM, respectively. This study confirmed the potential of peptides obtained from chicken blood hydrolysates to be used as DPP-IV inhibitors and, therefore, in the control or modulation of type 2 diabetes.

Keywords: DPP-IV inhibitor; hypoglycemic peptides; type 2 diabetes mellitus; enzymatic hydrolysis

Citation: Carrera-Alvarado, G.; Toldrá, F.; Mora, L. DPP-IV Inhibitory Peptides GPF, IGL, and GGGW Obtained from Chicken Blood Hydrolysates. *Int. J. Mol. Sci.* **2022**, *23*, 14140. https://doi.org/10.3390/ijms232214140

Academic Editor: Blanca Hernández-Ledesma

Received: 28 September 2022
Accepted: 9 November 2022
Published: 16 November 2022

1. Introduction

Type 2 diabetes mellitus is a common metabolic disorder, with a prevalence of 10.5% of adults worldwide [1]. It is characterized by elevated blood glucose levels due to complete or relative insufficiency of insulin secretion [2]. After food intake, glucagon-like peptide 1 (GLP-1) and gastric inhibitory polypeptide (GIP) secrete about two-thirds of total insulin [3]. However, both peptides are natural substrates of the enzyme DPP-IV and are degraded rapidly in vivo (1–2 min), causing the loss of their insulinotropic activity. Therefore, inhibition of the DPP-IV enzyme is an important strategy for the effective treatment of diabetes [4]. DPP-IV inhibitors aim to prolong the half-life of endogenous GLP-1 and GIP and, consequently, increase their plasma concentrations to decrease the postprandial blood glucose level [5,6]. Due to their biological origin, hypoglycemic peptides are considered safer as a treatment for diabetes, as they have fewer side effects than synthetic drugs [7,8]. Currently, the two most important agencies that regulate the access of drugs to the market, the Food and Drug Administration of the United States (FDA) and the European Medicines Agency (EMA) have approved more than 90 peptides as treatments for various diseases [9]. An example of these is lixisenatide (Lyxumia®), a polypeptide of 44 amino acids residues approved in 2013 by the EMA indicated for the treatment of diabetes.

Food bioactive peptides are generated from protein hydrolysis that occurs during the processing, cooking, and/or digestion of food. However, they can also be obtained through controlled hydrolysis with commercial proteolytic enzymes and according to their length and amino acid sequence, some of such peptides released may be bioactive [10]. There is evidence that some food protein hydrolysates inhibit DPP-IV in silico, in vitro, and in vivo.

For instance, α-lactalbumin hydrolysate inhibits DPP-IV activity with an IC_{50} value of 0.036 mg/mL [11]. A study with a hydrolyzed protein isolate (HPI) of black beans and their pure peptides reported that glucose absorption decreased 21.5% after 24 h of treatment (10 mg HPI/mL) in a Caco-2 cell model, and in male Wistar rats a 24.5% reduction in postprandial glucose (50 mg HPI/kg body weight) was found [12]. A simulated duodenal digestion study with quinoa protein and fraction >5 kDa, obtained after 120 min of digestion showed high inhibition of DPP-IV and its IC_{50} was 0.84 mg protein/mL [13].

The development of bioactive peptides from inexpensive and readily available protein raw materials is currently being promoted [14], like by-products from the meat industry such as blood, bones, viscera, skin, organs, etc., with the aim of adding value to protein-rich raw materials and improving the sustainability of meat production. For example, blood represents approximately 3 to 5% of body weight [15], in addition to its nutritional value, it contains proteins with technological functions or bioactive substances that can be generated by enzymatic hydrolysis [16]. Hydrolysates derived from dietary proteins are generally 10^4 times less potent than gliptins, however, the combination of gliptins and hydrolysates may enhance the effect on their ability to inhibit DPP-IV [17].

Therefore, the objective of this work was to determine those DPP-IV inhibitory peptides obtained from the most active chicken blood hydrolysates using chromatographic separations and the subsequent identification of peptide sequences by mass spectrometry in tandem. The identified peptides were studied using in silico approaches and those sequences showing the best potential as DPP-IV inhibitors were evaluated to confirm their bioactivity.

2. Results and Discussion

2.1. Degree of Hydrolysis and Inhibitory Activity of DPP-IV

Enzymatic protein hydrolysis is extensively used in the food industry to enhance the functional properties and nutritional quality of products, such as the elimination of allergenicity, flavor production, detoxification, etc. [18,19]. The degree of hydrolysis of chicken blood hydrolysates is shown in Figure 1. The *DH* increased up to three times more when applying sequentially two or more enzymes and a longer hydrolysis time (16 h), being AFP (2% Alcalase + 1% Flavourzyme + 3% Protana UBoost) and AP (2% Alcalase + 5% Protana Prime), the samples with the highest *DH*, 30.29 and 29.51%, respectively. It is considered that in a process of sequential hydrolysis, performing a pre-digestion with alcalase increases the number of N-terminal sites available for the subsequent action of some exo-peptidases as it occurs in our study with Flavourzyme or Protana Prime [19].

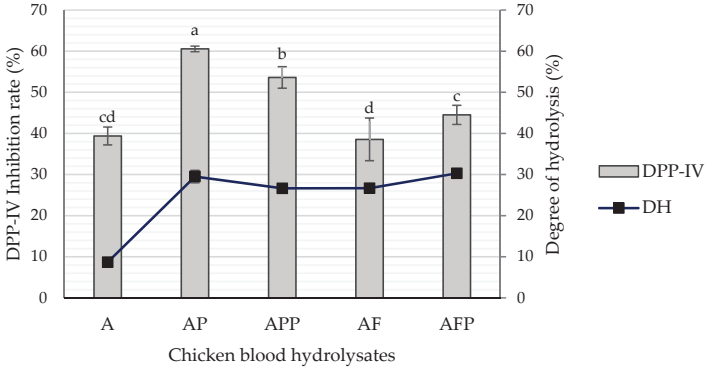

Figure 1. DPP-IV inhibition rate and degree of hydrolysis of different chicken blood hydrolysates: A (2% Alcalase), AP (2% Alcalase + 5% Protana Prime), APP (2% Alcalase + 5% Protana Prime + 3% Protana UBoost), AF (2% Alcalase + 1% Flavourzyme) and AFP (2% Alcalase + 1% Flavourzyme + 3% Protana UBoost). Bars with the same letter between samples are not statistically different. Tukey, $p < 0.05$.

Glycemic regulation and energy homeostasis can be improved by maintaining the incretin effect by inhibiting DPP-IV [20]. At a concentration of 10 mg/mL, the DPP-IV inhibition rate of the hydrolysates AP and APP showed the highest results ($p < 0.05$), with values of 60.55 and 53.61%, respectively. In the case of A hydrolysate, despite having the lowest degree of hydrolysis, it presented a DPP-IV inhibition rate of 39.38%. Regarding the hydrolysates AF and AFP, they showed DPP-IV inhibition values of 38.56 and 44.50%, respectively (Figure 1). Multiple sequential hydrolyses can produce peptides with improved or reduced activities [21]. In addition, it is known that Flavourzyme achieves aggressive hydrolysis, that could result in the hydrolysis of the bioactive peptide sequences obtained and decrease their bioactivity [7]. Bioactive peptides are released through different kinetics; the larger ones appear in the initial phase of hydrolysis and are cut into smaller peptides that, according to their characteristics, can show different bioactivity [22]. In addition, it has been reported that the DPP-IV inhibitory activity of a hydrolysate is determined by its peptide structure and sequence, which depends largely on the type and action of proteases used during hydrolysis [23]. For example, in a study with sheep serum hydrolysates, the inhibitory activity of DPP-IV was independent of the degree of hydrolysis, and they attributed the higher rate of inhibition (77.80%) to the characteristics of the peptides produced by the enzyme trypsin [8]. Mojica & de Mejía [24] reported that the best conditions to generate antidiabetic peptides from black bean protein isolate was by hydrolysis with Alcalase for 2 h and 1:20 enzyme/substrate, with a DPP-IV inhibition rate of 96.7%. In our study, AP and APP were hydrolyzed with Alcalase and Protana Prime, the first is an endo-protease, and the second is an exo-peptidase, two specific enzymes for the generation of peptides and small peptides/free amino acids, respectively. The inhibitory activity of DPP-IV has been attributed mainly to small peptides. According to the BIOPEP-UWM database, near 59% of the registered DPP-IV inhibitory peptides are dipeptides (Figure 2A).

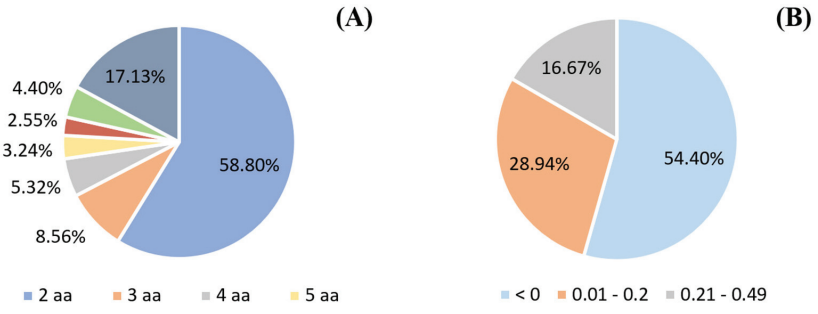

Figure 2. (**A**) DPP-IV inhibitory peptides contained in the bioactive peptides database BIOPEP-UWM grouped according to their amino acid (aa) length. (**B**) DPP-IV inhibitory peptides grouped according to their hydrophobicity, where low values indicate high hydrophobicity and higher values indicate low hydrophobicity. Data obtained from ToxinPred tool.

Due to AP and APP hydrolysates showing the best inhibitory results, these samples were selected for the subsequent separation into peptide fractions using RP-HPLC, and the DPP-IV inhibitory activity of each fraction was determined. From the HPLC chromatogram, the elution was separated into 20 main fractions according to the elution time (0–40 min). Of the 20 fractions tested of both hydrolysates, fraction 2 (elution time 3–4 min), corresponding to polar peptides, exhibited the highest inhibitory activity of DPP-IV with values of 44.01% in AP and 37.33% in APP (Figure 3). While in the rest of the chromatogram non-significant values of DPP-IV inhibition were observed. Consequently, 54.40% of the 432 DPP-IV inhibitory peptides registered in BIOPEP-UWM are hydrophilic (<0) and the rest are hydrophobic (<0.50) (Figure 2B). Therefore, these fractions were collected again, lyophilized,

and analyzed by LC-MS/MS to identify the sequences of DPP-IV inhibitory peptides contained in fraction 2 of the AP and APP hydrolysates.

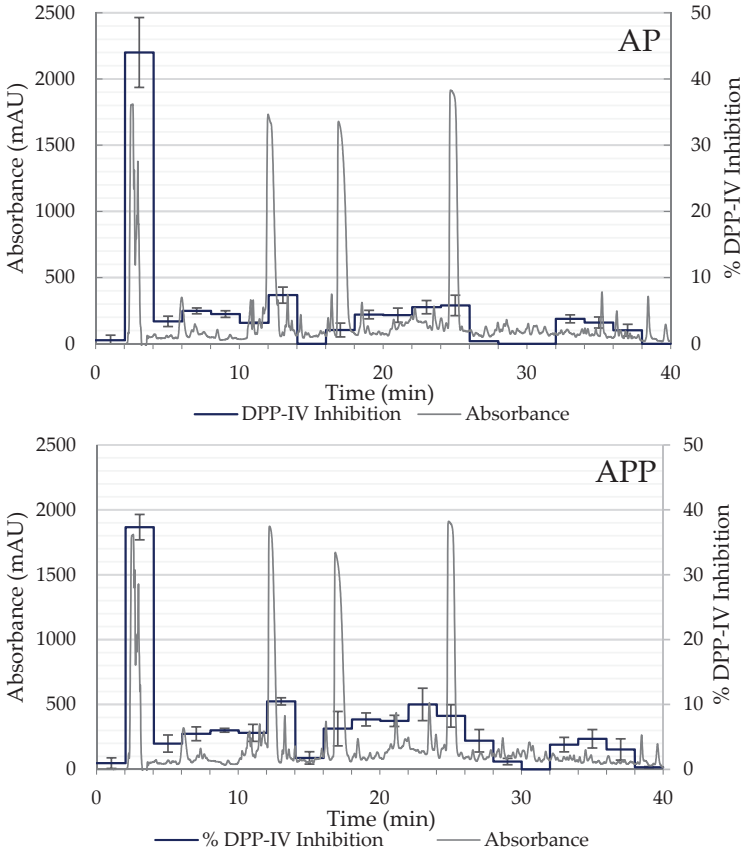

Figure 3. Elution profile and DPP-IV inhibition rate of the peptide fractions of the hydrolysates AP (2% Alcalase + 5% Protana Prime) and APP (2% Alcalase + 5% Protana Prime + 3% Protana UBoost) separated by RP-HPLC. The inhibition rate of DPP-IV was determined with each fraction at a concentration of 100 mg/mL hydrolysate.

2.2. Determination of Free Amino Acids (FAAs)

The protein content in food constitutes the source of essential amino acids in the diet. It has been reported that the bioactivity of antidiabetic peptides depends especially on their amino acid profile and their function is mainly based on inhibiting the activity of the DPP-IV enzyme [4]. Figure 4 shows the free amino acid content of hydrolysates A, AP, and APP. As expected for an endo-protease, the hydrolysis with Alcalase produced a low content of free amino acids; however, when combined with Protana Prime, a significant amount of amino acids were generated. Lys, Leu, Ala, Val, and Glu were found in greater concentration. A significant decrease in Gln was also found in AP with respect to APP hydrolysates, whereas, APP had a significantly higher Glu content than AP. These results are attributed to the specific hydrolytic action of Protana UBoost, which is based on the conversion of glutamine into glutamic acid. Xu et al. [25] state that a first hydrolysis with Alcalase allows several peptide bonds to be accessible and especially recognizes the Ala, Leu, and Val sites without affecting the residues of Pro amino acids in the hydrolysate, which has probably occurred in our hydrolysates. Similar to our results, the content of free amino acids in porcine blood hydrolysates increases after the enzymatic hydrolysis process, including branched-chain

amino acids such as Val, Ile, and Leu [26,27]. Sadri et al. [28] affirm that Leu and Val are involved in glycemic control, and Pro may increase the hypoglycemic activity of peptides.

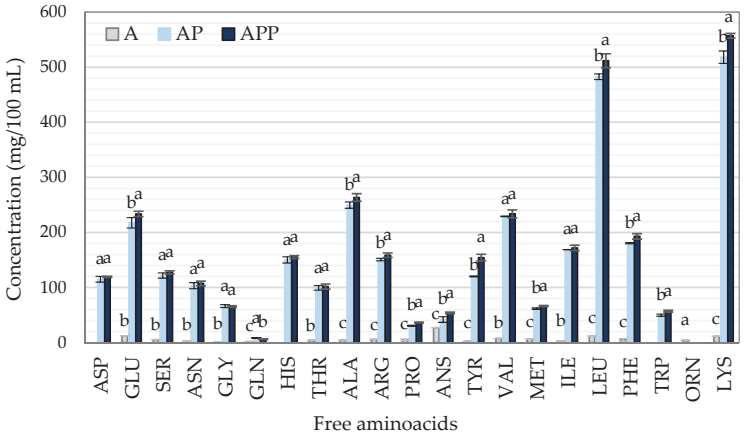

Figure 4. Concentration of free amino acids in three different hydrolysates: A (2% Alcalase), AP (2% Alcalase + 5% Protana Prime) and APP (2% Alcalase + 5% Protana Prime + 3% Protana UBoost). Bars with the same letter between samples are not statistically different. Tukey, $p < 0.05$.

2.3. In Silico Analysis of the Identified Peptides

The amino acid sequences of the peptides contained in fraction 2 of the AP and APP samples were identified by LC-MS/MS. A total of 79 and 12 peptide sequences were identified in AP and APP fractions, respectively. These peptides were studied using the Peptide Ranker tool to establish those sequences more able to exert DPP-IV inhibitory activity, obtaining 17 and 1 in AP and APP, respectively, with values greater than 0.5 (Supplementary Table S1). After simulating gastrointestinal digestion using in silico tools, novel peptides were generated, of which 21 have been previously described as bioactive with inhibitory activities of DPP-IV (18 peptides), ACE-I (13 peptides), renin (3 peptides), and antioxidant (3 peptides). Regarding DPP-IV inhibitors, peptides such as AT, GPA, GPAG, VN, AW, and PM are located at the N- or C-terminal of the identified AP hydrolysate sequences, which could also be active in their initial form before the simulated digestion (Table 1).

Table 1. In silico study of the identified peptides in chicken blood hydrolysates.

Sample	Peptide Ranker [1]	Peptide Sequence	MW (g/mol)	Enzyme Action [2]	Active Fragments	Bioactivity
AP	0.971435	GNGGGWGNSGGGG GGGGGGNGDGGGGDG CGNSGGCGGGGG	2926.42	GN–GGGW–GN– SGGGGGGGGGGN– GDGGGGDGCGN– SGGCGGGGG	-	-
AP	0.892122	NCFAAGF	728.90	N–CF–AAGF	CF	ACE inhibitor
AP	0.864842	PTWALLGCVLLLPSLR	1752.44	PTW–AL–L–GCVL–L–L– PSL–R	AL	Dipeptidyl peptidase IV inhibitor
AP	0.861194	FIGLFIGISKFMAT	1545.13	F–IGL–IGISK–F–M- AT	AT	Dipeptidyl peptidase IV inhibitor
AP	0.833521	LGPFSFSFGPAT	1227.54	L–GPF–SF–SF–GPAT	SF	ACE inhibitor, dipeptidyl peptidase IV inhibitor and renin inhibitor
AP	0.715609	PVGPMGPLGPA	992.36	PVGPM–GPL–GPA	GPL–GPA	ACE inhibitor and dipeptidyl peptidase IV inhibitor

Table 1. *Cont.*

Sample	Peptide Ranker [1]	Peptide Sequence	MW (g/mol)	Enzyme Action [2]	Active Fragments	Bioactivity
AP	0.704105	GPAGDAGAEGKPGIPG	1350.68	GPAGDAGAEGK–PGIPG	-	-
AP	0.690027	AWIRYSKVKFVSFNF	1892.68	AW–IR–Y–SK–VK–F–VSF–N–F	AW	ACE inhibitor, antioxidative, dipeptidyl peptidase IV inhibitor
					IR	ACE inhibitor, antioxidative, renin inhibitor, CaMPDE inhibitor and dipeptidyl peptidase IV inhibitor
					SK	Dipeptidyl peptidase IV inhibitor
					VK	ACE inhibitor, dipeptidyl peptidase IV inhibitor
AP	0.671755	GAGLLLLEALEKGYWV	1732.31	GAGL–L–L–L–EAL–EK–GY–W–V	EK–GY	ACE inhibitor, dipeptidyl peptidase IV inhibitor
AP	0.670104	GEKGPLGPNGPVGV	1277.66	GEK–GPL–GPN–GPVGV	GPL	ACE inhibitor
AP	0.63634	SPSKRFRGWRARTERT	1991.45	SPSK–R–F–R–GW–R–AR–TER–T	GW	ACE inhibitor, dipeptidyl peptidase IV inhibitor
					AR	ACE inhibitor
AP	0.607254	RDGPQGPLGPAG	1121.39	R–DGPQGPL–GPAG	GPAG	Dipeptidyl peptidase IV inhibitor
AP	0.571682	GPQGKVGPTGAPG	1122.44	GPQGK–VGPTGAP	-	-
AP	0.560064	GPAGAPGFPGAPGSKG EAGPTGARG	2121.65	GPAGAPGF–PGAPGSK–GEAGPTGAR -G	-	-
AP	0.551038	RAAELRPLR	1081.40	R–AAEL–R–PL–R	PL	ACE inhibitor and dipeptidyl peptidase IV inhibitor
AP	0.518296	PMADSGCLTEGEMGL IFVN	1984.57	PM–ADSGCL–TEGEM–GL–IF–VN	PM	Dipeptidyl peptidase IV inhibitor
					GL	ACE inhibitor and dipeptidyl peptidase IV inhibitor
					IF	ACE inhibitor
					VN	Dipeptidyl peptidase IV inhibitor
AP	0.50915	FSFLPQPPQEKAHD GGRYY	2237.73	F–SF–L–PQPPQEK–AH–DGGR–Y–Y	SF	ACE inhibitor, dipeptidyl peptidase IV inhibitor and renin inhibitor
					AH	ACE inhibitor, antioxidative and dipeptidyl peptidase IV inhibitor
18 APP	0.584356	KCYTPVCLK	1054.45	K–CY–TPVCL–K	-	-

[1] To predict the bioactivity potential of peptides, the Peptide Ranker tool was used to predict the potential bioactivity of peptides. [2] Gastrointestinal digestion was simulated with the BIOPEP-UWM database using the enzymes chymotrypsin (EC 3.4.21.1), trypsin (EC 3.4.21.4), and pepsin (EC 3.4.23.1).

According to previous reports, some of the characteristics of DPP-IV inhibitory peptides are (i) hydrophobicity in nature, (ii) length from 2 to 8 amino acids, and (iii) Pro residue located between the first four N-terminal positions [22,29,30], flanked by Gly, Phe, Leu, Val, and Ala [31]. In addition, Power et al. [6] mentioned that the DPP-IV enzyme also cleaves, although to a lesser degree, peptides containing Ser, Gly, Val, and Leu in the N-terminal position. Therefore, according to their amino acid sequence and physicochemical characteristics, a total of nine peptides generated in the simulated gastrointestinal digestion were selected as potential DPP-IV inhibitors and later synthesized: Gly-Trp (GW), Ala-Trp (AW), Gly-Pro-Phe (GPF), Gly-Gly-Gly-Trp (GGGW), Ile-Gly-Leu (IGL), Pro-Met (PM),

Pro-Leu (PL), Ile-Phe (IF), and Cys-Phe (CF). The best results are shown in Figure 5, where only those peptides with significant positive results were represented. In particular, three peptides showed outstanding inhibitory activity, with values of 65.19% (GPF), 43.64% (IGL), and 40.74% (GGGW) at a concentration of 2 mM. These results confirm the previously reported information as peptides GGGW, GPF, and GW contain Gly as an N-terminal residue, although GPF peptide contains a Pro residue in the second N-terminal position and is also flanked by Gly and Phe, which makes it the best potential DPP-IV inhibitor. Regarding hydrophobicity values shown in Table 2, they ranged from 0.21 to 0.47, since sequences were mainly composed of hydrophobic amino acids such as Trp, Ala, Ile, and Leu, making them potential sources of hypoglycemic peptides. According to the DPP-IV inhibition rate values, the IC_{50} of the three peptides with the highest inhibition was determined in vitro. The values obtained were 0.94 mM for GPF, 2.22 mM for IGL, and 2.73 mM for GGGW (Table 2, Figure 5). In the same trend, in a study with salmon skin gelatin hydrolysates, two peptides GPAE and GPGA were identified as DPP-IV inhibitory peptides, with IC_{50} values of 49.6 and 41.9 μM, respectively [23]. LPYPY, a peptide identified in milk proteins from in silico digestion with gastrointestinal proteins, was also identified as a potent DPP-IV inhibitor, with an IC_{50} value of 108 μM [30]. These peptides contained Pro as the second N-terminal residue, and the Pro residue was flanked by Ala, Gly, or Leu. In addition, the peptides were mainly composed of hydrophobic amino acid residues, such as Ala, Gly, and Pro. However, these peptides show a lower IC_{50} value than those obtained in this study, probably due to the primary sources from which they were obtained.

Table 2. Main physicochemical characteristics attributed to the peptides in this study.

Characteristics	GPF	GGGW	IGL	AW	GW
MW (g/mol)	319.39	375.44	301.43	275.32	261.30
Charge	0.00	0.00	0.00	0.00	0.00
Isoelectric point (pI)	5.88	5.88	5.88	5.88	5.88
Steric hindrance	0.58	0.64	0.64	0.51	0.59
Sidebulk	0.58	0.64	0.64	0.51	0.59
Hydrophobicity	0.23	0.21	0.47	0.31	0.27
Hydrophilicity	−0.83	−0.85	−1.20	−1.95	−1.70
Amphipathicity	0.00	0.00	0.00	0.00	0.00
IC_{50} (mM)	0.94	2.73	2.22		

Physicochemical property values obtained from ToxinPred.

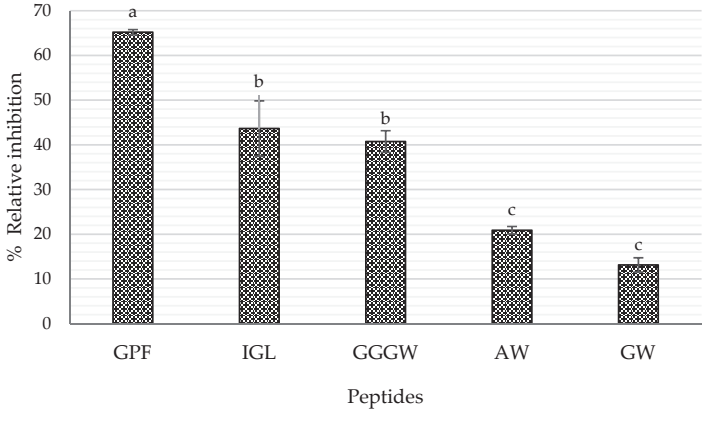

Figure 5. Relative DPP-IV inhibition rate of peptides at 2 mM. Bars with the same letter between samples are not statistically different. Tukey, $p < 0.05$.

3. Materials and Methods

3.1. Chemicals and Reagents

The Alcalase, Flavourzyme, Protana UBoost, and Protana Prime were purchased from Novozymes (Bagsvaerd, Denmark). Ile-Pro-Ile, o-phthaldialdehyde (OPA), Gly-Pro-7-amido-4-methylcoumarin (Gly-Pro-AMC) bromhydrate, trifluoroacetic acid (TFA), and DL-dithiotreitol (DTT) were from Sigma-Aldrich (Saint Louis, MO, USA). Dipeptidyl peptidase IV (from porcine kidney, EC 3.4.14.5), sodium dodecyl sulfate (SDS), and 2-mercaptoethanol were from Merck (Darmstadt, Germany). The synthetic peptides Gly-Pro-Phe (GPF), Gly-Gly-Gly-Trp (GGGW), Ile-Gly-Leu (IGL), Gly-Trp (GW), Ala-Trp (AW), Pro-Met (PM), Pro-Leu (PL), Ile-Phe (IF), and Cys-Phe (CF) were obtained from Bachem. Tris-(hydroxymethyl) aminomethane and formic acid (FA) were from Panreac Química S.A. (Barcelona, Spain). The supergrade HPLC grade acetonitrile (ACN) and supergrading HPLC grade methanol (MeOH) were from Scharlau Chemie (Barcelona, Spain). All other chemicals and reagents used were of analytical grade.

3.2. Enzymatic Hydrolysis

The hydrolysis process was carried out sequentially. In the first step, Alcalase, an endo-protease with an aggressive hydrolytic action, was used. In the second step, Flavourzyme and Protana Prime were used. Flavourzyme exerts moderate endo- and exo-peptidase activity being responsible for generating peptides and amino acids, whereas Protana Prime is mainly an exo-peptidase enzyme capable to generate free amino acids. In a third step, Protana UBoost was used with its main activity as a glutaminase enzyme. Thus, 1 g of boiled chicken blood was diluted in 2 mL of bidistilled water (500 mg/mL), brought to 80 °C for 15 min and a sequential hydrolysis process was applied. The first hydrolysis was prepared with 2% Alcalase (A) for 2 h at 55 °C. Subsequently, hydrolysate A was carried out to the second hydrolysis with 1% Flavourzyme (AF), 1% Flavourzyme + 3% Protana UBoost (AFP), 5% Protana Prime (AP), or 5% Protana Prime + Protana UBoost (APP) for 16 h at 55 °C. The digestion was stopped using heat in boiling water for 10 min. Finally, the hydrolysates were stored at −20 °C. All samples were prepared in triplicate.

3.3. Degree of Hydrolysis Determination

The OPA solution was made by mixing the following reagents: 50 mL of 100 mM sodium tetraborate decahydrate, 5 mL of 20% SDS (*w*/*w*), 80 mg of OPA dissolved in 2 mL of MeOH, 200 µL of 2-mercaptoethanol and adjusted to a final volume of 100 mL with bidistilled water. Each hydrolysate was diluted a hundred times in bidistilled water. For the reaction, 100 µL of the sample was incubated with 3.4 mL of OPA reagent for 2 min at room temperature. Absorbance was measured at 340 nm (Cary 60 UV-visible spectrophotometer, Agilent Technologies, CA, USA). The degree of hydrolysis (*DH*) was calculated according to the following equation:

$$DH\ (\%) = \frac{(ABS * 1.934 * d)}{c}$$

where *ABS* is the absorbance of the samples, *d* is the dilution factor and *c* is the protein concentration of the sample (g/L) [32]. All measurements were prepared in triplicate.

3.4. DPP-IV Inhibitory Activity

The DPP-IV inhibition assay was performed following the methodology proposed by Gallego et al. [5]. Briefly, in 96-well microplates, 45 µL of inhibitor, control, or sample (10 mg/mL) and 45 µL of DPP-IV at 5 mU/mL (diluted with 50 mM Tris-HCl + 5 mM of CaCl2 + 1µM of ZnCl2, pH 8.0) and 180 µL of 0.25 mM Gly-Pro-AMC (diluted with 50 mM Tris-HCl buffer + 0.5 mM DTT, pH 8.0). Fluorescence generation was measured in a CLARIOstar multimode microplate reader (BMG LABTECH, Ortenberg, Germany) using excitation wavelengths of 355 nm and emission of 460 nm at 0 and 20 min with an incubation temperature of 37 °C. Ile-Pro-Ile was used as a reference inhibitor and 50 mM

Tris-HCl buffer (pH = 8) was used as a control. The percentage of DPP-IV inhibition was calculated using the following formula:

$$\%\ Inhibition = \frac{Control\ fluorescence\ (t_{20} - t_0) - sample\ fluorescence(t_{20} - t_0)}{Control\ fluorescence\ (t_{20} - t_0)} \times 100$$

3.5. Peptide Separation by RP-HPLC

The hydrophobicity of the peptides was studied by reverse phase HPLC. A Symmetry C18 column (4.6 × 250 mm, 5 µm, Waters Co., Milford, MA, USA) was used. As solvent A 0.1% TFA in bidistilled water was used and as solvent B, 0.085% TFA in ACN (ACN:H_2O, 60:40, v/v). A 100 µL sample was injected at a concentration of 100 mg/mL. The elution was controlled at 214 nm. The peptides were run in a step gradient mode, where solvent B remained constant for 2 min, then it reached 50% in the next 50 min. The flow rate was 1 mL/min. Fractions were collected every two minutes. Each fraction was lyophilized and then re-dissolved in 50 µL of bidistilled H_2O to determine its DPP-IV inhibitory activity as indicated in Section 3.4.

3.6. Determination of Free Amino Acids (FAAs)

For sample preparation, 300 µL of hydrolysates A, AP, and APP were homogenized with HCl 0.01 N (1:4; w/v) in a vortex for 8 min and centrifuged at 10,000 g and 4 °C for 20 min. For the analysis of FAAs, the samples were pretreated following the methodology described by Aristoy & Toldrá [33], which includes chemical deproteinization and derivatization of the sample. A 5 mM norleucine solution was used as the internal standard. The chromatographic separation of the derivatized molecules was done following the methodology described by Flores et al. [34]. Briefly, using a reverse phase HPLC system (Series 1200; Agilent, Santa Clara, CA, USA), equipped with a Waters Pico Tag® C18 column (3.9 × 300 mm; Waters Corp., Milford, MA, USA) at a temperature of 52 °C and flow rate of 1 mL/min. Elution was monitored at 254 nm. As phase A, 70 mM sodium acetate with 2.5% ACN, pH 6.55 was used. As phase B, ACN:H_2O:MeOH was used in a ratio of 45:40:15. Quantification was carried out considering the response factors calculated for each amino acid/sample in the mixed standards series. The results were expressed as mg of FAAs/100 mL of hydrolysate.

3.7. Peptide Sequence Identification by LC-MS/MS

A 1 µL sample was injected into an Ekspert nanoLC 425 (Eksigent, Redwood City, CA, USA) using a trap column C18-CL (3 µ 120 Ă, 350 m × 0.5 mm; Eksigent), where it was desalted and concentrated with a mobile phase of 0.1% TFA at a flow of 5 µL/min for 5 min. Subsequently, the peptides were loaded onto a C18-CL analytical column (3 µ, 120 Ă, 0.075 × 150 mm; Eksigent) equilibrated with 5% ACN and 0.1% FA. Solvent A was 0.1% FA dissolved in bidistilled water, and solvent B was ACN in 0.1% FA. Elution was carried out using a linear gradient of 15 to 40% of B in A for 20 min at a flow rate of 300 nL/min. Peptides were then analyzed in a mass spectrometer nanoESI qQTOF (6600 plus TripleTOF, ABSCIEX), where the peptides were ionized in a Nano Optiflow Source Type applying 3.0 kV to the spray emitter at 200 °C. Mass spectrometry was carried out in the data-dependent acquisition mode. MS1 scans of 350–1400 m/z were obtained for 250 ms. The quadrupole resolution was set to "LOW" for MS2 experiments, which were acquired from 100–1500 m/z for 25 ms in high sensitivity mode. The criteria used for switch was a charge from 2+ to 5+, minimum intensity, and 100 cps. Up to 100 ions were selected for fragmentation after each survey scan. Dynamic exclusion was set to 15 s. Digestion of 500 ng K562 trypsin was used as a control for system sensitivity. Regarding the data analysis, the obtained spectra were analyzed using ProteinPilot v 5.0. (SCIEX) default parameters. The peak list was directly generated from 6600 plus TripleTOF wiff files. The Paragon algorithm of ProteinPilot v 5.0 was used to search the Uniprot_GallusGallus database with no enzyme specificity.

3.8. In Silico Analysis of Identified Peptides

Peptide Ranker tool was used to predict the potential bioactivity of the peptides [35], and values greater than 0.5 were considered for additional in silico analyses simulating gastrointestinal digestion. Gastrointestinal digestion was simulated using the BIOPEP-UWM database [36], using the enzymes chymotrypsin (EC 3.4.21.1), trypsin (EC 3.4.21.4) and pepsin (EC 3.4.23.1) accessed on 12.05.22. The potential allergenicity of the synthesized peptides was predicted using the AllerTOP v. 2.0 software [37]. ToxinPred tool [38] was accessed on 7 July 2022 to study the toxicity of peptides and their physicochemical properties (hydrophobicity, amphipathicity, pI, and steric hindrance).

3.9. Statistical Analysis

For data analysis, an analysis of variance (ANOVA) followed by Tukey's study range test was used, with a significance level of $p < 0.05$. Each data point represents the average of three samples.

4. Conclusions

The hydrolysates AP (2% Alcalase + 5% Protana Prime) and APP (2% Alcalase + 5% Protana Prime + 3% Protana UBoost) have a significant DPP-IV inhibitory activity (60.55% and 53.61%, respectively, assayed at a concentration of 10 mg/mL). The peptides GPF, IGL, and GGGW were identified after simulated GI digestion of the peptides identified in the fraction with the highest DPP-IV inhibitory activity, showing IC_{50} values of 0.94, 2.22, and 2.73 mM, respectively. These results confirm the potential of chicken blood hydrolysates as a source of bioactive peptides as GPF, IGL, and GGGW could be good candidates to be used in the control or modulation of type 2 diabetes, although in vivo analysis would be needed in order to confirm their antidiabetic activity.

Supplementary Materials: The following supporting information can be downloaded at: https://www.mdpi.com/article/10.3390/ijms232214140/s1.

Author Contributions: G.C.-A.; Methodology, Formal analysis, Investigation, Writing—Original draft preparation, Visualization. F.T.; Conceptualization, Writing—Reviewing and Editing, Supervision, Funding acquisition. L.M.; Conceptualization, Writing—Reviewing and Editing, Supervision, Funding acquisition. All authors have read and agreed to the published version of the manuscript.

Funding: This research was funded by Grant PID2020-119684RB-I00 funded by MCIN/AEI/10.13039/501100011033. Grant GRISOLIAP/2020/021 de la Consellería de Innovació, Universitats, Ciència i Societat Digital de la Generalitat Valenciana (GCA) is also acknowledged. The proteomic analysis was performed in the proteomics facility of SCSIE University of Valencia that belongs to Proteored.

Conflicts of Interest: The authors declare no conflict of interest.

References

1. IDF. International Diabetes Federation. Available online: www.diabetesatlas.org (accessed on 15 July 2022).
2. Nasri, M. Protein Hydrolysates and Biopeptides: Production, biological activities, and applications in foods and health benefits. A Review. *Adv. Food Nutr. Res.* **2017**, *81*, 109–159. [CrossRef] [PubMed]
3. Wajchenberg, B.L. β-Cell failure in diabetes and preservation by clinical treatment. *Endocr. Rev.* **2007**, *28*, 187–218. [CrossRef] [PubMed]
4. Elam, E.; Feng, J.; Lv, Y.M.; Ni, Z.J.; Sun, P.; Thakur, K.; Zhang, J.G.; Ma, Y.L.; Wei, Z.J. Recent advances on bioactive food derived anti-diabetic hydrolysates and peptides from natural resources. *J. Funct. Foods.* **2021**, *86*, 104674. [CrossRef]
5. Gallego, M.; Aristoy, M.C.; Toldrá, F. Dipeptidyl peptidase IV inhibitory peptides generated in Spanish dry-cured ham. *Meat Sci.* **2014**, *96*, 757–761. [CrossRef]
6. Power, O.; Nongonierma, A.B.; Jakeman, P.; Fitzgerald, R.J. Food protein hydrolysates as a source of dipeptidyl peptidase IV inhibitory peptides for the management of type 2 diabetes. *Proc. Nutr. Soc.* **2014**, *73*, 34–46. [CrossRef] [PubMed]
7. Wang, X.; Fan, Y.; Xu, F.; Xie, J.; Gao, X.; Li, L.; Tian, Y.; Sheng, J. Characterization of the structure, stability, and activity of hypoglycemic peptides from Moringa oleifera seed protein hydrolysates. *Food Funct.* **2022**, *13*, 3481–3494. [CrossRef] [PubMed]
8. Zhang, X.; Wang, R.; Cheng, C.; Zhang, Y.; Ma, Y.; Lu, W. Identification of two novel dipeptidyl peptidase-IV inhibitory peptides from sheep whey protein and inhibition mechanism revealed by molecular docking. *Food Biosci.* **2022**, *48*, 101733. [CrossRef]

9. Rodriguez, H.; Albericio, F.; Santiago Vispo, N. Iberoamerican network for the development of therapeutic peptides, REDIPEPT. *Rev. Bionatura* **2020**, *5*, 1177–1180. [CrossRef]
10. Toldrá, F.; Gallego, M.; Reig, M.; Aristoy, M.C.; Mora, L. Recent progress in enzymatic release of peptides in foods of animal origin and assessment of bioactivity. *J. Agric. Food Chem.* **2020**, *68*, 12842–12855. [CrossRef]
11. Lacroix, I.M.E.; Li-Chan, E.C.Y. Inhibition of dipeptidyl peptidase (DPP)-IV and α-glucosidase activities by pepsin-treated whey proteins. *J. Agric. Food Chem.* **2013**, *61*, 7500–7506. [CrossRef]
12. Mojica, L.; Gonzalez de Mejia, E.; Granados-Silvestre, M.Á.; Menjivar, M. Evaluation of the hypoglycemic potential of a black bean hydrolyzed protein isolate and its pure peptides using in silico, in vitro and in vivo approaches. *J. Funct. Foods* **2017**, *31*, 274–286. [CrossRef]
13. Vilcacundo, R.; Martínez-Villaluenga, C.; Hernández-Ledesma, B. Release of dipeptidyl peptidase IV, α-amylase and α-glucosidase inhibitory peptides from quinoa (*Chenopodium quinoa* Willd.) during in vitro simulated gastrointestinal digestion. *J. Funct. Foods* **2017**, *35*, 531–539. [CrossRef]
14. Daliri, E.B.M.; Lee, B.H.; Oh, D.H. Current trends and perspectives of bioactive peptides. *Crit. Rev. Food Sci. Nutr.* **2017**, *58*, 2273–2284. [CrossRef] [PubMed]
15. Wongngam, W.; Mitani, T.; Katayama, S.; Nakamura, S.; Yongsawatdigul, J. Production and characterization of chicken blood hydrolysate with antihypertensive properties. *Poult. Sci.* **2020**, *99*, 5163–5174. [CrossRef] [PubMed]
16. Toldrá, F.; Reig, M.; Mora, L. Management of meat by- and co-products for an improved meat processing sustainability. *Meat Sci.* **2021**, *181*, 108608. [CrossRef] [PubMed]
17. Nongonierma, A.B.; FitzGerald, R.J. Dipeptidyl peptidase IV inhibitory properties of a whey protein hydrolysate: Influence of fractionation, stability to simulated gastrointestinal digestion and food–drug interaction. *Int. Dairy J.* **2013**, *32*, 33–39. [CrossRef]
18. Clemente, A. Enzymatic protein hydrolysates in human nutrition. *Trends Food Sci. Technol.* **2000**, *11*, 254–262. [CrossRef]
19. Nchienzia, H.A.; Morawicki, R.O.; Gadang, V.P. Enzymatic hydrolysis of poultry meal with endo- and exopeptidases. *Poult. Sci.* **2010**, *89*, 2273–2280. [CrossRef]
20. Nongonierma, A.B.; Dellafiora, L.; Paolella, S.; Galaverna, G.; Cozzini, P.; FitzGerald, R.J. In silico approaches applied to the study of peptide analogs of Ile-Pro-Ile in relation to their dipeptidyl peptidase IV inhibitory properties. *Front. Endocrinol.* **2018**, *9*, 329. [CrossRef]
21. Agyei, D. Bioactive proteins and peptides from soybeans. *Recent Pat. Food Nutr. Agric.* **2015**, *7*, 100–107. [CrossRef]
22. Lammi, C.; Aiello, G.; Boschin, G.; Arnoldi, A. Multifunctional peptides for the prevention of cardiovascular disease: A new concept in the area of bioactive food-derived peptides. *J. Funct. Foods* **2019**, *55*, 135–145. [CrossRef]
23. Li-Chan, E.C.Y.; Hunag, S.L.; Jao, C.L.; Ho, K.P.; Hsu, K.C. Peptides derived from Atlantic salmon skin gelatin as dipeptidyl-peptidase IV Inhibitors. *J. Agric. Food Chem.* **2012**, *60*, 973–978. [CrossRef] [PubMed]
24. Mojica, L.; de Mejía, E.G. Optimization of enzymatic production of anti-diabetic peptides from black bean (Phaseolus vulgaris L.) proteins, their characterization and biological potential. *Food Funct.* **2016**, *7*, 713–727. [CrossRef] [PubMed]
25. Xu, F.; Yao, Y.; Xu, X.; Wang, M.; Pan, M.; Ji, S.; Wu, J.; Jiang, D.; Ju, X.; Wang, L. Identification and quantification of DPP-IV-inhibitory peptides from hydrolyzed-rapeseed-protein-derived napin with analysis of the interactions between key residues and protein domains. *J. Agric. Food Chem.* **2019**, *67*, 3679–3690. [CrossRef] [PubMed]
26. Jin, S.W.; Lee, G.H.; Kim, J.Y.; Kim, C.Y.; Choo, Y.M.; Cho, W.; Han, E.H.; Hwang, Y.P.; Kim, Y.A.; Jeong, H.G. Effect of porcine whole blood protein hydrolysate on slow-twitch muscle fiber expression and mitochondrial biogenesis via the AMPK/SIRT1 pathway. *Int. J. Mol. Sci.* **2022**, *23*, 1229. [CrossRef]
27. Young Park, J.; Kim, M.-Y.; Jeong, Y.-J. Changes in physicochemical characteristics of porcine blood under various conditions of enzyme hydrolysis. *Korean J. Food Preserv.* **2016**, *23*, 413–421. [CrossRef]
28. Sadri, H.; Larki, N.N.; Kolahian, S. Hypoglycemic and hypolipidemic effects of leucine, zinc, and chromium, alone and in combination, in rats with type 2 diabetes. *Biol. Trace Elem. Res.* **2017**, *180*, 246–254. [CrossRef]
29. Nielsen, S.D.; Beverly, R.L.; Qu, Y.; Dallas, D.C. Milk bioactive peptide database: A comprehensive database of milk protein-derived bioactive peptides and novel visualization. *Food Chem.* **2017**, *232*, 673–682. [CrossRef]
30. Nongonierma, A.B.; Fitzgerald, R.J. Susceptibility of milk protein-derived peptides to dipeptidyl peptidase IV (DPP-IV) hydrolysis. *Food Chem.* **2014**, *145*, 845–852. [CrossRef]
31. Boots, J.-W.P. US8273710B2—Protein Hydrolysate Enriched in Peptides Inhibiting DPP-IV and Their Use. Europen Patent EP1831361B1, 2006.
32. Church, F.C.; Swaisgood, H.E.; Porter, D.H.; Catignani, G.L. Spectrophotometric assay using o-phthaldialdehyde for determination of proteolysis in milk and isolated milk proteins. *J. Dairy Sci.* **1983**, *66*, 1219–1227. [CrossRef]
33. Aristoy, M.C.; Toldrá, F. Deproteinization techniques for HPLC amino acid analysis in fresh pork muscle and dry-cured ham. *J. Agric. Food Chem.* **1991**, *39*, 1792–1795. [CrossRef]
34. Flores, M.; Aristoy, M.C.; Spanier, A.M.; Toldrá, F. Non-volatile components effects on quality of "Serrano" dry-cured ham as related to processing time. *J. Food Sci.* **1997**, *62*, 1235–1239. [CrossRef]
35. Mooney, C.; Haslam, N.J.; Pollastri, G.; Shields, D.C. Towards the improved discovery and design of functional peptides: Common features of diverse classes permit generalized prediction of bioactivity. *PLoS ONE* **2012**, *7*, e45012. [CrossRef] [PubMed]
36. Minkiewicz, P.; Iwaniak, A.; Darewicz, M. BIOPEP-UWM Database of bioactive peptides: Current opportunities. *Int. J. Mol. Sci.* **2019**, *20*, 5978. [CrossRef]

37. Dimitrov, I.; Bangov, I.; Flower, D.R.; Doytchinova, I. AllerTOP v.2—A server for *in silico* prediction of allergens. *J. Mol. Model.* **2014**, *20*, 2278. [CrossRef]
38. Gupta, S.; Kapoor, P.; Chaudhary, K.; Gautam, A.; Kumar, R.; Raghava, G.P.S. *In silico* approach for predicting toxicity of peptides and proteins. *PLoS ONE* **2013**, *8*, e73957. [CrossRef]

International Journal of
Molecular Sciences

MDPI

Article

Effect of the Production Parameters and In Vitro Digestion on the Content of Polyphenolic Compounds, Phenolic Acids, and Antiradical Properties of Innovative Snacks Enriched with Wild Garlic (*Allium ursinum* L.) Leaves

Kamila Kasprzak-Drozd [1], Tomasz Oniszczuk [2,*], Iwona Kowalska [3], Jarosław Mołdoch [3], Maciej Combrzyński [2], Marek Gancarz [4,5], Bohdan Dobrzański, Jr. [6], Adrianna Kondracka [7] and Anna Oniszczuk [1,*,†]

1 Department of Inorganic Chemistry, Medical University of Lublin, Chodźki 4a, 20-093 Lublin, Poland
2 Department of Thermal Technology and Food Process Engineering, University of Life Sciences in Lublin, Głęboka 31, 20-612 Lublin, Poland
3 Department of Biochemistry and Crop Quality, Institute of Soil Science and Plant Cultivation, State Research Institute, 24-100 Puławy, Poland
4 Faculty of Production and Power Engineering, University of Agriculture in Kraków, Balicka 116B, 30-149 Kraków, Poland
5 Institute of Agrophysics, Polish Academy of Sciences, Doświadczalna 4, 20-290 Lublin, Poland
6 Pomology, Nursery and Enology Department, University of Life Sciences in Lublin, Głęboka 28, 20-400 Lublin, Poland
7 Department of Obstetrics and Pathology of Pregnancy, Medical University of Lublin, Staszica 16, 20-081 Lublin, Poland
* Correspondence: tomasz.oniszczuk@up.lublin.pl (T.O.); anoniszczuk@o2.pl (A.O.)
† Senior author.

Citation: Kasprzak-Drozd, K.; Oniszczuk, T.; Kowalska, I.; Mołdoch, J.; Combrzyński, M.; Gancarz, M.; Dobrzański, B., Jr.; Kondracka, A.; Oniszczuk, A. Effect of the Production Parameters and In Vitro Digestion on the Content of Polyphenolic Compounds, Phenolic Acids, and Antiradical Properties of Innovative Snacks Enriched with Wild Garlic (*Allium ursinum* L.) Leaves. *Int. J. Mol. Sci.* **2022**, *23*, 14458. https://doi.org/10.3390/ijms232214458

Academic Editor: David Arráez-Román

Received: 28 October 2022
Accepted: 19 November 2022
Published: 21 November 2022

Publisher's Note: MDPI stays neutral with regard to jurisdictional claims in published maps and institutional affiliations.

Abstract: A new type of corn snack has been created containing additions of wild garlic (*Allium ursinum* L.). This medicinal and dietary plant has a long tradition of use in folk medicine. However, studies on wild garlic composition and activity are fairly recent and scarce. This research aimed to investigate the influence of the screw speed and *A. ursinum* amounts on the antiradical properties as well as the content of polyphenolic compounds and individual phenolic acids of innovative snacks enriched with wild garlic leaves. The highest radical scavenging activity and content of polyphenols and phenolic acids were found in the snacks enriched with 4% wild garlic produced using screw speed 120 rpm. The obtained findings demonstrated that snacks enriched with wild garlic are a rich source of polyphenolic compounds. Since the concentration of such compounds is affected by many factors, e.g., plant material, presence of other compounds, and digestion, the second aim of this study was to determine radical scavenging activity, the content of polyphenols, and individual phenolic acids of snacks after in vitro simulated gastrointestinal digestion. Using an in vitro two-stage model, authors noted a significant difference between the concentration of polyphenolic compounds and the polyphenol content of the plant material before digestion.

Keywords: dietary polyphenols; high performance liquid chromatography; functional food; in vitro two-stage simulated gastrointestinal digestion; wild garlic; antioxidant activity; extrusion-cooking; processing parameters

1. Introduction

Polyphenolic compounds, of which more than 8000 chemical structures have been described, are one of the most diverse and widely distributed groups of secondary plant metabolites. They are an essential component of a balanced human diet [1]. The common feature of polyphenols is the presence of at least two hydroxyl groups attached to one or more aromatic rings [2,3]. The most adopted classification places the phenolics within one of two groups: flavonoids (e.g., flavanols, flavanones, and anthocyanins) and non-flavonoids

(e.g., phenolic acids, stilbenes, lignans) polyphenols. Phenolic acids are further subdivided into derivatives of benzoic and cinnamic acid in terms of their chemical structure [1].

Phenolic compounds are direct antioxidants but show indirect antioxidant activity by inducing endogenous protective enzymes and positive regulatory action with regard to the signaling pathways [4,5]. The antioxidant activity of polyphenols is determined by the presence of hydroxyl groups. The strength of this action depends on their number and position in the ring structure, esterification, or proximity to other substituents [3,6]. The predominant mechanism of the antioxidant activity of these compounds is believed to be radical scavenging via hydrogen atom donation, although other types of mechanisms are recognized [3,4].

Oxidative stress is an imbalance state between ROS (reactive oxygen species) and antioxidant defenses. It can lead to various pathological conditions in the body, such as tissue injury and accelerated cellular death. The potential of plant products to serve as antioxidants to protect against ROS and various diseases induced by free radicals has been explored [7]. Scavenging free radicals through the action of compounds with antioxidant properties (such as polyphenols) reduces and prevents damage caused by oxidative stress [8]. Due to the fact that polyphenols exhibit a number of properties that are beneficial to health, in this case, many times representing a specific therapeutic potential, they are a frequent topic of research work. In most plant materials, they occur as compounds accompanying other active substances. Therefore the possible synergistic effect of their action must be taken into account [6]. The DPPH (2,2-diphenyl-1-picrylhydrazyl radical) assay is used to determine the radical-scavenging activity of samples [7,9].

In addition to the antioxidant activity, the therapeutic effects of polyphenols have been proven: e.g., anti-inflammatory and analgesic activity [10], as inhibitors of neurodegenerative processes [6], dyslipidemia and cardiovascular disease [11], in treating overweight and obesity [12]. Of note, most naturally occurring ingredients with consistently reported anticancer efficacy contain high levels of polyphenols [1].

A plant rich in phenolic compounds is ramson (wild garlic or bear's garlic, *Allium ursinum* L.), a dietary and medicinal plant with a long tradition of use in folk medicine. However, studies on its composition and pharmacological activity are fairly recent and scarce [13]. The species name "ursinum" is of Latin origin, derived from "ursus" (bear). It is related to folk stories, according to which bears, after awakening from winter hibernation, consume this plant to regain strength [14].

Allium ursinum L. has a distinct garlic-like scent associated with the presence of sulfur-containing compounds. These compounds are undoubtedly the most important constituents of ramson, both in terms of chemotaxonomic value and pharmacological activity. Of the various sulfur compounds present in this plant, glutamyl peptides and sulfoxides are considered primary. Apart from sulfur-containing substances, *A. ursinum* has also been reported to be a good source of phenolic compounds. The leaves contain free and bound forms of phenolic acids (protokatechuic, 4-OH-benzoic, vanillic, caffeic, syringic, coumaric, ferulic, and sinapic). As far as flavonoids, the leaves of ramson are abundant, predominantly in kaempferol derivatives [15].

The addition of wild garlic leaves to food allows for obtaining products with an extraordinary concentration of substances promoting health. The benefits of such additives include increasing the amount of dietary fiber-containing polyphenolic compounds of the nature of antioxidants, as well as enhancing the levels of essential oils and sulfur compounds.

Ramson has a much milder effect on the gastrointestinal tract than in the case of the addition of common garlic (*Allium sativum* L.). Common garlic, unlike wild garlic, is characterized by a more pronounced spicy taste and aroma, and it also causes an unpleasant smell from the mouth. The latter effect—the sulfur smell of the breath after eating even small amounts of garlic—is the result of the presence of bactericidal, antiviral, and antifungal allicin, the metabolites of which are excreted through the lungs. This organosulfur chemical can also damage the digestive tract if ingested in large amounts. The literature data [15,16] shows that wild garlic contains more than two times less of this compound in favor of three times more content of other sulfur-organic compounds that are equally beneficial for health

but less burdensome to the gastrointestinal tract. The presence of antioxidant polyphenolic compounds in the plant—including phenolic acids—protects the body against the harmful effects of free radicals, the excess of which in the body can cause neurodegenerative diseases, cancer, or cardiovascular diseases. Due to its pro-health properties, high content of polyphenols, and the fact that no one has used 'bear's garlic' in the production of functional food so far, authors decided to use this plant as an addition to snacks.

In order to exhaustively assess the potential biological properties of polyphenolic compounds that naturally occurred in plants, it is essential to study their bioaccessibility, bioavailability, and release efficiency, as undegraded bioactive compounds during digestion (bioaccessibility) can be available for absorption, especially in the intestine and promote biological action (bioavailability). In addition, it is important to study their synergistic action and coexistence in the plant matrix. In vitro models of the gastrointestinal tract are used for this purpose [8,17]. The complex biotransformation of plant secondary metabolites after ingestion and their low bioavailability can lead to tissue concentrations well below those exhibiting antioxidant capacity in vitro. Importantly, inside the gastrointestinal tract, the antioxidant potential of dietary components may play a key role in the body's defense at the systemic level [18].

Factors in the bioaccessibility of polyphenols include their release from the food matrix, particle size, their hydrophilic/lipophilic balance as related to their glycosylation, different pH-dependent transformations (degradation, hydrolysis, and oxidation within the gastrointestinal tract), and also interactions between polyphenols and food components. The absorption of some the free polyphenols (e.g., phenolic acids) occurs in the stomach, and these compounds can conjugate with glucuronic acid. The contribution of the intestinal step to the bioaccessibility of polyphenols depends on many parameters. For example, impact of intestinal enzymes on the residual matrix could increase the level of phenolic compounds. Absorption of aglycones and their glucosylated forms by the small intestine the process can take place in two ways: by passive diffusion or active transport. Undigested polyphenols pass into the large intestine, where they are further degraded by colonic microflora. Finally, metabolites of all these compounds lead to benzoic acid generation [17].

This study was primarily aimed at investigating the influence of the production parameters (screw rotational speed and *A. ursinum* addition) on the content of polyphenolic compounds, individual phenolic acids, and antiradical properties of innovative snacks enriched with wild garlic leaves.

Before bioactive compounds can be used by human organisms, they must be processed in the digestive tract in order to be assimilated in the proper form. Therefore, studies that are based only on the determination of the concentration of phytochemicals in plant material do not give proper information about the bioavailable level of these compounds. In contrast, analyses using an in vitro digestion system provide more detailed data on the concentration of test components after ingestion and digestion in the gastrointestinal tract in vivo [17]. Therefore, the secondary aim of this study was to determine the content of polyphenolic compounds, individual phenolic acids, and antiradical properties of the snacks after in vitro simulated gastrointestinal digestion.

2. Results and Discussion

2.1. Influence of A. ursinum Addition and Screw Speed on Polyphenols Content, Free Phenolic Acid Content and Antioxidant Properties of Snacks

The wide spectrum of biological activities obtained from wild garlic and the presence of chemical compounds with high therapeutic possibilities make this plant a candidate for the development of functional food and food supplements. Here, the used extraction method can significantly affect the quality and concentration of the targeted compounds. Extraction of active compounds from wild garlic using an ultrasound-assisted (UAE) process was recommended by Tomšik et al. [16] as an efficient, inexpensive, and simple existing extraction system that could be suitably upscaled for largescale preparations. UAE at elevated temperatures with 80% aqueous ethanol as an extractant was also previously

used by authors [19,20] to obtain polyphenol extracts from snacks enriched with herbs. As UAE was demonstrated to be the optimum technique for isolating phenolic acids from functional foods, the authors decided to use it in this experiment.

The samples—corn snacks with different quantities of wild garlic leaves (0, 1, 2, 3, and 4%) were produced using extrusion cooking at various screw speeds. In the first phase of the experiment, the authors examined the total content of polyphenolic compounds. Polyphenols are secondary metabolites of plants, present in the human diet, and used for medicinal and cosmetic purposes. They have strong antioxidant, anti-radical and pharmacological properties. The results showed that their content had increased significantly due to wild garlic addition (Table 1), notably with increased screw speed. The highest total content of polyphenols (as per gallic acid equivalents; GAE) was reported in snacks with a 4% addition of the *A. ursinum*, while the lowest was seen in a sample without such functional additive.

Table 1. The total content of polyphenolic compounds (TPC mg GAE/g d.w.) in snacks enriched with wild garlic extruded at two different screw speeds—80 and 120 rpm (n = 3; mean ± SD).

Wild Garlic Addition	Polyphenols Content, 80 rpm	Polyphenols Content, 120 rpm
0%	0.288 ± 0.008	0.381 ± 0.002
1%	0.302 ± 0.007	0.400 ± 0.003
2%	0.388 ± 0.002	0.403 ± 0.022
3%	0.440 ± 0.011	0.445 ± 0.016
4%	0.603 ± 0.009	0.610 ± 0.018

A. ursinum leaves were previously reported by Djurdjevic et al. [21] to contain free forms of ferulic and vanillic acids and bound forms of coumaric, ferulic, and vanillic acids. Phenolic acids are present in plant, most often as glycosides and esters. Acid (or base) hydrolysis transforms glycosylated and esterified phenolics into their aglycones and is often used during the analysis of phenolic acids in plant material [22]. For this reason, in the first step of the experiment, the content of polyphenols and free phenolic acids in the product was determined after acid hydrolysis. The phenolic acid content in extracts was assessed by applying reversed-phase ultra-high pressure liquid chromatography using a photodiode array detector coupled to a triple-quadrupole mass spectrometer. The following phenolic acids were identified in the samples: protocatechuic, 4-OH-benzoic, vanillic, syringic, salicylic (benzoic acid derivatives), and caffeic, coumaric, ferulic, sinapic (cinnamic acid derivatives) (Table 2, Figures 1 and 2). Ferulic acid was the prevailing phenolic acid. These results are consistent with those obtained by Djurdjevic et al. [21], who identified three phenolic acids in wild garlic extracts (*p*-coumaric, ferulic and vanillic), and Pop et al. [23], who quantified coumaric, ferulic and sinapic acids. However, in this study, the authors determined five additional phenolic acids in all snacks enriched with wild garlic.

As in the analysis of total polyphenols, also in this research, the content of active compounds in general increased as wild garlic leaves were added to the snacks. The comparatively proportional increase in the content of phenolic acids demonstrates extrusion process, under conditions of high temperature and high pressure, did not degrade the active compounds present in snacks enhanced with this raw material. In this regard, slight deviations may indicate that the ingredients had not been mixed properly during the preparation or production stage.

Table 2. The content of phenolic acids (after hydrolysis) in snacks enriched with wild garlic extruded at two different screw speeds (n = 3; mean ± SD).

		Content of Phenolic Acid (μg/g d.w.)									
Screw Speed	**Garlic Addition**	**Protokatechuic**	**4-OH-Benzoic**	**Vanilic**	**Caffeic**	**Syringic**	**Coumaric**	**Ferulic**	**Sinapic**	**Salicylic**	**Sum**
80 rpm	0%	0.406 ± 0.01	4.012 ± 0.20	0.121 ± 0.00	30.358 ± 1.72	8.817 ± 0.21	64.058 ± 2.36	665.751 ± 3.22	63.950 ± 1.15	0.657 ± 0.02	838.130 ± 8.89
	1%	0.574 ± 0.02	3.915 ± 0.16	0.873 ± 0.01	49.192 ± 2.04	11.088 ± 0.54	165.700 ± 5.24	1159.250 ± 12.06	82.192 ± 0.97	0.877 ± 0.03	1473.677 ± 21.07
	2%	0.509 ± 0.02	4.961 ± 0.18	5.083 ± 0.05	63.217 ± 0.39	11.191 ± 0.27	184.117 ± 2.35	1216.350 ± 1.28	93.850 ± 0.89	0.909 ± 0.03	1580.187 ± 5.46
	3%	0.624 ± 0.03	5.026 ± 0.20	21.868 ± 0.19	66.137 ± 1.49	11.253 ± 0.09	196.575 ± 3.28	1260.917 ± 11.98	93.700 ± 2.08	1.065 ± 0.01	1657.165 ± 19.35
	4%	0.442 ± 0.02	5.124 ± 0.01	52,142 ± 2.04	77.700 ± 0.92	12.065 ± 0.02	212.340 ± 0.34	1322.666 ± 7.64	105.342 ± 2.97	1.155 ± 0.02	1788.975 ± 13.98
120 rpm	0%	0.443 ± 0.00	4.928 ± 0.19	0.123 ± 0.01	32.083 ± 1.13	9.521 ± 0.18	66,875 ± 1.14	516.583 ± 7.09	62.108 ± 2.59	0.635 ± 0.01	693.299 ± 12.34
	1%	0.666 ± 0.01	4.955 ± 0.11	2.609 ± 0.02	58.508 ± 2.32	11.098 ± 0.31	173.200 ± 2.54	1161.750 ± 1.59	81.883 ± 1.38	0.779 ± 0.00	1495.448 ± 8.28
	2%	0.656 ± 0.01	5.050 ± 0.09	10.038 ± 0.31	66.479 ± 1.22	11.266 ± 0.16	187.716 ± 1.18	1225.083 ± 12.58	91.633 ± 2.03	0.904 ± 0.00	1598.825 ± 17.58
	3%	0.714 ± 0.00	5.035 ± 0.21	25.296 ± 0.29	67.554 ± 0.38	10.694 ± 0.08	200.208 ± 5.19	1265.333 ± 7.22	89.525 ± 0.50	1.053 ± 0.02	1665.415 ± 13.89
	4%	0.751 ± 0.00	5.365 ± 0.12	96.375 ± 1.15	78.383 ± 3.09	11.413 ± 0.02	216.650 ± 1.94	1323.583 ± 0.93	102.700 ± 4.02	1.130 ± 0.03	1836.350 ± 11.71

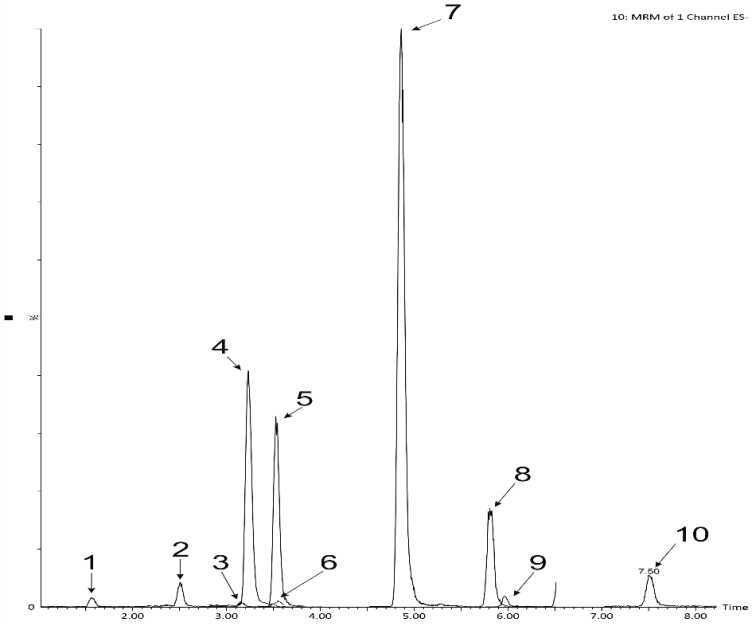

Figure 1. LC-MS-MRM chromatogram of phenolic acids found in snacks enriched with wild garlic (120 rpm, 3% of wild garlic, sample after hydrolysis): 1—protocatechuic, 2—4-OH-benzoic, 3—vanillic, 4—caffeic, 5—3-OH -benzoic (internal standard), 6—syringic, 7—*p*-coumaric, 8—ferulic, 9—sinapic, 10—salicylic.

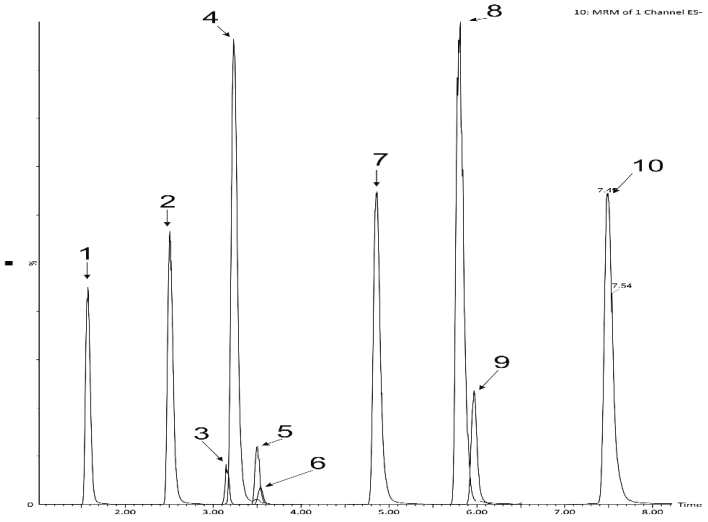

Figure 2. LC-MS-MRM chromatogram of phenolic acids standards: 1—protocatechuic, 2—4-OH-benzoic, 3—vanillic, 4—caffeic, 5—3-OH -benzoic (internal standard), 6—syringic, 7—*p*-coumaric, 8—ferulic, 9—sinapic, 10—salicylic.

A. ursinum is the source of many antioxidant molecules [23]. Therefore the quantity of total phenolic compounds (generally assumed to be responsible for the antioxidant activity of plant extracts) [23] was ascertained for snacks with the addition of wild garlic (Table 3). In the next phase of the experiment, the authors determined the DPPH free radical scavenging potential of the tested samples using a UV-VIS spectrophotometer. The obtained results showed that the antioxidant activity of snacks increased with the amount of added *A. ursinum*. The highest DPPH free radical scavenging activity was seen in the products supplemented with 4% of wild garlic and at 120 rpm. The maximum free radical scavenging ability by all extracts was obtained after 15 min. The results obtained by Pop et al. [23] by means of applying the DPPH radical-scavenging test, showed that wild garlic represents important sources of bioactive phenolic acids, volatile and sulfur compounds, and flavonoids) with strong in vitro antioxidant activity.

Table 3. DPPH radical scavenging activity of corn snacks enriched with wild garlic extruded at two different screw speeds (n = 3; mean ± SD).

	Radical Scavenging towards DPPH (%)									
Time (min)	**Wild Garlic Addition (%), 80 rpm**					**Wild Garlic Addition (%), 120 rpm**				
	0	**1**	**2**	**3**	**4**	**0**	**1**	**2**	**3**	**4**
0	19.21 ± 0.19	22.58 ± 0.15	24.69 ± 0.12	27.92 ± 0.46	28.95 ± 0.96	24.11 ± 0.44	25.39 ± 0.59	27.31 ± 0.71	28.92 ± 0.96	30.48 ± 0.71
5	60.75 ± 0.43	67.92 ± 1.72	69.95 ± 0.23	74.69 ± 1.29	77.63 ± 0.79	62.28 ± 2.72	69.15 ± 0.81	72.92 ± 0.84	75.97 ± 1.59	79.18 ± 0.16
10	62.32 ± 0.01	69.65 ± 0.98	76.58 ± 1.14	78.19 ± 0.21	83.16 ± 0.81	65.77 ± 1.34	71.53 ± 0.02	77.95 ± 0.93	80.18 ± 2.21	87.68 ± 0.93
15	62.32 ± 0.00	69.65 ± 0.81	76.50 ± 0.56	78.19 ± 0.93	83.16 ± 1.73	65.77 ± 0.20	71.53 ± 1.13	77.95 ± 1.07	80.18 ± 0.93	87.68 ± 0.13

Previous research have shown that aglycones have a higher antioxidant activity than their glycosidic compounds or are connected by other types of bonds [24]. Sani et al. [25] studied the influence of acidic hydrolysis on the yield, total phenolic content, and antioxidative

capacity of methanolic extract of germinated brown rice. These authors applied total phenolic content and DPPH radical scavenging for the measurement of antioxidant ability. In the study presented by Sani et al. [25], there were a significant difference in the total phenolic content and DPPH radical scavenging assay results when comparing neutral with acidic hydrolysis. Snack samples were further tested using high performance liquid chromatography to determine the individual phenolic compound levels in different hydrolytic media contributing to the antioxidant effects. This study revealed that acidic hydrolysis could improve the polyphenols content and antioxidant properties of germinated brown rice.

Furthermore, research has shown that the antioxidant activity of polyphenolic compounds is dependent on the number of hydroxyl groups in the molecules and can be changed by spherical effects, as well as by interactions of the compounds existing in the matrix and in the extracts [26]. In addition, it has been examined that the antioxidant activity of products is dependent on their composition. Korus et al. [27] found a lower antioxidant potential for red beans compared to black-brown and cream beans, even though dark-red bean extrudates demonstrated higher phenolic content compared to black-brown and creamy bean products. In the case of these innovative snacks enriched with *A. ursinum*, the product radical-scavenging activity measured after 15 min was positively correlated with the total content of polyphenols and free phenolic acids (Table 4). Very high positive correlations were established between the wild garlic leaves addition and radical-scavenging activity for both screw speeds.

Table 4. Pearson's correlation coefficients for snacks supplemented with wild garlic leaves addition.

	Total Polyphenols	Free Phenolic Acid	DPPH Radical Scavenging Activity
		80 rpm	
Wild garlic content	0.952	0.891	0.979
Total polyphenols		0.749	0.903
Free phenolic acids			0.945
		120 rpm	
Wild garlic content	0.849	0.873	0.991
Total polyphenols		0.623	0.859
Free phenolic acids			0.887

Polyphenols content can vary due to food manufacturing parameters [28]. Multari et al. [24] state that high-temperature treatment can improve the release of phenolic compounds bound to the cell wall structures. Furthermore, other compounds that have a beneficial effect on the human body can appear.

Extrusion-cooking is the short-time method of processing starchy raw materials under high-temperature (120–200 °C) and high pressure (20 MPa) conditions. The intense processing of mechanical shearing results in a deep transformation of individual components. Temperature, screw speed, moisture content, and residence time distribution during the process are crucial for the polyphenols content antioxidant activity of the product [29] and antinutritional factors level [30]. Khanal et al. [31] showed the effects of extrusion-cooking on procyanidin in grape seed and pomace. These authors have demonstrated that this method increases the levels of low-molecular-weight bioactive compounds (e.g., procyanidin) and releases biologically important monomers and dimers from polymer chains [31]. The intensity of changes therein depends on the properties of the raw material, e.g., humidity and the processing parameters. A high homogenization of ingredients leads to a decrease in diffusion barriers and the breaking down of chemical bonds. This factor results in the heightened reactivity of the components. Optimized extrusion-cooking conditions may therefore, release phenolic acids from the chemical bonds that they create with other compounds without deactivating aglycones [29–31]. This is due to the cracking of the rigid cell walls and other plant cell components. The breakdown of the glycosidic bonds, which leads to the formation of aglycons,

is also conducive to an increased antiradical capacity of products [32]. A Diagram of snack production using extrusion cooking is presented in Figure 3.

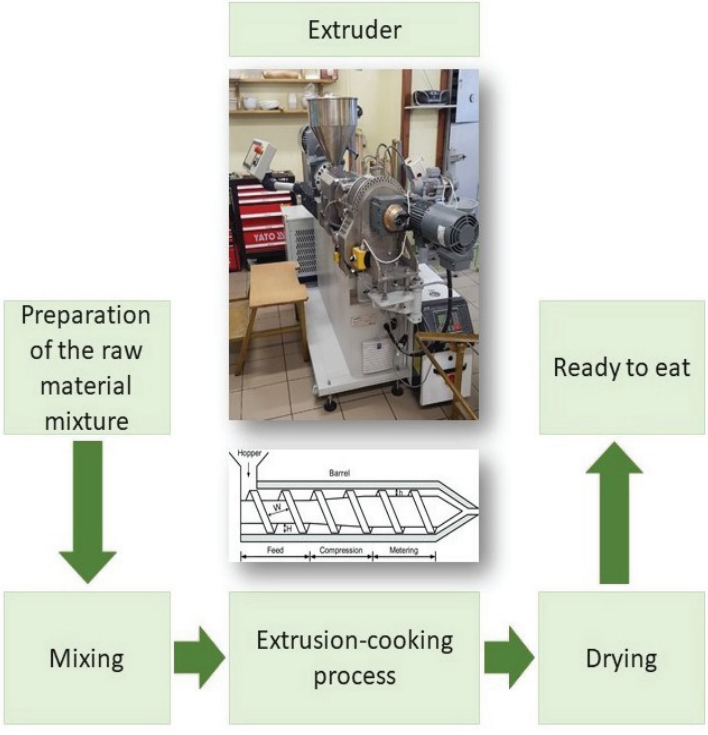

Figure 3. Diagram of the snack production process using extrusion-cooking.

The next stage of the research focused on the influence of one extrusion-cooking condition—the screw rotational speed, on the total content of polyphenols and free phenolic acids, as well as the antioxidant properties of extruded snacks. The obtained findings demonstrated that all snacks enriched with the wild garlic screw speed of 120 rpm resulted in a higher content of polyphenols and free phenolic acids and a higher ability to scavenge DPPH than the speed of 80 rpm (Tables 1–3). Alonso et al. [33] examined that the most important factors stimulating the transformation of raw material during the extrusion-cooking process are high temperatures and mechanical factors related to shear forces that increase along with the increase in screw rotational speed. It is possible that the extrusion conditions at 80 rpm are too mild, and they do not enable the release of some phenolics from the processed raw material. The rotation speed of 80 rpm was found to give higher contents than 120 rpm for only two phenolic acids. They were salicylic and sinapic acids, which have lower decomposition temperatures than most of the analyzed acids. So, it is possible that for these compounds, 120 rpm induced too drastic production conditions and brought about their decomposition.

Many previous studies have revealed antioxidant activity increase in extruded products with an increased temperature of processing [33–35]. This effect is explained due to the presence of products formed during Maillard reactions—which can have high radical scavenging activity.

Currently popular in food technology applications, the extrusion-cooking process can provide diversified properties within the final product. The effects of temperature, pressure, and shear forces on moist raw material induce profound changes in a very short time. They include the inactivation of anti-nutritive factors, enhanced digestibility of nutrients, and modified sensory characteristics. The type and intensification of these changes depend

on the parameters of the extrusion-cooking procedure (e.g., extruder screw rotational speed, temperature) as well as on the properties of the raw materials. The high degree of component mixing reduces diffusion barriers and breaks chemical bonds. This results in increased reactivity of the ingredients [36]. For this reason, the proper selection of parameters is crucial for the production process.

2.2. The Digestability of the Snack's Polyphenols Using Two-Stage In Vitro Human Digestion Model

Credible reports on the breakdown of food ingredients in the stomach are also crucial for assessing phytochemical bioaccessibility. Gastric digestion is multiple stages that includes mechanical actions and the effect of gastric fluids. Gastric juice contains hydrochloric acid, lipase, pepsinogens, mucus, electrolytes, and water. Hydrochloric acid supports the denaturation of proteins, and it activates pepsin. The duration of this phase lasts 2 to 4 h. The gastric pH in healthy human subjects in the fasted state is in the range of 1.3 to 2.5; the intake of a meal generally increases the pH to above 4.5. Unfortunately, most in vitro models include a pH below 2.5, which is a pH related to the human fasting state more than to real food digestion. The change in gastric pH is taken into consideration only in dynamic models [37,38]. The absorption of free phenolic acids occurs in the stomach, and phenolic acids can conjugate with glucuronic acid. The in vitro small intestinal digestion model simulates the time, temperature, pH, and composition of pancreatic juice, including electrolytes, bile salts, and enzymes. In the fed state, pH can be from 5.4–7.5 in the duodenum [39], to 5.3–8.1 in the jejunum, and up to 7.0–7.5 in the ileum. The contribution of the intestinal step to the bioaccessibility of polyphenols depends on many parameters. The effect of intestinal enzymes on the residual matrix could, for example, increase the concentration of phenolic compounds. Moreover, degradation or isomerization of these compounds can occur due to catalyzation by the presence of oxygen and/or transition metal ions. In addition, specific absorption of aglycones and their glucosylated forms by the small intestine can come about by passive diffusion or active transport [40].

In the human body, esterified polyphenols are degraded in the large intestine by microbial esterases. Undigested polyphenols pass into the large intestine, where they are further degraded by colonic microflora. Depending on the polyphenol's structure, a large variety of compounds can be formed. Finally, metabolites of all these compounds lead to benzoic acid generation [41].

In this study, a two-stage in vitro digestion model, including gastric and duodenal phases, was used. Before carrying out in vitro digestion, authors examined the total content of polyphenolic components, the content of free phenolic acids, and the antioxidant properties of the selected samples (Table 5, snacks enriched with 0%, 2%, and 4% of wild garlic extruded at 120 rpm) without prior hydrolysis, hence the much lower content of free phenolic acids before digestion (Table 6) in relation to its content after hydrolysis (Table 2). For all investigated snacks, the concentration of polyphenols after in vitro digestion was significantly reduced, both after gastric and duodenal digestion, compared with the samples before digestion (Table 5). The content of free phenolic acids also decreased drastically after the first stage of in vitro digestion (gastric), which was deepened during the second stage (duodenal). Acids such as protokatechuic, 4-OH-benzoic, vanillic, syringic, sinapic, and salicylic have not been found in the mixture after the first phase of digestion (Table 6).

Table 5. The total content of polyphenolic compounds (TPC mg GAE/g d.w.) in snacks enriched with wild garlic before and after two-stage digestion (n = 3; mean ± SD).

Wild Garlic Addition	Polyphenols Content		
	Before Digestion	Gastric Digestion	Duodendal Digestion
0%	0.221 ± 0.005	0.124 ± 0.002	0.042 ± 0.002
2%	0.307 ± 0.003	0.213 ± 0.0227	0.110 ± 0.0227
4%	0.542 ± 0.016	0.390 ± 0.0184	0.189 ± 0.0184

Table 6. The content of phenolic acids (without hydrolysis) in snacks enriched with wild garlic extruded at 120 rpm (n = 3; mean ± SD); I- gastric digestion stage, II- duodendal digestion stage.

		Content of Phenolic Acid (μg/g d.w.)									
Conditions	Garlic Addition	Protokatechuic	4-OH-benzoic	Vanillic	Caffeic	Syringic	Coumaric	Ferulic	Sinapic	Salicylic	Sum
Before digestion	0%	0.131 ± 0.003	0.235 ± 0.001	0.456 ± 0.002	1.374 ± 0.022	0.196 ± 0.000	4.374 ± 0.051	2.381 ± 0.003	0.324 ± 0.006	0.082 ± 0.000	9.553 ± 0.088
	2%	0.170 ± 0.001	0.272 ± 0.002	0.588 ± 0.008	1.387 ± 0.017	0.271 ± 0.004	6.121 ± 0.009	3.697 ± 0.071	0.362 ± 0.001	0.156 ± 0.004	13.024 ± 0.117
	4%	0.192 ± 0.002	0.296 ± 0.000	0.599 ± 0.010	1.808 ± 0.041	0.336 ± 0.003	7.878 ± 0.085	5.128 ± 0.011	0.556 ± 0.003	0.193 ± 0.002	16.986 ± 0.002
After digestion	0% I	-	-	-	0.079 ± 0.000	-	0.428 ± 0.001	0.236 ± 0.000	-	-	0.743 ± 0.157
	0% II	-	-	-	-	-	0.218 ± 0.000	-	-	-	0.218 ± 0.000
	2% I	-	-	-	0.132 ± 0.001	-	1.356 ± 0.023	0.397 ± 0.003	-	-	1.885 ± 0.027
	2% II	-	-	-	-	-	0.477 ± 0.001	-	-	-	0.477 ± 0.001
	4% I	-	-	-	0.144 ± 0.001	-	1.893 ± 0.003	0.502 ± 0.007	-	-	2.539 ± 0.011
	4% II	-	-	-	-	-	0.754 ± 0.008	-	-	-	0.754 ± 0.008

There are reports in which the total concentration of polyphenols was reduced during the gastric digestion stage, as in this study. This tendency has been observed for aqueous infusions from *Capparis spinosa* L., *Crithmum maritimum* L. [42], chamomile tea, yerba mate, coffee-like substitutes, and coffee blend. The decrease in active compounds content was further exacerbated in the subsequent intestinal part of the in vitro digestion [43]. Similarly, Dacrema et al. [44] observed a drop in the content of individual polyphenolic compounds after in vitro digestion of fireweed extract. These Authors reported a loss of individual polyphenolic compounds after the orogastric phase (in the range of 1.92–84.17%) and a decrease (11.83–98.07%) after the duodenal phase.

In plant-processing by-products of black carrot, a decrease in phenolic acids content (chlorogenic, neochlorogenic, and cryptochlorogenic) was also observed during the gastric stage of in vitro digestion, which escalated at further stages of digestion. Contrastingly, ferulic and caffeic acid mostly demonstrated an increase in bioavailability as compared to undigested samples [45]. As in the author's work, Majdoub et al. [46] have also noted a decrease in certain compounds post-in vitro gastric and gastric + duodenal digestion. In particular, caffeoylquinic acids were found to be partially decreased after 20 min of gastric digestion. Likewise, coumaroylquinic acids only minutely persisted throughout the simulated human digestion as a result of the degradation occurring in the gastric and duodenal compartments. However, quinic acid was only found in the samples obtained during duodenal digestion. This fact suggests that this compound was derived from the degradation of the more complex coumaroylquinic and caffeoylquinic acids. Moreover, the work of Majdoub et al. [46] saw that hibiscus acid was present in the undigested extract

and persisted, albeit in lower concentrations, throughout the simulated digestion. Other authors have indicated high polyphenol stability in the gastric phase and their degradation at the intestinal level. Gayoso et al. [47] examined the effect of in vitro gastrointestinal digestion methods using three static models on the stability and bioaccessibility of phenolic compounds. When the results were referred to mg/mg lyophilized digested sample, the remaining % of the sample decreased to 67% and 68% (oral and gastric, respectively) for rosmarinic acid, and 75% and 78% (oral and gastric, respectively) in the case of caffeic acid. No remarkable differences were observed for rutin between the initial level subjected to digestion and the levels recovered during the oral and gastric steps.

It is difficult to compare bioaccessibility studies due to the many variables that may influence gastrointestinal digestion. Differences in results can be dictated by the effect of the plant/food matrix, the heterogeneity of analyzed plant materials, their degree of processing, as well as the in vitro digestion methodology. Pure compounds also show high variability. For example, for rutin, the % of loss after intestinal digestion was found to be from only 3% to total loss. In the case of quercetin, the results ranged from 5.8% [48] to total loss [42], and for chlorogenic acid, from 44% to 95.7% [42]. It is certain that the digestion methodology is a key factor for assessing the bioaccessibility of polyphenols.

This research has shown the in vitro digestion procedure reduced the antioxidant activity of snacks (Table 7). The decrease in antioxidant activity is consistent with the results presented by other authors. The study of the effect of in vitro digestion on the antioxidant activity of phenolic demonstrated a decrease in activity for rosmarinic acid (24–36%), caffeic acid (12–19%) and no change in antioxidant capacity for rutin [47]. A similar tendency of the reduction in antioxidant potential for plant-processing by-products of black carrot was observed during the gastric stage of in vitro digestion. At the further phases of digestion, the results were divergent, indicating an increase or decrease depending on the method and raw material [45]. The reduction in antioxidant activity during the intestinal part of in vitro digestion was observed in this study and in the work of other authors. This fact can be explained by the structural reorganization of some compounds during a change in pH to slightly alkaline.

Table 7. DPPH radical scavenging activity of corn snacks enriched with wild garlic before and after two-stage digestion (n = 3; mean ± SD).

Time	Radical Scavenging (%) before Digestion			Radical Scavenging (%) after Gastric Digestion			Radical Scavenging (%) after Duodendal Digestion		
	Wild Garlic Addition (%)								
	0	2	4	0	2	4	0	2	4
0	15.41 ± 0.05	21.08 ± 0.54	25.91 ±1.06	11.21 ± 0.08	21.08 ± 0.54	28.10 ±0.67	10.32 ± 0.34	20.01 ± 1.15	24.91 ±0.39
5	58.73 ± 0.83	62.22 ± 0.49	75.16 ± 1.78	24.07 ± 0.34	32.76 ± 0.33	36.55 ± 1.17	18.07 ± 0.94	29.17 ± 0.13	31.79 ± 0.45
10	59.15 ± 0.24	73.56 ± 2.09	82.16 ± 0.78	38.23 ± 0.86	51.56 ± 0.76	59.98 ± 0.98	29.23 ± 0.89	38.56 ± 1.26	46.98 ± 0.57
15	59.15 ± 0.00	73.56 ± 0.08	82.16 ± 2.73	38.23 ± 0.12	51.56 ± 2.18	59.98 ± 1.11	29.23 ± 1.07	38.56 ± 1.19	46.02 ± 2.29

pH conditions have a significant influence on both in vitro and in vivo studies concerning the antioxidant activity of polyphenols. It is significantly different in acidic and alkaline environments in relation to neutral environments. This fact is crucial for the theoretical deliberation of the influence of the pH of individual parts of the digestive tract on the structures and activity of plant metabolites. However, available study results are limited. It is known that the antioxidant activity of extracts depends on the number of OH groups in their main compounds, as well as their hydrogen-donating abilities. Moreover, additional

OH groups in *ortho*-positions have a positive effect on the antioxidant activity of phenolic compounds, especially at pH 4. Thus, in order to analyze the pH influence on the activity of food polyphenols, each component must be considered [49].

Lettuce (*L. sativa*) extract is rich in polyphenols such as caffeic acid derivatives, chlorogenic acids, and flavonoids [50]. The results of a study involving lettuce extract showed that free radical scavenging potential increases with increasing pH [51]. Other results were obtained for sweet potato leaf extract [52]. This material is rich in chlorogenic and caffeic acid derivatives. In this case, a slightly alkaline (pH 8) environment had a negative influence on antioxidant ability, while neutral and weak acidic environments gave an increase in activity. Why regard to this effect, interesting experiments were performed for honey. The analysis confirmed that the substance is rich in flavonoids (quercetin, luteolin, hesperitin, and apigenin) and phenolic acids such as cinnamic, benzoic, vanillic, coumaric, caffeic, chlorogenic and ellagic, and the authors observed significantly decreasing activity with increasing pH.

These discrepancies can result from different species of analyzed plant raw materials, their distinct characteristics, chemical structure and initial concentration of bioactive compounds, the methodology for the determination of antioxidant potential, and the in vitro digestion procedure [37].

Phenolic compounds during gastrointestinal digestion can be hydrolyzed as a consequence of the acid environment of the stomach, the alkaline environment of the intestine, and the action of digestive enzymes [53]. Furthermore, these compounds have the ability to bind with other ingredients of the food matrix, resulting in the formation of complexes that may also contribute to the reduction in their antioxidant activity.

3. Materials and Methods

3.1. Plant Materials

Allium ursinum L. leaves (series nr 5902741007841) were purchased from "Dary Natury Sp z o.o." herbal industrial (Grodzisk, Poland). Before the extraction, the dry plant material was milled and sieved. Corn grits were purchased at the local market (distributor Vegetus, Poland).

3.2. Extrusion-Cooking Procedure

Blends of corn grits and ground wild garlic leaves were prepared by mixing dry components in the ratios of 100:0, 99:1, 98:2, 97:3, and 96:4 on a weight basis. The blended samples were conditioned to 15% of moisture content by spraying with a calculated amount of water and mixing continuously for 10 min. Recipes with different amounts of wild garlic leaves were processed using a single screw extrusion-cooker TS-45 (ZMCh Metalchem, Gliwice, Poland) with L:D = 12:1 (L is barrel length; D is screw diameter). The screw compression ratio was 3:1. The range of the temperatures of the extrusion-cooking process was as follows: 125/130/135 °C, respectively, in the three extruder sections. The extrusion-cooking was carried out at screw speeds: 80 and 120 rpm. A single-open forming die of 3 mm in diameter was used. Samples were stored in polyethylene bags at room temperature before tests [19].

3.3. Extraction Procedure

The extraction process was performed in an ultrasonic bath (Bandelin Electronic GmbH & Co. KG, Berlin, Germany). Accordingly, 2 g portions of samples were extracted 2-times with 40 mL of 80% ethanol for 40 min at a temperature of 60 °C, ultrasound frequency of 33 kHz, and a power of 320 W. The extracts were filtered, combined, evaporated to dryness, and dissolved in 10 mL of methanol [19].

3.4. Hydrolysis of the Samples

Hydrolysis of the samples was carried out according to the modified method of Czaban et al. [54]. Samples were treated with 2 M NaOH for 4 h at room temperature. At the beginning of hydrolysis, 4 µg of an internal standard (4-OH-benzoic acid) was

added to all samples. The hydrolyzed samples were subsequently cooled and acidified using ice-cold 6 M HCl to achieve a pH value of about 2. The resulting mixtures were centrifuged at 8000 rpm for 20 min, and supernatants were extracted with ethyl acetate. The organic phase was collected and evaporated to dryness. The residue was dissolved in methanol and stored in a refrigerator. After centrifugation, the samples were subjected to chromatographic analysis.

3.5. Determination of Phenolic Acids

The determination of phenolic acids was carried out according to the modified method of Burda and Oleszek [55]. The phenolic acid content in extracts was assessed by reversed-phase ultra-high pressure liquid chromatography, performed on a Waters ACQUITY UPLC® Systems chromatograph (Waters Corporation, Milford, MA, USA), equipped with a photodiode array detector and coupled to a triple-quadrupole mass spectrometer (Waters ACQUITY® TQD, Micromass, Manchester, GB). Samples were then separated on a Waters ACQUITY UPLC® HSS C18 column (1.0 mm × 100 mm; 1.8 µm) at 30 °C. The mobile phase consisted of 0.1% formic acid in MilliQ water (*v*/*v*) and 0.1% formic acid in acetonitrile (*v*/*v*). The analytes were eluted using a combination of isocratic and gradient steps.

The detection of phenolic acids was performed in the negative ionization mode, using a selected reaction monitoring method. The source temperature was 110 °C, while the desolvation temperature was 350 °C. Nitrogen was used as a desolvation gas (a flow of 1000 L/h) and as a cone gas (100 L/h). Argon was used as a collision gas (0.1 mL/min). Collision energies were optimized for particular phenolic acids. Concentrations of phenolic acids in wheat extracts were calculated on the basis of calibration curves.

3.6. Determination of the Total Content of Polyphenolic Compounds (TPC)

The total content of polyphenolic compounds (TPC) was resolved to utilize the modified Folin-Ciocalteu (FC) method [19]. Here, the number of polyphenols is expressed as mg gallic acid equivalents (GAE) per g of dry weight (d.w.).

3.7. Ability to Scavenge DPPH

Measurement of antiradical activity was carried out via DPPH stable radical (2,2-diphenyl-1-picrylhydrazyl) spectroscopy, according to the modified method of Burda and Oleszek [55]. Absorbance was measured at 517 nm wavelength every 5 min for 15 min, using a UV-VIS spectrophotometer (Genesys UV-VIS, Thermo Scientific, Waltham, MA, USA). This method enables tracking of absorbance changes over time and indicates the plateau phase. The free radical scavenging ability of the samples was calculated using the following formula:

$$\%\mathrm{RSA} = \left[\frac{(\mathrm{A}_0 - \mathrm{A}_{1)}}{\mathrm{A}_0}\right] \times 100 \quad (1)$$

A_0—the absorbance of the sample except for tested extracts
A_1—the absorbance of the sample with tested extracts

3.8. In Vitro Two-Stages Digestion Model

Authors applied a static in vitro digestion model comparing two-stages digestion (gastric and duodenal) according to Seraglio et al. [8] with minor modifications. In order to carry out the first gastric digestion step, 1.632 g of each sample was weighed and homogenized beforehand. To each of the samples, 5.84 mL of gastric solution was added and manually stirred for 4 min. Subsequently, 2.32 mL of hydrochloric acid (Chempur) at pH 2.5 ± 0.2 was added. Afterward, the samples were incubated in a water bath with shaking (GFL 1083) for two hours (37 °C, 100 rpm). The samples were then centrifuged (10 min, 8000 rpm), and the supernatant was collected for further analysis. Until the scheduled analysis was performed, the samples were refrigerated (−20 °C for 24 h).

The next step (duodenal digestion) was performed in the same way as the gastric but using a different amount of sample (2.246 g). After incubation (skipping the centrifugation step), 0.09 mL of 1 mol/L sodium bicarbonate (Chempur) (to increase the pH to 5.5) and 2.26 mL of duodenal solution were added to each sample. Then the samples were stirred for 1 min.

After this time, 0.72 mL of sodium bicarbonate solution for adjustment to pH 6.7 ± 0.2 was added to each flask. The samples were then incubated in a water bath with shaking for 2 h (37 °C, 100 rpm). After centrifugation (10 min, 8000 rpm), the supernatant was examined and further analyzed. The storage conditions were the same as for the first step.

The simulated gastric juice (gastric solution) was prepared as follows: 0.16 g of pepsin (Merck, Darmstadt, Germany) was dissolved in 0.35 mL of 12 M hydrochloric acid, and it was made up to 50 mL with ultrapure water. Simulated intestinal juice (duodenal solution) was prepared by connecting 0.25 g pancreatin with 0.047 g of sodium glycodeoxycholate, 0.0505 g of sodium taurocholate, and 0.029 g of sodium taurodeoxycholate (Merck) dissolved in 0.25 mL of 0.5 M sodium bicarbonate in 25 mL ultrapure water.

3.9. Statistical Analysis

All the measurements were done in three replications; the results were mean values of multiple repetitions and standard deviations (SD). Statistical analysis with ANOVA (Statistica 13.0, StatSoft Inc., Tulsa, OK, USA) was used to determine the significance of differences at $\alpha = 0.05$, with Duncan's test applied to evaluate the homogenous groups. Pearson's correlation coefficients and their significance were evaluated at 0.05 and 0.01 for the tested characteristics.

4. Conclusions

Interest in a healthy lifestyle and the prevention of lifestyle diseases have contributed to the advancement of new nutritional trends. This paper describes studies of newly developed innovative snacks enriched with *Allium ursinum* L. leaves. The influence of wild garlic addition and screw rotational speed on the content of polyphenols and biological properties was examined. The highest content of polyphenols and free phenolic acids and the highest radical scavenging activity was found in the fried snacks enriched with 4% of leaves. Polyphenols content and antiradical properties of the snacks exhibited a positive correlation with the addition of wild garlic leaves to the product.

Optimized extrusion-cooking process conditions may release phenolic acids from the chemical bonds that they create with other compounds without deactivating aglycones. The obtained findings demonstrated that for all snacks enriched with the wild garlic, a screw speed of 120 rpm resulted in the highest content of polyphenols and free phenolic acids, as well as a higher ability to scavenge DPPH.

Plant foods have diverse compositions and are often eaten in conjunction with other foods. Therefore, the food bolus ingredients can modulate the bioaccessibility and stability of phytochemicals. Hence, in bioavailability studies, biochemical and chemical reactions and physical barriers occurring within food must be considered. In this study, authors used a two-stage in vitro digestion model, including gastric and duodenal phases. For all the investigated snacks, the concentration of polyphenols after in vitro digestion was significantly reduced, after gastric and duodenal digestion, as compared with the samples before digestion. The content of free phenolic acids also decreased drastically after the first stage of in vitro digestion (gastric), which was deepened during the second stage (duodenal). In addition, the authors found that the in vitro digestion procedure reduced the snack's antioxidant activity.

This work is the first to comprehensively investigate the in vitro digestion of snacks incorporating polyphenol-rich plant material.

Author Contributions: Conceptualization, K.K.-D., T.O., A.O. and I.K.; methodology, K.K.-D., T.O., A.O. and J.M.; validation, K.K.-D., I.K. and J.M.; formal analysis K.K.-D., M.G. and B.D.J.; investigation, K.K.-D., T.O., M.C. and M.G.; resources, M.C. and J.M.; data curation, K.K, I.K., J.M., A.K. and A.O.; writing-original draft preparation, K.K.-D. and A.O.; supervision, A.O. All authors have read and agreed to the published version of the manuscript.

Funding: This research received no external funding.

Institutional Review Board Statement: Not applicable.

Informed Consent Statement: Not applicable.

Data Availability Statement: Not applicable.

Conflicts of Interest: The authors declare no conflict of interest.

References

1. Durazzo, A.; Lucarini, M.; Souto, E.B.; Cicala, C.; Caiazzo, E.; Izzo, A.A.; Novellino, E.; Santini, A. Polyphenols: A Concise Overview on the Chemistry, Occurrence, and Human Health. *Phytother. Res.* **2019**, *33*, 2221–2243. [CrossRef] [PubMed]
2. Ferreira, I.C.F.R.; Barros, L. (Eds.) *Functional Food Ingredients from Plants*, 1st ed.; Academic Press: Cambridge, MA, USA, 2019; ISBN 978-0-12-816567-6.
3. Olszowy, M. What Is Responsible for Antioxidant Properties of Polyphenolic Compounds from Plants? *Plant Physiol. Biochem.* **2019**, *144*, 135–143. [CrossRef]
4. Kumar, N.; Goel, N. Phenolic Acids: Natural Versatile Molecules with Promising Therapeutic Applications. *Biotechnol. Rep.* **2019**, *24*, e00370. [CrossRef] [PubMed]
5. Stevenson, D.E.; Hurst, R.D. Polyphenolic Phytochemicals—Just Antioxidants or Much More? *Cell. Mol. Life Sci.* **2007**, *64*, 2900–2916. [CrossRef]
6. Brewer, M.S. Natural Antioxidants: Sources, Compounds, Mechanisms of Action, and Potential Applications. *Compr. Rev. Food Sci. Food Saf.* **2011**, *10*, 221–247. [CrossRef]
7. Gulcin, İ. Antioxidants and Antioxidant Methods: An Updated Overview. *Arch. Toxicol.* **2020**, *94*, 651–715. [CrossRef] [PubMed]
8. Seraglio, S.K.T.; Valese, A.C.; Daguer, H.; Bergamo, G.; Azevedo, M.S.; Nehring, P.; Gonzaga, L.V.; Fett, R.; Costa, A.C.O. Effect of in Vitro Gastrointestinal Digestion on the Bioaccessibility of Phenolic Compounds, Minerals, and Antioxidant Capacity of Mimosa Scabrella Bentham Honeydew Honeys. *Food Res. Int.* **2017**, *99*, 670–678. [CrossRef]
9. Kasprzak, K.; Oniszczuk, T.; Wójtowicz, A.; Waksmundzka-Hajnos, M.; Olech, M.; Nowak, R.; Polak, R.; Oniszczuk, A. Phenolic Acid Content and Antioxidant Properties of Extruded Corn Snacks Enriched with Kale. *J. Anal. Methods Chem.* **2018**, *2018*, e7830546. [CrossRef]
10. Jucá, M.M.; Filho, F.M.S.C.; De Almeida, J.C.; Mesquita, D.D.S.; Barriga, J.R.D.M.; Dias, K.C.F.; Barbosa, T.M.; Vasconcelos, L.C.; Leal, L.K.A.M.; Ribeiro, J.E.; et al. Flavonoids: Biological Activities and Therapeutic Potential. *Nat. Prod. Res.* **2020**, *34*, 692–705. [CrossRef]
11. Kumari, P.; Kumar, V.; Kumar, R.; Pahuja, S.K. Sorghum Polyphenols: Plant Stress, Human Health Benefits, and Industrial Applications. *Planta* **2021**, *254*, 47. [CrossRef]
12. Kasprzak, K.; Wojtunik-Kulesza, K.; Oniszczuk, T.; Kuboń, M.; Oniszczuk, A. Secondary Metabolites, Dietary Fiber and Conjugated Fatty Acids as Functional Food Ingredients against Overweight and Obesity. *Nat. Prod. Commun.* **2018**, *13*, 1934578X1801300836. [CrossRef]
13. Sobolewska, D.; Podolak, I.; Makowska-Wąs, J. Allium Ursinum: Botanical, Phytochemical and Pharmacological Overview. *Phytochem. Rev.* **2015**, *14*, 81–97. [CrossRef]
14. Rejewski, M. Pochodzenie Łacińskich Nazw Roślin Polskich. In *Przewodnik Botaniczny*; Książka i Wiedza: Warszawa, Poland, 1996.
15. Oszmiański, J.; Kolniak-Ostek, J.; Wojdyło, A. Characterization and Content of Flavonol Derivatives of *Allium ursinum* L. Plant. *J. Agric. Food Chem.* **2013**, *61*, 176–184. [CrossRef] [PubMed]
16. Tomšik, A.; Pavlić, B.; Vladić, J.; Ramić, M.; Brindza, J.; Vidović, S. Optimization of Ultrasound-Assisted Extraction of Bioactive Compounds from Wild Garlic (*Allium ursinum* L.). *Ultrason. Sonochem* **2016**, *29*, 502–511. [CrossRef]
17. Wojtunik-Kulesza, K.; Oniszczuk, A.; Oniszczuk, T.; Combrzyński, M.; Nowakowska, D.; Matwijczuk, A. Influence of In Vitro Digestion on Composition, Bioaccessibility and Antioxidant Activity of Food Polyphenols—A Non-Systematic Review. *Nutrients* **2020**, *12*, 1401. [CrossRef] [PubMed]
18. Papillo, V.A.; Vitaglione, P.; Graziani, G.; Gokmen, V.; Fogliano, V. Release of Antioxidant Capacity from Five Plant Foods during a Multistep Enzymatic Digestion Protocol. *J. Agric. Food Chem.* **2014**, *62*, 4119–4126. [CrossRef]
19. Olech, M.; Kasprzak, K.; Wójtowicz, A.; Oniszczuk, T.; Nowak, R.; Waksmundzka-Hajnos, M.; Combrzyński, M.; Gancarz, M.; Kowalska, I.; Krajewska, A.; et al. Polyphenol Composition and Antioxidant Potential of Instant Gruels Enriched with *Lycium barbarum* L. Fruit. *Molecules* **2020**, *25*, 4538. [CrossRef]

20. Oniszczuk, A.; Wójtowicz, A.; Oniszczuk, T.; Olech, M.; Wojtunik-Kulesza, K.; Klimek, M.; Krawczyk, W.; Hajnos, M. Extruded Corn Gruels Containing Linden Flowers: Quantitation of Phenolic Compounds and Selected Quality Characteristics. *Open Chem.* **2015**, *13*, 1209–1217. [CrossRef]
21. Djurdjevic, L.; Dinic, A.; Pavlovic, P.; Mitrovic, M.; Karadzic, B.; Tesevic, V. Allelopathic Potential of *Allium ursinum* L. *Biochem. Syst. Ecol.* **2004**, *6*, 533–544. [CrossRef]
22. Rommel, A.; Wrolstad, R. Influence of Acid and Base Hydrolysis on the Phenolic Composition of Red Raspberry Juice. *J. Agric. Food Chem.* **1993**, *41*, 1237–1241. [CrossRef]
23. Pop, R.M.; Bocsan, I.C.; Buzoianu, A.D.; Chedea, V.S.; Socaci, S.A.; Pecoraro, M.; Popolo, A. Evaluation of the Antioxidant Activity of Nigella Sativa L. and Allium Ursinum Extracts in a Cellular Model of Doxorubicin-Induced Cardiotoxicity. *Molecules* **2020**, *25*, 5259. [CrossRef] [PubMed]
24. Multari, S.; Marsol-Vall, A.; Keskitalo, M.; Yang, B.; Suomela, J.P. Effects of Different Drying Temperatures on the Content of Phenolic Compounds and Carotenoids in Quinoa Seeds (*Chenopodium Quinoa*) from Finland. *J. Food Compos. Anal.* **2018**, *72*, 75–82. [CrossRef]
25. Sani, I.M.; Iqbal, S.; Chan, K.W.; Ismail, M. Effect of Acid and Base Catalyzed Hydrolysis on the Yield of Phenolics and Antioxidant Activity of Extracts from Germinated Brown Rice (GBR). *Molecules* **2012**, *17*, 7584–7594. [CrossRef] [PubMed]
26. Patrón-Vázquez, J.; Baas-Dzul, L.; Medina-Torres, N.; Ayora-Talavera, T.; Sánchez-Contreras, Á.; García-Cruz, U.; Pacheco, N. The Effect of Drying Temperature on the Phenolic Content and Functional Behavior of Flours Obtained from Lemon Wastes. *Agronomy* **2019**, *9*, 474. [CrossRef]
27. Korus, J.; Gumul, D.; Czechowska, K. Effect of Extrusion on the Phenolic Composition and Antioxidant Activity of Dry Beans of *Phaseolus vulgaris* L. *Food Technol. Biotechnol.* **2007**, *45*, 277375.
28. Bernardino-Nicanor, A.; Montañéz-Soto, J.L.; Vivar-Vera, M.A.; Juárez-Goiz, J.M.; Acosta-García, G.; González-Cruz, L. Effect of Drying on the Antioxidant Capacity and Concentration of Phenolic Compounds in Different Parts of the Erythrina Americana Tree. *BioResources* **2016**, *11*, 9741–9755. [CrossRef]
29. Guerrero, B.G.; Montero-Montero, J.C.; Fernández-Quintero, A.; Rivera-Agredo, Y.J.; Ospina-Patiño, B.; Gallego-Castillo, S. Assessing the Effect of Adding Maize and Rice Brans in the Development by Twin-Screw Extrusion of a Ready-to-Eat Cereal Formulated with Flours of Quality Protein Maize and Zinc Biofortified Rice. *DYNA* **2019**, *86*, 298–303. [CrossRef]
30. Schmid, V.; Trabert, A.; Schäfer, J.; Bunzel, M.; Karbstein, H.P.; Emin, M.A. Modification of Apple Pomace by Extrusion Processing: Studies on the Composition, Polymer Structures, and Functional Properties. *Foods* **2020**, *9*, 1385. [CrossRef]
31. Khanal, R.C.; Howard, L.R.; Prior, R.L. Procyanidin Content of Grape Seed and Pomace, and Total Anthocyanin Content of Grape Pomace as Affected by Extrusion Processing. *J. Food Sci.* **2009**, *74*, H174–H182. [CrossRef]
32. Ramírez-Anaya, J.D.P.; Samaniego-Sánchez, C.; Castañeda-Saucedo, M.C.; Villalón-Mir, M.; de la Serrana, H.L.-G. Phenols and the Antioxidant Capacity of Mediterranean Vegetables Prepared with Extra Virgin Olive Oil Using Different Domestic Cooking Techniques. *Food Chem.* **2015**, *188*, 430–438. [CrossRef]
33. Alonso, R.; Grant, G.; Dewey, P.; Marzo, F. Nutritional Assessment In Vitro and In Vivo of Raw and Extruded Peas (*Pisum sativum* L.). *J. Agric. Food Chem.* **2000**, *48*, 2286–2290. [CrossRef] [PubMed]
34. Yilmaz, Y.; Toledo, R. Antioxidant Activity of Water-Soluble Maillard Reaction Products. *Food Chem.* **2005**, *93*, 273–278. [CrossRef]
35. Brennan, C.; Brennan, M.; Derbyshire, E.; Tiwari, B.K. Effects of Extrusion on the Polyphenols, Vitamins and Antioxidant Activity of Foods. *Trends Food Sci. Technol.* **2011**, *22*, 570–575. [CrossRef]
36. Singh, S.; Gamlath, S.; Wakeling, L. Nutritional Aspects of Food Extrusion: A Review. *Int. J. Food Sci.* **2007**, *42*, 916–929. [CrossRef]
37. Doniec, J.; Florkiewicz, A.; Dziadek, K.; Filipiak-Florkiewicz, A. Hydrothermal Treatment Effect on Antioxidant Activity and Polyphenols Concentration and Profile of Brussels Sprouts (Brassica Oleracea Var. Gemmifera) in an In Vitro Simulated Gastrointestinal Digestion Model. *Antioxidants* **2022**, *11*, 446. [CrossRef]
38. Schulze, K. Imaging and Modelling of Digestion in the Stomach and the Duodenum. *Neurogastroenterol. Motil.* **2006**, *18*, 172–183. [CrossRef]
39. Clarysse, S.; Tack, J.; Lammert, F.; Duchateau, G.; Reppas, C.; Augustijns, P. Postprandial Evolution in Composition and Characteristics of Human Duodenal Fluids in Different Nutritional States. *J. Pharm. Sci.* **2009**, *98*, 1177–1192. [CrossRef]
40. Dupont, D.; Alric, M.; Blanquet-Diot, S.; Bornhorst, G.; Cueva, C.; Deglaire, A.; Denis, S.; Ferrua, M.; Havenaar, R.; Lelieveld, J.; et al. Can Dynamic In Vitro Digestion Systems Mimic the Physiological Reality? *Crit. Rev. Food Sci. Nutr.* **2019**, *59*, 1546–1562. [CrossRef]
41. Mateo Anson, N.; van den Berg, R.; Havenaar, R.; Bast, A.; Haenen, G.R.M.M. Bioavailability of Ferulic Acid Is Determined by Its Bioaccessibility. *J. Cereal Sci.* **2009**, *49*, 296–300. [CrossRef]
42. Siracusa, L.; Kulisic-Bilusic, T.; Politeo, O.; Krause, I.; Dejanovic, B.; Ruberto, G. Phenolic Composition and Antioxidant Activity of Aqueous Infusions from *Capparis spinosa* L. and *Crithmum maritimum* L. before and after Submission to a Two-Step In Vitro Digestion Model. *J. Agric. Food Chem.* **2011**, *59*, 12453–12459. [CrossRef]
43. Baeza, G.; Sarriá, B.; Bravo, L.; Mateos, R. Polyphenol Content, in Vitro Bioaccessibility and Antioxidant Capacity of Widely Consumed Beverages. *J. Sci. Food Agric.* **2018**, *98*, 1397–1406. [CrossRef]
44. Dacrema, M.; Sommella, E.; Santarcangelo, C.; Bruno, B.; Marano, M.G.; Insolia, V.; Saviano, A.; Campiglia, P.; Stornaiuolo, M.; Daglia, M. Metabolic Profiling, In Vitro Bioaccessibility and in Vivo Bioavailability of a Commercial Bioactive *Epilobium angustifolium* L. Extract. *Biomed Pharm.* **2020**, *131*, 110670. [CrossRef]

45. Kamiloglu, S.; Capanoglu, E.; Bilen, F.D.; Gonzales, G.B.; Grootaert, C.; Van de Wiele, T.; Van Camp, J. Bioaccessibility of Polyphenols from Plant-Processing Byproducts of Black Carrot (*Daucus carota* L.). *J. Agric. Food Chem.* **2016**, *64*, 2450–2458. [CrossRef]
46. Majdoub, Y.O.E.; Ginestra, G.; Mandalari, G.; Dugo, P.; Mondello, L.; Cacciola, F. The Digestibility of *Hibiscus sabdariffa* L. Polyphenols Using an In Vitro Human Digestion Model and Evaluation of Their Antimicrobial Activity. *Nutrients* **2021**, *13*, 2360. [CrossRef]
47. Gayoso, L.; Claerbout, A.-S.; Calvo, M.I.; Cavero, R.Y.; Astiasarán, I.; Ansorena, D. Bioaccessibility of rutin, caffeic acid and rosmarinic acid: Influence of the in vitro gastrointestinal digestion models. *J. Funct. Foods* **2016**. [CrossRef]
48. Tagliazucchi, D.; Verzelloni, E.; Bertolini, D.; Conte, A. In Vitro Bio-Accessibility and Antioxidant Activity of Grape Polyphenols. *Food Chem.* **2010**, *120*, 599–606. [CrossRef]
49. Cristea, E.; Sturza, R.; Jauregi, P.; Niculaua, M.; Ghendov-Moșanu, A.; Patras, A. Influence of PH and Ionic Strength on the Color Parameters and Antioxidant Properties of an Ethanolic Red Grape Marc Extract. *J. Food Biochem.* **2019**, *43*, e12788. [CrossRef] [PubMed]
50. Materska, M.; Olszówka, K.; Chilczuk, B.; Stochmal, A.; Pecio, Ł.; Pacholczyk-Sienicka, B.; Piacente, S.; Pizza, C.; Masullo, M. Polyphenolic Profiles in Lettuce (*Lactuca sativa* L.) after $CaCl_2$ Treatment and Cold Storage. *Eur. Food Res. Technol.* **2019**, *245*, 733–744. [CrossRef]
51. Altunkaya, A.; Gökmen, V.; Skibsted, L.H. PH Dependent Antioxidant Activity of Lettuce (*L. Sativa*) and Synergism with Added Phenolic Antioxidants. *Food Chem.* **2016**, *190*, 25–32. [CrossRef]
52. Sun, H.-N.; Mu, T.-H.; Xi, L.-S. Effect of PH, Heat, and Light Treatments on the Antioxidant Activity of Sweet Potato Leaf Polyphenols. *Int. J. Food Prop.* **2017**, *20*, 318–332. [CrossRef]
53. Kong, F.; Singh, R.P. A Human Gastric Simulator (HGS) to Study Food Digestion in Human Stomach. *J. Food Sci.* **2010**, *75*, E627–E635. [CrossRef] [PubMed]
54. Czaban, J.; Sułek, A.; Pecio, Ł.; Zuchowski, J.; Podolska, G. Effect of Genotype and Crop Management Systems on Phenolic Acid Content in Winter Wheat Grain. *J. Food Agric. Environ.* **2013**, *11*, 1201–1206.
55. Burda, S.; Oleszek, W. Antioxidant and Antiradical Activities of Flavonoids. *J. Agric. Food Chem.* **2001**, *49*, 2774–2779. [CrossRef] [PubMed]

International Journal of
Molecular Sciences

MDPI

Article

Selectively Halogenated Flavonolignans—Preparation and Antibacterial Activity

Martina Hurtová [1,2], Kristýna Káňová [1], Simona Dobiasová [2], Kateřina Holasová [2], Denisa Čáková [2], Lan Hoang [2], David Biedermann [1], Marek Kuzma [1], Josef Cvačka [3], Vladimír Křen [1], Jitka Viktorová [2] and Kateřina Valentová [1,*]

[1] Institute of Microbiology of the Czech Academy of Sciences, Vídeňská 1083, 142 20 Prague, Czech Republic
[2] Department of Biochemistry and Microbiology, University of Chemistry and Technology Prague, Technická 5, 166 28 Prague, Czech Republic
[3] Institute of Organic Chemistry and Biochemistry of the Czech Academy of Sciences, Flemingovo nám. 542, 160 00 Prague, Czech Republic
* Correspondence: kata.valentova@email.cz

Abstract: A library of previously unknown halogenated derivatives of flavonolignans (silybins A and B, 2,3-dehydrosilybin, silychristin A, and 2,3-dehydrosilychristin A) was prepared. The effect of halogenation on the biological activity of flavonolignans was investigated. Halogenated derivatives had a significant effect on bacteria. All prepared derivatives inhibited the AI-2 type of bacterial communication (quorum sensing) at concentrations below 10 μM. All prepared compounds also inhibited the adhesion of bacteria (*Staphyloccocus aureus* and *Pseudomonas aeruginosa*) to the surface, preventing biofilm formation. These two effects indicate that the halogenated derivatives are promising antibacterial agents. Moreover, these derivatives acted synergistically with antibiotics and reduced the viability of antibiotic-resistant *S. aureus*. Some flavonolignans were able to reverse the resistant phenotype to a sensitive one, implying that they modulate antibiotic resistance.

Keywords: flavonoids; flavonolignans; halogenation; biological activity; multidrug resistance; bacteria

Citation: Hurtová, M.; Káňová, K.; Dobiasová, S.; Holasová, K.; Čáková, D.; Hoang, L.; Biedermann, D.; Kuzma, M.; Cvačka, J.; Křen, V.; et al. Selectively Halogenated Flavonolignans—Preparation and Antibacterial Activity. *Int. J. Mol. Sci.* **2022**, *23*, 15121. https://doi.org/10.3390/ijms232315121

Academic Editor: Dmitry Aminin

Received: 9 November 2022
Accepted: 28 November 2022
Published: 1 December 2022

1. Introduction

Halogen-containing compounds have an outstanding position in medicinal chemistry. Natural products containing halogens are widely distributed in marine organisms and possess numerous interesting biological activities. For example, briarane diterpenoids containing chlorine have been shown to have antibacterial activity [1], hemigerans containing bromine exhibited antifungal activity against *Saccharomyces cerevisiae* [2], and prulonide A (containing both chlorine and bromine) isolated from *Synoicum* showed cytotoxicity against breast cancer cell lines at a concentration of 1 μM [3]. Synthetic halides are commonly used as drugs; e.g., the antimetabolite 5-fluorouracil is used in cancer treatment [4]. Natural products are often altered by synthetic modifications to improve their biological activity. Flavopiridol, a semisynthetic chlorinated flavonoid, is currently undergoing clinical trials as a potent cyclin-dependent kinase 2 inhibitor [5,6].

Flavonoids (e.g., taxifolin (**1**) and quercetin (**2**)) are phenolic secondary metabolites found in plants and fungi. They usually have beneficial biological effects, such as antioxidant, antimutagenic, and anti-inflammatory activities [7]. Flavonolignans form a small subclass of flavonoids, which are mainly isolated from silymarin (extract from the fruits of milk thistle *Silybum marianum*). Silymarin contains mainly silybin AB (**3**), silychristin A (**5**), silydianin, isosilybin AB, and, as minor components, 2,3-dehydrosilybin AB (**4**), 2,3-dehydrosilychristin A (**6**), (Figure 1), taxifolin (**1**), some minor flavonoids, and ca. 30% of a polymeric phenolic fraction [8,9]. These compounds and their derivatives generally have low toxicity and interesting biological activity, such as hepatoprotective activity, anti-inflammatory activity, antioxidant activity, and the ability to modulate the pumps associated with multidrug resistance [8,10–12].

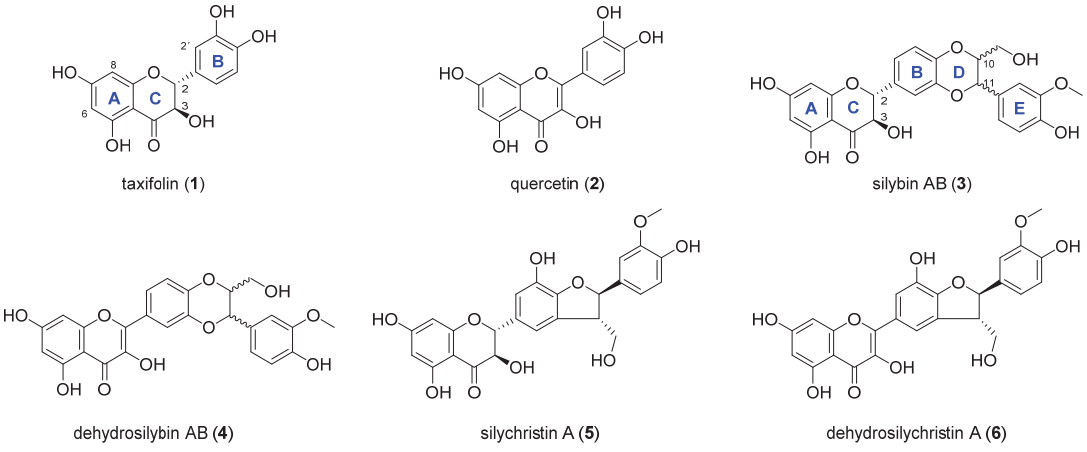

Figure 1. Structure of selected flavonols and flavonolignans.

The halogenation of flavonoids has been described only for taxifolin and quercetin. Brominated derivatives of quercetin can generally be prepared by the reaction with elemental bromine or with *N*-bromosuccinimide (NBS) [13]. The reaction with elemental bromine leads to a complex mixture of brominated compounds. High regioselectivity of bromination with NBS was achieved only when quercetin was protected at groups 5-OH and 7-OH (methyl, ethyl, isopropyl) [14]. Dibromination of taxifolin was carried out with two equivalents of NBS. Monobrominated taxifolin was prepared by selective debromination of 6,8-dibromotaxifolin with Na_2SO_3 and $NaHCO_3$ [15].

We have recently developed a new method using α,β-dibromohydrocinnamic acid (DBHCA) for the selective monobromination and dibromination of flavonoids [16]. This method allows substitution exclusively at C-6 in flavonoids saturated at C-2, C-3 (taxifolin (**1**), silybin AB (**3**), silychristin A (**5**)), and C-8 in 2,3-unsaturated flavonoids (quercetin (**2**), 2,3-dehydrosilybin AB (**4**), 2,3-dehydrosilychristin A (**6**)). Here, the bromine is eliminated in situ from DBHCA to form cinnamic acid. Dibromination of flavonolignans at C-6 and C-8 can be achieved at higher temperatures [16].

The chlorination of quercetin at C-6, C-8, and C-3 was previously performed with hypochlorous acid (HOCl) [17]. Freitas et al. described the mono- and dichlorination of quercetin at C-6, C-8, or C-3 with *N*-chlorosuccinimide (NCS) [18]. Iodinated derivatives were prepared with *N*-iodosuccinimide (NIS) on selectively protected quercetin (methyl, ethyl, isopropyl, and benzyl). This method yields an iodinated product at C-6 in the case of protection at group 7-OH. When both the 5-OH and 7-OH groups were protected, iodination occurred at C-8 [19].

Electrophilic fluorination of the A-ring of flavonoids has not yet been described. Fluorinated derivatives of flavones were prepared from fluorinated synthones by various semisynthetic methods, e.g., cyclodehydration of 1-(2-hydroxyphenyl-5-fluoro)-3-aryl-1,3-propanodiones [20] or a reaction of 1-(2-bromo-4-fluorophenyl)-3-phenylprop-2-yn-1-one with benzaldehyde oxime in the presence of a base [21]. In addition, 8-trifluoromethyl-3,5,7,3′,4′-*O*-pentamethyl-quercetin was prepared using Chen's reagent (methyl fluorosulfonyldifluoroacetate) [22].

Chlorination of quercetin substantially improved anti-inflammatory activity [23] and antioxidant activity [17], compared with that of the parent molecule. Mono- and dibromination of quercetin increased antiviral activity [13] and lipophilicity, which facilitated the transport across the cell membrane [24], while 8-trifluoromethyl-3,5,7,3′,4′-*O*-pentamethyl-quercetin blocked bladder cancer cell growth and promoted apoptotic progression more effectively than quercetin [22]. Unfortunately, some of the reported in vitro studies were performed using mixtures of products, not pure halogenated compounds.

Based on previously published work on the enhancement of biological activity by halogenation, our goal was to prepare a library of novel selectively halogenated derivatives of silymarin flavonolignans that would serve as a platform for further synthetic modifications and basic physicochemical and biological evaluations to identify new lead structures. Since the biological activity of halogenated derivatives of taxifolin (**1**) and quercetin (**2**) has been studied only in mixtures, we prepared their pure brominated derivatives to determine their biological activity. Specifically, the abilities of the halogenated derivatives to inhibit bacterial communication and biofilm formation and to modulate antibiotic resistance in bacteria, as well as their antiradical, reducing, anti-lipoperoxidant, cytotoxic, and anti-inflammatory activities and their ability to modulate doxorubicin-resistant phenotypes in human ovarian carcinoma cells, were evaluated and compared to their parent compounds.

2. Results and Discussion

2.1. Chemistry

Monobrominated derivatives were prepared from the respective flavonoid, employing our original method for selective monobromination using DBHCA in the presence of Cs_2CO_3. The selectivity of this reaction was controlled by using different bases, e.g., K_2CO_3, and higher temperatures to prepare dibrominated derivatives (Scheme 1) [16].

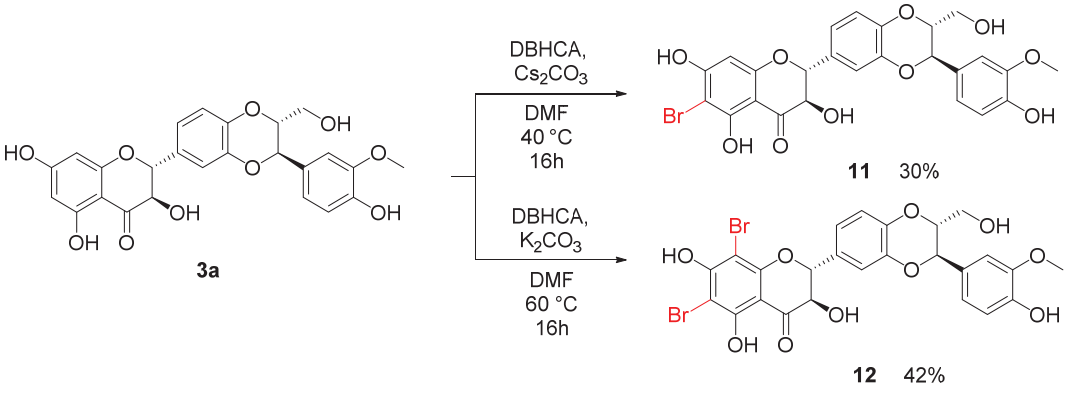

Scheme 1. Use of α,β-dibromohydrocinnamic acid (DBHCA) for bromination of silybin A [16]. Bromines are highlighted in red.

The bromination of silybin with one equivalent of NBS afforded the mixture of mono- and dibrominated product and unreacted starting material (ratio 1:1:1, determined by HPLC). The low yield and complicated separation made this reaction impractical. Di- and tribrominated derivatives were prepared by electrophilic substitution with different concentrations of NBS (Scheme 2).

The use of different concentrations of NBS revealed that the most reactive positions for an electrophilic attack in the flavonolignan structure are C-6 and C-8. The use of four equivalents of NBS with silychristin A (**5**) yielded a mixture of 6,8,19-tribromosilychristin A (**23**) and 6,8,12,19-tetrabromosilychristin A (**29**). The use of four equivalents of NBS with silybin A (**3a**) afforded a complex mixture of inseparable polybrominated products. Monobrominated derivatives at C-8 (8-bromosilybin A (**19**) and 8-bromosilybin B (**20**)) were prepared in good yields by selective dehalogenation reaction of 6,8-dibromosilybin A (**12**) and 6,8-dibromosilybin B (**14**) in the presence of Na_2SO_3 and $NaHCO_3$.

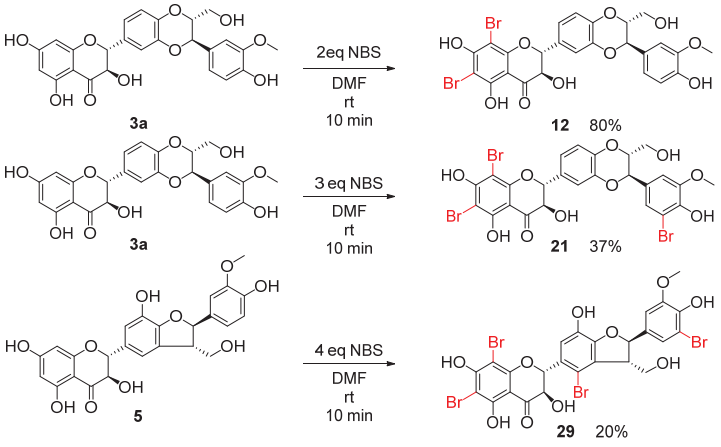

Scheme 2. Bromination of silybin A (**3a**) and silychristin A (**5**) using different concentrations of NBS. Bromines are highlighted in red.

Iodinated derivatives of 2,3-saturated flavonoids (taxifolin (**1**), silybin AB (**3**), silychristin A (**5**)) were prepared in good yields using NIS. Diiodinated derivatives were prepared using two equivalents of NIS and 8-iodosilybin B (**24**) was prepared by selective dehalogenation of 6,8-diiodosilybin B (**26**) with Na_2SO_3 and $NaHCO_3$ in excellent yields (97%) (Scheme 3).

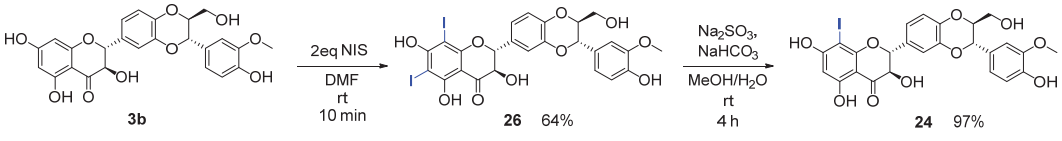

Scheme 3. The preparation of iodinated derivatives of silybin B (**24**, **26**). Iodines are highlighted in blue.

Iodinated 2,3-unsaturated derivatives (quercetin (**2**), 2,3-dehydrosilybin AB (**4**), 2,3-dehydrosilychristin A (**6**)) were highly unstable and their decomposition was observed by NMR analysis, yielding a complex mixture of uncharacterized products. All iodinated derivatives of 2,3-saturated flavonoids exhibited low stability during storage and were decomposed to a mixture of the respective 8-iodo derivative and/or the deiodinated compound.

A mixture of monochlorinated derivatives at C-6 and C-8 of silybin was prepared using one equivalent of NCS. The use of more equivalents of NCS resulted in a mixture of inseparable (poly)chlorinated compounds.

All derivatives prepared for the biological tests are summarized in Figures 2 and 3.

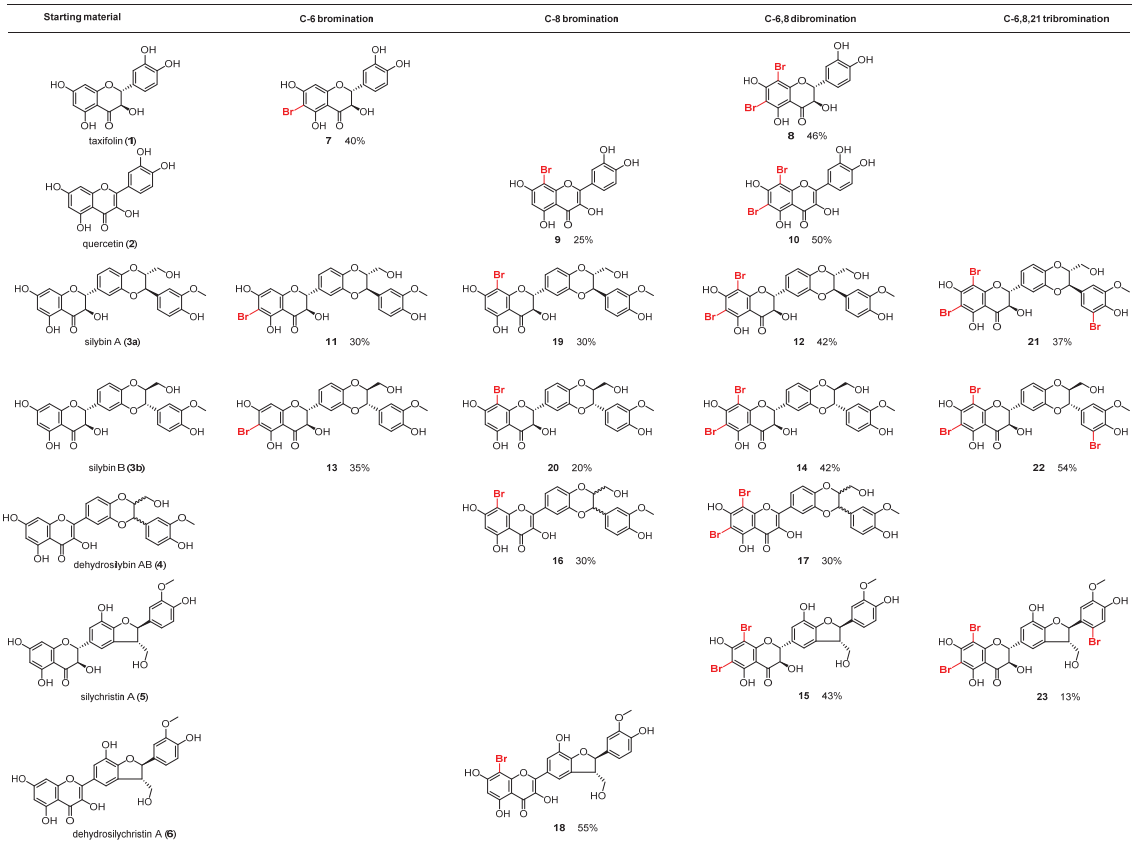

Figure 2. Prepared brominated derivatives of flavonoids. Bromines are highlighted in red.

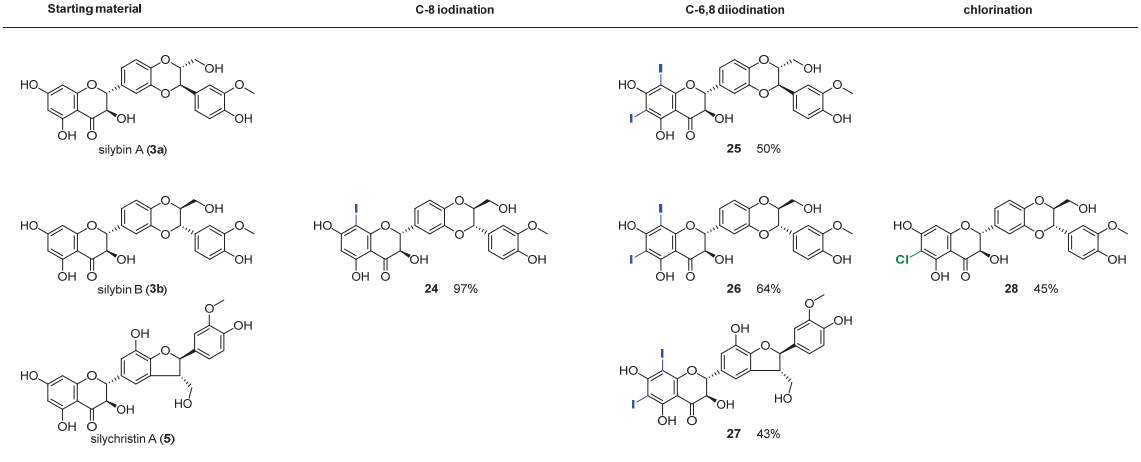

Figure 3. Prepared iodinated and chlorinated derivatives of flavonolignans. Iodinies are highlighted in blue.

Fluorination of silybin AB (**3**) with diethylaminosulfur trifluoride (DAST) yielded a mixture of products containing, mainly, the product of oxidation (dehydrogenation)

at C-2. The reaction of quercetin with Selectfluor (1-fluoro-4-methyl-1,4-diazoniabicyclo [2.2.2]octane-bis-(tetrafluoroborate)) led to the oxidation of the C-ring, forming a five-membered benzofuranone ring (Scheme 4).

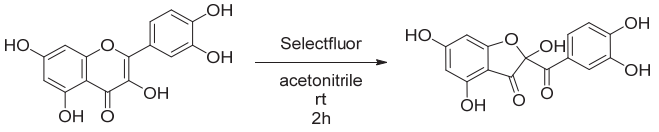

3 **29** 20%

Scheme 4. The reaction of quercetin (**2**) with Selectfluor led to the contraction of the C-ring, affording compound **29**.

All of the above fluorinating agents are very strong oxidative reagents that are not suitable for use with oxidation-prone compounds such as flavonoids. The formation of the Grignard reagent using Mg with 8-iodo-3,3′,4′,5,7-penta-*O*-isopropylquercetin or 8-bromo-3,3′,4′,5,7-penta-*O*-isopropylquercetin and the reaction with Xtalfluor were not successful. Therefore, the electrophilic fluorination of flavonoids remains a major challenge.

2.2. Biological Activity

Recently, we discovered that flavonolignans modulate antibiotic resistance and virulence of *Staphylococcus aureus* by affecting the corresponding efflux pumps [12]. Moderately lipophilic structures are required for this type of biological activity, which involves the interaction with cell membranes and transmembrane proteins [25]. Because bromination increases lipophilicity [24], all prepared compounds were tested for their potential to inhibit bacterial communication (quorum sensing), surface colonization (biofilm formation), and the modulation of antibiotic resistance in both Gram-positive and Gram-negative bacteria.

2.2.1. Inhibition of Bacterial Communication

Bacterial intercellular communication (quorum sensing) is the process by which bacteria determine (sense) the number (quorum) of bacterial cells in their environment. In this cell-to-cell chemical communication, bacteria produce small molecules—autoinducers (AI)—that are secreted into the extracellular environment and, at the same time, determine their quantity in their environment via transmembrane receptors. When autoinducers are present in sufficient concentrations, the signaling pathway is activated, significantly altering the expression profile of bacteria. As a result, bacterial toxins and virulence factors can be produced, or biofilm formation and sporulation may occur [26].

Commercially available strains of *Vibrio campbellii* were used to evaluate the ability of flavonoids and their derivatives to inhibit bacterial quorum sensing. *V. campbellii* uses two types of autoinducing molecules for its communication—*N*-acyl-homoserine lactones (Autoinducer I, AI-1, strain BAA 1118) and furanosyl borate diester (Autoinducer II, AI-2, strain BAA 1119) [27]. AI-1-based communication is mainly used by Gram-negative bacteria, while AI-2-based communication is found in both Gram-negative and Gram-positive bacteria. The mutant strains of *V. campbellii* BA1118 and BA1119 respond only to AI-1 or AI-2, respectively, and the response to the respective AI concentration is measured as luminescence. The higher the AI concentration, the higher the luminescence signal. The ability to inhibit the communication was expressed as the selectivity index (SI), calculated as the ratio between the concentration that halved the viability (IC_{50}) and the concentration that halved the communication (EC_{50}) of the respective *V. campbellii* strains. The higher the SI, the better the inhibitor, and this allows for better dosing at concentrations that are not themselves antimicrobial. The antimicrobial activity of quorum-sensing inhibitors is undesirable because it creates a selection pressure and can lead to the development of resistance. The measured data of the parent flavonoids and their halogenated derivatives are summarized in Table 1.

Table 1. The ability of flavonoids and their derivatives to inhibit communication was expressed as the selectivity index (SI), calculated as the ratio between the concentration that halved the viability (IC_{50}, μM) and the concentration that halved the communication (EC_{50}, μM) of *V. campbellii* BA1118 and BA1119 strains that respond only to autoinducer 1 (AI-1) or AI-2, respectively.

	Vibrio campbellii **BAA 1118 (AI-1)**				*Vibrio campbellii* **BAA 1119 (AI-2)**			
	EC_{50} [μM]	**IC_{50} [μM]**	**SI**	**SA $**	**EC_{50} [μM]**	**IC_{50} [μM]**	**SI**	**SA $**
Taxifolin (**1**)	63.7 ± 2.7	71.0 ± 3.0	1.1 ± 0.1	E	7.3 ± 0.3	80.0 ± 1.7	11.0 ± 0.6	A
6-Bromotaxifolin (**7**)	38.9 ± 1.6	59.0 ± 0.1	1.5 ± 0.1	*	11.9 ± 0.5	19.7 ± 1.0	1.7 ± 0.2	***
6,8-Dibromotaxifolin (**8**)	38.1 ± 2.0	55.5 ± 1.0	1.5 ± 0.1	*	10.1 ± 0.4	109.3 ± 0.8	10.8 ± 0.6	
Quercetin (**2**)	15.9 ± 0.5	24.5 ± 0.8	1.5 ± 0.1	C, D	4.8 ± 0.2	10.6 ± 0.5	2.2 ± 0.2	C
8-Bromoquercetin (**9**)	25.6 ± 0.5	27.8 ± 0.5	1.08 ± 0.04	*****	0.4 ± 0.02	1.1 ± 0.1	2.9 ± 0.3	*****
6,8-Dibromoquercetin (**10**)	7.3 ± 0.4	13.8 ± 0.5	1.9 ± 0.2	**	0.7 ± 0.02	3.5 ± 0.1	5.0 ± 0.3	**
Silybin A (**3a**)	97.1 ± 1.0	131.0 ± 3.7	1.3 ± 0.1	D	17.1 ± 0.5	119.6 ± 3.1	7.0 ± 0.4	B
6-Bromosilybin A (**11**)	24.4 ± 0.7	51.7 ± 0.7	2.1 ± 0.1	*****	9.4 ± 0.5	51.5 ± 0.6	5.5 ± 0.3	*
8-Bromosilybin A (**19**)	33.9 ± 1.8	114.9 ± 5.4	3.4 ± 0.3	***	4.6 ± 0.3	>200	≥43.1 ± 2.6	***
6,8-Dibromosilybin A (**12**)	12.2 ± 0.4	23.5 ± 1.0	1.9 ± 0.2	***	13.2 ± 0.3	80.5 ± 4.8	6.1 ± 0.5	
6,8,21-Tribromosilybin A (**21**)	>200	>200			30.7 ± 1.6	>200	≥6.5 ± 0.3	
Silybin B (**3b**)	121.5 ± 0.6	116.6 ± 0.9	0.96 ± 0.01	E	22.3 ± 0.5	152.4 ± 2.4	6.8 ± 0.2	B
6-Bromosilybin B (**13**)	14.5 ± 0.5	16.1 ± 0.1	1.11 ± 0.04	*	26.1 ± 1.3	52.7 ± 0.6	2.0 ± 0.1	*****
6-Chlorosilybin B (**28**)	114.2 ± 5.0	130.1 ± 5.9	1.1 ± 0.1		3.2 ± 0.2	>200	≥62.6 ± 3.6	***
8-Bromosilybin B (**20**)	44.2 ± 0.7	126.6 ± 4.0	2.9 ± 0.1	***	4.7 ± 0.2	200	≥42.9 ± 2.1	***
6,8-Dibromosilybin B (**14**)	14.7 ± 0.7	16.6 ± 0.8	1.1 ± 0.1		19.3 ± 0.5	60.2 ± 3.4	3.1 ± 0.3	*****
6,8,21-Tribromosilybin B (**22**)	4.3 ± 0.3	7.3 ± 0.1	1.7 ± 0.1	*	12.0 ± 0.5	34.4 ± 1.8	2.9 ± 0.3	****
2,3-Dehydrosilybin AB (**4**)	59.9 ± 2.0	163.2 ± 3.8	2.7 ± 0.2	A	10.2 ± 0.4	25.3 ± 1.0	2.5 ± 0.2	C
8-Bromo-2,3-dehydrosilybin AB (**16**)	>200	>200			6.9 ± 0.3	87.0 ± 2.5	12.7 ± 1.0	*****
6,8-Dibromo-2,3-dehydrosilybin AB (**17**)	55.5 ± 1.6	>200	≥3.6 ± 0.1	***	4.1 ± 0.2	126.8 ± 7.4	31.2 ± 3.5	****
Silychristin A (**5**)	>200	>200			>200	>200		
6,8-Dibromosilychristin A (**15**)	>200	>200			>200	>200		
2,3-dehydrosilychristin A (**6**)	22.3 ± 1.0	43.0 ± 1.5	1.9 ± 0.2	B	11.1 ± 0.1	11.0 ± 0.4	0.99 ± 0.05	D
8-Bromo-2,3-dehydrosilychristin A (**18**)	29.4 ± 0.7	80.1 ± 1.7	2.7 ± 0.1	**	10.5 ± 0.2	23.0 ± 0.2	2.2 ± 0.1	*****
5-Fluorouracil (PC)	(0.39 ± 0.05) × 10^{-3}	(0.68 ± 0.01) × 10^{-3}	1.73 ± 0.05	B, C	(0.44 ± 0.03) × 10^{-3}	(3.41 ± 0.03) × 10^{-3}	7.8 ± 0.5	B

The data are presented as the average of three repetitions with the standard error. $ Statistical analysis (SA): *t*-test was used for the comparison of the halogenated derivative and its parent compound (* $p \leq 0.05$, ** $p \leq 0.01$, *** $p \leq 0.005$, **** $p \leq 0.001$, ***** $p \leq 0.0005$). ANOVA with Duncan's post hoc test was used for the comparison of parent compounds and positive control (PC) 5-fluorouracil (different capital letters indicate significant differences).

AI-1-type communication was inhibited by 2,3-dehydrosilybin AB (**4**) (SI 2.7, EC_{50} = 59.9 μM) and 2,3-dehydrosilychristin A (**6**) (SI 1.9, EC_{50} = 22.3 μM) (Table 1), while 8-bromination significantly improved the activity, especially in the case of silybin A (**19**, SI 3.4), silybin B (**20**, SI 2.9), and 2,3-dehydrosilychristin A (**18**, SI 2.7). Of all the compounds, 6,8-dibromodehydrosilybin AB (**17**, SI > 3.6) was the most promising for inhibiting AI-1, which is consistent with the previously reported inhibition of AI-1-type quorum sensing by several flavonoids [28], along with the hypothesis that halogenation may enhance this ability [29].

AI-2-type communication was significantly inhibited by the parent compounds taxifolin (**1**) (SI 11.0, EC_{50} = 7.3 μM), silybin A (**3a**) (SI 7.0, EC_{50} = 17.1 μM), and silybin B (**3b**) (SI 6.8, EC_{50} = 22.3 μM). The ability of flavonolignans to inhibit AI-2-type communication was significantly increased for all 8-bromo derivatives, namely quercetin (**9**), silybin A (**19**), silybin B (**20**), 2,3-dehydrosilybin AB (**16**), and 2,3-dehydrosilychristin A (**18**), as well as in the cases of 6-chlorosilybin B (**28**), 6,8-dibromoquercetin (**10**), and 6,8,21-tribromosilybin A (**21**). In such cases, halogenation significantly improved the selectivity index.

This work contains the first study of the effects of halogenation on the ability of flavonoids to inhibit bacterial communication. In the case of AI-2-based communication, brominated derivatives inhibited activity with an EC_{50} value below 10 μM, and toxicity against bacteria was very low. Compounds capable of affecting bacterial communication have promising therapeutic potential in the field of regulating bacterial virulence [30]. We also suggest that chlorinated derivatives of flavonoids may be the most promising inhibitors of bacterial communication. Unfortunately, their preparation was not successfully optimized in this work, due to the high reactivity of chlorine in electrophilic substitutions.

2.2.2. Effect on Biofilm Formation

Biofilm formation is a fully organized, multistep process in which bacteria are constantly communicating with each other. We found that most tested flavonoids and their derivatives inhibited bacterial cell-to-cell communication; accordingly, their ability to affect the surface adhesion of Gram-positive (*S. aureus*) and Gram-negative (*Pseudomonas aeruginosa*) bacteria was also investigated.

The inhibition of *P. aeruginosa* biofilm formation was only observed for silybin A (**3a**, IC_{50} = 77 μM), silybin B (**3b**, IC_{50} = 105 μM), and silychristin A (**5**, IC_{50} = 73 μM). Except for quercetin (**2**), all compounds inhibited *S. aureus* biofilm formation, with an IC_{50} value of less than 100 μM. In all cases, halogenation resulted in a significant increase in inhibitory activity, compared with that of the parent compounds with an IC_{50} value mostly below 10 μM (Figure 4).

Disruption of the matured biofilm was not detected by any of the tested flavonoids or their derivatives, up to a concentration of 100 μM.

Flavonoids (myricetin, hesperetin, and phloretin) have previously been reported to inhibit *S. aureus* biofilm formation at concentrations of 4 μM and less [31]. Our work is the first to report the effect of halogenation on the ability of flavonoids to inhibit biofilm formation.

2.2.3. Modulation of Antibiotic-Resistant Phenotype in Resistant Bacteria

The ability of the compounds to modulate the antibiotic-resistant phenotype in resistant bacteria was also investigated. To use flavonoids as modulators of antibiotic resistance, they should not, themselves, possess antimicrobial activity. Multidrug-resistant clinical strains of *P. aeruginosa* and *S. aureus* were incubated with the concentration range of flavonoids and their halogenated derivatives to determine antimicrobial activity. Neither of the tested derivatives exhibited antimicrobial activity. None of the compounds tested were able to halve bacterial growth below a concentration of 100 μM.

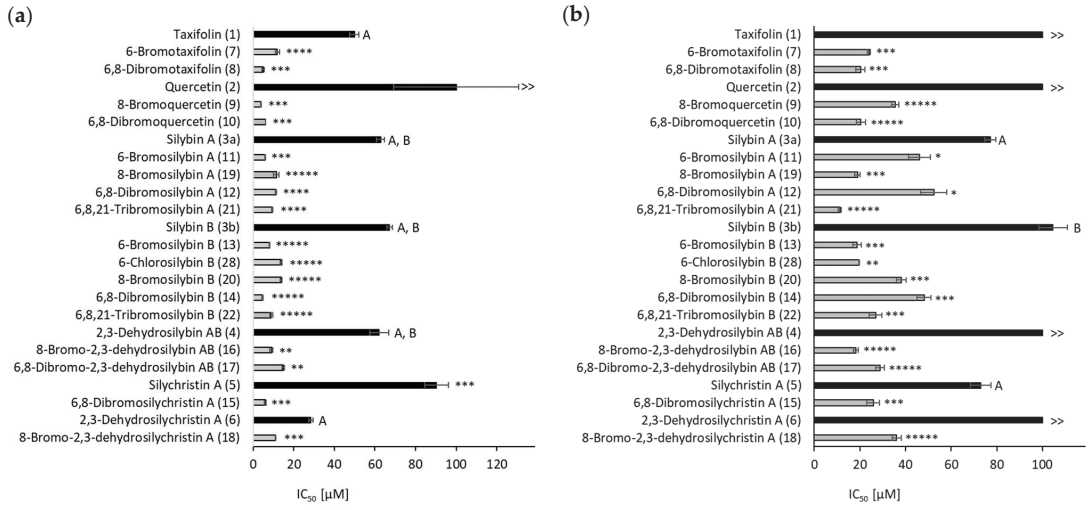

Figure 4. Inhibition of *S. aureus* (ATCC, 25923) (**a**) and *P. aeruginosa* (CCM, 3955) (**b**) surface colonization by flavonoids and their halogenated derivatives. The data are presented as the average of three repetitions with the standard error. A *t*-test was used for the comparison of the halogenated derivative and its parent compound (* $p \leq 0.05$, ** $p \leq 0.01$, *** $p \leq 0.005$, **** $p \leq 0.001$, ***** $p \leq 0.0005$). ANOVA with Duncan´s post hoc test was used for the comparison of the parent compounds (different capital letters to the right of the respective bars indicate significant differences).

Clinically relevant antibiotics were selected for sensitization testing according to the European Committee on Antimicrobial Susceptibility Testing (EUCAST). Neither colistin and imipenem at breakpoint concentrations (according to EUCAST, 4 mg/mL imipenem and 2 mg/mL colistin) affected the growth of the multidrug-resistant clinical strain of *P. aeruginosa*. Similarly, neither chloramphenicol and gentamicin at breakpoint concentrations (8 mg/mL and 1 mg/mL, respectively) affected the multidrug-resistant clinical strain of *S. aureus*. Flavonoids and their derivatives (1–40 μM) were used in combination therapy, along with the breakpoint concentration of antibiotics. After co-incubation, the minimum inhibitory concentration of flavonoids inhibiting the visible growth of bacteria was determined (Table 2).

None of the compounds tested affected the sensitivity of *P. aeruginosa* to imipenem: 8-bromo-2,3-dehydrosilybin AB (**16**) reversed the colistin-resistant phenotype in *P. aeruginosa* to a sensitive one, while 6,8-dibromo-2,3-dehydrosilybin AB (**17**) reduced growth to 47%. The chloramphenicol-resistant phenotype of *S. aureus* was not affected by the flavonoids or halogenated derivatives. Only 2,3-dehydrosilychristin A (**6**, 40 μM) reduced its growth, to 69%. The gentamicin-resistant phenotype of *S. aureus* was reversed by 5 μM 2,3-dehydrosilybin AB (**4**) and the growth of this multidrug-resistant strain was reduced to 37% by the addition of 40 μM taxifolin (**1**).

The 2,3-saturated parent flavonolignans (silybins and silychristin) had no sensitizing potential, but their bromination significantly enhanced this activity in gentamicin-resistant *S. aureus*. Moreover, the presence of an additional bromine atom on the E ring in 6,8,21-tribromosilybin A (**21**) and 6,8,21-tribromosilybin B (**22**) further enhanced this activity and reversed the resistant phenotype to a sensitive one, at 40 μM.

Table 2. Viability of multidrug-resistant *P. aeruginosa* and *S. aureus* cultivated in the combination of breakpoint antibiotic concentration (according to EUCAST) and flavonoid (40 μM, unless otherwise stated).

	Pseudomonas aeruginosa		*Staphylococcus aureus*	
	Imipenem	**Colistin**	**Chloramphenicol**	**Gentamicin**
	4 mg/L	**2 mg/L**	**8 mg/L**	**1 mg/L**
Taxifolin (1)	-	-	-	37 ± 1%
6-Bromotaxifolin (**7**)	-	-	-	46 ± 4%
6,8-Dibromotaxifolin (**8**)	-	-	-	54 ± 5%
Quercetin (2)	-	-	-	-
8-Bromoquercetin (**9**)	-	-	-	-
6,8-Dibromoquercetin (**10**)	-	-	-	-
Silybin A (**3a**)	-	-	-	-
6-Bromosilybin A (**11**)	-	-	-	37 ± 1%
8-Bromosilybin A (**19**)	-	-	-	41 ± 3%
6,8-Dibromosilybin A (**12**)	-	-	-	40 ± 1%
6,8,21-Tribromosilybin A (**21**)	-	-	-	reversion of resistance
Silybin B (**3b**)	-	-	-	-
6-Bromosilybin B (**13**)	-	-	-	67 ± 4%
6-Chlorosilybin B (**28**)	-	-	-	34 ± 2%
8-Bromosilybin B (**20**)	-	-	-	48 ± 9%
6,8-Dibromosilybin B (**14**)	-	-	-	41 ± 1%
6,8,21-Tribromosilybin B (**22**)	-	-	-	reversion of resistance
2,3-Dehydrosilybin AB (**4**)	-	-	-	reversion of resistance [5 μM]
8-Bromo-2,3-dehydrosilybin AB (**16**)	-	reversion of resistance	-	-
6,8-Dibromo-2,3-dehydrosilybin AB (**17**)	-	47 ± 3%	-	-
Silychristin A (**5**)	-	-	-	-
6,8-Dibromosilychristin A (**15**)	-	-	-	viability 63 ± 3%
2,3-Dehydrosilychristin A (**6**)	-	-	69 ± 4% [10 μM]	-
8-Bromo-2,3-dehydrosilychristin A (**18**)	-	-	-	-
Sulbactam (**PC**)	-	-	reversion of resistance	-

The data are presented as the average of three repetitions with the standard error. Neither antibiotic nor flavonoid affects the cell viability if applied separately. "-" indicates that no effect (100% viability) was observed up to the highest flavonolignan concentration tested (>40 μM); "reversion of resistance" indicates that the compound reversed the resistant phenotype to a sensitive one; "PC" positive control.

2.2.4. Antioxidant Capacity, Reducing Potential and Lipoperoxidation Inhibition

To further elucidate how halogenation affects other properties of the flavonoids studied, their 2,2′-azino-bis-(3-ethylbenzothiazoline-6-sulfonic acid) cation (ABTS) and 1,1-diphenyl-2-picrylhydrazyl (DPPH) radical scavenging, the Folin–Ciocalteu reagent (FCR) reducing, the ferric-reducing antioxidant power (FRAP), and the anti-lipoperoxidation activities were evaluated by in vitro methods (Supplementary Information Tables S1 and S2). The activity of the parent flavonoids was consistent with previously published data [32–38], with the 2,3-unsaturated compounds being more active. Halogenation did not affect these activities, with a few exceptions: 6,8-dibromotaxifolin (**8**) showed increased activity in FRAP and FCR assays, compared with taxifolin (**1**); 6,8-dibromoquercetin (**10**) showed much higher activity than both 8-bromoquercetin (**9**) and quercetin (**2**) in the FRAP test; and 8-iodosilybin B (**24**) showed 2.5-fold higher anti-lipoperoxidant activity than silybin B (**3b**). In the case of anti-lipoperoxidation activity, taxifolin (**1**) and 6,8-dibromotaxifolin (**8**) showed the highest inhibitory potential, with higher activity than that of quercetin and Trolox

(positive control) (Table S2). Quercetin (**2**), 8-bromoquercetin (**9**), and 6,8-dibromoquercetin (**10**) also showed high potential to inhibit lipid peroxidation, with activity increasing with an increasing number of bromines. The values for the parent compounds can be found in the literature, but the data presented here are new for halogenated flavonolignans. To date, only the DPPH scavenging activity of brominated flavonols has been studied [24]; however, because the authors used crude reaction mixtures and not pure brominated derivatives, their results are not comparable to ours.

2.2.5. Cytotoxicity and Anti-Inflammatory Activity

In addition, the cytotoxicity of these compounds was evaluated as the ability to decrease the viability of human dermal fibroblasts (HDF) and human ovarian carcinoma cells that are resistant to doxorubicin (HOC/DOX) (Table S3). Neither of the tested derivatives exhibited cytotoxicity against healthy or cancer cells. These results are consistent with our previous findings [34,38] that silybin and silychristin had no direct anticancer effect but showed the potential to act as adjuvant therapy to conventional chemotherapeutic agents and to modulate tumor resistance. Moreover, flavonoids and flavonolignans have been a common component of the human diet for centuries and have never shown adverse effects [39]. Halogenation did not improve the ability of flavonoids to modulate the drug-resistant phenotype in doxorubicin-resistant human ovarian carcinomas (Figure S2).

To our knowledge, this is the first report of the effects of bromination on the anti-inflammatory activity of flavonoids, which was evaluated as the ability of flavonoids to decrease nitric oxide production (Tables S4 and S5). The results indicate that nine of the 16 compounds tested were more active than the positive control, indomethacin.

3. Materials and Methods

3.1. General Experimental Procedures

Procedures using oxygen or moisture-sensitive materials were performed with anhydrous solvents (vide infra) under an atmosphere of argon in flame-dried flasks, using standard Schlenk techniques. Analytical TLC was performed on Al plates (Silica Gel 60 F254; Merck, Darmstadt, Germany). Purification was performed in a preparative HPLC system using an ASAHIPAK GS-310 20F column (Shodex, Munich, Germany), with MeOH as the mobile phase, a flow rate of 5 mL/min, and detection at 254 nm and 369 nm. The preparative HPLC system (Shimadzu, Kyoto, Japan) consisted of an LC-8A high-pressure pump with an SPD-20A dual wavelength detector (with a preparative cell), FRC-10A, and a fraction collector. The system was connected to a PC via a CBM-20A command module and controlled via the LabSolution 1.24 SPI software suite supplied with the instrument. All analytical HPLC separations were performed using a Shimadzu Prominence System (Shimadzu, Kyoto, Japan) consisting of a DGU-20A mobile phase degasser, two LC-20AD high-pressure pumps, a SIL-20AC refrigerated autosampler, a CTO-10AS column oven, and an SPDM20 A diode array detector. Shimadzu Solution software was used to acquire chromatographic data at a rate of 40 Hz. A monolithic Chromolith Performance RP-18e column (100 × 3 mm i.d., Merck, Darmstadt, Germany) was coupled with a guard column (5 × 4.6 mm, Merck, Darmstadt, Germany). Mobile phase A, $CH_3CN/H_2O/HCOOH$ (5:95:0.1), and phase B, $CH_3CN/H_2O/HCOOH$ (80:20:0.1), were used for the analyses with the following gradient: 0–6 min 10–80% B; 6–8 min 80% B; 10–12 min 80–10% A. The flow rate was 0.4 mL/min at 25 °C. MS parameters were as follows: negative mode; ESI interface voltage, 4.5 kV; detector voltage, 1.15 kV; nebulization gas flow, 1.5 mL/min; drying gas flow, 15 mL/min; heater block temperature, 200 °C; DL temperature, 250 °C; scan mode 300–800 m/z. PDA data were acquired in the 200 nm to 450 nm range, and the signal at 285 nm was used to monitor separation. Flash column chromatography was performed on Kieselgel 60 (60–200 mesh). NMR analyses were performed using Bruker Avance III 700 MHz (700.13 MHz for ^1H, 176.05 MHz for ^{13}C), Bruker Avance III 600 MHz (600.23 MHz for ^1H, 150.93 MHz for ^{13}C), and Bruker Avance III 400 MHz (399.87 MHz for ^1H, 100.55 MHz for ^{13}C) spectrometers in DMSO-d_6 at 30 °C and in $CDCl_3$ at 20 °C. The signals

in DMSO-d_6 and $CDCl_3$ were used as reference (δ_H 2.499, δ_C 39.46 for DMSO-d_6 and δ_H 7.263, δ_C 77.01 for $CDCl_3$). Spectra were recorded using the manufacturer's software. The ^1H and ^{13}C NMR spectra were zero filled to 4-fold data points and multiplied by a window function before Fourier transformation. To improve resolution, a double-exponential Lorentz–Gauss function with two parameters was applied for ^1H, and line broadening (1 Hz) was applied for ^{13}C to obtain a better signal-to-noise ratio. Chemical shifts were reported on the δ-scale, and the digital resolution justified the reported values to three (δ_H) or two (δ_C) decimal places.

High-resolution mass spectra (HRMS) were measured using a LTQ Orbitrap XL hybrid mass spectrometer (Thermo Fisher Scientific, Waltham, MA, USA) equipped with an electrospray ion source and operated at the resolution of 100,000. The samples were loop injected into methanol/water (4:1), with a flow rate of 100 µL/min.

Mono- and dibrominated compounds (compounds **7**–**17**) were prepared according to a previously published method for selective bromination [16]. Commercially available reagents, ligands, and pooled microsomes from male rat liver (M9066), 1,1-diphenyl-2-picrylhydrazyl (DPPH) radical, and tert-butyl hydroperoxide (tBH) were purchased from Sigma Aldrich (Darmstadt, Germany), Alfa Aesar (Ward Hill, MA, USA), Acros Organics (Morris Plains, NJ, USA), and TCI chemicals (Gurugram, India) and, unless stated otherwise, were used without further purification. Pure diastereomers of silybin were prepared using diastereomeric enzymatic resolution [40]. The 2,3-dehydrosilybin AB and 2,3-dehydrosilychristin A were prepared as described previously [36,41]. The FRAP (ferric reducing antioxidant power, KF-01-003) and the ABTS (2,2'-azino-bis-(3-ethylbenzothiazoline-6-sulphonic acid, KF-01-002) radical scavenging kits were acquired from Bioquochem (Llanera, Spain). The Folin–Ciocalteu reagent, human dermal fibroblasts (HDF), doxorubicin-resistant human ovarian carcinoma (HOC/DOX), Dulbecco's Modified Eagle's Medium, antibiotic antimycotic solution, murine macrophages (RAW 264.7), and Griess reagent were purchased from Merck (Darmstadt, Germany). Fetal bovine serum and MEM medium were purchased from Thermo Fisher Scientific (Waltham, MA, USA). *Vibrio campbellii* BAA-1118 and BAA-1119 strains (American Type Culture Collection, ATCC, Manassas, VA, USA) were used for the detection of bacterial communication inhibition. A SpectraMax i3x microplate reader (Molecular Devices, San Jose, CA, USA) was used for the biological activity measurements. GraphPad Prism software version 5.00 for Windows (GraphPad Software, San Diego, CA, USA) and Statext software ver. 2.1 (STATEXT LLC, Wayne, NJ, USA) were used for the evaluation of the results.

3.2. General Procedure A for Tribromination

NBS (3.0 eq) was added to a solution of starting material (1.0 eq) in DMF (2 mL) at room temperature and the mixture was stirred for 30 min. The reaction mixture was poured into water and extracted with ethyl acetate (3 × 10 mL). The combined organic fractions were washed with brine, dried over Na_2SO_4, and evaporated in vacuo. The residue was purified by preparative HPLC chromatography (ASAHIPACK, 5 mL/min MeOH isocratic) to afford the corresponding product.

For 6,8,21-tribromosilybin A (**21**), general procedure A was followed and yielded **21** as brown petals (110 mg, yield 37%, HPLC purity 96%—Figure S25); ^1H and ^{13}C NMR data (DMSO-d_6, 30 °C, 700.13 and 176.05 MHz, respectively), Table S7, Figures S7 and S8; HRMS (ESI, m/z) calcd for $C_{25}H_{18}O_{10}Br_3$ $[M-H]^-$ 714.84556, found 714.84382, Figure S35.

For 6,8,21-tribromosilybin B (**22**), general procedure A was followed and afforded **22** as a white solid (160 mg, yield 54%, HPLC purity 100%—Figure S26); ^1H and ^{13}C NMR data (DMSO-d_6, 30 °C, 399.87 and 100.55 MHz, respectively), Table S8, Figures S9 and S10; HRMS (ESI, m/z) calcd for $C_{25}H_{18}O_{10}Br_3$ $[M-H]^-$ 714.84556, found 714.84485, Figure S36.

For 6,8,20-tribromosilychristin A (**23**), general procedure A was followed and afforded **23** as a white solid (20 mg, yield 13%, HPLC purity 94%—Figure S27); ^1H and ^{13}C NMR data (DMSO-d_6, 30 °C, 600.23 and 150.93 MHz, respectively), Table S9, Figures S11 and S12; HRMS (ESI, m/z) calcd for $C_{25}H_{18}O_{10}Br_3$ $[M-H]^-$ 714.84556, found 714.84418, Figure S37.

3.3. General Procedure B for Diiodination

NIS (2.0 eq) was added to a solution of the starting material (1.0 eq) in DMF (2 mL) at room temperature and the mixture was stirred for 30 min. The reaction mixture was poured into water and extracted with ethyl acetate (3 × 10 mL). The combined organic fractions were washed with brine, dried over sodium sulfate, and evaporated in vacuo. The residue was purified by preparative HPLC chromatography (ASAHIPACK, 5 mL/min isocratic) to afford the corresponding product.

For 6,8-diiodosilybin A (**25**), general procedure B was followed and yielded **25** as a white solid (30 mg, yield 50%, HPLC purity 96%—Figure S29); ^{1}H and ^{13}C NMR data (DMSO-d_6, 30 °C, 600.23 and 150.93 MHz, respectively), Table S11, Figures S15 and S16; HRMS (ESI, m/z) calcd for $C_{25}H_{19}O_{10}I_2$ $[M - H]^-$ 732.90731, found 732.90678, Figure S39.

For 6,8-diiodosilybin B (**26**), general procedure B was followed and afforded **26** as a white solid (153 mg, yield 64%, HPLC purity 97%—Figure S30); ^{1}H and ^{13}C NMR data (DMSO-d_6, 30 °C, 600.23 and 150.93 MHz, respectively), Table S12, Figures S17 and S18; HRMS (ESI, m/z) calcd for $C_{25}H_{19}O_{10}I_2$ $[M - H]^-$ 732.90731, found 732.90619, Figure S40.

For 6,8-diiodosilychristin A (**27**), Ggeneral procedure B was followed and yielded **27** as a white solid (65 mg, yield 43%, HPLC purity 96%—Figure S31); ^{1}H and ^{13}C NMR data (DMSO-d_6, 30 °C, 600.23 and 150.93 MHz, respectively), Table S13, Figures S19 and S20; HRMS (ESI, m/z) calcd for $C_{25}H_{19}O_{10}I_2$ $[M - H]^-$ 732.90731, found 732.90620, Figure S41.

3.4. General Procedure C for Chlorination

NCS (1.0 eq) was added to a solution of starting material (1.0 eq) in DMF (2 mL) at room temperature and the mixture was stirred for 30 min. The reaction mixture was poured into water and extracted with EtOAc (3 × 10 mL). The combined organic fractions were washed with brine, dried over Na_2SO_4, and evaporated in vacuo. The residue was purified by preparative HPLC chromatography (ASAHIPACK, 5 mL/min isocratic) to afford the corresponding product.

For 6-chlorosilybin B (**28a**) and 8-chlorosilybin B (**28b**), general procedure C was followed and afforded an inseparable mixture containing 6-chlorosilybin B (66%, **28a**) and 8-chlorosilybin B (25%, **28b**) as a white solid (70 mg, 45%, HPLC chromatogram—Figure S32); ^{1}H and ^{13}C NMR data (DMSO-d_6, 30 °C, 600.23 and 150.93 MHz, respectively), Table S14, Figures S21 and S22; HRMS (ESI, m/z) calcd for $C_{25}H_{20}O_{10}Cl$ $[M - H]^-$ 515.07505, found 515.07385, Figure S42.

3.5. General Procedure D for Selective Dehalogenation

To a solution of dihalogenated compound (1.0 eq) in MeOH (1 mL) was added a solution of $NaHCO_3$ (1.0 eq) in water (0.5 mL), followed by dropwise addition of Na_2SO_3 (1 eq) in water (0.5 mL). The reaction mixture was stirred at room temperature for 4 h. The reaction mixture was evaporated and the residue was dissolved in EtOAc and extracted with water (3 × 10 mL). The combined organic fractions were washed with brine, dried over Na_2SO_4, and evaporated in vacuo. The residue was purified by preparative HPLC chromatography (ASAHIPACK, 5 mL/min isocratic) to give the corresponding product.

For 8-bromosilybin A (**19**), general procedure D was followed and afforded **19** as a white solid (50 mg, yield 30%, HPLC purity 96%—Figure S23); ^{1}H and ^{13}C NMR data (DMSO-d_6, 30 °C, 600.23 and 150.93 MHz, respectively), Table S5, Figures S3 and S4; HRMS (ESI, m/z) calcd for $C_{25}H_{20}O_{10}Br$ $[M - H]^-$ 559.02453, found 559.02344, Figure S33.

For 8-bromosilybin B (**20**) general procedure D was followed and yielded **20** as a white solid (20 mg, yield 20%, HPLC purity 97%—Figure S24); ^{1}H and ^{13}C NMR data (DMSO-d_6, 30 °C, 600.23 and 150.93 MHz, respectively), Table S6, Figures S5 and S6; HRMS (ESI, m/z) calcd for $C_{25}H_{20}O_{10}Br$ $[M - H]^-$ 559.02453, found 559.02355, Figure S34.

For 8-iodosilybin A (**24**), general procedure D was followed and yielded **24** as a white solid (112 mg, yield 97%, HPLC purity 92%—Figure S28); ^{1}H and ^{13}C NMR data (DMSO-d_6, 30 °C, 700.13 and 176.05 MHz, respectively), Table S10, Figures S13 and S14; HRMS (ESI, m/z) calcd for $C_{25}H_{20}O_{10}I$ $[M - H]^-$ 607.01066, found 607.00892, Figure S38.

3.6. Inhibition of Quorum Sensing

The inhibition of bacterial extracellular communication was measured using *Vibrio campbellii* strains BAA-1118 and BAA-1119. The experiment was performed according to the methods of Szemerédi et al. [42]. Briefly, 5 × 105 CFU/mL (colony-forming units per milliliter) were seeded in an Autoinducer Bioassay medium (NaCl 17.5 g/L, $MgSO_4$ 12.3 g/L, Casamino acids 2 g/L, 10 mL of 1 M potassium phosphate pH 7.0, 10 mL of 0.1 M L-arginine, and 10 mL of glycerol in 970 mL of deionized water) in a 96-well plate. Immediately, the tested compounds were added at the final concentration of 0.2–200 μM and luminescence was recorded for 16 h by a SpectraMax i3x microplate reader set at 30 °C, an integration time of 10,000 ms, and shaking for 60 s before measurement. The effective concentration of compounds halving the luminescence (EC_{50}) was determined from the sum of luminescence. At the same time, the viability of the culture was determined by the resazurin assay, which gave the IC_{50} value for each compound. The selectivity index was calculated as the ratio of EC_{50} (the concentration that halves the cell communication) and IC_{50} (the concentration halving the viability). The EC_{50} and IC_{50} were calculated using GraphPad Prism software version 5.00 for Windows with a nonlinear regression curve fit.

3.7. Sensitization of Antibiotic-Resistant Bacteria

Clinical isolates of *P. aeruginosa* and *S. aureus* were obtained from the General University Hospital in Prague (Prague, Czech Republic). *P. aeruginosa* was resistant to ciprofloxacin, oxacillin, ticarcillin, colistin, gentamicin, and imipenem. *S. aureus* was resistant to ciprofloxacin, gentamicin, erythromycin, chloramphenicol, clindamycin, oxacillin, cefotaxime, and vancomycin. Bacteria were cultivated in Mueller–Hinton broth (MH broth, Merck). The susceptibility of the bacteria was evaluated by the minimum inhibitory concentrations (MIC). The MIC of derivatives in the presence of the antibiotic cut-off concentration was determined according to ISO 20776-1: 2020. The antibiotic cut-off concentration was chosen according to the European Committee on Antimicrobial Susceptibility Testing (EUCAST, Clinical breakpoints—bacteria (ver. 11.0), 1 January 2021). The 40 μM concentration of the derivatives was chosen as the highest concentration for the tests. Cell viability was determined by measuring absorbance (A590 nm) after 24 h incubation at 37 °C, 150 rpm.

3.8. Inhibition of Biofilm Formation and Disruption of Maturated Biofilm

The activity of derivatives on biofilms was tested with *S. aureus* (ATCC, 25923) and *P. aeruginosa* (CCM, 3955), according to the previously described method [43]. The highest tested concentration of derivatives was 100 μM. The activity was evaluated using an IC_{50} comparison between the parent compound and its derivative.

3.9. Antioxidant Activity, Reducing Potential, and Lipid Peroxidation Inhibition

The antiradical activity was evaluated by the ability to scavenge ABTS and DPPH radicals [33,44,45]. Reducing capacity was assessed by the ability to reduce the Folin–Ciocalteu reagent (FCR) and ferric ions (FRAP) [36,46]. The ability to inhibit lipid peroxidation of pooled male rat microsomal liver membranes induced by tert-butyl hydroperoxide was also evaluated and the results were expressed as IC_{50} values [36,47].

3.10. Cytotoxicity

The cytotoxicity of flavonoids and their halogenated derivatives was determined as their ability to decrease the viability of human dermal fibroblasts (HDF) and doxorubicin-resistant human ovarian carcinomas (HOC/DOX). Both cell lines were cultivated in Dulbecco's Modified Eagle's Medium supplemented with fetal bovine serum (FBS, 10% v/v) and 1 × antibiotic antimycotic solution and incubated at 37 °C in the atmosphere of 5% CO2. The experiment was performed according to a previously published method [48]. Briefly, 1×10^5 cells/mL were seeded into a 96-well plate (100 μL/well). After 24 h, flavonoids and their derivatives were administered at the concentration range of 31.25–500 μM. After 72 h, the viability was determined by resazurin assay (0.03 mg/mL of resazurin in PBS), where

the fluorescence was measured after 2 h of incubation by the SpectraMax i3x microplate reader at a wavelength of 560/590 nm (excitation/emission). The concentration inhibiting half of the population (IC_{50}) was determined using nonlinear regression in GraphPad Prism software. The selectivity index was calculated as the ratio between the IC_{50} for HDF (control, non-cancerous cells) and the IC_{50} for HOC/DOX (cancer cells).

3.11. Inhibition of Nitric Oxide Production

The anti-inflammatory activity of the tested flavonolignans was determined as the ability to reduce nitric oxide production by murine macrophages (RAW 264.7) stimulated by bacterial lipopolysaccharides, as previously described [34]. Briefly, RAW 264.7 cells were cultivated in DMEM medium supplemented with 10% FBS and 1 × antibiotic antimycotic solution. For the experiment, 1×10^6 cells/mL was seeded into the 96-well plate (100 μL/well). After 48 h, LPS (100 ng/mL) and the samples (6.25–100 μM) were added to MEM medium (Eagle's Minimum Essential Media, no phenol red). After 24 h, the medium was mixed with Griess reagent (0.04 g/mL), prepared freshly in deionized water at the ratio of 1:1. The absorbance was measured after 15 min at 540 nm by the SpectraMax i3x microplate reader. Cell viability was determined by resazurin assay.

3.12. Sensitization of Doxorubicin-Resistant Human Ovarian Carcinoma Cells

The sensitization of doxorubicin-resistant human ovarian cancer cells (HOC/DOX) was performed, as previously described [38]. Briefly, the HOC/DOX cells were cultivated and seeded as described above. The concentration of doxorubicin that halved the viability (IC_{50}) of HOC/DOX was determined after 72 h incubation, using the resazurin assay, and then divided by the IC_{50} of doxorubicin in the presence of the tested compound (10 μM). This ratio is referred to as the sensitization fold (SF). The compound was able to sensitize HOC/DOX to doxorubicin when SF > 1. The higher the SF, the better the sensitizing agent.

3.13. Statistical Analysis

Data from the biological activity tests were analyzed using the statistical package Statext ver. 2.1 ANOVA, Scheffé, and least-square difference tests for post hoc comparisons between pairs of means. Data are presented as the average number of replicates (n) with the standard error (SE). A *t*-test was used for the comparison between the halogenated derivative and its parent compound (* $p \leq 0.05$, ** $p \leq 0.01$, *** $p \leq 0.005$, **** $p \leq 0.001$, ***** $p \leq 0.0005$). Differences were considered statistically significant when $p < 0.05$.

4. Conclusions

In conclusion, a library of new halogenated derivatives of flavonolignans was prepared. To understand how halogenation affects biological activity, all prepared derivatives were tested for their basic physicochemical properties and biological activity. Brominated derivatives of flavonoids were able to inhibit bacterial communication (quorum sensing) and biofilm formation with an IC_{50} below 10 μM. Halogenated derivatives were also able to inhibit the growth of gentamicin-resistant *S. aureus*, and 6,8,21-tribromosilybins A (**21**) and B (**22**) were able to revert the resistant phenotype into a sensitive one. In vitro results indicated that brominated derivatives are promising antibacterial derivatives, but further toxicological and pharmacological tests need to be performed. The prepared derivatives showed higher anti-inflammatory activity than the positive control. Possible mechanisms of action in biological assays are under further investigation. To our knowledge, this is the first paper dealing with the preparation and biological activity of brominated flavonolignans.

Supplementary Materials: The following supporting information can be downloaded at: https://www.mdpi.com/article/10.3390/ijms232315121/s1.

Author Contributions: Conceptualization, V.K., J.V. and K.V.; Data curation, M.H., D.Č., M.K. and J.C.; Formal analysis, M.H., K.H. and L.H.; Funding acquisition, J.V. and K.V.; Investigation, M.H., K.K., S.D., K.H., D.Č., L.H., D.B., M.K. and J.C.; Methodology, M.H., J.V. and K.V.; Project administration, J.V. and K.V.; Supervision, V.K.; Visualization, M.H., K.K. and L.H.; Writing—original draft, M.H., S.D., J.V. and K.V.; Writing—review and editing, M.H., K.K., S.D., K.H., D.Č., L.H., D.B., M.K., J.C., V.K., J.V. and K.V. All authors have read and agreed to the published version of the manuscript.

Funding: This work was supported by the Czech Science Foundation (project No. 21-00551S) and by the Ministry of Education, Youth and Sports of the Czech Republic (mobility project LTC20070). This study was also supported by COST Action CA17104 <STRATAGEM>, funded by COST (European Cooperation in Science and Technology, http://www.cost.eu, accessed on 8 November 2022).

Institutional Review Board Statement: Not applicable.

Informed Consent Statement: Not applicable.

Data Availability Statement: Not applicable.

Conflicts of Interest: All authors declare no conflict of interest.

References

1. Li, C.; La, M.P.; Tang, H.; Pan, W.H.; Sun, P.; Krohn, K.; Yi, Y.H.; Li, L.; Zhang, W. Bioactive briarane diterpenoids from the South China Sea gorgonian *Dichotella gemmacea*. *Bioorg. Med. Chem. Lett.* **2012**, *22*, 4368–4372. [CrossRef] [PubMed]
2. Singh, A.J.; Dattelbaum, J.D.; Field, J.J.; Smart, Z.; Woolly, E.F.; Barber, J.M.; Heathcott, R.; Miller, J.H.; Northcote, P.T. Structurally diverse hamigerans from the New Zealand marine sponge *Hamigera tarangaensis*: NMR-directed isolation, structure elucidation and antifungal activity. *Org. Biomol. Chem.* **2013**, *11*, 8041–8051. [CrossRef] [PubMed]
3. Smitha, D.; Kumar, M.M.K.; Ramana, H.; Rao, D.V. Rubrolide R: A new furanone metabolite from the ascidian *Synoicum* of the Indian Ocean. *Nat. Prod. Res.* **2014**, *28*, 12–17. [CrossRef] [PubMed]
4. Parker, W.B.; Cheng, Y.C. Metabolism and mechanism of action of 5-fluorouracil. *Pharmacol. Ther.* **1990**, *48*, 381–395. [CrossRef]
5. Senderowicz, A.M. Flavopiridol: The first cyclin-dependent kinase inhibitor in human clinical trials. *Investig. New Drugs* **1999**, *17*, 313–320. [CrossRef]
6. Deep, A.; Marwaha, R.K.; Marwaha, M.G.; Jyoti; Nandal, R.; Sharma, A.K. Flavopiridol as cyclin dependent kinase (CDK) inhibitor: A review. *New J. Chem.* **2018**, *42*, 18500–18507. [CrossRef]
7. Naderi, G.A.; Asgary, S.; Sarraf-Zadegan, N.; Shirvany, H. Anti-oxidant effect of flavonoids on the susceptibility of LDL oxidation. *Mol. Cell Biochem.* **2003**, *246*, 193–196. [CrossRef]
8. Chambers, C.S.; Holečková, V.; Petrásková, L.; Biedermann, D.; Valentová, K.; Buchta, M.; Křen, V. The silymarin composition . . . and why does it matter? *Food Res. Int.* **2017**, *100*, 339–353. [CrossRef]
9. Křen, V.; Valentová, K. Silybin and its congeners: From traditional medicine to molecular effects. *Nat. Prod. Rep.* **2022**, *39*, 1264–1281. [CrossRef]
10. Biedermann, D.; Vavříková, E.; Cvak, L.; Křen, V. Chemistry of silybin. *Nat. Prod. Rep.* **2014**, *31*, 1138–1157. [CrossRef]
11. Valentová, K.; Biedermann, D.; Křen, V. 2,3-Dehydroderivatives of silymarin flavonolignans: Prospective natural compounds for the prevention of chronic diseases. *Proceedings* **2019**, *11*, 21. [CrossRef]
12. Holasová, K.; Křížkovská, B.; Hoang, L.; Dobiasová, S.; Lipov, J.; Macek, T.; Křen, V.; Valentová, K.; Ruml, T.; Viktorová, J. Flavonolignans from silymarin modulate antibiotic resistance and virulence in *Staphylococcus aureus*. *Biomed. Pharmacother.* **2022**, *149*, 112806. [CrossRef] [PubMed]
13. Karimova, E.; Baltina, L.; Spirikhin, L.; Gabbasov, T.; Orshanskaya, Y.; Zarubaev, V. Synthesis and antiviral activity of quercetin brominated derivatives. *Nat. Prod. Commun.* **2015**, *10*, 1565–1568. [CrossRef] [PubMed]
14. Pan, G.; Yang, K.; Ma, Y.; Zhao, X.; Lu, K.; Yu, P. Synthesis of 6- or 8-bromo flavonoids by regioselective mono-bromination and deprotection protocol from flavonoid alkyl ethers. *Bull. Korean Chem. Soc.* **2015**, *36*, 1460–1466. [CrossRef]
15. Kiehlmann, E.; Szczepina, M.G. Epimerization, transacylation and bromination of dihydroquercetin acetates; synthesis of 8-bromodihydroquercetin. *Cent. Eur. J. Chem.* **2011**, *9*, 492–498. [CrossRef]
16. Hurtová, M.; Biedermann, D.; Kuzma, M.; Křen, V. Mild and selective method of bromination of flavonoids. *J. Nat. Prod.* **2020**, *83*, 3324–3331. [CrossRef]
17. Binsack, R.; Boersma, B.J.; Patel, R.P.; Kirk, M.; White, C.R.; Darley-Usmar, V.; Barnes, S.; Zhou, F.; Parks, D.A. Enhanced antioxidant activity after chlorination of quercetin by hypochlorous acid. *Alcohol. Clin. Exp. Res.* **2001**, *25*, 434–443. [CrossRef]
18. Freitas, M.; Ribeiro, D.; Tome, S.M.; Silva, A.M.; Fernandes, E. Synthesis of chlorinated flavonoids with anti-inflammatory and pro-apoptotic activities in human neutrophils. *Eur. J. Med. Chem.* **2014**, *86*, 153–164. [CrossRef]
19. Lu, K.; Chu, J.; Wang, H.; Fu, X.; Quan, D.; Ding, H.; Yao, Q.; Yu, P. Regioselective iodination of flavonoids by *N*-iodosuccinimide under neutral conditions. *Tetrahedron Lett.* **2013**, *54*, 6345–6348. [CrossRef]
20. Pérez, M.; Ruiz, D.; Autino, J.; Sathicq, A.; Romanelli, G. A very simple solvent-free method for the synthesis of 2-arylchromones using KHSO4 as a recyclable catalyst. *Comptes Rendus Chim.* **2016**, *19*, 551–555. [CrossRef]

21. Zhang, J.W.; Yang, W.W.; Chen, L.L.; Chen, P.; Wang, Y.B.; Chen, D.Y. An efficient tandem synthesis of chromones from *o*-bromoaryl ynones and benzaldehyde oxime. *Org. Biomol. Chem.* **2019**, *17*, 7461–7467. [CrossRef] [PubMed]
22. Tao, T.; He, C.; Deng, J.; Huang, Y.; Su, Q.; Peng, M.; Yi, M.; Darko, K.O.; Zou, H.; Yang, X. A novel synthetic derivative of quercetin, 8-trifluoromethyl-3,5,7,3′,4′-*O*-pentamethyl-quercetin, inhibits bladder cancer growth by targeting the AMPK/mTOR signaling pathway. *Oncotarget* **2017**, *8*, 71657–71671. [CrossRef] [PubMed]
23. Proenca, C.; Ribeiro, D.; Soares, T.; Tome, S.M.; Silva, A.M.S.; Lima, J.; Fernandes, E.; Freitas, M. Chlorinated flavonoids modulate the inflammatory process in human blood. *Inflammation* **2017**, *40*, 1155–1165. [CrossRef] [PubMed]
24. Justino, G.C.; Rodrigues, M.; Florencio, M.H.; Mira, L. Structure and antioxidant activity of brominated flavonols and flavanones. *J. Mass Spectrom.* **2009**, *44*, 1459–1468. [CrossRef] [PubMed]
25. Ahmed-Belkacem, A.; Pozza, A.; Muñoz-Martínez, F.; Bates, S.E.; Castanys, S.; Gamarro, F.; Di Pietro, A.; Pérez-Victoria, J.M. Flavonoid structure-activity studies identify 6-prenylchrysin and tectochrysin as potent and specific inhibitors of breast cancer resistance protein ABCG2. *Cancer Res.* **2005**, *65*, 4852–4860. [CrossRef]
26. Miller, M.B.; Bassler, B.L. Quorum sensing in bacteria. *Annu. Rev. Microbiol.* **2001**, *55*, 165–199. [CrossRef]
27. Girard, L. Quorum sensing in *Vibrio* spp.: The complexity of multiple signalling molecules in marine and aquatic environments. *Crit. Rev. Microbiol.* **2019**, *45*, 451–471. [CrossRef]
28. Paczkowski, J.E.; Mukherjee, S.; McCready, A.R.; Cong, J.P.; Aquino, C.J.; Kim, H.; Henke, B.R.; Smith, C.D.; Bassler, B.L. Flavonoids suppress *Pseudomonas aeruginosa* virulence through allosteric inhibition of quorum-sensing receptors. *J. Biol. Chem.* **2017**, *292*, 4064–4076. [CrossRef]
29. Manefield, M.; de Nys, R.; Naresh, K.; Roger, R.; Givskov, M.; Peter, S.; Kjelleberg, S. Evidence that halogenated furanones from *Delisea pulchra* inhibit acylated homoserine lactone (AHL)-mediated gene expression by displacing the AHL signal from its receptor protein. *Microbiology* **1999**, *145*, 283–291. [CrossRef]
30. Soukarieh, F.; Liu, R.; Romero, M.; Roberston, S.N.; Richardson, W.; Lucanto, S.; Oton, E.V.; Qudus, N.R.; Mashabi, A.; Grossman, S.; et al. Hit identification of new potent PqsR antagonists as inhibitors of quorum sensing in planktonic and biofilm grown *Pseudomonas aeruginosa*. *Front. Chem.* **2020**, *8*, 204. [CrossRef]
31. Lopes, L.A.A.; Dos Santos Rodrigues, J.B.; Magnani, M.; de Souza, E.L.; de Siqueira-Júnior, J.P. Inhibitory effects of flavonoids on biofilm formation by *Staphylococcus aureus* that overexpresses efflux protein genes. *Microb. Pathog.* **2017**, *107*, 193–197. [CrossRef] [PubMed]
32. Topal, F.; Nar, M.; Gocer, H.; Kalin, P.; Kocyigit, U.M.; Gülçin, İ.; Alwasel, S.H. Antioxidant activity of taxifolin: An activity–structure relationship. *J. Enzym. Inhib. Med. Chem.* **2016**, *31*, 674–683. [CrossRef] [PubMed]
33. Trouillas, P.; Marsal, P.; Svobodová, A.; Vostálová, J.; Gažák, R.; Hrbáč, J.; Sedmera, P.; Křen, V.; Lazzaroni, R.; Duroux, J.-L.; et al. Mechanism of the antioxidant action of silybin and 2,3-dehydrosilybin flavonolignans: A joint experimental and theoretical study. *J. Phys. Chem. A* **2008**, *112*, 1054–1063. [CrossRef] [PubMed]
34. Viktorová, J.; Dobiasová, S.; Řehořová, K.; Biedermann, D.; Káňová, K.; Šeborová, K.; Václavíková, R.; Valentová, K.; Ruml, T.; Křen, V.; et al. Antioxidant, anti-inflammatory, and multidrug resistance modulation activity of silychristin derivatives. *Antioxidants* **2019**, *8*, 303. [CrossRef]
35. Biedermann, D.; Buchta, M.; Holečková, V.; Sedlák, D.; Valentová, K.; Cvačka, J.; Bednárová, L.; Křenková, A.; Kuzma, M.; Škuta, C.; et al. Silychristin: Skeletal alterations and biological activities. *J. Nat. Prod.* **2016**, *79*, 3086–3092. [CrossRef]
36. Pyszková, M.; Biler, M.; Biedermann, D.; Valentová, K.; Kuzma, M.; Vrba, J.; Ulrichová, J.; Sokolová, R.; Mojović, M.; Popović-Bijelić, A.; et al. Flavonolignan 2,3-dehydroderivatives: Preparation, antiradical and cytoprotective activity. *Free Radic. Biol. Med.* **2016**, *90*, 114–125. [CrossRef]
37. Valentová, K.; Káňová, K.; Di Meo, F.; Pelantová, H.; Chambers, C.; Rydlová, L.; Petrásková, L.; Křenková, A.; Cvačka, J.; Trouillas, P.; et al. Chemoenzymatic preparation and biophysical properties of sulfated quercetin metabolites. *Int. J. Mol. Sci.* **2017**, *18*, 2231. [CrossRef]
38. Dobiasová, S.; Řehořová, K.; Kučerová, D.; Biedermann, D.; Káňová, K.; Petrásková, L.; Koucká, K.; Václavíková, R.; Valentová, K.; Ruml, T.; et al. Multidrug resistance modulation activity of silybin derivatives and their anti-inflammatory potential. *Antioxidants* **2020**, *9*, 455. [CrossRef]
39. Waheed Janabi, A.H.; Kamboh, A.A.; Saeed, M.; Xiaoyu, L.; BiBi, J.; Majeed, F.; Naveed, M.; Mughal, M.J.; Korejo, N.A.; Kamboh, R.; et al. Flavonoid-rich foods (FRF): A promising nutraceutical approach. *Iran J. Basic Med. Sci.* **2020**, *23*, 140–153.
40. Gažák, R.; Marhol, P.; Purchartová, K.; Monti, D.; Biedermann, D.; Riva, S.; Cvak, L.; Křen, V. Large-scale separation of silybin diastereoisomers using lipases. *Process Biochem.* **2010**, *45*, 1657–1663. [CrossRef]
41. Gažák, R.; Trouillas, P.; Biedermann, D.; Fuksová, K.; Marhol, P.; Kuzma, M.; Křen, V. Base-catalyzed oxidation of silybin and isosilybin into 2,3-dehydro derivatives. *Tetrahedron Lett.* **2013**, *54*, 315–317. [CrossRef]
42. Szemerédi, N.; Kincses, A.; Řehořová, K.; Hoang, L.; Salardón-Jiménez, N.; Sevilla-Hernández, C.; Viktorová, J.; Domínguez-Álvarez, E.; Spengler, G. Ketone- and cyano-selenoesters to overcome efflux pump, quorum-sensing, and biofilm-mediated resistance. *Antibiotics* **2020**, *9*, 896. [CrossRef] [PubMed]
43. Hoang, L.; Beneš, F.; Fenclová, M.; Kronusová, O.; Švarcová, V.; Řehořová, K.; Baldassarre Švecová, E.; Vosátka, M.; Hajšlová, J.; Kaštánek, P.; et al. Phytochemical composition and *in vitro* biological activity of iris spp. (iridaceae): A new source of bioactive constituents for the inhibition of oral bacterial biofilms. *Antibiotics* **2020**, *9*, 403. [CrossRef]

44. Joyeux, M.; Mortier, F.; Fleurentin, J. Screening of antiradical, antilipoperoxidant and hepatoprotective effects of nine plant extracts used in Caribbean folk medicine. *Phytother. Res.* **1995**, *9*, 228–230. [CrossRef]
45. Roubalová, L.; Purchartová, K.; Papoušková, B.; Vacek, J.; Křen, V.; Ulrichová, J.; Vrba, J. Sulfation modulates the cell uptake, antiradical activity and biological effects of flavonoids in vitro: An examination of quercetin, isoquercitrin and taxifolin. *Bioorg. Med. Chem.* **2015**, *23*, 5402–5409. [CrossRef] [PubMed]
46. Velioglu, Y.S.; Mazza, G.; Gao, L.; Oomah, B.D. Antioxidant activity and total phenolics in selected fruits, vegetables, and grain products. *J. Agric. Food Chem.* **1998**, *46*, 4113–4117. [CrossRef]
47. Vavříková, E.; Vacek, J.; Valentová, K.; Marhol, P.; Ulrichová, J.; Kuzma, M.; Křen, V. Chemo-enzymatic synthesis of silybin and 2,3-dehydrosilybin dimers. *Molecules* **2014**, *19*, 4115–4134. [CrossRef]
48. Tran, V.N.; Viktorová, J.; Augustýnková, K.; Jelenová, N.; Dobiasová, S.; Řehořová, K.; Fenclová, M.; Stránská-Zachariášová, M.; Vítek, L.; Hajšlová, J.; et al. In silico and in vitro studies of mycotoxins and their cocktails; their toxicity and its mitigation by silibinin pre-treatment. *Toxins* **2020**, *12*, 148. [CrossRef]

International Journal of
Molecular Sciences

MDPI

Review

Crosstalk between Resveratrol and Gut Barrier: A Review

Natalia Drabińska [1,*] and Elżbieta Jarocka-Cyrta [2]

[1] Department of Chemistry and Biodynamics of Food, Institute of Animal Reproduction and Food Research of Polish Academy of Sciences, 10-748 Olsztyn, Poland
[2] Department of Pediatrics, Gastroenterology and Nutrition, Faculty of Medicine, Collegium Medicum, University of Warmia and Mazury, Żołnierska 18A Str., 10-561 Olsztyn, Poland
* Correspondence: n.drabinska@pan.olsztyn.pl

Abstract: The plant-based nutraceuticals are receiving increasing interest in recent time. The high attraction to the phytochemicals is associated with their anti-inflammatory and antioxidant activities, which can lead to reduced risk of the development of cardiovascular and other non-communicable diseases. One of the most disseminated groups of plant bioactives are phenolic compounds. It was recently hypothesized that phenolic compounds can have the ability to improve the functioning of the gut barrier. The available studies showed that one of the polyphenols, resveratrol, has great potential to improve the integrity of the gut barrier. Very promising results have been obtained with in vitro and animal models. Still, more clinical trials must be performed to evaluate the effect of resveratrol on the gut barrier, especially in individuals with increased intestinal permeability. Moreover, the interplay between phenolic compounds, intestinal microbiota and gut barrier should be carefully evaluated in the future. Therefore, this review offers an overview of the current knowledge about the interaction between polyphenols with a special emphasis on resveratrol and the gut barrier, summarizes the available methods to evaluate the intestinal permeability, discusses the current research gaps and proposes the directions for future studies in this research area.

Keywords: intestinal permeability; gut barrier; leaky gut; polyphenols; resveratrol

Citation: Drabińska, N.; Jarocka-Cyrta, E. Crosstalk between Resveratrol and Gut Barrier: A Review. *Int. J. Mol. Sci.* **2022**, *23*, 15279. https://doi.org/10.3390/ijms232315279

Academic Editor: Alessandro Attanzio

Received: 20 November 2022
Accepted: 1 December 2022
Published: 3 December 2022

Publisher's Note: MDPI stays neutral with regard to jurisdictional claims in published maps and institutional affiliations.

1. Introduction

The interest in plant-based nutraceuticals is growing over the last decades. Many of the phytochemicals were found to exhibit anti-inflammatory and antioxidant effects, which can reduce the risk of the development of cardiovascular and other non-communicable diseases. One of the most disseminated groups of plant bioactives are phenolic compounds. Phenolic compounds are a very diverse group of secondary plant metabolites, which are widely distributed in vegetables, fruits, nuts and various plant-based food. The biological function of these compounds in plants is generally involved in protection against pathogens and herbivores, the attraction of pollinators, and the defence against ultraviolet radiation [1]. Phenolic compounds are formed from acetyl coenzyme A and amino acids as precursors or via the shikimic acid pathway. In the latter case, the carbohydrate precursors of the glycolysis and pentose phosphate pathway are converted into tyrosine, phenylalanine and tryptophan, which are then deaminated enzymatically to form cinnamic acid [1]. The group of phenolic compounds consists of approx. 8000 compounds, which can be further categorised into classes as presented in Figure 1. The simplest phenolic compound is phenol, which is a primary structural unit in phenolic compounds. The flavonoids consist of two benzene rings bound with a heterogenous pyrone C ring, and the subclasses of flavonoids differ with the number and the position of hydroxyl groups, which determine their biological functions [2]. The non-flavonoids consist of the simplest benzoic acid to very complex structures such as lignans and tannins. The main health-beneficial functions of phenolic compounds are associated with their anti-inflammatory and antioxidant properties due to the ability of phenolic compounds to donate hydrogen or electrons to free radicals.

Consequently, it leads to the stabilization of cell membranes, protects from cellular oxidative stress and limits the production of pro-inflammatory cytokines such as interleukin (IL) 6 and 8 as well as tumour necrosis factor α (TNF-α) [3,4]. The bioactive activity of polyphenols has been extensively studied and summarized in excellent reviews [5–7].

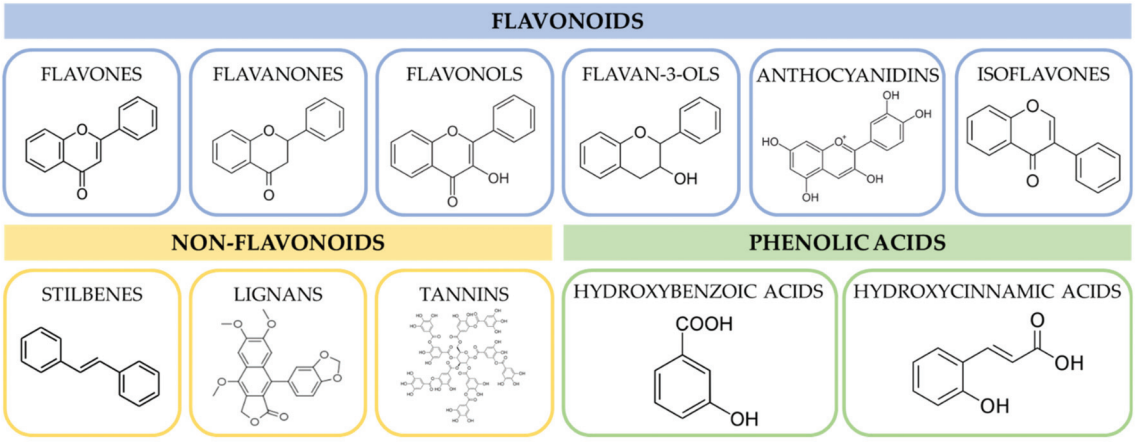

Figure 1. The classification of phenolic compounds.

Ingested phenolic compounds must be absorbed in the intestinal tract to exhibit their systemic effects. The absorption of phenolic compounds depends on the molecular weight, stereochemistry, presence of specific functional groups and lipophilicity [8]. Some of the phenolic compounds are present in free forms. However, generally, they are bound to proteins or sugars. Small molecular weight phenolic compounds, such as isoflavones and gallic acid, are easily absorbed into the intestinal epithelium [9]. Contrary, many of the phenolic compounds are absorbed only in 0.3–43%, therefore their concentration in the circulation is low [9]. It is hypothesized that phenolic compounds are transported by passive diffusion or by certain transporters such as sodium-dependent glucose transporter 1 (SGLT1), glucose transporter 2 (GLUT2) and P-glycoprotein, which are present in the cell membranes [10,11].

The metabolism and degradation of some phenolic compounds, such as anthocyanins, occur partly already in the oral cavity, which is moderately mediated by local microbiota [12]. Other compounds are hydrolysed in the stomach, and small intestine (5–10%), while many phenolic compounds reach the colon in the intact form [13]. The absorption of phenolic compounds in the duodenum and jejunum is closely related to the activity of digestive enzymes, which release aglycons from the food matrix. The enzymes involved in the transformation of the phenolic compound include among others lactase-phlorizin hydrolase and cytosolic β-glucosidase [14,15]. The majority of phenolic compounds is transported to the colon, where they are subjected to the enzymatic activity of gut microbiota. The intestinal bacteria degrade the aromatic ring and release aglycones facilitating the absorption of phenolic compound derivatives. Generally, the polymeric phenolics are hydrolysed to phenolic acids, flavones and flavanones to hydroxyphenylpropionic acid, flavanols to hydroxyphenyl acetic acid and proanthocyanidins to phenolic acids of a smaller molecular weight, which then can be absorbed [15].

A new branch of studies focuses on the interaction between polyphenols and gut microbiota. The mechanisms of these interactions are not fully understood. However, it is suggested that polyphenols have stimulating activity on the gut bacteria, and therefore according to the new classification of the International Scientific Association for Probiotics and Prebiotics (ISAPP) are classified as prebiotics [16]. Moreover, some studies reported that the simultaneous intake of polyphenols with probiotics can enhance the positive

effects of the latter [2]. On the other hand, gut bacteria are suggested to be involved in the metabolism of phenolic compounds, which can lead to their better bioavailability [17]. Recently, it is hypothesized that polyphenols can be potential modulators of intestinal permeability, although the mechanism is not fully understood. Therefore, this review offers an overview of the current knowledge about the interaction between polyphenols with a special emphasis on resveratrol and the gut barrier, discusses the current research gaps and proposes the directions for future studies in this research area. Moreover, the available methods used for the evaluation of the gut barrier integrity are summarized and their limitations are discussed.

2. Resveratrol—Overview

Resveratrol (3,5,4′-trihydroxystilbene) belongs to the group of stilbenes, which are characterized by two phenol rings linked by an ethylene bridge, and its structure is presented in Figure 2. Resveratrol can exist in two forms: *cis* and *trans*, and the latter is more prevalent and potent than the other. The interest in resveratrol is associated with its high antioxidant potential. Many studies have reported that resveratrol possesses anti-cancerogenic, anti-inflammatory and neuroprotective activity [18,19]. Resveratrol can be detected in over 70 plant species. However, the highest content is detected in grapes, peanuts and berries [19]. Early studies showed that high content of resveratrol was present in injured and infected plants. Currently it is known that stilbenes, in general, provide protection against microbial and fungal infections in plants and therefore they are classified as phytoalexins [20]. In plants, resveratrol is present in the glycosylated form to protect it from enzymatic oxidation and hence increasing its stability and consequently preserving the biological effects [19]. Resveratrol is suggested to be responsible for the "French paradox" defined by Renauld and Lorgeril in 1992 [21], who noticed a lower rate of heart diseases in Southern French who regularly drink red wine, despite their diet being rich in saturated fat.

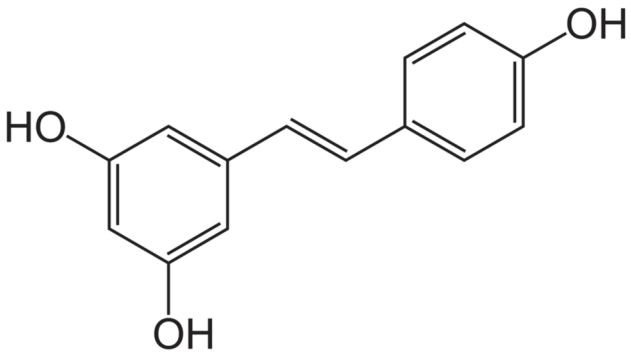

Figure 2. The chemical structure of resveratrol.

Resveratrol has the ability to activate sirtuin 1 (SIRT1), which deacetylates histones and nonhistone proteins, including transcription factors [22]. SIRT1 is involved in various metabolic processes, including stress resistance, cellular senescence, endothelial functions, and cell survival, thus it is suggested that resveratrol can be beneficial in diseases associated with inflammation, cell cycle defects and metabolic disturbances [18]. Moreover, resveratrol was found to influence the signalling pathways of the nuclear factor κβ (NF-κβ), insulin-like growth factor type 1 receptor (IGF-1R)/Wnt, the mechanistic target of rapamycin complex 1 (mTORC1), Akt/mTORC1/S6K1 and others [23–26], which are involved in carcinogenesis and the development of cardiovascular, metabolic and neurodegenerative diseases.

When discussing the health-beneficial potential of plant bioactive compounds, the concepts of bioaccessibility, bioavailability and bioactivity have to be defined. Bioaccessibility is defined as the quantity which is released from the food matrix in the intestinal tract and becomes available for absorption. Next, bioavailability can be defined as the

fraction of a compound and/or its bioactive metabolites which reach systemic circulation. Finally, bioactivity includes the specific physiological response to the presence of a certain substance [9]. The bioavailability of resveratrol was established as relatively low and this polyphenol is rapidly metabolised after oral ingestion [27]. Approx. 80% of resveratrol is absorbed in the intestine and the free form is bound to albumins and lipoproteins, which serve as a reservoir and distributor of resveratrol [28]. However, after absorption, resveratrol is metabolized by the liver, forming two forms of resveratrol, glucuronidated and sulphated, which can have lower beneficial activity compared to resveratrol itself [28]. Collectively, it is considered that from 80% absorbed, only approx. 1% of free resveratrol is bioavailable [27]. Furthermore, the absorbed resveratrol is rapidly excreted in approx. 75% in urine and cannot be utilized by the organism. Therefore, many of the results conducted in vitro where the substance is directly placed on the cells did not have the confirmation by in vivo studies applying the same doses, which results from the metabolic changes of the compound.

The study with isotopically-labelled resveratrol showed that next to glucuronidated and sulphated forms of resveratrol, a third conjugated form resulting from microbial activity is detected in human urine [29]. All three metabolites accounted for 25% of resveratrol ingested. It can suggest that the intestinal microbiota plays an important role in the bioavailability of resveratrol and its biological functions. Later studies discovered that resveratrol reaching the colon is converted by gut bacteria mainly to dihydroresveratrol (3,4-dihydroxystilbene) and lunularin (3,4′-dihydroxybibenzyl) [30]. The bacteria responsible for this conversion were identified as *Slackia equolifaciens* and *Adlercreutzia equolifaciens* [30]. It is hypothesized that the conjugated forms of resveratrol, especially the glucuronidated ones, serve as reservoirs of this compound from which it can be released locally by tissue β-glucuronidases. However, it was not confirmed experimentally yet [27]. In addition, it has to be kept in mind that also gut bacteria can produce this enzyme, increasing resveratrol bioavailability [31].

3. Gut Barrier—Structure and Importance

A gut barrier is a functional unit organized into intestinal microbiota, a mucus layer, intestinal epithelial cells (IECs) and lamina propria (Figure 3). A physical barrier consists of IECs, which are sealed by tight junctions (TJs), adherens junctions (AJs) and desmosomes [32]. TJs which are found on the side parts of enterocytes are built of transmembrane proteins such as claudins, occludins, peripheral membrane proteins, i.e., zonula occludens (ZO), and regulatory proteins. The most flexible part of the gut barrier is microbiota, which composition and count depend on lifestyle, diet and ongoing diseases. The microbiota plays an important role in the gut barrier integrity and function by adherence of commensal bacteria to the intestinal mucosa and forming an additional, protective layer [33,34].

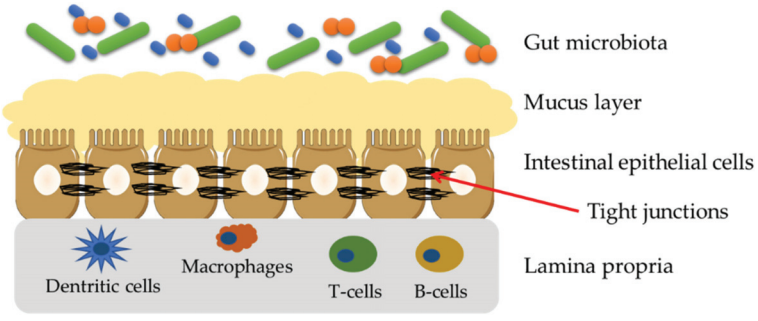

Figure 3. The scheme of the gut barrier.

The functioning of the intestinal barrier is a dynamic process, dependent on the activity of intercellular connections, regulated by both dietary components, the nervous system,

inflammatory mediators and hormones. The intestinal barrier is, therefore, responsible for maintaining the balance between the selective permeability of nutrients from the intestinal lumen into the circulation and the internal milieu as well as the protection of the organism against the penetration of harmful components of the external environment. Under physiological conditions, the selective absorption of nutrients through intercellular transport occurs, while unnecessary food components and harmful substances are removed from the gastrointestinal tract. The disruption of the proper functioning of the intestinal barrier by violating its integrity may result in the development of inflammation, as a consequence of uncontrolled penetration of antigens and products of bacterial metabolism. The impairment of the gut barrier has been associated with the development of various diseases, including celiac disease, obesity, non-alcoholic steatohepatitis (NASH) or non-alcoholic fatty liver disease (NAFLD), liver cirrhosis, chronic viral hepatitis B or C, HIV infection, inflammatory bowel diseases, irritable bowel syndrome and diverse autoimmune conditions [35]. Therefore, the maintenance of the integrity of the gut barrier is a crucial element for human health, and hence an increasing number of studies is conducted to understand the mechanisms involved in the improvement of the intestinal barrier integrity.

4. Non-Invasive Methods of Assessment of Gut Barrier in Clinical Trails

The important element in the gut barrier analysis is the selection of the appropriate analytical approach. Among various methods, the non-invasive techniques, which are based on the ingestion of specific molecules, or the analysis of circulating indirect markers which can evaluate the state of the gut barrier are the most commonly applied, especially in clinical trials. These methods can be easily applied in the clinical trials, in which the sampling of the tissues for histological analyses or local gene expression is impossible or too harmful. In this section, a brief presentation of the available methods is presented.

4.1. Absorption Methods for the Assessment of Gut Barrier Integrity

The integrity of the gut barrier can be assessed using various non-invasive approaches (Table 1). Among them, the most commonly used method in clinical trials is the sugar absorption test (SAT). SAT consists of the administration of a mixture of sugars with different molecular weights and different levels of penetration through the intestinal membrane. The most frequently used SAT includes the ingestion of high-molecular lactulose, which crosses the intestinal barrier to a small extent, through paracellular transport and low-molecular mannitol, which easily crosses the intestinal barrier by transcellular transport [36–39]. These molecules enter the bloodstream and then are excreted in the urine. The results of SAT are usually expressed as the ratio of lactulose to mannitol in the urine after 5–6 h of collection. The SAT accurately reflects the loss of intestinal barrier integrity in the small intestine [40]. The use of additional sugars, e.g., sucralose which is not metabolized by the gut microbiota, allows the assessment of integrity also in the colon [41]. Moreover, the ingestion of a certain amount of sucrose, which is easily metabolized by sucrases secreted by the duodenum, can be useful for the assessment of the integrity of the stomach and the proximal part of the duodenum. The sugars can be also replaced by other substances such as polyethylene glycols (PEG) with various molecular weights (400–4000 Da), ethylenediaminetetraacetic acid labelled with radioisotope chromium (^{51}Cr-EDTA) and dextran labelled with fluorescein isothiocyanate (FITC-dextran) [40]. All these methods similar to SAT are based on the selective permeability of the gut barrier to molecules dependent on their size.

Table 1. The characteristics of the methods for assessments of intestinal permeability.

Method	Analysed Marker	Localization	Type of Sample	Analytical Method	Disadvantages
Sugar absorption test (SAT)	Sugars of various molecular weights (lactulose, mannitol, sucralose, sucrose, raffinose)	Small intestine (can be extended to other parts of the intestinal tract by adding additional sugars to the mixture)	Urine	Chromatography	Time-consuming; requires chromatographical equipment for sugars analyses
PEG 400/4000	Polyethylene glycols (PEG)	The whole intestinal tract	Urine	Chromatography	Time-consuming; requires chromatographical equipment which can analyse PEG; big individual variation in response
^{51}Cr-EDTA	Isotopically labelled EDTA	The whole intestinal tract	Urine	Chromatography	Radioactivity
FITC-dextran	Fluorescent-labelled dextran	The whole intestinal tract	Urine/serum	Chromatography/ fluorimeter	Other substances (i.e., bilirubin) can give a fluorescence response
LAL	Endotoxin LPS	The whole intestinal tract	Plasma	ELISA	Low concentration—requires portal vein blood collection
EndoCAb	Antibodies anty-LPS	The whole intestinal tract	Serum	ELISA	Only in acute phase inflammations
D-lactate	Bacterial lactic acid	The whole intestinal tract	Plasma	ELISA/chromatography	Low specificity
Zonulin	Zonulin protein	-	Serum	ELISA	
DAO	Diamine oxidase	Small intestine	Plasma	ELISA	Requires the administration of heparin
Calprotectin	Calprotectin	Colon	Faeces	ELISA	Low specificity
AAT	Alfa-1-antitrypsin	Small intestine	Faeces/serum	ELISA	Unknown specificity
Citrulline	Citrulline	Small intestine	Plasma	ELISA/chromatography	Time-consuming; requires chromatographical equipment for amino acids analyses
GST	Glutathione S-transferases	-	Plasma/urine	ELISA	Low specificity
FABP	Fatty acid-binding proteins	Depending on the type of FABP	Plasma/urine	ELISA	Only in acute phase inflammations

4.2. Methods for the Assessment of Gut Barrier Integrity Related to Bacterial Metabolism

Another group of methods used for gut barrier assessment is the analysis of the indirect markers being the products of bacterial metabolism. The products of bacterial metabolism used as an intestinal permeability marker are lipopolysaccharides (LPS), which are amphiphilic bacterial endotoxins that are a component of the outer cell membrane of gram-negative bacteria [42]. The presence of LPS reflects the increased gut permeability as a result of damage to the intestinal barrier. An alternative to the analysis of LPS concentration is the analysis of antibodies against the endotoxin core—EndoCAb (Endotoxin Core Antibodies) in the peripheral blood. This method allows the quantification of antibodies against the inner core of bacterial endotoxin, which is responsible for its toxicity. EndoCAb can be used as an indirect indicator of intestinal barrier damage since the penetration of endotoxin into the bloodstream is related to the dysfunction of intestinal mucosa integrity [43]. Finally, the last marker of bacterial metabolism is D-lactic acid. D-lactic acid is a product of the metabolism of many bacteria, including the host microbiota. Initially, D-lactate was considered an indicator of bacterial infections [44], but low levels of D-lactic acid are also found in healthy people. When the intestinal barrier is injured, the concentration of D-lactic acid in the bloodstream increases, which is related to its increased transit through the damaged intestinal mucosa. Thus, D-lactic acid can be used as an indicator of the impairment of the intestinal barrier. An increased concentration of D-lactic acid may also be associated

with an increase in the number of bacteria in the gastrointestinal tract [45]. Therefore, the usefulness of this indicator for assessing intestinal permeability needs careful control.

4.3. Inflammation-Related Markers for the Assessment of Gut Barrier Integrity

The next group of intestinal permeability indicators are markers associated with inflammation. Zonulin is an analogue of the Zot toxin produced by *Vibrio cholerae*, which is involved in the regulation of TJ. Zonulin is an approximately 47 kDa protein that increases the permeability of the small intestine and contributes to the acquisition of primary intestinal immunity [42,46]. The molecular mechanism of zonulin action on the intestinal barrier is not fully understood. The Zot toxin activates the proteinase-activated receptor 2 (PAR2) followed by the epidermal growth factor receptor (EGFR) [47]. This signalling cascade results in the detachment of the peripheral ZO-1 protein from the occludins and claudins, the tight halo proteins [48]. It has been suggested that zonulin exhibits a similar mechanism of action, although this has not been conclusively confirmed. The concentration of zonulin in the bloodstream is elevated in the presence of disturbances in the integrity of the intestinal barrier, therefore zonulin is a useful marker of intestinal permeability [42,49].

The main enzyme catalysing the oxidation of diamines such as histamine, putrescine and cadaverine is diamine oxidase (DAO). This enzyme is synthesized in the intestinal mucosa, placenta, kidneys and thymus [50]. The majority of DAO in the bloodstream comes from the small intestine, where it is produced at the apical ends of the mature cells of the intestinal villi [51]. The determination of DAO activity was used to assess intestinal permeability in people suffering from Crohn's disease, ulcerative colitis or acute lymphoblastic leukaemia [52].

Calprotectin is a 32-kDa acute-phase calcium and zinc-binding protein. It is produced by leukocytes, mainly by neutrophils, but also by macrophages and monocytes [53]. Inflammation overexpresses calprotectin in cells of the immune system. The concentration of this protein in serum and faeces increases, and under physiological conditions the concentration of calprotectin in the faeces exceeds that in the serum several times. Numerous studies have identified faecal calprotectin as a sensitive marker of intestinal inflammation [54–56]. Intestinal inflammation leads to an increase in intestinal permeability and the penetration of calprotectin-secreting leukocytes, which in turn leads to a significant increase in its concentration in the faeces. In practice, faecal calprotectin testing is used to distinguish IBD from Irritable Bowel Syndrome, to diagnose necrotising enteritis and monitor response to treatment of inflammatory bowel conditions [57].

Alpha-1-antitrypsin (AAT) is a 52 kDa trypsin inhibitor and is one of the most potent serine protease inhibitors. In the bloodstream, it is present at a concentration of 1.5 to 3.5 g/L, although, during acute inflammation, the concentration of AAT may increase many times [58]. This protein protects tissues against the influence of inflammatory cell enzymes, especially neutrophilic elastase [42]. In contrast with other serum proteins, AAT is highly resistant to gastrointestinal proteolytic enzymes and is excreted intact in the faeces. A high concentration of AAT is found in the stool due to inflammation and ulceration of the intestinal mucosa and increased intestinal permeability, as AAT passes from the bloodstream into the intestinal lumen. For this reason, AAT has been recognized as a marker of intestinal permeability [59]. AAT concentration can be determined using a nephelometer [60], although commercially available enzyme immunoassays are most commonly used for this purpose [42].

4.4. Markers Associated with the Damage of the Mucosa

Citrulline is a non-protein amino acid, a derivative of ornithine, which is converted into arginine in the urea cycle. The concentration of citrulline in the plasma under physiological conditions is 20–50 μmol/L. Citrulline present in the bloodstream is produced mainly by cells of the small intestine. Therefore, the concentration of this amino acid in the blood is considered an indicator of the activity of enterocytes (functional enterocyte mass, FEM). The reduction of FEM in course of many pathological conditions is connected with

increased permeability of the gut barrier and leads to a decrease in the level of citrulline in the bloodstream. Numerous studies have shown a reduced level of citrulline in the plasma of people suffering from short bowel syndrome, HIV, adenovirus infections and during small intestine transplant rejection [61]. It should be emphasized that the proper functioning of the kidneys has a great influence on the concentration of citrulline in the bloodstream. Increased levels of citrulline have been found in people with moderate renal impairment [62], therefore the concentration of creatinine, which informs about the condition of the kidneys, should be monitored during the determination of citrulline.

Glutathione S-transferases (GSTs) are a family of detoxification enzymes that catalyse the nucleophilic coupling reactions of reduced glutathione with electrophilic compounds [63]. The catalytic activity of GSTs is associated with the detoxification of chemical compounds with electrophilic properties and reactive products of oxidative stress. Depending on the tissue they come from, there are four subgroups of GST: α, μ, π and θ. αGST is mainly present in the liver, kidneys and intestines. αGST has been proposed as a marker of intestinal epithelial cell damage [64]. Elevated levels of αGST in plasma and urine may indicate damage to the intestinal barrier, but also to the liver and kidneys since this enzyme is found in the epithelial cells of these organs. A disadvantage of αGST as a marker of intestinal barrier damage is its low specificity and it can be useful only if other diseases have been eliminated.

Fatty Acid Binding Proteins (FABPs) are small (14–15 kDa), water-soluble cytosolic proteins. Their function is to bind and transport fatty acids. There are several types of FABP, distinguished according to the tissues of origin [65]. Three types of fatty acid binding proteins have been found in the digestive tract: hepatic FABP (L-FABP) present in the liver, kidneys and intestines, bile acid binding proteins (BABPs) present in the ileum, and intestinal FABP (I-FABP) present mainly in the jejunum, and to a lesser extent in the colon. I-FABP is a 15-kDa protein produced in mature cells of the epithelium of the small intestine. Its function is to transfer fatty acids from the apical membrane of the enterocyte to the endoplasmic reticulum, where the biosynthesis of lipid complexes occurs. Due to its low molecular weight and relatively good solubility, I-FABP is easily released into the bloodstream when the intestinal epithelial membrane is damaged and is rapidly cleared by the kidneys (half-life is 11 min) [66]. Therefore, its presence can be measured in urine or plasma. The most common methods for determining I-FABP are enzyme immunoassay methods (ELISA). The physiological level of I-FABP reflects the exchange rate of intestinal epithelial cells [67], while an elevated level of I-FABP may indicate damage to the intestinal barrier [68]. Numerous studies have indicated that I-FABP can be considered a marker of epithelial cell damage. Increased levels of I-FABP in the urine have been found in people suffering from intestinal ischemia, systemic inflammatory response syndrome or necrotizing enterocolitis [67,69]. Due to the diversity of FABPs depending on the tissue from which they originate, the measurement of individual proteins in urine and/or plasma can be a valuable tool in locating tissue damage.

5. Principles of Polyphenols Action on the Gut Barrier

Dietary modification affects significantly the microbial ecosystem, which can influence the intestinal barrier [70,71]. For instance, it was reported that the Western diet aggravates the integrity of the gut barrier via modifications of the bacterial ecosystem, while individuals on the Mediterranean diet, rich in fruits, vegetables and unrefined cereals were found to have intact intestinal barriers [70]. The metabolites suggested to be involved in this process are short-chain fatty acids (SCFA), such as acetic, butyric, propionic and valeric acids, which are suggested as important factors in the functioning of the epithelium [72]. Recently, an increasing interest in the role of phenolic compounds, which are also consumed in large quantities in the Mediterranean diet, is observed in the gut barrier integrity [73,74].

The hypothesis about the involvement of phenolic compounds on the gut barrier results from the antioxidant and anti-inflammatory properties of these compounds. Since phenolic compounds are capable to downregulate inflammatory genes such as NF-κβ,

reduce the production of cytokine production and promote the internal antioxidant capacity [75], it can be assumed that phenolic compounds can locally reduce inflammation. The NF-κβ signalling is strongly connected with cytokines (which activate the NF-κβ) and the gut barrier functions (by TJ impairment) [76]. Other signalling pathways, which are affected by phenolic compounds and can influence the gut barrier are various kinases, which are regulators of epithelial cells, and TJ expressions. Some phenolic compounds were found to inhibit different kinases involved in the phosphorylation of proteins involved in gut barrier functioning, such as protein kinase C (PKC) and myosin light-chain kinase (MLKC) [75,77].

Moreover, phenolic compounds were repeatedly reported to modulate the intestinal microbiota [76,78,79]. This two-way interaction not only facilitates the metabolism of phenolic compounds but also phenolic compounds can stimulate the growth of beneficial intestinal bacteria [78,79]. The derivatives originating from phenolic compounds microbial metabolism may not only affect backwards the bacteria but can also influence the signalling pathways [80]. Another potential way of action is the role of phenolic compounds in the metabolism of other molecules present in a colon, including SCFA, sterols and products of bacterial metabolism, which exhibit pro- or anti-inflammatory properties [81].

6. Effect of Resveratrol on the Gut Barrier

6.1. In Vitro Studies

The main evidence about the potential positive effects of resveratrol for the gut barrier is based on the in vitro studies, which were focused on the changes in the regulatory pathways. The most commonly used cell line was Caco-2 [82–85] and intestinal porcine enterocytes (IPEC-J2) [86,87]. The intestinal permeability in these studies was assessed by the measurement of transepithelial electrical resistance (TEER) across the cellular monolayer and by the measurement of the expression of the genes and corresponding proteins.

Carasco-Pozo et al. [82] reported that phenolic compounds applied in the Caco-2 cells with indomethacin-induced disruption of epithelial integrity were able to reverse the functioning of the layer. Among the analysed compounds, quercetin was the most efficient, followed by epigallocatechin gallate and resveratrol. Only rutin was found to be neutral on the cell integrity. In another study, resveratrol was applied in 1, 10 and 20 μM in Caco-2 cells treated with hydrogen peroxide to induce hyperpermeability and oxidative stress [83]. The authors found that resveratrol increased the epithelial expression and phosphorylation of ZO-1 and occludins with the increasing dose of polyphenol. Additionally, resveratrol protected Caco-2 cells from oxidative stress, reducing the accumulation of malonaldehyde and oxygen species and increasing the expression of enzymes involved in protection against oxidative stress, such as superoxide dismutase and heme oxygenase-1. 20 μM of resveratrol was able to block the hydrogen peroxide-induced activation of PKC and phosphorylation of p38, which had a confirmation in the protein expression assessed by Western blot.

Two studies showed that resveratrol is capable to protect the intestinal barrier from disruption caused by deoxynivaleron, a mycotoxin produced by *Fusarium* genera [86,87]. Both these studies showed that resveratrol prevents the deoxynivaleron-induced degradation of TJ proteins, and decreases TEER and bacteria translocation. The modulation of IL-6 and IL-8 secretion via mitogen-activated protein kinase-dependent pathways was proposed as a potential route of resveratrol activity.

A recent study evaluated the effect of resveratrol and its metabolites resulting from microbiota metabolism, namely dihydroresveratrol and 3-(4-hydroxyphenyl)-propionic acid on the intestinal barrier in LPS-treated Caco-2 cells [85]. It was found that only resveratrol and 3-(4-hydroxyphenyl)-propionic acid have beneficial effects on the intestinal barrier by increasing the expression of TJ protein and Muc2, and the molecular mechanism proposed by authors to be involved is monophosphate-activated protein kinase (AMPK)-mediated activation of CDX2 and the regulation of the SIRT1/NF-κβ pathway. At the same time, dihydroxyresveratrol did not show any positive effect on the intestinal barrier. Another study on the resveratrol derivative was conducted by Jo et al. [84]. The authors

applied oxyresveratrol to the Caco-2 cells. Oxyresveratrol was found to upregulate the expression of genes and proteins related to TJ, such as claudin-1, ZO-1 and occludins. The improvement of the intestinal barrier by oxyresveratrol was associated with the activation of mitogen-activated protein kinase (MAPK) and PKC pathways.

6.2. Animal Studies

The results obtained in vitro needed confirmation in vivo, especially considering that resveratrol was applied directly on the cell lines, while in vivo the limited bioavailability of phenolic compounds has to be taken into consideration. The majority of studies were performed with rodents including Wistar and Sprague Dawley rats [83,88–91] and mice [85,92–98]. One study was performed with ducks [99]. Collectively, animal studies confirmed the beneficial effect of resveratrol on the gut barrier.

Wang et al. [83] reported that resveratrol restored intestinal integrity in rats with induced obstructive jaundice. The results of SAT in groups fed with resveratrol were significantly reduced compared to rats with obstructive jaundice and were closer to the control group. Moreover, the activity of superoxide oxidase was increasing with increasing doses of resveratrol (from 10 to 20 mg/kg) and in rats fed with 20 mg/kg was at the same level as in the control group. In another study, male Sprague-Dawley rats with high-fat diet (HFD)-induced NASH were fed with resveratrol for six weeks [91]. Resveratrol inhibited the development of NASH as well as attenuated the gut microbiota dysbiosis, colon inflammation and metabolic endotoxemia. An increase in the count of *Akkermansia muciniphila*, *Ruminococcaceae*, *Lachnospiraceae*, and a decrease in *Desulfovibrio* was noted in rats after resveratrol intake. Importantly, resveratrol ingestion led to the upregulation of TJ expression and decreased intestinal permeability, assessed based on bacterial translocation. HFD was used also to induce insulin resistance in mice [94]. The authors reported that resveratrol intake improved the lipid profile parameters in HFD-treated mice, as well as ameliorated endotoxemia, intestinal barrier dysfunction, glucose intolerance and inflammation. Similar to the previous study, the abundance of *Akkermansia* was increased after resveratrol administration. The confirmation of the positive effect of resveratrol on the gut barrier was found also in a study by Wang et al. [95], who observed the alleviation in HFD-induced NAFLD, improvement of intestinal barrier functions and gut microbiota composition after resveratrol intake. The expression of the TJ proteins and the intestinal mucosa morphology was improved after resveratrol administration, despite the HFD. The study conducted with cyclophosphamide-induced immunosuppressed mice confirmed that resveratrol can restore the intestinal microbiota dysbiosis, improve the gut barrier integrity and upregulate the expression of ZO-1, claudin-1 and occludin [98]. The authors confirmed that the TLR4-NF-κβ signalling pathway is involved in the resveratrol effect on the gut barrier. A very recent study by Hao et al. [97] evaluated the effect of resveratrol on intestinal permeability in mice exposed to aluminium chloride. Aluminium exposure induced depressive-like behaviour and increased intestinal permeability. The administration of resveratrol decreased depressive symptoms and upregulated the expression of SIRT1, which was found to reduce inflammation and restore intestinal permeability.

Finally, the study conducted with ducks with LPS-induced intestinal dysfunction showed that resveratrol in a dose of up to 500 mg/kg alleviated intestinal permeability established based on the increased expression of TJ genes and proteins [99]. The increasing dose of resveratrol resulted in the decrease of pro-inflammatory cytokine (IL-6, IL-18, TNF-α) levels and the expression of genes involved in inflammation (TLR4/NF-κβ signalling pathway, IKK, TXNIP, NLRP3, Caspase-1, IL-6, IL-18).

Interestingly, a recent study showed that resveratrol can act beneficially not only on the intestinal epithelium, but can also improve pulmonary epithelium functions. Alharris et al. [100] evaluated the effect of resveratrol in ovalbumin-induced murine allergic asthma. Resveratrol intake attenuated allergic asthma, improved pulmonary functions, and reduced inflammation in the lungs in ovalbumin-treated mice. Moreover, the administration of resveratrol affected not only the lung but also the intestinal tract. The administration

of resveratrol led to changes in intestinal microbiota with the enrichment of *Bacteroides acidifaciens* and SCFA concentration in the colon.

The assumption about the positive effects of resveratrol on the gut barrier is mainly based on the gene and protein expression and TEER. More studies with functional tests of the circulating level of indirect metabolites (see Section 4) need to be performed to show the effects of the expression modifications.

6.3. Human Studies

To date, there is a limited number of studies on the effect of phenolic compounds on the gut barrier. Although some studies have been registered in clinical trial databases [74], the number of available published reports is very low. The MaPLE (Microbiome mAnipulation through Polyphenols for managing Leakiness in the Elderly) project is an example of a study focused on the interaction between polyphenols, microbiota and gut barrier [101]. The authors reported that 700 mg of total polyphenols daily in a form of three small portions of selected polyphenol-rich foods daily for 8 weeks reduced the intestinal permeability expressed as a circulating level of zonulin in the elderly population [102,103]. Notably, the analysis of intestinal permeability was based on only the level of zonulin, without any functional tests, such as SAT. To date, despite the successful findings obtained with in vitro and in vivo studies, no clinical studies were performed aimed to evaluate the effect of resveratrol on the gut barrier. However, considering the positive effects of resveratrol on inflammation [104–106], oxidative stress [105,107] and gut microbiota composition [104,108], and the involvement of these factors in the gut barrier integrity, it can be assumed that the positive effect of resveratrol on the intestinal permeability obtained with in vitro and in vivo studies may be observed also in clinical trials. In addition, the studies using functional tests, not only indirect markers are needed to fully address the integrity of the gut barrier.

7. Summary and Future Perspectives

To summarize, the current studies showed that phenolic compounds, including resveratrol, have a great potential to improve the integrity of the gut barrier. Very promising studies have been conducted with in vitro and animal models, establishing the expression of TJ genes and proteins or TEER. Still, more clinical trials must be performed to evaluate the effect of resveratrol on the gut barrier, especially in individuals with increased intestinal permeability, using both indirect markers and functional tests. Moreover, considering the two-way interaction of this phytochemical with microbiota and the important role of gut microorganisms in the functioning of the intestinal barrier, the interplay between all these three compartments should be carefully evaluated in future.

Author Contributions: Conceptualization, N.D. and E.J.-C.; data curation, N.D.; writing—original draft preparation, N.D.; writing—review and editing, N.D. and E.J.-C.; visualization, N.D.; funding acquisition, N.D. All authors have read and agreed to the published version of the manuscript.

Funding: This research received no external funding.

Data Availability Statement: Not applicable.

Conflicts of Interest: The authors declare no conflict of interest.

References

1. Cutrim, C.S.; Cortez, M.A.S. A Review on Polyphenols: Classification, Beneficial Effects and Their Application in Dairy Products. *Int. J. Dairy Technol.* **2018**, *71*, 564–578. [CrossRef]
2. de Souza, E.L.; de Albuquerque, T.M.R.; dos Santos, A.S.; Massa, N.M.L.; de Brito Alves, J.L. Potential Interactions among Phenolic Compounds and Probiotics for Mutual Boosting of Their Health-Promoting Properties and Food Functionalities—A Review. *Crit. Rev. Food Sci. Nutr.* **2019**, *59*, 1645–1659. [CrossRef]
3. Jiang, B.; Guo, L.; Li, B.-Y.; Zhen, J.-H.; Song, J.; Peng, T.; Yang, X.-D.; Hu, Z.; Gao, H.-Q. Resveratrol Attenuates Early Diabetic Nephropathy by Down-Regulating Glutathione S-Transferases Mu in Diabetic Rats. *J. Med. Food* **2013**, *16*, 481–486. [CrossRef] [PubMed]

4. Li, A.N.; Li, S.; Zhang, Y.J.; Xu, X.R.; Chen, Y.M.; Li, H.B. Resources and Biological Activities of Natural Polyphenols. *Nutrients* **2014**, *6*, 6020–6047. [CrossRef]
5. Scalbert, A.; Manach, C.; Morand, C.; Rémésy, C.; Jiménez, L. Dietary Polyphenols and the Prevention of Diseases. *Crit. Rev. Food Sci. Nutr.* **2005**, *45*, 287–306. [CrossRef] [PubMed]
6. Quideau, S.; Deffieux, D.; Douat-Casassus, C.; Pouységu, L. Plant Polyphenols: Chemical Properties, Biological Activities, and Synthesis. *Angew. Chem. Int. Ed.* **2011**, *50*, 586–621. [CrossRef] [PubMed]
7. Teplova, V.; Isakova, E.P.; Klein, O.I.; Dergachova, D.I.; Gessler, N.N.; Deryabina, Y.I. Natural Polyphenols: Biological Activity, Pharmacological Potential, Means of Metabolic Engineering (Review). *Appl. Biochem. Microbiol.* **2018**, *54*, 221–237. [CrossRef]
8. Kobayashi, S.; Shinohara, M.; Nagai, T.; Konishi, Y. Transport Mechanisms for Soy Isoflavones and Microbial Metabolites Dihydrogenistein and Dihydrodaidzein Across Monolayers and Membranes. *Biosci. Biotechnol. Biochem.* **2013**, *77*, 2210–2217. [CrossRef]
9. Carbonell-Capella, J.M.; Buniowska, M.; Barba, F.J.; Esteve, M.J.; Frígola, A. Analytical Methods for Determining Bioavailability and Bioaccessibility of Bioactive Compounds from Fruits and Vegetables: A Review. *Compr. Rev. Food Sci. Food Saf.* **2014**, *13*, 155–171. [CrossRef]
10. Zhang, X.; Song, J.; Shi, X.; Miao, S.; Li, Y.; Wen, A. Absorption and Metabolism Characteristics of Rutin in Caco-2 Cells. *Sci. World J.* **2013**, *2013*, 382350. [CrossRef]
11. Li, S.; Liu, J.; Li, Z.; Wang, L.; Gao, W.; Zhang, Z.; Guo, C. Sodium-Dependent Glucose Transporter 1 and Glucose Transporter 2 Mediate Intestinal Transport of Quercetrin in Caco-2 Cells. *Food Nutr. Res.* **2020**, *64*, 3745. [CrossRef] [PubMed]
12. Kamonpatana, K.; Giusti, M.M.; Chitchumroonchokchai, C.; MorenoCruz, M.; Riedl, K.M.; Kumar, P.; Failla, M.L. Susceptibility of Anthocyanins to Ex Vivo Degradation in Human Saliva. *Food Chem.* **2012**, *135*, 738–747. [CrossRef] [PubMed]
13. Rodríguez-Daza, M.C.; Pulido-Mateos, E.C.; Lupien-Meilleur, J.; Guyonnet, D.; Desjardins, Y.; Roy, D. Polyphenol-Mediated Gut Microbiota Modulation: Toward Prebiotics and Further. *Front. Nutr.* **2021**, *8*, 689456. [CrossRef] [PubMed]
14. Shahidi, F.; Peng, H. Bioaccessibility and Bioavailability of Phenolic Compounds. *J. Food Bioact.* **2018**, *4*, 11–68. [CrossRef]
15. Cosme, P.; Rodríguez, A.B.; Espino, J.; Garrido, M. Plant Phenolics: Bioavailability as a Key Determinant of Their Potential Health-Promoting Applications. *Antioxidants* **2020**, *9*, 1263. [CrossRef]
16. Gibson, G.R.; Hutkins, R.; Sanders, M.E.; Prescott, S.L.; Reimer, R.A.; Salminen, S.J.; Scott, K.; Stanton, C.; Swanson, K.S.; Cani, P.D.; et al. Expert Consensus Document: The International Scientific Association for Probiotics and Prebiotics (ISAPP) Consensus Statement on the Definition and Scope of Prebiotics. *Nat. Rev. Gastroenterol. Hepatol.* **2017**, *14*, 491–502. [CrossRef]
17. Corrêa, T.A.F.; Rogero, M.M.; Hassimotto, N.M.A.; Lajolo, F.M. The Two-Way Polyphenols-Microbiota Interactions and Their Effects on Obesity and Related Metabolic Diseases. *Front. Nutr.* **2019**, *6*, 188. [CrossRef]
18. Berman, A.Y.; Motechin, R.A.; Wiesenfeld, M.Y.; Holz, M.K. The Therapeutic Potential of Resveratrol: A Review of Clinical Trials. *NPJ Precis. Oncol.* **2017**, *1*, 35. [CrossRef]
19. Salehi, B.; Mishra, A.P.; Nigam, M.; Sener, B.; Kilic, M.; Sharifi-Rad, M.; Fokou, P.V.T.; Martins, N.; Sharifi-Rad, J. Resveratrol: A Double-Edged Sword in Health Benefits. *Biomedicines* **2018**, *6*, 91. [CrossRef]
20. Bavaresco, L.; Trevisan, M.; Cinerea, B.; Bavaresco, I.L.; Petegolli, I.D.; Cantu, I.E.; Fregoni, M.; Chiusaz, G.; Trevisan, M. Elicitation and Accumulation of Stilbene Phytoalexins in Grapevine Berries Infected by Botrytis Cinerea. *Vitis* **2017**, *36*, 77–83.
21. Renaud, S.; de Lorgeril, M. Wine, Alcohol, Platelets, and the French Paradox for Coronary Heart Disease. *Lancet* **1992**, *339*, 1523–1526. [CrossRef]
22. Chung, S.; Yao, H.; Caito, S.; Hwang, J.; Arunachalam, G.; Rahman, I. Regulation of SIRT1 in Cellular Functions: Role of Polyphenols. *Arch. Biochem. Biophys.* **2010**, *501*, 79–90. [CrossRef]
23. Vanamala, J.; Reddivari, L.; Radhakrishnan, S.; Tarver, C. Resveratrol Suppresses IGF-1 Induced Human Colon Cancer Cell Proliferation and Elevates Apoptosis via Suppression of IGF-1R/Wnt and Activation of P53 Signaling Pathways. *BMC Cancer* **2010**, *10*, 238. [CrossRef]
24. Park, E.-S.; Lim, Y.; Hong, J.-T.; Yoo, H.-S.; Lee, C.-K.; Pyo, M.-Y.; Yun, Y.-P. Pterostilbene, a Natural Dimethylated Analog of Resveratrol, Inhibits Rat Aortic Vascular Smooth Muscle Cell Proliferation by Blocking Akt-Dependent Pathway. *Vascul. Pharmacol.* **2010**, *53*, 61–67. [CrossRef]
25. Alayev, A.; Doubleday, P.F.; Berger, S.M.; Ballif, B.A.; Holz, M.K. Phosphoproteomics Reveals Resveratrol-Dependent Inhibition of Akt/MTORC1/S6K1 Signaling. *J. Proteome Res.* **2014**, *13*, 5734–5742. [CrossRef]
26. Alayev, A.; Berger, S.M.; Holz, M.K. Resveratrol as a Novel Treatment for Diseases with MTOR Pathway Hyperactivation. *Ann. N. Y. Acad. Sci.* **2015**, *1348*, 116–123. [CrossRef]
27. Walle, T. Bioavailability of Resveratrol. *Ann. N. Y. Acad. Sci.* **2011**, *1215*, 9–15. [CrossRef]
28. Pannu, N.; Bhatnagar, A. Resveratrol: From Enhanced Biosynthesis and Bioavailability to Multitargeting Chronic Diseases. *Biomed. Pharmacother.* **2019**, *109*, 2237–2251. [CrossRef]
29. Walle, T.; Hsieh, F.; DeLegge, M.H.; Oatis, J.E.; Walle, U.K. High Absorption but Very Low Bioavailability of Oral Resveratrol in Humans. *Drug Metab. Dispos.* **2004**, *32*, 1377. [CrossRef]
30. Bode, L.M.; Bunzel, D.; Huch, M.; Cho, G.-S.; Ruhland, D.; Bunzel, M.; Bub, A.; Franz, C.M.A.P.; Kulling, S.E. In Vivo and in Vitro Metabolism of Trans-Resveratrol by Human Gut Microbiota. *Am. J. Clin. Nutr.* **2013**, *97*, 295–309. [CrossRef]

31. Candeliere, F.; Raimondi, S.; Ranieri, R.; Musmeci, E.; Zambon, A.; Amaretti, A.; Rossi, M. β-Glucuronidase Pattern Predicted From Gut Metagenomes Indicates Potentially Diversified Pharmacomicrobiomics. *Front. Microbiol.* **2022**, *13*, 826994. [CrossRef] [PubMed]
32. Kocot, A.M.; Jarocka-Cyrta, E.; Drabińska, N. Overview of the Importance of Biotics in Gut Barrier Integrity. *Int. J. Mol. Sci.* **2022**, *23*, 2896. [CrossRef] [PubMed]
33. Camilleri, M. Human Intestinal Barrier: Effects of Stressors, Diet, Prebiotics, and Probiotics. *Clin. Transl. Gastroenterol.* **2021**, *12*, e00308. [CrossRef] [PubMed]
34. Hsieh, C.-Y.; Osaka, T.; Moriyama, E.; Date, Y.; Kikuchi, J.; Tsuneda, S. Strengthening of the Intestinal Epithelial Tight Junction by Bifidobacterium Bifidum. *Physiol. Rep.* **2015**, *3*, e12327. [CrossRef] [PubMed]
35. Assimakopoulos, S.F.; Triantos, C.; Maroulis, I.; Gogos, C. The Role of the Gut Barrier Function in Health and Disease. *Gastroenterol. Res.* **2018**, *11*, 261–263. [CrossRef]
36. Rao, A.S.; Camilleri, M.; Eckert, D.J.; Busciglio, I.; Burton, D.D.; Ryks, M.; Wong, B.S.; Lamsam, J.; Singh, R.; Zinsmeister, A.R. Urine Sugars for in Vivo Gut Permeability: Validation and Comparisons in Irritable Bowel Syndrome-Diarrhea and Controls. *Am. J. Physiol. Gastrointest. Liver Physiol.* **2011**, *301*, G919–G928. [CrossRef]
37. Ordiz, M.I.; Davitt, C.; Stephenson, K.; Agapova, S.; Divala, O.; Shaikh, N.; Manary, M.J. EB 2017 Article: Interpretation of the Lactulose:Mannitol Test in Rural Malawian Children at Risk for Perturbations in Intestinal Permeability. *Exp. Biol. Med.* **2018**, *243*, 677–683. [CrossRef]
38. Musa, M.A.; Kabir, M.; Hossain, M.I.; Ahmed, E.; Siddique, A.; Rashid, H.; Mahfuz, M.; Mondal, D.; Ahmed, T.; Petri, W.A.; et al. Measurement of Intestinal Permeability Using Lactulose and Mannitol with Conventional Five Hours and Shortened Two Hours Urine Collection by Two Different Methods: HPAE-PAD and LC-MSMS. *PLoS ONE* **2019**, *14*, e0220397. [CrossRef]
39. Drabińska, N.; Krupa-kozak, U.; Jarocka-cyrta, E. Intestinal Permeability in Children with Celiac Disease after the Administration of Oligofructose-Enriched Inulin into a Gluten-Free Diet—Results of a Randomized, Placebo-Controlled, Pilot Trial. *Nutrients* **2020**, *12*, 1736. [CrossRef]
40. Grootjans, J.; Thuijls, G.; Verdam, F.; Derikx, J.P.; Lenaerts, K.; Buurman, W.A. Non-Invasive Assessment of Barrier Integrity and Function of the Human Gut. *World J. Gastrointest Surg.* **2010**, *2*, 61–69. [CrossRef]
41. van Wijck, K.; Verlinden, T.J.M.; van Eijk, H.M.H.; Dekker, J.; Buurman, W.A.; Dejong, C.H.C.; Lenaerts, K. Novel Multi-Sugar Assay for Site-Specific Gastrointestinal Permeability Analysis: A Randomized Controlled Crossover Trial. *Clin. Nutr.* **2013**, *32*, 245–251. [CrossRef]
42. Wang, L.; Llorente, C.; Hartmann, P.; Yang, A.-M.; Chen, P.; Schnabl, B. Methods to Determine Intestinal Permeability and Bacterial Translocation during Liver Disease. *J. Immunol. Methods* **2015**, *421*, 44–53. [CrossRef]
43. Bischoff, S.C.; Barbara, G.; Buurman, W.; Ockhuizen, T.; Schulzke, J.D.; Serino, M.; Tilg, H.; Watson, A.; Wells, J.M. Intestinal Permeability—A New Target for Disease Prevention and Therapy. *BMC Gastroenterol.* **2014**, *14*, 189. [CrossRef]
44. Smith, S.M.; Eng, R.H.K.; Buccini, F. Use of D-Lactic Acid Measurements in the Diagnosis of Bacterial Infections. *J. Infect. Dis.* **1986**, *154*, 658–664. [CrossRef]
45. Herrera, D.J.; Morris, K.; Johnston, C.; Griffiths, P. Automated Assay for Plasma D-Lactate by Enzymatic Spectrophotometric Analysis with Sample Blank Correction. *Ann. Clin. Biochem.* **2008**, *45*, 177–183. [CrossRef]
46. Fasano, A.; Not, T.; Wang, W.; Uzzau, S.; Berti, I.; Tommasini, A.; Goldblum, S.E. Zonulin, a Newly Discovered Modulator of Intestinal Permeability, and Its Expression in Coeliac Disease. *Lancet* **2000**, *355*, 1518–1519. [CrossRef]
47. Tripathi, A.; Lammers, K.M.; Goldblum, S.; Shea-Donohue, T.; Netzel-Arnett, S.; Buzza, M.S.; Antalis, T.M.; Vogel, S.N.; Zhao, A.; Yang, S.; et al. Identification of Human Zonulin, a Physiological Modulator of Tight Junctions, as Prehaptoglobin-2. *Proc. Natl. Acad. Sci. USA* **2009**, *106*, 16799–16804. [CrossRef]
48. Goldblum, S.E.; Rai, U.; Tripathi, A.; Thakar, M.; de Leo, L.; di Toro, N.; Not, T.; Ramachandran, R.; Puche, A.C.; Hollenberg, M.D.; et al. The Active Zot Domain (Aa 288–293) Increases ZO-1 and Myosin 1C Serine/Threonine Phosphorylation, Alters Interaction between ZO-1 and Its Binding Partners, and Induces Tight Junction Disassembly through Proteinase Activated Receptor 2 Activation. *FASEB J.* **2011**, *25*, 144–158. [CrossRef]
49. Moreno-Navarrete, J.M.; Sabater, M.; Ortega, F.; Ricart, W.; Fernández-Real, J.M. Circulating Zonulin, a Marker of Intestinal Permeability, Is Increased in Association with Obesity-Associated Insulin Resistance. *PLoS ONE* **2012**, *7*, e37160. [CrossRef]
50. Rangachari, P.K. Histamine: Mercurial Messenger in the Gut. *Am. J. Physiol.-Gastrointest. Liver Physiol.* **1992**, *262*, G1–G13. [CrossRef]
51. Luk, G.D.; Bayless, T.M.; Baylin, S.B. Diamine Oxidase (Histaminase). A Circulating Marker for Rat Intestinal Mucosal Maturation and Integrity. *J. Clin. Investig.* **1980**, *66*, 66–70. [CrossRef] [PubMed]
52. Honzawa, Y.; Nakase, H.; Matsuura, M.; Chiba, T. Clinical Significance of Serum Diamine Oxidase Activity in Inflammatory Bowel Disease: Importance of Evaluation of Small Intestinal Permeability. *Inflamm. Bowel. Dis.* **2011**, *17*, E23–E25. [CrossRef] [PubMed]
53. Pathirana, W.G.W.; Chubb, S.P.; Gillett, M.J.; Vasikaran, S.D. Faecal Calprotectin. *Clin. Biochem. Rev.* **2018**, *39*, 77–90. [PubMed]
54. Malcomson, F.C.; Willis, N.D.; McCallum, I.; Xie, L.; Ibero-Baraibar, I.; Leung, W.C.; Kelly, S.; Bradburn, D.M.; Belshaw, N.J.; Johnson, I.T.; et al. Effects of Supplementation with Nondigestible Carbohydrates on Fecal Calprotectin and on Epigenetic Regulation of SFRP1 Expression in the Large-Bowel Mucosa of Healthy Individuals. *Am. J. Clin. Nutr.* **2017**, *105*, 400–410. [CrossRef] [PubMed]

55. Casellas, F.; Borruel, N.; Torrejón, A.; Varela, E.; Antolin, M.; Guarner, F.; Malagelada, J.R. Oral Oligofructose-Enriched Inulin Supplementation in Acute Ulcerative Colitis Is Well Tolerated and Associated with Lowered Faecal Calprotectin. *Aliment. Pharm. Ther.* **2007**, *25*, 1061–1067. [CrossRef]
56. Montalto, M.; Santoro, L.; Curigliano, V.; D'Onofrio, F.; Cammarota, G.; Panunzi, S.; Ricci, R.; Gallo, A.; Grieco, A.; Gasbarrini, A.; et al. Faecal Calprotectin Concentrations in Untreated Coeliac Patients. *Scand. J. Gastroenterol.* **2007**, *42*, 957–961. [CrossRef]
57. D'Amico, F.; Nancey, S.; Danese, S.; Peyrin-Biroulet, L. A Practical Guide for Faecal Calprotectin Measurement: Myths and Realities. *J. Crohns. Colitis.* **2020**, *15*, 152–161. [CrossRef]
58. Kosek, M.; Haque, R.; Lima, A.; Babji, S.; Shrestha, S.; Qureshi, S.; Amidou, S.; Mduma, E.; Lee, G.; Yori, P.P.; et al. Fecal Markers of Intestinal Inflammation and Permeability Associated with the Subsequent Acquisition of Linear Growth Deficits in Infants. *Am. Soc. Trop. Med. Hyg.* **2013**, *88*, 390–396. [CrossRef]
59. Alam, A.N.; Sarker, S.A.; Wahed, M.A.; Khatun, M.; Rahaman, M.M. Enteric Protein Loss and Intestinal Permeability Changes in Children during Acute Shigellosis and after Recovery: Effect of Zinc Supplementation. *Gut* **1994**, *35*, 1707. [CrossRef]
60. Sharpstone, D.; Rowbottom, A.; Nelson, M.; Gazzard, B. Faecal Alpha 1 Antitrypsin as a Marker of Gastrointestinal Disease in HIV Antibody Positive Individuals. *Gut* **1996**, *38*, 206. [CrossRef]
61. Gondolesi, G.; Ghirardo, S.; Raymond, K.; Hoppenhauer, L.; Surillo, D.; Rumbo, C.; Fishbein, T.; Sansaricq, C.; Sauter, B. The Value of Plasma Citrulline to Predict Mucosal Injury in Intestinal Allografts. *Am. J. Transplant.* **2006**, *6*, 2786–2790. [CrossRef]
62. Ceballos, I.; Chauveau, P.; Guerin, V.; Bardet, J.; Parvy, P.; Kamoun, P.; Jungers, P. Early Alterations of Plasma Free Amino Acids in Chronic Renal Failure. *Clin. Chim. Acta* **1990**, *188*, 101–108. [CrossRef]
63. Wu, G.; Fang, Y.-Z.; Yang, S.; Lupton, J.R.; Turner, N.D. Glutathione Metabolism and Its Implications for Health. *J. Nutr.* **2004**, *134*, 489–492. [CrossRef]
64. McMonagle, M.P.; Halpenny, M.; McCarthy, A.; Mortell, A.; Manning, F.; Kilty, C.; Mannion, D.; Wood, A.E.; Corbally, M.T. Glutathione-S-Transferase: A Potential Marker of Ischemia-Reperfusion Injury of the Intestine after Cardiac Surgery? *J. Pediatr. Surg.* **2006**, *41*, 1526–1531. [CrossRef]
65. Niewold, T.A.; Meinen, M.; van der Meulen, J. Plasma Intestinal Fatty Acid Binding Protein (I-FABP) Concentrations Increase Following Intestinal Ischemia in Pigs. *Res. Vet. Sci.* **2004**, *77*, 89–91. [CrossRef]
66. van de Poll, M.C.G.; Derikx, J.P.M.; Buurman, W.A.; Peters, W.H.M.; Roelofs, H.M.J.; Wigmore, S.J.; Dejong, C.H.C. Liver Manipulation Causes Hepatocyte Injury and Precedes Systemic Inflammation in Patients Undergoing Liver Resection. *World J. Surg.* **2007**, *31*, 2033–2038. [CrossRef]
67. Derikx, J.P.M.; Blijlevens, N.M.A.; Donnelly, J.P.; Fujii, H.; Kanda, T.; van Bijnen, A.A.; Heineman, E.; Buurman, W.A. Loss of Enterocyte Mass Is Accompanied by Diminished Turnover of Enterocytes after Myeloablative Therapy in Haematopoietic Stem-Cell Transplant Recipients. *Ann. Oncol.* **2009**, *20*, 337–342. [CrossRef]
68. Adriaanse, M.P.M.; Tack, G.J.; Passos, V.L.; Damoiseaux, J.G.M.C.; Schreurs, M.W.J.; van Wijck, K.; Riedl, R.G.; Masclee, A.A.M.; Buurman, W.A.; Mulder, C.J.J.; et al. Serum I-FABP as Marker for Enterocyte Damage in Coeliac Disease and Its Relation to Villous Atrophy and Circulating Autoantibodies. *Aliment. Pharmacol. Ther.* **2013**, *37*, 482–490. [CrossRef]
69. Guthmann, F.; Börchers, T.; Wolfrum, C.; Wustrack, T.; Bartholomäus, S.; Spener, F. Plasma Concentration of Intestinal- and Liver-FABP in Neonates Suffering from Necrotizing Enterocolitis and in Healthy Preterm Neonates. *Mol. Cell Biochem.* **2002**, *239*, 227–234. [CrossRef]
70. Guerreiro, C.S.; Calado, Â.; Sousa, J.; Fonseca, J.E. Diet, Microbiota, and Gut Permeability—The Unknown Triad in Rheumatoid Arthritis. *Front. Med.* **2018**, *5*, 349. [CrossRef]
71. de Filippo, C.; Cavalieri, D.; di Paola, M.; Ramazzotti, M.; Poullet, J.B.; Massart, S.; Collini, S.; Pieraccini, G.; Lionetti, P. Impact of Diet in Shaping Gut Microbiota Revealed by a Comparative Study in Children from Europe and Rural Africa. *Proc. Natl. Acad. Sci. USA* **2010**, *107*, 14691–14696. [CrossRef] [PubMed]
72. Liu, W.; Luo, X.; Tang, J.; Mo, Q.; Zhong, H.; Zhang, H.; Feng, F. A Bridge for Short-Chain Fatty Acids to Affect Inflammatory Bowel Disease, Type 1 Diabetes, and Non-Alcoholic Fatty Liver Disease Positively: By Changing Gut Barrier. *Eur. J. Nutr.* **2021**, *60*, 2317–2330. [CrossRef] [PubMed]
73. Mrduljaš, N.; Krešić, G.; Bilušić, T. Polyphenols: Food Sources and Health Benefits. In *Functional Food*; Hueda, M.C., Ed.; IntechOpen: Rijeka, Croatia, 2017; Chapter 2; ISBN 978-953-51-3440-4.
74. Bernardi, S.; del Bo', C.; Marino, M.; Gargari, G.; Cherubini, A.; Andrés-Lacueva, C.; Hidalgo-Liberona, N.; Peron, G.; González-Dominguez, R.; Kroon, P.; et al. Polyphenols and Intestinal Permeability: Rationale and Future Perspectives. *J. Agric. Food Chem.* **2020**, *68*, 1816–1829. [CrossRef] [PubMed]
75. Kaulmann, A.; Bohn, T. Bioactivity of Polyphenols: Preventive and Adjuvant Strategies toward Reducing Inflammatory Bowel Diseases—Promises, Perspectives, and Pitfalls. *Oxid. Med. Cell Longev.* **2016**, *2016*, 9346470. [CrossRef] [PubMed]
76. Luescher, S.; Urmann, C.; Butterweck, V. Effect of Hops Derived Prenylated Phenols on TNF-α Induced Barrier Dysfunction in Intestinal Epithelial Cells. *J. Nat. Prod.* **2017**, *80*, 925–931. [CrossRef]
77. Das, J.; Ramani, R.; Suraju, M.O. Polyphenol Compounds and PKC Signaling. *Biochim. Biophys. Acta Gen. Subj.* **2016**, *1860*, 2107–2121. [CrossRef]
78. Boto-Ordóñez, M.; Urpi-Sarda, M.; Queipo-Ortuño, M.I.; Tulipani, S.; Tinahones, F.J.; Andres-Lacueva, C. High Levels of Bifidobacteria Are Associated with Increased Levels of Anthocyanin Microbial Metabolites: A Randomized Clinical Trial. *Food Funct.* **2014**, *5*, 1932–1938. [CrossRef]

79. Queipo-Ortuño, M.I.; Boto-Ordóñez, M.; Murri, M.; Gomez-Zumaquero, J.M.; Clemente-Postigo, M.; Estruch, R.; Cardona Diaz, F.; Andrés-Lacueva, C.; Tinahones, F.J. Influence of Red Wine Polyphenols and Ethanol on the Gut Microbiota Ecology and Biochemical Biomarkers. *Am. J. Clin. Nutr.* **2012**, *95*, 1323–1334. [CrossRef]
80. Mosele, J.I.; Macià, A.; Motilva, M.J. Metabolic and Microbial Modulation of the Large Intestine Ecosystem by Non-Absorbed Diet Phenolic Compounds: A Review. *Molecules* **2015**, *20*, 17429–17468. [CrossRef]
81. Edwards, C.A.; Havlik, J.; Cong, W.; Mullen, W.; Preston, T.; Morrison, D.J.; Combet, E. Polyphenols and Health: Interactions between Fibre, Plant Polyphenols and the Gut Microbiota. *Nutr. Bull.* **2017**, *42*, 356–360. [CrossRef]
82. Carrasco-Pozo, C.; Morales, P.; Gotteland, M. Polyphenols Protect the Epithelial Barrier Function of Caco-2 Cells Exposed to Indomethacin through the Modulation of Occludin and Zonula Occludens-1 Expression. *J. Agric. Food Chem.* **2013**, *61*, 5291–5297. [CrossRef] [PubMed]
83. Wang, N.; Han, Q.; Wang, G.; Ma, W.P.; Wang, J.; Wu, W.X.; Guo, Y.; Liu, L.; Jiang, X.Y.; Xie, X.L.; et al. Resveratrol Protects Oxidative Stress-Induced Intestinal Epithelial Barrier Dysfunction by Upregulating Heme Oxygenase-1 Expression. *Dig. Dis. Sci.* **2016**, *61*, 2522–2534. [CrossRef]
84. Jo, H.A.; Hwang, D.; Kim, J.K.; Lim, Y.H. Oxyresveratrol Improves Tight Junction Integrity through the PKC and MAPK Signaling Pathways in Caco-2 Cells. *Food Chem. Toxicol.* **2017**, *108*, 203–213. [CrossRef]
85. Zhang, B.; Zhang, Y.; Liu, X.; Yin, J.; Li, X.; Zhang, X.; Xing, X.; Wang, J.; Wang, S. Differential Protective Effect of Resveratrol and Its Microbial Metabolites on Intestinal Barrier Dysfunction Is Mediated by the AMPK Pathway. *J. Agric. Food Chem.* **2022**, *70*, 11301–11313. [CrossRef] [PubMed]
86. Ling, K.H.; Wan, M.L.Y.; El-Nezami, H.; Wang, M. Protective Capacity of Resveratrol, a Natural Polyphenolic Compound, against Deoxynivalenol-Induced Intestinal Barrier Dysfunction and Bacterial Translocation. *Chem. Res. Toxicol.* **2016**, *29*, 823–833. [CrossRef] [PubMed]
87. Li, E.; Horn, N.; Ajuwon, K.M. Mechanisms of Deoxynivalenol-Induced Endocytosis and Degradation of Tight Junction Proteins in Jejunal IPEC-J2 Cells Involve Selective Activation of the MAPK Pathways. *Arch. Toxicol.* **2021**, *95*, 2065–2079. [CrossRef]
88. Ergün, O.; Ergün, G.; Öktem, G.; Selvi, N.; Doğan, H.; Tunçyürek, M.; Saydam, G.; Erdener, A. Enteral Resveratrol Supplementation Attenuates Intestinal Epithelial Inducible Nitric Oxide Synthase Activity and Mucosal Damage in Experimental Necrotizing Enterocolitis. *J. Pediatr. Surg.* **2007**, *42*, 1687–1694. [CrossRef]
89. Etxeberria, U.; Arias, N.; Boqué, N.; Macarulla, M.T.; Portillo, M.P.; Martínez, J.A.; Milagro, F.I. Reshaping Faecal Gut Microbiota Composition by the Intake of Trans-Resveratrol and Quercetin in High-Fat Sucrose Diet-Fed Rats. *J. Nutr. Biochem.* **2015**, *26*, 651–660. [CrossRef]
90. Siu, F.Y.K.; Ye, S.; Lin, H.; Li, S. Galactosylated PLGA Nanoparticles for the Oral Delivery of Resveratrol: Enhanced Bioavailability and in Vitro Anti-Inflammatory Activity. *Int. J. Nanomed.* **2018**, *13*, 4133–4144. [CrossRef]
91. Chen, M.; Hou, P.; Zhou, M.; Ren, Q.; Wang, X.; Huang, L.; Hui, S.; Yi, L.; Mi, M. Resveratrol Attenuates High-Fat Diet-Induced Non-Alcoholic Steatohepatitis by Maintaining Gut Barrier Integrity and Inhibiting Gut Inflammation through Regulation of the Endocannabinoid System. *Clin. Nutr.* **2020**, *39*, 1264–1275. [CrossRef]
92. Bereswill, S.; Muñoz, M.; Fischer, A.; Plickert, R.; Haag, L.M.; Otto, B.; Kühl, A.A.; Loddenkemper, C.; Göbel, U.B.; Heimesaat, M.M. Anti-Inflammatory Effects of Resveratrol, Curcumin and Simvastatin in Acute Small Intestinal Inflammation. *PLoS ONE* **2010**, *5*, e15099. [CrossRef] [PubMed]
93. Cai, T.T.; Ye, X.L.; Li, R.R.; Chen, H.; Wang, Y.Y.; Yong, H.J.; Pan, M.L.; Lu, W.; Tang, Y.; Miao, H.; et al. Resveratrol Modulates the Gut Microbiota and Inflammation to Protect Against Diabetic Nephropathy in Mice. *Front. Pharmacol.* **2020**, *11*, 1249. [CrossRef] [PubMed]
94. Chen, K.; Zhao, H.; Shu, L.; Xing, H.; Wang, C.; Lu, C.; Song, G. Effect of Resveratrol on Intestinal Tight Junction Proteins and the Gut Microbiome in High-Fat Diet-Fed Insulin Resistant Mice. *Int. J. Food Sci. Nutr.* **2020**, *71*, 965–978. [CrossRef] [PubMed]
95. Wang, P.; Wang, J.; Li, D.; Ke, W.; Chen, F.; Hu, X. Targeting the Gut Microbiota with Resveratrol: A Demonstration of Novel Evidence for the Management of Hepatic Steatosis. *J. Nutr. Biochem.* **2020**, *81*, 108363. [CrossRef]
96. Zhang, B.; Xu, Y.; Lv, H.; Pang, W.; Wang, J.; Ma, H.; Wang, S. Intestinal Pharmacokinetics of Resveratrol and Regulatory Effects of Resveratrol Metabolites on Gut Barrier and Gut Microbiota. *Food Chem.* **2021**, *357*, 129532. [CrossRef]
97. Hao, W.; Zhu, X.; Liu, Z.; Song, Y.; Wu, S.; Lu, X.; Yang, J.; Jin, C. Resveratrol Alleviates Aluminum-Induced Intestinal Barrier Dysfunction in Mice. *Environ. Toxicol.* **2022**, *37*, 1373–1381. [CrossRef]
98. Song, X.; Liu, L.; Peng, S.; Liu, T.; Chen, Y.; Jia, R.; Zou, Y.; Li, L.; Zhao, X.; Liang, X.; et al. Resveratrol Regulates Intestinal Barrier Function in Cyclophosphamide-Induced Immunosuppressed Mice. *J. Sci. Food Agric.* **2022**, *102*, 1205–1215. [CrossRef]
99. Yang, H.; Wang, Y.; Jin, S.; Pang, Q.; Shan, A.; Feng, X. Dietary Resveratrol Alleviated Lipopolysaccharide-Induced Ileitis through Nrf2 and NF-KB Signalling Pathways in Ducks (Anas Platyrhynchos). *J. Anim. Physiol. Anim. Nutr.* **2022**, *106*, 1306–1320. [CrossRef]
100. Alharris, E.; Mohammed, A.; Alghetaa, H. The Ability of Resveratrol to Attenuate Ovalbumin-Mediated Allergic Asthma Is Associated With Changes in Microbiota Involving the Gut-Lung Axis, Enhanced Barrier Function and Decreased Inflammation in the Lungs. *Front. Immunol.* **2022**, *13*, 805770. [CrossRef]
101. Guglielmetti, S.; Bernardi, S.; del Bo', C.; Cherubini, A.; Porrini, M.; Gargari, G.; Hidalgo-Liberona, N.; Gonzalez-Dominguez, R.; Peron, G.; Zamora-Ros, R.; et al. Effect of a Polyphenol-Rich Dietary Pattern on Intestinal Permeability and Gut and Blood Microbiomics in Older Subjects: Study Protocol of the MaPLE Randomised Controlled Trial. *BMC Geriatr.* **2020**, *20*, 77. [CrossRef]

102. del Bo', C.; Bernardi, S.; Cherubini, A.; Porrini, M.; Gargari, G.; Hidalgo-Liberona, N.; González-Domínguez, R.; Zamora-Ros, R.; Peron, G.; Marino, M.; et al. A Polyphenol-Rich Dietary Pattern Improves Intestinal Permeability, Evaluated as Serum Zonulin Levels, in Older Subjects: The MaPLE Randomised Controlled Trial. *Clin. Nutr.* **2021**, *40*, 3006–3018. [CrossRef]
103. Peron, G.; Gargari, G.; Meroño, T.; Miñarro, A.; Lozano, E.V.; Escuder, P.C.; González-Domínguez, R.; Hidalgo-Liberona, N.; del Bo, C.; Bernardi, S.; et al. Crosstalk among Intestinal Barrier, Gut Microbiota and Serum Metabolome after a Polyphenol-Rich Diet in Older Subjects with "Leaky Gut": The MaPLE Trial. *Clin. Nutr.* **2021**, *40*, 5288–5297. [CrossRef]
104. Walker, J.M.; Eckardt, P.; Aleman, J.O.; Correa da Rosa, J.; Liang, Y.; Iizumi, T.; Etheve, S.; Blaser, M.J.; Breslow, J.L.; Holt, P.R. The Effects of Trans-Resveratrol on Insulin Resistance, Inflammation, and Microbiota in Men with the Metabolic Syndrome: A Pilot Randomized, Placebo Controlled Clinical Trial. *J. Clin. Transl. Res.* **2018**, *4*, 122–135. [CrossRef]
105. Tomé-Carneiro, J.; Larrosa, M.; Yáñez-Gascón, M.J.; Dávalos, A.; Gil-Zamorano, J.; Gonzálvez, M.; García-Almagro, F.J.; Ruiz Ros, J.A.; Tomás-Barberán, F.A.; Espín, J.C.; et al. One-Year Supplementation with a Grape Extract Containing Resveratrol Modulates Inflammatory-Related MicroRNAs and Cytokines Expression in Peripheral Blood Mononuclear Cells of Type 2 Diabetes and Hypertensive Patients with Coronary Artery Disease. *Pharmacol. Res.* **2013**, *72*, 69–82. [CrossRef] [PubMed]
106. Ghanim, H.; Sia, C.L.; Korzeniewski, K.; Lohano, T.; Abuaysheh, S.; Marumganti, A.; Chaudhuri, A.; Dandona, P. A Resveratrol and Polyphenol Preparation Suppresses Oxidative and Inflammatory Stress Response to a High-Fat, High-Carbohydrate Meal. *J. Clin. Endocrinol. Metab.* **2011**, *96*, 1409–1414. [CrossRef]
107. Apostolidou, C.; Adamopoulos, K.; Iliadis, S.; Kourtidou-Papadeli, C. Alterations of Antioxidant Status in Asymptomatic Hypercholesterolemic Individuals after Resveratrol Intake. *Int. J. Food Sci. Nutr.* **2016**, *67*, 541–552. [CrossRef]
108. Most, J.; Penders, J.; Lucchesi, M.; Goossens, G.H.; Blaak, E.E. Gut Microbiota Composition in Relation to the Metabolic Response to 12-Week Combined Polyphenol Supplementation in Overweight Men and Women. *Eur. J. Clin. Nutr.* **2017**, *71*, 1040–1045. [CrossRef]

International Journal of
Molecular Sciences

MDPI

Article

Ivermectin Attenuates CCl_4-Induced Liver Fibrosis in Mice by Suppressing Hepatic Stellate Cell Activation

Hanglu Ying [1], Long Li [1,2,*], Yufen Zhao [1,2] and Feng Ni [1,2,*]

[1] Institute of Drug Discovery Technology, Ningbo University, Ningbo 315211, China
[2] Qian Xuesen Collaborative Research Center of Astrochemistry and Space Life Sciences, Ningbo University, Ningbo 315211, China
* Correspondence: lilong@nbu.edu.cn (L.L.); nifeng@nbu.edu.cn (F.N.)

Abstract: Liver fibrosis, a common liver dysfunction with high morbidity and mortality rates, is the leading cause of cirrhosis and hepatocellular carcinoma, for which there are no effective therapies. Ivermectin is an antiparasitic drug that also has been showing therapeutic actions in many other diseases, including antiviral and anticancer actions, as well as treating metabolic diseases. Herein, we evaluated the function of ivermectin in regulating liver fibrosis. Firstly, carbon tetrachloride (CCl_4)-injected Balb/c mice were used to assess the antifibrosis effects of ivermectin in vivo. Further, CFSC, a rat hepatic stellate cell (HSC) line, was used to explore the function of ivermectin in HSC activation in vitro. The in vivo data showed that ivermectin administration alleviated histopathological changes, improved liver function, reduced collagen deposition, and downregulated the expression of profibrotic genes. Mechanistically, the ivermectin treatment inhibited intrahepatic macrophage accumulation and suppressed the production of proinflammatory factors. Importantly, the ivermectin administration significantly decreased the protein levels of α-smooth muscle actin (α-SMA) both in vivo and in vitro, suggesting that the antifibrotic effects of ivermectin are mainly due to the promotion of HSC deactivation. The present study demonstrates that ivermectin may be a potential therapeutic agent for the prevention of hepatic fibrosis.

Keywords: ivermectin; liver fibrosis; hepatic stellate cells; TGF-β1; inflammation

Citation: Ying, H.; Li, L.; Zhao, Y.; Ni, F. Ivermectin Attenuates CCl_4-Induced Liver Fibrosis in Mice by Suppressing Hepatic Stellate Cell Activation. *Int. J. Mol. Sci.* **2022**, *23*, 16043. https://doi.org/10.3390/ijms232416043

Academic Editor: Rolf Teschke

Received: 26 September 2022
Accepted: 14 December 2022
Published: 16 December 2022

1. Introduction

Liver fibrosis is a type of liver disorder sourced from a variety of chronic liver diseases, including nonalcoholic fatty liver disease (NAFLD), alcoholic liver disease, hepatitis B or C virus, and hepatic toxic damage [1,2]. It is mainly characterized by excessive collagen deposition associated with chronic liver injury and could progress to cirrhosis or hepatocellular carcinoma [3,4]. Currently, hepatic stellate cell (HSC) activation has been identified as the primary mechanism for the initiation and progression of hepatic fibrosis, while activated HSCs could convert into myofibroblasts and produce numerous extracellular matrix proteins [5,6]. As a worldwide health problem, there is still no effective agent for the treatment of liver fibrosis [7]. Therefore, it is necessary to develop novel therapies for the prevention of liver fibrosis [8].

The avermectins are a class of macrocyclic lactones, which can be naturally produced by *Streptomyces avermitilis* [9]. Ivermectin, a derivative of avermectin, is synthesized via the double-bond hydrogenation of avermectin at the C22–C23 positions, which are mainly composed of two components, 22,23-dihydroavermectin B1a (≥80%) and 22,23-dihydroavermectin B1b (≤20%) [10]. As an FDA-approved broad-spectrum anthelmintic agent, ivermectin is one of the most widely used antiparasitic drugs in veterinary and human medicine against many parasitic diseases, including onchocerciasis, lymphatic filariasis, strongyloidiasis, and trichinellosis [11,12]. In addition to its antiparasitic effect, ivermectin has also been reported to have a variety of other pharmacological functions against viral infection, cancer, asthma, and metabolic diseases [13–15]. The antivirus effects of ivermectin have been found in various flaviviruses, including yellow fever virus, tick-borne encephalitis virus, and Japanese encephalitis

virus [10]. Interestingly, ivermectin also exhibits antiviral activity against SARS-CoV-2, the coronavirus that causes coronavirus disease 2019 (COVID-19) [16]. The inhibition of NS3 helicase or the suppression of the importin α/β1-mediated nuclear import of viral proteins may be the antiviral mechanism of ivermectin [17,18]. Numerous studies have revealed the anticancer effects of ivermectin in a variety of cancers, such as leukemia, esophageal squamous cell carcinoma, melanoma, and breast cancer [19–22]. A pharmacological study in a mouse model of allergic asthma revealed the anti-inflammatory activities of ivermectin, suggesting that this compound may play a protective role in diseases closely related to inflammation [13]. As the progression of various liver diseases, including NAFLD, hepatic insulin resistance, and liver fibrosis, is closely related to the inflammatory response, ivermectin might play a beneficial role in liver diseases [23]. It has been reported that ivermectin could regulate glucose and lipid metabolism and has therapeutic effects on NAFLD. However, it is still unclear whether it affects the development of liver fibrosis [24,25].

In this study, we investigated the function and potential mechanisms of ivermectin in liver fibrosis in CCl_4-induced fibrotic model mice and in transforming growth factor β1 (TGF-β1)-stimulated HSCs.

2. Results

2.1. Ivermectin Ameliorated CCl_4-Induced Liver Injury in Mice

To explore the contribution of ivermectin to liver fibrosis, we first examined the protective effects of ivermectin on liver injury in the CCl_4-induced hepatic fibrosis model in mice. As shown in Figure 1, the CCl_4 injection caused severe architectural changes in Balb/c mice, while the ivermectin administration significantly attenuated these histopathological changes (Figure 1A). Meanwhile, the CCl_4-triggered upregulation of the liver index was markedly decreased after ivermectin treatment (Figure 1B). In addition, a significant elevation of the activity levels of aspartate aminotransferase (AST) and alanine aminotransferase (ALT) was observed in the CCl_4-treated mice. However, the ivermectin obviously reduced the increases in AST and ALT (Figure 1C,D). These results demonstrate that ivermectin could protect mice against CCl_4-induced liver injury.

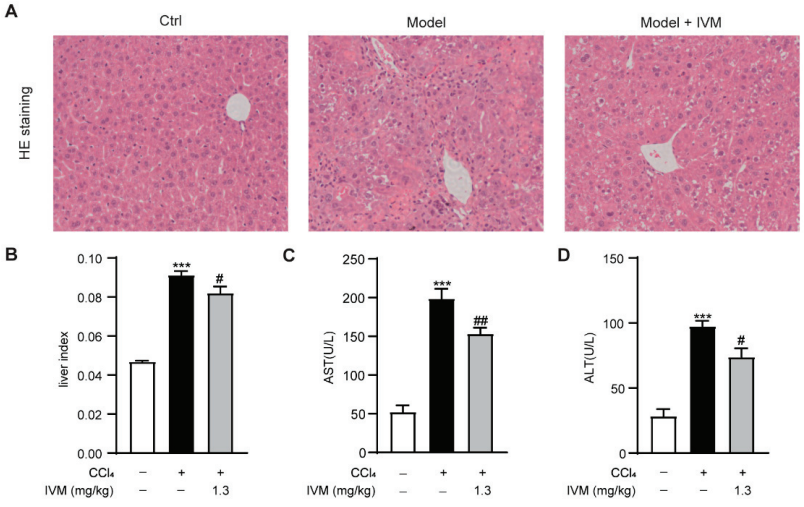

Figure 1. Effects of ivermectin on CCl_4-induced hepatic pathological and biochemical parameters in mice: (**A**) liver tissues were stained with hematoxylin and eosin (HE) for the histopathological analysis (original magnifications, ×200); (**B**) liver index values; (**C**,**D**) plasma AST and ALT levels. Data are expressed as means ± SEM (n = 6–8/group). Note: *** $p < 0.001$ vs. control group, # $p < 0.05$, ## $p < 0.01$ vs. CCl_4-treated model group.

2.2. Ivermectin Inhibits CCl_4-Induced Fibrogenesis in Mice

To investigate whether ivermectin could alleviate liver fibrosis in vivo, the collagen accumulation in the liver from sacrificed mice was detected via Sirius red staining. The results showed that the collagen deposition was significantly increased, while the ivermectin treatment led to a decrease in the fibrotic area (Figure 2A,B). In accordance with the collagen staining results, the ivermectin also greatly decreased the hepatic hydroxyproline levels in CCl_4-induced fibrosis mice (Figure 2C).

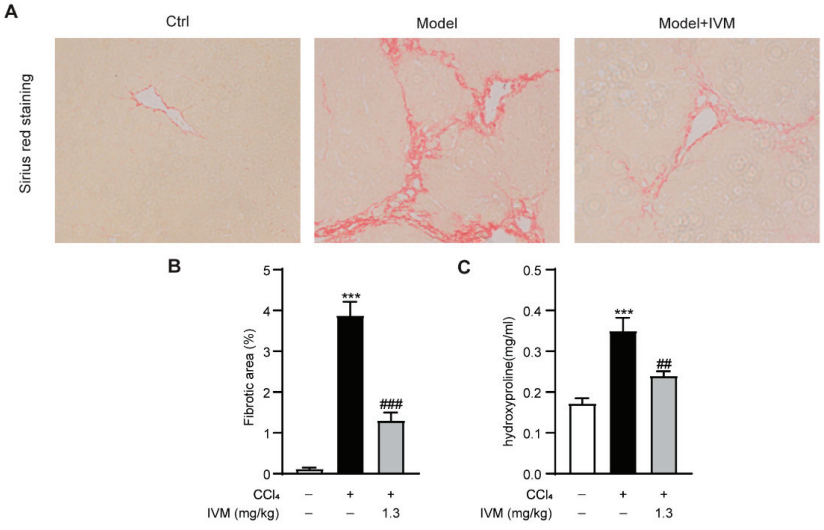

Figure 2. Ivermectin inhibited fibrosis in CCl_4-treated mice: (**A**) Sirius red staining (original magnification, ×200) of liver tissues; (**B**) quantitation of fibrotic areas in the liver; (**C**) hydroxyproline levels in the liver. Data are expressed as means ± SEM (n = 6–8/group). Note: *** $p < 0.001$ vs. control group, ## $p < 0.01$, ### $p < 0.001$ vs. CCl_4-treated model group.

2.3. Ivermectin Suppresses Inflammation

Intrahepatic macrophage and various inflammatory factors also play a key role in the development of liver fibrosis [26]. To ascertain whether ivermectin treatment affects inflammation in CCl_4-injected mice, macrophage accumulation and the expression of proinflammatory cytokines were detected. The results showed that in the livers of CCl_4 model mice, F4/80, the biomarker of activated macrophages, was markedly increased, whereas an obvious decrease was detected in mice that received the ivermectin treatment (Figure 3A,B). Moreover, the CCl_4-treated mice showed significant increases in the expression of interleukin 6 (IL-6), tumor necrosis factor α (TNF-α), interleukin-1β (IL-1β), monocyte chemoattractant protein-1 (MCP-1), and RANTES (regulated upon activation, normal T-cell expressed and secreted) compared to control mice. However, the levels of the above inflammatory mediators were obviously downregulated in ivermectin-treated mice (Figure 3C–G). Collectively, these data indicated that the inflammatory response in CCl_4 model mice is suppressed after ivermectin treatment.

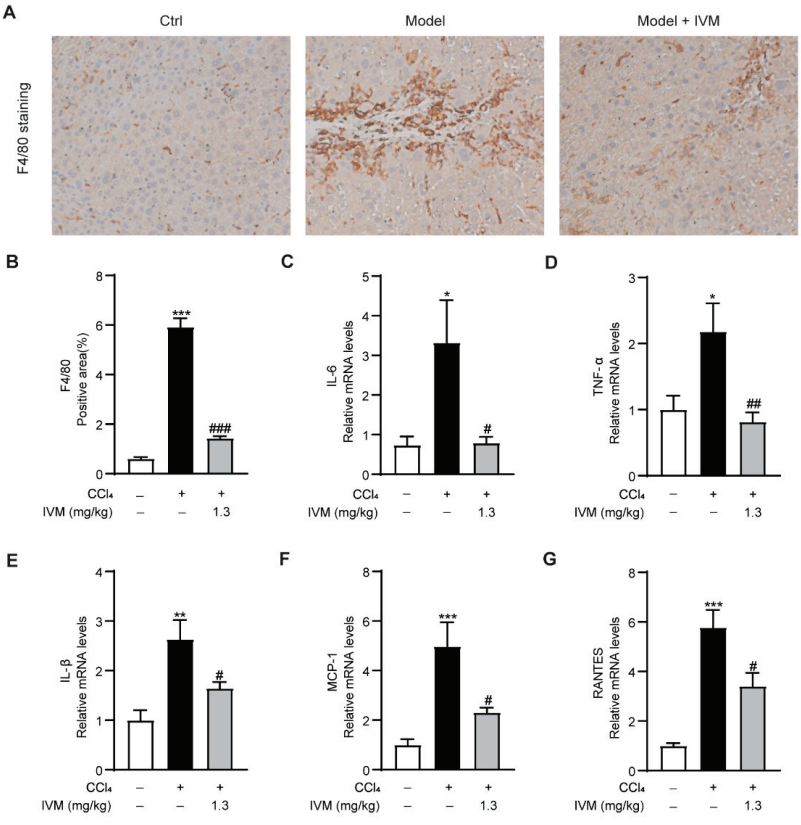

Figure 3. Anti-inflammatory effects of ivermectin in liver tissues from mice who received a CCl_4 injection: (**A**) hepatic F4/80 detection via immunohistochemistry (IHC) staining (original magnification, ×200) in liver tissues; (**B**) F4/80-positive area; (**C**–**G**) mRNA expression levels of IL-6, TNF-α, IL-1β, MCP-1, and RANTES in liver tissues. Data are expressed as means ± SEM (n = 6–8/group). Note: * $p < 0.05$, ** $p < 0.01$, *** $p < 0.001$ vs. control group, # $p < 0.05$, ## $p < 0.01$, ### $p < 0.001$ vs. CCl_4-treated model group.

2.4. Ivermectin Regulates the Expression of Fibrotic Genes

To explore whether fibrosis inhibition in ivermectin-treated mice was associated with the modulation of fibrotic genes, the mRNA expression levels of α-smooth muscle actin (α-SMA), connective tissue growth factor (CTGF), collagen type 1 α 1 (Col1α1), collagen type 3 α 1 (Col3α1), and TGF-β1 were examined. As shown in Figure 4, all of the above fibrosis-related genes were upregulated in CCl_4-injected mice. Interestingly, α-SMA, CTGF, and Col1α1 were markedly downregulated after the ivermectin treatment, while the expression levels of Col3α1 and TGF-β1 were also reduced but with less significance (Figure 4A–E). Furthermore, the Western blot results suggested that the Col1α1 and Col3α1 levels were elevated in CCl_4-injected mice and were decreased by the ivermectin treatment, which validated the real-time PCR data to some extent (Figure 4F).

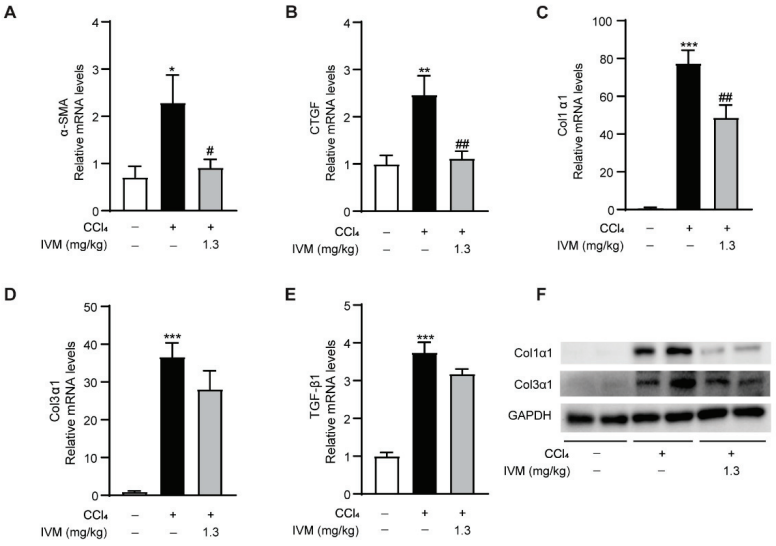

Figure 4. Impacts of ivermectin on the CCl_4-induced elevation of profibrogenic genes in the liver: (**A**–**E**) mRNA expression levels of α-SMA, CTGF, Col1α1, Col3α1, and TGF-β1 in liver tissues; (**F**) protein expression levels of Col1α1 and Col3α1 in the liver. Data are expressed as means ± SEM (n = 6–8/group). Note: * $p < 0.05$, ** $p < 0.01$, *** $p < 0.001$ vs. control group, # $p < 0.05$, ## $p < 0.01$ vs. CCl_4-treated model group.

2.5. Ivermectin Inhibits HSC Activation in the Livers of CCl_4-Treated Mice

To evaluate the change of the HSC phenotype in the liver, the expression of hepatic α-SMA was detected using IHC staining and Western blotting. As shown in Figure 5, the CCl_4-induced model mice treated with ivermectin exhibited significantly decreased α-SMA expression compared to those mice only treated with the vehicle. These data suggest that ivermectin inhibits HSC activation in the context of CCl_4-induced liver fibrosis.

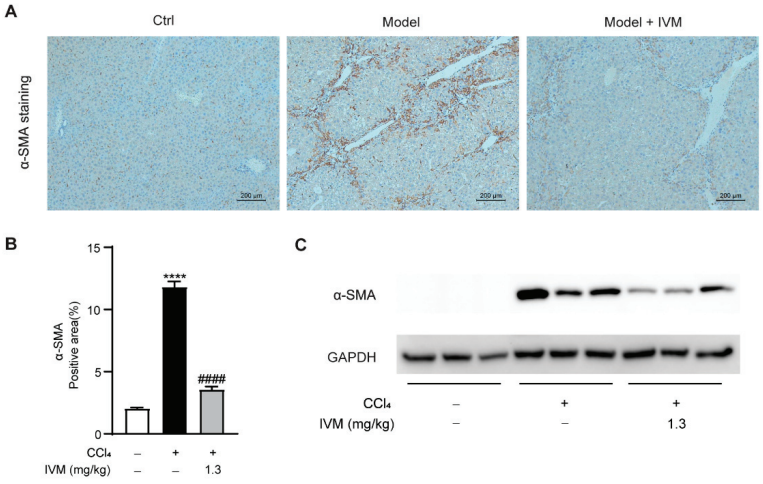

Figure 5. Effects of ivermectin on HSC activation in the liver in CCl_4-treated mice: (**A**) IHC staining of α-SMA in the liver; (**B**) α-SMA-positive areas; (**C**) the Western blot analysis of α-SMA protein expression in the liver. Data are expressed as means ± SEM (n = 6–8/group). Note: **** $p < 0.0001$ vs. control group, #### $p < 0.0001$ vs. CCl_4-treated model group.

2.6. Effects of Ivermectin on Cell Viability in CFSC Cells

To assess the cytotoxic effects of ivermectin on HSCs, CFSC (a rat HSC cell line) cells were incubated with growing doses of ivermectin (3, 6, 12, and 25 μM) or vehicle. The results showed that the low-dose ivermectin treatment (3 and 6 μM) had no significant effect on the cell survival, whereas the high-dose ivermectin treatment (12 and 25 μM) obviously reduced the cell viability (Figure 6).

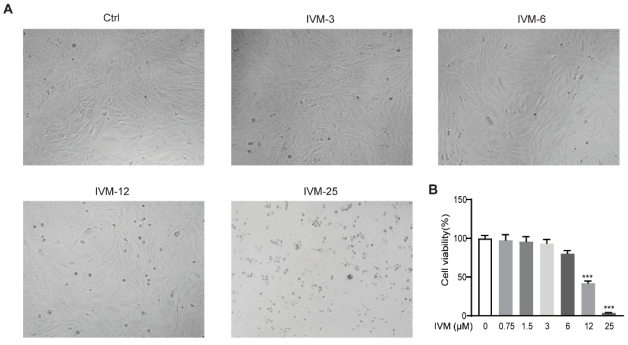

Figure 6. Impacts of ivermectin on cell viability in CFSC cells: (**A**) bright-field images of CFSC cells; (**B**) cell viability of CFSC cells assessed using a cell counting kit-8 (CCK-8) assay. Data are expressed as means ± SEM (n = 3). Note: *** $p < 0.001$.

2.7. Ivermectin Suppresses TGF-β1-Induced HSC Activation In Vitro

To further investigate whether ivermectin could directly regulate HSC activation, TGF-β1-stimulated CFSC cells were used in this study. As shown in Figure 7, the α-SMA expression was progressively upregulated in CFSC cells upon TGF-β1 stimulation, suggesting the activation of HSCs in vitro. However, the ivermectin pretreatment dose-dependently reduced the TGF-β1-induced elevation of the α-SMA protein levels, revealing that ivermectin could suppress TGF-β1-induced HSC activation in vitro.

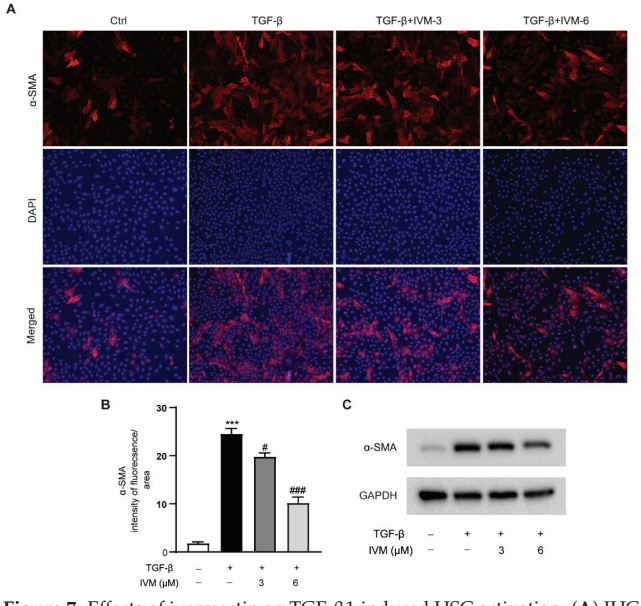

Figure 7. Effects of ivermectin on TGF-β1-induced HSC activation: (**A**) IHC staining of α-SMA in CFSC cells that received TGF-β1 stimulation and ivermectin treatment; (**B**) α-SMA intensity of fluorescence;

(**C**) the Western blot analysis of α-SMA protein expression in CFSC cells. Data are expressed as means ± SEM ($n = 3$). Note: *** $p < 0.001$ vs. control group, # $p < 0.05$, ### $p < 0.001$ vs. TGF-β1-treated model group.

3. Discussion

William C. Campbell and Satoshi Ōmura were awarded the 2015 Nobel Prize in Physiology and Medicine for their discoveries leading to ivermectin [27]. Ivermectin is a broad-spectrum antiparasitic drug against various nematodes and ectoparasites [15]. Recently, the pharmacological application of ivermectin has been extended to the treatment of multiple diseases, including cancer, inflammation, and viral infection [28–30]. Some previous reports have revealed that ivermectin displays glucose- and cholesterol-reducing, insulin-resistance-improving, and fatty-liver-ameliorating properties in rodents [14,24]. Our present study reveals a previously unrecognized crucial role of ivermectin in attenuating liver fibrosis through suppressing HSC activation. In this study, we found that ivermectin attenuated liver injury, reduced plasma levels of transaminase, suppressed hepatic accumulation of macrophages, inhibited the production of proinflammatory factors, and alleviated the expression of fibrotic genes. All of the above data demonstrated the beneficial effects of ivermectin on liver fibrosis.

As one of the most commonly used inducers of liver fibrosis, CCl_4 has hepatotoxicity and can cause hepatocyte injury [31]. In our present study, severe liver damage was observed in mice exposed to repeated CCl_4 injection, as evidenced by the presence of parenchymal necrotic zones, inflammatory cell infiltration, and elevated plasma AST and ALT activities. To our delight, the ivermectin treatment greatly alleviated hepatic histopathological changes in parallel with the improvement in liver function. Previous studies have found that a number of fibrogenesis-associated genes are involved in the occurrence and development of hepatic fibrosis [32,33]. Among these genes, α-SMA is the most classic biomarker of HSCs activation; CTGF could stimulate the production of extracellular matrix (ECM) components, while Col1a1 is the most important component of the ECM [34–36]. Our data revealed that ivermectin administration significantly reduced α-SMA, CTGF, and Col1α1 expression in CCl_4-injected hepatic tissues.

Numerous studies have reported that HSC activation is the key driving factor for the progression of liver fibrosis [37,38]. In the present study, ivermectin significantly reduced hepatic α-SMA expression in mice injected with CCl_4. The activation of HSC transdifferentiation in the liver is mainly due to the stimulation of TGF-β1, which is a member of the TGF-β superfamily and could be synthesized and released from various cell types during acute and chronic liver injury [39,40]. As a key regulator of liver physiology and pathology, the TGF-β1 signaling pathway is considered to be an important target for the treatment of liver fibrosis [41,42]. However, the effect of ivermectin on the expression of TGF-β1 was not significant in CCl_4-induced hepatic fibrosis mice in the present study, suggesting that the antifibrotic function of ivermectin may be independent of the regulation of TGF-β1 production. Interestingly, our in vitro study showed that ivermectin could obviously decrease the protein levels of α-SMA in TGF-β1-stimulated CFSC cells. These data imply that ivermectin attenuates hepatic fibrosis by suppressing HSC activation.

Ivermectin is known as a macrocyclic lactone with an antiparasitic function [43]. The macrocyclic lactones include two subfamilies, avermectins and milbemycins [44]. In addition to ivermectin, the avermectins also include abamectin, doramectin, selamectin, and eprinomectin, while the milbemycins include milbemycin oxime and moxidectin [45]. These antiparasitics have a similar structure, containing a 16-membered lactone ring [46–48]. To investigate which compound exerts the best anti fibrotic activity, we compared the regulatory effects of ivermectin, abamectin, doramectin, selamectin, moxidectin, and eprinomectin on the activation of HSCs, and found that ivermectin had the most significant inhibitory effect on the expression of α-SMA in TGF-β1-treated CFSC cells, indicating that among these macrocyclic lactones, ivermectin should be the most effective against liver fibrosis (Figure S1).

Farnesoid X receptor (FXR) is a nuclear receptor that plays a key role in the modulation of lipids, bile acid, cholesterol, and the glucose metabolism [49,50]. A previous study identified ivermectin as a ligand for FXR and revealed its function in regulating cholesterol and glucose homeostasis in an FXR-dependent manner [14]. The nuclear receptor small heterodimer partner (SHP) is an inductive target of FXR [51,52]. It has been reported that SHP mediated the protective effect of FXR against liver fibrosis through suppressing HSC activation [53]. To explore whether the FXR/SHP signaling pathway mediated the beneficial effect of ivermectin against hepatic fibrosis, we assessed the hepatic expression of SHP in CCl_4-treated mice and found that the CCl_4 injection significantly reduced the SHP mRNA expression. However, the ivermectin administration failed to elevate the expression of SHP in the liver (Figure S2). Our present data indicated that the protective effect of ivermectin on hepatic fibrosis may be independent of the FXR signaling pathway.

The accumulating evidence suggests that inflammation could drive the progression of liver fibrosis [54,55]. An intrahepatic macrophage is closely related to the initiation and development of liver fibrosis, which could be activated in the case of liver injury and could further promote the expression and secretion of proinflammatory cytokines, such as IL-6, TNF-α, and IL-1β, triggering inflammatory responses in the liver [56,57]. Consistent with previous studies, this study also found that a CCl_4 injection in mice significantly increased the hepatic expression of chemokines including MCP-1 and RANTES, which could recruit more immune cells into the liver, aggravating the progression of liver fibrosis [58,59]. Ivermectin has been reported to inhibit the infiltration of inflammatory cells and the expression of cytokines in asthmatic mice [13]. In addition, ivermectin has been shown to increase the survival rate of lipopolysaccharide-treated mice by suppressing the production of inflammatory cytokines [60]. Importantly, our present study found that ivermectin inhibited the number of F4/80-positive macrophages and decreased the expression levels of IL-6, TNF-α, IL-1β, MCP-1, and RANTES in CCl_4-treated mice. These results indicated that the anti-inflammatory effect of ivermectin may also contribute to its alleviation of liver fibrosis.

Together, we provide evidence that ivermectin alleviated CCl_4-induced liver injury, inflammation, and fibrogenesis in mice. The inhibition of TGF-β1-stimulated HSC activation is the main mechanism underlying the protective effects of ivermectin against liver fibrosis. These findings demonstrate that ivermectin, which is an FDA-approved drug, maybe a potential pharmacological agent for the therapy of hepatic fibrosis.

4. Materials and Methods

4.1. Animal Experiments

The Balb/c male mice were 6–8 weeks of age and were acquired from Vital River Laboratory Animal Technology Co., Ltd. (Beijing, China). The Animal Ethics and Welfare Committee of Ningbo University approved all animal experiments (Approval No. NBU20220121). The mice were housed at a controlled temperature range of 20–23 °C and 50–60% humidity with 12 h light/12 h dark cycles and ad libitum access to food and water. The mice in the control group only received intraperitoneal injections of olive oil (Sangon Biotech, Shanghai, China). The liver fibrosis model was established via CCl_4 (Macklin, Shanghai, China) injection (1 mL/kg body weight, i.p., dissolved in olive oil) for 4 weeks, twice a week, as previously reported [61]. A subset of model mice received daily intraperitoneal injections of ivermectin (1.3 mg/kg; Macklin, Shanghai, China) or vehicle during the period of liver fibrosis modeling.

4.2. Cell Culture

CFSC, a rat HSC cell line, was grown in DMEM supplemented with 10% FBS. The cells were maintained in a cell incubator with 5% CO_2 under 37 °C. For the cell viability assay, the CFSC cells were treated with ivermectin (3 μM, 6 μM, 12 μM, 25 μM) for 48 h. For the HSC activation assay, the CFSC cells were pretreated with ivermectin at concentrations of

3 μM and 6 μM for 1 h and then treated with TGFβ1 (10 ng/mL; Novoprotein, Shanghai, China) for another 48 h.

4.3. Histological Assessments

The liver tissues were fixed in a 4% paraformaldehyde (PFA) solution (Solarbio, Beijing, China) for 24 h at 4 °C and then embedded in paraffin (Sigma Aldrich, Shanghai, China). The paraffin-embedded liver tissues were sectioned (5 μm) and stained with HE to evaluate histological changes or stained with Sirius red to assess collagen deposition following standard procedures.

4.4. Immunofluorescence (IF) Analysis

The CFSC cells were fixed with 4% PFA and stained with the mouse anti-α-SMA antibody (Sigma Aldrich, Shanghai, China), then stained with the CoraLite594-conjugated goat anti-mouse IgG (Proteintech, Wuhan, China). The nuclei were counterstained with DAPI (Solarbio, Beijing, China). A Zeiss Axio Observer 5 microscope (Carl Zeiss, Oberkochen, Germany) was used for the observations.

4.5. Biochemistry Assay

The levels of AST, ALT, and hydroxyproline were determined using colorimetric assay kits (Nanjing Jiancheng Bioengineering Institute, Nanjing, China) according to the manufacturer's protocols.

4.6. IHC Assay

The harvested liver tissue samples were fixed in 4% PFA, embedded in paraffin, and sectioned to 5 μm for immunohistochemistry. The sections were deparaffinized in xylene and rehydrated in graded alcohol. Next, antigen retrieval was carried out by heating sections in citrate buffer for 10 min. Then, the sections were incubated with 0.3% H_2O_2 for 10 min to block the endogenous peroxidase activity. After blocking with 5% BSA, the anti-F4/80 antibody (Abcam, Shanghai, China) or anti-α-SMA antibody (Sigma Aldrich, Shanghai, China) was incubated overnight at 4 °C, followed by incubation with HRP-conjugated secondary antibodies (Proteintech, Wuhan, China) for 1 h. Finally, the sections were stained with the DAB substrate solution and co-stained with hematoxylin.

4.7. Western Blot Analysis

The protein extracts from liver tissues and CFSC cells were prepared in RIPA lysis buffer (Beyotime Biotechnology, Shanghai, China) supplemented with protease inhibitor cocktails (Roche, Shanghai, China). Then, the protein samples were separated using SDS-PAGE and transferred to PVDF membranes (Merck Millipore, Shanghai, China). After blocking with 5% skim milk, the membranes were incubated with mouse anti-α-SMA antibody (Sigma Aldrich, Shanghai, China) or rabbit anti-GAPDH antibody (Proteintech, Wuhan, China) overnight at 4 °C and subsequently incubated with HRP-conjugated goat anti-mouse IgG or HRP-conjugated goat anti-rabbit IgG (Proteintech, Wuhan, China) for 2 h at room temperature. Finally, the bands were examined with an ECL assay kit (NCM Biotech, Suzhou, China).

4.8. RNA Extraction, cDNA Synthesis, Real-Time PCR

The total RNA was isolated from liver tissues using a Total RNA Kit (Omega Bio-Tek, Norcross, GA, USA). The preparation of the cDNA was carried out with a FastQuant cDNA kit (Tiangen, Beijing, China). The real-time PCR was carried out with SuperReal PreMix Plus (SYBR Green) (Tiangen, Beijing, China) for the quantification of target gene expression and normalized to the expression of GAPDH using $2^{-\Delta\Delta}$Ct method.

4.9. Statistical Analyses

The statistical analyses were performed with a one-way analysis of variance (ANOVA) followed by the Tukey multiple comparison test in GraphPad prism 8.3.0 (GraphPad Software, La Jolla, CA, USA). The data are expressed as the means ± the standard error of the mean (SEM). Statistical significance was set as $p < 0.05$.

Supplementary Materials: The following supporting information can be downloaded at: https://www.mdpi.com/article/10.3390/ijms232416043/s1.

Author Contributions: Conceptualization, L.L., F.N. and Y.Z.; methodology, H.Y.; validation, L.L.; formal analysis, H.Y. and L.L.; resources, F.N., L.L. and Y.Z.; data curation, L.L.; writing—original draft preparation, H.Y.; writing—review and editing, L.L.; project administration, L.L. and F.N.; funding acquisition, L.L. and Y.Z. All authors have read and agreed to the published version of the manuscript.

Funding: This research was funded by the Natural Science Foundation of Zhejiang Province (No. LQ21H030002), the Scientific Research Grant of Ningbo University (215-432000282), and the Ningbo Top Talent Project (215-432094250).

Institutional Review Board Statement: The study was approved by the Experimental Animal Ethical Committee of Ningbo University (Approval No. NBU20220121).

Informed Consent Statement: Not applicable.

Data Availability Statement: All data generated for this research are included in the article or supplementary materials.

Conflicts of Interest: The authors declare no conflict of interest.

References

1. Kisseleva, T.; Brenner, D. Molecular and cellular mechanisms of liver fibrosis and its regression. *Nat. Rev. Gastroenterol. Hepatol.* **2021**, *18*, 151–166. [CrossRef] [PubMed]
2. Roehlen, N.; Crouchet, E.; Baumert, T.F. Liver Fibrosis: Mechanistic Concepts and Therapeutic Perspectives. *Cells* **2020**, *9*, 875. [CrossRef] [PubMed]
3. Acharya, P.; Chouhan, K.; Weiskirchen, S.; Weiskirchen, R. Cellular Mechanisms of Liver Fibrosis. *Front. Pharmacol.* **2021**, *12*, 671640. [CrossRef] [PubMed]
4. Dhar, D.; Baglieri, J.; Kisseleva, T.; Brenner, D.A. Mechanisms of liver fibrosis and its role in liver cancer. *Exp. Biol. Med.* **2020**, *245*, 96–108. [CrossRef] [PubMed]
5. Trivedi, P.; Wang, S.; Friedman, S.L. The Power of Plasticity-Metabolic Regulation of Hepatic Stellate Cells. *Cell Metab.* **2021**, *33*, 242–257. [CrossRef]
6. Kamm, D.R.; McCommis, K.S. Hepatic stellate cells in physiology and pathology. *J. Physiol.* **2022**, *600*, 1825–1837. [CrossRef]
7. Tan, Z.; Sun, H.; Xue, T.; Gan, C.; Liu, H.; Xie, Y.; Yao, Y.; Ye, T. Liver Fibrosis: Therapeutic Targets and Advances in Drug Therapy. *Front. Cell Dev. Biol.* **2021**, *9*, 730176. [CrossRef]
8. Zhao, M.; Wang, L.; Wang, M.; Zhou, S.; Lu, Y.; Cui, H.; Racanelli, A.C.; Zhang, L.; Ye, T.; Ding, B.; et al. Targeting fibrosis, mechanisms and cilinical trials. *Signal Transduct. Target. Ther.* **2022**, *7*, 206. [CrossRef]
9. Ashour, D.S. Ivermectin: From theory to clinical application. *Int. J. Antimicrob. Agents* **2019**, *54*, 134–142. [CrossRef]
10. Martin, R.J.; Robertson, A.P.; Choudhary, S. Ivermectin: An Anthelmintic, an Insecticide, and Much More. *Trends Parasitol.* **2021**, *37*, 48–64. [CrossRef]
11. Laing, R.; Gillan, V.; Devaney, E. Ivermectin—Old Drug, New Tricks? *Trends Parasitol.* **2017**, *33*, 463–472. [CrossRef] [PubMed]
12. Sharun, K.; Shyamkumar, T.S.; Aneesha, V.A.; Dhama, K.; Pawde, A.M.; Pal, A. Current therapeutic applications and pharmacokinetic modulations of ivermectin. *Vet. World* **2019**, *12*, 1204–1211. [CrossRef] [PubMed]
13. Yan, S.; Ci, X.; Chen, N.; Chen, C.; Li, X.; Chu, X.; Li, J.; Deng, X. Anti-inflammatory effects of ivermectin in mouse model of allergic asthma. *Inflamm. Res. Off. J. Eur. Histamine Res. Soc.* **2011**, *60*, 589–596. [CrossRef]
14. Jin, L.; Feng, X.; Rong, H.; Pan, Z.; Inaba, Y.; Qiu, L.; Zheng, W.; Lin, S.; Wang, R.; Wang, Z.; et al. The antiparasitic drug ivermectin is a novel FXR ligand that regulates metabolism. *Nat. Commun.* **2013**, *4*, 1937. [CrossRef] [PubMed]
15. Tang, M.; Hu, X.; Wang, Y.; Yao, X.; Zhang, W.; Yu, C.; Cheng, F.; Li, J.; Fang, Q. Ivermectin, a potential anticancer drug derived from an antiparasitic drug. *Pharmacol. Res.* **2021**, *163*, 105207. [CrossRef]
16. Caly, L.; Druce, J.D.; Catton, M.G.; Jans, D.A.; Wagstaff, K.M. The FDA-approved drug ivermectin inhibits the replication of SARS-CoV-2 in vitro. *Antiviral Res.* **2020**, *178*, 104787. [CrossRef]
17. Yang, S.N.Y.; Atkinson, S.C.; Wang, C.; Lee, A.; Bogoyevitch, M.A.; Borg, N.A.; Jans, D.A. The broad spectrum antiviral ivermectin targets the host nuclear transport importin alpha/beta1 heterodimer. *Antiviral Res.* **2020**, *177*, 104760. [CrossRef]

18. Mastrangelo, E.; Pezzullo, M.; De Burghgraeve, T.; Kaptein, S.; Pastorino, B.; Dallmeier, K.; de Lamballerie, X.; Neyts, J.; Hanson, A.M.; Frick, D.N.; et al. Ivermectin is a potent inhibitor of flavivirus replication specifically targeting NS3 helicase activity: New prospects for an old drug. *J. Antimicrob. Chemother.* **2012**, *67*, 1884–1894. [CrossRef]
19. Sharmeen, S.; Skrtic, M.; Sukhai, M.A.; Hurren, R.; Gronda, M.; Wang, X.; Fonseca, S.B.; Sun, H.; Wood, T.E.; Ward, R.; et al. The antiparasitic agent ivermectin induces chloride-dependent membrane hyperpolarization and cell death in leukemia cells. *Blood* **2010**, *116*, 3593–3603. [CrossRef]
20. Chen, L.; Bi, S.; Wei, Q.; Zhao, Z.; Wang, C.; Xie, S. Ivermectin suppresses tumour growth and metastasis through degradation of PAK1 in oesophageal squamous cell carcinoma. *J. Cell. Mol. Med.* **2020**, *24*, 5387–5401. [CrossRef]
21. Deng, F.; Xu, Q.; Long, J.; Xie, H. Suppressing ROS-TFE3-dependent autophagy enhances ivermectin-induced apoptosis in human melanoma cells. *J. Cell. Biochem.* **2018**, *120*, 1702–1715. [CrossRef]
22. Dou, Q.; Chen, H.N.; Wang, K.; Yuan, K.; Lei, Y.; Li, K.; Lan, J.; Chen, Y.; Huang, Z.; Xie, N.; et al. Ivermectin Induces Cytostatic Autophagy by Blocking the PAK1/Akt Axis in Breast Cancer. *Cancer Res.* **2016**, *76*, 4457–4469. [CrossRef] [PubMed]
23. Del Campo, J.A.; Gallego, P.; Grande, L. Role of inflammatory response in liver diseases: Therapeutic strategies. *World J. Hepatol.* **2018**, *10*, 1–7. [CrossRef] [PubMed]
24. Jin, L.; Wang, R.; Zhu, Y.; Zheng, W.; Han, Y.; Guo, F.; Ye, F.B.; Li, Y. Selective targeting of nuclear receptor FXR by avermectin analogues with therapeutic effects on nonalcoholic fatty liver disease. *Sci. Rep.* **2015**, *5*, 17288. [CrossRef]
25. Yang, J.S.; Qi, W.; Farias-Pereira, R.; Choi, S.; Clark, J.M.; Kim, D.; Park, Y. Permethrin and ivermectin modulate lipid metabolism in steatosis-induced HepG2 hepatocyte. *Food Chem. Toxicol. Int. J. Publ. Br. Ind. Biol. Res. Assoc.* **2019**, *125*, 595–604. [CrossRef] [PubMed]
26. Cheng, D.; Chai, J.; Wang, H.; Fu, L.; Peng, S.; Ni, X. Hepatic macrophages: Key players in the development and progression of liver fibrosis. *Liver Int.* **2021**, *41*, 2279–2294. [CrossRef] [PubMed]
27. Formiga, F.R.; Leblanc, R.; de Souza Reboucas, J.; Farias, L.P.; de Oliveira, R.N.; Pena, L. Ivermectin: An award-winning drug with expected antiviral activity against COVID-19. *J. Control. Release* **2021**, *329*, 758–761. [CrossRef]
28. Li, N.; Zhao, L.; Zhan, X. Quantitative proteomics reveals a broad-spectrum antiviral property of ivermectin, benefiting for COVID-19 treatment. *J. Cell. Physiol.* **2021**, *236*, 2959–2975. [CrossRef]
29. DiNicolantonio, J.J.; Barroso, J.; McCarty, M. Ivermectin may be a clinically useful anti-inflammatory agent for late-stage COVID-19. *Open Heart* **2020**, *7*, e001350. [CrossRef]
30. Markowska, A.; Kaysiewicz, J.; Markowska, J.; Huczynski, A. Doxycycline, salinomycin, monensin and ivermectin repositioned as cancer drugs. *Bioorg. Med. Chem. Lett.* **2019**, *29*, 1549–1554. [CrossRef]
31. Di Paola, R.; Modafferi, S.; Siracusa, R.; Cordaro, M.; D'Amico, R.; Ontario, M.L.; Interdonato, L.; Salinaro, A.T.; Fusco, R.; Impellizzeri, D.; et al. S-Acetyl-Glutathione Attenuates Carbon Tetrachloride-Induced Liver Injury by Modulating Oxidative Imbalance and Inflammation. *Int. J. Mol. Sci.* **2022**, *23*, 4429. [CrossRef] [PubMed]
32. Schuppan, D.; Ashfaq-Khan, M.; Yang, A.T.; Kim, Y.O. Liver fibrosis: Direct antifibrotic agents and targeted therapies. *Matrix Biol.* **2018**, *68–69*, 435–451. [CrossRef] [PubMed]
33. Zhan, Z.; Chen, Y.; Duan, Y.; Li, L.; Mew, K.; Hu, P.; Ren, H.; Peng, M. Identification of key genes, pathways and potential therapeutic agents for liver fibrosis using an integrated bioinformatics analysis. *PeerJ* **2019**, *7*, e6645. [CrossRef] [PubMed]
34. Ramazani, Y.; Knops, N.; Elmonem, M.A.; Nguyen, T.Q.; Arcolino, F.O.; van den Heuvel, L.; Levtchenko, E.; Kuypers, D.; Goldschmeding, R. Connective tissue growth factor (CTGF) from basics to clinics. *Matrix Biol.* **2018**, *68–69*, 44–66. [CrossRef]
35. Ai, L.; Wang, Q.; Cheng, K. Key genes in the liver fibrosis process are mined based on single-cell transcriptomics. *Biochem. Biophys. Res. Commun.* **2022**, *598*, 131–137. [CrossRef]
36. Carpino, G.; Morini, S.; Ginanni Corradini, S.; Franchitto, A.; Merli, M.; Siciliano, M.; Gentili, F.; Onetti Muda, A.; Berloco, P.; Rossi, M.; et al. Alpha-SMA expression in hepatic stellate cells and quantitative analysis of hepatic fibrosis in cirrhosis and in recurrent chronic hepatitis after liver transplantation. *Dig. Liver Dis.* **2005**, *37*, 349–356. [CrossRef]
37. Baghaei, K.; Mazhari, S.; Tokhanbigli, S.; Parsamanesh, G.; Alavifard, H.; Schaafsma, D.; Ghavami, S. Therapeutic potential of targeting regulatory mechanisms of hepatic stellate cell activation in liver fibrosis. *Drug Discov. Today* **2022**, *27*, 1044–1061. [CrossRef]
38. Tsuchida, T.; Friedman, S.L. Mechanisms of hepatic stellate cell activation. *Nat. Rev. Gastroenterol. Hepatol.* **2017**, *14*, 397–411. [CrossRef]
39. Fabregat, I.; Moreno-Caceres, J.; Sanchez, A.; Dooley, S.; Dewidar, B.; Giannelli, G.; Ten Dijke, P.; Consortium, I.-L. TGF-beta signalling and liver disease. *FEBS J.* **2016**, *283*, 2219–2232. [CrossRef]
40. McMillin, M.; Grant, S.; Frampton, G.; Petrescu, A.D.; Williams, E.; Jefferson, B.; Thomas, A.; Brahmaroutu, A.; DeMorrow, S. Elevated circulating TGFbeta1 during acute liver failure activates TGFbetaR2 on cortical neurons and exacerbates neuroinflammation and hepatic encephalopathy in mice. *J. Neuroinflamm.* **2019**, *16*, 69. [CrossRef]
41. Shi, N.; Wang, Z.; Zhu, H.; Liu, W.; Zhao, M.; Jiang, X.; Zhao, J.; Ren, C.; Zhang, Y.; Luo, L. Research progress on drugs targeting the TGF-beta signaling pathway in fibrotic diseases. *Immunol. Res.* **2022**, *70*, 276–288. [CrossRef]
42. Gyorfi, A.H.; Matei, A.E.; Distler, J.H.W. Targeting TGF-beta signaling for the treatment of fibrosis. *Matrix Biol.* **2018**, *68–69*, 8–27. [CrossRef] [PubMed]
43. Junco, M.; Iglesias, L.E.; Sagues, M.F.; Guerrero, I.; Zegbi, S.; Saumell, C.A. Effect of macrocyclic lactones on nontarget coprophilic organisms: A review. *Parasitol. Res.* **2021**, *120*, 773–783. [CrossRef] [PubMed]

44. Munoz-Munoz, L.; Shoen, C.; Sweet, G.; Vitoria, A.; Bull, T.J.; Cynamon, M.; Thompson, C.J.; Ramon-Garcia, S. Repurposing Avermectins and Milbemycins against *Mycobacteroides abscessus* and Other Nontuberculous Mycobacteria. *Antibiotics* **2021**, *10*, 381. [CrossRef] [PubMed]
45. Wolstenholme, A.J.; Neveu, C. The avermectin/milbemycin receptors of parasitic nematodes. *Pestic. Biochem. Physiol.* **2022**, *181*, 105010. [CrossRef]
46. El-Saber Batiha, G.; Alqahtani, A.; Ilesanmi, O.B.; Saati, A.A.; El-Mleeh, A.; Hetta, H.F.; Magdy Beshbishy, A. Avermectin Derivatives, Pharmacokinetics, Therapeutic and Toxic Dosages, Mechanism of Action, and Their Biological Effects. *Pharmaceuticals* **2020**, *13*, 196. [CrossRef]
47. Campbell, W.C. History of avermectin and ivermectin, with notes on the history of other macrocyclic lactone antiparasitic agents. *Curr. Pharm. Biotechnol.* **2012**, *13*, 853–865. [CrossRef]
48. Merola, V.M.; Eubig, P.A. Toxicology of Avermectins and Milbemycins (Macrocyclic Lactones) and the Role of P-Glycoprotein in Dogs and Cats. *Vet. Clin. N. Am. Small Anim. Pract.* **2018**, *48*, 991–1012. [CrossRef]
49. Panzitt, K.; Wagner, M. FXR in liver physiology: Multiple faces to regulate liver metabolism. *Biochim. Biophys. Acta Mol. Basis Dis.* **2021**, *1867*, 166133. [CrossRef]
50. Sun, L.; Cai, J.; Gonzalez, F.J. The role of farnesoid X receptor in metabolic diseases, and gastrointestinal and liver cancer. *Nat. Rev. Gastroenterol. Hepatol.* **2021**, *18*, 335–347. [CrossRef]
51. Jiang, L.; Zhang, H.; Xiao, D.; Wei, H.; Chen, Y. Farnesoid X receptor (FXR): Structures and ligands. *Comput. Struct. Biotechnol. J.* **2021**, *19*, 2148–2159. [CrossRef] [PubMed]
52. Zhang, T.; Feng, S.; Li, J.; Wu, Z.; Deng, Q.; Yang, W.; Li, J.; Pan, G. Farnesoid X receptor (FXR) agonists induce hepatocellular apoptosis and impair hepatic functions via FXR/SHP pathway. *Arch. Toxicol.* **2022**, *96*, 1829–1843. [CrossRef] [PubMed]
53. Fiorucci, S.; Antonelli, E.; Rizzo, G.; Renga, B.; Mencarelli, A.; Riccardi, L.; Orlandi, S.; Pellicciari, R.; Morelli, A. The nuclear receptor SHP mediates inhibition of hepatic stellate cells by FXR and protects against liver fibrosis. *Gastroenterology* **2004**, *127*, 1497–1512. [CrossRef] [PubMed]
54. Ramos-Tovar, E.; Muriel, P. Molecular Mechanisms That Link Oxidative Stress, Inflammation, and Fibrosis in the Liver. *Antioxidants* **2020**, *9*, 1279. [CrossRef]
55. Seki, E.; Schwabe, R.F. Hepatic inflammation and fibrosis: Functional links and key pathways. *Hepatology* **2015**, *61*, 1066–1079. [CrossRef]
56. Binatti, E.; Gerussi, A.; Barisani, D.; Invernizzi, P. The Role of Macrophages in Liver Fibrosis: New Therapeutic Opportunities. *Int. J. Mol. Sci.* **2022**, *23*, 6649. [CrossRef]
57. Wen, Y.; Lambrecht, J.; Ju, C.; Tacke, F. Hepatic macrophages in liver homeostasis and diseases-diversity, plasticity and therapeutic opportunities. *Cell. Mol. Immunol.* **2021**, *18*, 45–56. [CrossRef]
58. Queck, A.; Bode, H.; Uschner, F.E.; Brol, M.J.; Graf, C.; Schulz, M.; Jansen, C.; Praktiknjo, M.; Schierwagen, R.; Klein, S.; et al. Systemic MCP-1 Levels Derive Mainly from Injured Liver and Are Associated with Complications in Cirrhosis. *Front. Immunol.* **2020**, *11*, 354. [CrossRef]
59. Chen, L.; Zhang, Q.; Yu, C.; Wang, F.; Kong, X. Functional roles of CCL5/RANTES in liver disease. *Liver Res.* **2020**, *4*, 28–34. [CrossRef]
60. Zhang, X.; Song, Y.; Ci, X.; An, N.; Ju, Y.; Li, H.; Wang, X.; Han, C.; Cui, J.; Deng, X. Ivermectin inhibits LPS-induced production of inflammatory cytokines and improves LPS-induced survival in mice. *Inflamm. Res. Off. J. Eur. Histamine Res. Soc.* **2008**, *57*, 524–529. [CrossRef]
61. Salhab, A.; Amer, J.; Lu, Y.; Safadi, R. Sodium(+)/taurocholate cotransporting polypeptide as target therapy for liver fibrosis. *Gut* **2022**, *71*, 1373–1385. [CrossRef] [PubMed]

International Journal of
Molecular Sciences

MDPI

Article

Cannabidiol and Nano-Selenium Increase Microvascularization and Reduce Degenerative Changes in Superficial Breast Muscle in *C. perfringens*-Infected Chickens

Paweł Konieczka [1,2,*], Dominika Szkopek [1], Misza Kinsner [1], Paweł Kowalczyk [1], Monika Michalczuk [3], Damian Bień [3], Joanna Banach [4], Paulius Matusevičius [5] and Joanna Bogucka [6,7,*]

1 Department of Animal Nutrition, The Kielanowski Institute of Animal Physiology and Nutrition, Polish Academy of Sciences, Instytucka 3, 05-110 Jabłonna, Poland
2 Department of Poultry Science and Apiculture, University of Warmia and Mazury, Oczapowskiego 5, 10-718 Olsztyn, Poland
3 Department of Animal Breeding, Institute of Animal Sciences, Warsaw University of Life Sciences, Ciszewskiego 8, 02-786 Warsaw, Poland
4 Institute of Natural Fibres and Medicinal Plants-National Research Institute, Wojska Polskiego 71b, 60-630 Poznań, Poland
5 Department of Animal Nutrition, Lithuanian University of Health Sciences, Tilzes 18, LT-47181 Kaunas, Lithuania
6 The Independent Research Laboratory STANLAB LLC, Puchacza 1, 89-100 Nakło nad Notecią, Poland
7 Department of Health Sciences, University of Bydgoszcz, Unii Lubelskiej 4C, 85-059 Bydgoszcz, Poland
* Correspondence: p.konieczka@ifzz.pl (P.K.); j.bogucka@stanlab.pl (J.B.)

Abstract: Here, we demonstrated the potential of *Cannabis*-derived cannabidiol (CBD) and nanosized selenium (nano-Se) for the modulation of microvascularization and muscle fiber lesions in superficial breast muscle in *C. perfringens*-challenged chickens. The administration of CBD resulted in a decreased number of atrophic fibers (3.13 vs. 1.13/1.5 mm^2) compared with the control, whereas nano-Se or both substances resulted in a decreased split fiber number (4.13 vs. 1.55/1.5 mm^2) and in a lower number of necrotic myofibers (2.38 vs. 0.69/1.5 mm^2) in breast muscle than the positive control. There was a significantly higher number of capillary vessels in chickens in the CBD+Nano-Se group than in the control and positive control groups (1.31 vs. 0.97 and 0.98, respectively). Feeding birds experimental diets lowered the activity of DNA damage repair enzymes, including 3,N4-ethenodeoxycytosine (by 39.6%), 1,N6-ethenodeoxyadenosine (by 37.5%), 8-oxo-guanine (by 36.2%), formamidopyrimidine (fapy)-DNA glycosylase (by 56.2%) and human alkyl adenine DNA glycosylase (by 40.2%) in the ileal mucosa, but it did not compromise the blood mitochondrial oxygen consumption rate (−2.67 OD/min on average). These findings indicate a potential link between gut mucosa condition and histopathological changes in superficial pectoral muscle under induced inflammation and show the ameliorative effect of CBD and nano-Se in this cross-talk due to their protection from mucosal DNA damage.

Keywords: cannabis; selenium; necrotic enteritis; DNA damage; muscle abnormalities

Citation: Konieczka, P.; Szkopek, D.; Kinsner, M.; Kowalczyk, P.; Michalczuk, M.; Bień, D.; Banach, J.; Matusevičius, P.; Bogucka, J. Cannabidiol and Nano-Selenium Increase Microvascularization and Reduce Degenerative Changes in Superficial Breast Muscle in *C. perfringens*-Infected Chickens. *Int. J. Mol. Sci.* **2023**, *24*, 237. https://doi.org/10.3390/ijms24010237

Academic Editor: Maurizio Battino

Received: 25 November 2022
Revised: 20 December 2022
Accepted: 21 December 2022
Published: 23 December 2022

1. Introduction

Necrotic enteritis (NE), caused by the anaerobic bacterium *Clostridium perfringens* (or *C. perfringens*), is responsible for major economic losses in the poultry industry due to impaired bird performance and increased morbidity and mortality rates [1]. Due to the ban on the preventive use of antibiotics and antibiotic growth promoters in the EU (Regulation (EC) No. 1831/2003), health problems have arisen in broiler chicken flocks, including an outbreak of *Clostridium perfringens* infections. The acute form of the disease leads to increased mortality in broiler flocks [2]. In the subclinical form, there is damage to the intestinal mucosa caused by *C. perfringens*, leading to reduced digestion and absorption and

consequently to lower body weight gain and increased feed conversion ratio. Importantly, *C. perfringens* in poultry poses a risk of transmission to humans through the food chain [3].

In recent years, the poultry industry has made significant progress in breeding broiler chickens, resulting in shorter fattening times and faster weight gain. However, the rapid growth of birds results in histological and biochemical modifications of the muscle tissue, the occurrence of myopathies, and ischemic and degenerative changes in the muscles [4]. Histopathological lesions in myopathies include necrosis and atrophy of fibers, split fibers, giant fibers and connective tissue hyperplasia [5].

With the aim of minimizing the consumption of pharmaceuticals, possibilities have been sought to replace drugs with health-promoting preparations that are not medicines but exert similar effects. One bioactive substance that has been looked at in great detail is cannabidiol (CBD). Research on CBD has discovered a new, so-called endocannabinoid system, which regulates not only brain function but also the immune system. Studies examining the effects of cannabinoid-based drugs on immunity have shown that many cellular and cytokine mechanisms are suppressed by these agents [6]. This leads to the hypothesis that the aforementioned drugs may be of value in the treatment of chronic inflammatory diseases [7]. The mechanism underlying CBD action has not yet been fully elucidated, but it may represent biological activity in the regulation of inflammation through close affinity to the processes mediating necrosis and intestinal inflammation in chickens. Since NE is a serious problem in the poultry industry, CBD could be an interesting solution in prevention strategies. Therefore, additives that can help to improve birds' health while maintaining performance indicators are currently of great interest [8]. While it is overall consensus that the abuse of the most abundant bioactive substance found in *Cannabis* plants—tetrahydrocannabinol—is usually associated with toxicity to the host, current findings indicate that CBD, the second active compound in *cannabis* plants in terms of abundance (but without psychedelic effects on the host), is one of the most promising cannabinoids [9,10]. On the other hand, reports indicating CBD toxicity based on preclinical and clinical studies, as well as experiments involving animals and in vitro models, also exist [11]. More recently, an increasing body of evidence obtained using different models has suggested that CBD exposure (depending on dose) may affect the mitochondrial respiration efficiency of immune cells as well as mitochondrial fission and fusion, which are of key importance during response to high metabolic stress [12].

Selenium (Se) is another bioactive substance that has caught the attention of poultry producers. Selenium has been recognized as an essential trace element to animals and humans that is actively involved in oxidative stress resistance, reproductive performance and immune function [13]. Selenium is an important antioxidant mineral in animals and is known to affect feather production and maintain cellular integrity in bird tissues. Various Se forms are available for supplementation in animal and poultry feeds, e.g., inorganic sodium selenate (Na_2SeO_4) and sodium selenite (Na_2SeO_3) [14,15]. The organic form, such as that of selenized yeast, is similar to Se compounds found in cereals and feeds. However, selenium concentrations in feed ingredients vary widely depending on the plant species and, in particular, the Se status of the soil. Therefore, Se supplementation is necessary in poultry nutrition to provide a safety margin against its deficiency and to maintain production efficiency [16]. With the development of nanotechnology, the effect of particles in "nano" form has begun to be studied. Nanoscale selenium is of great interest as a food additive, especially for individuals with selenium deficiency, but also as a therapeutic agent without significant side effects in medicine. The nano form of selenium has attracted even more attention due to its high bioavailability and low toxicity compared with inorganic and organic forms, where inorganic compounds are more toxic than organic ones [17]. Studies have demonstrated the antimicrobial and antifungal activity of nano-Se [18]. In the context of potential bioactivity/toxicity of Se, it was evidenced, using Lilly Laboratories culture-Porcine Kidney 1 cell lines, that Se produced significant protection against Cd-induced apoptosis by mediating oxidative stress, which in turn had ameliorative effects on mitochondrial dysfunction [19]. In another study, it was shown that Se was effective in the

prevention of mitochondrial damage caused by Adriamycin in Sprague–Dawley rats [20]. Eventually, Se nanoparticles were used to investigate their potential in malignant ascites treatment using a mouse model. It was revealed that Se could influence mitochondrial function and induce cell apoptosis [21]. Taken together, the results suggests that both molecules (CBD and nano-Se) have a close affinity to mitochondrial function; thus, based on this interaction, their beneficial/toxic effects on the host can be assessed. Nano-Se can be obtained via chemical synthesis, physical methods or even in a biological way (green synthesis), using microorganisms or plant extracts, which indeed determine their biological action to a high extent [22]. Among others, nano-Se obtained via chemical synthesis seems to be the most suitable component for nutritional applications, because in this form, it is positively charged, biocompatible, non-immunogenic, nontoxic, pH sensitive and biodegradable [22].

To date, research has focused on the effects of cannabidiol and nano-selenium on the improvement of intestinal barrier function and bacterial enzyme activity in chickens. This study investigated the bioactive properties of CBD and nano-Se in broilers with potential beneficial effects on gut health and function. Konieczka et al. [8] found that CBD and nano-Se could modulate the response of chickens to *C. perfringens* infection, which in turn may provide time for effective intervention. The beneficial effects of both agents on host physiology were manifested in supporting intestinal barrier function through increased expression of genes that control intestinal integrity (tight junction proteins; TJPs). CBD and nano-Se promoted changes in extracellular bacterial enzyme activity toward increased energy uptake in challenged chickens but showed no counter-effects on mediating the host response to infection. Recently, an increasing number of studies have indicated a close relationship between intestine condition and processes determining the physicochemical properties of meat in poultry [23–25]. The metabolism of key elements, including peptides, fatty acids and amino acids, in the host depends to a high extend on gut barrier function [26]. As reported, both CBD and nano-Se manifest direct and indirect actions on the same mechanisms of the gut physiological status, particularly the modulation of gut bacterial composition and activities; thus, we speculated that both CBD and nano-Se could be more effective in supporting gut integrity and should thus affect meat properties, especially in challenged birds, as this condition leads to fermentation disturbance, as proven in various models [27–29]. For instance, chickens challenged with *C. perfringens* were shown to have a higher abundance of several foodborne pathogens in the gut, including *C. jejuni*, *E. coli* and *L. monocylogenes*; this treatment also affected the transcript levels of many genes regulating host metabolism [30]. In our previous study [31], in a turkey model, we found that challenging birds with *C. perfringens* had a significant effect on the sarcoplasmic protein profile of the breast muscle, indicating a strong association between *C. perfringens* infection and the function of glycolytic enzymes in turkeys, which could lead to significant consequences in cell metabolism [32]. In line with this, [33] showed a possible linkage between reduced vessel density and ultrastructural alterations in chicken breast muscle in early-stage wooden breast myopathy development, and the enlargement of the sarcoplasmic reticulum and greater severity of mitochondrial morphological alterations due to osmotic imbalance. The authors of [34] reported that skeletal muscles, including breast muscle, in chickens and turkeys can be affected by *C. perfringens* due to immune system failure caused by different stressors. In another report [35], it was shown that *C. perfringens* impairs the muscle regeneration process due to induced necrosis via the disturbance of collagen deposition in injured tissue, alternations in capillary vessels and nerves in infected muscle, as well as changes in the transcript levels of gene mediators of the inflammatory response and fibrosis in infected muscle. Both CBD and nano-Se may have the potential to interact with all of the mentioned pathogenesis factors.

However, the most significant correlation between host intestinal response and meat quality in chickens was found in our recent study, in which dietary CBD in *C. perfringens*-infected chickens reduced meat volatile compound levels correlated with bacterial activity [36]. In the latter study, we showed that the only group of birds with a differ-

ent VOC profile (including spoilage markers) was the *C. perfringens*-challenged group, indicating a strong impact of *C. perfringens* infection on meat properties. This could be attributed to the fact that *C. perfringens* affects lipid metabolism by downregulating the expression of fatty acid catabolism-related genes, including peroxisome proliferator-activated receptor-alpha, carnitine palmitoyl transferase 1 and acyl CoA oxidase 1 [37], which play important roles in lipid metabolism and thus strongly contribute to meat sensory properties. Eventually, Bień et al. [38] demonstrated that using different forms of selenium, including the nanosized form, in chicken diet was effective in the modulation of the fatty acid profile, and lipid and enzymatic indices of fatty acid metabolism in breast muscle as well as in the liver in birds.

Corresponding to the above reported findings, the aim of this study was to verify whether the use of CBD and Se in the form of nanoparticles in the diet of broiler chickens subjected to necrotic enteritis caused by *Clostridium perfringens* affected the degree of blood supply to the superficial breast muscle and the extent of pathological changes. At the same time, the study verified whether the use of the tested substances in the diet of chickens exerted toxic effects on selected markers of intestinal barrier function and mitochondria.

2. Results

2.1. Breast Meat Microstructure in Response to Treatment

There was a significantly higher number of capillary vessels in the muscle of chickens in the CBD + Nano-Se group than in CON and CON positive birds ($p < 0.05$) (Table 1). At the time of CBD and nano-Se administration to the chickens, a tendency of improved microvascularity of the muscle was observed. A lower number of necrotic myofibers was found in the chicken groups infected with *C. perfringens* after the addition of both bioactive substances, as well as selenium nanoparticles alone, compared with the CON positive group. The smallest number of atrophic fibers was observed in the muscle of CBD group birds compared with CON. Noteworthy is the number of split fibers, as a significant increase in the number of these lesions was observed after infecting chickens with *C. perfringens* compared with the control group. The administration of CBD, nano-Se and CBD + nano-Se reduced the extent of splitting compared with the CON positive group ($p < 0.05$). There were no differences in the content of giant fibers nor the thickness and number of fibers among the studied groups of birds (Table 1).

Table 1. Effects of dietary treatments and *Clostridium perfringens* challenge on the microstructure of the superficial breast muscle in 35-day-old broiler chickens.

Trait	Group				
	CON	CON Positive	CBD	Nano-Se	CBD + Nano-Se
Number of capillaries per muscle fiber	$0.97^{b} \pm 0.07$	$0.98^{b} \pm 0.05$	$1.20^{ab} \pm 0.10$	$1.11^{ab} \pm 0.09$	$1.31^{a} \pm 0.12$
Number of muscle fibers/1.5 mm^2	165.38 ± 5.89	177.75 ± 12.70	165.13 ± 10.07	172.88 ± 7.82	178.13 ± 12.67
Muscle fiber diameter (μm)	48.56 ± 2.99	44.95 ± 5.62	47.59 ± 5.60	48.29 ± 3.10	45.66 ± 6.09
Number of necrotic fibers/1.5 mm^2	$1.63^{ab} \pm 0.32$	$2.38^{a} \pm 0.53$	$1.50^{ab} \pm 0.60$	$0.38^{b} \pm 0.26$	$1.00^{b} \pm 0.38$
Number of atrophic fibers/1.5 mm^2	$3.13^{a} \pm 0.79$	$2.50^{ab} \pm 0.53$	$1.13^{b} \pm 0.30$	$2.25^{ab} \pm 0.60$	$2.50^{ab} \pm 0.42$
Number of split fibers /1.5 mm^2	$2.00^{b} \pm 0.65$	$4.13^{a} \pm 0.55$	$1.88^{b} \pm 0.40$	$1.63^{b} \pm 0.60$	$1.13^{b} \pm 0.40$
Number of giant fibers/1.5 mm^2	0.50 ± 0.27	0.63 ± 0.32	0.63 ± 0.32	0.75 ± 0.25	0.25 ± 0.16

CON—untreated control group; CON positive—birds fed a CON diet and challenged with *Clostridium perfringens* on days 15, 16, 17 and 18 of age; CBD—CON positive + dietary supplementation with cannabidiol; Nano-Se—CON positive + dietary supplementation with nano form of selenium; CBD+Nano-Se—CON positive + dietary supplementation with both additives. ^{ab}—statistically significant differences at $p < 0.05$.

2.2. Gut Barrier Condition as Response to Treatment

The activity of DNA damage repair enzymes in the ileum is shown in Figure 1. etC repair activity was significantly higher in the CON positive group than in the other groups ($p < 0.001$). With respect to the repair activity of the etA enzyme, no significant differences

were recorded between the CON and CON positive groups, and both groups showed higher enzyme activity than the Nano-Se and CBD + Nano-Se groups, with activity being higher in CON positive than in the CBD group ($p < 0.001$). The activity of the 8oxodG enzyme was the highest in the CON positive group and did not differ significantly between CON and CBD, while it was the lowest in the Nano-Se and CBD + Nano-Se groups ($p < 0.001$). Fpg activity was the highest in the CON positive group and did not differ significantly among the CON, CBD and CBD + Nano-Se groups, and it was the lowest in the Nano-Se group ($p < 0.001$). The activity of hAAG was significantly lower in the other groups compared with the CON positive group ($p < 0.001$).

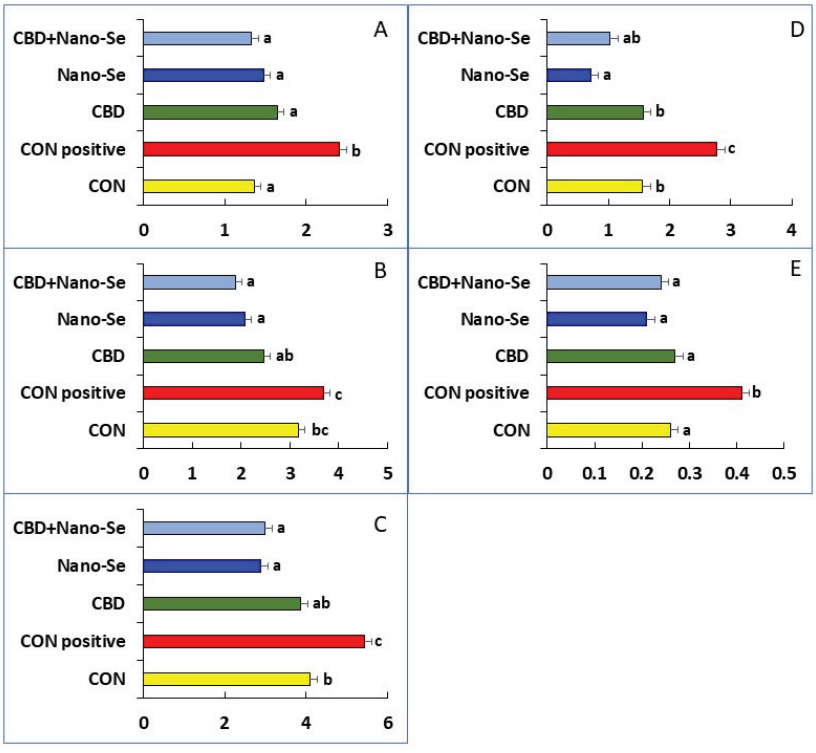

Figure 1. Excision activity (pmol/h/mg protein) of 3,N4-ethenodeoxycytosine (**A**), 1,N6- ethenodeoxyadenosine (**B**), 8-oxo-guanine (**C**), formamidopyrimidine (fapy)-DNA glycosylase (**D**) and human alkyl adenine DNA glycosylase (**E**). CON—untreated control group; CON positive—birds fed a CON diet challenged with *Clostridium perfringens* on days 15, 16, 17 and 18 of age; CBD—CON positive + dietary supplementation with cannabidiol; Nano-Se—CON positive + dietary supplementation with nano form of selenium; CBD + Nano-Se—CON positive + dietary supplementation with both additives. ^{a,b,c} Different letters represent significant differences ($p < 0.001$). Error bars represent mean standard error values for 8 birds in each dietary treatment.

2.3. Oxygen Consumption Rate in Platelet Mitochondria as a Response to Treatments

The rate of oxygen consumption in platelet mitochondria, expressed as a change in fluorescence signal over time (intensity inversely proportional to the level of extracellular oxygen), is shown in Figure 2. The results indicate that neither dietary treatments nor *C. perfringens* challenge significantly affected the oxygen use of platelet mitochondria ($p > 0.05$).

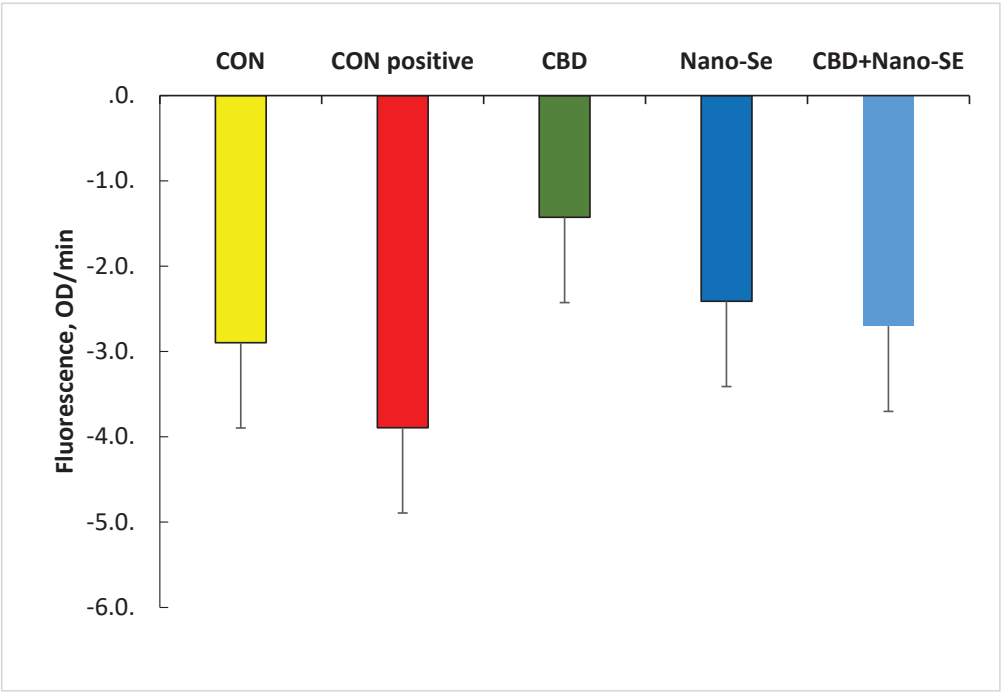

Figure 2. Oxygen consumption rate in platelet mitochondria expressed as the rate of fluorescence signal change per minute. CON—untreated control group; CON positive—birds fed a CON diet and challenged with *Clostridium perfringens* on days 15, 16, 17 and 18 of age; CBD—CON positive + dietary supplementation with cannabidiol; Nano-Se—CON positive + dietary supplementation with nano form of selenium; CBD + Nano-Se—CON positive + dietary supplementation with both additives. Error bars represent the mean standard errors for 8 birds in each dietary treatment (SEM = 0.318 and $p = 0.250$).

3. Discussion

The available literature indicates a positive effect of both CBD [39–41] and nano-Se [14,16,42,43] on the quality of broiler chicken meat. Studies in rats show that CBD can provide moderate analgesic and anti-inflammatory effects without suppressing muscle recovery [44]. Konieczka et al. [8] investigated the activity of cannabidiol derived from *Cannabis sativa* and selenium nanoparticles in modulating the host response to challenge with *Clostridium perfringens* in broiler chickens under mild infection conditions. It should be noted that the infected chickens showed no clinical signs, confirming the potential risk of pathogen transmission into the food chain in the commercial sector. However, both CBD and nano-Se had a positive effect on chickens' response to *C. perfringens*. The beneficial effect of both agents was manifested in the increased expression of genes determining intestinal barrier function. Both CBD and nano-Se promoted changes in gut bacterial enzyme activity to increase energy intake in challenged chickens and enhance potential collagenase activity. The results of the cited studies prompted the authors to conduct research concerning the effect of CBD and nano-Se on the microstructure of the breast muscle of chickens after infection with *C. perfringens*. There were no differences among the chicken groups in both the diameter and the number of muscle fibers, which was also confirmed by previous studies with other bioactive substances administered in feed and in ovo [5,45–47]. However, differences in muscle blood supply and changes in its microstructure were observed. There was a tendency of an increasing number of capillaries after CBD and nano-Se administration, and a significant improvement in blood supply was

observed after supplying both substances simultaneously. This was also reflected in the number of pathological changes in the muscle. After the addition of selenium nanoparticles, as well as both bioactive substances concurrently, decreased muscle fiber necrosis was observed compared with the CON positive group. Pelyhe and Mézes [48] emphasized the role of selenium in antioxidant defense systems, as well as the prevention of cell damage in farm animals, which might explain the lowest number of necrotic fibers in the selenium-supplemented group. As reported by Bilgili and Hess [49], and Velleman [50], necrosis is one of the degenerative lesions primarily caused by limited blood supply to the muscle fiber, which may be associated with fewer capillaries and limited angiogenesis. In addition, the administration of cannabidiol (CBD group) resulted in a small number of atrophic fibers in the muscle compared with CON. As is well known, CBD is a phytochemical that shows a strong potential in the control of neurodegenerative disorders, which are the main cause of muscle fiber atrophy [51]. However, the number of split fibers deserves attention, as the administration of CBD, nano-Se and CBD + nano-Se resulted in decreased fiber splitting compared with the CON positive group (p <0.05) (Table 1). Fiber splitting is a lesion that requires special attention in the muscles of fast-growing chickens. The longitudinal splitting of muscle fibers is one of the degenerative changes that may be identified in transverse sections of muscle tissue. McRae et al. [52] reported that this lesion occurs in chickens showing myopathic changes as a result of metabolic stress associated with, among others, the functioning of larger fibers. The study by Bogucka et al. [5,45] also showed a positive effect of probiotics and synbiotics as additives in the nutrition of broiler chickens on reducing the degree of muscle fiber splitting, which indicated a significant relationships between the environment of the digestive tract and the physicochemical properties of breast muscle in chickens.

In the present experiment, the activity of DNA repair enzymes was studied as a marker of intestinal barrier condition in relation to dietary treatments. Since DNA repair is an important risk factor in the etiology of pathogen challenge, it may also serve as a good indicator of the effectiveness of the treatment efficacy of test substances [53]. One of the important modulators of DNA changes is oxidative stress resulting from the increased sensitivity of cells to oxidizing and alkylating agents, which is associated with incomplete repair of single-strand breaks [54]. To the best of our knowledge, there are no data in the literature regarding changes in the activity of DNA repair enzymes in chickens infected with *C. perfringens*; however, in studies in a rat model challenged with lipopolysaccharide from S. typhimurium and E. coli, an increased rate of oxidative DNA damage was found to be originated by either a direct attack of ROS on DNA (8-oxoG) or the adduction of lipid peroxidation products (εA and εC), as well as a concomitant increase in DNA repair enzyme activity [55]. For this reason, it can be assumed that they are good markers of the effectiveness of treatments. Indeed, in our experiment, the repair activity of all enzymes except for etA was the highest in the CON positive group, indicating an increase in DNA damage in the ileum caused by *C. perfringens* compared with the non-infected group. In contrast, the repair activity in the experimental groups was significantly lower or did not differ from that in the CON group, suggesting an ameliorating effect of CBD and nano-Se on DNA damage in intestinal epithelial cells under *C. perfringens* challenge conditions. We speculated that both bioactive substances (CBD and nano-Se) could improve the integrity and function of the ileal barrier, as in a previous study, we showed that both additives increased the expression levels of TJP genes, including GLP-2, JAM-2, ZO-1 and TLR-4, in the intestines of *C. perfringens*-infected chickens [8]. A number of cases has indicated an association between stress-regulating factors of the host response and meat features, including myopathies such as white striping, wooden breast and spaghetti meat, which are associated with breast muscle vascularization and oxygen supply [56]. A report by Pampouille et al. [57] demonstrated that broiler meat disorders are associated with histological changes or transcript levels of oxygen carrier genes. Avian breast muscle disorders have also been linked to genes regulating the transition from the glycolysis pathway towards amino acid catabolism and lipid oxidation for the production of energy [58] and of

long- medium-chain and monounsaturated fatty acids, as well as lipid metabolism [59,60]. Although these mechanisms are complex and require further research, the present study contributes to research by reporting the fact that meat vacuolization is affected by intestinal barrier function.

Here, we used an oxygen consumption assay to investigate whether the bioactive agents used (CBD and/or nano-Se) exerted a toxic effect. Oxygen consumption assays allow respiration rates to be determined for the metabolic characterization and assessment of the toxic effects of treatments on mitochondrial function [61]. Lower extracellular oxygen levels indicate a higher rate of oxygen consumption in the mitochondria. Since mitochondria play a key role in the metabolic processes of the entire biological system, their impairment is the main mechanism of drug-induced toxicity, as has been demonstrated in various models [62–64]. In a recent study, we measured the rate of oxygen consumption in platelet mitochondria as an indicator of treatment effect, as this may have implications for further applications. Blood analysis is an easy-to-use approach; it can, therefore, be used to assess the effects of dietary treatment in birds [65]. Our findings indicated that neither CBD nor nano-Se (or their concurrent application) significantly affected mitochondrial function, as assessed in terms of oxygen consumption. Thus, it can be speculated that oral administration of CBD and nano-Se did not induce toxicity in birds at the doses tested under both optimal conditions and *C. perfringens*-induced inflammation; in particular, it did not impair platelet function during the inflammatory response to stress stimuli, and it has been suggested that platelets play a key role during antigen presentation [66,67].

4. Materials and Methods

4.1. Chemical Composition of Hemp Extract and Nano-Selenium

Hemp (*Cannabis sativa*) panicles were extracted from plants harvested in 2019 at Institute of Natural Fibers and Medicinal Plants in Poznań, Poland. Plants for the experiment were cultivated from certified seeds, and all procedures, including either plant cultivation or the collection of plant material, complied with institutional, national and international guidelines and legislation. The plants that were used for extract preparation were EU-registered (Research Centre for Cultivation Testing, Polish National List of Variety (NLI); Tygra No. R1865) and had a cannabinoid content below 0.2%. The plant material was collected, cut and dried at room temperature. The hemp extract was obtained at Supercritical Extraction Department, Institute of New Syntheses Institute, Puławy. Extraction parameters: pressure, 250 bar; temperature, 60 °C; flow rate, 40 kg CO_2/kg hemp. Hemp extract contained 12% CBD, 0.49% tetrahydrocannabinol and 0.38% tetrahydrocannabinolic acid. The plants used to prepare extracts were registered in the EU (Research Centre for Cultivation Testing, Polish National List of Variety (NLI); Tygra No. R1865) and had a cannabinoid content of less than 0.2%. In the present experiment, the desired result of extraction was to obtain the highest possible concentration of CBD in the extract, which in consequence increased the content of other cannabinoids in the final extract, including tetrahydrocannabinol. Therefore, considering the inclusion level (15 g/kg diet) of CBD extract in the diet, the final concentrations were 0.0735 g of tetrahydrocannabinol per 1 kg feed and 1.8 g of CBD per 1 kg feed.

Nano-Se obtained through chemical synthesis was used in the form of a nanopowder with an average particle size of 10–45 nm, specific surface area (SSA) of about 30–50 m^2/g and purity of 99.9%, as declared by the manufacturer (American Elements, Los Angeles, CA, USA).

4.2. Birds, Treatments and Challenge Model

A total of 360 birds (male broiler chickens of the Ross 308 line), reared from day 1 to 35, were used in the experiment. Chickens, from the first day of rearing, were placed in collective cages (9 individuals per cage) taking into account the average body weight. The study design included 5 experimental groups, with 8 replicates (cages) in each group—9 birds in each replicate. Chickens were fed a complete feed mix for broilers

divided into 3 feeding periods, starter (days 1 to 7), grower (days 8 to 35) and finisher (days 36 to 42), according to the Ross 308 chicken feeding recommendations [68]. The experiment used CBD extract obtained from industrial hemp (*Cannabis sativa*) and/or nano-Se, which were added to the experimental diets (Table 2).

Table 2. Dietary treatments applied in the chicken experiments.

Treatment	CON	CON Positive	CBD	Nano-Se	CBD+Nano-Se
Commercial diet for broiler Ross 308 with no additives	+	+	+	+	+
C. perfringens Challenge	−	+	+	+	+
Cannabidiol	−	−	+	−	+
Nanosized selenium	−	−	−	+	+

CON—untreated control group; CON positive—birds fed a CON diet and challenged with *Clostridium perfringens* on days 15, 16, 17 and 18 of age; CBD—CON positive + dietary supplementation with cannabidiol; Nano-Se—CON positive + dietary supplementation with nano form of selenium; CBD+Nano-Se—CON positive + dietary supplementation with both additives.

Birds from groups CON positive, CBD, Nano-Se and CBD+Nano-Se were infected with *Clostridium perfringens* on days 15, 16, 17 and 18, according to the methodology reported previously [8]. Briefly, at 15, 16, 17 and 18 days of age, birds were challenged with 1 mL (per os, directly into the crop using a probe) of a *C. perfringens* overnight culture inoculum, freshly prepared for each subsequent day; bacteria were cultivated anaerobically in sterile brain heart infusion broth medium (Sigma-Aldrich) containing beef heart (5 g/L), calf brain (12.5 g/L), disodium hydrogen phosphate (2.5 g/L), D (+)-glucose (2 g/L), peptone (10 g/L) and sodium chloride (5 g/L) at the temperature of 37 °C and were maintained overnight (14 h) in a jar containing an atmosphere of 10% CO2, 10% H2 and 80% N2. *C. perfringens* inoculum was confirmed according to ISO standard 7937:2005 (PN EN ISO 7937, 2005) and contained approximately 10^8 CFU/mL of *C. perfringens* type A strain 56 according to a pre-validated protocol [69], while chickens in the non-challenged group received the same dose of sterilized broth medium. Before *C. perfringens* challenge, 1 mL of coccidial cocktail containing *Eimeria* (E) species (*E. acervulina*, (5000 oocytes), *E. maxima* (3500 oocytes), *E. mitis* (5000 oocytes), *E. praecox* (5000 oocytes) and *E. tenella* (5000 oocytes)) was administered per os to all birds at 14 and 15 days of age to create a favorable intestinal environment [70] for the development of mild necrotic enteritis caused by *C. perfringens* colonization (Laboratorios HIPRA S.A., Spain). The chicken basal diet was composed of wheat (50.76%), soybean meal (21.76%), triticale (15.54%), fish meal (5.18%) and oilseed rape meal (4.15%) to create a favorable environment in the digestive tract for *C. perfringens* proliferation. The severity of infection in the intestinal tissue was assessed by a veterinarian based on necrotic lesions typical of *C. perfringens*. None of the birds showed severe necrosis, which is usually manifested by confluent necrosis of the mucosa of large parts of the gut segments, collapse of the intestinal lumen, lack of turgor, thin and fragile intestinal wall, advanced necrosis of the gut mucosa, and visible multifocal hemorrhage in various regions [71,72]. The experimental diets were supplemented with CBD at a level of 15 g/kg feed, while nano-Se was added in the amount sufficient to provide 0.3 mg Se/kg feed.

4.3. Evaluation of the Microstructure of the Breast Muscles of Broiler Chickens

Breast muscle samples were collected from chickens at 35 days of age (n = 8/group). The histological preparations that were used to evaluate the microstructure of broiler chicken breast muscles were prepared using the freezing technique. After fixation in liquid nitrogen (−196 °C), superficial breast muscle samples were cut in a cryostat (Thermo Shandon/Thermo Fisher Scientific, UK) into 10 μm thick sections. The thus-prepared sections were transferred onto slides and subjected to hematoxylin and eosin (HE) staining and reaction to alkaline phosphatase present in capillary endothelium. HE staining was

used to measure muscle fiber diameter and determine the number of normal and altered fibers. The number of lesions such as necrotic fibers, atrophic fibers, split fibers and giant fibers was calculated. The alkaline phosphatase method was used to determine the number of capillaries in the studied muscle. Ten fields of view with the highest number of vessels, the so-called "hot spots", were analyzed; subsequently, the number of capillaries per 1 muscle fiber was calculated (Figure 3). A Nikon Eclipse Ci microscope, equipped with a Delta Optical DLT-Cam PRO 6.3MP camera and DLT Cam Viewer software, was used to analyze histological images. Muscle analysis was performed on an area of 1.5 mm^2.

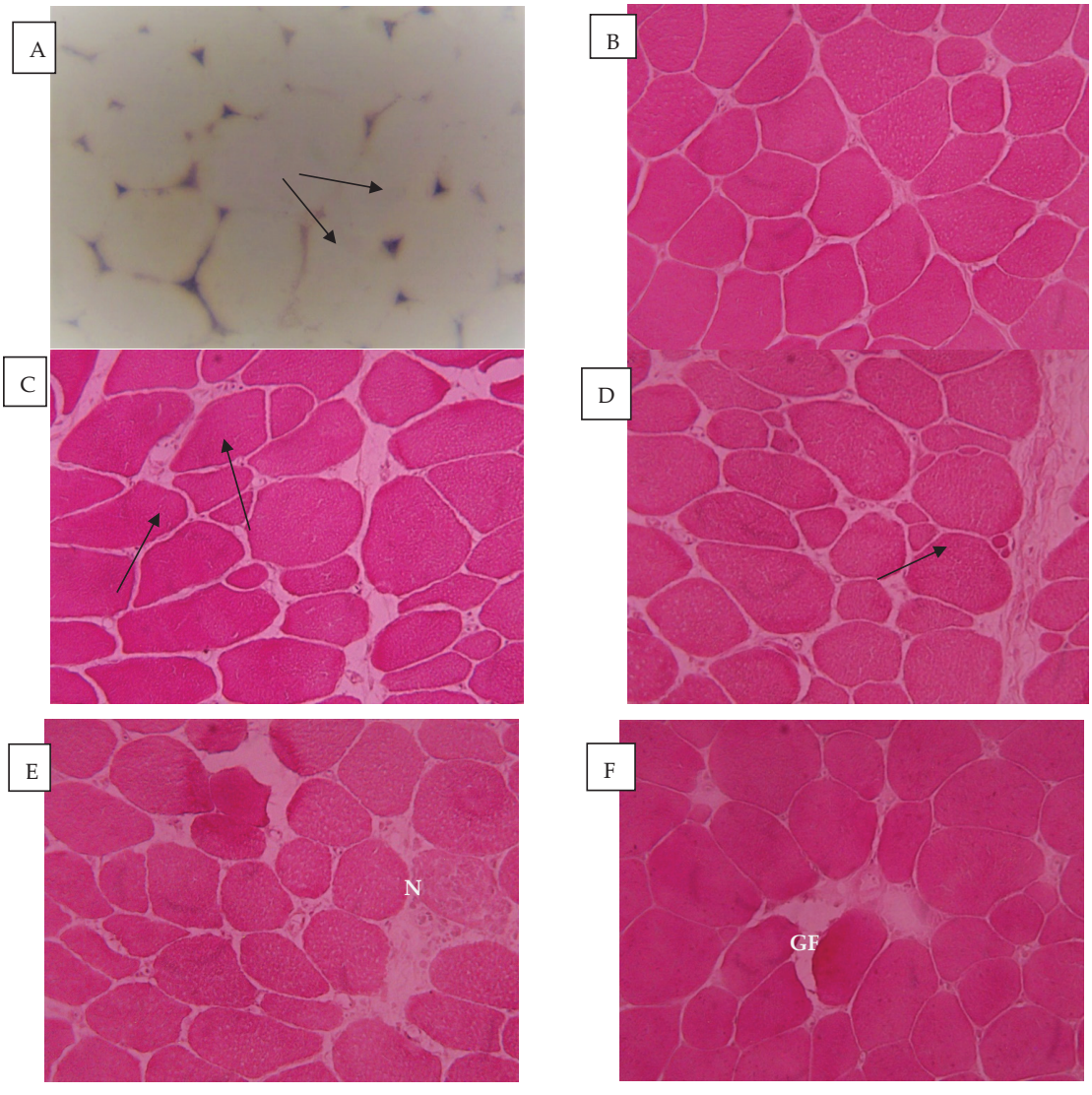

Figure 3. (**A**) Capillaries (arrows); alkaline phosphatase staining; magnification ×200. (**B**) Normal structure of superficial breast muscle. (**C**) Split fibers (arrows). (**D**) Atrophic fibers (arrow). (**E**) Necrosis (N). (**E**) Giant fiber (GF). (**B**–**F**) hematoxylin and eosin (HE) staining; magnification ×200.

4.4. Assessment of the Activity of DNA Damage Repair Enzymes in the Ileum

The condition of the intestinal barrier was assessed using the repair activity assay and nicking assay method. On day 23 of age (5 days after the last *C. perfringens* challenge), 8 birds from each treatment were sacrificed, and ileal samples were collected and fixed. Briefly, the condition of the intestinal barrier was assessed on the basis of the repair activity assay with the nicking assay method [55,73] using oligonucleotides (40-mers) containing a single 3,N^4-ethenodeoxycytosine (εC), 1,N6-ethenodeoxyadenosine (εA) and 8-oxo-guanine (8-oxoG) at position 20 in the sequence 5′-d(GCT ACC TAC CTA GCG ACC TXC GAC TGT CCC ACT GCT CGA)-3′. Oligonucleotides were obtained from Eurogentec Herstal (Herstal, Belgium) or Genset Oligos (Paris, France). Understanding the genotoxic properties of endogenous DNA damage as etheno-DNA adducts, such as 1,N^6-ethenoadenine (εA), 3,N^4-ethenocytosine (εC), N^2,3-ethenoguanine (εG) and 1,N^2-ethenoguanine (εG) and repair pathways, resulting in oxidative stress response, is fundamental to understand the mechanisms of diseases associated with chronic inflammation such as cancer, neurodegenerative diseases and aging. Due to the large range and pleiotropic effects of these products, knowledge about their molecular mechanisms of action is still fragmentary [55,73]. The principle of the nicking assay is based on the cleavage of an oligodeoxynucleotide at the site of modified bases (exocyclic DNA base adducts) such as etenoadenine (εA), etenocytosine (εC) and etenoguanine (εG) performed by glycosylases and AP-endonucleases present in tissue homogenates. The assay monitors the excision of εAde, εCyt and 8oxoG from a 5′-radiolabeled or phosphorescent synthetic DNA oligodeoxynucleotide performed by DNA glycosylases contained in tissue extracts, as well as the incision of abasic sites performed by AP endonucleases such as formamidopyrimidine (fapy)-DNA glycosylase (Fpg) and human alkyl adenine DNA glycosylase (hAAG) (Scheme 1).

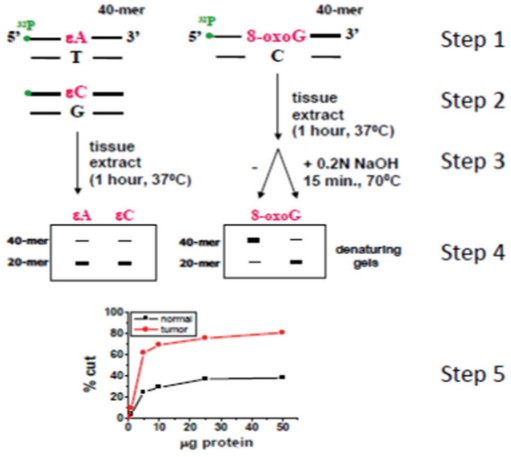

Scheme 1. The nicking assay involves 5 main steps: 1—labeling of oligodeoxynucleotides containing εA, εC and 8-oxoG; 2—hybridization; 3—excision of εA, εC and 8-oxoG from oligonucleotides performed by glycosylases present in tissue extracts; 4—separation of reaction products; 5—detection and quantification of the reaction products. The resulting reaction products were analyzed using Imane Quant 5.2 and Microcal Origin programs for reaction product quantification. The cleavage percentage of a known amount of ^{32}P-labeled oligonucleotides relative to the total content was evaluated and expressed as picomoles of product/hour/microgram of protein.

4.5. Analysis of Mitochondrial Oxygen Metabolism Using the Oxygen Consumption Assay

The rate of oxygen consumption in platelet mitochondria was assessed according to the previously described protocol [65]. Briefly, whole blood samples (2 mL) were collected from birds at 23 days of age (8 birds per group) into heparinized tubes. Blood was subsequently gently mixed to avoid microsphere formation, which could reduce the

number of platelets and impair the results, and was placed on ice for 2 h to allow the sedimentation of individual blood cells to be achieved. Once a visible phase boundary was established, approximately 150 µL of the upper layer containing the platelets was collected and transferred to new tubes containing 300 µL of 10 mM dimethyl sulfoxide (DMSO) for cryopreservation. Samples were stored at −20 °C for further analyses. Before the analyses, fixed platelets were centrifuged at 3500× *g* for 5 min at 2 °C to remove DMSO. Isolated platelets were dissolved in 300 µL of HEPES-buffered Tyrode's solution (119 mM NaCl, 5 mM KCl, 25 mM HEPES buffer, 2 mM $CaCl_2$, 2 mM $MgCl_2$ and 6 g/L glucose, adjusted with NaOH to final pH of 7.4). The extracellular oxygen consumption rate in platelet mitochondria was measured using a filter-based multi-mode microplate reader (FLUOstar OPTIMA; BMG Labtech, Ofenburg, Germany) using MitoXpress-Xtra HS kits (Luxcel Company, Cork, Ireland) according to the manufacturer's instructions. Fluorescence intensity was measured at 5 min intervals for 30 min at 37 °C in a sealed environment by applying 100 µL of mineral oil to reduce oxygen exchange. Tyrode's buffer with 10 µL of MitoXpress-Xtra HS compound was used as reference. Each sample was analyzed in duplicate. The rate of fluorescence signal change per minute was calculated for each 5-minute interval, and the average signal change per minute over the entire 30-minute period was calculated for each sample.

4.6. Statistical Analysis

The results were subjected to one-way analysis of variance (ANOVA), using STATGRAPHICS Centurion XVI ver. 16.1.03 software. Arithmetic means and standard errors of the mean (SEMs) were calculated using the aforementioned program. The significance of the differences among groups was verified with Tukey's test (HSD). The level of significance was set at $p < 0.05$, and data were presented as means ± standard errors of the mean (SEMs) ($n = 8$ for each group).

5. Conclusions

Our research showed a positive effect of CBD and nano-Se on the microstructure of the chicken breast muscle after *C. perfringens* infection. After adding these substances, an increase in the number of capillaries supplying individual muscle fibers was observed. The improvement in blood supply could have reduced degenerative changes in the muscles, i.e., fiber necrosis and splitting. This finding also indicated that a potential link between the condition of gut mucosa and histopathological changes in superficial pectoral muscle under induced inflammation may exist, and in this regard, CBD and nano-Se manifest ameliorative effects due to their protection against mucosal DNA damage. Further research is needed in this area to elucidate the mechanisms of action of the tested substances on skeletal muscles.

Author Contributions: Conceptualization, P.K. (Paweł Konieczka), M.M. and J.B. (Joanna Bogucka); data curation, P.K. (Paweł Konieczka), M.M. and J.B. (Joanna Bogucka); formal analysis, D.S., M.K., P.K. (Paweł Kowalczyk), J.B. (Joanna Banach), D.B. and J.B. (Joanna Bogucka); funding acquisition, P.K. (Paweł Konieczka); investigation, P.K. (Paweł Konieczka), M.M. and J.B. (Joanna Bogucka); methodology, P.K. (Paweł Konieczka), P.K. (Paweł Kowalczyk) and J.B. (Joanna Bogucka); project administration, P.K. (Paweł Konieczka); supervision, P.K. (Paweł Konieczka) and M.M.; writing—original draft, P.K. (Paweł Konieczka) and J.B. (Joanna Bogucka); writing—review and editing, P.K. (Paweł Konieczka), M.M., J.B. (Joanna Bogucka), P.M. and P.K. (Paweł Kowalczyk). All authors have read and agreed to the published version of the manuscript.

Funding: This work was supported by National Science Centre, grant No. 2018/29/B/NZ9/01351. This work was partially supported (preparation of microscopic slides) by the statutory funds of Department of Animal Physiology and Physiotherapy, Faculty of Animal Breeding and Biology, Bydgoszcz University of Science and Technology, grant No. BN 52/2019.

Institutional Review Board Statement: The protocol for this study was approved by the Local Ethics Committee for animal testing at UWM Olsztyn, Poland (Resolution No. 54/2019 of 30 July 2019), and all procedures involving animals were performed in accordance with EU regulations (recommendation 2007/526/CE) and the Polish Law on Animal Protection. All procedures in this study complied with the ARRIVE guidelines.

Data Availability Statement: All data generated during the study are available from the corresponding author upon reasonable request.

Conflicts of Interest: The authors declare no conflict of interest.

References

1. Skinner, J.T.; Bauer, S.; Young, V.; Pauling, G.; Wilson, J. An economic analysis of the impact of subclinical (Mild) necrotic enteritis in broiler chickens. *Avian Dis.* **2010**, *54*, 1237–1240. [CrossRef] [PubMed]
2. Goossens, E.; Dierick, E.; Ducatelle, R.; Van Immerseel, F. Spotlight on avian pathology: Untangling contradictory disease descriptions of necrotic enteritis and necro-haemorrhagic enteritis in broilers. *Avian Pathol.* **2020**, *49*, 423–427. [CrossRef] [PubMed]
3. Van Immerseel, F.; De Buck, J.; Pasmans, F.; Huyghebaert, G.; Haesebrouck, F.; Ducatelle, R. Clostridium perfringens in poultry: An emerging threat for animal and public health. *Avian Pathol.* **2004**, *33*, 537–549. [CrossRef] [PubMed]
4. Hasegawa, Y.; Hosotani, M.; Saito, M.; Nagasawa, T.; Mori, Y.; Kawasaki, T.; Yamada, M.; Maeda, N.; Watanabe, T.; Iwasaki, T. Mitochondrial characteristics of chicken breast muscle affected by wooden breast. *Comp. Biochem. Physiol.-Part A Mol. Integr. Physiol.* **2022**, *273*, 111296. [CrossRef]
5. Bogucka, J.; Dankowiakowska, A.; Stanek, M.; Stadnicka, K.; Kirkiłło-Stacewicz, K. Effect of synbiotics administered in ovo on microvascularization and histopathological changes in pectoral muscle and the biochemical profile of broiler chicken blood. *Poult. Sci.* **2022**, *101*, 101628. [CrossRef]
6. Yekhtin, Z.; Khuja, I.; Meiri, D.; Or, R.; Almogi-Hazan, O. Differential Effects of D9 Tetrahydrocannabinol (THC)- and Cannabidiol (CBD)-Based Cannabinoid Treatments on Macrophage Immune Function In Vitro and on Gastrointestinal Inflammation in a Murine Model. *Biomedicines* **2022**, *10*, 1793. [CrossRef]
7. Klein, T.W.; Cabral, G.A. Cannabinoid-induced immune suppression and modulation of antigen-presenting cells. *J. Neuroimmune Pharmacol.* **2006**, *1*, 50–64. [CrossRef]
8. Konieczka, P.; Szkopek, D.; Kinsner, M.; Fotschki, B.; Juśkiewicz, J.; Banach, J. Cannabis-derived cannabidiol and nanoselenium improve gut barrier function and affect bacterial enzyme activity in chickens subjected to C. perfringens challenge. *Vet. Res.* **2020**, *51*, 141. [CrossRef]
9. Varga, Z.V.; Ferdinandy, P.; Liaudet, L.; Pacher, P. Drug-induced mitochondrial dysfunction and cardiotoxicity. *Am. J. Physiol.-Heart Circ. Physiol.* **2015**, *309*, H1453–H1467. [CrossRef]
10. Fraguas-Sánchez, A.I.; Fernández-Carballido, A.; Delie, F.; Cohen, M.; Martin-Sabroso, C.; Mezzanzanica, D.; Figini, M.; Satta, A.; Torres-Suárez, A.I. Enhancing ovarian cancer conventional chemotherapy through the combination with cannabidiol loaded microparticles. *Eur. J. Pharm. Biopharm.* **2020**, *154*, 246–258. [CrossRef]
11. Huestis, M.A.; Solimini, R.; Pichini, S.; Pacifici, R.; Carlier, J.; Busardò, F.P. Cannabidiol Adverse Effects and Toxicity. *Curr. Neuropharmacol.* **2019**, *17*, 974–989. [CrossRef]
12. Chan, J.Z.; Duncan, R.E. Regulatory effects of cannabidiol on mitochondrial functions: A review. *Cells* **2021**, *10*, 1251. [CrossRef] [PubMed]
13. Yuan, D.; Zhan, X.A.; Wang, Y.X. Effect of selenium sources on the expression of cellular glutathione peroxidase and cytoplasmic thioredoxin reductase in the liver and kidney of broiler breeders and their offspring. *Poult. Sci.* **2012**, *91*, 936–942. [CrossRef]
14. Perić, L.; Milošević, N.; Žikić, D.; Kanački, Z.; Džinić, N.; Nollet, L.; Spring, P. Effect of selenium sources on performance and meat characteristics of broiler chickens. *J. Appl. Poult. Res.* **2009**, *18*, 403–409. [CrossRef]
15. Surai, P.F.; Kochish, I.I.; Fisinin, V.I.; Velichko, O.A. Selenium in poultry nutrition: From sodium selenite to organic selenium sources. *J. Poult. Sci.* **2018**, *55*, 79–93. [CrossRef] [PubMed]
16. Selim, N.A.; Radwan, N.L.; Youssef, S.F.; Salah Eldin, T.A.; Abo Elwafa, S. Effect of inclusion inorganic, organic or Nano selenium forms in Broiler diets on: 1-Growth Performance, carcass and Meat Characteristics. *Int. J. Poult. Sci.* **2015**, *14*, 135–143. [CrossRef]
17. Michalczuk, M.; Batorska, M.; Sikorska, U.; Bień, D.; Urban, J.; Capecka, K.; Konieczka, P. Selenium and the health status, production results, and product quality in poultry. *Anim. Sci. J.* **2021**, *92*, e13662. [CrossRef] [PubMed]
18. Hosnedlova, B.; Kepinska, M.; Skalickova, S.; Fernandez, C.; Ruttkay-Nedecky, B.; Donald Malevu, T.; Sochor, J.; Baron, M.; Melcova, M.; Zidkova, J.; et al. A summary of new findings on the biological effects of selenium in selected animal species—A critical review. *Int. J. Mol. Sci.* **2017**, *18*, 2209. [CrossRef]
19. Zhou, Y.; Zhang, S.; Liu, C.; Cai, Y. The protection of selenium on ROS mediated-apoptosis by mitochondria dysfunction in cadmium-induced LLC-PK1 cells. *Toxicol. Vitr.* **2009**, *23*, 288–294. [CrossRef]

20. Taskin, E.; Dursun, N. Recovery of adriamycin induced mitochondrial dysfunction in liver by selenium. *Cytotechnology* **2015**, *67*, 977–986. [CrossRef]
21. Liu, H.J.; Qin, Y.; Zhao, Z.H.; Zhang, Y.; Yang, J.H.; Zhai, D.H.; Cui, F.; Luo, C.; Lu, M.X.; Liu, P.P.; et al. Lentinan-functionalized selenium nanoparticles target tumor cell mitochondria via TLR4/TRAF3/MFN1 pathway. *Theranostics* **2020**, *10*, 9083–9099. [CrossRef] [PubMed]
22. Hosnedlova, B.; Kepinska, M.; Skalickova, S.; Fernandez, C.; Ruttkay-Nedecky, B.; Peng, Q.; Baron, M.; Melcova, M.; Opatrilova, R.; Zidkova, J.; et al. Nano-selenium and its nanomedicine applications: A critical review. *Int. J. Nanomed.* **2018**, *13*, 2107–2128. [CrossRef] [PubMed]
23. Kogut, M.H.; Yin, X.; Yuan, J.; Broom, L. Gut health in poultry. *CAB Rev. Perspect. Agric. Vet. Sci. Nutr. Nat. Resour.* **2017**, *12*, 1–7. [CrossRef]
24. Wang, Y.; Sun, J.; Zhong, H.; Li, N.; Xu, H.; Zhu, Q.; Liu, Y. Effect of probiotics on the meat flavour and gut microbiota of chicken. *Sci. Rep.* **2017**, *7*, 6400. [CrossRef]
25. Castro, F.L.D.S.; Kim, W.K. Secondary functions of arginine and sulfur amino acids in poultry health: Review. *Animals* **2020**, *10*, 2106. [CrossRef]
26. Bortoluzzi, C.; Rochell, S.J.; Applegate, T.J. Threonine, arginine, and glutamine: Influences on intestinal physiology, immunology, and microbiology in broilers. *Poult. Sci.* **2018**, *97*, 937–945. [CrossRef]
27. Celi, P.; Cowieson, A.J.; Fru-Nji, F.; Steinert, R.E.; Kluenter, A.M.; Verlhac, V. Gastrointestinal functionality in animal nutrition and health: New opportunities for sustainable animal production. *Anim. Feed Sci. Technol.* **2017**, *234*, 88–100. [CrossRef]
28. Fallahi, S.; Bobak, Ł.; Opaliński, S. Hemp in Animal Diets—Cannabidiol. *Animals* **2022**, *12*, 2541. [CrossRef]
29. Wang, Q.; Zhan, X.; Wang, B.; Wang, F.; Zhou, Y.; Xu, S.; Li, X.; Tang, L.; Jin, Q.; Li, W.; et al. Modified Montmorillonite Improved Growth Performance of Broilers by Modulating Intestinal Microbiota and Enhancing Intestinal Barriers, Anti-Inflammatory Response, and Antioxidative Capacity. *Antioxidants* **2022**, *11*, 1799. [CrossRef]
30. Lu, M.; Yuan, B.; Yan, X.; Sun, Z.; Lillehoj, H.S.; Lee, Y.; Baldwin-Bott, C.; Li, C. Clostridium perfringens-induced host-pathogen transcriptional changes in the small intestine of broiler chickens. *Pathogens* **2021**, *10*, 1607. [CrossRef]
31. Konieczka, P.; Żelechowska, E.; Przybylski, W.; Jaworska, D.; Sałek, P.; Kinsner, M.; Jankowski, J. The sarcoplasmic protein profile of breast muscle in Turkeys in response to different dietary ratios of limiting amino acids and Clostridium perfringens-induced inflammation. *Poult. Sci.* **2022**, *101*, 102195. [CrossRef] [PubMed]
32. Cai, K.; Shao, W.; Chen, X.; Campbell, Y.L.; Nair, M.N.; Suman, S.P.; Beach, C.M.; Guyton, M.C.; Schilling, M.W. Meat quality traits and proteome profile of woody broiler breast (pectoralis major) meat. *Poult. Sci.* **2018**, *97*, 337–346. [CrossRef] [PubMed]
33. Sihvo, H.K.; Airas, N.; Lindén, J.; Puolanne, E. Pectoral Vessel Density and Early Ultrastructural Changes in Broiler Chicken Wooden Breast Myopathy. *J. Comp. Pathol.* **2018**, *161*, 1–10. [CrossRef] [PubMed]
34. Gornatti-Churria, C.D.; Crispo, M.; Shivaprasad, H.L.; Uzal, F.A. Gangrenous dermatitis in chickens and turkeys. *J. Vet. Diagn. Investig.* **2018**, *30*, 188–196. [CrossRef] [PubMed]
35. Zúñiga-Pereira, A.M.; Santamaría, C.; Gutierrez, J.M.; Alape-Girón, A.; Flores-Díaz, M. Deficient skeletal muscle regeneration after injury induced by a clostridium perfringens strain associated with gas gangrene. *Infect. Immun.* **2019**, *87*, e00200-19. [CrossRef]
36. Konieczka, P.; Wojtasik-Kalinowska, I.; Poltorak, A.; Kinsner, M.; Szkopek, D.; Fotschki, B.; Juśkiewicz, J.; Banach, J.; Michalczuk, M. Cannabidiol affects breast meat volatile compounds in chickens subjected to different infection models. *Sci. Rep.* **2022**, *12*, 18940. [CrossRef]
37. Zhou, M.; Zeng, D.; Ni, X.; Tu, T.; Yin, Z.; Pan, K.; Jing, B. Effects of bacillus licheniformis on the growth performance and expression of lipid metabolism-related genes in broiler chickens challenged with clostridium perfringens-induced necrotic enteritis. *Lipids Health Dis.* **2016**, *15*, 48. [CrossRef]
38. Bień, D.; Michalczuk, M.; Szkopek, D.; Kinsner, M.; Konieczka, P. Changes in lipids metabolism indices as a result of different form of selenium supplementation in chickens. *Sci. Rep.* **2022**, *12*, 13817. [CrossRef]
39. Ullah Khan, R.; Durrani, F.-E.-R.; Chand, N.; Anwar, H.; Naz, S.; Farooqi, A.; Manzoor, M.N. Effect of cannabis sativa fortified feed on muscle growth and visceral organs in broiler chicks. *Int. J. Biol. Biotechnol.* **2009**, *6*, 179–182.
40. Skřivan, M.; Englmaierová, M.; Taubner, T.; Skřivanová, E. Effects of dietary hemp seed and flaxseed on growth performance, meat fatty acid compositions, liver tocopherol concentration and bone strength of cockerels. *Animals* **2020**, *10*, 458. [CrossRef]
41. Šťastník, O.; Jůzl, M.; Karásek, F.; Fernandová, D.; Mrkvicová, E.; Pavlata, L.; Nedomová, Š.; Vyhnánek, T.; Trojan, V.; Doležal, P. The effect of hempseed expellers on selected quality indicators of broiler chicken's meat. *Acta Vet. Brno* **2019**, *88*, 121–128. [CrossRef]
42. Cai, S.J.; Wu, C.X.; Gong, L.M.; Song, T.; Wu, H.; Zhang, L.Y. Effects of nano-selenium on performance, meat quality, immune function, oxidation resistance, and tissue selenium content in broilers. *Poult. Sci.* **2012**, *91*, 2532–2539. [CrossRef] [PubMed]
43. Li, J.L.; Zhang, L.; Yang, Z.Y.; Zhang, Z.Y.; Jiang, Y.; Gao, F.; Zhou, G.H. Effects of Different Selenium Sources on Growth Performance, Antioxidant Capacity and Meat Quality of Local Chinese Subei Chickens. *Biol. Trace Elem. Res.* **2018**, *181*, 340–346. [CrossRef] [PubMed]
44. Langer, H.T.; Mossakowski, A.A.; Pathak, S.; Mascal, M.; Baar, K. Cannabidiol does not impair anabolic signaling following eccentric contractions in rats. *Int. J. Sport Nutr. Exerc. Metab.* **2021**, *31*, 93–100. [CrossRef] [PubMed]

45. Bogucka, J.; Ribeiro, D.M.; Bogusławska-Tryk, M.; Dankowiakowska, A.; da Costa, R.P.R.; Bednarczyk, M. Microstructure of the small intestine in broiler chickens fed a diet with probiotic or synbiotic supplementation. *J. Anim. Physiol. Anim. Nutr.* **2019**, *103*, 1785–1791. [CrossRef] [PubMed]
46. Dankowiakowska, A.; Bogucka, J.; Sobolewska, A.; Tavaniello, S.; Maiorano, G.; Bednarczyk, M. Effects of in ovo injection of prebiotics and synbiotics on the productive performance and microstructural features of the superficial pectoral muscle in broiler chickens. *Poult. Sci.* **2019**, *98*, 5157–5165. [CrossRef]
47. Maiorano, G.; Stadnicka, K.; Tavaniello, S.; Abiuso, C.; Bogucka, J.; Bednarczyk, M. In ovo validation model to assess the efficacy of commercial prebiotics on broiler performance and oxidative stability of meat. *Poult. Sci.* **2017**, *96*, 511–518. [CrossRef]
48. Pelyhe, C.; Mézes, M. Myths and Facts About the Effects of Nano- Selenium in Farm Animals—Mini-Review. *Eur. Chem. Bull.* **2013**, *2*, 1049–1052.
49. Bilgili, S.F.; Hess, J.B. Green Muscle Disease in broilers increasing. *World Poult.* **2002**, *18*, 42–43.
50. Velleman, S.G. Relationship of Skeletal Muscle Development and Growth to Breast Muscle Myopathies: A Review. *Avian Dis.* **2015**, *59*, 525–531. [CrossRef]
51. Kaszyńska, A. Possibilities of therapeutic action of cannabinoids in neurodegenerative diseases. *Pharmacother. Psychiatry Neurol.* **2022**, *38*, 49–58. [CrossRef]
52. MacRae, V.E.; Mahon, M.; Gilpin, S.; Sandercock, D.A.; Mitchell, M.A. Skeletal muscle fibre growth and growth associated myopathy in the domestic chicken (Gallus domesticus). *Br. Poult. Sci.* **2006**, *47*, 264–272. [CrossRef] [PubMed]
53. Olmon, E.D.; Delaney, S. Differential Ability of Five DNA Glycosylases to Recognize and Repair Damage on Nucleosomal DNA. *ACS Chem. Biol.* **2017**, *12*, 692–701. [CrossRef] [PubMed]
54. Winczura, A.; Czubaty, A.; Winczura, K.; Masłowska, K.; Nałecz, M.; Dudzińska, D.A.; Saparbaev, M.; Staroń, K.; Tudek, B. Lipid peroxidation product 4-hydroxy-2-nonenal modulates base excision repair in human cells. *DNA Repair* **2014**, *22*, 1–11. [CrossRef]
55. Kowalczyk, P.; Jaworek, J.; Kot, M.; Sokolowska, B.; Bielen, A.; Janowska, B.; Ciesla, J.M.; Szparecki, G.; Sados, B.; Tudek, B. Inflammation increases oxidative DNA damage repair and stimulates preneoplastic changes in colons of newborn rats. *J. Physiol. Pharmacol.* **2016**, *67*, 277–286.
56. Soglia, F.; Petracci, M.; Davoli, R.; Zappaterra, M. A critical review of the mechanisms involved in the occurrence of growth-related abnormalities affecting broiler chicken breast muscles. *Poult. Sci.* **2021**, *100*, 101180. [CrossRef]
57. Pampouille, E.; Hennequet-Antier, C.; Praud, C.; Juanchich, A.; Brionne, A.; Godet, E.; Bordeau, T.; Fagnoul, F.; Le Bihan-Duval, E.; Berri, C. Differential expression and co-expression gene network analyses reveal molecular mechanisms and candidate biomarkers involved in breast muscle myopathies in chicken. *Sci. Rep.* **2019**, *9*, 14905. [CrossRef]
58. Abasht, B.; Mutryn, M.F.; Michalek, R.D.; Lee, W.R. Oxidative Stress and Metabolic Perturbations in Wooden Breast Disorder in Chickens. *PLoS ONE* **2016**, *11*, e0153750. [CrossRef]
59. Gratta, F.; Fasolato, L.; Birolo, M.; Zomeño, C.; Novelli, E.; Petracci, M.; Pascual, A.; Xiccato, G.; Trocino, A. Effect of breast myopathies on quality and microbial shelf life of broiler meat. *Poult. Sci.* **2019**, *98*, 2641–2651. [CrossRef]
60. Marchesi, J.A.P.; Ibelli, A.M.G.; Peixoto, J.O.; Cantão, M.E.; Pandolfi, J.R.C.; Marciano, C.M.M.; Zanella, R.; Settles, M.L.; Coutinho, L.L.; Ledur, M.C. Whole transcriptome analysis of the pectoralis major muscle reveals molecular mechanisms involved with white striping in broiler chickens. *Poult. Sci.* **2019**, *98*, 590–601. [CrossRef]
61. Hynes, J.; Nadanaciva, S.; Swiss, R.; Carey, C.; Kirwan, S.; Will, Y. A high-throughput dual parameter assay for assessing drug-induced mitochondrial dysfunction provides additional predictivity over two established mitochondrial toxicity assays. *Toxicol. Vitr.* **2013**, *27*, 560–569. [CrossRef] [PubMed]
62. De Paula Martins, R.; Glaser, V.; Da Luz Scheffer, D.; De Paula Ferreira, P.M.; Wannmacher, C.M.D.; Farina, M.; De Oliveira, P.A.; Prediger, R.D.; Latini, A. Platelet oxygen consumption as a peripheral blood marker of brain energetics in a mouse model of severe neurotoxicity. *J. Bioenerg. Biomembr.* **2013**, *45*, 449–457. [CrossRef] [PubMed]
63. Siewiera, K.; Kassassir, H.; Talar, M.; Wieteska, L.; Watala, C. Higher mitochondrial potential and elevated mitochondrial respiration are associated with excessive activation of blood platelets in diabetic rats. *Life Sci.* **2016**, *148*, 293–304. [CrossRef] [PubMed]
64. Vuda, M.; Kamath, A. Drug induced mitochondrial dysfunction: Mechanisms and adverse clinical consequences. *Mitochondrion* **2016**, *31*, 63–74. [CrossRef] [PubMed]
65. Konieczka, P.; Barszcz, M.; Kowalczyk, P.; Szlis, M.; Jankowski, J. The potential of acetylsalicylic acid and vitamin e in modulating inflammatory cascades in chickens under lipopolysaccharide-induced inflammation. *Vet. Res.* **2019**, *50*, 65. [CrossRef]
66. Ferdous, F.; Scott, T.R. A comparative examination of thrombocyte/platelet immunity. *Immunol. Lett.* **2015**, *163*, 32–39. [CrossRef]
67. Wigley, P. Immunity to bacterial infection in the chicken. *Dev. Comp. Immunol.* **2013**, *41*, 413–417. [CrossRef]
68. *Aviagen Ross 308: Broiler Performance Objectives*; Aviagen Inc.: Huntsville, AL, USA, 2019; pp. 1–15.
69. Konieczka, P.; Sandvang, D.; Kinsner, M.; Szkopek, D.; Szyryńska, N.; Jankowski, J. Bacillus-based probiotics affect gut barrier integrity in different ways in chickens subjected to optimal or challenge conditions. *Vet. Microbiol.* **2022**, *265*, 109323. [CrossRef]
70. Van Damme, L.; Cox, N.; Callens, C.; Haesebrouck, F.; Dargatz, M.; Ducatelle, R.; Van Immerseel, F.; Goossens, E.C. perfringens challenge reduces matrix metalloproteinase activity in the jejunal mucosa of Eimeria-infected broiler chickens. *Vet. Res.* **2020**, *51*, 100. [CrossRef]

71. Olkowski, A.A.; Wojnarowicz, C.; Chirino-Trejo, M.; Drew, M.D. Responses of broiler chickens orally challenged with Clostridium perfringens isolated from field cases of necrotic enteritis. *Res. Vet. Sci.* **2006**, *81*, 99–108. [CrossRef]
72. Timbermont, L.; Haesebrouck, F.; Ducatelle, R.; Van Immerseel, F. Necrotic enteritis in broilers: An updated review on the pathogenesis. *Avian Pathol.* **2011**, *40*, 341–347. [CrossRef] [PubMed]
73. Obtułowicz, T.; Winczura, A.; Speina, E.; Swoboda, M.; Janik, J.; Janowska, B.; Cieśla, J.M.; Kowalczyk, P.; Jawien, A.; Gackowski, D.; et al. Aberrant repair of etheno-DNA adducts in leukocytes and colon tissue of colon cancer patients. *Free Radic. Biol. Med.* **2010**, *49*, 1064–1071. [CrossRef] [PubMed]

International Journal of
Molecular Sciences

MDPI

Article

Differential Effects of Oligosaccharides, Antioxidants, Amino Acids and PUFAs on Heat/Hypoxia-Induced Epithelial Injury in a Caco-2/HT-29 Co-Culture Model

Puqiao Lian [1], Paul A. J. Henricks [1], Harry J. Wichers [2], Gert Folkerts [1] and Saskia Braber [1,*]

[1] Division of Pharmacology, Utrecht Institute for Pharmaceutical Sciences, Faculty of Science, Utrecht University, 3584 CG Utrecht, The Netherlands
[2] Food & Biobased Research, Wageningen University & Research, 6700 AA Wageningen, The Netherlands
* Correspondence: s.braber@uu.nl; Tel.: +31-302531599

Abstract: (1) Exposure of intestinal epithelial cells to heat and hypoxia causes a (heat) stress response, resulting in the breakdown of epithelial integrity. There are indications that several categories of nutritional components have beneficial effects on maintaining the intestinal epithelial integrity under stress conditions. This study evaluated the effect of nine nutritional components, including non-digestible oligosaccharides (galacto-oligosaccharides (GOS), fructo-oligosaccharides (FOS), chitosan oligosaccharides (COS)), antioxidants (α-lipoic acid (ALA), resveratrol (RES)), amino acids (l-glutamine (Glu), l-arginine (Arg)) and polyunsaturated fatty acids (PUFAs) (docosahexaenoic acid (DHA) and eicosapentaenoic acid (EPA)), on heat/hypoxia-induced epithelial injury. (2) Two human colonic cell lines, Caco-2 and HT-29, were co-cultured and pre-treated with the nutritional components for 48 h. After pre-treatment, the cells were exposed to heat/hypoxia (42 °C, 5% O_2) for 2 h. Epithelial integrity was evaluated by measuring trans-epithelial electrical resistance (TEER), paracellular Lucifer Yellow (LY) permeability, and tight junction (TJ) protein expression. Heat stress and oxidative stress levels were evaluated by determining heat-shock protein-70 (HSP-70) expression and the concentration of the lipid peroxidation product malondialdehyde (MDA). (3) GOS, FOS, COS, ALA, RES, Arg, and EPA presented protective effects on epithelial damage in heat/hypoxia-exposed Caco-2/HT-29 cells by preventing the decrease in TEER, the increase in LY permeability, and/or decrease in TJ proteins zonula occludens-1 (ZO-1) and claudin-3 expression. COS, RES, and EPA demonstrated anti-oxidative stress effects by suppressing the heat/hypoxia-induced MDA production, while Arg further elevated the heat/hypoxia-induced increase in HSP-70 expression. (4) This study indicates that various nutritional components have the potential to counteract heat/hypoxia-induced intestinal injury and might be interesting candidates for future in vivo studies and clinical trials in gastrointestinal disorders related to heat stress and hypoxia.

Keywords: intestinal epithelial cells; hypoxia; heat stress; epithelial integrity; nutritional components; tight junction

Citation: Lian, P.; Henricks, P.A.J.; Wichers, H.J.; Folkerts, G.; Braber, S. Differential Effects of Oligosaccharides, Antioxidants, Amino Acids and PUFAs on Heat/Hypoxia-Induced Epithelial Injury in a Caco-2/HT-29 Co-Culture Model. *Int. J. Mol. Sci.* **2023**, *24*, 1111. https://doi.org/10.3390/ijms24021111

Academic Editor: Alain Couvineau

Received: 25 November 2022
Revised: 30 December 2022
Accepted: 3 January 2023
Published: 6 January 2023

1. Introduction

The homeostasis of the human gastrointestinal (GI) tract is affected by multiple factors, including changes in diet and internal environment, and exposure to stressors, such as infectious agents and toxins. Strenuous exercise is an important stressor that predisposes athletes and other persons to different intestinal disorders [1,2]. During strenuous exercise such as marathon running and cycling, blood redistribution from the intestine to peripheral limbs combined with increased body temperature may lead to local hypoxic conditions and potential heat stress in the GI tract, which results in alterations in the integrity of the intestinal epithelial barrier [3].

Junctional complexes between adjacent intestinal epithelial cells form the critical structures responsible for the integrity of the intestinal barrier. This barrier is composed of

a series of tight junction (TJ), adherens junction (AJ), and desmosome proteins that regulate paracellular transport and stability and tightness of the epithelium [4]. Our previous study proved that 2-h exposure to heat (40 or 42 °C) and hypoxia (5% of oxygen) significantly decreased TJ protein expression and disturbed the cellular TJ distribution, while expression of the AJ protein E-cadherin was enhanced in a co-culture model using two human colonic epithelial cell lines, Caco-2 and HT-29 [5]. Furthermore, trans-epithelial electrical resistance (TEER) was decreased, and the epithelial permeability was increased after hypoxia and heat treatment [5]. A dysfunctional or leaky intestinal epithelial tight junction barrier allows augmented permeation of luminal antigens, endotoxins, and bacteria into the local tissues and blood circulation, possibly leading to severe local and systemic inflammatory conditions [6]. Any intervention, which prevents abnormal expression of TJ/AJ proteins or restores the epithelial integrity, may contribute to alleviate heat stress (HS)-induced intestinal injury and associated disorders.

A broad range of nutritional supplements, such as non-digestible oligosaccharides, polyunsaturated fatty acids (PUFAs), antioxidants, and amino acids, may be effective in the prevention and treatment of HS-induced intestinal disorders, not only by restoring the expression of TJ/AJ proteins, but also by modulating immune responses and stress resilience pathways [3]. Our group demonstrated that galacto-oligosaccharides (GOS) and α-lipoic acid (ALA) modulate heat shock protein (HSP)-70 expression, the key regulator of the HS response, in HS-exposed Caco-2 cells and chickens [7–9].

Although the association between exercise-induced heat and enhanced intestinal permeability is clear [10], the exact mechanism behind the pathology of hypoxia- and heat-induced epithelial breakdown still needs to be elucidated. The TJ protein claudin-1 can act as a target protein for hypoxia-inducible factors (HIFs) suggesting a direct relationship between hypoxia and intestinal barrier damage [11]. Additionally, hypoxia and heat can lead to increased ROS activity and thus cause peroxidative damage to epithelial cells and is one of the hypotheses proposed so far [11]. A suitable intervention strategy for this intestinal barrier injury is of great importance. In the present study, we used the combination of heat stress and hypoxia in an in vitro set up using a well-characterized Caco-2/HT-29 co-culture model (epithelial cells forming a tight intestinal epithelial barrier combined with mucus-producing cells) mimicking the human intestinal epithelial layer [12,13]. These monolayers were pre-treated with different nutritional components, including GOS, fructo-oligosaccharides (FOS), chitosan oligosaccharides (COS), ALA, resveratrol (RES), l-glutamine (Glu), l-arginine (Arg), docosahexaenoic acid (DHA), and eicosapentaenoic acid (EPA), prior to two hours of heat (42 °C) and hypoxia (5% of oxygen) treatment, followed by measuring markers of intestinal integrity, including TEER, Lucifer Yellow (LY) permeability, and the expression of TJ proteins. In addition, heat stress and oxidative stress was measured via determination of HSP-70 and HIF-1α expression levels and products of lipid peroxidation.

The goal of this study is to explore the possible impact of nutritional components on altered intestinal barrier function exerted by heat and hypoxia exposure. The outcome of this study might bring us one step closer to the goal of finding suitable dietary components for people with gastrointestinal problems that are related to heat stress and hypoxia.

2. Results

2.1. Hypoxia and Heat Exposure in Combination with the Nutritional Components Do Not Affect the Cell Viability of Caco-2/HT-29 Cell Monolayers

Cytotoxicity of all nutritional components on the Caco-2/HT-29 monolayers was evaluated in a concentration- and time-dependent manner by using the MTT assay. For each nutritional component, four biologically relevant concentrations and three time points (24, 48, and 72 h) were used (Supplementary Figure S1). These results demonstrated that after 48 h of incubation, none of the selected concentrations of the nutritional components used in the following study caused cytotoxicity in the Caco-2/HT-29 monolayers (Supplementary Figure S1).

Cytotoxicity of hypoxia and heat exposure in the presence of the promising nutritional components in Caco-2/HT-29 monolayers was further analyzed through the determination of LDH release at the end of the exposure time. No significant differences were observed between the different groups: control versus heat/hypoxia (model) and control versus model with the nutritional components (Figure 1). The results demonstrated that either heat/hypoxia exposure alone or combined with 48 h pre-incubation with one of the nutritional components did not result in lethal damage to the Caco-2/HT-29 cell monolayers.

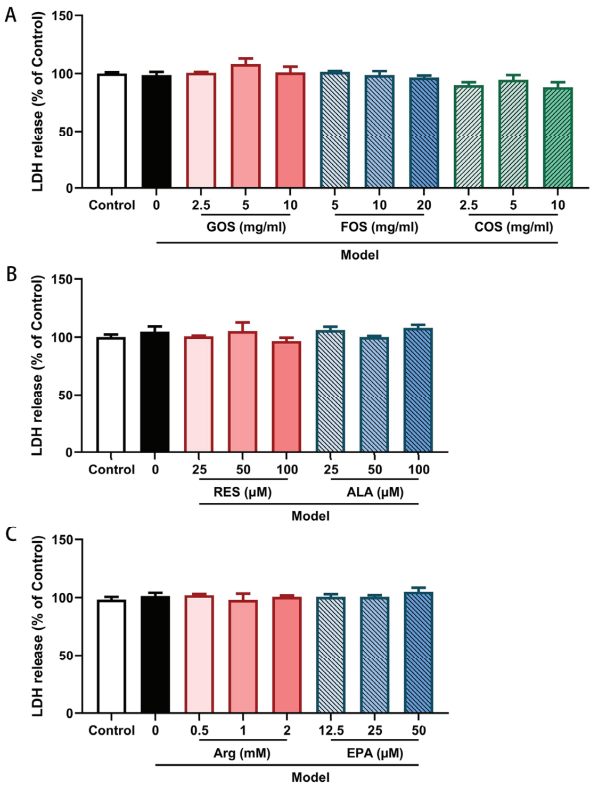

Figure 1. LDH release of Caco-2/HT-29 cell monolayers pre-incubated with GOS, FOS, COS (**A**), RES, ALA (**B**), arginine, and EPA (**C**) for 48 h then exposed to 2 h of hypoxia and heat treatment. LDH release into supernatants was assayed using a LDH assay. All values were presented as means ± SEM (N = 3, n = 2 (GOS, FOS, COS group) and n = 3 (all other groups)). Statistical differences were analyzed by two-way ANOVA followed by the Bonferroni's multiple comparison test. LDH, lactate dehydrogenase; GOS, galacto-oligosaccharides; FOS, fructo-oligosaccharides; COS, chitosan oligosaccharides; ALA, α-lipoic acid; RES, resveratrol; Arg, l-arginine; EPA, eicosapentaenoic acid. The detailed raw OD data are listed in Table S1.

2.2. GOS, FOS, COS, Arg, RES, ALA and EPA Prevent the Heat/Hypoxia-Induced TEER Decrease in Caco-2/HT-29 Cell Monolayers

TEER values are strong indicators of epithelial cell barrier integrity and permeability. The results showed that after 2 h of hypoxia and heat treatment, TEER values of the co-culture model decreased significantly, which indicates an increased leakiness of the monolayer (Figure 2). Forty-eight hours of pre-treatment with GOS (2.5 mg/mL, Figure 2A), FOS (10 and 20 mg/mL, Figure 2B), COS (2.5 and 5 mL/mg, Figure 2C), RES (25, 50, and 100 μM, Figure 2D), ALA (25, 50, and 100 μM, Figure 2E), Arg (0.5 mM, Figure 2F), and EPA (12.5, 25, and 50 μM, Figure 2G) prevented the heat/hypoxia-induced TEER decrease. It is

worth mentioning that after 48 h of pre-treatment, all these nutritional components (and DHA) already significantly increased the TEER values prior to hypoxia and heat exposure (Supplementary Figure S2A–C,E,G–I).

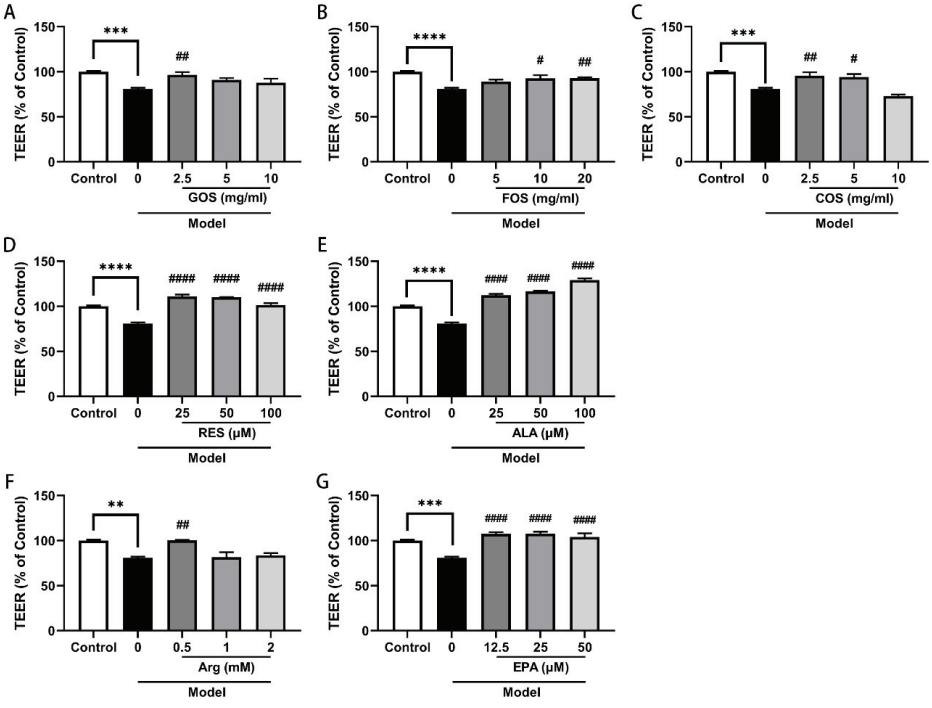

Figure 2. Relative TEER values of Caco-2/HT-29 cell monolayers pre-incubated with GOS (**A**), FOS (**B**), COS (**C**), RES (**D**), ALA (**E**), Arg (**F**), and EPA (**G**) for 48 h then exposed to hypoxia and heat treatment (2 h). After heat/hypoxia exposure, TEER values were determined by using an epithelial volt-ohm meter. All values were presented as means ± SEM (N = 3, n = 3). Same control and model values were depicted in separate figures for different nutritional components. Statistical differences were analyzed by two-way ANOVA followed by the Bonferroni's multiple comparison test. ** $p < 0.01$, *** $p < 0.001$, and **** $p < 0.0001$ versus control; # $p < 0.05$, ## $p < 0.01$, and #### $p < 0.0001$ versus model. TEER, trans-epithelial electrical resistance; GOS, galacto-oligosaccharides; FOS, fructo-oligosaccharides; COS, chitosan oligosaccharides; ALA, α-lipoic acid; RES, resveratrol; Arg, l-arginine; EPA, eicosapentaenoic acid. The detailed raw TEER readings are listed in Table S2.

No significant effect was observed in the Glu- and DHA-treated group after heat/hypoxia treatment (Supplementary Figure S2D,I). Therefore, Glu and DHA-treated groups were excluded from the subsequent measurements.

2.3. GOS, FOS, COS, ALA, and EPA Decrease the Heat/Hypoxia-Induced Paracellular Lucifer Yellow Flux in Caco-2/HT-29 Monolayers

The barrier function was also evaluated by the flux of LY (0.4 kD), an indicator of paracellular permeability, across the epithelial cell layers. After 2 h of hypoxia and heat exposure, LY flux increased significantly in Caco-2/HT-29 cell monolayer (Figure 3). This increase in LY flux was attenuated by pre-incubation with GOS (10 mg/mL, Figure 3A), FOS (20 mg/mL, Figure 3A), COS (5 mg/mL, Figure 3A), ALA (100 μM, Figure 3B), and EPA (25 and 50 μM, Figure 3C) for 48 h. Although RES and Arg prevented the heat/hypoxia-induced TEER decrease, these nutritional components did not significantly affect the increased LY permeability induced by hypoxia and heat exposure.

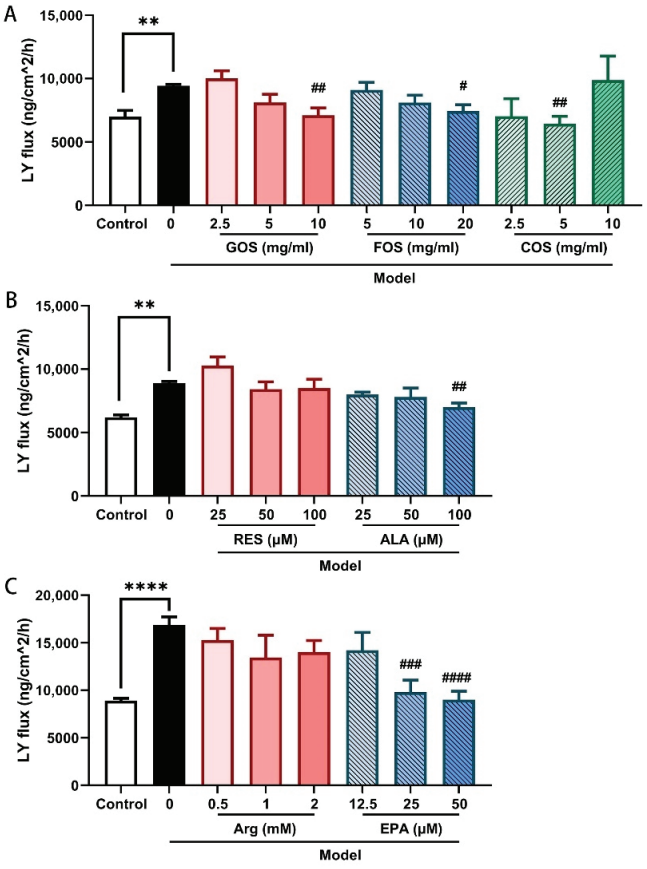

Figure 3. Lucifer Yellow flux of Caco-2/HT-29 cell monolayers pre-incubated with GOS, FOS, COS, (**A**), RES, ALA (**B**), Arg, and EPA (**C**) for 48 h then exposed to hypoxia and heat treatment (2 h). After hypoxia and heat treatment, Lucifer Yellow was added to the apical compartment, and the fluorescent intensity of the medium in the basolateral compartment was measured 4 h after application. All values were presented as means ± SEM (N = 3, n = 2 (GOS, FOS, COS group), and n = 3 (all other groups)). Statistical differences were analyzed by two-way ANOVA followed by the Bonferroni's multiple comparison test. ** $p < 0.01$ and **** $p < 0.0001$ versus control; # $p < 0.05$, ## $p < 0.01$, ### $p < 0.001$, and #### $p < 0.0001$ versus model. LY, Lucifer Yellow; GOS, galacto-oligosaccharides; FOS, fructo-oligosaccharides; COS, chitosan oligosaccharides; ALA, α-lipoic acid; RES, resveratrol; Arg, l-arginine; EPA, eicosapentaenoic acid. The detailed fluorescent readings are listed in Table S3.

2.4. GOS, ALA, and EPA Prevent the Heat/Hypoxia-Induced Decrease in ZO-1 Protein Expression in Caco-2/HT-29 Cell Monolayers

ZO-1, an important TJ protein, is a critical structural protein for maintaining intestinal barrier integrity. The ZO-1 protein expression was investigated in the Caco-2/HT-29 co-cultured monolayers via WB analysis. Two hours of heat and hypoxia exposure significantly decreased ZO-1 protein expression (Figure 4). Among all tested components, 5 and 10 mg/mL GOS (Figure 4A), 25–100 μM ALA (Figure 4B), and 25 and 50 μM EPA (Figure 4C) prevented the heat/hypoxia-induced decrease in ZO-1 expression in the Caco-2/HT-29 cells. There was no effect of FOS, COS, RES, and Arg on ZO-1 protein expression in the heat/hypoxia-stimulated Caco-2/HT-29 cell monolayers (Figure 4A–C).

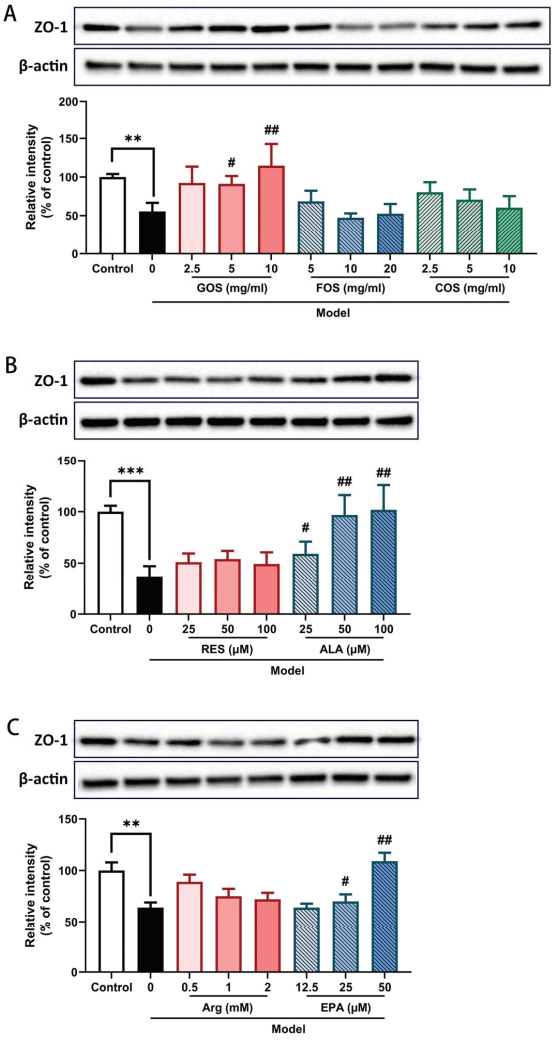

Figure 4. Relative ZO-1 protein expression level in Caco-2/HT-29 cell monolayers pre-incubated with GOS, FOS, COS (**A**), RES, ALA (**B**), Arg, and EPA (**C**) for 48 h then exposed to hypoxia and heat treatment (2 h). ZO-1 protein expression was determined by WB and normalized to β-actin. All values were presented as means ± SEM (N = 3, n = 2 (GOS, FOS, COS group), and n = 3 (all other groups)). Statistical differences were analyzed by two-way ANOVA followed by the Bonferroni's multiple comparison test. ** $p < 0.01$ and *** $p < 0.001$ versus control; # $p < 0.05$ and ## $p < 0.01$ versus model. GOS, galacto-oligosaccharides; FOS, fructo-oligosaccharides; COS, chitosan oligosaccharides; ALA, α-lipoic acid; RES, resveratrol; Arg, l-arginine; EPA, eicosapentaenoic acid. The original uncropped bands are included in the Supplementary Materials.

2.5. GOS, FOS, ALA, and EPA Prevent the Heat/Hypoxia-Induced Decrease in Claudin-3 Protein in Caco-2/HT-29 Cell Monolayers

In addition to ZO-1, CLDN3 is another member of the junctional complex that regulate paracellular intestinal barrier permeability. The CLDN3 protein expression was examined in the Caco-2/HT-29 co-cultured monolayers via WB analysis. The results showed that 2 h of heat and hypoxia exposure significantly decreased ZO-1 protein expression (Figure 5). Among all tested components, 2.5 and 5 mg/mL GOS (Figure 5A), 10 mg/mL

FOS (Figure 5A), 25–100 μM ALA (Figure 5B), and 50 μM EPA (Figure 5C) prevented the heat and hypoxia-induced decrease in CLDN3 expression in the Caco-2/HT-29 cells. No significant effect was observed for COS, RES, and Arg in regulating CLDN3 protein expression in this Caco-2/HT29 co-culture model (Figure 5A–C).

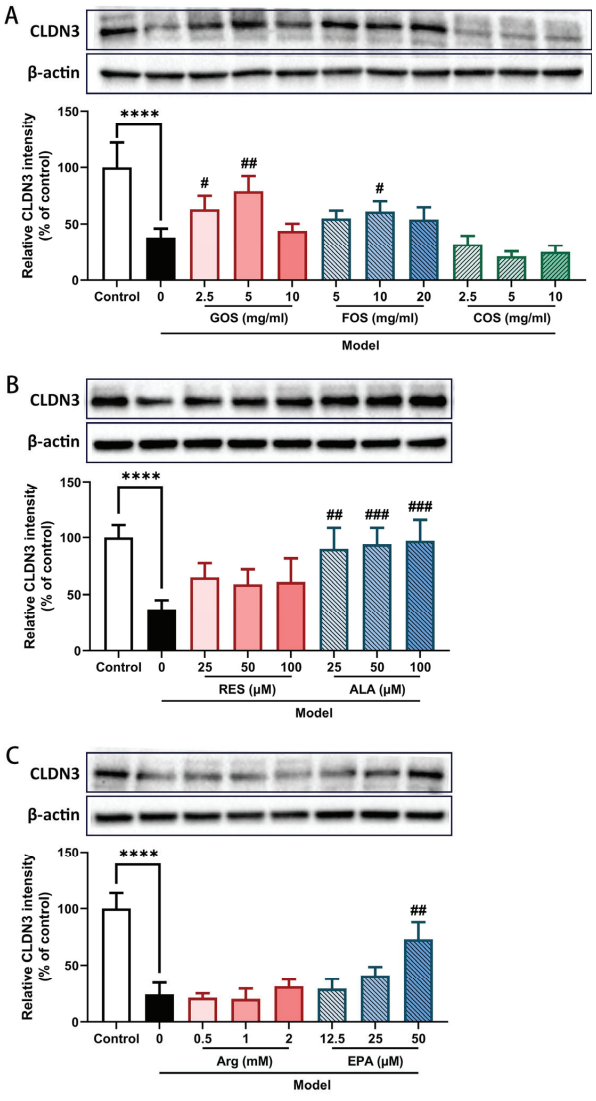

Figure 5. Relative CLDN3 protein expression level in Caco-2/HT-29 cell monolayer pre-incubated with GOS, FOS, COS (**A**), RES, ALA (**B**), Arg, and EPA (**C**) for 48 h then exposed to hypoxia and heat treatment (2 h). CLDN3 protein expression was determined by WB and normalized to β-actin. All values were presented as means ± SEM (N = 3, n = 2 (GOS, FOS, COS group), and n = 3 (all other groups)). Statistical differences were analyzed by two-way ANOVA followed by the Bonferroni's multiple comparison test. **** $p < 0.0001$ versus control; # $p < 0.05$, ## $p < 0.01$ and ### $p < 0.001$ versus model. GOS, galacto-oligosaccharides; FOS, fructo-oligosaccharides; COS, chitosan oligosaccharides; ALA, α-lipoic acid; RES, resveratrol; Arg, l-arginine; EPA, eicosapentaenoic acid. The original uncropped bands are included in the Supplementary Materials.

2.6. COS, RES and EPA Decrease the Heat/Hypoxia-Induced MDA Production in Caco-2/HT-29 Monolayers

HIF-1α, a critical regulator of the response to hypoxia, was determined via WB analysis. Two hours of heat and hypoxia exposure significantly increased the HIF-1α protein expression in the Caco-2/HT-29 monolayers (Supplementary Figure S3), indicating the occurrence of hypoxic stress. None of the components in this study affected heat/hypoxia-induced HIF-1α accumulation (Supplementary Figure S3).

The production of MDA, a biomarker for lipid peroxidation, was used to measure the cellular level of oxidative stress, as a result of hypoxia and subsequent reoxygenation, in the Caco-2/HT-29 co-culture model. The results showed that after 2 h of hypoxia and heat treatment, MDA production was significantly enhanced, indicating that lipid peroxidation occurred in Caco-2/HT-29 monolayers (Figure 6). Pre-incubation with COS (2.5 mg/mL, Figure 6A), RES (50 and 100 μM, Figure 6B), and EPA (50 μM, Figure 6C) for 48 h decreased the heat/hypoxia-induced MDA release compared to the model group. Contrary to the lower COS concentrations, supplementation of 10 mg/mL COS to the heat/hypoxia-exposed cells induced MDA production. The studied concentrations of GOS, FOS, ALA, and Arg did not show a significant effect on heat/hypoxia-induced MDA production (Figure 6A–C).

2.7. Arg Further Enhances the Heat/Hypoxia-Induced Increase in HSP-70 Protein Expression in Caco-2/HT-29 Monolayers

HSP-70 performs chaperone functions in protein folding and can protect cells from the adverse effects of (heat) stress. HSP-70 expression was determined by WB analysis. HSP-70 levels were significantly enhanced after 2 h of heat and hypoxia exposure compared to control Caco-2/HT-29 monolayers (Figure 7). High concentrations of Arg pre-treatment (1 and 2 mM) further increased HSP-70 expression (Figure 7C). The other nutritional components did not significantly alter the heat/hypoxia-induced increase in HSP-70 expression (Figure 7A–C).

The aforementioned effects of the nine nutritional components on preserving epithelial integrity, anti-lipid peroxidation, and regulating heat shock response are summarized in Table 1.

Table 1. The effects of nutritional components on heat/hypoxia-induced intestinal epithelial injury.

	GOS	FOS	COS	Glu	Arg	RES	ALA	DHA	EPA
Preserving epithelial integrity	+++	+++	++	-	+	+	+++	-	+++
Anti-lipid peroxidation	-	-	+	ND	-	+	-	ND	+
Regulating heat shock response	-	-	-	ND	+	-	-	ND	-

-, no significant effect was observed; ND, not determined. "Preserving epithelial integrity": +, significant effect was observed on TEER values; ++, significant effect was observed on TEER values and LY permeability; +++, significant effect was observed on TEER values, LY permeability, and TJ protein expression. "Anti-lipid peroxidation": +, MDA production was significantly decreased. "Regulating heat shock response": +, HSP-70 protein expression was significantly enhanced.

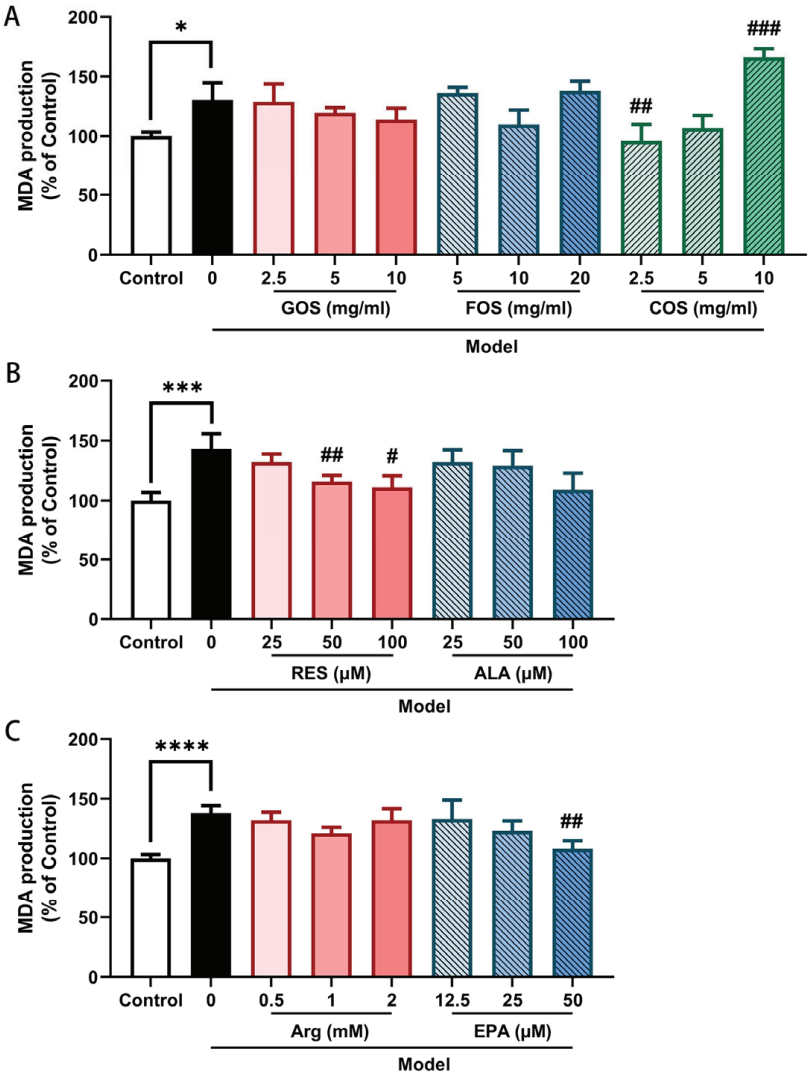

Figure 6. MDA production of Caco-2/HT-29 cell monolayers pre-incubated with GOS, FOS, COS (**A**), RES, ALA (**B**), Arg, and EPA (**C**) for 48 h then exposed to hypoxia and heat treatment (2 h). After hypoxia and heat treatment, MDA in the supernatant was determined by a thiobarbituric acid assay. All values were presented as means ± SEM (N = 3, n = 2 (GOS, FOS, COS group), and n = 3 (all other groups)). Statistical differences were analyzed by two-way ANOVA followed by the Bonferroni's multiple comparison test. * $p < 0.05$, *** $p < 0.001$, and **** $p < 0.0001$ versus control; # $p < 0.05$, ## $p < 0.01$, and ### $p < 0.001$ versus model. MDA, malondialdehyde; GOS, galacto-oligosaccharides; FOS, fructo-oligosaccharides; COS, chitosan oligosaccharides; ALA, α-lipoic acid; RES, resveratrol; Arg, l-arginine; EPA, eicosapentaenoic acid. The detailed raw OD data are listed in Table S4.

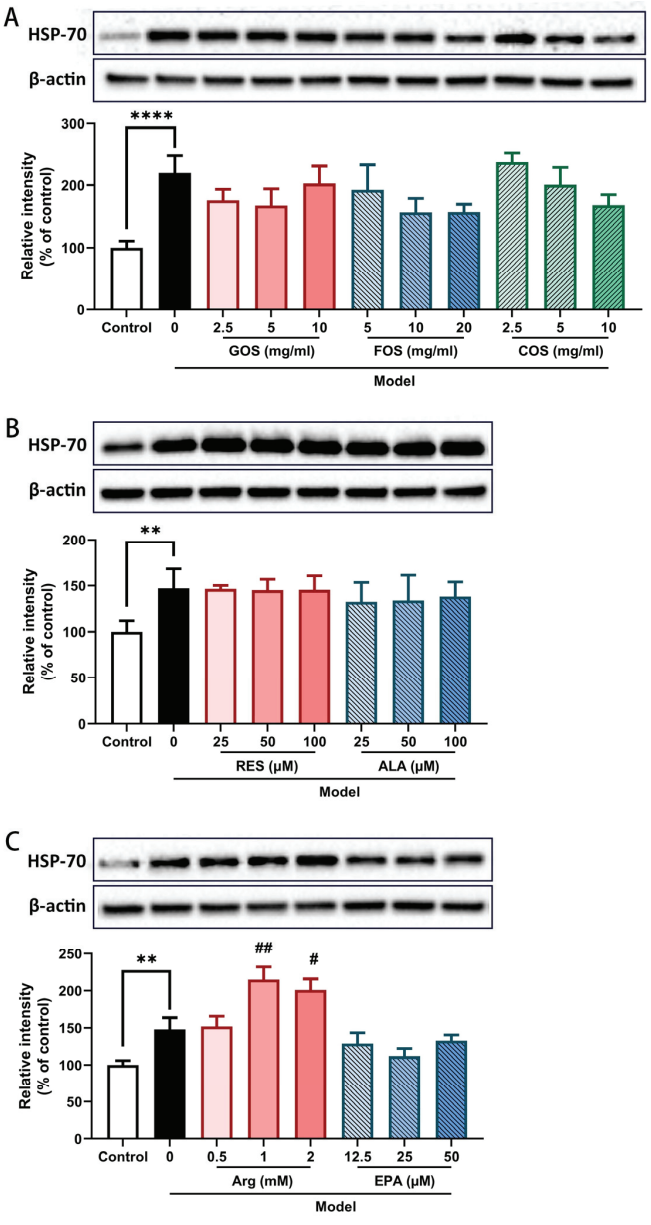

Figure 7. Relative HSP-70 protein expression levels in Caco-2/HT-29 cell monolayer pre-incubated with GOS, FOS, COS (**A**), RES, ALA (**B**), Arg, and EPA (**C**) for 48 h then exposed to hypoxia and heat treatment (2 h). HSP-70 protein expression was determined by WB and normalized to β-actin. All values were presented as means ± SEM (N = 3, n = 2 (GOS, FOS, COS group), and n = 3 (all other groups)). Statistical differences were analyzed by two-way ANOVA followed by the Bonferroni's multiple comparison test. ** $p < 0.01$ and **** $p < 0.0001$ versus control; # $p < 0.05$ and ## $p < 0.01$ versus model. GOS, galacto-oligosaccharides; FOS, fructo-oligosaccharides; COS, chitosan oligosaccharides; ALA, α-lipoic acid; RES, resveratrol; Arg, l-arginine; EPA, eicosapentaenoic acid. The original uncropped bands are included in the Supplementary Materials.

3. Discussion

In this study, an in vitro co-culture model comprising two human colonic cell lines, Caco-2 and HT-29, was used to investigate the effect of nine nutritional components on heat/hypoxia-induced intestinal epithelial injury by measuring intestinal barrier function, oxidative stress, and heat shock responses. We have reviewed potential promising nutritional intervention strategies and found evidence that non-digestible oligosaccharides GOS, FOS, and COS, antioxidants ALA and RES, amino acids Glu and Arg, and PUFAs DHA and EPA might be potential candidates to prevent HS/hypoxia-induced alterations in the integrity of the intestinal epithelial barrier and support intestinal homeostasis [3].

Our co-culture model consists of 10% HT-29 cells and 90% Caco-2 cells to simulate the environment of the human intestine. HT-29 cells are mucus-producing cells and represent the specialized secretory cells present in the intestinal epithelium, such as Goblet cells [14]. Goblet cells make up 10–20 percent of total intestinal cells in the epithelium and produce mucins to form a mucosal layer, which is an important physical and chemical barrier to preserve intestinal epithelial integrity [15]. The human intestinal absorptive enterocytes, the Caco-2 cells, form confluent monolayers consisting of well-polarized columnar cells representing a tight intestinal epithelial barrier [16]. Several previous studies have examined the optimal Caco-2:HT-29 ratio for in vitro studies mimicking the in vivo intestinal anatomy and physiology. The physiologically most relevant ratios are considered between 9:1 and 7:3 (Caco-2/HT-29), where TEER, indicative of the barrier properties of the monolayer, reached values quite similar to the human intestine [17–19]. Our previous study demonstrated that the addition of 25% HT-29 cells significantly reduced the TEER values of the Caco-2 monolayer and increased paracellular permeability, while 10% HT-29 cells had no effect on the epithelial integrity compared to only Caco-2 cells. The monolayer consisting of Caco-2/HT-29 in a 9:1 ratio expressed mucins, TJ/AJs and heat shock, and oxidative stress-related proteins and genes [5]. Therefore, this Caco-2/HT-29 co-culture model is a valid and versatile model for studying detrimental effects of heat and/or hypoxia on intestinal barrier function.

3.1. HSP-70, a Key Regulatory Protein in the HS Response Process Induced by Heat and Hypoxia

Generally, environmental heat or strenuous exercise results in vasodilation and blood re-distribution in the body, leading to hypoxia in different organs and tissues, including the intestinal epithelium [20]. Two hours of heat/hypoxia exposure resulted in a significantly increase in HSP-70 (Figure 5) and HIF-1α (Supplementary Figure S3) expression, indicating the occurrence of heat stress and hypoxia in this Caco-2/HT-29 co-culture model. The expression of HIF-1α, the key regulator of the cellular hypoxic response, can be upregulated by heat and is essential for heat acclimatisation [21]. HIF-1α mRNA levels significantly increased after 5 days of heat stress in the ilea of chickens [8]. On the other hand, hypoxia/reoxygenation increased superoxide generation, which induced cellular protein damage and protein HSP-70 production in Caco-2 cells [22]. Both protective proteins, HSP-70, and HIF-1α display a (synergistic) regulatory role in the heat shock and oxidative stress responses, which contribute to an increased resilience to these stressors [3].

In this study, none of the nine nutritional components affected heat/hypoxia-induced HIF-1α or HSP-70 protein expression, except Arg, which further enhanced the HSP-70 protein expression in heat/hypoxia-stimulated Caco-2/HT-29 cells (Figure 5C). HSP-70 is an important modulator of intestinal epithelial barrier function, performing chaperone functions and helping to protect cells from the adverse effects of physiological stresses [23]. Our previous study demonstrated that ALA stimulates intestinal epithelial recovery after heat stress by enhancing HSP-70 expression in Caco-2 cells [9]. Similarly, other studies proved that enhancement of HSP-70 or administration of exogenous HSP-70 significantly improved intestinal barrier integrity [24,25]. We show for the first time that the amino acid Arg contribute to the regulation of HSP-70 expression under hypoxia and hyperthermia conditions in the co-culture model, playing a potential modulatory role in the stress resilience pathways. HS-induced damage within the intestine is a complicated process

involving a benefit–damage balance and a complex modulatory network. Unfortunately, the upregulation of HSP-70 did not lead to improved intestinal epithelial integrity, which might be associated with the inhibition of Glu transport [26,27], as discussed in more detail below.

3.2. TEER Values and TJ Protein Expression, Indicators of Intestinal Epithelial Barrier Integrity

The hypoxia and heat-induced damage to the small intestinal epithelium is reflected by decreased TEER and increased paracellular permeability associated with decreased epithelial TJ protein expression. TJ proteins include claudins, occludins, and zonula occludens (ZO). Claudins and occludins interact with each other on their extracellular sides to promote junction assembly, while the ZO family provides intracellular structural support [28,29]. E-cadherin, the most essential cadherin present on the epithelial surface, is responsible for AJ formation by connecting to E-cadherin on the neighbouring cell [30]. Destruction and dissociation of epithelial TJ/AJ structures leads to increased leakage of luminal toxins or bacteria into blood circulation [31]. Therefore, attenuating or preventing the disruption of TJ/AJ protein breakdown in epithelial cells is critical for increasing cellular adaptation to hypoxia and heat. Our previous studies proved the beneficial effects of GOS, antioxidant ALA, and amino acid Arg in maintaining and supporting the intestinal homeostasis under heat stress conditions in Caco-2 cells [7,9,32].

Here, we observed that seven nutritional components (GOS, FOS, COS, RES, ALA, Arg, and EPA) prevented the heat/hypoxia-induced TEER decrease (Figure 2). After 48 h of pre-treatment, all these nutritional components (and DHA) already significantly increased the TEER values prior to hypoxia and heat exposure (Supplementary Figure S2). These results indicate that these nutritional components not only "treated" intestinal epithelial damage after heat/hypoxia exposure, but also exhibited a direct and preventive beneficial effect on barrier tightness prior to heat/hypoxia exposure.

In agreement with the TEER observations, GOS, FOS, COS, ALA, and EPA also attenuated the LY paracellular permeability (Figure 3). WB results showed that GOS, FOS, ALA, and EPA prevented the heat/hypoxia-induced decrease in claudin-3 and ZO-1 TJ protein expression in Caco-2/HT-29 cells (Figures 4 and 5).

Although the lack of in-depth mechanistic studies, there are some indications how non-digestible oligosaccharides, such as GOS, FOS, and COS, can reinforce intestinal epithelial integrity and TJ function. This reinforcing effect is mediated via direct interaction with epithelial cell receptors, such as Toll-like receptors, via stimulation of intracellular calcium signalling, via inhibition of pathogen-induced mitogen-activated protein kinase (MAPK) and downstream pro-inflammatory nuclear factor kappa B (NF-κB) hypersensitivity, or by promoting TJ re-assembly, for instance via 5′ adenosine monophosphate-activated protein kinase (AMPK) stimulation [33–37]. The antioxidant ALA preserves intestinal barrier integrity, in part, by regulating oxidative stress as oxidative stress is associated with a tyrosine-kinase-dependent dissociation of E-cadherin—β-catenin and occludin—ZO-1 complexes, which leads to barrier integrity loss [38]. The results related to members of the omega-3 fatty acid family, EPA, and DHA, are in agreement with two studies of Xiao et al., who showed that EPA is more potent than DHA in protecting against heat-induced permeability dysfunction and intestinal epithelial TJ damage in Caco-2 cells as well as in rats [39]. This protective effect of DHA might be related to inhibition of the necroptosis signalling pathway [40,41]. The improved intestinal barrier function induced by Arg observed in rats and IEC-6 cells during heat stress might be associated with AMPK signalling and promoting autophagy [42].

In addition to these direct barrier-protective mechanisms, suppressing local inflammatory responses might also play a role in ameliorating intestinal epithelial injury and enhancing intestinal barrier function as these nutritional components also demonstrate immune-regulatory and anti-inflammatory properties [3]. Further research is required to better understand the regulation of intestinal epithelial integrity by these nutritional components.

Surprisingly, the lower concentrations of GOS, COS, and Arg were more effective in preventing the heat/hypoxia-induced TEER decrease as compared to the higher concentrations. The decreased mitochondrial activity (Supplementary Figure S3) and the increased lipid peroxidation as measured by increased MDA levels in heat/hypoxia-stimulated cells incubated with the higher COS concentration (10 mg/mL) (Figure 6) might explain this lower efficacy of 10 mg/mL COS on intestinal epithelial barrier integrity.

The TEER values after GOS incubation were not in agreement with the LY flux data: the lowest GOS concentration restored the heat/hypoxia-decreased TEER values, while only the highest GOS concentration attenuated the paracellular LY permeability. Although these findings are difficult to interpret, TEER measurement is more sensitive as it captures changes in ionic permeability, implying that a small leakage is sufficient to alter TEER values [43]. In contrast, the LY flux is only affected when the intestinal epithelial damage is sufficient to cause leakage of this 0.4 kDa molecule.

Furthermore, our study showed that 1.4 mM to 2.4 mM Arg (including the 0.4 mM Arg already present in the medium) is not beneficial to heat/hypoxia-induced epithelial barrier dysfunction in intestinal epithelial cells in contrast to 0.9 mM Arg. Supra-physiological concentrations of Arg (>10 mM) are reported to be deleterious in the intestine [44,45]. In almost every cell type, Glu transport is partly inhibited by Arg [27]; therefore, it might be possible that the high Arg concentrations affect the basic Glu uptake from the culture medium. Glu is important for maintaining the intestinal mucosal barrier [46,47]. Moreover, the main glutamine transporter alanine-serine-cysteine transporter 2 (ASCT2) was significantly down-regulated in hypoxia-exposed Caco-2 cells [26], and deprivation of glutamine decreased expression of multiple TJ proteins, including ZO-1, in Caco-2 cells [48]. This can explain why no significant protective effect was observed in heat/hypoxia-stimulated Caco-2/HT-29 cells incubated with Glu in the current study (Supplementary Figure S2). This may also (partly) clarify why high concentrations of Arg induced HSP-70 protein expression under heat/hypoxia environment, but neither enhanced TEER values nor elevated tight junction protein expression. These findings point to an extreme narrow therapeutic window for these nutritional components, which should be further investigated and be taken into account in future in vivo or clinical studies.

3.3. Oxidative Stress, One of the Sources of Hypoxia and Heat Shock-Induced Tissue Injury

Under hypoxia/reoxygenation and hyperthermia conditions, the oxidative stress and heat shock responses induce excessive production of reactive oxygen species and reactive nitrogen species causing (intestinal) inflammation and tissue damage [49]. In this study, COS, RES, and EPA reversed the heat/hypoxia-induced increase in MDA, a product of lipid breakdown by oxidative stress, in Caco-2/HT-29 cells, demonstrating a promising role of these components in combating oxidative stress (Figure 4). COS, as non-digestible oligosaccharides, exert antioxidative properties, possibly via modulating the intestinal microbiota composition and subsequently the metabolism of short-chain fatty acids [3,50–52]. Here, we found that COS act directly as an antioxidant in this intestinal epithelial co-culture system without the presence of intestinal microbiota.

The polyphenolic compound RES, as an antioxidant, displays a strong antioxidant and anti-inflammatory capacity [53]. In addition, the PUFA EPA might also act as an antioxidant as EPA supplementation leads to a substantial antioxidant response, which might mainly occur via restoring imbalanced endogenous antioxidant moieties [54,55]. The role of oxidative stress in intestinal barrier dysfunction, e.g., following heat/hypoxia exposure, is well established [56] and therefore, restoring the imbalance of the antioxidative system by nutritional components might contribute to a stronger intestinal epithelial barrier, which can more easily deal with the adverse effects of heat/hypoxia.

3.4. Clinical Significance

One quarter to one half of elite athletes suffer from gastrointestinal symptoms, which may deter them from participating in training and competitive events. Strenuous exercise

and dehydrated states play an important role in the development of gastrointestinal symptoms referred by 70% of the athletes [57]. Recent research suggests that the gut microbiota may play a role in athlete health and performance [58]. Different studies reported increased intestinal permeability and/or endotoxemia during strenuous exercise and/or heat stress in humans [59–61].This is in agreement with the in vitro model described in this study showing heat/hypoxia-induced intestinal epithelial barrier disruption. Moreover, the heat/hypoxia-induced increase in HSP-70 protein expression in this Caco-2/HT-29 model is also in correspondence with several studies showing the upregulation of HSP-70 during different types of exercise in normal or increased temperatures, suggesting a role of HSP-70 in the cellular heat adaptation to heat acclimatization [62–65].

However, we need to be careful with the translation of this in vitro study using two intestinal epithelial cell lines to the more complex in vivo situation and ultimately to future clinic trials. The safety of the multiple nutritional components used in this study has been evaluated in different clinical trials [66–71], and these compounds are already available. A systematic review pointed out that in most of the studies probiotics, prebiotics and synbiotics induce positive health effects in athletes and active individuals, but these studies are currently limited in number and quality [72]. Our in vitro data suggest that a combination of non-digestible oligosaccharides (e.g., GOS, FOS), antioxidants (e.g., ALA, RES) and PUFAs (DHA) might be an interesting preventive (or therapeutic) approach to counteract heat/hypoxia-induced intestinal damage in humans. The clinical relevance of these nutritional components, the doses required, and the duration of treatment to exert potential influences on heat/hypoxia-induced intestinal damage remains to be elucidated.

4. Materials and Methods

4.1. Cell Culture

Caco-2 (HTB-37™, ATCC, Manassas, VA, USA) and HT-29 (HTB-38™, ATCC, Manassas, VA, USA) cells were separately grown in 75-cm^2 tissue culture flasks (#430641, Corning, Corning, NY, USA) at 37 °C, 5% CO_2, and 90% relative humidity environment. The cells were sub-cultured at ~90% confluence (~6 days) by 0.25% trypsin and 0.02% EDTA solution (#25200056, Thermo Fisher Scientific, Waltham, MA, USA). The DMEM culture medium (#42430025, Thermo Fisher Scientific), supplemented with 10% fetal calf serum (#10099, Thermo Fisher Scientific), 1 × non-essential amino acids (#11140035, Thermo Fisher Scientific), 2 mM L-glutamine (#25030081, Thermo Fisher Scientific), and 1% penicillin and streptomycin (#15140122, Thermo Fisher Scientific), was refreshed every 2 days [5].

4.2. Cell Co-Culture

Caco-2 and HT-29 cells were counted by an automated cell counter (Cellometer Auto T4, Nexcelom Bioscience, Lawrence, MA, USA), mixed in a ratio of 9:1 (Caco-2: HT-29) and seeded into the apical chambers of 24-well Transwell™ inserts (#353495, Corning, Corning, NY, USA) with a final density of 1×10^5 cells/cm^2 in each insert. Cells were cultured as described in Section 4.1 and allowed to grow for 17 days. The medium (300 µL in the apical chamber and 700 µL in the basolateral chamber) was refreshed every 2 days. Caco-2 and HT-29 co-cultures with TEER values > 300 Ω × cm^2 which reached a plateau (~17 days after seeding) were used for further experiments [5].

4.3. Pre-Treatment with the Nutritional Components

Chicory FOS (purity > 97%) were obtained from Orafti (Wijchen, The Netherlands). GOS (Vivinal® GOS Powder, purity > 70%) produced from lactose were provided by Friesland Campina (Amersfoort, The Netherlands). COS (purity > 90%) derived from marine biological sources, such as shrimp and crab shells, were purchased from BZ Oligo Biotech (Qingdao, China). FOS, GOS, and COS were dissolved in DMEM medium and sterilized by 0.2 µM pore filters (#431227, Corning, Corning, NY, USA) prior to each experiment. The acidic pH of the prepared COS solution was adjusted to 7.0 (pH neutral) with 1 M NaOH. DHA (#D2534, Sigma Aldrich, St. Louis, MO, USA), EPA (#E2011, Sigma

Aldrich), ALA (#T1395, Sigma Aldrich), and RES (#R5010, Sigma Aldrich, St. Louis, MO, USA) stock solutions (100 mM) were prepared with 100% ethanol. Arg (#A8094, Sigma Aldrich) and Glu (#G8540, Sigma Aldrich) stock solutions (400 mM) were prepared with PBS. The stock solutions were sterilised by 0.2 μM pore filters and kept in −20 °C (dark environment) and dissolved in the culture medium prior to each experiment.

4.4. Hypoxia and Heat Exposure

Hypoxia was induced by using a multi-functional incubator (Galaxy 48R, Eppendorf AG, Hamburg, Germany) for 2 h. The O_2 concentration in the chamber was maintained at 5%, with a residual gas mixture composed of 5% CO_2 and balanced N_2. For heat exposure, the environmental temperature was set at 42 °C. The relative humidity was kept at 90% as described before [5].

4.5. Cytotoxicity Assays

Possible cytotoxicity of the nutritional components on the co-cultured cells was evaluated with the 3-[4,5-dimethylthiazol-2-yl]-2,5-diphenyl-tetrazolium bromide (MTT) assay. At the end of nutritional component pre-treatment (48 h), the cells were refreshed with medium containing 0.1% (*w/v*) MTT (#M5655, Sigma-Aldrich, St. Louis, MO, USA) and incubated for an additional period of 4 h. The amount of violet formazan dye formed from MTT as a marker of changes in mitochondrial activity is proportional to the amount of viable cells. The supernatant was carefully removed, and 200 μL DMSO was added to the cells to terminate the MTT reaction and dissolve the formazan at the end of the 4 h incubation period. The absorbance (λ_{ab} 570 nm) of DMSO containing formazan was read using a microplate spectrophotometer. The group in which all cells were intentionally lysed by lysis buffer was included as a positive control.

Since hypoxia and heat treatment would interfere with mitochondrial function, cytotoxicity of the components after hypoxia and heat treatment was determined via the lactate dehydrogenase (LDH) production, indicating cytomembrane damage and intracellular contents release. After exposure to hypoxia and heat, the supernatants were collected and immediately assayed for cytotoxicity using CytoTox 96® Cytotoxicity Non-Radioactive Assay kit (Promega, Madison, WI, USA) according to manufacturer's instructions.

4.6. Trans-Epithelial Electrical Resistance (TEER) Measurement

The cell monolayer integrity was determined by TEER measurement using an epithelial volt-ohm meter (Millicell ERS-2, Merck, Rahway, MJ, USA). The electrodes were placed into two chambers of each Transwell™ insert. TEER values > 300 $\Omega \times cm^2$ were regarded as valid for further permeability studies.

4.7. Lucifer Yellow (LY) Permeability Test

The fluorescent chemical LY (0.44 kDa, L0144, Sigma-Aldrich) was used to measure the paracellular permeability across the co-culture monolayer. At the end of heat/hypoxia treatment, 30 μL LY (200 μg/mL) was added into the apical chamber of the Transwell™ inserts. The inserts were kept at 37 °C in the dark for 4 h, then the medium from the basolateral chamber was collected for fluorescent intensity measurements (λ_{ex} 428 nm, λ_{em} 540 nm) using a fluorometer (Fluoroskan Ascent® FL, Thermo Fisher Scientific). The fluorescent emission intensity was converted into fluorescein flux per hour by using a standard curve.

4.8. Lipid Peroxidation Assay

Lipid peroxidation was determined in the supernatant by the reaction of malondialdehyde (MDA) with thiobarbituric acid (TBA) following the instructions of the Lipid Peroxidation (MDA) Assay Kit (#MAK085, Sigma-Aldrich). The results were presented as MDA production, indicating oxidative attack and cytomembrane damage.

4.9. Protein Extraction

For total protein extraction, the cells were lysed using 50 µL Pierce™ RIPA buffer (#89901, Thermo Fisher Scientific) containing protease inhibitor cocktail (#11836170001, Roche, Basel, Switzerland). Total protein concentration was assessed and standardized with Pierce™ BCA Protein Assay Kit according to the manufacturer's instructions (Thermo Fisher Scientific). The protein samples used for determining hypoxia-inducible factor-1α (HIF-1α) expression were preincubated with dimethyloxalylglycine (DMOG; #D3695, Sigma-Aldrich), a HIF prolyl-hydroxylase inhibitor, which prevents HIF-1α degradation under normoxic conditions.

4.10. Western Blot (WB) Analysis

Equal amounts (20 µg) of boiled protein samples were separated by electrophoresis (Criterion™ Gel, 4–20% Tris-HCl, Bio-Rad, Hercules, CA, USA) and electrotransferred onto Trans-Blot® Turbo™ polyvinylidene difluoride (PVDF) membranes (midi format 0.2 µm, Bio-Rad, Hercules, CA, USA). After being blocked with 5% skimmed milk (in PBS containing 0.05% Tween-20 (PBST)), the membranes were incubated overnight at 4 °C with the primary antibodies of HSP-70 (1:1000, #C92F3A5, Enzo life science, Bruxelles , Belgium), HIF-1α (1:2000, #ab113642, Abcam, Cambridge, UK), claudin-3 (CLDN3) (1:1000, #341700, Invitrogen, Waltham, MA, USA), and ZO-1 (1:500, #339100, Invitrogen, Waltham, MA, USA). Housekeeping protein β-actin (1:2000, #13E5, Cell Signaling, Danvers, MA, USA) was also assessed in parallel with each target protein and used for normalization. Thereafter, the membranes were incubated with horseradish peroxidase (HRP)-conjugated secondary antibodies (1:10,000, Dako, Glostrup, Denmark) for 2 h at room temperature. After being rinsed with PBST and incubated with ECL detection reagent (#RPN2235, GE Healthcare, Chicago, IL, USA), the membranes were exposed to ECL imaging system (ChemiDoc MP, Bio-Rad, Hercules, CA, USA). The optical intensity of the blots was recorded and analyzed by using Image Lab (version 6.01, Bio-Rad, Hercules, CA, USA) and ImageJ (version 1.80, NIH, Bethesda, MD, USA) software. Membranes were stripped by using Restore PLUS Western Blot Stripping Buffer (#46430, Thermo Fisher Scientific) and re-blotted with the different primary antibodies.

4.11. Statistical Analysis

Results are expressed as means ± SEM of 3 independent experiments (N = 3), each performed in duplicate or triplicate unless otherwise stated. Statistical analyses were performed by using GraphPad Prism® (version 9.3.1, GraphPad, San Diego, CA, USA). Differences between groups were determined by using two-way analysis of variance (ANOVA), with Bonferroni post-hoc test. Results were considered statistically significant when $p < 0.05$.

5. Conclusions

In conclusion, the non-digestible oligosaccharides, especially GOS and FOS, the antioxidant ALA, and the PUFA EPA, exhibited the ability to protect Caco-2/HT29 cells from heat/hypoxia-induced intestinal injury, as these components preserved TEER values, inhibited paracellular LY permeability and increased tight junction protein expression. Amino acid Arg acts more like a "double-edged sword" as the beneficial effect of Arg on intestinal barrier function (TEER) was only confined close to its physiological level, while higher concentrations further enhanced the heat/hypoxia-induced increase in HSP-70 expression. Besides the barrier-protective properties of EPA and antioxidant RES under heat/hypoxia conditions, they also exhibited antioxidative activity. The amino acid Glu and the PUFA DHA were less effective in mitigating heat/hypoxia-induced intestinal injury in this specific Caco-2/HT-29 co-culture model. Combinations of non-digestible oligosaccharides (e.g., GOS, FOS), antioxidants (e.g., ALA, RES), and PUFAs (DHA) might be an interesting preventive (or therapeutic) approach to combat heat/hypoxia-induced intestinal injury and could be an important research area for future in vivo studies and clinical trials.

Supplementary Materials: The supporting information can be downloaded at: https://www.mdpi.com/article/10.3390/ijms24021111/s1.

Author Contributions: Conceptualization, S.B. and G.F.; methodology, S.B., G.F. and P.L.; formal analysis, P.L. writing—original draft preparation, P.L. and S.B.; writing—review and editing, S.B., G.F., H.J.W. and P.A.J.H.; supervision, S.B., G.F., H.J.W. and P.A.J.H. All the authors listed have made a significant contribution to writing the manuscript and approving it for publication. All authors have read and agreed to the published version of the manuscript.

Funding: This research was partly funded by China Scholarship Council (CSC), grant number 201706210064.

Institutional Review Board Statement: Not applicable.

Informed Consent Statement: Not applicable.

Data Availability Statement: The datasets used and/or analyzed during the current study are available from the corresponding author on reasonable request.

Acknowledgments: We wish to gratefully acknowledge the technical and intellectual support provided by Soheil Varasteh and Thirza van Deuren and Jan-Willem Versteeg at Utrecht Institute of Pharmaceutical Sciences (UIPS).

Conflicts of Interest: The authors declare no conflict of interest. The funders had no role in the design of the study; in the collection, analyses, or interpretation of data; in the writing of the manuscript; or in the decision to publish the results.

References

1. Costa, R.J.S.; Snipe, R.M.J.; Kitic, C.M.; Gibson, P.R. Systematic Review: Exercise-Induced Gastrointestinal Syndrome—Implications for Health and Intestinal Disease. *Aliment. Pharmacol. Ther.* **2017**, *46*, 246–265. [CrossRef] [PubMed]
2. Bilski, J.; Mazur-Bialy, A.; Brzozowski, B.; Magierowski, M.; Zahradnik-Bilska, J.; Wójcik, D.; Magierowska, K.; Kwiecien, S.; Mach, T.; Brzozowski, T. Can Exercise Affect the Course of Inflammatory Bowel Disease? Experimental and Clinical Evidence. *Pharmacol. Rep.* **2016**, *68*, 827–836. [CrossRef] [PubMed]
3. Lian, P.; Braber, S.; Garssen, J.; Wichers, H.J.; Folkerts, G.; Fink-Gremmels, J.; Varasteh, S. Beyond Heat Stress: Intestinal Integrity Disruption and Mechanism-Based Intervention Strategies. *Nutrients* **2020**, *12*, 734. [CrossRef]
4. Groschwitz, K.R.; Hogan, S.P. Intestinal Barrier Function: Molecular Regulation and Disease Pathogenesis. *J. Allergy Clin. Immunol.* **2009**, *124*, 3–20. [CrossRef]
5. Lian, P.; Braber, S.; Varasteh, S.; Wichers, H.J.; Folkerts, G. Hypoxia and Heat Stress Affect Epithelial Integrity in a Caco-2/HT-29 Co-Culture. *Sci. Rep.* **2021**, *11*, 13186. [CrossRef] [PubMed]
6. Dokladny, K.; Zuhl, M.N.; Moseley, P.L. Intestinal Epithelial Barrier Function and Tight Junction Proteins with Heat and Exercise. *J. Appl. Physiol.* **2016**, *120*, 692–701. [CrossRef]
7. Varasteh, S.; Braber, S.; Garssen, J.; Fink-Gremmels, J. Galacto-Oligosaccharides Exert a Protective Effect against Heat Stress in a Caco-2 Cell Model. *J. Funct. Foods* **2015**, *16*, 265–277. [CrossRef]
8. Varasteh, S.; Braber, S.; Akbari, P.; Garssen, J.; Fink-Gremmels, J. Differences in Susceptibility to Heat Stress along the Chicken Intestine and the Protective Effects of Galacto-Oligosaccharides. *PLoS ONE* **2015**, *10*, e0138975. [CrossRef]
9. Varasteh, S.; Fink-Gremmels, J.; Garssen, J.; Braber, S.; Nl, S.B. α-Lipoic Acid Prevents the Intestinal Epithelial Monolayer Damage under Heat Stress Conditions: Model Experiments in Caco-2 Cells. *Eur. J. Nutr.* **2018**, *57*, 1577–1589. [CrossRef]
10. Pires, W.; Veneroso, C.E.; Wanner, S.P.; Pacheco, D.A.S.; Vaz, G.C.; Amorim, F.T.; Tonoli, C.; Soares, D.D.; Coimbra, C.C. Association Between Exercise-Induced Hyperthermia and Intestinal Permeability: A Systematic Review. *Sport. Med.* **2017**, *47*, 1389–1403. [CrossRef]
11. Della Rocca, Y.; Fonticoli, L.; Rajan, T.S.; Trubiani, O.; Caputi, S.; Diomede, F.; Pizzicannella, J.; Marconi, G.D. Hypoxia: Molecular Pathophysiological Mechanisms in Human Diseases. *J. Physiol. Biochem.* **2022**, *78*, 739–752. [CrossRef] [PubMed]
12. Gagnon, M.; Zihler Berner, A.; Chervet, N.; Chassard, C.; Lacroix, C. Comparison of the Caco-2, HT-29 and the Mucus-Secreting HT29-MTX Intestinal Cell Models to Investigate Salmonella Adhesion and Invasion. *J. Microbiol. Methods* **2013**, *94*, 274–279. [CrossRef] [PubMed]
13. Huang, X.; Gao, Y.; Li, S.; Wu, C.; Wang, J.; Zheng, N. Modulation of Mucin (MUC2, MUC5AC and MUC5B) MRNA Expression and Protein Production and Secretion in Caco-2/HT29-MTX Co-Cultures Following Exposure to Individual and Combined Aflatoxin M1 and Ochratoxin A. *Toxins* **2019**, *11*, 132. [CrossRef]
14. Navabi, N.; McGuckin, M.A.; Lindén, S.K. Gastrointestinal Cell Lines Form Polarized Epithelia with an Adherent Mucus Layer When Cultured in Semi-Wet Interfaces with Mechanical Stimulation. *PLoS ONE* **2013**, *8*, e68761. [CrossRef] [PubMed]
15. Odenwald, M.A.; Turner, J.R. The Intestinal Epithelial Barrier: A Therapeutic Target? *Nat. Rev. Gastroenterol. Hepatol.* **2017**, *14*, 9–21. [CrossRef] [PubMed]

16. Meunier, V.; Bourrié, M.; Berger, Y.; Fabre, G. The Human Intestinal Epithelial Cell Line Caco-2; Pharmacological and Pharmacokinetic Applications. *Cell Biol. Toxicol.* **1995**, *11*, 187–194. [CrossRef] [PubMed]
17. Ferraretto, A.; Bottani, M.; de Luca, P.; Cornaghi, L.; Arnaboldi, F.; Maggioni, M.; Fiorilli, A.; Donetti, E. Morphofunctional Properties of a Differentiated Caco2/HT-29 Co-Culture as an In Vitro Model of Human Intestinal Epithelium. *Biosci. Rep.* **2018**, *38*, BSR20171497. [CrossRef]
18. Kleiveland, C.R.; Kleiveland, C.R. Co–Cultivation of Caco–2 and HT–29MTX. In *The Impact of Food Bioactives on Health: In Vitro and Ex Vivo Models*; Springer: Berlin/Heidelberg, Germany, 2015; pp. 135–140. [CrossRef]
19. Béduneau, A.; Tempesta, C.; Fimbel, S.; Pellequer, Y.; Jannin, V.; Demarne, F.; Lamprecht, A. A Tunable Caco-2/HT29-MTX Co-Culture Model Mimicking Variable Permeabilities of the Human Intestine Obtained by an Original Seeding Procedure. *Eur. J. Pharm. Biopharm.* **2014**, *87*, 290–298. [CrossRef]
20. Wu, D.; Cao, W.; Xiang, D.; Hu, Y.P.; Luo, B.; Chen, P. Exercise Induces Tissue Hypoxia and HIF-1α Redistribution in the Small Intestine. *J. Sport Health Sci.* **2020**, *9*, 82–89. [CrossRef]
21. Maloyan, A.; Eli-Berchoer, L.; Semenza, G.L.; Gerstenblith, G.; Stern, M.D.; Horowitz, M. HIF-1α-Targeted Pathways Are Activated by Heat Acclimation and Contribute to Acclimation-Ischemic Cross-Tolerance in the Heart. *Physiol. Genom.* **2005**, *23*, 79–88. [CrossRef]
22. Gebhardt, B.R.; Ries, J.; Caspary, W.F.; Boehles, H.; Stein, J. Superoxide: A Major Factor for Stress Protein Induction in Reoxygenation Injury in the Intestinal Cell Line Caco-2. *Digestion* **1999**, *60*, 238–245. [CrossRef] [PubMed]
23. Radons, J. The Human HSP70 Family of Chaperones: Where Do We Stand? *Cell Stress Chaperones* **2016**, *21*, 379. [CrossRef] [PubMed]
24. Akagi, R.; Ohno, M.; Matsubara, K.; Fujimoto, M.; Nakai, A.; Inouye, S. Glutamine Protects Intestinal Barrier Function of Colon Epithelial Cells from Ethanol by Modulating Hsp70 Expression. *Pharmacology* **2013**, *91*, 104–111. [CrossRef] [PubMed]
25. Yang, P.-C.; He, S.-H.; Zheng, P.-Y. Investigation into the Signal Transduction Pathway via Which Heat Stress Impairs Intestinal Epithelial Barrier Function. *J. Gastroenterol. Hepatol.* **2007**, *22*, 1823–1831. [CrossRef]
26. Huang, Q.; Li, N.; Zhu, W.; Li, Q.; Li, J. Glutamine Transporter ASCT2 Was Down-Regulated in Ischemic Injured Human Intestinal Epithelial Cells and Reversed by Epidermal Growth Factor. *J. Parenter. Enter. Nutr.* **2007**, *31*, 86–93. [CrossRef]
27. Heckel, T.; Bröer, A.; Wiesinger, H.; Lang, F.; Bröer, S. Asymmetry of Glutamine Transporters in Cultured Neural Cells. *Neurochem. Int.* **2003**, *43*, 289–298. [CrossRef] [PubMed]
28. Costantini, T.W.; Deree, J.; Loomis, W.; Putnam, J.G.; Choi, S.; Baird, A.; Eliceiri, B.P.; Bansal, V.; Coimbra, R. Phosphodiesterase Inhibition Attenuates Alterations to the Tight Junction Proteins Occludin and ZO-1 in Immunostimulated Caco-2 Intestinal Monolayers. *Life Sci.* **2009**, *84*, 18–22. [CrossRef]
29. Yonemura, S. Actin Filament Association at Adherens Junctions. *J. Med. Investig.* **2017**, *64*, 14–19. [CrossRef]
30. Brasch, J.; Harrison, O.J.; Honig, B.; Shapiro, L. Thinking Outside the Cell: How Cadherins Drive Adhesion. *Trends Cell Biol.* **2012**, *22*, 299–310. [CrossRef] [PubMed]
31. Chelakkot, C.; Ghim, J.; Ryu, S.H. Mechanisms Regulating Intestinal Barrier Integrity and Its Pathological Implications. *Exp. Mol. Med.* **2018**, *50*, 1–9. [CrossRef]
32. Varasteh, S.; Braber, S.; Kraneveld, A.D.; Garssen, J.; Fink-Gremmels, J. L-Arginine Supplementation Prevents Intestinal Epithelial Barrier Breakdown under Heat Stress Conditions by Promoting Nitric Oxide Synthesis. *Nutr. Res.* **2018**, *57*, 45–55. [CrossRef] [PubMed]
33. Cario, E.; Gerken, G.; Podolsky, D.K. Toll-like Receptor 2 Controls Mucosal Inflammation by Regulating Epithelial Barrier Function. *Gastroenterology* **2007**, *132*, 1359–1374. [CrossRef]
34. Vogt, L.; Ramasamy, U.; Meyer, D.; Pullens, G.; Venema, K.; Faas, M.M.; Schols, H.A.; de Vos, P. Immune Modulation by Different Types of B2→1-Fructans Is Toll-Like Receptor Dependent. *PLoS ONE* **2013**, *8*, e68367. [CrossRef]
35. Suzuki, T.; Hara, H. Various Nondigestible Saccharides Open a Paracellular Calcium Transport Pathway with the Induction of Intracellular Calcium Signaling in Human Intestinal Caco-2 Cells. *J. Nutr.* **2004**, *134*, 1935–1941. [CrossRef]
36. Wongkrasant, P.; Pongkorpsakol, P.; Ariyadamrongkwan, J.; Meesomboon, R.; Satitsri, S.; Pichyangkura, R.; Barrett, K.E.; Muanprasat, C. A Prebiotic Fructo-Oligosaccharide Promotes Tight Junction Assembly in Intestinal Epithelial Cells via an AMPK-Dependent Pathway. *Biomed. Pharmacother.* **2020**, *129*, 110415. [CrossRef]
37. Wu, R.Y.; Määttänen, P.; Napper, S.; Scruten, E.; Li, B.; Koike, Y.; Johnson-Henry, K.C.; Pierro, A.; Rossi, L.; Botts, S.R.; et al. Non-Digestible Oligosaccharides Directly Regulate Host Kinome to Modulate Host Inflammatory Responses without Alterations in the Gut Microbiota. *Microbiome* **2017**, *5*, 135. [CrossRef]
38. Rao, R.K.; Basuroy, S.; Rao, V.U.; Karnaky, K.J., Jr.; Gupta, A. Tyrosine Phosphorylation and Dissociation of Occludin-ZO-1 and E-Cadherin-β-Catenin Complexes from the Cytoskeleton by Oxidative Stress. *Biochem. J.* **2002**, *368*, 471–481. [CrossRef] [PubMed]
39. Xiao, G.; Tang, L.; Yuan, F.; Zhu, W.; Zhang, S.; Liu, Z.; Geng, Y.; Qiu, X.; Zhang, Y.; Su, L. Eicosapentaenoic Acid Enhances Heat Stress-Impaired Intestinal Epithelial Barrier Function in Caco-2 Cells. *PLoS ONE* **2013**, *8*, e73571. [CrossRef] [PubMed]
40. Xiao, K.; Liu, C.; Qin, Q.; Zhang, Y.; Wang, X.; Zhang, J.; Odle, J.; Lin, X.; Hu, C.A.A.; Liu, Y. EPA and DHA Attenuate Deoxynivalenol-Induced Intestinal Porcine Epithelial Cell Injury and Protect Barrier Function Integrity by Inhibiting Necroptosis Signaling Pathway. *FASEB J.* **2020**, *34*, 2483–2496. [CrossRef]
41. Huang, L.; Yin, P.; Liu, F.; Liu, Y.; Liu, Y.; Xia, Z. Protective Effects of L-Arginine on the Intestinal Epithelial Barrier under Heat Stress Conditions in Rats and IEC-6 Cell Line. *J. Anim. Physiol. Anim. Nutr.* **2020**, *104*, 385–396. [CrossRef] [PubMed]

42. Xia, Z.; Huang, L.; Yin, P.; Liu, F.; Liu, Y.; Zhang, Z.; Lin, J.; Zou, W.; Li, C. L-Arginine Alleviates Heat Stress-Induced Intestinal Epithelial Barrier Damage by Promoting Expression of Tight Junction Proteins via the AMPK Pathway. *Mol. Biol. Rep.* **2019**, *46*, 6435–6451. [CrossRef]
43. Srinivasan, B.; Kolli, A.R.; Esch, M.B.; Abaci, H.E.; Shuler, M.L.; Hickman, J.J. TEER Measurement Techniques for in Vitro Barrier Model Systems. *J. Lab. Autom.* **2015**, *20*, 107–126. [CrossRef]
44. Rhoads, J.M.; Chen, W.; Gookin, J.; Wu, G.Y.; Fu, Q.; Bliklslager, T.; Rippe, R.A.; Argenzio, R.A.; Cance, W.G.; Weaver, E.M.; et al. Arginine Stimulates Intestinal Cell Migration through a Focal Adhesion Kinase Dependent Mechanism. *Gut* **2004**, *53*, 514–522. [CrossRef]
45. Sharma, J.N.; Al-Omran, A.; Parvathy, S.S. Role of Nitric Oxide in Inflammatory Diseases. *Inflammopharmacology* **2007**, *15*, 252–259. [CrossRef] [PubMed]
46. Wu, G. Functional Amino Acids in Growth, Reproduction, and Health. *Adv. Nutr.* **2010**, *1*, 31–37. [CrossRef]
47. Windmueller, H.G.; Spaeth, A.E. Identification of Ketone Bodies and Glutamine as the Major Respiratory Fuels in Vivo for Postabsorptive Rat Small Intestine. *J. Biol. Chem.* **1978**, *253*, 69–76. [CrossRef] [PubMed]
48. Li, N.; Lewis, P.; Samuelson, D.; Liboni, K.; Neu, J. Glutamine Regulates Caco-2 Cell Tight Junction Proteins. *Am. J. Physiol. Liver Physiol.* **2004**, *287*, 726–733. [CrossRef]
49. Slimen, I.B.; Najar, T.; Ghram, A.; Dabbebi, H.; ben Mrad, M.; Abdrabbah, M. Reactive Oxygen Species, Heat Stress and Oxidative-Induced Mitochondrial Damage. A Review. *Int. J. Hyperth.* **2014**, *30*, 513–523. [CrossRef] [PubMed]
50. Guan, Z.; Feng, Q. Chitosan and Chitooligosaccharide: The Promising Non-Plant-Derived Prebiotics with Multiple Biological Activities. *Int. J. Mol. Sci.* **2022**, *23*, 6761. [CrossRef]
51. Abd El-Hack, M.E.; El-Saadony, M.T.; Shafi, M.E.; Zabermawi, N.M.; Arif, M.; Batiha, G.E.; Khafaga, A.F.; Abd El-Hakim, Y.M.; Al-Sagheer, A.A. Antimicrobial and Antioxidant Properties of Chitosan and Its Derivatives and Their Applications: A Review. *Int. J. Biol. Macromol.* **2020**, *164*, 2726–2744. [CrossRef] [PubMed]
52. Mei, Q.-X.; Hu, J.-H.; Huang, Z.-H.; Fan, J.-J.; Huang, C.-L.; Lu, Y.-Y.; Wang, X.-P.; Zeng, Y. Pretreatment with Chitosan Oligosaccharides Attenuate Experimental Severe Acute Pancreatitis via Inhibiting Oxidative Stress and Modulating Intestinal Homeostasis. *Acta Pharm. Sin.* **2021**, *42*, 942–953. [CrossRef]
53. Salehi, B.; Mishra, A.P.; Nigam, M.; Sener, B.; Kilic, M.; Sharifi-Rad, M.; Fokou, P.V.T.; Martins, N.; Sharifi-Rad, J. Resveratrol: A Double-Edged Sword in Health Benefits. *Biomedicines* **2018**, *6*, 91. [CrossRef] [PubMed]
54. Oppedisano, F.; Macrì, R.; Gliozzi, M.; Musolino, V.; Carresi, C.; Maiuolo, J.; Bosco, F.; Nucera, S.; Zito, M.C.; Guarnieri, L.; et al. The Anti-Inflammatory and Antioxidant Properties of n-3 PUFAs: Their Role in Cardiovascular Protection. *Biomedicines* **2020**, *8*, 306. [CrossRef] [PubMed]
55. Mollace, V.; Gliozzi, M.; Carresi, C.; Musolino, V.; Oppedisano, F. Re-Assessing the Mechanism of Action of n-3 PUFAs. *Int. J. Cardiol.* **2013**, *170*, S8. [CrossRef] [PubMed]
56. Wang, Y.; Chen, Y.; Zhang, X.; Lu, Y.; Chen, H. New Insights in Intestinal Oxidative Stress Damage and the Health Intervention Effects of Nutrients: A Review. *J. Funct. Foods* **2020**, *75*, 104248. [CrossRef]
57. de Oliveira, E.P.; Burini, R.C. The Impact of Physical Exercise on the Gastrointestinal Tract. *Curr. Opin. Clin. Nutr. Metab. Care* **2009**, *12*, 533–538. [CrossRef]
58. Hughes, R.L.; Holscher, H.D. Fueling Gut Microbes: A Review of the Interaction between Diet, Exercise, and the Gut Microbiota in Athletes. *Adv. Nutr.* **2021**, *12*, 2190–2215. [CrossRef]
59. Lambert, G.P. Intestinal Barrier Dysfunction, Endotoxemia, and Gastrointestinal Symptoms: The 'Canary in the Coal Mine' during Exercise-Heat Stress? *Med. Sport Sci.* **2008**, *53*, 61–73. [CrossRef]
60. Ribeiro, F.M.; Petriz, B.; Marques, G.; Kamilla, L.H.; Franco, O.L. Is There an Exercise-Intensity Threshold Capable of Avoiding the Leaky Gut? *Front. Nutr.* **2021**, *8*, 627289. [CrossRef]
61. Chantler, S.; Griffiths, A.; Matu, J.; Davison, G.; Jones, B.; Deighton, K. The Effects of Exercise on Indirect Markers of Gut Damage and Permeability: A Systematic Review and Meta-Analysis. *Sport. Med.* **2021**, *51*, 113–124. [CrossRef]
62. Gavrilov, V.; Borisova, N.; Anurov, V.; Chun-pu Chu, E. Pre-and Post-Exercise Blood Contents of HPS70 in Athletes Involved in Different Sports. *J. Phys. Educ. Sport (JPES)* **2022**, *22*, 2098–2105. [CrossRef]
63. Banfi, G.; Dolci, A.; Verna, R.; Corsi, M.M. Exercise Raises Serum Heat-Shock Protein 70 (Hsp70) Levels. *Clin. Chem. Lab. Med.* **2004**, *42*, 1445–1446. [CrossRef] [PubMed]
64. Alizadeh, A.M.; Isanejad, A.; Sadighi, S.; Mardani, M.; Kalaghchi, B.; Hassan, Z.M. High-Intensity Interval Training Can Modulate the Systemic Inflammation and HSP70 in the Breast Cancer: A Randomized Control Trial. *J. Cancer Res. Clin. Oncol.* **2019**, *145*, 2583–2593. [CrossRef] [PubMed]
65. Milne, K.J.; Noble, E.G. Exercise-Induced Elevation of HSP70 Is Intensity Dependent. *J. Appl. Physiol.* **2002**, *93*, 561–568. [CrossRef]
66. Meli, F.; Puccio, G.; Cajozzo, C.; Ricottone, G.L.; Pecquet, S.; Sprenger, N.; Steenhout, P. Growth and Safety Evaluation of Infant Formulae Containing Oligosaccharides Derived from Bovine Milk: A Randomized, Double-Blind, Noninferiority Trial. *BMC Pediatr.* **2014**, *14*, 306. [CrossRef]
67. Naveed, M.; Phil, L.; Sohail, M.; Hasnat, M.; Baig, M.M.F.A.; Ihsan, A.U.; Shumzaid, M.; Kakar, M.U.; Mehmood Khan, T.; Akabar, M.D.; et al. Chitosan Oligosaccharide (COS): An Overview. *Int. J. Biol. Macromol.* **2019**, *129*, 827–843. [CrossRef]

68. Fogacci, F.; Rizzo, M.; Krogager, C.; Kennedy, C.; Georges, C.M.G.; Knežević, T.; Liberopoulos, E.; Vallée, A.; Pérez-martínez, P.; Wenstedt, E.F.E.; et al. Safety Evaluation of α-Lipoic Acid Supplementation: A Systematic Review and Meta-Analysis of Randomized Placebo-Controlled Clinical Studies. *Antioxidants* **2020**, *9*, 1011. [CrossRef]
69. Singh, A.P.; Singh, R.; Verma, S.S.; Rai, V.; Kaschula, C.H.; Maiti, P.; Gupta, S.C. Health Benefits of Resveratrol: Evidence from Clinical Studies. *Med. Res. Rev.* **2019**, *39*, 1851–1891. [CrossRef]
70. Wichmann, M.W.; Thul, P.; Czarnetzki, H.D.; Morlion, B.J.; Kemen, M.; Jauch, K.W. Evaluation of Clinical Safety and Beneficial Effects of a Fish Oil Containing Lipid Emulsion (Lipoplus, MLF541): Data from a Prospective, Randomized, Multicenter Trial. *Crit. Care Med.* **2007**, *35*, 700–706. [CrossRef]
71. McNeal, C.J.; Meininger, C.J.; Wilborn, C.D.; Tekwe, C.D.; Wu, G. Safety of Dietary Supplementation with Arginine in Adult Humans. *Amino Acids* **2018**, *50*, 1215–1229. [CrossRef]
72. Calero, C.D.Q.; Rincón, E.O.; Marqueta, P.M. Probiotics, Prebiotics and Synbiotics: Useful for Athletes and Active Individuals? A Systematic Review. *Benef. Microbes* **2020**, *11*, 135–149. [CrossRef] [PubMed]

International Journal of
Molecular Sciences

MDPI

Article

A Mixture of Dietary Plant Sterols at Nutritional Relevant Serum Concentration Inhibits Extrinsic Pathway of Eryptosis Induced by Cigarette Smoke Extract

Ignazio Restivo [1], Alessandro Attanzio [1,*], Luisa Tesoriere [1], Mario Allegra [1], Guadalupe Garcia-Llatas [2] and Antonio Cilla [2]

[1] Department of Biological, Chemical and Pharmaceutical Sciences and Technologies, University of Palermo, Via Archirafi 28, 90123 Palermo, Italy
[2] Nutrition and Food Science Area, Faculty of Pharmacy, University of Valencia, Avda. Vicente Andrés Estellés s/n, 46100 Burjassot, Spain
* Correspondence: alessandro.attanzio@unipa.it; Tel.: +39-091-2386-2434

Abstract: Cell death program of red blood cells (RBCs), called eryptosis, is characterized by activation of caspases and scrambling of membrane phospholipids with externalization of phosphatidylserine (PS). Excessive eryptosis confers a procoagulant phenotype and is implicated in impairment of microcirculation and increased prothrombotic risk. It has recently been reported that cigarette smokers have high levels of circulating eryptotic erythrocytes, and a possible contribution of eryptosis to the vaso-occlusive complications associated to cigarette smoke has been postulated. In this study, we demonstrate how a mixture of plant sterols (MPtS) consisting of β-sitosterol, campesterol and stigmasterol, at serum concentration reached after ingestion of a drink enriched with plant sterols, inhibits eryptosis induced by cigarette smoke extract (CSE). Isolated RBCs were exposed for 4 h to CSE (10–20% v/v). When RBCs were co-treated with CSE in the presence of 22 μM MPtS, a significant reduction of the measured hallmarks of apoptotic death like assembly of the death-inducing signaling complex (DISC), PS outsourced, ceramide production, cleaved forms of caspase 8/caspase 3, and phosphorylated p38 MAPK, was evident. The new beneficial properties of plant sterols on CSE-induced eryptosis presented in this work open new perspectives to prevent the negative physio-pathological events caused by the eryptotic red blood cells circulating in smokers.

Keywords: cigarette smoke; plant sterols; eryptosis; DISC; caspases; p38 MAPK

Citation: Restivo, I.; Attanzio, A.; Tesoriere, L.; Allegra, M.; Garcia-Llatas, G.; Cilla, A. A Mixture of Dietary Plant Sterols at Nutritional Relevant Serum Concentration Inhibits Extrinsic Pathway of Eryptosis Induced by Cigarette Smoke Extract. *Int. J. Mol. Sci.* **2023**, *24*, 1264. https://doi.org/10.3390/ijms24021264

Academic Editor: Maurizio Battino

Received: 16 December 2022
Revised: 5 January 2023
Accepted: 6 January 2023
Published: 9 January 2023

1. Introduction

"Tobacco is one of the greatest emerging health disasters in the history of humanity". That is the sentence of Dr. Gro Brandtland, then Director General of the World Health Organization (WHO), in 1998. In 2019, WHO sources say that up to half of tobacco consumers, in all its forms, face death, and that every year, due to the direct use of tobacco or passive smoking, there are about 8 million deaths. Although tobacco continues to be a dramatic factor in the development of cardiovascular diseases and dysfunctions, which are the greatest cause of death in humans, in about twenty years, global tobacco consumption has fallen by only 4.3% (1397 billion consumers to 1337) [1].

A number of studies correlate cigarette smoke (CS) with dysfunction of endothelial cells [2], leukocytes [3], and platelet activation [4], as well as increased circulation of eryptotic RBCs [5] leading to damage of the cardiovascular system. Endothelial dysfunction is one of the main early pathophysiological biomarkers of smokers [6], and relatively recent studies show that excessive and dysfunctional eryptosis, or programmed death of red blood cells (RBCs), is associated with vase-occlusive events and physio-pathogenesis of the cardiovascular system such as atherosclerosis [7] and atherothrombosis [8,9], as well as being involved in chronic kidney disease [10] and metabolic syndrome [11]. Eryptosis is one

of the main ways of death of RBCs, and is characterized by loss of membrane asymmetry following scrambling of phospholipids with externalization of phosphatidylserine (PS), membrane shrinkage, membrane blebbing, and activation of proteases involved in cell death such as caspase 8 and caspase 3 (Figure 1) [12].

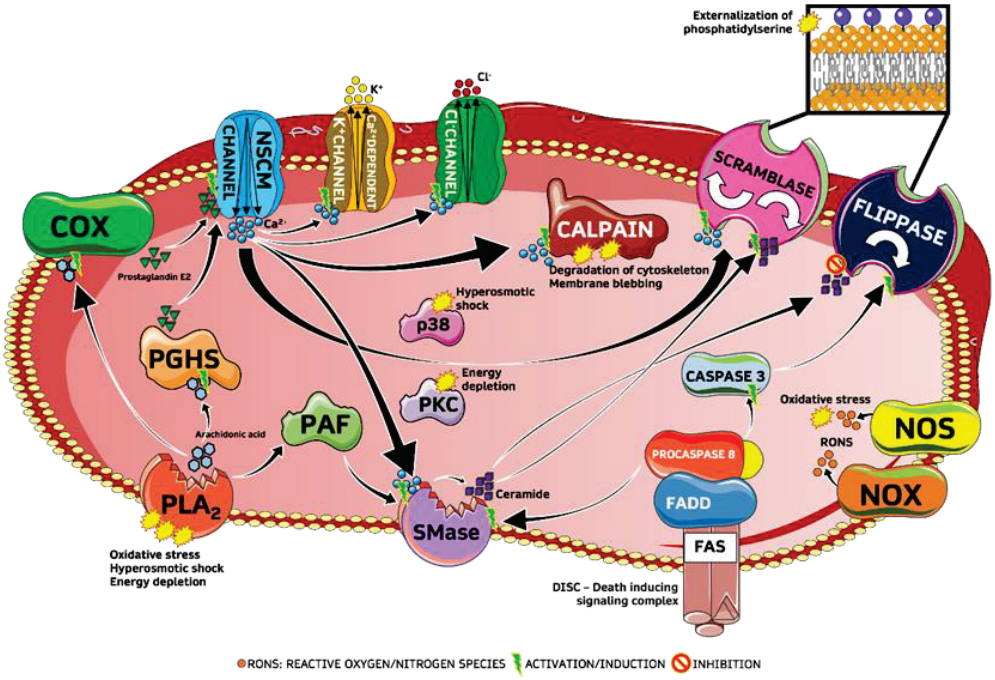

Figure 1. Synthetic scheme of eryptotic machinery. Sphingomyelinase (SMase), platelet-activating factor (PAF), phospholipase A_2 (PLA_2), prostaglandin endoperoxide synthase (PGHS), cyclooxygenase (COX), calcium sensitive non-selective (NSCM), protein kinase C (PKC), FAS-associated via death-domain (FADD), nitric oxide synthase (NOS), NADPH oxidase (NOX).

In a previous study of our research groups, we have shown that smokers have a higher level of circulating eryptotic erythrocytes associated with inflammatory status (high C-reactive protein levels) and RBCs' oxidative stress (low glutathione levels), suggesting a further relationship between cigarette smoke and vascular damage [5]. In this regard, we recently investigated, in isolated human RBCs, the molecular mechanism of the eryptosis induced by cigarette smoke extract (CSE). The study showed that CSE induces extrinsic eryptosis where assembly of the death-inducing signaling complex (DISC) is started by activating p38 MAPK, and followed by overproduction of ceramide and activation of caspase 8 and caspase 3. In vitro results were reinforced by ex vivo data where RBCs from smokers report higher levels of caspase 8 and FADD in the DISC, as well as increased phosphorylation of p38 MAPK than non-smokers [13].

According to the statistical office of the European Union (EUROSTAT), cardiovascular disease continues to be the main cause of death for humans [14], and it is a main objective of WHO to reduce deaths from these diseases [1]. Therefore, it is very important to implement prevention and try to inhibit all possible causes of cardiovascular disease, including eryptosis. Although efforts have been made to reduce the number of global smokers in order to reduce care costs and mortality, in recent years, the number of smokers has fallen by a few million. It is therefore very important and cost-effective to use nutrition to help reduce the onset of diseases, but above all, as a preventive tool.

Plant sterols (PtS) are important phytochemicals found in plant foods, and the most common present in foods are sitosterol, campesterol, and stigmasterol, which account for about 50–65%, 10–40%, and 0–35% of the total PtS fraction. PtS are well known for their positive health activities, so their beneficial role has been increasingly consolidated over the years [15,16]. PtS, naturally occurring mainly in vegetable oils, margarines, and nuts, are steroids associated with health benefits such as cholesterol-lowering, anti-inflammatory, and anti-proliferative effects [17]. PtS are normally absorbed with low efficiency, and different PtS-enriched foods are now commercialized to obtain the recommended daily quantity for healthy purposes. Previous study showed that four months of consumption of milk-based fruit beverage enriched with 1.5 g of mixture of plant sterols (MPtS) consisting of β-sitosterol, campesterol, and stigmasterol (Figure 2), resulted in an increase in serum concentration of plant sterols up to 22 μM [18]. At nutritional relevant serum concentration, MPtS was shown to prevent pro-eryptotic and hemolytic effects evoked by oxidative stress induced by tert-butyl hydroperoxide (tBOOH) in isolated human RBCs [19].

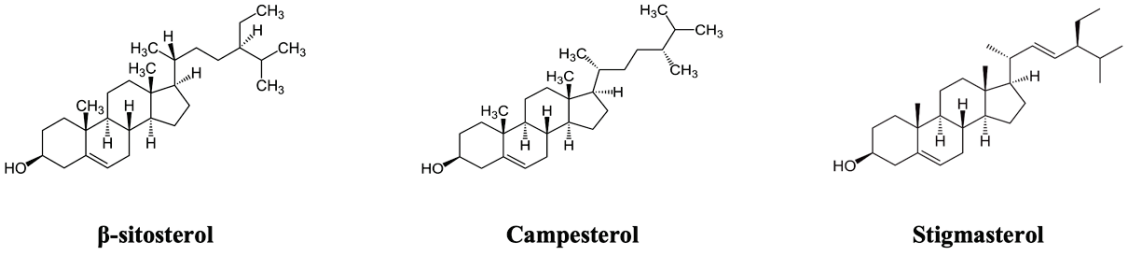

Figure 2. Structure of main dietary plant sterols.

The aim of this work is investigating, for the first time, the potential protective effect of MPtS, at serum concentration reached after the consumption of PtS-enriched milk-based fruit beverage, against eryptosis induced by CSE.

2. Results

2.1. MPtS Decreases PS Exposure and Ceramide Production in CSE-Induced Eryptosis

Since CSE-induced extrinsic eryptosis involves DISC in the first hours of treatment [10], 0.4% hematocrit of isolated RBCs were treated for 4 h with 10% CSE and 20% CSE (*v*/*v*), with the absence of treatment or after combination with 22 μM MPtS. Parameters characterizing eryptosis such as membrane scrambling with PS exposure, ceramide production, and cell volume variation measured by forward scatter (FS), were evaluated by flow cytometry. Co-treatment of erythrocytes with 22 μM MPtS, decreased ($p < 0.001$) the CSE-induced increase of annexin V-binding fluorescent cells with 20% CSE treatment (5.9% vs. 11%) and 10% CSE treatment (5.8% vs. 8.8%), reporting values on control levels (Figure 3A). Treatment of RBCs with only MPtS did not show any increase of PS exposure (4.7% vs. 4.6%). Likewise, ceramide formation was significantly ($p < 0.001$) inhibited by MPtS, as shown by the decrease of cells binding anti-ceramide labeled with fluorescein-5-isothiocyanate (FITC) probe with 20% CSE treatment (4.4% vs. 13.5%) and 10% CSE treatment (4.4% vs. 9.2%) (Figure 3B). In addition, FS measurements failed to pick a variation of cell volume with any treatment (Figure S1C in the Supplementary Materials).

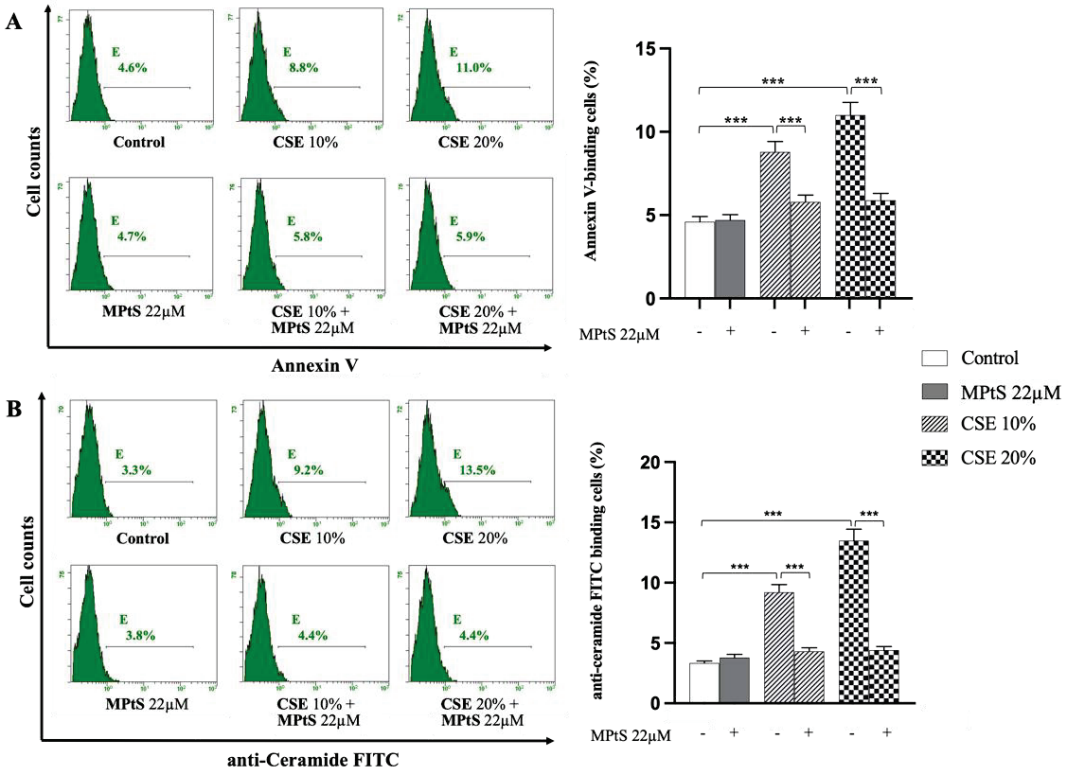

Figure 3. Mixture of plant sterols (MPtS) inhibits cigarette smoke extract (CSE)-induced eryptosis with decrease of PS exposure and ceramide production. (**A**) Percentage of PS-exposing erythrocytes and (**B**) ceramide formation in 10% or 20% CSE-treated RBCs incubated for 4 h in the absence or in co-treatment with 22 μM MPtS measured by flow cytometry. RBCs incubated with Ringer solution were used as control. Protocol of measurement at Section 4.4. Values are means ± SD of (n = 6) experiments carried out in triplicate. *** $p < 0.001$ (ANOVA associated with Tukey's test).

2.2. MPtS Inhibits CSE-Induced Extrinsic Eryptosis

To assess whether MPtS inhibited CSE-induced extrinsic eryptosis, co-immunoprecipitation experiments of RBCs treated with either 10% or 20% CSE in the absence or in the presence of 22 μM MPtS, were performed to assess formation of DISC in the membrane. After 4 h of treatment or co-treatment, the RBCs' lysates were immunoprecipitated with anti-FAS antibodies, followed by Western blotting with anti-FAS-associated via death-domain (FADD) or anti-caspase 8. Both caspase 8 and FADD were found in the immunoprecipitates of RBCs treated with CSE, in a concentration-dependent manner (Figure 4). Co-treatment with MPtS, on the other hand, showed an evident decrease almost to reach control levels ($p < 0.001$) in the amounts of both proteins analyzed with all the conditions of treatment (Figure 4B,C). The RBCs treated only with MPtS did not show any significant changes in the proteins' asset.

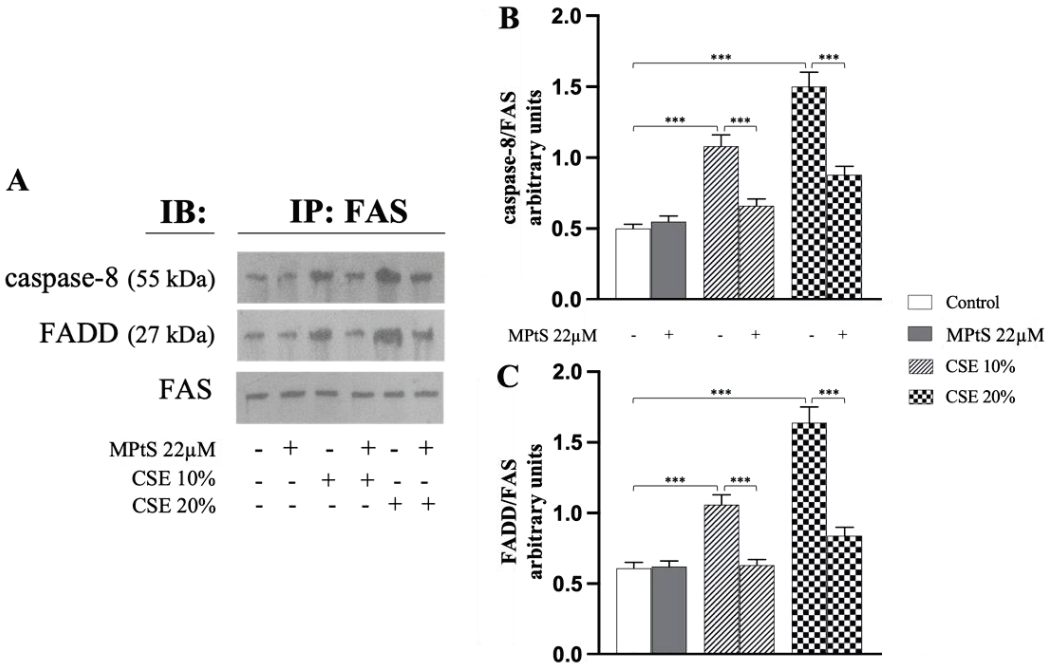

Figure 4. Mixture of plant sterols (MPtS) inhibits cigarette smoke extract (CSE)-induced extrinsic eryptosis. (**A**) Representative images of immunoblotting analysis of caspase 8 and FAS-associated via death-domain (FADD) after immunoprecipitation with anti-FAS antibody in 10% or 20% CSE-treated RBCs incubated for 4 h in absence or in co-treatment with 22 μM MPtS. Protocol of analysis at Sections 4.6 and 4.7. (**B**,**C**) densitometric analysis of caspase 8 and FADD levels normalized for FAS. Values are the means of bands' densitometry of three separate experiments with comparable results carried out on the same blood sample. *** $p < 0.001$ (ANOVA associated with Tukey's test).

2.3. MPtS Inhibits Caspase 8/Caspase 3 Cleavage and Phosphorylation of p38 MAPK in CSE-Induced Extrinsic Eryptosis

After treating the RBCs for 4 h, the cell lysates were immunoblotted with anti-caspase 8 or anti-caspase 3. When the RBCs were co-incubated with 22 μM MPtS, there was a significant reduction ($p < 0.001$) in the level of the active fragments of both caspase 8 and caspase 3 (Figure 5C,D), compared to cells treated only with CSE which showed a much higher level of the cleaved forms. Activation and signaling of the p38 MAP kinase pathway also appears to be involved in several eryptotic pathways and is characterized by the phosphorylation of the enzyme. Co-treatment at 4 h with MPtS showed an evident reduction ($p < 0.001$) in the phosphorylation of p38 MAPK, both with 10% CSE and 20% CSE treatment, compared to RBC only treated with CSE at both the concentrations (Figure 5B). RBCs treated only with MPtS did not report significant changes in the proteins analyzed above.

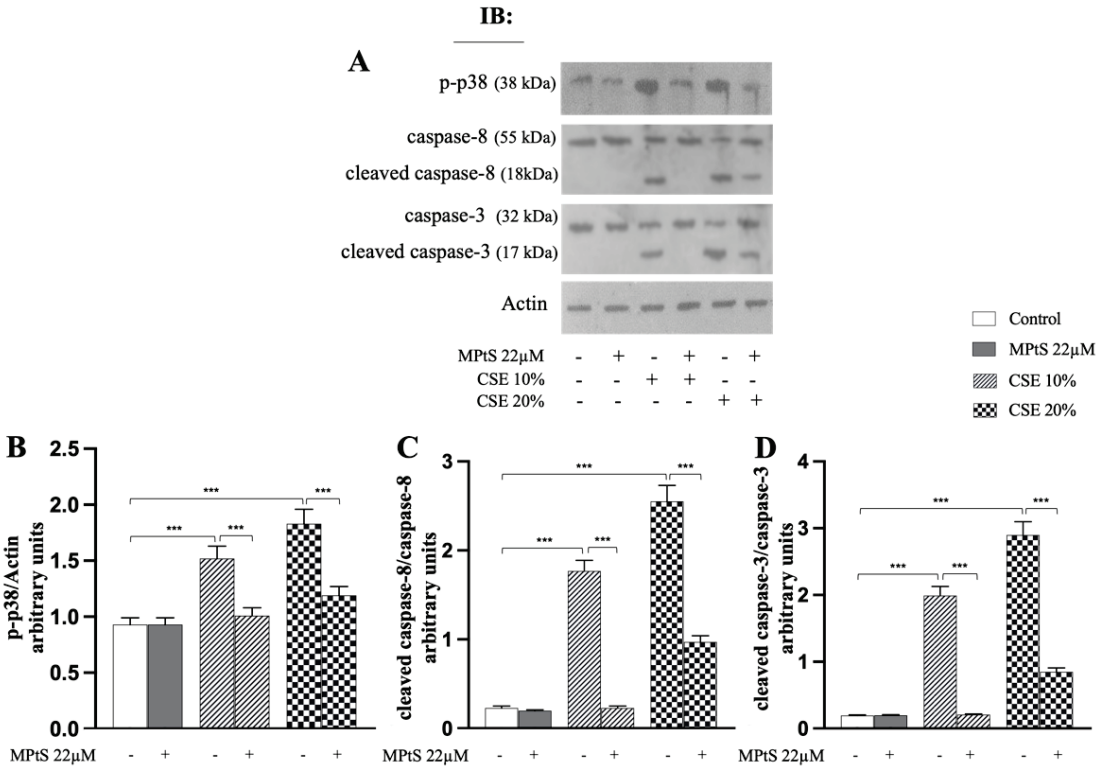

Figure 5. Mixture of plant sterols (MPtS) inhibits caspase 8/caspase 3 cleavage and phosphorylation of p38 MAPK in cigarette smoke extract (CSE)-induced eryptosis. (**A**) Representative images of immunoblotting analysis of p-p38 MAPK, cleaved caspase 8 and cleaved caspase 3 in 10% or 20% CSE-treated RBCs incubated for 4 h in absence or in co-treatment with 22 μM MPtS. Protocol of analysis at Section 4.7. (**B**–**D**) densitometric analysis of p-p38 MAPK, cleaved caspase 8 and cleaved caspase 3 levels normalized for actin. For (**C**,**D**), values are the ratio between cleaved and uncleaved caspases. Values are the means of bands' densitometry of three separate experiments with comparable results carried out on the same blood sample. *** $p < 0.001$ (ANOVA associated with Tukey's test).

3. Discussion

In the present study, we have shown that MPtS at 22 μM, used at this concentration as compatible with nutritional relevant serum concentrations obtained after the consumption of PtS-enriched milk-based fruit beverage [18], inhibits CSE-induced extrinsic eryptosis. MPtS counteracts eryptosis with the reduction of the pro-eryptotic bioactive lipid ceramide, the caspase 8 and caspase 3 proteases activation, the formation of the DISC in membrane and the phosphorylation of p38 (p-p38) MAPK. All these aspects lead to a reduction of the externalization of PS which is the key element of the eryptotic RBCs to be recognized by macrophages and to be removed from the bloodstream [20–22].

Although they represent hallmarks characteristic of the eryptotic process [8,9] changes in redox balance, intracellular Ca^{2+} levels and cell volume measured by FS, have not been observed (Figure S1). Present data confirm what has been observed previously [13]. However, the lack of variation of the FS could be partly attributed to the time of treatment in our model, since 4 h of treatment under experimental conditions could not be sufficient to unbalance the cellular volume. In recent work investigating the biochemical pathway leading to eryptosis in RBC treated with CSE [13] and in line with other studies [23,24], we have shown that the stimulation of p38 MAPK leads to the assembly of the membrane

DISC resulting in caspase activation. The mechanism in which this happens is unclear and deserves to be explored. Our data suggest that MPtS is able to inhibit the eryptotic process by inhibiting p-p38 MAPK which, as mentioned above, is the initiator of CSE-induced extrinsic eryptosis. In addition, the chemical-physical properties of PtS, could make them interact with the cell membrane of RBC going in some way to strengthen the inhibition of eryptosis avoiding the trimerization of FAS acting on membrane lipids-raft. It is quoted that MPtS can interact with the pathway involving Apoptosis Signal-Regulating Kinase 1 (ASK1)- MAPK kinases (MKK) 3/6 axis that in different experimental models leads to the phosphorylation and activation of p38 MAPK [25–27]. These assumptions would be in line with Zhang et al. [28] and Xu et al. [29] where the PtS like β-sitosterol and ergosterol appear to have modulated activities of p38 MAPK in gastric epithelial GES-1 and murine macrophages RAW 264.7 cells. However, to the best of our knowledge, this work is the first study in which it has been shown the inhibition of eryptosis by plant sterols acting on the extrinsic death pathway. For nucleated cells, many biochemical mechanisms are well known, while for anucleate cells such as RBCs, many mechanisms remain unknown or poorly studied. This study provides many ideas of reflection and deepening to fill the gap in the pathways shown above.

In conclusion, there are many pharmacological approaches and awareness campaigns aimed to reducing the harm of smoking. The new beneficial properties on RBC presented in this work involving plant sterols at nutritional relevant serum concentrations compatible with their well-known hypocholesterolemic effects, open new perspectives to prevent and treat part of the negative physio-pathological events caused by the eryptotic red blood cells circulating in smokers. Further confirmatory in vivo studies are warranted.

4. Materials and Methods

When not specified, all chemicals were purchased from Sigma-Aldrich (Milan, Italy) and were of the highest purity grade available.

4.1. Preparation of CSE

CSE was prepared by a modification of a methods previously published by Carnevali et al. [30]. In summary, 3 filtered Marlboro Red cigarettes (Philip Morris USA Inc., Richmond, VA, USA), each containing 0.8 mg nicotine, 10 mg tar and 10 mg carbon monoxide, were smoked consecutively through a system with a constant airflow (0.4 L/min) controlled by a vacuum pump. The smoke was gurgling through 30 mL of Ringer solution pre-heated to 37 °C. The Ringer solution consist of (mM) 125 NaCl, 5 KCl, 1 $MgSO_4$, 32 N-2-hydroxyethylpiperazine-N-2-ethanesulfonic acid (HEPES)/NaOH, 5 glucose, 1 $CaCl_2$, with a final pH 7.4. Cigarettes were torched up to 3 mm from the start of the filter. To ensure its sterility CSE was filtered through a 0.22-mm filter (Millipore, Billerica, MA, USA). This solution was considered to be 100% CSE. Concentration of nicotine, one of the stable constituents, was assessed by LC–MS analysis carried out using an Ultimate 3000 instrument coupled to a TSQ Quantiva (Thermo Fisher Scientific, San José, CA, USA) triple-stage quadrupole mass spectrometer. Nicotine mean concentration of four different CSE preparations was 32.13 ± 1.23 mg/L.

4.2. Preparation of MPtS

The PtS mixture at 22 μM final concentration in Ringer solution compatible with nutritional relevant serum concentrations obtained after the consumption of PtS-enriched milk-based fruit beverage, cointain β-sitosterol (13 μM), campesterol (8 μM), and stigmasterol (1 μM) and was prepared at 0.2% (*v*/*v*) ethanol, as reported in a previous study [18].

4.3. Red Blood Cells and Treatment

Fresh blood samples were collected in tubes coated with lithium heparin or sodium heparin to inhibit clotting from non-smoking healthy male volunteers (n = 6; age range 25–51 years; normal BMI range) with informed consent, and RBCs were immediately

isolated by centrifugation (2000× *g*, 4 °C, 20 min) over a Ficoll (Sigma-Aldrich, Milan, Italy, Cat. No. F5415) gradient [31]. Cells were washed twice in Ringer solution. The cell pellet aliquots were diluted in order to have a 0.4% hematocrit (HT) in the same simple Ringer solution (control) or in Ringer containing CSE at appropriate dilutions for the treatment. RBCs were then incubated at 37 °C, 5% CO_2 and 95% humidity for 4 h.

The experimental study protocol was approved by the Ethic Committee of Palermo 1, University Hospital (No. 8-09/2022) and performed in accordance with the Declaration of Helsinki and its amendments.

4.4. Measurement of PS Externalization

RBCs were washed once in Ringer solution, pH 7.4, and adjusted to 1.0×10^6 cells/mL with binding buffer following the manufacturer's instructions (eBioscience, San Diego, CA, USA, Cat No. 88-8005-74). In experiments designed to evaluate the percentage of PS externalization, suspension of RBCs (100 µL) was incubated with 5 µL of Annexin V-FITC at room temperature in the dark for 15 min. Subsequently, suspension samples of at least 1.0×10^4 cells were subjected to flow cytometric analysis by Epics XL™, using Expo32 software (Beckman Coulter, Fullerton, CA, USA). The annexin V-fluorescence intensity was measured in fluorescence channel FL-1 with an excitation wavelength of 488 nm and an emission wavelength of 530 nm.

4.5. Measurement of Ceramide

Abundance of ceramide levels was measured as follows. Briefly, after treatment, 1.0×10^5 erythrocytes were incubated for 1 h at 37 °C with 1 µg/mL of a mouse monoclonal anti-ceramide antibody (Sigma-Aldrich Chemical Co., St. Louis, MO, USA, Cat. No. C8104) in PBS containing 0.1% bovine serum albumin (BSA). RBCs after two washing steps with PBS-BSA, were stained for 30 min with 20 µL of a goat anti-mouse, polyclonal, fluorescein isothiocyanate-conjugated, secondary antibody (Millipore, Billerica, MA, USA, Cat. No. AQ502F) diluted 1/50 in PBS-BSA in the dark. Finally, erythrocytes were collected by centrifugation (2000× *g*, 4 °C, 5 min), washed twice, resuspended in PBS and analyzed by flow cytometer as reported in Section 4.4.

4.6. Immunoprecipitation

RBCs (2.0×10^8 cells) were washed twice with PBS and resuspended in lysis buffer (20 mM Tris-HCl, pH 7.6, 100 mM NaCl, 10 mM $MgCl_2$, 1% NP-40, 2 mM PMSF, 0.5 mM DTT and 2 mg/mL lysozyme) containing phosphatase (Roche, Basel, Switzerland, Cat. No. 4906845001) and protease inhibitors (Roche, Basel, Switzerland, Cat. No. 4693132001). Whole cell lysates were also sonicated (2 cycles, each for 30 s) with Labsonic LBS1-10 (Labsonic Falc, Treviglio, Italy) and after centrifugation (40,000× *g*, 4 °C, 1 h) were incubated overnight with mouse anti-FAS antibody (1:200) at 4 °C. Supernatants were then incubated with 20 µL of Protein G PLUS-Agarose (Santa Cruz Biotechnology, Inc., Dallas, TX, USA, sc-2002) for 3 h at 4 °C. Beads were pelleted, washed twice in lysis buffer and finally proteins were separated by SDS-PAGE for immunorecognition by western blotting [13].

4.7. Western Blotting

After treatment, erythrocytes (2.0×10^8 cells) were washed twice with PBS, resuspended in lysis buffer (20 mM Tris-HCl, pH 7.6, 100 mM NaCl, 10 mM MgCl2, 1% NP-40, 2 mM PMSF, 0.5 mM DTT and 2 mg/mL lysozyme) containing phosphatase and protease inhibitors and sonicated (2 cycles, each for 30 s) with Labsonic LBS1-10 (Labsonic Falc, Treviglio, Italy). Lysates were clarified by centrifugation (40,000× *g*, 4 °C, 1 h) and supernatants were collected and stored at −80 °C. Bradford protein assay (Bio-Rad, Hercules, CA, USA, Cat. No. 5000006) was used to quantify the total protein concentration in each sample. For each sample, equal amounts of proteins were loaded (50 µg/lane), separated on 10% gel by discontinuous SDS-PAGE and then electrotransferred to a polyvinylidene difluoride (PVDF) membrane (Millipore, Billerica, MA, USA, Cat. No. IPVH00010). Blots were treated

with blocking solution (5% nonfat dry milk) and then incubated overnight at 4 °C with primary antibodies (Santa Cruz Biotechnology, Inc., Dallas, TX, USA) in Tris-buffered saline (TBS; 25 mM Tris, 150 mM NaCl, pH 7.4) containing Tween 20 (1%, *v*/*v*) (TBST) and 5% (*w*/*v*) BSA. Mouse monoclonal anti-FADD (Santa Cruz Biotechnology, Inc., Dallas, TX, USA, sc-271748), anti-FAS (Santa Cruz Biotechnology, Inc., Dallas, TX, USA, sc-74540), anti-caspase 3 (Santa Cruz Biotechnology, Inc., Dallas, TX, USA, sc-56053), anti-caspase 8 (Santa Cruz Biotechnology, Inc., Dallas, TX, USA, sc-81657), and anti-p-p38 MAPK (Santa Cruz Biotechnology, Inc., Dallas, TX, USA, sc-166182) primary antibodies were used at a dilution of 1:200. After washing three times with TBST, immunoblots were incubated with a 1:2000 dilution of rabbit anti-mouse IgG antibody, horseradish peroxidase (HRP) conjugated (Sigma-Aldrich Chemical Co., St. Louis, MO, USA, Cat. No. AP160P) for 1 h at room temperature. Immunoblots were then washed five times with TBST and developed by enhanced chemiluminescence (Amersham, Milan, Italy, Cat. No. RPN2232). Mouse monoclonal anti-actin antibody (Santa Cruz Biotechnology, Inc., Dallas, TX, USA, sc-8432) was used as loading control. Densitometric analysis of protein spots was measured by Quantity One Imaging Software (Bio-Rad, Hercules, CA, USA, Cat. No. 1708265) and the results were reported as arbitrary densitometric units normalized to actin [32].

4.8. Statistical Analysis

Results are expressed as mean ± SD of (n = 6) separate experiments in triplicates. Statistical comparisons were performed by one-way analysis of variance (ANOVA) followed by Tukey's correction for multiple comparisons using Prism 8.4 (GraphPad Software Inc., San Diego, CA, USA). In all cases, significance was accepted if the null hypothesis was rejected at the $p < 0.05$ level.

Supplementary Materials: The following supporting information can be downloaded at: https://www.mdpi.com/article/10.3390/ijms24021264/s1.

Author Contributions: Conceptualization, A.C., A.A. and I.R.; methodology, A.C., A.A. and I.R.; software, I.R.; validation, A.C., A.A., G.G.-L. and L.T.; formal analysis, A.C. and L.T.; investigation, A.C. and I.R.; resources, M.A. and G.G.-L.; data curation, A.A. and I.R.; writing—original draft preparation, I.R.; writing—review and editing, A.C., A.A. and L.T.; visualization, L.T., M.A. and G.G.-L.; supervision, A.C. and L.T.; project administration, A.C. and A.A.; funding acquisition, G.G.-L. and A.A. All authors have read and agreed to the published version of the manuscript.

Funding: Grant PID2019-104167RB-I00 funded by MCIN/AEI/10.13039/501100011033 (Ministry of Science and Innovation (Spain)); European Union 2014–2020 Pon Ricerca E Innovazione Grant from the Italian Ministry of Education, University and Research, Entitled "Progema-Processi Green Per L'estrazione Di Principi Attivi E La Depurazione Di Matrici Di Scarto E Non" (ARS01_00432/).

Institutional Review Board Statement: The study was conducted in accordance with the Declaration of Helsinki and approved by the Ethics Committee of Palermo University Hospital (No. 8-09/2022).

Informed Consent Statement: Informed consent was obtained from all subjects involved in the study.

Data Availability Statement: All important data is included in the manuscript.

Conflicts of Interest: The authors declare no conflict of interest.

Abbreviations

Cigarette smoke (CS); cigarette smoke extract (CSE); death-induced signaling complex (DISC); statistical office of European Unit (EUROSTAT); FAS-associated via death-domain (FADD); fluorescein-5-isothiocyanate (FITC); forward scatter (FS); glutathione (GSH); mixture of plant sterols (MPtS); phosphorylated p-38 MAPK (p-38 MAPK); plant sterols (PtS); red blood cells (RBCs); reactive oxygen species (ROS); tert-butyl hydroperoxide (tBOOH); World Health Organization (WHO).

References

1. World Health Organization. *World Health Organization Global Report on Trends in Prevalence of Tobacco Smoking*; World Health Organization: Geneva, Switzerland, 2015.
2. Blann, A.D.; McCollum, C.N. Adverse Influence of Cigarette Smoking on the Endothelium. *Thromb. Haemost.* **1993**, *70*, 707–711. [CrossRef] [PubMed]
3. El-Mahdy, M.A.; Abdelghany, T.M.; Hemann, C.; Ewees, M.G.; Mahgoup, E.M.; Eid, M.S.; Shalaan, M.T.; Alzarie, Y.A.; Zweier, J.L. Chronic Cigarette Smoke Exposure Triggers a Vicious Cycle of Leukocyte and Endothelial-Mediated Oxidant Stress That Results in Vascular Dysfunction. *Am. J. Physiol. Heart Circ. Physiol.* **2020**, *319*, H51–H65. [CrossRef] [PubMed]
4. Nowak, J.; Murray, J.J.; Oates, J.A.; FitzGerald, G.A. Biochemical Evidence of a Chronic Abnormality in Platelet and Vascular Function in Healthy Individuals Who Smoke Cigarettes. *Circulation* **1987**, *76*, 6–14. [CrossRef] [PubMed]
5. Attanzio, A.; Frazzitta, A.; Vasto, S.; Tesoriere, L.; Pintaudi, A.M.; Livrea, M.A.; Cilla, A.; Allegra, M. Increased Eryptosis in Smokers Is Associated with the Antioxidant Status and C-Reactive Protein Levels. *Toxicology* **2019**, *411*, 43–48. [CrossRef]
6. Celermajer, D.S.; Sorensen, K.E.; Georgakopoulos, D.; Bull, C.; Thomas, O.; Robinson, J.; Deanfield, J.E. Cigarette Smoking Is Associated with Dose-Related and Potentially Reversible Impairment of Endothelium-Dependent Dilation in Healthy Young Adults. *Circulation* **1993**, *88*, 2149–2155. [CrossRef]
7. Cilla, A.; López-García, G.; Collado-Díaz, V.; Amparo Blanch-Ruiz, M.; Garcia-Llatas, G.; Barberá, R.; Martinez-Cuesta, M.A.; Real, J.T.; Álvarez, Á.; Martínez-Hervás, S. Hypercholesterolemic Patients Have Higher Eryptosis and Erythrocyte Adhesion to Human Endothelium Independently of Statin Therapy. *Int. J. Clin. Pract.* **2021**, *75*, e14771. [CrossRef]
8. Lang, F.; Qadri, S.M. Mechanisms and Significance of Eryptosis, the Suicidal Death of Erythrocytes. *Blood Purif.* **2012**, *33*, 125–130. [CrossRef]
9. Qadri, S.M.; Bissinger, R.; Solh, Z.; Oldenborg, P.-A. Eryptosis in Health and Disease: A Paradigm Shift towards Understanding the (Patho)Physiological Implications of Programmed Cell Death of Erythrocytes. *Blood Rev.* **2017**, *31*, 349–361. [CrossRef]
10. Lang, F.; Bissinger, R.; Abed, M.; Artunc, F. Eryptosis—The Neglected Cause of Anemia in End Stage Renal Disease. *Kidney Blood Press. Res.* **2017**, *42*, 749–760. [CrossRef]
11. Restivo, I.; Attanzio, A.; Tesoriere, L.; Allegra, M. Suicidal Erythrocyte Death in Metabolic Syndrome. *Antioxidants* **2021**, *10*, 154. [CrossRef]
12. Restivo, I.; Attanzio, A.; Tesoriere, L.; Allegra, M.; Garcia-Llatas, G.; Cilla, A. Anti-Eryptotic Activity of Food-Derived Phytochemicals and Natural Compounds. *IJMS* **2022**, *23*, 3019. [CrossRef] [PubMed]
13. Restivo, I.; Attanzio, A.; Giardina, I.C.; Di Gaudio, F.; Tesoriere, L.; Allegra, M. Cigarette Smoke Extract Induces P38 MAPK-Initiated, Fas-Mediated Eryptosis. *Int. J. Mol. Sci.* **2022**, *23*, 14730. [CrossRef]
14. Statistical office of the European Union (EUROSTAT). *Causes of Death—Deats by Country of Residence and Occurrence (HLTH_CD_ARO)*; Statistical office of the European Union (EUROSTAT): Luxembourg, 2022.
15. Gylling, H.; Plat, J.; Turley, S.; Ginsberg, H.N.; Ellegård, L.; Jessup, W.; Jones, P.J.; Lütjohann, D.; Maerz, W.; Masana, L.; et al. Plant sterols and plant stanols in the management of dyslipidaemia and prevention of cardiovascular disease. *Atherosclerosis* **2014**, *232*, 346–360. [CrossRef] [PubMed]
16. Danesi, F.; Ferioli, F.; Caboni, M.F.; Boschetti, E.; Di Nunzio, M.; Verardo, V.; Valli, V.; Astolfi, A.; Pession, A.; Bordoni, A. Phytosterol supplementation reduces metabolic activity and slows cell growth in cultured rat cardiomyocytes. *Br. J. Nutr.* **2011**, *106*, 540–548. [CrossRef]
17. Salehi, B.; Quispe, C.; Sharifi-Rad, J.; Cruz-Martins, N.; Nigam, M.; Mishra, A.P.; Konovalov, D.A.; Orobinskaya, V.; Abu-Reidah, I.M.; Zam, W.; et al. Phytosterols: From Preclinical Evidence to Potential Clinical Applications. *Front. Pharmacol.* **2020**, *11*, 599959. [CrossRef]
18. Garcia-Llatas, G.; Cilla, A.; Alegría, A.; Lagarda, M.J. Bioavailability of Plant Sterol-Enriched Milk-Based Fruit Beverages: In Vivo and in Vitro Studies. *J. Funct. Foods* **2015**, *14*, 44–50. [CrossRef]
19. Alvarez-Sala, A.; López-García, G.; Attanzio, A.; Tesoriere, L.; Cilla, A.; Barberá, R.; Alegría, A. Effects of Plant Sterols or β-Cryptoxanthin at Physiological Serum Concentrations on Suicidal Erythrocyte Death. *J. Agric. Food Chem.* **2018**, *66*, 1157–1166. [CrossRef]
20. Allen, T.M.; Williamson, P.; Schlegel, R.A. Phosphatidylserine as a Determinant of Reticuloendothelial Recognition of Liposome Models of the Erythrocyte Surface. *Proc. Natl. Acad. Sci. USA* **1988**, *85*, 8067–8071. [CrossRef]
21. Schroit, A.J.; Madsen, J.W.; Tanaka, Y. In Vivo Recognition and Clearance of Red Blood Cells Containing Phosphatidylserine in Their Plasma Membranes. *J. Biol. Chem.* **1985**, *260*, 5131–5138. [CrossRef]
22. Boas, F.E.; Forman, L.; Beutler, E. Phosphatidylserine Exposure and Red Cell Viability in Red Cell Aging and in Hemolytic Anemia. *Proc. Natl. Acad. Sci. USA* **1998**, *95*, 3077–3081. [CrossRef]
23. Lang, E.; Bissinger, R.; Gulbins, E.; Lang, F. Ceramide in the Regulation of Eryptosis, the Suicidal Erythrocyte Death. *Apoptosis* **2015**, *20*, 758–767. [CrossRef] [PubMed]
24. Kuo, W.-H.; Chen, J.-H.; Lin, H.-H.; Chen, B.-C.; Hsu, J.-D.; Wang, C.-J. Induction of Apoptosis in the Lung Tissue from Rats Exposed to Cigarette Smoke Involves P38/JNK MAPK Pathway. *Chem. Biol. Interact.* **2005**, *155*, 31–42. [CrossRef] [PubMed]
25. Rubiolo, C.; Piazzolla, D.; Meissl, K.; Beug, H.; Huber, J.C.; Kolbus, A.; Baccarini, M. A Balance between Raf-1 and Fas Expression Sets the Pace of Erythroid Differentiation. *Blood* **2006**, *108*, 152–159. [CrossRef] [PubMed]

26. Gatidis, S.; Zelenak, C.; Fajol, A.; Lang, E.; Jilani, K.; Michael, D.; Qadri, S.M.; Lang, F. P38 MAPK Activation and Function Following Osmotic Shock of Erythrocytes. *Cell Physiol. Biochem.* **2011**, *28*, 1279–1286. [CrossRef]
27. Tobiume, K.; Matsuzawa, A.; Takahashi, T.; Nishitoh, H.; Morita, K.; Takeda, K.; Minowa, O.; Miyazono, K.; Noda, T.; Ichijo, H. ASK1 Is Required for Sustained Activations of JNK/P38 MAP Kinases and Apoptosis. *EMBO Rep.* **2001**, *2*, 222–228. [CrossRef]
28. Zhang, Y.; Liang, J.; Jiang, H.; Qian, M.; Zhao, W.; Bai, W. Protective Effect of Sterols Extracted from Lotus Plumule on Ethanol-Induced Injury in GES-1 Cells in Vitro. *Food Funct.* **2021**, *12*, 12659–12670. [CrossRef]
29. Xu, J.; Xiao, C.; Xu, H.; Yang, S.; Chen, Z.; Wang, H.; Zheng, B.; Mao, B.; Wu, X. Anti-Inflammatory Effects of Ganoderma Lucidum Sterols via Attenuation of the P38 MAPK and NF-KB Pathways in LPS-Induced RAW 264.7 Macrophages. *Food Chem. Toxicol.* **2021**, *150*, 112073. [CrossRef]
30. Carnevali, S.; Petruzzelli, S.; Longoni, B.; Vanacore, R.; Barale, R.; Cipollini, M.; Scatena, F.; Paggiaro, P.; Celi, A.; Giuntini, C. Cigarette Smoke Extract Induces Oxidative Stress and Apoptosis in Human Lung Fibroblasts. *Am. J. Physiol. Lung Cell. Mol. Physiol.* **2003**, *284*, L955–L963. [CrossRef]
31. Allegra, M.; Restivo, I.; Fucarino, A.; Pitruzzella, A.; Vasto, S.; Livrea, M.A.; Tesoriere, L.; Attanzio, A. Proeryptotic Activity of 4-Hydroxynonenal: A New Potential Physiopathological Role for Lipid Peroxidation Products. *Biomolecules* **2020**, *10*, 770. [CrossRef]
32. Restivo, I.; Tesoriere, L.; Frazzitta, A.; Livrea, M.A.; Attanzio, A.; Allegra, M. Anti-Proliferative Activity of A Hydrophilic Extract of Manna from Fraxinus Angustifolia Vahl through Mitochondrial Pathway-Mediated Apoptosis and Cell Cycle Arrest in Human Colon Cancer Cells. *Molecules* **2020**, *25*, E5055. [CrossRef]

International Journal of
Molecular Sciences

MDPI

Article

Hyperforin Elicits Cytostatic/Cytotoxic Activity in Human Melanoma Cell Lines, Inhibiting Pro-Survival NF-κB, STAT3, AP1 Transcription Factors and the Expression of Functional Proteins Involved in Mitochondrial and Cytosolic Metabolism

Alessia Cardile [1,†], Valentina Zanrè [1,†], Rachele Campagnari [1], Francesca Asson [1], Solomon Saforo Addo [1], Elisa Orlandi [2] and Marta Menegazzi [1,*]

[1] Section of Biochemistry, Department of Neurosciences, Biomedicine and Movement Sciences, University of Verona, Strada Le Grazie, 8, 37134 Verona, Italy
[2] Section of Biology and Genetics, Department of Neurosciences, Biomedicine and Movement Sciences, University of Verona, Strada Le Grazie, 8, 37134 Verona, Italy
* Correspondence: marta.menegazzi@univr.it
† These authors contributed equally to this work.

Abstract: Hyperforin (HPF), the main component responsible for the antidepressant action of *Hypericum perforatum*, displays additional beneficial properties including anti-inflammatory, antimicrobic, and antitumor activities. Among its antitumor effects, HPF activity on melanoma is poorly documented. Melanoma, especially BRAF-mutated melanoma, is still a high-mortality tumor type and the currently available therapies do not provide solutions. We investigated HPF's antimelanoma effectiveness in A375, FO1 and SK-Mel-28 human BRAF-mutated cell lines. Cell viability assays documented that all melanoma cells were affected by low HPF concentrations (EC50% 2–4 μM) in a time-dependent manner. A Br-deoxy-uridine incorporation assay attested a significant reduction of cell proliferation accompanied by decreased expression of cyclin D1 and A2, CDK4 and of the Rb protein phosphorylation, as assessed by immunoblots. In addition, the expression of P21/waf1 and the activated form of P53 were increased in A375 and SK-Mel-28 cells. Furthermore, HPF exerts cytotoxic effects. Apoptosis is induced 24 h after HPF administration, documented by an increase of cleaved-PARP1 and a decrease of both Bcl2 and Bcl-xL expression levels. Autophagy is induced, attested by an augmented LC3B expression and augmentation of the activated form of AMPK. Moreover, HPF lowers GPX4 enzyme expression, suggesting ferroptosis induction. HPF has been reported to activate the TRPC6 Ca^{++} channel and/or Ca^{++} and Zn^{++} release from mitochondria stores, increasing cytosolic Ca^{++} and Zn^{++} concentrations. Our data highlighted that HPF affects many cell-signaling pathways, including signaling induced by Ca^{++}, such as FRA1, pcJun and pCREB, the expression or activity of which are increased shortly after treatment. However, the blockage of the TRPC6 Ca^{++} channel or the use of Ca^{++} and Zn^{++} chelators do not hinder HPF cytostatic/cytotoxic activity, suggesting that damages induced in melanoma cells may pass through other pathways. Remarkably, 24 h after HPF treatment, the expression of activated forms of the transcription factors NF-κB P65 subunit and STAT3 are significantly lowered. Several cytosolic (PGM2, LDHA and pPKM2) and mitochondrial (UQCRC1, COX4 and ATP5B) enzymes are downregulated by HPF treatment, suggesting a generalized reduction of vital functions in melanoma cells. In line with these results is the recognized ability of HPF to affect mitochondrial membrane potential by acting as a protonophore. Finally, HPF can hinder both melanoma cell migration and colony formation in soft agar. In conclusion, we provide evidence of the pleiotropic antitumor effects induced by HPF in melanoma cells.

Keywords: St. John's wort; cell cycle regulation; apoptosis; ferroptosis; autophagy; STAT3; NF-κB; HIF1α; CREB; metabolism

Citation: Cardile, A.; Zanrè, V.; Campagnari, R.; Asson, F.; Addo, S.S.; Orlandi, E.; Menegazzi, M. Hyperforin Elicits Cytostatic/Cytotoxic Activity in Human Melanoma Cell Lines, Inhibiting Pro-Survival NF-κB, STAT3, AP1 Transcription Factors and the Expression of Functional Proteins Involved in Mitochondrial and Cytosolic Metabolism. *Int. J. Mol. Sci.* **2023**, *24*, 1263. https://doi.org/10.3390/ijms24021263

Academic Editor: Sanjay K. Srivastava

Received: 18 November 2022
Revised: 31 December 2022
Accepted: 5 January 2023
Published: 9 January 2023

1. Introduction

Hyperforin (HPF) is an acylphloroglucinol abundantly present in the apical flowers of *Hypericum perforatum*, also known as St. John's wort (SJW). HPF has been assessed as the main component responsible for the antidepressant action of SJW extract [1].

Considering many experimental results present in the literature, three distinct modes of action can be ascribed to HPF. (i) It can activate the transient receptor potential cation channel (TRPC)-6, resulting in the modulation of synapsis plasticity [2–4]. (ii) It can induce calcium and zinc release from mitochondria stores, leading to an increase in their cytosolic concentration [5–7]. (iii) Acting as a protonophore, it can change the pH gradient and interfere with the driving force across a membrane (especially of the mitochondria) [8,9]. All these mechanisms may contribute to its biological effects, although each may do so to a different extent, depending on the cell type and the HPF concentrations used [10]. Accordingly, HPF displays a wide spectrum of biological effects besides its antidepressant activity. In the first studies, HPF has been reported to inhibit the activity of cyclooxygenase-1, 5-lypoxygenase and prostaglandin E2-synthase-1 [11,12] and to display antibacterial effects [13]. Subsequently, it was shown that the anti-inflammatory properties of HPF include its capability, in cells, to regulate gene expression and the activation of several cytokine-elicited kinases or transcription factors involved in inflammation [7,14–18] (reviewed by [19,20]). Other studies highlighted SJW and HPF protective effects against noxious stimuli in several animal models as well [21–23].

Remarkably, Manna et al. demonstrated that a diet with SJW extract can significantly improve the overall survival in a mouse model of azoxymethane-induced colorectal tumorigenesis [24]. In line with this result, a very large epidemiology study indicated that continued use of SJW extract is associated with a 65% decreased risk for colorectal cancer [25], suggesting that it may possess a protective effect in human carcinogenesis as well.

Importantly, HPF does not possess protective effects only before tumor formation. When tumor mass has already grown, HPF displays remarkable activity against tumor progression by downregulating survival signaling and by inducing programmed cell death. At the beginning of this century, Schempp et al. showed for the first time, in 17 cell lines from different tumor types, that HPF acts by triggering intrinsic apoptotic cell death and inhibiting cell proliferation, with half maximal effective concentration (EC50%) from 3 to 15 μM [26]. Again, the same authors assessed that HPF can hinder tumor growth in rats injected with MT-450 breast carcinoma cells in the absence of any signs of acute toxicity [26]. Subsequently, many studies confirmed the antitumor efficacy of HPF by examining the molecular targets of its cytotoxic effect.

HPF can affect leukemia cells (reviewed in [27]), such as the human acute promyelocytic leukemia cell line (HL60), by targeting mitochondrial membrane potential [28]. Again, HPF leads to apoptosis in chronic lymphocytic leukemia cells by inducing the pro-apoptotic protein Noxa [29]. HPF affects several acute myeloid leukemia (AML) cell lines, as well as primary cells from AML patients, through different mechanisms including upregulation of Noxa expression, mitochondrial membrane depolarization, activation of caspases and inhibition of protein kinase B (AKT) activity [30].

Regarding solid tumors, Hsu et al. showed that HPF can induce apoptosis in glioblastoma cells, with EC50% of 5–10 μM, by suppressing the expression of antiapoptotic-related proteins. Furthermore, they demonstrated that HPF can inactivate epithelial growth factor receptor (EGFR), extracellular signal-regulated kinases (ERK)1/2, and nuclear factor kappa B (NF-κB) [31]. HPF can inhibit cyclin D1 expression and can induce the loss of internal mitochondrial membrane potential in hepatocarcinoma cells [32]; in addition, it can affect tumor growth of non-small-cell lung cancer [33]. HPF decreases bladder cancer cell survival, with EC50% of 10–20 μM, by increasing reactive oxygen species (ROS), calcium signaling and apoptosis and by blocking NF-κB activity [34]. Recently, cytotoxicity of HPF and its derivatives was discovered in colon cancer cells by a mechanism involving the Wnt/β-catenin signaling pathway [35]. Donà et al. studied the HPF-elicited cytotoxic-

ity in many human and murine cell lines [36]. They found that HPF decreases ERK1/2 and metalloproteinases activity and affects cell viability at a concentration in the range of 5–20 μM, whereas untransformed endothelial cells were only marginally affected. Importantly, the authors reported that HPF concentrations 20-fold below the toxicity threshold were effective in hindering the invasive potential of malignant cells. Moreover, in mice injected with neoplastic cells, HPF administration reduced tumor growth and metastasis with persistence of healthy behavior [36].

Regarding melanoma, the HPF molecular mechanism has not yet been investigated, although its effectiveness in reducing the cell viability of some human or mouse melanoma cell lines has been previously reported [26,36,37].

Malignant melanoma is an aggressive skin tumor characterized by high metastatic potential and mortality [38]. In about 40–60% of patients with cutaneous melanoma, oncogenic mutations in BRAF kinase are found, which drive the constitutive activation of pro-survival kinases ERK1/2 [38]. Remarkably, patients harboring BRAF mutations showed poorer prognosis and survival [39]. BRAF inhibitors and mitogen-activated protein kinase (MEK)-inhibitors therapies are able to improve the lifespan of patients accompanied with the BRAF-mutated genotype [40]. Unfortunately, the effectiveness of targeted therapy has been shown to be time-restricted because melanoma becomes resistant to these drugs in a short time [41]. Therefore, new strategies to extend patients' survival should be discovered.

In the present work, three BRAF-mutated human melanoma cell lines are tested for their sensitivity to HPF administration. Data show that all cell lines are significantly affected by low μM concentration of HPF in contrast to normal human epithelial melanocytes. In addition, we documented pleiotropic effects by which HPF counteracts melanoma cell malignancy.

2. Results

2.1. A375, FO-1, SK-Mel-28 and MeWo Melanoma Cell Viability Was Affected by Hyperforin in a Time- and Concentration-Dependent Manner

To quantify the antitumor effect of HPF on melanoma cells, a sulforhodamine B (SRB) viability assay was carried out on SK-Mel-28, A375 and FO-1 BRAF-mutated melanoma cells and on P53-mutated MeWo cells after 24, 48 and 72 h of treatment with 1, 2, 3, 4 and 5 μM HPF. Results shown in Figure 1 reveal an evident time-dependent inhibition of cellular mass. Indeed, the effective HPF concentration able to achieve 50% cell viability (EC50%) of untreated cells was in a range from 2 to 4 μM after 48 or 72 h treatments (Figure 1). FO-1 was the most responsive melanoma cell line to HPF administration, with an EC50% of 2 μM after 72 h, while A375, SK-Mel-28 and MeWo cells displayed an EC50% of about 3–4 μM (Figure 1).

To investigate whether normal human epithelial melanocytes (NHEM) were affected by HPF treatment, increasing concentrations of HPF were added to NHEM culture medium and a cell viability assay was carried out after 24, 48 and 72 h. Results indicate that HPF at 5 μM, the highest concentration used on melanoma cells, reduces NHEM viability by 20% in comparison to a 70–80% reduction obtained in malignant cell lines (Figure 1).

Therefore, data suggest that HPF affects melanoma cell viability with higher specificity than normal melanocytes.

2.2. Hyperforin Affects the Morphology of Melanoma Cells

Morphological features acquired by melanoma cells after 24 and 48 h treatment with low micromolar concentrations of HPF were analyzed by microscopy examination.

Figure 2 shows that HPF can affect the natural shape of A375, FO-1, SK-Mel-28 and MeWo melanoma cells in 2D culture. Control cells turn out to be well adherent to the plate except for several cells in division showing rounded and translucent shapes (Figure 2, CTR). After 24 h treatment with 3 μM HPF, dividing cells as well as the total cell number were decreased. At 24/48 h after HPF administration, almost all remaining cells had lost

adherence to the plate and several cells showed blebbing of the plasma membrane, a typical morphology of cells undergoing late phase of apoptotic cell death (Figure 2). No change in morphology was detectable in NHEM after 24–48 h of HPF treatment (Figure 2).

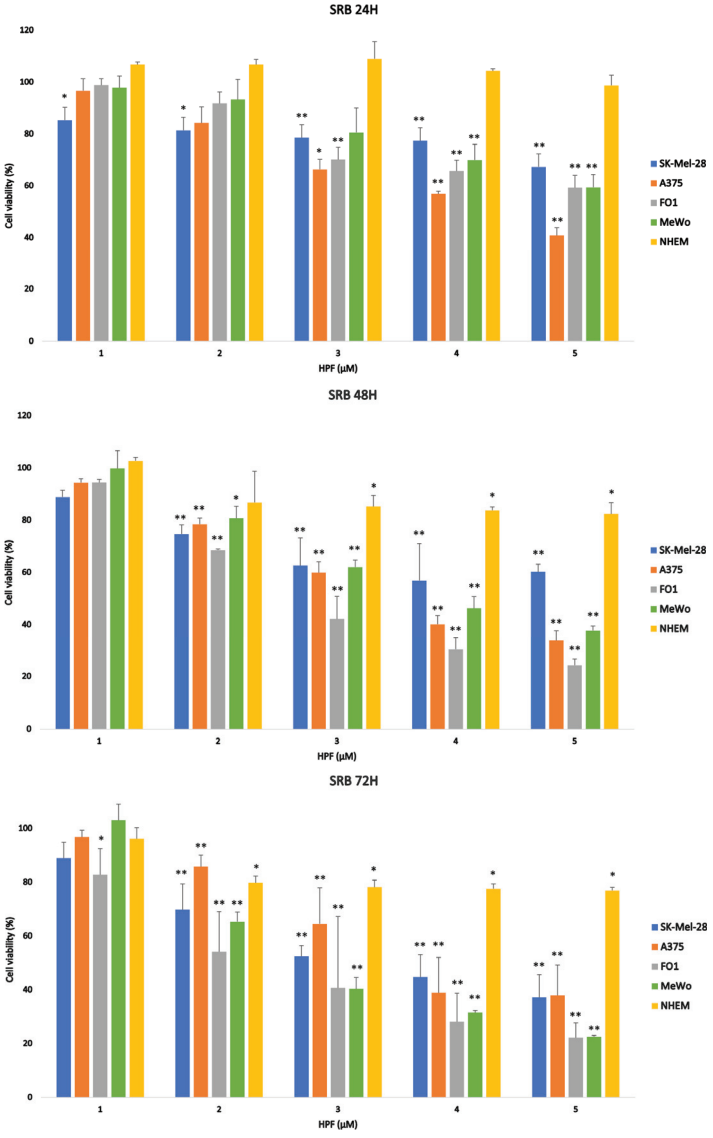

Figure 1. Histograms show time- and concentration-dependent reduction in cell viability after hyperforin treatment. SRB cell viability assay was performed on A375 (orange), FO-1 (grey), SK-Mel-28 (blue) and MeWo (green) melanoma cells treated with 1 to 5 μM hyperforin (HPF) for 24, 48 and 72 h. HPF induced a time- and concentration-dependent decrease in cell viability, in comparison with untreated cells (100%). Normal human epithelial melanocytes (NHEM, yellow), treated with HPF for 24, 48 and 72 h, was shown to be less affected by HPF than melanoma cells. Data acquired calculating the average ± S.D. of values obtained from at least four independent experiments were compared with the untreated control (* $p < 0.05$; ** $p < 0.01$).

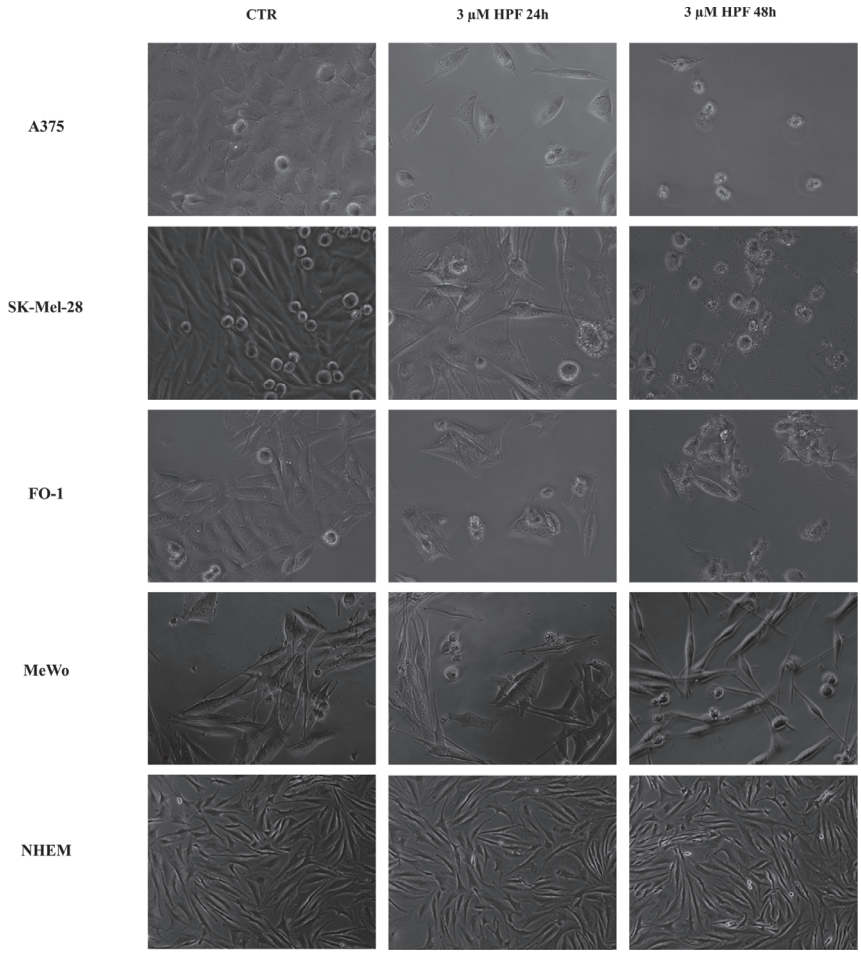

Figure 2. The images show melanoma cell morphological modifications after 24 and 48 h-treatment with 3 μM hyperforin. Representative images of A375, SK-Mel-28, FO-1 and MeWo melanoma cells and normal human epithelial melanocytes (NHEM), untreated (CTR) or treated with 3 μM hyperforin (HPF) for 24 and 48 h. In melanoma cells but not in NHEM, HPF induces a time-dependent decrease in cell number and a change in cell shape from elongated to round with membrane blebbing. Images were captured at 20× magnification (5× magnification only for NHEM) with an inverted microscope (Axio Vert A1, Zeiss, Oberkochen, Germany).

2.3. Hyperforin Inhibits Melanoma Cell Proliferation by Affecting the Expression of Cell Cycle-Regulating Proteins

SRB results ascertained that HPF can reduce total cell mass in melanoma cells, and morphological analysis suggested its effect on both cell proliferation and death. In order to investigate the HPF mechanism of action, we selected the most homogeneous cell lines presenting the mutation in the BRAF gene to perform all the following experiments.

Firstly, a cell proliferation assay was carried out by measuring Br-deoxy-uridine (BrdU) incorporation during the cell cycle DNA synthesis (S) phase. A375, FO-1 and SK-Mel-28 melanoma cells were treated with 2, 3 and 4 μM HPF for 48 h. At that time, BrdU was added to the culture medium and, after 8 h incubation, its incorporation in newly synthesized DNA was measured.

As shown in Figure 3A, HPF reduced A375, FO-1 and SK-Mel-28 cell proliferation rates. This result led us to investigate the underlying molecular mechanisms by immunoblots, carried out to discover the expression levels of target proteins controlling the cell cycle.

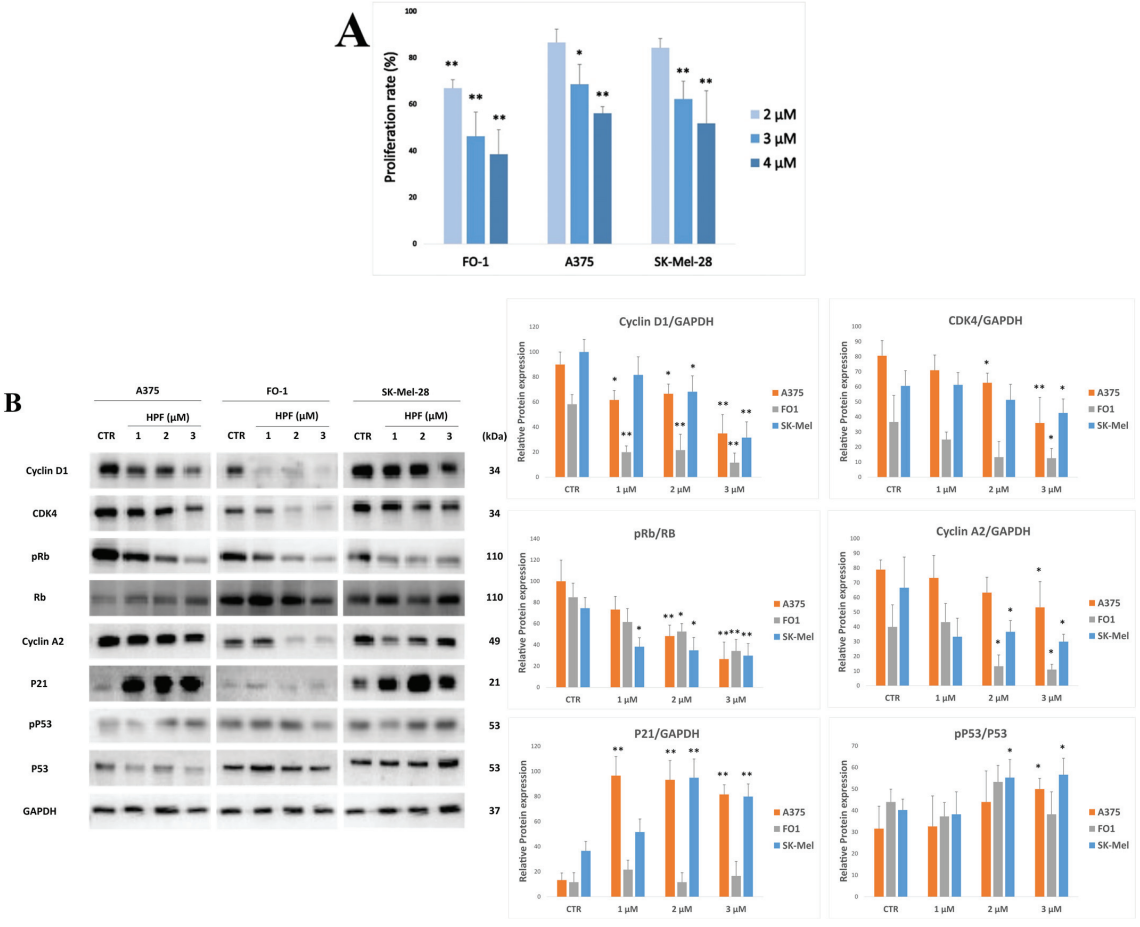

Figure 3. Hyperforin slows down melanoma cell proliferation by affecting the expression of several cell cycle-regulating proteins. (**A**) BrdU incorporation assay attesting the inhibition of cell proliferation of 2, 3 and 4 µM HPF on FO-1, A375 and SK-Mel-28 melanoma cell lines. (**B**) A375, FO-1 and SK-Mel-28 melanoma cells were treated with increasing concentrations of HPF for 24 h. In the left panel, representative immunoblots show the expression level of cyclin D1, cyclin-dependent kinase (CDK)-4, the phosphorylated form of retinoblastoma protein (pRb), total Rb protein, cyclin A2, P21/WAF1 (P21), phospho-Ser15-P53 (pP53), total P53 (P53) and glyceraldeide-3-phosphate dehydrogenase (GAPDH). On the right, histograms represent the mean values ± S.D. of protein expression level measured by densitometry deriving from three independent experiments and normalized with GAPDH expression, whereas pRb and pP53 results were normalized with total Rb and P53 protein level, respectively. All comparisons were performed vs. each control sample after data normalization; * $p < 0.05$; ** $p < 0.01$.

Cyclin D1 together with cyclin-dependent kinase (CDK)-4 are key regulators of the G1 phase of the cell cycle, and they are considered therapeutic targets in BRAF-mutated cancers [42]. Immunoblots showed a concentration-dependent decrease of cyclin D1 and CDK4

expression level in melanoma cells treated for 24 h with HPF (Figure 3B). Retinoblastoma (Rb) protein represents a major G1 restriction point aimed to block cell entry in S-phase. Cyclin D1/CDK4 activation determines hyperphosphorylation and inhibition of Rb protein, allowing cell cycle progression [43]. The phosphorylation level of Rb (pRb) was decreased in a concentration-dependent manner by a 24 h HPF treatment, whereas the total Rb protein level was unchanged (Figure 3B). Cyclin A2 is highly expressed in the S-phase when it is associated with CDK2 or CDK1 [44]. In addition to cyclin D1, cyclin A2 expression level was decreased after 24 h of treatment (Figure 3B). The cell cycle progression inhibitor P21/Waf1 (P21) protein can bind cyclin A2/CDK2 and cyclin D1/CDK4 complexes by hindering their activity. P21 protein binding makes cyclin D1/CDK4 complex inactive and unable to phosphorylate Rb protein [45]. Remarkably, P21 expression level was maximally increased after 24 h treatment in A375 and SK-Mel-28 cell lines (Figure 3B). Tumor suppressor P53 is a transcription factor able to induce the expression of many genes, including P21 protein, inhibiting, finally, cell cycle progression [46]. Immunoblots showed an increased expression of the active form of P53 (phospho-Ser15-P53) in the P53 wild type A375 and SK-Mel-28 cell lines concomitantly with an increase of P21 expression (Figure 3B). Instead, FO-1 cells expressed a very low level of P21 and the amount of P53 phosphorylation remains unchanged until 2 μM HPF, decreasing at higher concentrations (Figure 3B).

In summary, all data suggest a pleiotropic mechanism elicited by HPF able to hinder cell cycle progression in melanoma cells.

2.4. Hyperforin Induces Apoptotic Cell Death, as Well as Autophagy and Ferroptosis

Morphological analysis of melanoma cells showed several signs of cell death at 24 and 48 h after HPF administration (Figure 2). Therefore, we analyzed some molecular markers of programmed cell death. The cleaved form of poly (ADP-ribose) polymerase 1 (cleaved-PARP1) is obtained through the activity of caspase 3 or caspase 7 in cells undergoing apoptosis [47,48]. After 24 h of HPF treatment, in all melanoma cell lines, immunoblots showed a decrease of bands representing full-length PARP1 expression and a correspondent increase of higher mobility band displaying cleaved-PARP1 level (Figure 4). Thereby, data suggest induction of apoptotic cell death in a concentration-dependent manner. Proteins belonging to the B-cell lymphoma 2 (Bcl2) family are regulators of apoptosis. Bcl2 and Bcl-extra-large (Bcl-xL) are antiapoptotic proteins highly expressed in tumor cells [49,50]. Immunoblots showed a gradual decrease of both Bcl2 and Bcl-xL expression levels (Figure 4), explaining in part the high propensity of cells treated for 24 h with HPF to undergo apoptosis.

Then, the involvement of other types of programmed cell death was investigated. It has been reported that HPF augments AMP-activated kinase (AMPK) activity either in normal [51] or in cancer cells [28]. Immunoblot results showed an increase of the phosphorylated and activated form of AMPK (pAMPK) after 24 h of HPF treatment, whereas the total level of the kinase was not significantly affected (Figure 4). In agreement with the increased pAMPK level, acetylCoA carboxylase enzyme (ACC), which is a known target of AMPK activity, has been found phosphorylated as well (pACC, Figure 4). AMPK is an activator of mitophagy/autophagy in tumor cells, including melanoma [52]. Therefore, the expression level of microtubule-associated proteins 1A/1B light chain 3B (LC3B), a known marker of autophagy, was investigated by immunoblotting. Data show that LC3B increased after HPF treatment (Figure 4), suggesting activation of autophagy as well.

Glutathione peroxidase (GPX)-4 is an essential regulator of ferroptotic cell death since its knockdown or its overexpression can induce or antagonize, respectively, this form of cell death [53,54]. After 24 h treatment with HPF, the expression level of GPX4 enzyme was significantly reduced (Figure 4). Altogether, these data could suggest a co-presence of ferroptosis.

Finally, the phosphorylation level of eIF4E-binding protein 1 (4E-BP1) displayed a decrease, demonstrating that 24 h HPF treatment induces generalized translational repression in cells (Figure 4).

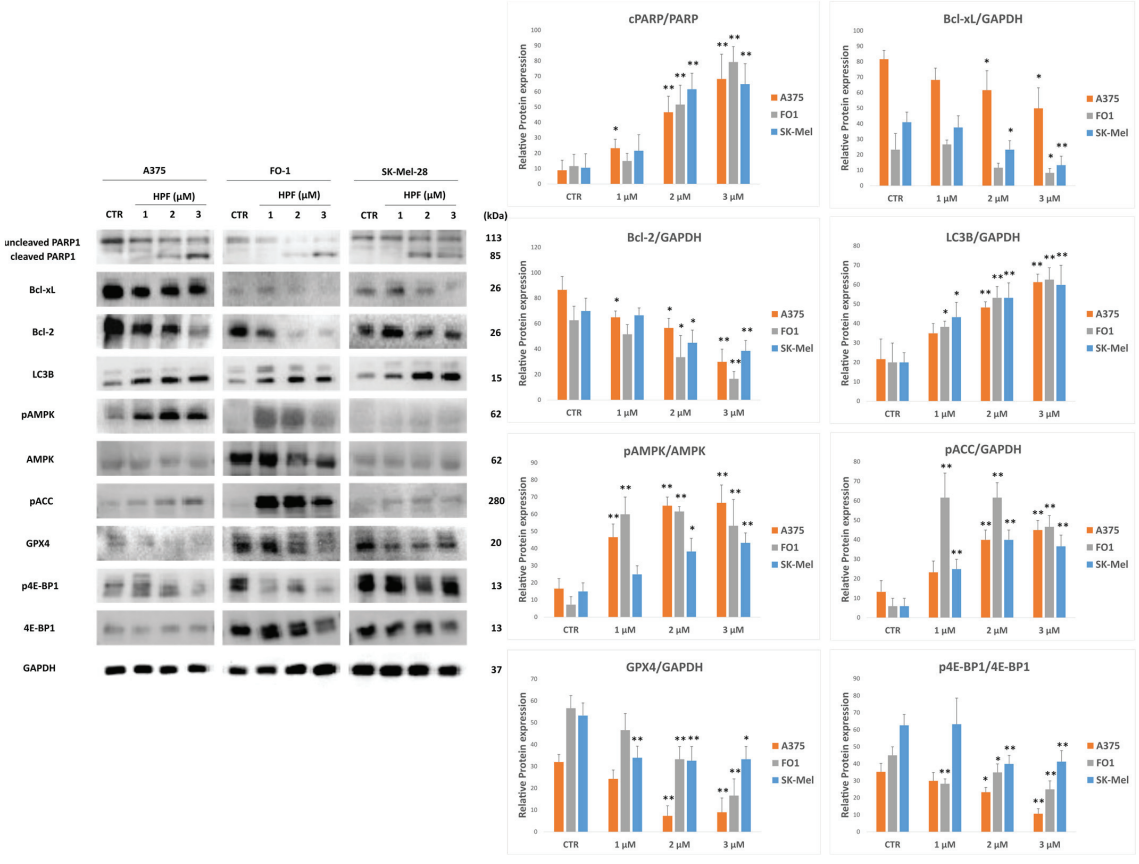

Figure 4. Hyperforin affects the expression of several proteins involved in apoptosis, autophagy and ferroptosis induction. A375, FO-1 and SK-Mel-28 melanoma cells were treated with increasing concentrations of HPF for 24 h. In the left panel, representative immunoblots show the expression level of cleaved and uncleaved PARP1, Bcl-extra-large (Bcl-xL), Bcl2, microtubule-associated proteins 1A/1B light chain 3B (LC3B), the phosphorylated form of AMP-activated kinase (pAMPK), total AMPK, the phosphorylated form of acetylCoA carboxylase (pACC), glutathione peroxidase 4 (GPX4), the phosphorylation level of eIF4E-binding protein 1 (4E-BP1), total 4E-BP1 and glyceraldeide-3-phosphate dehydrogenase (GAPDH). On the right, histograms represent the mean values ± S.D. of protein expression level measured by densitometry deriving from three or more independent experiments and normalized with GAPDH expression, unless otherwise stated. All comparisons were performed vs. each control sample after data normalization; * $p < 0.05$; ** $p < 0.01$.

2.5. Signaling Pathway Elicited by Hyperforin in Melanoma Cells

After establishing its antitumor activity, the mechanisms involved in the HPF-elicited cytotoxicity in melanoma cells were investigated.

As already mentioned, it has been reported that HPF acts as a specific activator of Ca^{++}-channel TRPC6 [2], it induces an increase of cytosolic Ca^{++} and Zn^{++} concentrations [5] and it facilitates proton flux between cell membranes acting as a protonophore [9].

Experiments were performed to verify if the Ca^{++} channel blocker SKF-96365 (SKF) could suppress the cytostatic/cytotoxic effects of HPF in melanoma cells. In addition, BAPTA and TPEN, the cell-permeable chelators of Ca^{++} and Zn^{++}, respectively, were used to ascertain whether the blockage of the HPF-elicited Ca^{++} and Zn^{++} cytosolic concentrations'

increase could suppress its antimelanoma activity. Thus, SRB viability assay was carried out on melanoma cells treated for 72 h with SKF, BAPTA or TPEN alone and in the co-presence of HPF, at concentrations corresponding approximately to the EC50% value measured in each cell line. All inhibitors were added to the cell culture medium 10 min before HPF addition.

The obtained data were very consistent considering the different sensitivity of each melanoma cell line to HPF.

As shown in Figure 5, the treatment with SKF alone at the lowest concentration used (1 μM) did not affect cell viability. Furthermore, SKF administration in association with HPF was not able to revert the cytostatic/cytotoxic activity of this acylphloroglucinol. Instead, the use of higher SKF concentrations alone (2.5 and 5 μM) induced a noticeable reduction of cell viability after 72 h of treatment. Remarkably, at these doses, HPF in association with SKF can increase, rather than hinder, its harmful effect in all melanoma cell lines (Figure 5).

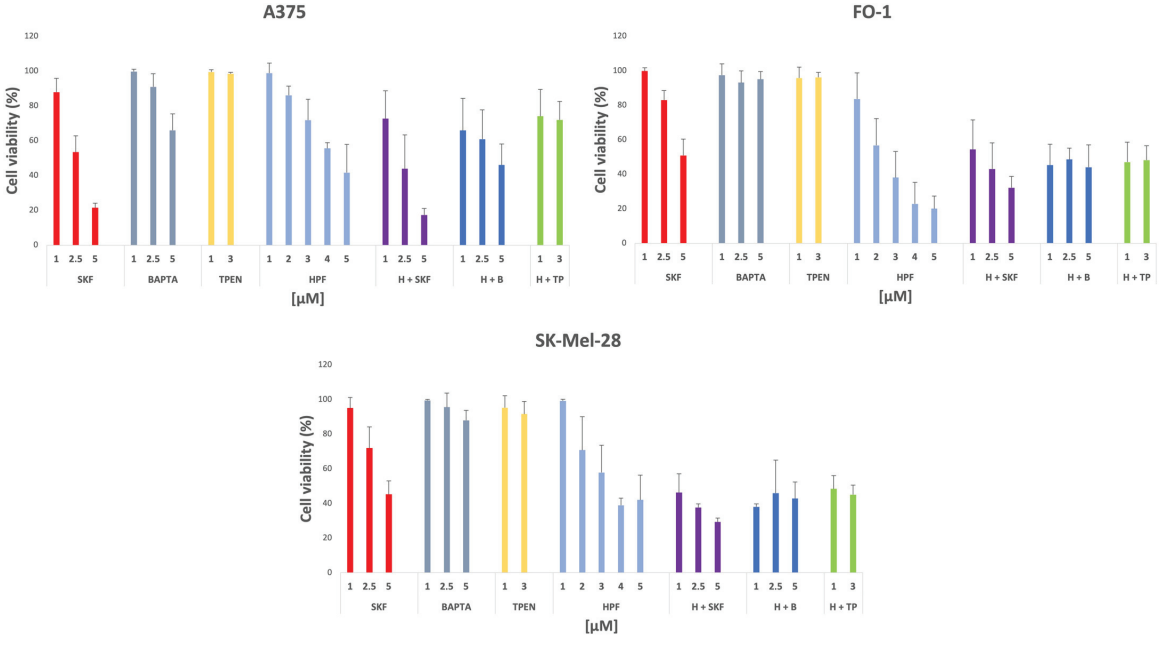

Figure 5. Histograms show the reduction in cell viability in presence of SKF, BAPTA and TPEN administered alone or in co-presence of hyperforin. SRB cell viability assay was performed on FO-1, SK-Mel-28 and A375 melanoma cells after 72 h of treatment with SKF-96365, an inhibitor of Ca^{++}-channel transient receptor canonical (TRPC)-6, or BAPTA-AM, a cell-permeable Ca^{++} chelator, or TPEN, a Zn^{++} chelator. The co-treatment was performed with each inhibitor singly, combined with HPF used at 2 μM for FO-1 and at 4 μM for A375 and SK-Mel-28 cells, accordantly with each EC50% value previously documented. Data acquired calculating the average ± S.D. of values were obtained from at least four independent experiments.

Again, cell viability was slightly affected by 1, 2.5 or 5 μM of BAPTA or by 1 or 3 μM of TPEN administered singly to the culture medium. Moreover, the co-presence of HPF with BAPTA or TPEN did not block the HPF cytostatic/cytotoxic effect (Figure 5).

Thus, for a longer time of treatment (72 h), data show that the antimelanoma activity of HPF was maintained even in the presence of either a TRPC6 blocker or a Ca^{++} or Zn^{++} chelator.

In addition to its effect on TRPC6 channel activity, HPF could affect the expression level of the TRPC6 channel. Immunoblotting data showed that TRPC6 protein level was

unchanged after 24 h treatment with HPF (Figure 6). In cells treated with HPF, SKF or both compounds for a short time (2 h), TRPC6 expression was unchanged as well (Figure 6). Data suggest that TRPC6 was not overexpressed after HPF treatment.

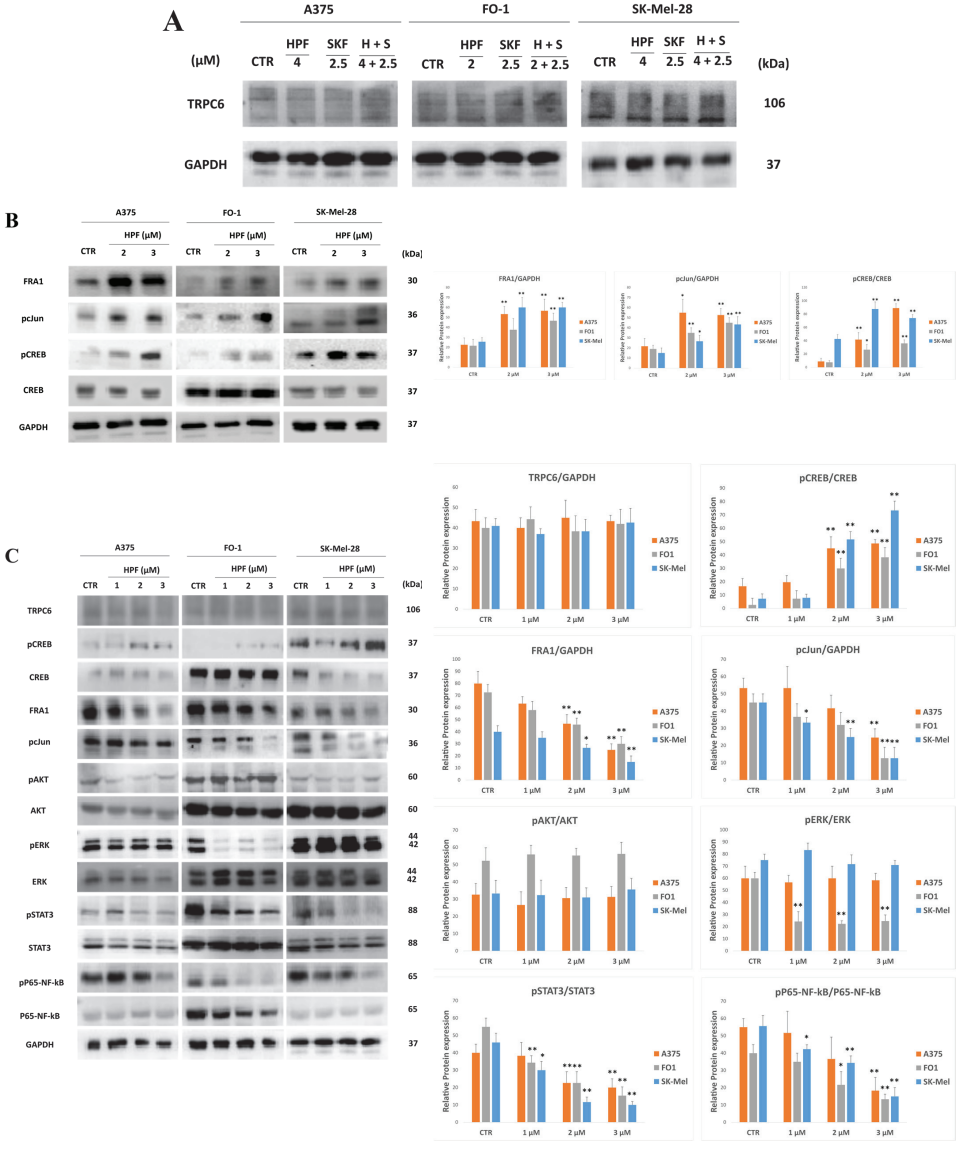

Figure 6. Hyperforin affects the expression levels of key proteins involved in signaling. (**A**) Represents immunoblots showing the expression level of TRPC6 in A375, FO-1 and SK-Mel-28 melanoma cells treated for 2 h with HPF, SKF, or both compounds. (**B**) Represents immunoblots showing the expression level of Fos-related antigen 1 (FRA1), the phosphorylated form of proto-oncogene c-Jun (pcJun) and of cyclic AMP response-element binding protein (pCREB), and total CREB in melanoma cells treated for 2 h with 0, 2 and 3 μM HPF concentrations. On the right, histograms represent the mean values ± S.D. of protein expression levels measured by densitometry deriving from three independent experiments and normalized with GAPDH expression, unless otherwise stated. All

comparisons were performed vs. each control sample after data normalization; * $p < 0.05$; ** $p < 0.01$. (**C**) Represents immunoblots showing the expression level of key proteins belonging to several signaling pathways activated in melanoma cells after 24 h HPF treatment. In particular, the expression of TRPC6, pCREB, total CREB, FRA1, pcJun, the phosphorylated form of protein kinase B (pAKT), total Akt, the phosphorylated form of extracellular signal-regulated kinases (ERK), total ERK, the phosphorylated form of signal transducer and activator of transcription 3 (STAT3), total STAT3, the phosphorylated form of nuclear factor kappa B P65 subunit (pP65 NF-κB), total P65 NF-κB and GAPDH. On the right, histograms represent the mean values ± S.D. of protein expression levels measured by densitometry deriving from three independent experiments and normalized. All comparisons were performed vs. each control sample after data normalization; * $p < 0.05$; ** $p < 0.01$.

At the molecular level, in different cancer models, several reports attested that many signaling pathways are affected by HPF administration (reviewed in [55]). Gibon et al. [7] reported that, in some tissues, HPF promotes the activation of the transcription factor cyclic-AMP response element-binding protein (CREB). In agreement with these previous data, in all the analyzed melanoma cell lines, 2 and 24 h after HPF administration, immunoblots showed a concentration-dependent increase of the phosphorylated and activated form of CREB (pCREB), whereas total CREB expression was unchanged or even decreased (Figure 6B,C).

After short time treatments, HPF was also able to increase the expression of proteins belonging to the transcription factor complex activating protein-1 (AP1). Immunoblots showed that HPF concentration dependently increases Fos-related antigen 1 (FRA1) expression and the phosphorylated and activated form of the proto-oncogene cJun (pcJun) (Figure 6B). However, after 24 h treatment, FRA1 and pcJun expression were decreased in a concentration-dependent manner in all the tested cell lines (Figure 6C).

Merhi et al. showed [30] a suppression of protein kinase B (AKT) activity in human myeloid cells at HPF concentrations similar to those used in the present work, whereas Hsu et al. proved that HPF can inhibit the extracellular signal-regulated kinases (ERK)-1/2 activity in glioblastoma cells [56]. Regarding pERK1/2 and pAKT, which are both constitutively active in the BRAF-mutated melanoma cell lines, no different expression levels were found at short times (not shown) and after 24 h treatment in A375 and SK-Mel-28 cells (Figure 6C). In FO-1 cells only, a reduction of pERK1/2 level was found 24 h after HPF administration (Figure 6C).

Key transcription factors largely involved in pro-survival signaling in melanoma are signal transducer and activator of transcription (STAT)-3 [57] and nuclear factor-kappa B (NF-κB) [58], which were shown to be activated by phosphorylation in melanoma cells. After 24 h of treatment, HPF concentration dependently decreased the expression levels of phospho-Ser475 of P65-NF-κB subunit and phospho-Tyr705 of STAT3, while total P65 and total STAT3 protein levels were unchanged (Figure 6C).

2.6. Metabolic Effects of Hyperforin in Melanoma Cells

Cancer cells are able to reprogram their metabolism by switching from the mitochondrial oxidative pathway (OXPHOS) to glycolytic anaerobic metabolism and vice versa [59]. The transcription factor hypoxia-inducible factor (HIF)-1α, among others, can control several enzymes regulating metabolic flux [59]. Firstly, we measured the HIF1α expression level after 24 h of HPF treatment. HIF1α protein level was decreased in all melanoma cells (Figure 7). Consistently, some cytosolic enzymes, such as lactate dehydrogenase A (LDHA), phosphoglucomutase 2 (PGM2) and the phosphorylated form of pyruvate kinase M2 (pPKM2) were downregulated (Figure 7).

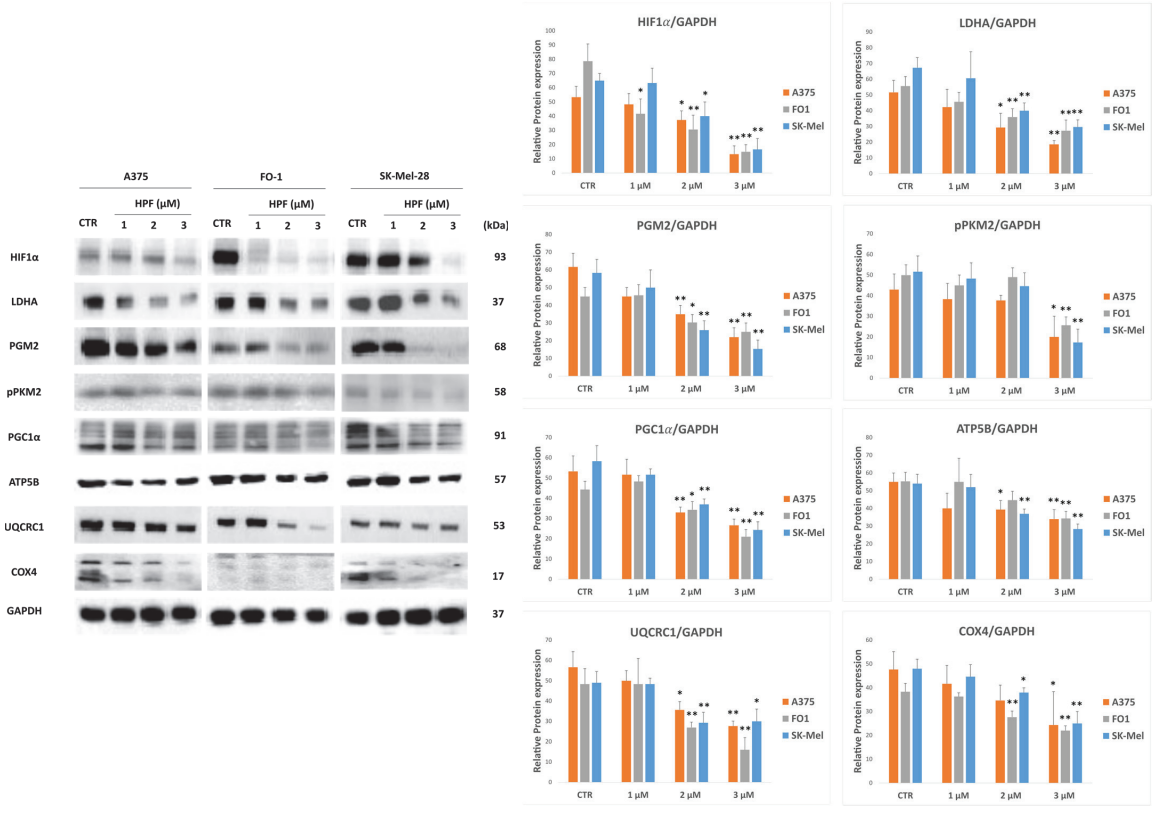

Figure 7. Hyperforin affects the expression levels of key proteins involved in cytosolic and mitochondria metabolic pathways. Represented immunoblots show the expression level of key proteins involved in melanoma cells metabolism after 24 h HPF treatment. In particular, the expression of hypoxia-inducible factor (HIF)-1α, lactate dehydrogenase A (LDHA), phospho-gluco-mutase2 (PGM2), the phosphorylated form of pyruvate kinase M2 (pPKM2), peroxisome proliferator-activated receptor-gamma coactivator (PGC)-1α, c1 subunit of the ubiquinol cytochrome c reductase (UQCRC1), ATP synthase F1 subunit β (ATP5B), cytochrome c oxidase subunit IV (COX4) and GAPDH. On the right, histograms represent the mean values ± S.D. of protein expression levels measured by densitometry deriving from three independent experiments and normalized. All comparisons were performed vs. each control sample after data normalization; * $p < 0.05$; ** $p < 0.01$.

Thus, expression levels of mitochondrial key proteins were measured. The expression level of peroxisome proliferator-activated receptor-gamma coactivator (PGC)-1α, which is a transcription factor stimulating mitochondria biogenesis, was decreased after 24 h treatment with HPF, as well as the expression of c1 subunit of the ubiquinol cytochrome c reductase (UQCRC1) and ATP synthase F1 subunit β (ATP5B). The protein level of the cytochrome c oxidase subunit IV (COX4) was increased 30 min after HPF addition (not shown), but its expression decreased after 24 h (Figure 7).

In summary, the expression levels of proteins regulating both cytosolic and mitochondrial metabolism are lowered by HPF treatment in all melanoma cells.

2.7. Hyperforin Affects the Rate of Cell Migration of FO-1 and SK-Mel-28 Melanoma Cells and It Hinders the Ability of Melanoma Cells to Form Colonies in Soft Agar

The wound healing assay is widely used to measure cell migration. The method is based on quantifying the rate at which cells can close an artificial scratch created in a confluent cell monolayer.

Figure 8 shows the ability of 2 and 3 μM HPF to slow down the migration rate of FO-1 and SK-Mel-28 melanoma cells. Instead, HPF did not delay the wound healing closure of the A375 cell line, although it decreased the density of cells filling the wound in comparison with the untreated sample (Figure 8).

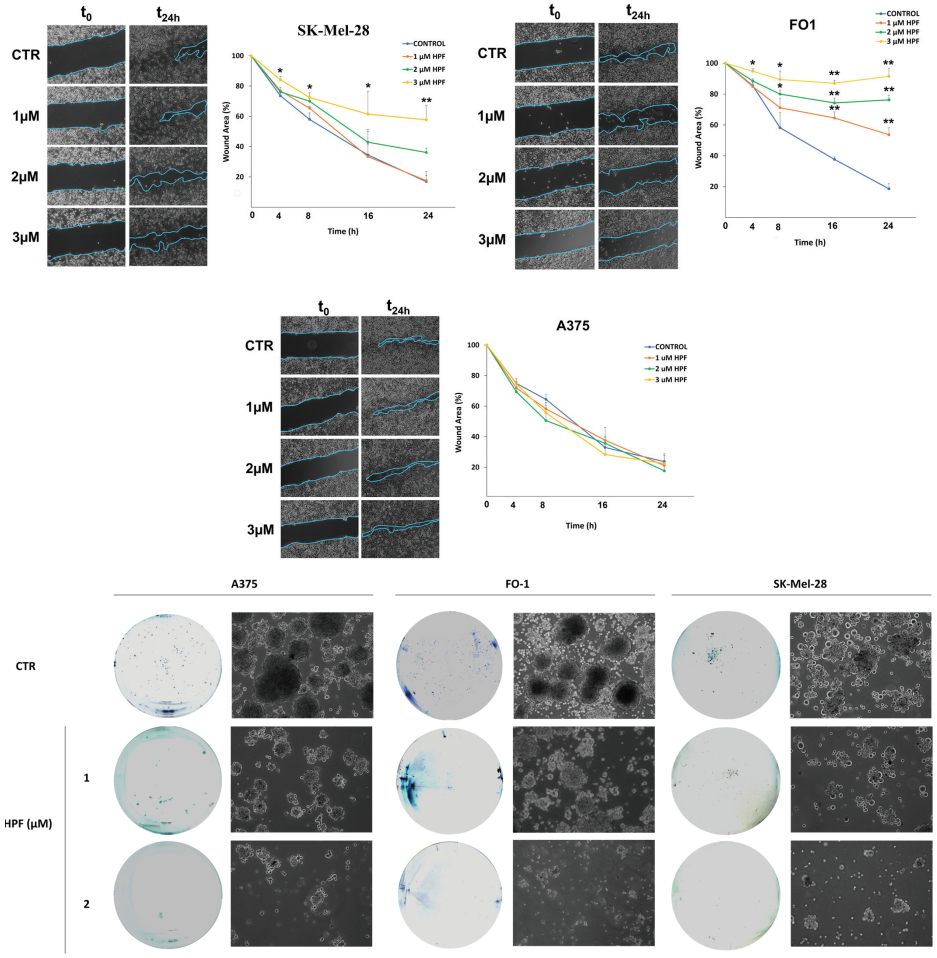

Figure 8. Hyperforin concentration dependently affects cell mobility and inhibits soft agar colony formation in melanoma cell lines. **Top**, wound healing assay attesting the inhibition of cell mobility by 2 and 3 μM HPF in FO-1 and SK-Mel-28 melanoma cells but not in A375 cell line. Images were recorded with an inverted microscope (Axio Vert A1, Zeiss, Oberkochen, Germany). The images were analyzed quantitatively using ImageJ computing software (NIH Image, Bethesda, MD, USA). **Bottom**, images of colonies taken from representative experiments of colonies formed in soft agar. Representative images showing growth and density of colonies were taken by an inverted microscope (5× magnification). * $p < 0.05$; ** $p < 0.01$.

To investigate if HPF can inhibit melanoma cell growth in an anchorage-independent manner, a soft agar colony formation assay was performed. Both 1 and 2 μM HPF can decrease the number and dimension of colonies formed in soft agar after 14–21 days of culture (Figure 8).

3. Discussion

HPF is the principal and active component of SJW extract, commonly used as an antidepressant medicament by many people around the world. In addition to this proven effect, SJW extract and HPF display additional beneficial properties including anti-inflammatory, antimicrobic and antitumor activities (reviewed by [19,20,55]). The large HPF bioavailability, the persistence of its protective benefits and the absence of adverse effects makes this compound suitable for both tumor prevention [25,60] and treatment [55].

Among the studies that investigate the antitumor activity of HPF, its mechanism of action on melanoma cells is poorly documented. Melanoma is still a high-mortality tumor type and the therapies currently available are not conclusive [38]. Therefore, we investigated HPF effects on three melanoma cell lines harboring the dangerous but frequent mutation in the BRAF gene, which makes downstream proliferative signaling pathways constitutively active [38,40]. The HPF antimelanoma activity was also documented on a BRAF wild-type but P53-mutated MeWo melanoma cell line.

Independently of their mutations, all melanoma cell lines tested were very responsive to the damaging effects of HPF, as their viability was affected by EC50% HPF concentrations in the range of 2–4 μM (Figure 1), lower than those previously registered in many other non-melanoma tumor cells [26,34–36,56]. Subsequently, we investigated the mechanism of HPF antimelanoma activity on the three BRAF-mutated cell lines.

In A375, FO-1 and SK-Mel-28 cells, HPF displays cytostatic activity hindering cell cycle progression, as demonstrated by the lower BrdU incorporation in comparison with untreated control cells (Figure 3A). HPF seems to move towards several targets in the cell cycle because it turns out to be able to decrease cyclins D1 and A2 and CDK4 protein expression (Figure 3B). These results are in line with the findings of Liu et al. [34], who registered a suppression of cyclin D1 expression in a human bladder cancer cell line. It is very significant that the activation of the cyclin D1/CDK4 complex passes through the G1/S checkpoint by triggering hyperphosphorylation of the Rb protein [43]. Notably, pRb expression level is concentration-dependently decreased by HPF, despite a stable total Rb protein level (Figure 3B), suggesting an early blockage of the cell cycle. In addition, HPF inhibits the expression of cyclin A2 that acts downstream of the G1/S checkpoint. At the same time HPF, driving a maximal induction of P21/Waf1 expression, would provide for a generalized blockage of all the phases of the cell cycle, since P21 can inhibit, in addition to the cyclin D1/CDK4 complex, the activity of cyclin E/CDK2, cyclin A2/CDK2 and cyclin B/CDK1 complexes [45]. P21 expression can be elicited in a P53-dependent or independent manner [46]. We found, indeed, a concomitant increase of P53 phosphorylation level in A375 and SK-Mel-28 but not in FO-1 melanoma cells. The activation of AMPK by phosphorylation, as we showed in Figure 4, can also participate in P21 induction, as previously reported by Ma et al. and Petti et al. [61,62].

In addition to cell cycle arrest, HPF induces a cytotoxic effect in melanoma cell lines, visible through cellular morphology analysis which highlighted several signs of cell death at both 24 and 48 h after treatment (Figure 2). Immunoblots showed a concentration-dependent increase of the cleaved PARP1 band and a concomitant decrease of its full-length band, in all BRAF-mutated melanoma cell lines (Figure 4). This evident marker of apoptotic cell death was accompanied by a decrease in expression levels of the antiapoptotic proteins Bcl2 and Bcl-xL (Figure 4). Many other authors reported that apoptosis is induced by HPF in different tumor types, with mechanisms involving other pro- or antiapoptotic effector proteins [29,30,32,56], or by mediating the Bcl2/Bcl-xL axis [63,64].

We also showed autophagic cell death, the marker of which, LC3B, was affected by HPF treatment (Figure 4). This result is in line with both the increase of AMPK phosphorylation

(Figure 4), an autophagy activator, and with data reported by Wiechmann et al., obtained in HL60 leukemic cells [28]. In a non-tumor context, HPF was recently reported to trigger thermogenesis in adipose tissue by activating autophagy via AMPK [51]. Notably, activated AMPK can inhibit the mechanistic target of the rapamycin (mTOR) complex, blocking the phosphorylation of its downstream substrate 4E-BP1, leading to protein synthesis repression [65]. Indeed, we found a hypo-phosphorylated 4E-BP1, which is unable to promote protein synthesis (Figure 4).

One novelty is the possible involvement of another form of regulated cell death, called ferroptosis, characterized by lipid peroxidation induced mainly by free iron. The principal molecular maker of ferroptosis is the antioxidant enzyme GPX4, whose depletion allows death process. Indeed, GPX4 knockdown triggers cell death accompanied by lipid peroxidation [53,54]. Treatment with HPF for 24 h decreased GPX4 expression level in a concentration-dependent manner (Figure 4). Although the involvement of ferroptosis needs further investigation, we could hypothesize that, after HPF-elicited depolarization of the mitochondrial inner membrane triggered by its activity as a protonophore, mitophagy/autophagy can be induced to remove injured mitochondria. Mitophagy/autophagy is reported to increase free iron through ferritin degradation, subsequently eliciting ferroptosis [66]. Indeed, the knockdown of ATG5, which is indispensable for autophagy, inhibits ferroptosis as well [54,66]. In this manner, autophagy and ferroptosis can both be induced in the same cell. Data suggest that HPF induces not only apoptosis but also other regulated cell deaths, such as autophagy and ferroptosis, with a mechanism that will be deeply investigated in the future.

For its extreme lipophilicity (XlogP 9.6), HPF does not need any membrane receptor to enter cells. Nevertheless, we considered the possibility that HPF's antitumor effect could depend on the binding and subsequent activation of the TRPC6 Ca^{++} channel, as previously reported by other authors [2–4]. The co-presence of Ca^{++} channel inhibitor SKF was not able to hinder the cytotoxic effects of HPF (Figure 5). In addition, TRPC6 expression level was not affected by HPF, both at early and late times of treatment (Figure 6). TRPC6 is a channel that allows Ca^{++} entry in cells. As reported by Shekhar et al. [67], the transcription factor CREB is a calcium sensor that can be activated by phosphorylation on its Ser133. Effectively, pCREB expression was increased by HPF in a concentration-dependent manner, whereas the expression of total CREB was unchanged or even decreased (Figure 6). These data are consistent with an HPF Ca^{++} dependence in our cell models, although these events do not hinder the antimelanoma effects of this natural compound. Recently, Scheuble et al. [68] reported that HPF stimulates the activity of the transcription factor AP1 via TRPC6. Indeed, in all melanoma cell lines, two components of AP1 complex, FRA1 and the phosphorylated and active form of cJun (pcJun), increased their expression at early times after HPF administration (Figure 6). Subsequently, the expression of both FRA1 and pcJun were strongly decreased (Figure 6), suggesting that the activation occurred but was transient.

Cytosolic concentrations of calcium and zinc can be increased by TRPC6-elicited calcium influx or by releasing them from the mitochondria stores, another recognized property of HPF [5–7]. The co-treatment of HPF with BAPTA and TPEN, able to chelate intracellular Ca^{++} and Zn^{++}, respectively, did not hinder the ability of HPF to affect cell viability (Figure 5).

Thus, other signaling pathways have been investigated. The activation of kinases ERK1/2 and AKT is very important for allowing a high rate of cell proliferation, especially in BRAF-mutated melanoma cells. BRAF- and MEK-inhibitors are highly effective targeted drugs in melanoma therapy, but they can induce drug resistance both in vitro and in patients [41]. As expected, A375, FO-1 and SK-Mel-28 cell lines showed activated pro-survival kinases ERK1/2 and AKT in control cells. In contrast with data obtained in other tumor cells [30,56], HPF cannot decrease the activity of these kinases, at least not with 24 h of treatment (Figure 6). The exception is the FO-1 cell line, in which only pERK1/2 expression was decreased.

HPF, instead, can block the activity of two transcription factors involved in the pro-survival signaling pathways NF-κB and STAT3.

We and other authors have previously reported that HPF and SJW extract had the ability to hinder NF-κB activation [33,34,56,69,70]. Many data demonstrate that NF-κB can be a specific target for counteracting melanoma progression [58]. Indeed, BMS-345541, a selective inhibitor of NF-κB, is known to induce an in vitro inhibition of cell proliferation and induction of apoptosis in three melanoma cell lines [71]. Constitutive activation of STAT3 plays a vital role in the development of melanoma [72]. Remarkably, in a melanoma mouse model, the silencing of STAT3 expression can reverse the malignant phenotype [73]. Tyr705 phosphorylation of STAT3 is an activating event since it allows STAT3 translocation into the nucleus. HPF can block STAT3 tyrosine phosphorylation in all the BRAF-mutated melanoma cell lines after 24 h treatment without affecting the total STAT3 protein level (Figure 6). In a cancer context, no data are available in the literature on STAT3 and HPF. Recently, Zhang et al. [74] reported that STAT3 inhibition is involved in the protective mechanism of HPF against psoriasis, and we previously demonstrated that the impediment of STAT3 transcriptional activity, elicited by SJW extract pre-treatment, can protect mice lungs injured by carrageenan [75]. Considering that many activation-signaling pathways converge on STAT3, such as EGFR, vascular endothelial growth factor, interleukin 6, focal adhesion kinase, proto-oncogene tyrosine kinase Src and others, we can state that STAT3 is an important target in melanoma therapy, and its blockage by HPF could be a crucial event among all the effects triggered by this natural compound.

Since HPF has been reported to affect mitochondrial membrane potential by acting as a protonophore [9], we investigated its effect on the expression of mitochondrial enzymes of the electron transport chain and of some enzymes belonging to the glucose metabolic pathway.

PGC1α is a transcription factor activating mitochondria biogenesis, but its expression is significantly reduced in the presence of HPF (Figure 7). The expression level of several key members of internal mitochondrial membrane functional complexes is similarly lowered, such as complex III (UQCRC1) and complex IV (COX4) components and the subunit β of ATP synthase (ATP5B) (Figure 7). All data are also in line with a possible dysfunction of the electron transport chain and the oxidative phosphorylation. Remarkably, the intrinsic apoptotic pathway is triggered by mitochondria membrane permeabilization. Moreover, in cells treated with HPF, studies that measured both apoptosis activity and mitochondrial membrane potential found a negative correlation among them [26,28,30,32,63]. The low expression levels of mitochondrial membrane functional proteins could be part of a general mechanism by which HPF leads to a drop in mitochondrial potential and functionality.

Despite the activation of AMPK, some cytosolic enzymes of glucose metabolism decreased their expression with the HPF treatment. LDHA, PGM2 and the phosphorylated form of pyruvate kinase M2, the level of which is high in tumor cells, are all less expressed (Figure 7). Indeed, the expression of HIF1α, a master activator of glucose metabolism, is strongly inhibited by HPF (Figure 7).

Finally, a wound healing assay and colony formation in soft agar demonstrated the ability of HPF to reduce cell mobility and colony growth in melanoma cell lines (Figure 8). This could suggest that HPF is able to counteract the metastatic potential of melanoma cells, as has been reported for other tumor cells [36,76,77].

4. Materials and Methods

4.1. Cell Cultures

A375 (CRL-1619) and FO1 (CRL-12177) melanoma cell lines (ATCC, Manassas, VA, USA) were cultured at 37 °C in a humidified atmosphere of 5% CO_2, in the presence of high glucose Dulbecco's modified Eagle Medium (DMEM, Gibco, BRL Invitrogen Corp., Carlsbad, CA, USA), supplemented with 10% heat-inactivated fetal bovine serum (FBS; Gibco, BRL Invitrogen Corp., Carlsbad, CA, USA) and with 1% antibiotic antimycotic solution (Gibco, BRL Invitrogen Corp., Carlsbad, CA, USA).

SK-Mel-28 (HTB-72), MeWo (HTB-65) melanoma cell lines and normal human epidermal melanocytes (NHEM, PCS-200-013) (ATCC, Manassas, VA, USA) were grown in Roswell Park Memorial Institute 1640 medium (RPMI-1640, Gibco, BRL Invitrogen Corp., Carlsbad, CA, USA) under the previously described conditions.

4.2. Melanoma Cell Treatments

Hyperforin-DCHA (*AG-CN2-0008*, AdipoGen Life Sciences, Fuellinsdorf, Switzerland) was dissolved in 100% dimethyl sulfoxide at a concentration of 5 mM. Many aliquots of the stock solution were stored at −20 °C, protected from the light. Cell lines were treated with different HPF concentrations (range 0.5–10 μM). At the end of each treatment, different types of assays were performed. Images of cells after 24 or 48 h of treatments were captured at 20× magnification with an inverted microscope (Axio Vert A1, Zeiss, Oberkochen, Germany). The TRPC6 Ca^{++} channel blocker, SKF 96,365 (CAY-10009312, Cayman Chemical, Ann Arbor, MI, USA) was used, as well as the chelators of Ca^{++} and Zn^{++}, respectively, BAPTA-AM (CDX-B0285, Biomol, Hamburg, Germany) and N,N,N,N,-tetrakis(2-pyridylmethyl) (TPEN) (Sigma-Merck, Milan, Italy).

4.3. Cell Viability Assay

A375, FO1, SK-Mel-28 and NHEM cells were seeded in 96-well plates (A375: 3.0×10^3 cells/well; FO1, SK-Mel-28, MeWo and NHEM: 6.0×10^3 cells/well). After 24 h, cells were treated with different concentrations of HPF and incubated for 24, 48 and 72 h. At the end of each treatment, cells were fixed by adding 25 μL/well of 50% (w/v) trichloroacetic acid directly into the culture medium. Plates were incubated at 4 °C for 1 h, washed 4 times with ddH_2O and dried at room temperature (RT). Staining was performed by adding 50 μL/well of 0.04% (w/v) sulforhodamine B (SRB) sodium salt solution (Sigma-Aldrich, Milan, Italy). After 1 h incubation at RT, plates were rinsed with 1% acetic acid and air-dried. SRB was solubilized in 10 mM Tris base solution, pH 10.5 and Abs 540 nm, measured in the plate reader TECAN NanoQuant Infinite M200 Pro (Tecan Group Ltd., Männedorf, Switzerland). Six replicates for each condition/data point were performed.

4.4. Br-deoxy-Uridine Cell Proliferation Assay

Cell proliferation was assessed with a colorimetric immunoassay based on the measurement of Br-deoxy-uridine (BrdU) incorporation during DNA synthesis. A375, FO1 and SK-Mel-28 cells were cultured in a 96-well plate as previously described, and after 24 h, incubated with or without HPF. After 48 h of treatment, the cells were incubated for 8 h with BrdU labelling solution (BrdU Cell Proliferation Kit, Roche, Merck, Milan, Italy), and then fixed with 200 μL/well of fix/denaturing solution for 30 min at RT. After washing 3 times, the peroxidase goat anti-mouse IgG conjugate was added, and the plate was incubated for 90 min at RT. Three washes were performed again, then 100 μL/well of TMB peroxidase substrate solution was added and plates were incubated at RT until color development was sufficient for photometric detection (5–30 min). Then, the absorbance of the samples was measured at Abs 370 nm (reference wavelength: approx. 492 nm) in a Tecan NanoQuant Infinite M200 Pro plate reader (Tecan Group Ltd., Männedorf, Switzerland). After many measurements at various time points (e.g., 5, 10 and 20 min), the reaction was stopped with 25 μL/well of 1 M H_2SO_4 and was measured in a plate reader at 450 nm (reference wavelength: 690 nm).

4.5. Total Protein Extracts

Cells were seeded in 6 cm Petri dishes (A375: 150×10^3 cells/dish; FO1 and SK-Mel-28: 300×10^3 cells/dish). After 24 h, cells were treated or not treated with increasing concentrations of HPF, alone or in presence of SKF, BAPTA and TPEN inhibitors. After 2 and 24 h of treatment, cells were scraped using warm 1× sample buffer (2% SDS, 10% glycerol, 50 mM Tris-HCl, 1.75% β-mercaptoethanol and bromophenol blue) and boiled at 99 °C for 10 min. Total protein extracts were kept at −80 °C until use.

4.6. Western Blot Analysis

Protein extracts were electrophoresed in a 10–12% polyacrylamide SDS-PAGE. Proteins were then transferred to a polyvinylidene difluoride membrane (PVDF, Merck-Millipore, Milan, Italy) and membranes were blocked at RT with TBST (10 mM Tris-HCl pH 7.5, 100 mM NaCl, 0.1% Tween 20) containing 5% milk for 1 h. Thereafter, they were incubated on a shaker overnight at 4 °C, with a 5% BSA solution containing the primary antibody against AMPK (#2532, 1:1000), Bcl-2 (#15071, 1:1000), GAPDH (#2118, 1:1000), LDHA (#3582, 1:2000), pACC (Ser79) (#11818, 1:1000), pAKT (Thr308) (#13038, 1:1000), pAMPK (Thr 172) (#2531, 1:1000), pERK (#9101, 1:1000), pP53 (#9286, 1:1000), pP65-NF-κB (Ser 536) (#3033, 1:1000), pRb (#8516, 1:2000), Rb (#9309, 1:2000), pSTAT3 (#9145, 1:2000) (Cell Signaling Technology, Danvers, MA, USA); AKT (GTX121937, 1:4000), ATP5B (GTX132925, 1:3000), CDK4 (GTX102993, 1:3000), COX4 (GTX114330, 1:3000), CREB (GTX112846, 1:3000), Cyclin A2 (GTX103042, 1:3000), Cyclin D1 (GTX108624, 1:10000), ERK1/2 (GTX134462, 1:10000), FRA1 (GTX134242, 1:4000), HIF1α (GTX127309, 1:3000), LC3B (GTX127375, 1:2000), P21/Waf1 (GTX629543, 1:3000), p4EBP1 (GTX133181, 1:6000), 4EBP1 (GTX116315, 1: 4000), P65-NF-κB (GTX102090, 1:3000), PARP1 (GTX628836, 1:3000), pcJun (GTX133873, 1:3000), pCREB (GTX130379, 1:3000), PGM2 (GTX119168, 1:3000), pPKM2 (GTX133886, 1:3000), STAT3 (GTX104616, 1:3000), TRPC6 (GTX113859, 1:3000), UQCRC1 (GTX630393, 1:1000) (Genetex, Alton Parkway, Irvine, CA, USA); GPX4 (67763-1, 1:3000) (Proteintech, Manchester, UK); P53 (sc-263, 1:3000) (Santa Cruz Biotechnology, Dallas, TX, USA); PGC1α (PA5-38022, 1:1000) (Invitrogen, Thermo Scientific, Waltham, MA, USA); and Bcl-xL (ab77571, 1:1000) (Abcam, Cambridge, UK). Then, membranes were washed 3 times with TBST buffer for 30 min and incubated for 1 h with a horseradish peroxidase-conjugated secondary antibody (anti-rabbit or anti-mouse, 1:6000-1:4000, Cell Signaling Technology, Danvers, MA, USA). Membranes were washed again 3 times for 30 min with TBST buffer. The expression of each protein was normalized with GAPDH protein level unless otherwise stated. Immuno-detection was carried out with an ECL kit (Merck-Millipore, Milan, Italy) and the chemiluminescence signals were visualized with ChemiDoc (Bio-Rad, Hercules, CA, USA).

4.7. Wound-Closure Cell Migration Assay

A375, FO1 and SK-Mel-28 cell migration was assessed by performing the wound-closure cell migration assay also known as a scratch test. Cells were seeded in a 12-well plate (A375: 150×10^3 cells/well, FO1 and SK-Mel-28: 4×10^5 cells/well). Once the cells had reached confluence, the wells were washed twice with PBS and once with complete medium. Then, the monolayers were scratched with a sterile pipette tip. To remove detached cells, wells were washed with a complete medium and refilled with fresh complete medium with or without HPF added. The cells were incubated for 24 h at 37 °C, in a humidified atmosphere with 5% CO_2. Images of cell movement were captured every 4 h using an inverted microscope (Axio Vert A1, Zeiss, Oberkochen, Germany). The acquired images were further quantitatively analyzed by using ImageJ computing software, MRI Wound Healing Tool.

4.8. Colony Formation Assay in Soft Agar

Anchorage-independent growth of A375, FO-1 and SK-Mel-28 melanoma cells was analyzed by colony formation in soft agar, as previously described [78]. Firstly, the bottom layer of 6 well-plates was filled with 1% low gelling temperature agarose (Sigma-Merck, Milan, Italy) dissolved in 2× DMEM, 20% FBS and 2% antibiotic, antimycotic solution. Thereafter, 0.6% low gelling temperature agarose dissolved in 2× DMEM, 20% FBS and 2% antibiotic, antimycotic solution, together with treated or not-treated cells (5000 cells/well) was placed over the 1% agarose layer. An amount of 100 µL–200 µL of fresh media were added to every well twice a week. After 15–21 days, the cell colonies that were formed were observed under an inverted microscope (Axio Vert A1, Zeiss, Oberkochen, Germany).

4.9. Statistics

All the results are reported as a mean value ± standard deviation (S.D.). Differences were analyzed with GraphPad Prism statistical program, using an unpaired, two-tailed Student's *t*-test. A *p*-value less than 0.05 (*) or less than 0.01 (**) was considered to be statistically significant. For each type of experiment, a minimum of 3 independent biological replicates were performed. The normal distribution of data was tested using the Shapiro–Wilk test.

5. Conclusions

In conclusion, HPF was shown to be a potent natural compound able to hinder the expression and function of different key proteins involved in pro-survival and pro-metastatic signaling of BRAF-mutated melanoma cells.

This study, far from being comprehensive, aims to provide evidence of pleiotropic effects of this interesting natural compound in highly malignant melanoma cells, in order to identify possible molecular mechanisms that will be studied more thoroughly in the future.

Additionally, an overview of HPF's mechanism of action in melanoma cells can pave the way for further studies to associate HPF with conventional antitumor drugs seeking synergistic effects.

Author Contributions: Conceptualization, M.M.; methodology, M.M.; formal analysis, M.M.; investigation, A.C., V.Z., R.C., F.A., S.S.A. and E.O.; data curation, A.C., V.Z., R.C., F.A. and S.S.A.; writing—original draft preparation, M.M.; writing—review and editing, M.M.; supervision, M.M.; funding acquisition, M.M. All authors have read and agreed to the published version of the manuscript.

Funding: This research received no external funding.

Institutional Review Board Statement: Not applicable.

Informed Consent Statement: Not applicable.

Data Availability Statement: Not applicable.

Conflicts of Interest: The authors declare no conflict of interest.

References

1. Chatterjee, S.S.; Bhattacharya, S.K.; Wonnemann, M.; Singer, A.; Müller, W.E. Hyperforin as a possible antidepressant component of hypericum extracts. *Life Sci.* **1998**, *63*, 499–510. [CrossRef]
2. Leuner, K.; Kazanski, V.; Müller, M.; Essin, K.; Henke, B.; Gollasch, M.; Harteneck, C.; Müller, W.E. Hyperforin—A key constituent of St. John's wort specifically activates TRPC6 channels. *FASEB J.* **2007**, *21*, 4101–4111. [CrossRef]
3. Müller, M.; Essin, K.; Hill, K.; Beschmann, H.; Rubant, S.; Schempp, C.M.; Gollasch, M.; Boehncke, W.H.; Harteneck, C.; Müller, W.E.; et al. Specific TRPC6 channel activation, a novel approach to stimulate keratinocyte differentiation. *J. Biol. Chem.* **2008**, *283*, 33942–33954. [CrossRef]
4. Freeman, H. Psychiatry in the National Health Service 1948-1998. *Br. J. Psychiatry J. Ment. Sci.* **1999**, *175*, 3–11. [CrossRef]
5. Tu, P.; Gibon, J.; Bouron, A. The TRPC6 channel activator hyperforin induces the release of zinc and calcium from mitochondria. *J. Neurochem.* **2010**, *112*, 204–213. [CrossRef]
6. Gibon, J.; Richaud, P.; Bouron, A. Hyperforin changes the zinc-storage capacities of brain cells. *Neuropharmacology* **2011**, *61*, 1321–1326. [CrossRef]
7. Gibon, J.; Deloulme, J.-C.; Chevallier, T.; Ladevèze, E.; Abrous, D.N.; Bouron, A. The antidepressant hyperforin increases the phosphorylation of CREB and the expression of TrkB in a tissue-specific manner. *Int. J. Neuropsychopharmacol.* **2013**, *16*, 189–198. [CrossRef]
8. Froestl, B.; Steiner, B.; Müller, W.E. Enhancement of proteolytic processing of the beta-amyloid precursor protein by hyperforin. *Biochem. Pharmacol.* **2003**, *66*, 2177–2184. [CrossRef]
9. Sell, T.S.; Belkacemi, T.; Flockerzi, V.; Beck, A. Protonophore properties of hyperforin are essential for its pharmacological activity. *Sci. Rep.* **2014**, *4*, 7500. [CrossRef]
10. Friedland, K.; Harteneck, C. Hyperforin: To Be or Not to Be an Activator of TRPC(6). In *Reviews of Physiology, Biochemistry and Pharmacology*; Nilius, B., Gudermann, T., Jahn, R., Lill, R., Petersen, O.H., de Tombe, P.P., Eds.; Springer International Publishing: Cham, Switzerland, 2015; Volume 169, pp. 1–24. ISBN 978-3-319-26563-6.
11. Albert, D.; Zündorf, I.; Dingermann, T.; Müller, W.E.; Steinhilber, D.; Werz, O. Hyperforin is a dual inhibitor of cyclooxygenase-1 and 5-lipoxygenase. *Biochem. Pharmacol.* **2002**, *64*, 1767–1775. [CrossRef]

12. Koeberle, A.; Rossi, A.; Bauer, J.; Dehm, F.; Verotta, L.; Northoff, H.; Sautebin, L.; Werz, O. Hyperforin, an Anti-Inflammatory Constituent from St. John's Wort, Inhibits Microsomal Prostaglandin E(2) Synthase-1 and Suppresses Prostaglandin E(2) Formation in vivo. *Front. Pharmacol.* **2011**, *2*, 7. [CrossRef]
13. Schempp, C.M.; Pelz, K.; Wittmer, A.; Schöpf, E.; Simon, J.C. Antibacterial activity of hyperforin from St John's wort, against multiresistant Staphylococcus aureus and gram-positive bacteria. *Lancet Lond. Engl.* **1999**, *353*, 2129. [CrossRef]
14. Krusekopf, S.; Roots, I. St. John's wort and its constituent hyperforin concordantly regulate expression of genes encoding enzymes involved in basic cellular pathways. *Pharmacogenet. Genom.* **2005**, *15*, 817–829. [CrossRef]
15. Thiel, G.; Rössler, O.G. Hyperforin activates gene transcription involving transient receptor potential C6 channels. *Biochem. Pharmacol.* **2017**, *129*, 96–107. [CrossRef]
16. Novelli, M.; Beffy, P.; Menegazzi, M.; De Tata, V.; Martino, L.; Sgarbossa, A.; Porozov, S.; Pippa, A.; Masini, M.; Marchetti, P.; et al. St. John's wort extract and hyperforin protect rat and human pancreatic islets against cytokine toxicity. *Acta Diabetol.* **2014**, *51*, 113–121. [CrossRef]
17. Novelli, M.; Menegazzi, M.; Beffy, P.; Porozov, S.; Gregorelli, A.; Giacopelli, D.; De Tata, V.; Masiello, P. St. John's wort extract and hyperforin inhibit multiple phosphorylation steps of cytokine signaling and prevent inflammatory and apoptotic gene induction in pancreatic β cells. *Int. J. Biochem. Cell Biol.* **2016**, *81*, 92–104. [CrossRef]
18. Novelli, M.; Beffy, P.; Gregorelli, A.; Porozov, S.; Mascia, F.; Vantaggiato, C.; Masiello, P.; Menegazzi, M. Persistence of STAT-1 inhibition and induction of cytokine resistance in pancreatic β cells treated with St John's wort and its component hyperforin. *J. Pharm. Pharmacol.* **2019**, *71*, 93–103. [CrossRef]
19. Novelli, M.; Masiello, P.; Beffy, P.; Menegazzi, M. Protective Role of St. John's Wort and Its Components Hyperforin and Hypericin against Diabetes through Inhibition of Inflammatory Signaling: Evidence from In Vitro and In Vivo Studies. *Int. J. Mol. Sci.* **2020**, *21*, 8108. [CrossRef]
20. Li, X.-X.; Yan, Y.; Zhang, J.; Ding, K.; Xia, C.-Y.; Pan, X.-G.; Shi, Y.-J.; Xu, J.-K.; He, J.; Zhang, W.-K. Hyperforin: A natural lead compound with multiple pharmacological activities. *Phytochemistry* **2022**, *206*, 113526. [CrossRef]
21. Di Paola, R.; Mazzon, E.; Muià, C.; Crisafulli, C.; Genovese, T.; Di Bella, P.; Esposito, E.; Menegazzi, M.; Meli, R.; Suzuki, H.; et al. Protective effect of Hypericum perforatum in zymosan-induced multiple organ dysfunction syndrome: Relationship to its inhibitory effect on nitric oxide production and its peroxynitrite scavenging activity. *Nitric Oxide Biol. Chem.* **2007**, *16*, 118–130. [CrossRef] [PubMed]
22. Dost, T.; Ozkayran, H.; Gokalp, F.; Yenisey, C.; Birincioglu, M. The effect of Hypericum perforatum (St. John's Wort) on experimental colitis in rat. *Dig. Dis. Sci.* **2009**, *54*, 1214–1221. [CrossRef]
23. Zdunić, G.; Godevac, D.; Milenković, M.; Vucićević, D.; Savikin, K.; Menković, N.; Petrović, S. Evaluation of Hypericum perforatum oil extracts for an antiinflammatory and gastroprotective activity in rats. *Phytother. Res. PTR* **2009**, *23*, 1559–1564. [CrossRef]
24. Manna, S.K.; Golla, S.; Golla, J.P.; Tanaka, N.; Cai, Y.; Takahashi, S.; Krausz, K.W.; Matsubara, T.; Korboukh, I.; Gonzalez, F.J. St. John's Wort Attenuates Colorectal Carcinogenesis in Mice through Suppression of Inflammatory Signaling. *Cancer Prev. Res.* **2015**, *8*, 786–795. [CrossRef] [PubMed]
25. Satia, J.A.; Littman, A.; Slatore, C.G.; Galanko, J.A.; White, E. Associations of herbal and specialty supplements with lung and colorectal cancer risk in the VITamins and Lifestyle study. *Cancer Epidemiol. Biomark. Prev.* **2009**, *18*, 1419–1428. [CrossRef]
26. Schempp, C.M.; Kirkin, V.; Simon-Haarhaus, B.; Kersten, A.; Kiss, J.; Termeer, C.C.; Gilb, B.; Kaufmann, T.; Borner, C.; Sleeman, J.P.; et al. Inhibition of tumour cell growth by hyperforin, a novel anticancer drug from St. John's wort that acts by induction of apoptosis. *Oncogene* **2002**, *21*, 1242–1250. [CrossRef]
27. Allegra, A.; Tonacci, A.; Spagnolo, E.V.; Musolino, C.; Gangemi, S. Antiproliferative Effects of St. John's Wort, Its Derivatives, and Other Hypericum Species in Hematologic Malignancies. *Int. J. Mol. Sci.* **2020**, *22*, 146. [CrossRef]
28. Wiechmann, K.; Müller, H.; Fischer, D.; Jauch, J.; Werz, O. The acylphloroglucinols hyperforin and myrtucommulone A cause mitochondrial dysfunctions in leukemic cells by direct interference with mitochondria. *Apoptosis Int. J. Program. Cell Death* **2015**, *20*, 1508–1517. [CrossRef] [PubMed]
29. Zaher, M.; Tang, R.; Bombarda, I.; Merhi, F.; Bauvois, B.; Billard, C. Hyperforin induces apoptosis of chronic lymphocytic leukemia cells through upregulation of the BH3-only protein Noxa. *Int. J. Oncol.* **2012**, *40*, 269–276. [CrossRef]
30. Merhi, F.; Tang, R.; Piedfer, M.; Mathieu, J.; Bombarda, I.; Zaher, M.; Kolb, J.-P.; Billard, C.; Bauvois, B. Hyperforin inhibits Akt1 kinase activity and promotes caspase-mediated apoptosis involving Bad and Noxa activation in human myeloid tumor cells. *PLoS ONE* **2011**, *6*, e25963. [CrossRef]
31. Hsu, S. Compounds Derived from Epigallocatechin-3-Gallate (EGCG) as a Novel Approach to the Prevention of Viral Infections. *Inflamm. Allergy Drug Targets* **2015**, *14*, 13–18. [CrossRef]
32. Chiang, I.-T.; Chen, W.-T.; Tseng, C.-W.; Chen, Y.-C.; Kuo, Y.-C.; Chen, B.-J.; Weng, M.-C.; Lin, H.-J.; Wang, W.-S. Hyperforin Inhibits Cell Growth by Inducing Intrinsic and Extrinsic Apoptotic Pathways in Hepatocellular Carcinoma Cells. *Anticancer Res.* **2017**, *37*, 161–167. [CrossRef] [PubMed]
33. Chen, W.-T.; Chen, Y.-K.; Lin, S.-S.; Hsu, F.-T. Hyperforin Suppresses Tumor Growth and NF-κB-mediated Anti-apoptotic and Invasive Potential of Non-small Cell Lung Cancer. *Anticancer Res.* **2018**, *38*, 2161–2167. [CrossRef]

34. Liu, Y.-C.; Lin, K.-H.; Hsieh, J.-H.; Chung, J.-G.; Tan, Z.-L.; Hsu, F.-T.; Chiang, C.-H. Hyperforin Induces Apoptosis Through Extrinsic/Intrinsic Pathways and Inhibits NF-κB-modulated Survival and Invasion Potential in Bladder Cancer. *Vivo Athens Greece* **2019**, *33*, 1865–1877. [CrossRef]
35. Knauthe, A.; Mittag, S.; Bloch, L.; Albring, K.F.; Schmidt, M.; Werz, O.; Huber, O. Hyperforin and Myrtucommulone Derivatives Act as Natural Modulators of Wnt/β-Catenin Signaling in HCT116 Colon Cancer Cells. *Int. J. Mol. Sci.* **2022**, *23*, 2984. [CrossRef] [PubMed]
36. Donà, M.; Dell'Aica, I.; Pezzato, E.; Sartor, L.; Calabrese, F.; Della Barbera, M.; Donella-Deana, A.; Appendino, G.; Borsarini, A.; Caniato, R.; et al. Hyperforin inhibits cancer invasion and metastasis. *Cancer Res.* **2004**, *64*, 6225–6232. [CrossRef]
37. Sun, F.; Liu, J.-Y.; He, F.; Liu, Z.; Wang, R.; Wang, D.-M.; Wang, Y.-F.; Yang, D.-P. In-vitro antitumor activity evaluation of hyperforin derivatives. *J. Asian Nat. Prod. Res.* **2011**, *13*, 688–699. [CrossRef]
38. Sabag, N.; Yakobson, A.; Retchkiman, M.; Silberstein, E. Novel Biomarkers and Therapeutic Targets for Melanoma. *Int. J. Mol. Sci.* **2022**, *23*, 11656. [CrossRef]
39. Ny, L.; Hernberg, M.; Nyakas, M.; Koivunen, J.; Oddershede, L.; Yoon, M.; Wang, X.; Guyot, P.; Geisler, J. BRAF mutational status as a prognostic marker for survival in malignant melanoma: A systematic review and meta-analysis. *Acta Oncol. Stockh. Swed.* **2020**, *59*, 833–844. [CrossRef]
40. Dhillon, S. Dabrafenib plus Trametinib: A Review in Advanced Melanoma with a BRAF (V600) Mutation. *Target. Oncol.* **2016**, *11*, 417–428. [CrossRef]
41. Pizzimenti, S.; Ribero, S.; Cucci, M.A.; Grattarola, M.; Monge, C.; Dianzani, C.; Barrera, G.; Muzio, G. Oxidative Stress-Related Mechanisms in Melanoma and in the Acquired Resistance to Targeted Therapies. *Antioxidants* **2021**, *10*, 1942. [CrossRef] [PubMed]
42. Yadav, V.; Chen, S.-H.; Yue, Y.G.; Buchanan, S.; Beckmann, R.P.; Peng, S.-B. Co-targeting BRAF and cyclin dependent kinases 4/6 for BRAF mutant cancers. *Pharmacol. Ther.* **2015**, *149*, 139–149. [CrossRef]
43. Giacinti, C.; Giordano, A. RB and cell cycle progression. *Oncogene* **2006**, *25*, 5220–5227. [CrossRef]
44. Liu, H.; Li, Z.; Huo, S.; Wei, Q.; Ge, L. Induction of G0/G1 phase arrest and apoptosis by CRISPR/Cas9-mediated knockout of CDK2 in A375 melanocytes. *Mol. Clin. Oncol.* **2020**, *12*, 9–14. [CrossRef]
45. Engeland, K. Cell cycle regulation: p53-p21-RB signaling. *Cell Death Differ.* **2022**, *29*, 946–960. [CrossRef]
46. el-Deiry, W.S.; Tokino, T.; Velculescu, V.E.; Levy, D.B.; Parsons, R.; Trent, J.M.; Lin, D.; Mercer, W.E.; Kinzler, K.W.; Vogelstein, B. WAF1, a potential mediator of p53 tumor suppression. *Cell* **1993**, *75*, 817–825. [CrossRef]
47. Pisano, M.; Dettori, M.A.; Fabbri, D.; Delogu, G.; Palmieri, G.; Rozzo, C. Anticancer Activity of Two Novel Hydroxylated Biphenyl Compounds toward Malignant Melanoma Cells. *Int. J. Mol. Sci.* **2021**, *22*, 5636. [CrossRef]
48. Raineri, A.; Fasoli, S.; Campagnari, R.; Gotte, G.; Menegazzi, M. Onconase Restores Cytotoxicity in Dabrafenib-Resistant A375 Human Melanoma Cells and Affects Cell Migration, Invasion and Colony Formation Capability. *Int. J. Mol. Sci.* **2019**, *20*, 5980. [CrossRef]
49. Hartman, M.L.; Czyz, M. Anti-apoptotic proteins on guard of melanoma cell survival. *Cancer Lett.* **2013**, *331*, 24–34. [CrossRef]
50. Lucianò, A.M.; Pérez-Oliva, A.B.; Mulero, V.; Del Bufalo, D. Bcl-xL: A Focus on Melanoma Pathobiology. *Int. J. Mol. Sci.* **2021**, *22*, 2777. [CrossRef]
51. Chen, S.; Liu, X.; Peng, C.; Tan, C.; Sun, H.; Liu, H.; Zhang, Y.; Wu, P.; Cui, C.; Liu, C.; et al. The phytochemical hyperforin triggers thermogenesis in adipose tissue via a Dlat-AMPK signaling axis to curb obesity. *Cell Metab.* **2021**, *33*, 565–580. [CrossRef]
52. Jin, J.; Chen, N.; Pan, H.; Xie, W.; Xu, H.; Lei, S.; Guo, Z.; Ding, R.; He, Y.; Gao, J. Triclosan induces ROS-dependent cell death and autophagy in A375 melanoma cells. *Oncol. Lett.* **2020**, *20*, 73. [CrossRef] [PubMed]
53. Yang, W.S.; SriRamaratnam, R.; Welsch, M.E.; Shimada, K.; Skouta, R.; Viswanathan, V.S.; Cheah, J.H.; Clemons, P.A.; Shamji, A.F.; Clish, C.B.; et al. Regulation of ferroptotic cancer cell death by GPX4. *Cell* **2014**, *156*, 317–331. [CrossRef] [PubMed]
54. Basit, F.; van Oppen, L.M.; Schöckel, L.; Bossenbroek, H.M.; van Emst-de Vries, S.E.; Hermeling, J.C.; Grefte, S.; Kopitz, C.; Heroult, M.; Hgm Willems, P.; et al. Mitochondrial complex I inhibition triggers a mitophagy-dependent ROS increase leading to necroptosis and ferroptosis in melanoma cells. *Cell Death Dis.* **2017**, *8*, e2716. [CrossRef]
55. Menegazzi, M.; Masiello, P.; Novelli, M. Anti-Tumor Activity of Hypericum perforatum L. and Hyperforin through Modulation of Inflammatory Signaling, ROS Generation and Proton Dynamics. *Antioxidants* **2020**, *10*, 18. [CrossRef] [PubMed]
56. Hsu, F.-T.; Chen, W.-T.; Wu, C.-T.; Chung, J.-G. Hyperforin induces apoptosis through extrinsic/intrinsic pathways and inhibits EGFR/ERK/NF-κB-mediated anti-apoptotic potential in glioblastoma. *Environ. Toxicol.* **2020**, *35*, 1058–1069. [CrossRef]
57. Laudisi, F.; Cherubini, F.; Monteleone, G.; Stolfi, C. STAT3 Interactors as Potential Therapeutic Targets for Cancer Treatment. *Int. J. Mol. Sci.* **2018**, *19*, 1787. [CrossRef]
58. Madonna, G.; Ullman, C.D.; Gentilcore, G.; Palmieri, G.; Ascierto, P.A. NF-κB as potential target in the treatment of melanoma. *J. Transl. Med.* **2012**, *10*, 53. [CrossRef]
59. Pouysségur, J.; Marchiq, I.; Parks, S.K.; Durivault, J.; Ždralević, M.; Vucetic, M. "Warburg effect" controls tumor growth, bacterial, viral infections and immunity—Genetic deconstruction and therapeutic perspectives. *Semin. Cancer Biol.* **2022**, *86*, 334–346. [CrossRef]
60. Imreova, P.; Feruszova, J.; Kyzek, S.; Bodnarova, K.; Zduriencikova, M.; Kozics, K.; Mucaji, P.; Galova, E.; Sevcovicova, A.; Miadokova, E.; et al. Hyperforin Exhibits Antigenotoxic Activity on Human and Bacterial Cells. *Molecules* **2017**, *22*, 167. [CrossRef]
61. Ma, Q.; Xiao, P.; Sun, L.; Wang, J.; Zhong, D. Liver kinase B1/adenosine monophosphate-activated protein kinase signaling axis induces p21/WAF1 expression in a p53-dependent manner. *Oncol. Lett.* **2018**, *16*, 1291–1297. [CrossRef]

62. Petti, C.; Vegetti, C.; Molla, A.; Bersani, I.; Cleris, L.; Mustard, K.J.; Formelli, F.; Hardie, G.D.; Sensi, M.; Anichini, A. AMPK activators inhibit the proliferation of human melanomas bearing the activated MAPK pathway. *Melanoma Res.* **2012**, *22*, 341–350. [CrossRef] [PubMed]
63. Quiney, C.; Billard, C.; Faussat, A.M.; Salanoubat, C.; Ensaf, A.; Naït-Si, Y.; Fourneron, J.D.; Kolb, J.-P. Pro-apoptotic properties of hyperforin in leukemic cells from patients with B-cell chronic lymphocytic leukemia. *Leukemia* **2006**, *20*, 491–497. [CrossRef]
64. You, M.-K.; Kim, H.-J.; Kook, J.H.; Kim, H.-A. St. John's Wort Regulates Proliferation and Apoptosis in MCF-7 Human Breast Cancer Cells by Inhibiting AMPK/mTOR and Activating the Mitochondrial Pathway. *Int. J. Mol. Sci.* **2018**, *19*, 966. [CrossRef] [PubMed]
65. Nakashima, K.; Ishida, A. AMP-activated Protein Kinase Activation Suppresses Protein Synthesis and mTORC1 Signaling in Chick Myotube Cultures. *J. Poult. Sci.* **2022**, *59*, 81–85. [CrossRef] [PubMed]
66. Hou, W.; Xie, Y.; Song, X.; Sun, X.; Lotze, M.T.; Zeh, H.J.; Kang, R.; Tang, D. Autophagy promotes ferroptosis by degradation of ferritin. *Autophagy* **2016**, *12*, 1425–1428. [CrossRef] [PubMed]
67. Shekhar, S.; Liu, Y.; Wang, S.; Zhang, H.; Fang, X.; Zhang, J.; Fan, L.; Zheng, B.; Roman, R.J.; Wang, Z.; et al. Novel Mechanistic Insights and Potential Therapeutic Impact of TRPC6 in Neurovascular Coupling and Ischemic Stroke. *Int. J. Mol. Sci.* **2021**, *22*, 2074. [CrossRef] [PubMed]
68. Scheuble, J.; Rössler, O.G.; Ulrich, M.; Thiel, G. Pharmacological and genetic inhibition of TRPC6-induced gene transcription. *Eur. J. Pharmacol.* **2020**, *886*, 173357. [CrossRef]
69. Yan, T.; Luo, Y.; Xia, Y.; Hamada, K.; Wang, Q.; Yan, N.; Krausz, K.W.; Ward, J.M.; Hao, H.; Wang, P.; et al. St. John's Wort alleviates dextran sodium sulfate-induced colitis through pregnane X receptor-dependent NFκB antagonism. *FASEB J.* **2021**, *35*, e21968. [CrossRef]
70. Menegazzi, M.; Novelli, M.; Beffy, P.; D'Aleo, V.; Tedeschi, E.; Lupi, R.; Zoratti, E.; Marchetti, P.; Suzuki, H.; Masiello, P. Protective effects of St. John's wort extract and its component hyperforin against cytokine-induced cytotoxicity in a pancreatic beta-cell line. *Int. J. Biochem. Cell Biol.* **2008**, *40*, 1509–1521. [CrossRef]
71. Yang, J.; Amiri, K.I.; Burke, J.R.; Schmid, J.A.; Richmond, A. BMS-345541 Targets Inhibitor of κB Kinase and Induces Apoptosis in Melanoma: Involvement of Nuclear Factor κB and Mitochondria Pathways. *Clin. Cancer Res.* **2006**, *12*, 950–960. [CrossRef]
72. Kaoud, T.S.; Mohassab, A.M.; Hassan, H.A.; Yan, C.; Van Ravenstein, S.X.; Abdelhamid, D.; Dalby, K.N.; Abdel-Aziz, M. NO-releasing STAT3 inhibitors suppress BRAF-mutant melanoma growth. *Eur. J. Med. Chem.* **2020**, *186*, 111885. [CrossRef]
73. Ehexige, E.; Bao, M.; Bazarjav, P.; Yu, X.; Xiao, H.; Han, S.; Baigude, H. Silencing of STAT3 via Peptidomimetic LNP-Mediated Systemic Delivery of RNAi Downregulates PD-L1 and Inhibits Melanoma Growth. *Biomolecules* **2020**, *10*, 285. [CrossRef]
74. Zhang, S.; Zhang, J.; Yu, J.; Chen, X.; Zhang, F.; Wei, W.; Zhang, L.; Chen, W.; Lin, N.; Wu, Y. Hyperforin Ameliorates Imiquimod-Induced Psoriasis-Like Murine Skin Inflammation by Modulating IL-17A-Producing γδ T Cells. *Front. Immunol.* **2021**, *12*, 635076. [CrossRef] [PubMed]
75. Menegazzi, M.; Di Paola, R.; Mazzon, E.; Muià, C.; Genovese, T.; Crisafulli, C.; Suzuki, H.; Cuzzocrea, S. Hypericum perforatum attenuates the development of carrageenan-induced lung injury in mice. *Free Radic. Biol. Med.* **2006**, *40*, 740–753. [CrossRef]
76. Martínez-Poveda, B.; Quesada, A.R.; Medina, M.A. Hyperforin, a bio-active compound of St. John's Wort, is a new inhibitor of angiogenesis targeting several key steps of the process. *Int. J. Cancer* **2005**, *117*, 775–780. [CrossRef]
77. Quiney, C.; Billard, C.; Mirshahi, P.; Fourneron, J.-D.; Kolb, J.-P. Hyperforin inhibits MMP-9 secretion by B-CLL cells and microtubule formation by endothelial cells. *Leukemia* **2006**, *20*, 583–589. [CrossRef]
78. Zanrè, V.; Campagnari, R.; Cerulli, A.; Masullo, M.; Cardile, A.; Piacente, S.; Menegazzi, M. Salviolone from Salvia miltiorrhiza Roots Impairs Cell Cycle Progression, Colony Formation, and Metalloproteinase-2 Activity in A375 Melanoma Cells: Involvement of P21(Cip1/Waf1) Expression and STAT3 Phosphorylation. *Int. J. Mol. Sci.* **2022**, *23*, 1121. [CrossRef]

International Journal of
Molecular Sciences

MDPI

Review

Biological Activity of Selenium and Its Impact on Human Health

Giuseppe Genchi [1,†], Graziantonio Lauria [1,†], Alessia Catalano [2], Maria Stefania Sinicropi [1,*] and Alessia Carocci [2]

[1] Dipartimento di Farmacia e Scienze della Salute e della Nutrizione, Università della Calabria, Arcavacata di Rende, 87036 Cosenza, Italy
[2] Dipartimento di Farmacia-Scienze del Farmaco, Università degli Studi di Bari "A. Moro", 70125 Bari, Italy
* Correspondence: s.sinicropi@unical.it
† These authors equally contributed to this work.

Abstract: Selenium (Se) is a naturally occurring metalloid element essential to human and animal health in trace amounts but it is harmful in excess. Se plays a substantial role in the functioning of the human organism. It is incorporated into selenoproteins, thus supporting antioxidant defense systems. Selenoproteins participate in the metabolism of thyroid hormones, control reproductive functions and exert neuroprotective effects. Among the elements, Se has one of the narrowest ranges between dietary deficiency and toxic levels. Its level of toxicity may depend on chemical form, as inorganic and organic species have distinct biological properties. Over the last decades, optimization of population Se intake for the prevention of diseases related to Se deficiency or excess has been recognized as a pressing issue in modern healthcare worldwide. Low selenium status has been associated with an increased risk of mortality, poor immune function, cognitive decline, and thyroid dysfunction. On the other hand, Se concentrations slightly above its nutritional levels have been shown to have adverse effects on a broad spectrum of neurological functions and to increase the risk of type-2 diabetes. Comprehension of the selenium biochemical pathways under normal physiological conditions is therefore an important issue to elucidate its effect on human diseases. This review gives an overview of the role of Se in human health highlighting the effects of its deficiency and excess in the body. The biological activity of Se, mainly performed through selenoproteins, and its epigenetic effect is discussed. Moreover, a brief overview of selenium phytoremediation and rhizofiltration approaches is reported.

Keywords: selenium; selenoproteins; selenium deficiency; human diseases; epigenetics; phytoremediation; rhizofiltration

Citation: Genchi, G.; Lauria, G.; Catalano, A.; Sinicropi, M.S.; Carocci, A. Biological Activity of Selenium and Its Impact on Human Health. *Int. J. Mol. Sci.* **2023**, *24*, 2633. https://doi.org/10.3390/ijms24032633

Academic Editor: Ryszard Lobinski

Received: 9 January 2023
Revised: 25 January 2023
Accepted: 26 January 2023
Published: 30 January 2023

1. Introduction

Selenium (Se) is a trace mineral, ubiquitously occurring in the environment that is of fundamental importance to human health. Initially regarded as a toxic element, its role as an essential element in the body was not established until 150 years after its discovery in 1957, when Klaus Schwartz and Calvin Foltz recognized it as a substance responsible for preventing lesions in the liver, blood vessels, and muscles in rats and chickens [1,2]. Since then, its impact on the human body and the mechanisms involved have been thoroughly investigated, being the link between Se deficiency, as well as its excess, and disease occurrence an important aspect. Despite its very low level in humans, Se plays an important and unique role among the trace essential elements being the only one for which incorporation into proteins is genetically encoded, as the constitutive part of the 21st amino acid, selenocysteine. In the form of selenocysteine, it is present in the active centers of Se-dependent enzyme (glutathione peroxidases, thioredoxin reductases, and iodothyronine deiodinases). Proteins having at least one selenocysteine residue in their structure are called selenoproteins that perform many important physiological roles, their main function being the maintenance of the redox balance in cells [3]. Data from mainly murine and cell-based,

but also some human studies, show that Se supplementation modifies epigenetic marks. Conceivably, this occurs through DNA methyltransferase inhibition by Se and its interaction with one-carbon metabolism [4]. Adequate levels of Se are functionally important for several aspects of human biology including male reproductive biology, endocrine system, muscle function, central nervous and cardiovascular systems, and immunity [5]. Prolonged Se deficiency in human organisms leads to serious diseases, since it adversely affects the cardiovascular system functioning, and can be a direct cause of myocardial infarction. The best-known endemic diseases caused by Se deficiency, otherwise known as "geochemical diseases", are Keshan and Kashin-Beck [6]. Low levels of Se in the body are also responsible for impaired fetal development, infertility in men [7], and increased risk of suffering from asthma because of the reduction in antioxidant defense and the decrease in glutathione peroxidase (Gpx) activity [8]. There is also evidence that Se deficiency weakens the immune system [9] and affects the proper functioning of the nervous system [10]. The main natural source of Se is food where it can exist in inorganic (such as selenates or selenites) and organic forms (selenomethionine, SeMet, and selenocysteine, SeC) [11]. Se deficiency, which affects about one billion people in the world, is due to its insufficient consumption. This factor mainly depends on the geographical area and correlates with the low content of this microelement in the soil, being climate-soil interaction as the main controlling factor [12]. According to World Health Organization (WHO) standards, the recommended dose of Se for adults is 55 μg/day, while the maximum tolerable adult intake without side effects is set at 400 μg/day [13]. Recently the reference values for Se intake have been revised, using the saturation of selenoprotein P (SePP) in plasma as a criterion for the derivation of such values [14]. The integration of selenium-rich food into the diet represents a meaningful measure to avoid deficiency; however, supplemental intake beyond the amounts needed for the full expression of selenoproteins potentially increases health risks therefore, it is not recommended. Excessive supplementation or a diet rich in products with a high content of Se may result in poisoning. In Venezuela, the consumption of the fruit of the species *Lecythis ollaria* which accumulates huge amounts of Se (7–12 g Se/kg of dry matter) caused acute Se poisoning with hair loss, diarrhea, and emesis [15]. Se toxicity depends on its chemical form, besides ingested dose, interactions with other dietary components, and physiological condition of the body. The inorganic forms of Se exhibit higher toxicity than the organic ones. Inorganic Se has a prooxidant effect on thiols, producing free oxygen radicals (ROS), while organic forms are excreted more easily [16]. Acute Se poisoning is difficult to diagnose since its symptoms are rather non-specific. These include hypotension, tachycardia, and neurological disorders such as tremor and muscle contractions [17]. Chronic Se toxicity, otherwise known as selenosis, is characterized by hair loss, changes, and fragility of fingernails, skin rash, joint pain, tooth decay, and a specific garlic odor in the exhaled breath due to the presence of the volatile compound dimethyl selenide [18]. Furthermore, a recent study showed the link between increased Se intake and the risk of type 2 diabetes mellitus [19]. Plants can absorb, assimilate, and accumulate Se in leaves and roots. The capability of plants to take up a substantial amount of Se is now being utilized to remove excess Se from contaminated areas in a process known as 'phytoremediation'. Phytoremediation of Se-contaminated soils can be a non-polluting and cost-effective way to remove Se that might otherwise be leached out of the soil by excessive irrigation or rainwater to contaminate groundwater, surface waters, or drainage waters [20]. The efficiency of phytoremediation may be greatly increased through the application of recent technological advances in plant breeding, and genetic engineering, and by manipulation of agronomic practices. With this review, we aim to underline the role of Se in the modulation of numerous biological effects, mainly performed through selenoproteins, along with its epigenetic effect. Furthermore, the most recent line of evidence concerning the human health effects of selenium is summarized highlighting the effects of its deficiency and excess in the body which represent the key issue currently at the forefront of this research.

2. Selenium Chemistry

Se is a chemical element with atomic number 34 and an atomic weight of 78.96 (Table 1). Se is a nonmetal with properties between sulfur and tellurium (elements above and below in the periodic table) and belongs to the main Group 16 (IV A). Se is a constituent of rare minerals, including crookesite [$Cu_7(Tl,Ag)Se_4$], berzelianite (Cu_2Se), tiemannite (HgSe), antimonselite (Sb_2Se_3) [21,22], and it is obtained during the electrolytic refining of copper. Se was discovered in 1817 by J.J. Berzelius, who was working with sulfuric acid. Berzelius was intrigued by a red sediment collected at the bottom of the container in which the sulfuric acid was prepared. Se is present in different allotropes (gray, red and black) that interconvert with temperature changes and on the rate of temperature change. Prepared in a chemical reaction, selenium is present as an amorphous brick-red powder; rapidly melted, it forms black vitreous beads. Black selenium is a brittle and lustrous solid. The structure of the black form of selenium is irregular and consists of polymeric rings with more than 1000 atoms per ring. Upon heating, it softens and about at 180 °C converts to gray. Gray selenium is the most stable and dense form with a chiral hexagonal crystal lattice consisting of a helical polymeric chain and behaves as a semiconductor with an appreciable photoconductivity. Selenium resists oxidation by air and it is not attacked by oxidizing acids, while with strong reducing agents it forms polyselenides $(Se_n)^{2-}$. Natural selenium has five stable isotopes (^{74}Se, ^{76}Se, ^{77}Se, ^{78}Se, and ^{80}Se); of which the most abundant isotopes are ^{80}Se and ^{78}Se (50% and 23.5%. natural abundance, respectively). Sixteen radioactive isotopes have been synthesized by irradiating selenium nuclei with neutrons. ^{79}Se occurs in very little quantities in uranium ores as a product of nuclear fission; it emits beta particles forming ^{79}Br with a half-life of 3.27×10^5 years. ^{82}Se has a half-life of 9.2×10^{19} years and emits double beta particles forming ^{82}Kr. It is an extremely rare element; in fact, it is the 59th most common in the Earth's crust. The average selenium content in the Earth's crust is about 50 μg/kg, and its concentration in different geographic regions (China, Japan, Russia, Canada, USA) varies from 10 to 2000 μg/kg [15]. In Europe, the major producers of selenium are Finland, Belgium, Germany and England. Se is present in the atmosphere as a component of the volcanic activity and burning of fossil fuel [23]. Se and its inorganic compounds can be found in several geographical sites, such as the lithosphere, hydrosphere, atmosphere, and biosphere. Its chemical form depends on pH and redox properties of the soil, absorption and deposition effects, and biological processes in the presence of microorganisms [24]. Se is present in all living organisms (humans, animals, and plants) as inorganic and organic compounds. The inorganic forms are elementary selenide (Se^{2-}), selenite (SeO_3^{2-}), and selenate (SeO_4^{2-}); while the main organic compounds are selenomethionine, selenocysteine, methylselenocysteine, selenocystathionine (Table 2) and proteins containing these amino acids. Plants can absorb and transform inorganic and organic Se forms. The amounts of Se in plants are determined by the type of soil and its pH and salinity, levels in the soil, temperature, and amount of precipitation [25,26]. The mechanisms of intestinal absorption of Se are different in relation to its chemical form. Selenite is absorbed by simple diffusion, while selenate is imported by a cotransport sodium/selenate, OH^- antiporter. Se-containing aminoacids are absorbed by Na-dependent aminoacid transport [27]. Some elements (sulfur, lead, arsenic, calcium, and iron) decrease the uptake of selenium. Indeed, Fe^{3+} precipitates Se to an inassimilable complex form; sulfur decreases the absorption of selenium by steric competitiveness.

Table 1. Chemical and physical properties of selenium.

Atomic number	34
Atomic weight	78.96 u
Electronic configuration	[Ar] $3d^{10}4s^24p^4$
Melting point	221 °C
Boiling point	685 °C
Density at 20 °C	4.81 g/cm^3
Covalent radius	120 ± 4 pm
Van der Waals radius	190 pm
Heat of fusion (gray)	6.69 KJ/mol
Heat of vaporization	95.48 KJ/mol
Pauling electronegativity number	2.55
First ionization energy	941.0 KJ/mol
Second ionization energy	2045.0 KJ/mol
Third ionization energy	2973.0 KJ/mol
Fourth ionization energy	4144.0 KJ/mol
Standard potential	0.823 V (VI/IV)
Allotropes	Gray, Red, Black
Mohs hardness	2.0
Cristal structure (gray)	Hexagonal
Oxidation states	−2, 0, 2, 4, 6

Table 2. Organic forms of selenium.

Molecular Structure	Name
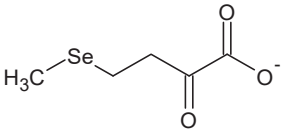	α-Keto-γ-methylselenobutyrate
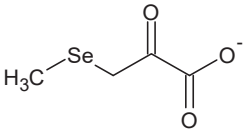	β-Methylselenopyruvate
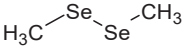	Dimethyldiselenide
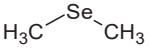	Dimethylselenide
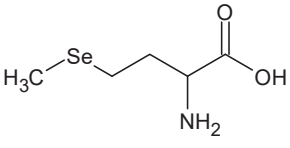	Selenomethionine
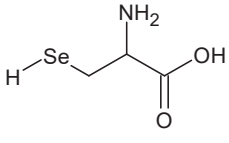	Selenocysteine
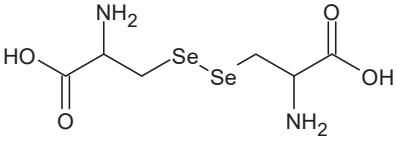	Selenocystine

Table 2. *Cont.*

Molecular Structure	Name
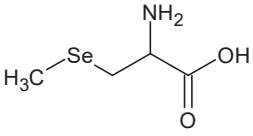	Methylselenocysteine
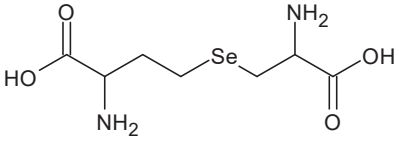	Selenocystathionine

3. Selenium Uses and Applications

In nature, Se is found in sulfide ores of copper, lead, nickel, gold, and silver. Se is commonly produced from selenide in many sulfide ores of copper, nickel, and lead. It is also obtained as a byproduct from the anode mud of copper electrolytic refineries in the proportion of 5 to 25%. Se can be extracted from sludge with the process of roasting with sod crystal or with sulfuric acid treatment. The largest commercial use of selenium (about 50%) is for the production of glass. Selenite (SeO_3^{2-}) and selenate (SeO_4^{2-}) sodium compounds are used in the production of glasses to give them a pink or red color and to hide the green tint that arises in the presence of iron impurities [28]. Se is used as a pigment also for ceramics and plastics. Furthermore, Se is used in photocells, solar cells, and photocopiers. The lithium-selenium battery is in electric vehicles one of the most promising systems for energy storage. It is an alternative to lithium-sulfur batteries with a good advantage of high electrical conductivity and better electrochemical performance [29]. It has been found that the use of Se as fertilizer nullifies the accumulation of lead and cadmium in lettuce. In low doses, Se has shown a beneficial effect on plant resistance to various environmental stress such as drought, UVB, soil salinity, and hot temperatures [30]. Se can also be used to reduce the transmission of sunlight in glass giving it a bronze tint. Se converts light to electricity (photovoltaic action) and has a photoconductive action (electrical resistance decreases with an increase in illumination). Organoselenium compounds are used as a catalyst in some chemical reactions such as selenocyclization, oxyselenenylation, oxidation, and reduction [31]. As a catalyst, it has the advantages of mild conditions, low cost, and it can be recycled and used more and more times. In metallurgy, Se is used to prepare alloys to provide resistance to corrosion and oxidation of metals. It is used for the vulcanization of rubber, for the preparation of pharmaceutical products, and for veterinary uses. Se is involved in the preparation of dietary supplements, and in the treatment of seborrheic dermatitis and dandruff; ^{75}Se is applied and used as a gamma source in industrial radiography of welds for steel thickness over 5 mm [32]. ^{75}Se is utilized also in biochemistry to follow the metabolism of selenocysteine and selenoproteins [33].

4. Selenium in Human Health and Diseases

Humans and animals require Se in trace quantities, being a component of the amino acid selenocysteine present in the active site of the enzymes. At high concentrations, it becomes toxic since it replaces sulfur in enzymes. Se participates in many metabolic processes in the human and animal bodies. In the immune system, Se stimulates the activity of immune cells such as helper T, cytotoxic T, and Natural Killer (NK) [34]. In the human body, selenium deficiency can cause or induce diseases such as Keshan and Kashin-Beck diseases [35]. Furthermore, Se deficiency is associated with muscle necrosis, hypothyroidism, cardio-cerebrovascular disease, male infertility, increased incidence of various cancer, and an improved immune system [21,36]. Se deficiency has supposed to

be linked also to infections such as Coronavirus disease 2019 (COVID-19) and acquired immune deficiency syndrome (AIDS) [37]. The Institute of Medicine (USA 2000) has proposed for adult humans a recommended dietary allowance of 55–75 μg/day. Unfortunately, the diet of about one billion people lacks sufficient Se for their good health [35,38]. A large part of dietary selenium in human beings derives directly and indirectly from plants and vegetables (The occurrence of Se in food products has been reported in Table 3). Se levels in soil generally reflect its presence in food; consequently, the lack of this element in human consumption is usually attributed to crop production in geographical areas with low selenium content, and to the amount that edible plants can extract from this soil [21,35,39]. On the other hand, excessive dietary selenium intake may impose risks and damage on human health. The symptoms of selenosis in humans include garlicky breath, dermatitis, hair and fingernail loss, acute respiratory distress, myocardial infarction, and renal failure [21,35,36,40]. The loss of human hair and nails was observed with a very high dietary selenium intake of 2000 μg/day in people of Enshi (Hubei, China) [41,42]. Se, as an antioxidant agent, shows great potential for redox regulation and the maintenance of cellular homeostasis and metabolism [43]. In recent years, the primary role of an excess of reactive oxygen species in the complex pathogenesis of metabolic diseases has been unveiled [44]. Recently, several studies have reported that serum Se status is related to the risk of metabolic diseases therefore, Se supplementation has supposed to be a promising approach in patients with low Se levels. Moreover, the crucial role of Se in chronic metabolic diseases, including cardiovascular disease [45], type 2 diabetes mellitus (T2DM) [46], and nonalcoholic fatty liver disease (NAFLD) [47] has been reported. Several prospective investigations have declared the association between Se level and coronary heart disease (CHD) risk and outcomes. These studies indicate an inverse correlation between Se plasma levels and CHD risk and suggest that moderate Se supplementation may be beneficial in preventing CHD risk. However, the preliminary results of studies conducted on animal models may not truly reflect the effectiveness of Se supplementation in preventing or treating CHD [48]. Se has been reported to play a significant role in glucose and lipid metabolism. Recent studies indicate that high levels of Se are associated with insulin resistance and dyslipidemia. A large cross-sectional study of 8198 rural Chinese reported that serum Se levels were positively correlated with total cholesterol, triglyceride, high-density lipoprotein, and low-density lipoprotein levels, and elevated serum Se levels were related to an increased risk of dyslipidemia [49]. On the other hand, a cross-sectional analysis of 4339 participants found that Se levels were positively associated with insulin resistance and blood glucose; indeed, a 10 μg/L increase in Se was associated with a 1.5% increase in insulin [50]. Based on the role of Se in glucose metabolism and antioxidant defense, Se may be involved in the pathogenesis of type 2 diabetes mellitus (T2DM). Several studies have reached a consensus that high Se exposure is a risk factor for T2DM however, the relationship between dose and effect in observational studies, and its specific role and mechanism have yet to be fully elucidated [50–53]. NAFLD, the most common cause of liver disease worldwide, is a complex disease that is modulated by numerous mechanisms, including metabolic factors. Some injurious processes, such as oxidative stress contribute to liver damage. Due to the role of Se in lipid metabolism and antioxidant defense, extensive evidence has suggested that Se may contribute to the development of NAFLD. Several animal studies have indicated that Se exposure could induce increased serum liver enzyme levels, the activation of Kupffer cells, and higher hepatic insulin resistance and triglyceride levels in animals, suggesting that Se exposure may be associated with the development of NAFLD [54]. In contrast, Reja et al. reported an inverse relationship between serum Se levels and the risk of advanced liver fibrosis, indicating that Se may be beneficial for the prevention of liver fibrosis in the development of NAFLD [55]. Therefore, whether Se levels are positively or negatively associated with NAFLD risk in humans remains unclear and research opinion regarding the protective action of Se in NAFLD remains inconsistent. Several recent manuscripts reviewed the antioxidant role of nutritional supplementation of selenium in the management of major chronic metabolic disorders including hyperlipi-

demia and hyperglycemia, highlighting the complex physiological role of Se [43,56,57]. Although the role of Se in metabolic diseases remains unclear, the antioxidant activity of Se in the pathogenesis of diseases cannot be ignored, and the molecular mechanisms underlying these paradoxical effects need to be further explored. Therefore, the relationship between Se status and various health outcomes, especially in metabolic diseases, requires close attention.

Table 3. Selenium content in food products according to reference [1].

Food	Selenium Content (μg/g)	References
Yeast	500–4000	[18,58,59]
Brazil Nuts	0.2–512	[60]
Beef Kidney	1.45	[61]
Liver	0.3–0.4	[62]
Beef	0.01–0.73	[59,63]
Fish	0.06–0.63	[59,61,64,65]
Bread	0.09–0.20	[64,66]
Eggs	0.09–0.25	[59,63,67]
Chicken	0.15	[64]
Pork	0.27–0.35	[64,66]
Broccoli	0.012	[63]
Milk	0.01–0.06	[64,65]
Chocolate	0.04	[59,61,63–65]

5. Biosynthesis of Selenocysteine and Selenoproteins

Se is an essential trace element to human health whose beneficial effects are mostly due to its incorporation in the form of selenocysteine (SeC) into a group of proteins called selenoproteins. SeC (considered as a 21st amino acid) is a functional analog of cysteine in which the sulfur atom is replaced by a selenium one. Selenoprotein biosynthesis is a complex process. Since there is no free SeC in the body, its synthesis occurs on specific tRNA (selenocysteinyl $tRNA^{SeRSeC}$) with the UCA anticodon complementary to the UGA stop codon as represented in Figure 1 [27,68]. SeC is incorporated into proteins via $tRNA^{SerSeC}$ that decodes the UGA codon as selenocysteine instead of a stop codon [69–71]. In eukaryotes, the synthesis of SeC begins so that seryl-tRNA synthetase charges $tRNA^{SerSeC}$ with serine in the presence of ATP. Subsequently, the hydroxyl mojety of serine is phosphorylated by *O*-phosphoseryl-tRNA kinase (PSTK) in the presence of ATP; finally, *O*-phosphoseryl $tRNA^{SerSeC}$ is substituted by Se atom in the presence of seleno phosphate and the enzymes seleno phosphate synthetase 2 (SPS2) and selenocysteinyl-tRNA synthase (SepSerS) (see Figure 1) [70,72]. The selenocystenyl $tRNA^{SerSeC}$ read UGA codon and is used for the integration of SeC into the amino acid sequence forming selenoprotein. SeC is encoded by the UGA codon, one of the three stop codons necessary for ending the polypeptide chain. The UGA codon encodes selenoprotein only in the presence of SeC insertion sequence (SECIS) element, and protein factors including the SECIS binding protein 2 (SBP2) [73–75], which is a nuclear protein, although it functions as a SECIS binding protein 2 in the cytoplasm [76].

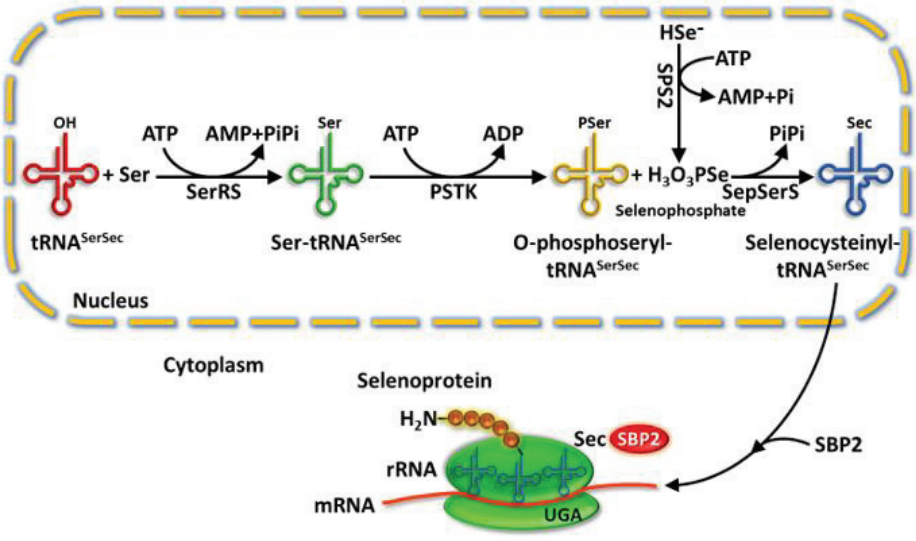

Figure 1. Selenoprotein biosynthesis pathway. SerRS catalyzes the reaction between $tRNA^{SerSec}$ and Ser in the presence of ATP to yield Ser-$tRNA^{SerSec}$, which in turn is phosphorylated in the presence of ATP and PSTK to give O-phosphoseryl- $tRNA^{SerSec}$. Thus, O-phosphoseryl- $tRNA^{SerSec}$ is replaced by Se in the presence of selenophosphate and SepSerS to synthesize Sec-$tRNA^{SerSec}$. Sec-$tRNA^{SerSec}$ is transferred to the ribosome thanks to SECIS and SBP2. Finally, the UGA codon is recognized as the Sec integration codon into the amino acid sequence of selenoprotein. Abbreviations: SeC = Selenocysteine; SerRS = Seryl-tRNA synthetase; mRNA = messenger RNA; rRNA = ribosomal RNA; PSTK = O-phosphoseryl tRNA kinase; SPS2 = selenophosphate synthetase 2; SepSerS = O-phosphoseryl tRNA: selenocysteinyl tRNA synthase; SECIS = SeC Insertion Sequence; SBP2 = SECIS Binding Protein 2.

6. Selenoproteins and Selenoenzymes

Se is incorporated as SeC into proteins and 25 selenoproteins and selenoenzymes have been identified in humans. These proteins include enzymes such as five glutathione peroxidases (GPX), three iodothyronine deiodinases, three thioredoxin reductases, selenophosphate synthetase 2, methionine sulfoxide reductase B1 and selenoproteins F, H, I, K, M, N, O, P, S, T, V, and W [77,78]. Glutathione peroxidase, iodothyronine deiodinase, and thioredoxin reductase are the best-known and the more important selenoenzymes. Among the selenoproteins, glutathione peroxidases are a family of mammalian antioxidant enzymes. Their most important functions are to reduce the hydrogen peroxide to water and lipid hydroperoxides to corresponding ethers in the intracellular and extracellular compartments. These enzymes have glutathione (GSH) as a cofactor, and, in turn, GS-SG (the oxidized form of GSH) is reduced by glutathione reductase [79]. In humans, five GPXs (GPX1-GPX4, and GPX6) contain selenocysteine in the catalytic site, while other GPXs, including GPX5, GPX7 and GPX8, contain a cysteine residue. GPX1 is expressed in the lungs, kidneys, liver, and erythrocytes [80]. GPX2 is localized in the gastrointestinal-specific tissue; it is also present in other tissues, such as lung, liver, and skin. GPX3 is a glycosylated enzyme secreted in the plasma and extracellular fluid; its enzymatic activity is commonly used to evaluate the levels of Se in the organism. Strong activity of GPX4 is deserved in the testes. GPX4 has been found in mitochondria, cytoplasmic, and nuclear cellular compartments [81]. This enzyme is particularly active during cellular differentiation in embryonic development and in spermatogenesis [5]. Finally, GPX6 is found only in embryonic tissues. The three iodothyronine deiodinases (DIOs) are integral membrane proteins; DIO1 and DIO3 are plasma membrane proteins [82], while DIO2 is localized in the endoplasmic reticulum (ER) membrane. All these three DIOs participate in oxidoreduction enzymatic

reactions with SeC residue in the catalytic site. These three enzymes are active in thyroid hormone metabolism by activating (DIO1 and DIO2) or inactivating (DIO3) tetraiodotyronine (T4), triiodothyronine (T3), and reverse-triiodothyronine (rT3) (Figure 2). Three DIOs exhibit different tissue distributions; indeed, DIO1 is present in the thyroid, liver, kidneys, and pituitary gland, while DIO2 is expressed in the thyroid, central nervous system, and skeletal muscle. Finally, DIO3 is present in the embryonic and neonatal tissues, uterus, and central nervous system. These thyroid hormones regulate also lipid metabolism, thermogenesis, and growth [83]. Three thioredoxin reductase (TrxR1, TrxR2, and TrxR3) are known, they are selenoproteins with the SeC at the penultimate position at the C-terminal end of the enzymes [84]. TrxR1 and TrxR2 are found in the cytoplasm and mitochondria, respectively, while TrxR3 is localized in testes [85]. Each monomer of these enzymes includes a FAD prosthetic group, an NADPH binding site, and a redox active disulfide site. During the reaction, the electrons are transferred from NADPH and FAD to the disulfide active site of TrxR, which reduces the various substrates as in Figure 3. TrxR reduces oxidized thioredoxin that provides a reducing equivalent to the disulfide bond of thioredoxin reductase, ribonucleotide reductase, thioredoxin peroxidase, and some transcription factors acting as a cell growth factor in DNA synthesis [5]. Many other substrates have been identified for this reductase, such as lipoic acid, lipid hydroperoxides, Ca-binding proteins, and glutaredoxin 2 [5]. Selenophosphate synthetase 2 (SPS2) catalyzes the synthesis of selenophosphate (Figure 1) in the presence of ATP, which transfer a phosphoryl group to hydrogen selenide (HSe^-). Selenoprotein P is a very abundant glycoprotein in plasma and is formed by two domains: the C-terminal very rich in selenocysteine (10 residues) and the N-terminal, larger than the C-terminal. It is also present in the liver, brain, and testes [86]. The high level of selenocysteine suggests that it can play an important role in selenium transport and storage in tissues [87]. Selenoprotein P has antioxidant properties and helps to eliminate peroxynitrite formed in the reaction of superoxide and nitric oxide.

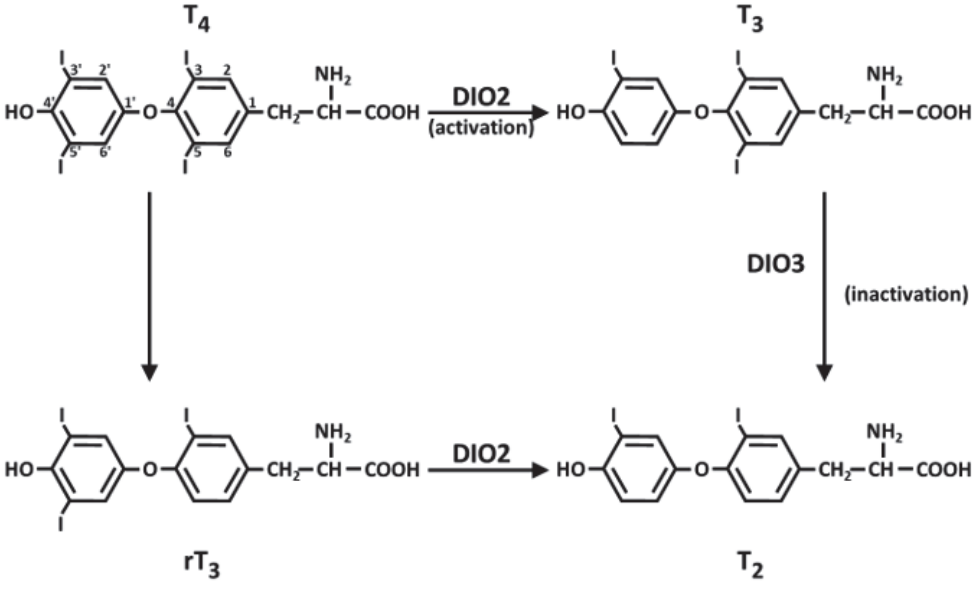

Figure 2. Deiodinases and metabolism of thyroid hormones. DIO2 deiodinase converts T4 into T3. DIO3 deiodinase mediates inner-ring deiodination of T4 or T3 to form the inactive metabolites rT3 and T2, respectively. Abbreviations. T4: thyroxine or 3,3′,5,5′-tetraiodotyronine; T3: 3,3′,5-triiodotyronine; rT3: reverse-3,3′,5′-triiodotyronine; T2: 3,3′-diiodotyronine.

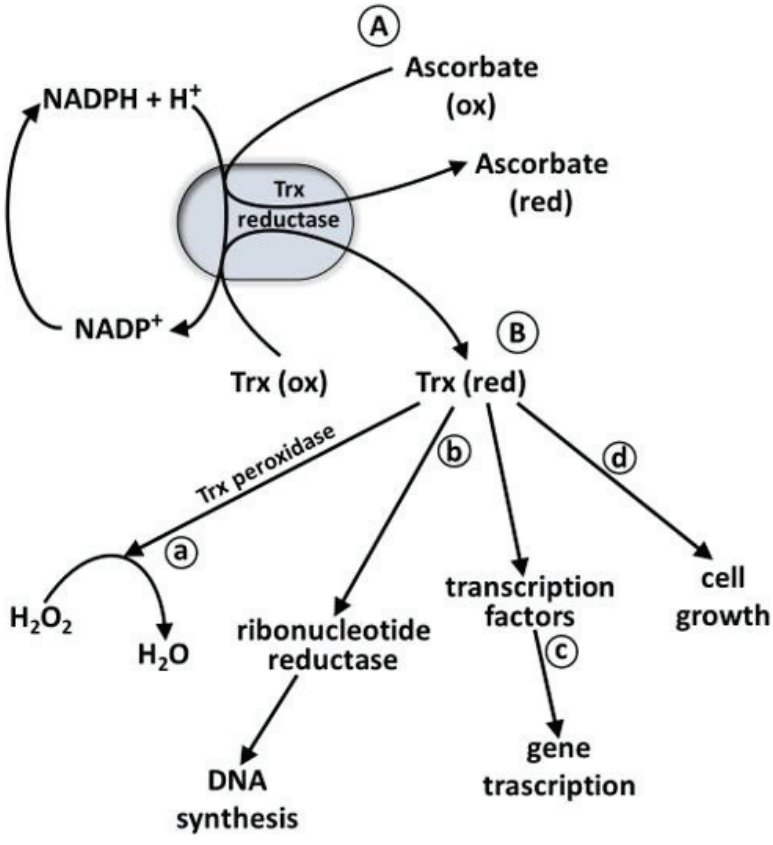

Figure 3. Reactions and functions of TrxR. (**A**) NADPH + H^+ catalyzed in the presence of TrxR the reaction of Trx (Ox) into Trx(Red) to reduce ascorbate (Ox) into ascorbate (Red). (**B**) Reduced Trx supplies reducing equivalents to break down H_2O_2 to H_2O in the presence of Trx peroxidase (**a**); reduced Trx in the presence of ribonucleotides reductase reduces ribonucleotides to deoxiribonucleotides for DNA synthesis (**b**); Trx (Red) provides reducing equivalent for transcription factors resulting in their increased binding to DNA leading to altered gene transcription (**c**); reduced Trx increase cell growth (**d**). Abbreviations: $NADP^+$: Nicotinamide Adenine Dinucleotide Phosphate; NADPH: Nicotinamide Adenine Dinucleotide Phosphate (reduced form); Trx: thioredoxin; Trx (Ox): thioredoxin oxidized; Trx (Red): thioredoxin reduced; TrxR: thioredoxin reductase.

7. Selenium Deficiencies in Food: Keshan and Kashin–Beck Diseases

Keshan disease is a juvenile cardiomyopathy with pulmonary edema caused by a combination of both a nutritional deficiency of the essential mineral Se and a mutated strain of the Coxsackie B virus [88,89]. The name of the disease derives from Keshan County of Heilongjiang province, Northeast China, where the symptoms were first noted: precordial oppression and pain, nausea and vomiting (yellowish fluid), and myocardial necrotic lesions. Afterwards, these symptoms were found prevalently in a region extending from northeast to southwest China, where the soil is deficient in Se. Keshan disease may lead to cancer, hypertension, strokes, and, in addition, eczema, psoriasis, arthritis, and cataracts. Supplementations with Se reduce these conditions. In regions in which Se is present in low amounts, human beings can increase their intake of selenium with food, such as Brazil nuts, onions, canned tuna, beef, cod, turkey, chicken breast, eggs, cottage cheese, oatmeal, white or brown rice, and garlic. Moreover, human beings must be advised to have a diet rich in selenium that includes seafood and meats (kidney and liver). Onions,

mushrooms, broccoli, tomatoes, and radishes are good sources of selenium if the soil, in which they are cultivated, contains it. Moreover, vitamin E deficiency is considered to have a relationship with the occurrence of Keshan disease, thus it is recommended to take vitamin E along with Se. Kashin-Beck disease is also due to the deficiency of Se and involves children between 5 and 15 years old living in areas with low Se levels. Kashin-Beck disease is a chronic osteochondropathy (disease of bones), mainly distributed from Northeastern to Southwestern China; other affected areas are Southeast Siberia and North Corea. Se and iodine have been considered the major nutritional deficiencies of this disease [90,91]. Furthermore, other causes of Kashin-Beck disease include mycotoxins trichotecene, produced by fungi (*Alternaria* sp. and *Fusarium* sp.), that contaminate barley grain in the diet, and fulvic acid in drinking water. Morning stiffness joints, limited motion in many joints of the body, disturbances of flexion and extension of the elbow, and enlarged interphalangical joints can be included among the symptoms of this disease. There are several Se supplements for treating Kashin-Beck disease in children, such as sodium selenite, sodium selenite, and vitamin E, sodium selenite and vitamin C, selenium salts, and selenium-enriched yeast. All these types of supplementations are highly effective compared to placebo/no treatment in treating Kashin-Beck disease in children. However, the content of Se must be strictly controlled to prevent harmful health effects, since Se in high doses may be poisoning [92].

8. Selenium Epigenetics: DNA, Histones, and Micrornas

There has been increased concern surrounding exposure to heavy metals (Cd, Cr, Hg, Fe, Ni, Pb) due to the evolving understanding of their role in the development of cancer [93–95]. Furthermore, the interaction between metalloids, such as Se and As, and the human body is correlated with the risk of lung, liver, urinary tract, kidney, and prostate cancers [96–99]. The essential trace element Se influences gene expression via different epigenetic pathways. Epigenetics refers to alterations in gene expression without involving any change in the DNA sequence but modifying the structural organization of chromatin. The mechanisms that mediate epigenetic regulation of gene expression are DNA hypo- or hyper-methylation, post-translational modifications of histone tail, and small non-coding RNA molecules (microRNA, miRNA). Eukaryotic DNA is packaged in the form of chromatin with the nucleosomes as a basic repeating unit. Each nucleosome is formed from 147 DNA base pairs wrapped around histones H2A, H2B, H3, and H4, which aggregate each other forming the histone octamer. The N-terminal end of these histones may undergo a variety of post-translational modifications promoted by specific enzymes with covalent reactions of acetylation and deacetylation, methylation and demethylation, phosphorylation, citrullination, sumoylation, biotinylation and ubiquitination processes. These reactions influence the chromatin structure facilitating gene transcription or its inhibition. DNA methyltransferases, histone methyltransferases, histone acetyltransferases, and histone deacetylases are the enzymes implicated in epigenetic mechanisms [94,95,97,100]. Dietary Se affects covalent reactions of DNA methylation and demethylation as well as histone methylation and demethylation, acetylation, and deacetylation. Se exerts its effects via the methionine-homocysteine cycle (one-carbon cycle) [4] (Figure 4). In this cycle, methionine is converted, in the presence of ATP and methionine adenosyltransferase (MAT), to S-adenosyl methionine (SAM), which is utilized as a methyl donor for methylation reactions of cytosine fifth carbon to 5-methylcytosine in DNA, and Se to dimethylselenide and dimethyldiselenide. During these methylation processes, SAM is transformed to S-adenosylhomocysteine which, in turn, is converted to homocysteine in the presence of the enzyme hydrolase (HY). Moreover, in this cycle, the methylation process of homocysteine to methionine takes place [101]. DNA methylation status is dependent on dietary intake of folate and vitamin B12, involved in the one-carbon cycle. The covalent methylation of DNA, in the presence of DNA methyltransferase and SAM, involves the transfer of a methyl group to the cytosine forming 5-methylcytosine; moreover, 5-methylcytosine can be actively or passively demethylated. Arai and coauthors [102] treated murine embryonic

stem cells with Se supplementation at concentrations found in human maternal serum. These authors found that Se induced a reversible alteration of the cell heterochromatin status and decreased the DNA methylation level in the Aebp2 gene (a component of the epigenetic regulator polycomb repression complex) and Piekle2gene (related to neural differentiation) without acting on the cell potential to form embryonic bodies. To test if Se affects the reaction of DNA methylation and the gene regulation, Uthus et al. [103] use a methylation array in the human epithelial Caco-2 cells (immortalized cell line of colorectal adenocarcinoma cells). DNA from cells grown with 250 nM methylselenocysteine solutions was incubated with methylation-binding protein labeled with biotin and then hybridized to the methylation array. DNA genes with methylated promoters will produce higher chemiluminescence than those genes without a methylated promoter. The methylation reaction of the von Lippel–Lindau tumor gene suppressor, among the genes profiled, was decreased, and that this results in the downregulation of this tumor suppressor. de Miranda and collaborators [104] in their study demonstrate that methylselenic acid (MSA) and selenite are promoting anti-breast cancer, acting in a dose-dependent manner on MCF-7 human breast adenocarcinoma cells, and showing modulation of DNA methylation and histone post-translation covalent modification. MSA (2 μM) and selenite (8 μM) altered epigenetic marks involving decreased expression of DNMT1 and histone modification. In particular, MSA decreased trimethylation reaction on H3K9 (H3K9me3) and increased the acetylation reaction of H4K16 (H4K16ac), while selenite acted decreasing the H4K16ac histone mark [104]. The H3 and H4 histone tails undergo post-translational covalent reactions that include methylation, acetylation, phosphorylation, ubiquitination, and sumoylation. The acetylation of the N-terminal lysine residue is a major histone modification involved in transcription, chromatin structure, and DNA repair. Histones acetylation and deacetylation are reactions allowed by histone acetyltransferases and histone deacetylases (HDAC). Histones are also methylated on arginine and histidine residues. Methylation, unlike acetylation, does not alter the charge of the histone molecules. In the acetylation reaction, in the presence of acetyl coenzyme A, an acetyl group is transferred on the $–NH^{3+}$ of the N-terminal lysine residue of histones that loses its ability to bind the DNA-negative phosphate group. This process releases negative charges of the phosphate groups of DNA, destabilizing the compact DNA-histone structure, and leading to a relaxed chromatin structure. Lee and collaborators [105] found that organoselenium compounds, such as methylselenocysteine and selenomethionine (Table 2), are metabolized to HDAC inhibitors in human prostate cancer cells (LNCaP cells). The selenocompounds methylselenocysteine and selenomethionine undergo transamination reaction in the presence of the enzymes glutamine transaminase K and aminoacid oxidase producing β-methylselenopyruvate and α-keto-γ-methylselenobutyrate, that are structurally similar to butyrate, a known HDAC inhibitor. These selenoketoacids decreased HDAC activity and increased the level of histone H3 acetylation in LNCaP cells. In a paper by Narayan and coauthors it has been shown, that in the presence of selenite and selenomethionine, the acetylation reaction of histone H4 (H4-K5, H4-K8, H4-K12, and H4-K16) was decreased in murine RAW 264.7 cells, macrophages and COX-2 promoter [106]. Finally, small noncoding microRNAs (miRNAs) are single-stranded, and are formed by 25–30 nucleotides. They play a central role in cell differentiation and proliferation and are involved in the post-transcriptional regulation of proteins expression binding to complementary target messenger RNA (mRNA) and silencing their translation, also reducing expression through induced decapping and deadenylation [107,108]. miRNAs are subjected to a covalent methylation modification (6-methyladenosine; 6MeA) and demethylation coordinated by methyltransferases and demethylases. Maciel-Dominguez and coauthors [109] studied the effect of Se on the gene expression of miRNA. Caco-2 cells were grown in Se-deficient or Se-supplemented medium [109]. After 72 h, RNA was extracted and subjected to microarray analysis (737 microRNA). Among 145 miRNA expressed in Caco-2 cells, 12 miRNA showed altered expression after Se-depletion. In the same study, the authors found that the expression of 50 mRNA was altered after Se depletion, and several mRNAs were

targeted by the Se-responsive miRNA. MicroRNA-185, whose expression was silenced after Se-depletion, was confirmed to regulate the expression of glutathione peroxidase 2 (GPX-2) and selenophosphate synthetase 2 (SPS-2). SPS-2 contributes to selenoprotein biosynthesis machinery. In a recent study, Matouskova et al. predicted several miRNAs as putative regulators of many glutathione peroxidases [110]. Moreover, miRNA-185 is a target of Se, since it has been found as a tumor suppressor in ovarian, breast, prostate, and gastric cancer [111,112]. In hepatocarcinoma cell lines, Se treatment modulated miRNA-544a expression interacting with selenoprotein K [113]. Xiang et al., treating LNCaP (Limph Node Carcinoma of the Prostate, androgen-sensitive human prostate adenocarcinoma) cells with 1.5 μM selenite for one week, found an important reduced HDAC activity and, at the same time, an increase of H3-K49 acetylation [114]. Telomeres are sequences at both the end of eukaryotic chromosomes. Human telomeres end is formed of about 100 base pairs of repeated sequences (TTAGGG)n; in mammals, n is generally ten of thousand. The end of the linear chromosomes is not replicated by DNA polymerase, but a special mechanism, in the presence of the enzyme telomerase, adds telomeres to chromosome ends. In the absence of this mechanism, telomeres could be shortened progressively with cell divisions. In any case, the telomere length is an important strategy to prolong life and to act against free radicals and aging. In 2004 Liu et al. showed that sodium selenite (2.5 μmol/L) prolongs life and anti-aging enhancing the activity of telomerase and length of telomere of human hepatocytes L-02 [115]. Furthermore, sodium selenite at a relatively high level (10 μmol/kg) increased the activity and the expression of telomerase in rat hepatocites [116].

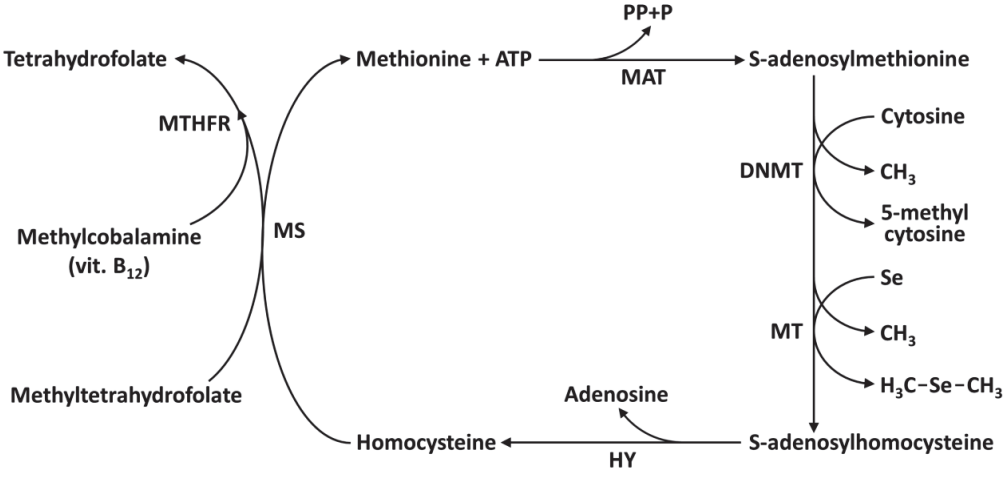

Figure 4. One-carbon metabolism cycle: DNA methylation and Se metabolism. Abbreviations: MAT: Methionine Adenosyl Transferase; MS: Methionine Synthase; MT: Methyl transferase; DNMT: DNA Methyl Transferase; HY: Hydrolase; MTHFR: Methylene Tetra Hydro Folate Reductase; PP: Pyrophosphate; P: phosphate.

9. Phytoremediation and Rhizofiltration

Anthropogenic activities (industrialization, mining, cement plants, and burning coal to produce energy) and natural activities (seepages and weathering from rocks, volcanic activity, and forest fires) are the major causes of the presence of toxic metals in the environment [117]. Toxic heavy metals are not degradable and their accumulation in the soil and water can contaminate drinking water, v and fruits with deleterious effects on human health. Physical, chemical, and biochemical approaches for heavy metals removal from water and soil are expensive and invasive and do not provide solutions to this problem. It is not yet clear, whether Se is essential and important for vegetation growth; however, plants are able to absorb and accumulate Se in roots and leaves. The capacity of plants to uptake Se is utilized to remove this element from contaminated soils and water [94,95,97].

This process is termed phytoremediation and its popularity is increasing as a low-cost and friendly technology for remediating contaminated environments (soils, groundwater and surface water). Among different phytoremediation strategies, the processes of phytovolatilization, phytoextract,tion and rizhofiltration are well known. With the process of phytovolatilization, green plants are able to absorb inorganic Se and release it into the atmosphere as volatile selenocompounds, which are less toxic than original inorganic forms. It has been demonstrated that the volatile Se compound dimethyldiselenide (DMDSe, Table 2) is released by Astragalus bisulcatus and *Astragalus Racemosus*, while broccoli (*Brassica oleracea*) release dimethylselenide (DMSe, Table 2) from their leaves [118]. These organic selenocompounds are almost 600 times less toxic than elemental Se. The capability of different plant species in volatilizing selenium has been reported, showing that *A. bisulcatus* and *B. oleracea* have the highest rates of volatilization followed by tomatoes (*Solanum lycopersicum*), tall fescue (*Festuca arundinacea*) and alfalfa (*Medicago sativa*). Broccoli and cabbages (*B. oleracea)* are capable of volatilize daily at a Se quantity of 10g/ha [119,120]. In plants, Se detoxification takes place by methylation of selenocysteine and selenomethionine (Table 2) in the presence of the enzyme selenocysteine methyltransferase and S-adenosyl methionine (SAM) [121,122]. Among different crops grown on selenite silty soil, Indian mustard (*Brassica juncea*), corn (*Zea mays*), rice (*Oriza sativa*), and wheat (*Triticum aestivum*) proved a good tolerance to Se in the phytoextraction process. The Se accumulation in this plant was 104.8 mg/kg in Indian mustard, 76.9 mg/kg in rice, and 18.9 mg/kg in wheat [123]. The highest accumulation of Se for *Heliantus annuus*, *Gaillardia aristata*, *Calendula officinalis*, *Tagetes erecta*, *Coreopis gladiate*, and *Helichrysum orientale* make these flowers potentially attractive for phytoextraction from seleniferous soils [124]. The great advantage obtained by using flowers in the phytoextraction process derives from the consideration that they do not become part of the food chain of humans and animals. Rhizofiltration is another remediation process of absorption and concentration of contaminants from aquatic environments into the roots and shoots of both aquatic and land plants [125,126]. For the making of this method, plants are grown on the contaminated site (in situ) or they are grown off-site and later introduced to the contaminated aquatic ecosystems environment (ex situ). Rhizofiltration can treat the agricultural runoff, industrial discharge, and acid mine drainage released as a result of anthropogenic activities. Contaminants are absorbed through plant roots until saturation is reached, and finally, the plants are harvested with their roots. The plant species such as iris-leaved rush (*Juncus xiphioides*), cattail (*Typha latifolia*), hydrilla (*Hydrilla verticillata*), dotted duckweed (*Landoltia punctata*), common reed (*Phragmites australis*) and saltmarsh bulrush (*Scirpus robustus*) have given great results for Se rhizofiltration in wetlands.

10. Conclusions

Se is considered an essential trace element of fundamental importance for human health and its multifaceted aspects have attracted worldwide clinical and research interest in the last few decades. It is very important to maintain an adequate level of Se since both deficiency and excess are dangerous for human health. However, the crucial factor is that this micronutrient has a narrow range of safety. Indeed, while additional Se intake may benefit people with low status, those of adequate-to-high status may be affected adversely and should not take selenium supplements. Se performs its biological activity mainly through selenoproteins which are responsible for thyroid hormone management, fertility, the aging process, and immunity, and which play a key role in the maintenance of a redox balance in cells. Several studies have shown the interference of Se with epigenetic marks that are associated with the risk of diseases, or predict them. This is a relatively new field of the investigation thus, a detailed and comprehensive understanding of epigenetic processes elicited by Se is required to clarify and predict its impact on health outcomes. Se has been shown to act as anticarcinogenic in experimental settings and also in some human studies; however further extensive research in this field is necessary to determine the exact involved mechanisms. In this context, uncovering the putative roles of miRNAs as mediators of

Se-dependent tumor protection against malignant transformation could be an interesting area of future studies.

Author Contributions: Writing-original draft preparation, G.G.; writing-review and editing, A.C. (Alessia Carocci); Conceptualization, A.C. (Alessia Catalano); funding acquisition and supervision, M.S.S.; literature review, G.L. All authors have read and agreed to the published version of the manuscript.

Funding: This research received no external funding.

Acknowledgments: The authors gratefully acknowledge the financial support provided by Ministero dell'Istruzione, dell'Università e della Ricerca (MIUR, Italia).

Conflicts of Interest: The authors declare that they have no conflict of interest.

References

1. Kieliszek, M. Selenium—Fascinating microelement, properties and sources in food. *Molecules* **2019**, *24*, 1298. [CrossRef]
2. Schwarz, K.; Foltz, C.M. Selenium as an integral part of factor 3 against dietary necrosis liver degeneration. *J. Am. Chem. Soc.* **1957**, *79*, 3292–3293. [CrossRef]
3. Kuršvietienė, L.; Mongirdienė, A.; Bernatonienė, J.; Šulinskienė, J.; Stanevičienė, I. Selenium Anticancer Properties and Impact on Cellular Redox Status. *Antioxidants* **2020**, *9*, 80. [CrossRef] [PubMed]
4. Speckmann, B.; Grune, T. Epigenetic effects of selenium and their implications for health. *Epigenetics* **2015**, *10*, 179–190. [CrossRef] [PubMed]
5. Roman, M.; Jitaru, P.; Barbante, C. Selenium biochemistry and its role for human health. *Metallomics* **2014**, *6*, 25–54. [CrossRef] [PubMed]
6. Shahid, M.; Niazi, N.K.; Khalid, S.; Murtaza, B.; Bibi, I.; Rashid, M.I. A critical review of selenium biogeochemical behavior in soil-plant system with an inference to human health. *Environ. Pollut.* **2018**, *234*, 915–934.
7. Mistry, H.D.; Broughton Pipkin, F.; Redman, C.W.; Poston, L. Selenium in reproductive health. *Am. J. Obstet. Gynecol.* **2012**, *206*, 21–30. [CrossRef] [PubMed]
8. Fitzpatrick, A.M.; Jones, D.P.; Brown, L.A. Glutathione redox control of asthma: From molecular mechanisms to therapeutic opportunities. *Antioxid. Redox Signal.* **2012**, *17*, 375–408. [CrossRef]
9. Avery, J.C.; Hoffmann, P.R. Selenium, Selenoproteins, and Immunity. *Nutrients* **2018**, *10*, 1203. [CrossRef]
10. Ellwanger, J.H.; Franke, S.I.; Bordin, D.L.; Prá, D.; Henriques, J.A. Biological functions of selenium and its potential influence on Parkinson's disease. *An. Acad. Bras. Cienc.* **2016**, *88*, 1655–1674. [CrossRef]
11. Lobinski, R.; Edmonds, J.; Suzuki, K.; Uden, P. Species-selective determination of selenium compounds in biological materials. *Pure Appl. Chem.* **2000**, *72*, 447–461. [CrossRef]
12. Jones, G.D.; Droz, B.; Greve, P.; Gottschalk, P.; Poffet, D.; McGrath, S.P.; Seneviratne, S.I.; Smith, P.; Winkel, L.H.E. Selenium deficiency risk predicted to increase under future climate change. *Proc. Natl. Acad. Sci. USA* **2017**, *114*, 2848–2853. [CrossRef]
13. Institute of Medicine. *Dietary Reference Intakes for Vitamin C, Vitamin E, Selenium, and Carotenoids*; The National Academies Press: Washington, DC, USA, 2000; p. 528.
14. Kipp, A.P.; Strohm, D.; Brigelius-Flohé, R.; Schomburg, L.; Bechthold, A.E.; Leschik-Bonnet, E.; Heseker, H.; German Nutrition Society (DGE). Revised reference values for selenium intake. *J. Trace Elem. Med. Biol.* **2015**, *32*, 195–199. [CrossRef] [PubMed]
15. Fordyce, F. Selenium geochemistry and health. *Ambio* **2007**, *36*, 94–97. [CrossRef] [PubMed]
16. Misra, S.; Boylan, M.; Selvam, A.; Spallholz, J.E.; Bjornstedt, M. Redox-active selenium compounds—From toxicity and cell death to cancer treatment. *Nutrients* **2015**, *7*, 3536–3556. [CrossRef]
17. MacFarquhar, J.K.; Broussard, D.L.; Melstrom, P.; Hutchinson, R.; Wolkin, A.; Martin, C.B.; Burk, R.F.; Dunn, J.R.; Green, A.L.; Hammond, R.; et al. Acute selenium toxicity associated with a dietary supplement. *Arch. Intern. Med.* **2010**, *170*, 256–261. [CrossRef] [PubMed]
18. Kieliszek, M.; Błażejak, S. Current knowledge on the importance of selenium in food for living organisms: A review. *Molecules* **2016**, *21*, 609. [CrossRef]
19. Kim, J.; Chung, H.S.; Choi, M.-K.; Roh, Y.K.; Yoo, H.J.; Park, J.H.; Kim, D.S.; Yu, J.M.; Moon, S. Association between Serum Selenium Level and the Presence of Diabetes Mellitus: A Meta-Analysis of Observational Studies. *Diabetes Metab. J.* **2019**, *43*, 447–460. [CrossRef]
20. Dhillon, K.S.; Bañuelos, G.S. Overview and prospects of selenium phytoremediation approaches. In *Selenium in Plants. Plant Ecophysiology*; Pilon-Smits, E., Winkel, L., Lin, Z.Q., Eds.; Springer: Cham, Switzerland, 2017; Volume 11.
21. Fordyce, F.M. Selenium deficiency and toxicity in the environment. In *Essentials of Medical Geology*; Springer: Dordrecht, The Netherlands, 2013; pp. 375–416.
22. Barone, G.; Storelli, A.; Mallamaci, R.; Storelli, M.M. Comparative study on trace metal accumulation in liver of Mediterranean deep-sea fish and their selenium/mercury molar ratios. *Water Air Soil Pollut.* **2017**, *228*, 211. [CrossRef]

23. Winkel, L.H.; Vriens, B.; Jones, G.D.; Schneider, L.S.; Pilon-Smits, E.; Bañuelos, G.S. Selenium cycling across soil-plant-atmosphere interfaces: A critical review. *Nutrients* **2015**, *7*, 4199–4239. [CrossRef]
24. Sharma, V.K.; Mcdonald, T.J.; Sohn, M.; Anquandah, G.A.K.; Pettine, M.; Zboril, R. Biogeochemistry of selenium. A review. *Environ. Chem. Lett.* **2015**, *13*, 49–58. [CrossRef]
25. Terry, N.; Zayed, A.M.; De Souza, M.P.; Tarun, A.S. Selenium in higher plants. *Annu. Rev. Plant Biol.* **2000**, *51*, 401–432. [CrossRef]
26. Pilon-Smits, E.A.H. On the ecology of selenium accumulation in plants. *Plants* **2019**, *8*, 197. [CrossRef]
27. Minich, W.B. Selenium metabolism and biosynthesis of selenoproteins in the human body. *Biochemistry* **2022**, *87*, S168–S177. [CrossRef] [PubMed]
28. Langner, B.E. Selenium and selenium compounds. In *Ullmann's Encyclopedia of Industrial Chemistry*; John Wiley and Sons: Hoboken, NJ, USA, 2000.
29. Eftekhari, A. The rise of lithium–selenium batteries. *Sustain. Energy Fuels* **2017**, *1*, 14–29. [CrossRef]
30. Feng, R.; Wei, C.; Tu, S. The roles of selenium in protecting plants against abiotic stresses. *Environ. Exp. Bot.* **2013**, *87*, 58–68. [CrossRef]
31. Singh, F.V.; Wirth, T. Selenium reagents as catalysts. *Catal. Sci. Technol.* **2019**, *9*, 1073–1091. [CrossRef]
32. Hayward, P.; Currie, D. Radiography of welds using selenium 75, IR 192 and X-rays. In Proceedings of the 12th A-PCNDT 2006—Asia-Pacific Conference on NDT, Auckland, New Zealand, 5–10 November 2006.
33. Evenson, J.K.; Sunde, R.A. Metabolism of Tracer ^{75}Se Selenium from Inorganic and Organic Selenocompounds into Selenoproteins in Rats, and the Missing ^{75}Se Metabolites. *Front. Nutr.* **2021**, *8*, 699652. [CrossRef] [PubMed]
34. Razaghi, A.; Poorebrahim, M.; Sarhan, D.; Björnstedt, M. Selenium stimulates the antitumour immunity: Insights to future research. *Eur. J. Cancer* **2021**, *155*, 256–267. [CrossRef]
35. Fairweather-Tait, S.J.; Bao, Y.; Broadley, M.R.; Collings, R.; Ford, D.; Hesketh, J.E.; Hurst, R. Selenium in human health and disease. *Antioxid. Redox Signal.* **2011**, *14*, 1337–1383. [CrossRef] [PubMed]
36. Rayman, M.P. Selenium and human health. *Lancet* **2012**, *379*, 1256–1268. [CrossRef] [PubMed]
37. Zhang, J.; Taylor, E.W.; Bennett, K.; Saad, R.; Rayman, M.P. Association between regional selenium status and reported outcome of COVID-19 cases in China. *Am. J. Clin. Nutr.* **2020**, *111*, 1297–1299. [CrossRef] [PubMed]
38. Stoffaneller, R.; Morse, N.L. A review of dietary selenium intake and selenium status in Europe and the Middle East. *Nutrients* **2015**, *7*, 1494–1537. [CrossRef] [PubMed]
39. Joy, E.J.; Broadley, M.R.; Young, S.D.; Black, C.R.; Chilimba, A.D.; Ander, E.L.; Barlow, T.S.; Watts, M.J. Soil type influences crop mineral composition in Malawi. *Sci. Total Environ.* **2015**, *505*, 587–595. [CrossRef] [PubMed]
40. Naderi, M.; Puar, P.; Zonouzi-Marand, M.; Chivers, D.P.; Niyogi, S.; Kwong, R.W. A comprehensive review on the neuropathophysiology of selenium. *Sci. Total Environ.* **2021**, *767*, 144329. [CrossRef]
41. Huang, Y.; Wang, Q.; Gao, J.; Lin, Z.; Banuelos, G.S.; Yuan, L.; Yin, X. Daily dietary selenium intake in a high selenium area of Enshi, China. *Nutrients* **2013**, *5*, 700–710. [CrossRef]
42. Qin, H.B.; Zhu, J.M.; Liang, L.; Wang, M.S.; Su, H. The bioavailability of selenium and risk assessment for human selenium poisoning in high-Se areas China. *Environ Int.* **2013**, *52*, 66–74. [CrossRef]
43. Wang, N.; Tan, H.Y.; Li, S.; Xu, Y.; Guo, W.; Feng, Y. Supplementation of micronutrient selenium in metabolic diseases: Its role as an antioxidant. *Oxidative Med. Cell. Longev.* **2017**, *2017*, 7478523. [CrossRef]
44. Carrier, A. Metabolic syndrome and oxidative stress: A complex relationship. *Antioxid. Redox Signal.* **2017**, *26*, 429–431. [CrossRef]
45. Yin, T.; Zhu, X.; Xu, D.; Lin, H.; Lu, X.; Tang, Y.; Shi, M.; Yao, W.; Zhou, Y.; Zhang, H.; et al. The association between dietary antioxidant micronutrients and cardiovascular disease in adults in the United States: A cross-sectional study. *Front. Nutr.* **2022**, *8*, 1256. [CrossRef]
46. Kohler, L.N.; Florea, A.; Kelley, C.P.; Chow, S.; Hsu, P.; Batai, K.; Saboda, K.; Lance, P.; Jacobs, E.T. Higher plasma selenium concentrations are associated with increased odds of prevalent type 2 diabetes. *J. Nutr.* **2018**, *148*, 1333–1340. [CrossRef] [PubMed]
47. Xu, L.; Lu, Y.; Wang, N.; Feng, Y. The Role and Mechanisms of Selenium Supplementation on Fatty Liver-Associated Disorder. *Antioxidants* **2022**, *11*, 922. [CrossRef] [PubMed]
48. Zhang, X.; Liu, C.; Guo, J.; Song, Y. Selenium status and cardiovascular diseases: Meta-analysis of prospective observational studies and randomized controlled trials. *Eur. J. Clin. Nutr.* **2016**, *70*, 162–169. [CrossRef]
49. Ju, W.; Ji, M.; Li, X.; Li, Z.; Wu, G.; Fu, X.; Yang, X.; Gao, X. Relationship between higher serum selenium level and adverse blood lipid profile. *Clin. Nutr.* **2018**, *37*, 1512–1517. [CrossRef]
50. Cardoso, B.R.; Braat, S.; Graham, R.M. Selenium status is associated with insulin resistance markers in adults: Findings from the 2013 to 2018 National Health and Nutrition Examination Survey (NHANES). *Front. Nutr.* **2021**, *8*, 365. [CrossRef]
51. Huang, Y.-Q.; Shen, G.; Lo, K.; Huang, J.-Y.; Liu, L.; Chen, C.-L.; Yu, Y.-L.; Sun, S.; Zhang, B.; Feng, Y.-Q. Association of circulating selenium concentration with dyslipidemia: Results from the NHANES. *J. Trace Elem. Med. Biol.* **2020**, *58*, 126438. [CrossRef] [PubMed]
52. Vinceti, M.; Bonaccio, M.; Filippini, T.; Costanzo, S.; Wise, L.A.; Di Castelnuovo, A.; Ruggiero, E.; Persichillo, M.; Cerletti, C.; Donati, M.B.; et al. Dietary selenium intake and risk of hospitalization for type 2 diabetes in the Moli-sani study cohort. *Nutr. Metab. Cardiovasc. Dis.* **2021**, *31*, 1738–1746. [CrossRef] [PubMed]
53. Steinbrenner, H.; Duntas, L.H.; Rayman, M.P. The role of selenium in type-2 diabetes mellitus and its metabolic comorbidities. *Redox Biol.* **2022**, *50*, 102236. [CrossRef] [PubMed]

54. Yang, Z.; Yan, C.; Liu, G.; Niu, Y.; Zhang, W.; Lu, S.; Li, X.; Zhang, H.; Ning, G.; Fan, J.; et al. Plasma selenium levels and nonalcoholic fatty liver disease in Chinese adults: A cross-sectional analysis. *Sci. Rep.* **2016**, *6*, 37288. [CrossRef]
55. Reja, M.; Makar, M.; Visaria, A.; Marino, D.; Rustgi, V. Increased serum selenium levels are associated with reduced risk of advanced liver fibrosis and all-cause mortality in NAFLD patients: National Health and Nutrition Examination Survey (NHANES) III. *Ann. Hepatol.* **2020**, *19*, 635–640. [CrossRef]
56. Huang, J.; Xie, L.; Song, A.; Zhang, C. Selenium Status and Its Antioxidant Role in Metabolic Diseases. *Oxidative Med. Cell. Longev.* **2022**, *2022*, 7009863. [CrossRef] [PubMed]
57. Hu, W.; Zhao, C.; Hu, H.; Yin, S. Food sources of selenium and its relationship with chronic diseases. *Nutrients* **2021**, *13*, 1739. [CrossRef] [PubMed]
58. Kieliszek, M.; Błażejak, S. Selenium: Significance, and outlook for supplementation. *Nutrition* **2013**, *29*, 713–718. [CrossRef] [PubMed]
59. Navarro-Alarcon, M.; Cabrera-Vique, C. Selenium in food and the human body: A review. *Sci. Total Environ.* **2008**, *400*, 115–141. [CrossRef] [PubMed]
60. Junior, E.S.; Wadt, L.H.O.; Silva, K.E.; Lima, R.M.B.; Batista, K.D.; Guedes, M.C.; Carvalho, G.S.; Reis, A.R.; Lopes, G.; Guilherme, L.R.G. Natural variation of selenium in Brazil nuts and soils from the Amazon region. *Chemosphere* **2017**, *188*, 650–658. [CrossRef] [PubMed]
61. Reilly, C. Selenium: A new entrant into the functional food arena. *Trends Food Sci. Technol.* **1998**, *9*, 114–118. [CrossRef]
62. Pilarczyk, B.; Tomza-Marciniak, A.; Mituniewicz-Małek, A.; Wieczorek-Dąbrowska, M.; Pilarczyk, R.; Wójcik, J.; Balicka-Ramisz, A.; Bąkowska, M.; Dmytrów, I. Selenium content in selected products of animal origin and estimation of the degree of cover daily Se requirement in Poland. *Int. J. Food Sci. Technol.* **2010**, *45*, 186–191. [CrossRef]
63. Pappa, E.C.; Pappas, A.C.; Surai, P.F. Selenium content in selected foods from the Greek market and estimation of the daily intake. *Sci. Total Environ.* **2006**, *372*, 100–108. [CrossRef] [PubMed]
64. Skalny, A.V.; Burtseva, T.I.; Salnikova, E.V.; Ajsuvakova, O.P.; Skalnaya, M.G.; Kirichuk, A.A.; Tinkov, A.A. Geographic variation of environmental, food, and human hair selenium content in an industrial region of Russia. *Environ. Res.* **2009**, *171*, 293–301. [CrossRef]
65. Klapec, T.; Mandić, M.L.; Grgić, J.; Primorac, L.; Perl, A.; Krstanović, V. Selenium in selected foods grown or purchased in eastern Croatia. *Food Chem.* **2004**, *85*, 445–452. [CrossRef]
66. Dos Santos, M.; da Silva Júnior, F.M.R.; Muccillo-Baisch, A.L. Selenium content of Brazilian foods: A review of the literature values. *J. Food Compost. Anal.* **2017**, *58*, 10–15. [CrossRef]
67. Pilarczyk, B.; Tomza-Marciniak, A.; Pilarczyk, R.; Kuba, J.; Hendzel, D.; Udała, J.; Tarasewicz, Z. Eggs as a source of selenium in the human diet. *J. Food Compost. Anal.* **2019**, *78*, 19–23. [CrossRef]
68. Flohé, L. The labour pains of biochemical selenology: The history of selenoprotein biosynthesis. *Biochim. Biophys. Acta* **2009**, *1790*, 1389–1403. [CrossRef] [PubMed]
69. Squires, J.E.; Berry, M.J. Eukaryotic selenoprotein synthesis: Mechanistic insight incorporating new factors and new functions for old factors. *IUBMB Life* **2008**, *60*, 232–235. [CrossRef]
70. Bulteau, A.L.; Chavatte, L. Update on selenoprotein biosynthesis. *Antioxid. Redox Signal.* **2015**, *23*, 775–794. [CrossRef]
71. Vindry, C.; Ohlmann, T.; Chavatte, L. Translation regulation of mammalian selenoproteins. *Biochim. Biophys. Acta Gen. Subj.* **2018**, *1862*, 2480–2492. [CrossRef] [PubMed]
72. Turanov, A.A.; Xu, X.M.; Carlson, B.A.; Yoo, M.H.; Gladyshev, V.N.; Hatfield, D.L. Biosynthesis of selenocysteine, the 21st amino acid in the genetic code, and a novel pathway for cysteine biosynthesis. *Adv. Nutr.* **2011**, *2*, 122–128. [CrossRef]
73. Lu, J.; Holgren, A. Selenoproteins. *J. Biol. Chem.* **2009**, *284*, 723–727. [CrossRef]
74. Seeher, S.; Mahdi, Y.; Schweizer, U. Post-transcriptional control of selenoprotein biosynthesis. *Curr. Protein Pept. Sci.* **2012**, *13*, 337–346. [CrossRef]
75. Hatfield, D.L.; Tsuji, P.A.; Carlson, B.A.; Gladyshev, V.N. Selenium and selenium cysteine: Roles in cancer, health, and development. *Trends Biochem. Sci.* **2014**, *39*, 112–120. [CrossRef]
76. Bubenik, J.L.; Miniard, A.C.; Driscoll, D.M. Characterization of the UGA-recoding and SECIS-binding activities of SECIS-binding protein 2. *RNA Biol.* **2014**, *11*, 1402–1413. [CrossRef] [PubMed]
77. Kryukov, G.V.; Castellano, S.; Novoselov, S.V.; Lobanov, A.V.; Zehtab, O.; Guigo, R.; Gladyshev, V.N. Characterization of mammalian selenoproteomes. *Science* **2003**, *300*, 1439–1443. [CrossRef] [PubMed]
78. Zoidis, E.; Seremelis, I.; Kontopoulos, N.; Danezis, G.P. Selenium-dependent antioxidant enzymes: Actions and properties of selenoproteins. *Antioxidants* **2018**, *7*, 66. [CrossRef] [PubMed]
79. Brigelius-Flohé, R.; Maiorino, M. Glutathione peroxidases. *Biochim. Biophys. Acta* **2013**, *1830*, 3289–3303. [CrossRef]
80. Akahoshi, N.; Anan, Y.; Hashimoto, Y.; Tokoro, N.; Mizuno, R.; Hayashi, S.; Yamamoto, S.; Shimada, K.-i.; Kamata, S.; Ishii, I. Dietary selenium deficiency or selenomethionine excess drastically alters organ selenium contents without altering the expression of most selenoproteins in mice. *J. Nutr. Biochem.* **2019**, *69*, 120–129. [CrossRef]
81. Maiorino, M.; Scapin, M.; Ursini, F.; Biasolo, M.; Bosello, V.; Flohé, L. Distinct promoters determine alternative transcription of gpx-4 into phospholipid-hydroperoxide glutathione peroxidase variants. *J. Biol. Chem.* **2003**, *278*, 34286–34290. [CrossRef]

82. Baqui, M.; Botero, D.; Gereben, B.; Curcio, C.; Harney, J.W.; Salvatore, D.; Sorimachi, K.; Larsen, P.R.; Bianco, A.C. Human Type 3 iodothyronine selenodeiodinase is located in the plasma membrane and undergoes rapid internalization to endosomes. *J. Biol. Chem.* **2003**, *278*, 1206–1211. [CrossRef]
83. Arrojo, E.; Drigo, R.; Bianco, A.C. Type 2 deiodinase at the crossroads of thyroid hormone action. *Int. J. Biochem. Cell Biol.* **2011**, *43*, 1432–1441. [CrossRef]
84. Arner, E.S. Focus on mammalian thioredoxin reductases—Important selenoproteins with versatile functions. *Biochim. Biophys. Acta* **2009**, *1790*, 495–526. [CrossRef]
85. Sun, Q.A.; Wu, Y.; Zappacosta, F.; Jeang, K.T.; Lee, B.J.; Hatfield, D.L.; Gladyshov, V.N. Redox regulation of cell signaling by selenocysteine in mammalian thioredoxin reductases. *J. Biol. Chem.* **1999**, *274*, 24522–24530. [CrossRef]
86. Burk, R.F.; Hill, K.E. Selenoprotein P: An extracellular protein with unique physical characteristics and a role in selenium homeostasis. *Annu. Rev. Nutr.* **2005**, *25*, 215–235. [CrossRef] [PubMed]
87. Saito, Y. Selenium transport mechanism via selenoprotein P—Its physiological role and related diseases. *Front. Nutr.* **2021**, *8*, 685517. [CrossRef] [PubMed]
88. Loscalzo, J. Keshan disease, selenium deficiency, and the selenoproteome. *N. Engl. J. Med.* **2014**, *370*, 1756–1760. [CrossRef] [PubMed]
89. Ren, L.Q.; Li, X.J.; Li, G.S.; Zhao, Z.T.; Sun, B.; Sun, F. Coxsackievirus B3 infection and its mutation in Keshan disease. *World J. Gastroenterol.* **2004**, *10*, 3299–3302. [CrossRef] [PubMed]
90. Yao, Y.; Pei, F.; Kang, P. Selenium, iodine, and the relation with Kashin-Beck disease. *Nutrition* **2011**, *27*, 1095–1100. [CrossRef] [PubMed]
91. Moreno-Reyes, R.; Suetens, C.; Mathieu, F.; Begaux, F.; Zhu, D.; Rivera, M.T.; Boelaert, M.; Neve, J.; Perlmutter, N.; Vanderpas, J. Kashin–Beck osteoarthropathy in rural Tibet in relation to selenium and iodine status. *N. Engl. J. Med.* **1998**, *339*, 1112–1120. [CrossRef]
92. Xie, D.; Liao, Y.; Yue, J.; Zhang, C.; Wang, Y.; Deng, C.; Chen, L. Effects of five types of selenium supplementation for treatment of Kashin-Beck disease in children: A systematic review and network meta-analysis. *BMJ Open* **2018**, *8*, e017883. [CrossRef]
93. Carocci, A.; Catalano, A.; Lauria, G.; Sinicropi, M.S.; Genchi, G. Lead toxicity, antioxidant defense and environment. In *Reviews of Environmental Contamination and Toxicology*; Springer: Berlin/Heidelberg, Germany, 2016; pp. 45–67.
94. Genchi, G.; Carocci, A.; Lauria, G.; Sinicropi, M.S.; Catalano, A. Nickel: Human health and environmental toxicology. *Int. Environ. Res. Public Health* **2020**, *17*, 679. [CrossRef]
95. Genchi, G.; Lauria, G.; Catalano, A.; Carocci, A.; Sinicropi, M.S. The double face of metals: The intriguing case of chromium. *Appl. Sci.* **2021**, *11*, 638. [CrossRef]
96. Palma-Lara, I.; Martínez-Castillo, M.; Quintana-Pérez, J.C.; Arellano-Mendoza, M.G.; Tamay-Cach, F.; Valenzuela-Limón, O.L.; García-Montalvo, E.A.; Hernández-Zavala, A. Arsenic exposure: A public health problem leading to several cancers. *Regul. Toxicol. Pharmacol.* **2020**, *110*, 104539. [CrossRef]
97. Genchi, G.; Lauria, G.; Catalano, A.; Carocci, A.; Sinicropi, M.S. Arsenic: A review on a great health issue worldwide. *Appl. Sci.* **2022**, *12*, 6184. [CrossRef]
98. Letavayová, L.; Vlčková, V.; Brozmanová, J. Selenium: From cancer prevention to DNA damage. *Toxicology* **2006**, *227*, 1–14. [CrossRef] [PubMed]
99. Vinceti, M.; Filippini, T.; Wise, L.A. Environmental selenium and human health: An update. *Curr. Environ. Health Rep.* **2018**, *5*, 464–485. [CrossRef] [PubMed]
100. Koturbash, I.; Zemp, F.J.; Pogribny, I.; Kovalchuk, O. Small molecules with big effects: The role of the microRNAome in cancer and carcinogenesis. *Mutat. Res. Genet. Toxicol. Environ. Mutagen.* **2011**, *722*, 94–105. [CrossRef]
101. Jabłońska, E.; Reszka, E. Selenium and epigenetics in cancer: Focus on DNA methylation. *Adv. Cancer Res.* **2017**, *136*, 193–234.
102. Arai, Y.; Ohgane, J.; Yagi, S.; Ito, R.; Iwasaki, Y.; Saito, K.; Akutsu, K.; Takatori, S.; Ishii, R.; Hayashi, R.; et al. Epigenetic assessment of environmental chemicals detected in maternal peripheral and cord blood samples. *J. Reprod. Dev.* **2011**, *57*, 507–517. [CrossRef]
103. Uthus, E.; Begaye, A.; Ross, S.; Zeng, H. The von Hippel-Lindau (VHL) tumor-suppressor gene is down-regulated by selenium deficiency in Caco-2 cells and rat colon mucosa. *Biol. Trace Elem. Res.* **2011**, *142*, 223–231. [CrossRef]
104. de Miranda, J.X.; Andrade, F.D.; Conti, A.D.; Dagli, M.L.; Moreno, F.S.; Ong, T.P. Effects of selenium compounds on proliferation and epigenetic marks of breast cancer cells. *J. Trace Elem Med. Biol.* **2014**, *28*, 486–491. [CrossRef]
105. Lee, J.I.; Nian, H.; Cooper, A.J.; Sinha, R.; Dai, J.; Bisson, W.H.; Dashwood, R.H.; Pinto, J.T. Alpha-keto acid metabolites of naturally ocurring organoselenium compounds as inhibitors of histone deacetylase in human prostate cancer cells. *Cancer. Prev. Res.* **2009**, *2*, 683–693. [CrossRef]
106. Narayan, V.; Ravindra, K.C.; Liao, C.; Kaushal, N.; Carlson, B.A.; Prabhu, K.S. Epigenetic regulation of inflammatory gene expression in macrophages by selenium. *J. Nutr. Biochem.* **2014**, *26*, 138–145. [CrossRef]
107. Pillai, R.S.; Bhattacharyya, S.N.; Filipowicz, W. Repression of protein synthesis by miRNAs: How many mechanisms? *Trends Cell Biol.* **2007**, *17*, 118–126. [CrossRef] [PubMed]
108. Mohr, A.M.; Mott, J.L. Overview of microRNA biology. In *Seminars in Liver Disease*; Thieme Medical Publishers: Leipzig, Germany, 2015; Volume 35, pp. 3–11.
109. Maciel-Dominguez, A.; Swan, D.; Ford, D.; Hesketh, J. Selenium alters miRNA profile in an intestinal cell line: Evidence that miR-185 regulates expression of *GPX2* and *SEPSH2*. *Mol. Nutr. Food Res.* **2013**, *57*, 2195–2205. [CrossRef] [PubMed]

110. Matoušková, P.; Hanousková, B.; Skálová, L. MicroRNAs as potential regulators of glutathione peroxidases expression and their role in obesity and related pathologies. *Int. J. Mol. Sci.* **2018**, *19*, 1199. [CrossRef]
111. Qu, F.; Cui, X.; Hong, Y.; Wang, J.; Li, Y.; Chen, L.; Liu, Y.; Gao, Y.; Xu, D.; Wang, Q. MicroRNA-185 suppresses proliferation, invasion, migration, and tumorigenicity of human prostate cancer cells through targeting androgen receptor. *Mol. Cell. Biochem.* **2013**, *377*, 121–130. [CrossRef] [PubMed]
112. Li, Q.; Wang, J.X.; He, Y.Q.; Feng, C.; Zhang, X.J.; Sheng, J.Q.; Li, P.F. MicroRNA-185 regulates chemotherapeutic sensitivity in gastric cancer by targeting apoptosis repressor with caspase recruitment domain. *Cell Death Dis.* **2014**, *5*, e1197. [CrossRef] [PubMed]
113. Potenza, N.; Castiello, F.; Panella, M.; Colonna, G.; Ciliberto, G.; Russo, A.; Costantini, S. Human miR.544 modulates SELK expression in hepatocarcinoma cell lines. *PLoS ONE* **2016**, *11*, e0156908. [CrossRef] [PubMed]
114. Xiang, N.; Zhao, R.; Song, G.; Zhong, W. Selenite reactivates silenced genes by modifying DNA methylation and histones in prostate cancer cells. *Carcinogenesis* **2008**, *29*, 2175–2218. [CrossRef]
115. Liu, Q.; Wang, H.; Hu, D.; Ding, C.; Xu, H.; Tao, D. Effects of trace elements on the telomere lengths of hepatocytes L-02 and hepatoma cells SMMC-7721. *Biol. Trace Elem. Res.* **2004**, *100*, 215–227. [CrossRef]
116. Yu, R.A.; Chen, H.J.; He, L.F.; Chen, B.; Chen, X.M. Telomerase activity and telomerase reverse transcriptase expression induced by selenium in rat hepatocytes. *Biomed. Environ. Sci.* **2009**, *22*, 311–317. [CrossRef]
117. Gautam, P.K.; Gautam, R.K.; Banerjee, S.; Chattopadhyaya, M.C.; Pandey, J.D. Heavy metals in the environment: Fate, transport, toxicity and remediation technologies. In *Heavy Metals*; Nova Science Publishers: Hauppage, NY, USA, 2016; Volume 60, pp. 101–130.
118. Guignardi, Z.; Schiavon, M. Biochemistry of plant selenium uptake and metabolism. In *Selenium in Plants*; Springer: Cham, Switzerland, 2017; pp. 21–34.
119. Duckart, E.C.; Waldron, L.J.; Doner, H.E. Selenium uptake and volatilization from plants growing in soil. *Soil Sci.* **1992**, *153*, 94–99. [CrossRef]
120. Zayed, A.; Pilon-Smits, E.; deSouza, M.; Lin, Z.Q.; Terry, N. Remediation of selenium-polluted soils and waters by phytovolatilization. In *Phytoremediation of Contaminated Soil and Water*; CRC Press: Boca Raton, FL, USA, 2020; pp. 61–83.
121. Pilon-Smits, E.A.H.; LeDuc, D.L. Phytoremediation of selenium using transgenic plants. *Curr. Opin. Biotechnol.* **2009**, *20*, 207–2012. [CrossRef] [PubMed]
122. White, P.J. Selenium metabolism in plants. *Biochim. Biophys. Acta Gen. Subj.* **2018**, *1862*, 2333–2342. [CrossRef] [PubMed]
123. Rani, N.; Dhillon, K.S.; Dhillon, S.K. Critical levels of selenium in different crops grown in an alkaline silty loam soil treated with selenite-Se. *Plant Soil* **2005**, *27*, 367–374. [CrossRef]
124. Dhillon, K.S.; Dhillon, S.K. Selenium concentrations of common weeds and agricultural crops grown in the seleniferous soils of northwestern India. *Sci. Total Environ.* **2009**, *407*, 6150–6156. [CrossRef] [PubMed]
125. Carvalho, K.M.; Martin, D.M. Removal of aqueous selenium by four aquatic plants. *J. Aquat. Plant Manag.* **2001**, *39*, 33–36.
126. Miranda, A.F.; Muradov, N.; Gujar, A.; Stevenson, T.; Nugegoda, D.; Ball, A.S.; Mouradov, A. Application of aquatic plants for the treatment of selenium-rich mining wastewater and production of renewable fuels and petrochemicals. *J. Sustain. Bioenergy Syst.* **2014**, *4*, 97–112. [CrossRef]

International Journal of
Molecular Sciences

MDPI

Article

Differential Roles of Cystathionine Gamma-Lyase and Mercaptopyruvate Sulfurtransferase in Hapten-Induced Colitis and Contact Dermatitis in Mice

Noriyuki Akahoshi, Ryoka Hasegawa, Shingo Yamamoto, Rintaro Takemoto, Toshiki Yoshizawa, Waka Kamichatani and Isao Ishii *

Department of Health Chemistry, Showa Pharmaceutical University, Machida, Tokyo 194-8543, Japan
* Correspondence: i-ishii@ac.shoyaku.ac.jp; Tel.: +81-42-721-1563

Abstract: Hydrogen sulfide (H_2S) has been shown to act as both anti-inflammatory and pro-inflammatory mediators. Application of H_2S donors generally protects against inflammation; however, experimental results using mice lacking endogenous H_2S-producing enzymes, such as cystathionine γ-lyase (CTH) and mercaptopyruvate sulfurtransferase (MPST), are often contradictory. We herein examined two types of model hapten-induced inflammation models, colitis (an inflammatory bowel disease model of mucosal immunity) and contact dermatitis (a type IV allergic model of systemic immunity), in CTH-deficient ($Cth^{-/-}$) and MPST-deficient ($Mpst^{-/-}$) mice. Both mice exhibited no significant alteration from wild-type mice in trinitrobenzene sulfonic acid (Th1-type hapten)-induced colitis (a Crohn's disease model) and oxazolone (Th1/Th2 mix-type; Th2 dominant)-induced colitis (an ulcerative colitis model). However, $Cth^{-/-}$ (not $Mpst^{-/-}$) mice displayed more exacerbated phenotypes in trinitrochlorobenzene (TNCB; Th1-type)-induced contact dermatitis, but not oxazolone, at the delayed phase (24 h post-administration) of inflammation. CTH mRNA expression was upregulated in the TNCB-treated ears of both wild-type and $Mpst^{-/-}$ mice. Although mRNA expression of pro-inflammatory cytokines (IL-1β and IL-6) was upregulated in both early (2 h) and delayed phases of TNCB-triggered dermatitis in all genotypes, that of Th2 (IL-4) and Treg cytokines (IL-10) was upregulated only in $Cth^{-/-}$ mice, when that of Th1 cytokines (IFNγ and IL-2) was upregulated in wild-type and $Mpst^{-/-}$ mice at the delayed phase. These results suggest that (upregulated) CTH or H_2S produced by it helps maintain Th1/Th2 balance to protect against contact dermatitis.

Keywords: contact dermatitis; cystathionine γ-lyase; cytokine; hydrogen sulfide; inflammatory bowel disease; mercaptopyruvate sulfurtransferase; systemic immunity; Th1/Th2 balance; trinitrochlorobenzene; ulcerative colitis

Citation: Akahoshi, N.; Hasegawa, R.; Yamamoto, S.; Takemoto, R.; Yoshizawa, T.; Kamichatani, W.; Ishii, I. Differential Roles of Cystathionine Gamma-Lyase and Mercaptopyruvate Sulfurtransferase in Hapten-Induced Colitis and Contact Dermatitis in Mice. *Int. J. Mol. Sci.* **2023**, *24*, 2659. https://doi.org/10.3390/ijms24032659

Academic Editor: Maurizio Battino

Received: 31 December 2022
Revised: 27 January 2023
Accepted: 29 January 2023
Published: 31 January 2023

1. Introduction

Inflammatory bowel disease (IBD) is a serious chronic condition of the colon and small intestine associated with severe pain, bleeding, and diarrhea, comprising two common forms: Crohn's disease (CD) and ulcerative colitis (UC) [1]. CD is characterized by patchy lesions, potentially scattered in any area of the gastrointestinal tract, and transmural inflammation involving all bowel wall layers that leads to fibrosis, stricture, and fistula [2]. UC is characterized by mucosal inflammation from the rectum and continuously extends to the proximal colon [3]. Although both environmental and genetic factors, as well as several inflammatory mediators (cytokines and chemokines), have been implicated in their pathogenesis [2,4,5], the underlying molecular mechanisms are not yet fully elucidated.

Several clinical studies have suggested that colonic luminal hydrogen sulfide (H_2S), with levels regulated by sulfate-reducing bacteria or colonic enzymes, such as H_2S-producing enzymes, cystathionine γ-lyase (CTH; also known as CSE), and mercaptopyruvate sulfurtransferase (MPST; 3-MST), and H_2S-degrating thiosulfate sulfurtransferase (TST; rhodanese)

could be implicated in the IBD pathogenesis, especially UC [6,7]. Several experimental findings show that H_2S (or its effects via persulfidation/polysulfidation [8,9]) plays important (patho)physiological roles in the neuronal, cardiovascular, and endocrine systems, as well as inflammation; importantly, exogenous/endogenous H_2S could act as both anti-inflammatory and pro-inflammatory mediators, like a coin with two sides, perhaps depending on its doses or circumstances [10–12]. Therefore, this study examined the regulatory roles of CTH and MPST in experimental colitis induced by different model haptens, trinitrobenzene sulfonic acid (TNBS) and oxazolone, as mucosal immunity models [13], and experimental contact dermatitis induced by trinitrochlorobenzene (TNCB) and oxazolone, as systemic immunity models, using the previously established CTH-deficient ($Cth^{-/-}$) and MPST-deficient ($Mpst^{-/-}$) mice [14,15].

Contact dermatitis is the most common inflammatory condition caused by the exposure to exogenous substances that elicit skin and/or mucous membrane inflammation, and is estimated to affect 15–20% of the adult general population throughout a lifetime [16,17]. Although the therapeutic efficacy of H_2S is expected for skin diseases [18], allergic contact dermatitis from diallyl trisulfide, a fast H_2S donor, has been reported [19]. We herein found that $Cth^{-/-}$ and $Mpst^{-/-}$ mice and wild-type (WT) mice have similar responses to both TNBS- and oxazolone-induced colitis; however, $Cth^{-/-}$ mice displayed the most severe phenotype in TNCB (not oxazolone)-induced contact dermatitis.

2. Results

2.1. Normal Responses of $Cth^{-/-}$ and $Mpst^{-/-}$ Mice in TNBS or Oxazolone-Induced Colitis

Experimental colitis was induced by the initial topical sensitization, followed by rectal administration of TNBS (as a Th1/Th17-associated CD model [20]; Figure 1A) or oxazolone (as a Th1/Th2-associated UC model [20]; Figure 1E) in adult male WT, $Cth^{-/-}$, and $Mpst^{-/-}$ mice. All TNBS-treated groups displayed granulomatous ulcers in the colonic lumens (Figure 1B), which resemble CD phenotypes [2], and thus, had higher Wallace scores than the respective vehicle-treated groups (Figure 1C), similar in all genotypes. Histological analyses of hematoxylin/eosin (HE)-stained sections revealed transmural inflammation that extends into the muscular layers of the colon (Supplementary Figure S1), similar to higher Ameho scores (Figure 1D), in all TNBS-treated groups. Challenges with the oxazolone challenge caused more superficial ulcers (like UC patients [3]) that continue from the anuses to the colonic lumens (Figure 1F) in all three genotypes. Oxazolone treatment also increased Wallace scores (Figure 1G) and induced extensive erosive inflammation (Supplementary Figure S2), resulting in increased inflammation scores to the equivalent levels in the three genotypes (Figure 1H).

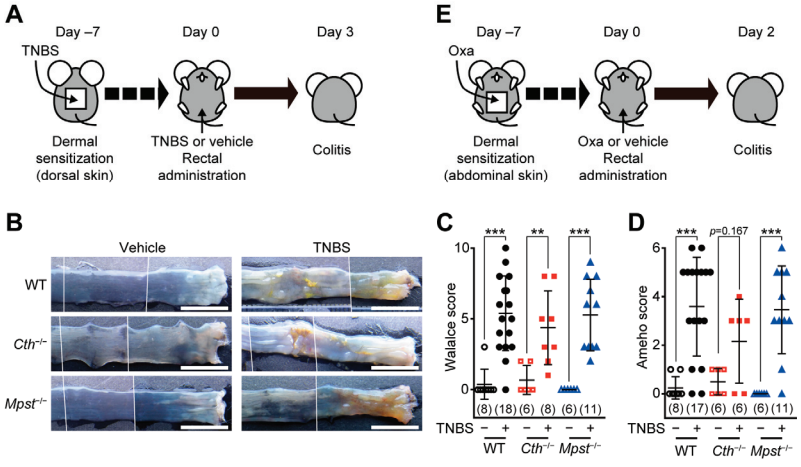

Figure 1. *Cont.*

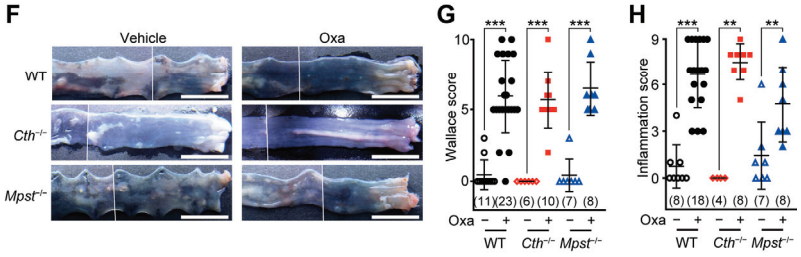

Figure 1. Two types of hapten-induced mouse IBD models: trinitrobenzene sulfonic acid (TNBS)-induced Crohn's disease-like model (**A**–**D**) and oxazolone (Oxa)-induced ulcerative colitis-like model (**E**–**H**). (**A**,**E**) Experimental Design. Adult male wild-type (WT), CTH-deficient ($Cth^{-/-}$), and MPST-deficient ($Mpst^{-/-}$) mice were sensitized on the (dorsal or abdominal) skin and then (7 days later) challenged per rectum with those haptens. (**B**–**D**) Typical pictures of colonic lumens (**B**), Wallace scores (**C**), and Ameho scores (**D**), obtained with histological examination of colonic sections (Supplementary Figure S1) at day 3 after the TNBS challenge. (**F**–**H**) Typical pictures of colonic lumens (**F**), Wallace scores (**G**), and inflammation scores (**H**), obtained with histological examination of colonic sections (Supplementary Figure S2) at day 2 after the Oxa challenge. Data are the mean ± standard derivation (SD) with sample numbers in parentheses. Differences between non-sensitized (vehicle alone) and pre-sensitized (with hapten) are significant in a Mann–Whitney U test at ** $p < 0.01$ and *** $p < 0.001$ (**C**,**D**,**G**,**H**). Bars indicate 1 cm (**B**,**F**).

2.2. Exacerbated TNCB (not Oxazolone)-Induced Contact Dermatitis in $Cth^{-/-}$ Mice

Experimental contact dermatitis was induced by the initial sensitization of TNCB or oxazolone on the abdominal skin, followed by the elicitation with the same hapten on one of the ears and the vehicle on another ear (Figure 2A), as models, to evaluate Th1- and Th1/Th2 mix-type allergic responses, respectively [21]. The elicitation response can be divided into two phases: the early phase at 2 h and the delayed phase at 24 h, after the challenge [21]. Allergic responses caused by TNCB-induced acute ear thickening after 2 h, followed by the delayed responses with additional thickening after 24 h in all three genotypes, although $Cth^{-/-}$ mice exhibited more severe thickening than WT and $Mpst^{-/-}$ mice at the delayed phase (Figure 2B–D). Closer examination of HE-stained sections revealed that TNCB induced acanthosis (epidermal hyperplasia; black arrowheads in Figure 2F,J) and spongiosis (red arrowheads in Figure 2F,J) in both WT and $Mpst^{-/-}$ mice, but induced immune cell infiltration only in $Cth^{-/-}$ mice (green arrowheads in Figure 2H). However, acanthosis and immune cell infiltration (especially lymphocyte and granule cell infiltration into the dermis) were more pronounced, whereas spongiosis was rather inconspicuous in $Cth^{-/-}$ mice (Figure 2G,H).

Immunostaining of ear sections revealed the most massive infiltration of CD4-positive T cells (Figure 3A,C), CD8-positive T cells (Figure 3B,D), and myeloperoxidase (MPO)-positive neutrophils (Figure 3A,B,E) in $Cth^{-/-}$ mice, compared to WT and $Mpst^{-/-}$ mice. Acute allergic responses (within 2 h) were not observed with oxazolone treatment, although the levels of their delayed responses (at 24 h) were comparable to those with TNCB and equivalent among the three genotypes (Figure 4A). HE staining revealed similar levels of acanthosis, dermal spongiosis, and immune cell infiltration in the three genotypes (Figure 4B–H).

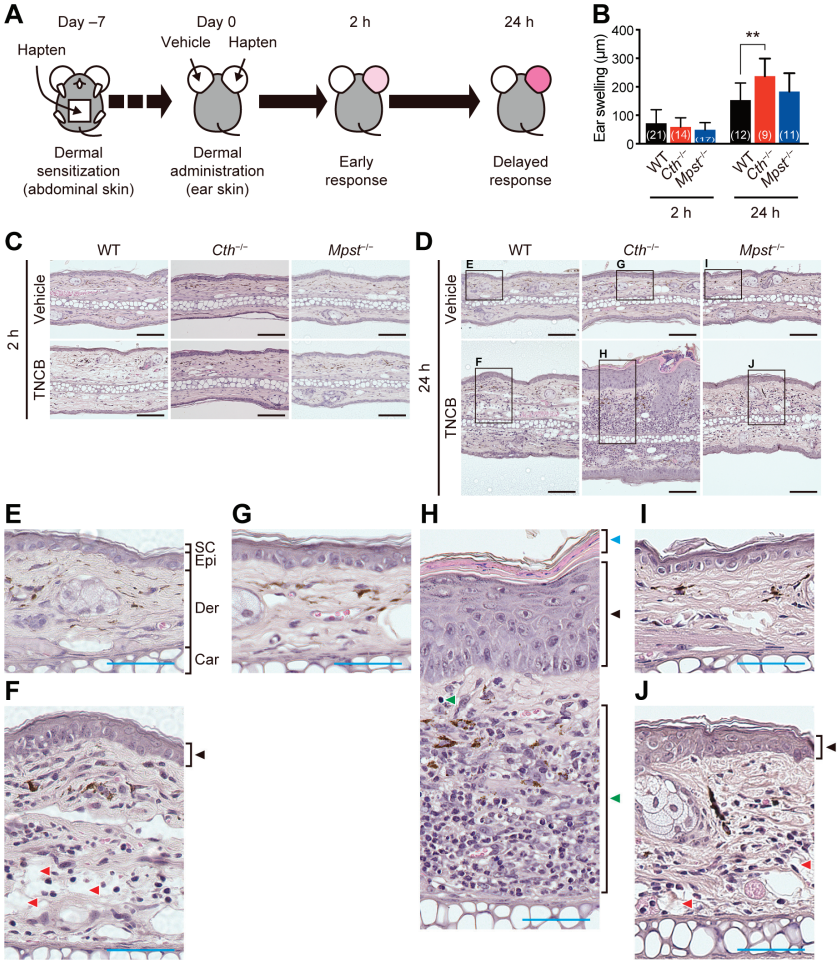

Figure 2. Trinitrochlorobenzene (TNCB)-induced contact dermatitis. (**A**) Experimental design. Adult male wild-type (WT), CTH-deficient (*Cth*$^{-/-}$), and MPST-deficient (*Mpst*$^{-/-}$) mice were sensitized on the skin and then (7 days later) challenged with TNCB on single ear (another ear with the vehicle) to examine Th1-type allergic responses. (**B**–**J**) Increased thickness of the ear (ear swelling = thickness difference between the TNCB-treated right ear and the vehicle-treated left ear) at 2 h and 24 h after the challenge (**B**) and their typical section images of HE-stained sagittal sections (**C**,**D**) with magnified images (**E**–**J**). Data are the mean ± SD (sample numbers). Differences are significant between the groups at each point by a one-way analysis of variance (ANOVA) with Tukey's multiple comparison test; ** $p < 0.01$ (**B**). Black bars indicate 100 μm (**C**,**D**), and blue bars indicate 50 μm (**E**–**J**). SC, stratum corneum; Epi, epidermis; Der, dermis; and Car, cartilage (**E**). Black arrowheads indicate TNCB-induced acanthosis (**F**,**H**,**J**); blue and green arrowheads indicate parakeratosis and immune cell infiltration, respectively (**H**); and red arrowheads indicate spongiosis (**F**,**I**).

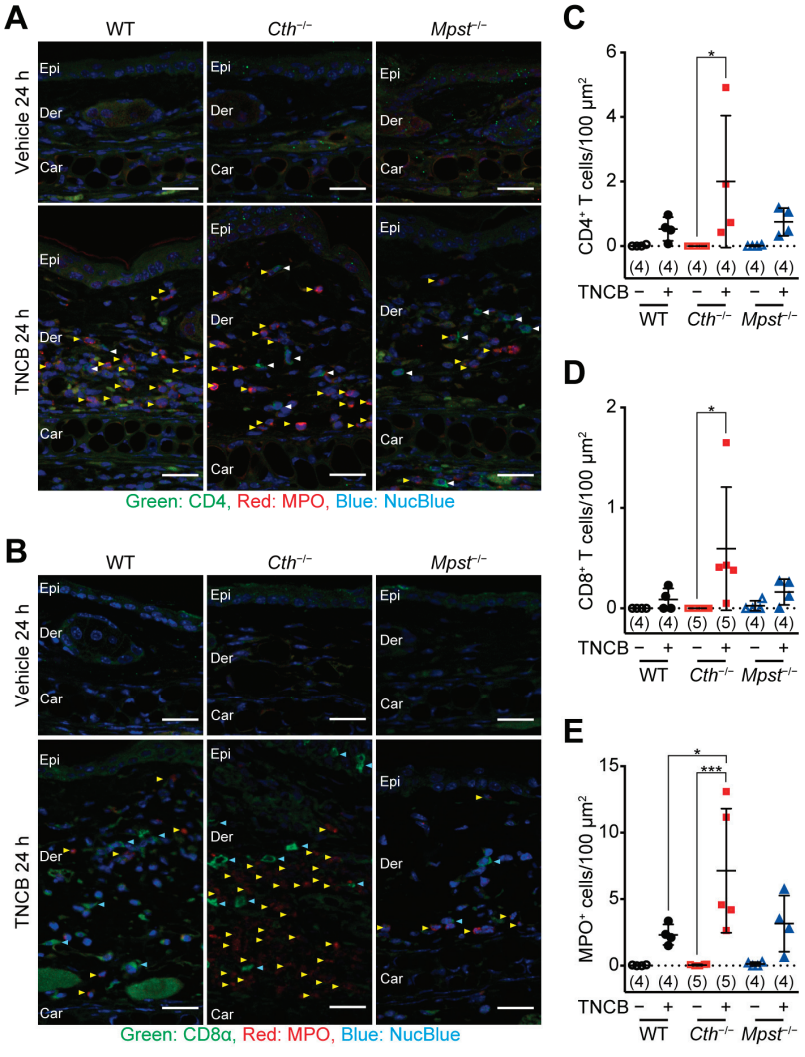

Figure 3. Immunohistochemical analysis of ear sagittal sections at 24 h after the trinitrochlorobenzene (TNCB) challenge. (**A**) Coimmunostaining with anti-CD4 antibody (green), anti-myeloperoxidase (MPO) antibody (red), and NucBlue (to stain nuclei, blue). White and yellow arrowheads indicate $CD4^+$ cells and MPO^+ cells, respectively. (**B**) Coimmunostaining with anti-CD8α antibody (green), anti-MPO antibody (red), and NucBlue (blue). Light blue and yellow arrowheads represent $CD8^+$ and MPO^+ cells, respectively. SC, stratum corneum; Epi, epidermis; Der, dermis; and Car, cartilage in (**A**,**B**). (**C**–**E**) Distribution density of $CD4^+$ (**C**), $CD8^+$ (**D**), and MPO^+ (**D**) cells per 100 μm^2. Data are the mean ± SD (sample numbers). Differences between groups in each time point are significant by a one-way ANOVA with Tukey's multiple comparison test at * $p < 0.05$ and *** $p < 0.001$ (**C**–**E**). White bars indicate 25 μm (**A**,**B**).

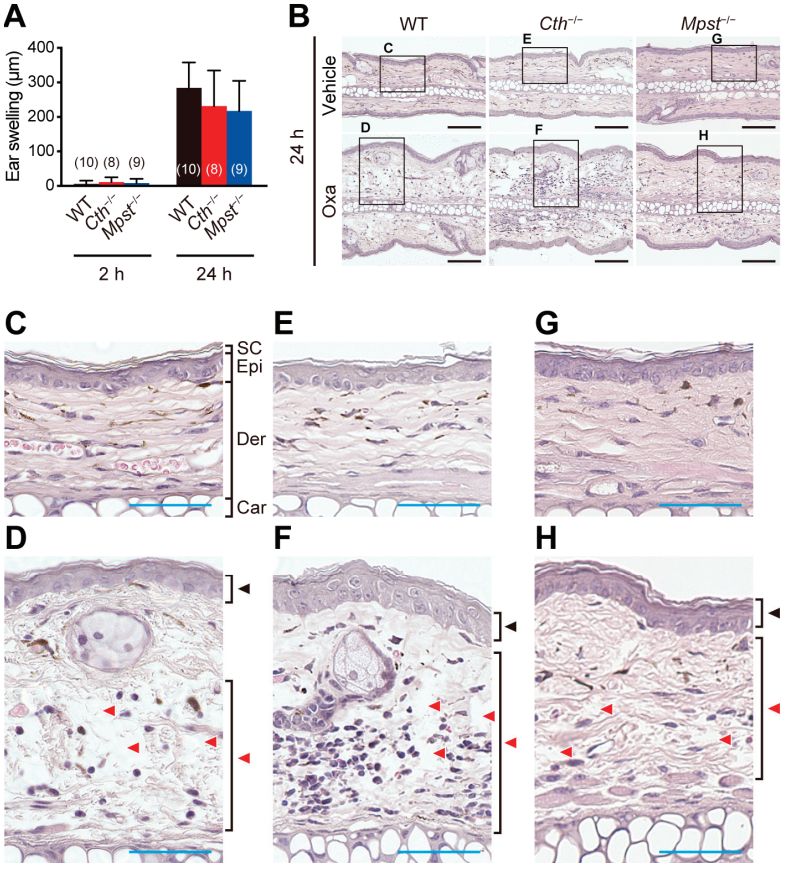

Figure 4. Oxazolone-induced contact dermatitis. Adult male wild-type (WT), CTH-deficient (*Cth*$^{-/-}$), and MPST-deficient (*Mpst*$^{-/-}$) mice were sensitized on the skin and then (7 days later) challenged with oxazolone (Oxa) on a single ear (another ear with the vehicle) to examine Th1/Th2-type allergic responses. (**A**) Increased ear thickness (the difference between oxazolone-treated right ear and vehicle-treated left ear) at 2 h and 24 h after oxazolone challenge. Data are the mean ± SD (sample numbers). (**B**–**H**) Typical section images of HE-stained sagittal sections of ears at 24 h after oxazolone challenge (**B**) with their magnified images (**C**–**H**). SC, stratum corneum; Epi, epidermis; Der, dermis; and Car, cartilage in (**A**,**B**). Black arrowheads indicate oxazolone-induced acanthosis, whereas red arrowheads indicate spongiosis (**D**,**F**,**H**). Bars indicate 100 μm (black, **B**) or 50 μm (blue, **C**–**H**).

2.3. CTH mRNA Induction in the Delayed Phase of TNCB-Induced Contact Dermatitis

Quantitative reverse transcription-polymerase chain reaction (RT-PCR) analyses revealed no level changes in both CTH and MPST mRNA in the TNCB- and vehicle-treated ears of WT, *Mpst*$^{-/-}$ (without *Mpst*), and *Cth*$^{-/-}$ mice (without *Cth*) at the early phase (2 h) (Figure 5A,B). However, at the delayed phase (24 h), CTH mRNA was upregulated in the TNCB-treated ears of WT and *Mpst*$^{-/-}$ mice, whereas MPST mRNA was downregulated in the TNCB-treated ears of WT and *Cth*$^{-/-}$ mice (Figure 5C,D), suggesting protective roles of CTH against the delayed phase of TNCB-induced contact dermatitis. MPST downregulation was also found in the delayed phase (not the early phase) of oxazolone-treated ears of WT and *Cth*$^{-/-}$ mice (but not significant in *Cth*$^{-/-}$) (Figure 5E,F); therefore, MPST mRNA downregulation may not be implicated in the disease condition.

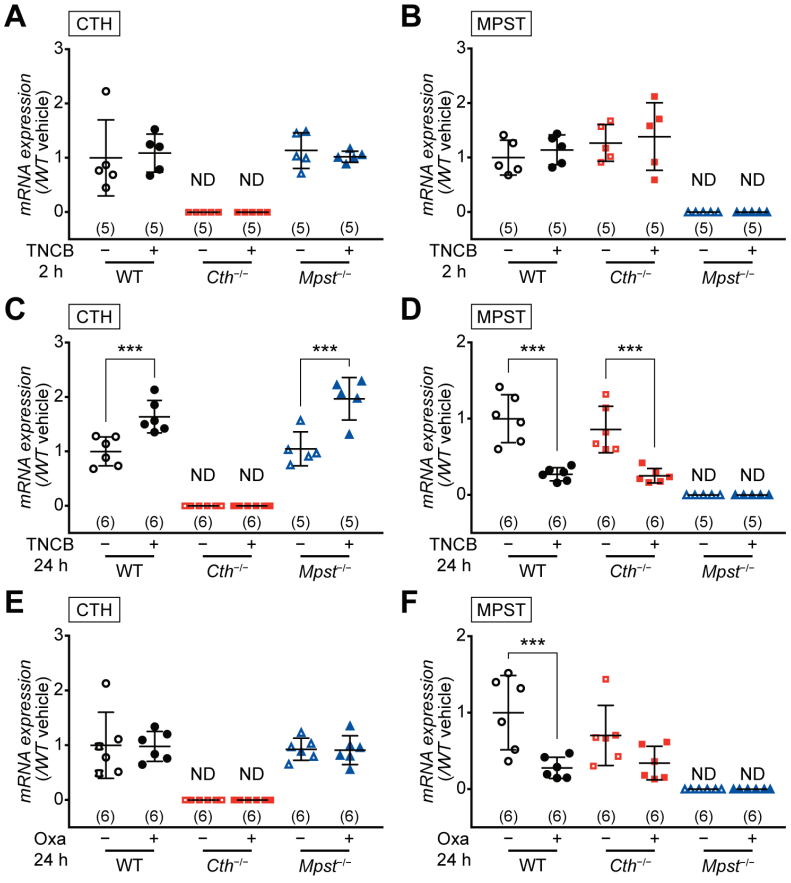

Figure 5. Expression levels of CTH and MPST mRNAs in the ear during hapten-induced contact dermatitis. The total RNA was extracted from each ear at 2 h (**A**,**B**) or 24 h (**C**–**F**) after trinitrochlorobenzene (TNCB; **A**–**D**) or oxazolone (Oxa; **E**,**F**) challenge. CTH (**A**,**C**,**E**) and MPST (**B**,**D**,**F**) mRNA levels were normalized by the housekeeping HPRT1 mRNA levels, and the relative expression versus vehicle-treated wild-type samples were calculated. Data are the mean ± SD (sample numbers) in parentheses. Differences are significant by a one-way ANOVA with Tukey's multiple comparison test at *** $p < 0.001$. ND, not detectable.

2.4. Marked Induction of Pro-inflammatory/Th2 Cytokine mRNA in the Delayed Phase of TNCB-Induced Contact Dermatitis in Cth$^{-/-}$ Mice

RT-PCR analyses revealed mRNA upregulation of pro-inflammatory cytokines, interleukin 1 beta (IL-1β), interleukin 6 (IL-6), and TNFα (but not significant), without apparent mRNA alterations in cytokines that regulate T-cell differentiation, such as interferon gamma (IFNγ), interleukin 2 (IL-2), interleukin 4 (IL-4), tumor growth factor beta (TGFβ), interleukin 17 (IL-17), and interleukin 10 (IL-10), in the early phase of TNCB- and vehicle-treated ears of all genotypes (Supplementary Figure S3; except for slight IL-4 mRNA upregulation in *Cth*$^{-/-}$ mice). In contrast, at the delayed phase, mRNA upregulation of IL-1β and IL-6 was the most pronounced and that of Th2 cytokines (IL-4 and IL-10) was only observed in the TNCB-treated ears of *Cth*$^{-/-}$ mice (Figure 6A–I). In the TNCB-treated ears of WT and *Mpst*$^{-/-}$ mice, Th1 cytokines (IFNγ and IL-2) expression was somewhat upregulated (Figure 6D,E, respectively), whereas that of Th2 cytokine IL-4 was downregulated (Figure 6F), supporting TNCB as a Th1-type inflammation-inducing hapten. Conversely,

such changes were not apparent in *Cth*$^{-/-}$ mice (Figure 6D–F). Both TGFβ and IL-17 mRNA were not upregulated in TNCB-treated ears of all genotypes (Figure 6G,H, respectively), and therefore, Th17 responses may not be involved. RT-PCR analyses also revealed mRNA upregulation of pro-inflammatory cytokines (IL-1β and IL-6) and some Th1 or Th2 cytokines (IFNγ, IL-4, and IL-10), but not that of IL-2, TGFβ, and IL-17, at the delayed phase of oxazolone-induced contact dermatitis, similar within the three genotypes (Figure 7A–I).

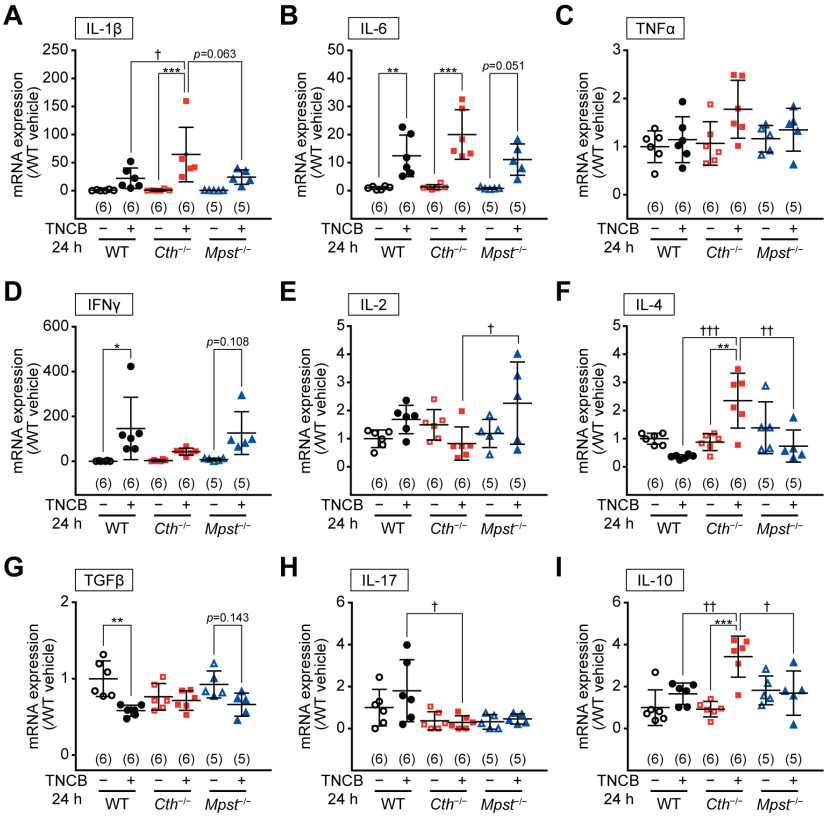

Figure 6. Expression levels of various cytokine mRNAs in the ear during trinitrochlorobenzene (TNCB)-induced contact dermatitis at 24 h after the challenge. IL-1β (**A**), IL-6 (**B**), TNFα (**C**), IFNγ (**D**), IL-2 (**E**), IL-4 (**F**), TGFβ (**G**), IL-17 (**H**), and IL-10 (**I**) mRNA levels were normalized by the housekeeping HPRT1 mRNA levels, and the relative expression versus vehicle-treated wild-type samples were calculated. Data are the mean ± SD with sample numbers in parentheses. Differences are significant by a one-way ANOVA with Tukey's multiple comparison test at * $p < 0.05$, ** $p < 0.01$, and *** $p < 0.001$ versus vehicle-treated samples of each genotype; † $p < 0.05$, †† $p < 0.01$, and ††† $p < 0.001$ between genotypes.

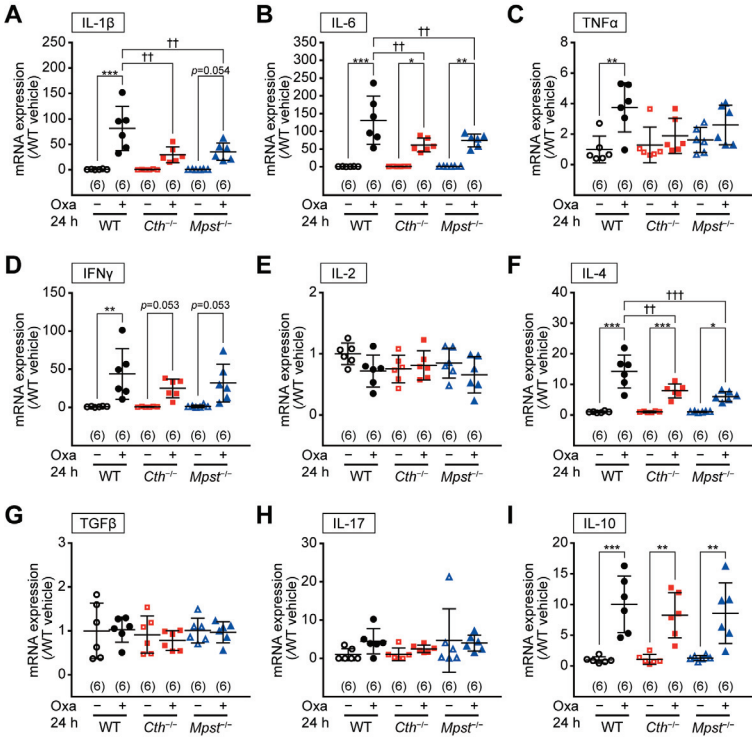

Figure 7. Expression levels of various cytokine mRNAs in the ear during oxazolone (Oxa)-induced contact dermatitis at 24 h after the challenge. IL-1β (**A**), IL-6 (**B**), TNFα (**C**), IFNγ (**D**), IL-2 (**E**), IL-4 (**F**), TGFβ (**G**), IL-17 (**H**), and IL-10 (**I**) mRNA levels were normalized by the housekeeping HPRT1 mRNA levels, and the relative expression versus vehicle-treated wild-type samples were calculated. Data are the mean ± SD with sample numbers in parentheses. Differences are significant by a one-way ANOVA with Tukey's multiple comparison test at * $p < 0.05$, ** $p < 0.01$, and *** $p < 0.001$ versus vehicle-treated samples of each genotypes; †† $p < 0.01$ and ††† $p < 0.001$ between genotypes.

3. Discussion

The first quarter of a century has passed since the first identification of H_2S as the signaling gaseous molecule; to date, >60,000 publications (in PubMed) have reported its versatile roles in regulating neural, cardiovascular, and endocrine systems, as well as inflammation (reviewed in [10,22]). Notably, H_2S could function as either an anti-inflammatory or pro-inflammatory mediator [10–12]. H_2S is apt to show anti-inflammatory effects at relatively low or physiological concentrations, whereas it exerts pro-inflammatory effects when the tissues/cells are exposed to high concentrations or under particular disease conditions, such as some types of inflammation [10–12]. Although applications of the so-called H_2S donors generally exert anti-inflammatory, cytoprotective, and antioxidant effects in the cells and animals [10], they often result in enhanced inflammation [23]. Indeed, our *Cth*$^{-/-}$ mice displayed the systemic resistance against caerulein-induced acute pancreatitis [24], cecal-ligation and puncture-induced sepsis [25], and acute renal ischemia/reperfusion injury and its associated inflammatory responses [26], suggesting the pro-inflammatory roles of endogenous H_2S produced by CTH at those inflammation loci.

As for experimental colitis, H_2S donor application has been shown to alleviate DSS-induced colitis in mice [27,28] and rats [29], and TNBS-induced colitis in mice [30] and rats [31,32]. DSS-induced colitis is one of the most commonly used IDB models to evaluate drug candidates because this model can be easily induced by administering DSS by drink-

ing water, although this model is fundamentally different from hapten-induced colitis [13]. Treatment with a nonspecific CTH inhibitor propargylglycine exacerbated DSS-induced colitis in mice [33], and mRNA expression of three H_2S-producing enzymes (CTH, MPST, and cystathionine β-synthase [CBS]) and H_2S production was upregulated in the colon mucosa in the experimental colitis of mice/rats [29,33–35]. *Cth*$^{-/-}$ mice of different origins were more susceptible to DSS-induced colitis [28] and dinitrobenzene sulfonic acid (DNBS [TNBS analog]; single intracolonic administration)-induced colitis [36], whereas *Mpst*$^{-/-}$ mice of a different origin [37] were more vulnerable to both TNBS- and DSS-induced colitis [35]. In this study, both *Cth*$^{-/-}$ and *Mpst*$^{-/-}$ mice (on the same C57BL/6J background) did not show significantly altered responses to TNBS and oxazolone (Figure 1A–F). Discrepancies between these studies could be attributable to the differences of experimental procedures, stimulants (DSS, DNBS, or TNBS), administration routes (oral or per rectum), a single administration or the challenge after sensitization, and fasted or not before the challenge.

On the other hand, the aberrant H_2S metabolism has been involved in the pathogenesis of various skin diseases, including vascular disorders, pigmentation disorders, melanoma, ulcers, and psoriasis [18]. Psoriasis, which is characterized by hyper-proliferative keratinocytes and auto-reactive immune cells, was associated with low serum levels of H_2S and high IL-6, IL-8, and TNFα [38]. H_2S donor application to mice alleviated chemically induced itch [39], promoted skin wound healing via oxidative stress inhibition and vascular endothelial growth factor enhancement [40], and improved diabetic wound healing by inhibiting NETosis and NETs release [41]. In contrast, the mean disulfide levels were found to be significantly higher in the rosacea patients than in the control group [42], and the serum levels of H_2S were significantly higher in atopic dermatitis patients compared to healthy controls [43]. Based on those somewhat contradictory findings, hapten-induced contact dermatitis (also referred to as contact hypersensitivity) was first investigated in *Cth*$^{-/-}$ and *Mpst*$^{-/-}$ mice as another inflammation model of the systemic immunity. Experimental contact dermatitis consists of the early phase dominated by complement and innate immune cells and the delayed phase governed by adaptive immune cells, such as CD4$^+$ T cells (Th1 and Th2 cells), CD8$^+$ T cells (Tc1 cells), and B cells, as a typical type IV allergic response [44,45].

Our *Cth*$^{-/-}$ mice (but not *Mpst*$^{-/-}$ mice) displayed higher sensitivity against TNCB at the delayed inflammation phase, as revealed by ear thickening (Figure 2B,D,H), infiltration of CD4$^+$ and CD8$^+$ T cells and MPO$^+$ neutrophils (Figure 3A–E), and mRNA induction of pro-inflammatory cytokines (IL-1β and IL-6) and Th2-type cytokines (IL-4 and IL-10) (Figure 6A,B,F,I). Conversely, both *Cth*$^{-/-}$ and *Mpst*$^{-/-}$ mice did not display marked alteration from WT mice in oxazolone-induced contact dermatitis at the delayed phase (Figure 4A–H) and mRNA upregulation of cytokines in all phases (Figure 7A–I). Notably, CTH mRNA was upregulated, whereas MPST mRNA was downregulated at the delayed phase of TNCB-treated ears (Figure 5C,D), when CTH mRNA upregulation was not observed in the early phase of TNCB-treated ears (Figure 5A) and the delayed phase of oxazolone-induced ears (Figure 5E), and MPST mRNA downregulation, was evident in the delayed phase of oxazolone-induced ears (Figure 5F).

These results suggest that CTH in the ear protected against the delayed phase of TNCB-induced inflammation by suppressing Th1-to-Th2 shift, whereas CTH deletion in mice exacerbated the inflammation by Th1/Th2 imbalance. Because acute ear canal responses to passive cutaneous anaphylaxis were equivalent between WT, *Cth*$^{-/-}$, and *Mpst*$^{-/-}$ mice in our previous study [15], CTH or H_2S might play more roles in the antigen-specific delayed phase of inflammation, rather than the antigen nonspecific early phase that mainly involves innate immune cells [46]. Pro-inflammatory M1 macrophages are activated by Th1 cytokines, whereas anti-inflammatory M2 macrophages are activated by Th2 cytokines. H_2S produced by CBS has been shown to suppress the polarization of mouse primary microglia (macrophages in the brain) toward M1 phenotypes [47]. H_2S regulated the expression of methylcytosine dioxygenases Tet1/Tet2 to promote regulatory T-cell differentiation in immune cells, and H_2S deficiency led to systemic autoimmune disease [48]. Therefore, H_2S

produced by CTH could help maintain the Th1/Th2 balance against challenges with the specific model hapten (TNCB) in this study.

Hyperhomocysteinemia (a highly elevated blood homocysteine level) should also be considered in $Cth^{-/-}$ mice; total serum homocysteine levels are 83.6 ± 18.6 μM (n = 5) and 5.78 ± 1.22 μM (n = 10) in WT mice, and 5.90 ± 2.05 μM (n = 7) in $Mpst^{-/-}$ mice [15]. Elevated blood homocysteine levels are an independent risk factor for cardiovascular diseases and the risk of hyperhomocysteinemia is significantly higher in patients with IBD [49]. Diet (high methionine)-induced hyperhomocysteinemia exacerbated DSS-induced colitis in rats [50], and homocysteine promoted $CD4^+$ T cell differentiation (lamina propria lymphocytes in the colonic mucosa of Wistar rats) into Th17 cells [51]. As for the skin, patients with psoriasis have significantly higher serum homocysteine levels [52], although the relationship between homocysteinemia and contact dermatitis remains unknown. Therefore, the exacerbated phenotypes in TNCB-induced contact dermatitis may not be solely attributable to H_2S deficiency in $Cth^{-/-}$ mice.

In conclusion, we have found that CTH plays important roles in protecting against contact dermatitis, induced by the specific model hapten (TNCB but not oxazolone). In this study, endogenous H_2S produced by CTH could act as a specific anti-inflammatory mediator. Our previous study demonstrated the altered serum amino acid profiles in $Cth^{-/-}$ and $Mpst^{-/-}$ mice [15], and further studies are warranted to explain the complex and often opposing roles of H_2S in inflammatory responses.

4. Materials and Methods

4.1. Animals

C57BL/6J inbred strain (C57BL/6JJcl; CLEA Japan, Tokyo, Japan) were used as WT mice. $Cth^{+/-}$ mice were generated by homologous recombination in embryonic stem cells and blastocyte injection, and backcrossed for 12 generations to C57BL/6JJcl [14]. $Mpst^{+/-}$ mice were generated using CRISPR/Cas9 technology on fertilized C57BL/6JJcl embryos by Setsurotech Inc. (Tokushima, Japan) [15]. Heterologous mice were bred to obtain homozygous mice, and these mice (8–22-week-old males) were used for comparative analyses on the same C57BL/6JJcl background. Preoperatively, mice were housed in an air-conditioned room (23 ± 1 °C, 55 ± 5% humidity), kept in a 12 h dark/light cycle, and allowed free access to a CE-2 standard dry rodent diet (CLEA Japan) and water. Before the surgeries, mice were anaesthetized with isoflurane inhalation.

4.2. Hapten-Induced Colitis

Hapten-induced experimental colitis was established as IBD models in mice. Adult male mice (aged 7–21 weeks) were anesthetized with isoflurane and sensitized by the topical application of 150 μL of 1% (*v/v*) TNBS (Sigma-Aldrich, Burington, MA, USA; cat no. P2297) in the vehicle (acetone-olive oil, 4:1 [*v/v*]) to the shaved dorsal skin (1.5 × 1.5-cm^2) between the shoulders. After 7 days, mice were weighed, anesthetized with isoflurane, and administered (~30 s) with 100 μL of 50% ethanol (vehicle) or 2.5% (*w/v*) TNBS in the vehicle, per rectum, using a 3.5-Fr. catheter system (Nippon Sherwood Medical Industries, Osaka, Japan). Mice were also sensitized by topical application of 150 μL of 3% (*w/v*) oxazolone (Sigma-Aldrich; cat no. 862207) in ethanol to the shaved ventral skin (2 × 2-cm square). After 7 days, they were weighed, anesthetized with isoflurane, and administered (~30 s) with 100 μL of 50% ethanol (vehicle) and or 1% (*w/v*) oxazolone in the vehicle, per rectum, using a 3.5-Fr. catheter system. After the administration, mice were kept upside-down for 30 s to prevent backflow. Mice were weighed daily and sacrificed at day 3 (for TNBS) or day 2 (for oxazolone), post-administration. The colons, including rectums, were quickly removed from the anesthetized mice, measured for their lengths, washed in saline, spread inside-out on a black paper, and examined for macroscopic lesions using the Wallace score, which scores on a scale from 0 to 10 based on the following criteria: hyperemia, bowel wall thickening, and the extent of ulceration and inflammation [53]. Then, the colon was fixed in either 10% formalin, dehydrated in an ascending ethanol series (from 75% to 100%), and

then xylene, and embedded in paraffin. About 3-μm sections were cut, deparaffinized, and stained with HE. TNBS-induced colitis was examined using the Ameho score [54]. Oxazolone-induced colitis was examined using the inflammation score defined in this study to evaluate tissue anomaly with reference to Bendtsen et al. [55]. The anomaly in the mucosal surface (epithelial cell loss, depletion of mucin producing goblet cells, and/or reduction of tubular density) was defined as ulcer, and scores of 0–3 (0 = no change, 1 = mild, 2 = moderate, and 3 = general) were given by one person. Similarly, anomalies in the mucosal intrinsic layer (immune cell filtration) and submucosal layer (edema) were independently defined and scored 0–3 each. Thus, the maximum inflammation score is summed up to 9 (Figure 1H).

4.3. Hapten-Induced Contact Dermatitis

Hapten-induced contact dermatitis was examined for contact hypersensitivity. Adult male mice (7–21 weeks) were anesthetized with isoflurane and sensitized by the topical application of 100 μL of 7% (*v/v*) TNCB (Tokyo Chemical Industry, Tokyo, Japan) in acetone-olive oil (4:1, *v/v*) to the shaved abdomen (approximately 2 cm^2). After 7 days, mice were challenged with 10 μL of 1% TNCB in acetone-olive oil (9:1, *v/v*) onto each side of the left ear, and the right ear was administered with the vehicle alone. The ear thickness was measured using a digital SMD-565J-L thickness gauge (Teclock, Nagano, Japan) before the induction (T_0), and at 2 h (T_1) and 12 h (T_2) after the induction. The ear swelling (μm thickness) was calculated as ($T_{1\ or\ 2} - T_0$ of the left ear)–($T_{1\ or\ 2} - T_0$ of the right ear). After 24 h measurement, the entire pinna was collected and weighed. The ear was cut lengthwise into two pieces; one was fixed in 10% formalin for hematoxylin-eosin staining of paraffin sections and one for mRNA expression assays. Mice were also sensitized with 100 μL of 3% oxazolone in ethanol and then (5 days later) challenged with 10 μL of 1% oxazolone in ethanol.

4.4. Immunohistochemistry

Paraffin sections were deparaffinized with xylene and ethanol, antigen-activated in Immunosaver (Fujifilm-Wako, Osaka, Japan) at 98 °C for 45 min, and then blocked with 5% normal donkey serum in phosphate-buffered saline-0.5% Tween 20. Sections were incubated with goat anti-myeloperoxidase (MPO) polyclonal antibody (1:500; Santa Cruz; cat no. sc-16129), rabbit anti-CD4 (BLR167J) monoclonal antibody (1:500; Bethyl Laboratories, Waltham, MA, USA; cat no. A700-167-T), or rabbit anti-CD8 alpha (BLR173J) monoclonal antibody (1:500; Bethyl Laboratories; cat no. A700-173-T) in Can Get Signal A (Toyobo, Osaka, Japan) as the primary antibody, and donkey anti-rabbit IgG conjugated Alexa 488 (1:500; Invitrogen, Waltham, MA, USA) and donkey anti-goat IgG conjugated Alexa 568 (1:500; Invitrogen) was used in the blocking solution as the secondary antibody. Sections were sealed with ProLong Glass Antifade Mountant with NucBlue Stain (ThermoFisher Scientific, Waltham, MA, USA) and observed by a BZ-9000 microscope (Keyence, Osaka, Japan) equipped with Nikon objectives.

4.5. Quantitative RT-PCR

The total RNA was isolated from the tissues using a TRI reagent (Molecular Research Center, Cincinnati, OH, USA), and cDNA was synthesized using a ReverTra Ace qPCR RT Master Mix with random hexamers (Toyobo). Quantitative real-time PCR assay was performed using THUNDERBIRD qPCR Mix (Toyobo) with a CFX Connect Real-Time PCR Detection System (Bio-Rad). Primers were designed using the Primer3 program (https://primer3.ut.ee, accessed on 1 January 2020) (Supplementary Table S1). The cycling conditions consisted of initial denaturation at 95 °C for 10 s, followed by 50 cycles of 95 °C for 5 s and 60 °C for 30 s.

4.6. Statistical Analyses

Data were expressed as mean ± SD with sample numbers in parentheses. Statistical comparison was performed by a Mann–Whitney U test or a one-way analysis of variance (ANOVA) with Tukey's multiple comparison test using Prizm 5 software (GraphPad, San Diego, CA, USA). All p-values of <0.05 denoted a significant difference.

Supplementary Materials: The following supporting information can be downloaded at: https://www.mdpi.com/article/10.3390/ijms24032659/s1.

Author Contributions: Conceptualization; validation; formal analysis; data curation; writing—original draft preparation; visualization; project administration; funding acquisition, N.A. and I.I.; methodology, N.A.; investigation, N.A., R.H., S.Y., R.T., T.Y. and W.K.; resources; supervision, I.I. All authors have read and agreed to the published version of the manuscript.

Funding: This work was partly supported by Grants-in-Aid for Scientific Research (17K08287 to N.A.) and Transformative Research Areas (A) (22H05577 to I.I.) from the Japan Society for the Promotion of Science.

Institutional Review Board Statement: All animal procedures conformed to the Guide for the Care and Use of Laboratory Animals, 8th Edition published by the US National Research Council and were approved by the Animal Care Committees of Showa Pharmaceutical University (No. P-2016-10, P-2018-07 and P-2021-2; approval dates: 22 July 2016, 12 April 2018 and 31 March 2022, respectively).

Informed Consent Statement: Not applicable.

Data Availability Statement: Not applicable.

Conflicts of Interest: The authors declare no conflict of interest.

References

1. M'Koma, A.E. Inflammatory Bowel Disease: Clinical Diagnosis and Surgical Treatment-Overview. *Medicina (Kaunas)* **2022**, *58*, 567. [CrossRef] [PubMed]
2. Roda, G.; Chien, N.S.; Kotze, P.G.; Argollo, M.; Panaccione, R.; Spinelli, A.; Kaser, A.; Peyrin-Biroulet, L.; Danese, S. Crohn's disease. *Nat. Rev. Dis. Prim.* **2020**, *6*, 22–40. [PubMed]
3. Kobayashi, T.; Siegmund, B.; Le Berre, C.; Wei, S.C.; Ferrante, M.; Shen, B.; Bernstein, C.N.; Danese, S.; Peyrin-Biroulet, L.; Hibi, T. Ulcerative colitis. *Nat. Rev. Dis. Prim.* **2020**, *6*, 74–93. [PubMed]
4. Kofla-Dłubacz, A.; Pytrus, T.; Akutko, K.; Sputa-Grzegrzółka, P.; Piotrowska, A.; Dzięgiel, P. Etiology of IBD-Is it still a mystery? *Int. J. Mol. Sci.* **2022**, *23*, 12445–12457. [PubMed]
5. Kakuta, Y.; Naito, T.; Kinouchi, Y.; Masamune, A. Current Status and Future Prospects of Inflammatory Bowel Disease Genetics. *Digestion* **2023**, *104*, 7–15. [CrossRef] [PubMed]
6. Rowan, F.E.; Docherty, N.G.; Coffey, J.C.; O'Connell, P.R. Sulphate-reducing bacteria and hydrogen sulphide in the aetiology of ulcerative colitis. *Br. J. Surg.* **2009**, *96*, 151–158. [CrossRef] [PubMed]
7. Stummer, N.; Weghuber, D.; Feichtinger, R.G.; Huber, S.; Mayr, J.A.; Kofler, B.; Neureiter, D.; Klieser, E.; Hochmann, S.; Lauth, W.; et al. Hydrogen Sulfide Metabolizing Enzymes in the Intestinal Mucosa in Pediatric and Adult Inflammatory Bowel Disease. *Antioxid* **2022**, *11*, 2235. [CrossRef]
8. Murphy, B.; Bhattacharya, R.; Mukherjee, P. Hydrogen sulfide signaling in mitochondria and disease. *FASEB J.* **2019**, *33*, 13098–13125. [CrossRef]
9. Sawa, T.; Motohashi, H.; Ihara, H.; Akaike, T. Enzymatic Regulation and Biological Functions of Reactive Cysteine Persulfides and Polysulfides. *Biomolecules* **2020**, *10*, 1245. [CrossRef]
10. Dilek, N.; Papapetropoulos, A.; Toliver-Kinsky, T.; Szabo, C. Hydrogen sulfide: An endogenous regulator of the immune system. *Pharmacol. Res.* **2020**, *161*, 105119–105157. [CrossRef]
11. Li, M.; Mao, J.; Zhu, Y. New Therapeutic Approaches Using Hydrogen Sulfide Donors in Inflammation and Immune Response. *Antioxid. Redox Signal.* **2021**, *35*, 341–356. [CrossRef] [PubMed]
12. Bhatia, M.; Gaddam, R.R. Hydrogen Sulfide in Inflammation: A Novel Mediator and Therapeutic Target. *Antioxid. Redox Signal.* **2021**, *34*, 1368–1377. [CrossRef] [PubMed]
13. Nagaoka, M.; Radi, Z.A. Pharmacologic efficacy in inflammatory bowel disease models. *Front. Biosci (Sch. Ed)* **2012**, *4*, 1295–1314. [CrossRef]
14. Ishii, I.; Akahoshi, N.; Yamada, H.; Nakano, S.; Izumi, T.; Suematsu, M. Cystathionine gamma-lyase-deficient mice require dietary cysteine to protect against acute lethal myopathy and oxidative injury. *J. Biol. Chem.* **2010**, *285*, 26358–26368. [CrossRef]

15. Akahoshi, N.; Minakawa, T.; Miyashita, M.; Sugiyama, U.; Saito, C.; Takemoto, R.; Honda, A.; Kamichatani, W.; Kamata, S.; Anan, Y.; et al. Increased Urinary 3-Mercaptolactate Excretion and Enhanced Passive Systemic Anaphylaxis in Mice Lacking Mercaptopyruvate Sulfurtransferase, a Model of Mercaptolactate-Cysteine Disulfiduria. *Int. J. Mol. Sci.* **2020**, *21*, 818. [CrossRef]
16. Scheinman, P.L.; Vocanson, M.; Thyssen, J.P.; Johansen, J.D.; Nixon, R.L.; Dear, K.; Botto, N.C.; Morot, J.; Goldminz, A.M. Contact dermatitis. *Nat. Rev. Dis. Prim.* **2021**, *7*, 38–63. [PubMed]
17. Johansen, J.D.; Bonefeld, C.M.; Schwensen, J.F.B.; Thyssen, J.P.; Uter, W. Novel insights into contact dermatitis. *J. Allergy Clin. Immunol.* **2022**, *149*, 1162–1171. [CrossRef]
18. Xiao, Q.; Xiong, L.; Tang, J.; Li, L.; Li, L. Hydrogen Sulfide in Skin Diseases: A Novel Mediator and Therapeutic Target. *Oxidative Med. Cell. Longev.* **2021**, *2021*, 6652086–6652096. [CrossRef]
19. Fernández-Vozmediano, J.M.; Hita, J.C.A.; Manrique-Plaza, A. Allergic contact dermatitis from diallyl disulfide. *Contact Dermat.* **2000**, *42*, 108–109.
20. Shi, Y.; Liu, Z.; Cui, X.; Zhao, Q.; Liu, T. Intestinal vitamin D receptor knockout protects from oxazolone-induced colitis. *Cell Death Dis.* **2020**, *11*, 461–471. [CrossRef]
21. Christensen, A.D.; Haase, C. Immunological mechanisms of contact hypersensitivity in mice. *Apmis* **2011**, *120*, 1–27. [CrossRef] [PubMed]
22. Kimura, H. Hydrogen sulfide (H2S) and polysulfide (H2Sn) signaling: The first 25 years. *Biomolecules* **2021**, *11*, 896. [CrossRef] [PubMed]
23. Di Villa Bianca, R.; Coletta, C.; Mitidieri, E.; De Dominicis, G.; Rossi, A.; Sautebin, L.; Cirino, G.; Bucci, M.; Sorrentino, R. Hydrogen sulphide induces mouse paw oedema through activation of phospholipase A2. *Br. J. Pharmacol.* **2010**, *161*, 1835–1842. [CrossRef]
24. Ang, A.D.; Rivers-Auty, J.; Hegde, A.; Ishii, I.; Bhatia, M. The effect of CSE gene deletion in caerulein-induced acute pancreatitis in the mouse. *Am. J. Physiol. Gastrointest Liver Physiol.* **2013**, *305*, G712–G721. [CrossRef] [PubMed]
25. Gaddam, R.R.; Fraser, R.; Badiei, A.; Chambers, S.; Cogger, V.C.; Le Couteur, D.G.; Ishii, I.; Bhatia, M. Cystathionine-Gamma-Lyase Gene Deletion Protects Mice against Inflammation and Liver Sieve Injury following Polymicrobial Sepsis. *PLoS ONE* **2016**, *11*, e0160521–e0160541. [CrossRef]
26. Markó, L.; Szijártó, I.A.; Filipovic, M.R.; Kaßmann, M.; Balogh, A.; Park, J.-K.; Przybyl, L.; N'Diaye, G.; Krämer, S.; Anders, J.; et al. Role of Cystathionine Gamma-Lyase in Immediate Renal Impairment and Inflammatory Response in Acute Ischemic Kidney Injury. *Sci. Rep.* **2016**, *6*, 27517–27526. [CrossRef]
27. Zhao, H.; Yan, R.; Zhou, X.; Ji, F.; Zhang, B. Hydrogen sulfide improves colonic barrier integrity in DSS-induced inflammation in Caco-2 cells and mice. *Int. Immunopharmacol.* **2016**, *39*, 121–127. [CrossRef]
28. Qin, M.; Long, F.; Wu, W.; Yang, D.; Huang, M.; Xiao, C.; Chen, X.; Liu, X.; Zhu, Y.Z. Hydrogen sulfide protects against DSS-induced colitis by inhibiting NLRP3 inflammasome. *Free. Radic. Biol. Med.* **2019**, *137*, 99–109. [CrossRef]
29. Liu, Y.; Liao, R.; Qiang, Z.; Yang, W.; Cao, J.; Zeng, H. Exogenous H_2S Protects Colon Cells in Ulcerative Colitis by Inhibiting *NLRP3* and Activating Autophagy. *DNA Cell Biol.* **2021**, *40*, 748–756. [CrossRef]
30. Fiorucci, S.; Orlandi, S.; Mencarelli, A.; Caliendo, G.; Santagada, V.; Distrutti, E.; Santucci, L.; Cirino, G.; Wallace, J.L. Enhanced activity of a hydrogen sulphide-releasing derivative of mesalamine (ATB-429) in a mouse model of colitis. *Br. J. Pharmacol.* **2007**, *150*, 996–1002. [CrossRef]
31. Wallace, J.L.; Vong, L.; McKnight, W.; Dicay, M.; Martin, G.R. Endogenous and Exogenous Hydrogen Sulfide Promotes Resolution of Colitis in Rats. *Gastroenterology* **2009**, *137*, 569–578. [CrossRef] [PubMed]
32. Kupai, K.; Almási, N.; Kósa, M.; Nemcsók, J.; Murlasits, Z.; Török, S.; Al-Awar, A.; Baráth, Z.; Pósa, A.; Varga, C. H2S confers colonoprotection against TNBS-induced colitis by HO-1 upregulation in rats. *Inflammopharmacology* **2017**, *26*, 479–489. [CrossRef] [PubMed]
33. Hirata, I.; Naito, Y.; Takagi, T.; Mizushima, K.; Suzuki, T.; Omatsu, T.; Handa, O.; Ichikawa, H.; Ueda, H.; Yoshikawa, T. Endogenous Hydrogen Sulfide Is an Anti-inflammatory Molecule in Dextran Sodium Sulfate-Induced Colitis in Mice. *Dig. Dis. Sci.* **2010**, *56*, 1379–1386. [CrossRef]
34. Flannigan, K.L.; Ferraz, J.G.P.; Wang, R.; Wallace, J.L. Enhanced Synthesis and Diminished Degradation of Hydrogen Sulfide in Experimental Colitis: A Site-Specific, Pro-Resolution Mechanism. *PLoS ONE* **2013**, *8*, e71962–e71970. [CrossRef]
35. Zhang, J.; Cen, L.; Zhang, X.; Tang, C.; Chen, Y.; Zhang, Y.; Yu, M.; Lu, C.; Li, M.; Li, S.; et al. MPST deficiency promotes intestinal epithelial cell apoptosis and aggravates inflammatory bowel disease via AKT. *Redox Biol.* **2022**, *56*, 102469–102484. [CrossRef] [PubMed]
36. Motta, J.-P.; Flannigan, K.L.; Agbor, T.A.; Beatty, J.K.; Blackler, R.W.; Workentine, M.L.; Da Silva, G.J.; Wang, R.; Buret, A.G.; Wallace, J.L. Hydrogen Sulfide Protects from Colitis and Restores Intestinal Microbiota Biofilm and Mucus Production. *Inflamm. Bowel Dis.* **2015**, *21*, 1006–1017. [CrossRef]
37. Li, M.; Xu, C.; Shi, J.; Ding, J.; Wan, X.; Chen, D.; Gao, J.; Li, C.; Zhang, J.; Lin, Y.; et al. Fatty acids promote fatty liver disease via the dysregulation of 3-mercaptopyruvate sulfurtransferase/hydrogen sulfide pathway. *Gut* **2018**, *67*, 2169–2180. [CrossRef]
38. Alshorafa, A.K.; Guo, Q.; Zeng, F.; Chen, M.; Tan, G.; Tang, Z.; Yin, R. Psoriasis Is Associated with Low Serum Levels of Hydrogen Sulfide, a Potential Anti-inflammatory Molecule. *Tohoku J. Exp. Med.* **2012**, *228*, 325–332. [CrossRef]

39. Coavoy-Sánchez, S.A.; Rodrigues, L.; Teixeira, S.A.; Soares, A.G.; Torregrossa, R.; Wood, M.E.; Whiteman, M.; Costa, S.K.P.; Muscará, M.N. Hydrogen sulfide donors alleviate itch secondary to the activation of type-2 protease activated receptors (PAR-2) in mice. *Pharmacol. Res.* **2016**, *113*, 686–694. [CrossRef]
40. Xu, M.; Hua, Y.; Qi, Y.; Meng, G.; Yang, S. Exogenous hydrogen sulphide supplement accelerates skin wound healing via oxidative stress inhibition and vascular endothelial growth factor enhancement. *Exp. Dermatol.* **2019**, *28*, 776–785. [CrossRef]
41. Yang, C.-T.; Chen, L.; Chen, W.-L.; Li, N.; Chen, M.-J.; Li, X.; Zheng, X.; Zhao, Y.-Z.; Wu, Y.-X.; Xian, M.; et al. Hydrogen sulfide primes diabetic wound to close through inhibition of NETosis. *Mol. Cell. Endocrinol.* **2019**, *480*, 74–82. [CrossRef]
42. Sener, S.; Akbas, A.; Kilinc, F.; Erel, O.; Aktas, A. Thiol/disulfide homeostasis as a marker of oxidative stress in rosacea: A controlled spectrophotometric study. *Cutan. Ocul. Toxicol.* **2019**, *38*, 55–58. [CrossRef]
43. Moniaga, C.S.; Kamata, Y.; Ogawa, H.; Suga, Y.; Tominaga, M.; Takamori, K. Hydrogen sulfide modulates the expression of axon-guidance molecules in human keratinocytes. *J. Dermatol. Sci.* **2020**, *97*, 232–235. [CrossRef] [PubMed]
44. Kimber, I.; Basketter, D.A.; Gerberick, G.F.; Dearman, R.J. Allergic contact dermatitis. *Int. Immunopharmacol* **2002**, *2*, 201–211. [CrossRef] [PubMed]
45. Vocanson, M.; Hennino, A.; Rozières, A.; Poyet, G.; Nicolas, J.F. Effector and regulatory mechanisms in allergic contact dermatitis. *Allergy* **2009**, *64*, 1699–1714. [CrossRef]
46. Honda, T.; Egawa, G.; Grabbe, S.; Kabashima, K. Update of Immune Events in the Murine Contact Hypersensitivity Model: Toward the Understanding of Allergic Contact Dermatitis. *J. Investig. Dermatol.* **2013**, *133*, 303–315. [CrossRef] [PubMed]
47. Du, C.; Jin, M.; Hong, Y.; Li, Q.; Wang, X.H.; Xu, J.M.; Wang, F.; Zhang, Y.; Jia, J.; Liu, C.F.; et al. Downregulation of cystathionine beta-synthase/hydrogen sulfide contributes to rotenone-induced microglia polarization toward M1 type. *Biochem. Biophys. Res. Commun* **2014**, *451*, 239–245. [CrossRef]
48. Yang, R.; Qu, C.; Zhou, Y.; Konkel, J.E.; Shi, S.; Liu, Y.; Chen, C.; Liu, S.; Liu, D.; Chen, Y.; et al. Hydrogen Sulfide Promotes Tet1- and Tet2-Mediated Foxp3 Demethylation to Drive Regulatory T Cell Differentiation and Maintain Immune Homeostasis. *Immunity* **2015**, *43*, 251–263. [CrossRef]
49. Oussalah, A.; Guéant, J.-L.; Peyrin-Biroulet, L. Meta-analysis: Hyperhomocysteinaemia in inflammatory bowel diseases. *Aliment. Pharmacol. Ther.* **2011**, *34*, 1173–1184. [CrossRef]
50. Zhu, S.; Li, J.; Bing, Y.; Yan, W.; Zhu, Y.; Xia, B.; Chen, M. Diet-Induced Hyperhomocysteinaemia Increases Intestinal Inflammation in an Animal Model of Colitis. *J. Crohn's Colitis* **2015**, *9*, 708–719. [CrossRef]
51. Gao, X.; Li, J.; Chen, M. Effect of Homocysteine on the Differentiation of CD4(+) T Cells into Th17 Cells. *Dig. Dis. Sci.* **2018**, *63*, 3339–3347. [CrossRef] [PubMed]
52. Lin, X.; Meng, X.; Song, Z. Homocysteine and psoriasis. *Biosci. Rep.* **2019**, *39*, BSR20190867–BSR20190881. [CrossRef] [PubMed]
53. Wallace, J.L.; MacNaughton, W.K.; Morris, G.P.; Beck, P.L. Inhibition of leukotriene synthesis markedly accelerates healing in a rat model of inflammatory bowel disease. *Gastroenterology* **1989**, *96*, 29–36. [CrossRef] [PubMed]
54. Ameho, C.K.; Adjei, A.A.; Harrison, E.K.; Takeshita, K.; Morioka, T.; Arakaki, Y.; Ito, E.; Suzuki, I.; Kulkarni, A.D.; Kawajiri, A.; et al. Prophylactic effect of dietary glutamine supplementation on interleukin 8 and tumour necrosis factor α production in trinitrobenzene sulphonic acid induced colitis. *Gut* **1997**, *41*, 487–493. [CrossRef]
55. Bendtsen, K.M.; Tougaard, P.; Hansen, A.K. An Early Life Mucosal Insult Temporarily Decreases Acute Oxazolone-Induced Inflammation in Mice. *Inflammation* **2018**, *41*, 1437–1447. [CrossRef]

International Journal of
Molecular Sciences

MDPI

Communication

Cornelian Cherry (*Cornus mas* L.) Iridoid and Anthocyanin-Rich Extract Reduces Various Oxidation, Inflammation, and Adhesion Markers in a Cholesterol-Rich Diet Rabbit Model

Maciej Danielewski [1,*], Agnieszka Gomułkiewicz [2], Alicja Z. Kucharska [3], Agnieszka Matuszewska [1], Beata Nowak [1], Narcyz Piórecki [4,5], Małgorzata Trocha [1], Marta Szandruk-Bender [1], Paulina Jawień [6], Adam Szeląg [1], Piotr Dzięgiel [2,7] and Tomasz Sozański [1,*]

1 Department of Pharmacology, Wroclaw Medical University, J. Mikulicza-Radeckiego 2, 50-345 Wroclaw, Poland
2 Division of Histology and Embryology, Department of Human Morphology and Embryology, Wroclaw Medical University, T. Chalubinskiego 6a, 50-368 Wroclaw, Poland
3 Department of Fruit, Vegetable, and Plant Nutraceutical Technology, Wroclaw University of Environmental and Life Sciences, J. Chelmonskiego 37, 51-630 Wroclaw, Poland
4 Bolestraszyce Arboretum and Institute of Physiography, Bolestraszyce 130, 37-722 Wyszatyce, Poland
5 Institute of Physical Culture Sciences, Medical College, University of Rzeszow, A. Towarnickiego 3, 35-959 Rzeszow, Poland
6 Department of Biostructure and Animal Physiology, Wroclaw University of Environmental and Life Sciences, C.K. Norwida 25/27, 50-375 Wroclaw, Poland
7 Department of Physiotherapy, Wroclaw University School of Physical Education, I.J. Paderewskiego 35, 51-612 Wroclaw, Poland
* Correspondence: maciej.danielewski@umw.edu.pl (M.D.); tomasz.sozanski@umw.edu.pl (T.S.)

Citation: Danielewski, M.; Gomułkiewicz, A.; Kucharska, A.Z.; Matuszewska, A.; Nowak, B.; Piórecki, N.; Trocha, M.; Szandruk-Bender, M.; Jawień, P.; Szeląg, A.; et al. Cornelian Cherry (*Cornus mas* L.) Iridoid and Anthocyanin-Rich Extract Reduces Various Oxidation, Inflammation, and Adhesion Markers in a Cholesterol-Rich Diet Rabbit Model. *Int. J. Mol. Sci.* **2023**, *24*, 3890. https://doi.org/10.3390/ijms24043890

Academic Editors: Antonio González-Sarrías and Juan Antonio Giménez-Bastida

Received: 21 December 2022
Revised: 7 February 2023
Accepted: 9 February 2023
Published: 15 February 2023

Abstract: Atherogenesis leads to the development of atherosclerosis, a progressive chronic disease characterized by subendothelial lipoprotein retention and endothelial impairment in the arterial wall. It develops mainly as a result of inflammation and also many other complex processes, which arise from, among others, oxidation and adhesion. Cornelian cherry (*Cornus mas* L.) fruits are abundant in iridoids and anthocyanins—compounds with potent antioxidant and anti-inflammatory activity. This study aimed to determine the effect of two different doses (10 mg and 50 mg per kg of body weight, respectively) of iridoid and anthocyanin-rich resin-purified Cornelian cherry extract on the markers that are important in the progress of inflammation, cell proliferation and adhesion, immune system cell infiltration, and atherosclerotic lesion development in a cholesterol-rich diet rabbit model. We used biobank blood and liver samples that were collected during the previous original experiment. We assessed the mRNA expression of MMP-1, MMP-9, IL-6, NOX, and VCAM-1 in the aorta, and the serum levels of VCAM-1, ICAM-1, CRP, PON-1, MCP-1, and PCT. The application of the Cornelian cherry extract at a dose of 50 mg/kg bw resulted in a significant reduction in MMP-1, IL-6, and NOX mRNA expression in the aorta and a decrease in VCAM-1, ICAM-1, PON-1, and PCT serum levels. The administration of a 10 mg/kg bw dose caused a significant decrease in serum ICAM-1, PON-1, and MCP-1. The results indicate the potential usefulness of the Cornelian cherry extract in the prevention or treatment of atherogenesis-related cardiovascular diseases, such as atherosclerosis or metabolic syndrome.

Keywords: Cornelian cherry; iridoids; anthocyanins; atherosclerosis; atherogenesis; inflammation; oxidation; adhesion

1. Introduction

The search for new, effective, and safe therapies is a consistent task in medicine. Despite continuous scientific progress in the diagnosis and treatment of many medical

conditions, the use of more and more advanced pharmaceuticals, and the growing awareness of the pathogenesis and treatment of various diseases, there is still a need for new specifics that will meet emerging therapeutic challenges. This especially applies to conditions commonly referred to as civilization diseases, the prevalence of which is increasing, with widespread intensity in new groups of patients, e.g., they appear in a spiral number of cases in younger people, and the financial and social costs of treating these diseases are starting to burden national health systems. Such conditions can result, to a greater or lesser extent, from an incorrect lifestyle, primarily a small amount of physical activity and an incorrect (Western) diet rich in simple sugars and cholesterol—i.e., atherosclerosis, type 2 diabetes, or metabolic syndrome.

Atherosclerosis is a progressive chronic disease characterized by subendothelial lipoprotein retention and endothelial impairment in the arterial wall. It is considered one of the most important types of arteriosclerotic vascular diseases [1]. Atherosclerosis develops mainly as a result of inflammation but also from many other complex processes, which arise from, among others, oxidation and adhesion. Pro-oxidant substances, in general, may be divided into reactive oxygen species (ROS) and reactive nitrogen species (RNS). ROS contributes to several aspects of atherosclerosis development, including endothelial cell dysfunction, immune cell recruitment and activation, stimulation of inflammation, and smooth muscle cell migration and proliferation. In addition, they are involved in low-density lipoprotein (LDL-C) oxidative modification, the inactivation of nitric oxide, and the modulation of redox-sensitive signaling pathways [2].

The nicotinamide adenine dinucleotide phosphate (NADPH) oxidases (NOX) family is considered a major source of ROS in eukaryotic cells [3,4]. The correct production of NOX isoforms fulfills multiple processes that are important for normal physiology, but its up-regulation is involved in many different pathologies, including atherosclerosis, cancer, and neurodegenerative diseases [5]. NOX enzymes occur in macrophages, vascular smooth muscle cells (VSMCs), and endothelial cells, and are involved in smooth muscle cell proliferation, the production of ROS/RNS, and low-density lipoprotein oxidation [6]. The production of ROS in the blood vessels is essential for redirecting the bloodstream to the most active tissues and thus maintaining vascular homeostasis. On the other hand, the overproduction of ROS contributes to the development of cardiovascular diseases such as hypertension, atherosclerosis, diabetes, hypertrophy, and cardiac arrest [3]. VSMCs, the most predominant component cells of the blood vessel wall, play a pivotal role in regulating vascular function [7]. LDL-C oxidation and proinflammatory cytokines, such as TNF-alpha, IL-1, IL-4 or IL-6, and IFN-gamma, may induce endothelial dysfunction, migration, and the proliferation of smooth muscle cells, the emergence of foam cells, and the expression of leukocyte and monocyte adhesion molecules, primarily vascular cell adhesion molecule-1 (VCAM-1), intercellular adhesion molecule-1 (ICAM-1), and E-selectin [6]. These molecules form an integrated system that transports leukocytes and monocytes into the vascular wall, promotes their accumulation in the vascular wall intima, and contributes to the development of atherosclerotic plaques [8]. Afterward, monocytes are differentiated into macrophages through chemotactic proteins, mainly monocyte chemotactic protein-1 (MCP-1) [9].

Matrix metalloproteinases (MMPs) are part of a large family of zinc-dependent endopeptidases. The major role of MMPs is to degrade and deposit structural proteins within the extracellular matrix (ECM). The production of MMPs is stimulated mainly by oxidative stress, various growth factors, and inflammation. The up- or down-regulation of MMPs can be conducive to vascular diseases, such as hypertension or atherosclerosis, and leads to subsequent ECM remodeling. In atherosclerosis, MMPs are primarily implicated in atherosclerotic plaque formation and instability and in promoting the migration and proliferation of smooth muscle cells [10–12]. Moreover, the degradation of native collagen induced by MMPs augmentation results in decreased resistance of the vessels to various stresses, including mechanical damage and intimal thickening [13,14].

Human serum paraoxonase-1 (PON-1) is a calcium-dependent hydrolytic enzyme primarily synthesized in the liver. It is an antioxidant protein protecting high-density lipoproteins from oxidation [15,16]. This HDL-associated enzyme can hydrolyze oxidized LDL-cholesterol (ox-LDL), thereby exhibiting potential antiatherosclerotic properties.

One of the raw materials of natural origin that can provide compounds that are potentially effective in the prevention and treatment of atherosclerosis is Cornelian cherry (*Cornus mas* L.) fruits, which are rich in substances from the group of polyphenols, flavonoids, anthocyanins, and iridoids [17–26]. Compounds from these groups are widely known for their potential antioxidant and anti-inflammatory effects.

Our previous work proved that Cornelian cherry extract is an efficacious therapeutic agent in a cholesterol-rich diet rabbit model. We have shown, among others, the positive impact of the extract on the levels of triglycerides and adipokines, PPAR alpha and gamma expression in the aorta, and LXR expression in the liver, as well as on the reduction of the intima/media ratio in the thoracic and abdominal aorta [27]. In this study, and continuing the evaluation of this potentially effective natural remedy, we focused more on assessing the influence of the extract on the inflammatory aspect of atherosclerosis. This study aimed to determine the effect of two different doses (10 mg or 50 mg per kg of body weight, respectively) of iridoid and anthocyanin-rich resin-purified Cornelian cherry extract on the markers important in the progression of inflammation, cell proliferation, immune system cells infiltration, and atherosclerotic lesion development in a cholesterol-rich diet rabbit model. We assessed the levels of the above-mentioned markers: the mRNA expression of MMP-1, MMP-9, IL-6, NOX, and VCAM-1 in the aorta, the serum concentrations of VCAM-1, ICAM-1, PON-1, and MCP-1, and classic inflammation markers, such as C-reactive protein (CRP) and procalcitonin (PCT).

2. Results

We have studied the effects of the oral administration of resin-purified Cornelian cherry extract in a cholesterol-rich diet rabbit model on mRNA expression of MMP-1, MMP-9, IL-6, NOX, and VCAM-1 in the aorta. Additionally, we have indicated the levels of VCAM-1, ICAM-1, CRP, PON-1, MCP-1, and PCT in the serum.

2.1. Assessment of MMP-1, MMP-9, IL-6, NOX, and VCAM-1 mRNA Expression in the Aorta by Real-Time PCR

When compared to the baseline, feeding a cholesterol-rich diet caused a significant increase in the CHOL group compared to the P group in MMP-1 ($p = 0.006$), MMP-9 ($p < 0.001$), NOX ($p = 0.023$), and VCAM ($p = 0.002$) expressions. In the assessment, the IL-6 upregulation in the CHOL group was also observed but to a lesser extent ($p = 0.056$). In the case of groups receiving the extract compared to the P group, significant increases in the expression of the tested substances were observed in the following samples: MMP-1 (a relevant difference in EXT 10 group, $p = 0.019$), MMP-9 (EXT 10 and EXT 50, respectively $p < 0.001$ and $p = 0.034$) and VCAM (EXT 10 and EXT 50, respectively $p < 0.001$ and $p = 0.033$). It is worth noticing that the determination of MMP-9 and VCAM expression in the EXT 10 group showed higher levels than in the CHOL group compared to the P group, while in the remaining cases, the increases were lower than those recorded in the CHOL group.

When compared to the CHOL group, significant positive changes were observed in the EXT 50 group in three out of the five analyses. The relevant decreases in expression levels concerned MMP-1 ($p = 0.005$), IL-6 ($p = 0.029$), and NOX ($p = 0.001$). Although in the MMP-9 and VCAM-1 assay, the statistical analysis did not show significance; a noticeable favorable decrease in the EXT 50 group was observed. However, when comparing the results of the EXT 10 group with the CHOL group, no relevant differences were obtained, and the assessed levels were, as mentioned earlier, in some cases higher and, in other cases, lower than in the CHOL group. The outcomes of the mRNA expression of MMP-1, MMP-9, IL-6, NOX, and VCAM in the aorta testing are presented in Table 1 and Figure 1.

Table 1. mRNA expression of MMP-1, MMP-9, IL-6, NOX, and VCAM-1 in the aorta. Values are presented as mean ± SD.

Group	MMP-1	MMP-9	IL-6	NOX	VCAM-1
P	1.365 ± 0.918	1.082 ± 0.430	1.099 ± 0.400	1.153 ± 0.543	1.076 ± 0.429
CHOL	3.333 ± 2.709	3.556 ± 1.688	1.623 ± 0.921	1.971 ± 1.140	2.663 ± 0.787
EXT 10	3.017 ± 1.613	3.969 ± 1.287	1.125 ± 0.363	1.580 ± 0.995	2.807 ± 1.148
EXT 50	1.337 ± 0.885	2.470 ± 2.316	1.021 ± 0.606	0.757 ± 0.528	2.122 ± 1.872
SIMV 5	0.702 ± 0.335	0.773 ± 0.153	1.344 ± 0.518	0.553 ± 0.384	0.662 ± 0.266

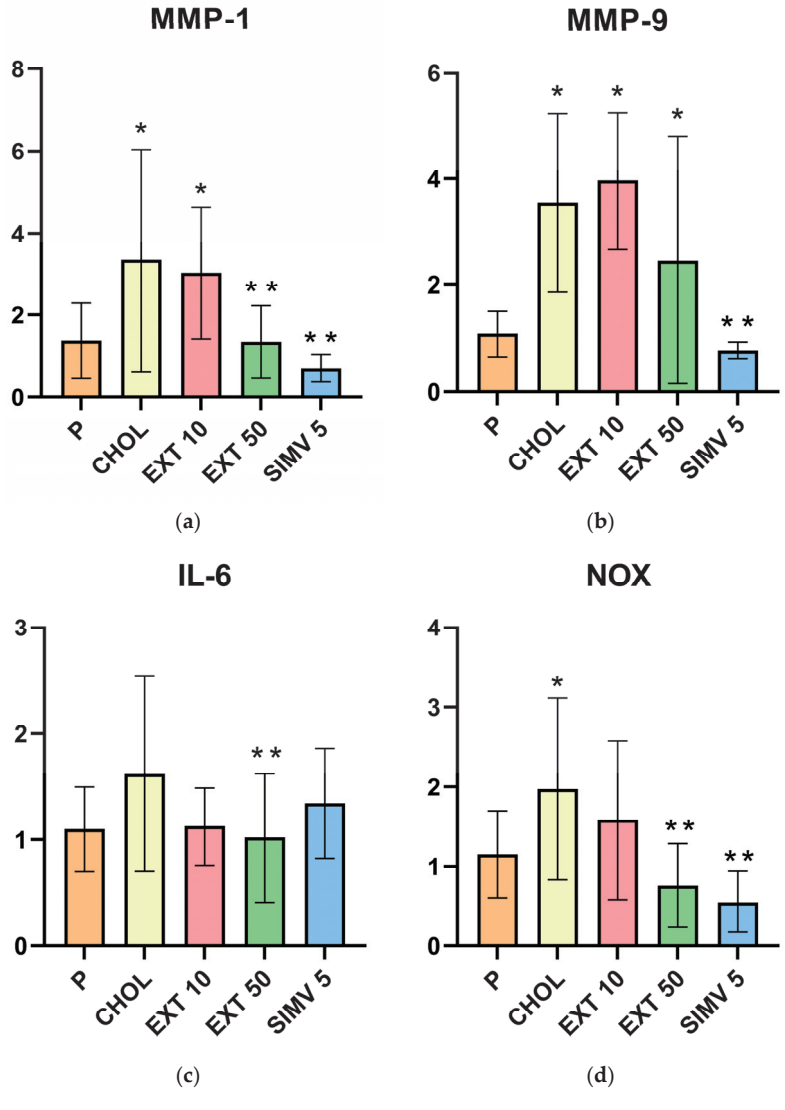

Figure 1. *Cont.*

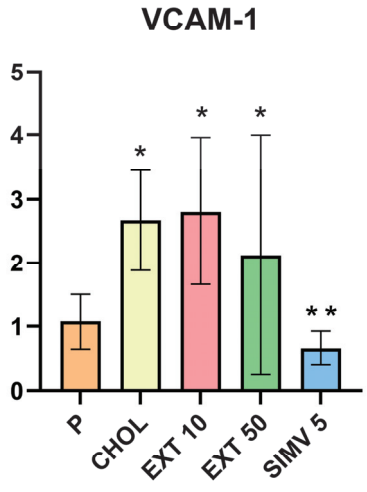

(**e**)

Figure 1. mRNA expression of MMP-1, MMP-9, IL-6, NOX, and VCAM-1 in the aorta. (**a**) MMP-1, (**b**) MMP-9, (**c**) IL-6, (**d**) NOX, and (**e**) VCAM-1. P—standard chow; CHOL—standard chow + 1% cholesterol; EXT 10—standard chow + 1% cholesterol + Cornelian cherry extract 10 mg/kg bw; EXT 50—standard chow + 1% cholesterol + Cornelian cherry extract 50 mg/kg bw; SIMV 5—standard chow + 1% cholesterol + simvastatin 5 mg/kg bw Values are presented as mean ± SD. * $p < 0.05$ vs. P. ** $p < 0.05$ vs. CHOL.

2.2. Assessment of VCAM-1, ICAM-1, CRP, PON-1, MCP-1, and PCT Serum Levels by ELISA

When compared to the baseline, feeding a cholesterol-rich diet caused a significant increase in the CHOL group compared to the P one in VCAM-1 ($p < 0.001$), ICAM-1 ($p < 0.001$), CRP ($p < 0.001$), PON-1 ($p < 0.001$), MCP-1 ($p = 0.032$), and PCT ($p = 0.002$) groups, i.e., in the serum levels of all the ELISA-assessed compounds. In the groups receiving the extract, the levels were also elevated compared to the P group but, in the vast majority of cases, they were lower than in the CHOL group. The only exception was the VCAM-1 concentration in the EXT 10 group, which was slightly higher than in the CHOL group. Significant increases in the serum levels of the tested substances were observed in the following samples: VCAM-1 (a relevant difference in EXT 10 and EXT 50 group, respectively $p < 0.001$ and $p = 0.026$), CRP (EXT 10 and EXT 50, respectively $p = 0.014$ and $p = 0.005$), PON-1 (EXT 10, $p = 0.038$), and PCT (EXT 10, $p = 0.018$).

When compared to the CHOL group, it was possible to notice a particularly positive effect regarding the administration of the Cornelian cherry extract on the serum levels of ICAM-1 and PON-1, where relevant differences were noted for both applied doses. The following statistical analysis results were obtained for ICAM-1: EXT 10—$p = 0.006$ and EXT 50—$p = 0.036$; for PON-1: EXT 10—$p = 0.010$ and EXT 50—$p < 0.001$. In the case of VCAM-1, MCP-1, and PCT, a significant reduction in the serum concentration was obtained in one of the extract doses, with 50 mg/kg bw twice and 10 mg/kg bw once. The specific values of the analysis results in comparison to the CHOL group are as follows: VCAM-1 (EXT 50, $p = 0.003$), MCP-1 (EXT 10, $p = 0.019$), and PCT (EXT 50, $p = 0.043$). Only in the CRP study were no significant differences observed; however, the levels of this compound in the extract groups were noticeably lower, with a greater decrease in the EXT 10 group compared to the CHOL group. The outcomes of the ELISA assessment of VCAM-1, ICAM-1, CRP, PON-1, MCP-1, and PCT serum levels are presented in Table 2 and Figure 2.

Table 2. Serum levels of VCAM-1, ICAM-1, CRP, PON-1, MCP-1, and PCT by ELISA method. Values are presented as mean ± SD. VCAM-1, ICAM-1, CRP, PON-1, and PCT concentrations are expressed as ng/mL and MCP-1 as pg/mL.

Group	VCAM-1	ICAM-1	CRP	PON-1	MCP-1	PCT
P	6.490 ± 0.923	0.381 ± 0.123	6.241 ± 3.039	20.700 ± 1.828	137.949 ± 34.880	0.750 ± 0.331
CHOL	8.421 ± 0.644	0.557 ± 0.121	14.734 ± 5.797	25.135 ± 1.868	180.805 ± 51.942	1.585 ± 0.524
EXT 10	8.532 ± 0.931	0.424 ± 0.064	11.720 ± 4.535	22.660 ± 1.880	133.751 ± 36.279	1.358 ± 0.649
EXT 50	7.310 ± 0.801	0.458 ± 0.059	12.568 ± 5.080	21.114 ± 1.904	150.531 ± 49.552	1.068 ± 0.665
SIMV 5	7.630 ± 0.648	0.405 ± 0.122	9.239 ± 5.052	19.684 ± 2.643	132.770 ± 41.303	0.850 ± 0.539

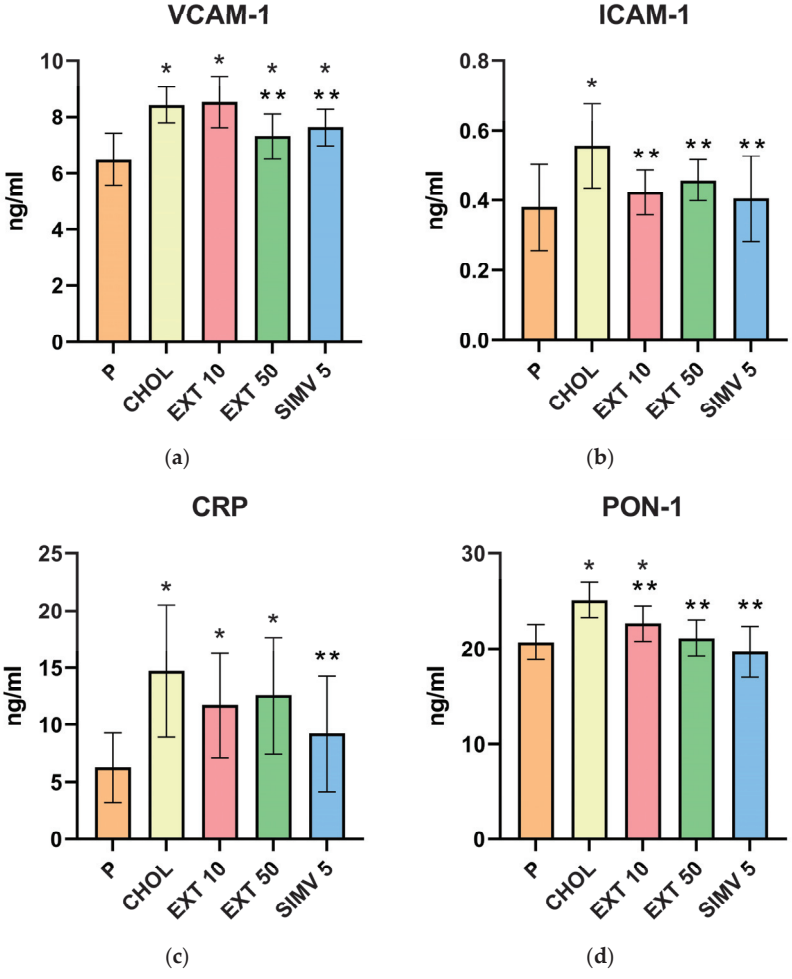

Figure 2. *Cont.*

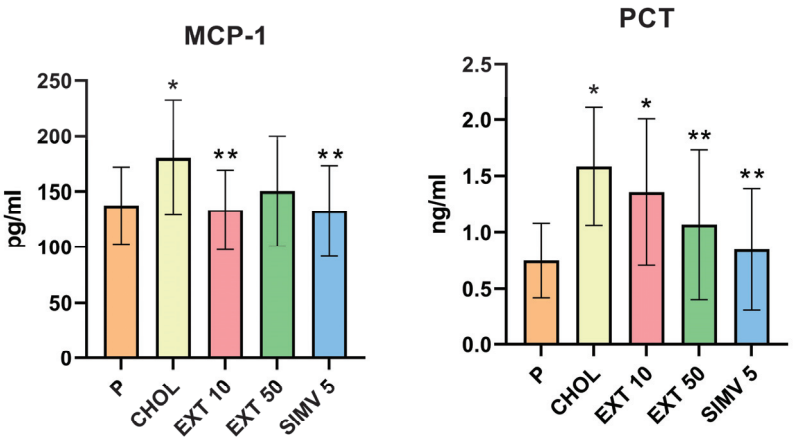

(**e**) (**f**)

Figure 2. Serum levels of VCAM-1, ICAM-1, CRP, PON-1, MCP-1, and PCT by ELISA method. (**a**) VCAM-1, (**b**) ICAM-1, (**c**) CRP, (**d**) PON-1, (**e**) MCP-1, and (**f**) PCT. P—standard chow; CHOL—standard chow + 1% cholesterol; EXT 10—standard chow + 1% cholesterol + Cornelian cherry extract 10 mg/kg bw; EXT 50—standard chow + 1% cholesterol + Cornelian cherry extract 50 mg/kg bw; SIMV 5—standard chow + 1% cholesterol + simvastatin 5 mg/kg bw Values are presented as mean ± SD. * $p < 0.05$ vs. P. ** $p < 0.05$ vs. CHOL.

3. Discussion

In this study, we examined a cholesterol-fed rabbit model and the effects of administering two doses (10 mg/kg bw or 50 mg/kg bw) of resin-purified Cornelian cherry (*Cornus mas* L.) extract on the mRNA expression of MMP-1, MMP-9, IL-6, NOX, and VCAM-1 in the thoracic aorta and the serum levels of VCAM-1, ICAM-1, CRP, PON-1, MCP-1, and PCT, which represent the compounds that may loom large in the pathogenesis and progress of atherosclerotic lesions. The main conclusion of our study is that oral administration of resin-purified Cornelian cherry extract has a positive, lowering impact on various markers that are important in the progression of inflammation, cell proliferation and adhesion, immune system cell infiltration, and atherosclerotic lesion development, which may contribute to the limitation of the pathogenesis and development of atherogenesis-related cardiovascular diseases, such as atherosclerosis or metabolic syndrome. The key findings are that Cornelian cherry extract, particularly at a dose of 50 mg/kg bw, significantly reduces the mRNA expression of MMP-1, IL-6, and NOX in the aorta and decreases the serum levels of VCAM-1, ICAM-1, PON-1, MCP-1, and PCT. These findings allow us to better understand the beneficial influence of Cornelian cherry extract on the formation of atherosclerotic changes, which we reported on in our previous studies [27].

Metalloproteinases that play a key role in atherosclerotic plaque vulnerability and rupture are, i.a., MMP-1 and MMP-9 [28]. Butoi et al. [29] found that crosstalk between macrophages and smooth muscle cells precisely enhances the expression of MMP-1 and MMP-9. One of the functions of MMPs is the generation of matrices—peptides originating from the fragmentation of extracellular matrix proteins. Matrikines can substantially impact inflammatory processes and atherosclerosis development due to their ability to alter cellular migration, chemotaxis, and mitogenesis. Both MMP-1 and MMP-9 (also MMP-2, MMP-8, and MMP-12) regulate, among others, the elastin peptide (val-gly-val-ala-pro-gly matrikine) [30]. Elastin peptide may stimulate the enhancement of vascular intimal wall thickness and wall diameter [31,32]. Moreover, Hu et al. proved that MMP-1 levels are positively correlated with the occurrence of cardiovascular and cerebrovascular events in the course of carotid atherosclerosis [33].

In our study, we observed an increase in the expression of MMP-1 and MMP-9 mRNA in the aorta in the CHOL group, which is consistent with the data described above, as well as a decrease in the expression level of MMP-1 and MMP-9 in the case of the 50 mg/kg bw dose application, with a statistically relevant difference in the MMP-1 level. However, in the case of a dose of 10 mg/kg bw, there was a slight mitigation (MMP-1) and a slight enhancement (MMP-9) in expression compared to the CHOL group. It appears that these relatively small disparities can be considered as within the statistical error, and it is allowed to assume that the lower dose of the extract is too small to obtain a noticeable effect on the expression level of the enzymes tested. On the other hand, the higher dose of the extract reduces the occurrence of the factors generating an increase in the level of metalloproteinases, i.e., oxidative stress or inflammation, thus demonstrating a beneficial effect on the development and stability of atherosclerotic lesions resulting from a diet rich in cholesterol. Most of the studies conducted so far on the impact of the extract or active compounds obtained from the genus *Cornus* on metalloproteinases mainly concern MMP-3 and MMP-13 [34–37], and a diminution in the expression of these enzymes was also observed; ergo, our results are consistent with the earlier outcomes, concomitantly expanding the knowledge on this subject.

As for the adhesion molecules tested, we observed the mitigation of expression of VCAM-1 in the aorta (dose of 50 mg/kg bw) and the depletion of VCAM-1 (dose of 50 mg/kg bw) and ICAM-1 (both the dose of 10 mg/kg and 50 mg/kg bw) concentrations in the serum. Interestingly, we noted a slight augmentation of VCAM-1 expression in the aorta and serum concentration in the case of the 10 mg/kg bw dose of the extract (which additionally confirms the consistency of the results received) and the concomitantly stronger beneficial effect of this dose on ICAM-1 serum concentration. This variable impact of the 10 mg/kg bw dose on both of the adhesion molecules requires further research. However, it can be overall admitted that Cornelian cherry extract reduces the levels of VCAM-1 and ICAM-1. Similar results were obtained in a human model by Kang et al. [38] with cornuside—an iridoid glucoside isolated from the fruits of *Cornus officinalis*, where the suppression of both molecules was also observed. It is worth mentioning that, in a review of the available literature, we found only this one study assessing the effect of the raw materials obtained from the genus *Cornus* on VCAM-1 and ICAM-1.

During one of the initial phases of atherosclerosis, the recruitment of inflammatory cells from the circulation and their transendothelial migration was observed. Cellular adhesion molecules, which appear on the vascular endothelium and the circulating leukocytes in response to various inflammatory factors, play a major role in this process. Both VCAM-1 and ICAM-1 induce the potent adhesion of inflammatory cells to the surface of blood vessels. The expression of these molecules is, consequently, apparent in atherosclerotic plaques [9]. VCAM-1 expression is enhanced in endothelial cells under proinflammatory conditions, as observed in the early stages of atherosclerosis [39]. Moreover, VCAM-1 may be associated with the severity of atherosclerosis and the prediction of cardiovascular disease [8]. Similarly, although ICAM-1 is constitutively present in endothelial cells, its expression is significantly enhanced in inflammatory conditions by proinflammatory cytokines. The endothelial expression of ICAM-1 is increased in atherosclerotic tissue and animal models of atherosclerosis. Elevated levels of the circulating or soluble form of ICAM-1 are observed in various body fluids in patients with atherosclerosis, heart failure, coronary artery disease, and transplant vasculopathy. ICAM-1 directly contributes to inflammatory responses within the blood vessel wall by increasing endothelial cell activation and augmenting atherosclerotic plaque formation [40]. It also plays an essential role in the regulation of vascular permeability [41].

In our previous work [27], we reported that a diet rich in cholesterol results in an increase in PPAR-alpha and PPAR-gamma expression in the aorta, and feeding the Cornelian cherry extract lowers the levels of expression of both of these transcription factors. Currently, we proved that the expression of VCAM-1 in the aorta and serum concentrations of VCAM-1 and ICAM-1 also decreased from the use of the extract. Meanwhile, Wei

et al. [1] informed that VCAM-1-targeted and PPAR-delta-agonist-loaded nanomicelles had a suppressing effect on apoptosis and the migration of oxidized LDL-C-induced human aortic vascular smooth muscle cells. It can therefore be hypothesized that the application of Cornelian cherry extract may be, to a certain extent, a comparable and valuable alternative to the above therapeutic approach, as well as a natural and feasibly cheaper treatment option for compounds obtained using synthetic or biotechnological methods, which are based on curative effects on the expression levels of receptors from the PPAR group and adhesion molecules, including VCAM-1.

In the reported study, we measured the expression levels in the aorta of IL-6, which belongs to proinflammatory and proatherogenic cytokines [42]. The administration of Cornelian cherry extract at a dose of 50 mg/kg bw caused a relevant reduction in Il-6 expression compared to the CHOL group. Interestingly, the level of IL-6 in the EXT 50 group turned out to be lower than in the positive control, i.e., the SIMV 5 group. This is a very favorable alteration as an elevated level of IL-6 is associated with cardiovascular risk [43,44]. It was proven that IL-6 signaling has a causative role in atherothrombosis [45]. A diminution in IL-6 level was also observed in at least a few other studies, but these mainly concerned *Cornus officinalis* rather than *Cornus mas* [46–50].

Chronic inflammation is a major contributor to age-related atherosclerosis. This may result from the associated increase in the aging of adipocytes in the bone marrow accompanied by an elevation of proinflammatory cytokines, including IL-6, and the synergy between the myeloid cells of the immune system and the vasculature via IL-6 signaling. Currently, the clinically approved agents that target this pathway (such as anti-IL-6 therapies) are already available and could reduce the risk of cardiovascular disease in elderly people [51,52]. Due to its ability to reduce the level of IL-6 expression, Cornelian cherry extract may constitute a valuable supplement for such therapy.

One of the most important reactive oxygen species that produce enzymes is the NOX group. In physiological conditions, NOX presents a low basal activity in blood vessels [53]. The augmentation of NOX-derived ROS is mainly caused by cytokines, growth factors, or high glucose levels and plays a key role in the pathogenesis of atherosclerosis [3]. In our study, we observed a significant increase in the level of NOX expression in the aorta in the CHOL group compared to the P group. Expression levels were lower in the extract groups, with the EXT 50 group noting a relevant difference compared to the CHOL group and similar to that observed in the simvastatin group. The fundamental NOX feature is the generation of reactive oxygen species in the vascular cells and in the circulating immune cells interacting with the blood vessels. While the physiological production of NOX-derived ROS contributes to the maintenance of vascular homeostasis, the hyperactivity of NOX triggers oxidative stress. In atherosclerosis, lipid peroxidation induced by activated NOX is highly deleterious and expands the free radical reactions [54,55].

Iridoids and anthocyanins possess considerable antioxidant activity. It is both indirect, through the stimulation of the antioxidant defense system, and direct, through the removal of reactive oxygen species. As for NADPH oxidase, it was shown that iridoids might modulate the AMPK/NOX4/PI3-K/AKT pathway, and anthocyanin metabolites may alter NOX activity in the endothelium [24]. The elevated level of LDL-C often observed in the course of atherosclerosis results in the increased binding of LDL-C and increased uptake by cell surface LDL receptors and may be responsible for the direct activation of NOX. NOX-generated superoxide stimulates lipid endocytosis, thus promoting plaque formation [3]. Therefore, it can be hypothesized that one of the factors that contributed to the diminished NOX expression in the extract groups was the lower LDL-C concentration when compared to the CHOL group, showed in our previous report [27]. The limited activity of NOX enzymes could have contributed to a reduction in ROS production, which may be confirmed by the favorable changes observed in the case of other markers, directly or indirectly, dependent on oxidative stress, as described in this article.

In two different studies of the active ingredients isolated from *Corni fructus* by Park et al., a positive impact on NOX levels was confirmed. 7-O-galloyl-D-sedoheptulose

reduced the renal protein expression of NOX-4 and one of the subunits of NADPH oxidase-p22(phox) [56], while the administration of loganin led to a significant decrease in the expression of both NOX-4 and p22(phox) in the liver of diabetic db/db mice [57]. Comparable results were obtained among others by Lee et al. [58], Chen et al. [59], and Fang et al. [60].

Although the C-reactive protein (CRP) level enhances after various unspecific inflammatory stimuli, it is also considered one of the leading biomarkers of cardiovascular risk prediction [45]. Concomitantly, it is ambiguous to state whether CRP itself plays any causal role in atherogenesis [61]. In the CHOL group, we noted a significant increase in serum CRP level compared to the P group. In the groups fed with the extract, the CRP concentrations were slightly lower (and lesser in the EXT 10 group), but were still essentially higher compared to the control group. Thus, a certain positive trend of extract administration can be noticed, but the final result obtained in our model is relatively modest. Similarly, no significant differences in C-reactive protein levels between the studied groups were determined in the *Cornus mas* randomized controlled trial [62].

A variety of studies have been performed to investigate the clinical relevance of PON-1 in cardiovascular disease, diabetes, cancer, or neurologic diseases; however, the received data are still insufficient and, in some cases, contradictory [63]. Nonetheless, Kunutsor et al. [64] stated that there is an approximately log-linear inverse association between PON-1 activity and CVD risk, which is partly dependent on HDL-C levels. Additionally, Gautier et al. recently confirmed the association between an increase in HDL-C level and PON-1 activity and a decrease in lipid oxidation markers [65].

In the assessment of serum PON-1 level, we obtained a significant reduction in the extract-fed groups compared to the CHOL group (greater in the EXT 50). It is worth noting that, while in the case of the EXT 10 group, the measured level was still essentially higher than in the control group, the concentration of PON-1 in the EXT 50 group was comparable to that determined in the P group. In a previous study, we found that there is a noticeable dose-dependent impact of Cornelian cherry extract on cholesterol fraction levels (reduction in LDL-C and augmentation of HDL-C), although these changes, at least in the doses applied, are not statistically significant compared to the CHOL group. Nevertheless, they constitute the starting point for the assessment of serum PON-1 concentration in the present study, and the obtained results are a logical consequence of the earlier ones. A more substantial increase in HDL-C was observed in the case of a 50 mg/kg bw dose translates into the greater activity of HDL-associated PON-1, which results in a boost in LDL-C hydrolysis and a more significant reduction in its level in the serum. To our knowledge, to date, only one study of the effects of *Cornus mas* on PON-1 has been carried out and resulted in the opposite to our outcomes [66]. This supports the above-mentioned statement about the insufficient and contradictory data on PON-1 and the necessity for further research.

For the monocyte chemotactic protein-1 MCP-1, we noted lower serum levels than in the CHOL group for both doses of the extract, and interestingly, the difference was significant in the EXT 10 group. It is also worth mentioning that the MCP-1 level obtained in EXT 10 group was almost identical to that in the positive control group, SIMV 5. MCP-1, also referred to as chemokine (C-C motif) ligand 2 (CCL2), is expressed by mainly inflammatory and endothelial cells [67]. This chemokine regulates monocyte chemotaxis and T-lymphocyte differentiation and plays a crucial role in the pathogenesis of various inflammatory diseases, atherosclerosis, and cancer [68]. Its level is upregulated as a result of proinflammatory stimuli and the tissue injury associated with atherosclerotic lesions [67]. According to one of the recent studies on inflammatory atherosclerosis pathogenesis, isolated human monocytes, via trained immunity induced by the primary stimulation of ox-LDL during secondary stimulation with agonists of toll-like TLR2 and TLR4 receptors, showed an increase in the production of proinflammatory cytokines such as TNF-alpha, interleukins -6, -8, and -18 and precisely the MCP-1 chemokine [69].

The explanation for the beneficial effect of the extract on the level of MCP-1 may be due to the fact that it is rich in compounds from the anthocyanin group. Anthocyanins mediate

the redox state and inflammation via various pathways. One of the most important factors is the elevation of the Nrf2 factor, the nuclear factor erythroid 2-related factor 2. It is an inducible, specific transcription factor that is a key regulator of many antioxidant responses. The Nrf2 factor contributes, among others, to a reduction in MCP-1 levels [24,70]. Other available reports on the impact of compounds or derivatives acquired from the *Cornus* genus are consistent with our results and confirm the MCP-1 lowering effect [38,49,57,71,72]. A separate matter is the fact that, in our study, the lower dose of the extract appeared to be more effective. Whether the obtained outcome is either a result of the adopted model, e.g., its length, feeding pattern, or the laboratory animals used, or results directly from the doses of the extract applied is an issue that certainly requires additional clarification.

Procalcitonin (PCT) is considered a classic marker of inflammation and is, therefore, useful in determining the pathogenesis of atherosclerosis as an inflammatory-grounded disease. We observed a significant increase in PCT levels in the CHOL group compared to the P group. In the EXT 10 group, the augmentation was also significant, but in the EXT 50 group, we noted a relevant decrease in PCT levels compared to the CHOL group. Under physiological conditions, procalcitonin is a precursor of calcitonin, i.e., a thyroid hormone involved in the regulation of calcium and phosphate metabolism in the body. However, PCT also plays a very important role in pathological conditions, being a sensitive marker of inflammation. In the course of an inflammatory reaction, procalcitonin is synthesized, i.a., by macrophages, monocytes, and hepatocytes; therefore, the evaluation of its level may be a relatively simple way of assessing the presence of inflammation in the body. Procalcitonin is suggested to be a useful marker for the assessment of inflammation related to atherosclerosis or metabolic syndrome and a risk factor for future cardiovascular events [73,74]. It is associated with several other established cardiovascular risk factors, such as C-reactive protein, hypertension, diabetes, and renal function, which limits the value of PCT as an independent cardiovascular risk predictor. PCT is also inversely correlated with HDL-C levels [75]. Additionally, procalcitonin concentration may be a useful instrument for assessing carotid wall thickening and stenosis in ischemic stroke and also the severity of coronary artery disease (CAD) [73,76].

As mentioned, the use of PCT as an individual marker for the assessment of cardiovascular diseases is limited; therefore, the determination of another classical marker of inflammation, for example, CRP, is often performed as well. Interestingly, the level of procalcitonin is usually elevated at earlier stages of pathogenesis than in the case of CRP [77,78]. This may explain the results we obtained: a more significant difference in the levels of PCT than CRP as the 60-day model of feeding with a cholesterol diet and administration of Cornelian cherry extract can be considered relatively short when considering the development of chronic inflammatory diseases such as atherosclerosis, and it can be discussed as a limitation of the experiment. However, to our knowledge, this is the first study to assess the effect of *Cornus*-derived products on PCT levels, so despite its limitations, it is certainly an important step forward in broadening the knowledge in this aspect.

Another examination constraint worth mentioning is the application of two doses of the extract, which in the case of assessing as many parameters as there were in the described study, limits to a certain extent the possibility of a proper dose-dependence determination in comparison to, for example, using three doses. On the other hand, the strength of our study is that we assessed the impact of Cornelian cherry extract on the parameters for which there are relatively few reports or no reports at all. In addition, we did not observe any side effects during the experiment, which, combined with a relatively large number of significant changes in the levels of parameters evaluated, presents Cornelian cherry extract as a promising therapeutic alternative in the prevention and treatment of atherogenesis-related diseases.

4. Materials and Methods

4.1. Animal Model

In the current study, we used biobank blood and liver samples that were collected during the original experiment described in our previous article [27]. A total of 50 sexually mature male New Zealand rabbits aged 8 to 12 months were used in the 60-day experiment. The animals were housed in individual chambers with temperatures maintained at 21–23 °C. After four weeks of acclimatization and observation, the rabbits were randomly divided into 5 groups of 10 animals. The animals in group P were fed the standard chow for rabbits. Animals in other groups: CHOL, EXT 10, EXT 50, and SIMV 5 were fed with the standard chow enriched with 1% cholesterol. During the experiment, rabbits had free access to drinking water and received the same daily portion of chow (40 g/kg). Once daily, in the morning, for the consecutive 60 days of the study, the following substances were administered orally to the rabbits: groups P and CHOL—normal saline solution, group EXT 10—*Cornus mas* L. extract 10 mg per kg bw, group EXT 50—*Cornus mas* L. extract 50 mg per kg bw, and group SIMV 5—simvastatin 5 mg per kg bw as a positive control. The feeding schema is presented in Table 3.

Table 3. Experimental groups and the feeding schema used in the experiment.

Group	Chow	Dose of Tested Substance
P	standard chow	none (normal saline solution)
CHOL	standard chow +1% cholesterol	none (normal saline solution)
EXT 10	standard chow +1% cholesterol	Cornelian cherry extract 10 mg/kg bw
EXT 50	standard chow +1% cholesterol	Cornelian cherry extract 50 mg/kg bw
SIMV 5	standard chow +1% cholesterol	simvastatin 5 mg/kg bw

Blood samples were taken from each animal at the beginning and the end of the experiment from the marginal vein of the ear or the saphenous vein. At the end of the study, the rabbits were put under terminal anesthesia. The aortas were harvested afterward and cleaned, then frozen and stored at −70 °C pending further analysis.

4.2. Plant Materials and Preparation of Extract

The research material was resin-purified Cornelian cherry fruit extract (*Cornus mas* L.). Fruits were collected at the Arboretum and the Institute of Physiography in Bolestraszyce, Poland. Before analysis, fruits were stored at −20 °C. The herbarium specimen (BDPA 3967) was authenticated and deposited at the Herbarium of the Arboretum and the Institute of Physiography in Bolestraszyce, Poland.

Frozen ripe *Cornus mas* L. fruits were ground and heated for 5 min at 95 °C with Thermomix (Vorwerk, Wuppertal, Germany). The pulp was cooled to 40 °C and depectinized at 50 °C for 2 h by adding 0.5 mL of Panzym Be XXL (Begerow GmbH & Co., Darmstadt, Germany) per 1 kg. After depectinization and pitting, the pulp was pressed in a laboratory hydraulic press (Zodiak, SRSE, Warsaw, Poland). The pressed juice was then filtered and passed through an Amberlite XAD-16 resin column (Rohm and Haas, Chauny Cedex, France). The impurities were rinsed with distilled water, while the pigments and iridoids were eluted with 80% ethanol. The eluate was concentrated under a vacuum at 40 °C. The solvent was evaporated using Rotavapor (Unipan, Warsaw, Poland). The concentrated dye and iridoid extract was purified with ethyl acetate to remove nonpolar impurities and other flavonoids. The purification procedure was repeated three times. A sample of the purified

compounds was concentrated under a vacuum at 40 °C and lyophilized (Alpha 1-4 LSC, Christ, Germany) [79].

The main active ingredients of the obtained extract were iridoids, anthocyanins, phenolic acids, and flavonols. The quantitative composition of compounds in the EXT was determined by the HPLC-PDA method [80] and presented in our previous study [27].

4.3. RNA Isolation, Reverse Transcription, and Assessment of mRNA Expression of MMP-1, MMP-9, IL-6, NOX, and VCAM-1 in the Aorta by Real-Time PCR

Total RNA was isolated from studied tissue samples with RNeasy Fibrous Mini Kit (Qiagen, Hilden, Germany) according to the manufacturer's protocol. To eliminate genomic DNA contamination, on-column DNase digestion was performed using RNase-Free DNase Set (Qiagen, Hilden, Germany). Quantity and purity of RNA samples were assessed by measuring the absorbance at 260 and 280 nm with a NanoDrop1000 spectrophotometer (Thermo Fisher Scientific, Wilmington, DE, USA). First-strand cDNA was synthesized using the High Capacity cDNA Reverse Transcription Kit (Applied Biosystems, Carlsbad, CA, USA) as described in the protocol. The mRNA expression of MMP-1, MMP-9, IL-6, NOX, and VCAM-1 was determined by quantitative real-time PCR with 7500 Real-Time PCR System and Power SYBR Green PCR Master Mix (Applied Biosystems, Carlsbad, CA, USA). Glyceraldehyde 3-phosphate dehydrogenase (GAPDH) was used as the reference gene. The reactions were performed with RT^2 qPCR Primer Assays (Qiagen, Hilden, Germany) for rabbit MMP-1 (PPN00411A), MMP-9 (PPN00307A), IL-6 (PPN00115A), NOX (PPN00200A), VCAM-1 (PPN00241A), and GAPDH (PPN00377A). All the reactions were performed in triplicates under the following conditions: activation of the polymerase at 50 °C for 2 min, initial denaturation at 94 °C for 10 min, and 40 cycles of denaturation at 94 °C for 15 s followed by annealing and elongation at 60 °C for 1 min. The specificity of the PCR was determined by melt–curve analysis for each reaction. The relative mRNA expression of the examined factors was calculated with the ΔΔCt method.

4.4. Quantification of Serum Levels of VCAM-1, ICAM-1, CRP, PON-1, MCP-1, and PCT by Enzyme-Linked Immunosorbent Assay (ELISA)

ELISA method was used in the evaluation of serum levels of VCAM-1 (Rabbit VCAM-1 ELISA kit, CSB-E10092Rb, Cusabio Technology LLC, Houston, TX, USA), ICAM-1 (ELISA kit for Rabbit ICAM-1, ERB0114, Fine Test, Wuhan Fine Biotech Corp., Wuhan, China), CRP (C Reactive Protein Rabbit ELISA Kit, AB157726-1X, Abcam, Cambridge, UK), PON-1 (Elisa kit PON1 Rabbit, E0011Rb, Bioassay Technology Laboratory, Shanghai, China), MCP-1 (ELISA kit for Rabbit MCP-1, ERB0074, Fine Test, Wuhan Fine Biotech Corp., Wuhan, China) and PCT (ELISA kit for Rabbit PCT, ERB0144, Fine Test, Wuhan Fine Biotech Corp., Wuhan, China). All tests were performed according to the manufacturer's instructions. All concentrations were expressed as ng/mL or pg/mL.

4.5. Statistical Analysis

Parametric data were expressed as mean ± standard deviation (mean ± SD). The statistical analysis was conducted using Statistica v. 13.3 software (TIBCO Software Inc., Palo Alto, CA, USA). One-way analysis of variance (ANOVA) with least significant difference (LSD) Fisher's post hoc test was performed for a comparison between multiple groups. The p-values < 0.05 were considered statistically significant. Graphical representations of the statistical data were created using the Statistica v. 13.3 software (TIBCO Software Inc., Palo Alto, CA, USA).

5. Conclusions

The application of the iridoid and anthocyanin-rich resin-purified Cornelian cherry extract in a cholesterol-rich diet rabbit model resulted in a significant reduction in MMP-1, IL-6, and NOX mRNA expression in the aorta and a decrease in VCAM-1, ICAM-1, PON-1, MCP-1, and PCT serum levels, especially in the case of the 50 mg/kg bw dose. The results obtained, in conjunction with no observed side effects, indicate the potential usefulness of

the Cornelian cherry extract either in the prevention or treatment of atherogenesis-related cardiovascular diseases, such as atherosclerosis or metabolic syndrome.

Author Contributions: Conceptualization, M.D. and T.S.; methodology, M.D. and T.S.; investigation, M.D., A.G., A.Z.K., P.J. and T.S.; resources, A.Z.K. and N.P.; statistical analysis, M.D.; visualization, M.D.; supervision, M.D. and T.S.; literature search, M.D.; writing-original draft preparation, M.D. and T.S.; writing-review and editing, M.D., A.G., A.Z.K., A.M., B.N., A.S., N.P., P.D., M.S.-B., P.J., M.T. and T.S. All authors have read and agreed to the published version of the manuscript.

Funding: This work was supported by the statutory budget of Wroclaw Medical University (SUBZ.A080.22.076).

Institutional Review Board Statement: The study was conducted according to the guidelines of the Declaration of Helsinki and approved by the Local Ethics Committee for Animal Experiments at the Hirszfeld Institute of Immunology and Experimental Therapy of the Polish Academy of Science in Wroclaw (Approval code 21/2015).

Informed Consent Statement: Not applicable.

Data Availability Statement: The data underlying this article will be shared upon request with the corresponding authors.

Acknowledgments: The authors are grateful to Joanna Kwiatkowska for her support with the experiment's conduction.

Conflicts of Interest: The authors declare no conflict of interest.

References

1. Wei, G.; Hao, L.; Li, X.; Xu, W.; Liu, F.; Peng, Q.; Lv, S. VCAM-1-targeted and PPARδ-agonist-loaded nanomicelles enhanced suppressing effects on apoptosis and migration of oxidized low-density lipoprotein-induced vascular smooth muscle cells. *Biosci. Rep.* **2020**, *40*, BSR20200559. [CrossRef]
2. Bryk, D.; Olejarz, W.; Zapolska-Downar, D. The role of oxidative stress and NADPH oxidase in the pathogenesis of atherosclerosis. *Postep. Hig. Med. Dosw.* **2017**, *71*, 57–68. [CrossRef]
3. Vermot, A.; Petit-Härtlein, I.; Smith, S.M.E.; Fieschi, F. NADPH Oxidases (NOX): An Overview from Discovery, Molecular Mechanisms to Physiology and Pathology. *Antioxidants* **2021**, *10*, 890. [CrossRef]
4. Fukai, T.; Ushio-Fukai, M. Cross-Talk between NADPH Oxidase and Mitochondria: Role in ROS Signaling and Angiogenesis. *Cells* **2020**, *9*, 1849. [CrossRef]
5. Singel, K.L.; Segal, B.H. NOX2-dependent regulation of inflammation. *Clin. Sci.* **2016**, *130*, 479–490. [CrossRef]
6. Malekmohammad, K.; Sewell, R.D.E.; Rafieian-Kopaei, M. Antioxidants, and Atherosclerosis: Mechanistic Aspects. *Biomolecules* **2019**, *9*, 301. [CrossRef]
7. Mazzuca, M.Q.; Wlodek, M.E.; Dragomir, N.M.; Parkington, H.C.; Tare, M. Uteroplacental insufficiency programs regional vascular dysfunction and alters arterial stiffness in female offspring. *J. Physiol.* **2010**, *588*, 1997–2010. [CrossRef]
8. Santos, J.C.D.; Cruz, M.S.; Bortolin, R.H.; Oliveira, K.M.; Araújo, J.N.G.; Duarte, V.H.R.; Silva, A.M.G.D.; Santos, I.C.C.D.; Dantas, J.M.O.; Paiva, M.S.M.O.; et al. Relationship between circulating VCAM-1, ICAM-1, E-selectin and MMP9 and the extent of coronary lesions. *Clinics* **2018**, *73*, e203. [CrossRef]
9. Blankenberg, S.; Barbaux, S.; Tiret, L. Adhesion molecules and atherosclerosis. *Atherosclerosis* **2003**, *170*, 191–203. [CrossRef]
10. Amin, M.; Pushpakumar, S.; Muradashvili, N.; Kundu, S.; Tyagi, S.C.; Sen, U. Regulation and involvement of matrix metalloproteinases in vascular diseases. *Front. Biosci.* **2016**, *21*, 89–118.
11. Macarie, R.D.; Vadana, M.; Ciortan, L.; Tucureanu, M.M.; Ciobanu, A.; Vinereanu, D.; Manduteanu, I.; Simionescu, M.; Butoi, E. The expression of MMP-1 and MMP-9 is up-regulated by smooth muscle cells after their cross-talk with macrophages in high glucose conditions. *J. Cell. Mol. Med.* **2018**, *22*, 4366–4376. [CrossRef]
12. Dollery, C.M.; Libby, P. Atherosclerosis and proteinase activation. *Cardiovasc. Res.* **2006**, *69*, 625–635. [CrossRef]
13. Varani, J.; Perone, P.; Fligiel, S.E.; Fisher, G.J.; Voorhees, J.J. Inhibition of type I procollagen production in photodamage: Correlation between presence of high molecular weight collagen fragments and reduced procollagen synthesis. *J. Investig. Dermatol.* **2002**, *119*, 122–129. [CrossRef]
14. Newby, A.C. Dual role of matrix metalloproteinases (matrixins) in intimal thickening and atherosclerotic plaque rupture. *Physiol. Rev.* **2005**, *85*, 1–31. [CrossRef]
15. Bayrak, A.; Bayrak, T.; Tokgözoglu, S.L.; Volkan-Salanci, B.; Deniz, A.; Yavuz, B.; Alikasifoglu, M.; Demirpençe, E. Serum PON-1 activity but not Q192R polymorphism is related to the extent of atherosclerosis. *J. Atheroscler. Thromb.* **2012**, *19*, 376–384. [CrossRef]

16. Wu, T.; Mazhar, Z.; Alsayrafi, D.; Garelnabi, M. p-Cymene Modulate Oxidative Stress and Inflammation in Murine Macrophages: Potential Implication in Atherosclerosis. *Cardiovasc. Hematol. Agents Med. Chem.* **2020**, *18*, 151–157. [CrossRef]
17. Sozański, T.; Kucharska, A.Z.; Rapak, A.; Szumny, D.; Trocha, M.; Merwid-Ląd, A.; Dzimira, S.; Piasecki, T.; Piórecki, N.; Magdalan, J.; et al. Iridoid-loganic acid versus anthocyanins from the *Cornus mas* fruits (cornelian cherry): Common and different effects on diet-induced atherosclerosis, PPARs expression and inflammation. *Atherosclerosis* **2016**, *254*, 151–160. [CrossRef]
18. Sozański, T.; Kucharska, A.Z.; Szumny, D.; Magdalan, J.; Merwid-Ląd, A.; Nowak, B.; Piórecki, N.; Dzimira, S.; Jodkowska, A.; Szeląg, A.; et al. Cornelian cherry consumption increases the L-arginine/ADMA ratio, lowers ADMA and SDMA levels in the plasma, and enhances the aorta glutathione level in rabbits fed a high-cholesterol diet. *J. Funct. Food.* **2017**, *34*, 189–196. [CrossRef]
19. Sozański, T.; Kucharska, A.Z.; Dzimira, S.; Magdalan, J.; Szumny, D.; Matuszewska, A.; Nowak, B.; Piórecki, N.; Szeląg, A.; Trocha, M. Loganic acid and anthocyanins from cornelian cherry (*Cornus mas* L.) fruits modulate diet-induced atherosclerosis and redox status in rabbits. *Adv. Clin. Exp. Med.* **2018**, *27*, 1505–1513. [CrossRef]
20. Sozański, T.; Kucharska, A.Z.; Wiśniewski, J.; Fleszar, M.G.; Rapak, A.; Gomułkiewicz, A.; Dzięgiel, P.; Magdalan, J.; Nowak, B.; Szumny, D.; et al. The iridoid loganic acid and anthocyanins from the cornelian cherry (*Cornus mas* L.) fruit increase the plasma l-arginine/ADMA ratio and decrease levels of ADMA in rabbits fed a high-cholesterol diet. *Phytomedicine* **2019**, *52*, 1–11. [CrossRef]
21. Nowak, B.; Matuszewska, A.; Tomanik, M.; Filipiak, J.; Kucharska, A.Z.; Piórecki, N.; Jędrzejuk, D.; Zduniak, K.; Trocha, M.; Bolanowski, M.; et al. Cornelian cherry extract ameliorates osteoporosis associated with hypercholesterolemia in New Zealand rabbits. *Adv. Clin. Exp. Med.* **2020**, *29*, 1389–1397. [CrossRef]
22. Nowak, B.; Matuszewska, A.; Szeląg, A.; Danielewski, M.; Dziewiszek, W.; Nikodem, A.; Filipiak, J.; Jędrzejuk, J.; Bolanowski, M.; Kucharska, A.; et al. Cornelian cherry (*Cornus mas* L.) extract reduces cardiovascular risk and prevents bone loss in ovariectomized Wistar rats. *J. Funct. Food.* **2022**, *90*, 104974. [CrossRef]
23. Szandruk-Bender, M.; Rutkowska, M.; Merwid-Ląd, A.; Wiatrak, B.; Szeląg, A.; Dzimira, S.; Sobieszczańska, B.; Krzystek-Korpacka, M.; Kucharska, A.Z.; Matuszewska, A.; et al. Cornelian Cherry Iridoid-Polyphenolic Extract Improves Mucosal Epithelial Barrier Integrity in Rat Experimental Colitis and Exerts Antimicrobial and Antiadhesive Activities in vitro. *Oxid. Med. Cell. Longev.* **2020**, *2020*, 7697851. [CrossRef]
24. Danielewski, M.; Matuszewska, A.; Nowak, B.; Kucharska, A.Z.; Sozański, T. The Effects of Natural Iridoids and Anthocyanins on Selected Parameters of Liver and Cardiovascular System Functions. *Oxid. Med. Cell. Longev.* **2020**, *2020*, 2735790. [CrossRef]
25. Park, E.; Sozański, T.; Lee, C.G.; Kucharska, A.Z.; Przybylska, D.; Piórecki, N.; Jeong, S.Y. A Comparison of the Antiosteoporotic Effects of Cornelian Cherry (*Cornus mas* L.) Extracts from Red and Yellow Fruits Containing Different Constituents of Polyphenols and Iridoids in Osteoblasts and Osteoclasts. *Oxid. Med. Cell. Longev.* **2022**, *2022*, 4122253. [CrossRef]
26. Przybylska, D.; Kucharska, A.Z.; Sozański, T. A Review on Bioactive Iridoids in Edible Fruits—From Garden to Food and Pharmaceutical Products. *Food Rev. Int.* **2022**. [CrossRef]
27. Danielewski, M.; Kucharska, A.Z.; Matuszewska, A.; Rapak, A.; Gomułkiewicz, A.; Dzimira, S.; Dzięgiel, P.; Nowak, B.; Trocha, M.; Magdalan, J.; et al. Cornelian Cherry (*Cornus mas* L.) Iridoid and Anthocyanin Extract Enhances PPAR-α, PPAR-γ Expression and Reduces I/M Ratio in Aorta, Increases LXR-α Expression and Alters Adipokines and Triglycerides Levels in Cholesterol-Rich Diet Rabbit Model. *Nutrients* **2021**, *13*, 3621. [CrossRef]
28. Rao, V.H.; Kansal, V.; Stoupa, S.; Agrawal, D.K. MMP-1 and MMP-9 regulate epidermal growth factor-dependent collagen loss in human carotid plaque smooth muscle cells. *Physiol. Rep.* **2014**, *2*, e00224. [CrossRef]
29. Butoi, E.; Gan, A.M.; Tucureanu, M.M.; Stan, D.; Macarie, R.D.; Constantinescu, C.; Calin, M.; Simionescu, M.; Manduteanu, I. Cross-talk between macrophages and smooth muscle cells impairs collagen and metalloprotease synthesis and promotes angiogenesis. *Biochim. Biophys. Acta* **2016**, *1863*, 1568–1578. [CrossRef]
30. Wells, J.M.; Gaggar, A.; Blalock, J.E. MMP generated matrikines. *Matrix Biol.* **2015**, *44–46*, 122–129. [CrossRef]
31. Nackman, G.B.; Karkowski, F.J.; Halpern, V.J.; Gaetz, H.P.; Tilson, M.D. Elastin degradation products induce adventitial angiogenesis in the Anidjar/Dobrin rat aneurysm model. *Surgery* **1997**, *122*, 39–44. [CrossRef]
32. Hinek, A.; Boyle, J.; Rabinovitch, M. Vascular smooth muscle cell detachment from elastin and migration through elastic laminae is promoted by chondroitin sulfate-induced "shedding" of the 67-kDa cell surface elastin binding protein. *Exp. Cell. Res.* **1992**, *203*, 344–353. [CrossRef]
33. Hu, W.; Wei, R.; Wang, L.; Lu, J.; Liu, H.; Zhang, W. Correlations of MMP-1, MMP-3, and MMP-12 with the degree of atherosclerosis, plaque stability and cardiovascular and cerebrovascular events. *Exp. Ther. Med.* **2018**, *15*, 1994–1998. [CrossRef]
34. Park, S.; Moon, B.R.; Kim, J.E.; Kim, H.J.; Zhang, T. Aqueous Extracts of *Morus alba* Root Bark and *Cornus officinalis* Fruit Protect against Osteoarthritis Symptoms in Testosterone-Deficient and Osteoarthritis-Induced Rats. *Pharmaceutics* **2020**, *12*, 1245. [CrossRef]
35. Park, E.; Lee, C.G.; Yun, S.H.; Hwang, S.; Jeon, H.; Kim, J.; Yeo, S.; Jeong, H.; Yun, S.H.; Jeong, S.Y. Ameliorative Effects of Loganin on Arthritis in Chondrocytes and Destabilization of the Medial Meniscus-Induced Animal Model. *Pharmaceuticals* **2021**, *14*, 135. [CrossRef]
36. Park, E.; Lee, C.G.; Han, S.J.; Yun, S.H.; Hwang, S.; Jeon, H.; Kim, J.; Choi, C.W.; Yang, S.; Jeong, S.Y. Antiosteoarthritic Effect of Morroniside in Chondrocyte Inflammation and Destabilization of Medial Meniscus-Induced Mouse Model. *Int. J. Mol. Sci.* **2021**, *22*, 2987. [CrossRef]

37. Yang, Y.; Gu, Y.; Zhao, H.; Zhang, S. Loganin Attenuates Osteoarthritis in Rats by Inhibiting IL-1β-Induced Catabolism and Apoptosis in Chondrocytes Via Regulation of Phosphatidylinositol 3-Kinases (PI3K)/Akt. *Med. Sci. Monit.* **2019**, *25*, 4159–4168. [CrossRef]
38. Kang, D.G.; Moon, M.K.; Lee, A.S.; Kwon, T.O.; Kim, J.S.; Lee, H.S. Cornuside suppresses cytokine-induced proinflammatory and adhesion molecules in the human umbilical vein endothelial cells. *Biol. Pharm. Bull.* **2007**, *30*, 1796–1799. [CrossRef]
39. Fallon, M.E.; Hinds, M.T. Single cell morphological metrics and cytoskeletal alignment regulate VCAM-1 protein expression. *Biochem. Biophys. Res. Commun.* **2021**, *555*, 160–167. [CrossRef]
40. Lawson, C.; Wolf, S. ICAM-1 signaling in endothelial cells. *Pharmacol. Rep.* **2009**, *61*, 22–32. [CrossRef]
41. Sumagin, R.; Lomakina, E.; Sarelius, I.H. Leukocyte-endothelial cell interactions are linked to vascular permeability via ICAM-1-mediated signaling. *Am. J. Physiol. Heart Circ. Physiol.* **2008**, *295*, H969–H977. [CrossRef] [PubMed]
42. Ridker, P.M. Anticytokine Agents: Targeting Interleukin Signaling Pathways for the Treatment of Atherothrombosis. *Circ. Res.* **2019**, *124*, 437–450. [CrossRef] [PubMed]
43. Roy, N.; Rosas, S.E. IL-6 Is Associated with Progression of Coronary Artery Calcification and Mortality in Incident Dialysis Patients. *Am. J. Nephrol.* **2021**, *52*, 745–752. [CrossRef] [PubMed]
44. Libby, P. Targeting Inflammatory Pathways in Cardiovascular Disease: The Inflammasome, Interleukin-1, Interleukin-6 and Beyond. *Cells* **2021**, *10*, 951. [CrossRef]
45. Moriya, J. Critical roles of inflammation in atherosclerosis. *J. Cardiol.* **2019**, *73*, 22–27. [CrossRef] [PubMed]
46. Quah, Y.; Lee, S.J.; Lee, E.B.; Birhanu, B.T.; Ali, M.S.; Abbas, M.A.; Boby, N.; Im, Z.E.; Park, S.C. *Cornus officinalis* Ethanolic Extract with Potential Anti-Allergic, Anti-Inflammatory, and Antioxidant Activities. *Nutrients* **2020**, *12*, 3317. [CrossRef]
47. Xu, R.; Zeng, M.; Wu, Y.; Wang, S.; Zhang, B.; Zhang, J.; Kan, Y.; Li, B.; Cao, B.; Zheng, X.; et al. Acetone Extract of *Cornus officinalis* Leaves Exerts Anti-Melanoma Effects via Inhibiting STAT3 Signaling. *Onco Targets Ther.* **2021**, *14*, 3487–3501. [CrossRef] [PubMed]
48. Wen, H.; Xing, L.; Sun, K.; Xiao, C.; Meng, X.; Yang, J. Loganin attenuates intestinal injury in severely burned rats by regulating the toll-like receptor 4/NF-κB signaling pathway. *Exp. Ther. Med.* **2020**, *20*, 591–598. [CrossRef]
49. Liu, S.; Shen, H.; Li, J.; Gong, Y.; Bao, H.; Zhang, J.; Hu, L.; Wang, Z.; Gong, J. Loganin inhibits macrophage M1 polarization and modulates sirt1/NF-κB signaling pathway to attenuate ulcerative colitis. *Bioengineered* **2020**, *11*, 628–639. [CrossRef]
50. Shi, J.Z.; Zheng, X.M.; Zhou, Y.F.; Yun, L.Y.; Luo, D.M.; Hao, J.J.; Liu, P.F.; Zhang, W.K.; Xu, J.K.; Yan, Y.; et al. Cornuside Is a Potential Agent against Alzheimer's Disease via Orchestration of Reactive Astrocytes. *Nutrients* **2022**, *14*, 3179. [CrossRef]
51. Tyrrell, D.J.; Blin, M.G.; Song, J.; Wood, S.C.; Zhang, M.; Beard, D.A.; Goldstein, D.R. Age-Associated Mitochondrial Dysfunction Accelerates Atherogenesis. *Circ. Res.* **2020**, *126*, 298–314. [CrossRef] [PubMed]
52. Tyrrell, D.J.; Goldstein, D.R. Ageing and atherosclerosis: Vascular intrinsic and extrinsic factors and potential role of IL-6. *Nat. Rev. Cardiol.* **2021**, *18*, 58–68. [CrossRef] [PubMed]
53. Burtenshaw, D.; Hakimjavadi, R.; Redmond, E.M.; Cahill, P.A. Nox, Reactive Oxygen Species and Regulation of Vascular Cell Fate. *Antioxidants* **2017**, *6*, 90. [CrossRef] [PubMed]
54. Manea, A.; Simionescu, M. Nox enzymes and oxidative stress in atherosclerosis. *Front. Biosci. Sch.* **2012**, *4*, 651–670.
55. Zhang, Y.; Murugesan, P.; Huang, K.; Cai, H. NADPH oxidases and oxidase crosstalk in cardiovascular diseases: Novel therapeutic targets. *Nat. Rev. Cardiol.* **2020**, *17*, 170–194. [CrossRef]
56. Park, C.H.; Noh, J.S.; Tanaka, T.; Yokozawa, T. 7-O-galloyl-D-sedoheptulose ameliorates renal damage triggered by reactive oxygen species-sensitive pathway of inflammation and apoptosis. *J. Pharm. Pharmacol.* **2012**, *64*, 1730–1740. [CrossRef]
57. Park, C.H.; Tanaka, T.; Kim, J.H.; Cho, E.J.; Park, J.C.; Shibahara, N.; Yokozawa, T. Hepato-protective effects of loganin, iridoid glycoside from Corni Fructus, against hyperglycemia-activated signaling pathway in liver of type 2 diabetic db/db mice. *Toxicology* **2011**, *290*, 14–21. [CrossRef]
58. Lee, J.A.; Shin, M.R.; Roh, S.S. Corni Fructus Alleviates UUO-Induced Renal Fibrosis via TGF-β/Smad Signaling. *BioMed Res. Int.* **2022**, *2022*, 5780964. [CrossRef]
59. Chen, Y.; Chen, J.; Jiang, M.; Fu, Y.; Zhu, Y.; Jiao, N.; Liu, L.; Du, Q.; Wu, H.; Xu, H.; et al. Loganin and catalpol exert cooperative ameliorating effects on podocyte apoptosis upon diabetic nephropathy by targeting AGEs-RAGE signaling. *Life Sci.* **2020**, *252*, 117653. [CrossRef]
60. Fang, W.J.; Feng, J.F.; Lu, X.M.; Lv, M.P.; Cao, S.S.; Li, R.F.; Li, Y.; Li, X.M. Effect of *Cornus officinalis* fruit core extract on the cardiac hypertrophy induced by two kidney two clip. *Zhong Yao Cai Zhongyaocai J. Chin. Med. Mater.* **2012**, *35*, 1985–1989.
61. Libby, P. Inflammation in atherosclerosis. *Arterioscler. Thromb. Vasc. Biol.* **2012**, *32*, 2045–2051. [CrossRef] [PubMed]
62. Asgary, S.; Kelishadi, R.; Rafieian-Kopaei, M.; Najafi, S.; Najafi, M.; Sahebkar, A. Investigation of the lipid-modifying and antiinflammatory effects of *Cornus mas* L. supplementation on dyslipidemic children and adolescents. *Pediatr. Cardiol.* **2013**, *34*, 1729–1735. [CrossRef] [PubMed]
63. Shunmoogam, N.; Naidoo, P.; Chilton, R. Paraoxonase (PON)-1: A brief overview on genetics, structure, polymorphisms and clinical relevance. *Vasc. Health Risk Manag.* **2018**, *14*, 137–143. [CrossRef]
64. Kunutsor, S.K.; Bakker, S.J.; James, R.W.; Dullaart, R.P. Serum paraoxonase-1 activity and risk of incident cardiovascular disease: The PREVEND study and meta-analysis of prospective population studies. *Atherosclerosis* **2016**, *245*, 143–154. [CrossRef] [PubMed]
65. Gautier, T.; Deckert, V.; Aires, V.; Le Guern, N.; Proukhnitzky, L.; Patoli, D.; Lemaire, S.; Maquart, G.; Bataille, A.; Xolin, M.; et al. Human apolipoprotein C1 transgenesis reduces atherogenesis in hypercholesterolemic rabbits. *Atherosclerosis* **2021**, *320*, 10–18. [CrossRef]

66. Francik, R.; Kryczyk, J.; Krośniak, M.; Berköz, M.; Sanocka, I.; Francik, S. The neuroprotective effect of cornus MAS on brain tissue of Wistar rats. *Sci. World J.* **2014**, *2014*, 847368. [CrossRef] [PubMed]
67. Lin, J.; Kakkar, V.; Lu, X. Impact of MCP-1 in atherosclerosis. *Curr. Pharm. Des.* **2014**, *20*, 4580–4588. [CrossRef]
68. Bianconi, V.; Sahebkar, A.; Atkin, S.L.; Pirro, M. The regulation and importance of monocyte chemoattractant protein-1. *Curr. Opin. Hematol.* **2018**, *25*, 44–51. [CrossRef]
69. Bekkering, S.; van den Munckhof, I.; Nielen, T.; Rutten, J.; Graaf, J.; Joosten, L.; Netea, M.; Gomes, M.; Riksen, N. Innate immune cell activation in symptomatic and asymptomatic atherosclerosis in humans in vivo. *Atherosclerosis* **2016**, *252*, e256. [CrossRef]
70. Danielewski, M.; Matuszewska, A.; Szeląg, A.; Sozański, T. The Impact of Anthocyanins and Iridoids on Transcription Factors Crucial for Lipid and Cholesterol Homeostasis. *Int. J. Mol. Sci.* **2021**, *22*, 6074. [CrossRef]
71. Cui, Y.; Wang, Y.; Zhao, D.; Feng, X.; Zhang, L.; Liu, C. Loganin prevents BV-2 microglia cells from $A\beta_{1\text{-}42}$-induced inflammation via regulating TLR4/TRAF6/NF-κB axis. *Cell Biol. Int.* **2018**, *42*, 1632–1642. [CrossRef] [PubMed]
72. Babu, D.; Thapa, D.; Lee, J.S.; Park, S.Y.; Kim, A.R.; Kim, Y.H.; Yang, H.C.; Kim, J.A. Inhibitory effects of an aqueous extract of *Cornus kousa* Burg. leaves on TNF-alpha-induced chemokine expression and monocyte adhesion to human colonic epithelial cells. *Arch. Pharm. Res.* **2009**, *32*, 91–98. [CrossRef]
73. Zhang, Y.; Chen, Z.; Tang, Y.; Shan, W.; Wang, L.; Shi, J.; Luo, Q.; Duan, J.; Xu, G. Association between procalcitonin levels and carotid atherosclerosis in acute ischemic stroke patients. *Int. J. Neurosci.* **2018**, *128*, 237–242. [CrossRef]
74. Ilhan, F.; Akbulut, H.; Karaca, I.; Godekmerdan, A.; Ilkay, E.; Bulut, V. Procalcitonin, c-reactive protein and neopterin levels in patients with coronary atherosclerosis. *Acta Cardiol.* **2005**, *60*, 361–365. [CrossRef]
75. Schiopu, A.; Hedblad, B.; Engström, G.; Struck, J.; Morgenthaler, N.G.; Melander, O. Plasma procalcitonin and the risk of cardiovascular events and death: A prospective population-based study. *J. Intern. Med.* **2012**, *272*, 484–491. [CrossRef]
76. Ertem, A.G.; Efe, T.H.; Yayla, Ç.; Akboğa, M.K.; Açar, B.; Ünal, S.; Kirbaş, Ö.; Sezer Tekce, Y.; Maden, O.; Selcuk, H.; et al. The Association between Serum Procalcitonin Levels and Severity of Coronary Artery Disease Assessed by SYNTAX Score in Patients with Acute Coronary Syndrome. *Angiology* **2017**, *68*, 40–45. [CrossRef] [PubMed]
77. Kraśniak, A.; Drozdz, M.; Pasowicz, M.; Chmiel, G.; Kowalczyk-Michałek, M.; Szumilak, D.; Podolec, P.; Klimeczek, P.; Konieczyńska, M.; Wicher-Muniak, E.; et al. Influence of microinflammation and oxidative stress on atherosclerosis progression and calcifications in cardiovascular system of hemodialyzed patients during two years follow-up. *Przegl Lek.* **2007**, *64*, 140–147.
78. Ozkan, H.; Celik, O.; Hatipoglu, E.; Kantarci, F.; Kadioglu, P. Procalcitonin can be used as a marker of premature atherosclerosis in acromegaly. *Pituitary* **2012**, *15*, 358–364. [CrossRef]
79. Kucharska, A.Z.; Szumny, A.; Sokół-Łętowska, A.; Piórecki, N.; Klymenko, S.V. Iridoids and anthocyanins in cornelian cherry (*Cornus mas* L.) cultivars. *J. Food Compos. Anal.* **2015**, *40*, 95–102. [CrossRef]
80. Kucharska, A.Z.; Sokół-Łętowska, A.; Oszmiański, J.; Piórecki, N.; Fecka, I. Iridoids, phenolic compounds and antioxidant activity of edible honeysuckle berries (*Lonicera caerulea* var. kamtschatica Sevast.). *Molecules* **2017**, *22*, 405. [CrossRef] [PubMed]

International Journal of
Molecular Sciences

MDPI

Article

Isolation and NMR Scaling Factors for the Structure Determination of Lobatolide H, a Flexible Sesquiterpene from *Neurolaena lobata* †

Tibor Kovács [1,2], Ildikó Lajter [3], Norbert Kúsz [3], Zsuzsanna Schelz [4], Noémi Bózsity-Faragó [4], Anikó Borbás [5], István Zupkó [4], Georg Krupitza [6], Richard Frisch [7], Judit Hohmann [3,8], Andrea Vasas [3,8,*] and Attila Mándi [1,*]

1 Department of Organic Chemistry, University of Debrecen, P.O. Box 400, 4002 Debrecen, Hungary
2 Doctoral School of Chemistry, University of Debrecen, Egyetem tér 1, 4032 Debrecen, Hungary
3 Institute of Pharmacognosy, University of Szeged, Eötvös u. 6, 6720 Szeged, Hungary
4 Institute of Pharmacodynamics and Biopharmacy, University of Szeged, Eötvös u. 6, 6720 Szeged, Hungary
5 Department of Pharmaceutical Chemistry, University of Debrecen, Egyetem tér 1, 4032 Debrecen, Hungary
6 Department of Pathology, Medical University of Vienna, Waehringer Guertel 18-20, 1090 Vienna, Austria
7 Institute for Ethnobiology, Playa Diana, San José GT-170, Guatemala
8 ELKH-USZ Biologically Active Natural Products Research Group, University of Szeged, Eötvös u. 6, 6720 Szeged, Hungary
* Correspondence: vasas.andrea@szte.hu (A.V.); mandi.attila@science.unideb.hu (A.M.)
† Dedicated to Professor Dr. Katalin E. Kövér.

Abstract: A new flexible germacranolide (**1**, lobatolide H) was isolated from the aerial parts of *Neurolaena lobata*. The structure elucidation was performed by classical NMR experiments and DFT NMR calculations. Altogether, 80 theoretical level combinations with existing ^{13}C NMR scaling factors were tested, and the best performing ones were applied on **1**. ^{1}H and ^{13}C NMR scaling factors were also developed for two combinations utilizing known exomethylene containing derivatives, and the results were complemented by homonuclear coupling constant (J_{HH}) and TDDFT-ECD calculations to elucidate the stereochemistry of **1**. Lobatolide H possessed remarkable antiproliferative activity against human cervical tumor cell lines with different HPV status (SiHa and C33A), induced cell cycle disturbance and exhibited a substantial antimigratory effect in SiHa cells.

Keywords: natural product; stereochemistry; NMR shift parameter development; DFT calculations; ECD calculations; antiproliferative activity; antimigratory effect

Citation: Kovács, T.; Lajter, I.; Kúsz, N.; Schelz, Z.; Bózsity-Faragó, N.; Borbás, A.; Zupkó, I.; Krupitza, G.; Frisch, R.; Hohmann, J.; et al. Isolation and NMR Scaling Factors for the Structure Determination of Lobatolide H, a Flexible Sesquiterpene from *Neurolaena lobata* † *Int. J. Mol. Sci.* **2023**, *24*, 5841. https://doi.org/10.3390/ijms24065841

Academic Editor: Azzurra Stefanucci

Received: 24 January 2023
Revised: 11 March 2023
Accepted: 13 March 2023
Published: 19 March 2023

1. Introduction

Sesquiterpene lactones (SLs) constitute a large and diverse group of biologically active plant specialized metabolites that have been identified in several plant families. The greatest numbers are found in the family Asteraceae with over 3000 reported different structures [1–3]. They are primarily classified on the basis of their carbocyclic skeletons. From over 40 structural types of sesquiterpene lactones known to date, the most widespread are germacrane, guaiane, eudesmane, and pseudoguaiane [4]. An important structural feature of the SLs is the presence of a γ-lactone ring containing in many cases an α-methylene group. The biological activity (e.g., cytotoxic [1,5–8], anti-inflammatory [2,9–11]) of SLs is mainly due to the presence of this structural element [12–14]. Furthermore, there are also reports on neuroprotective [15,16], antimicrobial [17] or antiparasitic [18,19] activities of SL derivatives.

Neurolaena lobata (L.) R.Br. ex Cass. (Asteraceae) is a perennial plant occurring mainly in Central and South America. It is a rich source of SLs; previously 24 sesquiterpenes, among them 22 SLs having germacranolide, *seco*-germacranolide, furanoheliangolide and eudesmanolide skeletons were isolated from the aerial parts of the plant. Several of them possessed remarkable antiproliferative and anti-inflammatory activities [20–24].

Although DFT NMR calculations of ^{1}H and ^{13}C chemical shifts and the associated statistical methods [25,26] are a powerful tool which allowed the structure elucidation [27–30] or even structure revision [31–34] of a large number of natural and synthetic derivatives, they have several limitations [26,33,35,36]. Regardless of one's aims to apply a scaling factor approach or an inner reference approach, for a successful determination of the relative/absolute configuration, the difference between the experimental values of the sample and computed data of the correct isomer should be small, while the wrong isomers should show larger differences from the experimental data. It is known that some atoms or groups can cause large deviations in the computed values, preventing a good reproduction of the experimental NMR data in the vicinity [37,38]. If there is no chirality center next to the problematic atom or group, one can neglect the highly affected atoms, which is usually applied for the training sets, too [27]. If the problematic region is far from the chirality center(s) to be determined, even truncated models can be applied for the NMR calculations [28,29,39]. There are, however, a few examples in the literature, where even for rather problematic cases, such as halogen atoms, well performing scaling factors could be prepared [40]. Exomethylene groups are less problematic than halogen atoms, but still capable of exerting a distortion of several ppm, which is comparable with the difference between the possible stereoisomers and, hence, thwarts a safe assignment [24,41,42]. For example, in our previous study on lobatolide derivatives, the ^{13}C NMR chemical shift data of lobatolide A could be well reproduced, but for most of the other exomethylene containing lobatolides, large differences were found in the vicinity of the exomethylene group preventing utilization of the calculated NMR scaling factors in structure elucidation [24]. Since a large number of level combinations with NMR scaling factors are already available in the literature [27,43], and for some of them, even exomethylene containing derivatives were considered in the training set [41], we hoped to find a few well applicable combinations for germacranolides including the novel flexible natural product (**1**). On the other hand, the vast majority of the combinations found in the literature apply B3LYP or other classical functionals for DFT optimization, and almost all combinations were prepared for gas-phase optimized conformers [44]. These combinations can work well for rigid molecules, but for open chain compounds or macrolides with high flexibility they can be problematic [45,46]. To this end, we developed scaling factors by applying the ωB97XD long-range corrected hybrid functional [47,48] for geometry optimization both in vacuo and with SMD (solvation model based on density) for chloroform.

2. Results and Discussion

Multistep chromatography of the dichloromethane-soluble phase of the methanolic extract prepared from the aerial parts of *N. lobata* resulted in the isolation of a pure compound (**1**, Figure 1). The structure elucidation of **1** was carried out by one- and two-dimensional NMR spectroscopy (^{1}H–^{1}H COSY, HSQC, HMBC and NOESY) and HRESIMS experiments and TDDFT-ECD calculations.

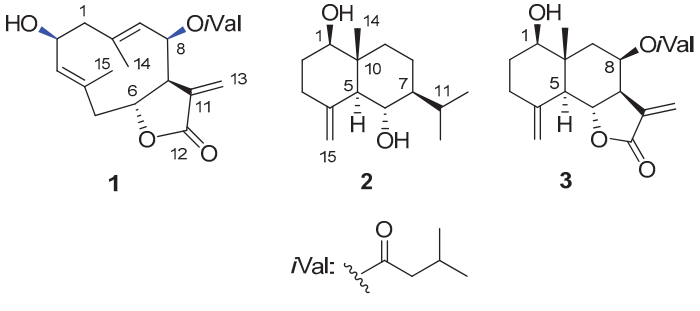

Figure 1. Structures of the novel compound (**1**) and the known NMR test compounds (**2**, volenol, and **3**, 8β-isovaleroyloxyreynosin) isolated from *N. lobata*. Blue indicates the problematic chirality centers.

Compound **1** (lobatolide H) was isolated as a yellow gum with $[\alpha]^{27}_{D}$ + 31 (*c* 0.1, $CHCl_3$). Its HRESIMS displayed a quasi-molecular ion peak at *m*/*z* 349.2012 $[M + H]^+$ (calcd. for 349.2010), indicating the molecular formula $C_{20}H_{28}O_5$. The ^1H and ^{13}C NMR spectra of **1** showed the presence of an isovaleroyl group (Table 1). Additionally, the 1D and 2D NMR spectra (Figures S1–S6) exhibited that this compound is very similar to the germacranolide-type sesquiterpene lactone 2*α*-hydroxy-8*β*-isovaleroyloxycostunolide, isolated previously from *Helianthus gracilentus* (Asteraceae) [49]. The ^{13}C NMR data of the two compounds were completely in agreement. Only two differences could be detected between the two compounds. Firstly, the positions of the double bonds differ. These were present at C-3–C-4 and C-9–C-10 in **1**, but at C-4–C-5 and C-1–C-10 in 2*α*-hydroxy-8*β*-isovaleroyloxycostunolide. Secondly, the orientation of OH-2 group in **1** differs from the proposed *α*-orientation of this substituent in case of the costunolide derivative. The position of the double bond was proved by ^1H-^1H COSY correlations. The ^1H-^1H COSY spectrum defined two structural fragments with correlated protons: –CH_2-CH(OH)-CH= (A) (δ_H 2.72, 2.07, 4.75, 5.25) (C-1–C-3) and –CH_2–CH(OR)–CH(R)–CH(OR)–CH= (B) (δ_H 2.76, 2.32, 5.76, 2.93, 5.50, and 4.98) (C-5–C-9). These two structural parts, tertiary methyls (δ_H 1.79 and 1.53), and quaternary carbons (δ_C 135.1, 136.4, 142.7, and 169.4) were connected by inspection of the HMBC correlations. The two- and three-bond correlations between the quaternary carbon C-4 and H-2, H-5a, H-6, and H-15; between C-10 and H-1a, H-1b, H-8, and H-14; and between C-7 and H-13a, H-13b revealed the presence of a germacranolide-3,9-diene structure substituted with a hydroxy group at C-2, and an isovaleroyloxy group at C-8.

Table 1. ^1H and ^{13}C NMR data of compound **1** in $CDCl_3$ (δ in ppm, mult. *J* in Hz).

Position	^1H	^{13}C
1a	2.72 dd (11.0, 5.9)	48.6
1b	2.07 m	
2	4.75 td (9.8, 5.9)	69.2
3	5.25 d (9.8)	133.9
4	-	135.1
5a	2.76 dd (14.3, 5.1)	44.0
5b	2.32 dd (14.3, 1.6)	
6	5.76 brd (5.1)	70.8
7	2.93 d (7.9)	52.9
8	5.50 t (9.9, 7.9)	75.3
9	4.98 brd (9.9)	129.3
10	-	142.7
11	-	136.4
12	-	169.4
13a	6.30 d (3.2)	121.2
13b	5.60 d (3.2)	
14	1.79 s	18.7
15	1.53 s	20.0
8-iVal		
1′	-	171.8
2′	2.15–2.17 m (2H)	43.3
3′	2.05 m	25.4
4′	0.92 d (6.2)	22.3
5′	0.90 d (6.3)	22.3

The *β*-orientation of the 2-OH and 8-isovaleroyl group was indicated by the NOE correlations between H-2/H-1a, H_3-14; H_3-14/H-1a, and H-8; and H-8/H-2. The *E* configuration of the olefinic bonds was demonstrated by the NOESY cross-peaks between H-14/H-1*α* and H-9/H-1*β*, and between H-15/H-2*α* and H-3/H-1*β*. All the above data suggested lobatolide H to have the structure **1**.

Although NOE correlations work well in smaller rings, for flexible systems or macrolides one should be careful with the interpretations to avoid misassignments [24,50,51]. Therefore, we tested a large number of available DFT NMR methods, developed parameters for two combinations and augmented the NMR studies with TDDFT-ECD calculations to verify the stereochemistry of **1**. To help the reader navigate between the tested and developed NMR chemical shift scaling factor combinations, we named approach A the test of three known DFT combinations on lobatolide H (**1**), which we used successfully lately on various heterocycles, including lobatolides A and B [24,28,29,52,53]. In approach B we tested 80 available combinations first on the known derivative volenol (**2**, step 1), and then the best performing ones on 8*β*-isovaleroyloxyreynosin (**3**, step 2) and **1** (step 3). In approach C we developed chemical shift scaling factors for two further combinations based on eleven exomethylene containing derivatives and tested them for **2**, **3** and **1**.

Approach A

Since in our previous work we could predict the ^{13}C chemical shifts of lobatolides A and B with a good approximation but encountered problems for other lobatolide derivatives [24], we tested three DFT combinations with available scaling factors on **1**, namely, the mPW1PW91/6-311+G(2d,p)//B3LYP/6-31+G(d,p) [27], the mPW1PW91/6-311+G(2d,p) SMD/$CHCl_3$//B3LYP/6-31+G(d,p) [27] and the mPW1PW91/6-311+G(2d,p) SMD/$CHCl_3$//mPW1PW91/6-311+G(2d,p) SMD/$CHCl_3$ [54] combinations, which were successfully utilized by us for other derivatives, recently [28,29,52,53]. The absolute configuration of the C-6, C-7 and C-10 chirality centers seems to be biosynthetically conserved in lobatine and related derivatives if applicable; thus, four possible diastereomers of **1** were considered with different configurations at the C-2 and C-8 chirality centers, namely, (2*R*,6*R*,7*S*,8*R*)-**1**, (2*R*,6*R*,7*S*,8*S*)-**1**, (2*S*,6*R*,7*S*,8*R*)-**1** and (2*S*,6*R*,7*S*,8*S*)-**1**. The experimentally most plausible isomer, (2*S*,6*R*,7*S*,8*R*)-**1**, was denoted as **isomer 1**, (2*R*,6*R*,7*S*,8*R*)-**1** as **isomer 2**, (2*R*,6*R*,7*S*,8*S*)-**1** as **isomer 3** and (2*S*,6*R*,7*S*,8*S*)-**1** as **isomer 4**. The results obtained at the three combinations were contradictory (Tables 2 and S3–S5). While the mPW1PW91/6-311+G(2d,p)//B3LYP/6-31+G(d,p) level suggested **isomer 2**, the mPW1PW91/6-311+G(2d,p) SMD/$CHCl_3$//B3LYP/6-31+G(d,p) level gave similarly good results for **isomer 1** and **isomer 2**, and only **isomer 4** yielded a considerably higher mean absolute error (MAE) value. The mPW1PW91/6-311+G(2d,p) SMD/$CHCl_3$//mPW1PW91/6-311+G(2d,p) SMD/$CHCl_3$ level gave similar results to mPW1PW91/6-311+G(2d,p)//B3LYP/6-31+G(d,p), preferring **isomer 2** and rating **isomer 1** the second best. The DP4+ [26] results suggested **isomer 2** with two combinations and **isomer 1** with 1 combination as the most plausible structure, but in the latter case, both **isomer 2** and **isomer 3** had considerable possibilities. It is important to note here, that ECD calculations allow exclusion of **isomer 3** (vide infra).

Table 2. MAE and DP4+ results calculated from the ^{13}C isotropic shielding constants of the four possible diastereomers of **1** vs. the experimental data of the naturally occurring **1** determined by three usually well performing combinations of theoretical levels.

NMR Level//DFT Optimization Level	MAE (Isomer 1; Isomer 2; Isomer 3, Isomer 4)	sDP4+ (Isomer 1; Isomer 2; Isomer 3, Isomer 4)
mPW1PW91/6-311+G(2d,p)//B3LYP/6-31+G(d,p)	2.32; 2.10; 2.57; 2.49	5.28%; 93.00%; 0.25%; 1.47%
mPW1PW91/6-311+G(2d,p) SMD/$CHCl_3$//B3LYP/6-31+G(d,p)	2.06; 2.07; 2.16; 2.34	55.91%; 30.41%; 12.46%; 1.22%
mPW1PW91/6-311+G(2d,p) SMD/$CHCl_3$//mPW1PW91/6-311+G(2d,p) SMD/$CHCl_3$	2.15; 1.89; 2.38; 2.41	3.40%; 96.26%; 0.19%; 0.16%

Approach B

Parallel with approach A, we also performed a three-step test for a large number of DFT combinations with available NMR chemical shift parameters. In the first evaluation step, 79 combinations were selected from the CHESHIRE Chemical Shift Repository

database as of 5 October 2018 [27,43,44,55–57]. Basically, all combinations were selected with available ^{13}C NMR scaling factors that were developed with reference to experimental data measured in $CDCl_3$ and either in gas-phase or based on Gaussian 09 solvent model calculations. (Solvent model implementations in previous versions of the software package were different; therefore, parameters developed with earlier versions are not comparable with calculations obtained by more recent versions). The scaling factors found in the CHESHIRE database are usually developed on a larger set of small, rigid but diverse organic compounds (e.g., a few dozens in Tantillo et al. [27] and Pierens [43] works). Since the CHESHIRE database did not contain the third combination applied in approach A, we supplemented the 79 combinations with the mPW1PW91/6-311+G(2d,p) SMD/$CHCl_3$//mPW1PW91/6-311+G(2d,p) SMD/$CHCl_3$ method. Thus the 80 combinations in total (see Table S1 in the Supplementary Materials) were tested for volenol (**2**) in the first step. The initial 24 MMFF conformers of (1*R*,5*S*,6*S*,7*S*,10*R*)-**2** were optimized independently at all the given DFT optimization levels (Tables S30–S37) and chemical shifts were computed at the corresponding NMR levels with the GIAO method [58]. The resulting values were Boltzmann averaged and corrected according Equation 1 utilizing the corresponding scaling factors (Table S1). The resulting computed ^{13}C NMR chemical shift values were compared with the experimental values of **2** [24,59]. Mean absolute error (MAE) values were calculated from the absolute differences of the calculated and experimental data (see Table S2 in the Supplementary Materials), and the methods were ranked according to their MAE values while taking also the maximum absolute errors ($\Delta\delta_{max}$) into account. The best performing four combinations were chosen for the second evaluation step, namely, mPW1PW91/6-31G(d)//M06-2X/6-31G(d), mPW1PW91/6-31G(d) SMD/$CHCl_3$//M06-2X/6-31G(d), M06/6-31G(d)//B3LYP/6-31+G(d,p) and OPBE0/6-31G(d)//B3LYP/6-31+G(d,p). It is interesting to note, that none of the three combinations of approach A were among the best ones for **2**.

$$\delta = (Intercept - \sigma)/-Slope \quad (1)$$

In the second evaluation step, the four best performing combinations of the first step were tested for 8β-isovaleroyloxyreynosin (**3**) that contains two exomethylene moieties, one in a five-membered and one in a six-membered ring. Since **3** contains a chirality center at C-8 with the same substitution pattern as **1** and C-8 was one of the problematic chirality centers in **1**, we aimed to differentiate the two C-8 epimers with the four NMR combinations. The calculations were performed similarly to **2** for the 65 and 92 initial MMFF conformers of (1*R*,5*S*,6*R*,7*R*,8*R*,10*R*)-**3** and (1*R*,5*S*,6*R*,7*R*,8*S*,10*R*)-**3**, respectively. The resulting MAE and DP4+ values indicated the mPW1PW91/6-31G(d) SMD/$CHCl_3$//M06-2X/6-31G(d) and the M06/6-31G(d)//B3LYP/6-31+G(d,p) methods to be better than the other two (Tables 3 and S6–S9). The mPW1PW91/6-31G(d)//M06-2X/6-31G(d) combination, which is similar to mPW1PW91/6-31G(d) SMD/$CHCl_3$//M06-2X/6-31G(d) but lacks the solvent model in the NMR calculation step, showed less difference between the epimers, while the last OPBE0/6-31G(d)//B3LYP/6-31+G(d,p) combination yielded much larger MAE values than the others. Here we want to note that the DP4+ method was developed for 24 combinations utilizing only the B3LYP and mPW1PW91 functionals with various basis sets, and application of the method for chemical shifts calculated at considerably different combinations can be misleading [26,35]. Therefore, the DP4+ values of all other combinations are shown only for information and where contradictory, the MAE values should be considered.

In the third step, the best performing two combinations of step 2 were applied for the above four isomers of **1**. While the mPW1PW91/6-31G(d) SMD/$CHCl_3$//M06-2X/6-31G(d) combination showed the best agreement for **isomer 1**, it rated **isomer 2** and **isomer 3** with similar MAE values the second best. The M06/6-31G(d)//B3LYP/6-31+G(d,p) method rated **isomer 4** and **isomer 2** similarly good and yielded considerably higher MAE values for **isomer 1** and **isomer 3** (Tables 4, S10 and S11).

Table 3. MAE and DP4+ results calculated from the ^{13}C isotropic shielding constants of the 8-epimers of **3** vs. the experimental data of naturally occurring **3** determined by the four best performing combinations of theoretical levels.

NMR Level//DFT Optimization Level	MAE [(8*R*)-Epimer; (8*S*)-Epimer]	sDP4+ [(8*R*)-Epimer; (8*S*)-Epimer]
mPW1PW91/6-31G(d)//M06-2X/6-31G(d)	1.63; 1.68	(69.35%; 30.65%)
mPW1PW91/6-31G(d) SMD/$CHCl_3$//M06-2X/6-31G(d)	1.40; 1.54	(93.58%; 6.42%)
M06/6-31G(d)//B3LYP/6-31+G(d,p)	1.68; 2.01	(99.13%; 0.87%)
OPBE0/6-31G(d)//B3LYP/6-31+G(d,p)	1.93; 2.35	(99.79%; 0.21%)

Table 4. MAE and DP4+ results calculated from the ^{13}C isotropic shielding constants of the four possible diastereomers of **1** vs. the experimental data of naturally occurring **1** determined by the two best performing combinations of theoretical levels.

NMR Level//DFT Optimization Level	MAE (Isomer 1; Isomer 2; Isomer 3, Isomer 4)	sDP4+ (Isomer 1; Isomer 2; Isomer 3, Isomer 4)
mPW1PW91/6-31G(d) SMD/$CHCl_3$//M06-2X/6-31G(d)	2.42; 2.59; 2.62; 2.85	(90.66% 3.14% 5.16% 1.04%)
M06/6-31G(d)//B3LYP/6-31+G(d,p)	3.12; 2.83; 3.19; 2.76	(2.54%; 69.71%; 9.58%; 18.17%)

Approach C

The contradictory results indicate that flexibility of **1** can play a significant role in the low reproducibility of the chemical shift values. If we consider the widely available or the tested 80 combinations, it is obvious that almost all of them use classical (mostly B3LYP) functionals for DFT geometry optimization, and there is only one combination (mPW1PW91/6-311+G(2d,p) SMD/$CHCl_3$//B3LYP/6-31+G(d,p) SMD/$CHCl_3$) [27] in the CHESHIRE chemical shift database which also applies a solvent model for the optimization level [44]. The additionally tested functional (mPW1PW91/6-311+G(2d,p) SMD/$CHCl_3$//mPW1PW91/6-311+G(2d,p) SMD/$CHCl_3$) was not part of the database, perhaps due to the very limited reference compound set utilized for creating the chemical shift parameters [54]. Although for small and rigid molecules, which usually constitute the reference set of the NMR scaling parameters, the available level combinations seem to be sufficient, for flexible molecules, however, better performing functionals and consideration of the solvent effect also for the DFT optimization can be crucial to obtaining the low-energy conformers and estimate their Boltzmann populations correctly. To this end, we selected the ωB97XD functional [40,47,48] for DFT optimization level both in vacuo and with SMD solvent model for chloroform, and combined it with the well performing mPW1PW91 functional as an NMR calculation level with the same or no solvent model as in the corresponding DFT optimization step (Tables S38 and S39). As reference set, we have chosen 11 exomethylene containing molecules with different flexibilities (**2**, **4**–**13**, Figures 2 and S14) [23,24,59–71]. One of the molecules contained no chirality centers (**12**), one had only one chirality center (**13**), while the relative or absolute configuration of the others was known from the literature, secured by X-ray measurements, synthetic or biosynthetic considerations.

As Figure 3 shows, the computed ^{13}C NMR data shows an excellent correlation with the experimental chemical shift data for the reference set at both level combinations. On the other hand, larger deviations were observed for the ^{1}H shift values of a few protons in both cases. We investigated the most discordant cases, such as H-7 of **2**, H-2 of **5**, H-13a and b of **9** or H-4 of **4**, but no better assignments could be found than those described in the literature. Unfortunately, some of these hydrogens are connected to a chirality center, which limits the application of the ^{1}H chemical shift data as a solid proof. Accordingly, we will rely more on the better performing ^{13}C parameters and the corrected shift values obtained by these if the results are contradictory.

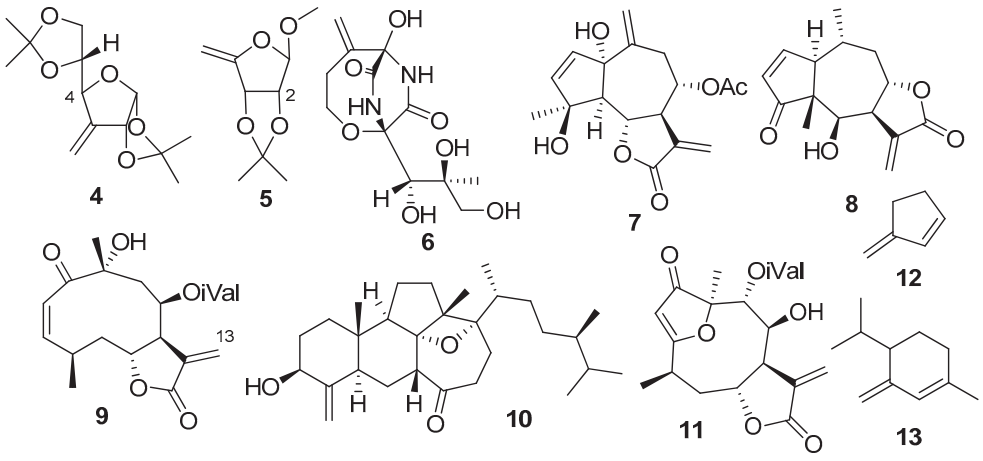

Figure 2. Structures of the compounds considered only in the reference set of the novel NMR shift methods: 3-deoxy-1,2;5,6-di-*O*-isopropylidene-3-*C*-methylene-*α*-D-*ribo*-hexofuranose (**4**), methyl 5-deoxy-2,3-*O*-isopropylidene-*β*-D-*erythro*-pent-4-enofuranoside (**5**), bicyclomycin (**6**), 1*α*,4*β*-dihydroxy-8*α*-acetoxy-guaia-2,10(14),11(13)-triene-6,12-olide (**7**), mexicanin I (**8**), neurolenin A (**9**), swinhoeisterol F (**10**), lobatolide A (**11**), 3-methylenecyclopent-1-ene (**12**), 4-isopropyl-1-methyl-3-methylenecyclohex-1-ene (**13**).

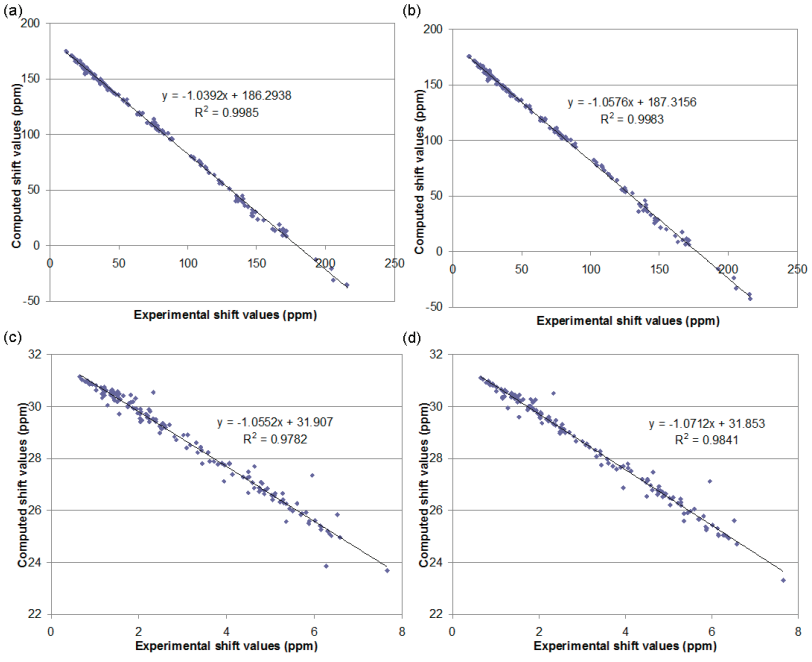

Figure 3. Correlation plots for computed ^{13}C and ^{1}H NMR data for the reference set: (**a**) ^{13}C gas phase, (**b**) ^{13}C SMD, (**c**) ^{1}H gas phase and (**d**) ^{1}H SMD.

The novel parameters were first tested back on **2** (Figure S11). The calculated chemical shifts of most carbons both in the gas phase and the SMD combination showed close agreement with the experimental values (Tables 5 and 6). Only the exomethylene carbons

exhibited larger deviations. However, most importantly, the carbons in the vicinity of the exomethylene moiety showed good correlation with the experimental data. The MAE values derived from the difference of the experimental and the computed ^{1}H chemical shift data are relatively small (0.18 and 0.19), but larger differences were found for the H-3, H-8 and H-9 hydrogens, and H-7 showed a particularly large difference as this hydrogen was one of the most problematic in the reference set already (see Tables S12 and S13 in the Supplementary Materials).

Table 5. Test of the mPW1PW91/6-311+G(2d,p)//ωB97XD/6-31+G(d,p) level ^{13}C parameters for **2**.

Numbering	δ_{Exp} (ppm)	δ_{Calc} (ppm)	Δδ (ppm)
C-1	79.28	78.78	0.50
C-2	32.17	31.26	0.91
C-3	35.34	36.89	1.55
C-4	146.48	152.97	6.49
C-5	56.15	56.06	0.09
C-6	67.25	64.33	2.92
C-7	49.59	48.55	1.04
C-8	18.43	19.65	1.22
C-9	36.55	35.90	0.65
C-10	41.93	44.33	2.40
C-11	26.26	27.81	1.55
C-12	21.32	19.60	1.72
C-13	16.44	15.72	0.72
C-14	11.82	10.57	1.25
C-15	108.03	105.99	2.04
MAE	N/A	N/A	1.67

Table 6. Test of the mPW1PW91/6-311+G(2d,p) SMD/$CHCl_3$//ωB97XD/6-31+G(d,p) SMD/$CHCl_3$ level ^{13}C parameters for **2**.

Numbering	δ_{Exp} (ppm)	δ_{Calc} (ppm)	Δδ (ppm)
C-1	79.28	77.99	1.29
C-2	32.17	31.72	0.45
C-3	35.34	36.68	1.34
C-4	146.48	152.90	6.42
C-5	56.15	55.65	0.50
C-6	67.25	64.65	2.60
C-7	49.59	48.49	1.10
C-8	18.43	19.48	1.05
C-9	36.55	35.92	0.63
C-10	41.93	44.70	2.77
C-11	26.26	28.01	1.75
C-12	21.32	19.80	1.52
C-13	16.44	15.27	1.17
C-14	11.82	11.13	0.69
C-15	108.03	104.29	3.74
MAE	N/A	N/A	1.80

Thereafter, the novel chemical shift parameters were also tested on the two above epimers of **3** (Figures S12 and S13). The computed ^{13}C chemical shift data obtained with both the novel in vacuo and SMD level parameters favored the (1*R*,5*S*,6*R*,7*R*,8*R*,10*R*)-**3** epimer, but the solvent model calculations showed substantially larger difference between the isomers and smaller MAE for the correct one (Tables 7, S14 and S15). In contrast to **2**, the results of the ^{1}H NMR chemical shift calculations at both levels gave excellent agreement for almost all protons of the correct isomer, and higher differences were found for some characteristic protons in the vicinity of the epimeric center in the wrong stereoisomer (see

Tables S16 and S17 in the Supplementary Materials). That is, both the carbon and proton results favored the correct (1*R*,5*S*,6*R*,7*R*,8*R*,10*R*)-**3** epimer at both novel combinations of levels.

Table 7. MAE and DP4+ results calculated from the ^{13}C isotropic shielding constants of the 8-epimers of **3** vs. the experimental data of naturally occurring **3** determined by the two novel combinations.

NMR Level//DFT Optimization Level	MAE [(8*R*)-Epimer; (8*S*)-Epimer]	sDP4+ [(8*R*)-Epimer; (8*S*)-Epimer]
mPW1PW91/6-311+G(2d,p)//ωB97XD/6-31+G(d,p)	1.82; 1.87	(66.38%; 33.62%)
mPW1PW91/6-311+G(2d,p) SMD/$CHCl_3$//ωB97XD/6-31+G(d,p) SMD/$CHCl_3$	1.60; 1.91	(99.26%; 0.74%)

Finally, the initial 133, 124, 252 and 201 MMFF conformers of the four possible stereoisomers of **1** were also re-optimized at the ωB97XD/6-31+G(d,p) and ωB97XD/6-31+G(d,p) SMD/$CHCl_3$ levels (Figures S7–S10). NMR shift data were calculated for the conformers above 1% Boltzmann distribution at the mPW1PW91/6-311+G(2d,p) and mPW1PW91/6-311+G(2d,p) SMD/$CHCl_3$ levels, respectively, and corrected with the novel parameters. The ^{13}C data obtained at both combinations of levels favored **isomer 1** (Tables 8, S18 and S19), while the ^{1}H data suggested **isomer 2** (see Tables S20 and S21 in the Supplementary Materials). As indicated above, the DP4+ statistical analysis gave unexpected results in contrast to the MAE values similar to the second combination in Table 3, due to the large difference in the combinations the method was originally developed for, and thus, the sDP4+ percentages were neglected.

Table 8. MAE results calculated from the ^{13}C isotropic shielding constants of the four possible diastereomers of **1** vs. the experimental data of naturally occurring **1** determined by the two novel combinations.

NMR Level//DFT Optimization Level	MAE (Isomer 1; Isomer 2; Isomer 3, Isomer 4)
mPW1PW91/6-311+G(2d,p)//ωB97XD/6-31+G(d,p)	2.33; 2.48; 2.58; 3.11
mPW1PW91/6-311+G(2d,p) SMD/$CHCl_3$//ωB97XD/6-31+G(d,p) SMD/$CHCl_3$	2.26; 2.42; 2.48; 3.23

Coupling constant calculations

To verify the result of the ^{13}C data, homonuclear coupling constants were also calculated with the last SMD combination for key protons in the macrolide ring of the two favored stereoisomers (**isomer 1** and **isomer 2**), and compared with the experimental values (Table 9). The results significantly preferred **isomer 1 in line with the ^{13}C calculations of approach C. Especially $J_{1aH\text{-}2H}$ and $J_{2H\text{-}3H}$ showed large differences between the calculated data of the two isomers and also in comparison with the experimental values, where isomer 1** reproduced the experimental data well. This also leads to the conclusion that the calculations better reproduced the conformation of the western part of the molecule than the eastern part, and that macrocycles are still a tough target to study even with otherwise well performing DFT functionals. At the suggestion of one of the reviewers, we tested the J-DP4 method [72] for the coupling constant data of the two isomers, resulting in a 98.21% probability for **isomer 1**. However, we have to indicate that similarly to the DP4+ method there are differences in the applied level and the level the method was developed for.

Table 9. Comparison of the experimental and computed coupling constant values of **isomer 1** and **isomer 2** of **1** vs. the experimental data of naturally occurring **1** determined by the mPW1PW91/6-311+G(2d,p) SMD/$CHCl_3$//ωB97XD/6-31+G(d,p) SMD/$CHCl_3$ level. J_{in} indicates the coupling constant data of **isomer n**.

Coupling Atoms	J_{Exp} (Hz)	J_{i1} (Hz)	J_{i2} (Hz)	ΔJ_{i1}	ΔJ_{i2}
1aH-2H	5.90	6.62	0.93	0.72	4.97
2H-3H	9.80	10.08	6.51	0.28	3.29
5aH-6H	5.10	6.58	2.82	1.48	2.28
7H-8H	7.90	4.33	3.28	3.57	4.62
8H-9H	9.90	7.36	8.73	2.54	1.17
MAE				1.72	3.27

TDDFT-ECD calculations

To elucidate the absolute configuration and further verify the NMR results, TDDFT-ECD calculations [73–75] were performed on the MMFF conformers of the four possible isomers of 1. The initial conformers were re-optimized at the CAM-B3LYP/TZVP [76] PCM/MeCN level (Table S40) and rotatory strength values were computed at four different levels similarly to the recently described lobatolides [24]. While the Boltzmann average for three isomers (isomer 1, isomer 2 and isomer 4) gave acceptable agreement with the experimental ECD spectrum (the high wavelength n-π^* transitions were reported to be hard to reproduce in several cases in the literature [77,78]), isomer 3 showed a mirror-image relationship (Figure 4). That is, assuming homochirality with the known lobatolides at the conserved chirality centers C-6 and C-7, isomer 3 can be excluded as a possible isomer, and accepting the results of the novel NMR combinations and the coupling constant calculations, the homochiral nature of 1 with the known lobatolides can be verified. Based on the above-described NMR and ECD calculations, the (2*S*,6*R*,7*S*,8*R*) absolute configuration was assigned for 1.

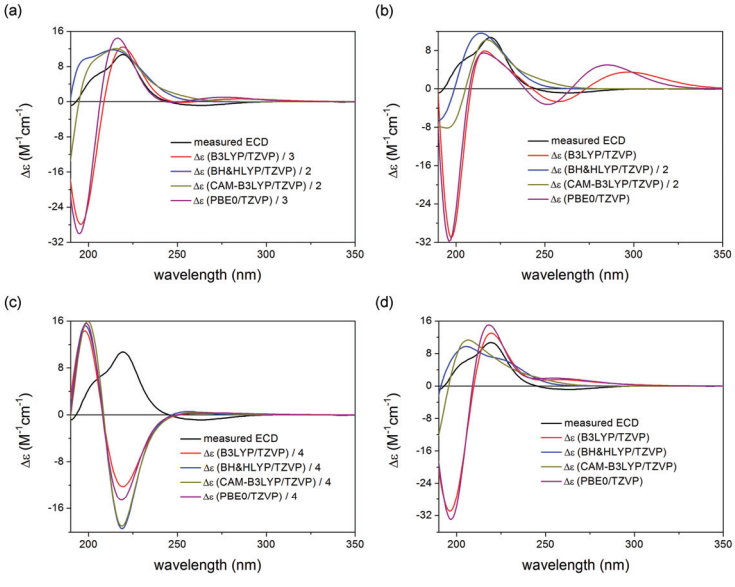

Figure 4. Comparison of the experimental ECD spectrum of **1** with the calculated spectra obtained at various levels of theory for the (**a**) 16 low-energy CAM-B3LYP/TZVP PCM/MeCN conformers of **isomer 1**, (**b**) 10 low-energy CAM-B3LYP/TZVP PCM/MeCN conformers of **isomer 2**, (**c**) 22 low-energy CAM-B3LYP/TZVP PCM/MeCN conformers of **isomer 3**, and (**d**) 25 low-energy CAM-B3LYP/TZVP PCM/MeCN conformers of **isomer 4**.

Antiproliferative activity

The antiproliferative activity of compound **1** was tested on three cervical cancer cell lines of different human papilloma virus (HPV) of different status (HeLa, SiHa, and C33A) and on non-cancerous (NIH/3T3 (mouse embryonic fibroblast) and MRC-5 (human fibroblast)) cell lines. Cisplatin was used as a positive control. Lobatolide H (1) showed remarkable growth-inhibitory effects against SiHa (IC_{50} 2.82 μM) and C33A (IC_{50} 4.43 μM) cells, whereas it exerted weak activity against HeLa (IC_{50} 16.62 μM) cell line (Table 10). These results were comparable to that of the reference agent cisplatin. According to the calculated IC_{50} values on the two non-cancerous fibroblast cell lines, cancer selectivity could be determined. The best selectivity was obtained in the case of the Siha cells (SI = 5.26).

Table 10. Antiproliferative activity (IC50 values) of compound **1**. The selectivity indices (SI) were calculated as the ratio of the IC50 value in the non-tumor cells and the IC50 in the cancer cell lines. The compound's activity towards cancer cells is considered as strongly selective if the selectivity index (SI) value is higher than 6, moderately selective if 3 < SI < 6, slightly selective if 1 < SI < 3, and non-selective if SI is lower than 1.

Compound	IC_{50} Values (μM) [95% CI]				
	HeLa	C33A	SiHa	NIH-3T3	MRC-5
1	16.62 [14.55–18.99]	4.43 [3.62–5.43]	2.82 [2.40–3.32]	13.05 [11.44–14.90]	14.82 [13.90–15.80]
cisplatin	12.14 [10.18–14.46]	5.85 [5.37–6.38]	4.29 [3.72–4.95]	5.49 [4.76–6.35]	5.17 [3.88–6.89]
SI for **1** NIH-3T3/cell line	0.79	2.95	4.63		
SI for **1** MRC-5/cell line	0.89	3.35	5.26		

The most sensitive SiHa cell line was chosen to further investigate the possible mechanisms behind the antiproliferative effects, and cell-cycle analysis was performed. The cell-cycle analysis showed only slight differences in the distribution of cell cycle phases compared with the untreated control cells. After 24 h, 3 μM of compound **1** elicited a significant depression in the S phase population with no relevant change in other cell phases. After a longer exposure (72 h), the sub G1 population had grown significantly but to a modest extent when treated with 3 μM (Figure 5).

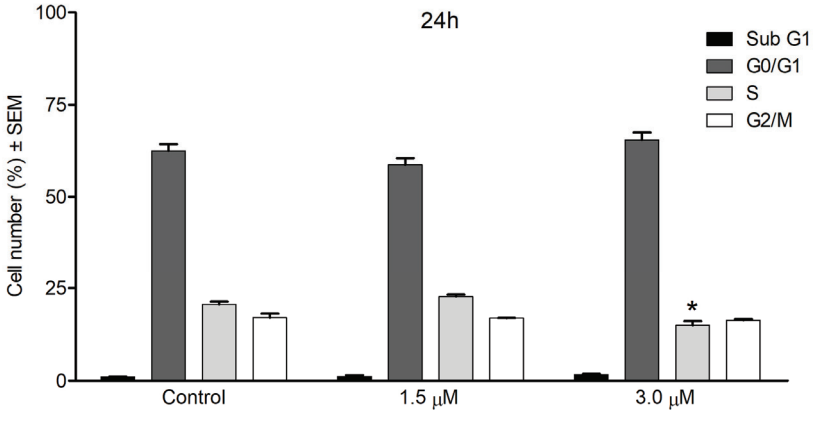

Figure 5. *Cont*.

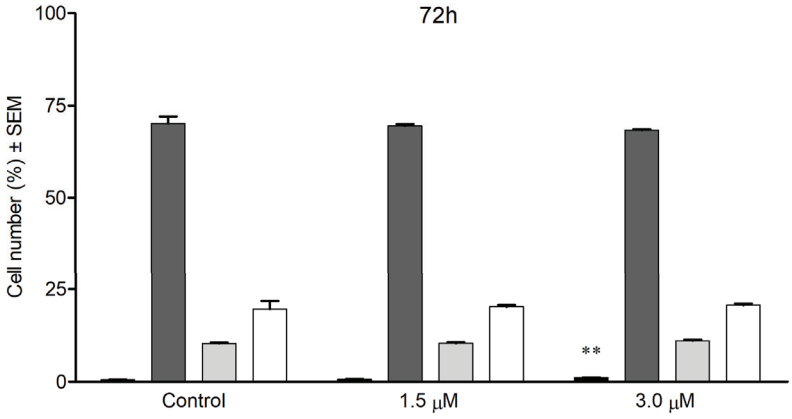

Figure 5. Cell cycle distributions of SiHa cells after treatment with compound **1** for 24 (**upper panel**) or 72 h (**lower panel**). Distribution of cell populations in different cell cycle phases. * and ** indicate $p < 0.05$ and $p < 0.01$, respectively, by means of one-way ANOVA followed by Dunnett's post hoc test.

Based on the results of the antiproliferative assay, compound **1** was additionally investigated for its antimetastatic activity. A wound healing assay was performed on the SiHa cell line in 1.5 μM and 3.0 μM concentrations.

Treatment with compound **1** resulted in no significant reduction in the migration of cervical cancer cells (Figure 6). A longer exposure, however, elicited a substantial and concentration-dependent decrease in the closure of the cell-free area, which indicates the inhibition of migration of the treated cells.

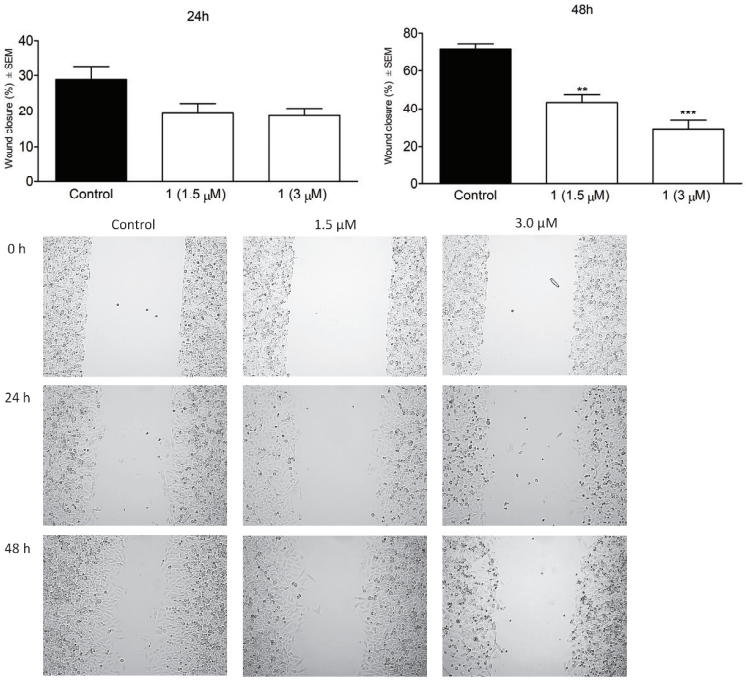

Figure 6. Wound healing assay. Effect of compound **1** on the migration of SiHa cancer cells after 24 and 48 h of incubation (**left and right upper panels**, respectively). ** and *** indicate $p < 0.01$ and $p < 0.001$,

respectively, by means of one-way ANOVA followed by Dunnett's post hoc test. **Lower panel**: representative images of reduced wound healing at 0, 24 and 48 h post-treatment.

3. Materials and Methods

3.1. General Procedures

The high-resolution MS spectra were acquired on a Thermo Scientific Q-Exactive Plus orbitrap mass spectrometer equipped with an ESI ion source in positive ionization mode. The samples were dissolved in MeOH. Data acquisition and analysis were accomplished with Xcalibur software version 2.0 (Thermo Fisher Scientific). A Bruker Avance DRX 500 spectrometer (500 MHz (^{1}H) and 125 MHz (^{13}C)) was used for recording the NMR spectra. The signals of the deuterated solvent $CDCl_3$ were taken as the reference. 2D NMR data were acquired and processed with standard Bruker software TopSpin 3.6.1. Gradient-enhanced versions were used in the ^{1}H–^{1}H COSY, HSQC and HMBC experiments. Optical rotations were determined in $CHCl_3$ by using a Perkin-Elmer 341 polarimeter. UV and ECD spectra were recorded on a JASCO J-810 spectropolarimeter.

For column chromatography (CC), polyamide (MP Polyamide, 50–160 μm, MP Biomedicals, Irvine, CA, USA) and silica gel (Kieselgel 60, 63–200 μm, Merck, Darmstadt, Germany) were used. Preparative thin-layer chromatography (prep. TLC) was carried out using RP-18 (F_{254s}, Merck) pre-coated plates.

3.2. Plant Material

Neurolaena lobata (L.) R.Br. ex Cass. (Asteraceae) was collected by R. Diaz, and R. O. Frisch (Institute for Ethnobiology, Playa Diana, GT-170 San José/Petén, Guatemala), in the flowering period, in the area of the Chakmamantok rock formation (16 59′16″ N, 89 53′45″ W) in San José, Guatemala. A voucher specimen (No. 813) has been deposited at the Herbarium of Department of Pharmacognosy, University of Szeged, Szeged, Hungary.

3.3. Extraction and Isolation

The dried and ground material from the aerial parts of the plant (3.00 kg) was percolated with MeOH (50 L) at room temperature. The extract was concentrated under reduced pressure and solvent–solvent partition was performed with 5 × 1 L petroleum ether (A), 5 × 1 L of CH_2Cl_2 (B), and finally with 5 × 1 L of EtOAc (C). The CH_2Cl_2 phase (95.4 g) was separated on a polyamide column (287 g) with mixtures of MeOH and H_2O (1:4, 2:3, 3:2 and 4:1, 3 L of each) as eluents to afford seven fractions (BI–BVII). Fraction BIII (7.6 g) obtained from the polyamide column with MeOH–H_2O (3:2) was subjected to silica gel VLC, using a gradient system of cyclohexane–EtOAc–EtOH (from 30:5:0 to 30:30:2) to yield 10 fractions (BIII/1–10). Fraction BIII/8 (0.6 g) was rechromatographed on VLC with a gradient system of cyclohexane–EtOAc–EtOH (from 3:1:0 to 30:30:3) and 10 subfractions (BIII/8/1–10) were obtained. Purification of subfraction BIII/8/8 by preparative RP-TLC (MeOH–H_2O 7:3) resulted in the isolation of compound **1** (28.7 mg).

3.4. Physical Characteristics of the New Compound

Lobatolide H (**1**): a yellow gum; $[\alpha]^{27}_D$ +31 (*c* 0.1, $CHCl_3$); UV (MeCN, λ_{max} (nm)) 204sh, <190; ECD (MeCN, λ (nm) (Δε), c 6.65 × 10^{-4} M): 263 (-0.87), 219 (+10.73), 206sh (+6.41); ^{1}H NMR and ^{13}C NMR data, see Table 1; HRESIMS *m*/*z* 349.2012 $[M + H]^+$ (calcd. for $C_{20}H_{29}O_5$, 349.2015).

3.5. Computational Section

Mixed torsional/low-mode conformational searches were carried out by means of the Macromodel 10.8.011 software using the MMFF with an implicit solvent model for $CHCl_3$ and applying a 21 kJ/mol energy window [79]. Geometry re-optimizations of the resultant conformers (CAM-B3LYP/TZVP PCM/MeCN for the ECD calculations, ωB97XD/6-31+G(d,p) in vacuo and ωB97XD/6-31+G(d,p) SMD/$CHCl_3$ for the novel NMR parameters, see Table S1 for tests of the 80 NMR combinations), TDDFT-ECD (B3LYP/TZVP

PCM/MeCN, BH&HLYP/TZVP PCM/MeCN, CAM-B3LYP/TZVP PCM/MeCN and PBE0/TZVP PCM/MeCN), and DFT-NMR calculations (mPW1PW91/6-311+G(2d,p) in vacuo and mPW1PW91/6-311+G(2d,p) SMD/$CHCl_3$ for the novel NMR parameters, see Table S1 for test of the 80 NMR combinations) were performed with the Gaussian 09 package [80–82]. ECD spectra were generated as sums of Gaussians with 3000 cm^{-1} width at half-height, using dipole-velocity-computed rotational strength values [83]. Computed NMR shift data were corrected with the scaling factors listed in Table S1 or determined in the current work. Boltzmann distributions were estimated from the DFT energies. Visualization of the results was performed by the MOLEKEL 5.4 software package [84].

3.6. Antiproliferative MTT Assay

The antiproliferative effects of the isolated compounds were determined in vitro using SiHa (HPV 16+), HeLa (HPV 18+), and C33A (HPV negative) human cervical cell lines, and NIH-3T3 mouse embryonic and MRC-5 human fibroblast cells by means of the MTT ([3-(4,5-dimethylthiazol-2-yl)-2,5-diphenyltetrazolium bromide]) assay. Briefly, a limited number of human cancer cells (5000/well for the SiHa and HeLa cells, 10,000/well in the case of C33A cells) were seeded onto a 96-well microplate and became attached to the bottom of the well overnight. On the second day of the procedure, the test substances were added in two concentrations (10.0, 30.0 μM) in order to obtain preliminary data and then the compounds were applied in serial dilutions (the final concentrations were 0.1, 0.3, 1.0, 3.0, 10.0 and 30.0 μM). After an incubation period of 72 h, the living cells were assayed by the addition of 20 μL of 5 mg/mL MTT solution. After a 4 h incubation, the medium was removed, and the precipitated formazan was dissolved in 100 μL/well of DMSO during a 60 min period of shaking. Finally, the reduced MTT was assayed at 545 nm, using a microplate reader. Untreated cells were taken as the negative control, and cisplatin (Ebewe Pharma GmbH, Unterach, Austria) was used as a reference active compound. All the cell lines were purchased from the European Collection of Cell Cultures (Salisbury, UK). Stock solutions (10 mM) of the tested compounds were prepared with DMSO. The highest DMSO concentration (0.3%) of the medium did not have any substantial effect on the cell proliferation. All in vitro experiments were carried out on two 96-well dishes with at least five parallel wells [24,85].

3.7. Cell Cycle Analysis by Flow Cytometry

Cellular DNA content was determined by means of flow cytometric analysis, using a DNA-specific fluorescent dye, propidium iodide (PI). The SiHa cells were seeded in 6-well plates and cultured overnight. The cultured cells were treated with various concentrations (1.5 or 3.0 μM) of the tested compound for 24 h or 72 h. The medium was then removed, and the cells were washed with phosphate-buffered saline (PBS) and trypsinized. The harvested cells were suspended in medium and centrifuged at 1500 rpm for 15 min at 4 °C. The supernatant was then removed and the cells were resuspended in 1 mL of PBS. After the second centrifugation, 1 mL of −20 °C 70% EtOH was added dropwise to the cell pellet. The cells were stored at −20 °C until DNA staining. On the day of measurement, the samples were washed with PBS and suspended in 1 mL of DNA staining buffer containing PI, ribonuclease-A, Triton-X and sodium citrate. After incubation for 1 h at room temperature, protected from light, the samples were analyzed with a Partec CyFlow instrument (Partec GmbH, Münster, Germany). For each experiment, 20,000 events were counted, and the percentages of the cells in the different cell-cycle phases (subG1, G1, S and G2/M) were determined by means of ModFit LT software 3.3.11 (Verity Software House, Topsham, ME, USA) [86–88].

3.8. Wound Healing Assay

In order to assess the antimetastatic activity of the tested compound, a wound healing assay was performed. The assay was performed with specific wound healing assay chambers (Ibidi GmbH, Martinsried, Germany). SiHa cells were collected and 35,000 cells were

seeded into both chambers of the insert. The cells were left to attach to the plate surface during an overnight incubation at 37 °C in 5% CO_2 atmosphere and then the inserts were removed. Cell debris was removed by a washing step with PBS. Test compounds were added to the wells in increasing concentrations in 2% FBS containing medium for 24 and 48 h. Migration of the cells into the wound site was visualized by a phase-contrast inverted microscope (Axiovert 40, Zeiss, Thornwood, NY, USA). The images were taken with CCD camera at defined intervals and the migration of the cells was calculated as the ratio of wound closure using ImageJ software 1.53a [89].

3.9. Statistical Analysis

Statistical analysis of the obtained data was performed by analysis of variance (ANOVA) followed by Dunnett's test. All analyses were performed with GraphPad Prism 5 (GraphPad Software; San Diego, CA, USA).

4. Conclusions

A new flexible, biologically active germacranolide (**1**, lobatolide H) was isolated from the aerial parts of *Neurolaena lobata*. In order to elucidate the relative configuration of the two problematic chirality centers, a large number of known NMR shift parameters with the corresponding theoretical level combinations were tested, and novel parameters were also developed. Although several methods were found among the existing ones which performed well for the rigid test molecules, also verifying the relative configuration of **3** at C-8 that was recently found to be problematic with standard DFT-NMR methods [24], the flexibility of **1** required the development of novel combinations with newer DFT functionals and solvent models, also in the geometry optimization step. The novel ^{13}C parameters combined with the coupling constant and TDDFT-ECD calculations allowed elucidation of the relative and absolute configuration of **1**. This example is a warning that similar to ECD [74,90], one should be careful with the DFT optimization level applied for NMR shift calculations of flexible compounds (Tables S22–S29). A novel type functional and solvent model or an independent verification of the results is recommended, if possible. Concerning the anticancer properties of **1**, the antiproliferative action determined on cervical cancer cells is comparable to that of the reference agent cisplatin with less pronounced action against non-cancerous cells. The modest treatment-related change in the cell-cycle distribution of the exposed cells provides limited information on the mechanism of the action, but the increase in the hypodiploid (sub G1) population indicates induction of apoptosis. Moreover, the compound inhibits the migration of SiHa cells in a concentration-dependent way, which may be the base of its antimetastatic action.

Supplementary Materials: The following supporting information can be downloaded at: https://www.mdpi.com/article/10.3390/ijms24065841/s1. References [23,24,27,43,44,54–57,59,64–71] are cited in the supplementary materials.

Author Contributions: Conceptualization, A.M., A.V., G.K., R.F. and I.Z.; methodology, A.M., T.K. and A.V.; software, T.K., A.M. and Z.S.; investigation, T.K., A.M., I.L., N.K., Z.S. and N.B.-F.; formal analysis, T.K. and A.M.; resources, A.V., A.M., I.Z. and J.H.; data curation, A.M., A.V., A.B. and J.H.; visualization, T.K., A.M., A.V. and Z.S.; writing—original draft preparation, A.M., A.V., T.K. and Z.S.; writing—review and editing, A.M., A.B., J.H. and I.Z.; supervision, A.M. and A.V.; project administration, A.M. and A.V. All authors have read and agreed to the published version of the manuscript.

Funding: Financial support from the National Research Development and Innovation Office (Grant numbers FK-134653, K-128963 and K-143690) is gratefully acknowledged.

Institutional Review Board Statement: Not applicable.

Informed Consent Statement: Not applicable.

Data Availability Statement: Not applicable.

Acknowledgments: The Governmental Information-Technology Development Agency (KIFÜ) is acknowledged for CPU time.

Conflicts of Interest: The authors declare no conflict of interest.

References

1. Babaei, G.; Aliarab, A.; Abroon, S.; Rasmi, Y.; Aziz, S.G.G. Application of sesquiterpene lactone: A new promising way for cancer therapy based on anticancer activity. *Biomed. Pharmacother.* **2018**, *106*, 239–246. [CrossRef]
2. Paço, A.; Brás, T.; Santos, J.O.; Sampaio, P.; Gomes, A.C.; Duarte, M.F. Anti-Inflammatory and Immunoregulatory Action of Sesquiterpene Lactones. *Molecules* **2022**, *27*, 1142. [CrossRef] [PubMed]
3. Shulha, O.; Zidorn, C. Sesquiterpene lactones and their precursors as chemosystematic markers in the tribe Cichorieae of the Asteraceae revisited: An update (2008–2017). *Phytochemistry* **2019**, *163*, 149–177. [CrossRef]
4. Zorrilla, J.G.; Cala, A.; Rial, C.; Mejias, F.J.R.; Molinillo, J.M.G.; Varela, R.M.; Macias, F.A. Synthesis of Active Strigolactone Analogues Based on Eudesmane- and Guaiane-Type Sesquiterpene Lactones. *J. Agric. Food Chem.* **2020**, *68*, 9636–9645. [CrossRef] [PubMed]
5. Laurella, L.C.; Mirakian, N.T.; Garcia, M.N.; Grasso, D.H.; Sülsen, V.P.; Papademetrio, D.L. Sesquiterpene Lactones as Promising Candidates for Cancer Therapy: Focus on Pancreatic Cancer. *Molecules* **2022**, *27*, 3492. [CrossRef] [PubMed]
6. Moujir, L.; Callies, O.; Sousa, P.M.C.; Sharopov, F.; Seca, A.M.L. Applications of Sesquiterpene Lactones: A Review of Some Potential Success Cases. *Appl. Sci.* **2020**, *10*, 3001. [CrossRef]
7. Liu, J.; Yang, Z.; Kong, Y.; He, Y.; Xu, Y.; Cao, X. Antitumor activity of alantolactone in lung cancer cell lines NCI-H1299 and Anip973. *J. Food Biochem.* **2019**, *43*, 12972. [CrossRef]
8. Zhu, N.L.; Tang, C.; Xu, C.; Ke, C.Q.; Lin, G.; Jenis, J.; Yao, S.; Liu, H.; Ye, Y. Cytotoxic germacrane-type sesquiterpene lactones from the whole plant of *Carpesium lipskyi*. *J. Nat. Prod.* **2019**, *82*, 919–927. [CrossRef]
9. Wang, J.; Su, S.; Zhang, S.; Zhai, S.; Sheng, R.; Wu, W.; Guo, R. Structure-activity relationship and synthetic methodologies of α-santonin derivatives with diverse bioactivities: A mini-review. *Eur. J. Med. Chem.* **2019**, *175*, 215–233.
10. Matos, M.S.; Anastácio, J.D.; dos Santos, C.N. Sesquiterpene Lactones: Promising Natural Compounds to Fight Inflammation. *Pharmaceutics* **2021**, *13*, 991. [CrossRef] [PubMed]
11. Yuan, J.; Wen, X.; Ke, C.Q.; Zhang, T.; Lin, L.; Yao, S.; Goodpaster, J.D.; Tang, C.; Ye, Y. Tricarabrols A-C, three anti-inflammatory sesquiterpene lactone trimers featuring a methylene-tethered linkage from *Carpesium faberi*. *Org. Chem. Front.* **2020**, *7*, 1374–1382. [CrossRef]
12. Li, Q.; Wang, Z.; Xie, Y.; Hu, H. Antitumor activity and mechanism of costunolide and dehydrocostus lactone: Two natural sesquiterpene lactones from the Asteraceae family. *Biomed. Pharmacother.* **2020**, *125*, 109955. [CrossRef] [PubMed]
13. Bailly, C. Anticancer targets and signaling pathways activated by britannin and related pseudoguaianolide sesquiterpene lactones. *Biomedicines* **2021**, *9*, 1325. [CrossRef]
14. Liu, X.N.; Li, H.M.; Wang, S.P.; Zhang, J.Z.; Liu, D.L. Sesquiterpene lactones of *Aucklandia lappa*: Pharmacology, pharmacokinetics, toxicity, and structure-activity relationship. *Chin. Herb. Med.* **2021**, *13*, 167–176. [CrossRef]
15. Ma, C.; Meng, C.W.; Zhou, Q.M.; Peng, C.; Liu, F.; Zhang, J.W.; Zhou, F.; Xiong, L. New sesquiterpenoids from the stems of *Dendrobium nobile* and their neuroprotective activities. *Fitoterapia* **2019**, *138*, 104351. [CrossRef]
16. Tang, J.J.; Huang, L.F.; Deng, J.L.; Wang, Y.M.; Guo, C.; Peng, X.N.; Liu, Z.; Gao, J.M. Cognitive enhancement and neuroprotective effects of 1,6-*O*,*O*-diacetylbritannilactone, a sesquiterpene lactone in 5xFAD Alzheimer's disease mice model. *Redox Biol.* **2022**, *50*, 102229. [CrossRef]
17. Abdelwahab, S.I.; Taha, M.M.E.; Alhazmi, H.A.; Ahsan, W.; Rehman, Z.U.; Bratty, M.A.; Makeen, H. Phytochemical profiling of costus (*Saussurea lappa* Clarke) root essential oil, and its antimicrobial and toxicological effects. *Trop. J. Pharm. Res.* **2019**, *18*, 2155–2160. [CrossRef]
18. Sülsen, V.P.; Martino, V.S. Overview. In *Sesquiterpene Lactones: Advances in Their Chemistry and Biological Aspects*; Sülsen, V.P., Martino, V.S., Eds.; Springer International Publishing: Cham, Switzerland, 2018; pp. 3–17.
19. Sosa, A.; Diaz, M.; Salvatore, A.; Bardon, A.; Borkosky, S.; Vera, N. Insecticidal effects of *Vernonanthura nebularum* against two economically important pest insects. *Saudi J. Biol. Sci.* **2019**, *26*, 881–889. [CrossRef] [PubMed]
20. Lajter, I.; Vasas, A.; Beni, Z.; Forgo, P.; Binder, M.; Bochkov, V.; Zupko, I.; Krupitza, G.; Frisch, R.; Kopp, B.; et al. Sesquiterpenes from Neurolaena lobata and their antiproliferative and anti-inflammatory activities. *J. Nat. Prod.* **2014**, *77*, 576–582. [CrossRef]
21. Passreiter, C.M.; Wendisch, D.; Gondol, D. Sesquiterpene lactones from *Neurolaena lobata*. *Phytochemistry* **1995**, *39*, 133–137. [CrossRef]
22. Borges-del-Castillo, J.; Manresa-Ferrero, M.T.; Rodríguez-Luis, F.; Vázquez-Bueno, P. Panama Flora. II. New Sesquiterpene Lactones from *Neurolaena lobata*. *J. Nat. Prod.* **1982**, *45*, 762–765. [CrossRef]
23. Manchand, P.S.; Blount, J.F. Stereostructures of Neurolenins A and B, Novel Germacranolide Sesquiterpenes from *Neurolaena lobata* (L.) R.Br. *J. Org. Chem.* **1978**, *43*, 4352–4354. [CrossRef]
24. Vasas, A.; Lajter, I.; Kúsz, N.; Király, S.B.; Kovács, T.; Kurtán, T.; Bózsity, N.; Nagy, N.; Schelz, Z.; Zupkó, I.; et al. Isolation, Structure Determination of Sesquiterpenes from *Neurolaena lobata* and Their Antiproliferative, Cell Cycle Arrest-Inducing and Anti-Invasive Properties against Human Cervical Tumor Cells. *Pharmaceutics* **2021**, *13*, 2088. [CrossRef]

25. Smith, S.G.; Goodman, J.M. Assigning Stereochemistry to Single Diastereoisomers by GIAO NMR Calculation: The DP4 Probability. *J. Am. Chem. Soc.* **2010**, *132*, 12946–12959. [CrossRef] [PubMed]
26. Grimblat, N.; Zanardi, M.M.; Sarotti, A.M. Beyond DP4: An Improved Probability for the Stereochemical Assignment of Isomeric Compounds using Quantum Chemical Calculations of NMR Shifts. *J. Org. Chem.* **2015**, *80*, 12526–12534. [CrossRef]
27. Lodewyk, M.W.; Siebert, M.R.; Tantillo, D.J. Computational Prediction of ^{1}H and ^{13}C Chemical Shifts: A Useful Tool for Natural Product, Mechanistic, and Synthetic Organic Chemistry. *Chem. Rev.* **2012**, *112*, 1839–1862. [CrossRef]
28. Li, W.S.; Yan, R.J.; Yu, Y.; Shi, Z.; Mándi, A.; Shen, L.; Kurtán, T.; Wu, J. Determination of the Absolute Configuration of Super-Carbon-Chain Compounds by a Combined Chemical, Spectroscopic, and Computational Approach: Gibbosols A and B. *Angew. Chem. Int. Ed.* **2020**, *59*, 13028–13036. [CrossRef] [PubMed]
29. Jiang, Z.P.; Sun, S.H.; Yu, Y.; Mándi, A.; Luo, J.Y.; Yang, M.H.; Kurtán, T.; Chen, W.H.; Shen, L.; Wu, J. Discovery of benthol A and its challenging stereochemical assignment: Opening up a new window for skeletal diversity of super-carbonchain compounds. *Chem. Sci.* **2021**, *12*, 10197–10206. [CrossRef] [PubMed]
30. Kawka, A.; Hajdaś, G.; Kułaga, D.; Koenig, H.; Kowalczyk, I.; Pospieszny, T. Molecular structure, spectral and theoretical study of new type bile acid–sterol conjugates linked via 1,2,3-triazole ring. *J. Mol. Struct.* **2023**, *1273*, 134313. [CrossRef]
31. Lodewyk, M.W.; Soldi, C.; Jones, P.B.; Olmstead, M.M.; Rita, J.; Shaw, J.T.; Tantillo, D.J. The Correct Structure of Aquatolide-Experimental Validation of a Theoretically-Predicted Structural Revision. *J. Am. Chem. Soc.* **2012**, *134*, 18550–18553. [CrossRef]
32. Liu, Y.; Holt, T.A.; Kutateladze, A.; Newhouse, T.R. Stereochemical revision of xylogranatin F by GIAO and DU8+ NMR calculations. *Chirality* **2020**, *32*, 515–523. [CrossRef]
33. Sarotti, A.M. In Silico Reassignment of (+)-Diplopyrone by NMR Calculations: Use of a DP4/J-DP4/DP4+/DIP Tandem to Revise Both Relative and Absolute Configuration. *J. Org. Chem.* **2020**, *85*, 11566–11570. [CrossRef]
34. Zhou, T.; Zheng, A.; Zhang, W.; Lu, X.; Chen, H.; Tan, H. Concise total syntheses of two flavans and structure revision assisted by quantum NMR calculations. *Org. Biomol. Chem.* **2022**, *20*, 4096–4100. [CrossRef] [PubMed]
35. Marcarino, M.O.; Cicetti, S.; Zanardi, M.M.; Sarotti, A.M. A critical review on the use of DP4+ in the structural elucidation of natural products: The good, the bad and the ugly. A practical guide. *Nat. Prod. Rep.* **2022**, *39*, 58–76. [CrossRef] [PubMed]
36. Xiong, J.; Zhou, P.J.; Jiang, H.W.; Huang, T.; He, Y.H.; Zhao, Z.Y.; Zang, Y.; Choo, Y.M.; Wang, X.; Chittiboyina, A.G.; et al. Forrestiacids A and B, Pentaterpene Inhibitors of ACL and Lipogenesis: Extending the Limits of Computational NMR Methods in the Structure Assignment of Complex Natural Products. *Angew. Chem. Int. Ed.* **2021**, *60*, 22270–22275. [CrossRef]
37. Dybiec, K.; Gryff-Keller, A. Remarks on GIAO-DFT predictions of ^{13}C chemical shifts. *Magn. Reson. Chem.* **2009**, *47*, 63–66. [CrossRef]
38. Autschbach, J.; Zheng, S. Relativistic Computations of NMR Parameters from First Principles: Theory and Applications. *Annu. Rep. NMR Spectrosc.* **2009**, *67*, 1–95. [CrossRef]
39. Forster, L.C.; Pierens, G.K.; Garson, M.J. Elucidation of Relative and Absolute Configurations of Highly Rearranged Diterpenoids and Evidence for a Putative Biosynthetic Intermediate from the Australian Nudibranch *Goniobranchus geometricus*. *J. Nat. Prod.* **2019**, *82*, 449–455. [CrossRef] [PubMed]
40. Kutateladze, A.G.; Reddy, D.S. High-Throughput in Silico Structure Validation and Revision of Halogenated Natural Products Is Enabled by Parametric Corrections to DFT-Computed ^{13}C NMR Chemical Shifts and Spin−Spin Coupling Constants. *J. Org. Chem.* **2017**, *82*, 3368–3381. [CrossRef]
41. Dračínský, M.; Buděšínský, M.; Warżajtis, B.; Rychlewska, U. Solution and Solid-State Effects on NMR Chemical Shifts in Sesquiterpene Lactones: NMR, X-ray, and Theoretical Methods. *J. Phys. Chem. A* **2012**, *116*, 680–688. [CrossRef]
42. Li, W.S.; Mándi, A.; Liu, J.J.; Shen, L.; Kurtán, T.; Wu, J. Xylomolones A−D from the Thai Mangrove *Xylocarpus moluccensis*: Assignment of Absolute Stereostructures and Unveiling a Convergent Strategy for Limonoid Biosynthesis. *J. Org. Chem.* **2019**, *84*, 2596–2606. [CrossRef]
43. Pierens, G.K. ^{1}H and ^{13}C NMR Scaling Factors for the Calculation of Chemical Shifts in Commonly Used Solvents Using Density Functional Theory. *J. Comput. Chem.* **2014**, *35*, 1388–1394. [CrossRef]
44. CHESHIRE CCAT, The Chemical Shift Repository for Computed NMR Scaling Factors. Available online: https://cheshirenmr.info/index.htm (accessed on 5 October 2018).
45. Bohle, F.; Grimme, S. Hydrocarbon Macrocycle Conformer Ensembles and ^{13}C-NMR Spectra. *Angew. Chem. Int. Ed.* **2022**, *61*, e202113905. [CrossRef] [PubMed]
46. Begnini, F.; Poongavanam, V.; Atilaw, Y.; Erdelyi, M.; Schiesser, S.; Kihlberg, J. Cell Permeability of Isomeric Macrocycles: Predictions and NMR Studies. *ACS Med. Chem. Lett.* **2021**, *12*, 983–990. [CrossRef] [PubMed]
47. Chai, J.D.; Head-Gordon, M. Long-range corrected hybrid density functionals with damped atom–atom dispersion corrections. *Phys. Chem. Chem. Phys.* **2008**, *10*, 6615–6620. [CrossRef]
48. Brémond, É.; Savarese, M.; Su, N.Q.; Pérez-Jiménez, Á.J.; Xu, X.; Sancho-García, J.C.; Adamo, C. Benchmarking Density Functionals on Structural Parameters of Small-/Medium-Sized Organic Molecules. *J. Chem. Theory Comput.* **2016**, *12*, 459–465. [CrossRef] [PubMed]
49. Melek, F.R.; Gershenzon, J.; Lee, E.; Mabry, T.J. Sesquiterpene lactones of *Helianthus gracilentus*. *Phytochemistry* **1984**, *23*, 2277–2279. [CrossRef]
50. Liang, L.F.; Lan, L.F.; Taglialatela-Scafati, O.; Guo, Y.W. Sartrolides A-G and bissartrolide, new cembranolides from the South China Sea soft coral *Sarcophyton trocheliophorum* Marenzeller. *Tetrahedron* **2013**, *69*, 7381–7386. [CrossRef]

51. Liang, L.F.; Kurtán, T.; Mándi, A.; Yao, L.G.; Li, J.; Lan, L.F.; Guo, Y.W. Structural, stereochemical, and bioactive studies of cembranoids from Chinese soft coral *Sarcophyton trocheliophorum*. *Tetrahedron* **2018**, *74*, 1933–1941. [CrossRef]
52. Kicsák, M.; Mándi, A.; Varga, S.; Herczeg, M.; Batta, G.; Bényei, A.; Borbás, A.; Herczegh, P. Tricyclanos: Conformationally constrained nucleoside analogues with a new heterotricycle obtained from a D-ribofuranose unit. *Org. Biomol. Chem.* **2018**, *16*, 393–401. [CrossRef]
53. Mándi, A.; Wu, J.; Kurtán, T. TDDFT-ECD and DFT-NMR studies of thaigranatins A–E and granatumin L isolated from *Xylocarpus granatum*. *RSC Adv.* **2020**, *10*, 32216–32224. [CrossRef]
54. Qiu, S.; de Gussem, E.; Tehrani, K.A.; Sergeyev, S.; Bultinck, P.; Herrebout, W. Stereochemistry of the Tadalafil Diastereoisomers: A Critical Assessment of Vibrational Circular Dichroism, Electronic Circular Dichroism, and Optical Rotatory Dispersion. *J. Med. Chem.* **2013**, *56*, 8903–8914. [CrossRef]
55. Rablen, P.R.; Pearlman, S.A.; Finkbiner, J. A comparison of density functional methods for the estimation of proton chemical shifts with chemical accuracy. *J. Phys. Chem. A* **1999**, *103*, 7357–7363. [CrossRef]
56. Jain, R.J.; Bally, T.; Rablen, P.R. Calculating accurate proton chemical shifts of organic molecules with density functional methods and modest basis sets. *J. Org. Chem.* **2009**, *74*, 4017–4023. [CrossRef]
57. Konstantinov, I.A.; Broadbelt, L.J. Regression Formulas for Density Functional Theory Calculated ^{1}H and ^{13}C NMR Chemical Shifts in Toluene-d8. *J. Phys. Chem. A* **2011**, *115*, 12364–12372. [CrossRef] [PubMed]
58. Ditchfield, R. Self-consistent perturbation theory of diamagnetism. *Mol. Phys.* **1974**, *27*, 789–807. [CrossRef]
59. Lee, K.H.; Min, Y.D.; Choi, S.Z.; Kwon, H.C.; Cho, O.R.; Lee, K.C.; Lee, K.R. A new sesquiterpene lactone from *Artemisia rubripes* nakai. *Arch. Pharmacal. Res.* **2004**, *27*, 1016–1019. [CrossRef]
60. Jewell, J.S.; Szarek, W.A. The light-induced addition of 1,3-dioxolan to unsaturated carbohydrates. *Tetrahedron Lett.* **1969**, *10*, 43–46. [CrossRef]
61. Hough, L.; Otte, B. Furanoid Vinyl Ethers. *Chem. Commun.* **1966**, 173–174. [CrossRef]
62. Miyoshi, T.; Miyairi, N.; Aoki, H.; Kohsaka, M.; Sakai, H.I.; Imanaka, H. Bicyclomycin, a new antibiotic I. Taxonomy, isolation and characterization. *J. Antibiot.* **1972**, *25*, 569–575. [CrossRef]
63. Domínguez, E.; Romo, J. Mexicanin—I. A new sesquiterpene lactone related to tenulin. *Tetrahedron* **1963**, *19*, 1415–1421. [CrossRef]
64. Li, J.; Tang, H.; Kurtán, T.; Mándi, A.; Zhuang, C.L.; Su, L.; Zheng, G.L.; Zhang, W. Swinhoeisterols from the South China Sea Sponge *Theonella swinhoei*. *J. Nat. Prod.* **2018**, *81*, 1645–1650. [CrossRef]
65. Kobayashi, S.; Lu, C.; Hoye, T.R.; Hillmyer, M.A. Controlled Polymerization of a Cyclic Diene Prepared from the Ring-Closing Metathesis of a Naturally Occurring Monoterpene. *J. Am. Chem. Soc.* **2009**, *131*, 7960–7961. [CrossRef]
66. Nishida, T.; Satoh, K.; Kamigaito, M. Biobased polymers via radical homopolymerization and copolymerization of a series of terpenoid derived conjugated dienes with exo-methylene and 6-membered ring. *Molecules* **2020**, *25*, 5890. [CrossRef]
67. Raghavendra, S.; Tadiparthi, K.; Yadav, J.S. Total syntheses of Prelactone V and Prelactone B. *Carbohydr. Res.* **2017**, *442*, 17–19. [CrossRef] [PubMed]
68. Doboszewski, B.; Herdewijn, P. Carbohydrate chiral-pool approach to four enantiomerically pure 2-naphthylmethyl 3-hydroxy-2-methylbutanoates. *Tetrahedron* **2008**, *64*, 5551–5562. [CrossRef]
69. Ivanova, N.A.; Valiullina, Z.R.; Shitikova, O.V.; Miftakhov, M.S. Reaction of methyl-4-methylene-2,3-*O*-isopropylidene-β-D-ribofuranoside with *N*-bromosuccinimide in aqueous tetrahydrofurane. *Russ. J. Org. Chem.* **2007**, *43*, 742–746. [CrossRef]
70. Kohn, H.; Abuzar, S.; Korp, J.D.; Zektzer, A.S.; Martin, G.E. Structural studies of bicyclomycin. *J. Heterocyclic. Chem.* **1988**, *25*, 1511–1517. [CrossRef]
71. Błoszyk, E.; Dudek, A.; Kosturkiewicz, Z.; Rychłewska, U.; Daniewski, W.M.; Gumulka, M.; Nawrot, J.; Buděšínský, M.; Vašíčková, S.; Holub, M. Sesquiterpene lactones of *Cephalophora aromatica* (HOOK.) SCHRADER and their deterrent activity. The stereostructure of geigerinin. *Collect. Czech. Chem. Commun.* **1989**, *54*, 1903–1918. [CrossRef]
72. Grimblat, N.; Gavín, J.A.; Daranas, A.H.; Sarotti, A.M. Combining the Power of J Coupling and DP4 Analysis on Stereochemical Assignments: The J-DP4 Methods. *Org. Lett.* **2019**, *21*, 4003–4007. [CrossRef] [PubMed]
73. Mándi, A.; Kurtán, T. Applications of OR/ECD/VCD to the structure elucidation of natural products. *Nat. Prod. Rep.* **2019**, *36*, 889–918. [CrossRef]
74. Superchi, S.; Scafato, P.; Górecki, M.; Pescitelli, G. Configuration Determination by Quantum Mechanical Calculation of Chiroptical Spectra: Basics and Applications to Fungal Metabolites. *Curr. Med. Chem.* **2018**, *25*, 287–320. [CrossRef] [PubMed]
75. De, B.C.; Zhang, W.; Yang, C.; Mándi, A.; Huang, C.; Zhang, L.; Liu, W.; Ruszczycky, M.W.; Zhu, Y.; Ma, M.; et al. Flavin-enabled reductive and oxidative epoxide ring opening reactions. *Nat. Commun.* **2022**, *13*, 4896. [CrossRef]
76. Yanai, T.; Tew, D.; Handy, N. A new hybrid exchange–correlation functional using the Coulomb-attenuating method (CAM-B3LYP). *Chem. Phys. Lett.* **2004**, *393*, 51–57. [CrossRef]
77. Pecul, M.; Marchesan, D.; Ruud, K.; Coriani, S. Polarizable continuum model study of solvent effects on electronic circular dichroism parameters. *J. Chem. Phys.* **2005**, *122*, 024106. [CrossRef]
78. Szabó, K.E.; Kun, S.; Mándi, A.; Kurtán, T.; Somsák, L. Glucopyranosylidene-Spiro-Thiazolinones: Synthetic Studies and Determination of Absolute Configuration by TDDFT-ECD Calculations. *Molecules* **2017**, *22*, 1760. [CrossRef]
79. MacroModel. Schrödinger LLC. 2015. Available online: http://www.schrodinger.com/MacroModel (accessed on 10 January 2023).

80. Frisch, M.J.; Trucks, G.W.; Schlegel, H.B.; Scuseria, G.E.; Robb, M.A.; Cheeseman, J.R.; Scalmani, G.; Barone, V.; Mennucci, B.; Petersson, G.A.; et al. *Gaussian 09, Revision B.01*; Gaussian Inc.: Wallingford, CT, USA, 2010.
81. Frisch, M.J.; Trucks, G.W.; Schlegel, H.B.; Scuseria, G.E.; Robb, M.A.; Cheeseman, J.R.; Scalmani, G.; Barone, V.; Mennucci, B.; Petersson, G.A.; et al. *Gaussian 09, Revision C.01*; Gaussian Inc.: Wallingford, CT, USA, 2010.
82. Frisch, M.J.; Trucks, G.W.; Schlegel, H.B.; Scuseria, G.E.; Robb, M.A.; Cheeseman, J.R.; Scalmani, G.; Barone, V.; Mennucci, B.; Petersson, G.A.; et al. *Gaussian 09, Revision E.01*; Gaussian Inc.: Wallingford, CT, USA, 2013.
83. Stephens, P.J.; Harada, N. ECD cotton effect approximated by the Gaussian curve and other methods. *Chirality* **2010**, *22*, 229–233. [CrossRef] [PubMed]
84. Varetto, U. *MOLEKEL, 5.4*; Swiss National Supercomputing Centre: Manno, Switzerland, 2009.
85. Mosmann, T. Rapid colorimetric assay for cellular growth and survival: Application to proliferation and cytotoxicity assays. *J. Immunol. Methods* **1983**, *65*, 55–63. [CrossRef]
86. Vermes, I.; Haanen, C.; Reutelingsperger, C. Flow cytometry of apoptotic cell death. *J. Immunol. Methods* **2000**, *243*, 167–190. [CrossRef] [PubMed]
87. Latif, D.A.; Gonda, T.; Vágvölgyi, M.; Kúsz, N.; Kulmány, Á.; Ocsovszki, I.; Zomborszki, P.Z.; Zupkó, I.; Hunyadi, A. Synthesis and In Vitro Antitumor Activity of Naringenin Oxime and Oxime Ether Derivatives. *Int. J. Mol. Sci.* **2019**, *20*, 2184. [CrossRef]
88. Kuo, C.Y.; Schelz, Z.; Tóth, B.; Vasas, A.; Ocsovszki, I.; Chang, F.R.; Hohmann, J.; Zupkó, I.; Wang, H.C. Investigation of natural phenanthrenes and the antiproliferative potential of juncusol in cervical cancer cell lines. *Phytomedicine* **2019**, *58*, 152770. [CrossRef] [PubMed]
89. Behrens, J.; Kameritsch, P.; Wallner, S.; Pohl, U.; Pogoda, K. The carboxyl tail of Cx43 augments p38 mediated cell migration in a gap junction-independent manner. *Eur. J. Cell Biol.* **2010**, *89*, 828–838. [CrossRef] [PubMed]
90. Sun, P.; Xu, D.X.; Mándi, A.; Kurtán, T.; Li, T.J.; Schulz, B.; Zhang, W. Structure, Absolute Configuration, and Conformational Study of 12-Membered Macrolides from the Fungus *Dendrodochium* sp. Associated with the Sea Cucumber *Holothuria nobilis* Selenka. *J. Org. Chem.* **2013**, *78*, 7030–7047. [CrossRef] [PubMed]

International Journal of
Molecular Sciences

MDPI

Article

Biofilm-Based Biocatalysis for Galactooligosaccharides Production by the Surface Display of β-Galactosidase in *Pichia pastoris*

Tianpeng Chen [1,2,†], Shimeng Wang [1,2,†], Huanqing Niu [1,2], Guanjia Yang [1,2], Sinan Wang [1,2], Yuqi Wang [1,2], Chaowei Zhou [1,2], Bin Yu [1,2], Pengpeng Yang [1,2], Wenjun Sun [1,2,*], Dong Liu [1,2], Hanjie Ying [1,2] and Yong Chen [1,2,*]

[1] National Engineering Research Center for Biotechnology, College of Biotechnology and Pharmaceutical Engineering, Nanjing Tech University, Nanjing 211816, China; chentianpeng@njtech.edu.cn (T.C.)
[2] State Key Laboratory of Materials-Oriented Chemical Engineering, College of Biotechnology and Pharmaceutical Engineering, Nanjing Tech University, Nanjing 211816, China
* Correspondence: sunwenjun@njtech.edu.cn (W.S.); chenyong1982@njtech.edu.cn (Y.C.); Tel.: +86-25-86990001 (Y.C.); Fax: +86-25-58139389 (Y.C.)
† These authors contributed equally to this work.

Abstract: Galactooligosaccharides (GOS) are one of the most important functional oligosaccharide prebiotics. The surface display of enzymes was considered one of the most excellent strategies to obtain these products. However, a rough industrial environment would affect the biocatalytic process. The catalytic process could be efficiently improved using biofilm-based fermentation with high resistance and activity. Therefore, the combination of the surface display of β-galactosidase and biofilm formation in *Pichia pastoris* was constructed. The results showed that the catalytic conversion rate of GOS was up to 50.3% with the maximum enzyme activity of 5125 U/g by screening the anchorin, and the number of the continuous catalysis batches was up to 23 times. Thus, surface display based on biofilm-immobilized fermentation integrated catalysis and growth was a co-culture system, such that a dynamic equilibrium in the consolidated integrative process was achieved. This study provides the basis for developing biofilm-based surface display methods in *P. pastoris* during biochemical production processes.

Keywords: yeast surface display; *Pichia pastoris*; biofilm; galactooligosaccharides; β-galactosidase

Citation: Chen, T.; Wang, S.; Niu, H.; Yang, G.; Wang, S.; Wang, Y.; Zhou, C.; Yu, B.; Yang, P.; Sun, W.; et al. Biofilm-Based Biocatalysis for Galactooligosaccharides Production by the Surface Display of β-Galactosidase in *Pichia pastoris*. *Int. J. Mol. Sci.* **2023**, *24*, 6507. https://doi.org/10.3390/ijms24076507

Academic Editor: Sergey Dobretsov

Received: 10 March 2023
Revised: 23 March 2023
Accepted: 27 March 2023
Published: 30 March 2023

1. Introduction

Galactooligosaccharides (GOS) are functional oligosaccharides with a molecular structure consisting of one to seven galactose groups attached to a galactose or glucose molecule, i.e., Gal-(Gal) n-Glc/Gal (n = 0–6) [1]. GOS are an excellent source of nutrients and could be an effective proliferation factor for beneficial bacteria such as *Bifidobacterium* and *Lactobacillus acidophilus* in the human intestinal tract, which could improve the functions of digestion and absorption of the intestinal tract of infants and children. Moreover, there are trace amounts of GOS found in animal milk and human breast milk [2]. Hence, GOS were approved to be added to infant formula as important nutrients. Lactose was generally used as the substrate for the industrial production of GOS, which was catalyzed by the trans-glycosylation of β-galactosidase [3]. In nature, microorganisms such as *Aspergillus oryzae* [4], *Bacillus circulans* [5], *Bifidobacterium infantis* [6], and *Kluyveromyces lactis* [7] are reported to have β-galactosidase glycosyltransferase activity [8,9]. In particular, the immobilized β-galactosidase from *A. oryzae* is relatively inexpensive and readily available, with the high specificity and trans-glycosylation activity, as well as being reusable and continuous, compared to the free enzyme [4,10]. However, the deficiencies such as the loss of enzyme activity and the isolation and purification of products have limited the progress of the traditional immobilized enzyme catalysis of β-galactosidase.

Surface display has gained worldwide attention as an available strategy for circumvention of the above deficiency during its green and efficient process [11]. The surface display of enzymes could save the steps of enzyme extraction and purification and the overall cost. For instance, the surface display of α-galactosidase derived from *Aspergillus niger* was carried out in *Pichia pastoris* for isomaltooligosaccharide (IMO) production from 30% maltose feedstock with the conversion rate of approximately 49% and three repeated catalysis cycles [12]. Hence, we used the surface display technique of *P. pastoris* in this study because it has well-established protein folding and secretory expression mechanisms. It can perform many of the post-translational modifications found in eukaryotes and is a good host choice due to its ease of handling, rapid reproduction, and high expression of heterologous proteins.

However, environmental stress on the cells and cell autolysis in the fermentation broth could result in reducing enzyme activity and catalytic efficiency in surface-displayed strains. To address this issue, biofilm-based immobilized fermentation has been proposed as an alternative to free-cell fermentation owing to advantages such as the protection provided by the multicellular aggregate matrix, enhanced cell viability, and repeated use of the cells [13]. Moreover, these cell cultures are adapted to adverse external environments such as high osmolarity, heat shock, oxidative stress, and nutrient deficiencies [14]. Based on this, some microorganisms such as *Clostridium acetobutylicum*, *Escherichia coli,* and *Saccharomyces cerevisiae* were used for immobilized batch or continuous (repeated-batch) fermentation effectively [15–20]. More specifically, we aimed to understand the effects of cell wall proteins, adhesion factors, and signaling molecules on biofilms [21,22]. For example, we previously identified the biofilm-related gene *PAS_chr1-3_0226* (Gene ID: 8196458) in *P. pastoris*, which encodes a GPI protein with high homology to GAS1p in *S. cerevisiae* [23], that was anchored to the cell surface and could counteract intracellular pressure and maintain normal cell morphology [24]. After the knockout of *PAS_chr1-3_0226*, the results showed increased levels of chitin and the greater resistance to lysozyme, suggesting the gene was associated with cell adhesion [25]. Gene knockout was shown to enhance the efficiency of surface display in *P. pastoris*; therefore, we selected this gene for studies related to biofilm and surface display.

In this study, we aimed to solve the potential deficiency of biofilm-immobilized fermentation and surface display methods by addressing the problem of reduced enzyme activity and catalytic efficiency together. To achieve this, genetic engineering was performed on *P. pastoris* to knock out the *PAS_chr1-3_0226* gene and enhance biofilm formation (Figure 1). Then, biofilm-based immobilized fermentation was constructed by using cotton fiber material as the carrier. In addition, the screenings of different anchorins resulted in the increased efficiency of the β-galactosidase surface-displayed strain. The combination of the surface-displayed system and biofilm-immobilized fermentation enabled continuous (repeated-batch) catalysis, which significantly shortened the catalytic cycle and improved production efficiency. Here, we successfully demonstrated for the first time the efficient biochemical production of GOS using biofilm-immobilized surface-display enzyme catalysis in industrial conditions.

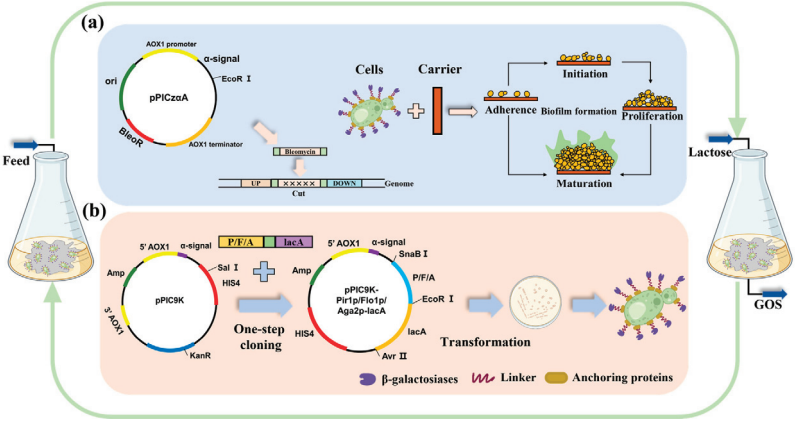

Figure 1. Biofilm-based biocatalysis for surface-displayed strains in dynamic growth and catalytic GOS production. (**a**) A schematic illustration of construction for the knockout of *PAS_chr1-3_0226* and biofilm formation in *P. pastoris*. (**b**) The DNA components of the surface-displayed plasmids used in this study and a schematic diagram of the yeast surface display.

2. Results and Discussion

2.1. The Impact of PAS_chr1-3_0226 Gene Deletion on Biofilm Formation in P. pastoris

In this study, the gene *PAS_chr1-3_0226* was deleted from the *P. pastoris* GS115 genome by homologous recombination. The knockdown effect on the biofilm was observed by significantly darker crystalline violet staining in the Δ0226 strain when compared to that of the WT strain (Figure 2a). Readings were taken at OD_{570}, where the biofilm of Δ0226 increased by 56% (Figure 2b), while the YPD medium was slightly better than the fermentation medium for biofilm production. We also observed that when the Δ0226 strain was grown on YPD plates, there was little effect on its growth (Figure 2c).

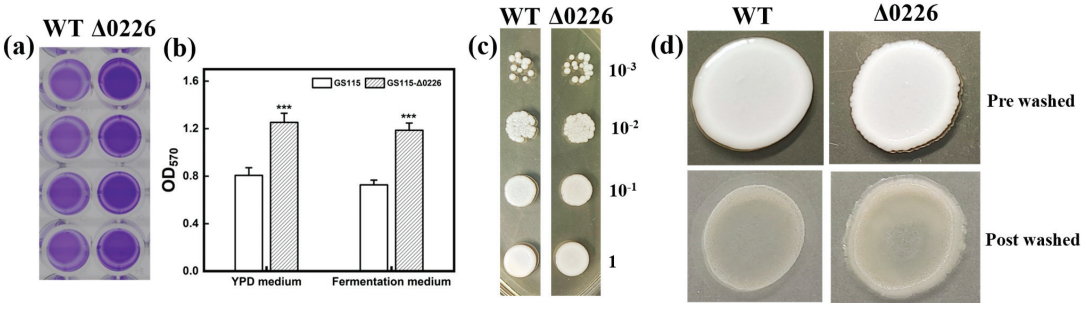

Figure 2. The impact of the knockout of *PAS_chr1-3_0226* gene on biofilm formation and cell adhesion. (**a**) GS115 and GS115-Δ0226 strains were cultivated in 96-well plates for 72 h and tested for adhesion ability. Free cells were removed and washed twice with PBS buffer and stained with 0.1% crystal violet. The samples were washed repeatedly with water, lysed with glacial acetic acid, and then photographed. (**b**) Adhesion expressed as the optical density at 570 nm (OD_{570}) of solubilized crystal violet in acetic acid. Data are reported as the means and standard deviation of three independent experiments. The *p*-values were computed using Student's *t*-test (*** $p < 0.001$). (**c**) Growth of GS115 and GS115-Δ0226 on YPD at an $OD_{600} = 1$ and used to make 10^{-1}, 10^{-2}, and 10^{-3} gradient dilutions in sterile water. (**d**) Standard plate-wash assay of GS115 and GS115-Δ0226.

The cell infestation ability assay was used to observe the ability of the recombinant strains to adhere to the YPD plates. The WT strains had a flat and smooth surface after rinsing and left little residue on the plates. Whereas, the recombinant strains all had a thick wall around the edges of the cells, with the GS115-Δ0226 strain showing a significant retention effect on the plates. The infection range of strain Δ0226 on the plate was larger than that of the WT strain, indicating that gene knockout improved the ability of infection (Figure 2d). This result was consistent with the tendency of biofilm formation in 96-well plates, suggesting that GS115-Δ0226 has a facilitative effect on the growth of biofilms.

2.2. Biofilm Formation on Carriers and Cell Morphological Changes

To further explore the amount of biofilm formation, the carriers were removed after fermentation of 24 h, the surface medium and free cells were removed with PBS, and the biofilms were fixed with 2.5% glutaraldehyde and immediately freeze-dried before observation with SEM. A few cells could be seen on the carrier of the WT strain but they did not form clusters (Figure 3a(II,V)), while the GS115-Δ0226 strain had significantly enhanced biofilm formation and the adsorption on the vector increased, with clusters of cells forming the biofilm (Figure 3a(III,VI)). These results further demonstrated that the Δ0226 strain had a facilitative effect on biofilm formation. The enhanced ability of biofilm formation laid the foundation for the strategy of biofilm-based surface display.

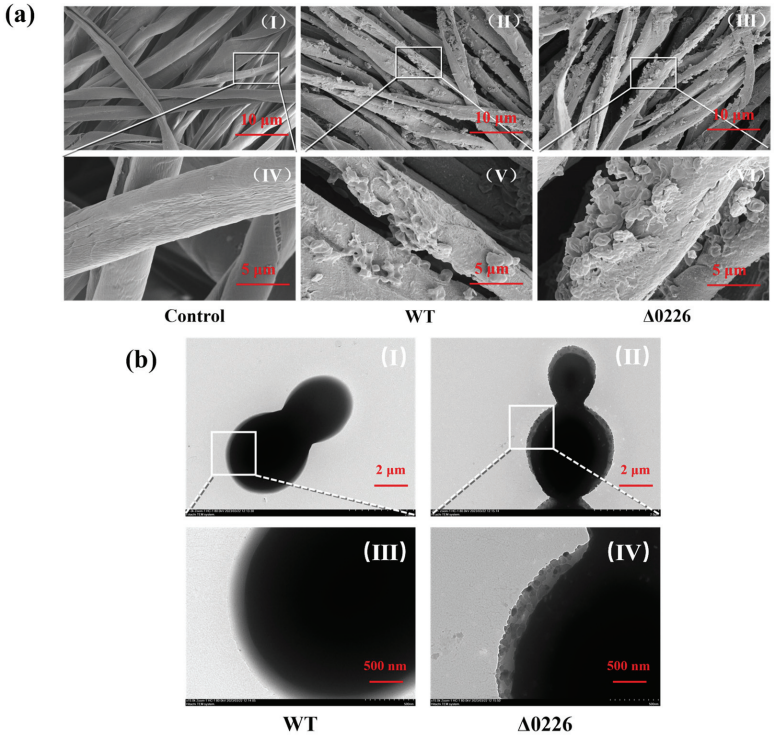

Figure 3. SEM (**a**) and TEM (**b**) images of cells after 48 h of fermentation. (**a**) The biofilm formation on the cotton fibers of the control, GS115 wild type, and GS115-Δ0226. The observation scale was 10 μm in I to III and 5 μm in IV to VI. The deletion of *PAS_chr1-3_0226* could enhance biofilm formation. (**b**) The microstructure of cell morphology of GS115 wild type and GS115-Δ0226. WT was normal with smooth surface, while strain Δ0226 was rough and the specific surface area was increased. The observation scale was 2 μm in I to II and 500 nm in III to IV.

In order to investigate the microstructure changes of cell morphology, a TEM test was carried out. Generally speaking, the beta-1,3-glucanosyltransferase encoded by *PAS_chr1-3_0226* was required for cell wall assembly in *Pichia pastoris* [24,26]. The results of TEM showed that the morphology of WT was normal with a smooth surface (Figure 3b(I,III)). Meanwhile, the substances similar to biofilm matrix were observed on the surface of strain Δ0226 (Figure 3b(II,IV)). These results were consistent with the conclusion that the deletion of *PAS_chr1-3_0226* could enhance biofilm formation in Figure 2. The surface of strain Δ0226 was rough and the specific surface area was increased, which could be beneficial to form more anchorin on the surface of the cell wall in the following surface display.

2.3. Construction of Strains for Surface Display

The β-galactosidase surface display system was constructed from three different anchorins with the *P. pastoris* methanol-inducible plasmid pPIC9K, which contained an α-signal peptide (Figure 1). The active center of β-galactosidase is in the C-terminus and therefore, β-galactosidase was fused to the C-termini of the anchorins Pir1p, Aga2p, and Flo1p. In order to prevent the signal peptide of the protein from being excised by the signal peptidase during cellular secretion, the signal peptide of both was removed. The terminator of the anchorins was also removed and a FLAG tag was added in front of the terminator of *lacA* for subsequent immunofluorescence and flow cytometry detection. All three recombinant strains were constructed successfully.

2.4. Expression of Surface-Displayed β-Galactosidase

The β-galactosidase in situ staining kit was used to verify the successful expression of β-galactosidase on the cell surface using X-Gal as a substrate, in which a dark blue product was observed as shown in Figure 4a. We could see the darkest blue color in sample III, indicating that strain Δ0226-Pir1p-lacA had the higher expression of β-galactosidase.

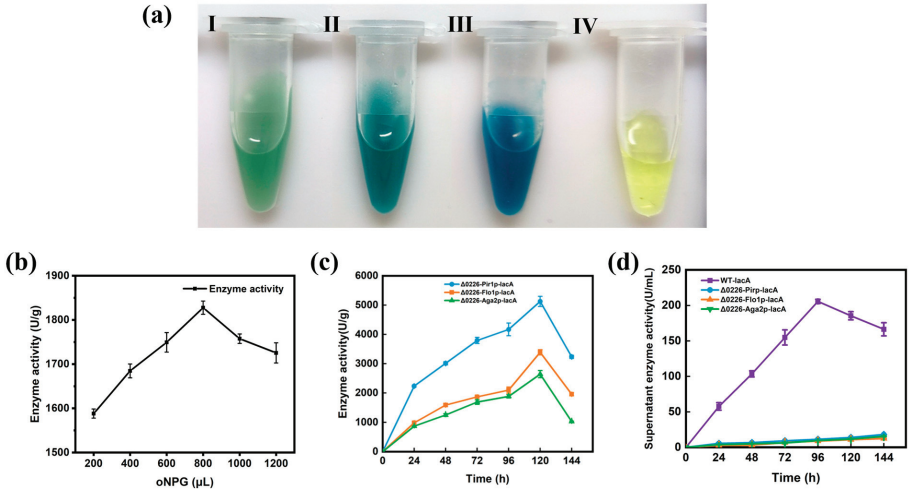

Figure 4. Expression and enzyme activity of surface-displayed β-galactosidase in *P. pastoris*. (**a**) β-galactosidase expression in (I) Δ0226-Aga2p-lacA, (II) Δ0226-Flo1p-lacA, (III) Δ0226-Pir1p-lacA, and (IV) the control. The darker the color of the sample, the higher the expression of β-galactosidase. (**b**) Enzyme activity was determined by adding 200–1200 μL *o*NPG to precipitate to determine the optimum substrate concentration. (**c**) The enzyme activities of precipitate by the strains Δ0226-Pir1p-lacA, Δ0226-Flo1p-lacA, and Δ0226-Aga2p-lacA. (**d**) The enzyme activity of supernatant by the free expression of WT-lacA and the three surface-displayed strains.

2.5. Enzyme Activity of Surface-Displayed β-Galactosidase

β-Galactosidase is an extracellular enzyme that is secreted out of the cell to the supernatant. Whereas, to achieve the surface display of β-galactosidase, it should stay on the cell surface. The effect of different substrates on enzyme activity was first screened by measuring the enzyme activity of the precipitate. The highest enzyme activity was measured when 800 μL *o*NPG was added to the sample, reaching 1828 U/g enzymatic activity (Figure 4b). Therefore, 800 μL *o*NPG was selected for the subsequent enzyme activity assays to determine whether the cell surface and supernatant had enzymatic activity. Subsequently, the samples of 1 mL were taken every 24 h to react in a water bath at pH 6.0 and 50 °C. The enzyme activity was determined in the precipitate and supernatant of the surface-displayed strains compared with that of the free type strain. The enzyme activity of the precipitate was defined by U/g, whereas that of the supernatant was defined as U/mL. We found that the Δ0226-Pir1p-lacA precipitate had the highest enzyme activity (5125 U/g) of the strains measured; however, Δ0226-Flo1p-lacA and Δ0226-Aga2p-lacA had relatively weak enzyme activities of 3389 U/g and 2643 U/g, respectively (Figure 4c). We also found that the enzymatic activity of Δ0226-Pir1p-lacA, Δ0226-Flo1p-lacA, and Δ0226-Aga2p-lacA was higher than that of WT-Pir1p-lacA, WT-Flo1p-lacA, and WT-Aga2p-lacA, indicating that the surface display efficiency was increased in the Δ0226 knockout strain, which allowed for more anchorin expression on the cell wall of *P. pastoris* (Figure S1). This result was consistent with those of the in situ staining experiments, so we selected the Δ0226-Pir1p-lacA strain with the highest enzyme activity for subsequent experiments.

We also performed free expression of β-galactosidase as a supernatant enzyme activity control. When we measured the supernatant enzyme activity of the recombinant surface-displayed strains and the free type strain, we found that the free expressed enzyme activity reached a maximum of 206 U/mL at 96 h, while the highest enzyme activity of all recombinant surface-displayed strains was 18 U/mL at 144 h (Figure 4d), which was much lower than the free expression. This result suggested that most of the surface-displayed enzyme was on the cell surface and only a minimal amount was present in the supernatant, probably due to the natural lysis of the cells and the release of some of the enzymes into the fermentation broth.

2.6. Verification of Surface-Displayed β-Galactosidase by Immunofluorescence Microscopy and Flow Cytometry

A 24 bp FLAG tag (DYKDDDDK) was added in front of the target protein β-galactosidase terminator to accurately localize the fusion protein within the cell in immunofluorescence (IF) experiments. The results of immunofluorescence microscopy further confirmed that the fusion protein localized to the surface of *P. pastoris*. Fluorescence microscopy showed that the cell surface emitted a visible signal (Figure 5a(IV)), whereas the no fluorescence was observed in the control (Figure 5a(I)), indicating that the flag tag on β-galactosidase successfully bound to the antibody and glowed under FITC excitation light successfully. Flow cytometry showed that a significant rightward shift in the strain Δ0226-Pir1p-lacA in the peak plot of the cytometry histogram compared to the control. Meanwhile, an increase in fluorescence intensity and a high display efficiency of 80.63% were detected. This experiment had demonstrated that the fusion proteins with high fusion efficiency were covered on the surface of *P. pastoris* (Figure 5b).

2.7. Characterization of Surface-Displayed β-Galactosidase Activity

We next tested the effect of different temperatures, pH, and metal ions on the relative activity and thermal stability of surface-displayed β-galactosidase. The surface-displayed β-galactosidase activity was highest at 50 °C and reached 94.2% and 75.9% at 60 °C and 70 °C (Figure 6a), respectively. This was similar to that of *A. oryzae* and *B. coagulans* reported by Gerhartz et al. [27,28], but 10 °C higher than the optimum reaction temperature of the immobilized enzyme previously reported by Matella et al. [29]. As the temperature continued to increase, the relative activity of surface-displayed β-galactosidase decreased,

indicating a loss of enzyme activity. In particular, the thermostability of the surface-displayed β-galactosidase was important in the catalytic process. The enzyme was most stable at 50 °C and 40 °C; after 120 min at 50 °C, it maintained 84.6% of the enzyme activity. However, at temperatures above 60 °C, the enzyme activity dropped abruptly and was almost inactive (Figure 6d).

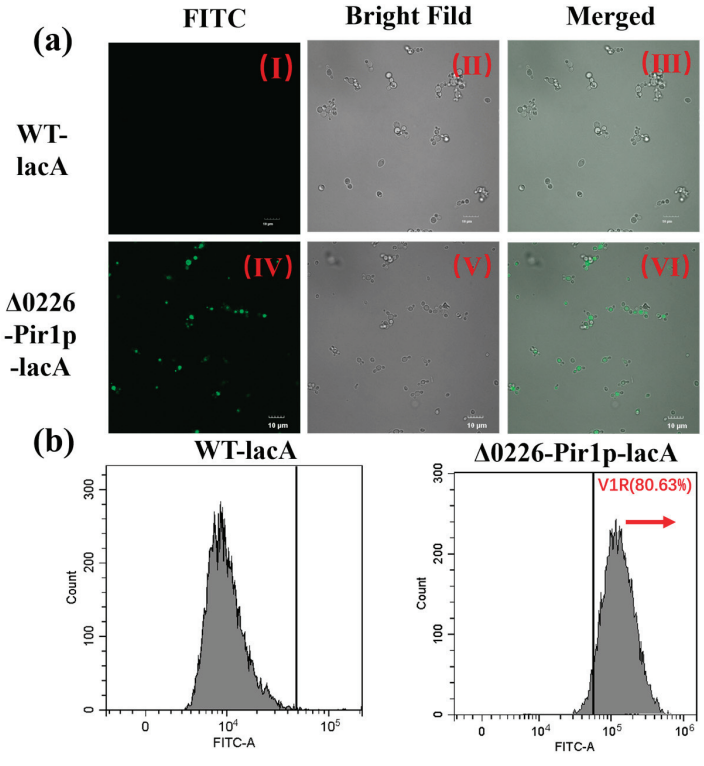

Figure 5. The characterization of β-galactosidase by (**a**) immunofluorescence microscopy and (**b**) flow cytometry in WT-lacA and Δ0226-Pir1p-lacA strains. (**a**) Panels I and IV show representative immunofluorescence micrographs of the free expression WT-lacA and surface-displayed strain Δ0226-Pir1p-lacA using FITC excitation wavelengths; II and V show the visible light images, and III and VI are merged composites of the visible light and FITC excitation images. All micrographs shown were taken at 1000× magnification and at the same angle. Scale bar = 10 μm. (**b**) Flow cytometry histograms reflect the fluorescence signal of the surface-displayed strain, with the *x*-axis indicating fluorescence intensity and the *y*-axis indicating the cell count. Red arrow: the peak shifted to the right indicated that the efficiency of surface display reached 80.63%.

The maximum enzymatic activity of β-galactosidase was demonstrated at pH 5.0 and was maintained at 93.5% and 68.6% at pH 6.0 and pH 7.0, respectively. The enzyme activity dropped sharply when was below pH 5.0 and above pH 7.0, such that the maximum activity was only 19.8% (Figure 6b). Although the optimal enzyme activity was achieved at pH 5.0, it was decreased to 36.5% after 120 min. As shown in Figure 6e, pH 6.0 was the most stable. Hence, it was chosen as the catalytic pH. The optimum pH for β-galactosidase was similar to that of the genetically recombinant strains studied by Katrolia et al. [30] and Lite et al. [31]. This indicated that either too high or low a pH had a significant effect on the enzyme displayed on the surface. We found that the half-life of the surface-display enzyme was still above 70% enzyme activity at 24 h, indicating its stability and role in later catalysis events (Figure 6f).

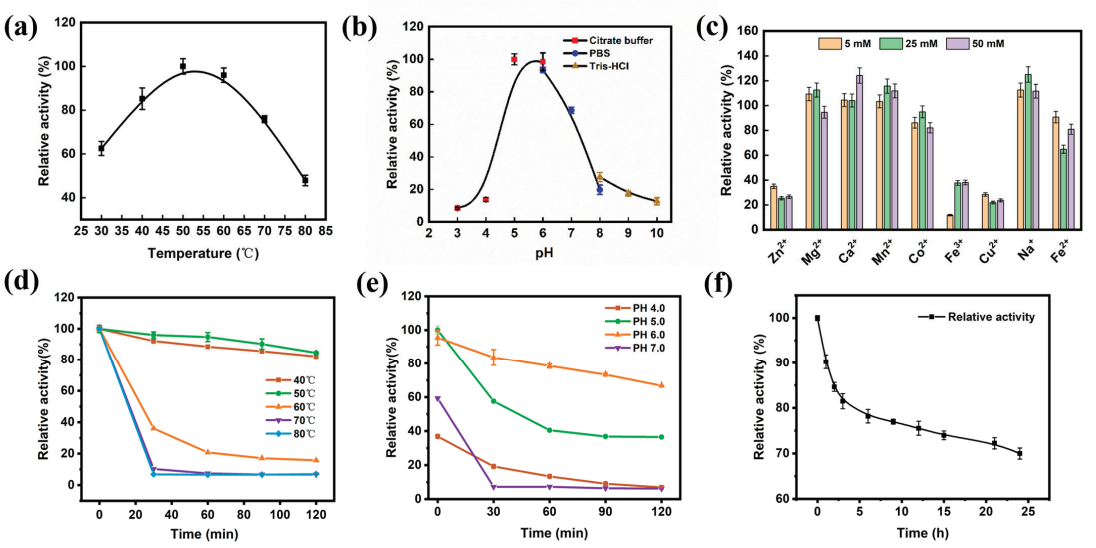

Figure 6. The characterization of surface-displayed β-galactosidase enzyme activity. (**a**) The influence of temperature on the relative activity of recombinant strain. (**b**) Effect of pH on the relative activity of recombinant strain. (**c**) Effect of exogenous addition by different concentrations of metal ions at 5 mmol/L, 25 mmol/L, and 50 mmol/L on the relative activity of recombinant strain, calculated assuming 100% enzyme activity without the addition of metal ions. (**d**) The surface-displayed enzyme was maintained at 40–80 °C for 120 min and the relative enzyme activity was measured every 30 min. (**e**) The surface-displayed enzyme was maintained at pH 4.0–7.0 for 120 min and the relative enzyme activity was measured every 30 min. (**f**) The surface-displayed enzyme was held at pH 6.0 and 50 °C for 24 h and sampled at intervals to measure the enzyme activity. Calculations assumed 100% activity at 0 h.

Metal ions can change the ionic strength of solutions, which in turn affects the ionization of amino acids and can change the protein structure. In addition, metal ions can affect the active site of enzymes, thereby affecting the enzymatic reaction. We found that different concentrations of metal ions had little effect on overall enzyme activity, where Ca^{2+}, Mn^{2+}, and Na^{+} at 5, 25, and 50 mmol/L all promoted enzyme activity (Figure 6c). Indeed, low concentrations of Mg^{2+} promoted enzyme activity, while high concentrations of Mg^{2+} slightly inhibited enzyme activity. Zn^{2+}, Co^{2+}, Fe^{3+}, Cu^{2+}, and Fe^{2+} had inhibitory effects on enzyme activity, with Zn^{2+}, Fe^{3+}, and Cu^{2+} having the most significant inhibitory effect on enzyme activity. These results indicated that some metal ions such as Ca^{2+}, Mn^{2+}, and Na^{+} can act as cofactors of β-galactosidase to enhance its activity, while others such as Cu^{2+} and Fe^{3+} can induce structural changes in the enzyme that inhibit its activity.

2.8. Optimizing the Process of Increasing GOS Yields

To ensure that the free and immobilized surface-display cells had the same amount of enzyme, both dry cells need to be weighed. The dry weight of the free cells was 0.92 g/100 mL and the immobilized cells was 1.72 g/100 mL, suggesting the amount of enzyme added for catalysis was 1.87-fold higher than that of the immobilized cells (Figure 7a). Cells in biofilm-based fermentation could produce more products during the same incubation time. Moreover, the biofilm-immobilized fermentation process maintained the cell activity, slowed down cell degradation, and improved catalytic efficiency.

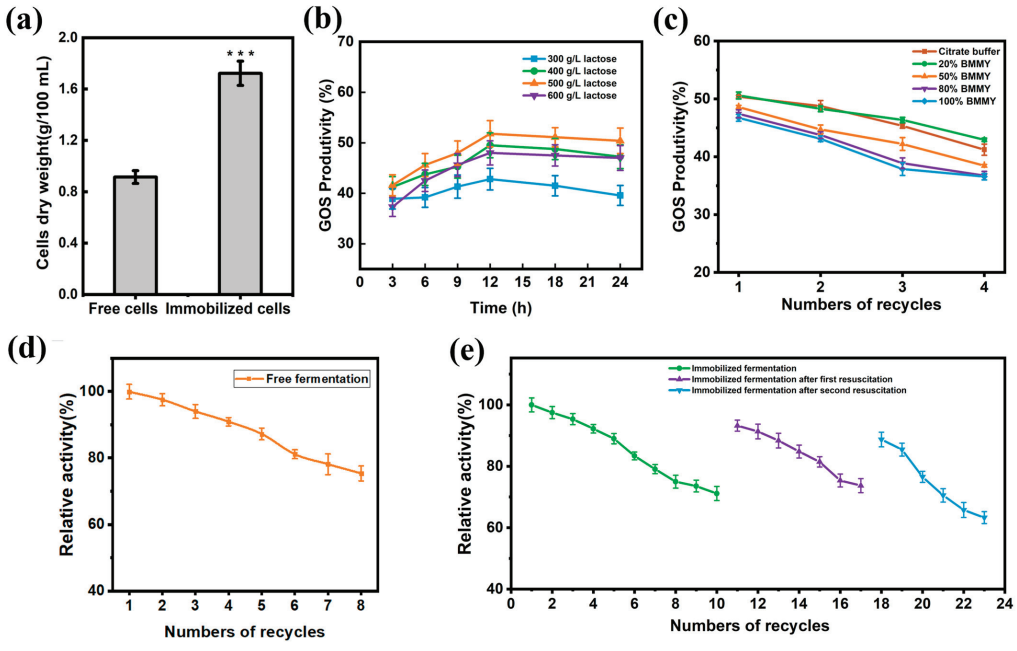

Figure 7. Optimization of GOS production and cell reuse times. (**a**) Comparison of immobilized and free cell dry weights. Data are reported as the means and standard deviation of three independent experiments. The *p*-values were computed using Student's *t*-test (*** $p < 0.001$). (**b**) Effect of lactose concentration and catalytic time on GOS production by the surface-displayed strains. GOS production was increased in a lactose concentration-dependent manner, with the highest production of 251 g/L GOS at 500 g/L lactose (50.3% yield), before a sudden drop in production at concentrations above 500 g/L lactose. The optimal production time for GOS was 12 h, after which the yield stabilizes. (**c**) Influence of different volumes of BMMY medium on GOS yield in multi-batch catalysis. A total of 4 catalysis batches were conducted, with the highest catalytic efficiency starting in the third batch with 20% BMMY. Adding more than 20% BMMY negatively impacted GOS yield. (**d**) Number of reuses in the free cell catalysis. (**e**) Number of reuses in the immobilized cell catalysis. When the GOS yield drops to a certain level, the immobilized cells were resuscitated for 48 h and before catalysis was resumed.

β-galactosidase could convert the high concentration of lactose substrate into GOS. Therefore, the initial lactose concentration is an important factor that affects the production of GOS. The reaction was carried out at 50 °C at lactose concentrations of 300–600 g/L, which showed that at higher concentrations of lactose, GOS production increased continuously with the highest yield achieved at a lactose concentration of 500 g/L. This suggested that the glycosyltransferase activity increased with increasing concentrations of lactose substrate. As the lactose concentration rose, the conversion rate slowly decreased. The lactose was not completely soluble, which could have affected the final trans-glycosylation reaction. The yield of the product was measured by sampling the liquid phase every 3 h, and the yield increased steadily during the first 12 h before it reached a maximum of 251 g/L at 12 h (Figure 7b), with a conversion rate of 50.3%. No significant change in yield was observed with an increasing reaction time, so 500 g/L for 12 h was used as the optimal experimental condition.

Different volumes of BMMY medium were added to the catalytic reaction to observe which condition ensured the growth of cells without affecting the catalytic activity. Lactose was added in citrate buffer at 20%, 50%, 80%, and 100% of BMMY medium and re-added

every 12 h to observe the effect of GOS yield in four consecutive batches. The GOS yield was higher with citrate buffer and 20% BMMY, where the yield was almost the same as that collected from the first two batches of catalysis, while the third batch the GOS yield was slightly higher in a system with 20% BMMY medium than in the citrate buffer (Figure 7c). This result showed that adding 20% BMMY medium ensured that cells remained enzymatically active during growth. The catalytic efficiency was inhibited when more than 20% of the volume of BMMY was added, presumably due to competition between growth and enzyme catalysis. Therefore, a buffer that was 20% of the volume of BMMY medium was used as the buffer.

2.9. Free and Immobilized Cell Biocatalytic GOS Production

Immobilized cotton fiber material was selected as the carrier [21]. Immobilized cells and free cells catalyzed 500 g/L of lactose at 40 °C. The product yield was measured using HPLC. After each batch of reaction, the buffer was removed and fresh culture with lactose was added. The number of reusable batches was recorded.

High concentrations of lactose led to trans-glycosylation reactions in which glucose, galactose, transferred disaccharides, trisaccharides, and tetrasaccharides were produced. Table 1 shows that in the first batch of catalysis, there was almost no difference between the yields of free and immobilized cells, with immobilization slightly higher than that of free cells. The highest proportion of GOS trisaccharides, which accounted for 23.6% of the composition, was the same as found by Gao Xin et al. [32]. Moreover, when the free cells were reused 8 times, the GOS yield dropped to 75%; the first 4 batches maintained a yield above 90%, whereas, the 5th batch showed reduced enzyme activity and the yield dropped more rapidly (Figure 7d). The immobilized cells were reused 10 times, which was 2 times more than the free cells, demonstrating that the addition of 20% BMMY could maintain cell activity and slow down enzyme activity loss. When the yield was dropped to 71%, the carriers were taken out and the fresh medium was added to reaction for 48 h to restore cell viability. A second catalysis was then conducted, which was stopped when the yield dropped to 73% at the end of the 7th batch and the recovery was continued for 48 h. A total of 6 catalysis repeats was achieved at 3rd batch, of which the recovery was stopped once the yield was dropped to 63%. The immobilized cells maintained catalytic activity for a total of 23 times in 3 batches, which is 15 times more than free cells (Figure 7e). The catalytic time and efficiency were both important aspects in the industrial production process. A total of 120 h of growth time was needed for every batch in free fermentation with 8 catalytic repeats. Although 120 h of growth time was still needed in the initial immobilized fermentation, the next growth time was instead a time of 48 h with the total of 23 catalytic times in 3 batches. The productivity of immobilized and free fermentation were 0.44 g/L/h and 0.33 g/L/h, respectively, showing how the production efficiency was significantly improved. Furthermore, the dry weight of immobilized fermentation cells was nearly twice than that of the free type, which is a great advantage in industrial production that was achieved. Overall, biofilm-based biocatalysis using surface display obtained a higher efficient productivity of GOS, shortened culture time, and the persistent cell activity.

Table 1. Analysis of reaction products.

	Yield of GOS (%)							Time-Space Yields of GOS (g/L/h)
	Lactose	Glucose	Galactose	Transfer Disaccharide	Trisaccharide	Tetrasaccharides	GOS	
Free surface-displayed enzyme	34.2 ± 0.2	10.6 ± 0.3	6.6 ± 0.6	15 ± 0.2	24.6 ± 0.1	9 ± 0.2	48.6 ± 0.6	0.33 [a]
Immobilized surface -displayed enzyme	33.8 ± 0.2	9.8 ± 0.2	6 ± 0.3	18.1 ± 0.1	23.6 ± 0.2	8.6 ± 0.1	50.3 ± 0.3	0.44 [b]

[a]: Total GOS production: 3934.5 g, catalytic volumes: 24 L, total time: 504 h. [b]: Total GOS production: 3613.7 g, catalytic volumes: 23 L, total time: 354 h.

3. Materials and Methods

3.1. Strains and Plasmids

P. pastoris GS115 was selected for this study. The gene *lacA* (GenBank: FM955406.1) coded β-galactosidase, which was synthesized by Tsingke Biotechnology Co., Ltd. (Beijing, China). The anchorins Pir1p, Aga2p, and Flo1p were all derived from *S. cerevisiae* S288c [33–35]. The plasmids were derived from the *P. pastoris* inducible plasmid pPIC9K and the expression plasmid pPICZαA. pPIC9K was used for the construction of surface-display strains and pPICZαA was used for the knockdown of the gene *PAS_chr1-3_0226* (Table 2).

Table 2. Strains and plasmids used in this study.

Strains or Plasmids	Relevant Characteristics	Sources
Strains		
Escherichia coli	DH5α	Stored in our lab
GS115	*P. pastoris*	Stored in our lab
GS115-Δ0226	*P. pastoris* with the deletion of *PAS_chr1-3_0226*	This study
GS115-lacA	*lacA* comes from *Aspergillus oryzae* BK03	This study
Δ0226-Pir1p-lacA	Pir1p comes from *S. cerevisiae* S288c	This study
Δ0226-Aga2p-lacA	Aga2p comes from *S. cerevisiae* S288c	This study
Δ0226-Flo1p-lacA	Flo1p comes from *S. cerevisiae* S288c	This study
Plasmids		
pPIC9K	Resistance to Ampicillin	Stored in our lab
pPICZαA	Resistance to Bleomycin	Stored in our lab

3.2. Media and Growth Conditions

The host for the molecular manipulation in this study was *E. coli* DH5α, which was grown in LB medium composed of yeast extract (5 g/L), peptone (10 g/L), and NaCl (5 g/L). *P. pastoris* was cultured in Yeast Extract Peptone Dextrose (YPD) medium composed of yeast extract (10 g/L), peptone (20 g/L), and glucose (20 g/L). Solid media were prepared in all cases by adding 1.5% (*w*/*v*) agar. Buffered Minimal Glycerol YP (BMGY) medium was composed of yeast extract (10 g/L), peptone (20 g/L), biotin (0.0004 g/L), 10% glycerol, $K_2HPO_4 \cdot 3H_2O$ (3 g/L), KH_2PO_4 (11.8 g/L), and Yeast Nitrogen Base (13.4 g/L) (YNB). Buffered Minimal Methanol Medium (BMMY) was composed of yeast extract (10 g/L), peptone (20 g/L), biotin (0.0004 g/L), $K_2HPO_4 \cdot 3H_2O$ (3 g/L), KH_2PO_4 (11.8 g/L), YNB (13.4 g/L), and methanol (AR, 5 mL/L. The initial pH was adjusted to 6.5 ± 0.2.

3.3. Construction of Gene Knock-Out and Surface-Displayed Strains

The homologous recombination was selected for the construction of a *P. pastoris* GS115 strain mutant as previously described [36]. The fragment of bleomycin was amplified by PCR using BleoR-F/R primers with the pPICZαA plasmid as a template. Similarly, the upper and lower homology arms (500 bp) of *PAS_chr1-3_0226* were obtained using primers from the genome of *P. pastoris* GS115. The sequences of primers are listed in Table 3. The *PAS_chr1-3_0226* gene in the GS115 genome was replaced by the gene of bleomycin successfully.

The encoding genes of anchorin Pir1p, Aga2p, and Flo1p were amplified by PCR from *S. cerevisiae* S288c with the fusion of the *lacA* gene, which was inserted into the pPIC9K plasmid. Competent cells of GS115-Δ0226 were prepared using the sorbitol method, and then the recombinant plasmids were electroporated into GS115-Δ0226 strain.

Table 3. Primers used in this study and their sequences.

Primer Name	Primer Sequence	Source
Δ0226-UP-F	CCTAGTGATTCCTGTGATGTATTCACGGCTGCGCAAAACT	This work
Δ0226-UP-R	GCTATGGTGTGTGGGGGATCATTTTGATTATCTTTGTGAG	This work
Δ0226-DOWN-F	GCTCGAAGGCTTTAATTTGCGCGGTTCACATTAATTAAAG	This work
Δ0226-DOWN-R	AAATTTAAAGAGATGCGAAACTTGACAGCTTGAGCGTGAC	This work
BleoR-F	CTCACAAAGATAATCAAAATGATCCCCCACACACCATAGC	This work
BleoR-R	CTTTAATTAATGTGAACCGCGCAAATTAAAGCCTTCGAGC	This work
Pir1p-UP	AAAGAGAGGCTGAAGCTTACGTATATGCTCCAAAGGACCC	This work
Pir1p-DOWN	CCAGAACCACCACCACCGAATTCACAGTTGAGCAAATCGA	This work
lacA-UP	GCTCAACTGTGAATTCGGTGGTGGTGGTTCTGGTGGTGGTGGA TCTGGTGGTGGAGGTTCTTCTATTAAGCATAGA	This work
lacA-DOWN	TTAATTCGCGGCCGCCCTAGGTTACTTATCATCATCATCCTTGTA ATCGTAAGCACCCTTTCTT	This work
FS-UP	TACGTAGCCACAGAGGCGTGCTTACCAGCAGGCCAGAGGAAAA	This work
FS-DOWN	GAATTCAGAGCTGGTGATTTGTCCTGAAGATGATGATGAC	This work
Aga2p-UP	AAAGAGAGGCTGAAGCTTACGTACAGGAACTGACAACTAT	This work
Aga2p-DOWN	CCAGAACCACCACCACCGAATTCAAAAACATACTGTGTGT	This work
Δ0226-UP100 bp	TGAGACACATTTAACCATCGC	This work

The lacA-UP redlined section is a 45 bp linker, and the lacA-DOWN redlined section is a 24 bp FLAG tag.

3.4. Characterization of Biofilm Formation

3.4.1. Biofilm Formation on Plastics

A crystal violet (CV) assay was performed to measure biofilm formation with minor modifications [37]. Yeast strains were grown in YPD and fermentation liquid media overnight at 30 °C with 150 rpm. After collection, washing, and discarding supernatant, the cells were resuspended in YPD and fermentation medium at an OD_{600} = 1. Cell suspensions (20 μL) were transferred to a 96-well microtiter plate (Corning, Kennebunk, ME, USA) containing 180 μL medium per well. The plate was then incubated for 72 h at 30 °C. Four replicate wells were used for each treatment. The biofilm-containing wells were washed twice with 200 μL PBS to remove free cells, after which the biofilms were stained with 200 μL 0.1% CV solution for 15 min at room temperature (about 25 °C), followed by repeated washing of the wells with PBS. Then, 200 μL 33% acetic acid was added to each well and the plate was incubated at room temperature for 20 min with slight shaking to elute the CV. Finally, the absorbance was measured at 570 nm using a microplate reader (SpectraMax® iD5; Molecular Devices, San Jose, CA, USA).

3.4.2. Cell Growth and Infiltration Capacity Analysis

P. pastoris strains were grown in YPD at 30 °C for 2 days. After collection, washing and discarding supernatant, the cells were resuspended in YPD at an OD_{600} = 1 and used to make 10^{-1}, 10^{-2}, and 10^{-3} gradient dilutions in sterile water. Each dilution (1 μL) was then dropped on YPD agar and incubated for 24 h at 30 °C.

The GS115 and GS115-Δ0226 strains were isolated in 5 mL/50 mL centrifuge tubes and cultured overnight at 30 °C and 250 rpm. The optical density of the strains was measured with a UV spectrophotometer and diluted to OD_{600} = 1 in YPD. A total of 10 μL was cultured in a YPD plate at 30 °C for 3–4 days. The cultured strains were slowly washed with running water until the cells could not be eluted and observed to remain on the medium [38].

3.4.3. Characterization of Scanning Electron Microscopy and Transmission Electron Microscopy

The GS115 and GS115-Δ0226 strains were incubated in BMMY fermentation medium on cotton fiber material for 24 h. After immobilization, the carriers were removed and cut into suitable-sized squares and repeatedly rinsed 2–3 times with PBS buffer to ensure that no medium or yeast remained on the surface of the carriers. Immediately afterward, the samples were fixed in 2.5% glutaraldehyde with triton for 30 min at room temperature, and then washed 2–3 times with PBS and placed in a −80 °C freezer before they were dried overnight in a freeze drier (Labconco, Fort Scott, Kansas, USA). Freeze-dried

samples were sputter-coated with gold and observed with a scanning electron microscope (TM3000, Hitachi, Tokyo, Japan) and transmission electron microscope (HT7820, Hitachi, Tokyo, Japan) [13].

3.5. Surface-Displayed β-Galactosidase Assay

3.5.1. β-Galactosidase In Situ Staining Assay

An in situ β-galactosidase staining kit is a tool for the in situ staining of cells for β-galactosidase detection. The mutant strains were induced with methanol in BMMY medium for 48 h. Then, the fermentation broth was centrifuged at 6000 rpm for 5 min to remove the supernatant. The cells were washed twice with PBS and centrifuged again to remove the supernatant. An aliquot of 500 μL staining solution (Beyotime Biotechnology Co., Ltd., Shanghai, China) was added to each 1.5 mL centrifuge tube. The cells were incubated at 50 °C until the color stabilized and the cell morphology was observed under an optical microscope.

3.5.2. β-Galactosidase Enzyme Activity

The enzymatic activity of β-galactosidase was determined as described previously [32]. The *P. pastoris* GS115 strain and the positive transformants were incubated overnight in 5 mL YPD, which was then used to inoculate 25 mL BMGY in conical flasks. These cultures were incubated at 30 °C for 21–24 h until OD_{600} = 2–6. The supernatants were removed by centrifugation at 6000 rpm for 5 min, and the precipitate was washed twice with sterile water before it was transferred to 100 mL BMMY. The enzyme activity was measured every 24 h by taking 1 mL of the solution after the expression was induced with 1% methanol.

The enzyme activity was measured by hydrolysis of o-nitrophenyl-β-galactoside (*o*NPG). The different volume of *o*NPG liquid was added to the precipitate of 1 mL to determine enzyme activity. The extract was centrifuged to remove the supernatant, and the cells were washed twice with PBS to remove any residual supernatant. A total of 1.2 mL citrate buffer at pH 6.0 and 800 μL 20 mmol/L *o*NPG were added to the bacterial precipitate and incubated in a water bath at 50 °C for 10 min. After the reaction, 1 mL of 1 mol/L Na_2CO_3 was added to inactivate the enzyme. The *o*-nitrophenol (*o*NP) was observed at 420 nm. One unit of enzyme activity was defined as hydrolyzing 1 μmol *o*NPG to *o*NP per minute.

3.5.3. Immunofluorescence Microscopy and Flow Cytometry Analysis

To verify β-galactosidase display on the surface of *P. pastoris*, the recombinant strains were observed under an immunofluorescence microscope (Mshot, MF52-N, Guangzhou, China) and with flow cytometry (CytoFLEX, Beckman Coulter, Bria, California, USA). After 120 h of methanol-induced fermentation, 1 mL cells were collected by centrifugation at 6000 rpm for 5 min, washed three times with PBS (pH 7.4), and suspended in PBS containing 2% BSA (pH 7.4). Then, 1 μL FLAG-tagged mouse monoclonal antibody (1:100) was added to a suspension of 200 μL. After incubation for 3 h at 37 °C and shaking at 60 rpm, the cells were washed three times with PBS and suspended in PBS containing 2% BSA. Then, 1 μL FITC-labeled goat anti-mouse IgG antibody (1:500) was added to the cells and incubated for 3 h at 37 °C with shaking at 60 rpm. The cells were washed again with PBS three times and observed under an immunofluorescence microscope. Additionally, 200 μL cells were filtered through a 600 mesh sieve (aperture is 0.025 mm) to disperse the cell clusters, and the samples were measured with a flow cytometer. We collected 10,000 cells for the assay using an excitation light wavelength was 488 nm, and the channel signal was recorded [39].

3.5.4. Enzymatic Properties of β-Galactosidase

One milliliter of cells was collected after 72 h of induced expression, centrifuged at 6000 rpm for 5 min to remove the supernatant, and the cells were washed three times with PBS. To investigate the effect of temperature on enzyme activity, 800 μL 20 mmol/L *o*NPG and pH 6.0 citrate buffer was added for 10 min at 30–80 °C. The β-galactosidase enzyme activity was measured at 420 nm at the end of the reaction. To investigate the effect of pH

on enzyme activity, the reaction was conducted in a 50 °C water bath at pH 3.0 to 9.0. The same number of cells were taken and held at 40–70 °C and pH 4.0–7.0 for 120 min, with samples taken every 30 min to measure the enzyme activity. Samples were also taken at the optimum temperature and pH to measure the activity and half-life of the enzyme. In addition, 5 mmol/L, 25 mmol/L, and 50 mmol/L Na^+, Ca^{2+}, Mg^{2+}, Fe^{2+}, Fe^{3+}, Mn^{2+}, Co^{2+}, Cu^{2+}, and Zn^{2+} were added to pH 6.0 buffer and the enzyme activity of β-galactosidase was measured after 10 min of reaction at 50 °C in a water bath.

3.6. Free and Immobilized Fermentation for GOS Synthesis

The dry weight of the cells at the end of fermentation was measured to ensure uniformity in the experiment. For cells on immobilized carriers, 100 mL carriers and free cells at the end of fermentation was washed twice with PBS buffer, centrifuged at 6000 rpm for 5 min, dried at 105 °C, and weighed. To determine the optimum substrate concentration and reaction time for GOS production by fermentation, concentrations ranging from 300–600 g/L lactose were made in citrate buffer (pH 6.0). The substrate was catalyzed at 40 °C by strain Δ0226-Pir1p-lacA. The samples were taken every 3 h. The GOS, glucose, galactose, and lactose content were analyzed using HPLC.

In order to optimize the catalytic process and verify whether the cells could achieve growth and catalysis at the same time, citrate buffer (pH 6.0) and 20–100% BMMY (pH 6.0) were added to the buffer. After 4 batches of catalysis, the production of GOS and enzyme activity of the cells were tested. The number of reused free and immobilized cells was examined using the same catalytic system, to which the lactose substrate was re-added every 6 h to determine the lactose conversion rate. When the catalytic efficiency of the immobilized cells dropped below 70%, the immobilized carriers were placed back into a fresh medium to recover, then taken out to continue catalysis. This cycle was repeated several times until the catalytic effect was greatly reduced. The total time–space yield of free and immobilized cells was calculated as follows:

① Free cells (g/L/h) = $\frac{\text{Total production of GOS}}{\text{Total cell growth time+catalytic time}}$

② Immobilized cells (g/L/h) = $\frac{\text{“Total production of GOS”}}{\text{“Total cell growth time+resuscitation+catalytic time”}}$

3.7. The Methods of Product Detection

The analysis of glucose, galactose, and GOS was performed on an Agilent 1260 Infinity II RID instrument and an Aminex HPX-87H analytical HPLC column at 60 °C with 5 mmol/L H_2SO_4 as the mobile phase and a flow rate of 0.4 mL/min.

4. Conclusions

The biofilm-based fermentation of *P. pastoris* was developed by using the advantages of biofilm formation. Knocking out the cell wall protein gene *PAS_chr1-3_0226* successfully enhanced biofilm formation, which provided excellent growth conditions for the cells to maintain high activity during prolonged fermentation, which was applicable to continuous (repeated-batch) fermentation. In addition, the optimal surface-displayed strains with anchorin were selected based on strain GS115-Δ0226, with the enzyme activity of 5125 U/g and 23 repeats of continuous catalysis batches. This could improve catalytic efficiency and repeated batches compared with the free fermentation. A co-culture system integrated catalysis and growth, so that a dynamic equilibrium in the consolidated integrative process was achieved. These results indicated that biofilm-based fermentation using surface display will be of great value for immobilized GOS production. Overall, this study provides a reference for the development of more biofilm-based surface display methods in *P. pastoris* for biochemical production processes.

Supplementary Materials: The following supporting information can be downloaded at https://www.mdpi.com/article/10.3390/ijms24076507/s1.

Author Contributions: Designing the experiments and writing original draft preparation, T.C. and S.W. (Shimeng Wang); experiments and analysis, H.N., G.Y., S.W. (Sinan Wang) and Y.W.; resources of strains, C.Z., B.Y., P.Y. and D.L.; revising the manuscript, Y.C. and W.S.; funding acquisition, H.Y. and Y.C. All authors have read and agreed to the published version of the manuscript.

Funding: This work was supported by the National Key R&D Program of China 2022YFC2105400; the National Key R&D Program of China (Grant No. 2021YFC2101100); the National Natural Science Foundation of China (22178176); the National Key Research and Development Program of China (Grant No. 2018YFB1501705); the key program of the National Natural Science Foundation of China (Grant No. 21636003); the Program for Changjiang Scholars and Innovative Research Team in University (IRT_14R28); Jiangsu National Synergetic Innovation Center for Advanced Materials (SICAM); the Priority Academic Program Development of Jiangsu Higher Education Institutions (PAPD); Key Research and Development Program of Nanjing Jiangbei New Area (ZDYF20200220); Key R & D plan of Jiangsu Province (BE2019001); Youth Fund of Natural Science Foundation of Jiangsu Province (BK20220334); the National Natural Science Foundation of China (Grant No. 22208157).

Institutional Review Board Statement: Not applicable.

Informed Consent Statement: Not applicable.

Data Availability Statement: Not applicable.

Conflicts of Interest: The authors declare no conflict of interest.

References

1. Tzortzis, G.; Vulevic, J. Galacto-Oligosaccharide Prebiotics. In *Prebiotics and Probiotics Science and Technology*; Charalampopoulos, D., Rastall, R.A., Eds.; Springer: New York, NY, USA, 2009; pp. 207–244.
2. Nawaz, A.; Bakhsh Javaid, A.; Irshad, S.; Hoseinifar, S.H.; Xiong, H. The functionality of prebiotics as immunostimulant: Evidences from trials on terrestrial and aquatic animals. *Fish Shellfish. Immunol.* **2018**, *76*, 272–278. [CrossRef]
3. Panesar, P.S.; Kaur, R.; Singh, R.S.; Kennedy, J.F. Biocatalytic strategies in the production of galacto-oligosaccharides and its global status. *Int. J. Biol. Macromol.* **2018**, *111*, 667–679. [CrossRef] [PubMed]
4. Schwab, C.; Lee, V.; Sørensen, K.I.; Gänzle, M.G. Production of galactooligosaccharides and heterooligosaccharides with disrupted cell extracts and whole cells of lactic acid bacteria and bifidobacteria. *Int. Dairy J.* **2011**, *21*, 748–754. [CrossRef]
5. Güleç, H.A.; Gürdaş, S.; Albayrak, N.; Mutlu, M. Immobilization of Aspergillus oryzae β-galactosidase on low-pressure plasma-modified cellulose acetate membrane using polyethyleneimine for production of galactooligosaccharide. *Biotechnol. Bioprocess Eng.* **2010**, *15*, 1006–1015. [CrossRef]
6. Onishi, N.; Tanaka, T. Purification and Properties of a Galacto- and Gluco-Oligosaccharide-Producing P-Glycosidase from Rhodotorula minuta IF0879. *J. Ferment. Bioeng.* **1996**, *82*, 439–443. [CrossRef]
7. Kaczyński, L.K.; Cais-Sokolińska, D.; Szwengiel, A. Kinetics of lactose hydrolysis and galactooligosaccharides formation in beverages based on goat's milk and its permeate. *Food Sci. Biotechnol.* **2019**, *28*, 1529–1534. [CrossRef] [PubMed]
8. Van Loo, J.; Cummings, J.; Delzenne, N.; Englyst, H.; Franck, A.; Hopkins, M.; Kok, N.; Macfarlane, G.; Newton, D.; Quigley, M.; et al. Functional food properties of non-digestible oligosaccharides: A consensus report from the ENDO project (DGXII AIRII-CT94-1095). *Br. J. Nutr.* **1999**, *81*, 121–132. [PubMed]
9. Vera, C.; Córdova, A.; Aburto, C.; Guerrero, C.; Suárez, S.; Illanes, A. Synthesis and purification of galacto-oligosaccharides: State of the art. *World J. Microbiol. Biotechnol.* **2016**, *32*, 197. [CrossRef]
10. Guidini, C.Z.; Fischer, J.; Santana, L.N.S.; Cardoso, V.L.; Ribeiro, E.J. Immobilization of Aspergillus oryzae β-galactosidase in ion exchange resins by combined ionic-binding method and cross-linking. *Biochem. Eng. J.* **2010**, *52*, 137–143. [CrossRef]
11. Tanaka, T.; Yamada, R.; Ogino, C.; Kondo, A. Recent developments in yeast cell surface display toward extended applications in biotechnology. *Appl. Microbiol. Biotechnol.* **2012**, *95*, 577–591. [CrossRef] [PubMed]
12. Zhao, N.; Xu, Y.; Wang, K.; Zheng, S. Synthesis of Isomalto-Oligosaccharides by Pichia pastoris Displaying the Aspergillus niger α-Glucosidase. *J. Agric. Food Chem.* **2017**, *65*, 9468–9474. [CrossRef]
13. Li, Z.; Chen, Y.; Liu, D.; Zhao, N.; Cheng, H.; Ren, H.; Guo, T.; Niu, H.; Zhuang, W.; Wu, J.; et al. Involvement of glycolysis/gluconeogenesis and signaling regulatory pathways in Saccharomyces cerevisiae biofilms during fermentation. *Front. Microbiol.* **2015**, *6*, 139. [CrossRef] [PubMed]
14. Blankenship, J.R.; Mitchell, A.P. How to build a biofilm: A fungal perspective. *Curr. Opin. Microbiol.* **2006**, *9*, 588–594. [CrossRef] [PubMed]
15. Zhao, N.; Ren, H.; Li, Z.; Zhao, T.; Shi, X.; Cheng, H.; Zhuang, W.; Chen, Y.; Ying, H. Enhancement of nuclease P1 production by Penicillium citrinum YL104 immobilized on activated carbon filter sponge. *Appl. Microbiol. Biotechnol.* **2015**, *99*, 1145–1153. [CrossRef]
16. Chen, T.; Liu, N.; Ren, P.; Xi, X.; Yang, L.; Sun, W.; Yu, B.; Ying, H.; Ouyang, P.; Liu, D.; et al. Efficient Biofilm-Based Fermentation Strategies for L-Threonine Production by Escherichia coli. *Front. Microbiol.* **2019**, *10*, 1773. [CrossRef]

17. Chen, Y.; Liu, Q.; Zhou, T.; Li, B.; Yao, S.; Li, A.; Wu, J.; Ying, H. Ethanol production by repeated batch and continuous fermentations by Saccharomyces cerevisiae immobilized in a fibrous bed bioreactor. *J. Microbiol. Biotechnol.* **2013**, *23*, 511–517. [CrossRef]
18. Shi, X.; Chen, Y.; Ren, H.; Liu, D.; Zhao, T.; Zhao, N.; Ying, H. Economically enhanced succinic acid fermentation from cassava bagasse hydrolysate using Corynebacterium glutamicum immobilized in porous polyurethane filler. *Bioresour. Technol.* **2014**, *174*, 190–197. [CrossRef]
19. Sun, W.; Yu, Y.; Chen, J.; Yu, B.; Chen, T.; Ying, H.; Zhou, S.; Ouyang, P.; Liu, D.; Chen, Y. Light Signaling Regulates Aspergillus niger Biofilm Formation by Affecting Melanin and Extracellular Polysaccharide Biosynthesis. *Mol. Biol. Physiol.* **2021**, *12*, e03434-20. [CrossRef] [PubMed]
20. Liu, D.; Chen, Y.; Li, A.; Ding, F.; Zhou, T.; He, Y.; Li, B.; Niu, H.; Lin, X.; Xie, J.; et al. Enhanced butanol production by modulation of electron flow in Clostridium acetobutylicum B3 immobilized by surface adsorption. *Bioresour. Technol.* **2013**, *129*, 321–328. [CrossRef]
21. Ding, S.; Zhang, D.; Sha, Y.; Wang, F.; Liang, C.; Chen, T.; Sun, W.; Zhuang, W.; Yu, B.; Liu, D.; et al. Efficient preparation of phytase from genetically modified Pichia pastoris in immobilised fermentation biofilms adsorbed on surface-modified cotton fibres. *Process Biochem.* **2021**, *111*, 69–78. [CrossRef]
22. Zhang, D.; Wang, F.; Yu, Y.; Ding, S.; Chen, T.; Sun, W.; Liang, C.; Yu, B.; Ying, H.; Liu, D.; et al. Effect of quorum-sensing molecule 2-phenylethanol and ARO genes on Saccharomyces cerevisiae biofilm. *Appl. Microbiol. Biotechnol.* **2021**, *105*, 3635–3648. [CrossRef]
23. Juturu, V.; Wu, J.C. Heterologous Protein Expression in Pichia pastoris: Latest Research Progress and Applications. *Chembiochem* **2018**, *19*, 7–21. [CrossRef] [PubMed]
24. Ha, C.W.; Kim, K.; Chang, Y.J.; Kim, B.; Huh, W.K. The beta-1,3-glucanosyltransferase Gas1 regulates Sir2-mediated rDNA stability in Saccharomyces cerevisiae. *Nucleic. Acids Res.* **2014**, *42*, 8486–8499. [CrossRef]
25. Lipke, P.N.; Mathelié-Guinlet, M.; Viljoen, A.; Dufréne, Y.F. A New Function for Amyloid-Like Interactions: Cross-Beta Aggregates of Adhesins form Cell-to-Cell Bonds. *Pathogens* **2021**, *10*, 1013. [CrossRef]
26. Klis, F.M.; Mol, P.; Hellingwerf, K.; Brul, S. Dynamics of cell wall structure in Saccharomyces cerevisiae. *FEMS Microbiol. Rev.* **2002**, *26*, 239–256. [CrossRef]
27. Schwartz, R. Enzymes in Industry Production and Application. *Biochem. Educ.* **1991**, *19*, 98. [CrossRef]
28. Batra, N.; Singh, J.; Joshi, A.; Sobti, R.C. Improved Properties ofBacillus coagulans β-Galactosidase through Immobilization. *Eng. Life Sci.* **2005**, *5*, 581–584. [CrossRef]
29. Matella, N.J.; Dolan, K.D.; Lee, Y.S. Comparison of Galactooligosaccharide Production in Free-Enzyme Ultrafiltration and in Immobilized-Enzyme Systems. *J. Food Sci.* **2006**, *71*, C363–C368. [CrossRef]
30. Katrolia, P.; Zhang, M.; Yan, Q.; Jiang, Z.; Song, C.; Li, L. Characterisation of a thermostable family 42 β-galactosidase (BgalC) family from Thermotoga maritima showing efficient lactose hydrolysis. *Food Chem.* **2011**, *125*, 614–621. [CrossRef]
31. Li, L.; Zhang, M.; Jiang, Z.; Tang, L.; Cong, Q. Characterisation of a thermostable family 42 β-galactosidase from Thermotoga maritima. *Food Chem.* **2009**, *112*, 844–850. [CrossRef]
32. Gao, X.; Wu, J.; Wu, D. Rational design of the beta-galactosidase from Aspergillus oryzae to improve galactooligosaccharide production. *Food Chem.* **2019**, *286*, 362–367. [CrossRef] [PubMed]
33. Jacobs, P.P.; Ryckaert, S.; Geysens, S.; De Vusser, K.; Callewaert, N.; Contreras, R. Pichia surface display: Display of proteins on the surface of glycoengineered Pichia pastoris strains. *Biotechnol. Lett.* **2008**, *30*, 2173–2181. [CrossRef] [PubMed]
34. Jiang, Z.-B.; Song, H.-T.; Gupta, N.; Ma, L.-X.; Wu, Z.-B. Cell surface display of functionally active lipases from Yarrowia lipolytica in Pichia pastoris. *Protein Expr. Purif.* **2007**, *56*, 35–39. [CrossRef]
35. Wang, Q.; Li, L.; Chen, M.; Qi, Q.; Wang, P.G. Construction of a novel Pichia pastoris cell-surface display system based on the cell wall protein Pir1. *Curr. Microbiol.* **2008**, *56*, 352–357. [CrossRef] [PubMed]
36. Jiao, L.; Zhou, Q.; Yan, Y. Efficient gene disruption by posttransformational directed internal homologous recombination in Pichia pastoris. *Anal. Biochem.* **2019**, *576*, 1–4. [CrossRef] [PubMed]
37. Yang, L.; Zheng, C.; Chen, Y.; Ying, H. FLO Genes Family and Transcription Factor MIG1 Regulate Saccharomyces cerevisiae Biofilm Formation During Immobilized Fermentation. *Front. Microbiol.* **2018**, *9*, 1860. [CrossRef]
38. Liang, C.; Ding, S.; Sun, W.; Liu, L.; Zhao, W.; Zhang, D.; Ying, H.; Liu, D.; Chen, Y. Biofilm-based fermentation: A novel immobilisation strategy for Saccharomyces cerevisiae cell cycle progression during ethanol production. *Appl. Microbiol. Biotechnol.* **2020**, *104*, 7495–7505. [CrossRef]
39. Zhang, L.; Liang, S.; Zhou, X.; Jin, Z.; Jiang, F.; Han, S.; Zheng, S.; Lin, Y. Screening for glycosylphosphatidylinositol-modified cell wall proteins in Pichia pastoris and their recombinant expression on the cell surface. *Appl. Environ. Microbiol.* **2013**, *79*, 5519–5526. [CrossRef]

International Journal of
Molecular Sciences

MDPI

Article

Hepatic, Muscle and Intestinal Oxidative Status and Plasmatic Parameters of Greater Amberjack (*Seriola dumerili*, Risso, 1810) Fed Diets with Fish Oil Replacement and Probiotic Addition

Maria Consolación Milián-Sorribes [1,*], Helena Peres [2,3], Ana Tomás-Vidal [1], Sara Moutinho [2,3], David S. Peñaranda [1], Miguel Jover-Cerdá [1], Aires Oliva-Teles [2,3] and Silvia Martínez-Llorens [1]

[1] Aquaculture and Biodiversity Group, Institute of Animal Science and Technology, Universitat Politècnica de València, Camino de Vera, 14, 46071 Valencia, Spain
[2] Departamento de Biologia, Faculdade de Ciências da Universidade do Porto, Rua do Campo Alegre s/n, Edifício FC4, 4169-007 Porto, Portugal
[3] CIIMAR, Centro Interdisciplinar de Investigação Marinha e Ambiental, Universidade do Porto, Terminal de Cruzeiros do Porto de Leixões, Avenida General Norton de Matos, s/n, 4450-208 Matosinhos, Portugal
* Correspondence: mamisor@etsia.upv.es

Abstract: The present study was conducted to investigate the effects of dietary fish oil replacement with a mixture of vegetable oils and probiotic supplementation on plasma biochemical parameters, oxidative stress, and antioxidant ability of *Seriola dumerili*. Specimens with an initial weight of 175 g were used. Four feeds were formulated with 0% (FO-100), 75% (FO-25), and 100% (FO-0 and FO-0+ with the addition of *Lactobacillus* probiotics) substitution of fish oil with a mixture of linseed, sunflower, and palm oils. After 109 days, no significant differences were observed in the activity of antioxidant enzymes in the liver, foregut, and hindgut, only glucose-6-phosphate dehydrogenase activity in the liver was higher in the fish fed the FO-100 diet than in those fed the FO-0 diet. No significant differences were observed in the total, reduced, and oxidized glutathione and the oxidative stress index in the liver. In addition, lipid peroxidation in the liver and red muscle values were higher in the fish fed the FO-100 diet than in the fish fed the FO-0+ diet, however, the foregut of the fish fed the FO-100 diet presented lower values than that of the fish fed the FO replacement diet, with and without probiotics. There were significant differences in cholesterol levels in the FO-100 group; they were significantly higher than those observed with the fish diets without fish oil. To sum up, fish oil can be replaced by up to 25% with vegetable oils in diets for *Seriola dumerili* juveniles, but total fish oil substitution is not feasible because it causes poor survival. The inclusion of probiotics in the FO-0+ diet had no effects on the parameters measured.

Keywords: fish oil replacement; *Seriola dumerili*; greater amberjack; antioxidant enzymes; blood parameters; fish health

Citation: Milián-Sorribes, M.C.; Peres, H.; Tomás-Vidal, A.; Moutinho, S.; Peñaranda, D.S.; Jover-Cerdá, M.; Oliva-Teles, A.; Martínez-Llorens, S. Hepatic, Muscle and Intestinal Oxidative Status and Plasmatic Parameters of Greater Amberjack (*Seriola dumerili*, Risso, 1810) Fed Diets with Fish Oil Replacement and Probiotic Addition. *Int. J. Mol. Sci.* **2023**, *24*, 6768. https://doi.org/10.3390/ijms24076768

Academic Editor: Maurizio Battino

Received: 1 March 2023
Revised: 1 April 2023
Accepted: 2 April 2023
Published: 5 April 2023

1. Introduction

In recent years, a large number of studies has focused on replacing fish oil (FO) in aquafeeds using fats or oils from plant or animal sources [1]. Nevertheless, high FO substitution in aquafeeds without compromising fish performance and health remains a challenge, especially in carnivorous species. Due to their low price and high and constant market availability, vegetable oils (VO) have been traditionally presented as the main option to solve the dependence on FO for aquafeeds, further contributing to more environmentally sustainable aquafeeds [2]. Furthermore, partial FO replacement with a mixture of VO sources allows for a reduction of FO dependency in fish [3–6]. Nevertheless, some VOs are rich in n-6 and n-9 fatty acids, mainly linoleic acid (18:2n-6) and oleic acid (OA, 18:1n-9), but lack n-3 long-chain polyunsaturated fatty acids (LC-PUFA), which are essential to achieve optimal fish growth [7]. Further, lack of n-3 might trigger negative effects on feed utilization,

induce inflammatory reactions, and depress oxidative capacity and, consequently, may reduce fish survival [8–10].

High dietary FO replacement has been linked to several side effects on fish health and stress [11–13] depending on the level of FO replacement, alternative oils included in the diet, dietary fatty acid profile, and fish species. An imbalance of n-3/n-6 LC-PUFAs triggers a stress response via altered eicosanoid production [9]. In addition, previous studies also reported negative effects in fish feed VOs, such as an increase in plasma cortisol levels [14] and a high hepatic triacylglycerol level [15]. Continuous cortisol secretion to the bloodstream has negative effects on fish feed intake, alters lipid and protein metabolism, and induces immunosuppression, increasing susceptibility to pathogens and infection [14,16,17].

On the other hand, the improvement of fish health through optimum nutrition is mandatory in smart aquaculture. In this sense, additives such as probiotics have been included in diets to counterbalance the negative effects caused by FO substitution, resulting in the strengthening of the immune system [18,19], nutrient digestibility [20], and increased fish stress resistance and survival [21].

FO substitution caused the alterations of the activities of digestive enzymes, antioxidant enzymes and the integrity of the mucosal barrier as well as in the intestinal microbiota, which participates and plays a key role in the recovery process [22–24]. Therefore, one of the strategies to palliate the alterations in intestinal health is to add a probiotic in the diet to improve the digestive process and fish health [22,25]. In aquaculture, the use of probiotics is very important as they colonize the intestinal mucosa and can displace pathogens and thus improve the health of the fish. This is an important aspect to better cope with the occurrence of diseases, especially in fish fed FO-free diets [26].

The greater amberjack (*Seriola dumerili*) is an excellent candidate for aquaculture diversification due to its higher growth as compared to other Mediterranean species and excellent sensory properties [6]. As marine fish have adapted to be fed high-lipid diets formulated with FO as the main lipid source, when dietary FO is substituted by vegetable oils, aspects such as immunological status, health, and welfare should be considered as they may be compromised [27–29].

Thus, this study aims to assess the effect of fish oil replacement with vegetable oils in diets for *Seriola dumerili* juveniles and its possible relation to oxidative stress alteration and health as well as to evaluate the potential benefits of *Lactobacillus brevis* and *L. buchneri* in fish fed with a complete FO replacement diet in different parameters to measure oxidative stress.

2. Results

2.1. Oxidative Status

Diet composition did not affect the oxidative stress enzyme activity in the liver and intestines except for glucose-6-phosphate dehydrogenase, where activity was higher in the liver in the FO-100 group and lower in the FO-0 group (Table 1). The dietary inclusion of probiotics in the FO-0 diet increased the glucose-6-phosphate dehydrogenase activity, which showed no differences compared to the other groups.

Table 1. Antioxidant enzyme activities [1] in the liver, foregut, and hindgut of Mediterranean yellowtail (*Seriola dumerili*) fed the experimental diets for 109 days.

	Diets			
	FO-100	**FO-25**	**FO-0**	**FO-0+**
Catalase				
Liver	808 ± 97.1	695 ± 125.9	596 ± 90.4	746 ± 137.5
Foregut	65.8 ± 13.27	72.8 ± 14.07	64.0 ± 14.07	42.3 ± 15.05
Hindgut	26.6 ± 12.15	30.5 ± 14.94	37.7 ± 11.50	12.0 ± 15.30
Superoxide dismutase				

Table 1. *Cont.*

	Diets			
	FO-100	**FO-25**	**FO-0**	**FO-0+**
Liver	127 ± 18.8	152 ± 18.8	121 ± 18.8	141 ± 91.8
Hindgut	74.7 ± 15.75	77.5 ± 19.42	56.5 ± 15.03	39.9 ± 19.22
Glutathione reductase				
Liver	12.4 ± 0.749	12.0 ± 0.764	13.3 ± 0.746	11.6 ± 0.765
Foregut	58.6 ± 8.56	55.5 ± 8.56	42.5 ± 8.56	30.0 ± 10.48
Hindgut	24.0 ± 2.98	23.3 ± 3.70	25.2 ± 2.80	22.0 ± 4.05
Glutathione peroxidase				
Liver	50.6 ± 5.87	55.8 ± 7.66	58.2 ± 5.49	52.9 ± 7.98
Foregut	435 ± 70.1	443 ± 70.1	324 ± 70.1	289 ± 79.4
Hindgut	154 ± 22.0	144 ± 22.0	126 ± 25.4	116 ± 20.7
Glucose-6-phosphate dehydrogenase				
Liver	98.6 ± 11.89 ^{a}	88.4 ± 15.35 ^{ab}	54.7 ± 11.16 ^{b}	93.0 ± 15.19 ^{ab}
Foregut	6.42 ± 1.40	5.24 ± 1.48	6.04 ± 1.40	4.03 ± 1.71
Hindgut	2.00 ± 0.595	2.85 ± 0.557	3.36 ± 0.557	2.40 ± 0.525

[1] Enzyme activities expressed as U/mg protein^{-1} for catalase and superoxide dismutase and mU/mg protein^{-1} for glutathione reductase, glutathione peroxidase, and glucose-6-phosphate dehydrogenase. Values represent the mean ± standard error (n = 9). Different superscript letters indicate significant differences between the treatments ($p < 0.05$), Bonferroni test.

No differences were observed in the liver for the total, reduced, or oxidized glutathione levels and for the oxidative stress index (Table 2). On the other hand, lipid peroxidation (expressed as nmols MDA per gram of tissue) was affected by diet composition in the liver, foregut, and red muscle (Table 3). In the liver, MDA was higher in the control group (FO-100) than in the FO-0+ group, while the opposite was observed in the foregut. In red muscle, MDA levels were higher in the fish fed FO-100 diets than in those fed the FO-0 and FO-0+ diets.

Table 2. Total glutathione (tGSH), reduced glutathione (GSH), oxidized glutathione (GSSG) and oxidative stress index (OSI) in the liver of Mediterranean yellowtail (*Seriola dumerili*) fed the experimental diets for 109 days.

	Diets			
	FO-100	**FO-25**	**FO-0**	**FO-0+**
tGSH (nmol g^{-1} tissue)	1254 ± 92.8	1161 ± 84.7	936 ± 92.8	1025 ± 92.8
GSH (nmol g^{-1} tissue)	1211 ± 91.8	1125 ± 83.8	914 ± 91.8	987 ± 91.8
GSSG (nmol g^{-1} tissue)	43.3 ± 6.26	35.5 ± 5.72	22.0 ± 6.26	37.7 ± 6.26
GSH/GSSG	44.4 ± 14.4	51.9 ± 14.4	72.6 ± 14.4	27.1 ± 17.1
OSI (%)	7.09 ± 1.14	6.28 ± 1.04	4.52 ± 1.14	7.44 ± 1.14

Values represent the mean ± standard error (n = 9).

Table 3. Lipid peroxidation levels (nmols MDA/g^{-1} tissue) in the liver, foregut, hindgut, white muscle, and red muscle of Mediterranean yellowtail (*Seriola dumerili*) fed the experimental diets for 109 days.

	Diets			
	FO-100	**FO-25**	**FO-0**	**FO-0+**
Liver	14.2 ± 0.949 ^{a}	11.8 ± 0.837 ^{ab}	11.3 ± 0.837 ^{ab}	10.7 ± 0.837 ^{b}
Foregut	10.8 ± 1.86 ^{b}	12.6 ± 2.36 ^{ab}	11.7 ± 1.72 ^{ab}	18.2 ± 2.44 ^{a}
Hindgut	11.0 ± 1.59	12.5 ± 1.59	12.6 ± 1.50	11.4 ± 1.59
White muscle	7.74 ± 1.33	6.25 ± 1.54	7.28 ± 1.33	7.15 ± 1.33
Red muscle	8.44 ± 0.468 ^{a}	7.18 ± 0.505 ^{ab}	5.90 ± 0.438 ^{b}	6.16 ± 0.413 ^{b}

Values represent the mean ± standard error (n = 9). Different superscript letters indicate significant differences between the treatments ($p < 0.05$), Bonferroni test.

2.2. Blood Parameters

As FO substitution increased, the cholesterol level reduced, and was significantly lower in the fish fed the diets deprived of fish oil than in the control (Table 4). No further differences were observed regarding the other parameters measured.

Table 4. Hematological parameters of Mediterranean yellowtail (*Seriola dumerili*) fed the experimental diets for 109 days.

	Diets			
	FO-100	**FO-25**	**FO-0**	**FO-0+**
Hemoglobin (g/dL)	10.1 ± 0.56	9.56 ± 0.63	9.85 ± 0.46	9.10 ± 0.50
RBC [1] (number × 10^6/μL)	2.59 ± 0.38	2.46 ± 0.44	2.66 ± 0.38	2.52 ± 0.41
Hematocrit (%)	30.4 ± 6.00	32.1 ± 6.95	30.9 ± 6.08	29.6 ± 6.42
Glucose (mg/dL)	97.3 ± 14.2	129.1 ± 12.0	97.2 ± 12.0	88.4 ± 12.5
Cholesterol (mg/dL)	168.2 ± 7.40 [a]	151.4 ± 7.40 [ab]	128.4 ± 7.40 [b]	124.4 ± 7.40 [b]
Triglycerides (mg/dL)	105.8 ± 7.06	103.8 ± 6.54	107.6 ± 6.54	106.6 ± 6.54
LDH [2] (U/L)	16,278 ± 3241.6	10,210 ± 2873.4	7049 ± 2981.9	12,155 ± 2873.4
Cortisol (μg/dL)	10.8 ± 5.14	13.9 ± 5.70	10.4 ± 5.30	13.8 ± 5.57

[1] Red blood cells; [2] lactate dehydrogenase. Values represent the mean ± standard error (n = 14). Different superscript letters indicate significant differences between the treatments ($p < 0.05$), Bonferroni test.

3. Discussion

Previous studies in fish reported an improvement of antioxidant defenses when the level of marine fatty acids was increased in the diet for seabream [30], and likewise, n-3 HUFA levels influenced the antioxidant capacity of juvenile black seabream, increased n-3 HUFA levels in the diet lead to increased MDA content in the liver and serum [31]. Further, fish oil replacement with vegetable oils can negatively affect lipid peroxidation and oxidative stress, which could lead to impaired membrane function and the reduction of endogenous antioxidant enzyme activity in fish [32]. For instance, in a previous study with *Nibea coibor* [33], it was observed that both SOD and CAT activities increased as the levels of fish oil substitution increased, being higher in fish fed a palm oil diet rather than a fish oil diet. Furthermore, in *Oncorhynchus mykiss* broodstock [34], SOD and GPX increased with increasing levels of fish oil substitution with vegetable oils. In the same study, liver CAT activity followed a negative relationship with FO substitution. During the last few years, measures have been sought to increase the antioxidant defense activity in different fish species. Among them, microbial feed additives showed promising effects on the antioxidant enzyme activity [35].

Nevertheless, in the present study, no significant differences in oxidative stress parameters were found despite the different dietary marine fatty acids in the diets, though a tendency to decrease the antioxidant enzyme activity as fish oil substitution increased was noticed, suggesting a detriment of oxidative defenses. This trend was statistically significant only for liver glucose-6-phosphate dehydrogenase (G6PD) activity. The major physiological role of G6PD is to produce NADPH [36], crucial for reductive biosynthesis [37] required to renew reduced glutathione (GSH), preserve the integrity of cell membrane sulfhydryl groups, and detoxify hydrogen peroxide and oxygen radicals in cells [38]. Nevertheless, the differences in G6PD were only observed in the fish fed the FO-0 diet, although the highest mortality was in the fish fed the FO-0+ diet.

MDA levels indirectly reflect the antioxidant capacity and the overall oxidative status of fish [39]. In the present study, the oxidation status was different depending on the tissue studied. Lipid peroxidation levels were higher in the FO-100 diet in the liver and red muscle than in the other tissues examined. These findings agree with observations in black sea buckthorn (*Acanthopagrus schlegelii*): increased MDA content along with an increase in dietary long-chain polyunsaturated fatty acids levels (n-3 LC-HUFAs) [31]. Previous studies demonstrated that excess n-3 LC-PUFAs in the liver are more likely to cause lipid peroxidation [40].

Comparing FO-0 with FO-0+, no significant differences were found, the CAT and SOD enzyme activities increased and the decrease in MDA concentrations in the liver in the fish fed FO-0+ may suggest a slight improvement in the antioxidant capacity of the fish. Similar results to those were found in common carp [41] in which probiotics increased CAT and SOD activity, as well as antioxidant capacity. Furthermore, in *Pangasianodon hypophthalmus* [42], they found that the addition of probiotics caused an increase in digestive enzymes and enzyme activity. However, in these studies, the difference was notable between the diets containing the probiotic and the control. In our study, the poor effect of probiotics could be due to the fact that the probiotic species were not the most suitable for *Seriola dumerili* or because the concentration of probiotics was not adequate.

The MDA contents of the liver and muscle of the fish fed with high levels of vegetable oils significantly decreased, as previously reported in other species [43–45], but in the case of the liver, this decrease was only observed when the probiotic was added. To the best of our knowledge, this is the first study that reports the antioxidant capacity of *Lactobacillus* as a probiotic in diets with high fish oil replacement, but the results are not conclusive as the oxidative status levels in response to the dietary inclusion of probiotics were tissue-dependent.

Probiotics in fish should produce metabolites with antioxidative abilities such as glutathione, folate, and butyrate [35]. These processes could positively influence the antioxidant capacity. However, the specific roles of each probiotic species and their effects on antioxidant capacity in fish need further study.

Blood metabolites have been widely used to provide information on the nutritional status and health of fish [46–48]. Hematological parameters can be considered good indicators of changes in fish. Situations of anemia, nutritional deficiencies or malnutrition affect hematocrit values [5]. To our knowledge, no previous studies assessed blood parameters in response to fish oil substitution in diets for greater amberjack. In this study, except for cholesterol, blood parameters were not affected by diet composition. Plasma cholesterol significantly decreased with the increase in vegetable oils in the diets. Similar results have been found in other species when fish oil was substituted with vegetable oils, for instance, in sea bass *D. labrax* and black sea bream *Acanthopagrus schlegeli* [49,50]. This was expected as VOs are rich in phytosterols which reduce cholesterol levels [51,52].

The hemoglobin and hematocrit values were lower than those observed in another study in the same species [53], probably due to the differences in fish weight (136 g compared to the 422 g average weight in the present experiment). This has also been noticed in other fish species, such as siluroid (*Heteropneustes fossilis*) [54], where the erythrocyte and leucocyte counts and hemoglobin concentration are higher in smaller fish and decrease as the animal grows and the hematocrit values and the mean corpuscular volumes decrease with the increase in fish weight.

In this study, plasma triglycerides levels are within the range reported for greater amberjack under good nutritional status [53]. Plasma cortisol, LDH, and glucose variations can be related to differences in diet composition and physiological changes related to stress. In the present study, no differences among treatments were observed in these parameters. This is similar to what was observed in *S. quinqueradiata* [55] juveniles fed diets where fish oil was replaced by a vegetable oil. Increases in glucose and cortisol levels normally appear as a response to chronic stress in fish. In our study, the addition of probiotics caused an increase in cortisol and a decrease in glucose in the groups without FO in the diet, therefore, probiotics had no stress-mitigating effect according to the parameters studied in the blood. This is different from the results obtained in many studies in which the addition of probiotics reduced the stress in fish [35,56–59]. The lack of differences in these plasma parameters also indicates that the fish were not suffering from stress related to diet.

The results of this study indicate that full substitution of fish oil for vegetable oils does not significantly affect the *Seriola dumerili* oxidative stress. The inclusion of a *Lactobacillus* probiotic in the diet with complete FO replacement did not have positive effects on oxidative

stress, and no significant differences were found in antioxidant enzyme activity, lipid peroxidation, or hematological parameters.

4. Materials and Methods

4.1. Fish and Experimental Diets

Greater amberjack juveniles (*Seriola dumerili*) (160 ± 5.3 g) were obtained from Futuna Blue SA (Cádiz, Spain) and moved to Universitat Politècnica de València facilities. Before starting the experiment, the animals were acclimatized to the laboratory conditions for one month and fed a standard feed (52% protein and 15% lipids).

After acclimatization, 25 fish (175 g ± 3.62 g) per tank were randomly distributed in 12 tanks, three per diet, with a capacity of 1750 L. The fish were fed until apparent satiation, twice daily (9:00 a.m.–16:00 p.m.), six days a week, for 109 days. The photoperiod was natural, and all the tanks had similar light conditions. Water temperature was maintained between 17.0 °C and 19.1 °C, salinity—around 30 ± 1 g/L^{-1}, oxygen level—6.7 ± 0.04 mg/L^{-1}, and pH—between 7.5 and 7.8. Ammonium, nitrite, and nitrate levels were maintained at 0.18 ± 0.07, 0.37 ± 0.05, and 93.2 ± 6.88 mg/L^{-1}, respectively.

Four isoproteic (52% crude protein) and isolipidic (15% crude lipids) feeds were formulated (Table 5): a control diet (FO-100) without FO substitution, a diet with 25% of FO (FO-25), and another diet without FO inclusion (FO-0). FM provided 3% of CL in all diets. Additionally, a fourth diet was prepared (FO-0+), with the same formulation as FO-0 but adding *Lactobacillus brevis* and *L. buchneri* (5.0×10^7 UCF g^{-1}) with a mix of 50% of each species as probiotic bacteria.

Table 5. Formulation (g/kg^{-1}) of the experimental diets. Feed ingredients and proximate composition.

	FO-100	FO-25	FO-0 [1]
Ingredients (g/kg)			
Fish meal	350	350	350
Wheat	100	100	100
Defatted soybean meal	185	185	185
Iberian meat meal	110	110	110
Fish oil	95	24	0
Linseed oil	–	28	38
Sunflower oil	–	21	28
Palm oil	–	22	29
Multivitamins and minerals mix [2]	20	20	20
Analyzed composition (% dry weight)			
Dry matter (%DM)	89.3	89.7	89.4
Crude protein (%CP)	52.2	52.5	52.1
Crude lipid (CL)	14.5	14.4	14.4
Ash (%)	7.3	9.1	7.4
EPA (% total FA)	5.8	4.3	2.8
DHA (% total FA)	13	7.6	4.3

[1] The FO-0+ diet details are not shown in the table because it had the same ingredients as FO 0 except for the addition of probiotics *Lactobacillus brevis* and *Lactobacillus buchneri* (concentration of 5 mL per each 500 g). [2] Vitamins and minerals mixture (g/kg^{-1}): premix, 25; Hill, 10; DL-a-tocopherol, 5; ascorbic acid, 5; $(PO_4)_2Ca_3$, 5. Pre-mixture composition: retinol acetate, 1,000,000 IU/kg^{-1}; calcipherol, 500 IU/kg^{-1}; DL-a-tocopherol, 10; menadione sodium bisulfite, 0.8; thiamine hydrochloride, 2.3; riboflavin, 2.3; pyridoxine hydrochloride, 15; cyanocobalamin, 25; nicotinamide, 15; pantothenic acid, 6; folic acid, 0.65; biotin, 0.07; ascorbic acid, 75; inositol, 15; betaine, 100; 12 polypeptides.

4.2. Diets' Hemical Analysis

Diets' chemical analyses were carried out in the Animal Science Technology at Universitat Politècnica de Valencia. The fatty acid composition was analyzed by gas chromatography on a FINNIGAN FOCUS 6C chromatograph (AI 3000) after direct synthesis of methyl esters (FAME) prepared according to O'Fallon [60]. Dry matter (105 °C to constant weight), ash (by incineration at 550 °C to constant weight), fat (Ankom XT10 extraction system), and

protein content (Dumas method) were determined according to the AOAC [61]. The Dumas method consists in the transformation of nitrogen into the gaseous state by calcination and its determination by thermal conductivity using a LECO CN 628 protein analyzer. All the analyses were performed in triplicate.

4.3. Enzyme Activity and Lipid Peroxidation Determination in Muscle, Liver, and Intestines

At the end of the experiment, liver, foregut, and hindgut samples of three fish per tank (nine fish per group) were collected and immediately frozen using liquid nitrogen and stored at –80 °C for later analysis. Muscle was also collected; red muscle was carefully dissected from white muscle, and both tissues were immediately frozen with liquid nitrogen and stored at −80 °C for later analysis.

Liver and intestine samples were diluted 1:9 and 1:4, respectively, and homogenized at pH 7.8 in an ice-cold 100 mM Tris HCl buffer containing 0.1 mM EDTA and 0.1% (*v*/*v*) Triton X-100. Homogenates were centrifuged at 30,000× *g* for 30 min at 4 °C and the resulting supernatants were separated into aliquots and stored at –80 °C for further enzyme assays. All enzyme activities were measured at 37 °C on a Multiskan GO microplate reader (Model 5111 9200; Thermo Scientific, Nanjing, China).

Glucose-6-phosphate dehydrogenase (G6PDH; EC 1.1.1.49) activities were assayed as described in [62]. Enzyme activities were determined by monitoring changes in NADH or NADP absorbance at 340 nm.

Oxidative stress enzymes were assayed as follows: superoxide dismutase (SOD; EC 1.15.1.1) activity was measured at 550 nm by the ferricytochrome C method using xanthine/xanthine oxidase as a source of superoxide radicals [63]. Catalase activity (CAT; EC 1.11.1.6) was determined according to [64] by measuring the decrease in hydrogen peroxide concentration at 240 nm. Glutathione reductase activity (GR; EC 1.6.4.2) was determined at 340 nm by measuring NADPH oxidation as described in [65]. Glutathione peroxidase activity (GPX; EC 1.11.1.9) was assayed as described. The GSSG generated by GPX was reduced according to [66]. GR and the rate of NADPH consumption were monitored at 340 nm.

One unit of SOD enzyme activity was defined as the amount of enzyme required to produce a 50% inhibition of the reduction rate of ferricytochrome C. All other enzyme activities were expressed as units (CAT) or milliunits (G6PDH, GPX, and GR) per milligram of soluble protein (specific activity). One unit of enzyme activity was defined as the amount of enzyme required to transform 1 µmol of substrate per minute under the assay conditions. Total protein concentration was determined according to [67] as described above.

Hepatic, intestinal (foregut and hindgut), and muscle (white and red) lipid peroxidation levels were determined as malondialdehyde concentration (MDA) according to [68]. A 100 µL aliquot of supernatant from the homogenate was mixed with 500 µL of a prepared solution (15% (*w*/*v*) TCA (Sigma, St. Louis, MO, USA), 0.375% (*w*/*v*) thiobarbituric acid (Sigma), 80% (*v*/*v*) HCl 0.25 N, and 0.01% (*w*/*v*) butylated hydroxytoluene (BTH) (Sigma)). The mixture was heated to 100 °C for 15 min, cooled to ambient temperature, and centrifuged at 1500 g for 10 min. The supernatant was collected and the absorbance was measured at 535 nm. Concentration was expressed as nmol MDA per g of wet tissue.

4.4. Glutathione and Oxidative Stress Index in the Liver

Portions of the liver were homogenized in nine volumes of an ice-cold solution containing 1.3% 5-sulphosalicylic acid (*w*/*v*) and 10 mM HCl. The homogenates were centrifuged at 14,000× *g* for 10 min at 4 °C, and the supernatants were analyzed.

Total glutathione (tGSH) and GSSG were measured following the method described in [69] and [70] with modifications. Both tGSH and GSSG analyses were carried out at 37 °C, and changes in absorbance due to the reduction of 5,5′-dithiobis (2-nitrobenzoic acid) (DTNB) were monitored at 405 nm in a Multiskan GO microplate reader. The molar extinction coefficient used for DTNB was 13,600 $M^{-1} \times cm^{-1}$. Total GSH was determined using a reaction mixture containing 133 mM phosphate buffer with 5.8 mM EDTA at pH 7.4,

0.71 mM DTNB, 0.24 mM NADPH, and 1.2 IU/mL GR. GSSG was measured using an aliquot from the solution obtained after 60 min of incubation of 100 µL of the sample with 2 µL vinylpyridine and 6 µL 1.5 M triethanolamine. The reaction mixture contained 122 mM phosphate buffer with 5.4 mM EDTA at pH 7.4, 0.71 mM DTNB, 0.24 mM NADPH, and 1.2 IU/mL^{-1} GR.

The results were calculated using standard curves of reduced glutathione (GSH) and GSSG for tGSH and GSSG measurements, respectively. The GSH level was calculated by subtracting GSSG from the tGSH values. The data are expressed as nmol per gram of tissue. The oxidative stress index (OSI) was calculated as follows: OSI (%) = 100 × (2 × GSSG/tGSH).

4.5. Blood Parameters

At the end of the experiment, 15 fish per experimental group were anesthetized and blood samples were collected by puncturing the caudal vein using heparinized syringes with an anticoagulant. The samples were immediately stored at 4 °C for later analysis.

The glucose, LDH, cholesterol, and triglyceride concentrations were determined by ultraviolet spectrophotometry (Ortho Clinical Diagnostics, Raritan, NJ, EUA), the cortisol concentration—by chemiluminescence. The red blood cell count was determined in a Neubauer chamber, the hematocrit percentage—using a manual microhematocrit method, and hemoglobin—by means of spectrophotometry. All the analyses were performed by the ICTIOVET S.C.P. laboratory.

4.6. Statistical Analysis

The data were evaluated by analysis of variance (ANOVA), following a completely randomized design. To determine significant differences between the treatments, the Bonferroni test was applied at the 5% significance level, using the statistical program Statgraphics Centurion XVII.

Author Contributions: Conceptualization, S.M.-L. and A.T.-V.; methodology, S.M.-L. and A.T.-V.; formal analysis, S.M., H.P. and M.C.M.-S.; investigation, S.M.-L. and A.T.-V.; resources, S.M.-L. and A.T.-V.; data curation, M.C.M.-S.; writing—original draft preparation, S.M. and M.C.M.-S.; writing—review and editing, D.S.P., H.P. and A.O.-T.; visualization, S.M-L.; supervision, H.P., A.O.-T. and S.M.-L.; project administration, M.J.-C.; funding acquisition, M.J.-C. and A.T.-V. All authors have read and agreed to the published version of the manuscript.

Funding: Valencian government (Conselleria d'Educació, Cultura i Esport) provided financial support (reference No. AICO/2015/123). AYUDAS PARA INVESTIGADORES PREDOCTORALES PARA PUBLICACIÓN PAID-12-21.-"Seriola dumerili". Universitat Politècnica de València.

Institutional Review Board Statement: This study complies with the 2010/63/EU directive, on which the Spanish regulations on the protection of animals in experimentation (Spanish Royal Decree 53/2013) are based. UPV Ethics and Animal Welfare Committee approved the protocol for the conduct of this experimental study. During the experiment, the fish were checked twice a day. Every month, their weight and health status were checked individually, and to do so, they were anesthetized with clove oil dissolved in water (0.01 mg/L^{-1} of water). Finally, the animals were euthanized with an excess of clove oil (150 mg/L^{-1}) and then dissected to collect liver and intestine samples.

Informed Consent Statement: Not applicable.

Data Availability Statement: Not applicable.

Conflicts of Interest: The authors declare no conflict of interest.

References

1. Bowyer, J.N.; Qin, J.G.; Smullen, R.P.; Stone, D.A.J. Replacement of fish oil by poultry oil and canola oil in yellowtail kingfish (*Seriola lalandi*) at optimal and suboptimal temperatures. *Aquaculture* **2012**, *356*, 211–222. [CrossRef]
2. Bordignon, F.; Trocino, A.; Sturaro, E.; Martínez-Llorens, S.; Tomas-Vidal, A.; Xiccato, G.; Berton, M. Fish oil substitution with vegetable oils in diets for greater amberjack (*Seriola dumerili*): A consequential life cycle assessment approach. *Aquaculture* **2023**, *563*, 738903. [CrossRef]

3. Oliva-Teles, A.; Enes, P.; Peres, H. Replacing fishmeal and fish oil in industrial aquafeeds for carnivorous fish. *Feed. Feed. Pract. Aquac.* **2015**, *2015*, 203–233.
4. Nogales-Mérida, S.; Tomás-Vidal, A.; Cerdá, M.J.; Martínez-Llorens, S. Growth performance, histological alterations and fatty acid profile in muscle and liver of sharp snout sea bream (*Diplodus puntazzo*) with partial replacement of fish oil by pork fat. *Aquac. Int.* **2011**, *19*, 917–929. [CrossRef]
5. Ribeiro, L.; Moura, J.; Santos, M.; Colen, R.; Rodrigues, V.; Bandarra, N.; Soares, F.; Ramalho, P.; Barata, M.; Dias, J.; et al. Effect of vegetable based diets on growth, intestinal morphology, activity of intestinal enzymes and haematological stress indicators in meagre (*Argyrosomus regius*). *Aquaculture* **2015**, *447*, 116–128. [CrossRef]
6. Monge-Ortiz, R.; Tomás-Vidal, A.; Rodriguez-Barreto, D.; Martínez-Llorens, S.; Pérez, J.A.; Jover-Cerdá, M.; Lorenzo, A. Replacement of fish oil with vegetable oil blends in feeds for greater amberjack (*Seriola dumerili*) juveniles: Effect on growth performance, feed efficiency, tissue fatty acid composition and flesh nutritional value. *Aquac. Nutr.* **2018**, *24*, 605–615. [CrossRef]
7. Turchini, G.M.; Torstensen, B.E.; Ng, W.K. Fish oil replacement in finfish nutrition. *Rev. Aquac.* **2009**, *1*, 10–57. [CrossRef]
8. Du, J.; Xu, H.; Li, S.; Cai, Z.; Mai, K.; Ai, Q. Effects of dietary chenodeoxycholic acid on growth performance, body composition and related gene expression in large yellow croaker (*Larimichthys crocea*) fed diets with high replacement of fish oil with soybean oil. *Aquaculture* **2017**, *479*, 584–590. [CrossRef]
9. Hundal, B.K.; Liland, N.S.; Rosenlund, G.; Höglund, E.; Araujo, P.; Stubhaug, I.; Sissener, N.H. Increasing the dietary n-6/n-3 ratio alters the hepatic eicosanoid production after acute stress in Atlantic salmon (*Salmo salar*). *Aquaculture* **2021**, *534*, 736272. [CrossRef]
10. Chen, Y.; Sun, Z.; Liang, Z.; Xie, Y.; Su, J.; Luo, Q.; Zhu, J.; Liu, Q.; Han, T.; Wang, A. Effects of dietary fish oil replacement by soybean oil and L-carnitine supplementation on growth performance, fatty acid composition, lipid metabolism and liver health of juvenile largemouth bass, *Micropterus salmoides*. *Aquaculture* **2020**, *516*, 734596. [CrossRef]
11. Serradell, A.; Torrecillas, S.; Makol, A.; Valdenegro, V.; Fernández-Montero, A.; Acosta, F.; Montero, D. Prebiotics and phytogenics functional additives in low fish meal and fish oil based diets for European sea bass (*Dicentrarchus labrax*): Effects on stress and immune responses. *Fish Shellfish. Immunol.* **2020**, *100*, 219–229. [CrossRef]
12. Calduch-Giner, J.A.; Sitjà-Bobadilla, A.; Davey, G.C.; Cairns, M.T.; Kaushik, S.; Pérez-Sánchez, J. Dietary vegetable oils do not alter the intestine transcriptome of gilthead sea bream (*Sparus aurata*), but modulate the transcriptomic response to infection with Enteromyxum leei. *BMC Genom.* **2012**, *13*, 470. [CrossRef]
13. Oxley, A.; Jolly, C.; Eide, T.; Jordal, A.-E.O.; Svardal, A.; Olsen, R.-E. The combined impact of plant-derived dietary ingredients and acute stress on the intestinal arachidonic acid cascade in Atlantic salmon (*Salmo salar*). *Br. J. Nutr.* **2010**, *103*, 851–861. [CrossRef]
14. Ganga, R.; Montero, D.; Bell, J.G.; Atalah, E.; Ganuza, E.; Vega-Orellana, O.; Izquierdo, M. Stress response in sea bream (*Sparus aurata*) held under crowded conditions and fed diets containing linseed and/or soybean oil. *Aquaculture* **2011**, *311*, 215–223. [CrossRef]
15. Alvheim, A.R.; Torstensen, B.E.; Lin, Y.H.; Lillefosse, H.H.; Lock, E.-J.; Madsen, L.; Malde, M.K. Dietary linoleic acid elevates endogenous 2-arachidonoylglycerol and anandamide in Atlantic salmon (*Salmo salar* L.) and mice, and induces weight gain and inflammation in mice. *Br. J. Nutr.* **2013**, *109*, 1508–1517. [CrossRef] [PubMed]
16. Turchini, G.M.; Ng, W.; Tocher, D. *Fish Oil Replacement and Alternative Lipid Sources in Aquaculture Feeds*; CRC Press: Boca Raton, FL, USA, 2011.
17. Estruch, G.; Collado, M.C.; Peñaranda, D.S.; Tomás-Vidal, A.; Jover-Cerdá, M.; Pérez Martínez, G.; Martinez-Llorens, S. Impact of fish meal replacement in diets for gilthead sea bream (*Sparus aurata*) on the gastrointestinal microbiota determined by pyrosequencing the 16S rRNA gene. *PLoS ONE* **2015**, *10*, e0136389. [CrossRef] [PubMed]
18. Amoah, K.; Huang, Q.C.; Tan, B.P.; Zhang, S.; Chi, S.Y.; Yang, Q.H.; Dong, X.H. Dietary supplementation of probiotic *Bacillus coagulans* ATCC 7050, improves the growth performance, intestinal morphology, microflora, immune response, and disease confrontation of Pacific white shrimp, *Litopenaeus vannamei*. *Fish Shellfish. Immunol.* **2019**, *87*, 796–808. [CrossRef]
19. Verschuere, L.; Rombaut, G.; Sorgeloos, P.; Verstraete, W. Probiotic Bacteria as Biological Control Agents in Aquaculture. *Microbiol. Mol. Biol. Rev.* **2000**, *64*, 655–671. [CrossRef] [PubMed]
20. Akhter, N.; Wu, B.; Memon, A.M.; Mohsin, M. Probiotics and prebiotics associated with aquaculture: A review. *Fish Shellfish. Immunol.* **2015**, *45*, 733–741. [CrossRef] [PubMed]
21. Aly, S.M.; Abdel-Galil Ahmed, Y.; Abdel-Aziz Ghareeb, A.; Mohamed, M.F. Studies on *Bacillus subtilis* and *Lactobacillus acidophilus*, as potential probiotics, on the immune response and resistance of Tilapia nilotica (*Oreochromis niloticus*) to challenge infections. *Fish Shellfish. Immunol.* **2008**, *25*, 128–136. [CrossRef]
22. Kong, Y.; Liao, Z.; Ma, X.; Liang, M.; Xu, H.; Mai, K.; Zhang, Y. Response of Intestinal Microbiota of Tiger Puffer (*Takifugu rubripes*) to the Fish Oil Finishing Strategy. *Microorganisms* **2023**, *11*, 208. [CrossRef]
23. Rimoldi, S.; Torrecillas, S.; Montero, D.; Gini, E.; Makol, A.; Victoria Valdenegro, V.; Terova, G. Assessment of dietary supplementation with galactomannan oligosaccharides and phytogenics on gut microbiota of European sea bass (*Dicentrarchus labrax*) fed low fishmeal and fish oil based diet. *PLoS ONE* **2020**, *15*, e0231494. [CrossRef] [PubMed]
24. Torrecillas, S.; Mompel, D.; Caballero, M.J.; Montero, D.; Merrifield, D.; Rodiles, A.; Izquierdo, M. Effect of fishmeal and fish oil replacement by vegetable meals and oils on gut health of European sea bass (*Dicentrarchus labrax*). *Aquaculture* **2017**, *468*, 386–398. [CrossRef]

25. Baumgärtner, S.; James, J.; Ellison, A. The supplementation of a prebiotic improves the microbial community in the gut and the skin of Atlantic salmon (*Salmo salar*). *Aquac. Rep.* **2022**, *25*, 101204. [CrossRef] [PubMed]
26. Milián-Sorribes, M.C.; Martínez-Llorens, S.; Cruz-Castellón, C.; Jover-Cerdá, M.; Tomás-Vidal, A. Effect of fish oil replacement and probiotic addition on growth, body composition and histological parameters of yellowtail (*Seriola dumerili*). *Aquac. Nutr.* **2021**, *27*, 3–16. [CrossRef]
27. Kiron, V.; Fukuda, H.; Takeuchi, T.; Watanabe, T. Essential fatty acid nutrition and defence mechanisms in rainbow trout *Oncorhynchus mykiss*. *Comp. Biochem. Physiol. A Physiol.* **1995**, *111*, 361–367. [CrossRef]
28. Kiron, V.; Thawonsuwan, J.; Panigrahi, A.; Scharsack, J.P.; Satoh, S. Antioxidant and immune defences of rainbow trout (*Oncorhynchus mykiss*) offered plant oils differing in fatty acid profiles from early stages. *Aquac. Nutr.* **2011**, *17*, 130–140. [CrossRef]
29. Montero, D.; Grasso, V.; Izquierdo, M.S.; Ganga, R.; Real, F.; Tort, L.; Acosta, F. Total substitution of fish oil by vegetable oils in gilthead sea bream (*Sparus aurata*) diets: Effects on hepatic Mx expression and some immune parameters. *Fish Shellfish. Immunol.* **2008**, *24*, 147–155. [CrossRef]
30. Magalhães, R.; Martins, N.; Fontinha, F.; Couto, A.; Serra, C.R.; Santos, R.A.; Oliva-Teles, A. Effects of dietary ARA, DHA, and carbohydrates levels on gilthead sea bream liver and intestine oxidative stress, tissue histomorphology, and gut microbiota. *Aquaculture* **2022**, *552*, 738014. [CrossRef]
31. Jin, M.; Lu, Y.; Yuan, Y.; Li, Y.; Qiu, H.; Sun, P.; Zhou, Q.C. Regulation of growth, antioxidant capacity, fatty acid profiles, hematological characteristics and expression of lipid related genes by different dietary n-3 highly unsaturated fatty acids in juvenile black seabream (*Acanthopagrus schlegelii*). *Aquaculture* **2017**, *471*, 55–65. [CrossRef]
32. Peng, X.; Li, F.; Lin, S.; Chen, Y. Effects of total replacement of fish oil on growth performance, lipid metabolism and antioxidant capacity in tilapia (*Oreochromis niloticus*). *Aquac. Int.* **2016**, *24*, 145–156. [CrossRef]
33. Huang, Y.; Wen, X.; Li, S.; Li, W.; Zhu, D. Effects of Dietary Fish Oil Replacement with Palm Oil on the Growth, Feed Utilization, Biochemical Composition, and Antioxidant Status of Juvenile Chu's Croaker, *Nibea coibor*. *J. World Aquac. Soc.* **2016**, *47*, 786–797. [CrossRef]
34. Khezrian, S.; Salati, A.P.; Agh, N.; Pasha-Zanoosi, H. Effect of replacement of fish oil with different plant oils in *oncorhynchus mykiss* broodstocks diets on egg and larval antioxidant defense development. *Vet. Res. Forum* **2020**, *11*, 83–88. [PubMed]
35. Hoseinifar, S.H.; Yousefi, S.; Van Doan, H.; Ashouri, G.; Gioacchini, G.; Maradonna, F.; Carnevali, O. Oxidative Stress and Antioxidant Defense in Fish: The Implications of Probiotic, Prebiotic, and Synbiotics. *Rev. Fish. Sci. Aquac.* **2021**, *29*, 198–217. [CrossRef]
36. Çiltaş, A.; Erdoğan, O.; Hisar, O.; Çiftçi, M. Effects of Chloramine-T and $CuSO_4$ on Enzyme Activity of Glucose 6-Phosphate Dehydrogenase From Rainbow Trout (*Oncorhynchus Myskiss*) Erythrocytes In Vitro an In Vivo. *Isr. J. Aquac. Bamidgeh* **2003**, *55*, 187–196. [CrossRef]
37. Bianchi, D.; Bertrand, O.; Haupt, K.; Coello, N. Effect of gluconic acid as a secondary carbon source on non-growing L-lysine producers cells of Corynebacterium glutamicum. Purification and properties of 6-phosphogluconate dehydrogenase. *Enzym. Microb. Technol.* **2001**, *28*, 754–759. [CrossRef]
38. Das, J.; Ghosh, J.; Manna, P.; Sil, P.C. Taurine protects rat testes against doxorubicin-induced oxidative stress as well as p53, Fas and caspase 12-mediated apoptosis. *Amino Acids* **2012**, *42*, 1839–1855. [CrossRef]
39. Tan, X.; Sun, Z.; Liu, Q.; Ye, H.; Zou, C.; Ye, C.; Wang, A.; Lin, H. Effects of dietary ginkgo biloba leaf extract on growth performance, plasma biochemical parameters, fish composition, immune responses, liver histology, and immune and apoptosis-related genes expression of hybrid grouper (*Epinephelus lanceolatus*♂ × *Epinephelus fuscoguttatus*♀) fed high lipid diets. *Fish Shellfish. Immunol.* **2018**, *72*, 399–409.
40. Lu, K.L.; Xu, W.N.; Wang, L.N.; Zhang, D.D.; Zhang, C.N.; Liu, W.B. Hepatic β-oxidation and regulation of carnitine palmitoyltransferase (CPT) I in blunt snout bream *Megalobrama amblycephala* fed a high fat diet. *PLoS ONE* **2014**, *9*, e93135. [CrossRef] [PubMed]
41. Wang, L.; Ge, C.; Wang, J.; Dai, J.; Zhang, P.; Li, Y. Effects of different combinations of *Bacillus* on immunity and antioxidant activities in common carp. *Aquac. Int.* **2017**, *25*, 2091–2099. [CrossRef]
42. Abdel-Latif, H.M.R.; Chaklader, M.R.; Shukry, M.; Ahmed, H.A.; Khallaf, M.A. A multispecies probiotic modulates growth, digestive enzymes, immunity, hepatic antioxidant activity, and disease resistance of *Pangasianodon hypophthalmus* fingerlings. *Aquaculture* **2023**, *563*, 738948. [CrossRef]
43. Gou, N.; Ji, H.; Zhong, M.; Chang, Z.; Deng, W. Effects of dietary fish oil replacements with three vegetable oils on growth, fatty acid composition, antioxidant capacity, serum parameters and expression of lipid metabolism related genes in juvenile *Onychostoma macrolepis*. *Aquac. Nutr.* **2021**, *27*, 163–175. [CrossRef]
44. Bordignon, F.; Tomás-Vidal, A.; Trocino, A.; Milián Sorribes, M.C.; Jover-Cerdá, M.; Martínez-Llorens, S. Fatty Acid Signatures in Different Tissues of Mediterranean Yellowtail, *Seriola dumerili* (Risso, 1810), Fed Diets Containing Different Levels of Vegetable and Fish Oils. *Animals* **2020**, *10*, 198. [CrossRef]
45. Benedito-Palos, L.; Navarro, J.C.; Kaushik, S.; Pérez-Sánchez, J. Tissue-specific robustness of fatty acid signatures in cultured gilthead sea bream (*Sparus aurata* L.) fed practical diets with a combined high replacement of fish meal and fish oil. *J. Anim. Sci.* **2010**, *88*, 1759–1770. [CrossRef] [PubMed]
46. Bonvini, E.; Bonaldo, A.; Parma, L.; Mandrioli, L.; Sirri, R.; Grandi, M.; Gatta, P.P. Feeding European sea bass with increasing dietary fibre levels: Impact on growth, blood biochemistry, gut histology, gut evacuation. *Aquaculture* **2018**, *494*, 1–9. [CrossRef]

47. Guardiola, F.A.; Saraiva-Fraga, M.; Cuesta, A.; Esteban, M.A. Changes in natural haemolytic complement activity induced by stress in gilthead seabream (*Sparus aurata* L.). *Fish Shellfish. Immunol.* **2018**, *78*, 317–321. [CrossRef] [PubMed]
48. Peres, H.; Santos, S.; Oliva-Teles, A. Selected plasma biochemistry parameters in gilthead seabream (*Sparus aurata*) juveniles. *J. Appl. Ichthyol.* **2013**, *29*, 630–636. [CrossRef]
49. Richard, N.; Mourente, G.; Kaushik, S.; Corraze, G. Replacement of a large portion of fish oil by vegetable oils does not affect lipogenesis, lipid transport and tissue lipid uptake in European seabass (*Dicentrarchus labrax* L.). *Aquaculture* **2006**, *261*, 1077–1087. [CrossRef]
50. Peng, S.; Chen, L.; Qin, J.G.; Hou, J.; Yu, N.; Long, Z.; Sun, X. Effects of replacement of dietary fish oil by soybean oil on growth performance and liver biochemical composition in juvenile black seabream, *Acanthopagrus schlegeli*. *Aquaculture* **2008**, *276*, 154–161. [CrossRef]
51. Fernandez, M.L.; West, K.L. Mechanisms by which Dietary Fatty Acids Modulate Plasma Lipids. *J. Nutr.* **2005**, *135*, 2075–2078. [CrossRef]
52. Plaza, I. Los fitosteroles, el colesterol y la prevención de las enfermedades cardiovasculares. *Clínica E Investig. En Arterioscler.* **2001**, *13*, 209–218. [CrossRef]
53. Dawood, M.A.O.; Koshio, S.; Ishikawa, M.; Yokoyama, S. Effects of partial substitution of fish meal by soybean meal with or without heat-killed lactobacillus plantarum (LP20) on growth performance, digestibility, and immune response of amberjack, *Seriola dumerili* juveniles. *Biomed. Res. Int.* **2015**, *2015*, 514196. [CrossRef]
54. Pandey, B.N.; Pandey, P.K.; Choubey, B.J.; Datta Munshi, J.S. Studies on blood components of an air-breathing siluroid fish, *Heteropneustes fossilis* (Bloch) in relation to body weight. *Folia Haematol.* **1976**, *103*, 101–116.
55. Seno-o, A.; Takakuwa, F.; Hashiguchi, T.; Morioka, K. Replacement of dietary fish oil with olive oil in young yellowtail *Seriola quinqueradiata*: Effects on growth, muscular fatty acid composition and prevention of dark muscle discoloration during refrigerated storage. *Fish. Sci.* **2008**, *74*, 1297–1306. [CrossRef]
56. Mohapatra, S.; Chakraborty, T.; Prusty, A.K.; Kumar, K.; Pani Prasad, K.; Mohanta, K.N. Fenvalerate induced stress mitigation by dietary supplementation of multispecies probiotic mixture in a tropical freshwater fish, *Labeo rohita* (Hamilton). *Pestic. Biochem. Physiol.* **2012**, *104*, 28–37. [CrossRef]
57. Gonçalves, A.T.; Maita, M.; Futami, K.; Endo, M.; Katagiri, T. Effects of a probiotic bacterial Lactobacillus rhamnosus dietary supplement on the crowding stress response of juvenile Nile tilapia *Oreochromis niloticus*. *Fish. Sci.* **2011**, *77*, 633–642. [CrossRef]
58. Paray, B.A.; Hoseini, S.M.; Hoseinifar, S.H.; Van Doan, H. Effects of dietary oak (*Quercus castaneifolia*) leaf extract on growth, antioxidant, and immune characteristics and responses to crowding stress in common carp (*Cyprinus carpio*). *Aquaculture* **2020**, *524*, 735276. [CrossRef]
59. Gabr, G.A.; Ibrahim, Y.S.; Al-Shawi, S.G.; Abosaooda, M.; Gupta, J.; Oudaha, K.H.; Dadras, M. Single or combined consumption of resveratrol and the probiotic, Lactobacillus acidophilus attenuate the effects of crowding stress on growth, immune characteristics, and antioxidant defense in the common carp, (*Cyprinus carpio*). *Aquac. Rep.* **2023**, *29*, 101471. [CrossRef]
60. O'Fallon, J.V.; Busboom, J.R.; Nelson, M.L.; Gaskins, C.T. A direct method for fatty acid methyl ester synthesis: Application to wet meat tissues, oils, and feedstuffs. *J. Anim. Sci.* **2007**, *85*, 1511–1521. [CrossRef]
61. AOAC. *Official Methods of Analysis*, 15th ed.; Associatio: Arlington, VA, USA, 1990.
62. Morales, A.E.; García-Rejón, L.; de La Higuera, M. Influence of handling and/or anaesthesia on stress response in rainbow trout. Effects on liver primary metabolism. *Comp. Biochem. Physiol. A Physiol.* **1990**, *95*, 87–93. [CrossRef]
63. McCord, J.M.; Fridovich, I. Superoxide Dismutase. *J. Biol. Chem.* **1969**, *244*, 6049–6055. [CrossRef] [PubMed]
64. Aebi, H. Catalase in Vitro. *Methods Enzym.* **1984**, *105*, 121–126.
65. Morales, A.E.; Pérez-Jiménez, A.; Carmen Hidalgo, M.; Abellán, E.; Cardenete, G. Oxidative stress and antioxidant defenses after prolonged starvation in Dentex dentex liver. *Comp. Biochem. Physiol. C Toxicol. Pharmacol.* **2004**, *139*, 153–161. [CrossRef] [PubMed]
66. Flohé, L.; Günzler, W.A. [12] Assays of Glutathione Peroxidase. *Methods Enzym.* **1984**, *105*, 114–120.
67. Bradford, M.M. A rapid and sensitive method for the quantitation of microgram quantities of protein utilizing the principle of protein-dye binding. *Anal. Biochem.* **1976**, *72*, 248–254. [CrossRef] [PubMed]
68. Buege, J.A.; Aust, S.D. [30] Microsomal lipid peroxidation. *Methods Enzym.* **1978**, *52*, 302–310.
69. Griffith, O.W. Determination of glutathione and glutathione disulfide using glutathione reductase and 2-vinylpyridine. *Anal. Biochem.* **1980**, *106*, 207–212. [CrossRef]
70. Vandeputte, C.; Guizon, I.; Genestie-Denis, I.; Vannier, B.; Lorenzon, G. A microtiter plate assay for total glutathione and glutathione disulfide contents in cultured/isolated cells: Performance study of a new miniaturized protocol. *Cell Biol. Toxicol.* **1994**, *10*, 415–421. [CrossRef]

International Journal of
Molecular Sciences

MDPI

Article

Bioactive Constituents of *Verbena officinalis* Alleviate Inflammation and Enhance Killing Efficiency of Natural Killer Cells

Xiangdong Dai [1,†], Xiangda Zhou [2,†], Rui Shao [1], Renping Zhao [2], Archana K. Yanamandra [2,3], Zhimei Xing [1], Mingyu Ding [4], Junhong Wang [5], Tao Liu [1], Qi Zheng [1], Peng Zhang [1], Han Zhang [1], Yi Wang [6], Bin Qu [2,*] and Yu Wang [1,5,*]

[1] State Key Laboratory of Component-Based Chinese Medicine, Tianjin University of Traditional Chinese Medicine, Tianjin 301617, China
[2] Department of Biophysics, Center for Integrative Physiology and Molecular Medicine (CIPMM), School of Medicine, Saarland University, 66421 Homburg, Germany
[3] Leibniz Institute for New Materials, 66123 Saarbrücken, Germany
[4] Institute for Immunology, School of Medicine, Tsinghua University, Beijing 100084, China
[5] School of Integrative Medicine, Tianjin University of Traditional Chinese Medicine, Tianjin 301617, China
[6] Pharmaceutical Informatics Institute, College of Pharmaceutical Sciences, Zhejiang University, Hangzhou 310058, China
* Correspondence: bin.qu@uks.eu (B.Q.); wangyu@tjutcm.edu.cn (Y.W.); Tel.: +49-6841-16-16310 (B.Q.); +86-22-59596171 (Y.W.); Fax: +49-6841-16-16302 (B.Q.); +86-22-27493265 (Y.W.)
† These authors contributed equally to this work.

Abstract: Natural killer (NK) cells play key roles in eliminating pathogen-infected cells. *Verbena officinalis* (*V. officinalis*) has been used as a medical plant in traditional and modern medicine for its anti-tumor and anti-inflammatory activities, but its effects on immune responses remain largely elusive. This study aimed to investigate the potential of *V. officinalis* extract (VO extract) to regulate inflammation and NK cell functions. We examined the effects of VO extract on lung injury in a mouse model of influenza virus infection. We also investigated the impact of five bioactive components of VO extract on NK killing functions using primary human NK cells. Our results showed that oral administration of VO extract reduced lung injury, promoted the maturation and activation of NK cells in the lung, and decreased the levels of inflammatory cytokines (IL-6, TNF-α and IL-1β) in the serum. Among five bioactive components of VO extract, Verbenalin significantly enhanced NK killing efficiency in vitro, as determined by real-time killing assays based on plate-reader or high-content live-cell imaging in 3D using primary human NK cells. Further investigation showed that treatment of Verbenalin accelerated the killing process by reducing the contact time of NK cells with their target cells without affecting NK cell proliferation, expression of cytotoxic proteins, or lytic granule degranulation. Together, our findings suggest that VO extract has a satisfactory anti-inflammatory effect against viral infection in vivo, and regulates the activation, maturation, and killing functions of NK cells. Verbenalin from *V. officinalis* enhances NK killing efficiency, suggesting its potential as a promising therapeutic to fight viral infection.

Keywords: *Verbena officinalis*; natural killer cells; killing efficiency

Citation: Dai, X.; Zhou, X.; Shao, R.; Zhao, R.; Yanamandra, A.K.; Xing, Z.; Ding, M.; Wang, J.; Liu, T.; Zheng, Q.; et al. Bioactive Constituents of *Verbena officinalis* Alleviate Inflammation and Enhance Killing Efficiency of Natural Killer Cells. *Int. J. Mol. Sci.* **2023**, *24*, 7144. https://doi.org/10.3390/ijms24087144

Academic Editor: Fabio Virgili

Received: 29 January 2023
Revised: 28 March 2023
Accepted: 7 April 2023
Published: 12 April 2023

1. Introduction

Verbena officinalis (*V. officinalis*), also known as common vervain, is a medicinal herb that is widely distributed in the temperate climate zone across the globe [1]. In China, *V. officinalis* is widely distributed in the southern part of the Yellow River and has been used for centuries as traditional Chinese medicine to treat rheumatism, bronchitis, depression, insomnia, anxiety, liver, and gallbladder diseases [2,3]. Moreover, it has a long-standing record of use in food and cosmetics, which validates its safety [3]. The bioactive constituents

of V. officinalis mainly include flavonoids, terpenoids, phenolic acids, phenylpropanoids, and iridoids [2–5]. Recent reports have shown various activities of *V. officinalis*, including anti-oxidation, anti-bacteria, anti-fungi, and anti-inflammation properties [1,6–8].

Inflammation is an immune response that can be triggered by a range of factors, including virus, bacteria, and transformed cells. During the inflammatory process, the permeability of blood vessels is enhanced, which facilitates the recruitment of immune cells to the site of inflammation. The recruited immune cells release cytokines that further activate and recruit other effector immune cells. Inflammatory responses are essential for fighting pathogens; however, uncontrolled inflammatory responses can have severe consequences, such as organ dysfunction, particularly in the lungs, and the potentially life-threatening cytokine storm syndrome. Innate immune cells are the primary initiators of inflammatory responses.

In the innate immune system, natural killer (NK) cells are specialized immune killer cells, which play key roles in eliminating tumorigenic and pathogen-infected cells. In response to virus infection, NK cells are recruited to the lung and contribute to the immune response to fight pathogens. Several studies have highlighted the pivotal role of NK cells in controlling influenza virus infection. Defects in NK cell activity or depletion of NK cells result in delayed viral clearance, increased morbidity, and mortality [9,10]. However, there are also examples in which NK cells exacerbate morbidity and pathology during lethal dose influenza virus infection in mice [11,12]. These suggest that overactivation of NK cells may lead to undesirable effects. In addition, NK cells are important in bridging the innate and adaptive immune responses to virus infection [13].

In this work, we investigated the anti-inflammatory effect of VO extract in vivo using virus-infected mice with low (0.5 g/kg) and high (1 g/kg) doses. We found that both doses significantly reduced the release of inflammatory cytokines (TNFα, IL-6, and IL-1β), induced by virus infection. Notably, the low dose provided better protection of the lung tissue and induced a higher level of NK activation. Further analysis of bioactive constituents from *V. officinalis* revealed that Verbenalin substantially enhanced the killing efficiency of NK cells.

2. Results

2.1. VO Extract Attenuated the Acute Lung Damage Induced by Virus Infection

Infections caused by viruses, such as influenza or SARS-CoV (severe acute respiratory syndrome coronavirus)-1/2, can result in lung damage, leading to severe breathing problems or even respiratory failure [14]. Acute lung damage caused by virus infection may also result in persistent lung abnormalities, including pulmonary fibrosis, which can lead to long-term respiratory impairments in patients who have recovered from the infection [15]. This type of lung damage is, to a large extent, owing to the massive inflammation initiated by an overactivated immune system. The well-established anti-inflammatory activity of *V. officinalis* prompted us to examine its effect on infection-induced lung damage. To this end, we infected C57BL/6J mice with the influenza virus A/PR8/34 (H1N1) and orally administered VO extract upon viral infection once per day for 3 days (Figure 1A). We chose the low dose (0.5 g/kg) and the high dose (1 g/kg) based on the doses in previous studies in mice [2,16], without any detectable toxicity to tissues, including heart, liver, and kidneys (Supplementary Figure S1). Body weight was monitored daily, and we observed loss of weight in the virus-infected group, which was significantly alleviated by VO extract administration for both the low and high doses (Figure 1B). Using H&E staining of lung sections, we examined changes in alveolar morphology and immune cell infiltration on day 3 post-viral infection. We observed massive immune cell infiltration, thickening of alveolar walls, and disrupted lung parenchyma in virus-infected mice (Figure 1C, Virus group vs. Control group). However, these infection-induced symptoms in the lung were considerably reduced by VO extract administration for both the low and high doses (Figure 1D, Low/High group vs. Virus group). Interestingly, the low dose appeared to achieve a better attenuation of symptoms than the high dose (Figure 1D, Low group vs. High group).

Moreover, the administration of VO extract reduced the release of inflammatory cytokines (TNF-α, IL-1β and IL-6) triggered by viral infection to a level comparable to that of the Control group (Figure 1E–G). No significance was identified between the high and low doses (Figure 1E–G). Taken together, our findings indicate that VO extract is a potent agent for reducing infection-induced acute lung damage and inflammatory response.

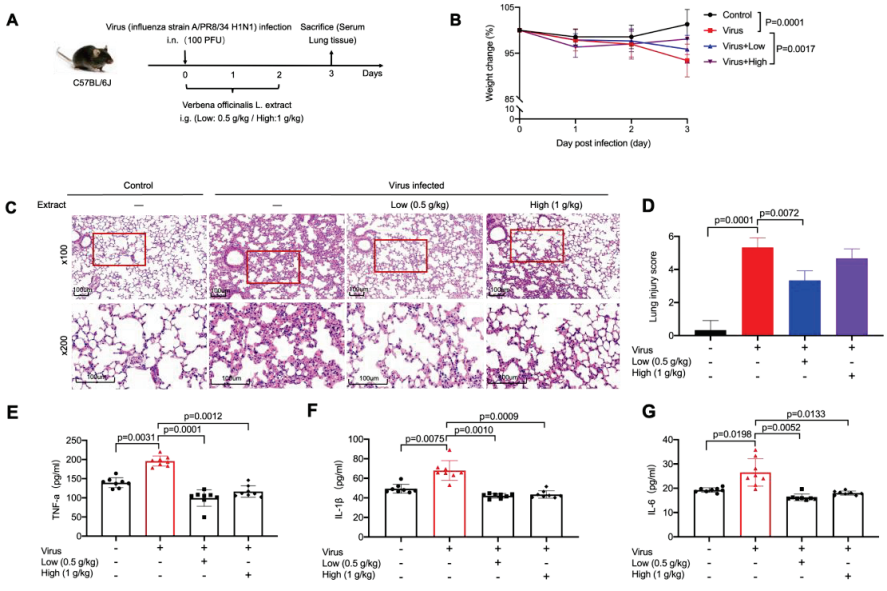

Figure 1. Analysis of the effects of VO extract on infection-induced acute lung damage and inflammation in vivo. (**A**) C57BL/6J mice were intranasally challenged with the influenza virus A/PR8/34 (H1N1) (100 PFU) on day 0 and then orally administered a single dose of VO extract (low dose/Low: 0.5 g/kg; high dose/High: 1 g/kg) every day for 3 days. Mice were sacrificed on day 3. (**B**) Loss of body weight caused by viral infection was ameliorated by VO extract. The body weight of mice was measured daily for three days. $n = 8$ for each group. (**C**) Administration of VO extract alleviated virus-induced inflammation in the lung. Histological analysis of lung tissues was carried out on day 3. Two magnifications are shown: 100× (scale bars: 100 μm) and 200× (scale bars: 100 μm). One representative sample from each group is shown ($n = 3$). (**D**) A total of 50 alveoli were counted on each slide at ×200 magnification ($n = 3$). (**E–G**) Administration of VO extract abolished viral infection-triggered release of proinflammatory cytokines. Blood samples were taken on day 3. Cytokine concentration was determined using ELISA. Circles, triangles, squares and diamonds represent the number of mice in each group. Statistical analysis was performed using SPSS version 19.0 and GraphPad Prism software 5.0. Results were presented as mean ± SD.

2.2. VO Extract Promoted Maturation and Activation of NK Cells in the Lungs in Response to Viral Infection

NK cells are key players in the elimination of pathogen-infected cells. To evaluate the effect of VO extract on NK functions, we examined the frequency and activation of NK cells isolated from lung tissues on day 3 post-infection (Figure 2A). We found no significant alteration in the frequency of lung-residing NK cells following VO extract administration (Figure 2B). To further evaluate NK cell activation, we used surface markers CD11b and CD69, as their expression is indicative of the effector functions and cytotoxicity of murine NK cells [17,18]. We found that viral infection substantially enhanced the frequency of the $CD11b^+$ and $CD69^+$ NK subsets (Figure 2C,D). Interestingly, this tendency was further elevated by the administration of the low dose of VO extract, but not by the high dose

(Figure 2C,D). These results indicated that VO extract at a low dose specifically promoted the activation of NK cells during viral infection.

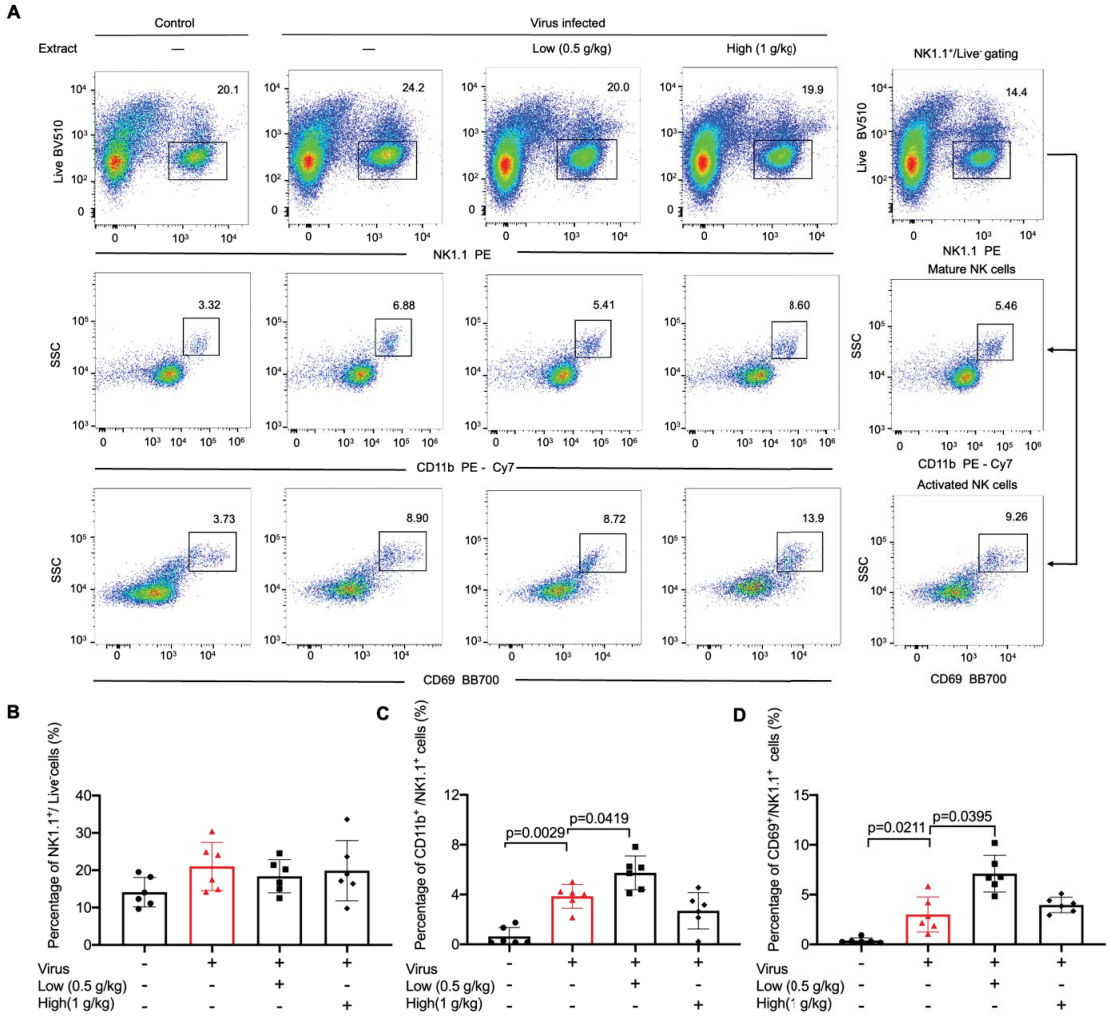

Figure 2. Low dose of VO extract enhances NK activation in response to viral infection. C57BL/6J mice were intranasally challenged with influenza virus A/PR8/34 (H1N1) (100 PFU) on day 0, followed by daily oral administration of a single dose of VO extract (Low: 0.5 g/kg; High: 1 g/kg) for 3 days. On day 3, lung samples were collected, homogenized, and filtered with a 70μm cell filter. (**A**) The cell suspension was stained with control antibodies (PE−conjugated anti−NK1.1 antibody, PE−Cy7−conjugated anti−CD11b antibody, BB700−conjugated anti−CD69 antibody) and analyzed using flow cytometry. (**B**) The $CD45^+NK1.1^+$ population was gated for NK cells. (**C**) $NK1.1^+CD11b^+$ were used to determine maturation of NK cells. (**D**) $NK1.1^+CD69^+$ were used to determine activation of NK cells. Circles, triangles, squares and diamonds represent the number of mice in each group. Statistical analysis was performed using SPSS version 19.0 and GraphPad Prism software 5.0. Results are presented as mean ± SD (n = 6).

2.3. Identification of Chemical Composition from VO Extract by UPLC-Q-TOF-MS

To identify the active ingredients in VO extract, we employed ultra-high-performance liquid chromatography-quadrupole time-of-flight mass spectrometry (UPLC-Q-TOF-MS).

A representative base peak chromatogram (BPC) of VO extract in positive and negative ion modes was shown in Figure 3. We successfully identified thirteen ingredients, including 3,4-dihydroverbenalin, Verbeofflin I, Hastatoside, Verbenalin, Quercetin, Acteoside, Luteolin, Isorhamnetin, Luteolin 7-O-β-gentiobioside, Isoacteoside, Leucosceptoside A, Apigenin, and Kaempferol (Supplementary Table S1). At the same time, we determined the relative content of key bioactive components in VO extract (Supplementary Figure S2).

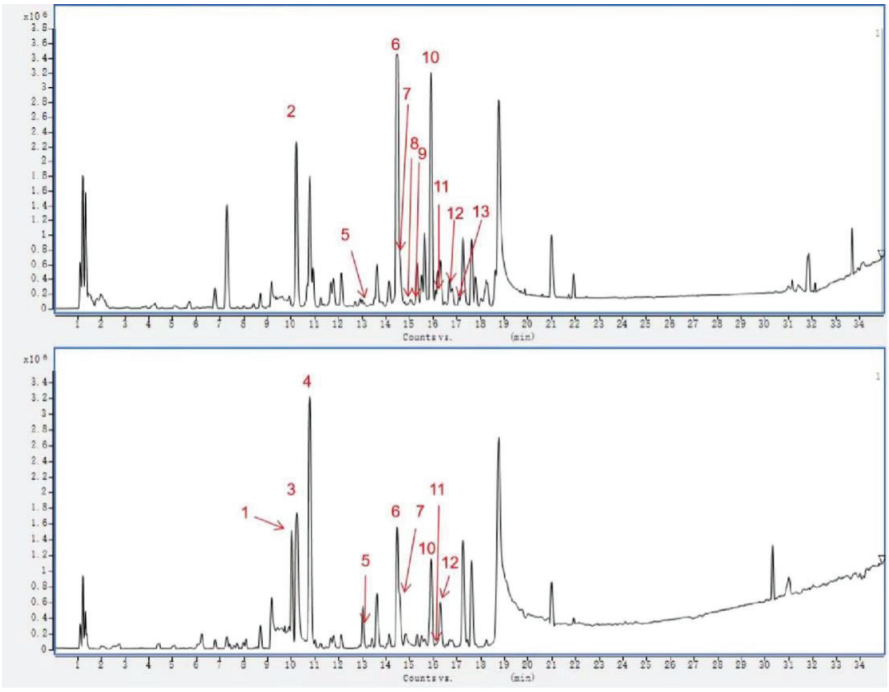

Figure 3. Chemical base peak intensity (BPI) chromatogram of key compounds in VO extract characterized in positive and negative ion modes. UPLC-Q-TOF/MS was employed. The identified compounds were numbered as follows: 3,4-dihydroverbenalin (1); Verbeofflin I (2); Hastatoside (3); Verbenalin (4); Quercetin (5); Acteoside (6); Luteolin (7); Isorhamnetin (8); Luteolin 7-*O*-*β*-gentiobioside (9); Isoacteoside (10); Leucosceptoside A (11); Apigenin (12); and Kaempferol (13). See Supplementary Table S1 for additional details.

2.4. Bioactive Components of V. officinalis Enhanced NK Killing Efficiency

To assess the effect of bioactive compounds from *V. officinalis* on NK cell functions, we cultured primary human NK cells with specific compounds (10 μM and 30 μM) in the presence of IL-2 for three days. We first analyzed the killing kinetics of NK cells using a plate-reader-based real-time killing assay [19]. We found that Acteoside, Apigenin, and Kaempferol slightly reduced NK cells' killing efficiency, whereas Verbenalin and Hastatoside enhanced it (Figure 4A). Notably, Verbenalin exhibited the highest potency in elevating NK cells' killing efficiency (Figure 4A). In addition, the presence of three negative bioactive constituents (Acteoside, Apigenin, and Kaempferol) did not counteract the effect of Verbenalin on NK cell killing (Supplementary Figure S3). To further confirm the effect of Verbenalin on NK cell killing, we performed a 3D killing assay. Target cells expressing FRET-based apoptosis reporter pCasper were embedded in a collagen matrix and NK cells were added from the top. Target cells were yellow when alive and turned green when undergoing apoptosis [20]. Our results showed that Verbenalin-treated NK cells exhibited significantly faster killing kinetics, compared to their counterparts treated with

the vehicle. Thus, we concluded that Verbenalin was capable of increasing NK cells' killing efficiency under physiologically relevant conditions, and among the bioactive constituents of *V. officinalis*, it has the most significant impact on NK cells' killing function.

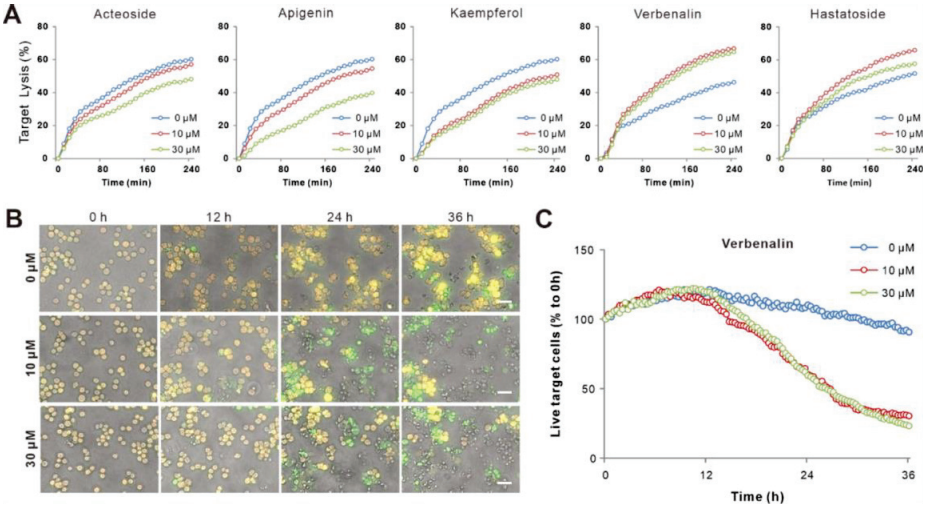

Figure 4. Effect of bioactive constituents of VO extract on NK cells' killing efficiency. (**A**) Primary human NK cells were cultured with different compounds of *V. officinalis* (10 μM and 30 μM) for three days in the presence of IL-2, and their killing kinetics were determined using a plate-reader-based real-time killing assay. (**B**,**C**) Verbenalin accelerates NK killing kinetics in 3D. K562-pCasper target cells were embedded in collagen matrices, and NK cells were added from the top. The killing events were visualized at 37 °C every 20 min for 36 h. Yellow indicates live target cells. Turning green indicates that they were undergoing apoptosis. Fully lysed target cells lost fluorescence signals. Selected time points are shown in (**B**), and the change in live target cells is shown in (**C**). Scale bars are 40 μm. Results from one representative donor out of four is shown.

2.5. Verbenalin Accelerated NK Killing Processes

Next, we sought out the underlying mechanisms regulating the increase in NK killing efficiency by Verbenalin. We examined proliferation, expression of cytotoxic proteins (perforin and granzyme B), and degranulation of lytic granules. We found that Verbenalin did not significantly impact those processes (Figure 5A–C). We then analyzed the time required for killing by visualizing the killing events every 70 s for 12 h using high-content imaging (Figure 6A, Movie S1). The time required for killing is defined as the duration from the initiation of NK/target contact to the target cell apoptosis. The quantification showed that for the NK cells treated with 30 μM of Verbenalin, the time required for NK cells to kill was considerably reduced (Figure 6B). Concomitantly, the number of target cells killed per NK cell was almost doubled in the Verbenalin-treated NK cells relative to their vehicle-treated counterpart (Figure 6C). It has been reported that a portion of NK cells can serve as serious killers, which are able to kill several target cells in a row [21,22]. We thus also analyzed the frequency of serial killers (NK cells that killed more than one target cell), single killers (NK cells that killed only one target cell), and non-killers (NK cells that did not kill any target cells). We found that Verbenalin treatment substantially increased the portion of serial killers while decreasing the portion of non-killers (Figure 6D). For the NK cells treated with 10 μM of Verbenalin, the time required for NK cells to kill was also reduced (Supplementary Figure S4A,B), with no significant change in the number of target cells killed per NK cell (Supplementary Figure S4C). The frequency of serial killers was enhanced and that of non-killers was decreased (Supplementary Figure S4D). In summary, our results suggested that Verbenalin potentiated NK cell activation upon target recognition

and shortened the time required to initiate target cell destruction, leading to an increase in killing efficiency of NK cells.

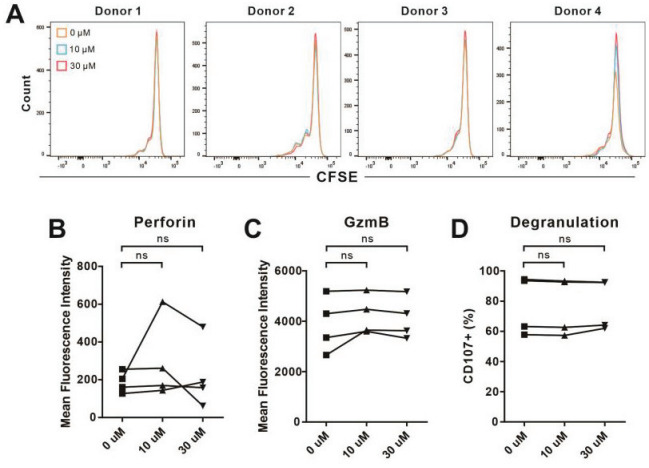

Figure 5. Verbenalin did not affect the proliferation and lytic granule pathway of NK cells. Primary human NK cells were stimulated with IL−2 in the presence of Verbenalin at the indicated concentrations for 3 days prior to experiments. (**A**) Proliferation of NK cells. Freshly isolated NK cells were stained with CFSE and then cultured as described above. (**B**,**C**) Expression of cytotoxic proteins. On day 3, NK cells were fixed, permeabilized, and stained with BV510 anti−human perforin antibody and PerCP/Cyanine5.5 anti-human granzyme B antibody. (**D**) Release of lytic granules was determined by CD107a degranulation assay. Results are shown as a percentage of $CD107a^+$ NK cells. Fluorescence was analyzed using flow cytometry and FlowJo. Results were from four donors. Statistical analysis was performed using paired Student's *t*-test. ns: not significant.

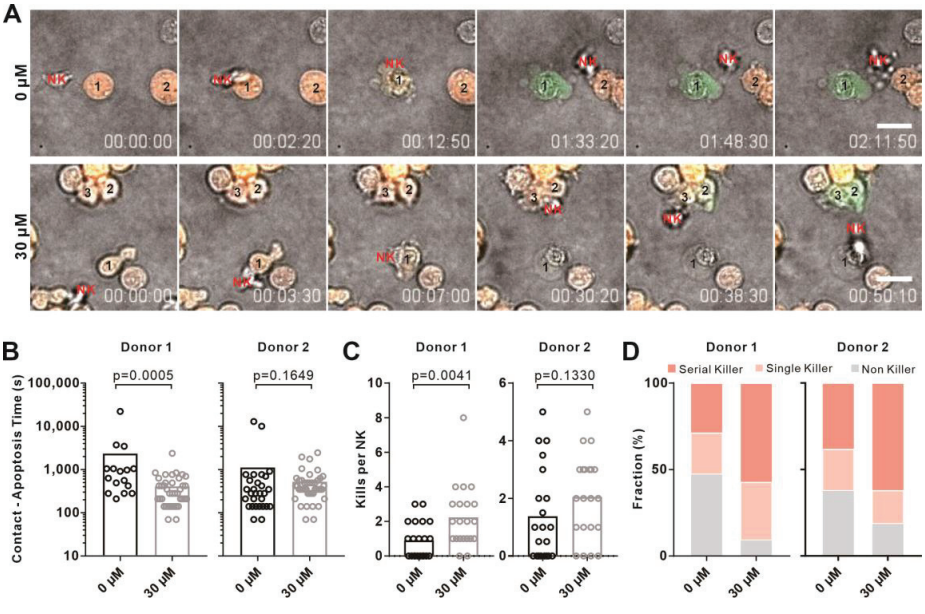

Figure 6. Verbenalin shortened the time required for NK cell killing and increased killing events per NK cell. Primary human NK cells were stimulated with IL−2 in the presence of Verbenalin (30 μM)

at the indicated concentrations for 3 days prior to experiments. K562-pCasper target cells were embedded in collagen and NK cells were added from the top. Killing events were visualized at 37 °C every 70 s for 14 h. (**A**) NK cells made multiple contacts with target cells. One representative NK cell from each condition was shown. NK cells (marked in red) were not fluorescently labeled. The corresponding target cells in contact were numbered. Scale bars were 20 μm. (**B**) Verbenalin shortened the time required for NK cell killing. The time from NK/target contact to target cell apoptosis was quantified. (**C**) Verbenalin treatment enhanced the number of target cells killed per NK cell. Both apoptosis and necrosis were considered as killing events. (**D**) The fraction of serial killers was elevated by Verbenalin treatment. The fraction of serial killers (NK cells that killed more than one target cell), single killers (NK cells that killed only one target cell), and non−killers (NK cells that did not kill any target cells) for each donor was analyzed. Results were from two donors. A total of 21 NK cells were randomly chosen from each condition. Statistical analysis was performed using a Mann−Whitney test.

To explore underlying mechanisms, we investigated potential interaction of Verbenalin with NK inhibitory receptors, especially NKG2A and KIR2DL1, using an in silico molecular docking analysis. Our results showed that Verbenalin could bind to both NKG2A and KIR2DL1 (Supplementary Figure S5). This finding suggested that Verbenalin might enhance NK cell killing by reducing inhibitory receptor-mediated signaling, thus facilitating the rapid activation of NK cells for efficient elimination of target cells.

3. Discussion

Uncontrolled immune responses induced by infection are often associated with life-threatening consequences, such as respiratory failure due to lung damage and cytokine storm syndrome. In this process, exacerbated inflammatory responses initiated by innate immunity play an essential role. Thus, early interventions that minimize undesired inflammation without compromising immune responses to fight pathogens are of great significance to achieve optimal clinical outcomes. In this work, we demonstrated that the extract of *V. officinalis*, a medical herb with a long history of utilization in traditional Chinese medicine and alternative medicine in Western countries, significantly reduced viral infection-induced acute lung damage as well as release of proinflammatory cytokines. At the same time, administration of a low dose of VO extract considerably enhanced NK activation in response to viral infection. In addition, we identified that Verbenalin, a biologically active constituent of *V. officinalis*, substantially elevated NK cell-mediated cytotoxicity by shortening the time required for killing and, consequently, enhancing the frequency of serial killers. These findings suggest that *V. officinalis* and Verbenalin are promising therapeutic agents for early intervention to protect lung function, avoid cytokine storm, and facilitate clearance of virus-infected cells.

The beneficial effect of VO extract on lung injury may arise from multiple mechanisms. Previous studies have shown that treatment with *V. officinalis* inhibits the replication of respiratory syncytial virus [23], and that treatment of active constituents of *V. officinalis* increases phagocytotic activity of neutrophils in vitro [23]. In our study, we administered VO extract orally, and its concentration in the lungs might have reached levels that affected viral replication to some extent. We postulated that the enhanced phagocytic activity of neutrophils in the VO extract-treated group might have contributed to the efficient removal of viral particles from the lungs. Although our study used a mouse model of influenza virus infection, we speculated that the effect of VO extract on acute lung injury induced by viral infection would be applicable to other respiratory viral infections that result in severe respiratory complications. This hypothesis is bolstered by a recent study that reported that a newly developed formula, Xuanfei Baidu, composed of thirteen medical herbs including *V. officinalis* has shown very positive clinical outcomes in treating patients with SARS-CoV-2 infection [23,24]. In addition, CD8+ cytotoxic T lymphocytes (CTLs) play critical roles in the adaptive immune defense against viral infection. However, we would like to emphasize

that the effect we have observed was on day 3, which is earlier than the peak of the primary murine CTL response upon influenza virus infection, typically observed on day 5 [25]. It is worth noting that NK cells can mount a cytotoxic response without prior priming, allowing them to respond to a viral infection immediately. Therefore, it is unlikely that CTLs are the primary targets of VO extract in attenuating the acute lung damage induced by viral infections.

Release of proinflammatory cytokines triggered by viral infection recruits immune cells to inflammation sites. In this study, we found that VO extract administration led to reduced levels of proinflammatory cytokines, including TNF-α, IL-1β, and IL-6, in serum. TNF-α is primarily released by M1-type macrophages and T cells [26], and is mainly regulated by the NF-κB pathway [27]. IL-1β is commonly released by monocytes, macrophages, and mast cells; however, non-immune cells, such as epithelial cells, endothelial cells, fibroblasts, and neuronal and glial cells, can also synthesize and release IL-1β during cell injury or inflammation [28]. IL-1β is regulated by the NF-κB, c-Jun N-terminal kinase (JNK), and p38 MAPK pathways [29]. IL-6 can be released by myocardial and immune cells [30], and is primarily triggered and regulated by signaling pathways such as NF-κB and MAPK [31]. It is reported that total glucosides of *V. officinalis* attenuate chronic nonbacterial prostatitis in rat models by reducing the release of IL-2, IL-1β, and TNF-α in the prostate [32]. Additionally, Verbenalin, a bioactive constituent of *V. officinalis*, can effectively reduce airway inflammation in asthmatic rats by inhibiting the activity of the NF-κB/MAPK signaling pathway [33]. These pathways and molecules are possible targets for *V. officinalis* to regulate the release of proinflammatory cytokines.

In this work, we observed that Verbenalin-treated NK cells were able to destroy target cells more quickly than their vehicle-treated counterparts. To successfully execute their killing function, NK cells need to identify their target cells using surface receptors, followed by the formation of a tight junction, termed the immunological synapse (IS), between the NK cell and the target cells. At the IS, lytic granules (LGs) containing cytotoxic proteins, including pore-forming protein perforin and serine protease granzymes, are enriched and released to induce target cell destruction [34,35]. Thus, the time required for killing is determined by several steps: engagement of surface-activating/inhibitory receptors, formation of the IS, enrichment and release of LGs, and uptake of cytotoxic proteins by target cells.

Both activating and inhibitory receptors are expressed on NK cells to control their activation [36]. Engagement of activating receptors, such as NKp46, NKp30, NKp44, and NKG2D, triggers signaling pathways for NK activation [37]. Inhibitory receptors bind to major histocompatibility complex (MHC) Class I molecules, which are expressed on healthy self-cells. Loss or down-regulation of MHC-I molecules leads to activation of NK cells to initiate killing processes [38]. Formation of the IS between NK cells and target cells largely depends on the interaction between LFA-1 and ICAM-1 [39]. Enrichment of LGs at the IS is regulated by reorganization of the cytoskeleton, especially reorientation of MTOC towards the contact site [40]. LG release requires proper docking at the plasma membrane and vesicle fusion with the plasma membrane, which are tightly regulated by SNARE and related proteins [41,42]. Uptake of cytotoxic proteins by target cells requires Ca^{2+}-dependent endocytosis [43]. Enhancement in any of the above-mentioned steps could accelerate killing processes, such as sensitizing activating receptors, up-regulating effector molecules downstream of activating receptors, promoting LG accumulation at the IS, reducing the dwell time for docking, or enhancing the efficiency of LG release. Our results suggested that Verbenalin bound to NK inhibitory receptors NKG2A and KIR2DL1, indicating that enhancement of NK cell killing by Verbenalin could be a result of its ability to reduce inhibitory signaling. Engagement of surface receptors is important to initiate and regulate the following steps: IS formation, LG enrichment and release, etc. Further investigation is needed to characterize how each step is affected by Verbenalin to accelerate killing.

4. Materials and Methods

4.1. Preparation of VO Extract

Verbena officinalis was obtained from Anhui Zehua China Pharmaceutical Slices Co., Ltd. The whole plant (4.5 kg) was extracted with 4.5 L of 70% ethanol for 2 h by refluxing extraction repeated three times. The combined extract was filtrated with ceramic membrane and concentrated using vacuum evaporation apparatus at a temperature not exceeding 45 °C. The resulting extract was then lyophilized to obtain the VO extract powder.

4.2. UPLC-Q-TOF-MS Analysis

Quantitative analysis was performed using an Agilent 1290 UHPLC system (Agilent Technologies Inc., Palo Alto, CA, USA) coupled to an Agilent 6520 Q-TOF instrument with electrospray ionization (ESI) source. Chromatographic separation was achieved using an ACQUITY UPLC® BEH C18 (2.1 × 150 mm, 1.7 μm; Waters, Milford, MA, USA). The mobile phase consisted of 0.1% aqueous formic acid (A) and methanol (B). The elution condition involved holding the starting mobile phase at 95% A and 5% B and applying a gradient of 5% A and 95% B for 35 min. The flow rate was set at 0.3 mL/min, and the injection volume for all the sample was 2 μL. Experiments were performed in positive and negative ESI mode with the following parameters: ESI temperature, 100 °C; collision energy, 10 V; collision pressure, 135 V; fragmentor voltage, 135 V; nebulizer gas, 40.0 psi; dry gas, 11.0 L/min at a temperature of 350 °C; scan range, m/z 100–1700.

4.3. Quantification of the Active Compounds from VO Extract

The prepared samples were injected into a Waters ACQUITY UPLC system (Waters, Milford, MA, USA) with a photodiode array (PDA) detector. The chromatographic separation was performed with a BEH C18 column (2.1 mm × 150 mm, 1.7 μm, Waters), operated at 35 °C, and the sample injection volume was set at 2 μL. The flow rate was kept constant at 0.3 mL/min and UV measurements were obtained at 254 nm. The mobile phases were methanol (solvent A) and water containing 0.1% formic acid (solvent B) with gradient elution using the following program: 0–35 min, 5–95% A.

A 10 mg/mL sample solution was formed from weighed VO extract powder and added methanol, swirled for 30 s, ultrasonic dissolved for 3 min, and centrifuged at 13,000 rpm for 10 min. The supernatant was filtered by 0.22 μm microporous filter membrane and then sampled to inject for UPLC and LC-MS analysis.

The mixed standard solution was composed of methanol solution with 0.1 mg each of hastatoside, verbenalin, and acteoside, and 0.01 mg each of apigenin and kaempferol per mL.

$$C = Pr \times Cx$$

C: the concentration of the compounds in the sample; Pr: peak area ratio of compounds in sample and in mixed standard; Cx: the concentration of compounds in a mixed standard.

4.4. Mice and Virus

Female C57BL/6 mice (6–10 weeks old, weighing 20 to 25 g) were purchased from Beijing Vital River Laboratory Animal Technology Co., Ltd. (Beijing, China), and housed in standard microisolator cages in a centralized animal care facility. Animal care and experimental procedures were performed in accordance with experimental animal guidelines. Mice were given ad libitum access to food and water and subjected to a 12 h light/dark cycle. All mice were adapted to the environment for seven days before the experiments. Virus (H1N1) was stored at −80 °C.

4.5. Virus Infection

Mice were anesthetized with isoflurane and intranasally inoculated with 100 PFU H1N1 in 40 μL PBS. The number of mice in each group ranged from 6 to 8. The Vehicle group received an intranasal challenge with 40 μL PBS. All the animal experiments were

approved, and efforts were made to minimize suffering and to reduce the number of animals used.

4.6. Administration of VO Extract

To administer the VO extract, VL (0.5 mg/kg) and VH (1 mg/kg) doses were given orally via gavage once daily for three consecutive days. The VO extract was freshly prepared each day and stored at 4 °C until administration. Distilled water was orally administered to mice in the Vehicle group simultaneously. On the third day, the mice were sacrificed, and their blood and lung tissues were collected for further analysis. During these three days, mice were monitored and changes in body weight were recorded.

4.7. Flow Cytometry Assay

To perform the flow cytometry analysis, nonspecific receptors were blocked with anti-CD16/CD32, and then surface markers (CD45, NK1.1, CD11b, and CD69) were stained. Cells were fixed and then incubated with specific surface-binding antibodies for 30 min at 4 °C. Samples were analyzed using BD FACScalibur and FlowJo software. Cells were gated according to forward scatter and side scatter, and NK cells were identified by the $CD45^+NK1.1^+$ population.$NK1.1^+CD11b^+$ were used to determine maturation of NK cells and $NK1.1^+CD69^+$ were used to determine activation of NK cells.

4.8. Hematoxylin–Eosin (HE) Staining

To assess pathological changes, the mice were sacrificed on the third day, and their lung, heart, liver, and kidney tissues were collected, fixed in 10% buffered formalin, and embedded in paraffin. Each tissue was cut into 4 μm sections and stained with hematoxylin and eosin. Lung injury was evaluated according to a quantitative scoring system that assesses infiltration of immune cells, thickening of alveolar walls, and disruption of lung parenchyma [44–46]. The scoring for lung damage was performed by three researchers independently according to standard protocols.

4.9. Detection of IL-6, TNF-α, and IL-1β Levels in Serum

To obtain the serum, blood samples were centrifuged at 3000 rpm and 4 °C for 15 min. The concentrations of IL-6, TNF-α, and IL-1β in serum were measured using corresponding ELISA kits (Sino Best Biological Technology Co., Ltd., Shanghai, China) according to the manufacturer's instructions with a microplate reader (Tecan Trading AG, männedorf, Switzerland).

4.10. NK Celsl Preparation and Cell Culture

Primary human NK cells were isolated from peripheral blood mononuclear cells (PBMCs) of healthy donors using the Human NK Cell Isolation Kit (Miltenyi Biotec, Bergisch Gladbach, Germany). The isolated NK cells were cultured in AIM V medium (Thermo Fischer Scientific, Waltham, MA, US) with 10% FCS and 100 U/mL of recombinant human IL-2 (Miltenyi Biotec, Bergisch Gladbach, Germany). K562 and K562-pCasper cells were cultured in RPMI-1640 medium (Thermo Fischer Scientific, Waltham, MA, US) with 10% FCS. For K562-pCasper cells, 1.25 mg/mL G418 was added. All cells were kept at 37 °C with 5% CO_2.

4.11. Real-Time Killing Assay

The real-time killing assay was conducted as previously reported [19]. Briefly, target cells (K562 cells) were loaded with Calcein-AM (500 nM, Thermo Fisher Scientific, Waltham, MA, US) and settled into a 96-well plate (2.5×10^4 target cells per well). NK cells were subsequently added with an effector-to-target (E:T) ratio of 2.5:1, if not otherwise specified. Fluorescence intensity was determined using the bottom-reading mode at 37 °C every 10 min for 4 h with a GENios Pro microplate reader (TECAN). The target lysis percentage was calculated using the formula:

Target lysis (t) % = 100 × (F_{live}(t) − F_{exp}(t))/(F_{live}(t) − F_{lysed}(t)). (F: fluorescence intensity)

4.12. 3D Killing Assay and Live Cell Imaging

Target cells (K562-pCasper cells) were embedded into 2 mg/mL of pre-chilled neutralized bovine type I collagen solution (Advanced Biomatrix) in a 96-well plate. The collagen was solidified at 37 °C with 5% CO_2 for 40 min, after which NK cells were added to the top of the collagen as effector cells. The cells were visualized using ImageXpress Micro XLS Widefield High-Content Analysis System (Molecular Devices) at 37 °C with 5% CO_2. For the 3D killing assay, as described previously [47], killing events were visualized every 20 min for 36 h, and live target cell numbers were normalized to hour 0 based on area. For live cell imaging to determine time required for killing and the average kills per NK cell, the cells were visualized every 70 s for 14 h and tracked manually. ImageJ software was used to process and analyze the images.

4.13. Proliferation Assay

To examine proliferation, freshly isolated primary human NK cells were labelled with CFSE (1 μM, Thermo Fischer Scientific, Waltham, MA, US) and then stimulated with recombinant human IL-2 in the presence of Verbenalin at indicated concentrations for 3 days. Fluorescence was determined with a FACSVerse™ flow cytometer (BD Biosciences, San Jose, CA, US) and analyzed with FlowJo v10 (FLOWJO, Ashland, OR, US).

4.14. Determination of Cytotoxic Protein Expression

To test perforin and granzyme B expression, NK cells were fixed in pre-chilled 4% paraformaldehyde. Permeabilization was carried out using 0.1% saponin in PBS containing 0.5% BSA and 5% FCS. FACSVerse™ flow cytometer (BD Biosciences, San Jose, CA, US) was used to acquire data. FlowJo v10 (FLOWJO, Ashland, OR, US) was used for analysis.

4.15. CD107a Degranulation Assay

For the degranulation assay, K562 cells were co-cultured with vehicle-treated or Verbenalin-treated NK cells in the presence of Brilliant Violet 421™ anti-human CD107a (LAMP1) antibody (Biolegend, San Diego, CA, US) and GolgiStop™ (BD Biosciences). The incubation was carried out at 37 °C with 5% CO_2 for 4 h. The cells were then stained with PerCP anti-human CD16 antibody (Biolegend) and APC mouse anti-human CD56 antibody (BD Biosciences) to define NK cells. Data were obtained with a FACSVerse™ flow cytometer (BD Biosciences) and analyzed with FlowJo v10 (FLOWJO, LLC).

4.16. Molecular Docking

To investigate the interactions between small molecules and receptor proteins, the CDOCKER module in Discovery Studio software was used for molecular docking. The three-dimensional structures of verbenalin molecules were downloaded from TCMSP (https://tcmsp-e.com/, accessed on 13 March 2023), and then we performed hydrogenation through the Prepare Ligand module and optimized the energy with the CHARMM force field. The three-dimensional structure of the target protein was downloaded from the PDB database (https://www.rcsb.org/, accessed on 13 March 2023). Then we ran the Prepare Protein module to optimize the protein structure: deleting redundant protein conformations, deleting water molecules, and completing incomplete residues, hydrogenation, and distribution of related charges. The prepared target proteins and small molecules were introduced into Discovery Studio and docked using the CDOCKER module. The semi-flexible docking method and simulated annealing algorithm were used to find the optimal conformation of ligand and receptor. According to the level of CDOCKER Interaction Energy, we evaluated the degree of docking: the lower score function value indicating the stronger affinity between compound and its receptor.

4.17. Statistical Analysis

Data were analyzed using SPSS version 19.0 and GraphPad Prism software 5.0 and presented as mean ± standard deviation (SD). Significant differences among the multiple group comparisons were performed using one-way analysis of variance (ANOVA), and the ANOVA comparisons were analyzed through Tukey's honest significant difference test. Data with a partial distribution were examined using the nonparametric Kruskal–Wallis test with Dunn's multiple comparison as a post-test. A p value less than 0.05 indicated a significant difference.

5. Conclusions

The present study provided evidence that VO extract had the ability to ameliorate lung injury induced by viral infection and enhance the maturation and activation of NK cells in the lungs. Moreover, our in vitro study with primary human NK cells showed that Verbenalin significantly reduced the required contact time for killing, thereby enhancing the total number of killing events per NK cell. The findings of this study established a direct link between Verbenalin, a bioactive constituent of VO extract, and the killing efficiency of NK cells, suggesting its promising potential for therapeutic applications in combating viral infections and, potentially, cancer.

Supplementary Materials: The following supporting information can be downloaded at: https://www.mdpi.com/article/10.3390/ijms24087144/s1.

Author Contributions: R.S., H.Z., Y.W. (Yu Wang) and B.Q. conceived of this study. X.Z., R.Z., X.D., T.L., M.D., Q.Z. and A.K.Y. performed the experiments. R.S. and B.Q. wrote the manuscript. X.D., X.Z. and Y.W. (Yi Wang) edited the pictures. Yu Wang., J.W., Z.X., B.Q. and P.Z. revised the manuscript. All authors have read and agreed to the published version of the manuscript.

Funding: This project was funded by the National Key R&D Program of China (No. 2021YFE0200300 to Y.W., and No. 2020YFA0708004 to H.Z.), by Tianjin University of Traditional Chinese Medicine (No.YJSKC-20211015), by the Deutsche Forschungsgemeinschaft (SFB 1027 A2 to B.Q., Forschungsgroßgeräte (GZ: INST 256/423-1 FUGG for the flow cytometer and GZ: INST 256/429-1 FUGB for ImageXpress), by the Leibniz-Gemeinschaft (INM Fellow to B.Q.), and by the National Natural Science Foundation of China (No. 82204878 to R.S.).

Institutional Review Board Statement: Research carried out for this study with material from healthy donors (leukocyte reduction system chambers from human blood donors) is authorized by the local ethics committee (declaration from 16.4.2015 (84/15, Rettig-Stürmer).

Informed Consent Statement: Not applicable.

Data Availability Statement: The datasets used and/or analyzed during the current study are available from the corresponding author upon reasonable request.

Acknowledgments: We thank the Institute for Clinical Hemostaseology and Transfusion Medicine at Saarland University for providing donor blood; Carmen Hässig, Cora Hoxha, and Gertrud Schäfer for excellent technical help; Markus Hoth for inspiring discussion and continuous support, as well as K562-pCasper cells (with Eva C. Schwarz). The sketches were made in BioRender.

Conflicts of Interest: The authors declare no conflict of interest.

Abbreviations

IS	immunological synapse
LG	lytic granules
MHC	major histocompatibility complex
NK	natural killer
PBMCs	peripheral blood mononuclear cells
VO extract	Verbena officinalis extract.

References

1. Kubica, P.; Szopa, A.; Kokotkiewicz, A.; Miceli, N.; Taviano, M.F.; Maugeri, A.; Cirmi, S.; Synowiec, A.; Gniewosz, M.; Elansary, H.O.; et al. Production of Verbascoside, Isoverbascoside and Phenolic Acids in Callus, Suspension, and Bioreactor Cultures of *Verbena officinalis* and Biological Properties of Biomass Extracts. *Molecules* **2020**, *25*, 5609. [CrossRef] [PubMed]
2. Khan, A.W.; Khan, A.U.; Ahmed, T. Anticonvulsant, Anxiolytic, and Sedative Activities of *Verbena officinalis*. *Front. Pharmacol.* **2016**, *7*, 499. [CrossRef] [PubMed]
3. Kubica, P.; Szopa, A.; Dominiak, J.; Luczkiewicz, M.; Ekiert, H. *Verbena officinalis* (Common Vervain)—A Review on the Investigations of This Medicinally Important Plant Species. *Planta Medica* **2011**, *86*, 1241–1257. [CrossRef] [PubMed]
4. Kubica, P.; Szopa, A.; Ekiert, H. Production of verbascoside and phenolic acids in biomass of *Verbena officinalis* L. (vervain) cultured under different in vitro conditions. *Nat. Prod. Res.* **2017**, *31*, 1663–1668. [CrossRef]
5. Shu, J.; Chou, G.; Wang, Z. Two New Iridoids from *Verbena officinalis* L. *Molecules* **2014**, *19*, 10473–10479. [CrossRef]
6. Casanova, E.; Garcia-Mina, J.M.; Calvo, M.I. Antioxidant and Antifungal Activity of *Verbena officinalis* L. Leaves. *Plant Foods Hum. Nutr.* **2008**, *63*, 93–97. [CrossRef]
7. Lopez-Jornet, P.; Camacho-Alonso, F.; Gómez-Garcia, F.; Miñano, F.M.; Cañas, X.; Serafín, A.; Castillo, J.; Vicente-Ortega, V. Effects of potassium apigenin and verbena extract on the wound healing process of SKH-1 mouse skin. *Int. Wound J.* **2014**, *11*, 489–495. [CrossRef]
8. Speroni, E.; Cervellati, R.; Costa, S.; Guerra, M.C.; Utan, A.; Govoni, P.; Berger, A.; Müller, A.; Stuppner, H. Effects of differential extraction of *Verbena officinalis* on rat models of inflammation, cicatrization and gastric damage. *Planta Med.* **2007**, *73*, 227–235. [CrossRef]
9. Gazit, R.; Gruda, R.; Elboim, M.; Arnon, T.; Katz, G.; Achdout, H.; Hanna, J.H.; Qimron, U.; Landau, G.; Greenbaum, E.; et al. Lethal influenza infection in the absence of the natural killer cell receptor gene Ncr1. *Nat. Immunol.* **2006**, *7*, 517–523. [CrossRef]
10. Nogusa, S.; Ritz, B.W.; Kassim, S.H.; Jennings, S.R.; Gardner, E.M. Characterization of age-related changes in natural killer cells during primary influenza infection in mice. *Mech. Ageing Dev.* **2008**, *129*, 223–230. [CrossRef]
11. Stein-Streilein, J.; Guffee, J. In vivo treatment of mice and hamsters with antibodies to asialo GM1 increases morbidity and mortality to pulmonary influenza infection. *J. Immunol.* **1986**, *136*, 1435–1441. [CrossRef] [PubMed]
12. Zhou, G.; Juang, S.W.W.; Kane, K.P. NK cells exacerbate the pathology of influenza virus infection in mice. *Eur. J. Immunol.* **2013**, *43*, 929–938. [CrossRef] [PubMed]
13. Abdul-Careem, M.F.; Mian, M.F.; Yue, G.; Gillgrass, A.; Chenoweth, M.; Barra, N.G.; Chew, M.V.; Chan, T.; Al-Garawi, A.A.; Jordana, M.; et al. Critical Role of Natural Killer Cells in Lung Immunopathology During Influenza Infection in Mice. *J. Infect. Dis.* **2012**, *206*, 167–177. [CrossRef] [PubMed]
14. Domizio, J.D.; Gulen, M.F.; Saidoune, F.; Thacker, V.V.; Yatim, A.; Sharma, K.; Nass, T.; Guenova, E.; Schaller, M.; Conrad, C.; et al. The cGAS-STING pathway drives type I IFN immunopathology in COVID-19. *Nature* **2022**, *603*, 145–151. [CrossRef]
15. Kiener, M.; Roldan, N.; Machahua, C.; Sengupta, A.; Geiser, T.; Guenat, O.T.; Funke-Chambour, M.; Hobi, N.; Julio, M.K.-D. Human-Based Advanced in vitro Approaches to Investigate Lung Fibrosis and Pulmonary Effects of COVID-19. *Front. Med.* **2021**, *8*, 644678. [CrossRef] [PubMed]
16. Sisay, M.; Bussa, N.; Gashaw, T. Evaluation of the Antispasmodic and Antisecretory Activities of the 80% Methanol Extracts of *Verbena officinalis* L: Evidence From In Vivo Antidiarrheal Study. *J. Evid.-Based Integr. Med.* **2019**, *24*, 2515690X19853264. [CrossRef]
17. Laura, C.; Julie, C.; Nicolas, F.; Claude, R.; Eric, V.; Thierry, W. Maturation of mouse NK cells is a 4-stage developmental program. *Blood* **2009**, *113*, 5488–5496.
18. Borrego, F.; Robertson, M.J.; Ritz, J.; Peña, J.; Solana, R. CD69 is a stimulatory receptor for natural killer cell and its cytotoxic effect is blocked by CD94 inhibitory receptor. *Immunology* **1999**, *97*, 159–165. [CrossRef]
19. Kummerow, C.; Schwarz, E.C.; Bufe, B.; Zufall, F.; Hoth, M.; Qu, B. A simple, economic, time-resolved killing assay. *Eur. J. Immunol.* **2014**, *44*, 1870–1872. [CrossRef]
20. Backes, C.S.; Friedmann, K.S.; Mang, S.; Knörck, A.; Hoth, M.; Kummerow, C. Natural killer cells induce distinct modes of cancer cell death: Discrimination, quantification, and modulation of apoptosis, necrosis, and mixed forms. *J. Biol. Chem.* **2018**, *293*, 16348–16363. [CrossRef]
21. Bhat, R.; Watzl, C. Serial Killing of Tumor Cells by Human Natural Killer Cells—Enhancement by Therapeutic Antibodies. *PLoS ONE* **2007**, *2*, e326. [CrossRef] [PubMed]
22. Prager, I.; Liesche, C.; van Ooijen, H.; Urlaub, D.; Verron, Q.; Sandström, N.; Fasbender, F.; Claus, M.; Eils, R.; Beaudouin, J.; et al. NK cells switch from granzyme B to death receptor-mediated cytotoxicity during serial killing. *Exp Med.* **2019**, *216*, 2113–2127. [CrossRef] [PubMed]
23. Ross, S.M. An integrative approach to rhinosinusitis in children, part II. *Holist. Nurs. Pract.* **2010**, *24*, 49–51. [CrossRef] [PubMed]
24. Xiong, W.-Z.; Wang, G.; Du, J.; Ai, W. Efficacy of herbal medicine (Xuanfei Baidu decoction) combined with conventional drug in treating COVID-19:A pilot randomized clinical trial. *Integr. Med. Res.* **2020**, *9*, 100489. [CrossRef] [PubMed]
25. Jiang, J.; Fisher, E.M.; Murasko, D.M. CD8 T cell responses to influenza virus infection in aged mice. *Ageing Res. Rev.* **2011**, *10*, 422–427. [CrossRef]
26. Tian, X.; Eikmans, M.; van der Hoorn, M.-L. The Role of Macrophages in Oocyte Donation Pregnancy: A Systematic Review. *Int. J. Mol. Sci.* **2020**, *21*, 939. [CrossRef]
27. Maeda, S.; Omata, M. Inflammation and cancer: Role of nuclear factor-kappaB activation. *Cancer Sci.* **2008**, *99*, 836–842. [CrossRef]

28. Fontenelle, T.P.C.; Lima, G.C.; Mesquita, J.X.; Lopes, J.L.D.S.; de Brito, T.V.; Júnior, F.D.C.V.; Sales, A.B.; Aragão, K.S.; Souza, M.H.L.P.; Barbosa, A.L.D.R.; et al. Lectin obtained from the red seaweed Bryothamnion triquetrum: Secondary structure and anti-inflammatory activity in mice. *Int. J. Biol. Macromol.* **2018**, *112*, 1122–1130. [CrossRef]
29. Weber, A.; Wasiliew, P.; Kracht, M. Interleukin-1 (IL-1) Pathway. *Sci. Signal.* **2010**, *3*, cm1. [CrossRef]
30. Koppinger, M.P.; Lopez-Pier, M.A.; Skaria, R.; Harris, P.R.; Konhilas, J.P. *Lactobacillus reuteri* attenuates cardiac injury without lowering cholesterol in low-density lipoprotein receptor-deficient mice fed standard chow. *Am. J. Physiol. Heart Circ. Physiol.* **2020**, *319*, H32–H41. [CrossRef]
31. Viji, V.; Shobha, B.; Kavitha, S.K.; Ratheesh, M.; Kripa, K.; Helen, A. Betulinic acid isolated from *Bacopa monniera* (L.) Wettst suppresses lipopolysaccharide stimulated interleukin-6 production through modulation of nuclear factor-kappaB in peripheral blood mononuclear cells. *Int. Immunopharmacol.* **2010**, *10*, 843–849. [CrossRef] [PubMed]
32. Wang, L.L.; Li, H.B.; Miao, M.S. Effect of total glucosides of *Verbena officinalis* L. on rat model for chronic nonbacterial prostatitis. *China Med. Herald.* **2016**, *13*, 4–7.
33. Dong, S.M.; Gao, P.H.; Liang, W.H. Effects of Verbenalin on Airway Inflammation, Airway Smooth Muscle Cell Proliferation and RhoA Expression in Rats with Bronchial Asthma Through NF-κB/MAPK Signaling Pathway. *Guid. J. Tradit. Chin. Med. Pharm.* **2021**, *27*, 23–27.
34. Prager, I.; Watzl, C. Mechanisms of natural killer cell-mediated cellular cytotoxicity. *J. Leukoc. Biol.* **2019**, *105*, 1319–1329. [CrossRef]
35. Orange, J.S. Formation and function of the lytic NK-cell immunological synapse. *Nat. Rev. Immunol.* **2008**, *8*, 713–725. [CrossRef]
36. Pegram, H.J.; Andrews, D.M.; Smyth, M.J.; Darcy, P.K.; Kershaw, M.H. Activating and inhibitory receptors of natural killer cells. *Immunol. Cell Biol.* **2011**, *89*, 216–224. [CrossRef]
37. Lanier, L.L. On guard–activating NK cell receptors. *Nat. Immunol.* **2001**, *2*, 23–27. [CrossRef]
38. Sivori, S.; Vacca, P.; Del Zotto, G.; Munari, E.; Mingari, M.C.; Moretta, L. Human NK cells: Surface receptors, inhibitory checkpoints, and translational applications. *Cell. Mol. Immunol.* **2019**, *16*, 430–441. [CrossRef]
39. Gross, C.C.; Brzostowski, J.A.; Liu, D.; Long, E.O. Tethering of Intercellular Adhesion Molecule on Target Cells Is Required for LFA-1–Dependent NK Cell Adhesion and Granule Polarization. *J. Immunol.* **2010**, *185*, 2918–2926. [CrossRef]
40. Mentlik, A.N.; Sanborn, K.B.; Holzbaur, E.L.; Orange, J.S. Rapid Lytic Granule Convergence to the MTOC in Natural Killer Cells Is Dependent on Dynein But Not Cytolytic Commitment. *Mol. Biol. Cell* **2010**, *21*, 2241–2256. [CrossRef]
41. Qu, B.; Pattu, V.; Junker, C.; Schwarz, E.C.; Bhat, S.S.; Kummerow, C.; Marshall, M.; Matti, U.; Neumann, F.; Pfreundschuh, M.; et al. Docking of Lytic Granules at the Immunological Synapse in Human CTL Requires Vti1b-Dependent Pairing with CD3 Endosomes. *J. Immunol.* **2011**, *186*, 6894–6904. [CrossRef] [PubMed]
42. Bertrand, F.; Müller, S.; Roh, K.-H.; Laurent, C.; Dupré, L.; Valitutti, S. An initial and rapid step of lytic granule secretion precedes microtubule organizing center polarization at the cytotoxic T lymphocyte/target cell synapse. *Proc. Natl. Acad. Sci. USA* **2013**, *110*, 6073–6078. [CrossRef] [PubMed]
43. Tuomela, K.; Ambrose, A.R.; Davis, D.M. Escaping Death: How Cancer Cells and Infected Cells Resist Cell-Mediated Cytotoxicity. *Front. Immunol.* **2022**, *13*, 867098. [CrossRef]
44. Kong, L.; Deng, J.; Zhou, X.; Cai, B.; Zhang, B.; Chen, X.; Chen, Z.; Wang, W. Sitagliptin activates the p62–Keap1–Nrf2 signalling pathway to alleviate oxidative stress and excessive autophagy in severe acute pancreatitis-related acute lung injury. *Cell Death Dis.* **2021**, *12*, 928. [CrossRef]
45. Schmidt, J.; Rattner, D.W.; Lewandrowski, K.; Compton, C.C.; Mandavilli, U.; Knoefel, W.T.; Warshaw, A.L. A Better Model of Acute Pancreatitis for Evaluating Therapy. *Ann. Surg.* **1992**, *215*, 44–56. [CrossRef] [PubMed]
46. Matute-Bello, G.; Winn, R.K.; Jonas, M.; Chi, E.Y.; Martin, T.R.; Liles, W.C. Fas (CD95) Induces Alveolar Epithelial Cell Apoptosis in Vivo: Implications for Acute Pulmonary Inflammation. *Am. J. Pathol.* **2001**, *158*, 153–161. [CrossRef]
47. Zhao, R.; Zhou, X.; Khan, E.S.; Alansary, D.; Friedmann, K.S.; Yang, W.; Schwarz, E.C.; del Campo, A.; Hoth, M.; Qu, B. Targeting the Microtubule-Network Rescues CTL Killing Efficiency in Dense 3D Matrices. *Front. Immunol.* **2021**, *12*, 729820. [CrossRef]

International Journal of
Molecular Sciences

MDPI

Review

Exploring the Impact of Cyanidin-3-Glucoside on Inflammatory Bowel Diseases: Investigating New Mechanisms for Emerging Interventions

Maximos Frountzas [1], Eva Karanikki [2], Orsalia Toutouza [3], Demosthenis Sotirakis [1], Dimitrios Schizas [4], Panagiotis Theofilis [5], Dimitris Tousoulis [5] and Konstantinos G. Toutouzas [1,*]

1 First Propaedeutic Department of Surgery, Hippocration General Hospital, School of Medicine, National and Kapodistrian University of Athens, 11527 Athens, Greece
2 Department of Clinical Nutrition, Hippocration General Hospital, 11527 Athens, Greece; karanikki.eva@gmail.com
3 School of Medicine, Imperial College of London, London SW7 2AZ, UK
4 First Department of Surgery, Laikon General Hospital, School of Medicine, National and Kapodistrian University of Athens, 11527 Athens, Greece
5 First Cardiology Department, "Hippocration" General Hospital, University of Athens Medical School, 11527 Athens, Greece
* Correspondence: tousur@hotmail.com; Tel.: +30-6970801370

Abstract: Cyanidin-3-O-glucoside (C3G), the most widely distributed anthocyanin (ACN) in edible fruits, has been proposed for several bioactivities, including anti-inflammatory, neuro-protective, antimicrobial, anti-viral, anti-thrombotic and epigenetic actions. However, habitual intake of ACNs and C3G may vary widely among populations, regions, and seasons, among individuals with different education and financial status. The main point of C3G absorption occurs in the small and large bowel. Therefore, it has been supposed that the treating properties of C3G might affect inflammatory bowel diseases (IBD), such as ulcerative colitis (UC) and Crohn's disease (CD). IBDs develop through complex inflammatory pathways and sometimes may be resistant to conventional treatment strategies. C3G presents antioxidative, anti-inflammatory, cytoprotective, and antimicrobial effects useful for IBD management. In particular, different studies have demonstrated that C3G inhibits NF-κB pathway activation. In addition, C3G activates the Nrf2 pathway. On the other hand, it modulates the expression of antioxidant enzymes and cytoprotective proteins, such as NAD(P)H, superoxide dismutase, heme-oxygenase (HO-1), thioredoxin, quinone reductase-oxide 1 (NQO1), catalase, glutathione S-transferase and glutathione peroxidase. Interferon I and II pathways are downregulated by C3G inhibiting interferon-mediating inflammatory cascades. Moreover, C3G reduces reactive species and pro-inflammatory cytokines, such as C reactive protein, interferon-γ, tumor necrosis factor-α, interleukin (IL)-5, IL-9, IL-10, IL-12p70, and IL-17A in UC and CD patients. Finally, C3G modulates gut microbiota by inducing an increase in beneficial gut bacteria and increasing microbial abundances, thus mitigating dysbiosis. Thus, C3G presents activities that may have potential therapeutic and protective actions against IBD. Still, in the future, clinical trials should be designed to investigate the bioavailability of C3G in IBD patients and the proper therapeutic doses through different sources, aiming to the standardization of the exact clinical outcome and efficacy of C3G.

Keywords: C3G; anthocyanin; IBD; ulcerative colitis; Crohn's disease

Citation: Frountzas, M.; Karanikki, E.; Toutouza, O.; Sotirakis, D.; Schizas, D.; Theofilis, P.; Tousoulis, D.; Toutouzas, K.G. Exploring the Impact of Cyanidin-3-Glucoside on Inflammatory Bowel Diseases: Investigating New Mechanisms for Emerging Interventions. *Int. J. Mol. Sci.* **2023**, *24*, 9399. https://doi.org/10.3390/ijms24119399

Academic Editor: Massimiliano Gasparrini

Received: 11 April 2023
Revised: 16 May 2023
Accepted: 19 May 2023
Published: 28 May 2023

1. Introduction

Over the last years, scientific data support that many non-communicable chronic diseases (NCCDs) could be prevented through sufficient dietary intake of bioactive molecules derived from fruits and vegetables. Soluble and insoluble dietary fibers, antioxidants,

functional carbohydrates and polyunsaturated fatty acids are responsible for several health benefits. More specifically, dietary antioxidants (AOX), such as pro-vitamins and phenolic compounds (PC), including anthocyanins (ACNs; anthos = flower, kianos = blue), could alleviate the oxidative stress associated with different molecular events in the body [1]. ACNs are responsible for several bioactivities, including anti-inflammatory, neuro-protective, antimicrobial, anti-viral, anti-thrombotic, and epigenetic actions [2]. However, ACNs differ in terms of metabolic fate and bioactivity. Several physiological barriers in the human body as well as various physical and chemical components in natural or prepared plant foods could influence their metabolic action [3]. In fact, the structure of ACNs is responsible for their nutraceutical potential, which has been associated with their specific physicochemical behavior within foods and biological systems [4]. Similarly, lots of data about Cyanidin-3-O-glucoside (C3G), the most widely distributed anthocyanin in edible fruits, have been published over the previous ten years and will be discussed in the following paragraphs [5].

Inflammatory bowel disease (IBD), which mainly presents as Crohn's disease (CD) or ulcerative colitis (UC), is a heterogenous chronic bowel inflammation without clear etiologic factors. Typically, the first manifestation is a complicated immune response that comprises a number of inflammatory cells, including macrophages, monocytes, neutrophils, natural killer cells, cytokines, and chemokines [6]. The subacute course of this clinical entity is further characterized by chronic immunological reactions that aim to balance local provocative factors and healing processes [7]. Alterations in gut microbiota seem to play a role in maintaining the above-mentioned immunological balance. Several therapeutic agents, such as corticosteroids, immunomodulatory drugs or targeted therapies, have been suggested through years, but there is still lack of clear evidence about the efficacy of several therapeutic regimens [8].

In recent years, the need for more effective therapeutic strategies against IBD has emerged. Under these circumstances, several biological agents with anti-inflammatory or antioxidative functions have been investigated in terms of their safety and efficacy against IBD [9]. The aim of this review is to investigate the possible therapeutic properties of Cyanidin-3-O-glucoside (C3G) in IBD.

2. Cyanidin-3-O-Glucoside

2.1. Chemical Structure

ACNs are anthocyanidin glycosides. Their backbone consists of a benzopyran core [benzoyl ring (A), pyran ring (C)], a phenolic ring (ring B) attached to its 2-position, and a sugar moiety, mainly, at its 3-position in the C-ring. Some 31 anthocyanidins (aglycones) and more than 600 ACNs have been determined thus far [10]. However, the majority of ACNs are based on six aglycones that differ in their B-ring substitution pattern: cyanidin (Cy), delphinidin (Dp), pelargodin (Pg), peonidin (Pn), petunidin (Pt) and malvidin (Mv). These aglycons are further divided into groups based on the type and amount of bonded sugars, as well as the presence of aliphatic or aromatic carboxylates (attached to their sugar moieties). The three non-methylated aglycones (Cy, Dp, and Pg) are further classified as 3-monosides (mostly glucosides), 3-biosides, 3,5- and 3,7-diglucosides [11]. Moreover, the heterogeneity in ACNs' structure represents a challenge for their isolation and identification. However, according to Flamini et al., the mass spectral fingerprint of Cy and the majority of its glycosides have been established so far [12].

The processes of glycosylation and methylation affect Cy's hydrophobic (octanol)/hydrophilic (water) partition coefficient (LogP), its polar surface area ($Å^2$), and its molecular weight (MW). All of these have important implications in the metabolic fate of Cy-derivates (ADME: absorption, distribution, metabolism and excretion). Cy has a lower MW (287.24 g/mol), and $Å^2$ (114.3) is less hydrophilic (LogP = 3.05) than C3G (449.4 g/mol, $Å^2$ = 191, LogP = 0.39). A second glycosylation (Cy-3,5-O-diglucoside, Cy3,5GG) increases its hydrophilic character, but compromises its absorption capacity, while an extra malonyl group (Cy3MG) has the opposite effect [13]. In addition, other structural features in C3G

have important implications for its chemical reactivity in vitro. STD-NMR spectroscopy and molecular dynamics simulations have been utilized to show that the absence of an extra hydroxyl at $R^{5'}$ in C3G affects its binding capacity toward citrus pectins, when compared to Dp3G [14]. Moreover, it has been demonstrated that C3G (as a flavylium cation, pH 3.4) binds spontaneously within 1 min to bacterial (*Gluconacetobacter xylinus* ATCC 53524)-derived cellulose [15]. It has also been reported that this binding behavior is not limited by the available interacting sites in cellulose, but it is limited by the number of free C3G molecules. Therefore, a Langmuir binding isotherm model is proposed:

$$Q = Q_{max} \times [(K_L \cdot C) \times (1 + K_L \times C)^{-1}].$$

where Q represents the amount of absorbed C3G per unit mass of cellulose ($\mu g \cdot mg^{-1}$), Q_{max} is the apparent max adsorption capacity (1109 $\mu g \cdot mg^{-1}$ of cellulose), K_L is the apparent binding affinity constant, and C is the free C3G concentration at equilibrium (mM). By applying this equation, a "C3G saturation effect" could be observed at about 200 mM. Furthermore, utilizing an in vitro model to simulate GI conditions demonstrated a "bind–release" behavior between C3G and pectin/chitosan at each digestion step (oral, gastric, and intestinal). On the other hand, it is suggested that this polymeric mixture functions as a protective mechanism against G3G degradation, as it is gradually released from protein and polysaccharide bonds and eventually becomes available for absorption by GI epithelial cells [16].

It is highly important that C3G binds to proteins in vitro as well. ACNs present different binding capacities to human serum albumin (HSA; Dp3G > C3G > Pg3G), but their capability to induce structural changes to this protein is also different (Pg3G > C3G > Dp3G) [17]. In addition, C3G–protein interactions are established by hydrogen bonding and van der Waals forces; thus, the secondary structure of bovine serum albumin (BSA), hemoglobin (Hb), and myoglobin (Mb) are almost destroyed (less% α-helixes) [18]. C3G is usually represented as a cation, which is only possible under acidic conditions, such as those created by gastric juice, and in silico assays, which have revealed that cationic C3G cannot be absorbed through passive diffusion. Nevertheless, only a substitution at $R3^1$ [–H (Pg3G) by –OH (C3G)] modifies C3G's bioaccessibility, absorptivity, and metabolism within enterocytes [19].

Finally, rare types of anthocyanidins, such as 3-deoxy-anthocyanidins, hydroxylated at the 6th position, 5, 7, 3^1, 5^1-*O*-glycosilated, *C*-glycosylated, or aliphatic (mainly malonic and pyruvic acids)- and PC-acylated ACNs are also currently studied, as they seem to be more bioactive than their conventional counterparts [20]. For example, Cy-malonyl-glucoside (Cy-Mal-3G) demonstrates stronger anticancer (colon, liver, prostate, and breast) activity than C3G [21]. Moreover, C3G acylated with lauric acid improves its stability due to its ester group, which is more stable than a hydroxyl group [22].

2.2. Dietary Sources

C3G is one of the commonest but not the major cyanidin; black elderberry, blue hybrid maize and Korean black raspberry are exceptions to this rule [23]. The daily intake and further bioactivity of C3G are highly affected by the proper selection of their plant sources. Some classic fruits characterized by increased C3G bioavailability are pomegranate and blackberry, while some exotic fruits are bilberry, elderberry and mulberry [24]. Although C3G is widely known to be found in fruits, mainly in berries and other blue and red fruits and vegetables, it is not necessarily the main ACN. For example, strawberry has 15 times more Pg3G, and raspberry (fresh/pomace) has 1.4–1.5 times more Cy-3-*O*-sophoriside (Cy3So) than C3G [25].

Dietary surveys with detailed information on the total and specific intake of ACNs are also scarce. Daily intake of ACNs, mainly C3G, does not depend on the richness of their sources. Mean daily intake per capita of ACNs was approximately 12.5 mg in US adults in 2000–2002, 80% coming from blueberry, grape, onion, grape 100% juices, raspberry, red cabbage, wine, and cherry sweet. In 2007–2008, the mean daily intake was 11.2 mg,

adding red/purple vegetables, bananas, and yogurt to the list [26]. In Europeans, the mean intake of total ACNs is about 20 mg/d, with Cy being the most common, and in Polish adults participants of the HAPPIEE study, 56% of daily ACN intake came from blackcurrants, beans, and strawberries [27]. Eastern countries present a higher intake of flavonoids than Americans or Europeans, but their ACN sources appear to be lesser than their isoflavone/proantocyanidin sources [28]. According to KNHANES 2007–2012, the mean daily intake of flavonoids was 318 mg/d/person. Some 23% of this mean daily intake was from proanthocyanidins, and 11.6% from anthocyanidins, while 20.3% was from flavonones, and 0.3% from flavones. The major contributing food groups to flavonoid intake were vegetables (20.5%) such as onions (9.6%) and fruits (54.4%) such as apples (21.9%), mandarins (12.5%), grapes (9.0%), and other fruits (1.4%) [29]. It should be noted that habitual intake of ACNs and C3G may vary widely among populations, regions, and seasons, and among individuals with different education and financial status, and depends on adequate dietary assessment tools (e.g., 24FR vs. FFQ) [30].

In conclusion, dietary choices could have an important impact on both ACN (and C3G) intake and the following health effects. In this sense, recent progress in agricultural and food technology has driven the international market of berry fruits at a lower cost [31]. According to the report of the Agri-Food and Fisheries Service, the production of berries in Mexico has increased almost three-fold in recent years [32]. Therefore, intake of ACNs and particularly of C3G is expected to gradually increase over the next years.

2.3. Bowel Metabolism

The small bowel is the third location of C3G metabolism, after the oral cavity and stomach. Unlike gastric conditions, the physical and chemical microenvironment in the small intestine reduces C3G's bioavailability by 40–50% [33]. Factors such as pH, C3G's ability to release from the food matrix, pancreatic and brush border enzyme action, transportation processes and enterocyte metabolism in phase I/II are crucial for the bioavailability of C3G, Cy and their metabolites (degradation products or phase II metabolites). At intestinal pH (8.2 ± 0.2), C3G becomes negatively changed and highly unstable, returning to its quinoidal form, while its glucose moiety remains neutral. Moreover, further de-glucosylation of C3G is performed with neither lactase-phlorizin hydrolase (LPH; EC 3.2.1.62) nor cytosolic β-glucosidases [34]. It is worth mentioning that the cleavage of its glucose moiety is not a prerequisite for C3G chemical breakdown and splanchnic metabolism, although it is an important mediator of its trans-epithelial transport [35].

Once inside the enterocyte, Cy and C3G could be either transformed to other PC (particular phenolic acids) and derivatives in phase I metabolism or to several conjugates (methylated, glucuronidated or sulphated) in phase II metabolism [36]. Microbials, with the exception of metabolic machinery, are responsible for producing phase I metabolites, although there is controversy as to whether this process occurs in the small intestine or as a product of the enterohepatic cycle (EHC) [37]. In phase II metabolism, many enzymes, such as phenyl sulfotransferases (PST), uridine 51diphosphate glucuronosyltransferases (UGT) and catechol-O-methyltransferase (COMT), may modify the Cy (and other anthocyanidins) structure, making it more water-soluble and thus facilitating their further elimination by the kidneys [13].

The main derivatives of Cy's metabolism/degradation are protocatechuic acid (PCA) and phloroglucinaldehyde (PGA) [38]. Cy and PGA, due to their hydrophobic nature in comparison to PCA, can passively diffuse through biological membranes, reaching the plasma in the first 2 h. Another reported reaction involves Cy (or C3G) methylation to produce Pn (or Pn3G), with both having almost the same in vivo bioactivity [39]. Recently, the major pathways for C3G metabolism in liver microsomes have been proposed. After deglycosylation, Cy produces PGA from its A-ring, ferulic acid (FA), 3,4-dihydroxyphenyl acetic and 4-hydroxyphenylacetic acids from its B-ring, and 3,4-dihydroxybenzaldehyde (PCA immediate precursor) also from its B-ring [40].

C3G and derived metabolites that surpassed absorption from the small bowel can finally be released from fibrous food matrices (also known as macromolecular antioxidants), transformed by the microbiome, and then absorbed by colonocytes [41]. The large bowel contributes to the remaining deglycosylation, phenolic acid production, and phase II conjugation events, resulting in the excretion of, intact, less than 0.005% of C3G. As occurred in the small bowel, the C-ring rupture and the Cy chalcone formation lead to the apparition of hydroxybenzoic's (OH-BA) and phenylacetic acids' derivatives, VA, IVA, FA, and HA, which can further be eliminated in feces and urine (by means of EHC) [42]. These metabolic transformations are mediated by the slightly basic pH present at this level, where C3G and Cy are highly unstable. On the other hand, certain metabolites such as 2-OH-4-methoxybenzoic acid, 4-methoxybenzaldehyde, methyl-VA, and caffeic acid are specifically produced within the large bowel [43].

2.4. Health Effects

C3G's bioactivity has been further investigated in clinical studies in humans. For instance, C3G benefits cardiovascular health [44–46]. A double-blind, randomized crossover study indicated that some ACNs peaked within 1–3 h, just as HDL-cholesterol did [placebo vs. 640 mg/d/4 weeks (purified ACNs supplement)] [47]. However, when different ACN sources were utilized in the same protocol [placebo vs. 486 mg/d/4 weeks (Delphinol® from maqui berry, Huechuruba, Santiago, Chile], a decrement in LDLox and F2-isoprostanes levels was highlighted [48]. However, both studies did not report any other noticeable benefit for CVD markers [49]. According to this, the significant changes that were reported were upregulation in serum HDL and downregulation in LDL cholesterol; in addition, soluble vascular cell adhesion molecule-1 (sVCAM-1) and high sensitivity C-reactive protein (hsCRP) levels were observed after 24-week ACNs = supplementation [50]. The same results have been reported with ACNs from strawberries, which modulated these inflammatory biomarkers and indirectly improved insulin action [51]. It is noteworthy that endothelial health is correlated to the regulation of nitric oxide production, and the latter could be altered by several types of flavonoids, including ACNs [52]. As for C3G's anticancer activity, Cy derivatives (including C3G) from black raspberries (BRB) are extensively metabolized and retained within the oral cavity of healthy humans. In addition, administrating per os troches of freeze-dried BRB to oral squamous cell carcinomas patients (OSCCs) for 14 days improves the expression of pro-survival genes (AURKA, BIRC5, EGFR). It reduces other pro-inflammatory genes (NFKB1, PTGS2) [53]. Moreover, the acute intake of a blueberry dry extract regulates DNA methylation in patients with colorectal adenocarcinomas, despite the inter-individual variability [54].

The radical scavenging capacity (RSC) and molecular competition ability of C3G (and Cy) may help prevent certain inflammatory processes, CVD, aging, and cancer [55]. For instance, senescent and cancer cells are also susceptible to DNA cleavage due to epigenetic factors that induce the production of free radicals and activate oxidative enzymes, such as xanthine oxidase, which can be attenuated by Cy and C3G [56]. Additionally, some animal studies have suggested that C3G may slow or inhibit the absorption of carbohydrates (glucose) and lipids in the intestine, confirming the postulated mechanisms in cells and the physiological impact on humans [57]. It has been observed that C3G provides protection against CVD related to oxidative stress, due to its transportation in EA.hy926 cells via a specific bilitranslocase, and it accumulates in the vascular endothelium wherein it exerts anti-ischemic properties on isolated rat heart [58]. It is worth mentioning that C3G's metabolic bioactivity in adipose cells has been extensively studied, both in vivo and in vitro. C3G and Cy both upregulate human adiponectin, uncoupling acylCoA oxidase-1, protein-2, and perilipin, while they downregulate IL-6 and plasminogen activator inhibitor-1 [59]. When adipose cells are exposed to the omega-3-fatty acid docosahexaenoic acid, C3G suppresses the secretion of interleukin-6 and monocyte chemoattractant protein-1 (MCP-1/CCL2) and decreases its basal lipolytic activity [60]. However, C3G and Cy upregulate the hormone-sensitive lipase gene and enhance the lipolytic activity of rat adipocytes [61].

On the other hand, the biological effects demonstrated in laboratory animals and in vitro assays do not precisely reflect their efficacy in humans. In a great number of cases, the amount required to achieve a specific biological action in general is much larger than that obtained from dietary sources. For example, the average amount of C3G employed in rat/mice bioassays far exceeds (by around 30–60 times) the amount that can be obtained from a single dietary source. On the other hand, in different cases, the amount derived from a habitual diet is sufficient to achieve certain benefits [62]. Moreover, C3G from natural sources or manufactured nutraceuticals is seriously restricted by its splanchnic metabolism, and thus its efficacy in targeting internal tissues is limited. Taking C3G's low bioaccessibility and bioavailability into account, entrapping agents such as malto/cyclodextrins or liposomes may be efficient alternatives to preserve its properties within the GI tract. Under these circumstances, concentrated sources of C3G, such as purees or freeze-dried fruits, provide a much higher intake of C3G, but also preserve its bioactive ability within the GI tract [63].

The previously stated bioactivities of C3G, its aglycone (Cy), and derived metabolites mostly rely on the following mechanisms: RSC, epigenetic action, competitive protein-binding, and enzyme inhibition. Flavonoids seem to exert regulatory effects on gene expression. Some examples are naringenin, kaempferol, and quercetin. The combination of flavonoids and chemotherapy seems to be an interesting approach to cancer treatment too [64]. However, molecular studies involving C3G or Cy as epigenetic effectors are still scarce. Many in vivo and in silico studies using pure DNA or protein systems have indicated their macromolecular-binding and enzyme inhibition capacities [65]. A $\Delta\lambda$ to the ultraviolet-visible spectra of this nucleic acid has been demonstrated while studying the binding capacity of Cy and C3G to calf thymus DNA, indicating the formation of the DNA-Cy and DNA-C3G complexes with an intercalative binding mode evidenced in their fluorescence spectra, and with C3G binding to DNA more efficiently than Cy [66].

Both molecules also bind salivary and blood proteins, which might modify their fate within GI and their bloodstream transport. Spectroscopic studies suggest that C3G spontaneously binds albumins by means of weak forces such as hydrogen bonds and Van der Waals forces, as well as hydrophobic interaction on a minor scale [17]. C3G binds to BSA to its IIA sub domain and is surrounded by key hydrophobic and non-polar (Ala, Leu, Tyr Phe, Trp and Gly) and polar (Arg, Glu, Lys and Asp) residues within the hydrophobic cavity of site II' [67]. Similarly, the abovementioned phenomenon has been reported in HAS. Certain structural features of both anthocyanidins/ACNs modify their binding capacity toward HAS; at increased pH 7.0 and at reduced pH 4.0, there is a differential electrostatic environment resulting in differences regarding the binding capacity of ACNs in their quinoidal form [68]. In addition, the binding constant of C3G has been reported to be higher for myoglobin than for BSA hemoglobin, which is structurally associated with its binding capacity toward α-helices. Finally, evidence on the differential binding and inhibitory capacity of Cy and C3G toward GI enzymes has been elucidated. C3G is a much stronger inhibitor of both intestinal α-glucosidase and pancreatic α-amylase as compared to Cy [69], whereas glucose substitution at the 3-O (increases) and 5-O (reduces) positions in Cy modifies its inhibitory activity toward α-glucosidase.

3. Inflammatory Bowel Disease (IBD)

Inflammatory bowel disease (IBD) is a term that describes disorders involving long-standing (chronic) inflammation of tissues within the GI tract. Types of IBD include ulcerative colitis (UC) and Crohn's disease (CD). As far as ulcerative colitis is concerned, it involves inflammation and sores (ulcers) along the lining of large intestine (colon) and rectum [70–72]. On the other hand, Crohn's disease is characterized by inflammation of the lining of digestive tract, which often may involve its deeper layers. Despite the fact that Crohn's disease most commonly affects the small intestine, it can also affect the large intestine, and, rarely, the GI tract. Both are typically characterized by abdominal pain, diarrhea, rectal bleeding, fatigue and weight loss. Moreover, they are associated with

extraintestinal manifestations, such as anemia, fever, weight loss, arthritis, ankylosing spondylitis, sclerosing cholangitis, uveitis, iritis, pyoderma gangrenosum and erythema nodosum. IBD patients also have a higher risk of colon cancer [71]. The extent of the symptoms is not the same for every patient, as it may range from mild illness to life-threatening complications.

3.1. Epidemiology

The number of children living with IBD is growing rapidly; in Canada, the diagnosis of young people increased 50% in the first decade of 21st century [73]. In 2018, there were over 7000 children and youth under 18 years old living with IBD in Canada alone, and 600 to 650 young children (under 16 years) diagnosed every year [73]. Several reports have been drafted on the prevalence of IBD in developed Western countries. Asia has a lower prevalence of IBD, whereas a recent increase in its incidence and prevalence has been observed in Eastern Europe and Asia [74]. Previous studies have demonstrated that the prevalence of Crohn's disease (CD) is higher than that of ulcerative colitis (UC) in pediatric patients in Northern California. However, in French pediatric patients, the observed rate for UC was higher than that for CD [75]. In a survey in Western Europe, IBD was found to affect 0.5–1% of the population, with 56 and 104 new cases per million inhabitants per year for CD and UC, respectively [76]. In addition, IBD affects approximately 1.4 million patients in the USA and 2.4 million in Europe [77]. In another investigation, the incidence of UC was reported to be around 10–20 per 1,000,000 per year, with a prevalence of 100–200 per 1,000,000 in Western countries [78].

3.2. Pathogenesis

The etiology of IBD is still not completely understood. Several studies support the hypothesis that its onset originates from the combination and interplay of immune dysregulation (chronic or relapsing), genetic factors, environmental triggers, psychological factors, smoking, host immune system and microbiota dysbiosis. However, the exact etiology of IBD is still not fully understood [79–82]. CD involves all parts of the GI tract from the mouth to the anus, whereas UC is confined to the colon. Activation of these cells in the intestinal mucosa contributes to elevated local levels of pro-inflammatory cytokines, such as tumor necrosis factor alpha (TNF-α), interleukin 1β (IL-1β), interferon-γ (IFN-γ), and interleukin-23 (IL-23), among which TNF-α attracts more attention due to its remarkable pro-inflammatory and proapoptotic effects [83]. Therefore, TNF-α blockers are central in IBD therapy. Besides cytokine production, the overproduction of different reactive oxygen species, including superoxide anion radicals, hydroxyl radicals, singlet oxygen, and triplet oxygen from activated leukocytes, overwhelm the tissue's antioxidant defenses and could be another molecular event involved in IBD pathogenesis [84]. Oxidative stress is also suggested to have a crucial role in apoptosis. It has been exhibited that the concentration of antioxidants (vitamins, flavonoids and trace elements) in patients with CD and rat experimental models of UC is markedly lower [85]. Antioxidants, defined as substances that significantly delay or inhibit oxidation of an oxidizable substrate, can be beneficial in IBD therapy even when used at concentrations lower than the oxidized substrate [86]. More than 230 genes predisposing people to IBD have been discovered [87]. Many of these IBD susceptibility genetic polymorphisms are associated with host mucosal barrier function and are involved in host–microbiome interactions [88–90], thus supporting the hypothesis that alterations in the gut microbiome are essential for triggering chronic inflammation, and not merely a consequence [91,92].

In addition, nuclear factor-kappa B (NF-κB)-signaling significantly contributes to multiple host responses underlying IBD pathogenesis. The NF-κB family of transcription factors are regulators of inflammation and gut epithelial integrity, and activators of antigen-presenting cells and effector leukocytes [93]. Upon activation, NF-κB dimers translocate to the nucleus, where they modulate the transcription of several genes, including those involved in inflammatory and immune responses [94]. Several IBD genetic risk alleles,

including nucleotide-binding oligomerization domain-containing protein 2 (NOD2), TNF-α-induced protein 3 (TNFAIP3/A20), and Toll-interacting protein (TOLLIP), promote gut pathogenesis, at least partly, through dysregulated NF-κB signaling [95]. Epithelial cells and macrophages isolated from the inflamed intestine of IBD patients show increased activation and nuclear localization of NF-κB-p65 [96]. Aryl hydrocarbon receptor (AHR)–NF-κB–CCAAT enhancer-binding protein beta (C/EBP-β)-signaling axis is found to operate in T cells and dendritic cells to promote intestinal inflammation [97].

Last but not least, the nuclear-related factor 2/ Kelch-like ECH associated protein 1 (Nrf2/Keap1) signaling pathway seems to regulate GI tract function, and therefore may moderate the course of IBD. According to Arisawa et al. [98], an Nrf2 gene polymorphism may be associated with the development of UC, while Myers et al. [99] supported that Nrf2 levels are found to be decreased in UC patients and those with active CD compared to healthy controls. On the other hand, higher Nrf2 levels are positively linked to antioxidative enzymes such as peroxiredoxin-1 and glutathione S-transferase A4, and negatively linked to pro-inflammatory IL-17a [100]. A study reported that persistent Nrf2 activation is the adaptation of colonic epithelial cells to oxidative stress during chronic inflammation of active IBD [101]. Stimulation of Nrf2 may be linked to the excessive mobilization of NF-kB during inflammatory reactions [68,69] and, in turn, may increase ROS production and enhance immediate early response-3 protein (IER3) expression [102,103]. The effect of Nrf2 on IBD development and progression should be further investigated.

3.3. Therapeutic Options

5-Aminosalicylic acid, sulfasalazine, glucocorticoids, azathioprine, 6mercaptopurine, thioguanine, methotrexate, cyclosporine, infliximab, and tacrolimus are all used for IBD treatment. However, the long-term usage of these drugs is limited due to several side and adverse effects, such as diarrhea, abdominal pain, nausea, and vomiting (sulfasalazine), pancreatitis, hepatotoxicity, and hematologic problems (methotrexate, azathioprine), leucopenia (6-mercaptopurine), nephrotoxicity, cardiotoxicity, hypertension, gingival hyperplasia, and arteriolopathy (cyclosporine and tacrolimus) [104]. Moreover, about 30–50% of CD patients and 15–20% of UC patients are not sufficiently controlled with conventional anti-inflammatory treatment, and most of these treatments are inadequate [105]. Conventional anti-inflammatory agents serve as symptomatic therapeutic means, whereas concerns have been raised regarding the efficacy of novel biologic and small molecule-targeted therapeutics. Consequently, heterogenous recommendations have been provided, which usually do not include them [106]. Surgical intervention is required in complicated cases, or when pharmacological treatment is not successful. Regarding the cited problems, new therapeutic strategic approaches should be used for IBD therapy. Targeting of CD4+ T-cell cytokines, inhibition of leucocyte adhesion and gene therapy are amongst the newest treatments proposed for IBD; however, it should be mentioned that many patients (from 39% in Austria to 51% in Germany) turn to herbal therapy in addition to conventional treatments [107].

3.4. Natural Products

Various herbal products, such as Portuguese blueberries and dark purple rice extract, have been used for IBD treatment [108–111]. Many investigations have reported that plant derivatives, such as polyphenols, are involved in a wide range of biological activities, such as anti-inflammatory and antioxidative activities, as secondary plant metabolites [112]. Dietary fiber showed an anti-IBD effect through the modification of TNF-α, IL-2, and nitric oxide (NO). Natural supplementation has a central role in cytokine production regulation.

4. Therapeutic Effects of C3G in IBD

Nowadays, more and more patients with IBD prefer an alternative medical approach to their condition, and turn to plant-based drugs; thus, anthocyanin-rich foods are highly emphasized. ACNs and anthocyanidin glycosides have presented an important role

in preventing and treating IBD. C3G has been recognized to have antioxidative, anti-inflammatory, cytoprotective, and antimicrobial effects that can be useful for IBD management (Table 1). In particular, C3G has been shown to act directly as an antioxidant and free radical scavenger [36,113,114]. Additionally, it has been found to regulate several detoxification enzyme pathways [115,116], modulate cytokine levels [117] and affect IFN pathways [39,117]. It also has an indirect effect via modulation of transcriptional factors, including NF-κB [114,118–121] and MAPK [122,123] activation and the Nrf2 pathway [116,119]. G3C can also improve intestinal microbiota composition [120,124].

Table 1. The protective effects of C3G against IBD.

Year; Author	Study Type	Subjects (Animal/Cell Models/Individuals)	Dose	IBD Indicators	Related Molecular Mechanisms in Regulation of IBD
[125]	In vitro	CM stimulated T84 cells	25, 50, 100 μM for 4 h	NA	↓ IP-10 (CXCL10)
[115]	In vitro	Cytokine stimulated HT-29 cells	12.5 to 50 μM for 24 h	NA	↓ NO,↓ PGE2, ↓ IL-8, ↓ iNOS ↓ COX-2↓ STAT1
[116]	In vitro	Cytokine stimulated HT-29 cells	25 μM, for 1 h	↑ Nrf2 pathway, ↑ HO-1,↑ GCLC and GCLM ↑ GSH/GSSG	↓ Reactive species
[114]	In vitro	Caco-2 cells + TNF-α	20–40 μM for24 h	↑ Nrf2 pathway, ↑ GSH ↑ HO-1 and NQO-1 mRNA Levels	↓ TNF-α, ↓ IKKα/β phosphorylation/activation and IκBα, ↓ NF-κB pathway ↓ Il-6 induced by TNF-α, COX-2, PGE2 and TXB2
[118]	In vitro	Caco-2 cells	0.25, 0.5 and 1 μM for 24 h	↑ FITC-dextran permeability	↓ IKKα, ↓ p65 phosphorylation, ↓ MLC, ↓ TNFα, ↓ NF-kB pathway, ↓ TEER
[121]	In vitro	Caco-2-HUVECs	20 or 40 μM for 24 h	NA	↓ NF-κB pathway, ↓ TNF-α, ↓ IL-8 ↓ endothelial cells activation: ↓ E-selectin, ↓ VCAM-1 mRNA, ↓ leukocyte adhesion
[39]	In vivo and in vitro	BALB/c TNBS-induced colitic mice Caco-2 cell monolayer model +LPS	200 μL for 12 h before TNBS injection 24.2–96.8 g/kgBW daily for 3 days	NA	↓ MPO, ↓ TEER, ↓ LY flux values. ↓ NO, ↓ TNF-α, ↓ IL-1b, ↓ IL-6, ↓ IFN-γ ↓ histological damage
[117]	In vitro	(Cell culture: RAW 264.7 cells+ IFNα+ IFNβ, 24 h) Naïve mouse peritoneal macrophages, lymphocytes removed + 1 ug/mL LPS, 24 h	1 ug/mL for 24 h	NA	Direct inhibition of CD80 and CD86 Inhibition of CD169 Expression induced by Type I IFN ↓ IL-1β, IL-18, IL-6, IL-17, and TNF-α

Table 1. *Cont.*

Year; Author	Study Type	Subjects (Animal/Cell Models/Individuals)	Dose	IBD Indicators	Related Molecular Mechanisms in Regulation of IBD
[36]	In vitro	Caco-2 cells + 100 μM PA (basolateral side)	10 or 20 μM for 24 h	↑ Nrf2/EpRE pathway ↑ NQO-1	↓ NF-κB pathway ↓ IL-6 and IL-8 mRNA levels ↓ COX-2 ↓ ROS
[113]	In vitro	Caco-2 cells+ LPS ± HPP	C3G-BP complexes (100–100 μg/mL)	↑ IL-10	↓ depolarization of mitochondria, ↓ ROS ↓ IL-1β, TNF-α, and IL-8 ↓ iNOS, COX-2, Bcl-2 and cleaved caspase-3 levels Inhibition of apoptosis
[119]	In vitro	Caco-2 cells +TNF- α	0.18, 0.37, 0.75, 1.5 μg C3G eq./mL for 24 h (ACN-rich purified and standardized bilberry and blackcurrant extract (BBE))	Activation of Nrf2/ Keap1 pathway	Inhibition of NF-κB pathway activated by TNF-α ↓ IL-8 and ↓ IL-6 mRNA levels
[124]	In vivo	DSS-induced colitic UC mice + HHP treatment	HPP 200 mg/kg C3G+ blueberry pectin complex (Oral administration)	↑ protein levels of the ratio Bcl-2/Bax and caspase-3/cleaved caspase-3 genes ↑ *Bacteroidetes, Verrucomicrobia Candidatus Saccharibacteria.*	↓ mRNA expression of pro-inflammatory factors ↓ NF-κB P65, ↓ NF-κB pathway ↓ *Firmicutes, Proteobacteria*, ↓ *Firmicutes to Bacteroidetes (F/B)* ratio
[126]	Cohort study	47 IBD patients Administration of a purple corn supplement to IBD patients receiving infliximab	Purple corn supplement composed by 2 mg GAE/g DW (gallic acid equivalents per g of dry weight) and total anthocyanin content of 0.5 mg cyanidin 3-glucoside (C3G)	NA	CD group only, not UC: ↓ CRP, ↓ IFN-γ ↓ TNF-α, IL-5, IL-9, IL-10, IL-12p70, and IL-17A

PA: palmitic acid, HHP: high hydrostatic pressure treatment, BP: blueberry pectin, HUVECs: human umbilical vein endothelial cells, TEER: transepithelial electrical resistance, LY flux: Lucifer yellow flux, TNF-α: tumor necrosis factor-a, IL-6: interleukin-6, IL1b: interleukin-1b, IFN-γ: interferon-γ, PGE2: prostaglandin E2, iNOS: nitric oxide synthase, COX-2: cyclooxygenase-2, HO-1: hemoxygenase-1, MLC: phosphorylation of myosin light chain. GCLM: glutamate cysteine ligase mRNA; ↑, increase; ↓, decrease.

4.1. C3G Inhibits NF-κB Pathway Activation

NF-κB is the main redox-sensitive nuclear transcriptional factor involved in the intestinal inflammation process [127], and plays a role in the regulation of several pro-inflammatory mediators, including interleukins (IL-6, IL-8, IL-12, IL-1β), TNF-α and IFN-γ [128]. Although NF-κB is involved in preserving intestinal epithelial cell homeostasis and regulating intestinal permeability [129], the chronic activation of NF-κB is typical of IBD and may play a critical role in the aggravation of inflammatory conditions in the intestinal

epithelium [96,130]. Many drugs for IBD interfere with the activation of NF-κB [131,132]; thus, natural antioxidants and their compounds that modulate the NF-κB pathway, such as C3G, have great potential as efficient complementary approaches for IBD [133,134].

Numerous in vitro studies have demonstrated the association between C3G and the NF-κB pathway [36,114,118,119,121]. A study by Cremonini et al. [118] indicated that C3G was able to completely prevent TNFα-mediated increases in IKKα and p65 phosphorylation in Caco-2 cells. Protection of TNF-α-induced activation of NF-κB led to a 1,4-fold increase in the MLC kinase-mediated phosphorylation and activation of MLC. It was therefore suggested that inhibition of the NF-κB pathway was the primary mechanism of monolayer protection from TNFα-induced decreases in TEER and increases in FITC-dextran permeability. Likewise, Speciale et al. [119] claimed that C3G's anti-inflammatory effects on TNF-α-induced Caco-2 cells were mediated via inhibition of the NF-κB pathway activated by TNF-α, and a reduction in IL-8 and IL-6 mRNA levels.

A study by Bashllari et al. [36] indicated a dose-dependent inhibition of the upregulation of palmitic acid (PA)-induced transcriptional activity of p65, IL-6, and IL-8 mRNA levels in PA-induced Caco-2 cells; thus, C3G helped in restoring gene expression levels to control values. Cytokines' downregulation was also reported in cells not exposed to PA. During the same study, the anti-inflammatory effect of C3G was further evaluated, considering another NF-κB downstream target, COX-2. It is worth mentioning that the human gene encoding COX-2 has two binding sites for NF-κB, in correspondence with the promoter region. It is activated by TNF-a, IL-1, IFN-γ via the NF-κB and AP-1 pathway, and upregulated in IBD intestinal mucosa. According to Bashllari et al., C3G reduced COX-2 protein levels in a dose-dependent manner, confirming the protective effect of C3G against PA-induced Caco-2 cells.

Regarding inflammation, a recent study by Tan et al. [113] reported that C3G monomer and C3G-BP complexes have been found to downregulate iNOS and COX-2 protein expression in Caco-2 cells. The greatest anti-inflammatory effect has been observed in HHP-treated C3G-BP complexes. According to Ferrari et al. [114], a C3G dose of 20–40 μM administered to intestinal Caco-2 cells exposed to TNF-α has anti-inflammatory properties through inhibition of the NF-kB pathway. C3G reduces TNF-α levels, IIKKα/β phosphorylation/activation and IκB, the two upstream kinases regulating NF-kB. Furthermore, it inhibits the expression of Il-6 induced by TNF-α, and downregulates COX-2, PGE2, and TXB2 [114]. Noting that the endothelium is closely linked to the initiation and propagation of IBD pathology, while distinctive features of the intestinal endothelium contribute to these conditions [135], Ferrari et al. [121] investigated C3G's modulatory effects on in vitro inflammatory crosstalk between intestinal epithelial and endothelial cells, using Caco-2 and HUVECs cells.

IBD initiation and progression stages are well known to involve changes in mucosal immunity and gastrointestinal physiology. Endothelial cells adjust structurally and functionally to modulate vascular supply, immune cell emigration, and the tissue environment [136]. In active IBD, angiogenesis of the endothelium mediated by chemokines and cytokines might correlate with disease severity. The newly formed endothelium or inflamed vessels differ from normal vessels in the terms of production of and response to pro-inflammatory cytokines, adhesion molecules and growth factors [137]. As a result, barrier function, coagulant capacity and blood cell recruitment after injury might be altered in the newly formed endothelium. Thus, Ferrari et al. [121] concluded that selective inhibition of the NF-κB pathway in epithelial cells represents the main mechanism by which C3G exerts its protective effects. C3G has been reported to downregulate TNF-α-induced nuclear translocation of NF-κB, reduce TNF-α and IL-8 gene expression in Caco-2 cells, and subsequently downregulate endothelial cells' activation, while decreasing E-selectin and VCAM-1 mRNA levels, leukocyte adhesion, and NF-κB levels in HUVECs [121].

Min et al. [122], using RAW 264.7 cells exposed to LPS, confirmed the downregulatory effects of C3G on TNF-α, L-1β, NO expression, LPS-induced PGE2, and NOS levels. Several IBD model studies have shown that C3G exhibits anti-inflammatory activity via NF-κB

inhibition [122,124]. According to Tan et al. [124], high-pressure threatened (HHP)-C3G-BP complexes have more enhanced anti-colitic effects than C3G monomers in DSS-induced colitic UC mice; HHP treatment increases ACNs' stability and availability in the body [138]. In the study, C3G administered orally at 200 mg/kg together with blueberry pectin was reported to be effective in alleviating inflammation by inhibiting NF-κB, as indicated in the significantly reduced levels of p65 expression [124]. In the study by Min et al. [122], in which oral administration of C3G was evaluated in BALB/c carrageenan-induced inflamed mice, C3G led to inhibition of NF-κB activation and pro-inflammatory mediation of COX-2 expression. Similarly, administration of C3G at a dose of 40 mg/kg for five days to antibiotic-associated diarrhea BALBc mice seemed to have anti-inflammatory effects through reducing the level of p65 phosphorylation and TNF-α, IL-6, and IL 12 levels, thus inhibiting the inflammatory facilitation of the NF-κB pathway [120].

Activation of the redox-sensitive signals IKK/NF-kB and increased expression of the PTP1B phosphatase regulated by NF-kB are cited in a study conducted by Daveri et al. [139] on mice fed with a high-fat diet and an AC-rich blend. Increased NF-kB p65 nuclear translocation of TNF-α challenged cells was additionally confirmed in in vitro studies using human umbilical vein endothelial cells [123]. A study by Fratantonio et al. [140] similarly found that C3G significantly inhibited the NF-κB pro-inflammatory pathway and adhesion molecules induced by PA; therefore, these effects have been attributed to the activation of Nrf2/EpRE pathway.

4.2. C3G Activates Nrf2 Pathway and Modulates Cytoprotective Enzymes Expression

Some bioactive components of food, including ACNs, exert indirect antioxidant activity by regulating the expression of antioxidant enzymes and cytoprotective proteins, such as NAD(P)H, superoxide dismutase, heme-oxygenase (HO-1), thioredoxin, quinone reductase-oxide 1 (NQO1), catalase, glutathione S-transferase and glutathione peroxidase, which are essential for cell protection [123,141]. Increased expression of these molecules could be modulated by Nrf2, a member of the NF-E2 family (transcription factors with basic leucine zipper domains). Nrf2 and its target genes mainly exert antioxidative effects or protective effects from chemical-induced cellular damage. Nrf2 is sequestered in the cytoplasm by Keap1; phase II enzyme inducers and prooxidants can induce its modification and disrupt the Nrf2–Keap1 complex, causing Nrf2 translocation into the nucleus, where it binds to the antioxidant responsive element (ARE), which is a cis-acting enhancer element that stimulates gene expression [142].

A study conducted by Speciale [119] indicates that C3G exerts an indirect antioxidant cell-adaptive response through the activation of the Nrf2/ Keap1 pathway in Caco-2 cells exposed or not to TNF-α. Pretreatment with 0.75–1.5μg C3G eq./mL induced overexpression of NQO1, which is a gene present in the ARE sequence in cells exposed to TNF-α or not. Another in vitro study conducted using Caco-2 cells and palmitate to induce a lipotoxic environment [36] illustrated that C3G has been able to increase the expression of NQO1. In addition, it seemed to activate the Nrf2 pathway. According to Bashllari et al. [36], C3G's anti-inflammatory effects may be attributed to an antioxidant adaptive cell response mainly regulated by the Nrf2 pathway. On the other hand, given the inhibitory effect that the Nrf2/EpRE pathway may have on NF-κB transcription machinery [140], a hypothesis of the crosstalk between Nrf2 and NF-κB pathways that could modulate the transcription or function of target proteins has been supported. In a study by Ferrari et al. [114], Caco-2 cells were exposed to TNF-α and treated with 20–40 μM C3G for 24 h. C3G was able to increase Nrf2 translocation in a dose-dependent manner, and HO-1 and NQO-1 mRNA Levels both in TNF-α treated and unexposed cells. Therefore, Ferrari et al. [114] support that the upregulation of the Nrf2 pathway is involved in C3G's protective effect on epithelial inflammation induced by TNF-α.

The In vitro study by Serra et al" [116] indicates that C3G can induce the activation of Nrf2 in cytokine-stimulated HT-29 cells. In fact, the stimulatory effect of C3G alone has been shown to be significantly higher than that assigned to 5-ASA, particularly when

considering differing concentrations (25 μM C3G vs. 500 μM 5-ASA). Notably, the combination of 5-ASA with C3G failed to reveal an additional/synergistic effect. Finally, C3G was found to be responsible for the increase in the HO-1 mRNA expression Moreover, it enhanced the GSH/GSSG ratio and slightly increased the mRNA expression of catalytic and modified subunits of GCL in cytokine-exposed cells. Nrf2/ARE activation by C3G was also confirmed in endothelial cells [123]. The results of the in vitro study conducted by Speciale et al. suggest that C3G activated the NRf2/ARE pathway at baseline and after TNF-α treatment of HUVECs, which in turn regulated several detoxification enzyme pathways such as HO-1. The study suggested the involvement of specific mitogen-activated protein kinases (MAPKs) (ERK1/2) in C3G's induction of the Nrf2/ARE pathway. Finally, an inhibitor's inactivation of ERK1/2 activity abolished the increase in Nrf2 nuclear accumulation induced by C3G [123].

4.3. C3G Modulates IFN Pathways

CD169 is expressed by some specific immune cells, especially dendritic cells (DCs) and macrophages. CD169+ macrophage subsets are mostly located in secondary lymphoid organs such as the subcapsular sinus. Medullary macrophages in lymph nodes (LN) highly express CD169, just as marginal metallophilic macrophages in the spleen do [143–146]. CD169+ macrophages encounter and engulf invading microbes at the entry sites of lymph or blood, acting as a gatekeeper within their special location at which antigens enter, and also act as activators of T and B cells to mount an immune response against pathogens [147,148]. Colonic CD169+ macrophages are mostly located in the lamina propria of the colon. After epithelial injuries, CD169+ macrophages produce CCL8 to initiate mucosal inflammation by recruiting inflammatory monocytes [143,149,150]. CD169-DTR mice with deleting or decreasing CD169+ macrophages did not display the typical clinical symptoms of colitis induced by DSS. Some studies have indicated that CD169+ macrophages play a crucial role in the development of colitis [151,152].

Xia et al. [117] evaluated the effects of orally administered C3G on DSS-induced colitic mice to conclude that C3G prevents the increase in CD169 cells. Furthermore, in vitro C3G administration could have directly inhibited macrophage activation and CD169+ cells' numerical increase. In the colon and mLNs, C3G has been found to reduce pro-inflammatory cytokine expression, including IL-6, IL-1β, IL-18, IL-17, TNF-α, and IFN-γ, to reduce CD169+ macrophages, and to increase CCL22 expression; some anti-inflammatory cytokines were also increased, e.g., IL-10 and TGF-β. C3G administration resulted in a reduction in CD80 and CD86 expression and induction of Tregs, together with an increase in CCL22 expression levels in both the colon and mLNs. The activation of peritoneal macrophages has been reported to be inhibited by C3G in vivo, while the expression of CD80 and CD86 is decreased. Thus, C3G is reported to be able to reduce the number of peritoneal CD169+ macrophages and also to inhibit their activation. In the same study [117], C3G inhibited the CD169 expression induced by type I IFN. Thus, Xia et al. support the hypothesis of Lee et al., stating that NF-κB inhibition after administration of C3G [153] is a critical factor in the type I IFN pathway [154]. On the other hand, for the inhibition of the type II IFN pathway, a few studies have reported downregulation of IFN-γ caused by C3G [39,115,125,126]. The in vitro study of Triebel et al. [125] conducted using CM-stimulated T84 cells reported a downregulation of IP-10 (CXCL10) by C3G and a decrease in IFN-γ-induced protein levels, while reporting no significant downregulation of TNF-α and IL-8.

4.4. C3G Reduces Reactive Species and Pro-Inflammatory Cytokines

Reductions in pro-inflammatory cytokines after C3G administration have been confirmed by several studies. Such pro-inflammatory cytokines include IL-6 [36,117,119–121], IL-8 [36,113,115,119], IL-1β [36,116,117,122], TNF-α [117,119,120,124], IL-17, and IL-18 [117]. A cohort study by Liso et al. [126] on IBD patients receiving infliximab reported that supplementary administration of purple corn, which includes 0.5mg C3G equivalents/g DW, to

their normal diet was associated with the downregulation of inflammatory biomarkers such as CRP, IFN-γ, TNF-α, IL-5, IL-9, IL-10, IL-12p70, and IL-17A, in CD but not UC patients. In addition, Serra et al. [115] claim that stimulation of a cytokine cocktail may be related to the suppression of an alternative cell signaling, one other than NF-kB. Administration of C3G to cytokine-stimulated HT-29 cells led to downregulation of NO, PGE2, IL-8, iNOS, COX-2, and STAT1 [115]. Similarly, according to Ferrari et al. [121], the downregulation of IL-6 induced by TNF-α, COX-2, PGE2, and TXB2, and the upregulation of GSH, HO-1, and NQO-1 mRNA levels induced by C3G underline C3G's activity as a direct redox scavenger downregulating TNF-α. Many in vitro studies have revealed the reactive oxygen species (ROS)-mitigating potential of C3G [36,113,116]. C3G is claimed to induce a direct reduction in reactive species and an upregulation in several detoxification enzyme pathways, such as HO-1 [114,116], NQO-1 mRNA levels [36,114], GCLC, GCLM (glutamate cysteine ligase mRNA expression) [116] and GSH [114], and a change in the ratio of GSH/GSSG [116]. It has also been found that C3G and/or complexes with the monomer exert antiapoptotic properties [113,124,155]. Tan et al. reported increased protein levels of Bcl-2/Bax and the caspase-3/cleaved caspase-3 gene ratio, thus indicating the enhanced therapeutic effect of HHP-treated C3G on mice enteritis [113,124], the inhibition of the depolarization of mitochondria, and the reduction of the produced ROS, as demonstrated by the reduced mRNA expression of IL-1β, TNF-α, and IL-8. Increased expression of IL-10 and reduced iNOS, COX-2, Bcl-2, and cleaved caspase-3 levels were also observed [113]. However, a study by Xia et al. [117] found no significant effect of C3G administration in apoptosis.

4.5. C3G Modulates Gut Microbiota

Anthocyanins may modulate gut microbiota by inducing an increase in special gut bacteria [156] and increasing microbial abundances [157], thus mitigating dysbiosis. Anthocyanins have been claimed to increase the relative abundance of beneficial bacteria, such as *Bifidobacterium* and *Akkermansia*, which are believed to have anti-inflammatory effects [156,158]. In a previously referenced study by Wang et al. [120], C3G extracted from the Chinese bayberry has been positively correlated with an increase in richness and diversity of gut microbiota. Moreover, it was related to increased *Bacteroides* species, which are widely known for its beneficial effects and ability to reduce harmful bacteria, *Enterococcus* and *Clostridium sensu stricto 1*. C3G has been claimed to contribute to restoring the homeostasis of gut microbiota [120]. In detail, *Enterococcus* represented by *E. faecium* and *E. faecalis* is an opportunistic pathogen that helps the adhesion, colonization and invasion of host tissue, the modulation of host immunity, and the production of toxins and extracellular enzymes [159,160]. *Clostridium sensu stricto 1* has been found to proliferate in IBD, and is considered a potential biomarker of intestinal inflammation [161]. In addition, administration of C3G was positively correlated with the relative abundance of *Lachnoclostridium*, known for propionate and butyrate production, which contributes to restoring SCFAs concentration in the gut [162]. SCFAs are the ligands of two G protein-coupled receptors, Gpr43 and Gpr41, which participate in glycolysis and protein synthesis by modulating the level of some endocrine peptides. Moreover, they promote the proliferation, differentiation and apoptosis of intestinal epithelial cells. Finally, they protect the intestinal epithelial barrier [163,164]. *Parabacteroides* and *Blautia*, some beneficial bacteria, were also positively correlated with C3G administration. Tan et al. [124] indicated an increase in species diversity after C3G administration + HC treatment of DSS-induced colitic UC mice. C3G was found to induce a decrease in the relative abundance of *Firmicutes* and *Proteobacteria*, and an increase in *Bacteroidetes*, *Verrucomicrobia* and *Candidatus Saccharibacteria* of an HHP-treated C3G-BP group was the biggest change, resulting in a smaller *Firmicutes* to *Bacteroidetes (F/B)* ratio, which is related to the degree of inflammation in colitis [165]. In a study by Wu et al. that did not involve IBD directly [166], a mouse model of experimental non-alcoholic fatty liver disease was used. They demonstrated that the *Lonicera caerulea* L. berry, which is rich in C3G, was able to reduce inflammation due to the ratio change of *Firmicutes* to *Bacteroidetes*.

Aside from C3G, its metabolites have been investigated in a colitic environment. C3G's metabolites, as components of the monofloral honey Prunella Vulgaris, have been found to exert protective properties in DDS-induced UC colitic mice by restoring the relative abundance of *Lactobacillus* [167]. More studies on C3G metabolites as components of food products have confirmed their anti-inflammatory effects through a reduction in the population of Bacteroides spp. In DSS-induced colitic rats [168], and through growth inhibition of *E. coli*, *S. aureus*, and *P. aeruginosa* [169], and therefore mitigation of the growth of pathogenic bacteria. Finally, phenolic compounds can be used as substrates by bacteria to produce energy [170,171] and to produce fermentable metabolites, which can exert bioactive functions similar to those of parent anthocyanins [172]. Thus, the gut microbiota play a role in the metabolism of anthocyanins and secondary phenolic metabolites after the removal of anthocyanins' sugar moiety [173].

4.6. Clinical Aspects

The cause of IBD is still not well understood. Current knowledge on IBD pathogenesis suggests genetically susceptible individuals develop intolerance to dysregulated gut microbiota, and chronic inflammation develops as a result of environmental triggers. Thus, there is limited evidence based on randomized controlled trials (RCTs) supporting that a substance alone or a specific diet pattern can prevent the disease. However, the scientific community should aim to find ways to manage IBD symptoms and improve gut health, mainly through gut inflammation alleviation, regulation of the immune responses involved in IBD, and improvement of gut microbiota composition. Thus, even though C3G appears very promising in treating and/or preventing IBD, further clinical studies should be conducted. Regarding administration, in vivo experiments in mice have mainly practiced oral administration and intraperitoneal C3G injections. Both routes of administration resulted in impressive findings regarding inflammatory responses, oxidative indices, and microbiota composition, but the latter was related to a greater reduction in immunomodulatory modules such as CCL22 and Tregs induction [117]. Concerning human studies, a cohort study investigated the effects of oral administration of C3G as a complex with a nutritional supplement, resulting in reduced inflammatory biomarkers in CD, but not UC patients [126]. Administrating C3G as a complex with other nutritional regimens is not an uncommon practice [124]. The limited stability, bioaccessibility and colonic delivery of the compound are considered to restrict the wider oral supplementary use of C3G alone against IBD. Nevertheless, loading of bioactive phytochemicals in a robust carrier system might be crucial to increase stability, solubility, intestinal absorption, and bioaccessibility, or to improve the bioactivity in body circulation through specific targeting. According to Shishir et al. [174], an efficient carrier of C3G, named nanofibersolome, has recently been developed to provide protection during its passage through the simulated digestion processes, thus being a very promising approach.

In addition, there are no registered interventional clinical trials investigating C3G's effects on IBD patients. Regarding the wider category of anthocyanins, a randomized, double-blind, Phase iIa study was conducted by Rogler et al. [9], and evaluated the efficacy, safety and tolerability of an anthocyanin-rich extract (ACRE) in patients with UC (NCT04000139). During the trial, 3 g of anthocyanin-rich extract was administered daily in three doses of 2 $\times$ 500 mg, for 56 days. Another study regarding anthocyanins, expected to finish in 2024, is planning to evaluate the efficacy of Montmorency Tart Cherry Juice Supplementation on UC patients (NCT05486507). The administered dose reported in the majority of the in vivo studies in mice ranges from 24.2 to 96.8 g/kg BW or 1 ug daily [117]. However, during an aforementioned cohort study, 0.5mg C3G /g DW was administered to subjects as a complex with garlic acid [126]. Since clinical trials and cohort studies investigating the impact of C3G on IBD patients are limited, there are no clear recommendations on dosage. C3G levels can be evaluated via the plasma concentration of the compound, but also in urine and target tissues.

To assess therapeutic outcomes after administrating C3G, validated scores could be used alongside a report of a series of clinical symptoms, laboratory tests, and endoscopic and histological assessments. The first validated score recommended is the Mayo score/disease activity index (DAI) for ulcerative colitis [175,176]; it evaluates stool frequency, rectal bleeding, mucosal appearance at endoscopy, and the physician's rating of disease activity. The second one addressing CD patients is the Crohn's Disease activity index (CDAI) [177], which scores on a scale of 0 to 100 and includes aspects such as abdominal pain, general wellbeing, complications, abdominal mass, anemia, and weight change. This composite instrument divides patients with CD according to their score into categories of asymptomatic remission, mild-to-moderate CD, moderate-to-severe CD, severe-to-fulminant disease, and clinically significant improvement in disease activity. Other scores that could be used in CD patients [178] are the Harvey–Bradshaw index, Crohn's disease endoscopic index of severity (CDEIS) and the simple endoscopic score for Crohn's disease (SES-CD). Last but not least, the capsule endoscopy Crohn's disease activity index (CECDAI, or Niv score) [179] could be used to evaluate inflammation, the extent of CD, and the presence of strictures. Furthermore, therapeutic outcomes and clinical remission after administrating C3G could be assessed through evaluating parameters such as rectal bleeding, stool frequency, abdominal pain, endoscopic remission (colonic inflammation characterized by erythema, loss of normal vascular pattern, granularity, erosions, friability, bleeding [180] etc.), histological remission, physicians global assessment (PGA), fecal calprotectin, steroid dosage, and the SIBDQ (short inflammatory bowel disease questionnaire) [181]. Other parameters that could be evaluated include symptoms of urgency and fecal incontinence, weight loss and fever. As for laboratory tests, patients should be monitored for anemia, hypoalbuminemia, and elevated C-reactive protein (CRP). Elevated fecal calprotectin is a sensitive (but not specific) indicator of intestinal inflammation in IBD [182].

5. Conclusions

According to recent studies, mounting evidence suggests C3G might be a potential therapeutic target for preventing or controlling the progression of IBD, while alleviating symptoms (Figure 1) [113,114,117]. C3G is claimed to exert not only anti-inflammatory, antioxidative, and cytoprotective, but also immunomodulatory and anti-microbial effects. C3G acts both directly as a free radical scavenger, modulating detoxification enzymes and cytokine expression, and indirectly via downregulating the redox-dependent transcriptional factor NF-κB, upregulating the Nrf2 pathway, and improving the composition of the intestinal microbiota [116].

While current treatment options achieve sustained remission of IBD in most patients, upcoming treatment regimens involving different molecular pathways and modes of actions are further highlighting the need for personalized medicine [24]. In conclusion, C3G may represent a promising alleviating agent for IBD, while its metabolites may be important lead compounds for the development of new therapeutic tools against the disease. Although the potential effect of this compound has been reported across various in vitro and in vivo settings, more preclinical and clinical studies are required to validate its potency, determine the recommended therapeutic dose, frequency and route of administration, and to develop more efficient ways to exploit its several notable properties.

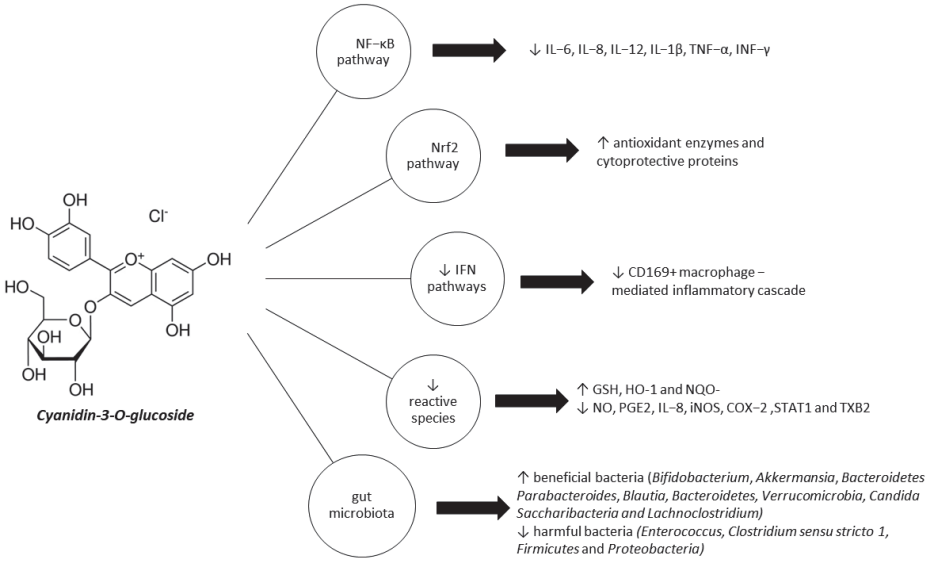

Figure 1. Therapeutic actions of C3G against IBD. NF-κB, nuclear factor-kappa B; Nrf2, nuclear factor erythroid 2–related factor 2; IFN, interferon; IL-6, interleukin 6; IL-8, interleukin 8; IL-12, interleukin 12; IL-1β, interleukin 1β; TNF-α, tumor necrosis factor alpha; IFN-γ, interferon-γ; GSH, glutathione; HO-1, heme oxygenase-1; NQO-, NAD(P)H Quinone Dehydrogenase 1; NO, nitric oxide; PGE2, prostaglandin 2; iNOS, inducible nitric oxide synthase; COX-2, cyclooxygenase 2; STAT1, signal transducer and activator of transcription 1; TXB2, thromboxane B2.

Author Contributions: Conceptualization, D.T., P.T. and K.G.T.; formal analysis, D.T.; investigation, E.K. and M.F.; resources, M.F. and E.K.; data curation, M.F., E.K., D.S. (Demosthenis Sotirakis) and D.S. (Dimitrios Schizas); writing—original draft preparation, E.K. and M.F.; writing—review and editing, M.F., E.K., O.T. and P.T.; visualization, M.F. and E.K.; supervision, K.G.T.; project administration, P.T. All authors have read and agreed to the published version of the manuscript.

Funding: This research received no external funding.

Institutional Review Board Statement: Not applicable.

Informed Consent Statement: Not applicable.

Data Availability Statement: Not applicable.

Conflicts of Interest: The authors report no conflict of interest.

Abbreviations

ACN, anthocyanidins; AhR, aryl hydrocarbon receptor; ARE, antioxidant response element; Bcl-2, B-cell lymphoma-2; CD, Crohn's disease; C/EBP-β, CCAAT enhancer binding protein beta; CM, cytokine mixture; COMT, catechol-O-methyltransferase; COX-2, cyclooxygenase 2; Cy, cyanidin; CVD, cardiovascular disease; C3G, cyanidin-3-O-glucoside; DC, dendritic cells; Dp, delphinidin; DSS, dextran sodium sulfate; DW, dry weight; EGFR, epidermal growth factor receptor; EHC, enterohepatic cycle; ERK, extracellular signal-regulated kinases; FA, ferulic acid; GCLC, glutamate cysteine ligase catalytic subunit; GCLM, glutamate cysteine ligase regulatory subunit; GI, gastrointestinal; GPCRs, G protein-coupled receptors; GSH, glutathione; GSSG, glutathione disulfide; HDL, high-density lipoprotein; HHP, high hydrostatic pressure; HO-1, heme oxygenase-1; HUVECs, human umbilical endothelial cells; IBD, inflammatory bowel disease; ICAM-1, intercellular adhesion molecule1; IFN-γ, interferon gamma; IL-1β, interleukin 1β; IL-6, interleukin 6; IL-17, interleukin 17; IL-8, interleukin 8;

IKK, inhibitor of nuclear factor kappa kinase; iNOS, nitric oxide synthetase; IP-10, inducible protein-10; IFN-γ, interferon-γ; KEAP1, Kelch-like ECH associated protein; LDL, low-density lipoprotein; LN, lymph node; LPH, lactase-phlorizin hydrolase; LPS, lipopolysaccharide; MAPK, mitogen-activated protein kinase; MCP-1, monocyte chemoattractant protein-1; MLC, myosin light chain; Mv, malvidin; NCCDs, non-communicable chronic diseases; NF-κB, nuclear factor-kappa B; NO, nitric oxide; NOD2, nucleotide-binding oligomerization domain-containing protein 2; NRF2, nuclear factor erythroid 2–related factor 2; OSCC, oral squamous cell carcinoma; PA, palmitic acid; PCA, protocatechuic acid; PC, phenolic compounds; PGA, phloroglucinaldehyde; Pg, pelargodin; PGE2, prostaglandin 2; Pn, peonidin; Pt, petunidin; PST, phenyl sulfotransferases; PTP1B, protein tyrosine phosphatase 1B; PGE2, prostaglandin E_2; ROS, reactive oxygen species; RSC, radical scavenging capacity; SCFAs, short-chain fatty acids; STAT1, signal transducer and activator of transcription 1; sVCAM-1, soluble vascular cell adhesion molecule-1; TEER, transepithelial electrical resistance; Th1, T helper cell 1; Th17 T helper cell 17; TNF-α, tumor necrosis factor alpha; TNFAIP3/A20, TNF-α-induced protein 3; TOLLIP, Toll interacting protein; TXB2, thromboxane B2; UC, ulcerative colitis; UGT, uridine 51 diphosphate glucuronosyltransferases; VCAM-1, vascular cell adhesion molecule 1.

References

1. Martins, I.; Maciel, M.G.; do Nascimento, J.L.M.; Mafra, D.; Santos, A.F.; Padilha, C.S. Anthocyanins-rich interventions on oxidative stress, inflammation and lipid profile in patients undergoing hemodialysis: Meta-analysis and meta-regression. *Eur. J. Clin. Nutr.* **2023**, *77*, 316–324. [CrossRef]
2. Pérez-Torres, I.; Castrejón-Téllez, V.; Soto, M.E.; Rubio-Ruiz, M.E.; Manzano-Pech, L.; Guarner-Lans, V. Oxidative Stress, Plant Natural Antioxidants, and Obesity. *Int. J. Mol. Sci.* **2021**, *22*, 1786. [CrossRef]
3. Fang, Z.; Luo, Y.; Ma, C.; Dong, L.; Chen, F. Blueberry Anthocyanins Extract Attenuates Acrylamide-Induced Oxidative Stress and Neuroinflammation in Rats. *Oxidative Med. Cell. Longev.* **2022**, *2022*, 7340881. [CrossRef] [PubMed]
4. Zheng, F.; Wang, Y.Z.; Wu, Y.X.; Zhang, M.Y.; Li, F.T.; He, Y.; Wen, L.K.; Yue, H. Effect of stabilization malvids anthocyanins on the gut microbiota in mice with oxidative stress. *J. Food Biochem.* **2021**, *45*, 4892–4902. [CrossRef] [PubMed]
5. Rahman, S.; Mathew, S.; Nair, P.; Ramadan, W.S.; Vazhappilly, C.G. Health benefits of cyanidin-3-glucoside as a potent modulator of Nrf2-mediated oxidative stress. *Inflammopharmacology* **2021**, *29*, 907–923. [CrossRef]
6. Higashiyama, M.; Hokaria, R. New and Emerging Treatments for Inflammatory Bowel Disease. *Digestion* **2023**, *104*, 74–81. [CrossRef]
7. Saez, A.; Herrero-Fernandez, B.; Gomez-Bris, R.; Sánchez-Martinez, H.; Gonzalez-Granado, J.M. Pathophysiology of Inflammatory Bowel Disease: Innate Immune System. *Int. J. Mol. Sci.* **2023**, *24*, 1526. [CrossRef]
8. Dai, C.; Huang, Y.H.; Jiang, M. Combination therapy in inflammatory bowel disease: Current evidence and perspectives. *Int. Immunopharmacol.* **2023**, *114*, 109545. [CrossRef]
9. Rogler, G.; Singh, A.; Kavanaugh, A.; Rubin, D.T. Extraintestinal Manifestations of Inflammatory Bowel Disease: Current Concepts, Treatment, and Implications for Disease Management. *Gastroenterology* **2021**, *161*, 1118–1132. [CrossRef] [PubMed]
10. Wu, X.; Prior, R.L. Systematic identification and characterization of anthocyanins by HPLC-ESI-MS/MS in common foods in the United States: Fruits and berries. *J. Agric. Food Chem.* **2005**, *53*, 2589–2599. [CrossRef]
11. Olivas-Aguirre, F.J.; Rodrigo-García, J.; Martínez-Ruiz, N.D.R.; Cárdenas-Robles, A.I.; Mendoza-Díaz, S.O.; Álvarez-Parrilla, E.; González-Aguilar, G.A.; De la Rosa, L.A.; Ramos-Jiménez, A.; Wall-Medrano, A. Cyanidin-3-O-glucoside: Physical-chemistry, foodomics and health effects. *Molecules* **2016**, *21*, 1264. [CrossRef]
12. Flamini, R.; De Rosso, M.; Bavaresco, L. Study of grape polyphenols by liquid chromatography-high-resolution mass spectrometry (UHPLC/QTOF) and suspect screening analysis. *J. Anal. Methods Chem.* **2015**, *2015*, 350259. [CrossRef] [PubMed]
13. Felgines, C.; Krisa, S.; Mauray, A.; Besson, C.; Lamaison, J.-L.; Scalbert, A.; Mérillon, J.-M.; Texier, O. Radiolabelled cyanidin 3-O-glucoside is poorly absorbed in the mouse. *Br. J. Nutr.* **2010**, *103*, 1738–1745. [CrossRef]
14. Fernandes, I.; Marques, F.; de Freitas, V.; Mateus, N. Antioxidant and antiproliferative properties of methylated metabolites of anthocyanins. *Food Chem.* **2013**, *141*, 2923–2933. [CrossRef] [PubMed]
15. Phan, A.D.T.; Netzel, G.; Wang, D.; Flanagan, B.M.; D'Arcy, B.R.; Gidley, M.J. Binding of dietary polyphenols to cellulose: Structural and nutritional aspects. *Food Chem.* **2015**, *171*, 388–396. [CrossRef]
16. Oliveira, A.; Pintado, M. In vitro evaluation of the effects of protein–polyphenol–polysaccharide interactions on (+)-catechin and cyanidin-3-glucoside bioaccessibility. *Food Funct.* **2015**, *6*, 3444–3453. [CrossRef]
17. Tang, L.; Zuo, H.; Shu, L. Comparison of the interaction between three anthocyanins and human serum albumins by spectroscopy. *J. Lumin.* **2014**, *153*, 54–63. [CrossRef]
18. Tang, L.; Li, S.; Bi, H.; Gao, X. Interaction of cyanidin-3-O-glucoside with three proteins. *Food Chem.* **2016**, *196*, 550–559. [CrossRef]
19. Kosińska-Cagnazzo, A.; Diering, S.; Prim, D.; Andlauer, W. Identification of bioaccessible and uptaken phenolic compounds from strawberry fruits in in vitro digestion/Caco-2 absorption model. *Food Chem.* **2015**, *170*, 288–294. [CrossRef]

20. Fernandes, A.; Brás, N.F.; Mateus, N.; de Freitas, V. Understanding the molecular mechanism of anthocyanin binding to pectin. *Langmuir* **2014**, *30*, 8516–8527. [CrossRef]
21. Urias-Lugo, D.A.; Heredia, J.B.; Muy-Rangel, M.D.; Valdez-Torres, J.B.; Serna-Saldívar, S.; Gutierrez-Uribe, J.A. Anthocyanins and phenolic acids of hybrid and native blue maize (*Zea mays* L.) extracts and their antiproliferative activity in mammary (MCF7), liver (HepG2), colon (Caco2 and HT29) and prostate (PC3) cancer cells. *Plant Foods Hum. Nutr.* **2015**, *70*, 193–199. [CrossRef]
22. Zhao, X.; Yuan, Z.; Feng, L.; Fang, Y. Cloning and expression of anthocyanin biosynthetic genes in red and white pomegranate. *J. Plant Res.* **2015**, *128*, 687–696. [CrossRef] [PubMed]
23. Vogiatzoglou, A.; Mulligan, A.A.; Lentjes, M.A.; Luben, R.N.; Spencer, J.P.; Schroeter, H.; Khaw, K.-T.; Kuhnle, G.G. Flavonoid intake in European adults (18 to 64 years). *PLoS ONE* **2015**, *10*, e0128132. [CrossRef]
24. Cheng, Z.; Si, X.; Tan, H.; Zang, Z.; Tian, J.; Shu, C.; Sun, X.; Li, Z.; Jiang, Q.; Meng, X.; et al. Cyanidin-3-O-glucoside and its phenolic metabolites ameliorate intestinal diseases via modulating intestinal mucosal immune system: Potential mechanisms and therapeutic strategies. *Crit. Rev. Food Sci. Nutr.* **2023**, *63*, 1629–1647. [CrossRef] [PubMed]
25. Orhan Dereli, B.; Türkyılmaz, M.; Özkan, M. Clarification of pomegranate and strawberry juices: Effects of various clarification agents on turbidity, anthocyanins, colour, phenolics and antioxidant activity. *Food Chem.* **2023**, *413*, 135672. [CrossRef] [PubMed]
26. Sebastian, R.S.; Wilkinson Enns, C.; Goldman, J.D.; Martin, C.L.; Steinfeldt, L.C.; Murayi, T.; Moshfegh, A.J. A new database facilitates characterization of flavonoid intake, sources, and positive associations with diet quality among US adults. *J. Nutr.* **2015**, *145*, 1239–1248. [CrossRef]
27. Grosso, G.; Stepaniak, U.; Micek, A.; Stefler, D.; Bobak, M.; Pająk, A. Dietary polyphenols are inversely associated with metabolic syndrome in Polish adults of the HAPIEE study. *Eur. J. Nutr.* **2017**, *56*, 1409–1420. [CrossRef]
28. Zamora-Ros, R.; Andres-Lacueva, C.; Lamuela-Raventós, R.M.; Berenguer, T.; Jakszyn, P.; Barricarte, A.; Ardanaz, E.; Amiano, P.; Dorronsoro, M.; Larrañaga, N.; et al. Estimation of dietary sources and flavonoid intake in a Spanish adult population (EPIC-Spain). *J. Am. Diet. Assoc.* **2010**, *110*, 390–398. [CrossRef]
29. Jun, S.; Shin, S.; Joung, H. Estimation of dietary flavonoid intake and major food sources of Korean adults. *Br. J. Nutr.* **2016**, *115*, 480–489. [CrossRef]
30. Peterson, J.J.; Dwyer, J.T.; Jacques, P.F.; McCullough, M.L. Improving the estimation of flavonoid intake for study of health outcomes. *Nutr. Rev.* **2015**, *73*, 553–576. [CrossRef] [PubMed]
31. Onwude, D.I.; Chen, G.; Eke-Emezie, N.; Kabutey, A.; Khaled, A.Y.; Sturm, B. Recent advances in reducing food losses in the supply chain of fresh agricultural produce. *Processes* **2020**, *8*, 1431. [CrossRef]
32. Huang, K.-M.; Guan, Z.; Hammami, A. The US Fresh Fruit and Vegetable Industry: An Overview of Production and Trade. *Agriculture* **2022**, *12*, 1719. [CrossRef]
33. Felgines, C.; Talavéra, S.; Texier, O.; Besson, C.; Fogliano, V.; Lamaison, J.-L.; La Fauci, L.; Galvano, G.; Rémésy, C.; Galvano, F. Absorption and metabolism of red orange juice anthocyanins in rats. *Br. J. Nutr.* **2006**, *95*, 898–904. [CrossRef] [PubMed]
34. Rodriguez-Mateos, A.; Vauzour, D.; Krueger, C.G.; Shanmuganayagam, D.; Reed, J.; Calani, L.; Mena, P.; Del Rio, D.; Crozier, A. Bioavailability, bioactivity and impact on health of dietary flavonoids and related compounds: An update. *Arch. Toxicol.* **2014**, *88*, 1803–1853. [CrossRef] [PubMed]
35. Woodward, G.M.; Needs, P.W.; Kay, C.D. Anthocyanin-derived phenolic acids form glucuronides following simulated gastrointestinal digestion and microsomal glucuronidation. *Mol. Nutr. Food Res.* **2011**, *55*, 378–386. [CrossRef] [PubMed]
36. Bashllari, R.; Molonia, M.S.; Muscarà, C.; Speciale, A.; Wilde, P.J.; Saija, A.; Cimino, F. Cyanidin-3-O-glucoside protects intestinal epithelial cells from palmitate-induced lipotoxicity. *Arch. Physiol. Biochem.* **2023**, *129*, 379–386. [CrossRef]
37. Feng, J.; Wu, Y.; Zhang, L.; Li, Y.; Liu, S.; Wang, H.; Li, C. Enhanced Chemical Stability, Intestinal Absorption, and Intracellular Antioxidant Activity of Cyanidin-3-O-glucoside by Composite Nanogel Encapsulation. *J. Agric. Food Chem.* **2019**, *67*, 10432–10447. [CrossRef]
38. Miyazawa, T.; Nakagawa, K.; Kudo, M.; Muraishi, K.; Someya, K. Direct intestinal absorption of red fruit anthocyanins, cyanidin-3-glucoside and cyanidin-3, 5-diglucoside, into rats and humans. *J. Agric. Food Chem.* **1999**, *47*, 1083–1091. [CrossRef]
39. Gan, Y.; Fu, Y.; Yang, L.; Chen, J.; Lei, H.; Liu, Q. Cyanidin-3-O-Glucoside and Cyanidin Protect Against Intestinal Barrier Damage and 2,4,6-Trinitrobenzenesulfonic Acid-Induced Colitis. *J. Med. Food* **2020**, *23*, 90–99. [CrossRef]
40. Fang, J. Some anthocyanins could be efficiently absorbed across the gastrointestinal mucosa: Extensive presystemic metabolism reduces apparent bioavailability. *J. Agric. Food Chem.* **2014**, *62*, 3904–3911. [CrossRef]
41. Hanske, L.; Engst, W.; Loh, G.; Sczesny, S.; Blaut, M.; Braune, A. Contribution of gut bacteria to the metabolism of cyanidin 3-glucoside in human microbiota-associated rats. *Br. J. Nutr.* **2013**, *109*, 1433–1441. [CrossRef]
42. Valdés, L.; Cuervo, A.; Salazar, N.; Ruas-Madiedo, P.; Gueimonde, M.; González, S. The relationship between phenolic compounds from diet and microbiota: Impact on human health. *Food Funct.* **2015**, *6*, 2424–2439. [CrossRef] [PubMed]
43. Alves Castilho, P.; Bracht, L.; Barros, L.; Albuquerque, B.R.; Dias, M.I.; Ferreira, I.; Comar, J.F.; Barlati Vieira da Silva, T.; Peralta, R.M.; Sá-Nakanishi, A.B.; et al. Effects of a Myrciaria jaboticaba peel extract on starch and triglyceride absorption and the role of cyanidin-3-O-glucoside. *Food Funct.* **2021**, *12*, 2644–2659. [CrossRef]
44. Shan, X.; Lv, Z.Y.; Yin, M.J.; Chen, J.; Wang, J.; Wu, Q.N. The Protective Effect of Cyanidin-3-Glucoside on Myocardial Ischemia-Reperfusion Injury through Ferroptosis. *Oxidative Med. Cell. Longev.* **2021**, *2021*, 8880141. [CrossRef] [PubMed]

45. Sivasinprasasn, S.; Pantan, R.; Thummayot, S.; Tocharus, J.; Suksamrarn, A.; Tocharus, C. Cyanidin-3-glucoside attenuates angiotensin II-induced oxidative stress and inflammation in vascular endothelial cells. *Chem. Biol. Interact.* **2016**, *260*, 67–74. [CrossRef] [PubMed]
46. Aloud, B.M.; Raj, P.; McCallum, J.; Kirby, C.; Louis, X.L.; Jahan, F.; Yu, L.; Hiebert, B.; Duhamel, T.A.; Wigle, J.T.; et al. Cyanidin 3-O-glucoside prevents the development of maladaptive cardiac hypertrophy and diastolic heart dysfunction in 20-week-old spontaneously hypertensive rats. *Food Funct.* **2018**, *9*, 3466–3480. [CrossRef]
47. Hassellund, S.; Flaa, A.; Kjeldsen, S.; Seljeflot, I.; Karlsen, A.; Erlund, I.; Rostrup, M. Effects of anthocyanins on cardiovascular risk factors and inflammation in pre-hypertensive men: A double-blind randomized placebo-controlled crossover study. *J. Hum. Hypertens.* **2013**, *27*, 100–106. [CrossRef]
48. Hidalgo, J.; Flores, C.; Hidalgo, M.A.; Perez, M.; Yañez, A.; Quiñones, L.; Caceres, D.D.; Burgos, R.A. Delphinol® standardized maqui berry extract reduces postprandial blood glucose increase in individuals with impaired glucose regulation by novel mechanism of sodium glucose cotransporter inhibition. *Panminerva Med.* **2014**, *56*, 1–7. [PubMed]
49. Davinelli, S.; Bertoglio, J.C.; Zarrelli, A.; Pina, R.; Scapagnini, G. A randomized clinical trial evaluating the efficacy of an anthocyanin–maqui berry extract (Delphinol®) on oxidative stress biomarkers. *J. Am. Coll. Nutr.* **2015**, *34*, 28–33. [CrossRef]
50. Zhu, Y.; Ling, W.; Guo, H.; Song, F.; Ye, Q.; Zou, T.; Li, D.; Zhang, Y.; Li, G.; Xiao, Y. Anti-inflammatory effect of purified dietary anthocyanin in adults with hypercholesterolemia: A randomized controlled trial. *Nutr. Metab. Cardiovasc. Dis.* **2013**, *23*, 843–849. [CrossRef]
51. Edirisinghe, I.; Banaszewski, K.; Cappozzo, J.; Sandhya, K.; Ellis, C.L.; Tadapaneni, R.; Kappagoda, C.T.; Burton-Freeman, B.M. Strawberry anthocyanin and its association with postprandial inflammation and insulin. *Br. J. Nutr.* **2011**, *106*, 913–922. [CrossRef]
52. Zhu, Y.; Xia, M.; Yang, Y.; Liu, F.; Li, Z.; Hao, Y.; Mi, M.; Jin, T.; Ling, W. Purified anthocyanin supplementation improves endothelial function via NO-cGMP activation in hypercholesterolemic individuals. *Clin. Chem.* **2011**, *57*, 1524–1533. [CrossRef]
53. Knobloch, T.J.; Uhrig, L.K.; Pearl, D.K.; Casto, B.C.; Warner, B.M.; Clinton, S.K.; Sardo-Molmenti, C.L.; Ferguson, J.M.; Daly, B.T.; Riedl, K.; et al. Suppression of Proinflammatory and Prosurvival Biomarkers in Oral Cancer Patients Consuming a Black Raspberry Phytochemical-Rich Troche. *Cancer Prev. Res. (Phila. Pa.)* **2016**, *9*, 159–171. [CrossRef] [PubMed]
54. Wang, L.-S.; Arnold, M.; Huang, Y.-W.; Sardo, C.; Seguin, C.; Martin, E.; Huang, T.H.-M.; Riedl, K.; Schwartz, S.; Frankel, W.; et al. Modulation of genetic and epigenetic biomarkers of colorectal cancer in humans by black raspberries: A phase I pilot study. *Clin. Cancer Res.* **2011**, *17*, 598–610. [CrossRef] [PubMed]
55. Cheynier, V.G.C.; Ageorges, A. Flavonoids: Anthocyanins. In *Handbook of Analysis of Active Compounds in Functional Foods*, 1st ed.; Nollet, L.M.C., Toldrá, F., Eds.; CRC Press/Taylor & Francis Group: Boca Raton, FL, USA, 2012; pp. 379–403.
56. Acquaviva, R.; Russo, A.; Galvano, F.; Galvano, G.; Barcellona, M.; Volti, G.L.; Vanella, A. Cyanidin and cyanidin 3-O-[beta]-D-glucoside as DNA cleavage protectors and antioxidants. *Cell Biol. Toxicol.* **2003**, *19*, 243. [CrossRef]
57. Guo, H.; Xia, M.; Zou, T.; Ling, W.; Zhong, R.; Zhang, W. Cyanidin 3-glucoside attenuates obesity-associated insulin resistance and hepatic steatosis in high-fat diet-fed and db/db mice via the transcription factor FoxO1. *J. Nutr. Biochem.* **2012**, *23*, 349–360. [CrossRef]
58. Ziberna, L.; Tramer, F.; Moze, S.; Vrhovsek, U.; Mattivi, F.; Passamonti, S. Transport and bioactivity of cyanidin 3-glucoside into the vascular endothelium. *Free Radic. Biol. Med.* **2012**, *52*, 1750–1759. [CrossRef]
59. Tsuda, T.; Ueno, Y.; Yoshikawa, T.; Kojo, H.; Osawa, T. Microarray profiling of gene expression in human adipocytes in response to anthocyanins. *Biochem. Pharmacol.* **2006**, *71*, 1184–1197. [CrossRef]
60. Björk, C.; Wilhelm, U.; Mandrup, S.; Larsen, B.D.; Bordoni, A.; Hedén, P.; Rydén, M.; Arner, P.; Laurencikiene, J. Effects of selected bioactive food compounds on human white adipocyte function. *Nutr. Metab.* **2016**, *13*, 4. [CrossRef] [PubMed]
61. Tsuda, T.; Ueno, Y.; Kojo, H.; Yoshikawa, T.; Osawa, T. Gene expression profile of isolated rat adipocytes treated with anthocyanins. *Biochim. Biophys. Acta (BBA)-Mol. Cell Biol. Lipids* **2005**, *1733*, 137–147. [CrossRef]
62. Neveu, V.; Perez-Jiménez, J.; Vos, F.; Crespy, V.; du Chaffaut, L.; Mennen, L.; Knox, C.; Eisner, R.; Cruz, J.; Wishart, D.; et al. Phenol-Explorer: An online comprehensive database on polyphenol contents in foods. *Database* **2010**, *2010*, bap024. [CrossRef] [PubMed]
63. Pimpao, R.C.; Ventura, M.R.; Ferreira, R.B.; Williamson, G.; Santos, C.N. Phenolic sulfates as new and highly abundant metabolites in human plasma after ingestion of a mixed berry fruit purée. *Br. J. Nutr.* **2015**, *113*, 454–463. [CrossRef] [PubMed]
64. Kiemlian Kwee, J. Yin and Yang of polyphenols in cancer prevention: A short review. *Anti-Cancer Agents Med. Chem. (Former. Curr. Med. Chem. -Anti-Cancer Agents)* **2016**, *16*, 832–840. [CrossRef] [PubMed]
65. Sheng, F.; Wang, Y.; Zhao, X.; Tian, N.; Hu, H.; Li, P. Separation and identification of anthocyanin extracted from mulberry fruit and the pigment binding properties toward human serum albumin. *J. Agric. Food Chem.* **2014**, *62*, 6813–6819. [CrossRef]
66. Zhang, C.; Guo, X.; Cai, W.; Ma, Y.; Zhao, X. Binding Characteristics and Protective Capacity of Cyanidin-3-Glucoside and its Aglycon to Calf Thymus DNA. *J. Food Sci.* **2015**, *80*, H889–H893. [CrossRef]
67. Shi, J.h.; Wang, J.; Zhu, Y.y.; Chen, J. Characterization of intermolecular interaction between cyanidin-3-glucoside and bovine serum albumin: Spectroscopic and molecular docking methods. *Luminescence* **2014**, *29*, 522–530. [CrossRef]
68. Cahyana, Y.; Gordon, M.H. Interaction of anthocyanins with human serum albumin: Influence of pH and chemical structure on binding. *Food Chem.* **2013**, *141*, 2278–2285. [CrossRef]

69. Akkarachiyasit, S.; Charoenlertkul, P.; Yibchok-Anun, S.; Adisakwattana, S. Inhibitory activities of cyanidin and its glycosides and synergistic effect with acarbose against intestinal α-glucosidase and pancreatic α-amylase. *Int. J. Mol. Sci.* **2010**, *11*, 3387–3396. [CrossRef]
70. Flynn, S.; Eisenstein, S. Inflammatory Bowel Disease Presentation and Diagnosis. *Surg. Clin. N. Am.* **2019**, *99*, 1051–1062. [CrossRef]
71. Butterworth, J. Chemoprevention of colorectal cancer in inflammatory bowel disease. *Dig. Liver Dis.* **2009**, *41*, 338–339. [CrossRef]
72. Yu, Y.R.; Rodriguez, J.R. Clinical presentation of Crohn's, ulcerative colitis, and indeterminate colitis: Symptoms, extraintestinal manifestations, and disease phenotypes. *Semin. Pediatr. Surg.* **2017**, *26*, 349–355. [CrossRef] [PubMed]
73. Carroll, M.W.; Kuenzig, M.E.; Mack, D.R.; Otley, A.R.; Griffiths, A.M.; Kaplan, G.G.; Bernstein, C.N.; Bitton, A.; Murthy, S.K.; Nguyen, G.C.; et al. The Impact of Inflammatory Bowel Disease in Canada 2018: Children and Adolescents with IBD. *J. Can. Assoc. Gastroenterol.* **2019**, *2*, S49–S67. [CrossRef] [PubMed]
74. Thia, K.T.; Loftus Jr, E.V.; Sandborn, W.J.; Yang, S.-K. An update on the epidemiology of inflammatory bowel disease in Asia. *Off. J. Am. Coll. Gastroenterol. | ACG* **2008**, *103*, 3167–3182. [CrossRef]
75. Chouraki, V.; Savoye, G.; Dauchet, L.; Vernier-Massouille, G.; Dupas, J.L.; Merle, V.; Laberenne, J.E.; Salomez, J.L.; Lerebours, E.; Turck, D. The changing pattern of Crohn's disease incidence in northern France: A continuing increase in the 10-to 19-year-old age bracket (1988–2007). *Aliment. Pharmacol. Ther.* **2011**, *33*, 1133–1142. [CrossRef] [PubMed]
76. Lakatos, P.L. Recent trends in the epidemiology of inflammatory bowel diseases: Up or down? *World J. Gastroenterol. WJG* **2006**, *12*, 6102. [CrossRef]
77. Cosnes, J.; Gower–Rousseau, C.; Seksik, P.; Cortot, A. Epidemiology and natural history of inflammatory bowel diseases. *Gastroenterology* **2011**, *140*, 1785–1794.e1784. [CrossRef]
78. Loftus Jr, E.V. Clinical epidemiology of inflammatory bowel disease: Incidence, prevalence, and environmental influences. *Gastroenterology* **2004**, *126*, 1504–1517. [CrossRef]
79. Dixon, L.J.; Kabi, A.; Nickerson, K.P.; McDonald, C. Combinatorial effects of diet and genetics on inflammatory bowel disease pathogenesis. *Inflamm. Bowel Dis.* **2015**, *21*, 912–922. [CrossRef] [PubMed]
80. Leone, V.; Chang, E.B.; Devkota, S. Diet, microbes, and host genetics: The perfect storm in inflammatory bowel diseases. *J. Gastroenterol.* **2013**, *48*, 315–321. [CrossRef]
81. Debnath, T.; Hasnat, M.A.; Pervin, M.; Lee, S.Y.; Park, S.R.; Kim, D.H.; Kweon, H.J.; Kim, J.M.; Lim, B.O. Chaga mushroom (Inonotus obliquus) grown on germinated brown rice suppresses inflammation associated with colitis in mice. *Food Sci. Biotechnol.* **2012**, *21*, 1235–1241. [CrossRef]
82. Baumgart, D.C.; Carding, S.R. Inflammatory bowel disease: Cause and immunobiology. *Lancet* **2007**, *369*, 1627–1640. [CrossRef]
83. Lucas, A.; Cobelens, P.; Kavelaars, A.; Heijnen, C.; Holtmann, G.; Haag, S.; Gerken, G.; Langhorst, J.; Dobos, G.; Schedlowski, M.; et al. Disturbed in vitro adrenergic modulation of cytokine production in inflammatory bowel diseases in remission. *J. Neuroimmunol.* **2007**, *182*, 195–203. [CrossRef]
84. Sies, H. Oxidative stress: Oxidants and antioxidants. *Exp. Physiol. Transl. Integr.* **1997**, *82*, 291–295. [CrossRef]
85. Lobo, V.; Patil, A.; Phatak, A.; Chandra, N. Free radicals, antioxidants and functional foods: Impact on human health. *Pharmacogn. Rev.* **2010**, *4*, 118–126. [CrossRef]
86. Halliwell, B.; Gutteridge, J.M. *Free Radicals in Biology and Medicine*; Pergamon: Oxford, UK, 1985.
87. Turpin, W.; Goethel, A.; Bedrani, L.; Croitoru Mdcm, K. Determinants of IBD Heritability: Genes, Bugs, and More. *Inflamm. Bowel Dis.* **2018**, *24*, 1133–1148. [CrossRef] [PubMed]
88. Lee, Y.K.; Mazmanian, S.K. Has the microbiota played a critical role in the evolution of the adaptive immune system? *Science* **2010**, *330*, 1768–1773. [CrossRef]
89. Elinav, E.; Strowig, T.; Kau, A.L.; Henao-Mejia, J.; Thaiss, C.A.; Booth, C.J.; Peaper, D.R.; Bertin, J.; Eisenbarth, S.C.; Gordon, J.I.; et al. NLRP6 Inflammasome Regulates Colonic Microbial Ecology and Risk for Colitis. *Cell* **2011**, *145*, 745–757. [CrossRef] [PubMed]
90. Dheer, R.; Santaolalla, R.; Davies, J.M.; Lang, J.K.; Phillips, M.C.; Pastorini, C.; Vazquez-Pertejo, M.T.; Abreu, M.T. Intestinal Epithelial Toll-Like Receptor 4 Signaling Affects Epithelial Function and Colonic Microbiota and Promotes a Risk for Transmissible Colitis. *Infect. Immun.* **2016**, *84*, 798–810. [CrossRef]
91. Hansen, J.J.; Sartor, R.B. Therapeutic Manipulation of the Microbiome in IBD: Current Results and Future Approaches. *Curr. Treat. Options Gastroenterol.* **2015**, *13*, 105–120. [CrossRef] [PubMed]
92. Lane, E.R.; Zisman, T.L.; Suskind, D.L. The microbiota in inflammatory bowel disease: Current and therapeutic insights. *J. Inflamm. Res.* **2017**, *10*, 63–73. [CrossRef]
93. Liu, T.; Zhang, L.; Joo, D.; Sun, S.C. NF-κB signaling in inflammation. *Signal Transduct. Target. Ther.* **2017**, *2*, 17023. [CrossRef]
94. Wullaert, A.; Bonnet, M.C.; Pasparakis, M. NF-kappaB in the regulation of epithelial homeostasis and inflammation. *Cell Res.* **2011**, *21*, 146–158. [CrossRef] [PubMed]
95. Zaidi, D.; Wine, E. Regulation of Nuclear Factor Kappa-Light-Chain-Enhancer of Activated B Cells (NF-kappabeta) in Inflammatory Bowel Diseases. *Front. Pediatr.* **2018**, *6*, 317. [CrossRef]
96. Rogler, G.; Brand, K.; Vogl, D.; Page, S.; Hofmeister, R.; Andus, T.; Knuechel, R.; Baeuerle, P.A.; Scholmerich, J.; Gross, V. Nuclear factor kappaB is activated in macrophages and epithelial cells of inflamed intestinal mucosa. *Gastroenterology* **1998**, *115*, 357–369. [CrossRef] [PubMed]

97. Sanmarco, L.M.; Chao, C.C.; Wang, Y.C.; Kenison, J.E.; Li, Z.; Rone, J.M.; Rejano-Gordillo, C.M.; Polonio, C.M.; Gutierrez-Vazquez, C.; Piester, G.; et al. Identification of environmental factors that promote intestinal inflammation. *Nature* **2022**, *611*, 801–809. [CrossRef]
98. Arisawa, T.; Tahara, T.; Shibata, T.; Nagasaka, M.; Nakamura, M.; Kamiya, Y.; Fujita, H.; Yoshioka, D.; Okubo, M.; Sakata, M.; et al. Nrf2 gene promoter polymorphism is associated with ulcerative colitis in a Japanese population. *Hepatogastroenterology* **2008**, *55*, 394–397.
99. Myers, J.N.; Schaffer, M.W.; Korolkova, O.Y.; Williams, A.D.; Gangula, P.R.; M'Koma, A.E. Implications of the colonic deposition of free hemoglobin-alpha chain: A previously unknown tissue by-product in inflammatory bowel disease. *Inflamm. Bowel Dis.* **2014**, *20*, 1530–1547. [CrossRef]
100. Sabzevary-Ghahfarokhi, M.; Shohan, M.; Shirzad, H.; Rahimian, G.; Soltani, A.; Ghatreh-Samani, M.; Deris, F.; Bagheri, N.; Shafigh, M.; Tahmasbi, K. The regulatory role of Nrf2 in antioxidants phase2 enzymes and IL-17A expression in patients with ulcerative colitis. *Pathol. Res. Pract.* **2018**, *214*, 1149–1155. [CrossRef]
101. Stachel, I.; Geismann, C.; Aden, K.; Deisinger, F.; Rosenstiel, P.; Schreiber, S.; Sebens, S.; Arlt, A.; Schafer, H. Modulation of nuclear factor E2-related factor-2 (Nrf2) activation by the stress response gene immediate early response-3 (IER3) in colonic epithelial cells: A novel mechanism of cellular adaption to inflammatory stress. *J. Biol. Chem.* **2014**, *289*, 1917–1929. [CrossRef] [PubMed]
102. Kim, J.; Cha, Y.N.; Surh, Y.J. A protective role of nuclear factor-erythroid 2-related factor-2 (Nrf2) in inflammatory disorders. *Mutat. Res.* **2010**, *690*, 12–23. [CrossRef]
103. Singh, S.; Vrishni, S.; Singh, B.K.; Rahman, I.; Kakkar, P. Nrf2-ARE stress response mechanism: A control point in oxidative stress-mediated dysfunctions and chronic inflammatory diseases. *Free. Radic. Res.* **2010**, *44*, 1267–1288. [CrossRef]
104. Joshi, R.; Kumar, S.; Unnikrishnan, M.; Mukherjee, T. Free radical scavenging reactions of sulfasalazine, 5-aminosalicylic acid and sulfapyridine: Mechanistic aspects and antioxidant activity. *Free Radic. Res.* **2005**, *39*, 1163–1172. [CrossRef]
105. Lakatos, P.L.; Lakatos, L. Ulcerative proctitis: A review of pharmacotherapy and management. *Expert Opin. Pharmacother.* **2008**, *9*, 741–749. [CrossRef] [PubMed]
106. State, M.; Negreanu, L. Defining the Failure of Medical Therapy for Inflammatory Bowel Disease in the Era of Advanced Therapies: A Systematic Review. *Biomedicines* **2023**, *11*, 544. [CrossRef]
107. Langhorst, J.; Anthonisen, I.B.; Steder-Neukamm, U.; Lüdtke, R.; Spahn, G.; Michalsen, A.; Dobos, G.J. Amount of systemic steroid medication is a strong predictor for the use of complementary and alternative medicine in patients with inflammatory bowel disease. Results from a German national survey. *Inflamm. Bowel Dis.* **2005**, *11*, 287–295. [CrossRef]
108. Santino, A.; Scarano, A.; De Santis, S.; De Benedictis, M.; Giovinazzo, G.; Chieppa, M. Gut Microbiota Modulation and Anti-Inflammatory Properties of Dietary Polyphenols in IBD: New and Consolidated Perspectives. *Curr. Pharm. Des.* **2017**, *23*, 2344–2351. [CrossRef] [PubMed]
109. Pereira, S.R.; Pereira, R.; Figueiredo, I.; Freitas, V.; Dinis, T.C.; Almeida, L.M. Comparison of anti-inflammatory activities of an anthocyanin-rich fraction from Portuguese blueberries (*Vaccinium corymbosum* L.) and 5-aminosalicylic acid in a TNBS-induced colitis rat model. *PLoS ONE* **2017**, *12*, e0174116. [CrossRef] [PubMed]
110. Zhang, G.; Gu, Y.; Dai, X. Protective Effect of Bilberry Anthocyanin Extracts on Dextran Sulfate Sodium-Induced Intestinal Damage in Drosophila melanogaster. *Nutrients* **2022**, *14*, 2875. [CrossRef] [PubMed]
111. Thipart, K.; Gruneck, L.; Phunikhom, K.; Sharpton, T.J.; Sattayasai, J.; Popluechai, S. Dark-purple rice extract modulates gut microbiota composition in acetic acid- and indomethacin-induced inflammatory bowel disease in rats. *Int. Microbiol.* **2023**, *26*, 423–434. [CrossRef]
112. Farzaei, M.H.; Khanavi, M.; Moghaddam, G.; Dolatshahi, F.; Rahimi, R.; Shams-Ardekani, M.R.; Amin, G.; Hajimahmoodi, M. Standardization of Tragopogon graminifolius DC. extract based on phenolic compounds and antioxidant activity. *J. Chem.* **2014**, *2014*, 425965. [CrossRef]
113. Tan, C.; Tong, Y.; Deng, H.; Wang, M.; Zhao, Y.; Wan, M.; Lin, S.; Liu, X.; Meng, X.; Ma, Y. Anti-apoptotic effects of high hydrostatic pressure treated cyanidin-3-glucoside and blueberry pectin complexes on lipopolysaccharide-induced inflammation in Caco-2 cells. *J. Funct. Foods* **2021**, *86*, 104709. [CrossRef]
114. Ferrari, D.; Speciale, A.; Cristani, M.; Fratantonio, D.; Molonia, M.S.; Ranaldi, G.; Saija, A.; Cimino, F. Cyanidin-3-O-glucoside inhibits NF-kB signalling in intestinal epithelial cells exposed to TNF-α and exerts protective effects via Nrf2 pathway activation. *Toxicol. Lett.* **2016**, *264*, 51–58. [CrossRef]
115. Serra, D.; Paixao, J.; Nunes, C.; Dinis, T.C.; Almeida, L.M. Cyanidin-3-glucoside suppresses cytokine-induced inflammatory response in human intestinal cells: Comparison with 5-aminosalicylic acid. *PLoS ONE* **2013**, *8*, e73001. [CrossRef] [PubMed]
116. Serra, D.; Almeida, L.M.; Dinis, T.C. Anti-inflammatory protection afforded by cyanidin-3-glucoside and resveratrol in human intestinal cells via Nrf2 and PPAR-gamma: Comparison with 5-aminosalicylic acid. *Chem. Biol. Interact.* **2016**, *260*, 102–109. [CrossRef]
117. Xia, Y.; Tian, L.M.; Liu, Y.; Guo, K.S.; Lv, M.; Li, Q.T.; Hao, S.Y.; Ma, C.H.; Chen, Y.X.; Tanaka, M. Low Dose of Cyanidin-3-O-Glucoside Alleviated Dextran Sulfate Sodium-Induced Colitis, Mediated by CD169+ Macrophage Pathway. *Inflamm. Bowel Dis.* **2019**, *25*, 1510–1521. [CrossRef]
118. Cremonini, E.; Mastaloudis, A.; Hester, S.N.; Verstraeten, S.V.; Anderson, M.; Wood, S.M.; Waterhouse, A.L.; Fraga, C.G.; Oteiza, P.I. Anthocyanins inhibit tumor necrosis alpha-induced loss of Caco-2 cell barrier integrity. *Food Funct.* **2017**, *8*, 2915–2923. [CrossRef]

119. Speciale, A.; Bashllari, R.; Muscara, C.; Molonia, M.S.; Saija, A.; Saha, S.; Wilde, P.J.; Cimino, F. Anti-Inflammatory Activity of an In Vitro Digested Anthocyanin-Rich Extract on Intestinal Epithelial Cells Exposed to TNF-α. *Molecules* **2022**, *27*, 5386. [CrossRef]
120. Wang, Y.; Chen, J.; Wang, Y.; Zheng, F.; Qu, M.; Huang, Z.; Yan, J.; Bao, F.; Li, X.; Sun, C.; et al. Cyanidin-3-O-glucoside extracted from the Chinese bayberry (Myrica rubra Sieb. et Zucc.) alleviates antibiotic-associated diarrhea by regulating gut microbiota and down-regulating inflammatory factors in NF-kappaB pathway. *Front. Nutr.* **2022**, *9*, 970530. [CrossRef] [PubMed]
121. Ferrari, D.; Cimino, F.; Fratantonio, D.; Molonia, M.S.; Bashllari, R.; Busa, R.; Saija, A.; Speciale, A. Cyanidin-3-O-Glucoside Modulates the In Vitro Inflammatory Crosstalk between Intestinal Epithelial and Endothelial Cells. *Mediat. Inflamm.* **2017**, *2017*, 3454023. [CrossRef]
122. Min, S.W.; Ryu, S.N.; Kim, D.H. Anti-inflammatory effects of black rice, cyanidin-3-O-beta-D-glycoside, and its metabolites, cyanidin and protocatechuic acid. *Int. Immunopharmacol.* **2010**, *10*, 959–966. [CrossRef]
123. Speciale, A.; Anwar, S.; Canali, R.; Chirafisi, J.; Saija, A.; Virgili, F.; Cimino, F. Cyanidin-3-O-glucoside counters the response to TNF-alpha of endothelial cells by activating Nrf2 pathway. *Mol. Nutr. Food Res.* **2013**, *57*, 1979–1987. [CrossRef]
124. Tan, C.; Wang, M.; Kong, Y.; Wan, M.; Deng, H.; Tong, Y.; Lyu, C.; Meng, X. Anti-inflammatory and intestinal microbiota modulation properties of high hydrostatic pressure treated cyanidin-3-glucoside and blueberry pectin complexes on dextran sodium sulfate-induced ulcerative colitis mice. *Food Funct.* **2022**, *13*, 4384–4398. [CrossRef]
125. Triebel, S.; Trieu, H.-L.; Richling, E. Modulation of inflammatory gene expression by a bilberry (Vaccinium myrtillus L.) extract and single anthocyanins considering their limited stability under cell culture conditions. *J. Agric. Food Chem.* **2012**, *60*, 8902–8910. [CrossRef]
126. Liso, M.; Sila, A.; Verna, G.; Scarano, A.; Donghia, R.; Castellana, F.; Cavalcanti, E.; Pesole, P.L.; Sommella, E.M.; Lippolis, A. Nutritional Regimes Enriched with Antioxidants as an Efficient Adjuvant for IBD Patients under Infliximab Administration, a Pilot Study. *Antioxidants* **2022**, *11*, 138. [CrossRef] [PubMed]
127. Hayden, M.S.; Ghosh, S. Regulation of NF-kappaB by TNF family cytokines. *Semin. Immunol.* **2014**, *26*, 253–266. [CrossRef] [PubMed]
128. Speciale, A.; Saija, A.; Bashllari, R.; Molonia, M.S.; Muscara, C.; Occhiuto, C.; Cimino, F.; Cristani, M. Anthocyanins As Modulators of Cell Redox-Dependent Pathways in Non-Communicable Diseases. *Curr. Med. Chem.* **2020**, *27*, 1955–1996. [CrossRef]
129. Pasparakis, M. IKK/NF-kappaB signaling in intestinal epithelial cells controls immune homeostasis in the gut. *Mucosal Immunol.* **2008**, *1* (Suppl. 1), S54–S57. [CrossRef] [PubMed]
130. Andresen, L.; Jorgensen, V.L.; Perner, A.; Hansen, A.; Eugen-Olsen, J.; Rask-Madsen, J. Activation of nuclear factor kappaB in colonic mucosa from patients with collagenous and ulcerative colitis. *Gut* **2005**, *54*, 503–509. [CrossRef]
131. Bernotti, S.; Seidman, E.; Sinnett, D.; Brunet, S.; Dionne, S.; Delvin, E.; Levy, E. Inflammatory reaction without endogenous antioxidant response in Caco-2 cells exposed to iron/ascorbate-mediated lipid peroxidation. *Am. J. Physiol. Gastrointest. Liver Physiol.* **2003**, *285*, G898–G906. [CrossRef]
132. Machado, A.; Geraldi, M.V.; do Nascimento, R.P.; Moya, A.; Vezza, T.; Diez-Echave, P.; Galvez, J.J.; Cazarin, C.B.B.; Marostica Junior, M.R. Polyphenols from food by-products: An alternative or complementary therapy to IBD conventional treatments. *Food Res. Int.* **2021**, *140*, 110018. [CrossRef]
133. Piechota-Polanczyk, A.; Fichna, J. Review article: The role of oxidative stress in pathogenesis and treatment of inflammatory bowel diseases. *Naunyn Schmiedebergs Arch. Pharmacol.* **2014**, *387*, 605–620. [CrossRef]
134. Kannan, N.; Guruvayoorappan, C. Protective effect of Bauhinia tomentosa on acetic acid induced ulcerative colitis by regulating antioxidant and inflammatory mediators. *Int. Immunopharmacol.* **2013**, *16*, 57–66. [CrossRef]
135. Cromer, W.E.; Mathis, J.M.; Granger, D.N.; Chaitanya, G.V.; Alexander, J.S. Role of the endothelium in inflammatory bowel diseases. *World J. Gastroenterol.* **2011**, *17*, 578–593. [CrossRef]
136. Dvornikova, K.A.; Platonova, O.N.; Bystrova, E.Y. Hypoxia and Intestinal Inflammation: Common Molecular Mechanisms and Signaling Pathways. *Int. J. Mol. Sci.* **2023**, *24*, 2425. [CrossRef]
137. Aggeletopoulou, I.; Marangos, M.; Assimakopoulos, S.F.; Mouzaki, A.; Thomopoulos, K.; Triantos, C. Vitamin D and Microbiome: Molecular Interaction in Inflammatory Bowel Disease Pathogenesis. *Am. J. Pathol.* 2023; *In press*. [CrossRef]
138. Czank, C.; Cassidy, A.; Zhang, Q.; Morrison, D.J.; Preston, T.; Kroon, P.A.; Botting, N.P.; Kay, C.D. Human metabolism and elimination of the anthocyanin, cyanidin-3-glucoside: A (13)C-tracer study. *Am. J. Clin. Nutr.* **2013**, *97*, 995–1003. [CrossRef] [PubMed]
139. Daveri, E.; Cremonini, E.; Mastaloudis, A.; Hester, S.N.; Wood, S.M.; Waterhouse, A.L.; Anderson, M.; Fraga, C.G.; Oteiza, P.I. Cyanidin and delphinidin modulate inflammation and altered redox signaling improving insulin resistance in high fat-fed mice. *Redox Biol.* **2018**, *18*, 16–24. [CrossRef] [PubMed]
140. Fratantonio, D.; Speciale, A.; Ferrari, D.; Cristani, M.; Saija, A.; Cimino, F. Palmitate-induced endothelial dysfunction is attenuated by cyanidin-3-O-glucoside through modulation of Nrf2/Bach1 and NF-kappaB pathways. *Toxicol. Lett.* **2015**, *239*, 152–160. [CrossRef] [PubMed]
141. Dinkova-Kostova, A.T.; Talalay, P. Direct and indirect antioxidant properties of inducers of cytoprotective proteins. *Mol. Nutr. Food Res.* **2008**, *52* (Suppl. 1), S128–S138. [CrossRef]
142. Lee, J.M.; Johnson, J.A. An important role of Nrf2-ARE pathway in the cellular defense mechanism. *J. Biochem. Mol. Biol.* **2004**, *37*, 139–143. [CrossRef]

143. Asano, K.; Takahashi, N.; Ushiki, M.; Monya, M.; Aihara, F.; Kuboki, E.; Moriyama, S.; Iida, M.; Kitamura, H.; Qiu, C.H.; et al. Intestinal CD169(+) macrophages initiate mucosal inflammation by secreting CCL8 that recruits inflammatory monocytes. *Nat. Commun.* **2015**, *6*, 7802. [CrossRef]
144. Junt, T.; Moseman, E.A.; Iannacone, M.; Massberg, S.; Lang, P.A.; Boes, M.; Fink, K.; Henrickson, S.E.; Shayakhmetov, D.M.; Di Paolo, N.C.; et al. Subcapsular sinus macrophages in lymph nodes clear lymph-borne viruses and present them to antiviral B cells. *Nature* **2007**, *450*, 110–114. [CrossRef] [PubMed]
145. Kuka, M.; Iannacone, M. The role of lymph node sinus macrophages in host defense. *Ann. N. Y. Acad. Sci.* **2014**, *1319*, 38–46. [CrossRef] [PubMed]
146. Saunderson, S.C.; Dunn, A.C.; Crocker, P.R.; McLellan, A.D. CD169 mediates the capture of exosomes in spleen and lymph node. *Blood* **2014**, *123*, 208–216. [CrossRef]
147. Ravishankar, B.; Shinde, R.; Liu, H.; Chaudhary, K.; Bradley, J.; Lemos, H.P.; Chandler, P.; Tanaka, M.; Munn, D.H.; Mellor, A.L.; et al. Marginal zone CD169+ macrophages coordinate apoptotic cell-driven cellular recruitment and tolerance. *Proc. Natl. Acad. Sci. USA* **2014**, *111*, 4215–4220. [CrossRef] [PubMed]
148. Hiemstra, I.H.; Beijer, M.R.; Veninga, H.; Vrijland, K.; Borg, E.G.; Olivier, B.J.; Mebius, R.E.; Kraal, G.; den Haan, J.M. The identification and developmental requirements of colonic CD169(+) macrophages. *Immunology* **2014**, *142*, 269–278. [CrossRef]
149. Makita, S.; Kanai, T.; Nemoto, Y.; Totsuka, T.; Okamoto, R.; Tsuchiya, K.; Yamamoto, M.; Kiyono, H.; Watanabe, M. Intestinal lamina propria retaining CD4+CD25+ regulatory T cells is a suppressive site of intestinal inflammation. *J. Immunol.* **2007**, *178*, 4937–4946. [CrossRef]
150. Sakuraba, A.; Sato, T.; Kamada, N.; Kitazume, M.; Sugita, A.; Hibi, T. Th1/Th17 immune response is induced by mesenteric lymph node dendritic cells in Crohn's disease. *Gastroenterology* **2009**, *137*, 1736–1745. [CrossRef]
151. Wang, D.; Li, Q.; Yang, Y.; Hao, S.; Han, X.; Song, J.; Yin, Y.; Li, X.; Tanaka, M.; Qiu, C.H. Macrophage Subset Expressing CD169 in Peritoneal Cavity-Regulated Mucosal Inflammation Together with Lower Levels of CCL22. *Inflammation* **2017**, *40*, 1191–1203. [CrossRef]
152. Li, Q.; Wang, D.; Hao, S.; Han, X.; Xia, Y.; Li, X.; Chen, Y.; Tanaka, M.; Qiu, C.H. CD169 Expressing Macrophage, a Key Subset in Mesenteric Lymph Nodes Promotes Mucosal Inflammation in Dextran Sulfate Sodium-Induced Colitis. *Front. Immunol.* **2017**, *8*, 669. [CrossRef]
153. Lee, S.G.; Kim, B.; Yang, Y.; Pham, T.X.; Park, Y.K.; Manatou, J.; Koo, S.I.; Chun, O.K.; Lee, J.Y. Berry anthocyanins suppress the expression and secretion of proinflammatory mediators in macrophages by inhibiting nuclear translocation of NF-kappaB independent of NRF2-mediated mechanism. *J. Nutr. Biochem.* **2014**, *25*, 404–411. [CrossRef]
154. Brennan, K.; Lyons, C.; Fernandes, P.; Doyle, S.; Houston, A.; Brint, E. Engagement of Fas differentially regulates the production of LPS-induced proinflammatory cytokines and type I interferons. *FEBS J.* **2019**, *286*, 523–535. [CrossRef] [PubMed]
155. Wang, Z.; Zhang, M.; Wang, Z.; Guo, Z.; Wang, Z.; Chen, Q. Cyanidin-3-O-glucoside attenuates endothelial cell dysfunction by modulating miR-204-5p/SIRT1-mediated inflammation and apoptosis. *Biofactors* **2020**, *46*, 803–812. [CrossRef] [PubMed]
156. Morais, C.A.; de Rosso, V.V.; Estadella, D.; Pisani, L.P. Anthocyanins as inflammatory modulators and the role of the gut microbiota. *J. Nutr. Biochem.* **2016**, *33*, 1–7. [CrossRef]
157. Lee, S.; Keirsey, K.I.; Kirkland, R.; Grunewald, Z.I.; Fischer, J.G.; de La Serre, C.B. Blueberry Supplementation Influences the Gut Microbiota, Inflammation, and Insulin Resistance in High-Fat-Diet-Fed Rats. *J. Nutr.* **2018**, *148*, 209–219. [CrossRef]
158. Zhao, S.; Liu, W.; Wang, J.; Shi, J.; Sun, Y.; Wang, W.; Ning, G.; Liu, R.; Hong, J. Akkermansia muciniphila improves metabolic profiles by reducing inflammation in chow diet-fed mice. *J. Mol. Endocrinol.* **2017**, *58*, 1–14. [CrossRef]
159. Rinttila, T.; Kassinen, A.; Malinen, E.; Krogius, L.; Palva, A. Development of an extensive set of 16S rDNA-targeted primers for quantification of pathogenic and indigenous bacteria in faecal samples by real-time PCR. *J. Appl. Microbiol.* **2004**, *97*, 1166–1177. [CrossRef] [PubMed]
160. Fiore, E.; Van Tyne, D.; Gilmore, M.S. Pathogenicity of Enterococci. *Microbiol. Spectr.* **2019**, *7*. [CrossRef]
161. Wen, X.; Wang, H.G.; Zhang, M.N.; Zhang, M.H.; Wang, H.; Yang, X.Z. Fecal microbiota transplantation ameliorates experimental colitis via gut microbiota and T-cell modulation. *World J. Gastroenterol.* **2021**, *27*, 2834–2849. [CrossRef] [PubMed]
162. Wang, C.; Li, W.; Wang, H.; Ma, Y.; Zhao, X.; Zhang, X.; Yang, H.; Qian, J.; Li, J. Saccharomyces boulardii alleviates ulcerative colitis carcinogenesis in mice by reducing TNF-alpha and IL-6 levels and functions and by rebalancing intestinal microbiota. *BMC Microbiol.* **2019**, *19*, 246. [CrossRef]
163. Sun, Q.; Ji, Y.C.; Wang, Z.L.; She, X.; He, Y.; Ai, Q.; Li, L.Q. Sodium Butyrate Alleviates Intestinal Inflammation in Mice with Necrotizing Enterocolitis. *Mediat. Inflamm.* **2021**, *2021*, 6259381. [CrossRef] [PubMed]
164. Hempel, S.; Newberry, S.J.; Maher, A.R.; Wang, Z.; Miles, J.N.; Shanman, R.; Johnsen, B.; Shekelle, P.G. Probiotics for the prevention and treatment of antibiotic-associated diarrhea: A systematic review and meta-analysis. *JAMA* **2012**, *307*, 1959–1969. [CrossRef]
165. Guo, M.; Li, Z. Polysaccharides isolated from Nostoc commune Vaucher inhibit colitis-associated colon tumorigenesis in mice and modulate gut microbiota. *Food Funct.* **2019**, *10*, 6873–6881. [CrossRef]
166. Wu, S.; Hu, R.; Nakano, H.; Chen, K.; Liu, M.; He, X.; Zhang, H.; He, J.; Hou, D.X. Modulation of Gut Microbiota by Lonicera caerulea L. Berry Polyphenols in a Mouse Model of Fatty Liver Induced by High Fat Diet. *Molecules* **2018**, *23*, 3213. [CrossRef]

167. Wang, K.; Wan, Z.; Ou, A.; Liang, X.; Guo, X.; Zhang, Z.; Wu, L.; Xue, X. Monofloral honey from a medical plant, Prunella Vulgaris, protected against dextran sulfate sodium-induced ulcerative colitis via modulating gut microbial populations in rats. *Food Funct.* **2019**, *10*, 3828–3838. [CrossRef]
168. Wang, K.; Jin, X.; Li, Q.; Sawaya, A.; Le Leu, R.K.; Conlon, M.A.; Wu, L.; Hu, F. Propolis from Different Geographic Origins Decreases Intestinal Inflammation and Bacteroides spp. Populations in a Model of DSS-Induced Colitis. *Mol. Nutr. Food Res.* **2018**, *62*, e1800080. [CrossRef]
169. Ajiboye, T.O.; Habibu, R.S.; Saidu, K.; Haliru, F.Z.; Ajiboye, H.O.; Aliyu, N.O.; Ibitoye, O.B.; Uwazie, J.N.; Muritala, H.F.; Bello, S.A.; et al. Involvement of oxidative stress in protocatechuic acid-mediated bacterial lethality. *Microbiologyopen* **2017**, *6*, e00472. [CrossRef] [PubMed]
170. Nishitani, Y.; Sasaki, E.; Fujisawa, T.; Osawa, R. Genotypic analyses of lactobacilli with a range of tannase activities isolated from human feces and fermented foods. *Syst. Appl. Microbiol.* **2004**, *27*, 109–117. [CrossRef] [PubMed]
171. Szwajgier, D.; Jakubczyk, A. Biotransformation of ferulic acid by Lactobacillus acidophilus KI and selected Bifidobacterium strains. *ACTA Sci. Pol. Technol. Aliment.* **2010**, *9*, 45–59.
172. Gowd, V.; Bao, T.; Chen, W. Antioxidant potential and phenolic profile of blackberry anthocyanin extract followed by human gut microbiota fermentation. *Food Res. Int.* **2019**, *120*, 523–533. [CrossRef] [PubMed]
173. Keppler, K.; Humpf, H.-U. Metabolism of anthocyanins and their phenolic degradation products by the intestinal microflora. *Bioorganic Med. Chem.* **2005**, *13*, 5195–5205. [CrossRef]
174. Shishir, M.R.I.; Suo, H.; Liu, X.; Kang, Q.; Xiao, J.; Wang, M.; Chen, F.; Cheng, K.W. Development and evaluation of a novel nanofibersolosome for enhancing the stability, in vitro bioaccessibility, and colonic delivery of cyanidin-3-O-glucoside. *Food Res. Int.* **2021**, *149*, 110712. [CrossRef]
175. Schroeder, K.W.; Tremaine, W.J.; Ilstrup, D.M. Coated oral 5-aminosalicylic acid therapy for mildly to moderately active ulcerative colitis. A randomized study. *N. Engl. J. Med.* **1987**, *317*, 1625–1629. [CrossRef]
176. Travis, S.P.; Schnell, D.; Krzeski, P.; Abreu, M.T.; Altman, D.G.; Colombel, J.F.; Feagan, B.G.; Hanauer, S.B.; Lichtenstein, G.R.; Marteau, P.R.; et al. Reliability and initial validation of the ulcerative colitis endoscopic index of severity. *Gastroenterology* **2013**, *145*, 987–995. [CrossRef]
177. Chen, M.; Shen, B. Overview of Diagnosis and Medical Treatment of Inflammatory Bowel Diseases. In *Interventional Inflammatory Bowel Disease: Endoscopic Management and Treatment of Complications*; Academic Press: Cambridge, MA, USA, 2018.
178. Jesse, K.; Liu, G.R.L. Inflammatory Bowel Disease. In *Clinical Gastrointestinal Endoscopy*, 2nd ed.; Elsevier: Amsterdam, The Netherlands, 2012; pp. 243–264.
179. Niv, Y.; Gal, E.; Gabovitz, V.; Hershkovitz, M.; Lichtenstein, L.; Avni, I. Capsule Endoscopy Crohn's Disease Activity Index (CECDAIic or Niv Score) for the Small Bowel and Colon. *J. Clin. Gastroenterol.* **2018**, *52*, 45–49. [CrossRef] [PubMed]
180. Burri, E.; Maillard, M.H.; Schoepfer, A.M.; Seibold, F.; Van Assche, G.; Riviere, P.; Laharie, D.; Manz, M. Treatment Algorithm for Mild and Moderate-to-Severe Ulcerative Colitis: An Update. *Digestion* **2020**, *101* (Suppl. 1), 2–15. [CrossRef]
181. Johnson, T.O.; Akinsanmi, A.O.; Ejembi, S.A.; Adeyemi, O.E.; Oche, J.R.; Johnson, G.I.; Adegboyega, A.E. Modern drug discovery for inflammatory bowel disease: The role of computational methods. *World J. Gastroenterol.* **2023**, *29*, 310–331. [CrossRef] [PubMed]
182. Chen, Y.; Zhang, G.; Yang, Y.; Zhang, S.; Jiang, H.; Tian, K.; Arenbaoligao; Chen, D. The treatment of inflammatory bowel disease with monoclonal antibodies in Asia. *Biomed. Pharmacother. Biomed. Pharmacother.* **2023**, *157*, 114081. [CrossRef] [PubMed]

International Journal of
Molecular Sciences

MDPI

Review

Biological and Catalytic Properties of Selenoproteins

Jean Chaudière

CBMN (CNRS, UMR 5248), University of Bordeaux, 33600 Pessac, France; jean.chaudiere@u-bordeaux.fr

Abstract: Selenocysteine is a catalytic residue at the active site of all selenoenzymes in bacteria and mammals, and it is incorporated into the polypeptide backbone by a co-translational process that relies on the recoding of a UGA termination codon into a serine/selenocysteine codon. The best-characterized selenoproteins from mammalian species and bacteria are discussed with emphasis on their biological function and catalytic mechanisms. A total of 25 genes coding for selenoproteins have been identified in the genome of mammals. Unlike the selenoenzymes of anaerobic bacteria, most mammalian selenoenzymes work as antioxidants and as redox regulators of cell metabolism and functions. Selenoprotein P contains several selenocysteine residues and serves as a selenocysteine reservoir for other selenoproteins in mammals. Although extensively studied, glutathione peroxidases are incompletely understood in terms of local and time-dependent distribution, and regulatory functions. Selenoenzymes take advantage of the nucleophilic reactivity of the selenolate form of selenocysteine. It is used with peroxides and their by-products such as disulfides and sulfoxides, but also with iodine in iodinated phenolic substrates. This results in the formation of Se-X bonds (X = O, S, N, or I) from which a selenenylsulfide intermediate is invariably produced. The initial selenolate group is then recycled by thiol addition. In bacterial glycine reductase and D-proline reductase, an unusual catalytic rupture of selenium–carbon bonds is observed. The exchange of selenium for sulfur in selenoproteins, and information obtained from model reactions, suggest that a generic advantage of selenium compared with sulfur relies on faster kinetics and better reversibility of its oxidation reactions.

Keywords: selenium; selenoenzyme; selenocysteine; catalytic mechanism; glutathione peroxidase; thioredoxin reductase; deiodinase; methionyl-sulfoxide reductase; glycine reductase; D-proline reductase; formate dehydrogenase; hydrogenase; antioxidant; redox regulation

Citation: Chaudière, J. Biological and Catalytic Properties of Selenoproteins. *Int. J. Mol. Sci.* **2023**, *24*, 10109. https://doi.org/10.3390/ijms241210109

Academic Editor: Yasumitsu Ogra

Received: 4 May 2023
Revised: 6 June 2023
Accepted: 8 June 2023
Published: 14 June 2023

1. Introduction

The development of selenium biochemistry was best summarized by Leopold Flohé, one of its major contributors [1]. Selenium is the 34th element in the periodic table, with an atomic mass of 78.96. It belongs to period 4 and group VIB of chalcogens. It was discovered in 1817 by Berzelius and Gahn, in the red-brown sediment of industrial tanks used for the preparation of sulfuric acid, where tellurium (from Latin *telluris* which means earth) had already been identified. Hence the choice of the name selenium, from the Greek *selene*, which meant "moon goddess". As shown in Figure 1, a wide range of structures are observed in selenium-containing metabolites and essential biomolecules, as well as in synthetic selenium-containing mimics of selenoenzymes. Selenite SeO_3^{2-} and selenate SeO_4^{2-} are sources of selenium in drinking water, selenide HSe^- is an end-product of their biological reduction, and it can be enzymatically transformed into selenophosphate by ATP, or mono-, di- and tri-methylated by S-adenosyl methionine. Dimethylselenide $Se(CH_3)_2$ is excreted in breath, trimethylselenonium $(CH_3)_3Se^+$ is excreted in urine, and selenophosphate is always used for specific incorporation of selenium into biomolecules. In most selenium-containing proteins, selenium is in the form of a selenocysteine residue. These are the "selenoproteins" discussed in this review, but there are also a few "selenium-binding proteins" in which selenium can be dissociated from the protein by thiol reagents, probably from persulfides of cysteine residues [2].

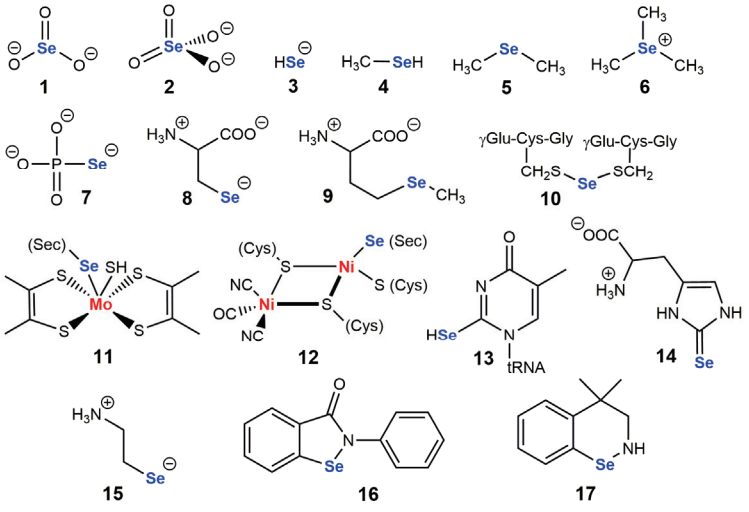

Figure 1. A few structures of selenium-containing molecules are of biological interest. (1) selenite; (2) selenate; (3) selenide; (4) methylselenol; (5) dimethylselenide; (6) trimethylselenonium; (7) selenophosphate; (8) selenocysteine; (9) selenomethionine; (10) glutathione selenotrisulfide; (11) dithiolene-molybdenum cluster of formate dehydrogenases; (12) nickel-sulfur cluster of bacterial hydrogenases; (13) 5-methyl-2-selenouridine in tRNA; (14) selenoneine, selenium analog of ergothioneine; (15) selenocysteamine; (16) and (17) are biomimetic catalysts (2-phenyl-1,2-benzisoselenazol-3-(2H)-one) and 4,4-dimethyl-benzisoselenazine, respectively known as ebselen and BXT-51072, which were tested in clinical development.

Selenium is an essential oligo-element in mammals including humans, but the window between deficiency and toxicity is rather narrow [3–5]. Signs of deficiency are observed for daily intakes of 18 µg or less, and signs of toxicity are observed above 400 µg. Depending on countries and organizations, the recommended daily intake varies between 30 and 75 µg in human adults. In humans, manifestations of severe deficiency include muscular and cardiovascular dysfunctions, osteochondropathy, and infertility. Moreover, large trials carried out among elderly persons have shown that a low selenium status is associated with a faster decline in cognitive functions [6]. The importance of selenoproteins in brain development, not only in aging, has been illustrated by reverse genetics [7]. A neurodevelopmental syndrome called progressive cerebello-cortical atrophy (PCCA) has also been shown to be caused by mutations in the selenocysteine synthase gene [8]. knock-out models have demonstrated that selenoproteins are specifically required in postmitotic neurons of the developing cerebellum [9].

Two endemic diseases which are associated with selenium deficiency have been largely studied in several Chinese regions, namely Keshan disease [10] which is severe cardiomyopathy, and Kashin–Beck disease [11] which is associated with degenerative lesions of joints and vertebral column. In deficient regions of China, Keshan disease was largely eradicated in the 1990s thanks to the addition of sodium selenite to table salt [12], and in Finland, the soil deficit in selenium has led to systematic addition of selenium in fertilization media [13].

In livestock, selenium deficiency also has severe consequences, and today, the selenium status of sheep, cows, pigs, and poultry is tightly controlled. Conversely, consequences of intoxication due to overload in bioavailable selenium—mainly selenite SeO_3^{2-}, selenate SeO_4^{2-}, selenomethionine and selenocysteine—i.e., selenium, which can be incorporated into natural selenoproteins or in place of sulfur in cysteine and methionine residues, may also be severe. The molecular origin of such toxic effects is mainly the nonspecific replacement of cysteine residues by selenocysteine residues whose selenol group may

induce deleterious reactions in such modified proteins. By comparison, the replacement of methionine residues by the isosteric selenomethionine is also observed, but it has no or minor deleterious effect. A recent work performed on mice indicates however that for some proteins which are not selenoproteins, selenium provided in the form of selenocysteine or selenomethionine—not as inorganic salts—can lead to the selective replacement of cysteine or methionine by their selenium homologs at specific sites [14]. Such facultative selenation would not be random and may explain some physiological effects attributable to shifts in dietary selenium.

The administration of selenium at normally toxic doses may serve as an antidote to intoxication by heavy metals such as mercury or cadmium, most likely by forming stable complexes which facilitate their elimination [15,16]. The other side of the coin is that such heavy metals inhibit selenoenzymes, which is also the case for gold salts [17].

In the early 1970s, the identification of an essential atom of selenium incorporated in the form of selenocysteine at the active site of glutathione peroxidases Se-GPx [18,19] provided a first explanation for the essential role of selenium in mammals. Such enzymes catalyze the reduction of hydroperoxides [H_2O_2 and/or ROOH] by glutathione GSH, thereby playing a central role in the antioxidant system of mammals.

Selenomethionine is synthesized in plants where it is randomly incorporated into proteins at Met positions. Selenium of plant selenoproteins is exclusively in the form of selenomethionine which is therefore not specifically coded in the genomic sequence. The partial replacement of one or several methionine [AUG codon] by selenomethionine as a competitive ligand of the tRNA acceptor has structural and functional effects which may be negligible. In archaea, bacteria, and animals, selenium is on the contrary specifically incorporated into selenoproteins by co-translational insertion of selenocysteine. Selenocysteine is therefore the 21st amino acid which is coded in the genome, and which can be inserted in a growing polypeptide chain by means of a specific tRNA [20]. Its codon is UGA—normally read as a termination "opal" codon—which will be read as a "selenocysteine codon" in the context of a control sequence carried by the mRNA. The requirement for selenocysteine-containing proteins is most puzzling in insects. For example, *Drosophila melanogaster* and most other fruit flies possess three selenoprotein genes, but in *Drosophila willistoni*, selenocysteine has been replaced by cysteine and the organism has lost the capacity to synthesize selenocysteine [21].

2. Co-Translational Incorporation of Selenocysteine

This is a complex process that is only partially identical in prokaryotes and eukaryotes [20,22–24]. In eukaryotes, decoding UGA as a selenocysteine codon requires a specific tRNA, a dedicated elongation factor EFsec, and a selenocysteine insertion sequence SECIS which is a hairpin present in the untranslated 3′ region [3′-UTR] of all selenoprotein mRNAs. SECIS recruits all the UGA recoding tools which will impose the recognition of UGA as a "selenocysteine codon" instead of a termination codon. The specific tRNA that binds UGA is called tRNA(Ser)Sec because it is initially aminoacylated by serine which is then transformed into selenocysteyl-t-RNA in a co-translational process. tRNA(Ser)Sec is much longer (a hundred nucleotides) than other tRNAs and it has a markedly distinct 3D structure. This prevents its binding to the canonical transporter of tRNA known as EF1A and enables its processing by the EFsec elongation factor. Clustering of the SECIS elements in the 3′-UTR region upstream from the first UGA codon enables the controlled decoding of several UGA/selenocysteine codons for a protein containing several selenocysteines, such as selenoprotein P in mammals. By contrast, in prokaryotes, SECIS elements are not in the 3′-UTR region, but immediately downstream from the UGA codon, so that the SECIS structure is required for the decoding of each UGA/selenocysteine codon. One should underline that the efficiency of UGA recoding and selenoprotein m-RNA translation is typically low, with a majority of ribosomes failing to incorporate selenocysteine and reach the termination codon. It is outside the scope of this review to discuss all factors involved in this process, but the reader is referred to the review of Copeland and Howard [25] in

which the role of accessory proteins and that of potential effectors of the No-Go Decay (NGD) mRNA pathway are discussed in detail.

The aminoacylation of tRNA-(Ser)Sec requires four enzymes instead of one, because the objective is not to load preformed selenocysteine, but to load serine (sidechain CH_2OH, not CH_2SeH) which will be transformed into selenocysteine on tRNA with an additional consumption of three ATP. These enzymes are seryl-tRNA synthetase, phosphoseryl-tRNA kinase, selenophosphate synthetase 2 which produces selenophosphate from selenide HSe^- and ATP, and Sec synthase.

This results in the following reactional sequence:

$$\text{tRNA} + \text{Ser} + \text{ATP} \rightarrow \text{tRNA-Ser} + \text{AMP} + \text{PPi Seryl-tRNA synthetase} \quad (1)$$

$$\text{tRNA-Ser} + \text{ATP} \rightarrow \text{tRNA-Ser-Ph} + \text{ADP Phosphoseryl-tRNA kinase} \quad (2)$$

$$HSe^- + \text{ATP} \rightarrow \text{AMP} + \text{PPi} + H_2SePO_3^- \text{ Selenophosphate synthetase} \quad (3)$$

$$\text{tRNA-Ser-Ph} + H_2SePO_3^- \rightarrow 2\ \text{Pi} + \text{tRNA-Sec Selenocysteine synthase} \quad (4)$$

Hydrogen selenide H_2Se is produced in the cell by the reduction of selenite SeO_3^{2-} through an intermediate selenodiglutathione GS-Se-SG, or from selenocysteine in the trans-selenation analog of the trans-sulfuration pathway.

The catalytic mechanism of mouse selenocysteine synthase [26] is shown in Figure 2. This pyridoxal phosphate-dependent enzyme would first produce an aminoacrylyl-tRNA(Ser)Sec intermediate, which agrees with the production of similar intermediates by serine dehydratase [27]. Selenophosphate would then attack this electrophilic intermediate, and the resulting selenoester would be hydrolyzed to phosphate and selenocysteinyl-t-RNA.

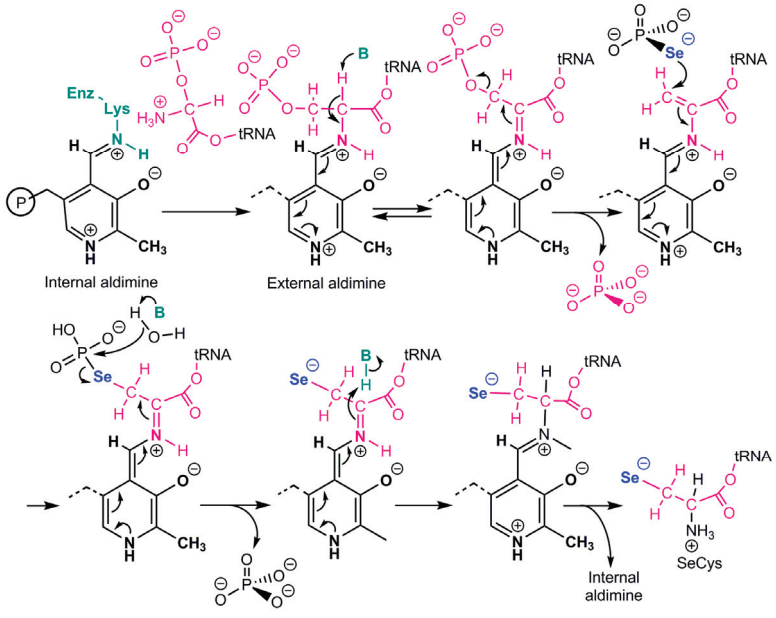

Figure 2. Catalytic mechanism of selenocysteine synthase. Adapted from Ganichkin et al. [26]. tRNA stands for tRNASer/Sec. Pyridoxal phosphate produces an aminoacrylyl-tRNA(Ser)Sec intermediate. Selenophosphate then attacks this electrophilic intermediate, and the resulting selenoester is hydrolyzed to phosphate and selenocysteinyl-t-RNA.

Hypermethylation by trimethylguanosine synthase TGS1 of the 5′-cap of mRNAs which code for selenoproteins is linked to the translation efficiency of the UGA/selenocysteine codon in vitro, and it is known that TGS1 activity is required for the biosynthesis of GPx1 in vivo [28]. Additionally, it seems that post-transcriptional modifications of tRNA-(Ser)Sec play a role in the regulation of its transferring activity as a function of selenium availability [24].

In mammals, knockout of the gene coding for tRNA(Ser)Sec is lethal. Higher plants, fungi, and many insect species do not have selenoproteins coded in their genome. Human genetic disorders resulting from mutations in genes essential for selenocysteine incorporation have been recently reviewed [29].

Because of distinct contexts of Secys/UGA reading in eucaryotes and procaryotes, the expression of mammalian selenoproteins in *E. coli* has been extremely difficult for many years, but this major difficulty was recently bypassed with a method of recombinant selenoprotein production which uses the amber codon UAG redefined as Sec codon in a specific strain of *E. coli* [30–33]. Other strategies use engineering of the *E. coli* selenium metabolism along with mutational changes in allo-tRNA and SelA in *E. coli* [34], or genetically encoded photocaged selenocysteines in yeast [35–38] or in human cell lines [39].

3. Mammalian Selenoproteins

Most selenoproteins identified in the living world were eventually discovered thanks to bioinformatic tools developed by Vadim Gladyshev and colleagues [40]. A total of 25 distinct genes coding for selenoproteins have been identified in mammals, and some of them code for several proteins [41]. Knock-out, knock-in, knock-down, and overexpression models plaid a major role in the functional characterization of several of these proteins. When selenium is limiting, the biosynthesis of some selenoproteins is maintained while that of others is not. This results in a well-defined selenoprotein hierarchy in terms of biosynthetic priority and production of selenoprotein m-RNA [42,43], which is generally assumed to reflect the relative biological importance of selenoproteins. When selenium supply is insufficient in cell culture experiments, however, activities of selenoproteins which are low in the hierarchy may be far below their physiological level and lead to misinterpretations. Selenoproteins that rank high in the hierarchy have the most stable m-RNA. Although initially based on radioactive ^{75}Se incorporation into selenoproteins, the selenoprotein hierarchy can now be analyzed by monitoring the incorporation of non-radioactive ^{76}Se and ^{77}Se isotopes using size-exclusion chromatography and mass spectrometry [44].

3.1. Selenophosphate Synthetase

Selenophosphate is essential for selenium insertion into biological macromolecules, it is not only used by selenocysteine synthase, but also by enzyme(s) that catalyze sulfur/selenium exchange on thiouridine in tRNA. Selenophosphate synthetase catalyzes the formation of selenophosphate, AMP, and orthophosphate, and it is itself a selenoprotein in some bacteria as well as in archeae and mammals [45,46]. This enigma of chicken and egg is similar to that of the current biosynthetic pathways of coenzymes in which a coenzyme is often required for its own biosynthesis. The enzyme is encoded by selenoprotein D (formerly called selD) gene in prokaryotes, whereas two isoenzymes exist in mammals and in many other animals [47,48]. The first one is a selenium-independent form (SEPHS1), which is also found in animals devoid of selenoproteins and which instead of being involved in selenophosphate synthesis [48,49] would play an important role in redox regulation. The second one is the selenoenzyme SEPHS2 which catalyzes selenophosphate synthesis. In addition to selenocysteine, bacterial SelD, and animal SEPHS2 both contain two essential residues in their active site which are lysine and cysteine.

Some important features of the catalytic mechanism of SelD have been inferred from structural studies, especially those from the enzyme from *E. coli* [46] and from *Aquifex aeolicus* [50]. It was found in vitro that a nucleophilic selenide derivative attacked the

gamma phosphorus of ATP to form selenophosphate, while ADP was hydrolyzed to form orthophosphate and AMP [45]. The first mechanistic proposal that was made is summarized in scheme IA of Figure 3.

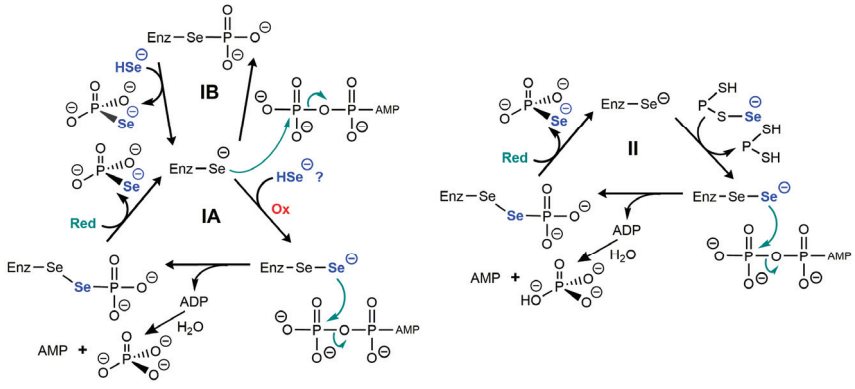

Figure 3. Putative catalytic mechanisms of selenophosphate synthetase. Adapted from studies on the enzyme from *E. coli* [46,50] and that from *Aquifex aeolicus* [45] which bear an essential SeCys residue. In (IA), a perselenide produced by oxidation attacks ATP. The oxidizing cofactor could be O_2, and the reducing cofactor could be a dithiol such as thioredoxin. (IB) suggests a simpler phosphorylation of SeCys but is not fully supported by structural data [51]. In (II), selenide would be incorporated by a protein partner in the form of a selenopersulfide directly producing a perselenide intermediate [51]. The reducing group "Red" could be a dithiol group of the protein partner.

This mechanism would require an oxidizing cofactor to produce a perselenide and a reducing cofactor, i.e., reduced thioredoxin. With a nucleophilic attack on the γ-phosphorus of ATP, the reason why this mechanism is costing two anhydride bonds of ATP instead of one is not obvious. One speculation is that this would prevent ADP to degrade the selenophosphate bond. One variant of this initial mechanism would involve phosphorylation of the active site selenocysteine (scheme IB) and it seems much simpler, although unfavored by the authors based on structural data [50].

A more important caveat is that the concentrations of HSe^- which are required in vitro (based on $K_M \simeq 7$–40 μM) would be highly cytotoxic in vivo, and it has been suggested that it might not be HSe^- itself which reacts with the enzyme, but instead a selenium-delivery protein in the form of a selenopersulfide Prot-S-Se^- [51]. The protein could be one of the cysteine desulfurases which are known to catalyze the conversion of cysteine into alanine and elemental S. They were shown in vitro to provide inorganic selenium to SelD from selenocysteine. Other ways to produce protein selenopersulfides have been described, for example with rhodanese, from selenite in the presence of GSH [52]. The protein-bound selenopersulfide would then transfer its selenium to the selenocysteine residue of selenophosphate synthase. Such possibilities are illustrated in scheme II of Figure 3.

3.2. Selenoprotein P (Selenop)

Selenoprotein P is a mammalian glycoprotein that typically contains 40 to 75% of selenium in circulating blood plasma. It is generally recognized that it serves as a selenium reservoir for the biosynthesis of other selenoproteins [53–56]. It is the only selenoprotein that contains several selenocysteine residues on a single polypeptide chain, ten residues in human as well as in rat and mouse, and the mode of co-translational insertion of these spaced selenocysteine residues is complex and only partially understood. One knows however that in this case, there are two SECIS elements in the 3'-UTR region, the first one controlling the incorporation of selenocysteine coded by the first UGA, and the next one

controlling the incorporation of selenocysteine coded by the other UGAs [24]. Once the first selenocysteine has been inserted, that of the others is much faster [56]. Selenoprotein P is mainly produced in the liver. In extra-hepatic tissues, its capture is under cothe ntrol of lipoprotein receptors. In the kidney, this is an LDL receptor named megalin, which is involved in its capture by proximal tubules [57], whereas in testicles and brain, this is a mechanism of endocytosis that is facilitated by the ApoER2 receptor [58,59]. Cerebral intake of selenium [58] is preceded by the capture of selenoprotein P by cerebral capillaries of the blood-brain barrier. Next, astrocytes that have captured this selenium in a form that remains to be determined synthesize their own selenoprotein P and secrete it in the interstitial medium where it will be used in priority by neurons which are the cells that express most ApoER2.

3.3. Selenium-Glutathione Peroxidases (Se-GPx)

Enzymes of the SeGPx family catalyze the reduction of hydroperoxides (H_2O_2 and some organic hydroperoxides ROOH) by GSH, and they constitute the largest family of selenoenzymes [60,61]. As shown in Table 1, they include five selenoenzymes in humans [GPx1–4 and GPx6], but it should be underlined that there are three sulfur homologs that have cysteine in place of selenocysteine, GPx5, GPx7 and GPx8, which have much lower or negligible GPx activities but may be involved in antioxidant protection through other enzyme activities.

GPx1, GPx2, and GPx3 are homotetramers, whereas GPx4 is a monomeric enzyme. Cytosolic GPx1 and GPx4 are ubiquitous, whereas GPx2 is mainly found in epithelial cells [62].

Tetrameric Se-GPx has a catalytic cycle that reduces from a kinetic point of view to that of Figure 4A. Everything happens as if no Michaelian complex was formed with each of the two substrates GSH and ROOH (or H_2O_2), which means that their rate of decomposition is much faster than their rate of formation. Consequently, such enzymes usually do not exhibit hyperbolic Michaelian rate curves, and they cannot be saturated by their substrates. Their steady-state initial rates are best described by the Dalziel equation [63]:

$$(E_T)/V = \phi_1/(ROOH) + \phi_2/(GSH) + \phi_{12}/[(ROOH).(GSH)] \quad (5)$$

In physiological conditions for which (GSH) is higher than 1 mM and (ROOH) less than 1 μM, the enzymatic hydroperoxide degradation rate is independent from (GSH).

3.3.1. GPx1

GPx1 is typically the dominant cytoplasmic form in most tissues. In this tetrameric enzyme which exclusively uses GSH in the reduction step of the selenenic intermediate Enz-SeOH, four arginine residues and a lysine residue of an adjacent subunit are involved in the binding of GSH at the active site of each subunit. The enzyme is most efficient to reduce H_2O_2 but is also efficient with many organic hydroperoxides [64]. I showed many years ago that mercaptosuccinate was a potent reversible inhibitor of GPx1 [65], and it is often used in cell culture to demonstrate the antioxidant or regulatory role of the enzyme. It was later shown that mercaptosuccinate forms a covalent selenenylsulfide adduct with the active selenocysteine, which eventually results in a sulfenylamide covalent adduct of the active site lysine [66], and it was shown more recently that mercaptosuccinate also inhibits recombinant GPx4 [67].

GPx1-deficient mice develop normally and show no increased sensitivity to hyperoxia [68], but they are markedly sensitive to H_2O_2-induced stress and to neurotoxic compounds such as malonate, 3-nitro-propionate or 1-methyl-4-phenyl-1,2,5,6-tetrahydropyridine [69]. Conversely, overexpression of GPx1 protects mice from acute oxidative stress [70], but these mice later develop hyperglycemia, hyperinsulinemia, increased β-cell mass, insulin resistance, and obesity [71]. This may be since activated oxygen species enhance sensitivity to insulin, as observed in $Gpx1^{-/-}$ mice [71–74]. The hyperinsulinemic effect of GPx1 overexpression is associated with the upregulation of pancreatic duodenal

homeobox-1 (PDX1) and the downregulation of uncoupling protein 2 (UCP2) in pancreatic islets. This at least tells us that persistently overexpressing a selenoenzyme to take advantage of its expected protective effects is potentially dangerous. Interestingly however, β-cell-specific overexpression of GPx1 reverses diabetes in db/db mice [75], which means that systemic and local modulations of GPx1 activity have markedly distinct effects. The explanation is still open to debate [76]. It may involve a major effect of GPx1 overexpression on the downregulation of protein tyrosine phosphatases, including the phosphatase and tensin homolog PTEN, in H_2O_2-mediated cell signaling [77,78]. But another rationale comes from a recent and remarkable study which has shown that skeletal muscle NOX4 is responsible for adaptive responses to physical exercise that prevent the development of insulin resistance in mice [79]. This study demonstrates that NOX4-derived H_2O_2 is essential to maintain adequate stimulation of Nrf2 with subsequent stimulation of mitochondrial biogenesis and transcriptional activation of antioxidant systems which include SOD2, peroxiredoxins Prdx1 and Prdx6, γ-glutamylcysteine ligase, glucose-6-phosphate dehydrogenase and NQQ1. As well, another important conclusion is that if the activity ratio GPx1/Nox4 is too high, the Nrf2-dependent stimulation of antioxidant protections is compromised, and insulin resistance develops.

Table 1. Main features of selenium-dependent glutathione peroxidases (Se-GPx) [1].

Type	Localization	Structure	Reducing Cosubstrate	Hydroperoxide Substrates	Inhibitors Inactivators	Function [2]
GPx1	Ubiquitous in cytosol and mitochondrial matrix	Homotetramer, five conserved residues at GSH binding site (four Arg, one Lys)	GSH	H_2O_2 and alkyl hydroperoxides	Mercaptosuccinate [3] $O_2^{\cdot -}$, HOCl Heavy metals	Antioxidant Redox regulator?
GPx2	Cytosol of epithelial cells	Homotetramer, extracellular glycoprotein	GSH	H_2O_2 and alkyl hydroperoxides	undocumented	Antioxidant Redox regulator?
GPx3	Mostly extracell. Blood plasma, Secreted/kidney mammary gland	Homotetramer, Glycoprotein	Thioredoxin; GSH (nonphysiological)	H_2O_2 and alkyl hydroperoxides	undocumented	Antioxidant Redox regulator?
GPx4	Membrane-bound Cytoplasm Mitochondria Nucleus (minor)	Monomer	Thioredoxin Protein thiols GSH (nonphysiological),	Phospholipid-OOH, Cholesterol-OOH, LDL-OOH	RSL3 ML162	Antiox/Redox regul? Anti-ferroptosis Spermatozoid specific-protein crosslinker
GpX6	Olfactory epithelium	Homotetramer, Strong sequence homology with GPx3	Thioredoxin; GSH?	undocumented	undocumented	Antioxidant Redox regulator?

[1] Essential selenocysteine at the active site. [2] The regulatory potential of SeGPx includes down-regulation of NFkB and lipoxygenase activities, and many other controversial targets. [3] Recombinant GPx4 would also be inhibited by mercaptosuccinate [67].

Finally, a decrease in endothelial GPx1 activity may be associated with homocysteinemia which induces arterial alterations and related cardiovascular and cerebral damage. In animal models of homocysteinemia, such as the heterozygous cystathionine-β-synthase-deficient ($CBS^{+/-}$) mouse, a two-fold increase in homocysteine is observed and is associated with impairment of endothelial-dependent relaxation of mesenteric arteries [80] and increased levels of oxidative stress markers such as aortic 3-nitrotyrosine and plasmatic F2-isoprostanes. Similar endothelial dysfunctions were observed in homozygous GPx1-deficient mice [81]. Overexpression of GPx1 in hyper-homocysteinemic mice restored normal endothelial-dependent relaxation and it was shown that the vascular effects of homocysteine were at least partly mediated by impairment of NO production [82,83]. Treatment of cultured endothelial cells with homocysteine did induce a decrease in GPx1

activity [84]. Homocysteine decreases GPx1 expression by a mechanism that does not affect transcription but involves the down-regulation of translation [84].

3.3.2. GPx2

GPx2 is cytosolic and mainly expressed in epithelial cells, especially in the gastrointestinal system and it uses GSH with high specificity [62,85,86]. Only two of the five residues involved in GSH binding by GPx1 are changed: lysine is replaced by glutamine and arginine is replaced by threonine [60]. GPx2 ranks higher than GPx4 and much higher than GPx1 and GPx3 in the selenium hierarchy of the SeGPx family [60]. A recombinant form of GPx2 has been characterized and found to follow typical ping-pong kinetics with H_2O_2-reducing activity being approximately 9-fold lower than those of GPx1 and GPx2 activities [87], but the expression strategy imposed to mutate four cysteine residues into serine.

Although GPx2 is mainly expressed in the gastrointestinal system, especially by epithelial cells of the esophagus, it is also expressed in other epithelia and in the human liver. It has been proposed that GPx2 prevented the absorption of food hydroperoxides [85], but the highest GPx2 protein concentrations are found in epithelial crypt bases [88] which are not the preferential location for absorption.

GPx2 knock-out mice develop normally [89], but the number of apoptotic cells is increased at crypt bases, even though GPx1 is markedly upregulated in this area [90]. This is an interesting example of partial compensation of GPx2 loss by GPX1 overexpression. Intestinal stem cells are in crypt bases where their growth and differentiation are regulated by the Wnt pathway [91]. Interestingly, GPx2 expression has been shown to be regulated by the Wnt pathway [92,93], which suggests that GPx2 may play a major role in the continuous self-regeneration of the intestinal epithelium.

The redox-sensitive matrix metalloproteinase-7 (MMP-7) which is required to produce microbicidal defensin peptides is modulated by intestine-specific GPx2 [94,95].

GPx2 knock-out mice show an increased allergic airway inflammatory response when challenged with ovalbumin [96], which reflects the fact that GPx2 is also expressed in epithelial cells which do not only belong to the gastrointestinal tract. GPx2 expression is increased in lungs exposed to hyperbaric oxygen [97] or to cigarette smoke [98] and upon treatment of mice with the lung protector and Nrf2 inducer sulforaphane [99].

In mouse embryos, preferential expression of GPx2 was found in rapidly growing tissues, which would again support the idea that GPx2 might play a role in cell proliferation [100]. This physiological function might become deleterious with cancer cells, and GPx2 has indeed been shown to be upregulated in several epithelial cancers [88,101–106], which may be all linked to Wnt activation. The link between GPx2-mediated Wnt activation and metastasis and cancer development is supported by recent studies [107,108]. It has also been shown that hydrogen peroxide neutralization by GPx2 is essential for maintaining metastatic capacity in colorectal cancer [109].

GPx2 is also upregulated by the transcription factor ΔNp63 which is abundant in undifferentiated cells [110], and more generally by Nrf2 [111] which stimulates cell protections against electrophilic and oxidative stresses [112]. Just as Wnt activation, Nrf2 activation may have undesirable effects on cancer cell survival [112–117], and this dual role of Nrf2 is indeed a reminder of what has been known for years with GSH [118], whose biosynthesis and reductive recycling are stimulated by Nrf2 activation. Finally, GPx2 overexpression is correlated with poor prognosis in patients with hepatocellular carcinoma [119].

The undesirable effect of GPx2 in cancer development may not be trivial, however. For example, GPx activity is known to down-regulate the activities of lipoxygenases [120–122], and 12-lipoxygenase promotes epithelial-mesenchymal transition via the Wnt/β-catenin signaling pathway in gastric cancer cells [123].

In addition to its supporting role in cell proliferation, GPx2 has obvious anti-inflammatory properties. Knock-down of GPx2 in adenocarcinoma HT29 cells indeed markedly stimulates

the production of COX2 and PGE2 [124]. Conversely, GPx2 is upregulated in models of inflammatory bowel disease and in human colitis [125].

A double knock-out of GPx1 and GPx2 was found to result in chronic colitis [126] and inflammation-driven intestinal cancer [127], mainly caused by Nox1 activation and its associated $O_2^{\cdot -}$ production [128]. Interestingly, $Gpx1^{[-/-]}/Gpx2^{[+/-]}$ mice were unaffected, which means that the GPx2 allele alone was able to prevent intestinal inflammation. Such results demonstrate that weak Gpx2 activity is sufficient to protect against ileocolitis [129].

Another inflammation-linked disease in which GPx2 is involved is viral hepatitis. Oxidative stress is always observed in HCV-infected hepatocytes [130–132] and this appears to be largely due to a marked decrease in cellular GPx2 [133]. Such oxidizing conditions are known to stimulate viral protein translation by hepatocytes as well as liver inflammation [134,135]. It has been shown that TP80—which is a retinoid derivative—exhibits an anti-HCV activity which is associated with its restoration of GPx2 activity [136].

3.3.3. GPx3

GPx3 is an extracellular glycoprotein mainly found in blood plasma but also in a few other extra-cellular fluids. It is secreted by the kidney in which the greatest levels of GPx-3 mRNA expression are found, within epithelial cells of the proximal tubule [137,138]. In vitro, GPx3 works well with GSH, but in plasma, GSH concentration is far too low to be used as a reducing coenzyme. GPx3 can use other thiols, for example, one of the reducing proteins thioredoxin, glutaredoxin, or thioredoxin reductase [139] which might be its reducing partners in extracellular compartments. The physiological role of GPx3 is uncertain, however, and this is the selenoprotein that disappears first (bottom of selenium hierarchy) in the situation of selenium deficiency. Some data suggest that an important function of GPx3 might be to preserve nitric oxide bioavailability and to promote an antithrombotic environment [140–142]. Other data suggest that GPx3 may behave as a tumor suppressor. In a model of murine inflammatory carcinogenesis, the number of intestinal tumors was indeed doubled in GPx3 knock-out mice [143]. Recent data show however that in a sub-population of murine alveolar epithelial cells from lung tumor, GPx3 has the opposite effect since it promotes metastasis by stabilizing HIF1-α which stimulates the production of Il-10 and thereafter cell migration [144].

3.3.4. GPx4

GPx4, also named PHGPx (Phospholipid Hydroperoxide Glutathione Peroxidase) was initially discovered in pig liver as a peroxidase working on phosphatidylcholine hydroperoxides in liposomes [145]. The sequence of discoveries that followed for four decades was recently summarized by major contributors [146]. This is a monomeric enzyme [147] which together with GPx2 ranks high in the selenium hierarchy of selenoproteins [60] and which occurs in cytosolic, mitochondrial, and nuclear forms. The cytosolic form of the enzyme prevails in somatic tissues, whereas the mitochondrial and nuclear forms are mainly found in testicular tissue [148,149]. The mitochondrial form mGPx4 is identical to the cytosolic form once the mitochondrial targeting sequence has been cleaved. A unique feature of GPx4 is to reduce efficiently lipid hydroperoxides of membranes and lipoproteins, such as hydroperoxides of phospholipids, cholesterol, and cholesterylesters [150,151]. Conversely, H_2O_2 and t-butyl hydroperoxide which are good substrates of GPx1 are not efficiently reduced by GPx4. In erythrocytes, hemolysis is inversely related to GPx4 activity during blood bank storage [152].

GPx4 has a unique property which is to accept protein thiols as reducing equivalents when the GSH pool becomes limiting. This situation is observed in spermatozoids during maturation [153,154] and here, oxidation of protein thiols by mitochondrial GPx4 induces the formation of protein polymers through inter-chain disulfides between reduced cysteine residues of GPx4 and cysteine residues of protein partners which have become oxidized to sulfenic acids PSOH. This leads to the fixation of the mitochondrial sheath found in the mid-piece of spermatozoids. Deletion of mGPx4 allows both normal embryogenesis

and postnatal development but causes male infertility which is associated with structural abnormalities in spermatozoa [155].

Homozygous Gpx4 knock-in mice obtained by mutation of Sec into Ala are not viable, but studies on heterozygous animals $Gpx4^{+/-}$ have confirmed that GPx4 deficiency is associated with spermatozoid structural abnormalities and reduced motility, and that the resulting infertility of males is markedly counteracted by concomitant knock-out of the Alox15 gene which codes for 15-lipoxygenase [156]. But systemic inactivation of the Alox15 gene does not prevent embryonic lethality in homozygous Sec46/Ala knock-in mice expressing catalytically silent Gpx4 [157].

Homozygous GPx4-deficient mice die in utero at midgestation [158,159], and the replacement of native GPx4Se/Se by a cysteine mutant GPx4S/S which conserves a weak but significant GPx4 activity does not prevent the development of embryos, but the animals die from epileptic seizures [160]. GPx4Se/Se is apparently required later for the survival of GABAergic interneurons whose disappearance is lethal.

GPx4 may play a down-regulating role in inflammation. In human dermal fibroblasts which have been transfected to overexpress GPx4, concentrations of phospholipid hydroperoxides are markedly decreased, and when such cells are treated with exogenous phosphatidylcholine hydroperoxides or exposed to UVA irradiation, the activation of the pro-inflammatory transcription factor NFκB and the release of interleukin 6 are also markedly reduced [161].

An active GPx4 is a requirement of a functional CGAS-STING pathway, a vital immune signaling pathway that is activated in response to infection by DNA viruses and which is also involved in tumor surveillance [162,163]. Here the phospholipid hydroperoxidase activity of GPx4 is required to observe the palmitoylation-induced STING activation and its subsequent migration from the endoplasmic reticulum to Golgi.

Finally, one major property of GPx4 is its ability to prevent ferroptosis [160,164]. Ferroptosis is a form of so-called "regulated cell death" which always involves a marked fall in GPx4 activity, and which differs from apoptosis or necrosis in terms of morphological and biochemical features. It mainly relies on the iron-dependent accumulation of lipid peroxides [165–167], which would be initiated by two major events, a decrease in GPx4 activity which may or may not be associated with intracellular GSH depletion as well as activation of 12,15-lipoxygenase [168]. Subsequently, non-enzymatic lipid autoxidation would be the final lethal trigger of ferroptosis. Much research work suggests that ferroptosis is involved in many physiopathological situations where GPx4 could be the focus of future drug design [169].

Although GPx4 is a monomer, GPx4 allosteric activators have been designed [170]. By increasing GPx4 activity, such allosteric activators suppress ferroptosis induced by erastin and cholesterol hydroperoxides, and they also down-regulate NFkB activation. Additionally, two potent inhibitors of ferroptosis, liproxstatin-1 and ferrostatin-1, have been independently identified in small molecule libraries [171,172]. Liproxstatin-1 is a spiroquinoxalinamine derivative that protects Gpx4 knockout mice from acute renal failure [171]. It was also shown to reduce myocardial infarct size and to restore cardiac GPx4 activity in isolated mouse hearts undergoing post-ischemic reperfusion [173]. The anti-ferroptotic activity of ferrostatin-1 was recently shown to be due to the scavenging of initiating alkoxyl radicals produced by Fe[II] complexes from lipid hydroperoxides [174]. In this process, ferrostatin-1 is not consumed and synergizes with GPx4 to inhibit iron- and hydroperoxide-dependent lipid peroxidation.

A critical discussion of ferroptosis is outside the scope of this review, but one should underline that the concept raises some fundamental questions which are still unsolved [175, 176]. Moreover, GPx4 may not be the only selenoprotein whose fall in activity triggers ferroptosis. Given their chloroacetamide warheads, the absolute GPx4 specificity of selenium-targeted inactivators RSL3 or ML162 is unlikely [177–179]. Recent experiments show that they do not inhibit purified recombinant GPx4, but instead inhibit thioredoxin reductase 1 [67]. It had been previously shown that the inactivation of GPx4 by RSL3 required the

adaptor protein 14-3-3ε in its reduced form [180], which depends on active TrxR1. This suggests that inhibition of TrxR1 might indirectly inhibit GPx4 by preventing the recycling of the reduced form of the adaptor protein [67]. In agreement with the link between ferroptosis and TrxR, another recent publication shows that the natural tetracyclic compound alterperylenol which is an inactivator of TrxR is also an inducer of ferroptosis [181]. Moreover, the idea that inhibition of the glutamate/cystine antiport xCT induces ferroptosis by decreasing GPx4 activity only through GSH depletion is probably an oversimplification. Data show that xCT is required for the extracellular reduction of selenite into selenide, the major form of inorganic selenium that can be internalized by cultured cells [182].

At any rate, GPx4 does prevent ferroptosis, and this may inspire cytoprotective pharmacological strategies, but this may also have deleterious effects on tumor growth and anti-cancer therapy. This is most obvious in epithelial-derived carcinomas in which tumor cells have been fixed in a therapy-resistant mesenchymal state which clearly relies on GPx4 expression [183,184]. In such extensive studies, statins—which inhibit GPx4 biosynthesis—were shown to decrease tumor cell resistance to cytotoxic antitumor drugs by synergizing with GPx4 inhibitors such as RSL3 [185]. These in vitro observations were also fully supported by in vivo experiments on tumor xenografts built from GPx4-wild type and GPx4 knock-out clones of such cells. The EMT regulator ZEB1 was strongly correlated with mesenchymal state sensitivity to GPx4 inhibition, and ZEB1 deletion abolished sensitivity to GPx4 inhibition. ZEB1 regulates the uptake and mobilization of lipids and affects the EMT-associated remodeling of sphingolipids in the plasma membrane [186], a process that plays a central role in intercellular connections.

Clear-cell carcinomas (CCC) are therapy-resistant malignant cells observed in a variety of cancers, most frequently in kidney and ovarian cancers. It was found that inhibitors of GPx4 were potent and selective killers of such cells [187], and this was related to their HIF2α-dependent enrichment in polyunsaturated lipids which made them highly vulnerable to ferroptosis.

3.3.5. Other Members of the GPx Family

GPx6 is the last member of the SeGPx family in humans, but it is not a selenoprotein in rats and mice where selenocysteine has been replaced by cysteine [60]. Human GPx6 exhibits a strong sequence homology with plasmatic GPx3, and it is expressed in the olfactory epithelium.

Finally, many homologous sequences of Se-GPx in which selenocysteine is replaced by cysteine have been identified in in non-vertebrate animals, higher plants, and fungi. Such sulfur homologs of Se-GPx are not all involved in hydroperoxide reduction, and most of them do not use GSH as a reducing co-enzyme but use instead the active-site cysteine dithiol group of thioredoxin, other redoxins, or protein disulfide isomerase [60,188–190], as further discussed in Section 6.

In mammals, GPx7 belongs to the CysGPx family, but it has a strong sequence homology with GPx4, and it also adopts a monomeric structure. It is localized in the lumen of the endoplasmic reticulum of epithelial cells where it acts as a catalyst of protein refolding, in association with protein disulfide isomerase [190]. In this mechanism, the active site cysteine thiol of GPx7 would be oxidized by hydroperoxide into a sulfenic acid intermediate PSOH which in turn would oxidize protein disulfide isomerase. But GSH and protein disulfide isomerase would compete as reducing cofactors of GPx7 in the endoplasmic reticulum [191].

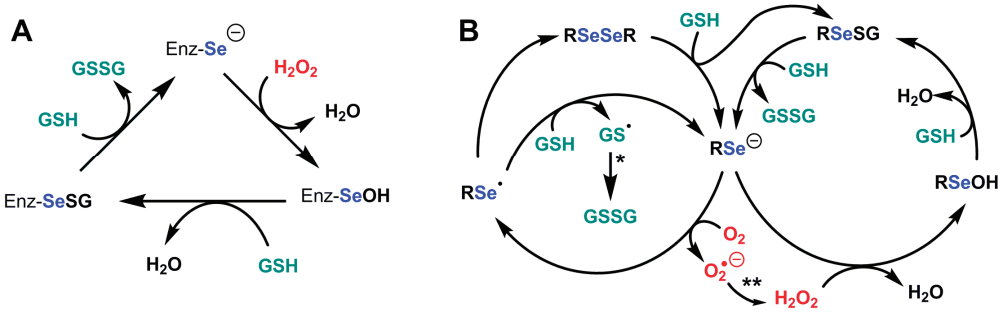

Figure 4. Catalytic cycles of glutathione peroxidases and of the model compound selenocystamine. (**A**) Catalytic cycle of glutathione peroxidases Se-GPx; (**B**) Catalytic cycles of glutathione peroxidase and glutathione oxidase activities of selenocystamine; adapted from Chaudière et al. [192]. (*) GSSG production most likely involves nucleophilic addition of GS^- to give a disulfide radical anion $GSSG^{\cdot -}$ which would decompose into GSSG by reducing O_2 into superoxide $O_2^{\cdot -}$. (**) The production of H_2O_2 from $O_2^{\cdot -}$ most likely results from dismutation.

3.3.6. Mechanistic Complexity of Glutathione Peroxidases

The generic mechanism of Se-GPx (see Figure 4A) does not exclude some surprises. For example, is the reactivity of the resting selenium with oxygen always negligible? with an apparent pKa of SeCys which is presumably lower than 5.5, it is usually postulated that the basic and highly reducing selenolate form is dominant in the resting enzyme. Selenolates can catalytically reduce dioxygen O_2 into superoxyde $O_2^{\cdot -}$ in the presence of GSH, which we first showed with selenocystamine [192] and which turned out to be a common feature of alkyl- and aryl-selenolates. Following the discovery of the GPx activity of ebselen [193,194], many biomimetic selenium catalysts have been studied, but only two of them—ebselen and BXT-51072—have been tested in clinical development, because of their anti-inflammatory properties and their very low toxicity [195–197]. In both cases, we observed that the peroxidase/oxidase ratio was high. Our study of half a dozen model compounds led to the conclusion that the rate of oxygen reduction in the presence of GSH was a major factor of cytotoxicity [197,198]. One cannot exclude the possibility that some GPx would maintain the selenocysteine residue in its protonated selenol form to avoid oxygen one-electron reduction in the resting enzyme. Additionally, the production of a selenenic enzyme intermediate EnzSe-OH in the hydroperoxide-reduction step (Figures 4A and 5A) seems unavoidable, but the reactivity of selenenic acids is so high that nobody ever observed the presumed selenenic intermediate in SeGPx active sites by mass spectrometry or spectrophotometric techniques. Sulfenic acid traps such as cyanide or dimedone have no effect on the enzyme but may be inappropriate for selenenic trapping [199,200]. At least one successful identification of a selenenic acid intermediate was obtained with dimedone for selenoprotein S, but this required that fast selenenic acid trapping as an internal selenenylsulfide be prevented by cysteine-to-serine mutation [186]. Direct observation of a transient selenenic acid has however been made in an ingenious molecular model [201].

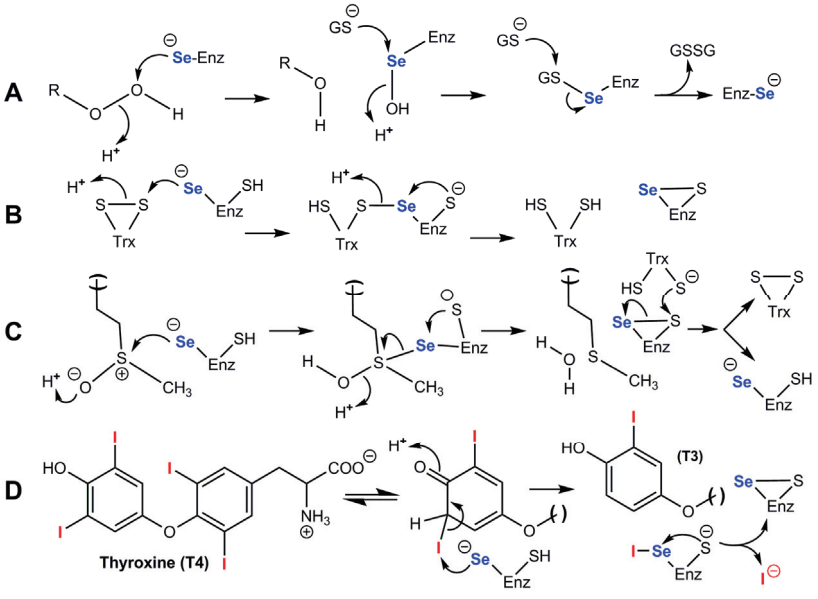

Figure 5. Catalytic mechanisms of the four main families of selenoenzymes in mammals. (**A**) Glutathione peroxidases SeGPx. (**B**) Thioredoxin reductases TrxR; the selenenylsulfide group present in the C-terminal region of a subunit is reduced to a selenol/thiol group by a dithiol group in the N-terminal region of the other subunit; the resulting disulfide is then recycled by flavin/NADPH. (**C**) R-methionine sulfoxide reductase MsrB1; a selenenic acid intermediate cannot be excluded in the second step. (**D**) Deiodinases DIO1 and DIO2; the reduced enzyme is recycled by thioredoxin or by glutaredoxin/GSH.

3.4. Thioredoxin Reductases (TrxR)

TrxR are NADPH-dependent enzymes that catalyze the reduction of the internal disulfide of thioredoxins (Trx) into a biologically active dithiol [202–204]. Trx are themselves 12-kDa reductases that catalyze the conversion of disulfide to dithiol in other protein targets and which have a conserved -Cys-Gly-Pro-Cys- active site motif [205–207]. They are ubiquitous in the living world, from archaea to mammals. Trx was first purified and characterized as the hydrogen donor for ribonucleotide reductase [RNR] in *Escherichia coli* [208,209]. This observation was later extended to mammals, confirming the importance of this reducing protein in DNA synthesis. In mammalian cells, there are two isoforms of Trx, Trx1 which is mainly cytosolic but can be translocated into the nucleus and sometimes secreted out of the cell, and mitochondrial Trx2.

Mammalian TrxR has a selenocysteine essential residue at the active site, which is not the case in prokaryotes. They include three selenoenzymes in humans, the cytosolic TrxR1, the mitochondrial TrxR2, and a specific isoenzyme TrxR3 also known as TGR in testicles. Each of the three enzymes includes isoforms due to extensive splicing.

Many questions are still puzzling concerning the relative importance of the three TrxR families. For example, knock-out models have shown that TrxR1 is essential for brain development, which is surprisingly not the case for TrxR2 [47].

As a rule, they play a major role in redox regulation of metabolism and cell functions, because Trx is used as a reducing cofactor of enzymes such as ribonucleotide reductase, peroxiredoxins, methionine sulfoxide reductases, and GPx3, and it interacts with many other target enzymes in which cysteine residues have been oxidized [210]. Such cysteine residues are normally reduced in their resting form but may be oxidized into sulfenic acid PSOH or disulfide during redox signaling or because of oxidative stress.

Although TrxRs are considered the major reducing system for thioredoxin, thioredoxin may also be reduced by the glutaredoxin/GSH couple which would act as a backup system [211,212]. This could only result in partial compensation, however, because the inactivation of each of these two systems leads to many distinct effects and to a large extent opposite metabolic effects [213]. A good illustration of this is that Trx is maintained in its reduced form in mouse embryonic fibroblasts lacking TrxR1, but that this is not the case if the cells are incubated with high glucose concentrations [214].

TrxR is usually antiparallel homodimers [215,216]. They have much structural homology with other NADPH- and flavin-dependent disulfide reductases such as glutathione reductase. The main difference is due to the presence of a C-terminal extension containing a Gly-Cys-Sec-Gly motif [215]. The catalytic mechanism of mammalian TrxR [202,216–219] involves the transfer of electrons from the active site flavin $FADH_2$ to an internal disulfide of the N-terminal domain of the same subunit. The resulting dithiol motif -Cys-Val-Asn-Val-Gly-Cys—is not interacting with the target protein used as a substrate, it rather transfers its electrons to the selenenylsulfide group present in the C-terminal region of the other subunit. This finally produces a selenol/thiol entity which is then responsible for the reduction of most substrates of the enzyme(s), which include Trx but also artificial disulfide such as 5,5′dithiobis[2-nitrobenzoate] known as DTNB. NADPH is of course used to recycle $FADH_2$. In this mechanism, a cysteine selenolate performs the final reduction of the disulfide substrate as illustrated in Figure 5B. Mutation of selenocysteine into cysteine results in an enzyme whose kcat is 100-fold lower than that of the wild-type selenoenzyme [220].

A distinctive mechanistic property of TrxR, compared with other selenoenzymes, is their ability to catalyze one-electron reductions. It was shown that TrxR2 was able to reduce ferric cytochrome c, ascorbyl radical, and dehydroascorbate by means of one-electron transfers [221]. Cysteine mutants did not conserve these properties, which means that in addition to reduced flavin which is known to be a one-electron-reducing coenzyme, selenium is essential for subsequent one-electron transfers. One exception is known however with juglone [5-hydroxy-1,4-naphthoquinone], a walnut toxin that is reduced by TrxR1 in a one-electron transfer which does not require selenocysteine and is coupled to the reduction of oxygen to superoxide [222].

TrxR is not fully dedicated to Trx reduction [223]. For example, TrxR1 also catalyzes the reduction of protein disulfide isomerase PDI, glutaredoxin Grx2, and small natural molecules such as selenite and lipoic acid [224]. Similar with selenoprotein P, we are dealing here with a selenoenzyme which may play a role in its own production since it is involved in the formation of hydrogen selenide from selenite. The easy accessibility of the highly reactive selenocysteine of TrxRs should explain their wide substrate specificity [223].

By ensuring the reduction of thioredoxins, TrxR is unavoidably major actors of a cascade of redox regulations in mammalian cells, with many protein targets of thioredoxins having essential functions. These redox-sensitive proteins form redox-dependent signaling pathways that are crucial for fundamental cellular processes, including metabolism, proliferation, differentiation, migration, and apoptosis [205].

As already mentioned, thioredoxin may be the main reducing cofactor of GPx3, but the biological link between TrxR1 and Gpx3 is not well documented. Thioredoxin is also the reducing cofactor of peroxiredoxins [205] and methionine sulfoxide reductases [225–227].

Peroxiredoxins have a cysteine-containing active site that catalyzes the intracellular reduction of H_2O_2 for signaling purposes [228] and act as extremely efficient H_2O_2 sensors. The active sites of Prx have an affinity for H_2O_2 which seems to have no equivalent in the world of peroxidases or a fortiori in that of catalases, and this markedly accelerates the oxidation of their essential cysteine. Second-order rate constants for the reduction of H_2O_2 by peroxiredoxins are close to 10^7 $M^{-1}.s^{-1}$, which is more than three orders of magnitude higher than those of small molecular-weight mercaptans. The role of Prx in H_2O_2-dependent signal transduction relies on the oxidation of target proteins. We do not know however if this is a generic function of Prx or only a specialized function of some of them.

It is not excluded that Prx also works as H_2O_2-dedicated antioxidants since they are abundant in mammalian cells. They are also able to reduce some hydroperoxides other than H_2O_2, although the physiological significance of these weaker activities is unknown. The distinctive feature of peroxiredoxins compared with other hydroperoxide reductases is that their active site does not require selenocysteine but only a dithiol that reduces their substrate with concomitant formation of an intersubunit disulfide [205]. Because TrxR reduces Trx which reduces Prx, they are unavoidably involved in the redox regulation of Prx, but other levels of Prx regulation involve kinase-mediated tyrosine phosphorylation [229] and H_2O_2-mediated hyperoxidation. Hyperoxidation of Prx occurs slowly when continuous exposure to H_2O_2 oxidizes the N-terminal catalytic cysteine into a sulfinic acid [230]. Trx is not able to reduce this sulfinylated form back to thiol, but this is achieved by sulfiredoxin Srx [231]. Hyperoxidation of Prxs leads to loss of peroxidase activity and stimulates chaperone activity [232]. Sulfinylated Prx activates transcription factors involved in sulfiredoxin biosynthesis [229].

Methionine sulfoxide reductases [225,227,233,234] are also using thioredoxin as a reducing cofactor, and they include the selenoenzyme MsrB1 discussed in the next section.

TrxR1 suppresses adipocyte differentiation and insulin responsiveness [235], which suggests that TrxR1 has synergistic effects on the antioxidant function of GPx1. The fact that TrxR1 protects tyrosine phosphatase 1B from inactivation by H_2O_2 also supports this hypothesis [236].

"Redox regulation" is probably the best functional descriptor of enzymes of the TrxR family, just as "antioxidant hydroperoxide degradation" is the best descriptor of enzymes of the SeGPx family. But this does not mean that SeGPx do not have a role in redox regulation, and here with TrxR, an important question is that of their role in antioxidant protection. The answer is that thioredoxin and thioredoxin reductases do have antioxidant functions [202], but those which are consequences of their regulatory functions may be as important as those which come from their intrinsic antioxidant properties as reducing cofactors of protective enzymes. Nrf2 is one of the regulatory targets which supports this concept. The idea that TrxR1 is probably a major gatekeeper of Nrf2 activation has been developed in a comprehensive review of TrxR1-Nrf2 interactions [204]. Inhibition of TrxR1 markedly activates Nrf2 which is the major transcriptional regulator of cellular responses to oxidative and electrophilic stress. As well, reciprocally, Nrf2 activation by electrophilic or oxidative stress induces the expression of both Trx and TrxR1.

TrxR1 is, however, itself a sensitive target of electrophilic species, and some of them, such as cis-diaminedichloroplatinum, transform the enzyme into SecTRAPs (selenium-compromised thioredoxin reductase-derived apoptotic proteins) which behave as harmful NADPH oxidases [237,238]. This is because they have lost their selenocysteine-dependent reducing properties but have kept their other redox components which are now able to catalyze redox cycling of quinonic substrates.

The complex redox network in which the TrxR/Trx system is involved is summarized in Figure 6. Trx1 can be translocated to the nucleus where it regulates the activity of several transcription factors which include Nrf2 [204,239], NFkB [240], p53 [241], AP-1 [242], and HIF-1 [243], as well as that of the glucocorticoid receptor [244]. The reduced form of Trx1 inhibits the phosphatase activities of the tumor suppressor PTEN, thereby stimulating cell proliferation and tumor growth [245]. PTEN (Phosphatase and Tensin Homolog 1) is a multi-domain protein that exerts its tumor-suppressive functions in a lipid phosphatase-dependent, protein phosphatase-dependent, or scaffold-dependent manner [246].

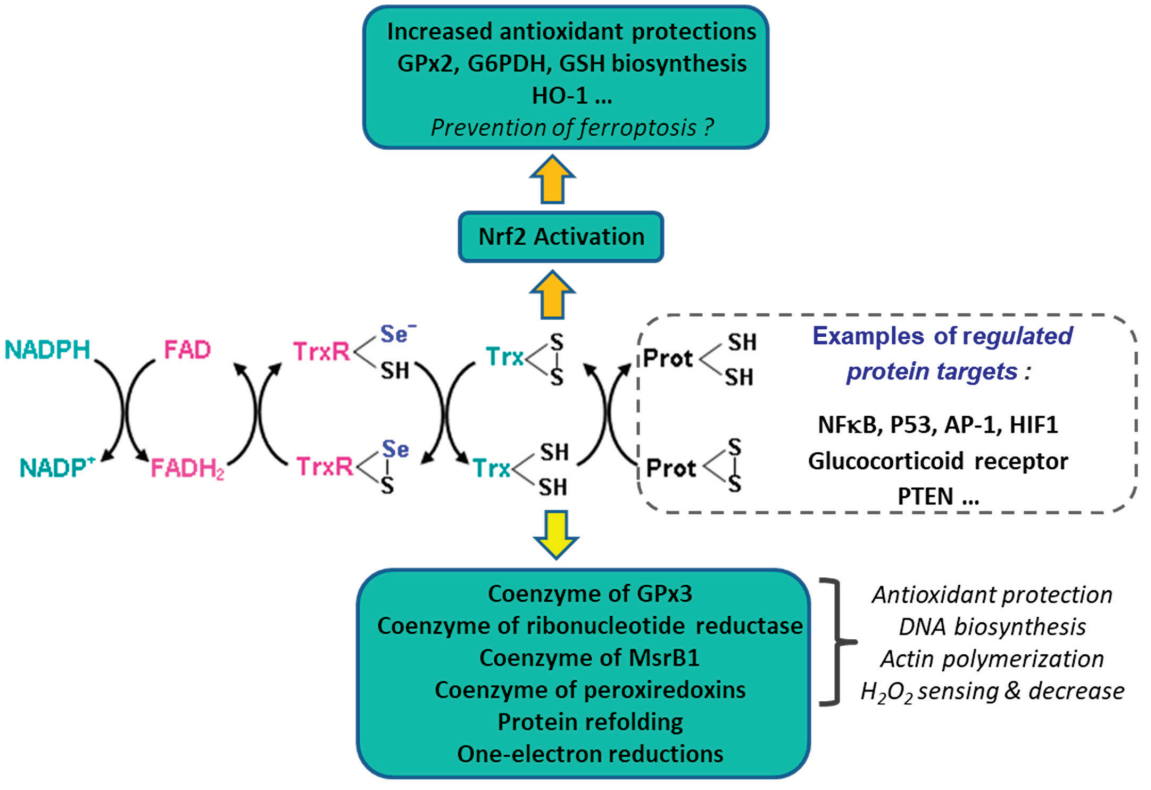

Figure 6. The TrxR/Trx system and its redox network of protein regulations. The reduced and oxidized forms of thioredoxin are involved in antioxidant protection, cell division, control of cytoskeleton structure, apoptosis, inflammation, and redox control of many regulatory proteins.

A final comment is required on the role of TrxR in cancer. In many tumors, TrxR1 is overexpressed, and they are believed to stimulate proliferation and inhibit apoptosis in cancer cells. This is why they have been considered an interesting target in cancer therapy [247]. An efficient and tolerable therapeutic window of TrxR inhibition may however be difficult to establish. It has been reported that 90% knocking down of TrxR1 has a negligible effect on cell growth in a human carcinoma cell line expressing high levels of TrxR1 [248], and it was also reported that 90% pharmacological inhibition of Trx1 had no effect on oxidized Trx1 in HeLa cells [249]. Such observations suggest that residual amounts of TrxR1 may be sufficient to maintain its essential functions in tumor cells. Nevertheless, intensive activities of anti-tumor drug design are currently going on in this area [250,251].

Trx1 is also regulating the apoptosis signal kinase 1 (ASK1). In its reduced form, Trx1 inhibits ASK1 and prevents apoptosis, whereas in the situation of oxidative stress, its oxidized form dissociates from ASK1 which results in apoptosis [252]. ASK1-Trx1 dissociation is not only achieved by oxidation but can also be induced by the Trx1-interacting protein TXNIP which competes with ASK1 by binding to the reduced form of Trx1 [253].

3.5. Selenium-Dependent Deiodinases

Selenium-dependent deiodinases catalyze the reductive deiodination of thyroxine [T4] or triiodothyronine [T3]. In mammals and in humans, they include three selenoenzymes [254–258], which are homodimeric structural homologs of thioredoxins [257–259]. They rank high in the selenium dependence hierarchy, such as GPx2 and GPx4.

The thyroid gland secretes a pro-hormone, tetra-iodothyronine, or thyroxine T4 which in target cells of peripheral tissues is converted into triiodothyronine T3, the active hormone. As shown in Figure 7, type 1 and type 2 deiodinases [DIO1 and DIO2] both produce T3 from T4, whereas type 3 deiodinase (DIO3) converts T4 into the inactive metabolite rT3 [reverse T3], and T3 into inactive 3,3′-T2. Selenium-dependent deiodinases, therefore, control the activity of T3, which interacts with nuclear receptors TRα and TRβ, and which is a major effector of lipid and sugar metabolism, as well as of respiration and mitochondrial biogenesis [260]. For example, the induction of DIO2 in brown adipose tissue exposed to cold stimulates energetic expenditure. This DIO2 increase is under the control of cAMP which binds regulatory subunits of PKA [259] and releases activated catalytic subunits. Conversely, DIO3 in the ischemic/hypoxic heart or brain decreases the energetic expenditure to cope with decreased oxygen delivery, and this other process is under the control of HIF-1α which interacts with the DIO3 promoter [259].

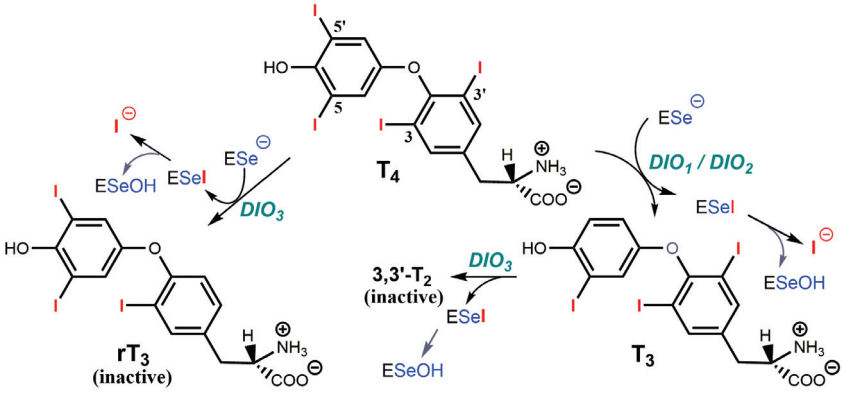

Figure 7. Reactions catalyzed by the three selenium-dependent deiodinases. DiO1 and DiO2 produce the active hormone T3 from T4, whereas DiO3 produces two inactive metabolites, rT3 [reverse T3] from T4, and 3,3′-T2 from T3.

DIO1 is a thyroxine 5′-deiodinase that is associated with the plasma membrane in cells of the liver, kidney, thyroid, and pituitary gland, whereas DIO2 is a thyroxine 5′-deiodinase that is associated with the endoplasmic reticulum and cells of the pituitary gland, thyroid, skeletal muscles, brown adipose tissue, heart, and CNS.

DIO2 expression is tightly regulated by transcriptional mechanisms [258] and deactivated by ubiquitination [261].

The three iodothyronine deiodinases catalyze similar reactions with distinct regiospecificity. Their structural and mechanistic analysis as integral membrane proteins has been difficult [255]. The crystal structure of the truncated catalytic domain of mouse Dio3 has been solved [256], and it shows that the enzyme has a close structural similarity to atypical 2-Cys peroxiredoxins. The structure is compatible with Sec170 extracting the 5-iodine as a selenenyl-iodide, which should then hydrolyze to a selenenic acid intermediate, as supported by model studies with a synthetic alkylselenenyl-iodide [262]. It also shows that the thyronine ring is protonated via a network of conserved amino acids. The oxidized enzyme can be directly reduced by exogenous dithiols in vitro, and it is reduced by physiological concentrations of either thioredoxin or glutaredoxin. There are still unanswered questions about possibly distinct catalytic and regulatory mechanisms of the three deiodinases [263]. In the catalytic mechanism of T4 to T3 conversion, which is illustrated in Figure 5D, an enzyme-catalyzed keto-enol tautomerization would fit with a direct attack of iodine by selenium with regiospecific proton exchange at the active site of DIO1 or DIO2. In the conversion of T4 to rT3 by DIO3, such a tautomerization mechanism seems unlikely because it would involve a much more unstable oxonium intermediate, but one cannot exclude its

stabilization through electrostatic interactions. In all cases, the internal selenenylsulfide which is produced is not reduced by glutathione GSH. It may be first reduced by a second proximal cysteine residue to form a mixed disulfide, but the reductant which can recycle the active site in vitro must be a dithiol such as a dithiothreitol or dithioerythritol which does not have the constraints of charges and steric hindrance of GSH. The physiological reduction is unknown but may be performed by thiol groups of proteins such as the Trx/TrxR system or the glutaredoxin/GSH system [256,257].

To complete our overview of selenoproteins in thyroid iodinated hormone production, we should underline that thyronine iodination to T4 is achieved on the thyroglobulin protein within the thyroid gland by means of thyroid peroxidase (TPO) which uses iodide I^- and H_2O_2 as cosubstrates [264,265]. Thyroxine T4 is then cleaved by proteolysis of thyroglobulin [266] within the thyroid gland, and then secreted into blood plasma and transported to peripheral tissues by specific carriers. It is then taken up by an anion transporter of its target cells where it diffuses to reach its nuclear receptor. The secretion of T4 is under the control of the hormone TSH which is produced by hypophysis.

H_2O_2 which is used by TPO is generated by NADPH oxidases DUOX1 and DUOX2, and its local concentration in the thyroid gland might be under the control of GPx1, GPx3, and TrxR, GPx4 being additionally present. Thus, the biosynthesis of T4 and its conversion into T3 might be under the control of half a dozen selenoproteins.

Congenital hypothyroidism is the most common congenital endocrine disorder in humans, and some of the associated genetic defects which have been identified include recessive mutations in the selenocysteine insertion sequence SBP2 [267], but genetic defects of the selenium-dependent deiodinases are not clearly documented. The main genetic defects associated with hypothyroidism bear on mutations of thyroglobulin, TPO, DUOX2, and tyrosine deiodinase [267,268] which are not selenoenzymes. The most characteristic thyroid phenotype exhibits low serum T3, high T4, and high rT3.

3.6. Methionine R-Sulfoxide Reductase B1 [MsrB1]

Methionine sulfoxide reductases catalyze the reduction of sulfoxide into thioether, using thioredoxin Trx as a reducing cofactor [269–272]. Methionine sulfoxide has a chiral center which is sulfur, and MsrA is preferentially reducing the S form whereas MsrB is preferentially reducing the R form. In addition to MsrB1, selenocysteine-containing MsrA has been identified in bacteria, algae, and invertebrate animals, but not in vertebrates [271]. They are extremely rare and not well understood. Most MsrA have an essential cysteine at the active site.

Among MsrB which have been identified in animals and especially in humans, only MsrB1 (formerly named selenoprotein R or selenoprotein X), is a selenoenzyme [219,269–272], and it is also the only one that has a strict specificity for the R form.

Sulfur homologs of MsrB1 exist, in which selenocysteine is replaced by cysteine, but their specific activities are 100- to 1000-fold smaller. Conversely, replacing the essential cysteine of MsrB2 and MsrB3 with selenocysteine increases their specific activities by more than 100-fold. Such observations confirm the catalytic advantage of selenium. Human MsrB1 has two Cys-X-X-Cys motifs that coordinate a zinc atom, but the latter is found in other MsrB and it is apparently not involved in catalysis. Upon reduction of methionine sulfoxide, a selenenylsulfide bond is formed and then reduced by thioredoxin [226,270,271]. Although not excluded, a selenenic acid intermediate has not been demonstrated. The main features of the catalytic mechanism of MsrB1 are summarized in Figure 5C.

Despite its former recognition as an antioxidant enzyme in $MsrB1^{-/-}$ mice [273], MsrB1 was found to perform a stereospecific reduction of each of the two methionine-R-sulfoxide residues which are produced on actin filaments by flavin-dependent monooxygenases of the MICAL family [234,274]. This MICAL-dependent oxidation triggers the dissociation of polymeric F-actin into globular monomers of G-actin, and conversely, MsrB1 triggers the polymerization of G-actin into F-actin. Thus, the MICAL/MsrB1 couple plays a central role in the regulation of the polymerization/depolymerization process, and it is in-

volved in many physiological events such as cell division, cytokinesis and cell contractions, as well as in hair development or muscle organization [272].

The MICAL/MsrB1 couple is likely to play important roles in physiopathology. For example, a strong increase in MsrB1 protein and MsrB activity is observed in LPS-treated macrophages where MsrB1 colocalizes with actin [275]. As well, MsrB1 has "anti-inflammatory properties" since LPS-treated MsrB1$^{-/-}$ macrophages have greatly reduced anti-inflammatory cytokines, such as Il10 and Il1rn, but increased pro-inflammatory cytokines such as Il12A and Il12B [276]. In the heart, the MICAL/MsrB1 couple regulates the Ca^{2+} calmodulin-dependent kinase (CAMKII). MICAL oxidizes methionine M308 of CAMKII, which prevents calmodulin binding and kinase activity [277].

Surprisingly, however, MsrB1$^{-/-}$ mice do not show strong phenotypic alterations [273], which suggests that compensatory activities may exist. Moreover, a quadrupole KO for MsrA/MsrB1/MsrB2/MsrB3 paradoxically results in mice more resistant to cardiac ischemia/reperfusion or treatment with paraquat [278], which is not explained, although suggesting some link with superoxide production or toxicity.

3.7. Other Mammalian Selenoproteins

Although there are still a few mammalian selenoproteins for which little information is available, our understanding of several mammalian selenoproteins substantially improved in recent years.

3.7.1. Selenoprotein O and Protein AMPylation

Selenoprotein O is a large size selenoprotein (73 kDa for the human mitochondrial protein) that is highly conserved in bacteria and eukaryotes. It belongs to the superfamily of pseudokinases which are generally believed to have non-catalytic functions, such as allosteric regulation or scaffolding [279]. It was found however that selenoprotein O is an active enzyme that transfers AMP instead of phosphate, to serine, threonine, or tyrosine residues of protein substrates [280]. Structural data obtained with *P. syringae* selenoprotein O show that it adopts a protein kinase-like fold in which ATP is positioned in a head-to-tail configuration, which explains why this is the α-phosphate (and its adenylyl substituent) which is transferred to protein targets [280]. Here, the γ-phosphate which is normally transferred by protein kinases is buried in an inaccessible pocket, which is largely due to its coordination by a highly conserved lysine residue. It was also found with *E. coli* selenoprotein O that the AMPylation activity required the reduction of an intramolecular disulfide bridge. In this work, selenoprotein O was further shown to protect S. cerevisiae in situations of oxidative stress triggered by either H_2O_2 or menadione. One of the protein substrates which was shown to be AMPylated by selenoprotein O is glutaredoxin which is known to remove glutathione from S-glutathionylated proteins. Reversible S-glutathionylation is an important mechanism of transient protection of proteins from overoxidation [281]. Under exposure of *E. coli* or yeast cells to GSSG or diamide, it was shown that the overall level of S-glutathionylation was markedly decreased in selenoprotein-O KO cells [280]. Thus, selenoprotein O-mediated AMPylation of glutaredoxin family members would regulate the S-glutathionylation of proteins in vivo.

3.7.2. Selenoprotein F and Endoplasmic Reticulum Glycoproteins

Selenoprotein F (previously called Sep15) is a 15 kDa protein which is an endoplasmic reticulum-resident protein, and which forms a 1:1 complex with UGGT (UDP-glucose:glycoprotein glucosyl transferase) [282]. It has a thioredoxin fold with selenocysteine present in the position of the redox-active cysteine of thioredoxin and a reduction potential of −225 mV/ENH, between that of thioredoxin and that of protein disulfide isomerase, which strongly suggests a redox function [283]. Data obtained in mice have shown that selenoprotein F plays the role of "gatekeeper" of disulfide-rich glycoproteins secreted by the endoplasmic reticulum [284]. This function would prevent the useless secretion and costly resynthesis of glycoproteins in which disulfide formation is incorrect,

such problems being well documented in the ER. The underlying mechanism is not well understood, however.

It was later shown that selenoprotein-F knockout mice developed nuclear cataracts at an early age, and it was assumed that this might be due to improper folding of lens proteins [285]. In a more recent study, it was shown that such selenoprotein-F knockout mice developed glucose intolerance and insulin reduction and that the deleterious effects induced by a high-fat diet (obesity, hyperglycemia, glucose intolerance, and hepatic steatosis) were markedly increased [286].

3.7.3. Selenoprotein N and Endoplasmic Reticulum Calcium Sensing

Selenoprotein N (also called SEPN1) is a 70 KDa transmembrane glycoprotein of the endoplasmic reticulum which contains one selenocysteine residue [287]. Mutations of the SELENON gene lead to myopathy of variable severity. High levels of selenoprotein N are observed in human fetal tissues and its high expression in cultured myoblasts is downregulated in differentiating myotubes, which suggests a role in cell proliferation. The sarcoplasmic/endoplasmic reticulum Ca^{2+}-ATPase (SERCA) mediates calcium uptake in the endoplasmic reticulum, whereas calcium release is mediated by inositol triphosphate and ryanodine receptors. The overall process must be tightly controlled, to maintain the steep calcium gradient required across ER and thereby rapid excitation/contraction coupling. It has been known for a long time that this is a redox control. The latter involves the dissociation of a disulfide of SERCA2, which in the oxidative conditions which prevail in the lumen of the ER, would require a reductase that was not identified [288]. A recent study shows that the N-terminal domain of selenoprotein N senses ER calcium fluctuations and that low luminal calcium triggers the dissociation of an oligomeric form of SEPN1 into monomers, which concomitant unmasking of its reductase activity toward protein CERCA2 [289]. Thus, selenoprotein N would be one of the long-sought reductases which mediate the replenishment of ER calcium stores during muscle contraction.

3.7.4. Selenoprotein I and Ethanolamine Phospholipids

Selenoprotein I is an ethanolamine phosphotransferase (EPT) involved in the synthesis of two distinct ethanolamine phospholipids, phosphatidylethanolamine (PE) and plasmenyl PE [290]. These transferase activities are not redox reactions and do not use the selenocysteine residue. The selenocysteine which is in the C-terminal region serves an unknown function. Deletion of SELENOI in mice prevents embryo development, while loss-of-function mutations of SELENOI in humans lead to hereditary spastic paraplegia [291]. The enzyme is required in the myelination process and neurodevelopment, and in the maintenance of normal homeostasis of ether-linked phospholipids in humans [291,292]. Selenoprotein I also plays an important role in metabolic reprogramming required for T cell activation/proliferation and optimal immunity [293]: T cell activation increases levels of selenoprotein I along with PE and plasmenyl PE, and selenoprotein-I deficiency in mouse T cells reduces the de novo synthesis of PE and plasmenyl PE as well as proliferation. T-cell activation in selenoprotein-I knockout resulted in an accumulation of ATP and decreased AMPK activation, which disrupted metabolic reprogramming and reduced cell cycle progression.

3.7.5. Selenoprotein K, Palmitoylation Cofactor and Inhibitor of ER-Induced Apoptosis

Selenoprotein K is a 10 KDa transmembrane protein associated with the endoplasmic reticulum, with a selenocysteine in the C-terminal region. It serves as a cofactor during protein palmitoylation by binding to the protein acyltransferase DHHC6, facilitating the addition of palmitate via a thioester bond to the sulfhydryl group of cysteine residues of target proteins [294]. This is illustrated by the essential role of a selenoprotein-K/DHHC complex in the palmitoylation of IP3 receptors in immune cells [295]. Thus, through specific interactions with distinct proteins, some selenoproteins may serve as cofactors of enzyme reactions rather than being used as selenoenzymes.

SELENOK gene knockout was shown to increase endoplasmic reticulum stress and induce apoptosis in neurons in vitro and in vivo, through intracellular calcium increase and activation of the m-calpain/caspase-12 cascade [296]. It was also shown that selenoprotein K expression was activated in myogenic cells during differentiation in vitro and in vivo [297]. Here, SiRNA-mediated silencing of selenoprotein K inhibited the development of myoblasts into myotubes and concomitantly increased apoptosis and autophagy in myogenic cells.

3.7.6. Selenoprotein W and EGF Regulation

Selenoprotein W is a cytoplasmic 9kDa thioredoxin-like protein that is required for cell cycle progression [298–300], and it has been shown that it is required for EGF-induced EGFR activation through suppression of EGFR ubiquitination and receptor degradation [301]. Interestingly, it interacts with the adaptor protein 14-3-3b [302]. This interaction requires the selenocysteine residue and is increased by diamide, which suggests that selenoprotein W is redox regulated.

3.7.7. Selenoprotein T

Selenoprotein T is a thioredoxin-like protein that is mostly expressed in endocrine organs, and which is involved in the production and release of hormones such as insulin and corticotropin [303]. Such effects are mediated by its role in ER proteostasis. It is essential during embryogenesis, and its knock-out in the mouse brain induces anatomical alterations and abnormal behavior. Recent experimental data support the involvement of selenoprotein-T dysfunction in Parkinson's disease [304,305].

3.7.8. Selenoprotein S

Selenoprotein-S is a protein of 189 amino acids which is prevalent in eukaryotic organisms. It is an intrinsically disordered membrane enzyme whose function is not established, but which is associated with the unfolded protein degradation complex ERAD (ER-associated degradation) of the endoplasmic reticulum [306]. It behaves in vitro as a disulfide reductase and as a peroxidase [200,306].

3.7.9. Selenoprotein-H

Selenoprotein-H is a 23kDa protein which is the only selenoprotein being exclusively localized in the nucleus [307], and it has been shown to protect human fibroblasts against replicative senescence by genome redox maintenance [308,309].

4. Bacterial Selenoenzymes

Several selenoenzymes exist in bacteria. Except for selenophosphate synthetase and selenoprotein O which are also found in mammals and catalyze reactions already described in Section 3, bacterial selenoenzymes are mostly involved in anaerobic metabolism [310, 311]. They include glycine reductase [312–315], D-proline reductase [316–318], formate dehydrogenase [319–325] and [NiFeSe]hydrogenase [326,327].

4.1. Glycine Reductase

This enzyme catalyzes the reductive deamination of glycine into acetylphosphate [312]:

$$\text{Glycine} + \text{Pi} + \text{Thioredoxin dithiol} \rightarrow \text{Acetylphosphate} + NH_4^+ + \text{Thioredoxin disulfide} + H_2O \quad (6)$$

It is the first bacterial enzyme that was identified as a selenoenzyme and it may be considered a terminal electron acceptor, acetylphosphate being converted to acetate and ATP by acetate kinase. It enables some anaerobic bacteria to conserve energy via a soluble substrate-level phosphorylation.

Glycine reductase is a trimeric enzyme composed of proteins named A, B. and C. Protein B contains selenocysteine and possibly a pyruvoyl residue. It binds glycine and is responsible for the extrusion of NH_3. Protein A also contains glycine, which is reduced by

thioredoxin, and it provides an intermediate that subunit C uses to produce acetylphosphate. In vitro, the enzyme works with dithiothreitol as a reducing agent, which means that biological reducing cofactors other than thioredoxin cannot be excluded.

The initial binding of glycine does not involve pyridoxal phosphate but is believed to involve a Schiff base with an activated carbonyl group of the enzyme which has never been clearly identified, due to its instability. It could be a pyruvoyl group, but its formation would require an additional enzyme that would not be within the glycine reductase operon. Some possible transformation steps summarized by Andreesen [314] are shown in Figure 8 in which we underlined that the formation of thioesters would likely require some additional activation step(s) that remain to be identified. In my view, the most interesting reaction here is the thiolate-mediated cleavage of the selenoether bond in the carboxymethylated derivative of selenocysteine, a reaction that had been initially proposed by Arkowitz and Abeles [315,317] without β activation of the distal carboxylate, even though they had in mind that β activation should have been expected. The important point is that the enzyme couples the cleavage of a selenoether carbon-selenium bond to the formation of a selenenylsulfide bond.

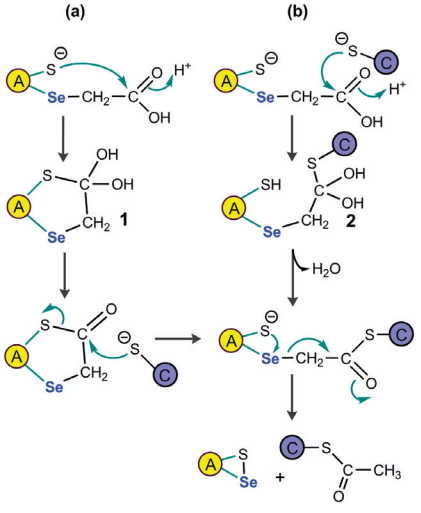

Figure 8. Two possible pathways of formation of the acetyl precursor in glycine reductase. Adapted from Andreesen [314]. The Schiff base formed from glycine and an activated carbonyl group in protein A would react first with a proximal selenocysteine selenolate to yield a carboxymethyl selenoether, whose C2 unit is transformed into an acetyl thioester on protein C, with the formation of a selenenylsulfide bond. Mechanistic options include a speculative keten-like intermediate CH_2=C=O, and an intramolecular carbonyl hydroxybase 1 in (**a**) or an intermolecular carbonyl hydroxybase 2 in (**b**).

4.2. D-Proline Reductase

This enzyme catalyzes the reductive cleavage of the D-proline cyclic sidechain into 5-aminopentanoate, which involves breaking of the Cα-N bond [316]:

$$\text{D-proline} + \text{Dithiol} \rightarrow \text{5-aminopentanoate} + \text{Disulfide} \quad (7)$$

This reductive deamination of aminoacid is similar to the reaction catalyzed by glycine reductase, but the existence of an analogous high-energy acyl-enzyme intermediate was excluded by $^{18}O_2$ labeling experiments [317], and D-proline reduction is not coupled to substrate-level phosphorylation. The reduction is also NADH-dependent, not NADPH-

dependent, which rules out thioredoxin as a biological partner, and is compatible with the use of a coenzyme such as lipoic acid.

D-Proline reductase is a membrane-bound protein composed of 10 subunits. A 46-aminoacid pyruvoyl-containing peptide is covalently attached to each subunit via an ester linkage [318].

The reaction sequence happens on a pyruvoyl-proline covalent adduct, as shown in Figure 9, but the hypothetical mechanism which was proposed [316] relies on two reactions that are not documented as such in organic chemistry. The first one is the nucleophilic attack of the non-activated α carbon of proline, and the second one is the nucleophilic attack of a non-activated selenoether intermediate by a cysteine thiolate, a mechanism that had been initially proposed by the group of Abeles for glycine reductase, as above mentioned [313]. Here again, the important point is that the unusual cleavage of a selenoether carbon-selenium bond is achieved by this selenoenzyme.

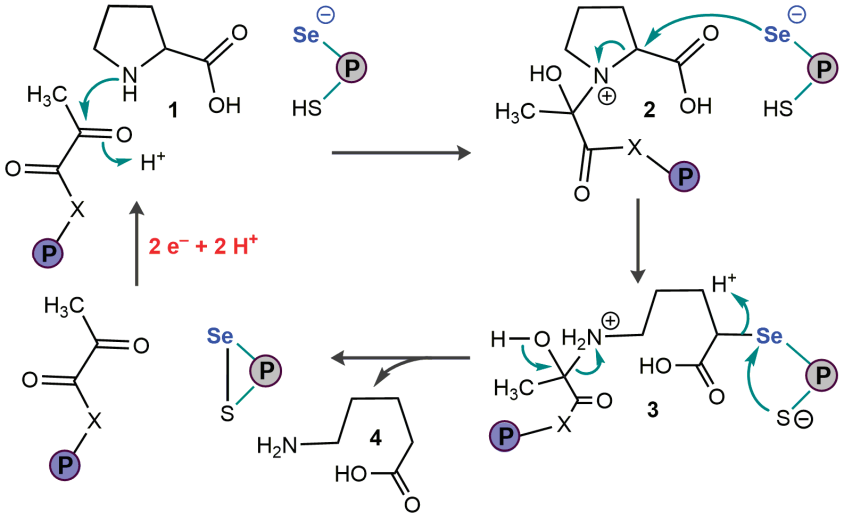

Figure 9. Putative catalytic mechanism of D-proline reductase. Adapted from Kabisch et al. for the enzyme of *Clostridium sticklandii* [316]. SeCys belongs to one protein of the enzyme complex, and pyruvate is covalently bound to another protein. Step 2 → 3 would require an iminium intermediate produced from 2. Step 3–4 involves two independent bond clivages.

4.3. Formate Dehydrogenase

Formate dehydrogenases [319–323] catalyze the reversible oxidation of formate to carbon dioxide and play an important role in the global fixation of carbon dioxide, as follows:

$$HCOOH \rightleftarrows CO_2 + 2\,H^+ + 2\,e^- \quad (8)$$

These enzymes are peripheral membrane proteins located on the cytoplasmic side and have several subunits. Their prosthetic group contains a cis-dithiolene structure which is bound to molybdenum by coordination (structure 11, Figure 1, where two pyranopterin guanine dinucleotides are not represented). The active site also contains an essential selenocysteine residue and a Fe_4S_4 cluster. The enzyme from *E. coli* is completely inactivated by iodoacetamide after reduction with formate, and the replacement of selenocysteine with cysteine decreases the activity by more than two orders of magnitude, which confirms the essential function of selenium [320]. Even though they are members of the dimethylsulfoxide reductase family, formate dehydrogenases do not catalyze oxygen-atom transfer reactions.

In its [+IV] oxidation state, molybdenum is pentacoordinate with the four pyranopterine ligands in equatorial positions and a fifth sulfido group in an axial position [324], which gives an approximate square pyramidal geometry. In its [+VI] oxidation state, it adopts a distorted hexacoordinated trigonal prismatic geometry, again with the four pyranopterine ligands plus a fifth ligand which is selenium from the selenocysteine residue and a sixth one which is the sulfido group.

The catalytic mechanism of formate dehydrogenases is still open to debate [323–325], but one should underline the existence of functional sulfur homologs in which selenocysteine has been replaced by cysteine.

Figure 10 shows a putative catalytic mechanism that is based on refined structural data as well as functional and theoretical analyses [323,324].

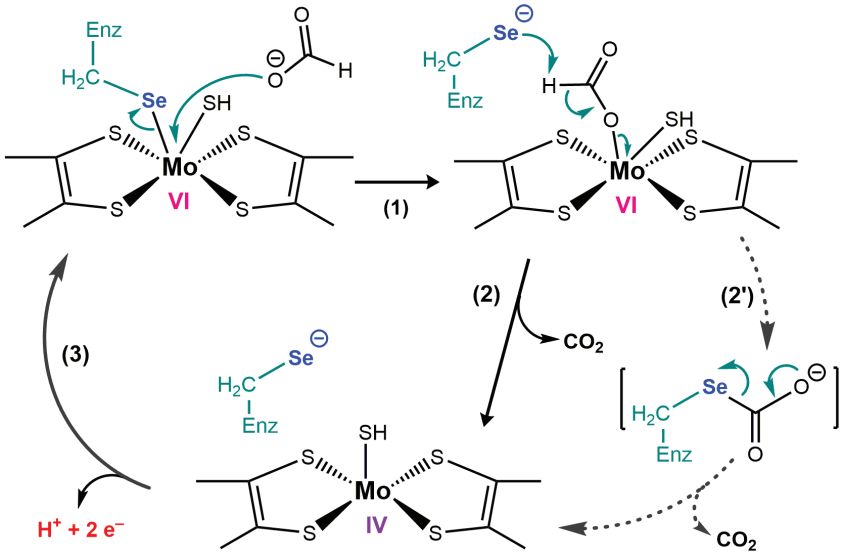

Figure 10. Putative catalytic mechanism of formate dehydrogenase. Formate displaces selenium of the SeCys ligand. It was assumed that the resulting selenolate would assist decarboxylation step (2) as a basic catalyst [323,324], which is unlikely with its low pKa and cannot explain the requirement for selenium. In the alternative of step (2′), the nucleophilic attack of the selenolate would yield a carboxylated SeCys which would decompose to selenolate and CO_2. The axial ligand of Mo[IV] is sulfide, not selenium.

4.4. [NiFeSe] Hydrogenases

The structures and functions of [NiFeSe] hydrogenases have been extensively reviewed [326,327]. They are a subclass of [NiFe]-hydrogenases with a selenocysteine residue coordinated to the active site nickel center in place of cysteine. They are exclusively found in sulfate-reducing and methanogenic microorganisms and catalyze the interconversion of hydrogen and protons:

$$H_2 \rightleftarrows 2\,H^+ + 2e^- \quad (9)$$

Most of them are heterodimers containing three iron-sulfur clusters in a small subunit and a nickel-iron-containing active site in a large subunit in which there is a selenocysteine ligand. Their prosthetic group was shown as Structure 12 in Figure 1.

They exhibit highly advantageous properties for applications in water splitting compared with other hydrogenases. They display a high H_2 evolution rate with marginal inhibition by H_2 and a high tolerance to O_2. [NiFeSe]-hydrogenases may therefore be the most efficient catalysts to produce H_2 by water splitting [291]. An interesting ap-

plication has been the development of a light-driven full water splitting system with a [NiFeSe]-hydrogenase wired to the water oxidation enzyme photosystem II [328,329].

The mechanism of [NiFeSe] hydrogenases is complex, but the specific advantage of selenocysteine in [NiFeSe] hydrogenase seems to bear in large part on the protection of nickel from irreversible overoxidation by O_2 [330–332]. As discussed in Section 6, one advantage of selenocysteine compared with cysteine may be the better reversibility of its oxidation reactions.

5. Is Redox Regulation an Essential Function of Most Mammalian Selenoproteins?

At least in mammals, selenoproteins are all involved in redox transformations. The involvement of GPx4 in redox regulation is supported by the fact that degeneration of GPx4-deficient neuronal cells relies on AIF- and not caspase3-dependent apoptosis [168]. We are dealing here with cell death regulation, however, not with cell function.

The involvement of TrxR and Msr in the redox regulation of cell function and structure is well established, and the same could be said of the role of deiodinases in metabolic regulations. But the situation is more ambiguous with selenium-glutathione peroxidases because they have major antioxidant properties. There are many arguments that can be used to suggest that they are involved in redox regulation [176,333,334], but one cannot give a detailed description of such regulations. In my view, an antioxidant enzyme could be envisaged as a redox regulator of cell function if its concentration or activity did markedly vary in response to anything else than oxidative stress, but such information is often missing with glutathione peroxidases. Because the information available on GPx3 is insufficient to be conclusive, a good starting point would be to assume that Gpx1 and GPx2 primarily deal with aqueous hydroperoxides, whereas GPx4 should be mainly involved in redox regulations as a phospholipid hydroperoxide reductase.

As early as 1987, we showed that the intoxication of rats with ethylmorphine, a metabolic source of H_2O_2 through cytochrome-P450 demethylases, induced an important increase in hepatic SeGPx after 24 to 48 h [335]. At that time, very little information was known about the mechanisms of transcriptional regulation of enzymes involved in antioxidant protection. One knows today that the promotor of GPx2 contains an ARE sequence (Antioxidant Response Elements) which enables its stimulation in the situation of oxidative stress by dissociation of the Nrf2/Keap1 assembly [111]. But it seems reasonable to assume that this is a purely antioxidant and detoxifying adaptation. GPx4 promoters do not contain any Nrf2 binding site [146], but oxidative stress stimulates the biosynthesis of several selenoproteins (GPx1, GPx4, Trx1, SelS, SelK, and Sps2) by improving the recoding efficiency of UGA/selenocysteine through relocation of the SBP2 elongation factor and the ribosomal protein L30 from the cytoplasm to the nucleus [336].

In mouse embryonic fibroblasts, the t-RNA methyltransferase Alkbh8 (mammalian alkylation repair homolog 8) was also shown to markedly induce the expression of several selenoproteins in situations of oxidative stress [337]. Enzymes of the Alkb family are iron-oxoglutarate dioxygenases which perform oxidative demethylation of various DNA and RNA bases and interact with transcription factors. Alkbh8 additionally contains a methyl transferase domain, it is induced in response to activated oxygen species, and it is apparently required for the efficient expression of at least GPx1, GPx2, GPx3, and TrxR1 in this situation [337].

A recent study on pure recombinant GPx1, GPx2 and GPx4 shows that they all have significant activities on H_2O_2, t-butylhydroperoxide, cumene hydroperoxide, and fatty acid hydroperoxides, but that GPx1 specific activities per selenium are much higher on such substrates [338]. On the other hand, GPx4 is the only one that is efficient on phosphatidylcholine hydroperoxides.

Sometimes, the coexistence of GPx1, GPx2, and GPx3 makes the picture very complex. For example, in the gastrointestinal tract, GPx1 is homogeneously expressed in the intestinal epithelium, whereas GPx2 expression is higher in crypts and mainly in the ileum and

cecum [94,339]. As well, GPx3 is also expressed in the gastrointestinal tract while plasma GPx3 binds to the basement membranes of intestinal epithelial cells [143].

Hydrogen peroxide H_2O_2 is produced by the stimulation of many hormone receptors, and it is believed to serve as an intracellular messenger by directly or indirectly oxidizing cysteine residues of target proteins [340,341]. Multiple H_2O_2 primary or secondary sensors contribute to the redox regulation of transcription factors which include among others AP-1, Nrf2, and NF-kB, and this complex network regulates major cellular events such as proliferation, differentiation, and apoptosis [342,343]. Thus, GPx1 and perhaps GPx2 might be involved in redox regulation by controlling H_2O_2 concentrations in space and time, but this is virtually impossible to prove without detailed information on the flux of H_2O_2 production by an activated enzyme such as NADPH oxidases as well as on their variations of activity. H_2O_2 may also have multiple time-dependent effects, for example, it acts as a biphasic modulator of NF-kB activation by other agents, not only as a direct activator [344,345].

At any rate, peroxiredoxins (Prx)—which are not selenoproteins may be more dedicated to H_2O_2 signaling than GPx1 or GPx2, and they use the small reducing pool of thioredoxin under the control of TrxR, not the pool of GSH which is generally in large excess. Given their reduction by the Trx/TrxR system, they are under the control of selenoenzymes, however.

One may have overlooked the importance of glutathione peroxidases in the control of organic hydroperoxide concentrations. Potential targets of such regulatory effects include at least lipoxygenases [120–122] and cyclooxygenases [346] whose activities require an initiation step induced by preformed organic hydroperoxides, and phosphatases, especially protein tyrosine phosphatase [347]. The latter invariably contains an essential cysteine thiolate in their active site which can be oxidized to specific sulfenic, sulfenylamide, or disulfides. The direct oxidation of such active site cysteines by H_2O_2 is very slow [347], but it was shown that physiological concentrations of bicarbonate which reacts with H_2O_2 to produce peroxymonocarbonate, facilitate the H_2O_2-mediated inactivation of protein tyrosine phosphatase 1B [348]. The observation that GPx1 or GPx4 overexpression can inhibit the activation of NFkB [161,349] would also fit with oxidative inactivation of a specific phosphatase. But with GPx1 as well as with GPx4, we do not know which hydroperoxides are directly involved and which target protein is affected.

Binding sites for transcription factors distinct from Nrf2 have been identified on GPx1 as well as GPx4 genes [176], but little is known about corresponding regulatory functions.

Finally, if the activity of a given SeGPx was not only upregulated for antioxidant protection but at least transiently downregulated for other purposes, for example by means of phosphorylation or mixed disulfide formation, it would certainly qualify as a redox regulator. We already mentioned that GPx4 might be under redox control of the adaptor protein 14-3-3e [180]. In cell culture, artificial inhibition of GPx1—and perhaps GPx2 and GPx4—by mercaptosuccinate markedly increases Ca^{2+}-mediated activation of monocyte 5-lipoxygenase [121]. At least one biological example of GPx4 down-regulation is associated with intestinal trans-epithelial neutrophil migration. This process is controlled by 12-lipoxygenase which produces the eicosanoid hepoxilin A3 and establishes a chemotactic gradient that guides PMN across the epithelial surface. Using Salmonella typhimurium to induce this process, it was found that the bacteria-induced apical secretion of hepoxilin A3 by decreasing the expression of GPx4, which in turn led to an increase in 12-lipoxygenase activity [350].

Mammalian tyrosine kinases c-Abl and Arg, which are devoid of receptors and play an important role in apoptosis induced by oxidative stress, form constitutive complexes with GPx1, thereby protecting the enzyme at non-lethal doses of H_2O_2, whereas lethal doses of H_2O_2 destroy such complexes and induce apoptosis [351]. This suggests that some growth factors may regulate SeGPx activities. At least one study showed that VEGFB strongly induced the expression of GPx1 and more modestly that of GPx5 in murine retinal cells [352].

Overall, we tentatively conclude that SeGPx is involved in major redox regulatory networks but may be more as local "kinetic buffers" of hydroperoxide concentrations than as dedicated transducers of redox signals such as protein regulators under the control of the Trx/TrxR system.

6. Advantages and Constraints Associated with the Choice of Selenocysteine at the Active Site of Selenoenzymes

Given the similarities between sulfur and selenium properties, a question that the biochemist cannot bypass is that of the expensive selection of selenium rather than that of sulfur [353–357]. Under its thiolate form, sulfur is indeed a good nucleophile and a good reductant. Contrary to vertebrates, non-vertebrate animals, higher plants, and fungi produce many protein homologs of our selenoproteins, in which selenocysteine is replaced by cysteine, but their peroxidase activities have been studied in detail only for non-vertebrate CysGPx. Such non-vertebrate CysGPx is not simple cysteine homologues as suggested by their name, because they contain an active site cysteine (peroxidatic Cp) in place of selenocysteine, but also a second cysteine (resolving Cr) which is used to form a disulfide from a putative cysteine sulfenic acid intermediate (reviewed in 188). This disulfide is then recycled by thioredoxin (or other redoxins), not by GSH. Some of these CysGPx/thioredoxin peroxidases are surprisingly efficient to reduce hydroperoxides, although not as efficient as the selenium-dependent GSH peroxidases, having typically second-order rate constants for the hydroperoxide reduction step which are at least two orders of magnitude smaller [188].

The case of peroxiredoxins already cited and which are very efficient peroxidases on H_2O_2 is another interesting example, even though such enzymes are not selenoprotein homologs.

If one inspects the key steps of the catalytic cycles of selenoenzymes that are best understood (see Figure 5), one would be tempted to say that a cysteine thiol group that would be activated to thiolate should be able to do the job. In selenoenzymes, the initial step is a nucleophilic attack by the selenolate group, and the final step is its restitution as leaving group. Conceivably, a thiolate group could replace the selenolate since the formation of a cysteine thiolate is generally observed in enzymes bearing a catalytic cysteine. Examples include glyceraldehyde-phosphate-dehydrogenase and disulfide reductases such as GSSG reductase, lipoamide dehydrogenases, thioredoxins, and glutaredoxins.

It is often underlined that the second-order rate constant of the active site selenolate of GPx1 with H_2O_2 is close to 5.10^7 $M^{-1}.s^{-1}$, whereas that of a non-enzymatic selenolate group is several orders of magnitude smaller. This would suggest that the protein environment of the active site selenocysteine is doing much of the job, and recent DFT calculations on a modelized H_2O_2/SeGPx or H_2O_2/SGPx interaction would support this concept [358,359]. In these model studies, it was found that the presence of one water molecule in the active site triggered a concerted deprotonation/reprotonation in which the proton dissociated from the selenol or thiol group was transferred by the bridging water to one oxygen of the peroxide bond, ensuring an optimal concerted nucleophilic attack of the peroxide bond by the selenolate or thiolate. This theoretical study does not explain however why the exchange of selenium for sulfur at the active site of GPx1 results in a 1000-fold decrease in GPx activity [360]. Similarly, a marked GPx activity often results from the exchange of native sulfur for selenium in cysteine-dependent enzymes which are not GPx and have no measurable GPx activities [361,362]. Such enzymes include subtilisin [363,364], GST [365], glutaredoxin [366,367], and even glyceraldehyde-3-phosphate dehydrogenase [368].

But one should admit that the example of peroxiredoxins whose second-order rate constants with H_2O_2 are close to 10^7 $M^{-1}.s^{-1}$ invalidates the concept of an absolute requirement for selenium in fast peroxide bond reduction.

If we compare the properties of oxygen, sulfur, and selenium, there is a drastic change in properties in going from oxygen to sulfur, whereas the changes are more modest in going from sulfur to selenium. The covalent radii change more between the first and the

second rows than between succeeding rows, which is illustrated by the abrupt change in electronegativity between oxygen and sulfur, much more modest from sulfur to selenium. In water, the nucleophilic selenolate form will predominate at neutral pH, which is not the case of the thiolate form, but given the ease of pKa lowering of cysteine thiols in enzyme active sites, a relevant comparison should bear on selenolate versus thiolate.

With its 3d-orbitals, a selenolate group is a softer nucleophile than a thiolate group, and this could be a major advantage for interaction with iodine in deiodinases, but to which extent this could facilitate the nucleophilic attack of a peroxide bond is not obvious. Perhaps a selenium-peroxide transition state of non-conventional geometry should be envisaged. Similar geometries of sulfur and selenium transition states have always been used in theoretical comparisons.

Another difference between thiols and selenols bears on their protonated form RSH and RSeH. Many years ago, Huber and Criddle [369] showed that the selenol form RSeH of selenocysteine had significant nucleophilic properties in water, which was not the case for the thiol form RSH of cysteine. Again, this is likely to come from filled 3d orbitals in selenium [empty in sulfur] and from the fact that with very similar covalent radii of sulfur and selenium, the electron density in the 3d and/or 4p orbitals of selenium should be much higher than that of the sulfur outer shell.

Many potentially discriminating properties have been extensively discussed in two reviews by Hondal and coworkers [356,357]. They confirm that selenolates are more nucleophilic than thiolates, and that selenides are more nucleophilic than sulfides. As well, selenium nucleophilicity may not be the main discriminating factor because electrophilic groups such as diselenides, selenenic acids, and selininic acids are also much better electrophiles than their sulfur analogs [356]. The reduction rate of seleninic acids by thiols is at least 10^6 times faster than the reduction rate of sulfinic acids by thiols [356] and this may be where the discrimination is most obvious. As underlined by Reich and Hondal [356], it would explain an observation that we had made on glutathione peroxidase [360]. By expressing the first sulfur/cysteine mutant (S-GPx) of GPx1 by directed mutagenesis, we had not only observed an enzyme activity that was decreased by three orders of magnitude, but also a fast auto-inactivation whose rate increased with the (hydroperoxide)/(GSH) ratio, and this had led us to envisage an irreversible mechanism of sulfur overoxidation which would not occur with selenium. At that time, our conclusion was that selenium solved a problem of irreversible oxidation that might induce sulfur loss by β-elimination, but we had no structural data to show. A specific method of immunodetection of dehydroalanine residues was developed only much later [370]. It was used to show that Sec in red blood cell GPx1 was increasingly replaced with dehydroalanine during blood storage.

It was also shown on the GPx4 cysteine mutant of *Schistosoma mansoni* that the active-site cysteine was oxidized to Cys-sulfonate, which did explain its inactivation [371]. Much more recently, it was shown that rat GPx4 was built to avoid irreversible overoxidation of selenium in the situation of GSH deficit thanks to the attack of the selenenic acid Enz-SeOH by a nucleophilic nitrogen from the polypeptide backbone [372]. The protective Se-N bond is broken by GSH when its physiological concentration is re-established, and the system is ready for new catalytic cycles.

Sulfur mutants of other selenocysteine-containing enzymes have been studied, including the [NiFeSe] hydrogenases discussed in Section 4.4, and as a rule, they were found to undergo oxidative inactivation which was not observed with the selenocysteine-containing enzymes [357]. Overall, it may be concluded that the catalytic advantage of selenium compared with sulfur relies in large part on a unique combination of faster kinetics and much better reversibility of its oxidation reactions.

7. Conclusions

The extensive investigations and multiple discoveries of the last four decades have been very exciting, and a few points deserve to be underlined:

- The co-translational incorporation of selenium in selenoproteins is probably unique among the elements situated below period 3 of the periodic table, and one of the major advantages of selenium compared with sulfur should be the better reversibility of its oxidation reactions in biological conditions.
- Selenoproteins are mostly involved in anaerobic metabolism in bacteria, whereas they are involved in antioxidant protection, protein repair, redox signaling, and regulation of cell proliferation/cell death, and energetic metabolism in mammals.
- Many functions of mammalian selenoproteins, especially those which are anti-inflammatory, anti-apoptotic, or anti-ferroptotic, or which interfere with energetic metabolism, require regulation in space and time. Specifically, most mammalian selenoenzymes should not only be regulating but also regulated, although, in this area, much information is probably still missing.
- With the recent development of new techniques of selenocysteine insertion into protein sequences, we can expect that new discoveries will shed light on the hidden face of the moon.

Funding: This work received no external funding.

Institutional Review Board Statement: Not relevant.

Informed Consent Statement: Not relevant.

Data Availability Statement: No original data available with this review article.

Conflicts of Interest: The author declares no conflict of interest.

Abbreviations

AIF, apoptosis inducing factor; Alkbh, mammalian alkylation repair homolog; Alox15 gene, gene encoding an arachidonate 15-lipoxygenase; AP-1, activator protein 1; ASK1, apoptosis signal kinase 1; CAMKII, Ca^{2+} calmodulin-dependent kinase; COX2, Type 2 cyclooxygenase; DIO, deiodinase; DUOX, dual oxidase; EFsec, selenocysteine dedicated elongation factor; EMT, epithelial-mesenchymal transition; GLS2, liver-type glutaminase; GPx, glutathione peroxidase; GR, glutathione reductase; HCV, hepatitis C virus; HIF, hypoxia inducible factor; Keap1, Kelch associated protein 1; LOX, Lipoxygenase; LPS, lipopolysaccharide; MAPK, mitogen-activated protein kinase; MICAL, molecules interacting with CasL; MsrB1, methionine sulfoxide reductase B1; NFκB, nuclear factor kB; Nox, NADPH oxidase; Nrf2, nuclear factor erythroid-2-related factor; NQQ1, NAD[P]H: Quinone oxidoreductase 1; PDI, protein disulfide isomerase; Prx, peroxiredoxin; PTEN, phosphatase and tensin homolog; SBP2, SECIS-binding protein 2; SecTRAPs, selenium compromised thioredoxin reductase-derived apoptotic proteins; SECYS, selenocysteine insertion sequence; Selenoprotein P, selenoprotein P; Sephs2, selenophosphate synthetase 2; TGS1, trimethylguanosine synthase 1; TNFα, tumor necrosis factor a; TPO, thyroid peroxidase; Trx, thioredoxin; TrxR, thioredoxin reductase; T4, thyroxine; T3 triiodothyronine; ZEB1, zinc-finger E-box binding protein 1.

References

1. Flohé, L. The labour pains of biochemical selenology: The history of selenoprotein biosynthesis. *Biochim. Biophys. Acta* **2009**, *1790*, 1389–1403. [CrossRef] [PubMed]
2. Elhodaky, M.; Diamond, A.M. Selenium-Binding Protein 1 in Human Health and Disease. *Int. J. Mol. Sci.* **2018**, *19*, 3437. [CrossRef] [PubMed]
3. Schrauzer, G.N.; Surai, P.F. Selenium in human and animal nutrition: Resolved and unresolved issues. *Crit. Rev. Biotechnol.* **2009**, *29*, 2–9. [CrossRef] [PubMed]
4. Wrobel, J.K.; Power, R.; Toborek, M. Biological activity of selenium: Revisited. *IUBMB Life* **2015**, *68*, 97–105. [CrossRef]
5. Genchi, G.; Lauria, G.; Catalano, A.; Sinicropi, M.S.; Carocci, A. Biological activity of selenium and its impact on human health. *Int. J. Mol. Sci.* **2023**, *24*, 2633. [CrossRef]

6. Steinbrenner, H.; Sies, H. Selenium homeostasis and antioxidant selenoproteins in brain: Implications for disorders in the central nervous system. *Arch. Biochem. Biophys.* **2013**, *536*, 152–157. [CrossRef]
7. Conrad, M.; Schweizer, U. Unveiling the molecular mechanisms behind selenium-related diseases through knockout mouse studies. *Antioxid. Redox Signal.* **2010**, *12*, 851–865. [CrossRef]
8. Agamy, O.; Ben Zeev, B.; Lev, D.; Marcus, B.; Fine, D.; Su, D.; Narkis, G.; Ofir, R.; Hoffmann, C.; Leshinsky-Silver, E.; et al. Mutations disrupting selenocysteine formation cause progressive cerebello-cerebral atrophy. *Am. J. Hum. Genet.* **2010**, *87*, 538–544. [CrossRef]
9. Wirth, E.K.; Bharathi, B.S.; Hatfield, D.; Conrad, M.; Brielmeier, M.; Schweizer, U. Cerebellar hypoplasia in mice lacking selenoprotein biosynthesis in neurons. *Biol. Trace Elem. Res.* **2014**, *158*, 203–210. [CrossRef]
10. Chen, J. An original discovery: Selenium deficiency and Keshan disease (an endemic heart disease). *Asia Pac. J. Clin. Nutr.* **2012**, *21*, 320–326.
11. Xie, D.; Liao, Y.; Yue, J.; Zhang, C.; Wang, Y.; Deng, C.; Chen, L. Effects of five types of selenium supplementation for treatment of Kashin-Beck disease in children: A systematic review and network meta-analysis. *BMJ Open* **2018**, *8*, e017883. [CrossRef]
12. Zhou, H.; Wang, T.; Li, Q.; Li, D. Prevention of Keshan Disease by Selenium Supplementation: A Systematic Review and Meta-analysis. *Biol. Trace Elem. Res.* **2018**, *186*, 98–105. [CrossRef]
13. Koivistoinen, P.; Huttunen, J.K. Selenium in food and nutrition in Finland: An overview on research and action. *Ann. Clin. Res.* **1986**, *18*, 13–17.
14. Jedrychowski, M.P.; Lu, G.Z.; Szpyt, J.; Mariotti, M.; Garrity, R.; Paulo, J.A.; Schweppe, D.K.; Laznik-Bogoslavski, D.; Kazak, L.; Murphy, M.P.; et al. Facultative protein selenation regulates redox sensitivity, adipose tissue thermogenesis, and obesity. *Proc. Natl. Acad. Sci. USA* **2020**, *117*, 10789–10796. [CrossRef]
15. Hosnedlova, B.; Kepinska, M.; Skalickova, S.; Fernandez, C.; Ruttkay-Nedecky, B.; Malevu, T.D.; Sochor, J.; Baron, M.; Melcova, M.; Zidkova, J.; et al. A summary of new findings on the biological effects of selenium in selected animal species—A critical review. *Int. J. Mol. Sci.* **2017**, *18*, 2209. [CrossRef]
16. Rahman, M.M.; Hossain, K.F.B.; Banik, S.; Sikder, M.T.; Akter, M.; Bondad, S.E.C.; Rahaman, M.S.; Hosokawa, T.; Saito, T.; Kurasaki, M. Selenium and zinc protections against metal-(loids)-induced toxicity and disease manifestations: A review. *Ecotoxicol. Environ. Saf.* **2019**, *168*, 146–163. [CrossRef]
17. Chaudière, J.; Tappel, A.L. Interaction of gold(I) with the active site of selenium-glutathione peroxidase. *J. Inorg. Biochem.* **1984**, *20*, 313–325. [CrossRef] [PubMed]
18. Flohé, L.; Günzler, W.A.; Schock, H.H. Glutathione peroxidase: A selenoenzyme. *FEBS Lett.* **1973**, *32*, 132–134. [CrossRef] [PubMed]
19. Rotruck, J.T.; Pope, A.L.; Ganther, H.E.; Swanson, A.B.; Hafeman, D.G.; Hoekstra, W.G. Selenium: Biochemical role as a component of glutathione peroxidase. *Science* **1973**, *179*, 588–590. [CrossRef] [PubMed]
20. Böck, A.; Forchhammer, K.; Heider, J.; Leinfelder, W.; Sawers, G.; Veprek, B.; Zinoni, F. Selenocysteine: The 21st amino acid. *Mol. Microbiol.* **1991**, *5*, 515–520. [CrossRef] [PubMed]
21. Chapple, C.E.; Guigó, R. Relaxation of selective constraints causes independent selenoprotein extinction in insect genomes. *PLoS ONE* **2008**, *3*, e2968. [CrossRef] [PubMed]
22. Squires, J.E.; Berry, M.J. Eukaryotic selenoprotein synthesis: Mechanistic insight incorporating new factors and new functions for old factors. *IUBMB Life* **2008**, *60*, 232–235. [CrossRef] [PubMed]
23. Allmang, C.; Wurth, L.; Krol, A. The selenium to selenoprotein pathway in eukaryotes: More molecular partners than anticipated. *Biochim. Biophys. Acta* **2009**, *1790*, 1415–1423. [CrossRef]
24. Vindry, C.; Ohlmann, T.; Chavatte, L. Translation regulation of mammalian selenoproteins. *Biochim. Biophys. Acta* **2018**, *1862*, 2480–2492. [CrossRef]
25. Copeland, P.R.; Howard, M.T. Ribosome fate during decoding of UGA-Sec codons. *Int. J. Mol. Sci.* **2021**, *22*, 13204. [CrossRef]
26. Ganichkin, O.M.; Xu, X.M.; Carlson, B.A.; Mix, H.; Hatfield, D.L.; Gladyshev, V.N.; Wahl, M.C. Structure and catalytic mechanism of eukaryotic selenocysteine synthase. *J. Biol. Chem.* **2008**, *283*, 5849–5865. [CrossRef]
27. Yamada, T.; Komoto, J.; Takata, Y.; Ogawa, H.; Pitot, H.C.; Takusagawa, F. Crystal structure of serine dehydratase from rat liver. *Biochemistry* **2003**, *42*, 12854–12865. [CrossRef]
28. Wurth, L.; Gribling-Burrer, A.S.; Verheggen, C.; Leichter, M.; Takeuchi, A.; Baudrey, S.; Martin, F.; Krol, A.; Bertrand, E.; Allmang, C. Hypermethylated-capped selenoprotein mRNAs in mammals. *Nucleic Acids Res.* **2014**, *42*, 8663–8677. [CrossRef]
29. Schoenmakers, E.; Chatterjee, K. Human Genetic Disorders Resulting in Systemic Selenoprotein Deficiency. *Int. J. Mol. Sci.* **2021**, *22*, 12927. [CrossRef]
30. Cheng, Q.; Arnér, E.S. Selenocysteine Insertion at a Predefined UAG Codon in a Release Factor 1 (RF1)-depleted Escherichia coli Host Strain Bypasses Species Barriers in Recombinant Selenoprotein Translation. *J. Biol. Chem.* **2017**, *292*, 5476–5487. [CrossRef] [PubMed]
31. Cheng, Q.; Arnér, E.S.J. Expressing recombinant selenoproteins using redefinition of a single UAG codon in an RF1-depleted *E. coli* host strain. *Methods Enzymol.* **2022**, *662*, 95–118. [CrossRef] [PubMed]
32. Chung, C.Z.; Miller, C.; Söll, D.; Krahn, N. Introducing selenocysteine into recombinant proteins in *Escherichia coli*. *Curr. Protoc.* **2021**, *1*, e54. [CrossRef] [PubMed]

33. Cheng, R.; Liu, J.; Wang, L.; Forstner, M.B.; Rozovsky, S. Methods | Re-engineering the site-specific Incorporation of selenocysteine into proteins. In *Encyclopedia of Biological Chemistry III*; Elsevier: Amsterdam, The Netherlands, 2021; pp. 757–765. [CrossRef]
34. Mukai, T.; Sevostyanova, A.; Suzuki, T.; Fu, X.; Söll, D. A facile method for producing selenocysteine-containing proteins. *Angew. Chem. Int. Ed. Engl.* **2018**, *57*, 7215–7219. [CrossRef] [PubMed]
35. Rakauskaitė, R.; Urbanavičiūtė, G.; Rukšėnaitė, A.; Liutkevičiūtė, Z.; Juškėnas, R.; Masevičius, V.; Klimašauskas, S. Biosynthetic selenoproteins with genetically encoded photocaged selenocysteines. *Chem. Commun.* **2015**, *51*, 8245–8248. [CrossRef]
36. Welegedara, A.P.; Adams, L.A.; Huber, T.; Graham, B.; Otting, G. Site-specific incorporation of selenocysteine by genetic encoding as a photocaged unnatural amino acid. *Bioconjug. Chem.* **2018**, *29*, 2257–2264. [CrossRef] [PubMed]
37. Liu, J.; Zheng, F.; Cheng, R.; Li, S.; Rozovsky, S.; Wang, Q.; Wang, L. Site-specific incorporation of selenocysteine using an expanded genetic code and palladium-mediated chemical deprotection. *J. Am. Chem. Soc.* **2018**, *140*, 8807–8816. [CrossRef]
38. Peeler, J.C.; Falco, J.A.; Kelemen, R.E.; Abo, M.; Chartier, B.V.; Edinger, L.C.; Chen, J.; Chatterjee, A.; Weerapana, E. Generation of recombinant mammalian selenoproteins through genetic code expansion with photocaged selenocysteine. *ACS Chem. Biol.* **2020**, *15*, 1535–1540. [CrossRef]
39. Peeler, J.C.; Weerapana, E. Expression of selenoproteins via genetic code expansion in mammalian cells. *Methods Enzymol.* **2022**, *662*, 143–158. [CrossRef]
40. Kryukov, G.V.; Gladyshev, V.N. Mammalian selenoprotein gene signature: Identification and functional analysis of selenoprotein genes using bioinformatics methods. *Methods Enzymol.* **2002**, *347*, 84–100. [CrossRef]
41. Kryukov, G.V.; Castellano, S.; Novoselov, S.V.; Lobanov, A.V.; Zehtab, O.; Guigó, R.; Gladyshev, V.N. Characterization of mammalian selenoproteomes. *Science* **2003**, *300*, 1439–1443. [CrossRef]
42. Wingler, K.; Böcher, M.; Flohé, L.; Kollmus, H.; Brigelius-Flohé, R. mRNA stability and selenocysteine insertion sequence efficiency rank gastrointestinal glutathione peroxidase high in the hierarchy of selenoproteins. *Eur. J. Biochem.* **1999**, *259*, 149–157. [CrossRef]
43. Low, S.C.; Grundner-Culemann, E.; Harney, J.W.; Berry, M.J. SECIS-SBP2 interactions dictate selenocysteine incorporation efficiency and selenoprotein hierarchy. *EMBO J.* **2000**, *19*, 6882–6890. [CrossRef]
44. Sonet, J.; Bulteau, A.L.; Touat-Hamici, Z.; Mosca, M.; Bierla, K.; Mounicou, S.; Lobinski, R.; Chavatte, L. Selenoproteome expression studied by non-radioactive isotopic selenium-labeling in human cell lines. *Int. J. Mol. Sci.* **2021**, *22*, 7308. [CrossRef]
45. Ehrenreich, A.; Forchhammer, K.; Tormay, P.; Veprek, B.; Böck, A. Selenoprotein synthesis in *E. coli* Purification and characterisation of the enzyme catalysing selenium activation. *Eur. J. Biochem.* **1992**, *206*, 767–773. [CrossRef]
46. Noinaj, N.; Wattanasak, R.; Lee, D.Y.; Wally, J.L.; Piszczek, G.; Chock, P.B.; Stadtman, T.C.; Buchanan, S.K. Structural insights into the catalytic mechanism of Escherichia coli selenophosphate synthetase. *J. Bacteriol.* **2012**, *194*, 499–508. [CrossRef] [PubMed]
47. Manta, B.; Makarova, N.E.; Mariotti, M. The selenophosphate synthetase family: A review. *Free Radic. Biol. Med.* **2022**, *192*, 63–76. [CrossRef] [PubMed]
48. Bang, J.; Kang, D.; Jung, J.; Yoo, T.J.; Shim, M.S.; Gladyshev, V.N.; Tsuji, P.A.; Hatfield, D.L.; Kim, J.H.; Lee, B.J. SEPHS1: Its evolution, function and roles in development and diseases. *Arch. Biochem. Biophys.* **2022**, *730*, 109426. [CrossRef]
49. Lobanov, A.V.; Hatfield, D.L.; Gladyshev, V.N. Selenoproteinless animals: Selenophosphate synthetase SPS1 functions in a pathway unrelated to selenocysteine biosynthesis. *Protein Sci.* **2008**, *17*, 176–182. [CrossRef]
50. Itoh, Y.; Sekine, S.; Matsumoto, E.; Akasaka, R.; Takemoto, C.; Shirouzu, M.; Yokoyama, S. Structure of selenophosphate synthetase essential for selenium incorporation into proteins and RNAs. *J. Mol. Biol.* **2009**, *385*, 1456–1469. [CrossRef]
51. Tobe, R.; Mihara, H. Delivery of selenium to selenophosphate synthetase for selenoprotein biosynthesis. *Biochim. Biophys. Acta. Gen. Subj.* **2018**, *1862*, 2433–2440. [CrossRef]
52. Ogasawara, Y.; Lacourciere, G.; Stadtman, T.C. Formation of a selenium-substituted rhodanese by reaction with selenite and glutathione: Possible role of a protein perselenide in a selenium delivery system. *Proc. Natl. Acad. Sci. USA* **2001**, *98*, 9494–9498. [CrossRef] [PubMed]
53. Motsenbocker, M.A.; Tappel, A.L. Selenocysteine-containing proteins from rat and monkey plasma. *Biochim. Biophys. Acta* **1982**, *704*, 253–260. [CrossRef] [PubMed]
54. Burk, R.F.; Hill, K.E. Selenoprotein P-expression, functions, and roles in mammals. *Biochim. Biophys. Acta* **2009**, *1790*, 1441–1447. [CrossRef]
55. Burk, R.F.; Hill, K.E. Regulation of selenium metabolism and transport. *Annu. Rev. Nutr.* **2015**, *35*, 109–134. [CrossRef]
56. Shetty, S.; Copeland, P.R. Molecular mechanism of selenoprotein P synthesis. *Biochim. Biophys. Acta* **2018**, *186*, 22506–22510. [CrossRef]
57. Olson, G.E.; Winfrey, V.P.; Hill, K.E.; Burk, R.F. Megalin mediates selenoprotein P uptake by kidney proximal tubule epithelial cells. *J. Biol. Chem.* **2008**, *283*, 6854–6860. [CrossRef]
58. Burk, R.F.; Hill, K.E.; Motley, A.K.; Winfrey, V.P.; Kurokawa, S.; Mitchell, S.L.; Zhang, W. Selenoprotein P and apolipoprotein E receptor-2 interact at the blood-brain barrier and also within the brain to maintain an essential selenium pool that protects against neurodegeneration. *FASEB J.* **2014**, *28*, 3579–3588. [CrossRef]
59. Olson, G.E.; Winfrey, V.P.; Nagdas, S.K.; Hill, K.E.; Burk, R.F. Apolipoprotein E receptor-2 (ApoER2) mediates selenium uptake from selenoprotein P by the mouse testis. *J. Biol. Chem.* **2007**, *282*, 12290–12297. [CrossRef]
60. Brigelius-Flohé, R.; Maiorino, M. Glutathione peroxidases. *Biochim. Biophys. Acta* **2013**, *1830*, 3289–3303. [CrossRef]
61. Labunsk, V.M.; Hatfield, D.L.; Gladyshev, V.N. Selenoproteins: Molecular pathways and physiological roles. *Physiol. Rev.* **2014**, *94*, 739–777. [CrossRef]

62. Esworthy, R.S.; Doroshow, J.H.; Chu, F.F. The beginning of GPX2 and 30 years later. *Free Radic. Biol. Med.* **2022**, *188*, 419–433. [CrossRef]
63. Dalziel, K.; Dickinson, F.M. The kinetics and mechanism of liver alcohol dehydrogenase with primary and secondary alcohols as substrates. *Biochem. J.* **1966**, *100*, 34–46. [CrossRef] [PubMed]
64. Chaudière, J.; Tappel, A.L. Purification and characterization of selenium-glutathione peroxidase from hamster liver. *Arch. Biochem. Biophys.* **1983**, *226*, 448–457. [CrossRef] [PubMed]
65. Chaudière, J.; Wilhelmsen, E.C.; Tappel, A.L. Mechanism of selenium-glutathione peroxidase and its inhibition by mercaptocarboxylic acids and other mercaptans. *J. Biol. Chem.* **1984**, *259*, 1043–1050. [CrossRef]
66. Hall, M.D.; Marshall, T.S.; Kwit, A.D.; Miller Jenkins, L.M.; Dulcey, A.E.; Madigan, J.P.; Pluchino, K.M.; Goldsborough, A.S.; Brimacombe, K.R.; Griffiths, G.L.; et al. Inhibition of glutathione peroxidase mediates the collateral sensitivity of multidrug-resistant cells to tiopronin. *J. Biol. Chem.* **2014**, *289*, 21473–21489. [CrossRef] [PubMed]
67. Cheff, D.M.; Huang, C.; Scholzen, K.C.; Gencheva, R.; Ronzetti, M.H.; Cheng, Q.; Hall, M.D.; Arnér, E.S.J. The ferroptosis inducing compounds RSL3 and ML162 are not direct inhibitors of GPX4 but of TXNRD1. *Redox Biol.* **2023**, *62*, 102703. [CrossRef]
68. Ho, Y.S.; Magnenat, J.L.; Bronson, R.T.; Cao, J.; Gargano, M.; Sugawara, M.; Funk, C.D. Mice deficient in cellular glutathione peroxidase develop normally and show no increased sensitivity to hyperoxia. *J. Biol. Chem.* **1997**, *272*, 16644–16651. [CrossRef] [PubMed]
69. Klivenyi, P.; Andreassen, O.A.; Ferrante, R.J.; Dedeoglu, A.; Mueller, G.; Lancelot, E.; Bogdanov, M.; Andersen, J.K.; Jiang, D.; Beal, M.F. Mice deficient in cellular glutathione peroxidase show increased vulnerability to malonate, 3-nitropropionic acid, and 1-methyl-4-phenyl-1,2,5,6-tetrahydropyridine. *J. Neurosci.* **2000**, *20*, 1–7. [CrossRef]
70. Cheng, W.H.; Ho, Y.S.; Valentine, B.A.; Ross, D.A.; Combs, G.F.; Lei, X.G. Cellular glutathione peroxidase is the mediator of body selenium to protect against paraquat lethality in transgenic mice. *J. Nutr.* **1998**, *128*, 1070–1076. [CrossRef]
71. McClung, J.P.; Roneker, C.A.; Mu, W.; Lisk, D.J.; Langlais, P.; Liu, F.; Lei, X.G. Development of insulin resistance and obesity in mice overexpressing cellular glutathione peroxidase. *Proc. Natl. Acad. Sci. USA* **2004**, *101*, 8852–8857. [CrossRef]
72. Wang, X.D.; Vatamaniuk, M.Z.; Wang, S.K.; Roneker, C.A.; Simmons, R.A.; Lei, X.G. Molecular mechanisms for hyperinsulinaemia induced by overproduction of selenium-dependent glutathione peroxidase-1 in mice. *Diabetologia* **2008**, *51*, 1515–1524. [CrossRef] [PubMed]
73. Huang, J.Q.; Zhou, J.C.; Wu, Y.Y.; Ren, F.Z.; Lei, X.G. Role of glutathione peroxidase 1 in glucose and lipid metabolism-related diseases. *Free Radic. Biol. Med.* **2018**, *127*, 108–115. [CrossRef] [PubMed]
74. Barquissau, V.; Capel, F.; Dardevet, D.; Feillet-Coudray, C.; Gallinier, A.; Chauvin, M.A.; Rieusset, J.; Morio, B. Reactive oxygen species enhance mitochondrial function, insulin sensitivity and glucose uptake in skeletal muscle of senescence accelerated prone mice SAMP8. *Free Radic. Biol. Med.* **2017**, *113*, 267–279. [CrossRef] [PubMed]
75. Harmon, J.S.; Bogdani, M.; Parazzoli, S.D.; Mak, S.S.; Oseid, E.A.; Berghmans, M.; Leboeuf, R.C.; Robertson, R.P. Beta-cell-specific overexpression of glutathione peroxidase preserves intranuclear MafA and reverses diabetes in db/db mice. *Endocrinology* **2009**, *150*, 4855–4862. [CrossRef] [PubMed]
76. Lein, X.G.; Vatamaniuk, M.Z. Two tales of antioxidant enzymes on beta cells and diabetes. *Antioxid. Redox Signal.* **2011**, *14*, 489–503.
77. Zhang, Y.; Han, S.J.; Park, I.; Kim, I.; Chay, K.O.; Kim, S.M.; Jang, D.I.; Lee, T.H.; Lee, S.R. Redox regulation of the tumor suppressor PTEN by hydrogen peroxide and tert-butyl hydroperoxide. *Int. J. Mol. Sci.* **2017**, *18*, 982. [CrossRef]
78. Han, S.J.; Zhang, Y.; Kim, I.; Chay, K.O.; Yoon, H.J.; Jang, D.I.; Yang, S.Y.; Park, J.; Woo, H.A.; Park, I.; et al. Redox regulation of the tumor suppressor PTEN by the thioredoxin system and cumene hydroperoxide. *Free Radic. Biol. Med.* **2017**, *112*, 277–286. [CrossRef]
79. Xirouchaki, C.E.; Jia, Y.; McGrath, M.J.; Greatorex, S.; Tran, M.; Merry, T.L.; Hong, D.; Eramo, M.J.; Broome, S.C.; Woodhead, J.S.T.; et al. Skeletal muscle NOX4 is required for adaptive responses that prevent insulin resistance. *Sci Adv.* **2021**, *7*, eabl4988. [CrossRef]
80. Eberhardt, R.T.; Forgione, M.A.; Cap, A.; Leopold, J.A.; Rudd, M.A.; Trolliet, M.; Heydrick, S.; Stark, R.; Klings, E.S.; Moldovan, N.I.; et al. Endothelial dysfunction in a murine model of mild hyperhomocyst(e)inemia. *J. Clin. Investig.* **2000**, *106*, 483–491. [CrossRef]
81. Forgione, M.A.; Weiss, N.; Heydrick, S.; Cap, A.; Klings, E.S.; Bierl, C.; Eberhardt, R.T.; Farber, H.W.; Loscalzo, J. Cellular glutathione peroxidase deficiency and endothelial dysfunction. *Am. J. Physiol. Heart Circ. Physiol.* **2002**, *282*, H1255–H1261. [CrossRef]
82. Weiss, N.; Zhang, Y.; Heydrick, S.; Bierl, C.; Loscalzo, J. Overexpression of cellular glutathione peroxidase rescues homocyst(e)ine-induced endothelial dysfunction. *Proc. Natl. Acad. Sci. USA* **2001**, *98*, 12503–12508. [CrossRef]
83. Upchurch, G.R., Jr.; Welch, G.N.; Fabian, A.J.; Freedman, J.E.; Johnson, J.L.; Keaney, J.F., Jr.; Loscalzo, J. Homocyst(e)ine decreases bioavailable nitric oxide by a mechanism involving glutathione peroxidase. *J. Biol. Chem.* **1999**, *272*, 17012–17017. [CrossRef]
84. Handy, D.E.; Zhang, Y.; Loscalzo, J. Homocysteine down-regulates cellular glutathione peroxidase (GPx1) by decreasing translation. *J. Biol. Chem.* **2005**, *280*, 15518–15525. [CrossRef] [PubMed]
85. Chu, F.F.; Doroshow, J.H.; Esworthy, R.S. Expression, characterization, and tissue distribution of a new cellular selenium-dependent glutathione peroxidase, GSHPx-GI. *J. Biol. Chem.* **1993**, *268*, 2571–2576. [CrossRef] [PubMed]

86. Esworthy, R.S.; Swiderek, K.M.; Ho, Y.S.; Chu, F.F. Selenium-dependent glutathione peroxidase-GI is a major glutathione peroxidase activity in the mucosal epithelium of rodent intestine. *Biochim. Biophys. Acta* **1998**, *1381*, 213–226. [CrossRef] [PubMed]
87. Guo, X.; Song, J.; Guan, T.; Wang, S.; Wang, Y.; Meng, Y.; Guo, J.; Li, T.; Ma, C.; Wei, J. Characterization of recombinant human gastrointestinal glutathione peroxidase mutant produced in *Escherichia coli*. *Free Radic. Res.* **2015**, *49*, 228–235. [CrossRef]
88. Florian, S.; Wingler, K.; Schmehl, K.; Jacobasch, G.; Kreuzer, O.J.; Meyerhof, W.; Brigelius-Flohé, R. Cellular and subcellular localization of gastrointestinal glutathione peroxidase in normal and malignant human intestinal tissue. *Free Radic. Res.* **2001**, *35*, 655–663. [CrossRef]
89. Esworthy, R.S.; Mann, J.R.; Sam, M.; Chu, F.F. Low glutathione peroxidase activity in Gpx1 knockout mice protects jejunum crypts from gamma-irradiation damage. *Am. J. Physiol. Gastrointest. Liver Physiol.* **2000**, *279*, G426–G436. [CrossRef]
90. Florian, S.; Krehl, S.; Loewinger, M.; Kipp, A.; Banning, A.; Esworthy, S.; Chu, F.F.; Brigelius-Flohé, R. Loss of GPx2 increases apoptosis, mitosis, and GPx1 expression in the intestine of mice. *Free Radic. Biol. Med.* **2010**, *49*, 1694–1702. [CrossRef]
91. Pinto, D.; Gregorieff, A.; Begthel, H.; Clevers, H. Canonical Wnt signals are essential for homeostasis of the intestinal epithelium. *Genes Dev.* **2003**, *17*, 1709–1713. [CrossRef]
92. Kipp, A.; Banning, A.; Brigelius-Flohé, R. Activation of the glutathione peroxidase2 (GPx2) promoter by beta-catenin. *Biol. Chem.* **2007**, *388*, 1027–1033. [CrossRef]
93. Kipp, A.P.; Müller, M.F.; Göken, E.M.; Deubel, S.; Brigelius-Flohé, R. The selenoproteins GPx2, TrxR2 and TrxR3 are regulated by Wnt signalling in the intestinal epithelium. *Biochim. Biophys. Acta* **2012**, *1820*, 1588–1596. [CrossRef]
94. Pérez, S.; Taléns-Visconti, R.; Rius-Pérez, S.; Finamor, I.; Sastre, J. Redox signaling in the gastrointestinal tract. *Free Radic. Biol. Med.* **2017**, *104*, 75–103. [CrossRef]
95. Wilson, C.L.; Ouellette, A.J.; Satchell, D.P.; Ayabe, T.; López-Boado, Y.S.; Stratman, J.L.; Hultgren, S.J.; Matrisian, L.M.; Parks, W.C. Regulation of intestinal alpha-defensin activation by the metalloproteinase matrilysin in innate host defense. *Science* **1999**, *286*, 113–117. [CrossRef]
96. Dittrich, A.M.; Meyer, H.A.; Krokowski, M.; Quarcoo, D.; Ahrens, B.; Kube, S.M.; Witzenrath, M.; Esworthy, R.S.; Chu, F.F.; Hamelmann, E. Glutathione peroxidase-2 protects from allergen-induced airway inflammation in mice. *Eur. Respir. J.* **2010**, *35*, 1148–1154. [CrossRef]
97. Cho, H.Y.; Jedlicka, A.E.; Reddy, S.P.; Kensler, T.W.; Yamamoto, M.; Zhang, L.Y.; Kleeberger, S.R. Role of Nrf2 in protection against hyperoxic lung injury in mice. *Am. J. Respir. Cell. Mol. Biol.* **2002**, *26*, 175–182. [CrossRef]
98. Singh, A.; Rangasamy, T.; Thimmulappa, R.K.; Lee, H.; Osburn, W.O.; Brigelius-Flohé, R.; Kensler, T.W.; Yamamoto, M.; Biswal, S. Glutathione peroxidase 2, the major cigarette smoke-inducible isoform of GPX in lungs, is regulated by Nrf2. *Am. J. Respir. Cell. Mol. Biol.* **2006**, *35*, 639–650. [CrossRef]
99. Cho, H.Y.; Miller-DeGraff, L.; Blankenship-Paris, T.; Wang, X.; Bell, D.A.; Lih, F.; Deterding, L.; Panduri, V.; Morgan, D.L.; Yamamoto, M.; et al. Sulforaphane enriched transcriptome of lung mitochondrial energy metabolism and provided pulmonary injury protection via Nrf2 in mice. *Toxicol. Appl. Pharmacol.* **2019**, *364*, 29–44. [CrossRef] [PubMed]
100. Baek, I.J.; Yon, J.M.; Lee, S.R.; Kim, M.R.; Hong, J.T.; Lee, B.J.; Yun, Y.W.; Nam, S.Y. Differential expression of gastrointestinal glutathione peroxidase (GI-GPx) gene during mouse organogenesis. *Anat. Histol. Embryol.* **2011**, *40*, 210–218. [CrossRef] [PubMed]
101. Al-Taie, O.H.; Uceyler, N.; Eubner, U.; Jakob, F.; Mörk, H.; Scheurlen, M.; Brigelius-Flohé, R.; Schöttker, K.; Abel, J.; Thalheimer, A.; et al. Expression profiling and genetic alterations of the selenoproteins GI-GPx and SePP in colorectal carcinogenesis. *Nutr. Cancer* **2004**, *48*, 6–14. [CrossRef] [PubMed]
102. Chiu, S.T.; Hsieh, F.J.; Chen, S.W.; Chen, C.L.; Shu, H.F.; Li, H. Clinicopathologic correlation of up-regulated genes identified using cDNA microarray and real-time reverse transcription-PCR in human colorectal cancer. *Cancer Epidemiol. Biomark. Prev.* **2005**, *14*, 437–443. [CrossRef]
103. Mörk, H.; al-Taie, O.H.; Bähr, K.; Zierer, A.; Beck, C.; Scheurlen, M.; Jakob, F.; Köhrle, J. Inverse mRNA expression of the selenocysteine-containing proteins GI-GPx and SeP in colorectal adenomas compared with adjacent normal mucosa. *Nutr. Cancer* **2000**, *37*, 108–116. [CrossRef]
104. Mörk, H.; Scheurlen, M.; Al-Taie, O.; Zierer, A.; Kraus, M.; Schöttker, K.; Jakob, F.; Köhrle, J. Glutathione peroxidase isoforms as part of the local antioxidative defense system in normal and Barrett's esophagus. *Int. J. Cancer* **2003**, *105*, 300–304. [CrossRef] [PubMed]
105. Serewko, M.M.; Popa, C.; Dahler, A.L.; Smith, L.; Strutton, G.M.; Coman, W.; Dicker, A.J.; Saunders, N.A. Alterations in gene expression and activity during squamous cell carcinoma development. *Cancer Res.* **2002**, *62*, 3759–3765. [PubMed]
106. Woenckhaus, M.; Klein-Hitpass, L.; Grepmeier, U.; Merk, J.; Pfeifer, M.; Wild, P.; Bettstetter, M.; Wuensch, P.; Blaszyk, H.; Hartmann, A.; et al. Smoking and cancer-related gene expression in bronchial epithelium and non-small-cell lung cancers. *J. Pathol.* **2006**, *210*, 192–204. [CrossRef] [PubMed]
107. Li, F.; Dai, L.; Niu, J. GPX2 silencing relieves epithelial-mesenchymal transition, invasion, and metastasis in pancreatic cancer by downregulating Wnt pathway. *J. Cell. Physiol.* **2019**, *235*, 7780–7790. [CrossRef] [PubMed]
108. Wang, Y.; Cao, P.; Alshwmi, M.; Jiang, N.; Xiao, Z.; Jiang, F.; Gu, J.; Wang, X.; Sun, X.; Li, S. GPx2 suppression of H_2O_2 stress regulates cervical cancer metastasis and apoptosis via activation of the β-catenin-WNT pathway. *Onco Targets Ther.* **2019**, *12*, 6639–6651. [CrossRef] [PubMed]

109. Emmink, B.L.; Laoukili, J.; Kipp, A.P.; Koster, J.; Govaert, K.M.; Fatrai, S.; Verheem, A.; Steller, E.J.; Brigelius-Flohé, R.; Jimenez, C.R.; et al. GPx2 suppression of H_2O_2 stress links the formation of differentiated tumor mass to metastatic capacity in colorectal cancer. *Cancer Res.* **2014**, *74*, 6717–6730. [CrossRef]
110. Yan, W.; Chen, X. GPX2, a direct target of p63, inhibits oxidative stress-induced apoptosis in a p53-dependent manner. *J. Biol. Chem.* **2006**, *281*, 7856–7862. [CrossRef]
111. Banning, A.; Deubel, S.; Kluth, D.; Zhou, Z.; Brigelius-Flohé, R. The GI-GPx gene is a target for Nrf2. *Mol. Cell. Biol.* **2005**, *25*, 4914–4923. [CrossRef]
112. Yamamoto, M.; Kensler, T.W.; Motohashi, H. The KEAP1-Nrf2 System: A thiol-based sensor-effector apparatus for maintaining redox homeostasis. *Physiol. Rev.* **2018**, *98*, 1169–1203. [CrossRef]
113. Brigelius-Flohé, R.; Müller, M.; Lippmann, D.; Kipp, A.P. The yin and yang of nrf2-regulated selenoproteins in carcinogenesis. *Int. J. Cell Biol.* **2012**, *2012*, 486147. [CrossRef]
114. Menegon, S.; Columbano, A.; Giordano, S. The Dual Roles of Nrf2 in Cancer. *Trends Mol. Med.* **2016**, *22*, 578–593. [CrossRef] [PubMed]
115. Wu, S.; Lu, H.; Bai, Y. Nrf2 in cancers: A double-edged sword. *Cancer Med.* **2019**, *8*, 2252–2267. [CrossRef] [PubMed]
116. DeNicola, G.M.; Karreth, F.A.; Humpton, T.J.; Gopinathan, A.; Wei, C.; Frese, K.; Mangal, D.; Yu, K.H.; Yeo, C.J.; Calhoun, E.S.; et al. Oncogene-induced Nrf2 transcription promotes ROS detoxification and tumorigenesis. *Nature* **2011**, *475*, 106–109. [CrossRef]
117. Zimta, A.A.; Cenariu, D.; Irimie, A.; Magdo, L.; Nabavi, S.M.; Atanasov, A.G.; Berindan-Neagoe, I. The Role of Nrf2 Activity in Cancer Development and Progression. *Cancers* **2019**, *11*, 1755. [CrossRef] [PubMed]
118. Narayanankutty, A.; Job, J.T.; Narayanankutty, V. Glutathione, an Antioxidant Tripeptide: Dual Roles in Carcinogenesis and Chemoprevention. *Curr. Protein Pept. Sci.* **2019**, *20*, 907–917. [CrossRef] [PubMed]
119. Liu, T.; Kan, X.F.; Ma, C.; Chen, L.L.; Cheng, T.T.; Zou, Z.W.; Li, Y.; Cao, F.J.; Zhang, W.J.; Yao, J.; et al. GPX2 overexpression indicates poor prognosis in patients with hepatocellular carcinoma. *Tumour Biol.* **2017**, *39*, 1010428317700410. [CrossRef]
120. Weitzel, F.; Wendel, A. Selenoenzymes regulate the activity of leukocyte 5-lipoxygenase via the peroxide tone. *J. Biol. Chem.* **1993**, *268*, 6288–6292. [CrossRef]
121. Bürkert, E.; Arnold, C.; Hammarberg, T.; Rådmark, O.; Steinhilber, D.; Werz, O. The C2-like beta-barrel domain mediates the Ca^{2+}-dependent resistance of 5-lipoxygenase activity against inhibition by glutathione peroxidase-1. *J. Biol. Chem.* **2003**, *278*, 42846–42853. [CrossRef]
122. Imai, H.; Narashima, K.; Arai, M.; Sakamoto, H.; Chiba, N.; Nakagawa, Y. Suppression of leukotriene formation in RBL-2H3 cells that overexpressed phospholipid hydroperoxide glutathione peroxidase. *J. Biol. Chem.* **1998**, *273*, 1990–1997. [CrossRef] [PubMed]
123. Yang, X.H.; Zhuang, M.K.; Xie, W.H.; Du, F.; Huang, Y.H.; Chen, Z.X.; Chen, F.L.; Wang, X.Z. 12-Lipoxygenase promotes epithelial-mesenchymal transition via the Wnt/β-catenin signaling pathway in gastric cancer cells. *Onco Targets Ther.* **2019**, *12*, 5551–5561. [CrossRef] [PubMed]
124. Banning, A.; Florian, S.; Deubel, S.; Thalmann, S.; Müller-Schmehl, K.; Jacobasch, G.; Brigelius-Flohé, R. GPx2 counteracts PGE2 production by dampening COX-2 and mPGES-1 expression in human colon cancer cells. *Antioxid Redox Signal.* **2008**, *10*, 1491–1500. [CrossRef] [PubMed]
125. Te Velde, A.A.; Pronk, I.; de Kort, F.; Stokkers, P.C. Glutathione peroxidase 2 and aquaporin 8 as new markers for colonic inflammation in experimental colitis and inflammatory bowel diseases: An important role for H_2O_2? *Eur. J Gastroenterol. Hepatol.* **2008**, *20*, 555–560. [CrossRef]
126. Esworthy, R.S.; Aranda, R.; Martín, M.G.; Doroshow, J.H.; Binder, S.W.; Chu, F.F. Mice with combined disruption of Gpx1 and Gpx2 genes have colitis. *Am. J. Physiol. Gastrointest. Liver Physiol.* **2001**, *281*, G848–G855. [CrossRef]
127. Chu, F.F.; Esworthy, R.S.; Chu, P.G.; Longmate, J.A.; Huycke, M.M.; Wilczynski, S.; Doroshow, J.H. Bacteria-induced intestinal cancer in mice with disrupted Gpx1 and Gpx2 genes. *Cancer Res.* **2004**, *64*, 962–968. [CrossRef]
128. Esworthy, R.S.; Kim, B.W.; Chow, J.; Shen, B.; Doroshow, J.H.; Chu, F.F. Nox1 causes ileocolitis in mice deficient in glutathione peroxidase-1 and -2. *Free Radic. Biol. Med.* **2014**, *68*, 315–325. [CrossRef]
129. Esworthy, R.S.; Yang, L.; Frankel, P.H.; Chu, F.F. Epithelium-specific glutathione peroxidase, Gpx2, is involved in the prevention of intestinal inflammation in selenium-deficient mice. *J. Nutr.* **2005**, *135*, 740–745. [CrossRef]
130. Choi, J.; Ou, J.H. Mechanisms of liver injury. III. Oxidative stress in the pathogenesis of hepatitis C virus. *Am. J. Physiol. Gastrointest. Liver Physiol.* **2006**, *290*, G847–G851. [CrossRef]
131. Choi, J. Oxidative stress, endogenous antioxidants, alcohol, and hepatitis C: Pathogenic interactions and therapeutic considerations. *Free Radic. Biol. Med.* **2012**, *52*, 1135–1150. [CrossRef] [PubMed]
132. Medvedev, R.; Ploen, D.; Hildt, E. HCV and Oxidative Stress: Implications for HCV Life Cycle and HCV-Associated Pathogenesis. *Oxid. Med. Cell. Longev.* **2016**, *2016*, 9012580. [CrossRef]
133. Morbitzer, M.; Herget, T. Expression of gastrointestinal glutathione peroxidase is inversely correlated to the presence of hepatitis C virus subgenomic RNA in human liver cells. *J. Biol. Chem.* **2005**, *280*, 8831–8841. [CrossRef]
134. MacCallum, P.R.; Jack, S.C.; Egan, P.A.; McDermott, B.T.; Elliott, R.M.; Chan, S.W. Cap-dependent and hepatitis C virus internal ribosome entry site-mediated translation are modulated by phosphorylation of eIF2alpha under oxidative stress. *J. Gen. Virol.* **2006**, *87 Pt 11*, 3251–3262. [CrossRef]
135. Jack, S.C.; Chan, S.W. The role of PERK and GCN2 in basal and hydrogen peroxide-regulated translation from the hepatitis C virus internal ribosome entry site. *Virus Genes* **2011**, *43*, 208–214. [CrossRef]

136. Nguyen, B.N.; Okuno, Y.; Ajiro, M.; Iida, K.; Denawa, M.; Yamamoto, M.; Sakamoto, N.; Kagechika, H.; Hagiwara, M. Retinoid derivative Tp80 exhibits anti-hepatitis C virus activity through restoration of GI-GPx expression. *J. Med. Virol.* **2017**, *89*, 1224–1234. [CrossRef]
137. Whitin, J.C.; Bhamre, S.; Tham, D.M.; Cohen, H.J. Extracellular glutathione peroxidase is secreted basolaterally by human renal proximal tubule cells. *Am. J. Physiol. Ren. Physiol.* **2002**, *283*, F20–F28. [CrossRef]
138. Avissar, N.; Kerl, E.A.; Baker, S.S.; Cohen, H.J. Extracellular glutathione peroxidase mRNA and protein in human cell lines. *Arch. Biochem. Biophys.* **1994**, *309*, 239–246. [CrossRef] [PubMed]
139. Björnstedt, M.; Xue, J.; Huang, W.; Akesson, B.; Holmgren, A. The thioredoxin and glutaredoxin systems are efficient electron donors to human plasma glutathione peroxidase. *J. Biol. Chem.* **1994**, *269*, 29382–29384. [CrossRef]
140. Freedman, J.E.; Loscalzo, J.; Benoit, S.E.; Valeri, C.R.; Barnard, M.R.; Michelson, A.D. Decreased platelet inhibition by nitric oxide in two brothers with a history of arterial thrombosis. *J. Clin. Investig.* **1996**, *97*, 979–987. [CrossRef] [PubMed]
141. Kenet, G.; Freedman, J.; Shenkman, B.; Regina, E.; Brok-Simoni, F.; Holzman, F.; Vavva, F.; Brand, N.; Michelson, A.; Trolliet, M.; et al. Plasma glutathione peroxidase deficiency and platelet insensitivity to nitric oxide in children with familial stroke. *Arterioscler. Thromb. Vasc. Biol.* **1999**, *19*, 2017–2023. [CrossRef] [PubMed]
142. Jin, R.C.; Mahoney, C.E.; Anderson, L.; Ottaviano, F.; Croce, K.; Leopold, J.A.; Zhang, Y.Y.; Tang, S.S.; Handy, D.E.; Loscalzo, J. Glutathione peroxidase-3 deficiency promotes platelet-dependent thrombosis in vivo. *Circulation* **2011**, *123*, 1963–1973. [CrossRef] [PubMed]
143. Barrett, C.W.; Ning, W.; Chen, X.; Smith, J.J.; Washington, M.K.; Hill, K.E.; Coburn, L.A.; Peek, R.M.; Chaturvedi, R.; Wilson, K.T.; et al. Tumor suppressor function of the plasma glutathione peroxidase GPx3 in colitis-associated carcinoma. *Cancer Res.* **2013**, *73*, 1245–1255. [CrossRef] [PubMed]
144. Wang, Z.; Zhu, J.; Liu, Y.; Wang, Z.; Cao, X.; Gu, Y. Tumor-polarized GPX3+ AT2 lung epithelial cells promote premetastatic niche formation. *Proc. Natl. Acad. Sci. USA* **2022**, *119*, e2201899119. [CrossRef] [PubMed]
145. Ursini, F.; Maiorino, M.; Valente, M.; Ferri, L.; Gregolin, C. Purification from pig liver of a protein which protects liposomes and biomembranes from peroxidative degradation and exhibits glutathione peroxidase activity on phosphatidylcholine hydroperoxides. *Biochim. Biophys. Acta* **1982**, *710*, 197–211. [CrossRef]
146. Ursini, F.; Bosello Travain, V.; Cozza, G.; Miotto, G.; Roveri, A.; Toppo, S.; Maiorino, M. A white paper on phospholipid Hydroperoxide Glutathione Peroxidase (GPx4) forty years later. *Free Radic. Biol. Med.* **2022**, *188*, 117–133. [CrossRef]
147. Maiorino, M.; Chu, F.F.; Ursini, F.; Davies, K.J.; Doroshow, J.H.; Esworthy, R.S. Phospholipid hydroperoxide glutathione peroxidase is the 18-kDa selenoprotein expressed in human tumor cell lines. *J. Biol. Chem.* **1991**, *266*, 7728–7732. [CrossRef]
148. Brigelius-Flohé, R.; Aumann, K.D.; Blöcker, H.; Gross, G.; Kiess, M.; Klöppel, K.D.; Maiorino, M.; Roveri, A.; Schuckelt, R.; Usani, F.; et al. Phospholipid-hydroperoxide glutathione peroxidase. Genomic DNA, cDNA, and deduced amino acid sequence. *J. Biol. Chem.* **1994**, *269*, 7342–7348. [CrossRef]
149. Pushpa-Rekha, T.R.; Burdsall, A.L.; Oleksa, L.M.; Chisolm, G.M.; Driscoll, D.M. Rat phospholipid-hydroperoxide glutathione peroxidase. cDNA cloning and identification of multiple transcription and translation start sites. *J. Biol. Chem.* **1995**, *270*, 26993–26999. [CrossRef]
150. Thomas, J.P.; Geiger, P.G.; Maiorino, M.; Ursini, F.; Girotti, A.W. Enzymatic reduction of phospholipid and cholesterol hydroperoxides in artificial bilayers and lipoproteins. *Biochim. Biophys. Acta* **1990**, *1045*, 252–260. [CrossRef]
151. Cozza, G.; Rossetto, M.; Bosello-Travain, V.; Maiorino, M.; Roveri, A.; Toppo, S.; Zaccarin, M.; Zennaro, L.; Ursini, F. Glutathione peroxidase 4-catalyzed reduction of lipid hydroperoxides in membranes: The polar head of membrane phospholipids binds the enzyme and addresses the fatty acid hydroperoxide group toward the redox center. *Free Radic. Biol. Med.* **2017**, *112*, 1–11. [CrossRef]
152. Stolwijk, J.M.; Stefely, J.A.; Veling, M.T.; van't Erve, T.J.; Wagner, B.A.; Raife, T.J.; Buettner, G.R. Red blood cells contain enzymatically active GPx4 whose abundance anticorrelates with hemolysis during blood bank storage. *Redox Biol.* **2021**, *46*, 102073. [CrossRef]
153. Pfeifer, H.; Conrad, M.; Roethlein, D.; Kyriakopoulos, A.; Brielmeier, M.; Bornkamm, G.W.; Behne, D. Identification of a specific sperm nuclei selenoenzyme necessary for protamine thiol cross-linking during sperm maturation. *FASEB J.* **2001**, *15*, 1236–1238. [CrossRef]
154. Maiorino, M.; Roveri, A.; Benazzi, L.; Bosello, V.; Mauri, P.; Toppo, S.; Tosatto, S.C.; Ursini, F. Functional interaction of phospholipid hydroperoxide glutathione peroxidase with sperm mitochondrion-associated cysteine-rich protein discloses the adjacent cysteine motif as a new substrate of the selenoperoxidase. *J. Biol. Chem.* **2005**, *280*, 38395–38402. [CrossRef] [PubMed]
155. Schneider, M.; Förster, H.; Boersma, A.; Seiler, A.; Wehnes, H.; Sinowatz, F.; Neumüller, C.; Deutsch, M.J.; Walch, A.; Hrabé de Angelis, M.; et al. Mitochondrial glutathione peroxidase 4 disruption causes male infertility. *FASEB J.* **2009**, *23*, 3233–3242. [CrossRef] [PubMed]
156. Brütsch, S.H.; Rademacher, M.; Roth, S.R.; Müller, K.; Eder, S.; Viertel, D.; Franz, C.; Kuhn, H.; Borchert, A. Male subfertility induced by heterozygous expression of catalytically inactive glutathione peroxidase 4 is rescued in vivo by systemic inactivation of the Alox15 gene. *J. Biol. Chem.* **2016**, *291*, 23578–23588. [CrossRef]
157. Brütsch, S.H.; Wang, C.C.; Li, L.; Stender, H.; Neziroglu, N.; Richter, C.; Kuhn, H.; Borchert, A. Expression of inactive glutathione peroxidase 4 leads to embryonic lethality, and inactivation of the Alox15 gene does not rescue such knock-in mice. *Antioxid. Redox Signal.* **2015**, *22*, 281–293. [CrossRef] [PubMed]

158. Borchert, A.; Wang, C.C.; Ufer, C.; Schiebel, H.; Savaskan, N.E.; Kuhn, H. The role of phospholipid hydroperoxide glutathione peroxidase isoforms in murine embryogenesis. *J. Biol. Chem.* **2006**, *281*, 19655–19664. [CrossRef]
159. Ufer, C.; Wang, C.C. The Roles of Glutathione Peroxidases during Embryo Development. *Front. Mol. Neurosci.* **2011**, *4*, 1–13. [CrossRef]
160. Ingold, I.; Berndt, C.; Schmitt, S.; Doll, S.; Poschmann, G.; Buday, K.; Roveri, A.; Peng, X.; Porto Freitas, F.; Seibt, T.; et al. Selenium utilization by GPX4 is required to prevent hydroperoxide-induced ferroptosis. *Cell* **2018**, *172*, 409–422. [CrossRef]
161. Wenk, J.; Schüller, J.; Hinrichs, C.; Syrovets, T.; Azoitei, N.; Podda, M.; Wlaschek, M.; Brenneisen, P.; Schneider, L.A.; Sabiwalsky, A.; et al. Overexpression of phospholipid-hydroperoxide glutathione peroxidase in human dermal fibroblasts abrogates UVA irradiation-induced expression of interstitial collagenase/matrix metalloproteinase-1 by suppression of phosphatidylcholine hydroperoxide-mediated NFkappaB activation and interleukin-6 release. *J. Biol. Chem.* **2004**, *279*, 45634–45642. [PubMed]
162. Wu, J.; Sun, L.; Chen, X.; Du, F.; Shi, H.; Chen, C.; Chen, Z.J. Cyclic GMP-AMP is an endogenous second messenger in innate immune signaling by cytosolic DNA. *Science* **2013**, *339*, 826–830. [CrossRef]
163. Jia, M.; Qin, D.; Zhao, C.; Chai, L.; Yu, Z.; Wang, W.; Tong, L.; Lv, L.; Wang, Y.; Rehwinkel, J.; et al. Redox homeostasis maintained by GPX4 facilitates STING activation. *Nat. Immunol.* **2020**, *21*, 727–735. [CrossRef] [PubMed]
164. Seibt, T.M.; Proneth, B.; Conrad, M. Role of GPX4 in ferroptosis and its pharmacological implication. *Free Radic. Biol. Med.* **2019**, *133*, 144–152. [CrossRef]
165. Hirschhorn, T.; Stockwell, B.R. The development of the concept of ferroptosis. *Free Radic. Biol. Med.* **2019**, *133*, 130–143. [CrossRef] [PubMed]
166. Dixon, S.J.; Lemberg, K.M.; Lamprecht, M.R.; Skouta, R.; Zaitsev, E.M.; Gleason, C.E.; Patel, D.N.; Bauer, A.J.; Cantley, A.M.; Yang, W.S.; et al. Ferroptosis: An iron-dependent form of nonapoptotic cell death. *Cell* **2012**, *149*, 1060–1072. [CrossRef]
167. Lei, P.; Bai, T.; Sun, Y. Mechanisms of ferroptosis and relations with regulated cell death: A review. *Front. Physiol.* **2019**, *10*, 139. [CrossRef]
168. Seiler, A.; Schneider, M.; Förster, H.; Roth, S.; Wirth, E.K.; Culmsee, C.; Plesnila, N.; Kremmer, E.; Rådmark, O.; Wurst, W.; et al. Glutathione peroxidase 4 senses and translates oxidative stress into 12/15-lipoxygenase dependent- and AIF-mediated cell death. *Cell Metab.* **2008**, *8*, 237–248. [CrossRef]
169. Weaver, K.; Skouta, R. The Selenoprotein Glutathione Peroxidase 4: From Molecular Mechanisms to Novel Therapeutic Opportunities. *Biomedicines* **2022**, *10*, 891. [CrossRef] [PubMed]
170. Li, C.; Deng, X.; Zhang, W.; Xie, X.; Conrad, M.; Liu, Y.; Angeli, J.P.F.; Lai, L. Novel allosteric activators for ferroptosis regulator glutathione peroxidase 4. *J. Med. Chem.* **2019**, *62*, 266–275. [CrossRef] [PubMed]
171. Friedmann Angeli, J.P.; Schneider, M.; Proneth, B.; Tyurina, Y.Y.; Tyurin, V.A.; Hammond, V.J.; Herbach, N.; Aichler, M.; Walch, A.; Eggenhofer, E.; et al. Inactivation of the ferroptosis regulator Gpx4 triggers acute renal failure in mice. *Nat. Cell. Biol.* **2014**, *16*, 1180–1191. [CrossRef]
172. Skouta, R.; Dixon, S.J.; Wang, J.; Dunn DEOrman, M.; Shimada, K.; Rosenberg, P.A.; Lo, D.C.; Weinberg, J.M.; Linkermann, A.; Stockwell, B.R. Ferrostatins inhibit oxidative lipid damage and cell death in diverse disease models. *J. Am. Chem. Soc.* **2014**, *136*, 4551–4556. [CrossRef] [PubMed]
173. Feng, Y.; Madungwe, N.B.; Imam Aliagan, A.D.; Tombo, N.; Bopassa, J.C. Liproxstatin-1 protects the mouse myocardium against ischemia/reperfusion injury by decreasing VDAC1 levels and restoring GPX4 levels. *Biochem. Biophys. Res. Commun.* **2019**, *520*, 606–611. [CrossRef] [PubMed]
174. Miotto, G.; Rossetto, M.; Di Paolo, M.L.; Orian, L.; Venerando, R.; Roveri, A.; Vučković, A.M.; Bosello Travain, V.; Zaccarin, M.; Zennaro, L.; et al. Insight into the mechanism of ferroptosis inhibition by ferrostatin-1. *Redox Biol.* **2020**, *28*, 101328. [CrossRef]
175. Gao, M.; Jiang, X. To eat or not to eat—The metabolic flavor of ferroptosis. *Curr. Opin. Cell Biol.* **2018**, *51*, 58–64. [CrossRef] [PubMed]
176. Brigelius-Flohé, R.; Flohé, L. Regulatory phenomena in the glutathione peroxidase superfamily. *Antioxid. Redox Signal.* **2020**, *33*, 498–516. [CrossRef] [PubMed]
177. Randolph, J.T.; O'Connor, M.J.; Han, F.; Hutchins, C.W.; Siu, Y.A.; Cho, M.; Zheng, Y.; Hickson, J.A.; Markley, J.L.; Manaves, V.; et al. Discovery of a Potent Chloroacetamide GPX4 Inhibitor with Bioavailability to Enable Target Engagement in Mice, a Potential Tool Compound for Inducing Ferroptosis In Vivo. *J. Med. Chem.* **2023**, *66*, 3852–3865. [CrossRef]
178. Moosmayer, D.; Hilpmann, A.; Hoffmann, J.; Schnirch, L.; Zimmermann, K.; Badock, V.; Furst, L.; Eaton, J.K.; Viswanathan, V.S.; Schreiber, S.L.; et al. Crystal structures of the selenoprotein glutathione peroxidase 4 in its apo form and in complex with the covalently bound inhibitor ML162. *Acta Crystallogr. D Struct. Biol.* **2021**, *77*, 237–248. [CrossRef]
179. Eaton, J.K.; Furst, L.; Cai, L.L.; Viswanathan, V.S.; Schreiber, S.L. Structure-activity relationships of GPx4 inhibitor warheads. *Bioorg. Med. Chem. Lett.* **2020**, *30*, 127538. [CrossRef]
180. Vučković, A.M.; Bosello Travain, V.; Bordin, L.; Cozza, G.; Miotto, G.; Rossetto, M.; Toppo, S.; Venerando, R.; Zaccarin, M.; Maiorino, M.; et al. Inactivation of the glutathione peroxidase GPx4 by the ferroptosis-inducing molecule RSL3 requires the adaptor protein 14-3-3ε. *FEBS Lett.* **2020**, *594*, 611–624. [CrossRef]
181. Xi, J.; Tian, L.L.; Xi, J.; Girimpuhwe, D.; Huang, C.; Ma, R.; Yao, X.; Shi, D.; Bai, Z.; Wu, Q.X.; et al. Alterperylenol as a novel thioredoxin reductase inhibitor induces liver cancer cell apoptosis and ferroptosis. *J. Agric. Food Chem.* **2022**, *70*, 15763–15775. [CrossRef]

182. Carlisle, A.E.; Lee, N.; Matthew-Onabanjo, A.N.; Spears, M.E.; Park, S.J.; Youkana, D.; Doshi, M.B.; Peppers, A.; Li, R.; Joseph, A.B.; et al. Selenium detoxification is required for cancer-cell survival. *Nat. Metab.* **2020**, *2*, 603–611. [CrossRef] [PubMed]
183. Viswanathan, V.S.; Ryan, M.J.; Dhruv, H.D.; Gill, S.; Eichhoff, O.M.; Seashore-Ludlow, B.; Kaffenberger, S.D.; Eaton, J.K.; Shimada, K.; Aguirre, A.J.; et al. Dependency of a therapy-resistant state of cancer cells on a lipid peroxidase pathway. *Nature* **2017**, *547*, 453–457. [CrossRef] [PubMed]
184. Liu, H.; Schreiber, S.L.; Stockwell, B.R. Targeting Dependency on the GPX4 Lipid Peroxide Repair Pathway for Cancer Therapy. *Biochemistry* **2018**, *57*, 2059–2060. [CrossRef]
185. Yang, W.S.; SriRamaratnam, R.; Welsch, M.E.; Shimada, K.; Skouta, R.; Viswanathan, V.S.; Cheah, J.H.; Clemons, P.A.; Shamji, A.F.; Clish, C.B.; et al. Regulation of ferroptotic cancer cell death by GPX4. *Cell* **2014**, *156*, 317–331. [CrossRef] [PubMed]
186. Mathow, D.; Chessa, F.; Rabionet, M.; Kaden, S.; Jennemann, R.; Sandhoff, R.; Gröne, H.J.; Feuerborn, A. Zeb1 affects epithelial cell adhesion by diverting glycosphingolipid metabolism. *EMBO Rep.* **2015**, *16*, 321–331. [CrossRef] [PubMed]
187. Zou, Y.; Palte, M.J.; Deik, A.A.; Li, H.; Eaton, J.K.; Wang, W.; Tseng, Y.Y.; Deasy, R.; Kost-Alimova, M.; Dančík, V.; et al. A GPX4-dependent cancer cell state underlies the clear-cell morphology and confers sensitivity to ferroptosis. *Nat. Commun.* **2019**, *10*, 1617. [CrossRef]
188. Toppo, S.; Flohé, L.; Ursini, F.; Vanin, S.; Maiorino, M. Catalytic mechanisms and specificities of glutathione peroxidases: Variations of a basic scheme. *Biochim. Biophys. Acta* **2009**, *1790*, 1486–1500. [CrossRef]
189. Passaia, G.; Margis-Pinheiro, M. Glutathione peroxidases as redox sensor proteins in plant cells. *Plant Sci.* **2015**, *234*, 22–26. [CrossRef]
190. Maiorino, M.; Bosello-Travain, V.; Cozza, G.; Miotto, G.; Roveri, A.; Toppo, S.; Zaccarin, M.; Ursini, F. Understanding mammalian glutathione peroxidase 7 in the light of its homologs. *Free Radic. Biol. Med.* **2015**, *83*, 352–360. [CrossRef]
191. Bosello-Travain, V.; Conrad, M.; Cozza, G.; Negro, A.; Quartesan, S.; Rossetto, M.; Roveri, A.; Toppo, S.; Ursini, F.; Zaccarin, M.; et al. Protein disulfide isomerase and glutathione are alternative substrates in the one Cys catalytic cycle of glutathione peroxidase 7. *Biochim. Biophys. Acta* **2013**, *1830*, 3846–3857. [CrossRef]
192. Chaudière, J.; Courtin, O.; Leclaire, J. Glutathione oxidase activity of selenocystamine: A mechanistic study. *Arch. Biochem. Biophys.* **1992**, *296*, 328–336. [CrossRef] [PubMed]
193. Müller, A.; Cadenas, E.; Graf, P.; Sies, H. A novel biologically active seleno-organic compound—I. Glutathione peroxidase-like activity in vitro and antioxidant capacity of PZ 51 (Ebselen). *Biochem. Pharmacol.* **1984**, *33*, 3235–3239. [CrossRef] [PubMed]
194. Wendel, A.; Fausel, M.; Safayhi, H.; Tiegs, G.; Otter, R. A novel biologically active seleno-organic compound—II. Activity of PZ 51 in relation to glutathione peroxidase. *Biochem. Pharmacol.* **1984**, *33*, 3241–3245. [CrossRef]
195. Chaudière, J.; Yadan, J.C.; Erdelmeier, I.; Tailhan-Lomont, C.; Moutet, M. Design of new selenium-containing mimics of glutathione peroxidase. In *Oxidative Stress and Antioxidants*; Raven Press, Ltd.: New York, NY, USA, 1994; pp. 165–184.
196. d'Alessio, P.; Moutet, M.; Coudrier, E.; Darquenne, S.; Chaudière, J. ICAM-1 and VCAM-1 expression induced by TNF-alpha are inhibited by a glutathione peroxidase mimic. *Free Radic. Biol. Med.* **1998**, *24*, 979–987. [CrossRef]
197. Moutet, M.; d'Alessio, P.; Malette, P.; Devaux, V.; Chaudière, J. Glutathione peroxidase mimics prevent TNF-alpha- and neutrophil-induced endothelial alterations. *Free Radic. Biol. Med.* **1998**, *25*, 270–281. [CrossRef] [PubMed]
198. Chaudière, J.; Erdelmeier, I.; Moutet, M.; Yadan, J.C. One- versus two-electron transfers: Cytotoxic and cytoprotective effects of seleno-organic catalysts. In *Phosphorus, Sulfur, and Silicon and the Related Elements*; Taylor & Francis: Oxfordshire, UK, 1998; Volume 136, pp. 467–470.
199. Payne, N.C.; Barber, D.R.; Ruggles, E.L.; Hondal, R.J. Can dimedone be used to study selenoproteins? An investigation into the reactivity of dimedone toward oxidized forms of selenocysteine. *Protein Sci.* **2018**, *28*, 41–55. [CrossRef]
200. Liu, J.; Rozovsky, S. Contribution of selenocysteine to the peroxidase activity of selenoprotein S. *Biochemistry* **2013**, *52*, 5514–5516. [CrossRef]
201. Masuda, R.; Kimura, R.; Karasaki, T.; Sase, S.; Goto, K. Modeling the catalytic cycle of glutathione peroxidase by nuclear magnetic resonance spectroscopic analysis of selenocysteine selenenic acids. *J. Am. Chem. Soc.* **2021**, *143*, 6345–6350. [CrossRef]
202. Lu, J.; Holmgren, A. The thioredoxin antioxidant system. *Free Radic. Biol. Med.* **2014**, *66*, 75–87. [CrossRef]
203. Dagnell, M.; Schmidt, E.E.; Arnér, E.S.J. The A to Z of modulated cell patterning by mammalian thioredoxin reductases. *Free Radic. Biol. Med.* **2018**, *115*, 484–496. [CrossRef]
204. Cebula, M.; Schmidt, E.E.; Arnér, E.S. TrxR1 as a potent regulator of the Nrf2-Keap1 response system. *Antioxid. Redox Signal.* **2015**, *23*, 823–853. [CrossRef]
205. Lee, S.; Kim, S.M.; Lee, R.T. Thioredoxin and thioredoxin target proteins: From molecular mechanisms to functional significance. *Antioxid. Redox Signal.* **2013**, *18*, 1165–1207. [CrossRef]
206. Lillig, C.H.; Holmgren, A. Thioredoxin and related molecules—From biology to health and disease. *Antioxid. Redox Signal.* **2007**, *9*, 25–47. [CrossRef]
207. Collet, J.F.; Messens, J. Structure, function, and mechanism of thioredoxin proteins. *Antioxid. Redox Signal.* **2010**, *13*, 1205–1216. [CrossRef]
208. Laurent, T.C.; Moore, E.C.; Reichard, P. Enzymatic synthesis of deoxyribonucleotides. IV: Isolation and characterization of thioredoxin, the hydrogen donor from *Escherichia coli* B. *J. Biol. Chem.* **1964**, *239*, 3436–3444. [CrossRef]
209. Holmgren, A.; Sengupta, R. The use of thiols by ribonucleotide reductase. *Free Radic. Biol. Med.* **2010**, *49*, 1617–1628. [CrossRef]

210. Nakao, L.S.; Everley, R.A.; Marino, S.M.; Lo, S.M.; de Souza, L.E.; Gygi, S.P.; Gladyshev, V.N. Mechanism-based proteomic screening identifies targets of thioredoxin-like proteins. *J. Biol. Chem.* **2015**, *290*, 5685–5695. [CrossRef] [PubMed]
211. Du, Y.; Zhang, H.; Lu, J.; Holmgren, A. Glutathione and glutaredoxin act as a backup of human thioredoxin reductase 1 to reduce thioredoxin 1 preventing cell death by aurothioglucose. *J. Biol. Chem.* **2012**, *287*, 38210–38219. [CrossRef] [PubMed]
212. Zhang, H.; Du, Y.; Zhang, X.; Lu, J.; Holmgren, A. Glutaredoxin 2 reduces both thioredoxin 2 and thioredoxin 1 and protects cells from apoptosis induced by auranofin and 4-hydroxynonenal. *Antioxid. Redox Signal.* **2014**, *21*, 669–681. [CrossRef] [PubMed]
213. López-Grueso, M.J.; González-Ojeda, R.; Requejo-Aguilar, R.; McDonagh, B.; Fuentes-Almagro, C.A.; Muntané, J.; Bárcena, J.A.; Padilla, C.A. Thioredoxin and glutaredoxin regulate metabolism through different multiplex thiol switches. *Redox Biol.* **2019**, *21*, 101049. [CrossRef] [PubMed]
214. Peng, X.; Mandal, P.K.; Kaminsk, V.O.; Lindqvist, A.; Conrad, M.; Arnér, E.S. Sec-containing TrxR1 is essential for self-sufficiency of cells by control of glucose-derived H_2O_2. *Cell Death Dis.* **2014**, *5*, e1235. [CrossRef] [PubMed]
215. Zhong, L.; Arnér, E.S.; Holmgren, A. Structure and mechanism of mammalian thioredoxin reductase: The active site is a redox-active selenolthiol/selenenylsulfide formed from the conserved cysteine-selenocysteine sequence. *Proc. Natl. Acad. Sci. USA* **2000**, *97*, 5854–5859. [CrossRef] [PubMed]
216. Cheng, Q.; Sandalova, T.; Lindqvist, Y.; Arnér, E.S. Crystal structure and catalysis of the selenoprotein thioredoxin reductase 1. *J. Biol. Chem.* **2009**, *284*, 3998–4008. [CrossRef] [PubMed]
217. Lacey, B.M.; Eckenroth, B.E.; Flemer, S.; Hondal, R.J. Selenium in thioredoxin reductase: A mechanistic perspective. *Biochemistry* **2008**, *47*, 12810–12821. [CrossRef]
218. Hondal, R.J. Using chemical approaches to study selenoproteins-focus on thioredoxin reductases. *Biochim. Biophys. Acta* **2009**, *1790*, 1501–1512. [CrossRef]
219. Arnér, E.S. Focus on mammalian thioredoxin reductases--important selenoproteins with versatile functions. *Biochim. Biophys. Acta* **2009**, *1790*, 495–526. [CrossRef]
220. Zhong, L.; Holmgren, A. Essential role of selenium in the catalytic activities of mammalian thioredoxin reductase revealed by characterization of recombinant enzymes with selenocysteine mutations. *J. Biol. Chem.* **2000**, *275*, 18121–18128. [CrossRef]
221. Barber, D.R.; Hondal, R.J. Gain of function conferred by selenocysteine: Catalytic enhancement of one-electron transfer reactions by thioredoxin reductase. *Protein Sci.* **2019**, *28*, 79–89. [CrossRef]
222. Xu, J.; Cheng, Q.; Arnér, E.S. Details in the catalytic mechanism of mammalian thioredoxin reductase 1 revealed using point mutations and juglone-coupled enzyme activities. *Free Radic. Biol. Med.* **2016**, *94*, 110–120. [CrossRef]
223. Turanov, A.A.; Hatfield, D.L.; Gladyshev, V.N. Characterization of protein targets of mammalian thioredoxin reductases. *Methods Enzymol.* **2010**, *474*, 245–254.
224. Lu, J.; Berndt, C.; Holmgren, A. Metabolism of selenium compounds catalyzed by the mammalian selenoprotein thioredoxin reductase. *Biochim. Biophys. Acta* **2009**, *1790*, 1513–1519. [CrossRef]
225. Lee, B.C.; Dikiy, A.; Kim, H.Y.; Gladyshev, V.N. Functions and evolution of selenoprotein methionine sulfoxide reductases. *Biochim. Biophys. Acta* **2009**, *1790*, 1471–1477. [CrossRef]
226. Kim, H.Y.; Gladyshev, V.N. Different catalytic mechanisms in mammalian selenocysteine- and cysteine-containing methionine-R-sulfoxide reductases. *PLoS Biol.* **2005**, *3*, e375. [CrossRef]
227. Lourenço Dos Santos, S.; Petropoulos, I.; Friguet, B. The oxidized protein repair enzymes methionine sulfoxide reductases and their roles in protecting against oxidative stress, in ageing and in regulating protein function. *Antioxidants* **2018**, *7*, 191. [CrossRef] [PubMed]
228. Rhee, S.G.; Woo, H.A.; Kang, D. The role of peroxiredoxins in the transduction of H_2O_2 signals. *Antioxid. Redox Signal.* **2018**, *28*, 537–557. [CrossRef]
229. Rhee, S.G.; Woo, H.A. Multiple functions of peroxiredoxins: Peroxidases, sensors and regulators of the intracellular messenger H_2O_2, and protein chaperones. *Antioxid. Redox Signal.* **2011**, *15*, 781–794. [CrossRef] [PubMed]
230. Yang, K.S.; Kang, S.W.; Woo, H.A.; Hwang, S.C.; Chae, H.Z.; Kim, K.; Rhee, S.G. Inactivation of human peroxiredoxin I during catalysis as the result of the oxidation of the catalytic site cysteine to cysteine-sulfinic acid. *J. Biol. Chem.* **2002**, *277*, 38029–38036. [CrossRef]
231. Biteau, B.; Labarre, J.; Toledano, M.B. ATP-dependent reduction of cysteine-sulphinic acid by *S. cerevisiae* sulphiredoxin. *Nature* **2003**, *425*, 980–984. [CrossRef] [PubMed]
232. Jang, H.H.; Lee, K.O.; Chi, Y.H.; Jung, B.G.; Park, S.K.; Park, J.H.; Lee, J.R.; Lee, S.S.; Moon, J.C.; Yun, J.W.; et al. Two enzymes in one; two yeast peroxiredoxins display oxidative stress-dependent switching from a peroxidase to a molecular chaperone function. *Cell* **2004**, *117*, 625–635. [CrossRef] [PubMed]
233. Weissbach, H.; Etienne, F.; Hoshi, T.; Heinemann, S.H.; Lowther, W.T.; Matthews, B.; St John, G.; Nathan, C.; Brot, N. Peptide methionine sulfoxide reductase: Structure, mechanism of action, and biological function. *Arch. Biochem. Biophys.* **2002**, *397*, 172–178. [CrossRef] [PubMed]
234. Kaya, A.; Lee, B.C.; Gladyshev, V.N. Regulation of protein function by reversible methionine oxidation and the role of selenoprotein MsrB1. *Antioxid. Redox Signal.* **2015**, *23*, 814–822. [CrossRef] [PubMed]
235. Peng, X.; Giménez-Cassina, A.; Petrus, P.; Conrad, M.; Rydén, M.; Arnér, E.S. Thioredoxin reductase 1 suppresses adipocyte differentiation and insulin responsiveness. *Sci. Rep.* **2016**, *6*, 28080. [CrossRef]

236. Dagnell, M.; Pace, P.E.; Cheng, Q.; Frijhoff, J.; Östman, A.; Arnér, E.S.J.; Hampton, M.B.; Winterbourn, C.C. Thioredoxin reductase 1 and NADPH directly protect protein tyrosine phosphatase 1B from inactivation during H_2O_2 exposure. *J. Biol. Chem.* **2017**, *292*, 14371–14380. [CrossRef]
237. Cenas, N.; Nivinskas, H.; Anusevicius, Z.; Sarlauskas, J.; Lederer, F.; Arner, E.S. Interactions of quinones with thioredoxin reductase: A challenge to the antioxidant role of the mammalian selenoprotein. *J. Biol. Chem.* **2004**, *279*, 2583–2592. [CrossRef]
238. Anestal, K.; Prast-Nielsen, S.; Cenas, N.; Arner, E.S. Cell death by SecTRAPs: Thioredoxin reductase as a prooxidant killer of cells. *PLoS ONE* **2008**, *3*, e1846. [CrossRef]
239. Hansen, J.M.; Watson, W.H.; Jones, D.P. Compartmentation of Nrf-2 redox control: Regulation of cytoplasmic activation by glutathione and DNA binding by thioredoxin-1. *Toxicol. Sci.* **2004**, *82*, 308–317. [CrossRef] [PubMed]
240. Hirota, K.; Murata, M.; Sachi, Y.; Nakamura, H.; Takeuchi, J.; Mori, K.; Yodoi, J. Distinct roles of thioredoxin in the cytoplasm and in the nucleus. A two-step mechanism of redox regulation of transcription factor NF-kappaB. *J. Biol. Chem.* **1999**, *274*, 27891–27897. [CrossRef] [PubMed]
241. Ueno, M.; Masutani, H.; Arai, R.J.; Yamauchi, A.; Hirota, K.; Sakai, T.; Inamoto, T.; Yamaoka, Y.; Yodoi, J.; Nikaido, T. Thioredoxin-dependent redox regulation of p53-mediated p21 activation. *J. Biol. Chem.* **1999**, *274*, 35809–35815. [CrossRef]
242. Hirota, K.; Matsui, M.; Iwata, S.; Nishiyama, A.; Mori, K.; Yodoi, J. AP-1 transcriptional activity is regulated by a direct association between thioredoxin and Ref-1. *Proc. Natl. Acad. Sci. USA* **1997**, *94*, 3633–3638. [CrossRef]
243. Go, Y.M.; Jones, D.P. Redox control systems in the nucleus: Mechanisms and functions. *Antioxid. Redox Signal.* **2010**, *13*, 489–509. [CrossRef]
244. Grippo, J.F.; Holmgren, A.; Pratt, W.B. Proof that the endogenous, heat-stable glucocorticoid receptor-activating factor is thioredoxin. *J. Biol. Chem.* **1985**, *260*, 93–97. [CrossRef]
245. Meuillet, E.J.; Mahadevan, D.; Berggren, M.; Coon, A.; Powis, G. Thioredoxin-1 binds to the C2 domain of PTEN inhibiting PTEN's lipid phosphatase activity and membrane binding: A mechanism for the functional loss of PTEN's tumor suppressor activity. *Arch. Biochem. Biophys.* **2004**, *429*, 123–133. [CrossRef]
246. Lee, Y.R.; Chen, M.; Pandolfi, P.P. The functions and regulation of the PTEN tumour suppressor: New modes and prospects. *Nat. Rev. Mol. Cell Biol.* **2018**, *19*, 547–562. [CrossRef]
247. Gencheva, R.; Arnér, E.S.J. Thioredoxin Reductase Inhibition for Cancer Therapy. *Annu. Rev. Pharmacol. Toxicol.* **2022**, *62*, 177–196. [CrossRef]
248. Eriksson, S.E.; Prast-Nielsen, S.; Flaberg, E.; Szekely, L.; Arnér, E.S. High levels of thioredoxin reductase 1 modulate drug-specific cytotoxic efficacy. *Free Radic. Biol. Med.* **2009**, *47*, 1661–1671. [CrossRef]
249. Watson, W.H.; Heilman, J.M.; Hughes, L.L.; Spielberger, J.C. Thioredoxin reductase-1 knock down does not result in thioredoxin-1 oxidation. *Biochem. Biophys. Res. Commun.* **2008**, *368*, 832–836. [CrossRef] [PubMed]
250. Zhang, J.; Li, X.; Han, X.; Liu, R.; Fang, J. Targeting the thioredoxin system for cancer therapy. *Trends Pharmacol. Sci.* **2017**, *38*, 794–808. [CrossRef] [PubMed]
251. Bian, M.; Fan, R.; Zhao, S.; Liu, W. Targeting the thioredoxin system as a strategy for cancer therapy. *J. Med. Chem.* **2019**, *62*, 7309–7321. [CrossRef]
252. Saitoh, M.; Nishitoh, H.; Fujii, M.; Takeda, K.; Tobiume, K.; Sawada, Y.; Kawabata, M.; Miyazono, K.; Ichijo, H. Mammalian thioredoxin is a direct inhibitor of apoptosis signal-regulating kinase (ASK) 1. *EMBO J.* **1998**, *17*, 2596–2606. [CrossRef]
253. Yoshihara, E.; Chen, Z.; Matsuo, Y.; Masutani, H.; Yodoi, J. Thiol redox transitions by thioredoxin and thioredoxin binding protein-2 in cell signaling. *Methods Enzymol.* **2010**, *474*, 67–82. [PubMed]
254. Kuiper, G.G.; Kester, M.H.; Peeters, R.P.; Visser, T.J. Biochemical mechanisms of thyroid hormone deiodination. *Thyroid* **2005**, *15*, 787–798. [CrossRef] [PubMed]
255. Callebaut, I.; Curcio-Morelli, C.; Mornon, J.P.; Gereben, B.; Buettner, C.; Huang, S.; Castro, B.; Fonseca, T.L.; Harney, J.W.; Larsen, P.R.; et al. The iodothyronine selenodeiodinases are thioredoxin-fold family proteins containing a glycoside hydrolase clan GH-A-like structure. *J. Biol. Chem.* **2003**, *278*, 36887–36896. [CrossRef] [PubMed]
256. Schweizer, U.; Schlicker, C.; Braun, D.; Köhrle, J.; Steegborn, C. Crystal structure of mammalian selenocysteine-dependent iodothyronine deiodinase suggests a peroxiredoxin-like catalytic mechanism. *Proc. Natl. Acad. Sci. USA* **2014**, *111*, 10526–10531. [CrossRef] [PubMed]
257. Schweizer, U.; Steegborn, C. New insights into the structure and mechanism of iodothyronine deiodinases. *J. Mol. Endocrinol.* **2015**, *55*, R37–R52. [CrossRef]
258. Bianco, A.C.; da Conceição, R.R. The Deiodinase Trio and Thyroid Hormone Signaling. *Methods Mol. Biol.* **2018**, *1801*, 67–83.
259. Köhrle, J.; Frädrich, C. Deiodinases control local cellular and systemic thyroid hormone availability. *Free Radic. Biol. Med.* **2022**, *193 Pt 1*, 59–79. [CrossRef]
260. Cicatiello, A.G.; Di Girolamo, D.; Dentice, M. Metabolic Effects of the Intracellular Regulation of Thyroid Hormone: Old Players, New Concepts. *Front. Endocrinol.* **2018**, *9*, 474. [CrossRef]
261. Zavacki, A.M.; Arrojo EDrigo, R.; Freitas, B.C.; Chung, M.; Harney, J.W.; Egri, P.; Wittmann, G.; Fekete, C.; Gereben, B.; Bianco, A.C. The E3 ubiquitin ligase TEB4 mediates degradation of type 2 iodothyronine deiodinase. *Mol. Cell. Biol.* **2009**, *29*, 5339–5347. [CrossRef]
262. Sase, S.; Kakimoto, R.; Kimura, R.; Goto, K. Synthesis of a stable primary-alkyl-substituted selenenyl iodide and its hydrolytic conversion to the corresponding selenenic acid. *Molecules* **2015**, *20*, 21415–21420. [CrossRef]

263. Steegborn, C.; Schweizer, U. Structure and Mechanism of Iodothyronine Deiodinases—What we know, what we don't know, and what would be nice to know. *Exp. Clin. Endocrinol. Diabetes* **2019**, *128*, 375–378. [CrossRef]
264. Di Jeso, B.; Arvan, P. Thyroglobulin from molecular and cellular biology to clinical endocrinology. *Endocr. Rev.* **2016**, *37*, 2–36. [CrossRef]
265. Ruf, J.; Carayon, P. Structural and functional aspects of thyroid peroxidase. *Arch. Biochem. Biophys.* **2006**, *445*, 269–277. [CrossRef]
266. Dunn, J.T.; Dunn, A.D. Update on intrathyroidal iodine metabolism. *Thyroid* **2001**, *11*, 407–414. [CrossRef] [PubMed]
267. Fu, J.; Dumitrescu, A.M. Inherited defects in thyroid hormone cell-membrane transport and metabolism. *Best Pract. Res. Clin. Endocrinol. Metab.* **2014**, *28*, 189–201. [CrossRef]
268. Fugazzola, L.; Muzza, M.; Weber, G.; Beck-Peccoz, P.; Persani, L. DUOXS defects: Genotype-phenotype correlations. *Ann. Endocrinol.* **2011**, *72*, 82–86. [CrossRef]
269. Kryukov, G.V.; Kumar, R.A.; Koc, A.; Sun, Z.; Gladyshev, V.N. Selenoprotein R is a zinc-containing stereo-specific methionine sulfoxide reductase. *Proc. Natl. Acad. Sci. USA* **2002**, *99*, 4245–4250. [CrossRef] [PubMed]
270. Aachmann, F.L.; Sal, L.S.; Kim, H.Y.; Marino, S.M.; Gladyshev, V.N.; Dikiy, A. Insights into function, catalytic mechanism, and fold evolution of selenoprotein methionine sulfoxide reductase B1 through structural analysis. *J. Biol. Chem.* **2010**, *285*, 33315–33323. [CrossRef]
271. Kim, H.Y. The methionine sulfoxide reduction system: Selenium utilization and methionine sulfoxide reductase enzymes and their functions. *Antioxid. Redox Signal.* **2013**, *19*, 958–969. [CrossRef]
272. Tarrago, L.; Kaya, A.; Kim, H.Y.; Manta, B.; Lee, B.C.; Gladyshev, V.N. The selenoprotein methionine sulfoxide reductase B1 (MSRB1). *Free Radic. Biol. Med.* **2022**, *191*, 228–240. [CrossRef]
273. Fomenko, D.E.; Novoselov, S.V.; Natarajan, S.K.; Lee, B.C.; Koc, A.; Carlson, B.A.; Lee, T.H.; Kim, H.Y.; Hatfield, D.L.; Gladyshev, V.N. MsrB1 (methionine-R-sulfoxide reductase 1) knock-out mice: Roles of MsrB1 in redox regulation and identification of a novel selenoprotein form. *J. Biol. Chem.* **2009**, *284*, 5986–5993. [CrossRef] [PubMed]
274. Wu, H.; Yesilyurt, H.G.; Yoon, J.; Terman, J.R. The MICALs are a Family of F-actin Dismantling oxidoreductases conserved from drosophila to humans. *Sci. Rep.* **2018**, *8*, 937. [CrossRef] [PubMed]
275. Lee, B.C.; Péterfi, Z.; Hoffmann, F.W.; Moore, R.E.; Kaya, A.; Avanesov, A.; Tarrago, L.; Zhou, Y.; Weerapana, E.; Fomenko, D.E.; et al. MsrB1 and MICALs regulate actin assembly and macrophage function via reversible stereoselective methionine oxidation. *Mol. Cell.* **2013**, *51*, 397–404. [CrossRef]
276. Lee, B.C.; Lee, S.G.; Choo, M.K.; Kim, J.H.; Lee, H.M.; Kim, S.; Fomenko, D.E.; Kim, H.Y.; Park, J.M.; Gladyshev, V.N. Selenoprotein MsrB1 promotes anti-inflammatory cytokine gene expression in macrophages and controls immune response in vivo. *Sci. Rep.* **2017**, *7*, 5119. [CrossRef]
277. Konstantinidis, K.; Bezzerides, V.J.; Lai, L.; Isbell, H.M.; Wei, A.C.; Wu, Y.; Viswanathan, M.C.; Blum, I.D.; Granger, J.M.; Heims-Waldron, D.; et al. MICAL1 constrains cardiac stress responses and protects against disease by oxidizing CaMKII. *J. Clin. Investig.* **2020**, *130*, 4663–4678. [CrossRef]
278. Lai, L.; Sun, J.; Tarafdar, S.; Liu, C.; Murphy, E.; Kim, G.; Levine, R.L. Loss of methionine sulfoxide reductases increases resistance to oxidative stress. *Free Radic. Biol. Med.* **2019**, *145*, 374–384. [CrossRef] [PubMed]
279. Dudkiewicz, M.; Szczepińska, T.; Grynberg, M.; Pawłowski, K. A novel protein kinase-like domain in a selenoprotein, widespread in the tree of life. *PLoS ONE* **2012**, *7*, e32138. [CrossRef]
280. Sreelatha, A.; Yee, S.S.; Lopez, V.A.; Park, B.C.; Kinch, L.N.; Pilch, S.; Servage, K.A.; Zhang, J.; Jiou, J.; Karasiewicz-Urbańska, M.; et al. Protein AMPylation by an evolutionarily conserved pseudokinase. *Cell* **2018**, *175*, 809–821.e19. [CrossRef]
281. Mieyal, J.J.; Gallogly, M.M.; Qanungo, S.; Sabens, E.A.; Shelton, M.D. Molecular mechanisms and clinical implications of reversible protein S-glutathionylation. *Antioxid. Redox Signal.* **2008**, *10*, 1941–1988. [CrossRef]
282. Labunskyy, V.M.; Ferguson, A.D.; Fomenko, D.E.; Chelliah, Y.; Hatfield, D.L.; Gladyshev, V.N. A novel cysteine-rich domain of Sep15 mediates the interaction with UDP-glucose:glycoprotein glucosyltransferase. *J. Biol. Chem.* **2005**, *280*, 37839–37845. [CrossRef]
283. Ferguson, A.D.; Labunskyy, V.M.; Fomenko, D.E.; Araç, D.; Chelliah, Y.; Amezcua, C.A.; Rizo, J.; Gladyshev, V.N.; Deisenhofer, J. NMR structures of the selenoproteins Sep15 and SelM reveal redox activity of a new thioredoxin-like family. *J. Biol. Chem.* **2006**, *281*, 3536–3543. [CrossRef] [PubMed]
284. Yim, S.H.; Everley, R.A.; Schildberg, F.A.; Lee, S.G.; Orsi, A.; Barbati, Z.R.; Karatepe, K.; Fomenko, D.E.; Tsuji, P.A.; Luo, H.R.; et al. Role of selenoprotein F as a gatekeeper of secreted disulfide-rich glycoproteins. *Cell Rep.* **2018**, *23*, 1387–1398. [CrossRef] [PubMed]
285. Kasaikina, M.V.; Fomenko, D.E.; Labunskyy, V.M.; Lachke, S.A.; Qiu, W.; Moncaster, J.A.; Zhang, J.; Wojnarowicz MWJr Natarajan, S.K.; Malinouski, M.; Schweizer, U.; et al. Roles of the 15-kDa selenoprotein (Sep15) in redox homeostasis and cataract development revealed by the analysis of Sep 15 knockout mice. *J. Biol. Chem.* **2011**, *286*, 33203–33212. [CrossRef] [PubMed]
286. Zheng, X.; Ren, B.; Li, X.; Yan, H.; Xie, Q.; Liu, H.; Zhou, J.; Tian, J.; Huang, K. Selenoprotein F knockout leads to glucose and lipid metabolism disorders in mice. *J. Biol. Inorg. Chem.* **2020**, *25*, 1009–1022. [CrossRef] [PubMed]
287. Petit, N.; Lescure, A.; Rederstorff, M.; Krol, A.; Moghadaszadeh, B.; Wewer, U.M.; Guicheney, P. Selenoprotein N: An endoplasmic reticulum glycoprotein with an early developmental expression pattern. *Hum. Mol. Genet.* **2003**, *12*, 1045–1053. [CrossRef]
288. Li, Y.; Camacho, P. Ca^{2+}-dependent redox modulation of SERCA 2b by ERp57. *J. Cell Biol.* **2004**, *164*, 35–46. [CrossRef]

289. Chernorudskiy, A.; Varone, E.; Colombo, S.F.; Fumagalli, S.; Cagnotto, A.; Cattaneo, A.; Briens, M.; Baltzinger, M.; Kuhn, L.; Bachi, A.; et al. Selenoprotein N is an endoplasmic reticulum calcium sensor that links luminal calcium levels to a redox activity. *Proc. Natl. Acad. Sci. USA* **2020**, *117*, 21288–21298. [CrossRef]
290. Horibata, Y.; Hirabayashi, Y. Identification and characterization of human ethanolaminephosphotransferase1. *J. Lipid Res.* **2007**, *48*, 503–508. [CrossRef]
291. Horibata, Y.; Elpeleg, O.; Eran, A.; Hirabayashi, Y.; Savitzki, D.; Tal, G.; Mandel, H.; Sugimoto, H. EPT1 (selenoprotein I) is critical for the neural development and maintenance of plasmalogen in humans. *J. Lipid Res.* **2018**, *59*, 1015–1026. [CrossRef]
292. Nunes, L.G.A.; Pitts, M.W.; Hoffmann, P.R. Selenoprotein I (selenoi) as a critical enzyme in the central nervous system. *Arch. Biochem. Biophys.* **2022**, *729*, 109376. [CrossRef]
293. Ma, C.; Hoffmann, F.W.; Marciel, M.P.; Page, K.E.; Williams-Aduja, M.A.; Akana, E.N.L.; Gojanovich, G.S.; Gerschenson, M.; Urschitz, J.; Moisyadi, S.; et al. Upregulated ethanolamine phospholipid synthesis via selenoprotein I is required for effective metabolic reprogramming during T cell activation. *Mol. Metab.* **2021**, *47*, 101170. [CrossRef]
294. Fredericks, G.J.; Hoffmann, P.R. Selenoprotein K and protein palmitoylation. *Antioxid. Redox Signal.* **2015**, *23*, 854–862. [CrossRef]
295. Fredericks, G.J.; Hoffmann, F.W.; Rose, A.H.; Osterheld, H.J.; Hess, F.M.; Mercier, F.; Hoffmann, P.R. Stable expression and function of the inositol 1,4,5-triphosphate receptor requires palmitoylation by a DHHC6/selenoprotein K complex. *Proc. Natl. Acad. Sci. USA* **2014**, *111*, 16478–16483. [CrossRef] [PubMed]
296. Jia, S.Z.; Xu, X.W.; Zhang, Z.H.; Chen, C.; Chen, Y.B.; Huang, S.L.; Liu, Q.; Hoffmann, P.R.; Song, G.L. Selenoprotein K deficiency-induced apoptosis: A role for calpain and the ERS pathway. *Redox Biol.* **2021**, *47*, 102154. [CrossRef]
297. Wang, S.; Zhao, X.; Liu, Q.; Wang, Y.; Li, S.; Xu, S. Selenoprotein K protects skeletal muscle from damage and is required for satellite cells-mediated myogenic differentiation. *Redox Biol.* **2022**, *50*, 102255. [CrossRef] [PubMed]
298. Hawkes, W.C.; Alkan, Z. Delayed cell cycle progression from S.E.PW1 depletion is p53- and p21-dependent in MCF-7 breast cancer cells. *Biochem. Biophys. Res. Commun.* **2011**, *413*, 36–40. [CrossRef] [PubMed]
299. Hawkes, W.C.; Printsev, I.; Alkan, Z. Selenoprotein W depletion induces a p53- and p21-dependent delay in cell cycle progression in RWPE-1 prostate epithelial cells. *J. Cell. Biochem.* **2012**, *113*, 61–69. [CrossRef]
300. Hawkes, W.C.; Alkan, Z. Delayed cell cycle progression in selenoprotein W depleted cells is regulated by a Mitogen-Activated Protein Kinase Kinase 4 (MKK4)-p38/c-Jun NH2-terminal kinase (JNK)-p53 pathway. *J. Biol. Chem.* **2012**, *287*, 27371–27379. [CrossRef]
301. Alkan, Z.; Duong, F.L.; Hawkes, W.C. Selenoprotein W controls epidermal growth factor receptor surface expression, activation and degradation via receptor ubiquitination. *Biochim. Biophys. Acta* **2015**, *1853*, 1087–1095. [CrossRef]
302. Jeon, Y.H.; Ko, K.Y.; Lee, J.H.; Park, K.J.; Jang, J.K.; Kim, I.Y. Identification of a redox-modulatory interaction between selenoprotein W and 14-3-3 protein. *Biochim. Biophys. Acta* **2016**, *1863*, 10–18. [CrossRef]
303. Anouar, Y.; Lihrmann, I.; Falluel-Morel, A.; Boukhzar, L. Selenoprotein T is a key player in ER proteostasis, endocrine homeostasis and neuroprotection. *Free Radic. Biol. Med.* **2018**, *127*, 145–152. [CrossRef]
304. Shao, Z.Q.; Zhang, X.; Fan, H.H.; Wang, X.S.; Wu, H.M.; Zhang, L.; Cheng, W.H.; Zhu, J.H. Selenoprotein T Promotes Proliferation and G1-to-S Transition in SK-N-SH Cells: Implications in Parkinson's Disease. *J. Nutr.* **2019**, *149*, 2110–2119. [CrossRef] [PubMed]
305. Zhang, X.; Liu, R.P.; Cheng, W.H.; Zhu, J.H. Prioritized brain selenium retention and selenoprotein expression: Nutritional insights into Parkinson's disease. *Mech. Ageing Dev.* **2019**, *180*, 89–96. [CrossRef]
306. Liu, J.; Li, F.; Rozovsky, S. The intrinsically disordered membrane protein selenoprotein S is a reductase in vitro. *Biochemistry* **2013**, *52*, 3051–3061. [CrossRef]
307. Novoselov, S.V.; Kryukov, G.V.; Xu, X.M.; Carlson, B.A.; Hatfield, D.L.; Gladyshev, V.N. Selenoprotein H is a nucleolar thioredoxin-like protein with a unique expression pattern. *J. Biol. Chem.* **2007**, *282*, 11960–11968. [CrossRef]
308. Wu, R.T.; Cao, L.; Chen, B.P.; Cheng, W.H. Selenoprotein H suppresses cellular senescence through genome maintenance and redox regulation. *J. Biol. Chem.* **2014**, *289*, 34378–34388. [CrossRef]
309. Zhang, X.; Zhang, L.; Zhu, J.H.; Cheng, W.H. Nuclear selenoproteins and genome maintenance. *IUBMB Life* **2016**, *68*, 5–12. [CrossRef]
310. Stadtman, T. Selenium biochemistry. *Annu. Rev. Biochem.* **1990**, *59*, 111–127. [CrossRef]
311. Stadtman, T.C. A gold mine of fascinating enzymes: Those remarkable, strictly anaerobic bacteria, Methanococcus vannielii and Clostridium sticklandii. *J. Biol. Chem.* **2002**, *277*, 49091–49100. [CrossRef]
312. Cone, J.E.; Del Rio, R.M.; Davis, J.N.; Stadtman, T.C. Chemical characterization of the selenoprotein component of clostridial glycine reductase: Identification of selenocysteine as the organoselenium moiety. *Proc. Natl. Acad. Sci. USA* **1976**, *73*, 2659–2663. [CrossRef] [PubMed]
313. Arkowitz, R.A.; Abeles, R.H. Identification of acetyl phosphate as the product of clostridial glycine reductase: Evidence for an acyl enzyme intermediate. *Biochemistry* **1989**, *28*, 4639–4644. [CrossRef] [PubMed]
314. Andreesen, J.R. Glycine reductase mechanism. *Curr. Opin. Chem. Biol.* **2004**, *8*, 454–461. [CrossRef]
315. Arkowitz, R.A.; Abeles, R.H. Mechanism of action of clostridial glycine reductase: Isolation and characterization of a covalent acetyl enzyme intermediate. *Biochemistry* **1991**, *30*, 4090–4097. [CrossRef]
316. Kabisch, U.C.; Gräntzdörffer, A.; Schierhorn, A.; Rücknagel, K.P.; Andreesen, J.R.; Pich, A. Identification of D-proline reductase from Clostridium sticklandii as a selenoenzyme and indications for a catalytically active pyruvoyl group derived from a cysteine residue by cleavage of a proprotein. *J. Biol. Chem.* **1999**, *274*, 8445–8454. [CrossRef] [PubMed]

317. Arkowitz, R.A.; Dhe-Paganon, S.; Abeles, R.H. The fate of the carboxyl oxygens during D-proline reduction by clostridial proline reductase. *Arch. Biochem. Biophys.* **1994**, *311*, 457–459. [CrossRef]
318. Bednarski, B.; Andreesen, J.R.; Pich, A. In vitro processing of the proproteins GrdE of protein B of glycine reductase and PrdA of D-proline reductase from Clostridium sticklandii: Formation of a pyruvoyl group from a cysteine residue. *Eur. J. Biochem.* **2001**, *268*, 3538–3544. [CrossRef] [PubMed]
319. Jones, J.B.; Stadtman, T.C. Selenium-dependent and selenium-independent formate dehydrogenases of Methanococcus vannielii. Separation of the two forms and characterization of the purified selenium-independent form. *J. Biol. Chem.* **1981**, *256*, 656–663. [CrossRef] [PubMed]
320. Axley, M.J.; Böck, A.; Stadtman, T.C. Catalytic properties of an Escherichia coli formate dehydrogenase mutant in which sulfur replaces selenium. *Proc. Natl. Acad. Sci. USA* **1991**, *88*, 8450–8454. [CrossRef]
321. Boyington, J.C.; Gladyshev, V.N.; Khangulov, S.V.; Stadtman, T.C.; Sun, P.D. Crystal structure of formate dehydrogenase H: Catalysis involving Mo, molybdopterin, selenocysteine, and a Fe_4S_4 cluster. *Science* **1997**, *275*, 1305–1308. [CrossRef]
322. Khangulov, S.V.; Gladyshev, V.N.; Dismukes, G.C.; Stadtman, T.C. Selenium-containing formate dehydrogenase H from Escherichia coli: A molybdopterin enzyme that catalyzes formate oxidation without oxygen transfer. *Biochemistry* **1998**, *37*, 3518–3528. [CrossRef]
323. Raaijmakers, H.C.; Romão, M.J. Formate-reduced *E. coli* formate dehydrogenase H: The reinterpretation of the crystal structure suggests a new reaction mechanism. *J. Biol. Inorg. Chem.* **2006**, *11*, 849–854. [CrossRef]
324. Leopoldini, M.; Chiodo, S.G.; Toscano, M.; Russo, N. Reaction mechanism of molybdoenzyme formate dehydrogenase. *Chemistry* **2008**, *14*, 8674–8681. [CrossRef] [PubMed]
325. Dong, G.; Ryde, U. Reaction mechanism of formate dehydrogenase studied by computational methods. *J. Biol. Inorg. Chem.* **2018**, *23*, 1243–1254. [CrossRef] [PubMed]
326. Baltazar, C.S.A.; Marques, M.C.; Soares, C.M.; DeLacey, A.M.; Pereira, I.A.C.; Matias, P.M. Nickel-iron-selenium hydrogenases—An Overview. *Eur. J. Inorg. Chem.* **2011**, *2011*, 948–962. [CrossRef]
327. Wombwell, C.; Caputo, C.A.; Reisner, E. [NiFeSe]-hydrogenase chemistry. *Acc. Chem. Res.* **2015**, *48*, 2858–2865. [CrossRef]
328. Mersch, D.; Lee, C.Y.; Zhang, J.Z.; Brinkert, K.; Fontecilla-Camps, J.C.; Rutherford, A.W.; Reisner, E. Wiring of photosystem II to hydrogenase for photoelectrochemical water splitting. *J. Am. Chem. Soc.* **2015**, *137*, 8541–8549. [CrossRef]
329. Nam, D.H.; Zhang, J.Z.; Andrei, V.; Kornienko, N.; Heidary, N.; Wagner, A.; Nakanishi, K.; Sokol, K.P.; Slater, B.; Zebger, I.; et al. Solar water splitting with a hydrogenase integrated in photoelectrochemical tandem cells. *Angew. Chem. Int. Ed. Engl.* **2018**, *57*, 10595–10599. [CrossRef]
330. Parkin, A.; Goldet, G.; Cavazza, C.; Fontecilla-Camps, J.C.; Armstrong, F.A. The difference a Se makes? Oxygen-tolerant hydrogen production by the [NiFeSe]-hydrogenase from Desulfomicrobium baculatum. *J. Am. Chem. Soc.* **2008**, *130*, 13410–13416. [CrossRef]
331. Marques, M.C.; Tapia, C.; Gutiérrez-Sanz, O.; Ramos, A.R.; Keller, K.L.; Wall, J.D.; De Lacey, A.L.; Matias, P.M.; Pereira, I.A.C. The direct role of selenocysteine in [NiFeSe] hydrogenase maturation and catalysis. *Nat. Chem. Biol.* **2017**, *13*, 544–550. [CrossRef]
332. Yang, X.; Elrod, L.C.; Le, T.; Vega, V.S.; Naumann, H.; Rezenom, Y.; Reibenspies, J.H.; Hall, M.B.; Darensbourg, M.Y. Controlling O_2 reactivity in synthetic analogues of [NiFeS]- and [NiFeSe]-hydrogenase active sites. *J. Am. Chem. Soc.* **2019**, *141*, 15338–15347. [CrossRef]
333. Hawkes, W.C.; Alkan, Z. Regulation of redox signaling by selenoproteins. *Biol. Trace Elem. Res.* **2010**, *134*, 235–251. [CrossRef]
334. Flohé, L. The impact of thiol peroxidases on redox regulation. *Free Radic. Res.* **2016**, *50*, 126–142. [CrossRef]
335. Chaudière, J.; Gérard, D.; Clément, M.; Bourre, J.M. Induction of selenium-glutathione peroxidase by stimulation of metabolic hydrogen peroxide production in vivo. *Bioelectrochem. Bioenerg.* **1987**, *18*, 247–256. [CrossRef]
336. Touat-Hamici, Z.; Legrain, Y.; Bulteau, A.L.; Chavatte, L. Selective up-regulation of human selenoproteins in response to oxidative stress. *J. Biol. Chem.* **2014**, *289*, 14750–14761. [CrossRef] [PubMed]
337. Endres, L.; Begley, U.; Clark, R.; Gu, C.; Dziergowska, A.; Małkiewicz, A.; Melendez, J.A.; Dedon, P.C.; Begley, T.J. Alkbh8 regulates selenocysteine-protein expression to protect against reactive oxygen species damage. *PLoS ONE* **2015**, *10*, e0131335. [CrossRef]
338. Schwarz, M.; Löser, A.; Cheng, Q.; Wichmann-Costaganna, M.; Schädel, P.; Werz, O.; Arnér, E.S.; Kipp, A.P. Side-by-side comparison of recombinant human glutathione peroxidases identifies overlapping substrate specificities for soluble hydroperoxides. *Redox Biol.* **2023**, *59*, 102593. [CrossRef] [PubMed]
339. Chu, F.F.; Esworthy, R.S. The expression of an intestinal form of glutathione peroxidase (GSHPx-GI) in rat intestinal epithelium. *Arch. Biochem. Biophys.* **1995**, *323*, 288–294. [CrossRef] [PubMed]
340. Marinho, H.S.; Real, C.; Cyrne, L.; Soares, H.; Antunes, F. Hydrogen peroxide sensing, signaling and regulation of transcription factors. *Redox Biol.* **2014**, *2*, 535–562. [CrossRef] [PubMed]
341. Sies, H. Hydrogen peroxide as a central redox signaling molecule in physiological oxidative stress: Oxidative eustress. *Redox Biol.* **2017**, *11*, 613–619. [CrossRef]
342. Espinosa-Diez, C.; Miguel, V.; Mennerich, D.; Kietzmann, T.; Sánchez-Pérez, P.; Cadenas, S.; Lamas, S. Antioxidant responses and cellular adjustments to oxidative stress. *Redox Biol.* **2015**, *6*, 183–197. [CrossRef]
343. Moldogazieva, N.T.; Mokhosoev, I.M.; Feldman, N.B.; Lutsenko, S.V. ROS and RNS signalling: Adaptive redox switches through oxidative/nitrosative protein modifications. *Free Radic. Res.* **2018**, *52*, 507–543. [CrossRef]

344. Oliveira-Marques, V.; Marinho, H.S.; Cyrne, L.; Antunes, F. Role of hydrogen peroxide in NF-kappaB activation: From inducer to modulator. *Antioxid. Redox Signal.* **2009**, *11*, 2223–2243. [CrossRef] [PubMed]
345. Nakajima, S.; Kitamura, M. Bidirectional regulation of NF-κB by reactive oxygen species: A role of unfolded protein response. *Free Radic. Biol. Med.* **2013**, *65*, 162–174. [CrossRef]
346. Kulmacz, R.J. Regulation of cyclooxygenase catalysis by hydroperoxides. *Biochem. Biophys. Res. Commun.* **2005**, *338*, 25–33. [CrossRef] [PubMed]
347. Netto, L.E.S.; Machado, L.E.S.F. Preferential redox regulation of cysteine-based protein tyrosine phosphatases: Structural and biochemical diversity. *FEBS J.* **2022**, *289*, 5480–5504. [CrossRef]
348. Dagnell, M.; Cheng, Q.; Rizvi, S.H.M.; Pace, P.E.; Boivin, B.; Winterbourn, C.C.; Arnér, E.S.J. Bicarbonate is essential for protein-tyrosine phosphatase 1B (PTP1B) oxidation and cellular signaling through EGF-triggered phosphorylation cascades. *J. Biol. Chem.* **2019**, *294*, 12330–12338. [CrossRef] [PubMed]
349. Kretz-Remy, C.; Mehlen, P.; Mirault, M.E.; Arrigo, A.P. Inhibition of I kappa B-alpha phosphorylation and degradation and subsequent NF-kappa B activation by glutathione peroxidase overexpression. *J. Cell Biol.* **1996**, *133*, 1083–1093. [CrossRef] [PubMed]
350. Agbor, T.A.; Demma, Z.; Mrsny, R.J.; Castillo, A.; Boll, E.J.; McCormick, B.A. The oxido-reductase enzyme glutathione peroxidase 4 (GPX4) governs Salmonella typhimurium-induced neutrophil transepithelial migration. *Cell. Microbiol.* **2014**, *16*, 1339–1353. [CrossRef]
351. Cao, C.; Leng, Y.; Huang, W.; Liu, X.; Kufe, D. Glutathione peroxidase 1 is regulated by the c-Abl and Arg tyrosine kinases. *J. Biol. Chem.* **2003**, *278*, 39609–39614. [CrossRef] [PubMed]
352. Arjunan, P.; Lin, X.; Tang, Z.; Du, Y.; Kumar, A.; Liu, L.; Yin, X.; Huang, L.; Chen, W.; Chen, Q.; et al. VEGF-B is a potent antioxidant. *Proc. Natl. Acad. Sci. USA* **2018**, *115*, 10351–10356. [CrossRef]
353. Chaudière, J. Selenium-Glutathione Peroxidase: Properties of the Active Site and Distribution in Mammals. Ph.D. Thesis, University of California, Davis, CA, USA, 1983. Available online: https://hdl.handle.net/2027/uc1.x15939 (accessed on 7 June 2023).
354. Wessjohann, L.A.; Schneider, A.; Abbas, M.; Brandt, W. Selenium in chemistry and biochemistry in comparison to sulfur. *Biol. Chem.* **2007**, *388*, 997–1006. [CrossRef]
355. Arnér, E.S. Selenoproteins-What unique properties can arise with selenocysteine in place of cysteine? *Exp. Cell Res.* **2010**, *316*, 1296–1303. [CrossRef]
356. Reich, H.J.; Hondal, R.J. Why nature chose selenium. *ACS Chem. Biol.* **2016**, *11*, 821–841. [CrossRef]
357. Maroney, M.J.; Hondal, R.J. Selenium versus sulfur: Reversibility of chemical reactions and resistance to permanent oxidation in proteins and nucleic acids. *Free Radic. Biol. Med.* **2018**, *127*, 228–237. [CrossRef]
358. Dalla Tiezza, M.; Bickelhaupt, F.M.; Flohé, L.; Maiorino, M.; Ursini, F.; Orian, L. A dual attack on the peroxide bond. The common principle of peroxidatic cysteine or selenocysteine residues. *Redox Biol.* **2020**, *34*, 101540. [CrossRef] [PubMed]
359. Flohé, L.; Toppo, S.; Orian, L. The glutathione peroxidase family: Discoveries and mechanism. *Free Radic. Biol. Med.* **2022**, *187*, 113–122. [CrossRef] [PubMed]
360. Rocher, C.; Lalanne, J.L.; Chaudière, J. Purification and properties of a recombinant sulfur analog of murine selenium-glutathione peroxidase. *Eur. J. Biochem.* **1992**, *205*, 955–960. [CrossRef] [PubMed]
361. Toscano, M.D.; Woycechowsky, K.J.; Hilvert, D. Minimalist active-site redesign: Teaching old enzymes new tricks. *Angew. Chem. Int. Ed. Engl.* **2007**, *46*, 3212–3236. [CrossRef] [PubMed]
362. Metanis, N.; Hilvert, D. Natural and synthetic selenoproteins. *Curr. Opin. Chem. Biol.* **2014**, *22*, 27–34. [CrossRef]
363. Bell, I.M.; Fisher, M.L.; Wu, Z.P.; Hilvert, D. Kinetic studies on the peroxidase activity of selenosubtilisin. *Biochemistry* **1993**, *32*, 3754–3762, Erratum in *Biochemistry* **1993**, *32*, 8980. [CrossRef]
364. Wang, T.; Li, J.; Xu, J.; Fan, X.; Zhao l Qiao, S.; Pan, T.; Liu, J. Rational redesign of the active site of selenosubtilisin with strongly enhanced glutathione peroxidase activity. *J. Catal.* **2018**, *359*, 27–35. [CrossRef]
365. Yu, H.J.; Liu, J.Q.; Bock, A.; Li, J.; Luo, G.M.; Shen, J.C. Engineering glutathione transferase to a novel glutathione peroxidase mimic with high catalytic efficiency: Incorporation of selenocysteine into a glutathione-binding scaffold using an auxotrophic expression system. *J. Biol. Chem.* **2005**, *280*, 11930–11935. [CrossRef]
366. Casi, G.; Roelfes, G.; Hilvert, D. Selenoglutaredoxin as a glutathione peroxidase mimic. *Chembiochem* **2008**, *9*, 1623–1631. [CrossRef] [PubMed]
367. Ge, Y.; Qi, Z.; Wang, Y.; Liu, X.; Li, J.; Xu, J.; Liu, J.; Shen, J. Engineered selenium-containing glutaredoxin displays strong glutathione peroxidase activity rivaling natural enzyme. *Int. J. Biochem. Cell Biol.* **2009**, *41*, 900–906. [CrossRef] [PubMed]
368. Boschi-Muller, S.; Muller, S.; Van Dorsselaer, A.; Böck, A.; Branlant, G. Substituting selenocysteine for active site cysteine of phosphorylating glyceraldehyde 3-phosphate dehydrogenase reveals a peroxidase activity. *FEBS Lett.* **1998**, *439*, 241–245. [CrossRef] [PubMed]
369. Huber, R.E.; Criddle, R.S. Comparison of the chemical properties of selenocysteine and selenocystine with their sulfur analogs. *Arch. Biochem. Biophys.* **1967**, *122*, 164–173. [CrossRef]
370. Rhee, S.G.; Cho, C.S. Blot-based detection of dehydroalanine-containing glutathione peroxidase with the use of biotin-conjugated cysteamine. *Methods Enzymol.* **2010**, *474*, 23–34. [CrossRef]

371. Dimastrogiovanni, D.; Anselmi, M.; Miele, A.E.; Boumis, G.; Petersson, L.; Angelucci, F.; Nola, A.D.; Brunori, M.; Bellelli, A. Combining crystallography and molecular dynamics: The case of Schistosoma mansoni phospholipid glutathione peroxidase. *Proteins Struct. Funct. Genet.* **2010**, *78*, 259–270. [CrossRef]
372. Orian, L.; Mauri, P.; Roveri, A.; Toppo, S.; Benazzi, L.; Bosello-Travain, V.; De Palma, A.; Maiorino, M.; Miotto, G.; Zaccarin, M.; et al. Selenocysteine oxidation in glutathione peroxidase catalysis: An MS-supported quantum mechanics study. *Free Radic. Biol. Med.* **2015**, *87*, 1–14. [CrossRef]

International Journal of
Molecular Sciences

MDPI

Article

Equol and Resveratrol Improve Bone Turnover Biomarkers in Postmenopausal Women: A Clinical Trial

Graziamaria Corbi [1], Vincenzo Nobile [2], Valeria Conti [3], Alessandro Cannavo [1], Vincenzo Sorrenti [4], Alessandro Medoro [5], Giovanni Scapagnini [5,*] and Sergio Davinelli [5]

[1] Department of Translational Medical Sciences, University of Naples "Federico II", 80138 Naples, Italy; graziamaria.corbi@unina.it (G.C.); alessandro.cannavo@unina.it (A.C.)
[2] Farcoderm S.r.l., 27028 San Martino Siccomario, Italy; vincenzo.nobile@complifegroup.com
[3] Department of Medicine Surgery and Dentistry, Scuola Medica Salernitana, University of Salerno, 84081 Baronissi, Italy; vconti@unisa.it
[4] Department of Pharmaceutical and Pharmacological Sciences, University of Padua, 35131 Padua, Italy; vincenzosorrenti88@gmail.com
[5] Department of Medicine and Health Sciences "V. Tiberio", University of Molise, 86100 Campobasso, Italy; alessandro.medoro@unimol.it (A.M.); sergio.davinelli@unimol.it (S.D.)
* Correspondence: giovanni.scapagnini@unimol.it; Tel.: +39-0874-404771

Abstract: Estrogen deficiency is a major cause of loss of postmenopausal bone mineral density (BMD). This study aimed to evaluate the effects of equol and resveratrol on bone turnover biomarkers in postmenopausal women. Sixty healthy postmenopausal women were randomly assigned to receive 200 mg fermented soy containing 10 mg equol and 25 mg resveratrol or a placebo for 12 months. Whole-body BMD and bone turnover biomarkers, such as deoxypyridinoline (DPD), tartrate-resistant acid phosphatase 5b (TRACP-5b), osteocalcin, and bone-specific alkaline phosphatase (BAP), were measured at baseline and after 12 months of treatment. At the end of treatment, DPD, osteocalcin, and BAP significantly improved in the active group ($p < 0.0001$ for all) compared to the placebo group. Conversely, TRACP-5b levels were unaffected by supplementation ($p = 0.051$). Statistically significant changes in the concentrations of DPD ($p < 0.0001$), osteocalcin ($p = 0.0001$), and BAP ($p < 0.0001$) compared to baseline were also identified. Overall, the intervention significantly increased BMD measured in the whole body ($p = 0.0220$) compared with the placebo. These data indicate that the combination of equol and resveratrol may positively modulate bone turnover biomarkers and BMD, representing a potential approach to prevent age-related bone loss in postmenopausal women.

Keywords: equol; resveratrol; menopause; bone metabolism markers; bone mineral density

Citation: Corbi, G.; Nobile, V.; Conti, V.; Cannavo, A.; Sorrenti, V.; Medoro, A.; Scapagnini, G.; Davinelli, S. Equol and Resveratrol Improve Bone Turnover Biomarkers in Postmenopausal Women: A Clinical Trial. *Int. J. Mol. Sci.* **2023**, *24*, 12063. https://doi.org/10.3390/ijms241512063

Academic Editor: Maurizio Battino

Received: 13 June 2023
Revised: 23 July 2023
Accepted: 24 July 2023
Published: 27 July 2023

1. Introduction

The prevalence of age-related bone loss is higher in women than in men, especially postmenopausal women. This loss is typically associated with osteoporosis, a common chronic disease responsible for reduced bone strength, disruption of bone architecture, and an increased risk of fracture. In postmenopausal women, the incidence of hospitalization due to osteoporotic fractures is higher than that of stroke, myocardial infarction, and breast cancer. After the age of 50 years, approximately 50% of women have at least one fracture due to osteoporosis [1]. The consequences of osteoporotic fractures include a poor quality of life, disability, and mortality. Therefore, the clinical and economic burden of osteoporosis is increasingly being recognized as a serious public health problem [2].

Accelerated loss of bone mineral density (BMD), which occurs during menopause due to estrogen deficiency, is a key contributor to the incidence of osteoporotic fractures [3]. Although it is well established that fracture risk is higher in menopausal women with low BMD, considerable attention has been paid to the role of bone turnover biomarkers in the clinical evaluation of osteoporosis. These biomarkers are released

during bone remodeling processes and fall into two categories: markers of bone formation produced by osteoblastic cells or derived from procollagen metabolism and markers of bone resorption, which are degradation products of osteoclasts or collagen degradation [4,5]. Although several biochemical markers of bone formation are currently in use, the measurement of osteocalcin and bone alkaline phosphatase (BAP) is recognized as a useful means for the management of osteoporosis and for the prediction of fracture risk in postmenopausal women [6]. To evaluate the response to pharmacologic treatment and to assist the clinical diagnosis of osteoporosis, among the most common markers of bone resorption, tartrate-resistant acid phosphatase 5b (TRACP-5b) and deoxypyridinoline (DPD) have shown great potential [5,7].

Recently, significant advances have been made in the development of nutraceutical agents to prevent age-related bone loss. Phytoestrogens are a group of plant polyphenols that are commonly used for the treatment of menopause-related conditions. They can be classified into four classes: isoflavones, lignans, coumestans, and stilbenes. The estrogenic activity of these compounds may exert a multitude of benefits in estrogen-deficient menopausal women, including beneficial effects on osteoporotic bone loss [8]. The health benefits of isoflavones in middle-aged women appear to be due to individual differences in their ability to produce equol in the intestine. In Western countries, only 30–50% of individuals metabolize the isoflavone daidzein into equol and are known as equol producers [9]. Some studies have reported that supplementation with equol contributes to improving bone health in postmenopausal women, including those who are not equol producers [10,11]. It was also shown that a combination of equol and resveratrol might attenuate menopausal symptoms and increase mitochondrial function [12,13]. Resveratrol is a phytoestrogen that modulates estrogenic activity through various mechanisms. It directly interacts with the estrogen receptor, acting as both an agonist and antagonist. This compound also affects the metabolism of estrogens in the intestines and liver, increasing their levels and enhancing their central and peripheral actions. Additionally, resveratrol inhibits key enzymes involved in steroidogenesis, influencing the plasma levels of steroids and their precursors. Resveratrol also exerts potent bone-protective effects, especially in experimental models that mimic postmenopausal osteoporosis caused by estrogen deficiency [14,15].

This randomized, placebo-controlled trial evaluated the efficacy of the combined use of resveratrol and equol on bone turnover biomarkers and whole-body BMD in postmenopausal women.

2. Results

The flowchart illustrating the study design is shown in Figure 1. A total of 76 healthy postmenopausal women were randomly allocated to receive the equol/resveratrol combination or placebo. At the end of the 12-month intervention phase, eight women in the placebo group and six in the active group were lost to follow-up. In the final analysis, two participants in the treatment group were excluded because the baseline data were lost and could not be recovered. The treatment was well tolerated by the patients, and none of the subjects experienced serious adverse events.

The characteristics of the participants are listed in Table 1. No significant baseline differences were observed between the active and placebo groups regarding the concentrations of osteocalcin, BAP, TRACP-5b, and DPD. All 60 participants who completed the study had a normal BMD at baseline. No baseline differences in whole-body BMD were found between the two groups. The control and intervention groups showed no change in compliance at baseline and follow-up.

After 12 months, the active group showed a statistically significant reduction in DPD levels from baseline ($p < 0.0001$, Figure 2A). Likewise, a significant change in the concentrations of OC and BAP compared to both the baseline and placebo ($p \leq 0.0001$ for all, Figure 2C,D) was observed after 12 months. Conversely, TRACP-5b levels were unaffected by the supplementation. However, after 12 months, the active group showed a

trend toward a reduction in TRACP-5b levels compared to the placebo group ($p = 0.051$, Figure 2B). The intervention significantly increased the BMD measured in the whole body ($p = 0.0220$, Figure 2E) compared to the placebo.

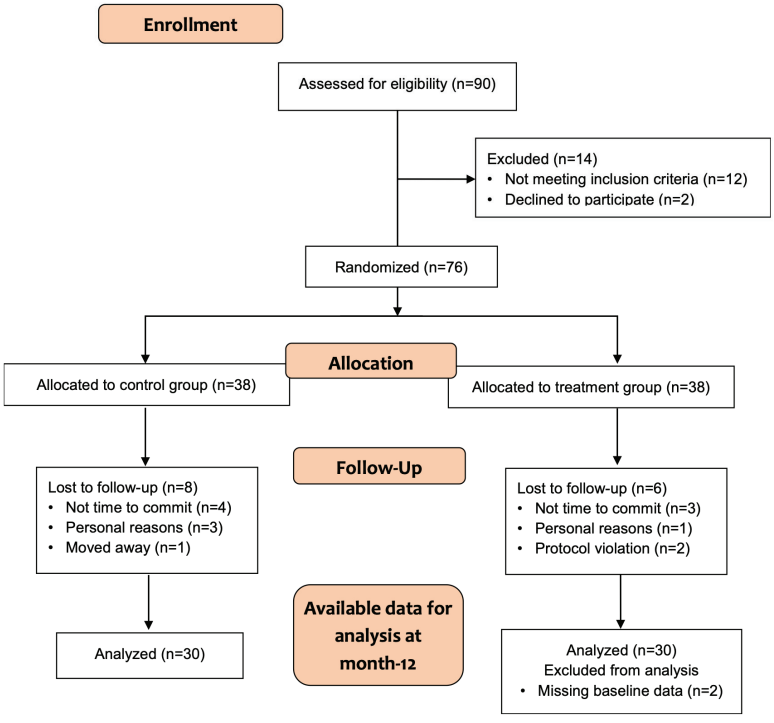

Figure 1. Flowchart of enrolment, intervention allocation, and data analysis.

Table 1. Baseline characteristics of study participants.

Characteristic	Placebo	Active	*p*
Age, years	52.69 ± 2.10	52.09 ± 1.71	0.931
SBP, mmHg	134.17 ± 12.87	134.26 ± 8.89	0.972
DBP, mmHg	85.17 ± 9.69	88.45 ± 8.46	0.171
BMI, Kg/m^2	23.84 ± 2.19	23.42 ± 1.81	0.355
Total Cholesterol, mg/dL	171.38 ± 29.23	178.03 ± 30.33	0.322
HDL Cholesterol, mg/dL	49.60 ± 21.94	50.64 ± 20.71	0.818
LDL Cholesterol, mg/dL	91.24 ± 34.78	98.08 ± 34.31	0.379
Triglycerides, mg/dL	108.43 ± 62.97	110.11 ± 66.97	0.904
ALT, U/L	22.95 ± 5.93	24.13 ± 9.49	0.217
AST, U/L	23.57 ± 4.41	24.47 ± 5.25	0.406
Glycemia, mg/dL	93.60 ± 28.98	91.08 ± 16.74	0.635
DPD, pmol/µmol	13.73 ± 2.98	14.40 ± 3.05	0.395
TRACP-5b, U/L	4.29 ± 0.81	4.11 ± 0.91	0.422
Osteocalcin, ng/mL	23.53 ± 5.67	22.95 ± 5.20	0.679
BAP, µ/mL	45.77 ± 2.30	45.13 ± 3.00	0.363
BMD, SD	0.827 ± 0.097	0.867 ± 0.119	0.211

Abbreviations: SBP, Systolic blood pressure; DBP, Diastolic blood pressure; BMI, body. mass index; LDL, low-density lipoprotein; HDL, high-density lipoprotein; ALT, alanine aminotransferase; AST, aspartate aminotransferase; DPD, deoxypyridinoline; TRACP-5b, tartrate-resistant acid phosphatase 5b; BAP, bone-specific alkaline phosphatase; BMD, bone mineral density.

To assess the efficacy of treatment, we calculated the percentage difference between the initial and final values. The percentage changes in all bone metabolism markers and BMD were significantly different between the placebo and active groups: DPD −32.63 ± 12.08%, $p < 0.0001$; TRACP-5b −8.78 ± 9.24%, $p = 0.0331$; osteocalcin +49.70 ± 28.54%, $p < 0.0001$; BAP +8.00 ± 4.64%, $p < 0.0001$; BMD +3.17 ± 2.74%, $p < 0.0001$ (Figure 3).

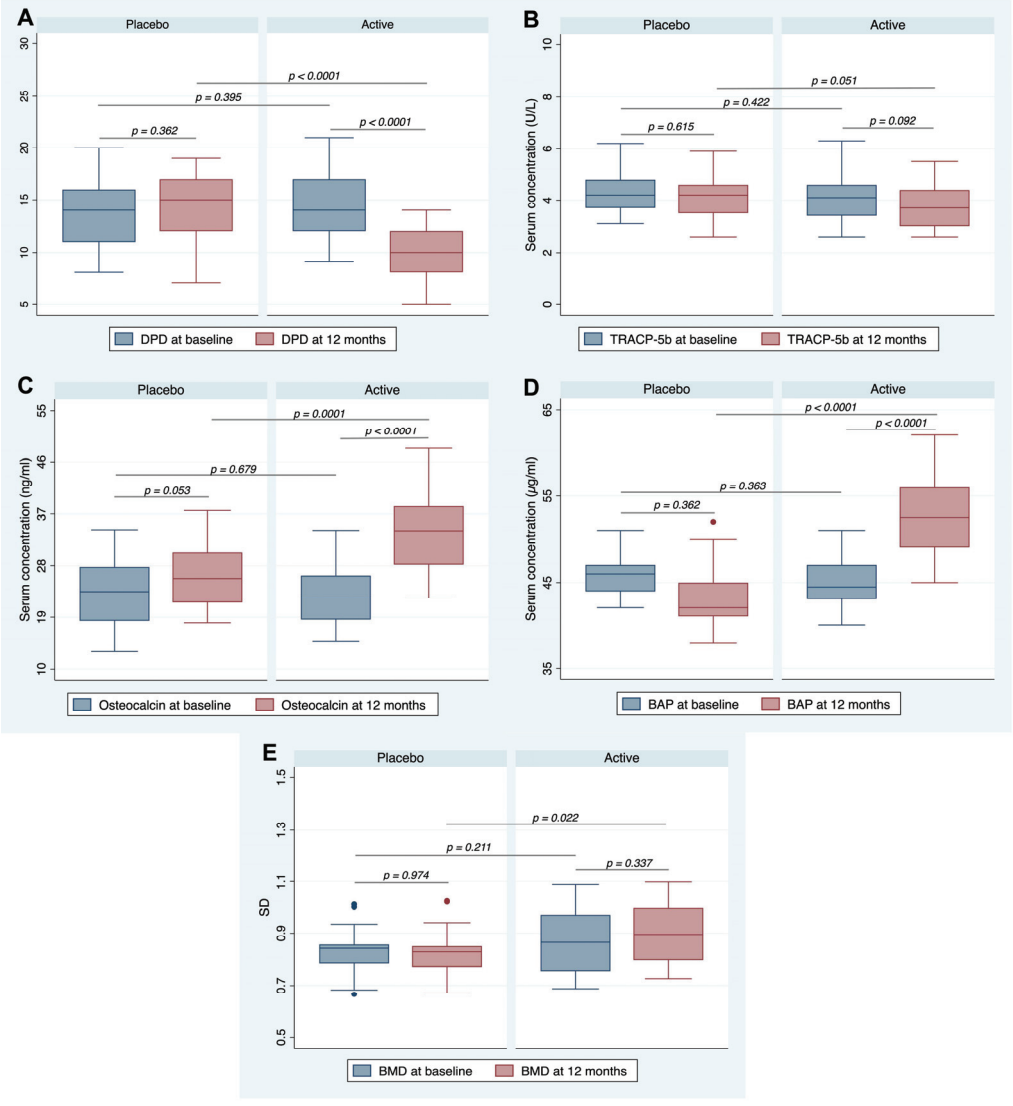

Figure 2. Concentrations of bone markers and BMD levels in the groups at baseline and after 12 months. The figure shows the concentration of (**A**) DPD, (**B**) TRACP-5b, (**C**) OC, (**D**) BAP levels, and (**E**) BMD measured in the whole body at baseline and after 12 months for both groups. The dots represent the outliner values.

To confirm these findings and determine the best predictive factor for percentage changes in BMD, multivariable linear regression analysis was conducted (Table 2). The

analysis examined whether percentage changes in OC, BAP, DPD, TRACP-5b, and being in the active group were significant predictors of percentage changes in BMD.

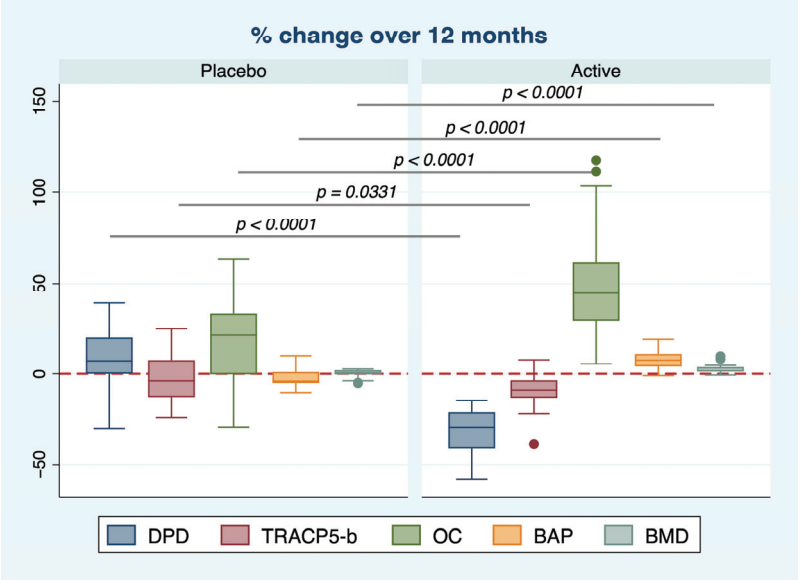

Figure 3. Percentage changes in all osteoblastic/osteoclastic parameters and BMD between the placebo and active groups were evaluated. The percentage changes in all bone metabolism markers and BMD were significantly different between the placebo and active groups. The dots represent the outliner values.

Table 2. Multivariable linear regression analysis.

Var_BMD	Beta	[95% Conf. Interval]		*p*
		Lowest	Highest	
Var_BAP	0.216	0.08	0.350	**0.002**
Var_OC	−0.014	−0.040	0.012	0.285
Var_TRACP-5b	0.008	−0.046	0.062	0.771
Var_DPD	0.052	0.008	0.095	**0.020**
Group				
Active	3.394	1.245	5.544	**0.003**

In bold the significant values are reported.

The fitted regression model was 0.495 + 0.216 × (% change in BAP) − 0.014 × (% change in OC) + 0.008 × (% change in TRACP-5b) + 0.052 × (% change in DPD) + 3.394 × (active group). The overall regression was statistically significant (r^2 = 0.4650, F (5.54), $p < 0.0001$). The best predictor of the percentage change in BMD was represented by the percentage changes in BAP (β = 0.216, 95% CI 0.0814–0.3498, $p = 0.002$), followed by participation in the active group (β = 3.394, 95% CI 1.245–5.544, $p = 0.003$), and percentage changes in DPD (β = 0.0516, 95% CI 0.008–0.095, $p = 0.020$). The analysis revealed that treatment with the equol/resveratrol combination was directly and significantly associated with higher percentage changes in BMD compared with placebo.

To better define the role of treatment in improving BMD, a linear regression analysis was performed by group. The analysis tested whether the percentage changes in OC, BAP, DPD, and TRPC-5b significantly predicted the percentage changes in BMD within each group. In the placebo group, no predictors of changes in BMD were identified. However,

in the intervention group, a statistically significant association was observed between percentage changes in BAP and percentage changes in BMD (Figure 4) (β = 0.337, 95% CI 0.139–0.536, $p = 0.002$). This finding suggested that the equol/resveratrol combination acted favorably through the BAP to induce an increase in BMD.

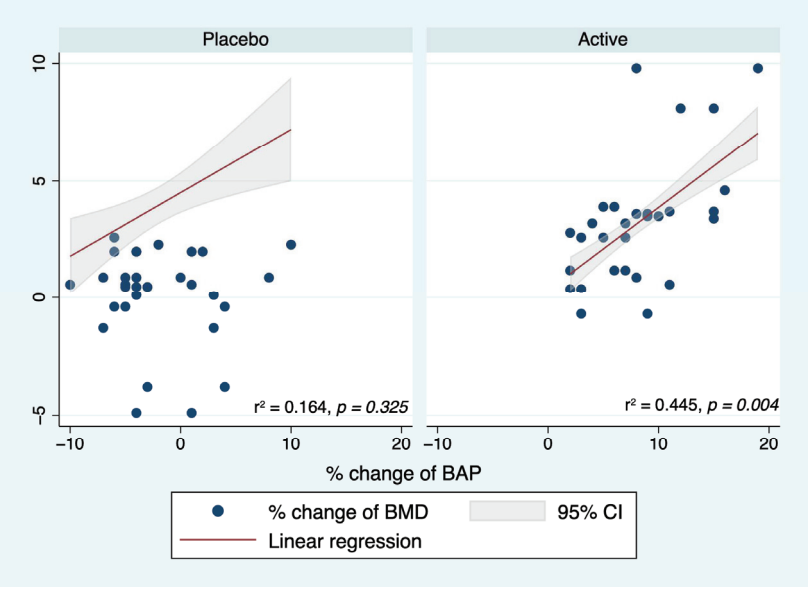

Figure 4. Linear regression analysis by group. In the placebo group, no predictors of changes in BMD were identified. Conversely, in the intervention group, a statistically significant association was found between the percentage changes in BAP and the percentage changes in BMD.

3. Discussion

In this randomized placebo-controlled trial, supplementation with an equol/resveratrol combination for 12 months improved the bone anabolism in postmenopausal women. This supplementation promoted an increase in osteoblast markers (osteocalcin and BAP) and a decrease in osteoclast markers (DPD and TRACP-5b) (Figures 2 and 3). These changes favorably counteracted the imbalance between excessive bone absorption and reduced bone formation in postmenopausal women. Moreover, these changes were also associated with an improvement in BMD, which generally exhibited a pathological reduction during menopause. These findings were confirmed by multilinear regression analysis, which identified the intervention group as a predictor of changes in BMD in a positive and direct manner (Table 2). When stratified by group, no association was found between changes in markers of bone absorption/resorption and BMD variations in the placebo group. In contrast, the active group showed a positive association between changes in BAP and BMD (Figure 4), suggesting that supplementation improved BMD by increasing BAP levels.

After menopause, women lose 3% of their BMD each year, resulting in osteopenia or osteoporosis [16]. Rapid BMD loss due to estrogen deficiency critically contributes to an increased incidence of fractures [3]. Although pharmacological options are available to counteract osteoporosis, considering the treatment duration for maintaining bone health during the postmenopausal period and the risks associated with the long-term use of estrogen therapy, it is clinically valuable to develop effective treatments with minimal side effects suitable for long-term use [17]. Therefore, dietary trends have been directed towards the utilization of health-protective and disease-preventive foods [18].

Equol is a daidzein metabolite produced by anaerobic bacteria with stronger estrogenic activity than any other isoflavone or isoflavone-derived metabolite [19]. Isoflavones have been repeatedly reported to help prevent osteoporosis [20,21], but the exact mechanism by which they preserve bone health is not completely understood. In a meta-analysis, Wei et al. found that soy isoflavones significantly increased bone mineral density by 54% and decreased the bone resorption marker urinary DPD by 23% compared to baseline in women. However, no significant effects on serum bone alkaline phosphatase activity have been observed [20]. In our study, the 12-month use of combined supplementation with equol and resveratrol was able to modify BMD and resorption and absorption bone markers.

Resveratrol has also been reported to act as a phytoestrogen. In a clinical study, resveratrol showed favorable effects on estrogen metabolism and circulating sex steroid hormones [22]. Recently, the Resveratrol for Healthy Aging in Women (RESHAW) trial demonstrated that a low dose of resveratrol (75 mg twice daily) supplementation in post-menopausal women, after 12 months, induced positive effects compared with placebo on bone density in the lumbar spine and neck of the femur. These effects were accompanied by a reduction in the levels of C-terminal telopeptide type-1 collagen, a bone resorption marker [23]. The significant benefits observed in our study may be the result of combining compounds, rather than the individual effects of equol or resveratrol. Although there are beneficial properties of equol and resveratrol against menopause-related symptoms, their effects on bone metabolism and prophylaxis of osteoporosis are poorly explored. To our knowledge, this is the first study to investigate the effects of combined supplementation of equol and resveratrol on bone metabolism in humans.

These compounds may act through multiple mechanisms, particularly through the estrogenic pathway. Resveratrol may exert its estrogen-like effect on bone by increasing the gene expression of osteoprotegerin, a protein that inhibits receptor activator of nuclear factor κB ligand (RANKL) to counteract osteoclast differentiation and activity [24]. Similarly, isoflavones have been reported to trigger the activity and proliferation of osteoblasts via insulin-like growth factor 1 (IGF-1), a key factor in maintaining bone mass against the action of osteoclasts [25]. In our study, multivariate analysis confirmed an association between the BMD improvement and increased BAP levels following supplementation, suggesting the involvement of this mechanism.

Soy isoflavones decrease RANKL levels and increase osteoprotegerin levels [26]. Therefore, isoflavones can improve bone metabolism and decrease bone resorption. Soy isoflavones decrease serum markers of bone resorption and improve bone metabolism. However, while the available data are promising, several studies have reported no change in RANKL and osteoprotegerin levels with isoflavone supplementation. In this regard, the current evidence is insufficient for conclusive approval of the efficacy of isoflavones in the RANKL/RANK/OPG pathway. Further research, including animal and human studies, is needed to confirm the effect of soy isoflavones on the RANKL/RANK/OPG pathway [26].

In most cases, supplementation included only isoflavones. Recently, Tousen et al. demonstrated that the combination of soy isoflavones and resveratrol prevented bone loss and decreased the RANKL/OPG gene expression ratio in bone marrow cells in unloaded mice [27], supporting the hypothesis of a beneficial multiplicative effect of these compounds on bone mass density.

Another factor that might have contributed to these effects could be related to the dosage. The dose of equol applied in this study has been used in several clinical trials and is reported to be effective for general menopausal symptoms without any serious adverse events. Tai et al. demonstrated that 24-month treatment with 300 mg/day isoflavones did not prevent the decline in BMD in postmenopausal women [28]. Kreijkamp-Kaspers et al. reported that a 12-month soy protein supplementation did not have any effect on BMD in postmenopausal women aged 60–75 years [29]. In contrast, Wu et al. assessed the positive effects of a 12-month intervention with soy isoflavones on the BMD of equol-producing postmenopausal Japanese women [30]. Consistent with our results, Wong et al. reported

that a 12-month supplementation with 75 mg of resveratrol twice daily has the potential to slow bone loss in postmenopausal women [23].

The present study has several strengths and limitations. The main strength is represented by the 100% retention rate for a 12-month intervention, associated with the investigation of the effects of simultaneous combined supplementation of equol and resveratrol on bone metabolism. The primary limitation of this study was its small sample size. However, several other similar studies did not include larger study populations. The second limitation is the duration of the study. Even though we conducted a 12-month study, a longer intervention duration may be helpful in further assessing the effects of equol and resveratrol on bone turnover and density. Finally, our study did not determine whether the enrolled subjects were equol producers. Therefore, even though the majority of Western women are not equol producers, we did not stratify the treatment and placebo groups based on equol-producing status.

In conclusion, our results suggest that combined supplementation of equol and resveratrol has some additional benefits on bone turnover biomarkers, especially in improving bone density formation in postmenopausal women. In the near future, larger studies should be conducted to confirm these results and investigate the molecular mechanisms underlying these effects. This non-pharmacological treatment represents a potential approach for preventing age-related bone loss in postmenopausal women.

4. Materials and Methods

4.1. Participants

Eligible subjects were all adult Caucasian menopausal women aged between 50 and 55 years old. The inclusion criteria were as follows: (1) menopause according to the WHO definition (after 12 consecutive months without menstruation) [31]; (2) case history characterized by menopausal complaints such as hot flushes, anxiety, emotional instability, sleep disorders, and depression; (3) 20 $kg/m^2 \geq$ BMI < 25 kg/m^2. Women were ineligible if any of the following criteria were present: (1) case history related to endometrial hyperplasia; (2) hormone replacement therapy (HRT); (3) metabolic syndrome; (4) pharmacological or nutritional treatments known to interfere with resveratrol and equol or affecting menopause symptoms. The subjects maintained their usual physical activity and diet pattern throughout the study. The study took place at Farcoderm S.r.l. facilities in San Martino Siccomario (PV), Italy. Subjects attended clinic visits at the time of randomization (baseline) and 12 months after supplementation initiation.

4.2. Study Design

A randomized, double-blind, placebo-controlled dietary intervention trial of 12 months duration was designed to evaluate the effects of equol and resveratrol supplementation on bone markers of in menopausal women. Of 90 eligible women, 12 were excluded because they did not meet the inclusion criteria, and 2 declined to participate (Figure 1). Thus, 76 menopausal women were included in the study. All the study procedures were carried out in accordance with the Declaration of Helsinki.

The study protocol was approved by the local ethics committee (study code: SI.02.DS.L; ref. no. 2011/3) and registered at the ISRCTN registry (ISRCTN10128742). All subjects provided written informed consent prior to the initiation of any study-related procedures.

4.3. Intervention and Randomization

The product was a commercially available dietary supplement (Equopausa D. Ulrich, Paladin Pharma S.p.A., Turin, Italy) containing 200 mg of fermented soy (including 80 mg of isoflavone aglycones and 10 mg of equol) and 25 mg of resveratrol from Vitis vinifera. The proposed level of equol intake has been used in several clinical trials and reported to be effective for menopausal symptoms [10,32,33]. The dosage of resveratrol was chosen because it was supported by several human studies showing that 25 mg of resveratrol per os was well absorbed and well tolerated [34–36]. Both active and placebo products were in

tablet form and identical in appearance. They were prepacked in blisters and consecutively numbered for each subject according to the randomization list. Subjects' compliance to treatment was assessed by means of product accountability as follows: at each visit, the expected number of consumed capsules was compared with the amount dispensed minus the quantity of the product that the subject returned.

Subjects were randomly assigned to receive the product or the placebo once a day. A restricted randomization list was created using PASS v.2008 (PASS, LLC. Kaysville, UT, USA) statistical software. The randomization sequence was stratified using a 10% maximum allowable % deviation with a 1:1 allocation ratio. The allocation sequence was concealed from the in-site study director in sequentially numbered, opaque, and sealed envelopes, reporting the unblinded treatment allocation. An independent technician dispensed either active or placebo products. Subjects, investigators, and collaborators were kept masked to product assignment.

The intervention period with phytoestrogens that would elicit a beneficial response in menopausal women is controversial and usually ranges from 3 to 12 months. Given that a short-term treatment of 3 months could have been a potential limitation, we chose 12 months of intervention as a in previous study investigating the effects of equol on bone metabolism in postmenopausal women [10].

4.4. Measurement of Bone Markers

Subjects were evaluated at baseline and after 12 months of treatment. Blood samples were centrifuged at 1200 g for 15 min at 4 °C, and serum samples were separated, divided into aliquots, and stored at −80 °C until analysis. Parameters of bone metabolism, such as OC and BAP, were measured by an electrochemiluminescence assay (ECLIA) (Roche Diagnostics, Mannheim, Germany). The serum level of TRACP-5b was measured using a fragment-absorbed immunocapture enzymatic assay (Quidel Corporation, San Diego, CA, USA). A complete 24 h urine collection was conducted at the beginning and end of the intervention and aliquots were stored at −80 °C until analysis. Urinary DPD concentrations were measured by high-performance liquid chromatography (HPLC) (Shimadzu, Kyoto, Japan).

4.5. Measurement of BMD

The whole-body BMD was assessed by dual-energy X-ray absorptiometry (DXA) using a Lunar Prodigy Primo device (GE Healthcare, Chicago, IL, USA) with the Encore v.1 Windows XP software platform. The measurements were performed at baseline and after 12 months of treatment. The device was regularly calibrated before each diagnostic block and all DXA scans were clinically performed in accordance with the manufacturer's recommendations.

4.6. Statistical Analysis

Categorical variables were summarized using frequencies and percentages, whereas, for continuous variables, means and standard deviations (SD) were used. For the univariate analysis, χ^2 tests to compare categorical variables between the groups and the Student's *t*-test for independent samples to compare continuous variables between the groups were used. To check the percentual change in all parameters, the following formula was used: [(Final value − baseline value)/baseline value] × 100. Multivariable linear regression was used to determine the independent predictive factors of % changes in BMD. Two-tailed $p < 0.05$ was considered statistically significant. Statistical analyses were performed using STATA 16 software (Stata Corp., College Station, TX, USA).

Author Contributions: Conceptualization, G.C. and S.D.; methodology, G.C. and S.D.; software, V.C. and A.M.; validation, A.C. and G.S.; formal analysis, G.C.; investigation, V.N.; resources, V.S.; data curation, A.M. and V.C.; writing—original draft preparation, G.C.; writing—review and editing, S.D. and G.C.; visualization, A.C.; supervision, G.S.; project administration, S.D.; funding acquisition, G.S. All authors have read and agreed to the published version of the manuscript.

Funding: This study was not supported by any industrial funds. PaladinPharma S.p.A. only provided the placebo and the active treatment. This company had no influence on the study design; in the collection, analysis or interpretation of data; or in the decision to submit the article for publication.

Institutional Review Board Statement: The study protocol and the informed consent form were approved by the local ethics committee (study code: SI.02.DS.L; ref. no. 2011/3, approved on March 2011). This study was registered at the ISRCTN registry (ISRCTN10128742; https://doi.org/10.1186/ISRCTN10128742, accessed on 25 January 2023).

Informed Consent Statement: Informed consent was obtained from all subjects involved in the study.

Data Availability Statement: The data presented in this study are available on request from the corresponding author. The data are not publicly available due to privacy.

Acknowledgments: We would like to acknowledge Manuela Visentin for her support and critical reading of the manuscript.

Conflicts of Interest: The authors declare no conflict of interest.

References

1. Singer, A.; Exuzides, A.; Spangler, L.; O'Malley, C.; Colby, C.; Johnston, K.; Agodoa, I.; Baker, J.; Kagan, R. Burden of illness for osteoporotic fractures compared with other serious diseases among postmenopausal women in the United States. *Mayo Clin. Proc.* **2015**, *90*, 53–62. [CrossRef] [PubMed]
2. Clynes, M.A.; Harvey, N.C.; Curtis, E.M.; Fuggle, N.R.; Dennison, E.M.; Cooper, C. The epidemiology of osteoporosis. *Br. Med. Bull.* **2020**, *133*, 105–117. [CrossRef]
3. Cheng, C.H.; Chen, L.R.; Chen, K.H. Osteoporosis Due to Hormone Imbalance: An Overview of the Effects of Estrogen Deficiency and Glucocorticoid Overuse on Bone Turnover. *Int. J. Mol. Sci.* **2022**, *23*, 1376. [CrossRef] [PubMed]
4. Kuo, T.R.; Chen, C.H. Bone biomarker for the clinical assessment of osteoporosis: Recent developments and future perspectives. *Biomark. Res.* **2017**, *5*, 18. [CrossRef] [PubMed]
5. Nishizawa, Y.; Miura, M.; Ichimura, S.; Inaba, M.; Imanishi, Y.; Shiraki, M.; Takada, J.; Chaki, O.; Hagino, H.; Fukunaga, M.; et al. From the Japan Osteoporosis Society Bone Turnover Marker Investigation Committee. Executive summary of the Japan Osteoporosis Society Guide for the Use of Bone Turnover Markers in the Diagnosis and Treatment of Osteoporosis (2018 Edition). *Clin. Chim. Acta* **2019**, *498*, 101–107. [CrossRef]
6. Lumachi, F.; Ermani, M.; Camozzi, V.; Tombolan, V.; Luisetto, G. Changes of bone formation markers osteocalcin and bone-specific alkaline phosphatase in postmenopausal women with osteoporosis. *Ann. N. Y. Acad. Sci.* **2009**, *1173* (Suppl. S1), E60–E63. [CrossRef]
7. Hlaing, T.T.; Compston, J.E. Biochemical markers of bone turnover—Uses and limitations. *Ann. Clin. Biochem.* **2014**, *51 Pt 2*, 189–202. [CrossRef]
8. Sansai, K.; Na Takuathung, M.; Khatsri, R.; Teekachunhatean, S.; Hanprasertpong, N.; Koonrungsesomboon, N. Effects of isoflavone interventions on bone mineral density in postmenopausal women: A systematic review and meta-analysis of randomized controlled trials. *Osteoporos. Int.* **2020**, *31*, 1853–1864. [CrossRef]
9. Fatima, A.; Khan, M.S.; Ahmad, M.W. Therapeutic Potential of Equol: A Comprehensive Review. *Curr. Pharm. Des.* **2020**, *26*, 5837–5843. [CrossRef]
10. Tousen, Y.; Ezaki, J.; Fujii, Y.; Ueno, T.; Nishimuta, M.; Ishimi, Y. Natural S-equol decreases bone resorption in postmenopausal, non-equol-producing Japanese women: A pilot randomized, placebo-controlled trial. *Menopause* **2011**, *18*, 563–574. [CrossRef]
11. Yoshikata, R.; Myint, K.Z.Y.; Ohta, H. Effects of Equol Supplement on Bone and Cardiovascular Parameters in Middle-Aged Japanese Women: A Prospective Observational Study. *J. Altern. Complement. Med.* **2018**, *24*, 701–708. [CrossRef]
12. Davinelli, S.; Scapagnini, G.; Marzatico, F.; Nobile, V.; Ferrara, N.; Corbi, G. Influence of equol and resveratrol supplementation on health-related quality of life in menopausal women: A randomized, placebo-controlled study. *Maturitas* **2017**, *96*, 77–83. [CrossRef]
13. Davinelli, S.; Sapere, N.; Visentin, M.; Zella, D.; Scapagnini, G. Enhancement of mitochondrial biogenesis with polyphenols: Combined effects of resveratrol and equol in human endothelial cells. *Immun. Ageing* **2013**, *10*, 28. [CrossRef]
14. Qasem, R.J. The estrogenic activity of resveratrol: A comprehensive review of in vitro and in vivo evidence and the potential for endocrine disruption. *Crit. Rev. Toxicol.* **2020**, *50*, 439–462. [CrossRef]
15. Tou, J.C. Evaluating resveratrol as a therapeutic bone agent: Preclinical evidence from rat models of osteoporosis. *Ann. N. Y. Acad. Sci.* **2015**, *1348*, 75–85. [CrossRef]

16. Majumder, M.I.; Harun, M.A.S.I. Alveolar Bone Changes in Post-menopausal Osteopenic and Osteoporosis Women: An Original Research. *Int. J. Dent. Med. Spec.* **2015**, *2*, 9–14. [CrossRef]
17. Lambert, M.N.T.; Thybo, C.B.; Lykkeboe, S.; Rasmussen, L.M.; Frette, X.; Christensen, L.P.; Jeppesen, P.B. Combined bioavailable isoflavones and probiotics improve bone status and estrogen metabolism in postmenopausal osteopenic women: A randomized controlled trial. *Am. J. Clin. Nutr.* **2017**, *106*, 909–920. [CrossRef]
18. Arooj, A.; Rabail, R.; Naeem, M.; Goksen, G.; Xu, B.; Aadil, R.M. A comprehensive review of the bioactive components of sesame seeds and their impact on bone health issues in postmenopausal women. *Food Funct.* **2023**, *14*, 4966–4980. [CrossRef]
19. Jackson, R.L.; Greiwe, J.S.; Schwen, R.J. Emerging evidence of the health benefits of S-equol, an estrogen receptor β agonist. *Nutr. Rev.* **2011**, *69*, 432–448. [CrossRef]
20. Wei, P.; Liu, M.; Chen, Y.; Chen, D.D. Systematic review of soy isoflavone supplements on osteoporosis in women. *Asian Pac. J. Trop. Med.* **2012**, *5*, 243–248. [CrossRef]
21. Pawlowski, J.W.; Martin, B.R.; McCabe, G.P.; McCabe, L.; Jackson, G.S.; Peacock, M.; Barnes, S.; Weaver, C.M. Impact of equol-producing capacity and soy-isoflavone profiles of supplements on bone calcium retention in postmenopausal women: A randomized crossover trial. *Am. J. Clin. Nutr.* **2015**, *102*, 695–703. [CrossRef] [PubMed]
22. Chow, H.H.; Garland, L.L.; Heckman-Stoddard, B.M.; Hsu, C.H.; Butler, V.D.; Cordova, C.A.; Chew, W.M.; Cornelison, T.L. A pilot clinical study of resveratrol in postmenopausal women with high body mass index: Effects on systemic sex steroid hormones. *J. Transl. Med.* **2014**, *12*, 223. [CrossRef] [PubMed]
23. Wong, R.H.; Thaung Zaw, J.J.; Xian, C.J.; Howe, P.R. Regular Supplementation with Resveratrol Improves Bone Mineral Density in Postmenopausal Women: A Randomized, Placebo-Controlled Trial. *J. Bone Miner. Res.* **2020**, *35*, 2121–2131. [CrossRef] [PubMed]
24. Zhao, H.; Li, X.; Li, N.; Liu, T.; Liu, J.; Li, Z.; Xiao, H.; Li, J. Long-term resveratrol treatment prevents ovariectomy-induced osteopenia in rats without hyperplastic effects on the uterus. *Br. J. Nutr.* **2014**, *111*, 836–846. [CrossRef]
25. Arjmandi, B.H.; Smith, B.J. Soy isoflavones' osteoprotective role in postmenopausal women: Mechanism of action. *J. Nutr. Biochem.* **2002**, *13*, 130–137. [CrossRef]
26. Hooshiar, S.H.; Tobeiha, M.; Jafarnejad, S. Soy Isoflavones and Bone Health: Focus on the RANKL/RANK/OPG Pathway. *Biomed. Res. Int.* **2022**, *2022*, 8862278. [CrossRef]
27. Tousen, Y.; Ichimaru, R.; Kondo, T.; Inada, M.; Miyaura, C.; Ishimi, Y. The Combination of Soy Isoflavones and Resveratrol Preserve Bone Mineral Density in Hindlimb-Unloaded Mice. *Nutrients* **2020**, *12*, 2043. [CrossRef]
28. Tai, T.Y.; Tsai, K.S.; Tu, S.T.; Wu, J.S.; Chang, C.I.; Chen, C.L.; Shaw, N.S.; Peng, H.Y.; Wang, S.Y.; Wu, C.H. The effect of soy isoflavone on bone mineral density in postmenopausal Taiwanese women with bone loss: A 2-year randomized double-blind placebo-controlled study. *Osteoporos. Int.* **2012**, *23*, 1571–1580. [CrossRef]
29. Kreijkamp-Kaspers, S.; Kok, L.; Grobbee, D.E.; de Haan, E.H.; Aleman, A.; Lampe, J.W.; van der Schouw, Y.T. Effect of soy protein containing isoflavones on cognitive function, bone mineral density, and plasma lipids in postmenopausal women: A randomized controlled trial. *JAMA* **2004**, *292*, 65–74. [CrossRef]
30. Wu, J.; Oka, J.; Ezaki, J.; Ohtomo, T.; Ueno, T.; Uchiyama, S.; Toda, T.; Uehara, M.; Ishimi, Y. Possible role of equol status in the effects of isoflavone on bone and fat mass in postmenopausal Japanese women: A double-blind, randomized, controlled trial. *Menopause* **2007**, *14*, 866–874. [CrossRef]
31. WHO. Menopause. Available online: https://www.who.int/news-room/fact-sheets/detail/menopause (accessed on 10 January 2023).
32. Ishiwata, N.; Melby, M.K.; Mizuno, S.; Watanabe, S. New equol supplement for relieving menopausal symptoms: Randomized, placebo-controlled trial of Japanese women. *Menopause* **2009**, *16*, 141–148. [CrossRef]
33. Oyama, A.; Ueno, T.; Uchiyama, S.; Aihara, T.; Miyake, A.; Kondo, S.; Matsunaga, K. The effects of natural S-equol supplementation on skin aging in postmenopausal women: A pilot randomized placebo-controlled trial. *Menopause* **2012**, *19*, 202–210. [CrossRef]
34. Walle, T.; Hsieh, F.; DeLegge, M.H.; Oatis, J.E., Jr.; Walle, U.K. High absorption but very low bioavailability of oral resveratrol in humans. *Drug Metab. Dispos.* **2004**, *32*, 1377–1382. [CrossRef]
35. Almeida, L.; Vaz-da-Silva, M.; Falcão, A.; Soares, E.; Costa, R.; Loureiro, A.I.; Fernandes-Lopes, C.; Rocha, J.F.; Nunes, T.; Wright, L.; et al. Pharmacokinetic and safety profile of trans-resveratrol in a rising multiple-dose study in healthy volunteers. *Mol. Nutr. Food Res.* **2009**, *53* (Suppl. S1), S7–S15. [CrossRef]
36. Cottart, C.H.; Nivet-Antoine, V.; Laguillier-Morizot, C.; Beaudeux, J.L. Resveratrol bioavailability and toxicity in humans. *Mol. Nutr. Food Res.* **2010**, *54*, 7–16. [CrossRef]

International Journal of
Molecular Sciences

MDPI

Article

Quercetins, Chlorogenic Acids and Their Colon Metabolites Inhibit Colon Cancer Cell Proliferation at Physiologically Relevant Concentrations

Alice Cattivelli, Angela Conte and Davide Tagliazucchi *

Department of Life Sciences, University of Modena and Reggio Emilia, Via Amendola, 2-Pad. Besta, 42100 Reggio Emilia, Italy; alice.cattivelli@unimore.it (A.C.); angela.conte@unimore.it (A.C.)
* Correspondence: davide.tagliazucchi@unimore.it

Abstract: Several studies have suggested that a phenolic-rich diet may be protective against colon cancer. Most phenolic compounds are not absorbed in the small intestine and reach the colon where they are metabolized by gut microbiota in simple phenolic acids. In this study, the anti-proliferative activity of quercetins, chlorogenic acids, their colon metabolites and mixtures of parent compounds/metabolites was assessed by using two colon cancer cell lines (Caco-2 and SW480) at physiologically relevant concentrations. Chlorogenic acids, quercetin and the metabolite 3-(3′,4′-dihydroxyphenyl)acetic acid exerted remarkable anti-proliferative activity against Caco-2, whereas quercetin derivatives and metabolites were the most active against SW480. Tested compounds arrested the cell cycle at the S phase in both the cell lines. The mixtures of parent compounds/metabolites, which mimic the colon human metabotypes that slowly or rapidly metabolize the parent compounds, similarly inhibited cell growth. SW480 cells metabolized parent phenolic compounds more rapidly and extensively than Caco-2, whereas colon metabolites were more stable. These results suggest that dietary phenolic compounds exert an anti-proliferative effect against human colon cancer cells that can be further sustained by the colon metabolites. Therefore, gut microbiota metabolism of phenolic compounds may be of paramount importance in explaining the protective effect of phenolic-rich foods against colon cancer.

Keywords: phenolic compounds; mass spectrometry; colon cancer; anti-proliferative activity; gut microbiota; metabolism

Citation: Cattivelli, A.; Conte, A.; Tagliazucchi, D. Quercetins, Chlorogenic Acids and Their Colon Metabolites Inhibit Colon Cancer Cell Proliferation at Physiologically Relevant Concentrations. *Int. J. Mol. Sci.* **2023**, *24*, 12265. https://doi.org/10.3390/ijms241512265

Academic Editor: Francesco Visioli

Received: 7 July 2023
Revised: 28 July 2023
Accepted: 29 July 2023
Published: 31 July 2023

1. Introduction

Colorectal cancer is one of the most frequent forms of cancer, playing an important role in mortality, lifestyle and economic costs worldwide [1]. Colorectal cancer is primarily affected by lifestyle (such as diets and low physical activity), genetic predisposition, and the presence of chronic intestinal inflammation conditions (such as inflammatory bowel diseases). This pathology is characterized by a low heritability level, with only 12–35% of CRC cases attributable to genetic predisposition, reflecting the crucial role of dietary and environmental factors [2]. Colorectal cancer prevention is one of the most essential priorities in public health, especially considering that modifiable lifestyle factors had a pivotal role in the occurrence and progression of colorectal cancer [3]. Several epidemiological and observational studies have highlighted the strong impact of diet on the risk of colorectal cancer [4–7]. Dietary factors and the type of diet are among the main determinants in the development of colorectal cancer [4]. For example, diets rich in fibers, calcium and dairy products as well as a plant-based diet rich in phenolic compounds can decrease the risk of developing colorectal cancer [4,5,8,9]. Vice versa, a low-fiber diet associated with a high intake of red and processed meat may increase the risk of the onset of colorectal cancer [4,5,8,9].

Among the different dietary patterns, the Mediterranean diet is widely recognized as a healthy diet that may be protective against the onset of several chronic diseases, including cancer [10,11]. For example, populations with a high adherence to the Mediterranean diet displayed a lower incidence of colorectal cancer, suggesting that the Mediterranean diet may be chemopreventive against this type of cancer [10,12,13]. Indeed, the Mediterranean diet is characterized by a high intake of vegetables, fiber-rich foods, fresh fruits and legumes together with a low intake of red and processed meat [11].

The beneficial consequences of a Mediterranean diet—and, more generally, a diet rich in vegetables and fruits—in preventing the onset of colorectal cancer may be in part ascribable to the high content in phenolic compounds of these foods [8,10]. For example, Zamora-Ros et al. [14] found a positive association between the intake of phenolic acids (mainly hydroxycinnamic acids) and a reduction in colon cancer, whereas Chang et al. [15] suggested that a high intake of flavonoids (especially flavonols) may decrease the onset of colon cancer.

Hydroxycinnamic acids are an important class of phenolic compounds which are mainly found in nature esterified with one or more quinic acid moieties, producing the so-called chlorogenic acids [16]. The most important chlorogenic acids found in nature are caffeoylquinic, feruloylquinic and dicaffeoylquinic acids [17]. In the context of the Mediterranean diet, they may account for 25–35% of total phenolic compound intake [18,19]. The main dietary sources of chlorogenic acids in the Mediterranean diet are coffee, vegetables (such as eggplant and carrots) and fruits (such as cherries and apples) [19–21].

Flavonols are another widespread class of dietary phenolic compounds that are mainly found in nature in the form of glycoside derivatives [22]. Flavonols may account for 7–15% of total phenolic compounds in the Mediterranean diet, where the main sources are fruits and vegetables and, in particular, onions, apples, berries and red wine [18,23]. The principal flavonols identified in vegetables are glycosylated quercetin derivatives, such as quercetin-3-*O*-glucoside and quercetin-3-*O*-rutinoside, as well as quercetin-4′-*O*-glucoside and quercetin-3-*O*-glucoside-4′-*O*-glucoside in onion [22,23].

Several meta-analyses of epidemiological studies as well as animal studies provide support for the protective effect of flavonols and hydroxycinnamic acids against colorectal cancer [15,24–26]. Nevertheless, the data extracted from human intervention studies are still inconclusive owing to the considerable inter-individual variability due largely to the different gut microbiota metabolism of phenolic compounds among individuals.

Quercetin and quercetin derivatives reaching the colon are subjected to microbiota metabolism that involves a deglycosylation reaction, followed by C-ring fission and β-oxidation generating some low-molecular-weight phenolic acids, mainly 3-(3′-hydroxyphenyl) propanoic acid, 3-(3′-hydroxyphenyl)acetic acid and 3-(3′,4′-dihydroxyphenyl)acetic acid [27,28]. Similarly, the colon metabolism of chlorogenic acids starts with the removal of the quinic acid moiety followed by reduction and de-hydroxylation, which results in the accumulation of 3-(3′-hydroxyphenyl)propanoic acid [29,30]. However, the amount and the type of the produced metabolites greatly differed among individuals depending on the microbiota composition [17,31]. Therefore, both the parent compounds and the microbial metabolites co-exist in the colon, and the ratio of parent compounds/metabolites strongly depends on the individual microbiota composition and on the ability to produce high or low amounts of phenolic metabolites and, therefore, on inter-individual variability and metabotype [32,33]. In the low-producers metabotype (i.e., individuals that produce low amounts of colon metabolites) the ratio of parent compounds/metabolites is strongly shifted towards the parent compounds, whereas in the high-producers metabotype (i.e., individuals that produce high amounts of colon metabolites) the equilibrium is directed towards a higher amount of colon metabolites.

Thus, the aim of this work was to study the anti-proliferative activity and the cell metabolism of selected quercetin derivatives (quercetin, quercetin-4′-*O*-glucoside and quercetin-3-*O*-glucoside-4′-*O*-glucoside) and chlorogenic acids (3-*O*-caffeoylquinic acid, 5-*O*-caffeoylquinic acid and 3,5-di-*O*-caffeoylquinic acid) as well as their most important

colon metabolites (3-(3′-hydroxyphenyl)propanoic acid, 3-(3′-hydroxyphenyl)acetic acid and 3-(3′,4′-dihydroxyphenyl)acetic acid) using colon adenocarcinoma Caco-2 and SW480 cell lines. Indeed, to understand the possible role of inter-individual variability, six different mixes were prepared, mimicking the low-producers (high amounts of parent compounds and low amounts of metabolites) and the high-producers (low amounts of parent compounds and high amounts of metabolites) metabotypes in comparison with a third mix with equimolar amounts of parent compounds and metabolites. The aim was to understand if colon metabolites may retain anti-proliferative activity against colon cancer cells sustaining the effect of the parent compounds and to shed light on the possible different impact of the diverse human metabotypes on the anti-cancer potential of phenolic-rich vegetables.

2. Results

2.1. Anti-Proliferative Activity of Phenolic Compounds and Metabolites

The tested parent phenolic compounds and metabolites at 100 µmol/L concentration exerted a time-dependent anti-proliferative activity against both the colon cancer cell lines, with the only exception being quercetin-3-*O*-glucoside-4′-*O*-glucoside which did not show any activity against Caco-2 cell proliferation at any time (Figure 1a,b).

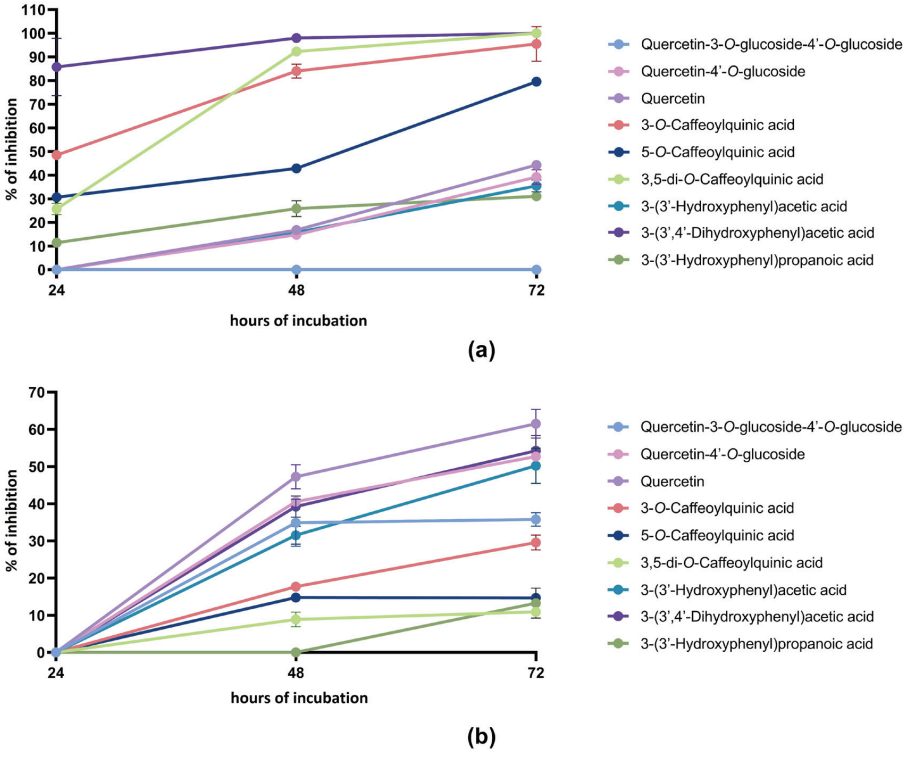

Figure 1. Antiproliferative activity of parent phenolic compounds and colon metabolites. All the compounds were tested at a final concentration of 100 µmol/L. (**a**) Percentage of inhibition of Caco-2 growth after 24, 48 and 72 h. (**b**) Percentage of inhibition of SW480 growth after 24, 48 and 72 h. Tested compounds were quercetins (quercetin-3-*O*-glucoside-4′-*O*-glucoside, quercetin-4′-*O*-lucoside and quercetin) and quercetin-derived colon metabolites (3-(3′-hydroxyphenyl)acetic acid, 3-(3′,4′-dihydroxyphenyl)acetic acid and 3-(3′-hydroxyphenyl)propanoic acid) as well as chlorogenic acids (3,5-di-*O*-caffeoylquinic acid, 3-*O*-caffeoylquinic acid and 5-*O*-caffeoylquinic acid) and the chlorogenic-acid-derived colon metabolite 3-(3′-hydroxyphenyl)propanoic acid. Data are presented as mean ± standard deviation.

In general, quercetin derivatives were more active against SW480 cell proliferation with respect to Caco-2 proliferation. The anti-proliferative activity started to be detectable after 48 h of incubation and increased in both the cell lines after 72 h of incubation. Among quercetin derivatives, the highest activity was found in both cell lines for quercetin, followed by quercetin-4′-*O*-glucoside. For both the compounds, the anti-proliferative effect was significantly higher ($p < 0.05$) against SW480 with respect to Caco-2 both after 48 and 72 h of incubation. As already mentioned, quercetin-3-*O*-glucoside-4′-*O*-glucoside displayed anti-proliferative activity only against the SW480 cell line, although it was significantly lower ($p < 0.05$) with respect to quercetin and quercetin-4′-*O*-glucoside.

An opposite trend was observed for chlorogenic acids, since they displayed a significantly higher ($p < 0.05$) anti-proliferative activity against Caco-2 with respect to the SW480 cell line at any time. In Caco-2 cells, 3,5-di-*O*-caffeoylquinic acid, 3-*O*-caffeoylquinic acid and 5-*O*-caffeoylquinic acid were active already after 24 h of incubation, and then the anti-proliferative activity increased over time, reaching an almost complete inhibition after 72 h of incubation. The anti-proliferative activity of 5-*O*-caffeoylquinic acid was significantly lower ($p < 0.05$) than that of its positional isomer 3-*O*-caffeoylquinic acid at any time. In the case of SW480, the maximum effect was observed after 72 h of incubation for both the compounds, with 3-*O*-caffeoylquinic acid more active than 3,5-di-*O*-caffeoylquinic acid and 5-*O*-caffeoylquinic acid (29.6%, 10.9% and 14.7% of inhibition at 72 h, respectively).

A similar trend was observed also for the phenolic metabolites, which exerted a higher anti-proliferative effect ($p < 0.05$) against Caco-2 with respect to SW480 at any incubation time, except for 3-(3′-hydroxyphenyl)acetic acid. The colon metabolite 3-(3′,4′-dihydroxyphenyl)acetic acid was the tested compound that exerted the highest anti-proliferative effect against the Caco-2 cell line. The metabolite 3-(3′-hydroxyphenyl)propanoic acid was more effective than 3-(3′-hydroxyphenyl)acetic acid after 24 and 48 h of incubation with the Caco-2 cell line. However, no significant differences ($p > 0.05$) were found in the anti-proliferative activity of these two colon metabolites after 72 h of incubation with Caco-2 cells. No anti-proliferative activity was observed in the SW480 cell line for all the tested colon metabolites after 24 h of incubation. After 48 and 72 h of incubation with SW480 cells, no significant differences ($p > 0.05$) were found between the anti-proliferative activity of 3-(3′,4′-dihydroxyphenyl)acetic acid and 3-(3′-hydroxyphenyl)acetic acid. Among the tested metabolites, 3-(3′-hydroxyphenyl)propanoic acid displayed the lowest anti-proliferative activity against SW480 cells, with a recorded 13.3% of inhibition after 72 h of incubation.

The IC_{50} values were calculated for the most active compounds and data are reported in Table 1.

Table 1. IC_{50} values (μmol/L) of the different tested compounds after 24, 48 and 72 h of incubation with Caco-2 and SW480 cell lines.

Compound	Caco-2 (μmol/L)			SW 480 (μmol/L)		
	24 h	48 h	72 h	24 h	48 h	72 h
Quercetin-3-*O*-glucoside-4′-*O*-glucoside	n.a.	n.a.	n.a.	n.a.	>200	~200
Quercetin-4′-*O*-glucoside	n.a.	>200	>200	n.a.	144.3 ± 6.6	102.2 ± 5.3 #
Quercetin	n.a.	>200	116.1 ± 4.9	n.a.	89.2 ± 3.1	58.2 ± 2.7
3-*O*-Caffeoylquinic acid	97.3 ± 2.9 #	42.8 ± 1.7 *	40.4 ± 2.0 *	n.a.	>200	>200
5-*O*-Caffeoylquinic acid	169.5 ± 8.3	98.8 ± 3.0 #	31.3 ± 2.1	n.a.	>200	>200
3,5-di-*O*-Caffeoylquinic acid	>200	27.5 ± 1.0	8.8 ± 0.2	n.a.	>200	>200
3-(3′-Hydroxyphenyl)acetic acid	n.a.	> 200	> 200	n.a.	>200	99.6 ± 4.8 #
3-(3′,4′-Dihydroxyphenyl)acetic acid	79.5 ± 1.4	14.7 ± 0.8	3.0 ± 0.1	n.a.	>200	92.2 ± 6.9 #
3-(3′-Hydroxyphenyl)propanoic acid	>200	>200	>200	n.a.	n.a.	>200

n.a. means not active compound. Number with the same superscript symbol (* or #) were not significantly different ($p > 0.05$). The maximum tested concentration was 200 μmol/L.

In the case of Caco-2 cells, the lowest IC_{50} values were calculated for the colon metabolite 3-(3′,4′-dihydroxyphenyl)acetic acid at any time of incubation. The IC_{50} values decreased according to the incubation time by 5.4 times from 24 to 48 h and by 4.9 times from 48 to 72 h. The IC_{50} values were also calculated for the three tested chlorogenic acids. At

24 h, 3-*O*-caffeoylquinic acid was more effective than 3,5-di-*O*-caffeoylquinic acid, whereas this last compound passed 3-*O*-caffeoylquinic acid in its anti-proliferative effect after 48 and 72 h of incubation. The IC_{50} value of 3-*O*-caffeoylquinic acid decreased by 2.3 times passing from 24 to 48 h of incubation, whereas no significant differences ($p > 0.05$) were detected in the IC_{50} values between 48 and 72 h of incubation.

The compound 5-*O*-caffeoylquinic acid displayed higher IC_{50} values (and therefore lower activity) than 3-*O*-caffeoylquinic acid at 24 and 48 h; however, at 72 h, the calculated IC_{50} value for 5-*O*-caffeoylquinic acid was significantly lower ($p < 0.05$) than that of 3-*O*-caffeoylquinic acid. The decrease in the IC_{50} values for 5-*O*-caffeoylquinic acid was 1.7-times from 24 to 48 h and 3.2-times from 48 to 72 h. For 3,5-di-*O*-caffeoylquinic acid, a 3.1-fold decrease in the IC_{50} value was recorded from 48 to 72 h of incubation.

In the case of SW480, the IC_{50} values were calculated only for two quercetin derivatives and two metabolites. In the case of quercetin derivatives, the lowest IC_{50} values were found for quercetin both after 48 and 72 h of incubation, with a recorded decrease of 1.5-fold passing from 48 to 72 h. A similar decrease in the IC_{50} values was observed for quercetin-4′-*O*-glucoside (1.4-fold) going from 48 to 72 h of incubation. The IC_{50} values calculated for the metabolites 3-(3′,4′-dihydroxyphenyl)acetic acid and 3-(3′-hydroxyphenyl)acetic acid after 72 h of incubation were not significantly different ($p > 0.05$).

2.2. Anti-Proliferative Activity of Quercetin Derivatives/Metabolites and Chlorogenic Acid/Metabolite Mixes

Exposure of Caco-2 and SW480 cell lines to the different mixes resulted in an anti-proliferative effect, the intensity of which was dependent on the cell line, mix composition, mix concentration and time of exposure (Figure 2).

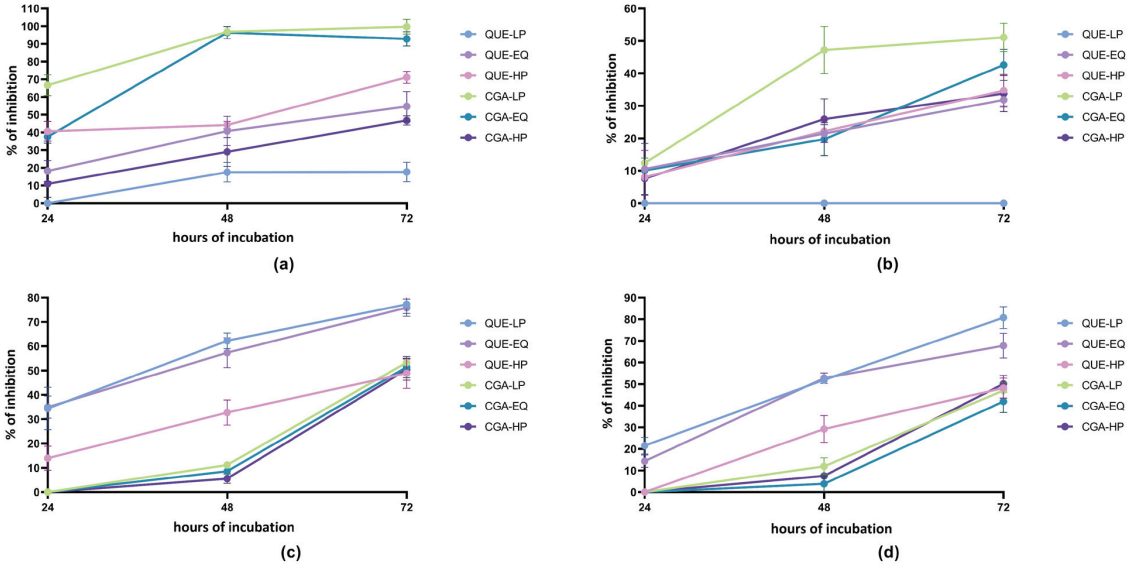

Figure 2. Antiproliferative activity of parent phenolic compound/metabolite mixtures. (**a**) Percentage of inhibition of Caco-2 growth after 24, 48 and 72 h by the different mixtures at a concentration of 200 µmol/L. (**b**) Percentage of inhibition of Caco-2 growth after 24, 48 and 72 h by the different mixtures at a concentration of 100 µmol/L. (**c**) Percentage of inhibition of SW480 growth after 24, 48 and 72 h by the different mixtures at a concentration of 200 µmol/L. (**d**) Percentage of inhibition of SW480 growth after 24, 48 and 72 h by the different mixtures at a concentration of 100 µmol/L. Quercetin derivative/metabolite mixtures (QUE mixes) were prepared by mixing the parent compounds quercetin-3-*O*-glucoside-4′-*O*-glucoside, quercetin-4′-*O*-glucoside and quercetin as well as the

colon metabolites 3-(3′-hydroxyphenyl)acetic acid, 3-(3′,4′-dihydroxyphenyl)acetic acid and 3-(3′-hydroxyphenyl)propanoic acid. Chlorogenic acid/metabolite mixtures (CGA mixes) were prepared by mixing the parent compounds 3,5-di-*O*-caffeoylquinic acid, 3-*O*-caffeoylquinic acid and 5-*O*-caffeoylquinic acid as well as the colon metabolite 3-(3′-hydroxyphenyl)propanoic acid. The mixtures which were formulated to mimic the metabotype of low-producers of colon metabolites (QUE-LP and CGA-LP), contained 90% of parent compounds and 10% of metabolites, and those formulated to mimic the metabotype of high-producers of colon metabolites (QUE-HP and CGA-HP) contained 10% of parent compounds and 90% of metabolites. Mixes QUE-EQ and CGA-EQ contained an equimolar amount of each compound. Data are presented as mean ± standard deviation.

As regards the quercetin derivative/metabolite mixes, the trend in the anti-proliferative activity was opposite considering the two cell lines. In the Caco-2 cell line, the cell-growth-inhibitory effect increased passing from the mix containing a higher amount of parent compounds (QUE-LP mix) to the mixture containing a higher amount of metabolites (QUE-HP mix).

This was particularly evident when the mixes were tested at a 200 μmol/L concentration. In particular, the mix QUE-HP reached 71% of cell growth inhibition after 72 h of incubation at 200 μmol/L. The opposite behavior was recorded with respect to the SW480 cell line, where the anti-proliferative activity decreased as the concentration of the metabolites in the mix increased (from QUE-LP to QUE-HP). The mixes QUE-LP and QUE-EQ attained an anti-proliferative activity of 77% and 76% after 72 h of incubation at 200 μmol/L, respectively. All this considered, the mix QUE-HP was still able to inhibit SW480 proliferation by about 50% after 72 h of incubation at 200 μmol/L.

Anti-proliferative activity was also observed for the chlorogenic acid/metabolite mixtures in both the cell lines. In the Caco-2 cell line, the highest anti-proliferative effect was observed with CGA-LP and CGA-EQ, which contained high amounts of the parent compounds. The effect was already observed after 24 h of incubation and reached values of more than 90% after 48 h of incubation. The mix with the highest amount of metabolites (CGA-HP) displayed lower inhibitory activity at any incubation time, with a maximum inhibitory activity of 47% after 72 h of incubation at 200 μmol/L.

Chlorogenic acid/metabolite mixtures did not show anti-proliferative activity after 24 h of incubation with SW480 cells, whereas they achieved the maximum effect after 72 h of incubation. No significant differences were observed among the inhibitory activities of the three mixes after 72 h of incubation with SW480 cells.

2.3. Cell Cycle Analysis

To obtain more information on the possible mechanism of anti-proliferative activity of phenolic compounds and metabolites, cell cycle analysis by flow cytometry was carried out on both the cell lines. Only those compounds for which an IC_{50} value was calculated were analyzed for their effect on cell cycle distribution. The active compounds were incubated for 72 h at a concentration equal to the calculated IC_{50} value.

Data displayed in Figure 3a shows that, after 72 h of incubation, the percentage of control Caco-2 cells in the G0/G1, S and G2/M phases was 57.8 ± 0.6%, 14.4 ± 2.3% and 23.3 ± 2.1%, respectively. All the tested compounds clearly triggered an increase in the percentage of Caco-2 cells in the S phase. This was particularly evident after treatments with 3-*O*-caffeoylquinic acid, quercetin and the metabolite 3-(3′,4′-dihydroxyphenyl)acetic acid where the increase in the percentage of Caco-2 cells in the S phase was associated to a significant ($p < 0.05$) decrease in the percentage of Caco-2 cells in the G2/M phase. Quercetin also significantly decreased ($p < 0.05$) the percentage of Caco-2 cells in the G0/G1 phase. The increase in the cell number in the S phase was less evident for 5-*O*-caffeoylquinic acid and 3,5-di-*O*-caffeoylquinic acid which, differently from the other compounds, were concomitant with a decrease in the percentage of Caco-2 cells in the G0/G1 phase.

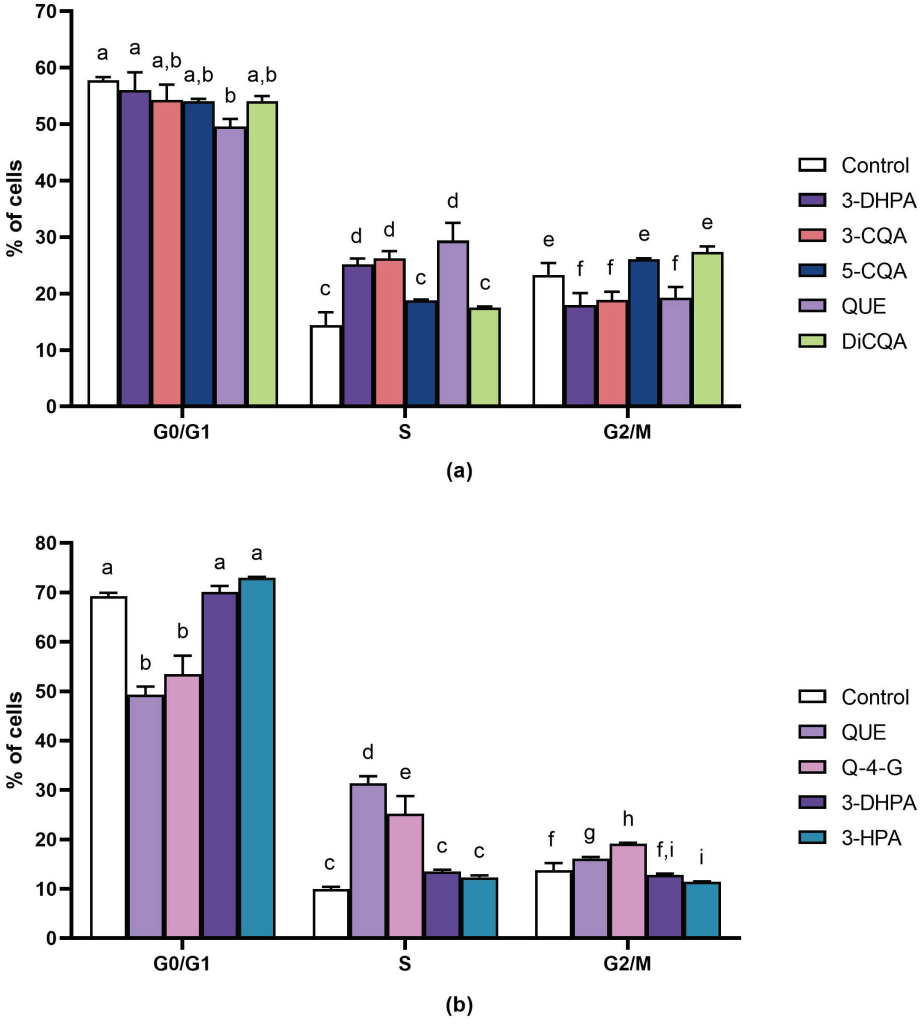

Figure 3. Effect of selected compounds on cell cycle progression in Caco-2 cells (**a**) and SW480 cells (**b**) after 72 h of incubation. The phases of the cell cycle are illustrated as control (cells incubated in absence of phenolic compounds) and as cells treated with the active compounds at a concentration equal to the calculated IC_{50} value. The data are expressed as mean ± SD. Significant differences were analyzed by the one-way ANOVA test. Different letters among samples denote significant differences ($p < 0.05$). 3-CQA: 3-*O*-caffeoylquinic acid; 5-CQA: 5-*O*-caffeoylquinic acid; DiCQA: 3,5-di-*O*-caffeoylquinic acid; QUE: quercetin; Q-4-G: quercetin-4′-*O*-glucoside; 3-DHPA: 3-(3′,4′-dihydroxyphenyl)acetic acid; 3-HPA: 3-(3′-hydroxyphenyl)acetic acid.

In the SW480 cell line control (Figure 3b), the percentage of cells in G0/G1, S and G2/M phases was 69.2 ± 0.7%, 10.0 ± 0.5% and 13.8 ± 1.5%, respectively. Quercetin and quercetin-4′-*O*-glucoside promoted an evident increase in the number of SW480 cells in the S phase (increase of 3.1 and 2.5 times, respectively), concomitant to a significant decrease ($p < 0.05$) in the percentage of SW480 cells in the G0/G1 phase. A lower increase in the number of SW480 cells in the S phase was also recorded after treatments with the metabolites 3-(3′,4′-dihydroxyphenyl)acetic acid and 3-(3′-hydroxyphenyl)acetic acid.

2.4. Cell Metabolism of Phenolic Compounds and Metabolites

Most of the tested phenolic compounds underwent substantial biotransformations depending on their chemical structure and cell line.

In the SW480 cell line, quercetin-3-*O*-glucoside-4′-*O*-glucoside was extensively metabolized, its amount decreasing by 14.4%, 26.0% and 53.6% after 24, 48 and 72 h of incubation (Table 2).

Table 2. Changes in the concentration of tested phenolic compounds and in the newly formed metabolites after 24, 48 and 72 h of incubation with the SW480 cell line.

	Compound	SW 480 (μmol/L)			
		0 h	24 h	48 h	72 h
Substrate	Quercetin-3-*O*-glucoside-4′-*O*-glucoside	50	42.77 ± 0.10	37.04 ± 0.35	23.22 ± 0.22
Metabolite	Quercetin-3-*O*-glucoside		3.35 ± 0.01	8.94 ± 0.03	9.34 ± 0.05
	Quercetin		n.d.	0.04 ± 0.00	0.07 ± 0.00
	Isorhamnetin		n.d.	0.01 ± 0.00	0.01 ± 0.00
	4′-*O*-methylquercetin		n.d.	0.01 ± 0.00	0.01 ± 0.00
Substrate	Quercetin-4′-*O*-glucoside	50	2.98 ± 0.07	0.07 ± 0.00	0.01 ± 0.00
Metabolite	Quercetin		52.70 ± 2.24	36.89 ± 0.52	12.78 ± 0.41
	Isorhamnetin		n.d.	0.79 ± 0.03	1.03 ± 0.04
	4′-*O*-methylquercetin		n.d.	0.49 ± 0.01	0.71 ± 0.04
	Quercetin-*O*-sulphate		n.d.	0.06 ± 0.00	0.12 ± 0.01
Substrate	Quercetin	50	47.39 ± 1.22	40.37 ± 1.20	14.83 ± 0.84
Metabolite	Isorhamnetin		1.61 ± 0.01	3.46 ± 0.08	3.76 ± 0.11
	4′-*O*-methylquercetin		0.97 ± 0.04	1.65 ± 0.04	1.83 ± 0.25
	Quercetin-*O*-sulphate		0.26 ± 0.01	0.48 ± 0.01	0.61 ± 0.01
Substrate	3-*O*-Caffeoylquinic acid *trans*	50	23.34 ± 0.07	19.54 ± 0.07	19.83 ± 0.05
Metabolite	5-*O*-Caffeoylquinic acid *trans*		4.95 ± 0.04	7.37 ± 0.07	11.32 ± 0.43
	4-*O*-Caffeoylquinic acid *trans*		6.89 ± 0.06	8.07 ± 0.24	12.02 ± 0.24
	3-*O*-Caffeoylquinic acid *cis*		4.72 ± 0.04	2.51 ± 0.01	3.27 ± 0.17
	Caffeic acid		0.44 ± 0.01	0.43 ± 0.01	0.57 ± 0.01
	3-*O*-Feruloylquinic acid		0.08 ± 0.00	0.12 ± 0.00	0.17 ± 0.00
	4-*O*-Feruloylquinic acid		0.02 ± 0.00	0.04 ± 0.00	0.07 ± 0.00
	5-*O*-Feruloylquinic acid		0.03 ± 0.00	0.03 ± 0.00	0.05 ± 0.00
Substrate	5-*O*-Caffeoylquinic acid *trans*	50	16.76 ± 0.01	17.52 ± 0.08	13.96 ± 0.03
Metabolite	5-*O*-Caffeoylquinic acid *cis*		2.50 ± 0.01	0.97 ± 0.05	1.42 ± 0.01
	3-*O*-Caffeoylquinic acid *trans*		2.21 ± 0.05	5.14 ± 0.07	5.55 ± 0.09
	4-*O*-Caffeoylquinic acid *trans*		12.69 ± 0.12	14.80 ± 0.09	11.93 ± 0.03
	3-*O*-Caffeoylquinic acid *cis*		0.41 ± 0.05	0.36 ± 0.04	0.72 ± 0.03
	Caffeic acid		n.d.	0.08 ± 0.00	0.09 ± 0.01
	3-*O*-Feruloylquinic acid		0.06 ± 0.00	0.07 ± 0.00	0.05 ± 0.00
	4-*O*-Feruloylquinic acid		0.04 ± 0.00	0.05 ± 0.00	0.04 ± 0.00
	5-*O*-Feruloylquinic acid		0.01 ± 0.00	0.03 ± 0.00	0.03 ± 0.00
	Ferulic acid		0.06 ± 0.02	0.33 ± 0.01	0.37 ± 0.01
Substrate	3,5-di-*O*-Caffeoylquinic acid	50	7.13 ± 0.13	5.41 ± 0.07	6.17 ± 0.05
Metabolite	1,3-di-*O*-Caffeoylquinic acid		8.97 ± 0.04	8.87 ± 0.05	10.98 ± 0.02
	3,4-di-*O*-Caffeoylquinic acid		10.12 ± 0.10	8.04 ± 0.14	9.05 ± 0.15
	4,5-di-*O*-Caffeoylquinic acid		3.30 ± 0.05	2.20 ± 0.02	1.71 ± 0.03
	1,4-di-*O*-Caffeoylquinic acid		0.91 ± 0.03	0.66 ± 0.03	0.55 ± 0.01
	3-*O*-Caffeoylquinic acid *trans*		0.09 ± 0.01	0.13 ± 0.01	0.27 ± 0.01
	4-*O*-Caffeoylquinic acid *trans*		0.07 ± 0.01	0.12 ± 0.01	0.25 ± 0.01
	5-*O*-Caffeoylquinic acid *trans*		0.08 ± 0.01	0.14 ± 0.01	0.29 ± 0.01
	Caffeic acid		n.d.	n.d.	1.07 ± 0.01
Substrate	3-(3′-hydroxyphenyl)acetic acid	50	42.23 ± 0.55	42.81 ± 0.10	39.28 ± 0.85
Substrate	3-(3′,4′-dihydroxyphenyl)acetic acid	50	21.62 ± 0.48	15.84 ± 0.09	10.30 ± 0.36
Substrate	3-(3′-hydroxyphenyl)propanoic acid	50	52.74 ± 0.44	50.70 ± 0.11	49.95 ± 0.37

n.d. means not detected.

Several new metabolites at *m/z* of 463.0888, 315.0513 and 301.0355 appeared already after 24 h of incubation. By comparing the *m/z* values, the fragmentation patterns and the retention times with authentic standards, the three compounds were identified as quercetin-3-*O*-glucoside, isorhamnetin (and the corresponding isomer 4′-*O*-methyl-quercetin) and quercetin, respectively. Similarly, quercetin-4′-*O*-glucoside was strongly metabolized to quercetin, isorhamnetin and 4′-*O*-methyl-quercetin, and quercetin metabolism resulted mainly in the formation of isorhamnetin and 4′-*O*-methyl-quercetin (Table 2). In these last two samples, a new compound having *m/z* 380.9921 was detected and identified as quercetin-*O*-sulphate. Concerning Caco-2 cells, quercetin-3-*O*-glucoside-4′-*O*-glucoside was found to be quite stable, without changes in its concentration during 72 h of incubation. Contrarywise, quercetin-4′-*O*-glucoside and quercetin cell medium concentrations had already strongly decreased during incubation with Caco-2 by 100% and 99.5%, respectively, after 24 h of incubation (Table 3). Nevertheless, no newly formed compounds were detected in the Caco-2 cell media.

Table 3. Changes in the concentration of tested phenolic compounds and in the newly formed metabolites after 24, 48 and 72 h of incubation with the Caco-2 cell line.

	Compound	Caco-2 (μmol/L)			
		0 h	24 h	48 h	72 h
Substrate	Quercetin-3-*O*-glucoside-4′-*O*-glucoside	50	53.05 ± 0.44	50.05 ± 0.32	50.18 ± 0.66
Substrate	Quercetin-4′-*O*-glucoside	50	n.d.	n.d.	n.d.
Substrate	Quercetin	50	0.61 ± 0.01	0.29 ± 0.01	0.52 ± 0.02
Substrate	3-*O*-Caffeoylquinic acid *trans*	50	2.80 ± 0.16	0.04 ± 0.00	0.02 ± 0.00
Metabolite	5-*O*-Caffeoylquinic acid *trans*		2.71 ± 0.09	0.02 ± 0.00	0.01 ± 0.00
	4-*O*-Caffeoylquinic acid *trans*		2.93 ± 0.10	0.03 ± 0.00	0.02 ± 0.00
	3-*O*-Caffeoylquinic acid *cis*		0.26 ± 0.01	0.02 ± 0.00	0.02 ± 0.00
Substrate	5-*O*-Caffeoylquinic acid *trans*	50	2.70 ± 0.01	0.02 ± 0.00	0.02 ± 0.00
Metabolite	5-*O*-Caffeoylquinic acid *cis*		0.12 ± 0.01	0.01 ± 0.00	0.01 ± 0.00
	3-*O*-Caffeoylquinic acid *trans*		2.35 ± 0.02	0.21 ± 0.00	0.19 ± 0.00
	4-*O*-Caffeoylquinic acid *trans*		3.46 ± 0.03	0.09 ± 0.00	0.09 ± 0.00
	3-*O*-Caffeoylquinic acid *cis*		0.15 ± 0.01	0.02 ± 0.00	0.02 ± 0.00
Substrate	3,5-di-*O*-Caffeoylquinic acid	50	0.15 ± 0.00	0.08 ± 0.00	0.18 ± 0.00
Metabolite	1,3-di-*O*-Caffeoylquinic acid		0.33 ± 0.01	0.16 ± 0.00	0.39 ± 0.00
	3,4-di-*O*-Caffeoylquinic acid		0.32 ± 0.00	0.18 ± 0.00	0.36 ± 0.00
	4,5-di-*O*-Caffeoylquinic acid		0.06 ± 0.00	0.03 ± 0.00	0.03 ± 0.00
	1,4-di-*O*-Caffeoylquinic acid		n.d.	n.d.	0.10 ± 0.00
Substrate	3-(3′-hydroxyphenyl)acetic acid	50	48.83 ± 0.85	47.02 ± 0.39	43.17 ± 0.06
Substrate	3-(3′,4′-dihydroxyphenyl)acetic acid	50	n.d.	n.d.	n.d.
	Hydroxybenzoic acid		n.d.	3.51 ± 0.07	15.73 ± 0.37
Substrate	3-(3′-hydroxyphenyl)propanoic acid	50	45.51 ± 0.41	46.27 ± 0.58	46.28 ± 0.76
	Hydroxybenzoic acid		n.d.	0.31 ± 0.01	0.30 ± 0.01

n.d. means not detected.

As reported in Tables 2 and 3, 3,5-di-*O*-caffeoylquinic acid, 3-*O*-caffeoylquinic acid and 5-*O*-caffeoylquinic acid underwent substantial isomerization during incubation with both the cell lines. Several positional isomers were already identified after 24 h of incubation of 3,5-di-*O*-caffeoylquinic acid with both the cell lines.

The two newly formed isomers detected in the highest amounts were 3,4-di-*O*-caffeoylquinic and 1,3-di-*O*-caffeoylquinic acids. Besides the isomerization, after incubation of 3,5-di-*O*-caffeoylquinic acid with both the cell lines, newly formed metabolites were detected; in particular, the different positional isomers of caffeoylquinic acids (i.e., 5-*O*-caffeoylquinic acid, 3-*O*-caffeoylquinic acid and 4-*O*-caffeoylquinic acid) deriving from

the hydrolysis of a caffeoyl moiety from the di-*O*-caffeoylquinic acids. Similarly to 3,5-di-*O*-caffeoylquinic acid, 3-*O*-caffeoylquinic acid and 5-*O*-caffeoylquinic acid were also partially transformed in the corresponding positional isomers as well as suffering trans–cis isomerization (Tables 2 and 3). After incubation with SW480, additional metabolites were detected such as caffeic acid (deriving from the hydrolysis of the quinic acid moiety from caffeoylquinic acids) and the different isomers of the methylated metabolites of feruloylquinic acids (Table 2). In addition, ferulic acid (deriving from the hydrolysis of the quinic acid moiety from feruloylquinic acids or from the methylation of caffeic acid) was detected after incubation of 5-*O*-caffeoylquinic acid with SW480 cells. No newly formed compounds were observed after incubation with Caco-2 cells.

Regarding the three tested colon metabolites, 3-(3′-hydroxyphenyl)acetic acid and 3-(3′-hydroxyphenyl)propanoic acid were quite stable after incubation with both the cell lines (Tables 2 and 3). Contrariwise, a decrease in 3-(3′,4′-dihydroxyphenyl)acetic acid concentration was observed after incubation with both the cell lines, with the values plummeting to zero already after 24 h of incubation with Caco-2. No newly formed compounds were observed in SW480 cell medium, whereas a strong production of hydroxybenzoic acid was detected after incubation with Caco-2 (Table 3). Small amounts of hydroxybenzoic acid were also revealed after incubation of 3-(3′-hydroxyphenyl)propanoic acid with Caco-2 (Table 3).

3. Discussion

Flavonols (such as glycosylated quercetin derivatives) and hydroxycinnamic acids (such as chlorogenic acids) are among the most widespread phenolic compounds in foods and among the most important phenolic compounds introduced through the diet [18]. For example, onion, apple, tea and red wine are rich in glycosylated quercetin derivatives, whereas coffee, eggplant, artichoke, apple and cherry contain high amounts of chlorogenic acids [16,20,21,23,31,34,35].

A plethora of studies have suggested that dietary phenolic compounds, such as glycosylated quercetin derivatives and chlorogenic acids, are poorly absorbed in the stomach and small intestine [16,31,34,36]. For example, only 20–30% of hydroxycinnamic acids present in coffee or other foods such as yerba mate and artichoke are absorbed in the small intestine, and appeared in plasma mainly as phase II conjugated metabolites [16,34,37]. The absorption of quercetin derivatives in the small intestine is dependent on the chemical structure of the compound itself. For example, quercetin aglycone was poorly absorbed (about 20%) whereas quercetin mono-glucosides were better absorbed, reaching 50% of the ingested dose [31,36]. Therefore, unabsorbed phenolic compounds reach the colon, where the gut microbiota may metabolize the parent phenolic compounds, producing a broad assortment of low-molecular-weight phenolic acids, mainly hydroxyphenylacetic, hydroxyphenylpropanoic and hydroxybenzoic acids [38].

Colon metabolism of glycosylated quercetin derivatives begins with the hydrolysis of the glucoside moiety, releasing the corresponding aglycone that undergoes C-ring fission generating the transient intermediate 3-(3′,4′-dihydroxyphenyl)propanoic acid that is further dehydroxylated to 3-(3′-hydroxyphenyl)propanoic acid or oxidated to 3-(3′,4′-dihydroxyphenyl)acetic acid. These last compounds may finally be converted into 3-(3′-hydroxyphenyl)acetic acid by oxidation and dehydroxylation, respectively (Figure 4) [27,28,39]. Similarly, the colon metabolism of chlorogenic acids starts with the hydrolysis of the ester bond between quinic acid and hydroxycinnamic acid, producing 3′,4′-dihydroxycinnamic acid which is further reduced and dehydroxylated to 3-(3′-hydroxyphenyl)propanoic acid (Figure 4) [27,30]. Thus, the most important metabolites identified after colon fermentation of glycosylated quercetin derivatives are quercetin aglycone, 3-(3′,4′-dihydroxyphenyl)acetic acid, 3-(3′-hydroxyphenyl)acetic acid and 3-(3′-hydroxyphenyl)propanoic acid, whereas colon metabolism of chlorogenic acids mainly results in the accumulation of 3-(3′-hydroxyphenyl)propanoic acid [27,28,30,39,40].

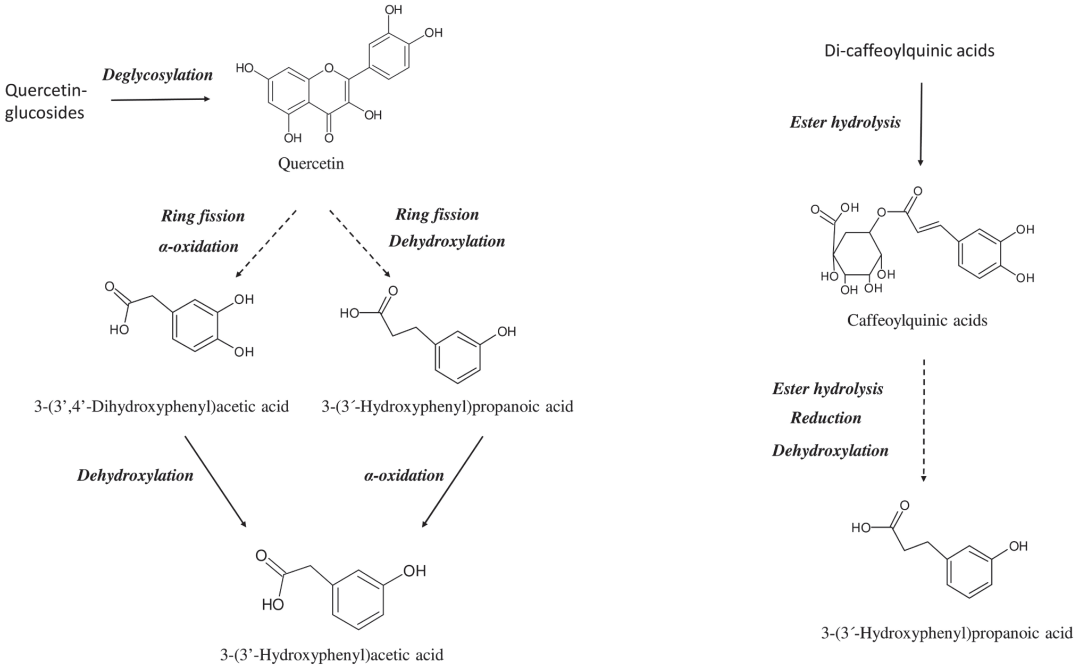

Figure 4. Simplified view of the colon metabolism of glycosylated quercetin derivatives and chlorogenic acids. Colon metabolism of glycosylated quercetin derivatives involves the hydrolysis of the glucose group, releasing the corresponding aglycone which undergoes C-ring fission followed by dehydroxylation or oxidation producing 3-(3′-hydroxyphenyl)propanoic acid and 3-(3′,4′-dihydroxyphenyl)acetic acid. The metabolism of these last compounds converges in the formation of 3-(3′-hydroxyphenyl)acetic acid. The colon metabolism of chlorogenic acids involved the hydrolysis of the quinic acid group, producing 3′,4′-dihydroxycinnamic acid, which is further reduced and dehydroxylated to 3-(3′-hydroxyphenyl)propanoic acid.

A comparison of the data previously reported in the in vitro studies of colonic fermentation of quercetin and quercetin derivatives highlighted the great inter-individual variability in the gut metabolism of these compounds.

For example, Juániz et al. [40] and Cattivelli et al. [28] identified 3-(3′-hydroxyphenyl) propanoic acid as the main metabolite produced after fecal fermentation of glycosylated quercetins in green pepper and red-skinned onion. On the other hand, Di Pede et al. [39] pointed out 3-(3′,4′-dihydroxyphenyl)acetic acid as the metabolite generated in higher amounts after quercetin fermentation by gut microbiota. Contrary to this, Serra et al. [27] detected 3-(3′-hydroxyphenyl)acetic acid as the major colon metabolite after fermentation of quercetin and quercetin-rhamnoside, and found almost equimolar amounts of 3-(3′-hydroxyphenyl)acetic acid and 3-(3′,4′-dihydroxyphenyl)acetic acid after fermentation of quercetin-rutinoside. In another study, Jaganath et al. [41] compared the colon metabolism of quercetin-rutinoside among three individual donors. Only one donor was able to produce both 3-(3′-hydroxyphenyl)acetic acid and 3-(3′,4′-dihydroxyphenyl)acetic acid, whereas the other two donors generated only 3-(3′,4′-dihydroxyphenyl)acetic acid. There were also differences in the rate of quercetin metabolic conversion. In some studies, quercetin aglycone was still present in high concentrations after 5-6 h of fermentation whereas, in others, quercetin completely disappeared after a few hours of fecal fermentation [28,39–42]. Therefore, inter-individual variability determined not only the type and concentration of produced metabolites but also the rate of bioconversion of quercetin.

Differently, chlorogenic acid metabolism seemed to be less sensitive to inter-individual variability, with 3-(3′-hydroxyphenyl)propanoic acid being the main metabolite identified in the majority of the studies [29,30,43]. However, there were also differences in the metabolic rate in this case. In some studies, chlorogenic acids totally disappeared after a few hours of incubation with colon bacteria, whereas in other studies they were found still present after 10 or 24 h of incubation [29,30,43–45]. Therefore, it can be inferred that both parent phenolic compounds and their colon metabolites co-exist in the colon, especially after repeated intake of phenolic-rich foods. Moreover, the relative amount of parent phenolic compounds and produced metabolites is greatly influenced by the individual composition of gut microbiota, showing great inter-individual variability [30,33].

In this study, we found that both parent compounds (i.e., glycosylated quercetin derivatives, quercetin aglycone and chlorogenic acids) as well as their most important colon metabolites were able to inhibit colon cancer cell proliferation at a concentration of 100 μmol/L. The tested concentration of 100 μmol/L is relevant from a physiological point-of-view, especially for the colon metabolites.

Previous studies reported in human fecal water or human fecal matrix a broad range of concentrations for the tested colon metabolites according to the inter-individual variability. Karlsson et al. [46] reported a concentration of 61 ± 34 μmol/L in human fecal water, whereas Jenner et al. [47] stated a mean value of 68 ± 93 μmol/L (range 0.72–209 μmol/L) for the colon metabolite 3-(3′-hydroxyphenyl)propanoic acid. Higher values of 3-(3′-hydroxyphenyl)propanoic acid (between 15 to 1076 μmol/L) were described by Knust et al. [48] in human fecal matrix. Lower concentrations were found for the colon metabolite 3-(3′-hydroxyphenyl)acetic acid (mean values from 30 to 110 μmol/L), with a wide range among individuals (from 4 to 294 μmol/L) and for 3-(3′,4′-dihydroxyphenyl)acetic acid (mean values from 7 to 64 μmol/L) and an individual range from 1 to 277 μmol/L [47–49]. It is important to note that the discussed studies have been carried out without any dietary restriction or supplementation, and thus represent values commonly found in a normal dietary regimen. Supplementation of phenolic-rich foods such as raspberry may further increase the amount of phenolic metabolites, as observed by Gill et al. [49] who found in human fecal water maximum values of 1810, 442 and 327 μmol/L of 3-(3′-hydroxyphenyl)propanoic acid, 3-(3′,4′-dihydroxyphenyl)acetic acid and 3-(3′-hydroxyphenyl) acetic acid. No available data were present in the literature about the fecal concentration of quercetin and its derivatives as well as of chlorogenic acids. However, as reported above, in vitro studies have suggested their presence in the colon in co-existence with their colon metabolites, especially following repeated ingestion of quercetin-rich or chlorogenic-acid-rich foods.

The anti-proliferative effect was time-dependent and increased in conjunction with increasing incubation time. The parent compounds 3,5-di-*O*-caffeoylquinic acid, 3-*O*-caffeoylquinic acid and 5-*O*-caffeoylquinic acid, as well as the metabolite 3-(3′,4′-dihydroxyphenyl) acetic acid, were the most active against Caco-2 cell proliferation at any incubation time. On the contrary, the parent compounds quercetin, quercetin-4′-*O*-glucoside and quercetin-3-*O*-glucoside-4′-*O*-glucoside, as well as the metabolites 3-(3′,4′-dihydroxyphenyl)acetic acid and 3-(3′-hydroxyphenyl)acetic acid, were the most active against SW480 cell proliferation.

In Caco-2 cells, the extent of the anti-proliferative effect seemed to be related to the presence of specific structural motifs. The most active molecules, i.e., 3,5-di-*O*-caffeoylquinic acid, 3-*O*-caffeoylquinic acid, 5-*O*-caffeoylquinic acid, 3-(3′,4′-dihydroxyphenyl)acetic acid and quercetin, displayed in their structure a catechol-type moiety, which was fundamental for exerting an anti-proliferative effect. For example, 3-(3′,4′-dihydroxyphenyl)acetic acid bearing a catechol moiety was clearly more active than the mono-hydroxylate 3-(3′-hydroxyphenyl)acetic acid. Similarly, quercetin showed a higher anti-proliferative activity than the glycosylated derivatives quercetin-4′-*O*-glucoside and quercetin-3-*O*-glucoside-4′-*O*-glucoside, where one of the two hydroxyl groups of the catechol moiety is esterified with a glucose molecule. Also, the presence of one or more glucose residues hampered the anti-proliferative effect, since quercetin showed a significantly higher effect than quercetin-

4′-*O*-glucoside whereas quercetin-3-*O*-glucoside-4′-*O*-glucoside was not active at any time. The effect of the tested compounds was quite different when incubated with SW480. In this case, quercetin and its glycosylated derivatives together with the metabolites 3-(3′,4′-dihydroxyphenyl)acetic acid and 3-(3′-hydroxyphenyl)acetic acid were the most active compounds, whereas the tested chlorogenic acids, although they present a certain degree of inhibition, were less effective in inhibiting SW480 proliferation.

Several previous studies reported the anti-proliferative effect of chlorogenic acids against human colon cancer cells. For example, 3-*O*-caffeoylquinic acid was found to be able to reduce Caco-2 and HT29 colon cancer cell proliferation, whereas dicaffeoylquinic acids inhibited the growth of HT29 and DLD-1 cancer cells [50–52].

Moreover, 3-(3′,4′-dihydroxyphenyl)acetic acid was found to be active against the proliferation of human colon cancer cells HCT116 and SNUC4 [53,54]. Furthermore, quercetin has already been found to be active against Caco-2 proliferation (as well as in other colon cancer cell models) at concentrations similar to those tested in this study [55,56].

As already mentioned, parent phenolic compounds and metabolites may co-exist in the colon and the ratio of parent phenolic compounds/metabolites is strongly dependent on the inter-individual variability related to the ability to metabolize the parent phenolic compounds slowly or rapidly. To better understand the potential impact of inter-individual variability, different mixtures of parent compounds and colon metabolites were prepared to mimic the low-producers and high-producers metabotypes. The quercetin derivative/metabolite mixes behaved differently depending on the tested cell line. The cell growth inhibition increased passing from the mix with the low amount of metabolites (i.e., low-producers) to the mix with the highest amount of metabolites (i.e., high-producers) after incubation with the Caco-2 cell line, whereas the trend was opposite for the SW480 cell line. However, the high-producers mix was still able to inhibit SW480 cell proliferation with values near to 50% at 200 μmol/L concentration. For the chlorogenic acid/metabolite mixes, the effect was more pronounced for the low-producers mix with respect to the high-producers mix in Caco-2 cells; nevertheless, the inhibitory effect of the high-producers mix was near to 50% at 200 μmol/L concentration. No difference in the anti-proliferative activity was observed in the SW480 cell line with the three chlorogenic acid/metabolite mixes. Therefore, our data support the hypothesis that parent phenolic compounds (i.e., quercetin derivatives and chlorogenic acids), once present in the colon after the consumption of phenolic-rich vegetables, may exert anti-proliferative activity against colon cancer cells. Later, when they begin to be metabolized, the formed colon metabolites may sustain and prolong the inhibitory effect towards colon cancer cell proliferation.

Cell cycle analysis pointed out that all the tested compounds arrest the cell cycle at the S phase in both the cell lines. The significant increase in the Caco-2 cell number in the S phase was concomitant with a decrease in the amount of cells in G2/M phase, indicating that quercetin, 3-*O*-caffeoylquinic acid and 3-(3′,4′-dihydroxyphenyl)acetic acid inhibited cell proliferation by arresting the cell cycle at the S phase, thus preventing Caco-2 cells from entering the G2 phase. In the case of SW480, the increase in the percentage of cells in the S phase was associated with a reduction in cell number for the G0/G1 phase.

Previous studies have found that quercetin and chlorogenic acid induced cell cycle arrest at the S phase in several colon cancer cell lines, including Caco-2 and SW480 [52,57]. Differently from this study, 3-(3′,4′-dihydroxyphenyl)acetic acid promoted cell cycle arrest at the G0/G1 phase in HT-29 colon cancer cells [58].

The different tested phenolic compounds and metabolites displayed different stability in the cell media and were differently metabolized accordingly to their structure and the specific cell line. Quercetin and glycosylated quercetin derivatives were strongly metabolized by SW480 cells, whereas no newly formed metabolites were detected after incubation with Caco-2 cells. In SW480 cells, quercetin-3-*O*-glucoside-4′-*O*-glucoside underwent extensive deglycosylation, suggesting the presence in these cells of a membrane-bound β-glucosidase. Moreover, the appearance of only the 3-*O*-glucoside derivative of quercetin suggested a strong preference of this β-glucosidase for the glycosidic linkage at the 4′-*O* position rather

than the 3-*O* position. This specificity was confirmed also by the data about quercetin-4′-*O*-glucoside metabolism in SW480 cells. This compound was rapidly hydrolyzed after 24 h in an equimolar amount of the corresponding aglycone quercetin. Furthermore, the fastest deglycosylation of quercetin-4′-*O*-glucoside with respect to quercetin-3-*O*-glucoside-4′-*O*-glucoside indicated that the presence of a 3-*O*-glucoside moiety in the molecule hampered the hydrolyzing ability of SW480 β-glucosidase. The appearance of small amounts of quercetin after 48 h of incubation of quercetin-3-*O*-glucoside-4′-*O*-glucoside pointed out the presence, also, of a β-glucosidase with specificity towards the 3-*O*-glucosidic linkage or the ability of the same β-glucosidase to also hydrolyze with less efficacy the 3-*O*-glucosidic linkage. Additional metabolites—and, in particular, isorhamnetin, 4′-*O*-methyl quercetin and quercetin-*O*-sulphate—were detected after incubation of quercetin and its derivatives with SW480 cell lines, suggesting the presence in these cells of a catechol-*O*-methyltransferase and a sulfotransferase. The appearance of higher amounts of isorhamnetin with respect to 4′-*O*-methyl quercetin pointed out a preference for the OH in position C3 for the catechol-*O*-methyltransferase. Due to the lack of authentic standards, it was not possible to identify the specific isomer of quercetin-sulphate. On the contrary, no β-glucosidase, as well as catechol-*O*-methyltransferase and sulfotransferase, activities were observed in Caco-2 cells after incubation with quercetin and glycosylated quercetin derivatives. In this cell line, quercetin-3-*O*-glucoside-4′-*O*-glucoside was stable in the cell media with a 100% recovery also after 72 h of incubation, whereas quercetin and quercetin-4′-*O*-glucoside rapidly disappeared already after 24 h of incubation. Since neither newly formed metabolites nor the known quercetin oxidation products were detected in the cell media, the most plausible explanation was that quercetin and quercetin-4′-*O*-glucoside were rapidly absorbed by Caco-2 cells. Previous studies demonstrated active absorption of quercetin and quercetin-4′-*O*-glucoside by Caco-2 cells [59]. The same consideration can be made for SW480 cells, where the final recovery of quercetin and its metabolites after 72 h of incubation of quercetin and quercetin-4′-*O*-glucoside was below 100%.

The cell metabolism of glycosylated quercetin derivatives may have an impact on their anti-proliferative activity. In SW480, quercetin was the most active compound and can also be considered responsible for the anti-proliferative activity of quercetin-4′-*O*-glucoside, since this last compound is rapidly hydrolyzed to the corresponding aglycone. Similarly, quercetin-3-*O*-glucoside-4′-*O*-glucoside was hydrolyzed to quercetin-3-*O*-glucoside, which can be responsible for its anti-proliferative effect against SW480 cells. The anti-proliferative activity of quercetin-3-*O*-glucoside has been already reported by several authors [60].

Likewise to what was noted for quercetins, chlorogenic acids were also extensively metabolized by SW480, whereas no metabolites were found after incubation with Caco-2. In addition to the obvious isomerization (acyl migration), which is dependent on the pH and not on the presence of cells [61], both 3,5-di-*O*-caffeoylquinic acid and the two caffeoylquinic acids (and their isomers) were hydrolyzed to caffeoylquinic acids and caffeic acid, respectively, suggesting the presence of esterase activity in SW480 cells [62]. Moreover, caffeoylquinic acids were methylated by SW480 catechol-*O*-methyltransferase, producing different isomers of feruloylquinic acids. In the Caco-2 cell line, 3,5-di-*O*-caffeoylquinic acid, 3-*O*-caffeoylquinic acid and 5-*O*-caffeoylquinic acid almost totally disappeared from the cell media already after 24 h of incubation. Some studies suggest that caffeoylquinic and dicaffeoylquinic acids can be transported in Caco-2 cells [61,63].

Concerning the phenolic metabolites, both 3-(3′-hydroxyphenyl)acetic acid and 3-(3′-hydroxyphenyl)propanoic acid were stable after incubation with Caco-2 and SW480, with recoveries of more than 80% after 72 h of incubation. On the contrary, 3-(3′,4′-dihydroxyphenyl)acetic acid concentration dropped to zero already after 24 h of incubation with Caco-2 cells. The only identified metabolite was hydroxybenzoic acid, which accounted for about the 30% of the initial amount of 3-(3′,4′-dihydroxyphenyl)acetic acid after 72 h of incubation. It is possible that this metabolite was formed by two consecutive reactions of de-hydroxylation and α-oxidation (or vice versa), which implies the uptake of 3-(3′,4′-dihydroxyphenyl)acetic in Caco-2 cells, as already suggested [64].

4. Materials and Methods

4.1. Materials

Chemicals and materials for cell culture were purchased from VWR International (Milan, Italy). The MTS cell proliferation assay kit was obtained from Promega (Milan, Italy). Mass spectrometry solvents were purchased from Bio-Rad (Hercules, CA, USA). The parent phenolic compounds 3-*O*-caffeoylquinic acid (purity ≥ 99%), 5-*O*-caffeoylquinic acid (purity ≥ 99%), 3,5-*O*-dicaffeoylquinic acid (purity ≥ 97%), quercetin (purity ≥ 99%), quercetin-4′-*O*-glucoside (purity ≥ 99%) and quercetin-3-*O*-glucoside-4′-*O*-glucoside (purity ≥ 98.5%) were obtained from Extrasynthese (Genay, France). Phenolic compound metabolites 3-(3′-hydroxyphenyl)propanoic acid (purity ≥ 98%), 3-(3′-hydroxyphenyl)acetic acid (purity ≥ 99%) and 3-(3′,4′-dihydroxyphenyl)acetic acid (purity ≥ 98%) were purchased from Thermo-Fisher Scientific (Waltham, MA, USA). All the other chemicals were purchased from Sigma-Aldrich (Milan, Italy).

4.2. Cell Cultures, Phenolic Compound Preparation and Anti-Proliferative Assay

Human colon cancer Caco-2 and SW480 cell lines were cultured and grown as previously reported [62]. All the phenolic compounds were dissolved in dimethyl-sulfoxide (DMSO) at a concentration of 50 mmol/L, diluted in the respective cell culture media at a concentration of 100 μmol/L (final DMSO concentration of 0.5%) and finally filtered at 0.2 μm.

For the anti-proliferative assay, cells were seeded in 96-well plates in the amount of 4000 and 8000 cells/cm^2 for Caco-2 and SW480, respectively. Cells were then left to adhere for 24 h before the addition of 200 μL of phenolic compounds (100 μmol/L). Incubation was carried out for 24, 48 and 72 h. Data were compared with a control solution containing 0.5% DMSO in cell medium and representing 100% proliferation. In addition, six different mixes were prepared to simulate the simultaneous presence of parent phenolic compounds and metabolites by mimicking the possible human inter-individual variability in colon metabolism of phenolic compounds. Two sets of mixes were prepared to consider the colon metabolism of quercetins and chlorogenic acids. The quercetin mixtures (QUE mixes) contained different amounts of quercetin-3-*O*-glucoside-4′-*O*-glucoside, quercetin-4′-*O*-glucoside and quercetin (the parent compounds) as well as the respective metabolites (3-(3′-hydroxyphenyl)acetic acid, 3-(3′,4′-dihydroxyphenyl)acetic acid and 3-(3′-hydroxyphenyl)propanoic acid). The chlorogenic acids mixtures (CGA mixes) were instead prepared by mixing the respective parent compounds (3-*O*-caffeoylquinic acid, 5-*O*-caffeoylquinic acid and 3,5-*O*-dicaffeoylquinic acid) with the metabolite 3-(3′-hydroxyphenyl)propanoic acid. For each set of mixtures (QUE and CGA mixtures), three different mixes were formulated. One set of mixes mimicked the low-producers metabotype and contained 90% parent compounds and 10% metabolites (mixes QUE-LP and CGA-LP). Another set of mixes was prepared to simulate the high-producers metabotype and contained 10% parent compounds and 90% metabolites (mixes QUE-HP and CGA-HP). Finally, a third set of mixes was prepared with equimolar amounts of all the compounds (mixes QUE-EQ and CGA-EQ). The anti-proliferative activity of the mixes was determined by using the final concentrations of 100 and 200 μmol/L (sum of the concentrations of the compounds present in the mixes). The composition of each mix is reported in Table 4.

Cell proliferation was assessed by the MTS assay as previously described [63].

For the most active compounds, the IC_{50} values (defined as the phenolic compound concentration able to inhibit cell proliferation by 50%) were calculated by carrying out the anti-proliferative activity assay with different concentrations of the specific phenolic compounds (ranging from 1.5 to 200 μmol/L). The IC_{50} values were calculated through non-linear regression analysis by plotting the base-10 logarithm of the phenolic compound concentration vs. the percentage of inhibition.

Table 4. Composition of the different mixes tested for their anti-proliferative effect against human colon carcinoma cell lines.

Compound	QUE-LP	QUE-EQ	QUE-HP	CGA-LP	CGA-EQ	CGA-HP
Quercetin-3-*O*-glucoside-4′-*O*-glucoside	60 μmol/L	33.3 μmol/L	6.7 μmol/L	/	/	/
Quercetin-4′-*O*-glucoside	60 μmol/L	33.3 μmol/L	6.7 μmol/L	/	/	/
Quercetin	60 μmol/L	33.3 μmol/L	6.7 μmol/L	/	/	/
3-*O*-Caffeoylquinic acid	/	/	/	60 μmol/L	50 μmol/L	6.7 μmol/L
5-*O*-Caffeoylquinic acid	/	/	/	60 μmol/L	50 μmol/L	6.7 μmol/L
3,5-di-*O*-Caffeoylquinic acid	/	/	/	60 μmol/L	50 μmol/L	6.7 μmol/L
3-(3′-Hydroxyphenyl)acetic acid	6.7 μmol/L	33.3 μmol/L	60 μmol/L	/	/	/
3-(3′,4′-Dihydroxyphenyl)acetic acid	6.7 μmol/L	33.3 μmol/L	60 μmol/L	/	/	/
3-(3′-Hydroxyphenyl)propanoic acid	6.7 μmol/L	33.3 μmol/L	60 μmol/L	20 μmol/L	50 μmol/L	180 μmol/L

The composition refers to the mixes prepared at the final concentration of 200 μmol/L considering all the added compounds. In the mixes prepared at the final concentration of 100 μmol/L, the concentration of each compound was halved.

4.3. Cell Cycle Analysis

Cell cycle analysis was carried out in both Caco-2 and SW480 cell lines as previously reported by Nicoletti et al. [65]. Cells were seeded in 6-well plates at a density of 4000 and 8000 cells/cm^2 for Caco-2 and SW480, respectively. Cells were then left to adhere for 24 h before the addition of 200 μL of the selected phenolic compounds at a concentration equal to the calculated IC_{50} values at 72 h of incubation. The tested phenolic compounds were 3-*O*-caffeoylquinic acid, 5-*O*-caffeoylquinic acid, 3,5-*O*-dicaffeoylquinic acid, quercetin and 3-(3′,4′-dihydroxyphenyl)acetic acid for Caco-2, and quercetin, quercetin-4′-*O*-glucoside, 3-(3′-hydroxyphenyl)acetic acid and 3-(3′,4′-dihydroxyphenyl)acetic acid for SW480.

After 72 h of incubation, the cells were washed with PBS, detached from the 6-well plates with 500 μL of trypsin and resuspended in 1000 μL of medium. Subsequently, they were centrifuged at 3500 rpm for 5 min. After removing the supernatant, the pellet was resuspended with 400 μL of Nicoletti's solution (sodium citrate 0.1%, Triton X-100 0.1% and 20 μg/mL propidium iodide). After 15 min of incubation at 4 °C in the dark, cell cycle analysis was performed with an Epics XL MCL flow cytometer (Beckman Coulter, Brea, CA, USA).

The data were compared with a control solution containing 0.5% DMSO in the cell medium.

4.4. High-Resolution Mass Spectrometry Analysis of Cell Media

To analyze the metabolism of phenolic compounds by Caco-2 and SW480 cells, the cell culture media were withdrawn after 0, 24, 48 and 72 h of incubation. Phenolic compounds were extracted from the culture media by following the procedure reported in Sala et al. [66]. Briefly, 100 μL of cold methanol was mixed with 100 μL of cell media and vortexed for 1 min. The mixture was then centrifuged at 10,000× *g* (4 °C, 5 min) and the supernatant was injected, after appropriate dilution, in an ultra-high-performance liquid chromatography high-resolution mass spectrometry system (UHPLC-HR-MS).

The HR-MS system consisted of a UHPLC Ultimate 3000 separation module, equipped with a C18 column (Acquity UPLC HSS C18 reversed phase, 2.1 × 100 mm, 1.8 μm particle size, Waters, Milan, Italy) and coupled with a Q Exactive Hybrid Quadrupole-Orbitrap Mass Spectrometer (Thermo Scientific, San Jose, CA, USA). Mobile phases consisted of a mixture of water containing formic acid (0.1%) (mobile phase A) and acetonitrile containing formic acid (0.1%) (mobile phase B). The gradient began at 1% B, reaching 40% B over 20 min. To wash the column, the mobile phase B concentration was raised to 99% over 6 min and kept at 99% for 3 min before returning to the initial conditions. The MS and MS/MS conditions are fully described in Martini et al. [67].

Quantification was carried out by building external calibration curves with the available standard compounds.

4.5. Statistical Analysis

All data are reported as mean ± standard deviation (SD) for three replicates for each prepared compound. Univariate analysis of variance (ANOVA) with Tukey post hoc test was applied using GraphPad Prism 6.0 (GraphPad Software, San Diego, CA, USA). The differences were considered significant with $p < 0.05$. The IC_{50} values were calculated by using GraphPad Prism 6.0.

5. Conclusions

For the first time, the anti-proliferative activity of the dietarily most relevant chlorogenic acids, quercetin derivatives, and their colon microbial metabolites against two different human colon cancer cell models was tested and compared. Generally, the reported data demonstrate that in-vivo-pertinent mixtures of parent compounds and metabolites at concentrations attainable in the human colon following the consumption of phenolic-rich vegetables exert anti-proliferative effects against colon cancer adenocarcinoma cell lines. Since the anti-proliferative activity was nearly comparable between mixes that mirror the low-producers and high-producers human metabotypes, it can be speculated that inter-individual variability does not substantially affect the potential in vivo anti-cancer activity of phenolic compounds.

The main limitation of this study is related to the use of 2D cell models that, somewhat, do not reflect the physiological tumor microenvironment with respect to more complex in vitro models such as 3D tumor spheroid models. Future research should be carried out to provide an even greater physiological significance to the reported data by using 3D colon cancer cell models.

However, these results suggest that gut microbiota metabolites may sustain the anti-proliferative effects observed for the parent compounds, playing an important role in the protective effect of phenolic compounds against colon cancer. The present manuscript, therefore, contributes to unveiling the fundamental role of the colonic metabolism in the context of the protective effect of phenolic compounds against colon cancer.

Author Contributions: Conceptualization, A.C. (Alice Cattivelli), A.C. (Angela Conte) and D.T.; methodology, A.C. (Alice Cattivelli) and D.T.; software, A.C. (Alice Cattivelli) and D.T.; validation, A.C. (Alice Cattivelli) and D.T.; formal analysis, A.C. (Alice Cattivelli); investigation, A.C. (Alice Cattivelli); data curation, A.C. (Alice Cattivelli) and D.T.; writing—original draft preparation, A.C. (Alice Cattivelli) and D.T.; writing—review and editing, A.C. (Alice Cattivelli), A.C. (Angela Conte) and D.T.; supervision, A.C. (Angela Conte) and D.T.; project administration, D.T. All authors have read and agreed to the published version of the manuscript.

Funding: This research received no external funding.

Institutional Review Board Statement: Not applicable.

Informed Consent Statement: Not applicable.

Data Availability Statement: The data presented in this study are available on request from the corresponding author.

Acknowledgments: The authors acknowledge the Fondazione Cassa di Risparmio di Modena for funding the HPLC-ESI-Q Exactive Hybrid Quadrupole-Orbitrap Mass Spectrometer system at the Centro Interdipartimentale Grandi Strumenti (CIGS). The authors also wish to thank Davide Malagoli at the Department of Life Sciences, University of Modena and Reggio Emilia, for his kind hospitality in his cell culture laboratory and Monica Montanari at the Cell-lab, University of Modena and Reggio Emilia, for her assistance in the cell cycle analysis.

Conflicts of Interest: The authors declare no conflict of interest.

References

1. Sung, H.; Ferlay, J.; Siegel, R.L.; Laversanne, M.; Soerjomataram, I.; Jemal, A.; Bray, F. Global Cancer Statistics 2020: GLOBOCAN Estimates of Incidence and Mortality Worldwide for 36 Cancers in 185 Countries. *CA Cancer J. Clin.* **2021**, *71*, 209–249. [CrossRef]
2. Czene, K.; Lichtenstein, P.; Hemminki, K. Environmental and heritable causes of cancer among 9.6 million individuals in the Swedish Family-Cancer Database. *Int. J. Cancer* **2002**, *99*, 260–266. [CrossRef] [PubMed]
3. Chan, A.T.; Giovannucci, E.L. Primary prevention of colorectal cancer. *Gastroenterology* **2010**, *138*, 2029–2043. [CrossRef] [PubMed]
4. Deng, Y.; Wei, B.; Zhai, Z.; Zheng, Y.; Yao, J.; Wang, S.; Xiang, D.; Hu, J.; Ye, X.; Yang, S.; et al. Dietary Risk-Related Colorectal Cancer Burden: Estimates from 1990 to 2019. *Front. Nutr.* **2021**, *8*, 690663. [CrossRef] [PubMed]
5. Papadimitriou, N.; Bouras, E.; van den Brandt, P.A.; Muller, D.C.; Papadopoulou, A.; Heath, A.K.; Critselis, E.; Gunter, M.J.; Vineis, P.; Ferrari, P.; et al. A Prospective Diet-Wide Association Study for Risk of Colorectal Cancer in EPIC. *Clin. Gastroenterol. Hepatol.* **2022**, *20*, 864–873. [CrossRef] [PubMed]
6. Sawicki, T.; Ruszkowska, M.; Danielewicz, A.; Niedźwiedzka, E.; Arłukowicz, T.; Przybyłowicz, K.E. A review of colorectal cancer in terms of epidemiology, risk factors, development, symptoms and diagnosis. *Cancers* **2021**, *13*, 2025. [CrossRef]
7. Thanikachalam, K.; Khan, G. Colorectal cancer and nutrition. *Nutrients* **2019**, *11*, 164. [CrossRef]
8. Amintas, S.; Dupin, C.; Boutin, J.; Beaumont, P.; Moreau-Gaudry, F.; Bedel, A.; Krisa, S.; Vendrely, V.; Dabernat, S. Bioactive food components for colorectal cancer prevention and treatment: A good match. *Crit. Rev. Food Sci. Nutr.* **2022**, *in press*. [CrossRef]
9. Schwingshackl, L.; Schwedhelm, C.; Hoffmann, G.; Knüppel, S.; Laure Preterre, A.; Iqbal, K.; Bechthold, A.; de Henauw, S.; Michels, N.; Devleesschauwer, B.; et al. Food groups and risk of colorectal cancer. *Int. J. Cancer* **2018**, *142*, 1748–1758. [CrossRef]
10. Farinetti, A.; Zurlo, V.; Manenti, A.; Coppi, F.; Mattioli, A.V. Mediterranean diet and colorectal cancer: A systematic review. *Nutrition* **2017**, *43–44*, 83–88. [CrossRef]
11. Finicelli, M.; Di Salle, A.; Galderisi, U.; Peluso, G. The Mediterranean Diet: An Update of the Clinical Trials. *Nutrients* **2022**, *14*, 2956. [CrossRef]
12. Mahmod, A.I.; Haif, S.K.; Kamal, A.; Al-Ataby, I.A.; Talib, W.H. Chemoprevention effect of the Mediterranean diet on colorectal cancer: Current studies and future prospects. *Front. Nutr.* **2022**, *9*, 924192. [CrossRef]
13. Morze, J.; Danielewicz, A.; Przybyłowicz, K.; Zeng, H.; Hoffmann, G.; Schwingshackl, L. An updated systematic review and meta-analysis on adherence to mediterranean diet and risk of cancer. *Eur. J. Nutr.* **2021**, *60*, 1561–1586. [CrossRef] [PubMed]
14. Zamora-Ros, R.; Cayssials, V.; Jenab, M.; Rothwell, J.A.; Fedirko, V.; Aleksandrova, K.; Tjønneland, A.; Kyrø, C.; Overvad, K.; Boutron-Ruault, M.C.; et al. Dietary intake of total polyphenol and polyphenol classes and the risk of colorectal cancer in the European Prospective Investigation into Cancer and Nutrition (EPIC) cohort. *Eur. J. Epidemiol.* **2018**, *33*, 1063–1075. [CrossRef]
15. Chang, H.; Lei, L.; Zhou, Y.; Ye, F.; Zhao, G. Dietary flavonoids and the risk of colorectal cancer: An updated meta-analysis of epidemiological studies. *Nutrients* **2018**, *10*, 950. [CrossRef]
16. Clifford, M.N.; Jaganath, I.B.; Ludwig, I.A.; Crozier, A. Chlorogenic acids and the acyl-quinic acids: Discovery, biosynthesis, bioavailability and bioactivity. *Nat. Prod. Rep.* **2017**, *34*, 1391–1421. [CrossRef]
17. Bento-Silva, A.; Koistinen, V.M.; Mena, P.; Bronze, M.R.; Hanhineva, K.; Sahlstrøm, S.; Kitrytė, V.; Moco, S.; Aura, A.M. Factors affecting intake, metabolism and health benefits of phenolic acids: Do we understand individual variability? *Eur. J. Nutr.* **2020**, *59*, 1275–1293. [CrossRef]
18. Godos, J.; Rapisarda, G.; Marventano, S.; Galvano, F.; Mistretta, A.; Grosso, G. Association between polyphenol intake and adherence to the Mediterranean diet in Sicily, southern Italy. *NFS J.* **2017**, *8*, 1–7. [CrossRef]
19. Vázquez-Ruiz, Z.; Toledo, E.; Vitelli-Storelli, F.; Goni, L.; de la O, V.; Bes-Rastrollo, M.; Martínez-González, M.Á. Effect of Dietary Phenolic Compounds on Incidence of Cardiovascular Disease in the SUN Project; 10 Years of Follow-Up. *Antioxidants* **2022**, *11*, 783. [CrossRef]
20. Martini, S.; Conte, A.; Cattivelli, A.; Tagliazucchi, D. Domestic cooking methods affect the stability and bioaccessibility of dark purple eggplant (*Solanum melongena*) phenolic compounds. *Food Chem.* **2021**, *341*, 128298. [CrossRef]
21. Martini, S.; Conte, A.; Tagliazucchi, D. Phenolic compounds profile and antioxidant properties of six sweet cherry (*Prunus avium*) cultivars. *Food Res. Int.* **2017**, *97*, 15–26. [CrossRef] [PubMed]
22. Del Rio, D.; Rodriguez-Mateos, A.; Spencer, J.P.E.; Tognolini, M.; Borges, G.; Crozier, A. Dietary (poly)phenolics in human health: Structures, bioavailability, and evidence of protective effects against chronic diseases. *Antiox. Redox Signal.* **2013**, *18*, 1818–1892. [CrossRef] [PubMed]
23. Cattivelli, A.; Conte, A.; Martini, S.; Tagliazucchi, D. Influence of cooking methods on onion phenolic compounds bioaccessibility. *Foods* **2021**, *10*, 1023. [CrossRef]
24. Coman, V.; Vodnar, D.C. Hydroxycinnamic acids and human health: Recent advances. *J. Sci. Food Agric.* **2020**, *100*, 483–499. [CrossRef] [PubMed]
25. Li, Y.; Zhang, T.; Chen, G.Y. Flavonoids and colorectal cancer prevention. *Antioxidants* **2018**, *7*, 187. [CrossRef]
26. Mihanfar, A.; Darband, S.G.; Sadighparvar, S.; Kaviani, M.; Mirza-Aghazadeh-Attari, M.; Yousefi, B.; Majidinia, M. In vitro and in vivo anticancer effects of syringic acid on colorectal cancer: Possible mechanistic view. *Chem. Biol. Interact.* **2021**, *337*, 109337. [CrossRef]
27. Serra, A.; Macià, A.; Romero, M.P.; Reguant, J.; Ortega, N.; Motilva, M.J. Metabolic pathways of the colonic metabolism of flavonoids (flavonols, flavones and flavanones) and phenolic acids. *Food Chem.* **2012**, *130*, 383–393. [CrossRef]

28. Cattivelli, A.; Nissen, L.; Casciano, F.; Tagliazucchi, D.; Gianotti, A. Impact of cooking methods of red-skinned onion on in vitro colon metabolic transformation of phenolic compounds and gut microbiota changes. *Food Funct.* **2023**, *14*, 3509–3525. [CrossRef]
29. Juániz, I.; Ludwig, I.A.; Bresciani, L.; Dall'Asta, M.; Mena, P.; del Rio, D.; Cid, C.; de Peña, M.P. Bioaccessibility of (poly)phenolic compounds of raw and cooked cardoon (*Cynara cardunculus* L.) after simulated gastrointestinal digestion and fermentation by human colonic microbiota. *J. Funct. Foods* **2017**, *32*, 195–207. [CrossRef]
30. Nissen, L.; Cattivelli, A.; Casciano, F.; Gianotti, A.; Tagliazucchi, D. Roasting and frying modulate the phenolic profile of dark purple eggplant and differently change the colon microbiota and phenolic metabolites after in vitro digestion and fermentation in a gut model. *Food Res. Int.* **2022**, *160*, 111702. [CrossRef]
31. Almeida, A.F.; Borge, G.I.A.; Piskula, M.; Tudose, A.; Tudoreanu, L.; Valentová, K.; Williamson, G.; Santos, C.N. Bioavailability of Quercetin in Humans with a Focus on Interindividual Variation. *Compr. Rev. Food Sci. Food Saf.* **2018**, *17*, 714–731. [CrossRef] [PubMed]
32. Cortés-Martín, A.; Selma, M.V.; Tomás-Barberán, F.A.; González-Sarrías, A.; Espín, J.C. Where to Look into the Puzzle of Polyphenols and Health? The Postbiotics and Gut Microbiota Associated with Human Metabotypes. *Mol. Nutr. Food Res.* **2020**, *64*, 1900952. [CrossRef] [PubMed]
33. Iglesias-Aguirre, C.E.; Cortés-Martín, A.; Ávila-Gálvez, M.A.; Giménez-Bastida, J.A.; Selma, M.V.; González-Sarrías, A.; Espín, J.C. Main drivers of (poly)phenol effects on human health: Metabolite production and/or gut microbiota-associated metabotypes? *Food Funct.* **2021**, *12*, 10324–10355. [CrossRef] [PubMed]
34. Domínguez-Fernández, M.; Young Tie Yang, P.; Ludwig, I.A.; Clifford, M.N.; Cid, C.; Rodriguez-Mateos, A. In vivo study of the bioavailability and metabolic profile of (poly)phenols after sous-vide artichoke consumption. *Food Chem.* **2022**, *367*, 130620. [CrossRef]
35. Feng, S.; Yi, J.; Li, X.; Wu, X.; Zhao, Y.; Ma, Y.; Bi, J. Systematic Review of Phenolic Compounds in Apple Fruits: Compositions, Distribution, Absorption, Metabolism, and Processing Stability. *J. Agric. Food Chem.* **2021**, *69*, 7–27. [CrossRef]
36. Hai, Y.; Zhang, Y.; Liang, Y.; Ma, X.; Qi, X.; Xiao, J.; Xue, W.; Luo, Y.; Yue, T. Advance on the absorption, metabolism, and efficacy exertion of quercetin and its important derivatives. *Food Front.* **2020**, *1*, 420–434. [CrossRef]
37. Gómez-Juaristi, M.; Martínez-López, S.; Sarria, B.; Bravo, L.; Mateos, R. Absorption and metabolism of yerba mate phenolic compounds in humans. *Food Chem.* **2018**, *240*, 1028–1038. [CrossRef]
38. Carregosa, D.; Pinto, C.; Ávila-Gálvez, M.Á.; Bastos, P.; Berry, D.; Santos, C.N. A look beyond dietary (poly)phenols: The low molecular weight phenolic metabolites and their concentrations in human circulation. *Compr. Rev. Food Sci. Food Saf.* **2022**, *21*, 3931–3962. [CrossRef]
39. Di Pede, G.; Bresciani, L.; Calani, L.; Petrangolini, G.; Riva, A.; Allegrini, P.; Del Rio, D.; Mena, P. The human microbial metabolism of quercetin in different formulations: An in vitro evaluation. *Foods* **2020**, *9*, 1121. [CrossRef]
40. Juániz, I.; Ludwig, I.A.; Bresciani, L.; Dall'Asta, M.; Mena, P.; Del Rio, D.; Cid, C.; De Peña, M.P. Catabolism of raw and cooked green pepper (*Capsicum annuum*) (poly)phenolic compounds after simulated gastrointestinal digestion and faecal fermentation. *J. Funct. Foods* **2016**, *27*, 201–213. [CrossRef]
41. Jaganath, I.B.; Mullen, W.; Lean, M.E.J.; Edwards, C.A.; Crozier, A. In vitro catabolism of rutin by human fecal bacteria and the antioxidant capacity of its catabolites. *Free Radic. Biol. Med.* **2009**, *47*, 1180–1189. [CrossRef]
42. Aura, A.M.; O'Leary, K.A.; Williamson, G.; Ojala, M.; Bailey, M.; Puupponen-Pimiä, R.; Nuutila, A.M.; Oksman-Caldentey, K.M.; Poutanen, K. Quercetin derivatives are deconjugated and converted to hydroxyphenylacetic acids but not methylated by human fecal flora in vitro. *J. Agric. Food Chem.* **2002**, *50*, 1725–1730. [CrossRef]
43. Gonthier, M.P.; Remesy, C.; Scalbert, A.; Cheynier, V.; Souquet, J.M.; Poutanen, K.; Aura, A.M. Microbial metabolism of caffeic acid and its esters chlorogenic and caftaric acids by human faecal microbiota in vitro. *Biomed. Pharmacother.* **2006**, *60*, 536–540. [CrossRef]
44. Ludwig, I.A.; de Peña, M.P.; Cid, C.; Crozier, A. Catabolism of coffee chlorogenic acids by human colonic microbiota. *Biofactors* **2013**, *39*, 623–632. [CrossRef]
45. Mills, C.E.; Tzounis, X.; Oruna-Concha, M.J.; Mottram, D.S.; Gibson, G.R.; Spencer, J.P.E. In vitro colonic metabolism of coffee and chlorogenic acid results in selective changes in human faecal microbiota growth. *Br. J. Nutr.* **2015**, *113*, 1220–1227. [CrossRef]
46. Karlsson, P.C.; Huss, U.; Jenner, A.; Halliwell, B.; Bohlin, L.; Rafter, J.J. Human fecal water inhibits COX-2 in colonic HT-29 cells: Role of phenolic compounds. *J. Nutr.* **2005**, *135*, 2343–2349. [CrossRef]
47. Jenner, A.M.; Rafter, J.; Halliwell, B. Human fecal water content of phenolics: The extent of colonic exposure to aromatic compounds. *Free Radic. Biol. Med.* **2005**, *38*, 763–772. [CrossRef]
48. Knust, U.; Erben, G.; Spiegelhalder, B.; Bartsch, H.; Owen, R.W. Identification and quantitation of phenolic compounds in faecal matrix by capillary gas chromatography and nano-electrospray mass spectrometry. *Rapid Commun. Mass. Spectrom.* **2006**, *20*, 3119–3129. [CrossRef]
49. Gill, C.I.R.; Mcdougall, G.J.; Glidewell, S.; Stewart, D.; Shen, Q.; Tuohy, K.; Dobbin, A.; Boyd, A.; Brown, E.; Haldar, S.; et al. Profiling of phenols in human fecal water after raspberry supplementation. *J. Agric. Food Chem.* **2010**, *58*, 10389–10395. [CrossRef]
50. Ekbatan, S.S.; Li, X.Q.; Ghorbani, M.; Azadi, B.; Kubow, S. Chlorogenic acid and its microbial metabolites exert anti-proliferative effects, S-phase cell-cycle arrest and apoptosis in human colon cancer caco-2 cells. *Int. J. Mol. Sci.* **2018**, *19*, 723. [CrossRef]
51. Glei, M.; Kirmse, A.; Habermann, N.; Persin, C.; Pool-Zobel, B.L. Bread enriched with green coffee extract has chemoprotective and antigenotoxic activities in human cells. *Nutr. Cancer* **2006**, *56*, 182–192. [CrossRef] [PubMed]

52. Rosa, L.d.S.; Silva, N.J.A.; Soares, N.C.P.; Monteiro, M.C.; Teodoro, A.J. Anticancer properties of phenolic acids in colon cancer—A review. *J. Nutr. Food Sci.* **2016**, *6*, 1000468.
53. Gao, K.; Xu, A.; Krul, C.; Venema, K.; Liu, Y.; Niu, Y.; Lu, J.; Bensoussan, L.; Seeram, N.P.; Heber, D.; et al. Of the major phenolic acids formed during human microbial fermentation of tea, citrus, and soy flavonoid supplements, only 3,4-dihydroxyphenylacetic acid has antiproliferative activity. *J. Nutr.* **2006**, *136*, 52–57. [CrossRef] [PubMed]
54. Kim, D.H.; Kim, S.Y.; Park, S.Y.; Han, M.J. Metabolism of quercitrin by human intestinal bacteria and its relation to some biological activities. *Biol. Pharm. Bull.* **1999**, *22*, 749–751. [CrossRef] [PubMed]
55. Dihal, A.A.; Woutersen, R.A.; Van Ommen, B.; Rietjens, I.M.C.M.; Stierum, R.H. Modulatory effects of quercetin on proliferation and differentiation of the human colorectal cell line Caco-2. *Cancer Lett.* **2006**, *238*, 248–259. [CrossRef] [PubMed]
56. Neamtu, A.A.; Maghiar, T.A.; Alaya, A.; Olah, N.K.; Turcus, V.; Pelea, D.; Totolici, B.D.; Neamtu, C.; Maghiar, A.M.; Mathe, E. A Comprehensive View on the Quercetin Impact on Colorectal Cancer. *Molecules* **2022**, *27*, 1873. [CrossRef] [PubMed]
57. Darband, S.G.; Kaviani, M.; Yousefi, B.; Sadighparvar, S.; Pakdel, F.G.; Attari, J.A.; Mohebbi, I.; Naderi, S.; Majidinia, M. Quercetin: A functional dietary flavonoid with potential chemo-preventive properties in colorectal cancer. *J. Cell Physiol.* **2018**, *233*, 6544–6560. [CrossRef]
58. Rosa, L.S.; Jordão, N.A.; da Costa Pereira Soares, N.; deMesquita, J.F.; Monteiro, M.; Teodoro, A.J. Pharmacokinetic, Antiproliferative and Apoptotic Effects of Phenolic Acids in Human Colon Adenocarcinoma Cells Using In Vitro and In Silico Approaches. *Molecules* **2018**, *23*, 2569. [CrossRef]
59. Zhang, H.; Hassan, Y.I.; Liu, R.; Mats, L.; Yang, C.; Liu, C.; Tsao, R. Molecular mechanisms underlying the absorption of aglycone and glycosidic flavonoids in a Caco-2 BBe1 cell model. *ACS Omega* **2020**, *5*, 10782–10793. [CrossRef]
60. Maiyo, F.C.; Moodley, R.; Singh, M. Cytotoxicity, Antioxidant and Apoptosis Studies of Quercetin-3-O Glucoside and 4-(β-D-Glucopyranosyl-1→4-α-L-Rhamnopyranosyloxy)-Benzyl Isothiocyanate from Moringa oleifera. *Anticancer. Agents Med. Chem.* **2016**, *16*, 648–656. [CrossRef]
61. Gómez-Juaristi, M.; Sarria, B.; Goya, L.; Bravo-Clemente, L.; Mateos, R. Experimental confounding factors affecting stability, transport, and metabolism of flavanols and hydroxycinnamic acids in Caco-2 cells. *Food Res. Int.* **2020**, *129*, 108797. [CrossRef]
62. Martini, S.; Conte, A.; Tagliazucchi, D. Antiproliferative Activity and Cell Metabolism of Hydroxycinnamic Acids in Human Colon Adenocarcinoma Cell Lines. *J. Agric. Food Chem.* **2019**, *67*, 3919–3931. [CrossRef]
63. Konishi, Y.; Kobayashi, S. Transepithelial transport of chlorogenic acid, caffeic acid, and their colonic metabolites in intestinal Caco-2 cell monolayers. *J. Agric. Food Chem.* **2004**, *52*, 2518–2526. [CrossRef]
64. Konishi, Y. Transepithelial transport of microbial metabolites of quercetin in intestinal Caco-2 cell monolayers. *J. Agric. Food Chem.* **2005**, *53*, 601–607. [CrossRef]
65. Nicoletti, I.; Migliorati, G.; Pagliacci, M.C.; Grignani, F.; Riccardi, C. A rapid and simple method for measuring thymocyte apoptosis by propidium iodide staining and flow cytometry. *J. Immunol. Methods* **1991**, *139*, 271–279. [CrossRef]
66. Sala, R.; Mena, P.; Savi, M.; Brighenti, F.; Crozier, A.; Miragoli, M.; Stilli, D.; Del Rio, D. Urolithins at physiological concentrations affect the levels of pro-inflammatory cytokines and growth factor in cultured cardiac cells in hyperglucidic conditions. *J. Funct. Foods* **2015**, *15*, 97–105. [CrossRef]
67. Martini, S.; Tagliazucchi, D.; Minelli, G.; Lo Fiego, D.P. Influence of linseed and antioxidant-rich diets in pig nutrition on lipid oxidation during cooking and in vitro digestion of pork. *Food Res. Int.* **2020**, *137*, 109528. [CrossRef]

International Journal of
Molecular Sciences

MDPI

Article

Overexpression of *BmJHBPd2* Repressed Silk Synthesis by Inhibiting the JH/Kr-h1 Signaling Pathway in *Bombyx mori*

Jikailang Zhang [1,†], Xia Zhang [1,†], Hui Zhang [1], Jiaojiao Li [1], Wei Li [1] and Chun Liu [1,2,*]

[1] State Key Laboratory of Resource Insects, Southwest University, Chongqing 400715, China; zhangjikailang@163.com (J.Z.)
[2] Jinfeng Laboratory, Chongqing 401329, China
* Correspondence: chunliu@swu.edu.cn
† These authors contributed equally to this work.

Abstract: The efficient production of silkworm silk is crucial to the silk industry. Silk protein synthesis is regulated by the juvenile hormone (JH) and 20-Hydroxyecdysone (20E). Therefore, the genetic regulation of silk production is a priority. JH binding protein (JHBP) transports JH from the hemolymph to target organs and cells and protects it. In a previous study, we identified 41 genes containing a JHBP domain in the *Bombyx mori* genome. Only one JHBP gene, *BmJHBPd2*, is highly expressed in the posterior silk gland (PSG), and its function remains unknown. In the present study, we investigated the expression levels of *BmJHBPd2* and the major silk protein genes in the high-silk-producing practical strain *872* (*S872*) and the low-silk-producing local strain *Dazao*. We found that *BmJHBPd2* was more highly expressed in *S872* than in the *Dazao* strain, which is consistent with the expression pattern of fibroin genes. A subcellular localization assay indicated that *BmJHBPd2* is located in the cytoplasm. In vitro hormone induction experiments showed that *BmJHBPd2* was upregulated by juvenile hormone analogue (JHA) treatment. *BmKr-h1* upregulation was significantly inhibited by the overexpression of *BmJHBPd2* (BmJHBPd2OE) at the cell level when induced by JHA. However, overexpression of *BmJHBPd2* in the PSG by transgenic methods led to the inhibition of silk fibroin gene expression, resulting in a reduction in silk yield. Further investigation showed that in the transgenic BmJHBPd2OE silkworm, the key transcription factor of the JH signaling pathway, Krüppel homolog 1 (Kr-h1), was inhibited, and 20E signaling pathway genes, such as broad complex (Brc), E74A, and ultraspiracle protein (USP), were upregulated. Our results indicate that *BmJHBPd2* plays an important role in the JH signaling pathway and is important for silk protein synthesis. Furthermore, our findings help to elucidate the mechanisms by which JH regulates silk protein synthesis.

Keywords: juvenile hormone; juvenile hormone binding protein; silk protein; *Bombyx mori*

Citation: Zhang, J.; Zhang, X.; Zhang, H.; Li, J.; Li, W.; Liu, C. Overexpression of *BmJHBPd2* Repressed Silk Synthesis by Inhibiting the JH/Kr-h1 Signaling Pathway in *Bombyx mori*. *Int. J. Mol. Sci.* **2023**, *24*, 12650. https://doi.org/10.3390/ijms241612650

Academic Editor: Clemente Capasso

Received: 24 May 2023
Revised: 24 July 2023
Accepted: 29 July 2023
Published: 10 August 2023

1. Introduction

The juvenile hormone (JH) plays a key role in insect development, metamorphosis, and reproduction [1,2]. Juvenile hormone binding protein (JHBP) is the first key factor in the JH signaling pathway. The JHBP or JH-JHBP complex is a vital member of the intricate JH signaling transmission chain that binds to membrane receptors [3,4]. It broadens our understanding of the crucial factors involved in the JH signaling pathway and its mode of action in target organs and has far-reaching importance in pest control and other practical applications.

JH is a hemiterpenoid compound secreted by the corpora allata [5]. JHBP is a carrier protein that works in the hemolymph and cells. This protein transports hormone molecules from the JH synthesis site in the corpora allata to the peripheral target cells and assists JH molecules in entering the circulatory system. JHBP can also reduce the non-specific binding of JH [6], protecting it from enzymatic degradation [7,8]. Intracellular JHBP can be divided into cytoplasmic and nuclear JHBP, which are both involved in the effects of JH on target

genes. However, to date, the progress of related research has been relatively slow [9,10]. The expression level of JHBP, which was found to be predominant in the fat body of the bamboo borer, was average from the third to the fifth stages. The expression level was the highest at the early diapause stage, which continued until the middle diapause stage and then decreased until the pupae stage [11]. In melon aphids, RNA interference has been used to silence the expression of JHBP and block the transmission of JH signals, resulting in mortality and thus allowing effective pest management [12]. Proteomic analysis of male accessory gland secretions has shown that JHBPs affect female reproduction in oriental fruit flies [13]. Therefore, these studies prove that JHBP is involved in metabolism, growth, and reproduction. The JHBPs from this gene family are found in many lepidopteran species and form a separate group from other genes [14,15]. To date, studies on the JHBP have focused on many lepidopteran insects, including the tobacco hornworm (*Manduca sexta*) [16,17], tobacco budworm (*Heliothis virescen*) [7,18], greater wax moth (*Galleria mellonella*) [19], and silkworm (*Bombyx mori*) [20,21].

The domesticated silkworm is a typical lepidopteran holometabolous insect model organism. As a natural protein fiber, the use of silk has been applied in many fields [22]. Silkworm silk glands primarily synthesize and secrete two types of silk proteins, namely fibroin and sericin. Fibroin is composed of a heavy (Fib-H) and light (Fib-L) chain, and glycoprotein 25 kDa (P25) is synthesized in the posterior silk gland (PSG) [23,24]. Previous studies have found that increasing the amount of silk protein, injection, smearing, and feeding on exogenous JH or JH analogs (JHAs) can prolong the larval stage of silkworms and increase the RNA and DNA contents of the silk protein gene [25–28]. The mechanism of action behind this remained unclear until recent results showed that Krüppel homolog 1 (Kr-h1) is involved in the repression of metamorphosis. In transgenic silkworms with *Kr-h1* overexpression, the silk glands were significantly enlarged [29]. Furthermore, JH induces extended expression of the *Bmfib-H* gene, and *BmKr-h1* may suppress larvae–pupae metamorphosis by activating the expression of *B. mori*-derived dimmed (*Bmdimm*). *Bmdimm* is a transcription factor involved in the regulation of silk gene transcription that activates the transcription of the *Bmfib-H* gene in *B. mori* posterior silk gland (PSG) cells [30].

In previous studies, 41 JHBP genes were identified in silkworms, which contained conserved structures of the binding proteins of JH. Microarray data have shown different JHBP gene expression trends in silkworms. The expression of *BmJHBP* genes was generally higher in the head, integument, midgut, fat body, testes, and ovaries. Expression levels also differed among different tissues. The PSG had a specific and high expression of *JHBPd2* [21]. Our study aimed to investigate the role of JHBPd2 in silk protein synthesis.

2. Results

2.1. Expression of BmJHBPd2 in Different Silk-Producing Strains

After many years of natural selection and artificial domestication, significant differences in silk production exist among different strains of silkworms. To analyze the mRNA levels of *BmJHBPd2* among different strains, the high-silk-producing practical strain 872 (*S872*) and low-silk-producing local strain *Dazao* were selected for further analysis to ascertain the differences between the strains. This study investigated the indicators of four main characteristics of *S872* and *Dazao*. The pupae and cocoons of *S872* were substantially larger than those of the *Dazao* strain (Figure S1A). The whole cocoon weight, pupae, and cocoon weight, particularly the shell weight percentage of *S872*, were significantly higher than those of *Dazao* (Figure S1B). Considering the high efficiency of silk protein synthesis by the silk glands of fifth instar larvae, the expression levels of genes in the PSG were investigated. In this study, we determined the expression levels of major silk protein genes using real-time quantitative reverse transcription polymerase chain reaction (qRT-PCR). *Bmfib-H*, *Bmfib-L*, and *BmP25* were specifically expressed in the PSG. The transcript levels of *Bmfib-H* and *Bmfib-L* were higher in the *S872* PSG than in that of *Dazao* at the third and fifth day of the fifth instar (Figure 1A,B). *BmP25* was expressed at the same level in both strains (Figure 1C). Differences in the *BmJHBPd2* expression were also analyzed. The transcript

level of *BmJHBPd2* in the *S872* PSG was higher than that in *Dazao* on the third and fifth day of the fifth instar. The expression level of *BmJHBPd2 in S872* on the fifth day of the fifth instar was significantly higher than that in *Dazao* (Figure 1D). These results suggest that *BmJHBPd2* may be involved in silk protein synthesis.

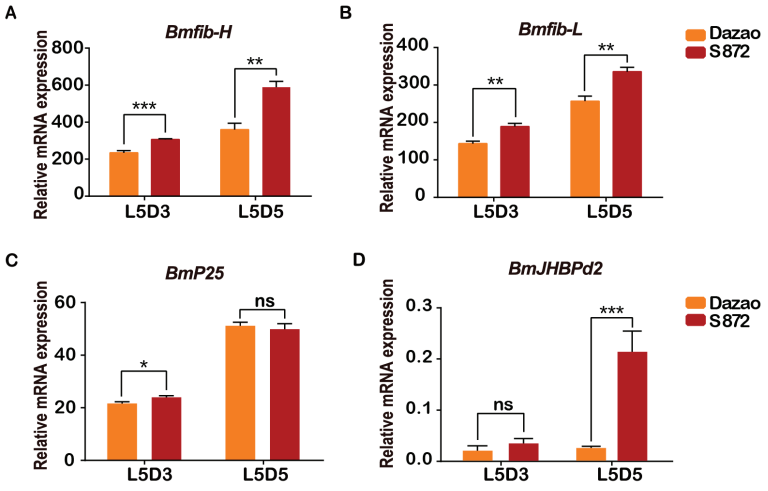

Figure 1. The expression of *BmJHBPd2* was different in the PSG among the two silk-producing strains *Dazao* and *S872*. (**A**–**D**). Relative *Bmfib-H*, *Bmfib-L*, *BmP25*, and *BmJHBPd2* mRNA levels in the PSG of *Dazao* and *S872* larvae on the 3rd and 5th day of the fifth instar as analyzed by real-time quantitative reverse transcription polymerase chain reaction (qRT-PCR). *BmRpl3* was used as an internal control. The results are expressed as means ± standard deviation (SD) of three independent experiments; * $p < 0.05$; ** $p < 0.01$; *** $p < 0.001$; ns, not significant.

2.2. Overexpression of BmJHBPd2 at the Cellular Level

JH regulates silk protein synthesis, and JHBP plays an important role in JH regulation as a vital response factor. To further explore how *BmJHBPd2* is involved in silk protein synthesis, the expression of the genes associated with the silk protein synthesis and those related to the JH signaling pathway in the exogenous JH induction were analyzed at the cellular level. First, the *BmJHBPd2* subcellular localization vector was constructed (Figure 2A). Immunofluorescence experiments showed that FLAG-tagged *BmJHBPd2* was localized in the cytoplasm (Figure 2B). This result is consistent with that reported by Li et al. [21] and implies that *BmJHBPd2* cannot be secreted and plays a physiological role in cells. The qRT-PCR analysis at the nucleic acid levels and Western blotting at the protein levels showed that the intracellular overexpression of BmJHBPd2 was successful (Figure 3A). BmE cells contain the signal transduction pathway for JH [30]. When adding JHA to BmE cells, the expression of *BmJHBPd2* was significantly upregulated. Furthermore, JHA significantly upregulated the expression of the early response factor *BmKr-h1*, suggesting that JHA significantly activated the JH downstream signaling pathway (Figure 3B). When only *BmJHBPd2* was overexpressed, *Bmkr-h1* was nearly unexpressed, and there was no change in the expression of the *B. mori* methoprene-tolerant 1 (*BmMet1)* gene (Figure 3C). However, the upregulated expression level of *BmKr-h1* in pSLfa1180-basic was higher than that in pSLfa1180-BmJHBPd2 (Figure 3D). These results infer that the excessive expression of BmJHBPd2 in the transfected cells reduced the amount of JH and then lowered the expression of *Bmkr-h1*, since the overexpression of BmJHBPd2 may be sufficiently high, as shown in Figure 3A, even though the expression of *Bmkr-h1* in Figure 3B increased. In addition, the expression of *Bmfib-H* was not detected in all experiments using BmE cells; this may have been caused by the lack of transcription factors specific to silk protein genes in the cells.

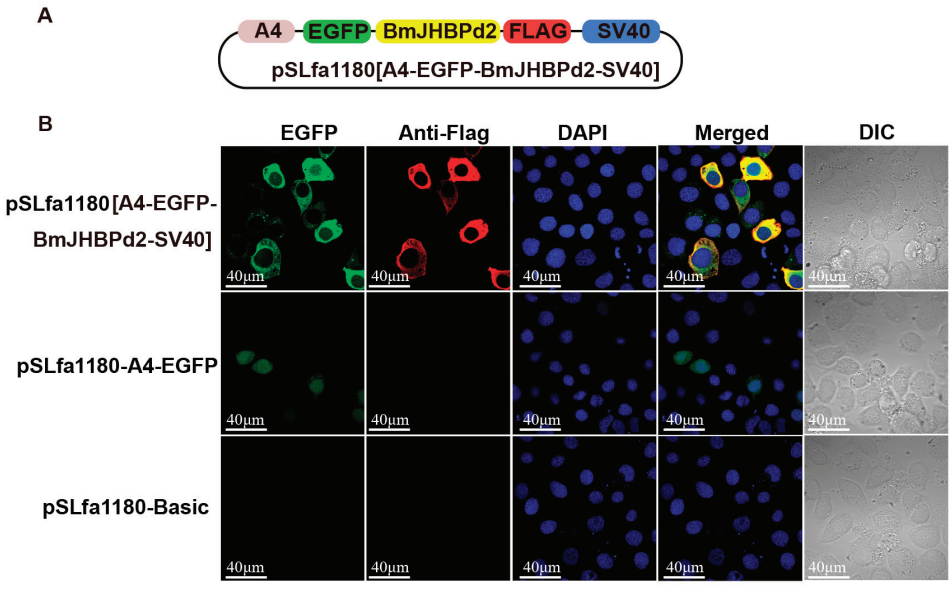

Figure 2. Overexpression of *BmJHBPd2* in BmE cells. (**A**). Structural map of subcellular-localized overexpression of the *BmJHBPd2* vector. (**B**). Immunofluorescence experiment of *BmJHBPd2* in BmE cells.

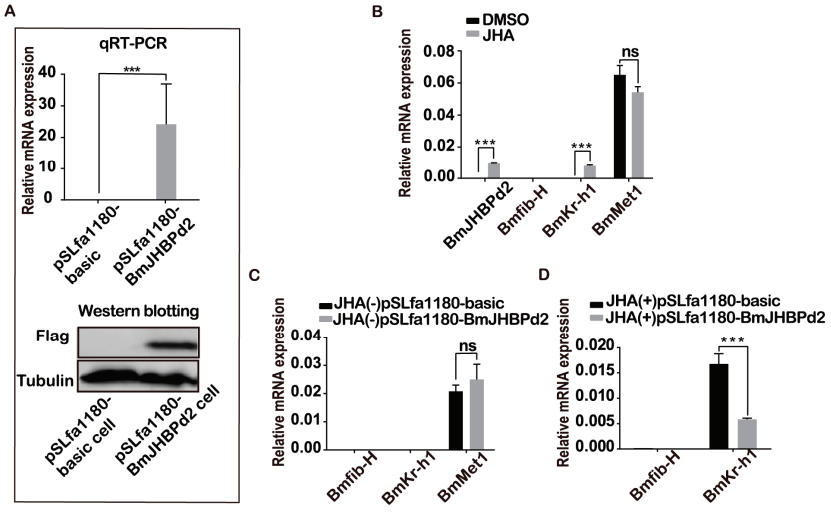

Figure 3. *BmJHBPd2* responds to juvenile hormone analogs (JHAs) in BmE cells. (**A**). Overexpression of *BmJHBPd2* in BmE cells assayed by qRT-PCR and Western blotting using the flag tag antibody and tubulin as a control. (**B**). Expression of *BmJHBPd2*, *Bmfib-H*, *BmKr-h1*, and *BmMet1* after adding JHA or DMSO to normal BmE cells. (**C**). Expression of *Bmfib-H*, *BmKr-h1*, and *BmMet1* after overexpression of *BmJHBPd2* assayed without adding JHA. (**D**). *Bmfib-H* and *BmKr-h1* expression level in BmE cells overexpressing *BmJHBPd2* after adding JHA. The experiments of (**B**–**D**) were assayed using qRT-PCR, and *BmRpl3* expression was used as an internal control. Results are expressed as the means ± S.D. of three independent experiments. *** $p < 0.001$; ns, not significant.

2.3. Transgenic Overexpression of BmJHBPd2 in the Silk Gland

To further explore the biological function of *BmJHBPd2* in the silk gland, a piggyBac transgenic vector containing a combination of *BmJHBPd2* and a Myc foreign label with the Fib-L promoter, Fib-L terminator, and *pBac [3xP3 EGFP]* was constructed (Figure 4A). The vector and helper plasmids were injected into 271 pre-blastoderm eggs, of which 136 hatched and developed to the adult stage. An EGFP-positive brood was obtained and used to establish the transgenic overexpression line (Figure 4B). Then, we obtained four positive G2 generations, and the results of the investigations on all four G2 generations showed that the synthesis of silk proteins was affected. One G3 generation was conserved and continued to be reared and investigated, and the result remained the same. The mRNA levels of *BmJHBPd2* in the PSG of larvae on the third day of the fifth instar larvae (L5D3) of the transgenic and wild-type (WT) lines were detected using qRT-PCR. The result showed that *BmJHBPd2* levels were substantially higher in the transgenic line than that in the WT line (Figure 4C). To confirm whether BmJHBPd2 with a Myc-tag was synthesized in the transgenic line, proteins were extracted from the PSG of L5D3 for Western blotting. The signals with the Myc antibody were only detected in the transgenic line (BmJHBPd2OE) but not in the WT line (Figure 4D). These results indicated that *BmJHBPd2* was overexpressed in the PSG.

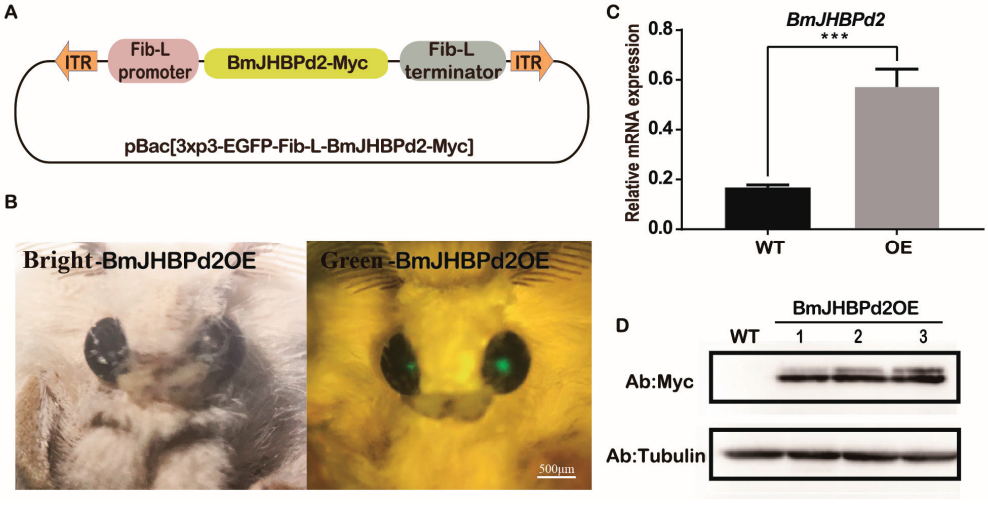

Figure 4. Overexpression of *BmJHBPd2* in the posterior silk gland. (**A**). Schematic diagram of carrier construction. (**B**). Screening of transgenic moths; transgenic-positive individual moths under white light and green fluorescence. (**C**). Overexpression of *BmJHBPd2* assayed using qRT-PCR; *BmRpl3* was used as an internal control. (**D**). Detection of BmJHBPd2 at the protein level using a Myc tag antibody and tubulin as a control. Results are expressed as means ± S.D. of three independent experiments. *** $p < 0.001$.

2.4. Overexpression of BmJHBPd2 Affects Silk Synthesis and Silk Yield

This study investigated the strain overexpressing the *BmJHBPd2* gene obtained above, predominantly focusing on the silk gland and yield of fifth instar larvae. The BmJHBPd2OE line was raised to the L5D3 stage, and its silk glands were dissected and observed. There was no pronounced difference in the biological characteristics of the silk glands (Figure 5A). However, we found that the overexpression of *BmJHBPd2* resulted in thinner and smaller cocoon shells than those in the WT lines (Figure 5B). Further observation of the cocoon shells of the two lines showed that the whole cocoon weight, cocoon weight, pupae weight, and cocoon shell rate were significantly reduced in the BmJHBPd2OE line (Figure 5C–F). Based on these differences in cocoon shells between the BmJHBPd2OE line and WT line, we chose

the L5D3 stage to determine the mRNA levels of silk protein-related transcription factors and silk fibroin genes in both lines. Among the silk fibroins tested, *Bmfib-H* and *Bmfib-L* were significantly downregulated at the L5D3 in the BmJHBPd2OE line (Figure 5G,H), except for *BmP25*, which did not differ significantly between the two lines (Figure 5I). Among the silk-related transcription factors, the expression of *Bmsage* and *Bmdimm* was significantly downregulated in the BmJHBPd2OE line (Figure 5J,K). However, the expression of *Bmsgf-1* was significantly upregulated (Figure 5L). These results indicate that this study successfully overexpressed the *BmJHBPd2* gene, although the expression of the silk fibroin gene and silk fibroin-related transcription factors in the BmJHBPd2OE line was significantly reduced, which affected the silk yield.

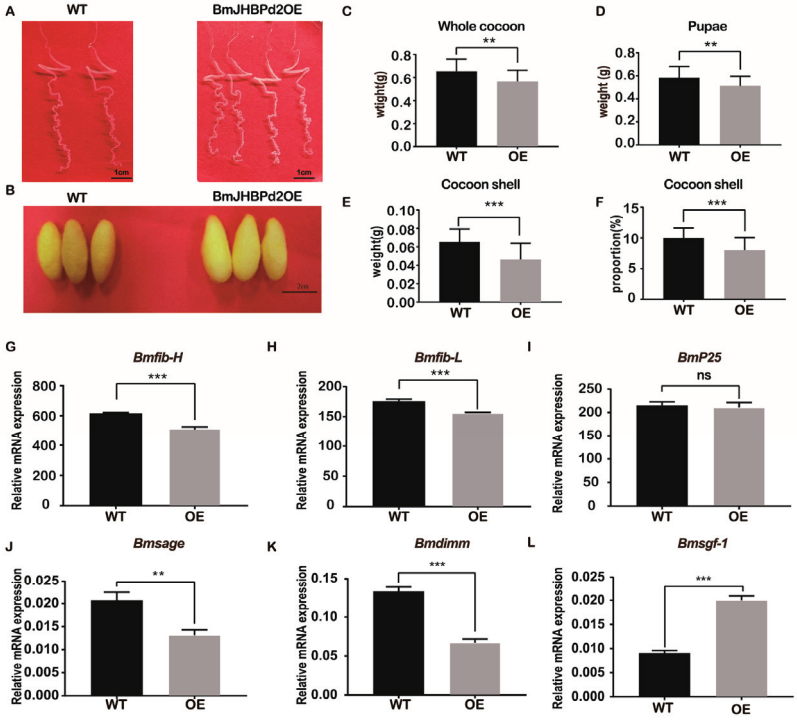

Figure 5. Analysis of fibroin gene expression and cocoon traits. (**A**–**F**). Phenotype of silk gland at the fifth instar and cocoon of the BmJHBPd2OE and WT lines. (**G**–**L**). Expression of silk fibroin protein gene and silk protein transcription factor in the WT and transgenic lines. *BmRpl3* expression was used as a control. Results are expressed as means ± S.D. of three independent experiments. ** $p < 0.01$; *** $p < 0.001$; ns, not significant.

2.5. Overexpression of BmJHBPd2 Led to Repression of Silk Synthesis by Inhibiting Bmkr-h1 Expression in the Silk Glands

JHBPd2 affected the expression of *Kr-h1* in the JH pathway at the cellular level. Therefore, the major JH regulatory pathway genes were investigated in the silk glands of the BmJHBPd2OE and WT lines. According to qRT-PCR, the relative expression level of the early response factor, *BmKr-h1*, in the JH pathway was significantly reduced in the BmJHBPd2OE line (Figure 6A). JH receptors, such as Met1, methoprene-tolerant 2 (Met2), and steroid receptor co-activator (SRC), were also downregulated (Figure 6C,D). The key enzymes of the JH metabolic pathway, JH esterase (JHE), and JH epoxide hydrolase (JHEH), were significantly downregulated (Figure S2A,B). Therefore, both the major genes in the

JH pathway and the JH-degrading enzymes were downregulated, indicating that the JH pathway was affected by overexpression of *BmJHBPd2*.

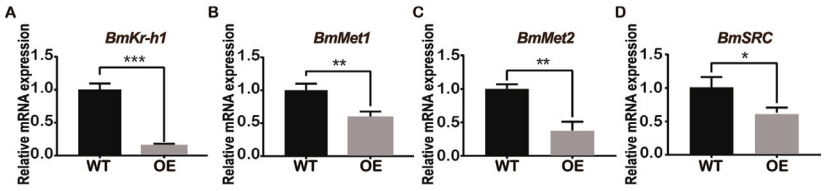

Figure 6. Overexpression of *BmJHBPd2* results in the inhibition of JH signaling pathway in silk glands assayed by qRT-PCR. The following JH signaling pathway–related genes were selected: Kr-h1 (**A**), Met1 (**B**), Met2 (**C**), and SRC (**D**). *BmRpl3* was used as a control. Results are expressed as means ± S.D. of three independent experiments. * $p < 0.05$; ** $p < 0.01$; *** $p < 0.001$.

Kr-h1 can directly inhibit the biosynthesis of 20-hydroxyecdysone (20E) and the expression of some early transcription factors in 20E [31]. Therefore, the expression of some early transcription factors in 20E was investigated. This study found that the early transcription factor *B. mori* broad complex (*BmBrc*) of 20E was significantly upregulated (Figure 7A). The relative expression levels of E74A and ultraspiracle protein (USP) were significantly upregulated in the BmJHBPd2OE line (Figure 7B,C). Meanwhile, those of the ecdysteroid receptor (EcR), hormone receptor 3 (HR3), and E75A did not differ significantly between the two lines (Figure 7D–F). These results suggest that overexpression of *BmJHBPd2* increases the expression of early transcription factors in the 20E signaling pathway.

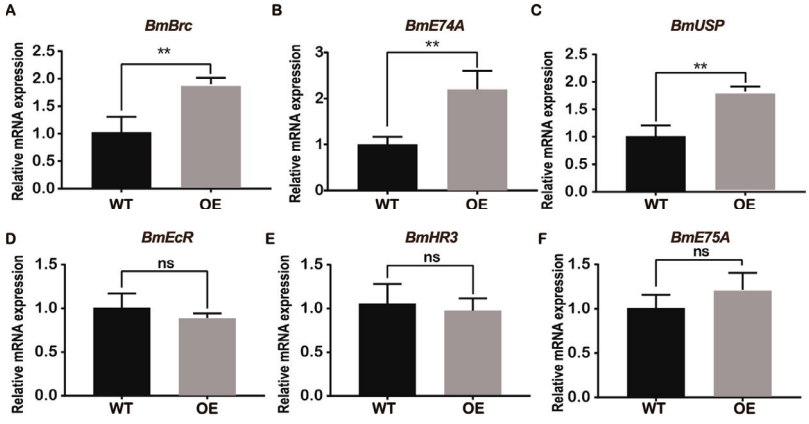

Figure 7. Overexpression of *BmJHBPd2* results in upregulation of the 20-hydroxyecdysone (20E) signaling pathway in silk glands assayed using qRT-PCR. The following 20E signaling pathway–related genes were selected: Brc (**A**), E74A (**B**), USP (**C**), EcR (**D**), HR3 (**E**), and E75A (**F**). *BmRpl3* was used as a control. Results are expressed as means ± S.D. of three independent experiments. ** $p < 0.01$; ns, not significant.

3. Discussion

The most valuable aspect of silkworm studies is the potential for increased production of silk [22]. In order to increase silk production, it is important to understand the process of silk protein synthesis [32]. In our study, we found a correlation between *BmJHBPd2* and silk protein gene expression and silk yield. At the cellular level, *BmJHBPd2* was induced by JHA and suppressed JH signaling by inhibiting the expression of *Bmkr-h1*. Individual experiments showed that overexpression of *BmJHBPd2* promoted the expression of 20E-related transcription factors by inhibiting the expression of *Bmkr-h1*, thereby decreasing the

expression of silk protein genes and silk production. Our results indicate that *BmJHBPd2* plays an important role in regulating JH signaling in silk glands. Simply increasing the expression of JHPBd2 does not increase silk yield; rather, silk protein synthesis is inhibited. Our research provides a reference for future genetic modifications to improve silk yield.

As a specific carrier of the endocrine hormone JH in silkworms, JHBP protects and transports synthesized and secreted JH from the corpora allata [6]. Given that the organs are used for silk protein synthesis and secretion, silk glands grow rapidly during the fifth instar. Although JH has been found to be largely absent from the blood of fifth instar silkworms [33], to date, there have been no reports on whether the silk glands of fifth instar silkworms contain JH. Based on the functional studies, the findings of this study suggest that the silk glands of fifth instar silkworms are likely to contain JH and that JHBPd2 may play a role in regulating the concentration gradient of JH in the functioning of silk glands. The rationale is that the overexpression of JHBPd2 alone in the PSG increases its protein production, and JH entering the silk gland without reaching the JH concentration in the blood binds to the overexpressed JHBPd2. This can result in a decrease in free JH in the silk gland, which, in turn, reduces the expression of *Kr-h1*. As a key transcription factor connecting the JH and the 20E pathways, *Kr-h1* can directly inhibit the biosynthesis of 20E [31], thereby inhibiting insect growth. *Kr-h1* also directly binds to the Kr-h1 binding site (KBS) elements of E93, Brc, and E75 promoters to inhibit their expression [34–37]. During crosstalk between the JH and 20E pathways, *Kr-h1* is located upstream of the 20E pathway genes and inhibits their expression. The 20E transcription factors, such as Brc, strongly repress silk protein synthesis [38]. Consequently, the expression of silk proteins is reduced, which then leads to decreased silk yield.

The expression pattern of the *JHBPd2* gene is highly similar to that of the silk fibroin gene, both of which are highly expressed at the fifth instar stage and are mainly expressed in the PSG. This indicates a close relationship with silk fibroin synthesis [39]. The larval stage of silkworms was found to be positively correlated with the silk yield [40,41]. The expression of JHBPd2 was significantly higher in high-silk-yield varieties than in low-silk-yield varieties, and there was a positive correlation between its expression and silk yield. However, the overexpression of JHBPd2 was found to inhibit silk yield. This study also conducted an in-depth analysis of this issue. This contradictory results suggest that JHBPd2 plays a role in the regulation of JH concentration. The larval stage of high-silk-yield *S872*, especially at the end of the fifth instar, is 2–3 days longer than that of the low-silk-yield variety *Dazao*. This suggests that *S872* contains more JH than *Dazao* in vivo, which can be inferred from applying JH to the silkworm body surface, prolonging the developmental time of the silkworm [30]. With more JH in the high-silk-yield *S872*, there is a corresponding increase in JH content in the silk gland, which requires more JHBPd2 protein to bind and protect JH. Therefore, the silk glands of the high-silk-yield *S872* have more time to synthesize more silk protein and, thus, produce more silk. After the overexpression of BmJHBPd2, because the JH signaling pathway in the silkworm was affected, the balance of JH concentration in the silk gland was disrupted, which inhibited silk protein synthesis. Our results also indicate that simply changing a gene that is positively associated with silk production may not improve silk yield. Silk yield is a quantitative trait controlled by multiple genes. Varieties with high silk yields can result from artificial selection, which is the result of the synergistic regulation of multiple genes. Altering only one gene, such as JHBPd2 in this study, may disrupt homeostasis in vivo, which, in turn, inhibits silk protein synthesis. Therefore, further research is required to determine how to improve silk production through genetic manipulation. Further research on the regulatory mechanism of silk protein synthesis is expected to identify the most critical factors affecting silk protein synthesis.

In this study, we did not measure JH in the silk glands of the JHBPd2OE line due to limited material availability; however, we performed JH assays on normal silk gland tissues and found that silk glands contained JH. We propose the following regarding the expression of *BmJHBPd2* in the PSG (Figure 8). JH is transported into PSG cells from the

hemolymph early in the fifth instar stage. Free JH then binds to the nuclear receptor *BmMet* and forms a complex with *BmSRC* [42]. This complex activates the expression of *BmKr-h1* and, subsequently, the expression of the transcription factor *Bmdimm* to regulate *Bmfib-H* [30]. Simultaneously, JH induces the upregulated expression of *BmJHBPd2* (Figure 3B). Cytoplasmic *BmJHBPd2* can bind to redundant JH and slowly release it to maintain the JH level, which continuously regulates gene expression for silk synthesis. Therefore, there are two potential sources of JH in the silk glands, one of which possibly originates from the blood. There is a consensus that JH is released into the blood after synthesis by the pharyngeal lateral body and that JH in the blood is bound by JHBP and transported to various tissues and organs. However, it is difficult to understand that at the fifth instar, JH is essentially undetectable in the blood. Therefore, it is unlikely that other tissues and organs contain JH. However, at the early age of the fifth instar, JH is likely synthesized by the corpora allata and then transported to other tissues and organs after being bound by JHBP in each organ. Here, JHBP functions as a sponge, which slowly releases JH and regulates the growth and development of each tissue and organ. The issue of the catch and release should be addressed in future research. However, the silk gland may synthesize JH independently. Although the corpora allata is the main JH-synthesizing organ, the possibility that other tissues and organs may synthesize JH cannot be excluded. In addition, a substantial number of JH synthesis enzymes have been detected in silk glands. Further confirmation of this is required.

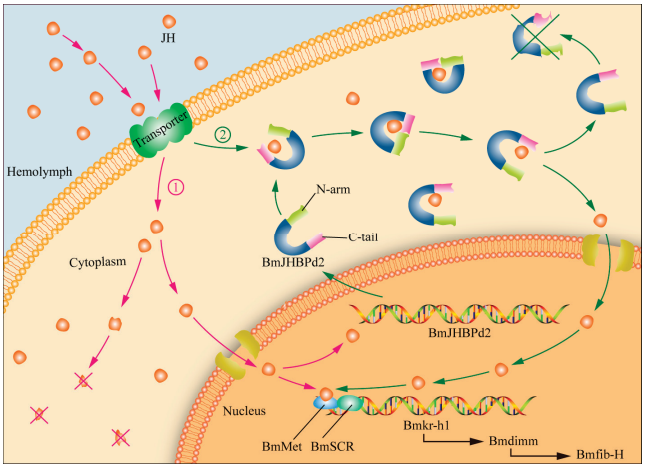

Figure 8. Function prediction model of BmJHBPd2 in the PSG. JH is transported into PSG cells from the hemolymph and functions in two ways. ①: Free JH binds to the nuclear receptor *BmMet* and forms a complex with *BmSRC*. ×: Free JH degradation in cytoplasm. ②: Cytoplasmic BmJHBPd2 can bind to redundant JH and slowly release it to maintain the JH level. And then, JH enters the nucleus and binds to the nuclear receptor *BmMet* and forms a complex with *BmSRC*.

4. Materials and Methods

4.1. Silkworm Strains and Cell Culture

Bombyx mori, the low-silk-producing strain *Dazao*, and the high-silk-producing strain *872* (*S872*), were provided by the State Key Laboratory of Silkworm Genome Biology, Southwest University in Chongqing, China. Silkworm eggs were cultured at a standard temperature of 25 °C under 12 h light and 12 h dark cycle conditions. The larvae were reared with fresh mulberry leaves with 75% relative humidity. The *B. mori* cell line, BmE [43], originally derived from embryo cells and was maintained at 27 °C in Grace's medium supplemented with 10% FBS (HyClone, San Angelo, TX, USA).

4.2. RNA Preparation and Quantitative Real Time-PCR (qRT-PCR)

Total RNA was extracted from the cells and silk glands using TRIzol™ reagent (Invitrogen, Waltam, MA, USA). The GoScrip™ Reverse Transcription system (Promega Madison, WI, USA) was used for RT-PCR. The semiquantitative RT-PCR conditions were as follows: 95 °C for 10 s, followed by 25 cycles at 95 °C for 10 s, 55 °C for 15 s, 72 °C for 1 min, 72 °C for 7 min, and then maintained at 16 °C. Reverse transcription was performed using the PrimeScript™ RT reagent Kit with gDNA Eraser (Takara, Shiga, Japan). Quantitative PCR was performed using SYBR® Premix Ex Taq™ II (Takara) and qPCR reaction under the following conditions: 95 °C for 10 s, followed by 40 cycles of treatment at 95 °C for 5 s, and 60 °C for 31 s. The silkworm ribosomal protein L3 (*BmRpl3*) was used as the internal marker gene. Three independent replicates were performed for each experiment.

4.3. Subcellular Localization

Primers for amplifying the ORF of *BmJHBPd2* are listed in Table S2. Target fragments were obtained by gel purification and cloned into an pSLfa1180 (pSLfa1180-A4-EGFP-SV40) expression vector (maintained in our laboratory) between *BamH*I and *Not*I sites. Highly purified plasmid DNA was prepared using Qiagen Plasmid Midi kits (Qiagen, Dusseldorf, Germany). For the subcellular localization assay of silkworm BmJHBPd2, BmE cells were seeded onto coverslips in 24-well plates. After 12 h of culture, pSLfa1180-Basic, pSLfa1180-A4-EGFP, and pSLfa1180[A4-EGFP-BmJHBPd2-SV40] were separately transfected into BmE cells at 1 μg per well. Cells were transfected with expression plasmids using the X-tremeGENE HP DNA Transfection Reagent (Roche Applied Science, Penzberg, Germany). After transfection for 48 h, cells were fixed for 10 min at room temperature with 4% (*v*/*v*) formaldehyde in PBS. They were then blocked for 30 min in PBS containing 0.1% (*w*/*v*) BSA and 5% (*v*/*v*) goat serum. The samples were treated with a primary antibody (anti-FLAG monoclonal M2 mouse (Sigma-Aldrich, St. Louis, MO, USA)) for 1 h before being incubated with a secondary antibody (anti-mouse Alexa 488) for 30 min at room temperature. The samples were then mounted using a mounting medium containing 4,6-diamidino-2-phenylindole (DAPI) and photographed using a confocal microscope (FV1000; Olympus, Tokyo, Japan).

4.4. Western Blotting

Radio-immunoprecipitation assay (RIPA) lysis buffer (Beyotime, Shanghai, China) was used to extract proteins from the cells and the PSG. The lysate was divided evenly and then centrifuged for 5 min at 12,000× *g*. Protease inhibitors were then added to the supernatants. Protein concentrations were measured using a bicinchoninic acid (BCA) protein assay kit (Beyotime, Shanghai, China). The proteins were separated using 10% sodium dodecyl sulfate-polyacrylamide gel electrophoresis (SDS-PAGE) and transferred onto a polyvinylidene difluoride (PVDF) membrane (Roche, Basel, Switzerland). The PVDF membrane was blocked using 5% skimmed milk overnight at 4 °C and incubated with a primary antibody against BmJHBPd2 (1:10,000) for 2 h at 37 °C. After washing the PVDF membrane six times at 5 min intervals, the membranes were incubated with the secondary antibody goat anti-rabbit IgG (1: 20,000), labeled with horseradish peroxidase (HRP) (Sigma-Aldrich, St. Louis, MO, USA), and visualized with SuperSignal™ West Femto Maximum Sensitivity Substrate (Thermo Fisher Scientific, Waltham, USA) using the automatic exposing pattern of Genome XRQ (Gene Company, Hong Kong, China).

4.5. Statistical Method for Cocoon Layer Proportion

The whole cocoon was weighed and then gently peeled; following this, the pupa was removed, the epidermis was shed, and the remaining cocoon was then weighed again. The ratio of this weight to the whole cocoon weight was determined as the cocoon layer ratio, which was measured in each of 15 individuals of transgenic and wild-type silkworms of *Dazao*.

4.6. Plasmid Construction to Obtain Transgenic Silkworms

To construct the transgenic overexpression lines, we used the *pBac [3xp3-EGFP]* system. JHBPd2 was driven by the PSG-specific Fib-L promoter to obtain the *pBac [3xp3-EGFP-Fib-L-BmJHBPd2-myc]* (Figure 4A). The target gene, *BmJHBPd2*, was amplified by PCR using cDNA from the silk gland tissue of the *Dazao* cultivar, using that of the third day of the fifth instar as the template. The 5′ end of *BmJHBPd2*-F was selected to add the *BamH* I (Takara, Tokyo, Japan) restriction endonuclease site. The 5′ end of *BmJHBPd2*-R was selected to add the *Not*I (Takara) restriction endonuclease site and Myc foreign label sequence for amplification. Full-length PCR products were digested with *BamH*I and *Not*I and connected to the 1180 vector skeleton with the Fib-L promoter to construct the *psl1180 [FibL-BmJHBPd2-myc]* expression vector. The *Asc*I (Takara) enzyme was used to digest the *psl1180 [FibL-BmJHBPd2-myc]* carrier and *pBac [3xp3-EGFP]* vector. Solution I (Takara) was used to construct an overexpression vector. The primers used to construct the plasmids are listed in Table S1 of the Supplementary Materials.

4.7. Silkworm Germline Transformation

For silkworm germline transformation, the ultrapure plasmid of *BmJHBPd2* overexpression transgenic vector and helper plasmid were mixed at a 1:1 volume ratio, and the final concentration for embryo injection was 300–500 ng/μL. After being sealed, they were moved into an artificial culture room and incubated at 25 °C for 10–12 days until the larvae hatched. After hatching by injecting the silkworm eggs, the G0 generation could not be screened for transgenic individuals [44]. Males and females were randomly mated and laid eggs for the G1 generation. The eggs of the G1 generation eggs were fluorescently screened at around the sixth day of development. Egg circles with eyes emitting green fluorescence were screened as positive individual egg circles and raised to produce the next generation. Homozygous third-generation transgenic silkworms were used for molecular-level detection in subsequent experiments.

4.8. Statistical Analysis

All the data were statistically analyzed using Student's *t*-tests. Asterisks indicate significant differences (* $p < 0.05$, ** $p < 0.01$, and *** $p < 0.001$). ns is not statistically different.

4.9. JHA Treatment

BmE cells were seeded onto coverslips in 24-well plates. After 12 h of culture, pSLfa1180-Basic and pSLfa1180-BmJHBPd2 were separately transfected into BmE cells at 1 μg per well. After transfection for 8 h, the medium was changed. JHA was melted in DMSO [30]. We then added 1 ng JHA (Sigma-Aldrich, Methoprene, 40596-69-8) to each well, and the cell RNA was extracted after hormone treatment for 12 h.

Supplementary Materials: The following supporting information can be downloaded at: https://www.mdpi.com/article/10.3390/ijms241612650/s1.

Author Contributions: Conceptualization, C.L.; methodology, X.Z., H.Z. and W.L.; validation, W.L., J.Z. and J.L.; formal analysis, J.Z.; visualization, J.Z.; writing—original draft preparation, J.Z., X.Z. and C.L.; writing—review and editing, J.Z. and C.L.; supervision, C.L.; project administration, C.L.; funding acquisition, C.L. All authors have read and agreed to the published version of the manuscript.

Funding: This research was funded by the National Natural Science Foundation of China (31972618), the Talent Plan Project of Chongqing (cstc2021ycjh-bgzxm0048), and the project of graduate innovation of Chongqing (CYB22159).

Institutional Review Board Statement: Not applicable.

Informed Consent Statement: Not applicable.

Data Availability Statement: The data presented in this study are available on request from the corresponding author.

Conflicts of Interest: The authors declare no conflict of interest.

References

1. Truman, J.W.; Riddiford, L.M. The origins of insect metamorphosis. *Nature* **1999**, *401*, 447–452. [CrossRef] [PubMed]
2. Shin, S.W.; Zou, Z.; Saha, T.T.; Raikhel, A.S. bHLH-PAS heterodimer of methoprene-tolerant and Cycle mediates circadian expression of juvenile hormone-induced mosquito genes. *Proc. Natl. Acad. Sci. USA* **2012**, *109*, 16576–16581. [CrossRef] [PubMed]
3. Wiśniewski, J.R.; Muszyńska-Pytel, M.; Grzelak, K.; Kochman, M. Biosynthesis and degradation of juvenile hormone in corpora allata and imaginal wing discs of *Galleria mellonella* (L.). *Insect Biochem.* **1987**, *17*, 249–254. [CrossRef]
4. Sok, A.J.; Andruszewska, G.; Niewiadomska-Cimicka, A.; Grad, I.; Rymarczyk, G.; Pajdzik, D.; Orłowski, M.; Schmidt, M.T.; Grajek, W.; Ozyhar, A.; et al. Regulatory elements in the juvenile hormone binding protein gene from Galleria mellonella–topography of binding sites for Usp and EcRDBD. *Biochim. Biophys. Acta* **2008**, *1779*, 390–401. [CrossRef] [PubMed]
5. Gilbert, L.I.; Granger, N.A.; Roe, R.M. The juvenile hormones: Historical facts and speculations on future research directions. *Insect Biochem. Mol. Biol.* **2000**, *30*, 617–644. [CrossRef]
6. Hammock, B.; Nowock, J.; Goodman, W.; Stamoudis, V.; Gilbert, L.I. The influence of hemolymph-binding protein on juvenile hormone stability and distribution in Manduca sexta fat body and imaginal discs in vitro. *Mol. Cell. Endocrinol.* **1975**, *3*, 167–184. [CrossRef] [PubMed]
7. Sanburg, L.L.; Kramer, K.J.; Kezdy, F.J.; Law, J.H.; Oberlander, H. Role of juvenile hormone esterases and carrier proteins in insect development. *Nature* **1975**, *253*, 266–267. [CrossRef]
8. Tauchman, S.J.; Lorch, J.M.; Orth, A.P.; Goodman, W.G. Effects of stress on the hemolymph juvenile hormone binding protein titers of Manduca sexta. *Insect Biochem. Mol. Biol.* **2007**, *37*, 847–854. [CrossRef]
9. Chang, E.S.; Bruce, M.J.; Prestwich, G.D. Further characterization of the juvenile hormone binding protein from the cytosol of a Drosophila cell line: Use of a photoaffinity label. *Insect Biochem.* **1985**, *15*, 197–204. [CrossRef]
10. Shemshedini, L.; Lanoue, M.; Wilson, T.G. Evidence for a juvenile hormone receptor involved in protein synthesis in Drosophila melanogaster. *J. Biol. Chem.* **1990**, *265*, 1913–1918. [CrossRef]
11. Ritdachyeng, E.; Manaboon, M.; Tobe, S.S.; Singtripop, T. Molecular characterization and gene expression of juvenile hormone binding protein in the bamboo borer, Omphisa fuscidentalis. *J. Insect Physiol.* **2012**, *58*, 1493–1501. [CrossRef]
12. Rebijith, K.B.; Asokan, R.; Ranjitha, H.H.; Rajendra Prasad, B.S.; Krishna, V.; Krishna Kumar, N.K. Diet-Delivered dsRNAs for Juvenile Hormone-Binding Protein and Vacuolar ATPase-H Implied Their Potential in the Management of the Melon Aphid (Hemiptera: Aphididae). *Environ. Entomol.* **2016**, *45*, 268–275. [CrossRef]
13. Wei, D.; Li, H.M.; Tian, C.B.; Smagghe, G.; Jia, F.X.; Jiang, H.B.; Dou, W.; Wang, J.J. Proteome analysis of male accessory gland secretions in oriental fruit flies reveals juvenile hormone-binding protein, suggesting impact on female reproduction. *Sci. Rep.* **2015**, *5*, 16845. [CrossRef] [PubMed]
14. Saito, K.; Su, Z.H.; Emi, A.; Mita, K.; Takeda, M.; Fujiwara, Y. Cloning and expression analysis of takeout/JHBP family genes of silkworm, *Bombyx mori*. *Insect Mol. Biol.* **2006**, *15*, 245–251. [CrossRef]
15. Whitmore, E.; Gilbert, L.I. Haemolymph lipoprotein transport of juvenile hormone. *J. Insect Physiol.* **1972**, *18*, 1153–1167. [CrossRef]
16. Kramer, K.J.; Sanburg, L.L.; Kézdy, F.J.; Law, J.H. The Juvenile Hormone Binding Protein in the Hemolymph of Manduca sexta Johannson (Lepidoptera: Sphingidae). *Proc. Natl. Acad. Sci. USA* **1974**, *71*, 493–497. [CrossRef]
17. Lerro, K.A.; Prestwich, G.D. Cloning and sequencing of a cDNA for the hemolymph juvenile hormone binding protein of larval Manduca sexta. *J. Biol. Chem.* **1990**, *265*, 19800–19806. [CrossRef]
18. Wojtasek, H.; Prestwich, G.D. Key disulfide bonds in an insect hormone binding protein: cDNA cloning of a juvenile hormone binding protein of *Heliothis virescens* and ligand binding by native and mutant forms. *Biochemistry* **1995**, *34*, 5234–5241. [CrossRef] [PubMed]
19. Rodriguez Parkitna, J.M.; Ozyhar, A.; Wiśniewski, J.R.; Kochman, M. Cloning and sequence analysis of Galleria mellonella juvenile hormone binding protein—A search for ancestors and relatives. *Biol. Chem.* **2002**, *383*, 1343–1355. [CrossRef]
20. Vermunt, A.M.; Kamimura, M.; Hirai, M.; Kiuchi, M.; Shiotsuki, T. The juvenile hormone binding protein of silkworm haemolymph: Gene and functional analysis. *Insect Mol. Biol.* **2001**, *10*, 147–154. [CrossRef] [PubMed]
21. Li, W.; Cheng, T.; Hu, W.; Peng, Z.; Liu, C.; Xia, Q. Genome-wide identification and analysis of JHBP-domain family members in the silkworm *Bombyx mori*. *Mol. Genet. Genom. MGG* **2016**, *291*, 2159–2171. [CrossRef] [PubMed]
22. Xia, Q.; Li, S.; Feng, Q. Advances in silkworm studies accelerated by the genome sequencing of *Bombyx mori*. *Annu. Rev. Entomol.* **2014**, *59*, 513–536. [CrossRef] [PubMed]
23. Gamo, T.; Inokuchi, T.; Laufer, H. Polypeptides of fibroin and sericin secreted from the different sections of the silk gland in *Bombyx mori*. *Insect Biochem.* **1977**, *7*, 285–295. [CrossRef]
24. Inoue, S.; Tanaka, K.; Arisaka, F.; Kimura, S.; Ohtomo, K.; Mizuno, S. Silk fibroin of *Bombyx mori* is secreted, assembling a high molecular mass elementary unit consisting of H-chain, L-chain, and P25, with a 6:6:1 molar ratio. *J. Biol. Chem.* **2000**, *275*, 40517–40528. [CrossRef] [PubMed]
25. Akai, H.; Kiguchi, K.; Mori, K. Increased Accumulation of Silk Protein Accompanying JH-Induced Prolongation of Larval Life in *Bombyx mori* L.(Lepidoptera: Bombycidae). *Appl. Entomol. Zool.* **1971**, *6*, 218–220. [CrossRef]

26. Akai, H.; Kobayashi, M. Induction of Prolonged Larval Instar by the Juvenile Hormone in *Bombyx mori* L.: Lepidoptera: Bombycidae. *Appl. Entomol. Zool.* **1971**, *6*, 138–139. [CrossRef]
27. Kurata, S.; Koga, K.; Sakaguchi, B. Nucleolar size in parallel with ribosomal RNA synthesis at diapause termination in the eggs of *Bombyx mori*. *Chromosoma* **1978**, *68*, 313–317. [CrossRef]
28. Kurata, K. Effect of a juvenile hormon analogue given at various ages of 5th instar larvae on RNA synthesis in the posterior silk gland of the silkworm, *Bombyx mori*. *J. Insect Biotechnol. Sericol.* **2010**, *53*, 421–426. [CrossRef]
29. Kayukawa, T.; Murata, M.; Kobayashi, I.; Muramatsu, D.; Okada, C.; Uchino, K.; Sezutsu, H.; Kiuchi, M.; Tamura, T.; Hiruma, K.; et al. Hormonal regulation and developmental role of Krüppel homolog 1, a repressor of metamorphosis, in the silkworm *Bombyx mori*. *Dev. Biol.* **2014**, *388*, 48–56. [CrossRef]
30. Zhao, X.M.; Liu, C.; Jiang, L.J.; Li, Q.Y.; Zhou, M.T.; Cheng, T.C.; Mita, K.; Xia, Q.Y. A juvenile hormone transcription factor Bmdimm-fibroin H chain pathway is involved in the synthesis of silk protein in silkworm, *Bombyx mori*. *J. Biol. Chem.* **2015**, *290*, 972–986. [CrossRef]
31. Zhang, T.; Song, W.; Li, Z.; Qian, W.; Wei, L.; Yang, Y.; Wang, W.; Zhou, X.; Meng, M.; Peng, J.; et al. Krüppel homolog 1 represses insect ecdysone biosynthesis by directly inhibiting the transcription of steroidogenic enzymes. *Proc. Natl. Acad. Sci. USA* **2018**, *115*, 3960–3965. [CrossRef] [PubMed]
32. Ma, L.; Xu, H.; Zhu, J.; Ma, S.; Liu, Y.; Jiang, R.J.; Xia, Q.; Li, S. Ras1(CA) overexpression in the posterior silk gland improves silk yield. *Cell Res.* **2011**, *21*, 934–943. [CrossRef]
33. Furuta, K.; Ichikawa, A.; Murata, M.; Kuwano, E.; Shinoda, T.; Shiotsuki, T. Determination by LC-MS of juvenile hormone titers in hemolymph of the silkworm, *Bombyx mori*. *Biosci. Biotechnol. Biochem.* **2013**, *77*, 988–991. [CrossRef]
34. Kayukawa, T.; Nagamine, K.; Ito, Y.; Nishita, Y.; Ishikawa, Y.; Shinoda, T. Krüppel Homolog 1 Inhibits Insect Metamorphosis via Direct Transcriptional Repression of Broad-Complex, a Pupal Specifier Gene. *J. Biol. Chem.* **2016**, *291*, 1751–1762. [CrossRef] [PubMed]
35. Kayukawa, T.; Jouraku, A.; Ito, Y.; Shinoda, T. Molecular mechanism underlying juvenile hormone-mediated repression of precocious larval-adult metamorphosis. *Proc. Natl. Acad. Sci. USA* **2017**, *114*, 1057–1062. [CrossRef]
36. Li, K.; Tian, L.; Guo, Z.; Guo, S.; Zhang, J.; Gu, S.H.; Palli, S.R.; Cao, Y.; Li, S. 20-Hydroxyecdysone (20E) Primary Response Gene E75 Isoforms Mediate Steroidogenesis Autoregulation and Regulate Developmental Timing in Bombyx. *J. Biol. Chem.* **2016**, *291*, 18163–18175. [CrossRef] [PubMed]
37. Liu, X.; Dai, F.; Guo, E.; Li, K.; Ma, L.; Tian, L.; Cao, Y.; Zhang, G.; Palli, S.R.; Li, S. 20-Hydroxyecdysone (20E) Primary Response Gene E93 Modulates 20E Signaling to Promote Bombyx Larval-Pupal Metamorphosis. *J. Biol. Chem.* **2015**, *290*, 27370–27383. [CrossRef]
38. Cong, J.; Tao, C.; Zhang, X.; Zhang, H.; Cheng, T.; Liu, C. Transgenic Ectopic Overexpression of Broad Complex (BrC-Z2) in the Silk Gland Inhibits the Expression of Silk Fibroin Genes of *Bombyx mori*. *Insects* **2020**, *11*, 374. [CrossRef]
39. Li, J.Y.; Yang, H.J.; Lan, T.Y.; Wei, H.; Zhang, H.R.; Chen, M.; Fan, W.; Ma, Y.Y.; Zhong, B.X. Expression profiling and regulation of genes related to silkworm posterior silk gland development and fibroin synthesis. *J. Proteome Res.* **2011**, *10*, 3551–3564. [CrossRef] [PubMed]
40. Zeng, B.; Huang, Y.; Xu, J.; Shiotsuki, T.; Bai, H.; Palli, S.R.; Huang, Y.; Tan, A. The FOXO transcription factor controls insect growth and development by regulating juvenile hormone degradation in the silkworm, *Bombyx mori*. *J. Biol. Chem.* **2017**, *292*, 11659–11669. [CrossRef]
41. Zhang, Z.; Liu, X.; Shiotsuki, T.; Wang, Z.; Xu, X.; Huang, Y.; Li, M.; Li, K.; Tan, A. Depletion of juvenile hormone esterase extends larval growth in *Bombyx mori*. *Insect Biochem. Mol. Biol.* **2017**, *81*, 72–79. [CrossRef] [PubMed]
42. Kayukawa, T.; Minakuchi, C.; Namiki, T.; Togawa, T.; Yoshiyama, M.; Kamimura, M.; Mita, K.; Imanishi, S.; Kiuchi, M.; Ishikawa, Y. Transcriptional regulation of juvenile hormone-mediated induction of Krüppel homolog 1, a repressor of insect metamorphosis. *Proc. Natl. Acad. Sci. USA* **2012**, *109*, 11729–11734. [CrossRef] [PubMed]
43. Pan, M.H.; Xiao, S.Q.; Chen, M.; Hong, X.J.; Lu, C. Establishment and characterization of two embryonic cell lines of *Bombyx mori*. *In Vitro Cell. Dev. Biol. Anim.* **2007**, *43*, 101–104. [CrossRef]
44. Tamura, T.; Thibert, C.; Royer, C.; Kanda, T.; Abraham, E.; Kamba, M.; Komoto, N.; Thomas, J.L.; Mauchamp, B.; Chavancy, G.; et al. Germline transformation of the silkworm *Bombyx mori* L. using a piggyBac transposon-derived vector. *Nat. Biotechnol.* **2000**, *18*, 81–84. [CrossRef] [PubMed]

International Journal of
Molecular Sciences

MDPI

Article

Pharmacological Inhibition and Genetic Deletion of Cystathionine Gamma-Lyase in Mice Protects against Organ Injury in Sepsis: A Key Role of Adhesion Molecules on Endothelial Cells

Sumeet Manandhar [1], Stephen Chambers [1], Andrew Miller [1], Isao Ishii [2] and Madhav Bhatia [1,*]

[1] Department of Pathology and Biomedical Science, University of Otago, Christchurch 8140, New Zealand; sumeet.manandhar@postgrad.otago.ac.nz (S.M.); steve.chambers@otago.ac.nz (S.C.); andrew.miller@otago.ac.nz (A.M.)
[2] Department of Health Chemistry, Showa Pharmaceutical University, Machida, Tokyo 194-8543, Japan; i-ishii@ac.shoyaku.ac.jp
* Correspondence: madhav.bhatia@otago.ac.nz; Tel.: +64-3-378-6238

Abstract: Hydrogen sulfide (H_2S), synthesized by cystathionine gamma-lyase (Cth), contributes to the inflammatory response observed in sepsis. This study examines the effect of Cth-derived H_2S in adhesion molecules on endothelial cells of vital organs in mice in a cecal ligation puncture (CLP)-induced model of sepsis, using two different and complementary approaches: Cth gene deletion and pharmacological inhibition. Our findings revealed a decreased level of H_2S-synthesizing activity (via Cth) in both $Cth^{-/-}$ mice and PAG-treated wild-type (WT) mice following CLP-induced sepsis. Both treatment groups had reduced MPO activity and expression of chemokines (MCP-1 and MIP-2α), adhesion molecules (ICAM-1 and VCAM-1), ERK1/2 phosphorylation, and NF-κB in the liver and lung compared with in CLP-WT mice. Additionally, we found that PAG treatment in $Cth^{-/-}$ mice had no additional effect on the expression of ERK1/2 phosphorylation, NF-κB, or the production of chemokines and adhesion molecules in the liver and lung compared to $Cth^{-/-}$ mice following CLP-induced sepsis. The WT group with sepsis had an increased immunoreactivity of adhesion molecules on endothelial cells in the liver and lung than the WT sham-operated control. The $Cth^{-/-}$, PAG-treated WT, and $Cth^{-/-}$ groups of mice showed decreased immunoreactivity of adhesion molecules on endothelial cells in the liver and lung following sepsis. Inhibition of H_2S production via both approaches reduced adhesion molecule expression on endothelial cells and reduced liver and lung injury in mice with sepsis. In conclusion, this study demonstrates that H_2S has an important role in the pathogenesis of sepsis and validates PAG use as a suited tool for investigating the Cth/H_2S-signalling axis in sepsis.

Keywords: hydrogen sulfide; cystathionine gamma-lyase; sepsis; adhesion molecules; endothelial cells

Citation: Manandhar, S.; Chambers, S.; Miller, A.; Ishii, I.; Bhatia, M. Pharmacological Inhibition and Genetic Deletion of Cystathionine Gamma-Lyase in Mice Protects against Organ Injury in Sepsis: A Key Role of Adhesion Molecules on Endothelial Cells. *Int. J. Mol. Sci.* **2023**, *24*, 13650. https://doi.org/10.3390/ijms241713650

Academic Editor: Maurizio Battino

Received: 13 July 2023
Revised: 29 August 2023
Accepted: 30 August 2023
Published: 4 September 2023

1. Introduction

Sepsis is a major public health problem with an overall mortality rate of 25–30% globally [1]. The most common cause is bacterial infection [2], which may trigger a systemic inflammatory response and multiple organ failure [3]. Severe liver injury and lung injury may be associated with sepsis. The underlying mechanisms of injury are not well understood but recent studies have shown H_2S is an important gaseous mediator of inflammation [4–7].

H_2S is synthesized through the metabolism of L-cysteine, in coordination with PLP (pyridoxal 5′-phosphate), via three enzymes: cystathionine γ-lyase (Cth), cystathionine β-synthase (CBS), and 3-mercaptopyruvate sulfurtransferase (MPST) [8]. Cth is predominantly responsible for H_2S synthesis in the liver, whereas CBS mainly regulates H_2S synthe-

sis in the brain and kidneys [9]. H_2S synthesized via Cth plays an essential role in physiological as well as in pathological processes [10]. It has been demonstrated that H_2S acts as a pro-inflammatory mediator during various acute inflammatory conditions [7,11,12], including cecal ligation and puncture (CLP)-induced sepsis [13–15] in mice as well as in patients with sepsis [16,17]. CLP-induced sepsis increased Cth expression/H_2S synthesis in these studies, promoting the inflammatory response by elevating pro-inflammatory cytokines, chemokines, and adhesion molecules [11–13]. These pro-inflammatory mediators were increased via the activation of NF-κB under the influence of Cth expression/H_2S synthesis during the inflammatory episode [18]. In addition, Cth expression/H_2S synthesis have been shown to regulate inflammation via the activation of extracellular signal-regulated kinase (ERK) [19], which is the primary upstream activator of NF-κB [18].

Recruitment of leukocytes is a key feature of inflammation. This involves a series of events that results in the recruitment of leukocytes to the site of inflammation via leukocyte–endothelial cell interactions [20]. This series of events is initiated by rolling and then adherence of leukocytes to the endothelial cells via the interaction between the adhesion molecules and their respective ligands. This, in turn, results in the infiltration of leukocytes to the site of injury [21,22]. Increased concentrations of H_2S have been reported to significantly increase pulmonary and hepatic concentrations of chemokines and adhesion molecules during sepsis [18,23].

Liver sinusoidal endothelial cells (LSECs) are the most abundant non-parenchymal cells in the liver, with unique functions, especially in leukocyte recruitment via various adhesion molecules expressed on their surface [24,25]. LYVE-1 (lymphatic vessel endothelial hyaluronan receptor-1) has been used as a potential maker for liver sinusoidal endothelial cells. Adhesion molecules such as intercellular adhesion molecule 1 (ICAM-1) and vascular cell adhesion molecule 1 (VCAM-1) [22,26] are highly expressed on inflamed LSECs [27]. We have found, in previous studies, that sepsis is associated with the disruption of the LSECs and the formation of gaps [4,28,29], which are large defects through the LSECs. Cth gene deletion protects mice against disruption of the LSECs caused by sepsis, suggesting disruption of LSECs' structure is an important consequence of H_2S-induced inflammation in sepsis [4]. In parallel, acute lung injury (ALI), and its more severe form ARDS (acute respiratory distress syndrome), are manifestations of lung injury that occur during sepsis [30]. Pulmonary endothelial cells have been identified as key modulators and orchestrators of ALI via leukocyte infiltration [31]. Expression of ICAM-1 and VCAM-1 are reported to be increased in the pulmonary endothelial cells during ARDS, which can be associated with septic shock and multiple organ failure [32]. Many studies have employed CD-31 (PECAM-1) as a potential marker for pulmonary endothelial cells. Inhibition of Cth expression/H_2S synthesis has been shown to protect against lung injury induced by sepsis [4,14,15,18,19]. To date, various methods have been used to understand the role of H_2S in inflammation related to sepsis, such as pharmacological tools [14,15,18,19], siRNA, and knockout mouse models [4]. These tools have opened up a new horizon for gaining deeper insights into the role of H_2S in inflammation. The most commonly used pharmacological tool is DL-propargylglycine (PAG). It is a specific inhibitor of Cth with no role in the inhibition of CBS. However, some studies have reported that PAG acts by inhibiting other PLP-dependent enzymes as well [33], leading to questions about its specificity.

Interestingly, a recent study with Cth deletion mice showed similar results to previous studies using PAG [14,15,18,19], indicating that the actions of PAG were indeed a result of Cth inhibition. The current study, therefore, uses two complementary and independent approaches to investigate the role of H_2S during sepsis. Moreover, so far, no study has explored the role of the Cth/H_2S signaling pathway on adhesion molecules expressed by the endothelial cells of vital organs during sepsis. Although previous studies have pointed to a key role of LSECs in the pro-inflammatory actions of H_2S, the mechanism by which they contribute to inflammation in sepsis remains unknown.

In this study, therefore, we aimed to investigate whether H_2S, synthesized via Cth, plays a role in the alteration of adhesion molecule expression on endothelial cells of the vital organs in CLP-induced septic mice. To achieve this, we utilized $Cth^{-/-}$ mice and PAG-treated wild-type $Cth^{-/-}$ mice, and examined the impact of different approaches to Cth inhibition on liver and lung pro-inflammatory mediators, injury, and adhesion molecule alteration in the endothelial cells in a mouse model of sepsis. This parallel use of two complementary and independent means of H_2S inhibition will help us to gain strong evidence of the role of endogenously synthesized H_2S in inflammation.

2. Results

2.1. Cth Expression and H_2S-Synthesizing Enzyme Activity

The expression of Cth protein in both the liver and lung was significantly higher in WT CLP-induced septic mice than in sham control mice (Figure 1A–D). However, treatment with the Cth pharmacological inhibitor PAG did not affect the expression of Cth protein in WT CLP-induced septic mice.

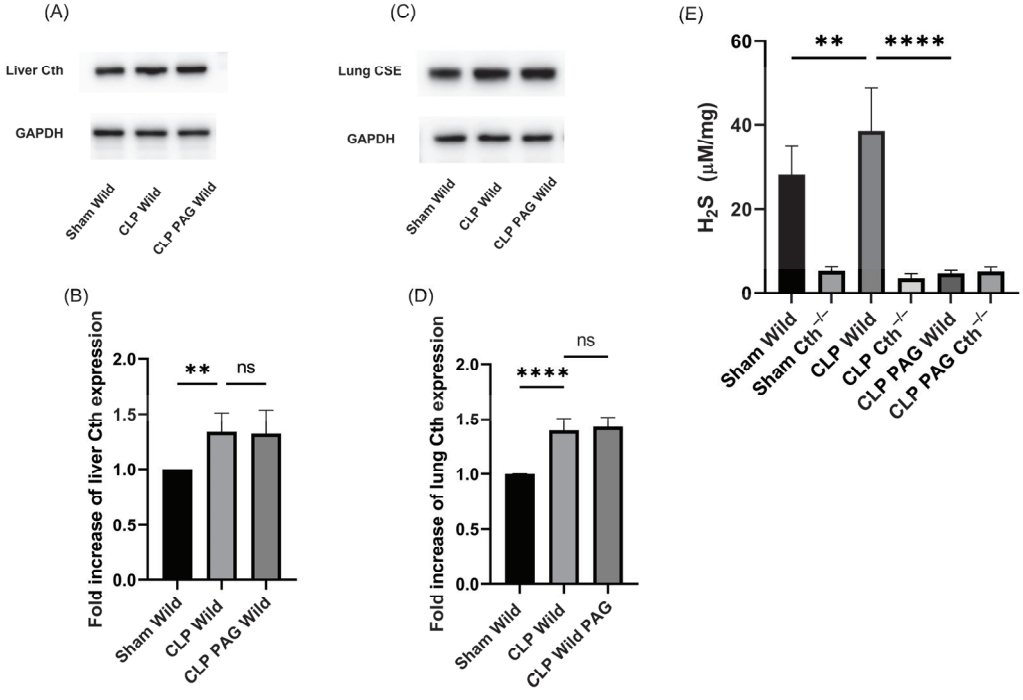

Figure 1. Cth expression in the liver (**A**,**B**) and lung (**C**,**D**) and liver H_2S production (**E**) after 8 h of CLP-induced sepsis. The expression of Cth protein in both liver and lungs was induced by CLP-induced sepsis. Cth band density was normalized to GAPDH band density. Results are expressed in relative fold increase. Representative Western blot images (**A**,**C**) were obtained from at least four independent experiments. (**E**) Liver H_2S-synthesizing activity measured over 30 min. In WT CLP-induced sepsis mice, H_2S-synthesizing activity was higher than in sham controls, whereas significantly lower concentrations were observed in $Cth^{-/-}$ mice. CLP-induced sepsis in WT and $Cth^{-/-}$ treated with demonstrated similar concentrations of H_2S-synthesizing activity to sham $Cth^{-/-}$. All data are represented as mean ± standard derivation (SD) (n = 8). One-way ANOVA with post hoc Tukey test was employed. Statistical significance was determined at ** $p < 0.01$; **** $p < 0.0001$; ns, not significant.

The liver H_2S-synthesizing enzyme activity in WT mice was significantly higher following CLP-induced sepsis than in the sham-operated control. It was significantly lower in $Cth^{-/-}$ mice than WT CLP-induced sepsis, and CLP-induced sepsis did not increase H_2S-synthesizing enzyme activity in $Cth^{-/-}$ mice compared with sham $Cth^{-/-}$. In addition, the treatment of PAG in both WT and $Cth^{-/-}$ mice showed similar H_2S-synthesizing activity in the liver. We could not detect any traces of H_2S-synthesizing activity in homogenized lung samples from any experimental group (Figure 1E).

2.2. Effect of PAG Treatment and $Cth^{-/-}$ on Myeloperoxidase (MPO) Activity and Sepsis-Associated Organ Injury

Liver and lung MPO activity were measured to assess neutrophil infiltration, and the increment in MPO activity over baseline was used as marker of neutrophil infiltration into these organs (Figure 2A,B). There was increased MPO activity in both the liver and lungs of mice with WT CLP-induced sepsis compared to sham control mice. PAG-treated WT and $Cth^{-/-}$ mice following CLP had significantly less MPO activity in both the liver and lung than mice with WT CLP-induced sepsis. Histological analysis of liver tissue sample from WT mice with sepsis showed more severe liver injury (ballooning degeneration) compared to sham WT, sham $Cth^{-/-}$, CLP $Cth^{-/-}$, CLP PAG WT, and CLP PAG $Cth^{-/-}$ (Figure 2C). Less lobular necrosis was observed in samples from mice in the CLP $Cth^{-/-}$, CLP PAG WT, and CLP PAG $Cth^{-/-}$ groups, but not in the sham WT and sham $Cth^{-/-}$ groups compared to WT mice with sepsis. Similarly, lung sections stained with H&E showed more evidence of lung injury (fibrin deposition, leukocyte infiltration, and thickening of alveolar walls) in septic WT mice compared to septic mice with $Cth^{-/-}$, PAG-treated WT, and $Cth^{-/-}$. Normal lung histological structure was seen in WT sham-operated and $Cth^{-/-}$ mice (Figure 2D,E).

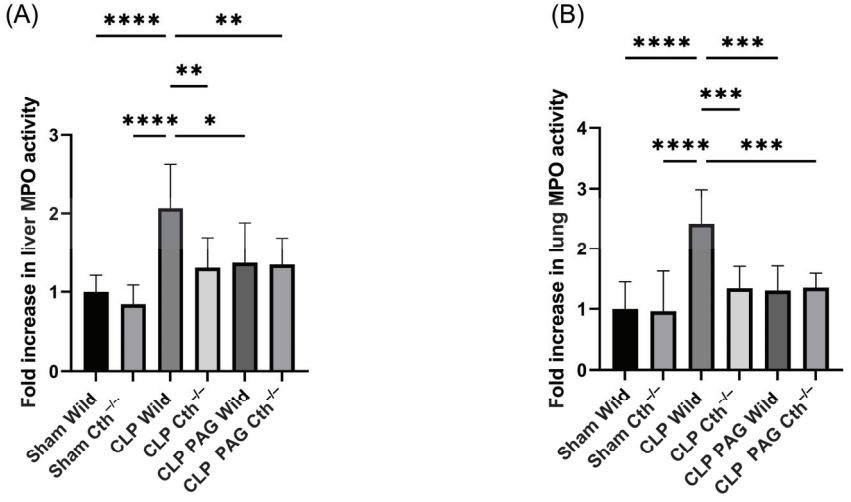

Figure 2. *Cont.*

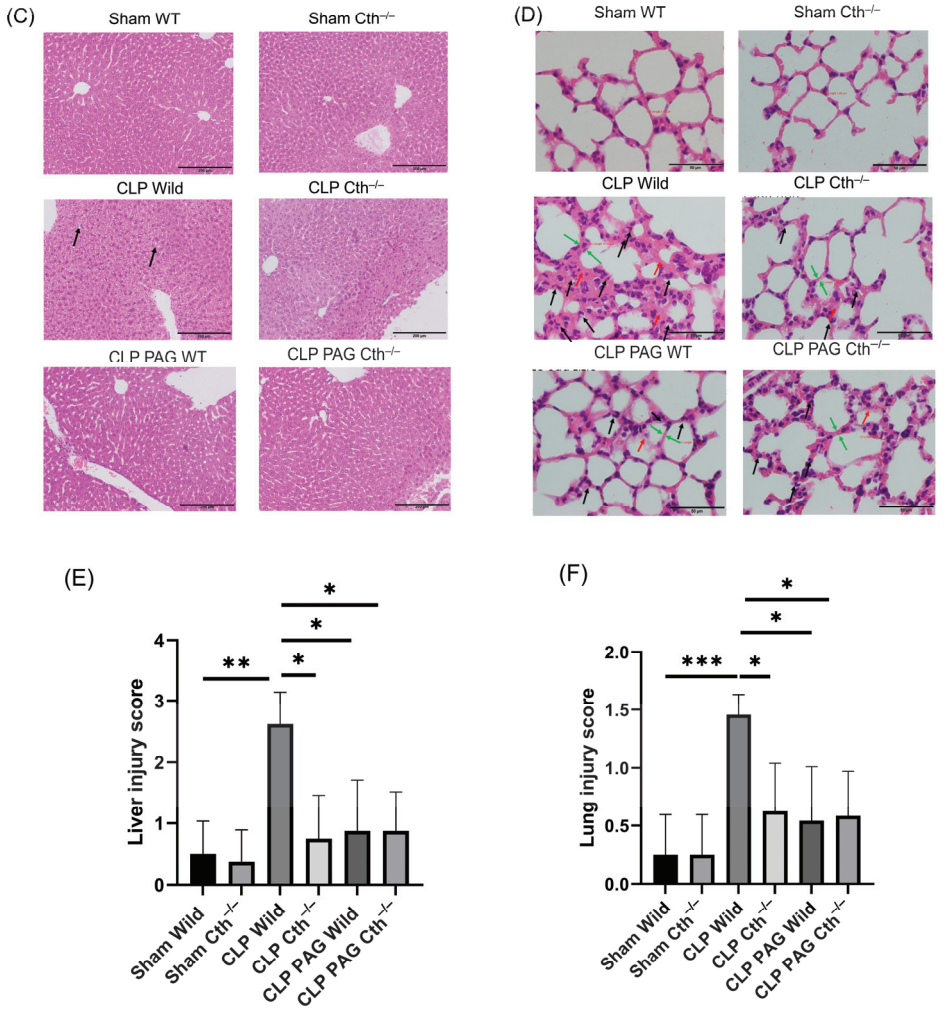

Figure 2. Impact of Cth inhibition or deletion on liver and lung injury after 8 hr of CLP-induced sepsis. MPO activity in the liver (**A**) and lung (**B**). Compared to sham operation controls, liver and lung MPO activity were higher in WT CLP-induced septic mice. CLP-induced sepsis in WT, $Cth^{-/-}$, PAG-treated WT, and PAG-treated $Cth^{-/-}$ significantly reduced MPO activity in the liver and lung. MPO activity was expressed as a relative fold increase over sham operations. (**C**) Representative histopathological images of the liver showed severe ballooning degeneration (liver injury) in WT CLP-induced sepsis mice (two large ballooned hepatocytes—black arrows) compared to sham control. CLP-induced $Cth^{-/-}$, PAG-treated WT, and PAG-treated $Cth^{-/-}$ mice revealed reduced level liver injury (less ballooning degeneration) (**E**); Scale bars = 200 µm. (**D**) Representative histopathological images of the lung. Histological analysis of lung sections showed prominent lung injury (fibrin deposition (red arrows), leukocyte (neutrophil) infiltration (black arrows), and alveolar thickening (green arrows)) (**F**) in WT mice following CLP-induced sepsis, compared to sham-operated controls. Notably, this effect was significantly diminished in $Cth^{-/-}$, PAG-treated WT, and PAG-treated $Cth^{-/-}$ mice following CLP-induced sepsis. Scale bars = 50 µm. One-way ANOVA with post hoc Tukey test was employed for liver and lung MPO activity, whereas non-parametric Kruskal–Wallis test was used to analyze liver and lung histology scores. All data are represented as mean ± SD ($n = 8$), and statistical significance was determined at * $p < 0.05$; ** $p < 0.01$; *** $p < 0.001$; and **** $p < 0.0001$.

2.3. Effect of PAG Treatment and Cth$^{-/-}$ on Liver and Lung ERK 1/2/NF-κB in Sepsis

ERK phosphorylation was higher in the liver and lung samples from WT mice with CLP-induced sepsis than WT sham-operated mice. As expected, phosphorylation was lower in samples from both the PAG-treated and Cth$^{-/-}$ with CLP-induced sepsis compared to the corresponding WT mice. No additional effect was observed with the treatment with PAG in Cth$^{-/-}$ mice followed by CLP-induced sepsis compared with either group alone (Figure 3A–D). Nuclear NF-κB DNA-binding activity in the lungs and liver was significantly increased in WT CLP-induced septic mice compared to WT sham-operated mice. Blockade of endogenous H_2S synthesis with PAG-treated or Cth$^{-/-}$ mice showed a marked inhibition of activation of NF-κB, and this was unaffected by PAG treatment in Cth$^{-/-}$ mice with sepsis (Figure 3E,F).

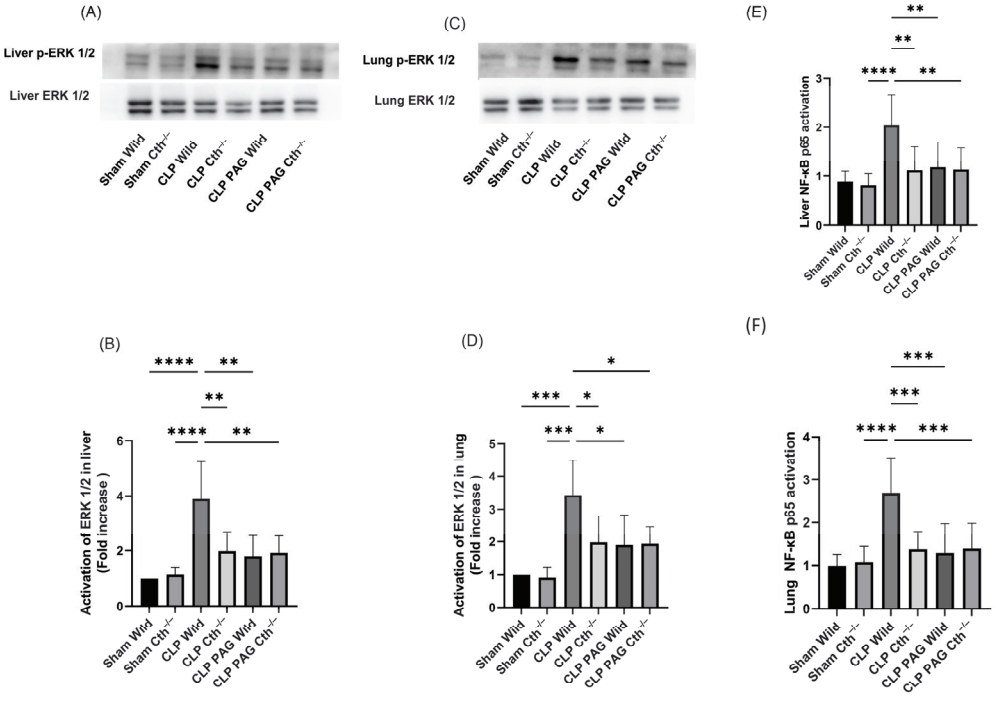

Figure 3. Impact of Cth inhibition or deletion on ERK1/2 and NF-κB activation after 8 h of CLP-induced sepsis. (**A**,**B**) p-ERK1/2 expression in the liver. WT CLP-induced septic mice showed increased phosphorylation of ERK1/2 as compared to the WT sham-operated mice. CLP-induced sepsis in Cth$^{-/-}$, PAG-treated WT, and PAG-treated Cth$^{-/-}$. ERK1/2 phosphorylation was significantly lower than WT CLP-induced sepsis. (**C**,**D**) p-ERK1/2 expression in the lung. WT CLP-induced septic mice showed increased phosphorylation of ERK1/2 compared to the WT sham-operated mice. CLP-induced sepsis in Cth$^{-/-}$, PAG-treated WT, and PAG-treated Cth$^{-/-}$. ERK1/2 phosphorylation was significantly lower than WT CLP-induced sepsis. p-ERK1/2 band density was normalized to ERK1/2 band density. Results are expressed in relative fold increase. Representative Western blot images were obtained from at least four independent experiments. (**E**,**F**) NF-κB p65 activation in the liver and lung. Activation of NF-κB p65 was higher in WT CLP-induced septic mice than WT sham-operated mice. CLP-induced sepsis in Cth$^{-/-}$, PAG-treated WT, and PAG-treated Cth$^{-/-}$ activation of NF-κB p65 was significantly lower than WT CLP-induced sepsis. The results are expressed as a relative fold increase. All data are represented as mean ± SD (n = 8). One-way ANOVA with post hoc Tukey test was employed. Statistical significance was determined at * $p < 0.05$; ** $p < 0.01$; *** $p < 0.001$; and **** $p < 0.0001$.

2.4. Effect of PAG Treatment and Cth$^{-/-}$ on Pro-Inflammatory Chemokines Synthesis on Liver and Lung Following Sepsis

The concentrations of pro-inflammatory chemokines (MCP-1 and MIP-2α) were significantly elevated in WT CLP mice as compared to WT sham mice (Figure 4A–D). PAG-treated and Cth$^{-/-}$ mice with CLP-induced sepsis demonstrated lower concentrations of pro-inflammatory chemokines in liver and lung homogenates than WT septic mice.

The concentrations of pro-inflammatory chemokines in liver and lung samples from PAG-treated Cth$^{-/-}$ mice were not significantly different from the Cth$^{-/-}$ group.

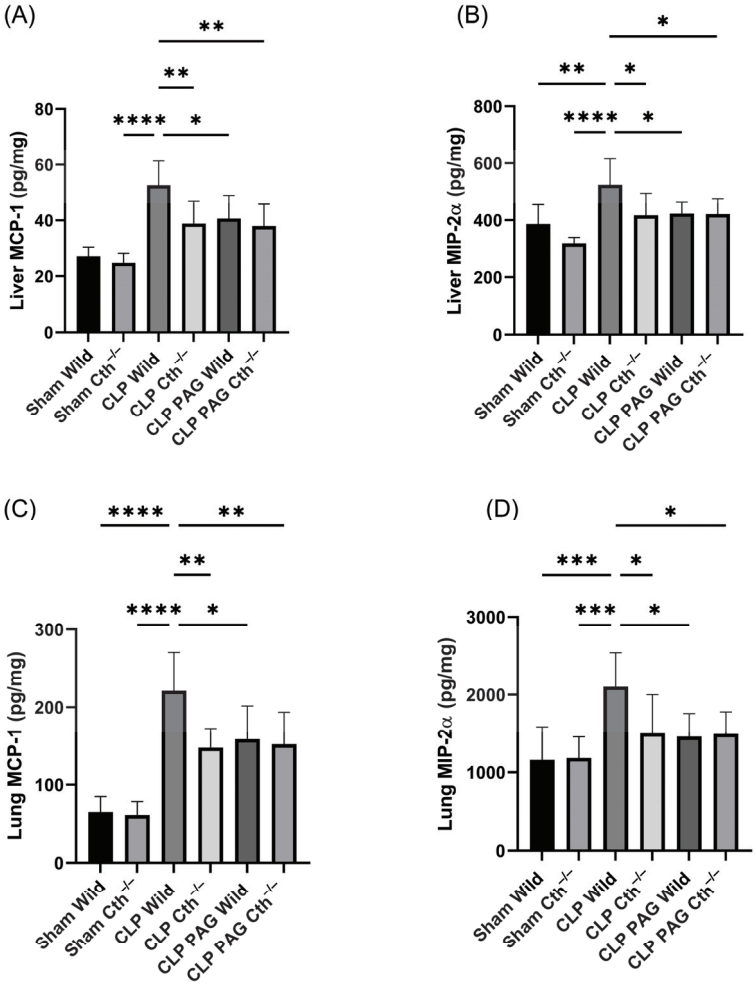

Figure 4. Impact of Cth inhibition or deletion on expression of liver MCP-1 (**A**) and MIP-2α (**B**) and lung MCP-1 (**C**) and MIP-2α (**D**) after 8 h of CLP-induced sepsis. CLP-induced sepsis in WT mice significantly elevated the pro-inflammatory chemokines MCP-1 and MIP-2α in the liver and lung more than in sham control. Cth$^{-/-}$, PAG-treated WT, and PAG-treated Cth$^{-/-}$ mice were demonstrated to reduce pro-inflammatory MCP-1 and MIP-2α expression in the liver and lung compared to WT CLP-induced septic mice. Results are expressed in pg/mg of protein. All data are represented as mean ± SD (n = 8). One-way ANOVA with post hoc Tukey test was employed. Statistical significance was determined at * $p < 0.05$; ** $p < 0.01$; *** $p < 0.001$; and **** $p < 0.0001$.

2.5. Effect of PAG Treatment and Cth$^{-/-}$ on Adhesion Molecule Synthesis in Liver and Lung Following Sepsis

The concentrations of pro-inflammatory adhesion molecules (ICAM-1 and VCAM-1) in liver and lung tissue were significantly elevated in WT CLP mice compared to WT sham-operated mice (Figure 5A–D). PAG-treated and Cth$^{-/-}$ mice with CLP-induced sepsis demonstrated lower protein concentrations of pro-inflammatory adhesion molecules in liver and lung homogenate than WT septic mice. The concentrations of pro-inflammatory adhesion molecules in liver and lung samples from PAG-treated Cth$^{-/-}$ mice were not significantly different from the Cth$^{-/-}$ group.

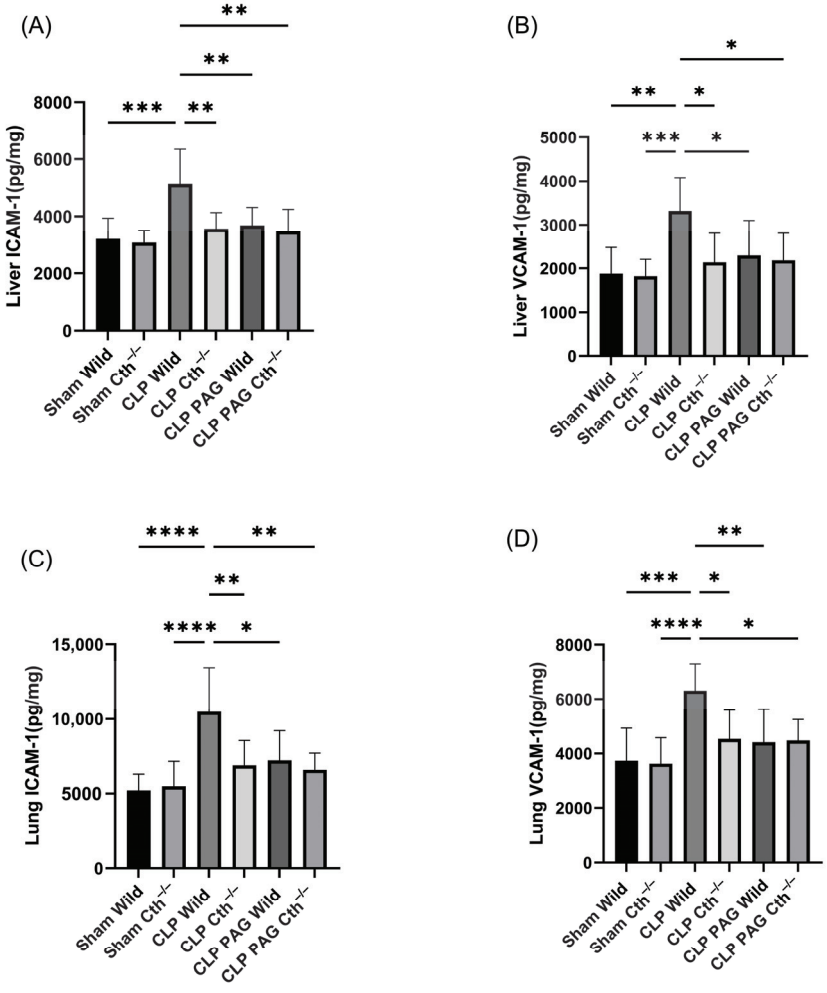

Figure 5. Impact of Cth inhibition or deletion on expression of liver ICAM-1 (**A**)/VCAM-1 (**B**) and lung ICAM-1 (**C**)/VCAM-1 (**D**) after 8 h of CLP-induced sepsis. WT CLP-induced septic mice significantly elevated pro-inflammatory adhesion molecules ICAM-1 and VCAM-1 in the liver and lung compared to sham operation controls. Cth$^{-/-}$, PAG-treated WT, and Cth$^{-/-}$ mice were shown to reduce pro-inflammatory ICAM-1 and VCAM-1 expression in the liver and lung compared to WT CLP-induced septic mice. Results are expressed in pg/mg of protein. All data are represented as mean ± SD (n = 8). One-way ANOVA with post hoc Tukey test was employed. Statistical significance was determined at * $p < 0.05$; ** $p < 0.01$; *** $p < 0.001$; and **** $p < 0.0001$.

2.6. Effect of PAG Treatment and Cth$^{-/-}$ on Immunoreactivity of Liver ICAM-1 and VCAM-1 Co-Localised with Liver Sinusoidal Endothelial Cells

To quantify the localized ICAM-1 and VCAM-1 immunoreactivity within the liver, co-localization was performed with LYVE-1 to identify liver sinusoidal endothelial cells. Immunofluorescence microscopy showed increased immunoreactivity of ICAM-1 (Figure 6A,C) and VCAM-1(Figure 6B,D) co-localized with LYVE-1 in WT CLP-induced septic mice compared with sham-operated control mice. Cth$^{-/-}$ and PAG treatment on WT and Cth$^{-/-}$ attenuated the expression of ICAM -1 and VCAM-1 co-localized with LYVE-1 compared to WT CLP mice.

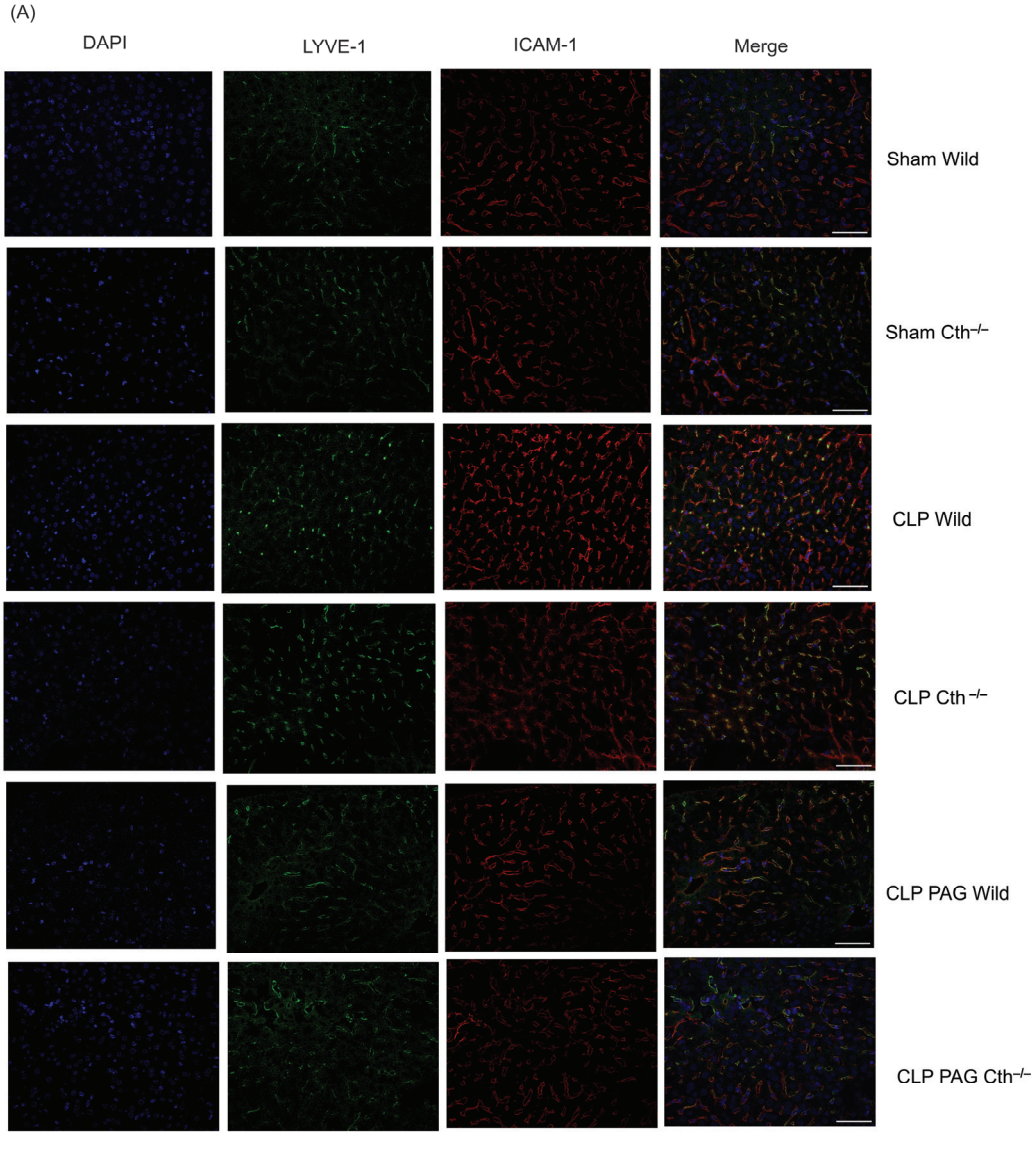

Figure 6. *Cont.*

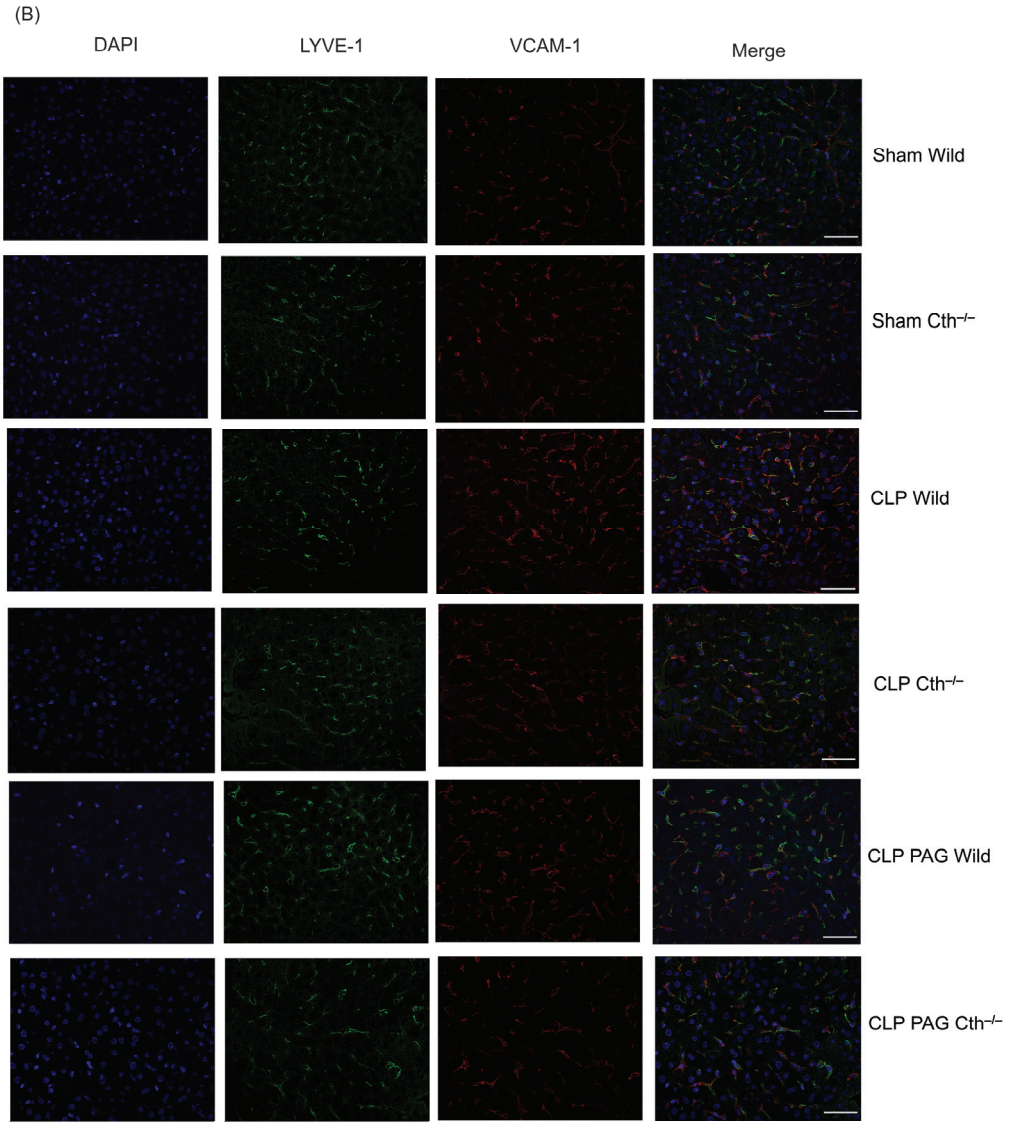

Figure 6. *Cont.*

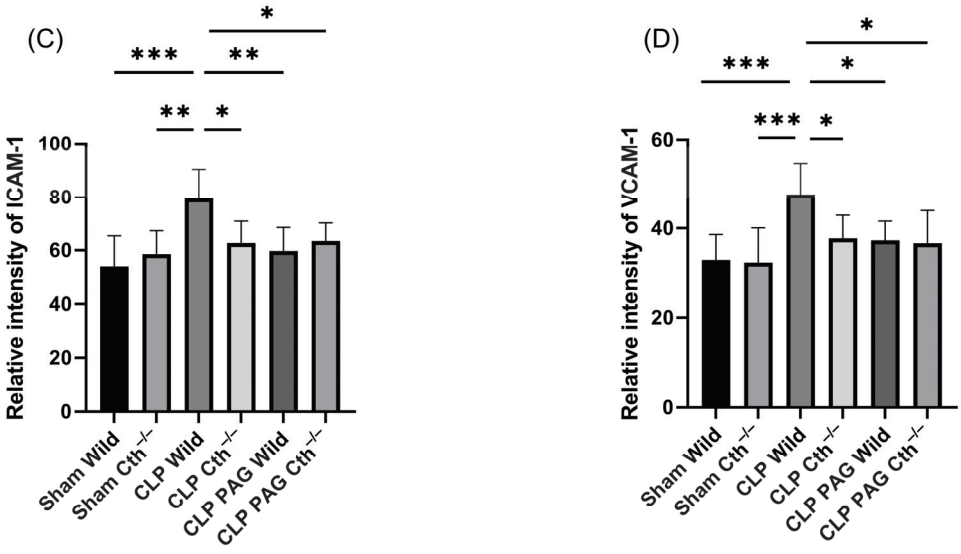

Figure 6. Representative images of ICAM-1 (**A**) and VCAM-1 (**B**) immunoreactivity (Cy3–red) co-localized with LYVE-1 (Alexa Fluor 488–green) after 8 h of CLP or sham operation. Scare bar: 50 μm. Semi-quantitative analysis of ICAM-1 (**C**) and VCAM-1 (**D**) immunoreactivity on LSEC were increased in CLP-induced WT mice compared to sham-operated control mice. $Cth^{-/-}$ and PAG treatment on the WT and $Cth^{-/-}$ group demonstrated decreased levels of ICAM-1 and VCAM-1 expression on LSECs compared to CLP-induced WT mice. All data are represented as mean ± SD (n = 8). One-way ANOVA with post hoc Tukey test was employed. Statistical significance was determined at * $p < 0.05$; ** $p < 0.01$; *** $p < 0.001$.

2.7. Effect of PAG Treatment and $Cth^{-/-}$ on Immunoreactivity of Lung ICAM-1 and VCAM-1 Co-Localised with Pulmonary Endothelial Cells

CD31 was used to identify the pulmonary endothelial cells, and the co-localized immunoreactivity of ICAM-1 and VCAM-1 with CD 31 was quantified. Immunofluorescence microscopy showed increased immunoreactivity of ICAM-1 (Figure 7A,C) and VCAM-1 (Figure 7B,D) co-localized with CD31 in WT CLP-induced septic mice than in sham-operated control mice. $Cth^{-/-}$ and PAG treatment on WT and $Cth^{-/-}$ attenuated the immunoreactivity of ICAM-1 and VCAM-1 co-localized with CD31 compared to WT CLP mice.

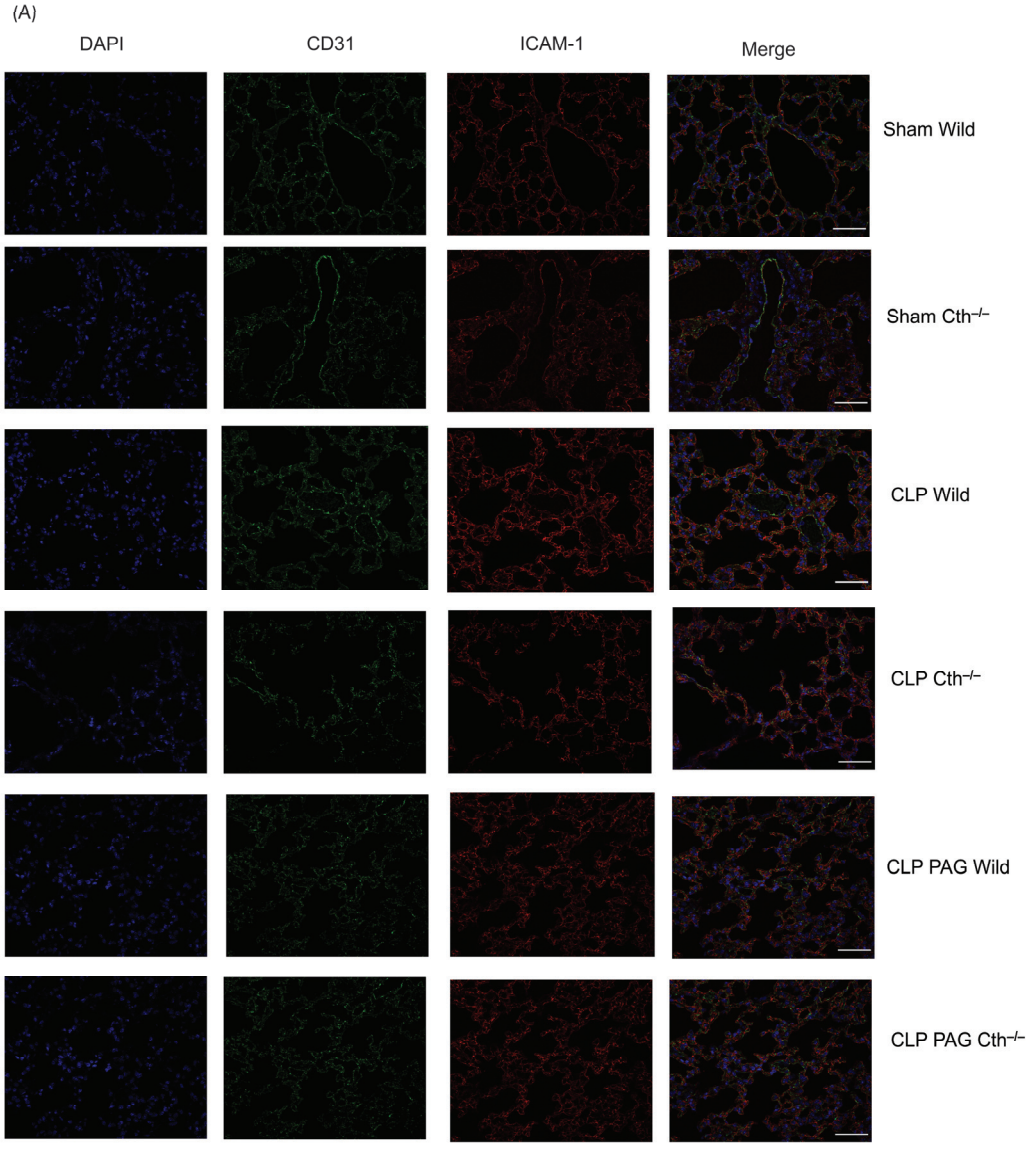

Figure 7. *Cont.*

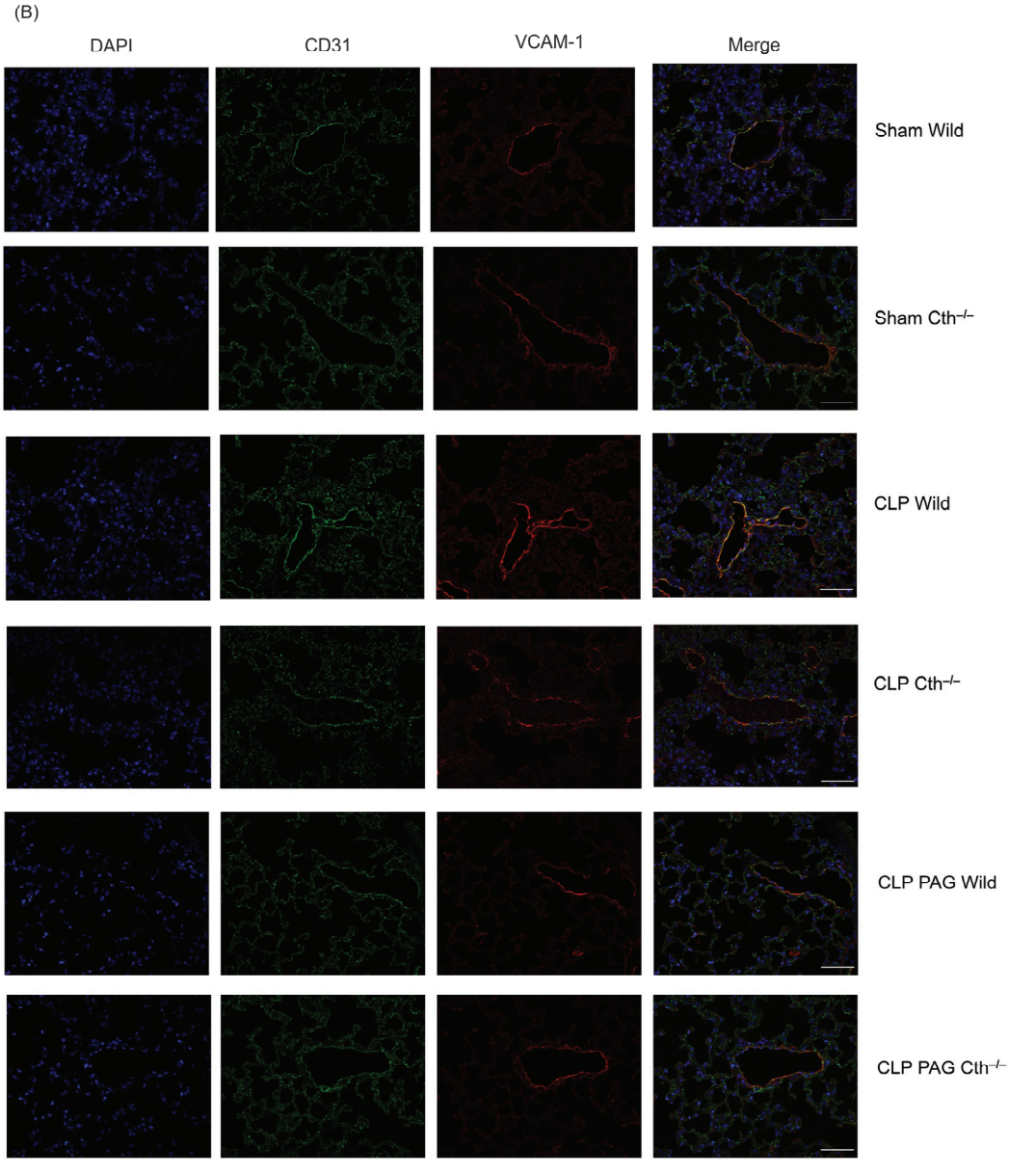

Figure 7. *Cont.*

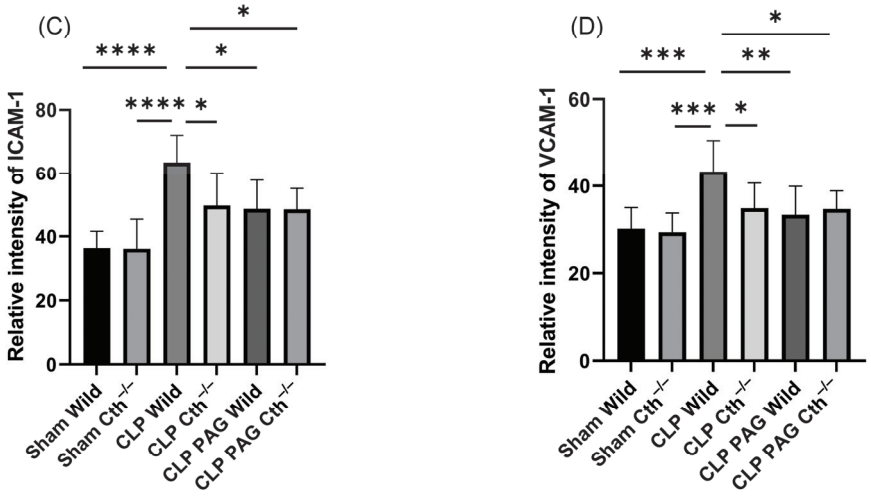

Figure 7. Representative images of ICAM-1 (**A**) and VCAM-1 (**B**) immunoreactivity (Cy3–red) co-localized with CD-31 (Alexa Fluor 488–green) after 8 h of CLP or sham operation. Scare bar: 50 µm. ICAM-1 (**C**) and VCAM-1 (**D**) immunoreactivity on pulmonary endothelial cells was significantly higher in WT CLP-induced septic mice than in WT sham-operated control mice. $Cth^{-/-}$ and PAG treatment on the WT and $Cth^{-/-}$ group showed lower levels of ICAM-1 and VCAM-1 immunoreactivity on pulmonary endothelial cells compared to CLP-induced WT mice. All data are represented as mean ± SD ($n = 8$). One-way ANOVA with post hoc Tukey test was employed. Statistical significance was determined at * $p < 0.05$; ** $p < 0.01$; *** $p < 0.001$; and **** $p < 0.0001$.

3. Discussion

Several studies have used different preclinical animal models to investigate the role of H_2S in sepsis. Both the CLP-induced sepsis and LPS-induced endotoxemia models resulted in increased synthesis of H_2S concentrations. PAG is the best-studied inhibitor of H_2S synthesis derived from Cth. Studies using PAG have pointed to Cth as a key enzyme responsible for elevating circulating and tissue H_2S, as well as tissue H_2S-synthesizing activity. This showed a systemic inflammatory response and multiple organ damage in sepsis, suggesting a pro-inflammatory role of H_2S in sepsis. In addition to Cth inhibition, PAG also inhibits other enzymes that use pyridoxal-5-phosphate as a co-factor [33]. Our recent study used $Cth^{-/-}$ mice to specifically target the Cth-H_2S pathway, and confirmed the key role of H_2S synthesized by Cth in sepsis [4]. The pleiotropic effect of other genes, however, could potentially compensate for the loss of Cth activity in the KO model, but this has not been shown previously. The present study therefore employs two complementary and independent means of H_2S inhibition in parallel to explore this over 8 h after CLP in a mouse model of polymicrobial sepsis. Furthermore, the effect of PAG treatment on $Cth^{-/-}$ mice will shed light on whether PAG primarily exerts its therapeutic action through Cth or if other mechanisms are also at play. We have selected an 8 h time point of CLP-induced sepsis in this study as there is a significant elevation of chemokines and cytokines at this time point, which has been shown to correlate with the severity of sepsis [19]. In addition, Cth activity in the liver is found to peak at 4–8 h after CLP. Post 8 h, there is a slow decline in the liver Cth activity and plasma H_2S concentration, leading to a restoration of levels similar to those observed in normal/sham-operated mice [19].

In this study, we found increased Cth expression and H_2S-synthesizing activity in the liver and lung following CLP-induced sepsis. This increase correlated with elevated MPO activity and histological alterations in the liver and lungs. Interestingly, $Cth^{-/-}$ and PAG-treated WT and $Cth^{-/-}$ mice demonstrated a similar reduction in liver H_2S-synthesizing activity and MPO activity in both organs, which reduced injury in these organs. Notably,

PAG treatment in CLP-induced sepsis WT mice did not affect Cth expression but inhibited its activity in synthesizing H_2S. These findings suggest that PAG does not affect Cth expression but rather inhibits the H_2S-synthesizing activity of the enzyme.

In response to sepsis, the immune system triggers increased production of various pro-inflammatory mediators (such as cytokines, chemokines, and adhesion molecules) through transcriptional activation, such as NF-κB [34,35], which is activated by ERK1/2 phosphorylation [36–38]. Our results confirm previous studies using PAG and NaHS that have demonstrated that an acute increase in H_2S concentrations is a key stimulus for the elevation of ERK1/2 phosphorylation and IκB deterioration, which subsequently induces the nuclear translocation of NF-κB in sepsis [19]. Recently, Cth deletion has been shown to attenuate liver and lung injury and the systemic inflammatory response by lowering ERK1/2 phosphorylation and the activation of NF-κB p65, as well as reducing the production of cytokines (TNF-α, IL-6, and IL-1β) and chemokines (MCP-1 and MIP-2α) [4]. These results suggest that the ERK1/2–NF-κB p65 signaling pathway may play a significant role in Cth/H_2S-mediated inflammation during sepsis.

This study demonstrated that $Cth^{-/-}$ CLP mice showed lower expression of ICAM-1 and VCAM-1 adhesion molecules compared to WT CLP mice in the liver and lung. Additionally, we found that PAG treatment in $Cth^{-/-}$ mice had no effect on the expression of ERK 1/2 phosphorylation, NF-κB p65, or the production of chemokines (MCP-1 and MIP-2α) and adhesion molecules (ICAM-1 and VCAM-1) compared to $Cth^{-/-}$ mice in liver and lung. However, a recent study has shown that PAG treatment in infected WT macrophages significantly reduced Mycobacterium tuberculosis CFU (colony-forming unit) counts even lower than in infected $Cth^{-/-}$ macrophages [39]. Differences in dosages, treatment conditions, and models may contribute to these discrepancies.

ICAM-1 and VCAM-1 are adhesion molecules primarily expressed on endothelial cells that respond to cytokines in a time- and dose-dependent manner. The transcription of these adhesion molecules is dependent on transcription factors such as NF-κB and AP-1, which play an important role in the activation of endothelial cells and the elevated expression of adhesion molecules in inflamed microvessels in response to various stimuli [40–42]. Our study showed increased ICAM-1 and VCAM-1 immunoreactivity in co-localization with LYVE-1 in a sepsis model. Similarly, ICAM-1 and VCAM-1 immunoreactivity in CLP-induced mice increased in co-localization with CD31. This suggested there was increased expression of ICAM-1 and VCAM-1 predominantly on liver sinusoidal endothelial cells and pulmonary endothelial cells, respectively, during sepsis. This increase could be from the elevated expressions of cytokines and the NF-κB transcription factor observed. Organ injury during inflammation is mainly induced by the selective infiltration of leukocytes, which is regulated by the expression of adhesion molecules and chemokines in the vascular endothelium [43–45]. Pharmacological inhibition of Cth and gene deletion both resulted in reduced immunoreactivity of ICAM-1 and VCAM-1 in co-localization with LYVE-1 and CD 31. This demonstrated that Cth is responsible in the regulation of adhesion molecules in both liver sinusoidal endothelial cells and pulmonary endothelial cells. In animal models and patients, liver injury is associated with the capillarization/defenestration (reduced porosity, frequency, and diameter) of LSECs [46]. $Cth^{-/-}$ mice demonstrated less defenestration and gap formation in LSECs following CLP-induced sepsis [4]. This indicates that Cth/H_2S synthesis regulates adhesion molecules in endothelial cells, which may be responsible for the alteration in fenestration and gap formation in LSECs, resulting in liver injury during sepsis. Similarly, the reduction in adhesion molecule expression in pulmonary endothelial cells following sepsis through Cth inhibition (both pharmacological and genetic) may be responsible for the attenuation of lung injury in sepsis, as reduced levels of adhesion molecules in endothelial cells decrease leukocyte infiltration to the site of infection, resulting in reduced injury. The histological evidence from the liver and lung further substantiates these results. Cth inhibition (both pharmacological and genetic) protected the liver from ballooning degeneration and focal hepatocyte necrosis in sepsis.

Similarly, there was a decrease in neutrophil infiltration, alveolar wall thickening, and fibrin deposition in Cth inhibition (both pharmacological and genetic) septic mice groups.

Employing two parallel complementary approaches has strengthened the evidence of H_2S involvement in sepsis. This study also validated the use of PAG as a proper tool in Cth/H_2S signaling in sepsis (inflammation), as no additional effect of PAG was observed in $Cth^{-/-}$ mice. Furthermore, this is the first study to demonstrate the Cth/H_2S signaling regulation of adhesion molecules in LSECs and pulmonary endothelial cells following sepsis. However, further investigation is needed to understand the precise mechanism of involvement of Cth/H_2S-synthesis-mediated changes in the expression of adhesion molecules in the LSECs and pulmonary endothelial cells.

This study and other studies have demonstrated the role of H_2S as a pro-inflammatory mediator in inflammation [5,7,13,47,48]. However, H_2S has also been suggested as having an anti-inflammatory action, pointing to contradictory outcomes in various inflammatory diseases [49–55]. H_2S may appear to have different pathogenic outcomes in different animal models but differences in the dosage, source of drug, and route and time of administration could also produce differing outcomes in the same model.

In conclusion, this study has demonstrated a key role of adhesion molecules expressed on endothelial cells in the pro-inflammatory action of H_2S in sepsis. PAG treatment in $Cth^{-/-}$ mice showed no additional effect in the activation of ERK1/2 and NF-κB p65 signaling, chemokines, and adhesion molecules, attenuating tissue damage in liver and lungs compared to Cth deletion mice during CLP-induced sepsis. The PAG-treated WT mice also showed similar results. $Cth^{-/-}$ mice and Cth inhibition using a pharmacological drug in both WT and KO mice demonstrated a decrease in the expression of adhesion molecules in LSECs and pulmonary endothelial cells (Figure 8). These results have important implications for our understanding of the mechanism by which H_2S contributes to inflammation in sepsis, and could contribute to the development of novel therapeutic approaches for sepsis.

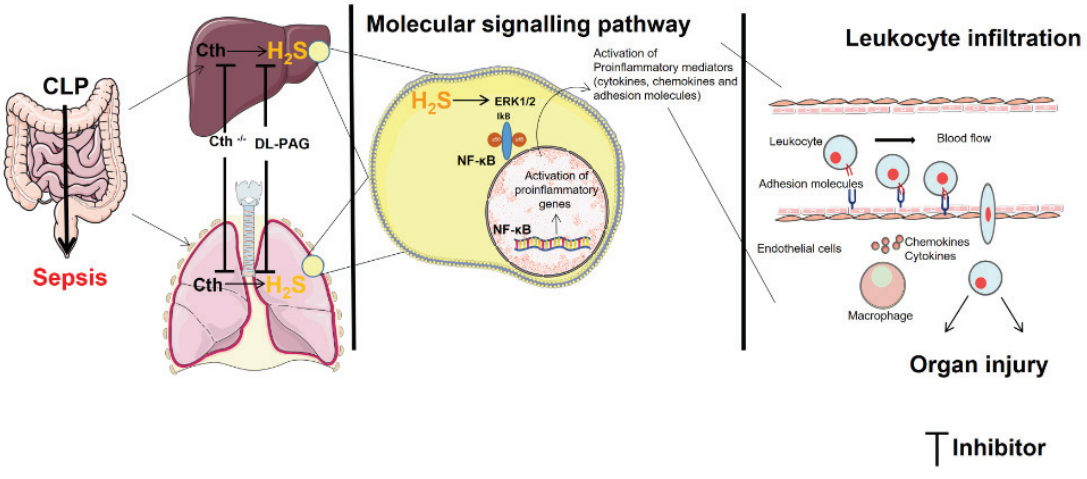

Figure 8. Hydrogen sulfide regulates liver and lung injury in CLP-induced sepsis. An increase in the expression of Cth results in the elevation in hydrogen sulfide synthesizing activity. This leads to the phosphorylation of ERK1/2, resulting in translocation and activation of NF-κB, thereby increasing the adhesion molecules' expression on liver sinusoidal endothelial cells and pulmonary endothelial cells that results in liver and lung injury. The figure incorporates images sourced from Servier Medical Art, which is licensed under a Creative Commons Attribution 3.0 Unported License (https://creativecommons.org/licenses/by/3.0/).

4. Materials and Methods

4.1. Induction of Polymicrobial Sepsis in Mice

All experimental procedures were authorized by the University of Otago Animal Welfare Office and Ethics Committee and conducted under the established guidelines. WT, $Cth^{-/-}$ [56], and PAG-treated WT and $Cth^{-/-}$ mice (C57BL/6J males, 25–30 g) were allocated to control or experimental groups in a randomized manner. WT mice were acquired from the Christchurch Animal Research Area, and the $Cth^{-/-}$ mice were bred by mating Cth heterozygous mice as previously described. Forty-eight mice were used in total, divided into WT saline sham, $Cth^{-/-}$ saline sham, WT saline sepsis, $Cth^{-/-}$ saline sepsis, PAG-treated $Cth^{-/-}$ sepsis, and PAG-treated WT sepsis (n = 8 each).

CLP-induced sepsis was performed with a few minor modifications to a previously described protocol [4]. Briefly, mice were mildly anesthetized using inhaled isoflurane (2%, 1 L/min O_2). Sterile surgical procedures were employed during the CLP operation. PAG (50 mg/kg) was dissolved in saline and intraperitoneally (i.p) administered 30 min before CLP (CLP PAG WT and CLP PAG $Cth^{-/-}$). Sham WT, sham $Cth^{-/-}$, CLP WT, and CLP $Cth^{-/-}$ were administered with saline intraperitoneally as a vehicle control. Disinfectant was applied after the removal of abdominal fur. A small midline incision through the skin, abdominal wall, and peritoneum was made to expose the caecum, which was ligated with 5.0 Silkam thread 8–10 mm from the end of the cecum without obstructing the bowel passage. Thereafter, a 22 gauge (22G)-sized needle was used to perforate the distal end of the cecum in two different locations. A small amount of feces was squeezed out through each hole; then, the bowel was repositioned. The abdomen was sutured with sterile permilene 5.0 thread. The same surgical procedure was performed on sham mice but without bowel perforation. Buprenorphine (Temgesic, 0.2 mg/kg) was administered by the subcutaneous route 45 min prior to and 3 h after the surgical procedure (sham or CLP) for analgesia. Eight hours after surgery, an IP injection of pentobarbital sodium (150 mg/kg) was administered to euthanize mice. Blood samples were taken from the right ventricle using heparinized syringes. Plasma was collected after centrifugation (1000× g, 5 min, at 4 °C). Sections of the liver and lung tissues were fixed in 10% formalin for more than 24 h, processed via a series of graded ethanol, and infused with paraffin wax. The rest of the tissue samples were kept at –80 °C for quantification of chemokines and adhesion molecules, H_2S-synthesizing activity, and tissue MPO.

4.2. Myeloperoxidase (MPO) Activity

Leukocyte sequestration into the liver and lung was quantified by measuring tissue MPO activity. Tissue samples were thawed, homogenized in 20 mM phosphate buffer (pH 7.4), centrifuged (13,000× g, 10 min, 4 °C), and the resulting pellet was resuspended in 50 mM phosphate buffer (pH 6.0) containing 0.5% w/v hexadecyltrimethylammonium bromide (Sigma-Aldrich, Dallas, TX, USA). The suspension was subjected to three cycles of freezing and thawing followed by sonication for 40 s. The reagent mixture consisted of supernatants (50 mL), tetramethylbenzidine (1.6 mM), sodium phosphate buffer (80 mM, pH 5.4), and hydrogen peroxide (0.3 mM) and this reagent was incubated at 37 °C for 110 s. The reaction was stopped with 50 µL of 2 M H_2SO_4, and absorbance was measured at 450 nm (Thermo Fisher Multiskan GO, Ratastie, Finland) and corrected for the protein content of the tissue sample using results from the Bradford protein assay [57]. The results are presented as a fold increase over a control group.

4.3. H_2S-Synthesizing Activity Assay

H_2S-synthesizing activity in liver tissue was measured, according to the protocol described previously with minor modifications [4]. The liver tissue was homogenized in 20mM mM sodium phosphate buffer (pH 7.4) while kept on ice. The reaction mixture is composed of sodium phosphate buffer (20 mM, pH 7.4), pyridoxyal 5′-phosphate (10 µL, 18 mM), and L-cysteine (10 µL, 250 mM) in 230 µL of tissue homogenate. The reaction was performed in a tightly parafilm-sealed microfuge tube and initiated by transferring the

tubes from ice to a water bath at 37 °C. An amount of 250 µL of zinc acetate (1% w/v) was added after 30 min of incubation in order to capture generated H_2S. Then, a mixture of *N*, *N*-dimethyl-*p*-phenylenediamine sulfate (20 mM) in 7.2 M HCl and $FeCl_3$ (30 mM) in 1.2 M HCl (133 µL, in 1:1 ratio) was added. Subsequently, the samples were incubated in the dark at room temperature for 20 min. After that, 10% (v/v) trichloroacetic acid was added to denature the protein and end the reaction. The supernatant was collected after the centrifugation and absorbance was measured with a 96-well microplate spectrophotometer at 670 nm. The H_2S concentration was measured against a calibration curve of Na_2S. The results are expressed as nmole H_2S/mg protein after being normalized for the tissue sample's protein concentrations as determined via the Bradford assay.

4.4. Western Blotting

Liver and lung tissue was lysed with homogenizer (Labserv, Fisher Scientific, Singapore) in lysis buffer (ice-cold RIPA buffer and protease inhibitor). Then, homogenates were centrifuged at 10,000× g for 10 min at 4 °C. Proteins (30 µg) were separated using 10% sodium dodecyl sulfate-polyacrylamide gel via electrophoresis and transferred onto a polyvinylidene difluoride (PVDF, Bio-Rad, Hercules, CA, USA) membrane via wet transfer for 1 h. After blocking the membrane with 0.1% (w/v) Tween 20 in tris-buffered saline (TBST) containing 5% (w/v) non-fat dry milk at room temperature for 1 h, the membrane was incubated overnight with primary antibody (Table 1) at 4 °C. The membrane was washed with TBST, incubated for 1.5 h with secondary antibody (Table 1) at room temperature, and detected with chemiluminescent reagent (Supersignal West Pico, Thermo Scientific, Waltham, MA, USA). The detection was carried out using a chemi-doc instrument (Uvitec, Cambridge, UK).

Table 1. Primary and secondary antibodies used in this study for Western blotting and immunofluorescence microscopy.

Product	Antibody/Type	Source Catalogue No.	Dilution
Western blotting			
CTH	Primary/Mouse monoclonal	Abnova, Taipei City, Taiwan/H00001491-M01	1:1000
GAPDH	Primary/Rabbit polyclonal	Santa Curz, Dallas, TX, USA/sc-25778	1:2000
ERK1/2	Primary/Rabbit monoclonal	Cell Signaling, Danvers, MA, USA/137F5	1:2000
p-ERK1/2	Primary/Rabbit monoclonal	Cell Signaling, Danvers, MA, USA/93H1	1:2000
Goat anti-mouse HRP	Secondary	Santa Curz, Dallas, TX, USA/sc-2005	1:20,000
Goat anti-rabbit HRP	Secondary	Abcam, Cambridge, UK/ad6721	1:20,000
Immunofluorescence			
ICAM-1	Primary/Goat polyclonal	R&D System, Minneapolis, MN, USA/AF796	1: 1000
VCAM-1	Primary/Goat polyclonal	R&D System, Minneapolis, MN, USA/AF643	1: 200
LYVE-1	Primary/Rabbit polyclonal	Abcam, Cambridge, UK/ab14917	1:100
CD31	Primary/Rabbit polyclonal	Abcam, Cambridge, UK/ab124432	1:500
Donkey anti-goat	Secondary/Texas Red	Abcam, Cambridge, UK/ab6883	1:1000
Donkey anti-rabbit	Secondary/FITC	Abcam, Cambridge, UK/ab6798	1:1000

4.5. Double-Immunofluorescence Staining of Paraffin Sections

Liver and lungs were extracted and fixed in 4% buffered paraformaldehyde. The fixed tissue was processed and embedded in paraffin. The paraffin-embedded tissues were sectioned to 4 µm thickness using a LEICA microtome (HistoCore BIOCUT R, Leica Biosystems, Mt Waverley, Australia) and attached to charged glass slide. Sections were deparaffined and hydrated followed by antigen retrieval by cooking slides in Tris EDTA pH 9.0 buffer at 100 °C for 4 min in a pressure cooker. The slides were left to cool in the buffer for 2 h. The slides were rinsed in water 3 times, followed by washing in PBS for 5 min. The tissue sections were permeabilized in 0.1% (w/v) Tween 20 in phosphate-buffered saline (PBST) buffer for 15 min at 4 °C. This was followed by washing sections with PBS

3 times for 5 min. The slides were drained properly without letting the section dry out. An ImmEdge pen (H-4000, Newark, CA, USA)was used to draw a hydrophobic barrier around the tissue section. Sections were blocked with 10% normal donkey serum at room temperature (humidifying chamber) for 1 h. After this, the sections were incubated in primary antibody (1:100 for LYVE-1, 1:1000 for ICAM-1, 1:200 VCAM-1, and 1:500 for CD31) diluted in 1% normal donkey serum overnight at 4 °C (in humidifying chamber) (Table 1). Slides were washed 3 times with PBS. This was followed by secondary antibody (Table 1) incubation for 2 h with DAPI (4′,6-diamidino-2-phenylindole) at room temperature. Slides were washed 3 times with PBS. Sections were mounted with anti-fading solution and observed with an epifluorescence microscope (Carl Zeiss, Oberkochen, Germany).

Mean fluorescence intensity (MFI) was measured using an automated region of interest selection based on a signal threshold using Fiji ImageJ (downloaded at https://fiji.sc/). This measurement procedure was followed according to a protocol described previously with minor modifications [58]. In the previous protocol, the interested stain (targeted protein) was selected using an automated region of interest based on a signal threshold and then mean intensity was directly measured. In this modified protocol, the selection of LYVE-1 or CD31 (Alexa Fluor 488–green) staining was performed with an automated region of interest based on a signal threshold. The mean intensity of staining of targeted proteins (Cy3–red), which was measured from the automated region of interest (e.g., yellow ROI's) selection obtained above from LYVE-1 or CD 31 (colonized of targeted protein in endothelial cells-LYVE-1). The background intensity for each image was calculated as the mean intensity within the blue regions of interest (ROIs). The intensity of layer-specific staining (ICAM-1 and VCAM-1) proteins was determined by subtracting the mean target protein staining intensity from the background staining intensity. This calculation was performed using 8 confocal images for each group and target protein (ICAM-1 and VCAM-1).

4.6. Histological Analysis

The liver and lung samples were extracted and fixed in 4% buffered paraformaldehyde. The fixed tissue was processed and embedded in paraffin. The samples were sectioned (4 μm), stained with hematoxylin/eosin (H&E), and examined via light microscopy using a Leica microscope. Organ (liver and lung) injury was scored double-blinded, involving an experienced pathologist (A.M.) as one of the individuals responsible for the assessment with regard to different treatment groups. Liver sections were assessed for liver injury (ballooning degeneration and focal hepatocyte necrosis) and scored for liver injury (ballooning degeneration) in 2 random fields at 10× magnification (n = 8 per condition) as previously described [59]. Lung pathology was assessed using a scoring system adapted from the American Thoracic Society guidelines [60]. The lung injury was based on the extent of fibrin deposition, leukocyte (neutrophil) infiltration, and alveolar wall thickening. For scoring, 3 random fields were counted per slide (n = 8 per condition) at 40× magnification.

4.7. NF-κB Activity Assay

NF-κB activation was measured in the nuclear extract of liver and lung tissues as per the manufacturer's instructions using a TransAM NF-κB p65 transcription factor assay kit (Active Motif, Wangarra, Australia). Nuclear extracts (20 μg) were incubated in a 96-well plate with complete lysis buffer for 1 h before being incubated with a specific primary antibody against NF-κB p65 for 1 h. After, a secondary antibody conjugated to horse radish peroxidase (HRP) was added for detection. The microplate reader measured the absorbance of the enzymatic product at 450 nm. The wild-type or mutated consensus oligonucleotides were incubated in the wells to determine the assay's specificity. The results are presented as a fold increase over a control group.

4.8. Enzyme-Linked Immunosorbent Assay

The protein concentrations of chemokines (MCP-1 and MIP-2α) and adhesion molecules (ICAM-1 and VCAM-1) were measured in liver and lung with a sandwich EILSA using Du-

oSet ELISA kits by R&D System (Minneapolis, MN, USA) as directed in the manufacturer's protocol. Liver and lung homogenates were prepared by homogenizing 20 mg of tissue in 1 mL of sodium phosphate buffer (20 mM, pH 7.4). The homogenates were centrifuged at 15,000× *g* for 15 min at 4 °C. The supernatant was used to measure adhesion molecule and chemokine concentrations. Measurements were corrected for the tissue sample's protein levels using Bradford protein assay and expressed as picogram per milligram of protein.

4.9. Statistical Analysis

The data are reported as mean ± SD and assessed for Gaussian or normal distribution using the Shapiro–Wilk test. For normally distributed data, one-way ANOVA with post hoc Tukey's test was performed. If the data were not normally distributed, the non-parametric Kruskal–Wallis test was used. Statistical analysis in this study was conducted using GraphPad Prism software (version 9, San Diego, CA, USA). Statistical significance was set at $p < 0.05$.

Author Contributions: Conceptualization, M.B.; methodology, S.M. and M.B.; formal analysis, S.M. and AM; investigation, S.M., A.M., S.C. and M.B.; resources, M.B. and I.I.; data curation, S.M.; writing—original draft preparation, S.M.; writing—review and editing, A.M., S.C., I.I. and M.B.; visualization, S.M. and A.M.; supervision, M.B. and S.C.; project administration, M.B.; funding acquisition, M.B. All authors have read and agreed to the published version of the manuscript.

Funding: This research was funded by support from the University of Otago Vice-Chancellor's Strategic Development Fund (M.B.), and Maurice and Phyllis Paykel Trust grant (M.B.). I.I. was supported by a Grant-in-Aid for Transformative Research Areas (A) (22H05577) from the Japan Society for the Promotion of Science.

Institutional Review Board Statement: The study was conducted according to the New Zealand guidelines on animal welfare and approved by the Animal Ethics Committee of University of Otago (AUP-19-104, date of approval 19 August 2019).

Informed Consent Statement: Not applicable.

Data Availability Statement: All data generated or analysed during this study are included in this published article.

Conflicts of Interest: The authors declare no conflict of interest. The funders had no role in the design of the study; in the collection, analyses, or interpretation of data; in the writing of the manuscript; or in the decision to publish the results.

References

1. Dugani, S.; Veillard, J.; Kissoon, N. Reducing the global burden of sepsis. *CMAJ* **2017**, *189*, E2–E3. [CrossRef]
2. Martin, G.S.; Mannino, D.M.; Eaton, S.; Moss, M. The epidemiology of sepsis in the United States from 1979 through 2000. *N. Engl. J. Med.* **2003**, *348*, 1546–1554. [CrossRef] [PubMed]
3. Remick, D.G. Pathophysiology of sepsis. *Am. J. Pathol.* **2007**, *170*, 1435–1444. [CrossRef] [PubMed]
4. Gaddam, R.R.; Fraser, R.; Badiei, A.; Chambers, S.; Cogger, V.C.; Le Couteur, D.G.; Ishii, I.; Bhatia, M. Cystathionine-Gamma-Lyase Gene Deletion Protects Mice against Inflammation and Liver Sieve Injury following Polymicrobial Sepsis. *PLoS ONE* **2016**, *11*, e0160521. [CrossRef] [PubMed]
5. Ang, A.D.; Rivers-Auty, J.; Hegde, A.; Ishii, I.; Bhatia, M. The effect of CSE gene deletion in caerulein-induced acute pancreatitis in the mouse. *Am. J. Physiol. Gastrointest. Liver Physiol.* **2013**, *305*, G712–G721. [CrossRef] [PubMed]
6. Muniraj, N.; Stamp, L.K.; Badiei, A.; Hegde, A.; Cameron, V.; Bhatia, M. Hydrogen sulfide acts as a pro-inflammatory mediator in rheumatic disease. *Int. J. Rheum. Dis.* **2017**, *20*, 182–189. [CrossRef] [PubMed]
7. Zhang, J.; Sio, S.W.S.; Moochhala, S.; Bhatia, M. Role of hydrogen sulfide in severe burn injury-induced inflammation in mice. *Mol. Med.* **2010**, *16*, 417–424. [CrossRef]
8. Kamoun, P. Endogenous production of hydrogen sulfide in mammals. *Amino Acids* **2004**, *26*, 243–254. [CrossRef]
9. Kabil, O.; Vitvitsky, V.; Xie, P.; Banerjee, R. The quantitative significance of the transsulfuration enzymes for H_2S production in murine tissues. *Antioxid. Redox Signal.* **2011**, *15*, 363–372. [CrossRef]
10. Manandhar, S.; Sinha, P.; Ejiwale, G.; Bhatia, M. Hydrogen Sulfide and its Interaction with Other Players in Inflammation. *Adv. Exp. Med. Biol.* **2021**, *1315*, 129–159.
11. Sidhapuriwala, J.N.; Hegde, A.; Ang, A.D.; Zhu, Y.Z.; Bhatia, M. Effects of S-propargyl-cysteine (SPRC) in caerulein-induced acute pancreatitis in mice. *PLoS ONE* **2012**, *7*, e32574. [CrossRef]

12. Collin, M.; Anuar, F.B.M.; Murch, O.; Bhatia, M.; Moore, P.K.; Thiemermann, C. Inhibition of endogenous hydrogen sulfide formation reduces the organ injury caused by endotoxemia. *Br. J. Pharmacol.* **2005**, *146*, 498–505. [CrossRef] [PubMed]
13. Zhang, H.; Zhi, L.; Moore, P.K.; Bhatia, M. Role of hydrogen sulfide in cecal ligation and puncture-induced sepsis in the mouse. *Am. J. Physiol. Lung Cell. Mol. Physiol.* **2006**, *290*, L1193–L1201. [CrossRef] [PubMed]
14. Zhang, H.; Zhi, L.; Moochhala, S.M.; Moore, P.K.; Bhatia, M. Endogenous hydrogen sulfide regulates leukocyte trafficking in cecal ligation and puncture-induced sepsis. *J. Leukoc. Biol.* **2007**, *82*, 894–905. [CrossRef] [PubMed]
15. Zhang, H.; Hegde, A.; Ng, S.W.; Adhikari, S.; Moochhala, S.M.; Bhatia, M. Hydrogen sulfide up-regulates substance P in polymicrobial sepsis-associated lung injury. *J. Immunol.* **2007**, *179*, 4153–4160. [CrossRef] [PubMed]
16. Gaddam, R.R.; Chambers, S.; Murdoch, D.; Shaw, G.; Bhatia, M. Circulating levels of hydrogen sulfide and substance P in patients with sepsis. *J. Infect.* **2017**, *75*, 293–300. [CrossRef]
17. Manandhar, S.; Scott-Thomas, A.; Harrington, M.; Sinha, P.; Pilbrow, A.; Richards, A.M.; Cameron, V.; Bhatia, M.; Chambers, S.T. Hydrogen Sulfide and Substance P Levels in Patients with Escherichia coli and Klebsiella pneumoniae Bacteraemia. *Int. J. Mol. Sci.* **2022**, *23*, 8639. [CrossRef]
18. Ang, S.F.; Moochhala, S.M.; MacAry, P.A.; Bhatia, M. Hydrogen sulfide and neurogenic inflammation in polymicrobial sepsis: Involvement of substance P and ERK-NF-κB signaling. *PLoS ONE* **2011**, *6*, e24535. [CrossRef]
19. Zhang, H.; Moochhala, S.M.; Bhatia, M. Endogenous hydrogen sulfide regulates inflammatory response by activating the ERK pathway in polymicrobial sepsis. *J. Immunol.* **2008**, *181*, 4320–4331. [CrossRef]
20. Nourshargh, S.; Alon, R. Leukocyte migration into inflamed tissues. *Immunity* **2014**, *41*, 694–707. [CrossRef]
21. Tanaka, Y.; Adams, D.H.; Hubscher, S.; Hirano, H.; Siebenlist, U.; Shaw, S. T-cell adhesion induced by proteoglycan-immobilized cytokine MIP-1 beta. *Nature* **1993**, *361*, 79–82. [CrossRef] [PubMed]
22. Campbell, J.J.; Hedrick, J.; Zlotnik, A.; Siani, M.A.; Thompson, D.A.; Butcher, E.C. Chemokines and the arrest of lymphocytes rolling under flow conditions. *Science* **1998**, *279*, 381–384. [CrossRef] [PubMed]
23. Ang, S.-F.; Sio, S.W.S.; Moochhala, S.M.; MacAry, P.A.; Bhatia, M. Hydrogen sulfide upregulates cyclooxygenase-2 and prostaglandin E metabolite in sepsis-evoked acute lung injury via transient receptor potential vanilloid type 1 channel activation. *J. Immunol.* **2011**, *187*, 4778–4787. [CrossRef] [PubMed]
24. Shetty, S.; Lalor, P.F.; Adams, D.H. Liver sinusoidal endothelial cells-gatekeepers of hepatic immunity. *Nat. Rev. Gastroenterol. Hepatol.* **2018**, *15*, 555–567. [CrossRef]
25. Wang, Y.; Liu, Y. Neutrophil-Induced Liver Injury and Interactions Between Neutrophils and Liver Sinusoidal Endothelial Cells. *Inflammation* **2021**, *44*, 1246–1262. [CrossRef]
26. Campbell, J.J.; Qin, S.; Bacon, K.B.; Mackay, C.R.; Butcher, E.C. Biology of chemokine and classical chemoattractant receptors: Differential requirements for adhesion-triggering versus chemotactic responses in lymphoid cells. *J. Cell Biol.* **1996**, *134*, 255–266. [CrossRef]
27. Lalor, P.F.; Adams, D.H. The liver: A model of organ-specific lymphocyte recruitment. *Expert Rev. Mol. Med.* **2002**, *4*, 1–16. [CrossRef]
28. Gaddam, R.R.; Fraser, R.; Badiei, A.; Chambers, S.; Cogger, V.C.; Le Couteur, D.G.; Bhatia, M. Differential Effects of Kupffer Cell Inactivation on Inflammation and the Liver Sieve Following Caecal-Ligation and Puncture-Induced Sepsis in Mice. *Shock* **2017**, *47*, 480–490. [CrossRef]
29. Gaddam, R.R.; Chambers, S.; Fraser, R.; Cogger, V.C.; Le Couteur, D.G.; Ishii, I.; Bhatia, M. Cystathionine-Gamma-Lyase-Derived Hydrogen Sulfide-Regulated Substance P Modulates Liver Sieve Fenestrations in Caecal Ligation and Puncture-Induced Sepsis. *Int. J. Mol. Sci.* **2019**, *20*, 3191. [CrossRef]
30. Boller, E.M.; Otto, C.M. *Chapter 107—Septic Shock, in Small Animal Critical Care Medicine*; Silverstein, D.C., Hopper, K., Eds.; W.B. Saunders: Saint Louis, MO, USA, 2009; pp. 459–463.
31. Millar, F.R.; Summers, C.; Griffiths, M.J.; Toshner, M.R.; Proudfoot, A.G. The pulmonary endothelium in acute respiratory distress syndrome: Insights and therapeutic opportunities. *Thorax* **2016**, *71*, 462–473. [CrossRef]
32. Müller, A.M.; Cronen, C.; Müller, K.-M.; Kirkpatrick, C.J. Heterogeneous expression of cell adhesion molecules by endothelial cells in ARDS. *J. Pathol.* **2002**, *198*, 270–275. [CrossRef] [PubMed]
33. Sun, Q.; Collins, R.; Huang, S.; Holmberg-Schiavone, L.; Anand, G.S.; Tan, C.H.; Van-den-Berg, S.; Deng, L.W.; Moore, P.K.; Karlberg, T.; et al. Structural basis for the inhibition mechanism of human cystathionine gamma-lyase, an enzyme responsible for the production of H_2S. *J. Biol. Chem.* **2009**, *284*, 3076–3085. [CrossRef] [PubMed]
34. Liu, S.F.; Malik, A.B. NF-κB activation as a pathological mechanism of septic shock and inflammation. *Am. J. Physiol. Lung Cell. Mol. Physiol.* **2006**, *290*, L622–L645. [CrossRef] [PubMed]
35. Li, X.; Su, J.; Cui, X.; Li, Y.; Barochia, A.; Eichacker, P.Q. Can we predict the effects of NF-kappaB inhibition in sepsis? Studies with parthenolide and ethyl pyruvate. *Expert Opin. Investig. Drugs* **2009**, *18*, 1047–1060. [CrossRef]
36. Jiang, B.; Xu, S.; Hou, X.; Pimentel, D.R.; Brecher, P.; Cohen, R.A. Temporal control of NF-κB activation by ERK differentially regulates interleukin-1β-induced gene expression. *J. Biol. Chem.* **2004**, *279*, 1323–1329. [CrossRef]
37. Roux, P.P.; Blenis, J. ERK and p38 MAPK-activated protein kinases: A family of protein kinases with diverse biological functions. *Microbiol. Mol. Biol. Rev.* **2004**, *68*, 320–344. [CrossRef]

38. Badiei, A.; Muniraj, N.; Chambers, S.; Bhatia, M. Inhibition of hydrogen sulfide production by gene silencing attenuates inflammatory activity by downregulation of NF-κB and MAP kinase activity in LPS-activated RAW 264.7 cells. *BioMed Res. Int.* **2014**, *2014*, 848570. [CrossRef]
39. Rahman, M.A.; Cumming, B.M.; Addicott, K.W.; Pacl, H.T.; Russell, S.L.; Nargan, K.; Naidoo, T.; Ramdial, P.K.; Adamson, J.H.; Wang, R.; et al. Hydrogen sulfide dysregulates the immune response by suppressing central carbon metabolism to promote tuberculosis. *Proc. Natl. Acad. Sci. USA* **2020**, *117*, 6663–6674. [CrossRef]
40. Granger, D.N.; Kubes, P. The microcirculation and inflammation: Modulation of leukocyte-endothelial cell adhesion. *J. Leukoc. Biol.* **1994**, *55*, 662–675. [CrossRef]
41. Panés, J.; Granger, D.N. Leukocyte-endothelial cell interactions: Molecular mechanisms and implications in gastrointestinal disease. *Gastroenterology* **1998**, *114*, 1066–1090. [CrossRef]
42. Henninger, D.D.; Panés, J.; Eppihimer, M.; Russell, J.; Gerritsen, M.; Anderson, D.C.; Granger, D.N. Cytokine-induced VCAM-1 and ICAM-1 expression in different organs of the mouse. *J. Immunol.* **1997**, *158*, 1825–1832. [CrossRef]
43. Lee, S.A.; Cozzi, M.; Bush, E.L.; Rabb, H. Distant Organ Dysfunction in Acute Kidney Injury: A Review. *Am. J. Kidney Dis.* **2018**, *72*, 846–856. [CrossRef]
44. Hillyer, P.; Mordelet, E.; Flynn, G.; Male, D. Chemokines, chemokine receptors and adhesion molecules on different human endothelia: Discriminating the tissue-specific functions that affect leucocyte migration. *Clin. Exp. Immunol.* **2003**, *134*, 431–441. [CrossRef] [PubMed]
45. Quarmby, S.; Kumar, P.; Kumar, S. Radiation-induced normal tissue injury: Role of adhesion molecules in leukocyte-endothelial cell interactions. *Int. J. Cancer* **1999**, *82*, 385–395. [CrossRef]
46. Szafranska, K.; Kruse, L.D.; Holte, C.F.; McCourt, P.; Zapotoczny, B. The wHole Story About Fenestrations in LSEC. *Front. Physiol.* **2021**, *12*, 735573. [CrossRef]
47. Dal-Secco, D.; Cunha, T.M.; Freitas, A.; Alves-Filho, J.C.; Souto, F.O.; Fukada, S.Y.; Grespan, R.; Alencar, N.M.N.; Neto, A.F.; Rossi, M.A.; et al. Hydrogen Sulfide Augments Neutrophil Migration through Enhancement of Adhesion Molecule Expression and Prevention of CXCR2 Internalization: Role of ATP-Sensitive Potassium Channels. *J. Immunol.* **2008**, *181*, 4287–4298. [CrossRef] [PubMed]
48. Dam, V.P.; Scott, J.L.; Ross, A.; Kinobe, R.T. Inhibition of cystathionine gamma-lyase and the biosynthesis of endogenous hydrogen sulphide ameliorates gentamicin-induced nephrotoxicity. *Eur. J. Pharmacol.* **2012**, *685*, 165–173. [CrossRef] [PubMed]
49. Zanardo, R.C.O.; Brancaleone, V.; Distrutti, E.; Fiorucci, S.; Cirino, G.; Wallace, J.L. Hydrogen sulfide is an endogenous modulator of leukocyte-mediated inflammation. *FASEB J.* **2006**, *20*, 2118–2120. [CrossRef] [PubMed]
50. Wallace, J.L.; Vong, L.; McKnight, W.; Dicay, M.; Martin, G.R. Endogenous and exogenous hydrogen sulfide promotes resolution of colitis in rats. *Gastroenterology* **2009**, *137*, 569–578, 578.e1. [CrossRef]
51. Tan, G.; Pan, S.; Li, J.; Dong, X.; Kang, K.; Zhao, M.; Jiang, X.; Kanwar, J.R.; Qiao, H.; Jiang, H.; et al. Hydrogen sulfide attenuates carbon tetrachloride-induced hepatotoxicity, liver cirrhosis and portal hypertension in rats. *PLoS ONE* **2011**, *6*, e25943. [CrossRef]
52. Esechie, A.; Kiss, L.; Olah, G.; Horváth, E.M.; Hawkins, H.; Szabo, C.; Traber, D.L. Protective effect of hydrogen sulfide in a murine model of acute lung injury induced by combined burn and smoke inhalation. *Clin. Sci.* **2008**, *115*, 91–97. [CrossRef] [PubMed]
53. Zeng, J.; Lin, X.; Fan, H.; Li, C. Hydrogen sulfide attenuates the inflammatory response in a mouse burn injury model. *Mol. Med. Rep.* **2013**, *8*, 1204–1208. [CrossRef] [PubMed]
54. Li, J.; Li, M.; Li, L.; Ma, J.; Yao, C.; Yao, S. Hydrogen sulfide attenuates ferroptosis and stimulates autophagy by blocking mTOR signaling in sepsis-induced acute lung injury. *Mol. Immunol.* **2022**, *141*, 318–327. [CrossRef] [PubMed]
55. Bhatia, M.; Sidhapuriwala, J.N.; Sparatore, A.; Moore, P.K. Treatment with H_2S-releasing diclofenac protects mice against acute pancreatitis-associated lung injury. *Shock* **2008**, *29*, 84–88. [CrossRef] [PubMed]
56. Ishii, I.; Akahoshi, N.; Yamada, H.; Nakano, S.; Izumi, T.; Suematsu, M. Cystathionine gamma-Lyase-deficient mice require dietary cysteine to protect against acute lethal myopathy and oxidative injury. *J. Biol. Chem.* **2010**, *285*, 26358–26368. [CrossRef] [PubMed]
57. Kruger, N.J. The Bradford method for protein quantitation. *Methods Mol. Biol.* **1994**, *32*, 9–15.
58. Shihan, M.H.; Novo, S.G.; Le Marchand, S.J.; Wang, Y.; Duncan, M.K. A simple method for quantitating confocal fluorescent images. *Biochem. Biophys. Rep.* **2021**, *25*, 100916. [CrossRef]
59. Muftuoglu, M.T.; Aktekin, A.; Ozdemir, N.C.; Saglam, A. Liver injury in sepsis and abdominal compartment syndrome in rats. *Surg. Today* **2006**, *36*, 519–524. [CrossRef]
60. Matute-Bello, G.; Downey, G.; Moore, B.B.; Groshong, S.D.; Matthay, M.A.; Slutsky, A.S.; Kuebler, W.M. An official American Thoracic Society workshop report: Features and measurements of experimental acute lung injury in animals. *Am. J. Respir. Cell Mol. Biol.* **2011**, *44*, 725–738. [CrossRef]

International Journal of
Molecular Sciences

MDPI

Article

Relationship between the Consumption of Fermented Red Beetroot Juice and Levels of Perfluoroalkyl Substances in the Human Body's Fluids and Blood Parameters

Magdalena Surma [1,*], Tomasz Sawicki [2], Mariusz Piskuła [3] and Wiesław Wiczkowski [3]

[1] Malopolska Centre of Food Monitoring, Faculty of Food Technology, University of Agriculture in Krakow, 122 Balicka St., 30-149 Krakow, Poland
[2] Department of Human Nutrition, Faculty of Food Sciences, University of Warmia and Mazury in Olsztyn, Słoneczna 45F St., 10-719 Olsztyn, Poland
[3] Institute of Animal Reproduction and Food Research, Polish Academy of Science, Tuwima 10 St., 10-748 Olsztyn, Poland
* Correspondence: magdalena.surma@urk.edu.pl

Abstract: Per- and polyfluoroalkyl substances (PFASs) are a group of fluorinated, organic, man-made chemicals; they do not occur naturally in the environment. This study aimed to determine the profile and content of PFASs in the volunteers' blood plasma and urine after the consumption of fermented red beetroot juice and then correlated it with the blood parameters. Over 42 days, 24 healthy volunteers ingested 200 mL/60 kg of body weight of fermented red beetroot juice. PFASs were analyzed using the micro-HPLC-MS/MS method. Five perfluoroalkyl substances were found in the volunteers' body fluids. After consuming the juice, it was discovered that regarding the perfluorocarboxylic acids, a downward trend was observed, while regarding the perfluoroalkane sulfonates, and their plasma content showed a statistically significant upward trend. Analysis of the hematology parameters indicated that the intake of fermented red beetroot juice showed a significant decrease in mean corpuscular volume (MCV), platelets concentration, mean platelet volume (MPV), platelet large cell ratio (P-LCR) at the significance level $p < 0.01$, and hematocrit ($p < 0.05$). On the other hand, the dietary intervention also indicated a significant ($p < 0.01$) increase in corpuscular/cellular hemoglobin concentration (MCHC). In the case of blood biochemistry, no significant change was observed in the blood samples after the intake of the fermented beetroot juice. However, a decreasing tendency of total cholesterol and low-density lipoprotein concentration (LDL-C) was observed. Based on the presented results, there is a need to analyze and monitor health-promoting food regarding undesirable substances and their impact on consumer health.

Keywords: perfluoroalkyl substances; fermented red beetroot juice; human body fluids; blood parameters

Citation: Surma, M.; Sawicki, T.; Piskuła, M.; Wiczkowski, W. Relationship between the Consumption of Fermented Red Beetroot Juice and Levels of Perfluoroalkyl Substances in the Human Body's Fluids and Blood Parameters. *Int. J. Mol. Sci.* **2023**, *24*, 13956. https://doi.org/10.3390/ijms241813956

Academic Editor: Francesco Visioli

Received: 3 August 2023
Revised: 30 August 2023
Accepted: 8 September 2023
Published: 11 September 2023

1. Introduction

Nowadays, it is believed that vegetables and the nutrients obtained from them are a crucial part of the daily human diet [1]. These products are considered to be among the best sources of essential nutrients and bioactive compounds [2]. In addition, many studies suggest that the intake of vegetables positively affects consumer health. The regular consumption of vegetables can positively affect the prevention of many diseases, such as cancer (colorectal and breast cancer) and cardiovascular diseases [3–5].

Red beetroot (*Beta vulgaris* L. subsp. *vulgaris*) is one of the most popular vegetables as a valuable source of vitamins, minerals, and bioactive compounds [6]. Due to the high phytochemical content, the intake of this vegetable may have positive, beneficial effects for consumers. Red beetroot shows anti-neurodegenerative, antitumor, anti-inflammatory, antibacterial, antiviral, cardioprotective, and lipid peroxidation inhibitory activities [7]. Moreover, this vegetable is trendy in the food industry. It produces many red beetroot

products or additives (such as drinks and concentrated juices, yoghurts, and frozen foods) and is used in the preparation of natural red dyes [6]. On the other hand, red beetroot may contain other compounds, such as perfluoroalkyl substances (PFASs) [2].

These molecules are a wide range of synthetic organofluorine compounds which have been used commonly in the industry [8]. They are a diverse group of compounds with high thermal, chemical, and biological inertness [9,10]. PFASs remain stable in the presence of acids, bases, oxidants, and reductants. Furthermore, they exhibit high resistance to degradation through photolytic or metabolic processes and microbial decomposition. Nevertheless, their widespread use has led to the contamination of the environment, which, as a consequence, has led to the exposure of these compounds in humans and animals [8,11]. They are a group of organofluorine compounds, aliphatic hydrocarbons, in which all or almost all hydrogen atoms are replaced with fluorine. They consist of a hydrophobic alkyl chain of varying lengths (typically C4 to C16) and a hydrophilic end group, which may be fully or partially fluorinated. PFASs are classified as persistent and bioaccumulative substances [12]. PFAAs are ubiquitous in various environmental media and are distributed globally. Due to their ability to migrate, they can be transferred from water to soils, taken up by plants, and thus enter the food chain. These substances enter the human body through the digestive and respiratory systems, as well as through the skin. Moreover, they are not metabolized and accumulate in the body [13]. Furthermore, direct and indirect contact with PFAS-containing materials such as oil- and water-resistant materials, detergents, paints, and fabrics causes a high exposure of humans to their toxic properties [10]. In living organisms, high absorption levels and low elimination rates of PFASs have been observed [14].

Researchers confirmed that PFASs can be present in human and animal tissues, and in blood (serum or plasma). Studies indicated that anionic PFASs were detected primarily in the human plasma/serum [15]. The biomonitoring of PFASs in the human body started in 2000. Many PFASs have been detected in human matrices, most commonly in blood samples [16,17]. In recent years, a number of papers have confirmed the occurrence of these compounds in human blood (both in serum and plasma), as well as in the umbilical cord and maternal blood [8,17–23]. In addition to blood, some PFASs have also been found in other human tissues. PFASs were predominantly found in the liver [24,25]. Furthermore, studies show some accumulation potential in the lungs, kidneys, bones, and the brain [26]. Numerous recent studies have confirmed their presence in seminal plasma [27], the breast milk [28] of lactating mothers, and umbilical cord blood, all drawing attention to their influence on the human reproductive system. However, in contrast to most other persistent organic pollutants (POPs), they do not tend to accumulate in fat tissues but bind to serum albumin and other cytosolic proteins and accumulate mainly in the liver, the kidneys, and in bile secretion [26,29]. In addition, positive associations were observed between levels of PFOS and PFOA detected in the serum, and total cholesterol, low-density lipoprotein cholesterol, and thyroxine and thyroid hormone concentrations [30,31].

In conjunction with the bioaccumulation and biomagnification potential of PFASs, these long half-lives can give rise to various processes within the living cell and lead to concern over their potential hazard to human health. Because of their capacity to modify surface properties, even at the molecular level, it is essential to elucidate their toxicity and toxicokinetic activity [32]. Both PFOA and PFOS have shown moderate acute toxicity via ingestion. The oral LD50 levels assessed for PFOS were 230 and 270 mg kg^{-1} bw for male and female rats, respectively [33]. In contrast to PFOS, PFOA is moderately toxic. The LD50 value in rats ranged from 430 to 680 mg kg^{-1} bw [34]. The suspected toxic effects of PFASs include the following: liver toxicity, including liver hypertrophy; liver cancer; disruption of lipid metabolism due to their effect on serum cholesterol and triglyceride levels; function of the immune system, causing atrophy of the thymus and spleen or suppressed antibody responses; function of the endocrine system due to their effects on thyroid hormone levels (triiodothyronine (T3) and thyroxine (T4)); induction of adverse neurobehavioral reactions; tumor formation; prenatal and neonatal toxicity; decreased birth weight and size; and even obesity [16,35–46]. Several studies cover the putative modes of action of PFASs on

a cellular level, but these mechanisms still need to be fully defined. Nevertheless, due to the structural similarities of PFASs to endogenous fatty acids, these reactions can be partly attributed to their morphology, and more precisely to activity resulting from their chemical structure. PFASs are characterized by the high tendency to noncovalent, intracellular binding to β-lipoproteins, albumin, and other plasma proteins, such as fatty acid-binding protein (L-FABP) [25]. The proliferation of peroxisomes is one of the main reasons for liver toxicity observed in laboratory animal studies.

PFASs are extensively applied in various industrial and consumer goods. Fluorosurfactants are more effective and efficient in surface activity than their hydrogenated analogues. These and other properties, such as high thermal, chemical, and biological stabilities, make PFASs a perfect material for industrial and domestic applications [47,48]. Typical applications encompass the automotive and aviation industries (hydraulic fluids, low-friction bearings and seals, and materials for car interiors), construction technology (paints and coating additives and glues), biocides (herbicides and pesticides), electronics (flame retardants, weather resistant coatings, and insulators), household products (wetting and cleaning agents, nonstick coatings, and components of cosmetic formulations), medical articles (stain and water repellents in surgical equipment, raw materials for implants), and packaging materials (oil and grease repellent materials) and textiles (impregnating agents for fabrics, leather, and breathable membranes) [10,49,50].

Due to the presence of PFAAs in ambient air, various consumer products, drinking water, and food, it has become necessary to assess their potential impact on human health accurately. Researchers have reviewed the occurrence of highly fluorinated compounds in human matrices in recent years, and there is indisputable evidence that their bioaccumulation potential in tissues is high [51,52]. However, there is uncertainty regarding the accumulation processes themselves and the acute or chronic toxicity effects due to variations in observed toxic response to PFAAs between species and genders within tested species. Considering all the aspects, this study aimed to determine the perfluoroalkyl substances' content in fermented red beetroot juice and human body fluids (blood plasma and urine) before and after intake of this product. The novelty of the work lies in linking dietary exposure to PFASs and blood parameters, bringing a new perspective to our understanding of these compounds. In this study, we wanted to observe whether, apart from compounds with beneficial properties for health, this product is a source of toxic substances and whether they can affect the biomarkers of the human body. In the case of the effect of the fermentation process on the PFAS content and bioavailability, there is no such scientific data. To our best knowledge, this paper is the first detailed and cross-sectional investigation of selected perfluoroalkyl substances in human body fluids after exposure to fermented red beetroot juice.

2. Results and Discussion

2.1. Perfluoroalkyl Substances Content

The content of perfluoroalkyl substances was tested in fermented red beetroot juice and the human body fluids (blood plasma and urine) of volunteers before and after the intake of these products (Table 1). In urine samples, the PFOA was the only perfluoroalkyl substance found in trace amounts (<LOQ). This confirms the information found in the literature, i.e., that these compounds metabolize very poorly, and thus they are excreted from the human body very poorly; they only accumulate in it, which makes them even more dangerous [13]. For PFASs, a high absorption level is observed with a low elimination rate of the substance [14]. Available epidemiological studies support an association between exposure to certain PFASs and various health outcomes, including altered immune and thyroid function, liver disease, lipid and insulin dysregulation, kidney disease, adverse reproductive and developmental effects, and cancer [53].

Table 1. PFASs detected in fermented red beetroot juice and the urine and blood plasma of volunteers.

No.	Compounds	R_t (min)	$[M]^-$ (*m*/*z*)	MS/MS (*m*/*z*)	Sample
		Perfluorocarboxilic acids			
1	PFOA	2.02	413	369	J, B, U
2	PFNA	2.43	463	419	B
3	PFDA	2.86	513	469	B
		Perfluoroalkane sulfonates			
4	PFOS	2.97	499	80	B
5	PFHS	2.11	399	80	B

R_t—retention time; J—red beetroot juice; B—blood plasma; U—urine.

In the tested fermented red beetroot juice, among the analyzed PFASs, only the most common perfluoroalkyl substance apart from the PFOS, i.e., the PFOA, was identified, the content of which was 0.099 ± 0.07 ng/mL. There are many scientific articles about fermented red beetroot juice. They concern the range of volatile or bioactive compounds of the polyphenols and red and yellow betalains. Still, none relate to the contained contaminants, in particular perfluoroalkyl substances. To the best of our knowledge, this paper is the first detailed and cross-sectional investigation of selected perfluoroalkyl substances in human bodily fluids after exposure to fermented red beetroot juice. Likewise, with red beetroot, recent modern studies have shown a variety of health benefits from it and its active compounds, and betalains (also betanin) having antioxidative, anti-inflammation, anticancer, blood pressure and lipid lowering, and also antidiabetic and anti-obesity effects. Still, it is hard to find information about its contamination, especially with PFASs. In her study, Sznajder-Karatzyńska et al. [2] investigated 55 samples of locally grown and imported fruits and vegetables. Among other things, they determined the content of 10 PFASs in red beetroot. In this case, the only identified PFAS was PFOA, and its content ranged from 0.050 to 0.090 (ng g^{-1} ww). For beetroot, the frequency of its occurrence was 100%. There is no possibility of comparing these data with the limits provided by the relevant agencies because they have not been established and do not exist. On 26 August 2022, the Commission Recommendation (EU) 2022/1431 on monitoring the presence of perfluoroalkyl substances in food was issued. Also, Herzke et al. [54] studied the contamination of vegetables by PFASs and reported that perfluorocarboxylic acids were the most frequently detected substances, with PFOA as the most abundant group. Its concentration was found to be between 0.008 and 0.121 ng g^{-1} of fresh weight. These findings are in agreement with our study.

In the case of the volunteers' blood plasma collected before and after intake of the fermented red beetroot juice, no statistical difference was observed in the median value of the content of perfluoroalkyl acids (Table 2). Among the twenty-four volunteers tested, an upward trend in the PFOA content was observed for five people. A downward trend in the median value was observed for the other identified perfluorocarboxylic acids, PFDA and PFNA (Table 2). And for individual results, in the case of PFNA and 10 volunteers, there was a statistically significant decrease in the analyte content in the tested blood plasma samples, and for PFDA in as many as 14. The sum of the determined acids also showed a statistically significant downward trend (Table 2), which can be explained by the fact that, excluding the consumption of certain products (which was required by the assumptions of the experiment), the supply of perfluoroalkyl acids was limited. These compounds are found in significant amounts in packaging dedicated to food storage [31], thus finding their way into the human body. Reducing the consumption of processed food thus resulted in a decrease in the supply of these specific compounds in the diet.

Table 2. Blood plasma profile of PFASs in volunteers before (T0) and after (T1) intake of fermented red beetroot juice. Values are expressed in ng/mL and are presented as median (P25–P75).

No.	Compounds	Blood Plasma Samples		*p* T0 vs. T1
		T0	T1	
		Acids		
1	PFOA	0.94 (0.76–1.56)	0.93 (0.77–1.52)	0.627
2	PFNA	0.39 (0.26–0.58)	0.34 (0.23–0.58)	<0.001 **
3	PFDA	0.30 (0.20–0.46)	0.23 (0.17–0.38)	<0.001 **
Total acids		1.65 (1.29–2.94)	1.49 (1.19–2.64)	0.009 **
		Sulfonates		
4	PFOS	0.59 (0.44–0.80)	0.71 (0.53–0.96)	<0.001 **
5	PFHS	0.11 (0.09–0.17)	0.25 (0.15–0.37)	<0.001 **
Total sulfonates		0.67 (0.53–0.92)	0.96 (0.68–1.37)	<0.001 **
Total of PFASs		2.66 (1.90–4.47)	2.62 (2.08–4.17)	0.031 *

* $p < 0.05$; ** $p < 0.01$.

In the case of the determined perfluoroalkane sulfonates, a statistically significant upward trend was observed ($p < 0.01$). Such a situation took place both for individually identified compounds, i.e., PFOS (14 volunteers) and PFHS (22 volunteers), and for their sum (Table 2). This slight but statistically significant increase could have been caused by the supply of other food products consumed by the volunteers.

2.2. Blood Parameters

To the best of the authors' knowledge, this study is the first to show the effect of a six-week intake of fermented beetroot juice on the twelve hematology and five blood biochemistry parameters.

The blood parameter values before and after the intervention are presented in Table 3. The analysis of the hematology parameters indicated that the intake of the fermented beetroot juice showed a significant decrease in MCV, platelets concentration, MPV, P-LCR at the significance level $p < 0.01$, and hematocrit ($p < 0.05$). On the other hand, the dietary intervention also indicated a significant ($p < 0.01$) increase in corpuscular/cellular hemoglobin concentration (MCHC). In the case of blood biochemistry, no significant change in blood samples after intake of the fermented beetroot juice was observed (Table 3). However, a decreasing tendency of total cholesterol and LDL-C concentration was observed. Previously published data showed an ambiguous influence of red beet products on blood parameters.

Nevertheless, the previous studies investigated only the three blood parameters: total cholesterol, LDL-C, and HDL-C [55,56]. The study by de Castro et al. [57], conducted on volunteers (n = 36) with overweight/obesity and dyslipidemia who consumed freeze-dried red beet leaves (2.5 g/day) for four weeks, showed a significant reduction in LDL. However, in our study, as mentioned above, the concentration of LDL showed only a decreased tendency. Also, no statistical difference in the total cholesterol concentration before and after the intervention was observed in the cited study. In turn, the study by Asgary et al. [58], conducted on 24 subjects, showed a significant reduction in total cholesterol and LDL-C after the consumption of raw beetroot juice (250 mL/day) for two weeks.

On the other hand, Asgary et al. [58] noticed no significant changes in the case of these same parameters (total cholesterol and LDL-C) after the intake of cooked beetroots (250 mg/day). The blood parameters may affect the red beet product (food matrix) type, dose, and intervention time. It should be mentioned that beetroot is rich in several bioactive compounds, i.e., betalains, phenolics, carotenoids, minerals, and vitamins [55], which may affect the blood parameters tested. The dominant substances present in beetroot products are betalains. Betalains are characterized by a strong antioxidant effect, which results from the structure of their molecule. Therefore, it is primarily thanks to these compounds that beetroot is among the ten vegetables with the strongest antioxidant properties [56]. Previous

studies indicate that the consumption of betalains has many positive aspects, including inhibiting lipid peroxidation, having a protective effect on red blood cells, preventing oxidative hemolysis, and having anti-carcinogenic properties [59].

Table 3. Descriptive statistics for blood parameters before (T0) and after (T1) consuming fermented red beet juice, expressed as median (P25–P75).

Blood Parameters	Samples		*p* T0 vs. T1
	T0	T1	
Hematology			
Leukocytes [k/μL]	5.2 (4.9–6.0)	5.1 (4.6–5.8)	0.961
Erythrocytes [mln/μL]	4.6 (4.3–5.1)	4.7 (4.3–4.9)	0.246
Hemoglobin [g/dL]	13.2 (12.9–14.7)	13.6 (12.7–14.1)	0.721
Hematocrit [%]	41.0 (39.0–45.0)	40.0 (37.0–42.0)	0.013 *
MCV [fl]	88.0 (85.0–92.0)	87.0 (84.0–90.0)	0.001 **
MCH [pg]	29.0 (28.0–30.0)	29.0 (28.0–31.0)	0.686
MCHC [g/dL]	32.9 (32.3–33.5)	33.4 (33.1–34.2)	<0.001 **
RDW–CV [%]	13.0 (12.0–14.0)	13.0 (12.0–13.0)	0.208
Platelets [k/μL]	273.0 (215.0–318.0)	262.0 (202.0–299.0)	0.002 **
PDW [fl]	14.0 (13.0–15.0)	14.0 (12.0–15.0)	0.083
MPV [fl]	11.2 (10.7–11.9)	10.9 (10.4–11.7)	<0.001 **
P–LCR [%]	34.0 (29.0–38.0)	32.0 (28.0–38.0)	<0.001 **
Blood biochemistry			
Total–C [mg/dL]	184.0 (165.0–197.0)	168.0 (155.0–194.0)	0.074
HDL–C [mg/dL]	69.0 (64.0–86.0)	73.0 (57.0–88.0)	0.897
LDL–C [mg/dL]	80.6 (64.8–109.8)	76.4 (66.4–98.4)	0.128
Triglycerides [mg/dL]	80.0 (48.0–102.0)	71.0 (58.0–81.0)	0.412
Glycated hemoglobin [%]	5.2 (5.0–5.3)	5.2 (5.1–5.3)	0.877

MCV—mean corpuscular volume; MCH—mean corpuscular hemoglobin; MCHC—mean corpuscular/cellular hemoglobin concentration; RDW-CV—red cell distribution width; PDW—platelet distribution width; MPV—mean platelet volume; P-LCR—platelet large cell ratio; Total-C—total cholesterol; HDL—high density lipoprotein; LDL—low density lipoprotein; * $p < 0.05$; ** $p < 0.01$.

Changes in blood parameters may signal adverse health effects caused by, e.g., nutritional intervention. One of the blood parameters that showed a decrease after the consumption of fermented beetroot juice was MCV. MCV is routinely measured in blood tests and is generally used to help classify the cause of anemia [60]. We observed that platelet-related parameters, such as platelet count, MPV, and P-LCR, decreased in blood samples analyzed after nutritional intervention. Generally, the platelet count determines the bleeding risk and monitors thrombopoiesis [61]. Moreover, increasing evidence describes the important role of platelets in physiological processes such as immune response, angiogenesis, and fibrosis formation [61,62]. This suggests that platelets independently influence morbidity and mortality, rather than merely reflecting underlying disease. An abnormal platelet count indicates poor prognosis in some patient groups, including in cancer and in critically ill patients [61,63,64].

The correlations between the individual PFAS compounds, total perfluorocarboxilic acids, perfluoroalkane sulfonates and PFASs and blood parameters are presented in Figure 1. Before intervention, moderate positive correlations ($0.3 \leq r < 0.5$) were observed between PFHS and erythrocytes, hemoglobin, and hematocrit. Also, a moderate positive correlation was calculated between total perfluoroalkane sulfonates and erythrocytes. A good negative correlation (0.5 to <0.7) was observed between RDW-CV and PFOA, while moderate negative correlations were determined between RDW-CV and PFNA, total perfluorocarboxilic acids, and total PFASs. Additionally, moderate positive correlations were observed between glycated hemoglobin, PFOS, PFHS, and total perfluoroalkane sulfonates. Moreover, before the intervention, a positive tendency was observed between PFOS and erythrocytes and LDL-C and between total perfluoroalkane sulfonates and hemoglobin, hematocrit, and LDL-C. A negative trend was found between total perfluoroalkane sulfonates and

HDL-C. On the other hand, after diet intervention, a moderate negative correlation was only observed between cholesterol HDL and PFHS (Figure 1). A negative tendency was observed between PFOS, total perfluoroalkane sulfonates, and HDL-C. Moreover, a positive tendency was noticed after the intake of the fermented beetroot juice between PFOS, total perfluoroalkane sulfonates and erythrocytes and total PFAs and hemoglobin.

A

Compounds	leukocytes	erythrocytes	hemoglobin	hematocrit	MCV	MCH	MCHC	platelets	RDW-CV	PDW	MPV	P-LCR	Total-C	HDL-C	LDL-C	triglycerides	glycated hemoglobin
PFOA	-0.06	0.07	0.19	0.21	0.27	0.24	0.01	-0.22	-0.53*	0.02	-0.06	-0.03	-0.30	-0.04	-0.25	-0.01	0.08
PFNA	0.02	-0.02	0.13	0.11	0.29	0.27	0.11	-0.22	-0.42*	0.05	0.08	0.11	-0.21	-0.13	-0.13	0.05	0.17
PFDA	-0.13	-0.21	-0.05	-0.07	0.33	0.29	0.07	-0.28	-0.35	0.08	0.11	0.14	-0.28	0.01	-0.24	-0.05	-0.01
Total acids	-0.07	-0.02	0.12	0.13	0.30	0.27	0.05	-0.25	-0.48*	0.04	0.01	0.04	-0.29	-0.05	-0.23	-0.01	0.08
PFOS	0.06	0.40	0.34	0.34	-0.14	-0.11	0.06	-0.12	-0.07	0.00	0.02	0.02	0.21	-0.35	0.41	0.06	0.49*
PFHS	0.15	0.47*	0.46*	0.46*	-0.08	0.02	0.09	-0.06	-0.19	0.07	0.07	0.06	0.01	-0.34	0.21	0.08	0.43*
Total sulfonates	0.07	0.42*	0.36	0.36	-0.14	-0.10	0.06	-0.11	-0.08	0.01	0.03	0.03	0.19	-0.36	0.40	0.07	0.49*
Total PFASs	-0.02	0.20	0.29	0.29	0.17	0.17	0.07	-0.26	-0.43*	0.04	0.02	0.05	-0.14	-0.23	0.02	0.03	0.33

B

Compounds	leukocytes	erythrocytes	hemoglobin	hematocrit	MCV	MCH	MCHC	platelets	RDW-CV	PDW	MPV	P-LCR	Total-C	HDL-C	LDL-C	triglycerides	glycated hemoglobin
PFOA	-0.12	0.19	0.31	0.24	0.21	0.16	-0.01	-0.17	-0.32	-0.13	-0.13	-0.21	-0.08	0.11	-0.20	0.02	0.03
PFNA	-0.05	0.10	0.27	0.09	0.22	0.21	0.09	-0.27	-0.17	0.01	0.02	-0.02	-0.13	0.01	-0.16	0.03	0.07
PFDA	-0.15	-0.06	0.12	0.05	0.23	0.24	0.12	-0.29	-0.20	0.10	0.08	0.02	-0.02	0.17	-0.14	-0.06	0.05
Total acids	-0.12	0.12	0.27	0.18	0.23	0.20	0.04	-0.23	-0.27	-0.05	-0.05	-0.12	-0.08	0.11	-0.18	0.00	0.04
PFOS	0.08	0.37	0.29	0.01	-0.08	-0.08	0.02	-0.12	0.27	-0.08	-0.01	0.04	-0.07	-0.37	0.19	0.13	0.12
PFHS	-0.11	0.23	0.14	0.20	-0.17	-0.08	0.09	-0.11	0.30	-0.02	0.05	0.13	-0.08	-0.43*	0.31	-0.04	0.19
Total sulfonates	0.05	0.37	0.28	0.04	-0.10	-0.09	0.03	-0.13	0.29	-0.08	0.00	0.06	-0.08	-0.40	0.22	0.11	0.13
Total PFASs	-0.06	0.31	0.39	0.16	0.12	0.10	0.05	-0.26	-0.05	-0.09	-0.04	-0.06	-0.11	-0.15	-0.02	0.07	0.12

r ≥ -1 -0.80 -0.60 -0.40 -0.20 0 0.20 0.40 0.60 0.80 1

Figure 1. Correlation heat map between individual compounds, total acids, sulfates and PFASs and blood parameters before (**A**) and after (**B**) intake of fermented red beetroot juice. (*)—Significant correlation, ($p < 0.05$).

However, some limitations of the study should be taken into account. First, the lack of control over food intake and potential sources of PFASs. Second, we assessed blood parameters on two points that may not account for intra-individual variability in blood parameters. Also, the number of participants participating in the study was relatively small, and could not show unambiguous statistical differences between individual parameters.

3. Materials and Methods

3.1. The Chemicals, Reagents, and Study Material

Gradient reagents, including methanol, acetonitrile, formic acid, and water, were purchased from Sigma Chemical Co. (St. Louis, MO, USA). A native standard mixture of PFASs containing seven perfluorocarboxylic acids (PFCAs) such as perfluorobutanoic acid (PFBA), perfluoropentanoic acid (PFPeA), perfluorohexanoic acid (PFHxA), perfluoroheptanoic acid (PFHpA), perfluorooctanoic acid (PFOA), perfluorononanoic acid (PFNA), and perfluorodecanoic acid (PFDA) and three perfluoroalkane sulfonates (PFSAs), namely perfluorobutane sulfonate (PFBS), perfluorohexane sulfonate (PFHxS), and perfluorooctane sulfonate (PFOS) prepared in methanol, with a chemical purity of >98% each, were purchased from Wellington Laboratories, Inc. (Guelph, ON, Canada). The isotopically labelled internal standards (ISs), perfluoro-n-[13C8] octanoic acid (13C8-PFOA) in methanol, with chemical purity of >98%, and sodium perfluoro-1-[13C8] octane sulfonate (13C8-PFOS) in methanol, with chemical purity of >98%, were obtained from Wellington Laboratories, Inc. (Guelph, ON, Canada). Auxiliary equipment such as an MPW-351R Centrifuge (MPW Med. Instruments, Warsaw, Poland), Vacuum Concentrator Plus (Eppendorf AG, Hamburg, Germany) and ultrasonicator were used for sample preparation.

Stock, intermediate, and working standard solutions of native PFASs and internal standards (13C8-PFOA and 13C8-PFOS named IS1 and IS2, respectively) were prepared in MeCN. Intermediate and working standard solutions of native PFASs with concentrations of 100 ng/mL and 1 ng/mL, respectively, were prepared by diluting the standards with a mixture of 20% MeOH in water (v/v) with the addition of 1% (v/v) of FA. Internal standard solutions were prepared according to the above procedure.

Fermented red beetroot juice was custom-prepared by a fruit and vegetable processing company in Poland.

3.2. Characteristic of Participants and Study Design

The subjects who met the inclusion criteria (body mass index (BMI) under 30; without gastrointestinal disturbances, including gastric and duodenal ulcers; and they could not have participated in other clinical trials within 90 days before the survey, take drugs, abuse alcohol, be pregnant and breast-feeding, or take any medications or vitamin supplements) and were certified healthy at a medical interview were accepted to the study. Ultimately, 24 healthy subjects, 5 males and 19 females, aged between 24 and 40, participated in the experiment (Table 4).

Table 4. Anthropometric parameters and demographic characteristics of the sample (% or mean and standard deviation, SD).

Characteristics	Total
Sample size	24
Sample percentage	100.0
Age (years), mean (SD)	29.5 (3.6)
Gender, n (%)	
Women	19 (79.2)
Men	5 (20.8)
BMI (kg/m^2), mean (SD)	24.9 (1.8)
Residence, n (%)	
Urban	17 (70.8)
Rural	7 (29.2)

The study was conducted for 6 weeks (42 days). For 42 days, once a day, volunteers consumed a dose of the fermented beetroot juice (200 mL/60 kg of body weight) directly after breakfast. Every 7 days, the health status of all volunteers was assessed by the doctor, and they received fermented beetroot juice for the next week. Under fasting conditions, before consumption (sample zero), and at the end of the experiment, the blood samples were taken into heparinized vacutainers and then centrifuged (1000× *g*, 10 min, 4 °C). According to the above sampling scheme (0 and 42 days), urine samples were collected from the volunteers. After that, the separated plasma and collected urine were frozen and stored at 80 °C until analysis. The study design is presented in Figure 2.

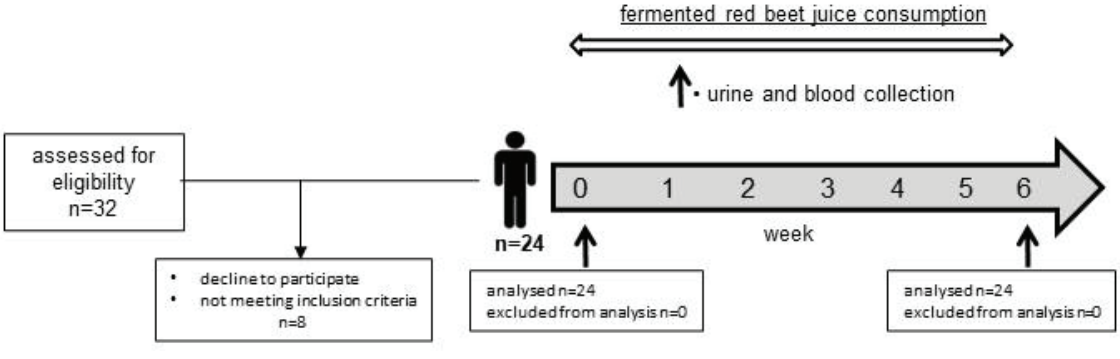

Figure 2. Flow diagram of participant recruitment during the study.

3.3. Ethical Aspects

The experimental design and procedure were accepted by the Bioethical Committee at the Faculty of Medical Science of the University of Warmia and Mazury in Olsztyn (Poland, No. 7/2015). All volunteers were fully informed about the potential benefits and risks

and signed an informed consent form. Moreover, the study was conducted under medical supervision in the NZOZ Atarax Clinic in Olsztyn, Poland.

3.4. Plasma and Urine Samples Preparation

The perfluoroalkyl substances content was determined in the plasma and urine samples. The plasma samples were prepared according to Rotander et al. [65]. Briefly, 200 μL of plasma with 4 μL of ISs solution (2.5 μg mL/1) was extracted with 1.5 mL 100% acetonitrile (MeCN) using ultrasonication followed by vortex extraction, centrifugation and evaporation to dryness in a vacuum concentrator. The residue was reconstituted with 100 μL of MeOH. Before the micro-HPLC-MS/MS analysis, samples were diluted fivefold in deionised water with 1% (*v*/*v*) of FA addition to the final volume of 500 μL. The same analytical procedure was applied to blank samples. Each sample for the assay was prepared in triplicate.

The urine samples were prepared according to Perez et al. [66]. Briefly, 500 μL of urine with 3.2 μL of ISs solution (2.5 μg mL/1) was mixed. The precipitation of traces of protein was induced by mixing the samples with acetonitrile (1:1). After centrifugation at 4000 rpm for 10 min, 400 μL of the supernatant was transferred to a PP tube and evaporation to dryness in a vacuum concentrator. The residue was reconstituted with 80 μL of MeOH. Before the micro-HPLC-MS/MS analysis, samples were diluted fivefold in deionised water with 1% (*v*/*v*) of FA addition to the final volume of 400 μL. The same analytical procedure was applied to blank samples. Each sample for the assay was prepared in triplicate.

3.5. Instrumental Analysis

The investigated substances were analyzed using micro-HPLC/MS/MS with the negative ion electrospray ionization (ESI) and Multiple Reaction Monitoring (MRM) mode. Chromatographic separation was carried out using an Eksigent LC200 System (AB SCIEX, Concord, ON, Canada). The column used was a HALO C18 column 50 mm × 0.5 mm × 2.7 μm (Eksigent, Concord, ON, Canada), and the thermostat was set at the temperature of 45 °C with the mobile phase flow rate of 20 μL/min. A binary gradient consisting of water (A) and MeCN (B) (both with 0.1% FA) was applied. The gradient was set as follows: 40% B (0–0.5 min), 40–90% B (0.5–3.0 min), 90% B (3.0–4.0 min), 90–40% B (4.0–4.2 min), and 40% B (4.2–5.0 min). The injection volume was 5 μL. The autosampler temperature was set at 40 °C. The mass spectrometer used was QTRAP 5500 with ESI (AB SCIEX, Concord, ON, Canada). The optimal sensitivity for the investigated PFASs was obtained under the following settings: curtain gas flow, 25 L/min; collision gas flow, 9 L/min; ion spray voltage, −4500 V; temperature, 350 °C; 1 ion source gas flow, 30 L/min; 2 ion source gas flow, 35 L/min; declustering potential range, −30 to −85 V; entrance potential, −10 V; collision energy range, −10 to −65 eV; and collision cell exit potential range, −10 to −38 V [67]. Quantitative analyses were performed using the multiple reaction monitoring (MRM) mode. Data analysis was carried out with Analyst Software (AB SCIEX, Concord, ON, Canada) (version 1.5.2).

3.6. Analysis of Blood Parameters

The analysis of blood samples was conducted by the Medical Diagnostic Laboratory of the Provincial Specialist Hospital in Olsztyn, Poland. The blood hematology parameters included leukocytes, erythrocytes, hemoglobin, platelets, hematocrit, mean corpuscular volume (MCV), mean corpuscular hemoglobin (MCH), mean corpuscular/cellular hemoglobin concentration (MCHC), red cell distribution width (RDW-CV), platelet distribution width (PDW), mean platelet volume (MPV), and platelet large cell ratio (P-LCR), and blood biochemistry parameters were also measured, which included lipid profile (total cholesterol, triglycerides, high-density lipoprotein (HDL), low-density lipoprotein (LDL)) and glycated hemoglobin.

3.7. Statistical Analyses

Statistical analyses were performed using Statistica software (v. 13, StatSoft, Tulsa, OK, USA). The normal distribution of the data was evaluated using a Shapiro–Wilk W test. The tested groups showed a non-normal distribution, and therefore quantitative variables were expressed as median (P25-P75). Comparisons within the groups, between the baseline and after the exposure to the fermented red beetroot juice, were performed using Wilcoxon signed-rank tests. Correlations between the concentration of individual PFASs, total acids, total sulfonates, total PFASs, and blood parameters (leukocytes, erythrocytes, hemoglobin, hematocrit, MCV, MCH, MCHC, platelets, RDW-CV, PDW, MPV, P-LCR, total cholesterol, cholesterol HDL, cholesterol LDL, triglycerides, glycated hemoglobin) were analyzed using a Pearson correlation coefficient test. Statistical significance thresholds were set at $p < 0.05$ (*) and $p < 0.01$ (**). The strength of the correlation was described as fair (<0.3), moderate (0.3 to <0.5), good (0.5 to <0.7), or very good ($\geq$0.7) [68].

4. Conclusions

This was the first time this type of experiment has been carried out, and although we cannot draw clear conclusions regarding the increase in the content of perfluoroalkyl substances in human bodily fluids due to the consumption of food contaminated with them, it proves that such research is necessary and should be continued. In the case of perfluorocarboxylic acids, a downward trend was observed, while perfluoroalkane sulfonates' plasma content showed a statistically significant upward trend. This confirms previous scientific data showing that these compounds metabolize very poorly; therefore, they are very poorly excreted from the human body—they only accumulate in it, which makes them even more dangerous for the consumer. On the other hand, it has been observed that fermented red beetroot juice can affect blood parameters. The effect of beetroot products depends on the type of food matrix, dose, and time of intervention. It is worth mentioning that beetroot is rich in several bioactive compounds (betalains, phenols, carotenoids, minerals, and vitamins) that can have a synergistic effect on the blood parameters tested.

More research is needed to determine the sources and impact of PFASs on consumer health. Ongoing research is critical to developing future strategies to control consumer exposure to PFASs and points to areas for the further improvement of multidisciplinary collaboration.

While preliminary, our study is among the first to explore the correlation between PFAS consumption and its potential accumulation in bodily fluids, highlighting an understudied area of consumer health.

Author Contributions: Conceptualization, M.S. and W.W.; methodology, M.S. and W.W.; formal analysis, M.S. and T.S.; investigation, M.S., W.W. and T.S.; resources, M.P. and W.W.; data curation, M.S.; writing—original draft preparation, M.S. and T.S.; writing—review and editing, M.P. and W.W.; visualization, T.S.; supervision, M.P.; project administration, W.W. and M.P.; funding acquisition, M.P. and W.W. All authors have read and agreed to the published version of the manuscript.

Funding: Institute of Animal Reproduction and Food Research Polish Academy of Science in Olsztyn project grants under the statutory subsidy—GW3.

Institutional Review Board Statement: The study was conducted in accordance with the Declaration of Helsinki, and approved by the Institutional Review Board (or Ethics Committee) of Bioethical Committee at the Faculty of Medical Science of the University of Warmia and Mazury in Olsztyn (Poland, No. 7/2015).

Informed Consent Statement: Not applicable.

Data Availability Statement: The datasets used and/or analyzed during the current study are available from the corresponding author upon reasonable request.

Acknowledgments: This work was supported by Institute of Animal Reproduction and Food Research Polish Academy of Science in Olsztyn project grants under the statutory subsidy—GW3, The impact of the consumption of food phytochemicals on the metabolomic profile of consumers.

Conflicts of Interest: The authors declare no conflict of interest.

References

1. Ellegrad, L.H.; Andersson, S.W.; Normen, A.L.; Andersson, H.A. Dietary plants sterols and cholesterol metabolism. *Nutr. Rev.* **2007**, *65*, 39–45. [CrossRef]
2. Sznajder-Katarzyńska, K.; Surma, M.; Cieślik, E.; Wiczkowski, W. The perfluoroalkyl substances (PFASs) contamination of fruits and vegetables. *Food Addit. Contam. Part A* **2018**, *35*, 1776–1786. [CrossRef] [PubMed]
3. Bradbury, K.E.; Appleby, P.N.; Key, T.J. Fruit, vegetable, and fiber intake in relation to cancer risk: Findings from the European Prospective Investigation into Cancer and Nutrition. *Am. J. Clin. Nutr.* **2014**, *100*, 394S–398S. [CrossRef] [PubMed]
4. Farvid, M.S.; Chen, W.Y.; Rosner, B.A.; Rulla, M.T.; Willett, W.C.; Eliassen, A.H. Fruit and vegetable consumption and breast cancer incidence: Repeated measures over 30 years of follow-up. *Int. J. Cancer* **2018**, *144*, 1496–1510. [CrossRef] [PubMed]
5. Zhan, J.; Liu, Y.J.; Cai, L.B.; Xu, F.-R.; Xie, T.; He, Q.-Q. Fruit and vegetable consumption and risk of cardiovascular disease: A meta-analysis of prospective cohort studies. *Crit. Rev. Food Sci. Nutr.* **2017**, *57*, 1650–1663. [CrossRef] [PubMed]
6. Płatosz, N.; Sawicki, T.; Wiczkowski, W. Profle of phenolic acids and flavonoids of red beet and its fermentation products. Does long-term consumption of fermented beetroot juice affect phenolics profle in human blood plasma and urine? *Polish J. Food Nutr. Sci.* **2020**, *70*, 55–65. [CrossRef]
7. Crawford, N.M.; Fenton, S.E.; Strynar, M.; Hines, E.P.; Pritchard, D.A.; Steiner, A.Z. Effects of perfluorinated chemicals on thyroid function, markers of ovarian reserve, and natural fertility. *Reprod. Toxicol.* **2017**, *69*, 53–59. [CrossRef] [PubMed]
8. Poothong, S.; Thomsec, C.; Padilla-Sanchez, J.A.; Papadopoulou, E.; Haug, L.S. Distribution of novel and well-know poly-and perfluoroalkyl substances (PFASs) in human serum, plasma, and whole blood. *Environ. Sci. Technol.* **2017**, *51*, 13388–13396. [CrossRef]
9. Lindstrom, A.B.; Strynar, M.J.; Libelo, E.L. Polyfluorinated compounds: Past, present, and future. *Environ. Sci. Technol.* **2011**, *45*, 7954–7961. [CrossRef]
10. Krafft, M.P.; Riess, J.G. Per- and polyfluorinated substances (PFASs): Environmental challenges. *Curr. Opin. Colloid Interface Sci.* **2015**, *20*, 192–212. [CrossRef]
11. Sznajder-Katarzyńska, K.; Surma, M.; Cieślik, I. A review of perfluoroalkyl AIDS (PFAAs) in terms of sources, applications, human exposure, dietary intake, toxicity, legal regulation, and methods of determination. *J. Chem.* **2019**, *2019*, 2717528. [CrossRef]
12. Jogsten, I.E.; Perello, G.; Llebaria, X.; Bigas, E.; Marti-Cid, R.; Karrman, A.; Domingo, J.L. Exposure to perfluorinated compounds in Catalonia, Spain, through consumption of various raw and cooked foodstuffs, including packaged food. *Food Chem. Toxicol.* **2009**, *47*, 1577. [CrossRef]
13. Giesy, J.P.; Kannan, K. Peer Reviewed: Perfluorochemical Surfactants in the Environment. *Environ. Sci. Technol.* **2008**, *36*, 146A–152A. [CrossRef] [PubMed]
14. Geueke, B. Dossier—Per- and polyfluoroalkyl substances (PFASs). *Food Packag. Forum* **2016**, 1–13. [CrossRef]
15. Ehresman, D.J.; Froehlich, J.W.; Olsen, G.W.; Chang, S.C.; Butenhoff, J.L. Comparison of human whole blood, plasma, and serum matrices for the determination of perfluorooctanesulfonate (PFOS), perfluorooctanoate (PFOA), and other fluorochemicals. *Environ. Res.* **2007**, *103*, 176–184. [CrossRef] [PubMed]
16. Lau, C.; Anitole, K.; Hodes, C.; Lai, D.; Pfahles-Hutchens, A.; Seed, J. Perfluoroalkyl acids: A review of monitoring and toxicological findings. *Toxicol. Sci.* **2007**, *99*, 366–394. [CrossRef]
17. Góralczyk, K.; Pachocki, K.A.; Hernik, A.; Struciński, P.; Czaja, K.; Lindh, C.H.; Jönsson, B.A.; Lenters, V.; Korcz, W.; Minorczyk, M.; et al. Perfluorinated chemicals in blood serum of inhabitants in central Poland in relation to gender and age. *Sci. Total Environ.* **2015**, *532*, 548–555. [CrossRef]
18. Kannan, K.; Corsolini, S.; Falandysz, J.; Fillmann, G.; Kumar, K.S.; Loganathan, B.G.; Mohd, M.A.; Olivero, J.; Van Wouwe, N.; Yang, J.H.; et al. Perfluorooctanesulfonate and related fluorochemicals in human blood from several countries. *Environ. Sci. Technol.* **2004**, *38*, 4489–4495. [CrossRef]
19. Wu, X.; Bennett, D.H.; Calafat, A.M.; Kato, K.; Strynar, M.; Andersen, E.; Moran, R.E.; Tancredi, D.J.; Tulve, N.S.; Hertz-Picciotto, I. Serum concentrations of perfluorinated compounds (PFC) among selected populations of children and adults in California. *Environ. Res.* **2015**, *136*, 264–273. [CrossRef]
20. Lien, G.-W.; Wen, T.-W.; Hsieh, W.-S.; Wu, K.-Y.; Chen, C.-Y.; Chen, P.-C. Analysis of perfluorinated chemicals in umbilical cord blood by ultra-high performance liquid chromatography/tandem mass spectrometry. *J. Chromatogr. B* **2011**, *879*, 641–646. [CrossRef]
21. Apelberg, B.J.; Witter, F.R.; Herbstman, J.B.; Calafat, A.M.; Halden, R.U.; Needham, L.L.; Goldman, L.R. Cord serum concentrations of perfluorooctane sulfonate (PFOS) and perfluorooctanoate (PFOA) in relation to weight and size at birth. *Environ. Health Perspect.* **2007**, *115*, 1670–1676. [CrossRef] [PubMed]
22. Monroy, R.; Morrison, K.; Teo, K.; Atkinson, S.; Kubwabo, C.; Stewart, B.; Foster, W.G. Serum levels of perfluoroalkyl compounds in human maternal and umbilical cord blood samples. *Environ. Res.* **2008**, *108*, 56–62. [CrossRef]

23. Hanssen, L.; Dudarev, A.A.; Huber, S.; Odland, J.Ř.; Nieboer, E.; Sandanger, T.M. Partition of perfluoroalkyl substances (PFASs) in whole blood and plasma, assessed in maternal and umbilical cord samples from inhabitants of arctic Russia and Uzbekistan. *Sci. Total Environ.* **2013**, *447*, 430–437. [CrossRef]
24. Kärrman, A.; Domingo, J.L.; Llebaria, X.; Nadal, M.; Bigas, E.; van Bavel, B.; Lindström, G. Biomonitoring perfluorinated compounds in Catalonia, Spain: Concentrations and trends in human liver and milk samples. *Environ. Sci. Pollut. Res.* **2010**, *17*, 750–758. [CrossRef]
25. He, J.-L.; Peng, T.; Xie, J.; Dai, H.-H.; Chen, D.-D.; Yue, Z.-F.; Fan, C.-L.; Li, C. Determination of 20 perfluorinated compounds in animal liver by HPLC-MS/MS. *Chin. J. Anal. Chem.* **2015**, *43*, 40–48. [CrossRef]
26. Pérez, F.; Nadal, M.; Navarro-Ortega, A.; Fàbrega, F.; Domingo, J.L.; Barceló, D.; Farré, M. Accumulation of perfluoroalkyl substances in human tissues. *Environ. Int.* **2013**, *59*, 354–362. [CrossRef]
27. Guruge, K.S.; Taniyasu, S.; Yamashita, N.; Wijeratna, S.; Mohotti, K.M.; Seneviratne, H.R.; Kannan, K.; Yamanaka, N.; Miyazaki, S. Perfluorinated organic compounds in human blood serum and seminal plasma: A study of urban and rural tea worker populations in Sri Lanka. *J. Environ. Monit.* **2005**, *7*, 371–377. [CrossRef]
28. Völkel, W.; Genzel-Boroviczény, O.; Demmelmair, H.; Gebauer, C.; Koletzko, B.; Twardella, D.; Raab, U.; Fromme, H. Perfluorooctane sulphonate (PFOS) and perfluorooctanoic acid (PFOA) in human breast milk: Results of a pilot study. *Int. J. Hyg. Environ. Health* **2008**, *211*, 440–446. [CrossRef]
29. Jones, P.D.; Hu, W.; De Coen, W.; Newsted, J.L.; Giesy, J.P. Binding of perfluorinated fatty acids to serum proteins. *Environ. Toxicol. Chem.* **2003**, *22*, 2639–2649. [CrossRef] [PubMed]
30. Frisbee, S.J.; Shankar, A.; Knox, S.; Steenland, K.; Savitz, D.A.; Fletcher, T.; Ducatman, A.M. Perfluorooctanoic acid, perfluorooctanesulfonate, and serum lipids in children and adolescents. *Arch. Pediatr. Adolesc. Med.* **2010**, *164*, 860–869. [CrossRef] [PubMed]
31. Clifford, T.; Howatson, G.; West, D.J.; Stevenson, E.J. The potential benefits of red beetroot supplementation in health and disease. *Nutrients* **2015**, *7*, 2801–2822. [CrossRef] [PubMed]
32. Rainieri, S.; Conlledo, N.; Langerholc, T.; Madorran, E.; Sala, M.; Barranco, A. Toxic effects of perfluorinated compounds at human cellular level and on a model vertebrate. *Food Chem. Toxicol.* **2017**, *104*, 14–25. [CrossRef] [PubMed]
33. Committee on Toxicity of Chemicals in Food, Consumer Products and the Environment (COT) (2006) COT Statement on the Tolerable Daily Intake for Perfluorooctane Sulfonate. COT Statement 2006/09, Committee on Toxicity of Chemicals in Food, London, UK, 2006. Available online: https://cot.food.gov.uk/sites/default/files/cot/cotstatementpfos200609.pdf (accessed on 3 August 2023).
34. Kennedy, G.L.; Butenhoff, J.L.; Olsen, G.W.; O'Connor, J.C.; Seacat, A.M.; Perkins, R.G.; Biegel, L.B.; Murphy, S.R.; Farrar, D.G. The toxicology of perfluorooctanoate. *Crit. Rev. Toxicol.* **2004**, *34*, 351–384. [CrossRef]
35. Seacat, A.M.; Thomford, P.J.; Hansen, K.J.; Olsen, G.W.; Case, M.T.; Butenhoff, J.L. Butenhoff Subchronic toxicity studies on perfluorooctanesulfonate potassium salt in cynomolgus monkeys. *Toxicol. Sci.* **2002**, *68*, 249–264. [CrossRef]
36. Zheng, L.; Dong, G.-H.; Jin, Y.-H.; He, Q.-C. Immunotoxic changes associated with a 7-day oral exposure to perfluorooctanesulfonate (PFOS) in adult male C57BL/6 mice. *Arch. Toxicol.* **2009**, *83*, 679–689. [CrossRef]
37. Benninghoff, A.D.; Orner, G.A.; Buchner, C.H.; Hendricks, J.D.; Duffy, A.M.; Williams, D.E. Promotion of hepatocarcinogenesis by perfluoroalkyl acids in rainbow trout. *Toxicol. Sci.* **2012**, *125*, 69–78. [CrossRef] [PubMed]
38. Nelson, J.W.; Hatch, E.E.; Webster, T.F. Exposure to polyfluoroalkyl chemicals and cholesterol, body weight, and insulin resistance in the general U.S. population. *Environ. Health Perspect.* **2010**, *118*, 197–202. [CrossRef]
39. DeWitt, J.C.; Peden-Adams, M.M.; Keller, J.M.; Germolec, D.R. Immunotoxicity of perfluorinated compounds: Recent developments. *Toxicol. Pathol.* **2012**, *40*, 300–311. [CrossRef]
40. Qazi, M.R.; Xia, Z.; Bogdanska, J.; Chang, S.C.; Ehresman, D.J.; Butenhoff, J.L.; Nelson, B.D.; DePierre, J.W.; Abedi-Valugerdi, M. The atrophy and changes in the cellular compositions of the thymus and spleen observed in mice subjected to short-term exposure to perfluorooctanesulfonate are high-dose phenomena mediated in part by peroxisome proliferator-activated receptoralpha (PPARα). *Toxicology* **2009**, *260*, 68–76. [CrossRef]
41. Grandjean, P.; Andersen, E.W.; Budtz-Jørgensen, E.; Nielsen, F.; Mølbak, K.; Weihe, P.; Heilmann, C. Serum vaccine antibody concentrations in children exposed to perfluorinated compounds. *JAMA* **2012**, *307*, 391–397. [CrossRef]
42. Lopez-Espinosa, M.-J.; Mondal, D.; Armstrong, B.; Bloom, M.S.; Fletcher, T. Thyroid function and perfluoroalkyl acids in children living near a chemical plant. *Environ. Health Perspect.* **2012**, *120*, 1036–1041. [CrossRef] [PubMed]
43. Johansson, N.; Fredriksson, A.; Eriksson, P. Neonatal exposure to perfluorooctane sulfonate (PFOS) and perfluorooctanoic acid (PFOA) causes neurobehavioural defects in adult mice. *Neurotoxicology* **2008**, *29*, 160–169. [CrossRef] [PubMed]
44. Filgo, A.J.; Quist, E.M.; Hoenerhoff, M.J.; Brix, A.E.; Kissling, G.E.; Fenton, S.E. Perfluorooctanoic acid (PFOA)-induced liver lesions in two strains of mice following developmental exposures. *Toxicol. Pathol.* **2015**, *43*, 558–568. [CrossRef]
45. Fei, C.; McLaughlin, J.K.; Tarone, R.E.; Olsen, J. Perfluorinated chemicals and fetal growth: A study within the Danish National Birth Cohort. *Environ. Health Perspect.* **2007**, *115*, 1677–1682. [CrossRef]
46. Halldorsson, T.I.; Rytter, D.; Haug, L.S.; Bech, B.H.; Danielsen, I.; Becher, G.; Henriksen, T.B.; Olsen, S.F. Prenatal exposure to perfluorooctanoate and risk of overweight at 20 years of age: A prospective cohort study. *Environ. Health Perspect.* **2012**, *120*, 668–673. [CrossRef] [PubMed]

47. Webster, G. *Potential Human Health Effects of Perfluorinated Chemicals (PFCs)*; National Collaborating Centre for Environmental Health-NCCEH: Vancouver, BC, Canada, 2010.
48. Wang, Z.; Cousins, I.T.; Scheringer, M.; Hungerbuehler, K. Hazard assessment of fluorinated alternatives to long-chain perfluoroalkyl acids (PFAAs) and their precursors: Status quo, ongoing challenges and possible solutions. *Environ. Int.* **2015**, *75*, 172–179. [CrossRef]
49. Organisation for Economic Co-operation and Development (OECD). Results of the 2006 survey on production and use of PFOS, PFAS, PFOA, PFCA, their related substances and products/mixtures containing these substances. In Proceedings of the Environment Directorate be Joint Meeting of the Chemicals Committee and Working Party on Chemicals, Pesticides and Biotechnology (ENV/JM/MONO 2006), Paris, France, February 2006; p. 36.
50. Krafft, M.P.; Riess, J.G. Highly fluorinated amphiphiles and colloidal systems, and their applications in the biomedical field. A contribution. *Biochimie* **1998**, *80*, 489–514. [CrossRef]
51. Ganesan, S.; Vasudevan, N. Impacts of perfluorinated compounds on human health. *Bull. Environ. Pharmacol. Life Sci.* **2015**, *4*, 183–191.
52. Maestri, L.; Negri, S.; Ferrari, M.; Ghittori, S.; Fabris, F.; Danesino, P.; Imbriani, M. Determination of perfluorooctanoic acid and perfluorooctanesulfonate in human tissues by liquid chromatography/single quadrupole mass spectrometry. *Rapid Commun. Mass Spectrom.* **2006**, *20*, 2728–2734. [CrossRef]
53. Fenton, S.E.; Ducatman, A.; Boobis, A. Per- and polyfluoroalhyl substances toxicity and human health review: Current state of knowledge and strategies for informing future research. *Environ. Toxicol. Chem.* **2021**, *40*, 606–630. [CrossRef]
54. Herzke, D.; Huber, S.; Bervoets, L.; D'Hollander, W.; Hajslova, J.; Pulkrabova, J.; Brambilla, G.; De Filippis, S.P.; Klenow, S.; Heinemeyer, G.; et al. Perfluorinated alkylated substances in vegetables collected in four European countries; occurrence and human exposure estimations. *Environ. Sci. Pollut. Res.* **2013**, *20*, 7930–7939. [CrossRef]
55. Nowacka, M.; Tappi, S.; Wiktor, A.; Rybak, K.; Miszczykowska, A.; Czyzewski, J.; Drozdzal, K.; Witrowa-Rajchert, D.; Tylewicz, U. The impact of pulsed electric field on the extraction of bioactive compounds from beetroot. *Foods* **2019**, *8*, 244. [CrossRef]
56. Carillo, C.; Rey, R.; Hendrickx, M.; Del Mar Cavia, M.; Alonso-Torre, S. Antioxidant capacity of beetroot: Traditional vs novel approaches. *Plant Foods Hum. Nutr.* **2017**, *72*, 266–273. [CrossRef] [PubMed]
57. de Castro, A.P.R.B.; da Cunha, D.T.; Antunes, A.E.C.; Corona, L.P.; Bezerra, R.M.N. Effect of freeze-dried red beet (*Beta vulgaris* L.) leaf supplementation on biochemical and anthropometrical parameters in overweight and obese individuals: A pilot study. *Plant Foods Hum. Nutr.* **2017**, *74*, 232–234. [CrossRef] [PubMed]
58. Asgary, S.; Afshani, M.R.; Sahebkar, A.; Keshvari, M.; Taheri, M.; Jahanian, E.; Rafieian-Kopaei, M.; Malekian, F.; Sarrafzadegan, N. Improvement of hypertension, endothelial function and systemic inflammation following short-term supplementation with red beet (*Beta vulgaris* L.) juice: A randomized crossover pilot study. *J. Hum. Hypertens.* **2016**, *30*, 627–632. [CrossRef]
59. Liñero, O.; Cidad, M.; Carrero, J.A.; Nguyen, C.; de Diego, A. Partitioning of nutrients and non-essential elements in Swiss chards cultivated in open-air plots. *J. Food Compos. Anal.* **2017**, *59*, 179–187. [CrossRef]
60. Nakamura, K.; Seishima, R.; Matsui, S.; Shiggeta, K.; Okabayashi, K.; Kitagawa, Y. The prognostic impact of preoperative mean corpuscular volume in colorectal cancer. *Jpn. J. Clin. Oncol.* **2022**, *52*, 562–570. [CrossRef]
61. Vinholt, P.J.; Hvas, A.M.; Frederiksen, H.; Bathum, L.; Jorgensen, M.K.; Nybo, M. Platelet count is associated with cardiovascular disease, cancer and mortality: A population-based cohort study. *Thromb. Res.* **2016**, *148*, 136–142. [CrossRef]
62. Semple, J.M.; Italiano, J.E., Jr.; Freedman, J. Platelets and the immune continuum. *Nat. Rev. Immunol.* **2011**, *11*, 264–274. [CrossRef] [PubMed]
63. Golebiewska, E.M.; Poole, A.W. Platelet secretion: From haemostasis to wound healing and beyond. *Blood Rev.* **2015**, *29*, 153–162. [CrossRef]
64. Gay, L.J.; Felding-Habermann, B. Contribution of platelets to tumour metastasis. *Nat. Rev. Cancer* **2011**, *11*, 123–134. [CrossRef]
65. Rotander, A.; Toms, L.-M.L.; Aylward, L.; Kay, M.; Mueller, J.F. Elevated levels of PFOS and PFHxS in firefighters exposed to aqueous film forming foam (AFFF). *Environ. Int.* **2015**, *82*, 28–34. [CrossRef] [PubMed]
66. Peraz, F.; Llorca, M.; Farré, M.; Barcelo, D. Automated analysis of perfluorinated compounds in human hair and urine samples by turbulent flow chromatography coupled to tandem mass spectrometry. *Anal. Bioanal. Chem.* **2012**, *402*, 2369–2378. [CrossRef] [PubMed]
67. Surma, M.; Wiczkowski, W.; Zieliński, H.; Cieślik, E. Determination of selected perfluorinated acids (PFCAs) and perfluorinated sulfonates (PFASs) in food contact materials using LC-MS/MS. *Packag. Technol. Sci.* **2015**, *28*, 789–799. [CrossRef]
68. Niedzwiedzka, E.; Wadolowska, L.; Kowalkowska, J. Reproducibility of a non-quantitative food frequency questionnaire (62-Item FFQ-6) and PCA-driven dietary pattern identification in 13–21-year-old females. *Nutrients* **2019**, *1*, 2183. [CrossRef] [PubMed]

International Journal of
Molecular Sciences

MDPI

Article

Cooking, Digestion, and In Vitro Colonic Fermentation of Nigerian Wholegrains Affect Phenolic Acid Metabolism and Gut Microbiota Composition

Oghenerukevwe Anne Obayiuwana [1,2], Volker Behrends [1], Yolanda Calle-Patino [1], Monica Barone [3], Silvia Turroni [4], Patrizia Brigidi [3], Adele Costabile [1,†] and Giulia Corona [1,*,†]

[1] School of Life and Health Sciences, University of Roehampton, London SW15 4JD, UK; anneobayiuwana@gmail.com (O.A.O.)
[2] Department of Medical Biochemistry, University of Benin, Benin 300283, Nigeria
[3] Microbiomics Unit, Department of Medical and Surgical Sciences, University of Bologna, 40138 Bologna, Italy
[4] Unit of Microbiome Science and Biotechnology, Department of Pharmacy and Biotechnology, University of Bologna, 40126 Bologna, Italy
* Correspondence: giulia.corona@roehampton.ac.uk
† These authors contributed equally to this work.

Abstract: Wholegrains contain both fibre and phenolic acids (PAs), and their gastrointestinal modifications are critical for their bioavailability and bioactivity. We evaluated the modifications on the PA profile and gut microbiota composition of selected Nigerian wholegrains, following cooking and gastrointestinal digestion. Red fonio, red millet, red sorghum, and white corn were cooked, digested, and fermented using an in vitro colonic model. A total of 26 PA derivatives were quantified in soluble and bound fractions using Ultraperformance Liquid Chromatography-Tandem Mass Spectrometry (UPLC-MS/MS) analysis. DNA samples were analysed using 16S rRNA amplicon sequencing to profile the microbiota composition. The results show that cooking and digestion significantly affected the levels of PAs in all grains ($p \leq 0.05$) compared to raw grains. Colonic fermentation resulted in a peak of total soluble PAs at 4–6 h for red sorghum and white corn and at 24 h for red millet and red fonio. *Enterobacteriaceae* genera were the most abundant at 24 h in all grains studied. 3-hydroxybenzaldehyde correlated positively with the relative abundance of *Dorea* and the mucus-degrader bacteria *Akkermansia* ($p \leq 0.05$), whereas hydroferulic acid and isoferulic acid levels correlated negatively with *Oscillospira* and *Ruminococcus* ($p \leq 0.05$), respectively. Our data indicate that cooking, digestion, and colonic fermentation affect the release of bound PAs from wholegrains and, consequently, their metabolic conversion. Furthermore, PA fermentation in the gut is associated with potentially relevant changes in the microbiota. This in vitro study provides the basis for the design of an in vivo human intervention study that can confirm the trends herein observed but also assess the impact on health outcomes.

Keywords: wholegrains; cooking; polyphenols; gut microbiota; digestion; fermentation; bioaccessibility; next-generation sequencing; UPLC-MS/MS

Citation: Obayiuwana, O.A.; Behrends, V.; Calle-Patino, Y.; Barone, M.; Turroni, S.; Brigidi, P.; Costabile, A.; Corona, G. Cooking, Digestion, and In Vitro Colonic Fermentation of Nigerian Wholegrains Affect Phenolic Acid Metabolism and Gut Microbiota Composition. *Int. J. Mol. Sci.* **2023**, *24*, 14111. https://doi.org/10.3390/ijms241814111

Academic Editor: Maurizio Battino

Received: 10 August 2023
Revised: 31 August 2023
Accepted: 6 September 2023
Published: 14 September 2023

1. Introduction

Cereal whole grains are part of the family *Poaceae* (also known as *Gramineae*), and their seeds are consumed as food. Wholegrains are a rich source of fibre and phenolic acids (PAs), and their consumption may be beneficial for the prevention of chronic illnesses, but this is subject to the bioaccessibility in the gastrointestinal tract and the subsequent bioavailability of their phenolic compounds [1]. In some continents, cereals serve as the major staple food for the population, and in Asia and Africa, sorghum and millet are known to be grown and consumed in addition to other grains [2]. Grains like fonio, sorghum, millet and corn are gluten-free and can be used as alternative grains in foods for different dietary needs. The

nutritional value of the above grains is within the range of other grains such as wheat, oats and barley, with carbohydrate content that can vary from 63 to 86 g/100 g, proteins ranging from 6 to 12 g/100 g, and fats levels ranging from 0.5 to 5 g/100 g [3–12]. Fonio, millet, corn and sorghum are consumed widely in Nigeria and are cultivated in the Northern regions of the country. The grains are often consumed as fermented porridge, which is eaten by all age groups, from infants to adults and the elderly. They can also be prepared and consumed in different forms, including fermented drinks and boiled or roasted.

PAs are a class of polyphenols consisting of an aromatic ring, a hydroxyl group and a carboxylic moiety. The two main groups of PAs are hydroxybenzoic acid (HBA) and hydroxycinnamic acid (HCA) (Figure 1). Phenolic compounds are known to possess bioactivity and health benefits [13].

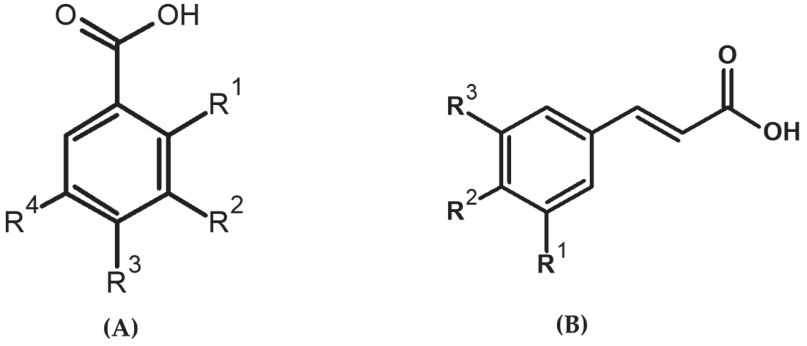

Figure 1. Basic structure of phenolic acids. (**A**) Hydroxybenzoic acid (vanillic acid (R2 = -OCH_3, R3 = -OH), 4-hydroxybenzoic acid (R3 = -OH), salicylic acid (R1 = -OH), syringic acid (R3 = -OH, R2, R4 = -OCH_3). (**B**) Hydroxycinnamic acid (p-coumaric acid (R2 = -OH), caffeic acid (R2, R3 = -OH), ferulic acid (R2 = OH, R3 = -OCH_3), R1–R4 = H, except where specified.

There is no research information on the PA content and bioaccessibility of Nigerian grains; previous studies focus on the total phenolic compounds in the grains [14,15]. The aim of this study was to investigate the PA content of Nigerian-grown grains. A pilot study was performed, where a variety of grains, including red and white fonio, red and white millet, red and white sorghum, ofada rice and corn, were screened for their PA and total dietary fibre (TDF) content; based on these results, red fonio, red millet, red sorghum and white corn were selected for digestion and fermentation studies.

We investigated the bioaccessibility of selected PAs using a standardised in vitro digestion model [16]. Furthermore, following digestion, grains were subjected to a 24 h fermentation to evaluate the impact of their phenolic extract on human colonic microbiota and vice versa using an in vitro colonic model. Samples were obtained from the fermentation vessel at time points 0, 4, 6, 8 and 24 h to determine the PA profile of the aliquot, while DNA profiling was performed using NGS for samples obtained at time points 0, 6, and 24 h [17].

2. Results

2.1. Phenolic Acid and Total Dietary Fiber Content of Raw Grains

2.1.1. UPLC-MS/MS Characterization of PAs

Supplementary Table S1 shows the MS detection parameters, and Supplementary Table S2 shows the calibration curve parameters for the 26 PA standards used in this study. For most compounds, at least three daughter fragments were generated from varying collision energies.

2.1.2. Total PA and TDF Content of Raw Grains

The TDF of the grains ranged from 3 to 26.7 g/100 g (Table 1). Red sorghum had the highest, while white fonio had the lowest TDF values.

Table 1. Total phenolic acid content, percentage of total soluble and bound phenolic acid fractions, and total dietary fibre in raw grains.

Raw Grain	Total PAs (ng/mg) FW	% Soluble PAs	% Bound PAs	TDF (g/100 g)
Red fonio	281.4 ± 10.8 [a]	17.2 ± 1.9	82.8 ± 1.9	6.7
White fonio	132.2 ± 12.1 [a]	5.1 ± 0.6	94.9 ± 9.7	3
Red millet	1631.2 ± 227.5 [b]	13.3 ± 0.2	86.7 ± 14.1	11.4
White millet	1466.1 ± 187.1 [b]	13.6 ± 1.0	86.4 ± 12.0	9.7
Red sorghum	1464.2 ± 184.2 [b]	26.8 ± 0.0	73.2 ± 8.0	26.7
White sorghum	693.3 ± 38.0 [c]	0.1 ± 0.0	99.9 ± 5.5	21.7
White corn	2202.5 ± 34.9 [d]	0.1 ± 0.0	99.9 ± 1.6	14.3
Ofada rice	276.64 ± 25.31 [a]	0.7 ± 0.3	99.3 ± 9.2	2.7

Samples were analysed in triplicates; results are expressed as mean ± SD. FW = fresh weight; PAs = phenolic acid; TDF = total dietary fibre. Values with different superscripts (a, b, c, d) differ significantly ($p \leq 0.05$).

Grain PAs were extracted in soluble and bound forms, with total PAs calculated as the sum of soluble and bound PAs and expressed as ng/mg fresh weight. Table 1 shows the total PAs in raw grains. The highest value of total PA concentration was seen in white corn compared to other grains (2202.5 ± 34.9 ng/mg, $p \leq 0.0001$). Apart from this, significantly high values of total PA concentration ($p \leq 0.0001$) were also seen in red millet (1631.2 ± 227.5 ng/mg), white millet (1466.1 ± 187.1 ng/mg) and red sorghum (1464.2 ± 18.2 ng/mg) compared to the rest grains. White Sorghum had a total PA concentration of 693.3 ± 38.0 ng/mg, which was significantly higher ($p \leq 0.05$) than that in Ofada rice and fonio, which had the lowest total PA concentrations, with values ranging from (132.2 ± 12.1 to 281.4 ± 10.8 ng/mg). PAs were mostly present in the bound form between 73.2% and 99.9% of total PAs. Millet and red sorghum had the highest proportions of soluble PAs (13.3% and 26.8%, respectively).

2.2. Impact of Cooking and Digestion on the Phenolic Acid Profile of Grains

Selected grains were cooked, subjected to simulated digestion and then freeze-dried. PAs were extracted from cooked and digested grains in soluble and bound forms, with total PAs calculated as the sum of soluble and bound PAs expressed as ng/mg fresh or dried weight. Table 2 shows the PA profile of raw, cooked, and digested grain samples.

Table 2. Individual phenolic acids (soluble + bound) in raw, cooked, and digested grains (ng/mg fresh or dried weight).

	Red Fonio			Red Millet			Red Sorghum			White Corn		
PA	**Raw**	**Cooked**	**Digested**	**Raw**	**Cooked**	**Digested**	**Raw**	**Cooked**	**Digested**	**Raw**	**Cooked**	**Digested**
VA	6.82 ± 1.33	1.02 ± 0.05	0.83 ± 0.12	37.60 ± 1.92	7.94 ± 1.23	8.20 ± 0.33	33.00 ± 3.52	4.60 ± 0.27	3.49 ± 0.45	5.87 ± 0.73	1.85 ± 0.66	1.28 ± 0.56
IVA	ND	0.00 ± 0.00	ND	ND	ND	ND	ND	ND	ND	ND	ND	ND
4-HBALD	2.25 ± 0.14	3.47 ± 0.53	1.69 ± 0.10	7.63 ± 0.84	8.10 ± 1.13	9.19 ± 0.42	15.54 ± 0.31	7.52 ± 2.67	9.36 ± 0.70	4.37 ± 0.08	3.20 ± 0.18	3.01 ± 0.72
3-HBALD	ND	ND	ND	ND	ND	ND	ND	ND	ND	ND	ND	ND
4-HBA	4.76 ± 0.41	2.57 ± 0.02	3.07 ± 0.03	43.58 ± 4.44	25.13 ± 0.63	21.22 ± 1.20	39.99 ± 0.02	41.57 ± 5.24	26.34 ± 2.10	2.03 ± 0.07	3.80 ± 0.24	1.92 ± 0.33
3-HBALD	0.05 ± 0.07	ND	0.03 ± 0.04	ND	ND	ND	ND	ND	ND	ND	ND	ND
SA	0.46 ± 0.01	0.55 ± 0.04	0.24 ± 0.04	0.29 ± 0.05	0.30 ± 0.09	0.27 ± 0.05	0.43 ± 0.01	0.30 ± 0.06	0.13 ± 0.00	0.26 ± 0.06	1.14 ± 0.04	0.40 ± 0.00
4-HPA	ND	ND	ND	ND	ND	ND	ND	ND	ND	0.26 ± 0.37	ND	ND
3-HPA	ND	ND	ND	ND	ND	ND	ND	ND	ND	ND	ND	ND
2-HPA	0.03 ± 0.04	ND	ND	0.41 ± 0.02	ND	ND	ND	ND	ND	ND	ND	ND
VN	0.50 ± 0.18	3.78 ± 1.15	2.32 ± 0.73	2.91 ± 0.20	13.92 ± 4.17	18.56 ± 1.49	1.08 ± 0.26	2.87 ± 1.82	2.94 ± 0.12	5.53 ± 0.21	9.57 ± 0.85	10.93 ± 3.58
3,4- and 3,5-DHBAs	0.37 ± 0.04	0.44 ± 0.04	0.46 ± 0.02	2.04 ± 0.03	1.11 ± 0.08	1.33 ± 0.14	2.46 ± 0.02	1.85 ± 0.01	1.65 ± 0.23	0.06 ± 0.02	0.18 ± 0.01	0.10 ± 0.04
2,5-DHBA	ND	ND	0.03 ± 0.05	0.03 ± 0.03	0.01 ± 0.02	ND	ND	0.05 ± 0.05	0.05 ± 0.02	0.02 ± 0.03	0.01 ± 0.02	ND
2,4-DHBA	0.42 ± 0.08	2.07 ± 0.00	0.12 ± 0.16	0.30 ± 0.07	0.12 ± 0.04	ND	0.03 ± 0.04	0.01 ± 0.01	ND	0.76 ± 0.36	2.60 ± 0.00	0.98 ± 0.06
pCA	11.48 ± 3.10	19.79 ± 5.98	11.76 ± 1.66	298.47 ± 50.15	581.74 ± 21.79	554.45 ± 5.21	120.78 ± 15.74	117.67 ± 9.20	106.07 ± 47.90	209.83 ± 8.63	341.28 ± 19.74	284.05 ± 29.83
GA	0.02 ± 0.02	0.36 ± 0.02	0.45 ± 0.31	0.01 ± 0.01	ND	ND	0.01 ± 0.02	0.09 ± 0.12	ND	ND	ND	ND
HA	ND	ND	1.04 ± 0.19	ND	ND	ND	0.08 ± 0.11	ND	ND	ND	ND	ND
CA	7.94 ± 0.37	17.31 ± 0.12	23.38 ± 2.96	96.89 ± 5.16	127.87 ± 9.14	133.89 ± 7.81	252.30 ± 55.92	177.14 ± 24.65	156.17 ± 3.34	8.15 ± 0.38	22.96 ± 2.84	11.75 ± 4.87
3,4-DHCA	ND	ND	ND	ND	ND	ND	0.03 ± 0.04	0.02 ± 0.03	ND	0.05 ± 0.07	0.02 ± 0.02	0.01 ± 0.01
HVA	0.79 ± 1.12	15.79 ± 0.32	19.47 ± 2.79	100.20 ± 10.55	134.05 ± 3.52	123.71 ± 24.40	264.16 ± 63.75	173.96	146.22 ± 8.09	7.85 ± 0.10	29.23 ± 11.49	9.30 ± 13.15
SYRALD	0.20 ± 0.23	ND	ND	0.92 ± 0.14	2.30 ± 1.58	3.40 ± 0.02	0.06 ± 0.04	ND	ND	0.85 ± 0.08	0.06 ± 0.08	0.76 ± 1.07
FA	170.90 ± 8.50	232.81 ± 7.03	300.29 ± 56.19	880.57 ± 166.10	1500.71 ± 230.04	2038.59 ± 30.01	640.55 ± 35.17	1306.02 ± 120.10	828.01 ± 53.40	1797.34 ± 27.50	2884.67 ± 922.74	2023.40 ± 225.61
IFA	45.85 ± 0.11	55.81 ± 4.39	54.26 ± 14.21	74.69 ±.88	7.50 ± 1.02	49.71 ± 1.38	72.63 ± 10.06	8.33 ± 3.98	24.49 ± 2.81	124.92 ± 9.22	10.41 ± 1.75	29.50 ± 8.58
HFA	ND	ND	0.58 ± 0.82	0.04 ± 0.07	ND	ND	ND	ND	ND	0.01 ± 0.02	ND	ND
SYRA	17.52 ± 2.47	13.40 ± 2.92	19.80 ± 2.95	34.05 ± 0.95	74.21 ± 12.02	56.66 ± 8.31	8.52 ± 1.69	15.19 ± 1.86	8.98 ± 2.79	5.37 ± 1.40	42.49 ± 13.99	19.74 ± 7.14
SNA	11.05 ± 0.85	6.06 ± 0.34	4.79 ± 0.03	50.61 ± 7.23	45.83 ± 5.66	58.54 ± 5.99	12.53 ± 0.98	6.19 ± 1.75	3.63 ± 0.75	28.96 ± 7.44	91.58 ± 3.00	36.20 ± 15.77
TOTAL	281.40 ± 10.78	375.23 ± 8.25	444.62 ± 45.25	1631.24 ± 227.46	2530.83 ± 248.11	3077.71 ± 2.20	1464.17 ± 184.19	1863.37 ± 185.37	1317.51 ± 2.21	2202.51 ± 34.93	3445.04 ± 913.04	2433.33 ± 311.17

Raw samples were analysed in triplicate, cooked and digested samples in duplicate. All results are expressed as mean ± standard deviation (SD). ND = not detected.

Soluble and Bound PAs in Cooked and Digested Grains

The impact of cooking and digestion on the soluble and bound PAs of the grains can be seen in Figure 2. Cooking significantly reduced the total soluble amount of PAs in red fonio and also in red millet and red sorghum samples ($p \leq 0.05$), whereas it led to a significant increase in white corn. The amount of soluble PAs measured in the grains after cooking varied from 1.8 ± 0.8 to 18.5 ± 7.1 ng/mg. The digested grains were also found to contain a lower amount of soluble forms of PA than raw grains, and this difference was significant for all grains ($p \leq 0.0001$), with the exception of white corn. The levels of soluble PAs in digested grains ranged from 0.1 ± 0.03 to 2.3 ± 3.2 ng/mg.

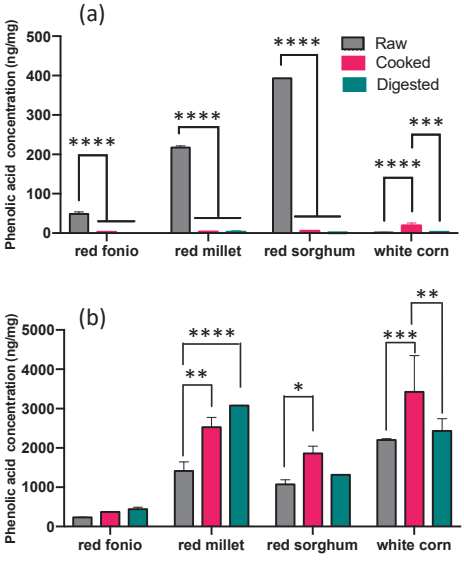

Figure 2. Total soluble (**a**) and bound (**b**) phenolic acids in raw, cooked, and digested grains. Raw samples were analysed in triplicate, cooked and digested samples in duplicate; all results are expressed as mean ± SD (2-way ANOVA, Tukey's multiple comparisons tests, * = $p \leq 0.05$, ** = $p \leq 0.01$, *** = $p \leq 0.001$, **** = $p \leq 0.0001$).

The amount of bound PAs measured in cooked grains varied from 373.1 ± 8.0 to 3426.6 ± 920.1 ng/mg. The cooking process significantly increased the levels of bound PAs in all grains ($p \leq 0.05$), with the exception of red fonio. The digestion process also had an impact on bound PA levels, and a significant increase was observed in red millet samples ($p \leq 0.001$). We also noted how the digestion of white corn samples induced a significant decrease in the levels of bound PAs when compared to the cooked samples ($p \leq 0.01$). Bound PA levels in digested grains varied from 444.5 ± 45.3 to 3075.4 ± 5.4 ng/mg.

The amount of selected bound HBAs in cooked and digested grains is shown in Figure 3. Homovanillic acid content was significantly higher in all grains after cooking, in comparison to the raw forms ($p \leq 0.01$), whereas we can notice how the amount of other bound forms, such as HBAs, increased only in some cooked grains. For example, in white corn, we measured increased levels of syringic acid, which were also higher in red fonio samples ($p \leq 0.0001$), whereas in red sorghum and millet, we observed increased levels of 4-OH benzoic acid ($p \leq 0.05$). The levels of vanillin in red millet samples and fonio samples were also increased ($p \leq 0.05$). In comparison to raw grains, the digestion process also affected the levels of PAs, with increases in syringic acid in white corn, red millet and red fonio ($p \leq 0.0001$) and increases in vanillin and homovanillic acid in red millet and red fonio ($p \leq 0.05$). The increase in homovanillic acid and syringic acid in red fonio was also significant when compared to cooked samples ($p \leq 0.0001$). Conversely, the

digestion process resulted in a significant decrease in homovanillic acid levels in white corn ($p \leq 0.0001$), sorghum ($p \leq 0.0001$) and red millet ($p \leq 0.05$), and decreased levels of 4-OH benzoic acid in sorghum ($p \leq 0.05$), as well as a decrease in syringic acid levels in red millet ($p \leq 0.0001$), compared to cooked grains.

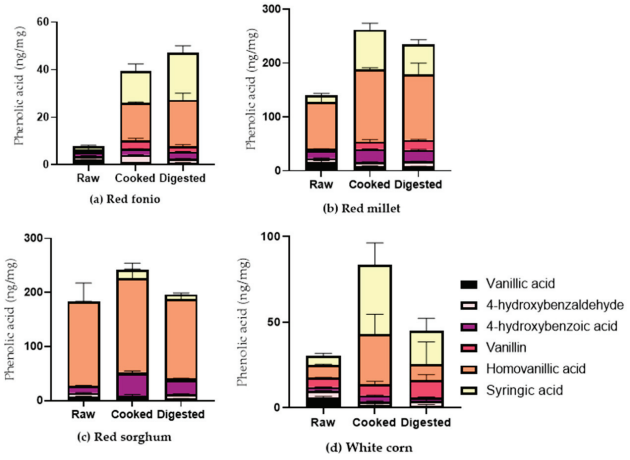

Figure 3. Amount of selected bound hydroxybenzoic acids in raw, cooked, and digested grains. Raw samples were analysed in triplicate, cooked and digested samples in duplicate. All results are expressed as mean ± SD.

For selected bound HCAs (Figure 4), the cooking process significantly increased ferulic acid levels in all grains ($p \leq 0.0001$). Additionally, a significant increase in p-coumaric acid levels was measured in red millet samples ($p \leq 0.001$). In comparison to the raw samples, the red fonio, sorghum and red millet grains subjected to digestion contained significantly higher amounts of ferulic acid ($p \leq 0.0001$), whereas the red millet samples contained significantly higher levels of p-coumaric acid ($p \leq 0.0001$). In comparison to the cooked samples, the digested ones were found to contain a significantly higher amount of ferulic acid for some grains (red millet and red fonio) but a significantly lower amount for others, such as sorghum and white corn ($p \leq 0.001$).

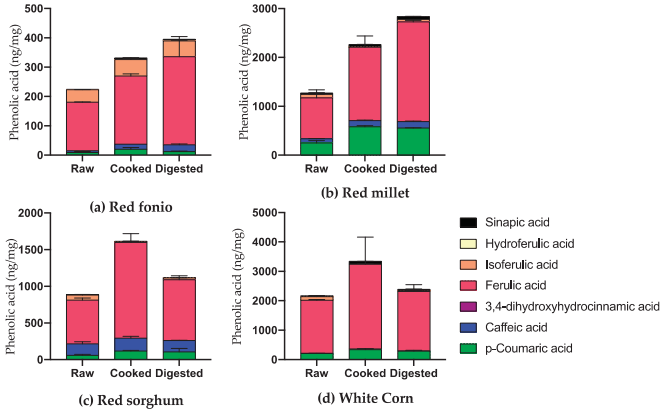

Figure 4. Amount of selected bound hydroxycinnamic acids in raw, cooked and digested grains. Raw samples were analysed in triplicate, cooked and digested samples in duplicate. All results are expressed as mean ± SD.

2.3. In Vitro Colonic Fermentation of Digested Grains

2.3.1. Phenolic Acid Content of Fermented Grains

Digested grains were subjected to in vitro colonic fermentation for 24 h, and aliquots were collected at 0, 2, 4, 6, 8, and 24 h for assessment of soluble PA content (Figure 5). The total soluble PA content did not differ significantly over time for any of the grains ($p > 0.05$), but the highest levels were measured at different time points for different grains (4 h, 6 h or 24 h for red sorghum, white corn, or red fonio and red millet, respectively. The total soluble PA forms released from each grain were significantly different in white corn, red sorghum and red millet in comparison to the negative control group ($p \leq 0.05$).

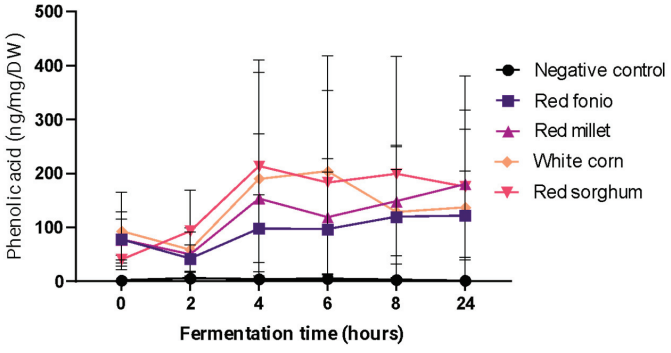

Figure 5. Total soluble phenolic acid concentration at different time points during in vitro colonic fermentation of digested grains. Samples were analysed in triplicate, except for red millet at 0 h, white corn at 6 h, and red sorghum at 0, 4, and 6 h, which were analysed in duplicate. All results are expressed as mean ± SD. DW, dry weight.

Looking at the changes in selected PAs over the fermentation period, 4-OH benzaldehyde increased significantly in red fonio, red millet, and red sorghum ($p \leq 0.05$) (Figure 6). In particular, peak levels of 4-OH benzaldehyde were observed at 6 h in red fonio and red sorghum and at 24 h in red millet. 4-OH benzoic acid levels were significantly higher in red millet and red sorghum ($p \leq 0.05$), with peak values measured after 24 h in both grains. In addition, the fermentation of white corn substrate resulted in the production of Isoferulic acid, which was significant ($p \leq 0.05$) after 4 h, 6 h, and 24 h.

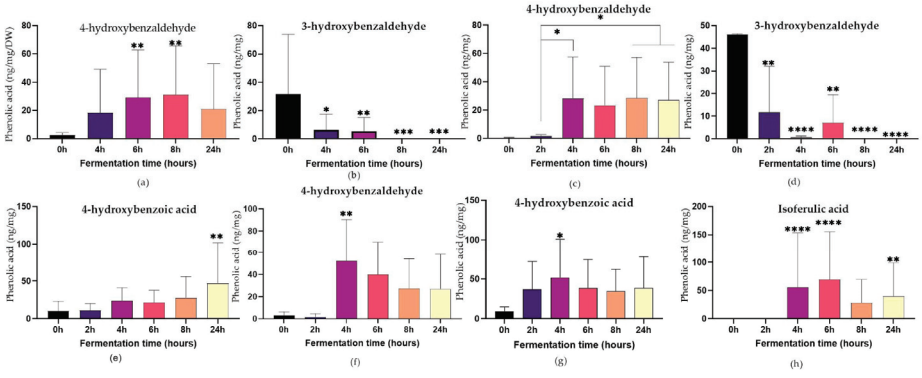

Figure 6. Changes in selected phenolic acids in red fonio (**a**,**b**), red millet (**c**–**e**), red sorghum (**f**,**g**) and white corn (**h**) during in vitro colonic fermentation of digested grains. 2-way ANOVA, Tukey's multiple comparisons tests, each time point vs. 0 h (unless otherwise indicated), * = $p \leq 0.05$, ** = $p \leq 0.01$, *** = $p \leq 0.001$, **** = $p \leq 0.0001$.

2.3.2. Impact of Digested Grains on Faecal-Derived Microbial Communities from Healthy Volunteers

The faecal microbial communities of three healthy volunteers were profiled over time during in vitro colonic fermentation of digested grains to assess whether the different dynamics of PA conversion were associated with different gut microbiota layouts and trajectories (Figure 7). The diversity of the microbial communities decreased remarkably over time for all grains, in parallel with an increase in the relative abundance of unclassified *Enterobacteriaceae* (relative abundance, 37% to 61% at 6 h, 55% to 87% at 24 h), particularly for white corn and red millet. The highest diversity at 24 h was found for red fonio, whose microbial communities were mainly composed of unclassified *Enterobacteriaceae* (55%), *Bacteroides* (10%), and *Veillonella* (9%).

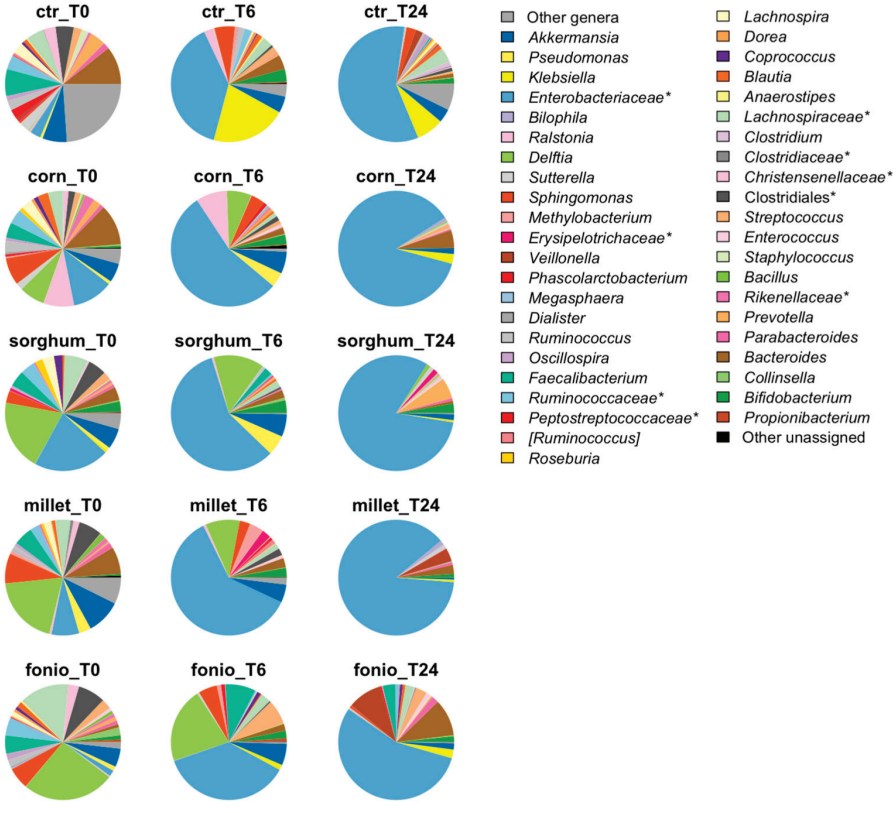

Figure 7. Genus-level relative abundance profiles of faecal microbial communities from healthy volunteers before (T0) and after 6 (T6) and 24 (T24) h of in vitro colonic fermentation with digested grains. Ctr, negative control (i.e., faecal slurry without any substrate addition). * = bacterial family with unclassified genera.

Correlation analysis between selected PAs and bacterial genera revealed some trends (Figure 8). In particular, 3-hydroxybenzaldehyde was positively correlated with *Dorea* and the mucus-degrader bacteria *Akkermansia* ($p \leq 0.05$), whereas both hydroferulic and isoferulic acids showed a negative correlation with the bacteria *Oscillospira* and *Ruminococcus*, respectively ($p \leq 0.05$). Both *Dorea* and *Oscillospira* tended to decrease over time in red fonio ($p \leq 0.1$), while *Ruminococcus* tended to decrease in white corn ($p \leq 0.1$).

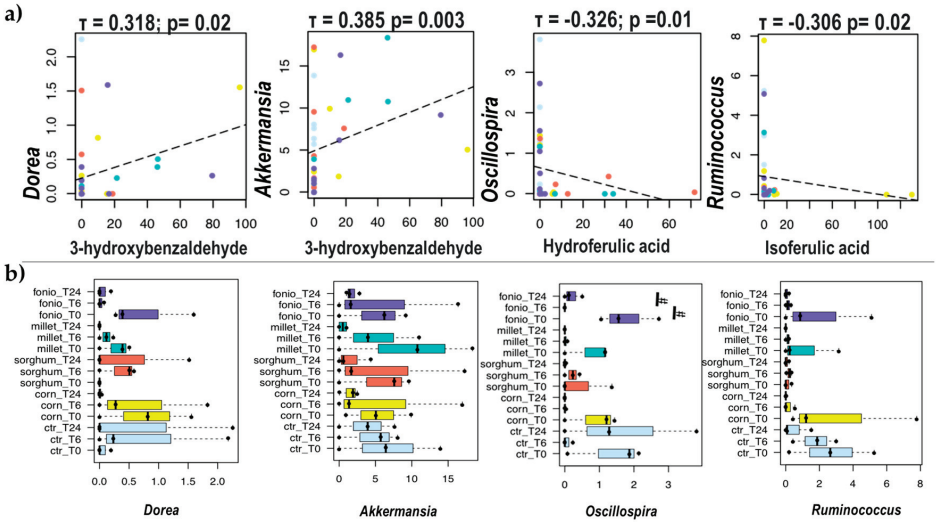

Figure 8. Associations between bacterial genera and phenolic acids during in vitro colonic fermentation of digested grains. (**a**) scatter plots showing the correlation between genus-level relative abundances and levels of selected phenolic acids. Only statistically significant correlations ($p \leq 0.05$) with absolute Kendall's tau ≥ 0.3 are shown. Samples are coloured based on the digested grains subjected to fermentation (see bottom panel). (**b**) Boxplots showing the relative abundance distribution of the genera significantly correlated with PAs. For each digested grain, samples were collected before (T0) and after 6 (T6) and 24 (T24) h of fermentation. Ctr, negative control (i.e., faecal slurry without any substrate addition). Wilcoxon test, # = $p \leq 0.1$.

3. Discussion

Dietary PAs have been found to beneficially affect health, but their bioaccessibility can have a significant impact on bioavailability and absorption. In this study, we provided a comprehensive and accurate assessment of extractable PAs in both soluble and bound forms in a panel of selected grains. The assessment was provided in raw grains but also in processed forms of nutritional interest (following cooking and simulated digestion), applying robust and validated analytical methods. As dietary fibre can bind and influence the mobility, transition and absorption of PAs in the digestive tract [18,19], ultimately affecting their bioavailability, the TDF content of the grains was assessed.

The TDF content of grains in this study was found to be as follows: red and white sorghum > white corn > red and white millet > ofada rice > red and white fonio. Our results are generally consistent with the available literature, which reports values of 3.3–8% in hulled fonio, 3.7–15% in pearl millet, 8.6–21.0% in sorghum, 1.4–3.5% in ofada rice, 11.1–15.34% and 2.1–10.1% in corn [3–12,20–22]

The total PA content of the grains selected for analysis in this study ranged from 276.64 to 2202.5 ng/mg, as the total PA amount in wholegrains can differ subject to the grain type, the environment and farming methods, as well as the different types of processing applied, the PAs selected for characterisation, as well as the extraction procedures and analytical methods applied. One study showed that total PAs differed significantly based on the type of corn [23] and rice cultivars [24]. Other studies showed differences in total PAs by grain type; for example, total PA content was 61.82 µg/g in raw fonio, 871.48 µg/g in raw millet, 678.36 µg/g in raw sorghum, and 832.2 µg/g in raw pearl millet [25,26].

The impact of cooking on the PA content in grain samples can vary in relation to several factors, including processing, for example, milling, and cooking procedures, including cooking duration and temperature levels, which could affect the bioaccessibility and amount of extractable PAs. During the process of cooking, the soluble PAs could be

leached into the cooking solution, making them susceptible to thermal degradation, or they could form complexes within the food matrix, causing a decrease in their amount. Furthermore, during the cooking process, cell wall polymers may, in turn, be broken down to facilitate the extraction of bound PAs [26,27]. Indeed, our results showed that cooking led to a decrease in soluble PAs and an increase in bound PAs in most grains. However, there is conflicting data in the literature. For example, a previous study found that cooking increased soluble PAs in sorghum and millet [26]. Differences in methods, especially cooking time (12 min for sorghum and 15 min for millet compared to 43 min and 36 min in this study), may explain the different observations. The study also reported that cooking fonio caused an increase in bound PAs, while cooking sorghum caused a decrease in bound PAs, with syringic and salicylic acids detected only in the bound cooked fractions [26]. A different study [28] observed that cooking durum wheat caused an increase in its bound PA content, and the authors suggested that this increase correlated with the increased antioxidant activity of their cooked samples. Other studies record that cooking waxy corn and rice caused a decrease in PA content in these grains [27,29]. Cooking was also reported to increase the total amount of free PAs [24].

The data presented in our study indicate how in vitro gastrointestinal digestion can reduce total soluble and increase total bound PA compared to raw grains. Literature data also indicate how boiling together with digestion can have an impact on PA levels, increasing the levels of ferulic acid in the intestinal digest compared to the digest of unprocessed sorghum samples [30]. The degradation of soluble PAs in the gastrointestinal tract (affected by the pH and also by the interaction with digestive enzymes) could result in the formation of new metabolic entities and a reduction in detectable soluble PA. Bond formation with cell wall constituents and resultant conversion or confinement of soluble PA may be a factor in the reduction in soluble PAs in digested samples. On the other hand, bound PAs can be more durable in the upper gastrointestinal tract due to their stronger association with cell wall structures, and the loosening of these structures during cooking, digestion or extraction may facilitate increased accessibility for extraction of bound PAs [26,30–32].

Bound PAs are not readily accessible in the upper part of the gastrointestinal tract, but in the lower part, the microbiota may also play a role, affecting their bioaccessibility and facilitating their release from the food matrix and subsequent biotransformation. Therefore, as part of the current study, we simulated the colonic fermentation of digested food in a controlled in vitro environment, which provided valuable insights into the bioaccessibility of PAs as well as other compounds. In this regard, several studies in the literature report changes in PA levels during in vitro human colonic fermentation of foods high in PA. For example, increases in protocatechuic acid and syringic acid and a decrease in vanillic acid levels have been observed, in addition to a gradual release of PAs from food substances supplemented with PA, while other reports show a decrease in PAs during the fermentation period [33–37]. Inter-individual variability in participants' gut microbiota is well known, and in combination with differences in the food matrix or experimental methods, may be an explanation for these differences in results.

In this study, after the cooking and digestion processes, the colonic fermentation process was also applied to the digested grain material using a validated in vitro intestinal model. Our results indicate that the total soluble PA content varies during the fermentation process, with a peak at 4–24 h; during this period, there was a gradual release of PAs measured during the 24 h fermentation period. Additionally, the analysis of pre-fermented samples also indicated a high content of bound PA (which was considered not bioaccessible prior to fermentation). The impact of the interaction between the bound PA forms and the food matrix and the resulting release of soluble forms from the matrix observed during the fermentation process could be explained as a result of the extended release of soluble PAs in the colonic environment. In addition, some specific PAs significantly decreased or increased over time during fermentation, while others were not detected in the fermented samples. For example, at 0 h, 3-hydroxybenzaldehyde was the highest PA observed in all the grains

studied. Thus, over time, its levels decreased significantly in red fonio samples, as well as in red millet samples, during the 24-h fermentation period. It can be speculated that it was utilised or metabolised to produce a different end product. On the other hand, 4-OH benzaldehyde, 4-OH benzoic acid, and isoferulic acid levels were observed to increase significantly during the 24-h fermentation period in some grains. This might suggest their release from the fibre into soluble forms or their synthesis through the biotransformation of other phenolic compounds in the grains by the action of the gut microbiota.

Once in the large intestine, the bound PA forms are degraded under the action of esterase activities, and the final metabolic product is likely to result from the synergistic action of the gut microbial taxa present. Biotransformation reactions that are likely to occur in the large intestine and affect the phenolic compounds present in the digesta can include hydrolysis, demethylation, reduction, decarboxylation, dihydroxylation and β-oxidation. These reactions can be carried out using bacterial species from the genera *Bifidobacterium* (phylum Actinobacteria), *Eggerthella*, *Lactobacillus*, *Clostridium*, *Eubacterium*, *Streptococcus*, *Ruminococcus* (phylum Firmicutes) *Peptostreptococcus*, and *Escherichia* (phylum Proteobacteria) [38–41]. β-oxidation reactions can also occur and cause the reduction in the hydrocarbon side chains in HCAs. A combination of different microbiota species, such as *Escherichia coli* and *Enterococcus faecalis*, was found to be responsible for the caffeic acid conversion to 3-hydroxyphenylpropionic acid, while benzoic acids can be measured as the end product [42]. A plausible pathway for the biotransformation of HCAs through the action of gut microbes is the degradation of HCAs to phenylpropionic acid derivatives, where demethylation can also occur. The formed metabolic derivatives can then be subjected to a series of β-oxidations to produce benzoic acids [43].

The results of in vitro colonic fermentation experiments showed an overall predominance of unclassified *Enterobacteriaceae* members at 6–24 h in all study groups, as reported in oat fermentation studies [44]. *Enterobacteriaceae* species are able to metabolise ferulic acid to produce vanillin [45]. In our study, prior to fermentation, soluble ferulic acid levels were seen in low amounts in all the forms of the grains, but these grains contained high levels of bound ferulic acid. For most grains, relatively low levels of soluble ferulic acid were also measured, except for white corn (14.57 ± 16.49 ng/mg at 6 h). It is, therefore, possible to hypothesise that, to some extent, the bound forms of ferulic acid may have been biotransformed into other products. For example, after fermentation of the white corn substrate, high levels of isoferulic acid were measured, whereas after fermentation of red millet and red sorghum substrates, high levels of hydroferulic acids were measured, probably suggesting that some of the bound ferulic acids were biotransformed to these related compounds. The microbiota analysis also showed reduced proportions of *Ruminococcus* spp. at 6 h in white corn. Interestingly, the relative abundance of *Ruminococcus* spp. correlated negatively with isoferulic acid. As anticipated, white corn had the highest amount of isoferulic acid compared to other grains during the fermentation period, with a peak at 6 h (69.55 ± 85.68 ng/mg), suggesting a possible inhibitory effect against *Ruminococcus*. No data are available in the literature, but it should be noted that ferulic acid, which was the highest in white corn at 6 h as well, can suppress the growth of cellulolytic bacteria, including *Ruminococcus* spp. [46].

A prolonged positive effect of the soluble PA compounds in the colonic environment may emerge from the progressive release of soluble PA from the food matrix throughout the fermentation process. Additionally, the ability of the microbiota to alter PAs results in a variety of metabolites that, if taken into systemic circulation, may be advantageous for colonic health and may produce advantageous bioactivity in vivo. The health benefit of phenolic compounds, including PAs, may be attributed to their antioxidant and anti-inflammatory nature, which makes them relevant in the prevention of chronic illnesses [47].

In addition to antioxidant and anti-inflammatory benefits, phenolic compounds exhibit antibacterial, neuroprotective, anticancer, and cardioprotective functions [48]. For instance, ferulic acid's metabolic product vanillic acid has been shown to have antibacterial, anticancer, and anti-inflammatory characteristics, while ferulic acid-4-O-sulfate and

dihydroferulic acid have also been shown to have anti-inflammatory and cardioprotective qualities [49–53]. According to a study, pro-inflammatory cytokines were observed to be inhibited using derived phenolic acid metabolites [41].

Research is still ongoing to determine the precise mechanisms underlying these actions, but some indications suggest that phenolic compounds and their metabolites may act as antioxidants by linking with free radicals and extinguishing them while promoting the production of endogenous antioxidant enzymes [48]. They also function as antimicrobial agents by creating hydrogen bonds with bacterial cell membrane bilayers or interacting with cell wall constituents to compromise the microbial cells' barrier of defence. Additionally, they might bind toxins and disrupt the bacterial cell's energy metabolism [54,55].

Finally, in this study, 3-hydroxybenzaldehyde, which decreased over time in red fonio and red millet, had a positive correlation with *Akkermansia*. This bacterial genus has been shown to promote metabolic health (and is now available as a postbiotic for weight management and glycemic control), but its ability to degrade mucus raises questions about its overall safety [56,57].

4. Materials and Methods

4.1. Chemical Reagents

Twenty-six PA compounds and some potential metabolites; (vanillic acid (VA), isovanillic acid (IVA), 4-hydroxybenzaldehyde (4-HBALD), 3-hydroxybenzaldehyde (3-HBALD), 4-hydroxybenzoic acid (4-HBA), 3-hydroxybenzoic acid (3-HBA), salicylic acid (SA), 4-hydroxyphenylacetic acid (4-HPA), 3-hydroxyphenylacetic acid (3-HPA), 2-hydroxyphenylacetic acid (2-HPA), vanillin (VN), 3,4- and 3,5-dihydroxybenzoic acid sum (3,4- and 3,5-DHBAs), 2,5-dihydroxy benzoic acid (2,5-DHBA), 2,4-dihydroxybenzoic acid (2,4-DHBA), p-coumaric acid (pCA), gallic acid (GA), hippuric acid (HA), caffeic acid (CA), 3,4-dihydroxyhydrocinnamic acid (3,4-DHCA), homovanillic acid (HVA), syringaldehyde (SYRALD), ferulic acid (FA), isoferulic acid (IFA), hydroferulic acid (HFA), syringic acid (SYRA), and sinapic acid (SNA), 3,5-dichloro-4-hydroxybenzoic acid (used as internal standard), bile extract, pancreatin, α-amylase and pepsin were purchased from Sigma-Aldrich (Gillingham, UK). Analytical grade NaOH, $CaCl_2$, and HCl were also used, in addition to LC-MS grade solvents (formic acid, ethyl acetate, acetonitrile methanol, ethanol) and water. Peptone water (BDH, Poole, UK), yeast extract (Oxoid, Basingstoke, UK), NaCl, K_2HPO_4 (BDH), KH_2PO_4 (BDH), $MgSO_4 \times 7H_2O$ (Fisher Scientific, Loughborough, UK), $CaCl_2 \times 6H_2O$ (0.01 g/L), $NaHCO_3$ (Fisher Scientific), tween-80, hemin (0.05 g/L), vitamin K (10 µL/L), L-cysteine HCl (0.5 g/L), bile salts (0.5 g/L) (Oxoid, Basingstoke, UK), resazurin solution 0.025 g/100 mL (4 mL/L, pH 7), QIAamp DNA Stool Kit (QIAGEN, Hilden, Germany), phosphate-buffered saline (Oxoid, Basingstoke, UK), inulin (P95-FOS, Orafti, Tienen, Belgium), were also used.

4.2. Wholegrains

All grains analysed in this study were purchased from a Nigerian market located in Jos (9.8965° N, 8.8583° E). The grains included red and white varieties of fonio (*Digitaria* spp. *Iburua* and *exilis*) (also known as acha), red and white varieties of millet (*Pennisetum glaucum*), red and white varieties of sorghum (*Sorghum bicolor*), white corn (*Zea mays*) (also known as maise), and ofada rice (*Oryza glabberimma*).

4.3. Total Dietary Fibre (TDF) Determination

The total dietary fibre (TDF) levels of the wholegrain samples were determined using the Association of Official Analytical Chemists (AOAC) Official method 991.43 [58]. The results were expressed as g/100 g.

4.4. Wholegrain Processing (Cooking and Digestion)

Raw grains were milled and used for PA extraction. A preliminary screening analysis of the raw grains was made and led to the selection of the 4 grains utilised for the study.

The selection was made to include grains with varied fibre and PA contents. Selected grains (red fonio, red millet, red sorghum and white corn) were further studied to assess the impact of cooking and in vitro digestion on PA levels. Selected raw samples (100 g) were weighed and boiled in water until tender, with cooking times of 15 min, 36 min, 43 min and 79 min for red fonio, red millet, red sorghum and white corn, respectively (Table 3). After cooking, the samples were kept at −20 °C until digestion.

Table 3. Cooking protocol for grains.

Cereal Grain	Initial Weight (g)	Volume of Water Used (mL)	Cooking Time (min)	Cooling Time (min)	Final Weight (g)
Red fonio	101.13	600	15	15	551.86
Red millet	100.29	550	36	15	178.92
Red sorghum	100.61	500	43	10	176.89
White corn	100.33	750	79	10	152.99

After cooking, the samples were further processed in order to simulate the different phases of the digestion process (oral, gastric, and intestinal), with a procedure similar to the one described in [16] with minor adjustments. The oral phase of the digestion was performed as follows: a 10 g aliquot of milled and boiled samples was mixed with distilled water, and α-amylase was added (5 mg dissolved in 10 mL of 1 mM $CaCl_2$). The mixture was then kept at 37 °C for 30 min on a shaker. The gastric digestion phase was then simulated by adjusting the pH of the oral digest to 2 and adding 12 M HCl. Pepsin (51.2 mg/mL of sample) was then added, and the mixture was incubated at 37 °C for 2 h on a shaker. After incubation, the pH was increased to 7.5 to simulate the small intestinal conditions, using 6 M NaOH. Pancreatin (4 mg/mL of sample) and bile extract (25 mg/mL of sample) were added, and the mixture was kept at 37 °C for 2 h on a shaker. The final digested material of each sample was subsequently freeze-dried and kept at −20 °C until the subsequent analysis for PA characterisation by UPLC-MS/MS and in vitro colonic fermentation.

4.5. Colonic Fermentation

4.5.1. Basal Media Composition

The basal media was made by mixing yeast extract (Oxoid, Hampshire, UK), Peptone water (BDH, Poole, UK), KH_2PO_4 (BDH), $MgSO_4 \times 7H_2O$ NaCl, K_2HPO_4 (BDH), (Fisher Scientific, Loughborough, UK), $CaCl_2 \times 6H_2O$ (0.01 g/L), $NaHCO_3$ (Fisher Scientific), tween-80, hemin (0.05 g/L), vitamin K (10 µL/L), L-cysteine HCl (0.5 g/L), bile salts (0.5 g/L) (Oxoid, Basingstoke, UK) and resazurin solution 0.025 g/100 mL (4 mL/L, pH 7). The obtained solution was heated, cooled, poured into Duran bottles, autoclaved and stored until use.

4.5.2. In Vitro Fermentation

Faecal samples obtained from three healthy volunteers who were not taking any medications or supplements were used for this study. Faecal samples were diluted (1:10 w/v) in phosphate-buffered saline (0.1 mol/L phosphate-buffered solution, pH 7.4) and homogenised (Stomacher 400, Seward, UK) for 2 min at 240 paddle beats per min in vitro colonic fermentation was performed according to [17] in an anaerobic pH-controlled batch culture system. Five vessels were used for each faecal slurry; four of these vessels were used to ferment the digested grains (red fonio, red millet, red sorghum and white corn), and one vessel for the negative control, i.e., faecal slurry without any substrate addition. Each vessel was inoculated with 5 mL of fresh faecal slurry (1/10 w/w). Digested freeze-dried grain substrates (1% w/w dry solid/total dietary fibre) prepared in basal medium (full description of the basal medium composition is indicated in 2.5.1) were fermented. Batch cultures were run in three replicates (n = 3) over a period of 24 h, and samples were

collected from each vessel at 0, 2, 4, 6, 8 and 24 h for PAs extraction. Microbiota profiling was performed for 0, 6 and 24 h aliquots.

4.6. PAs Extraction and Analysis

PAs were extracted in soluble (free and conjugated) and bound fractions from 100 mg of raw and digested milled grains according to the method of [59] with slight modifications. An aliquot of 100 mg of the milled whole grain samples was used for the extraction procedure, and it was spiked with 5 μL of internal standard solution. 1 mL of 80% water/ethanol solution was also added to the solution. The solution was agitated with a vortex mixer and then sonicated for 10 min. The obtained solution was then centrifuged at 13,200 rpm for 15 min. The supernatant was collected, 1 mL of 80% ethanol was added, and the process was repeated to extract the phenolic acids. The residue was collected and used for the extraction of bound phenolic acids, while the combined supernatants were evaporated with nitrogen steam. The samples were then further processed in order to extract the conjugated phenolic acids as follows: a 400 μL aliquot of 2 M NaOH was added, and the samples were agitated and kept in the dark for 4 h. After this step, the solution was acidified by adding 80 μL 12 M HCl and then vortexed. 500 μL of ethyl acetate was added, and the sample was mixed again to facilitate extraction of the PAs. The solution was centrifuged (13,200 rpm, 5 min), and the supernatant was collected and evaporated. Ethyl acetate (500 μL) was added to the samples, and the extraction process was repeated again. The supernatant was then collected and combined with the first supernatant aliquot and dried under a nitrogen stream. The dried samples were kept at −20 °C until the subsequent PAs analysis. Before the extraction of bound PAs, 10 μL of internal standard was added to the residue. An alkaline hydrolysis procedure was performed with the addition of 400 μL of NaOH (2 M). The samples were kept in the dark for 4 h during the hydrolysis. Following this step, an aliquot of HCl (120 μL) was added to the solution to adjust the pH. The PAs were then extracted in ethyl acetate (800 μL) and centrifuged (13,200 rpm, 5 min) twice. The two supernatants were combined and fully evaporated under a nitrogen stream. The evaporated samples were kept at −20 °C until the time of analysis.

The process described above was used for the extraction of PAs from cooked samples; 100 mg equivalent of cooked grains was used for the extraction. Fermented samples (200 μL) were extracted and assayed for soluble PAs as described above; extracts were evaporated to dryness and purified using solid phase extraction (see below).

4.6.1. Solid Phase Extraction (SPE)

The evaporated samples were reconstituted by adding 0.5 mL acidified water (1% formic acid) and subjected to SPE as follows: Phenomenex SPE cartridges (StrataTM-X 33 μm, polymeric, reverse phase, 100 mg 3 mL^{-1}) were used, and preconditioned by adding 3 mL acidified methanol (1% formic acid), followed by 3 mL acidified water. The acidified water was allowed to elute through the cartridge, and 0.5 mL of acidified water was then added to the column. A 0.5 mL aliquot of reconstituted sample was also loaded onto the column and eluted through the column. The column was rinsed twice with 0.5 mL of acidified water and then washed twice with 6 mL of water before applying the vacuum. After the washing steps, the sample eluent was collected into clean tubes using acidified methanol (2.5 + 0.75 mL) as an eluting solvent, and the vacuum was then applied. The eluted samples were evaporated and reconstituted with acidified water (100 μL), vortexed (1 min), sonicated (2 min), mixed again (1 min), and transferred into a 96-well plate for UPLC-MS/MS analysis.

4.6.2. Ultraperformance Liquid Chromatography-Tandem Mass Spectrometry (UPLC-MS/MS)

Samples were filtered using 0.45 μm Polytetrafluoroethylene (PTFE) membrane filters prior to injection into the UPLC system. The PAs characterised by the samples were performed on a Waters Acquity H class UPLC system coupled to a Waters Xevo TQ micro

Mass spectrometer (Waters, Milford, MA, USA). The chromatographic separations were performed on sample aliquots (2 µL) injected on an Acquity UPLC HSS T3 1.8 µm column (2.1 × 100 mm) with an HSS T3 1.8 µm Vanguard pre-column at 45 °C (0.65 mL min^{-1} flow rate). The mobile phase consisted of 0.1% v/v formic acid/water (phase A) and 0.1% v/v formic acid/acetonitrile. (Phase B) and the gradient was 99% A, 99% A, 70% A, 5% A, 5% A, 99% A, and 99% A scheduled at 0, 1, 10, 12, 13, 13.10 and 16 min, respectively. Twenty-six PA standards were infused for MS tuning and Multiple Reaction Monitoring (MRM) method optimisation. Three fragments were targeted for each analyte, and the one with the most intense signal was used for quantification. Calibration curves were used for the quantification of each compound using analytical grade standards (0.05–100 µg/mL range) and plotted against peak areas; R^2 values (all higher than 0.95), limit of detection (LOD) and limit of Quantification (LOQ) concentrations were estimated as part of the method development and validation, and signal to noise ratios limits were set to (S/N) ≥ 3 (LOD) and S/N ≥ 10 (LOQ). LC-MS data were analysed using MassLynx software (V4.1, Waters, Milford, MA, USA). Total PA content was reported as the sum of both soluble and bound forms of PAs and expressed as ng/g fresh or dry weight.

4.7. Gut Microbiota Profiling

The gut microbiota profiling of the fermented samples was performed using the QIAamp DNA Stool Kit (QIAGEN, Hilden, Germany) on the DNA extracted from sample aliquots (250 mg) according to the kit instructions. The DNA concentration was measured on a NanoDrop ND-1000 spectrophotometer (NanoDrop Technologies, Thermo Scientific, Waltham, MA, USA). 16S rRNA amplicon sequencing and bioinformatics were applied as previously reported [17].

4.8. Statistical Analysis

PA analyses were performed in datasets for analysis conducted in triplicate for each raw and fermented sample and in duplicate for cooked and digested samples. The statistical analysis for all PA data was conducted on GraphPad Prism version 8 software (GraphPad Software, Boston, MA, USA). One-way ANOVA was performed to determine any significant differences in PA levels between grains, whereas a two-way ANOVA was performed to verify any significant effect of cooking and digestion on PA levels. Post hoc Tukey's multiple comparison test ($p \leq 0.05$) was used for both analyses. All results have been reported as mean ± SD.

Statistical analysis for the gut microbiota was performed as reported by [17], using the packages stats and vegan on R software (v4.2.0, R Foundation for Statistical Computing, Vienna, Austria). Non-parametric tests (Kruskal–Wallis test followed by post hoc Wilcoxon test) were performed using the stats package. Kendall rank correlation test was used to assess the associations between genus-level relative abundances and PA levels. Only statistically significant correlations with absolute Kendall's tau ≥ 0.3 were considered. A p-value ≤ 0.05 was considered statistically significant; a p-value between 0.05 and 0.1 was considered a trend.

5. Conclusions

In this study, we investigated the PA profile of specific Nigerian-grown grains and further investigated how cooking, in vitro gastrointestinal digestion and in vitro colonic fermentation affected the PA profiles in selected grains. Our results indicated that in vitro gastrointestinal digestion of grains induced a decrease in total soluble PAs and an increase in total bound PA when compared to raw grains. The appearance of new metabolic forms not measured in the raw grains was also observed. Our data also suggest a relationship between the PA profiles of Nigerian grains and the configuration of the gut microbiota. However, further studies are needed to investigate the directionality of this relationship and the underlying mechanisms. Our data indicate how the PAs in the grains were able to significantly modulate the large intestine environment, and the current findings provide a

robust starting point for further confirmation of the observed trends. Our findings provide a basis for a future in vivo study that also focuses on the potential beneficial effects of grains and their PAs on host health.

Supplementary Materials: The following supporting information can be downloaded at: https://www.mdpi.com/article/10.3390/ijms241814111/s1.

Author Contributions: G.C. and O.A.O. designed the research. G.C., A.C., Y.C.-P. and V.B. organised and supervised the research. O.A.O. conducted most parts of the experimental work. O.A.O. and G.C. analysed and summarised all in vitro UPLC-MS/MS data. O.A.O. and A.C. carried out the in vitro fermentation experiments and DNA extraction. M.B., S.T. and P.B. carried out 16S rRNA amplicon sequencing and analysis and wrote the microbiota-related parts with A.C. oversight. O.A.O. drafted the manuscript, with major revisions from A.C. and G.C. and contributions from all authors. G.C. had primary responsibility for the final content, and all authors gave final approval of the version to be submitted. All authors have read and agreed to the published version of the manuscript.

Funding: This research was funded by The University of Roehampton and Schlumberger Foundation (Faculty for the Future).

Institutional Review Board Statement: The University of Roehampton Research Ethics Committee (LSC 18-241) approved this study in accordance with the Declaration of Helsinki.

Informed Consent Statement: Not applicable.

Data Availability Statement: Sequencing reads were deposited in the National Center for Biotechnology Information Sequence Read Archive (NCBI SRA; BioProject ID PRJNA993861).

Conflicts of Interest: The authors declare no conflict of interest.

References

1. Călinoiu, L.F.; Vodnar, D.C.; Călinoiu, L.F.; Vodnar, D.C. Whole Grains and Phenolic Acids: A Review on Bioactivity, Functionality, Health Benefits and Bioavailability. *Nutrients* **2018**, *10*, 1615. [CrossRef] [PubMed]
2. Mundia, C.W.; Secchi, S.; Akamani, K.; Wang, G. A regional comparison of factors affecting global sorghum production: The case of North America, Asia and Africa's Sahel. *Sustainability* **2019**, *11*, 2135. [CrossRef]
3. Cruz, J.-F.; Béavogui, F.; Dramé, D.; Diallo, T.A. *Fonio, an African Cereal*; CIRAD and IRAG Edition; CIRAD: Montpellier, France, 2016; 153p.
4. National Research Council. *Lost Crops of Africa*; National Academies Press: Washington, DC, USA, 1996.
5. Adebiyi, J.A.; Obadina, A.O.; Adebo, O.A.; Kayitesi, E. Comparison of nutritional quality and sensory acceptability of biscuits obtained from native, fermented, and malted pearl millet (*Pennisetum glaucum*) flour. *Food Chem.* **2017**, *232*, 210–217. [CrossRef] [PubMed]
6. Fliedel, G.; Ouattara, M.; Grabulos, J.; Drame, D.; Cruz, J. *Effect of Mechanical Bleaching on the Technological, Culinary and Nutritional Quality of Fonio, a West African Cereal*; CIRAD: Montpellier, France, 2004.
7. Grains and Legumes Nutrition Council. *Nutrient Database of Grains and Legumes Produced in Australia: Pilot Study Results*; Grains and Legumes Nutrition Council: South Perth, Australia, 2014.
8. Grains & Legumes Nutrition Council Ltd. *Nutrient Composition of Grains & Pseudo Grains*; Grains & Legumes Nutrition Council Ltd.: South Perth, Australia, 2012.
9. Mohapatra, D.; Patel, A.S.; Kar, A.; Deshpande, S.S.; Tripathi, M.K. Effect of different processing conditions on proximate composition, anti-oxidants, anti-nutrients and amino acid profile of grain sorghum. *Food Chem.* **2019**, *271*, 129–135. [CrossRef] [PubMed]
10. Adeyeye, S.A.O.; Bolaji, O.T.; Abegunde, T.A.; Idowu-Adebayo, F.; Tiamiyu, H.K.; Adebayo-Oyetoro, A.O. Nutritional composition and heavy metal profile of Nigerian rice varieties. *Curr. Res. Nutr. Food Sci.* **2019**, *7*, 576–583. [CrossRef]
11. Ebuehi, O.A.T.; Oyewole, A.C. Effect of cooking and soaking on physical, nutrient composition and sensory evaluation of indigenous and foreign rice varieties in Nigeria. *Afr. J. Biotechnol.* **2007**, *6*, 1016–1020.
12. Hiran, P.; Kerdchoechuen, O.; Laohakunjit, N. Combined effects of fermentation and germination on nutritional compositions, functional properties and volatiles of maize seeds. *J. Cereal Sci.* **2016**, *71*, 207–216. [CrossRef]
13. Rahman, M.M.; Rahaman, M.S.; Islam, M.R.; Rahman, F.; Mithi, F.M.; Alqahtani, T.; Almikhlafi, M.A.; Alghamdi, S.Q.; Alruwaili, A.S.; Hossain, M.S.; et al. Role of Phenolic Compounds in Human Disease: Current Knowledge and Future Prospects. *Molecules* **2021**, *27*, 233. [CrossRef]
14. Oluseyi, T.; Folarin, B.; Adegbola, R.; Olayinka, K. Proximate analysis, mineral element and total phenolic contents of some commonly consumed grains in Nigeria. *Ilorin J. Sci.* **2021**, *8*, 91–102.

15. Popoola, O.O. Phenolic compounds composition and in vitro antioxidant activity of Nigerian Amaranthus viridis seed as affected by autoclaving and germination. *Meas. Food* **2022**, *6*, 100028. [CrossRef]
16. Corona, G.; Ji, Y.; Anegboonlap, P.; Hotchkiss, S.; Gill, C.; Yaqoob, P.; Spencer, J.P.E.; Rowland, I. Gastrointestinal modifications and bioavailability of brown seaweed phlorotannins and effects on inflammatory markers. *Br. J. Nutr.* **2016**, *115*, 1240–1253. [CrossRef] [PubMed]
17. Corona, G.; Kreimes, A.; Barone, M.; Turroni, S.; Brigidi, P.; Keleszade, E.; Costabile, A. Impact of lignans in oilseed mix on gut microbiome composition and enterolignan production in younger healthy and premenopausal women: An in vitro pilot study. *Microb. Cell Fact.* **2020**, *19*, 82. [CrossRef] [PubMed]
18. Capuano, E. The behavior of dietary fiber in the gastrointestinal tract determines its physiological effect. *Crit. Rev. Food Sci. Nutr.* **2017**, *57*, 3543–3564. [CrossRef] [PubMed]
19. Mandalari, G.; Vardakou, M.; Faulks, R.; Bisignano, C.; Martorana, M.; Smeriglio, A.; Trombetta, D. Food Matrix Effects of Polyphenol Bioaccessibility from Almond Skin during Simulated Human Digestion. *Nutrients* **2016**, *8*, 568. [CrossRef]
20. Makame, J.; De Kock, H.; Emmambux, N.M. Nutrient density of common African indigenous/local complementary porridge samples. *LWT* **2020**, *133*, 109978. [CrossRef]
21. Ragaee, S.; Abdelaal, E.; Noaman, M. Antioxidant activity and nutrient composition of selected cereals for food use. *Food Chem.* **2006**, *98*, 32–38. [CrossRef]
22. Hager, A.S.; Wolter, A.; Jacob, F.; Zannini, E.; Arendt, E.K. Nutritional properties and ultra-structure of commercial gluten free flours from different botanical sources compared to wheat flours. *J. Cereal Sci.* **2012**, *56*, 239–247. [CrossRef]
23. Das, A.K.; Singh, V. Antioxidative free and bound phenolic constituents in pericarp, germ and endosperm of Indian dent (*Zea mays* var. *indentata*) and flint (*Zea mays* var. *indurata*) maize. *J. Funct. Foods* **2015**, *13*, 363–374.
24. Ryu, D.; Koh, E. Influence of Cooking Methods on Free and Bound Phenolic Acids in Korean Black Rice. *J. Food Process. Preserv.* **2017**, *41*, e12873. [CrossRef]
25. Hithamani, G.; Srinivasan, K. Effect of domestic processing on the polyphenol content and bioaccessibility in finger millet (*Eleusine coracana*) and pearl millet (*Pennisetum glaucum*). *Food Chem.* **2014**, *164*, 55–62. [CrossRef]
26. N'Dri, D.; Mazzeo, T.; Zaupa, M.; Ferracane, R.; Fogliano, V.; Pellegrini, N. Effect of cooking on the total antioxidant capacity and phenolic profile of some whole-meal African cereals. *J. Sci. Food Agric.* **2013**, *93*, 29–36. [CrossRef]
27. Harakotr, B.; Suriharn, B.; Tangwongchai, R.; Scott, M.P.; Lertrat, K. Anthocyanin, phenolics and antioxidant activity changes in purple waxy corn as affected by traditional cooking. *Food Chem.* **2014**, *164*, 510–517. [CrossRef]
28. Fares, C.; Platani, C.; Baiano, A.; Menga, V. Effect of processing and cooking on phenolic acid profile and antioxidant capacity of durum wheat pasta enriched with debranning fractions of wheat. *Food Chem.* **2010**, *119*, 1023–1029. [CrossRef]
29. Finocchiaro, F.; Ferrari, B.; Gianinetti, A.; Dall'Asta, C.; Galaverna, G.; Scazzina, F.; Pellegrini, N. Characterization of antioxidant compounds of red and white rice and changes in total antioxidant capacity during processing. *Mol. Nutr. Food Res.* **2007**, *51*, 1006–1019. [CrossRef] [PubMed]
30. Salazar-López, N.J.; González-Aguilar, G.A.; Rouzaud-Sández, O.; Robles-Sánchez, M. Bioaccessibility of hydroxycinnamic acids and antioxidant capacity from sorghum bran thermally processed during simulated in vitro gastrointestinal digestion. *J. Food Sci. Technol.* **2018**, *55*, 2021–2030. [CrossRef] [PubMed]
31. Palafox-Carlos, H.; Ayala-Zavala, J.F.; González-Aguilar, G.A. The Role of Dietary Fiber in the Bioaccessibility and Bioavailability of Fruit and Vegetable Antioxidants. *J. Food Sci.* **2011**, *76*, 6–15. [CrossRef]
32. Luzardo-Ocampo, I.; Campos-Vega, R.; Gaytán-Martínez, M.; Preciado-Ortiz, R.; Mendoza, S.; Loarca-Piña, G. Bioaccessibility and antioxidant activity of free phenolic compounds and oligosaccharides from corn (*Zea mays* L.) and common bean (*Phaseolus vulgaris* L.) chips during in vitro gastrointestinal digestion and simulated colonic fermentation. *Food Res. Int.* **2017**, *100*, 304–311. [CrossRef]
33. Ruíz-García, Y.; Beres, C.; Chávez, D.W.H.; Pereira, D.C.d.S.; Santiago, M.C.P.A.; Godoy, R.d.O.; Gomes, F.d.S.; Antoniassi, R.; Tonon, R.V.; Cabral, L.M.C. In vitro digestion and colonic fermentation of an Alicante Bouschet (*Vitis vinifera* L.) skin extract. *LWT* **2022**, *157*, 113083. [CrossRef]
34. Huang, G.; Wang, Z.; Wu, G.; Cao, X.; Zhang, R.; Dong, L.; Huang, F.; Zhang, M.; Su, D. In vitro simulated digestion and colonic fermentation of lychee pulp phenolics and their impact on metabolic pathways based on fecal metabolomics of mice. *Food Funct.* **2021**, *12*, 203–214. [CrossRef]
35. Cárdenas-Castro, A.P.; Zamora-Gasga, V.M.; Alvarez-Parrilla, E.; Ruíz-Valdiviezo, V.M.; Venema, K.; Sáyago-Ayerdi, S.G. In vitro gastrointestinal digestion and colonic fermentation of tomato (*Solanum lycopersicum* L.) and husk tomato (*Physalis ixocarpa* Brot.): Phenolic compounds released and bioconverted by gut microbiota. *Food Chem.* **2021**, *360*, 130051. [CrossRef]
36. Serra, A.; Maclà, A.; Romero, M.P.; Reguant, J.; Ortega, N.; Motilva, M.J. Metabolic pathways of the colonic metabolism of flavonoids (flavonols, flavones and flavanones) and phenolic acids. *Food Chem.* **2012**, *130*, 383–393. [CrossRef]
37. Hernández-Maldonado, L.M.; Blancas-Benítez, F.J.; Zamora-Gasga, V.M.; Cárdenas-Castro, A.P.; Tovar, J.; Sáyago-Ayerdi, S.G. In vitro gastrointestinal digestion and colonic fermentation of high dietary fiber and antioxidant-rich mango (*Mangifera indica* L.) "ataulfo"-based fruit bars. *Nutrients* **2019**, *11*, 1564. [CrossRef] [PubMed]
38. Rowland, I.; Gibson, G.; Heinken, A.; Scott, K.; Swann, J.; Thiele, I.; Tuohy, K. Gut microbiota functions: Metabolism of nutrients and other food components. *Eur. J. Nutr.* **2018**, *57*, 1–24. [CrossRef] [PubMed]

39. Chesson, A.; Provan, G.J.; Russell, W.R.; Scobbie, L.; Richardson, A.J.; Stewart, C. Hydroxycinnamic acids in the digestive tract of livestock and humans. *J. Sci. Food Agric.* **1999**, *79*, 373–378. [CrossRef]
40. Gaur, G.; Gänzle, M.G. Conversion of (poly)phenolic compounds in food fermentations by lactic acid bacteria: Novel insights into metabolic pathways and functional metabolites. *Curr. Res. Food Sci.* **2023**, *6*, 100448. [CrossRef]
41. Monagas, M.; Khan, N.; Andrés-Lacueva, C.; Urpí-Sardá, M.; Vázquez-Agell, M.; Lamuela-Raventós, R.M.; Estruch, R. Dihydroxylated phenolic acids derived from microbial metabolism reduce lipopolysaccharide-stimulated cytokine secretion by human peripheral blood mononuclear cells. *Br. J. Nutr.* **2009**, *102*, 201–206. [CrossRef]
42. Leonard, W.; Zhang, P.; Ying, D.; Fang, Z. Hydroxycinnamic acids on gut microbiota and health. *Compr. Rev. Food Sci. Food Saf.* **2021**, *20*, 710–737. [CrossRef]
43. Bustamante, L.; Pastene, E.; Duran-Sandoval, D.; Vergara, C.; Von Baer, D.; Mardones, C. Pharmacokinetics of low molecular weight phenolic compounds in gerbil plasma after the consumption of calafate berry (*Berberis microphylla*) extract. *Food Chem.* **2018**, *268*, 347–354. [CrossRef]
44. Kristek, A.; Wiese, M.; Heuer, P.; Kosik, O.; Schär, M.Y.; Soycan, G.; Alsharif, S.; Kuhnle, G.G.C.; Walton, G.; Spencer, J.P.E. Oat bran, but not its isolated bioactive β-glucans or polyphenols, have a bifidogenic effect in an in vitro fermentation model of the gut microbiota. *Br. J. Nutr.* **2019**, *121*, 549–559. [CrossRef]
45. Hunter, W.J.; Manter, D.K.; Van Der Lelie, D. Biotransformation of ferulic acid to 4-vinylguaiacol by *Enterobacter soli* and *E. aerogenes*. *Curr. Microbiol.* **2012**, *65*, 752–757. [CrossRef]
46. Wang, Y.-L.; Wang, W.-K.; Wu, Q.-C.; Yang, H.-J. The release and catabolism of ferulic acid in plant cell wall by rumen microbes: A review. *Anim. Nutr.* **2022**, *9*, 335–344. [CrossRef] [PubMed]
47. Rudrapal, M.; Khairnar, S.J.; Khan, J.; Bin Dukhyil, A.; Ansari, M.A.; Alomary, M.N.; Alshabrmi, F.M.; Palai, S.; Deb, P.K.; Devi, R. Dietary Polyphenols and Their Role in Oxidative Stress-Induced Human Diseases: Insights Into Protective Effects, Antioxidant Potentials and Mechanism(s) of Action. *Front. Pharmacol.* **2022**, *13*, 283. [CrossRef] [PubMed]
48. Yahfoufi, N.; Alsadi, N.; Jambi, M.; Matar, C. The immunomodulatory and anti-inflammatory role of polyphenols. *Nutrients* **2018**, *10*, 1618. [CrossRef] [PubMed]
49. Sova, M.; Saso, L. Natural sources, pharmacokinetics, biological activities and health benefits of hydroxycinnamic acids and their metabolites. *Nutrients* **2020**, *12*, 219. [CrossRef]
50. Keman, D.; Soyer, F. Antibiotic-resistant Staphylococcus aureus does not develop resistance to vanillic acid and 2-hydroxycinnamic acid after continuous exposure in vitro. *ACS Omega* **2019**, *4*, 15393–15400. [CrossRef]
51. Kim, M.-C.; Kim, S.-J.; Kim, D.-S.; Jeon, Y.-D.; Park, S.J.; Lee, H.S.; Um, J.-Y.; Hong, S.-H. Vanillic acid inhibits inflammatory mediators by suppressing NF-κB in lipopolysaccharide-stimulated mouse peritoneal macrophages. *Immunopharmacol. Immunotoxicol.* **2011**, *33*, 525–532. [CrossRef]
52. Van Rymenant, E.; Van Camp, J.; Pauwels, B.; Boydens, C.; Vanden Daele, L.; Beerens, K.; Brouckaert, P.; Smagghe, G.; Kerimi, A.; Williamson, G. Ferulic acid-4-O-sulfate rather than ferulic acid relaxes arteries and lowers blood pressure in mice. *J. Nutr. Biochem.* **2017**, *44*, 44–51. [CrossRef]
53. Baeza, G.; Bachmair, E.-M.; Wood, S.; Mateos, R.; Bravo, L.; De Roos, B. The colonic metabolites dihydrocaffeic acid and dihydroferulic acid are more effective inhibitors of in vitro platelet activation than their phenolic precursors. *Food Funct.* **2017**, *8*, 1333–1342. [CrossRef]
54. Bouarab-Chibane, L.; Forquet, V.; Lantéri, P.; Clément, Y.; Léonard-Akkari, L.; Oulahal, N.; Degraeve, P.; Bordes, C. Antibacterial properties of polyphenols: Characterization and QSAR (Quantitative structure-activity relationship) models. *Front. Microbiol.* **2019**, *10*, 829. [CrossRef]
55. Mithul Aravind, S.; Wichienchot, S.; Tsao, R.; Ramakrishnan, S.; Chakkaravarthi, S. Role of dietary polyphenols on gut microbiota, their metabolites and health benefits. *Food Res. Int.* **2021**, *142*, 110189. [CrossRef]
56. EFSA Panel on Nutrition, Novel Foods and Food Allergens (NDA); Turck, D.; Bohn, T.; Castenmiller, J.; De Henauw, S.; Hirsch-Ernst, K.I.; Maciuk, A.; Mangelsdorf, I.; McArdle, H.J.; Naska, A.; et al. Safety of pasteurised Akkermansia muciniphila as a novel food pursuant to Regulation (EU) 2015/2283. *EFSA J.* **2021**, *19*, e06780. [PubMed]
57. Depommier, C.; Everard, A.; Druart, C.; Plovier, H.; Van Hul, M.; Vieira-Silva, S.; Falony, G.; Raes, J.; Maiter, D.; Delzenne, N.M.; et al. Supplementation with Akkermansia muciniphila in overweight and obese human volunteers: A proof-of-concept exploratory study. *Nat. Med.* **2019**, *25*, 1096–1103. [CrossRef] [PubMed]
58. AOAC Official Methods of Analysis. *Annex G AOAC Official Method 991.43. Total, Soluble and Insoluble Dietary Fibre in Foods*; AOAC: Rockville, MD, USA, 1995; pp. 7–9.
59. Li, L.; Peter, R.S.; Jane, L.W. Phenolic Acids in Wheat Varieties in the HEALTHGRAIN Diversity Screen. *J. Agric. Food Chem.* **2008**, *56*, 9732–9739. [CrossRef] [PubMed]

International Journal of
Molecular Sciences

MDPI

Opinion

Current Challenges and Opportunities for Improved Cannabidiol Solubility

Khondker Rufaka Hossain [1], Amani Alghalayini [1,2] and Stella M. Valenzuela [1,2,*]

[1] School of Life Sciences, University of Technology Sydney, Sydney, NSW 2007, Australia; khondker.hossain@uts.edu.au (K.R.H.); amani.alghalayini@uts.edu.au (A.A.)
[2] ARC Research Hub for Integrated Device for End-User Analysis at Low-Levels (IDEAL), Faculty of Science, University of Technology Sydney, Sydney, NSW 2007, Australia
* Correspondence: stella.valenzuela@uts.edu.au; Tel.: +61-2-95141917

Abstract: Cannabidiol (CBD), derived from the cannabis plant, has gained significant attention due to its potential therapeutic benefits. However, one of the challenges associated with CBD administration is its low bioavailability, which refers to the fraction of an administered dose that reaches systemic circulation. This limitation necessitates the exploration of various approaches to enhance the bioavailability of CBD, thus helping to maximize its therapeutic potential. A variety of approaches are now emerging, including nanoemulsion-based systems, lipid-based formulations, prodrugs, nanocarriers, and alternative routes of administration, which hold promise for improving the bioavailability of CBD and pave the way for novel formulations that maximize the therapeutic potential of CBD in various medical conditions. This opinion piece presents the current understanding surrounding CBD bioavailability and considers strategies aimed at improving both its absorption and its bioavailability.

Keywords: bioavailability; cannabidiol; CBD; solubility; stability

Citation: Hossain, K.R.; Alghalayini, A.; Valenzuela, S.M. Current Challenges and Opportunities for Improved Cannabidiol Solubility. *Int. J. Mol. Sci.* **2023**, *24*, 14514. https://doi.org/10.3390/ijms241914514

Academic Editor: Maurizio Battino

Received: 24 August 2023
Revised: 20 September 2023
Accepted: 22 September 2023
Published: 25 September 2023

1. Introduction

Cannabidiol (CBD) is a phytocannabinoid extracted from cannabis plant species, including *Cannabis indica*, *Cannabis sativa*, or *Cannabis ruderalis* (also commonly known as hemp or marijuana) [1]. Although structurally similar to the psychoactive cannabinoid delta-9-tetrahydrocannabinol (THC), CBD does not cause intoxication or euphoric states and thus has low abuse potential while exhibiting a wide range of pharmacological effects [2]. A number of studies and clinical trials are now emerging that show CBD exhibits various therapeutic effects in conditions that range from epilepsy, psychotic disorders, anxiety, diabetes, sleep disorders, cardiovascular diseases, rheumatoid arthritis, pain, skin aging, antioxidant, and inflammation to cancer therapy [3–5]. As the therapeutic virtues of CBD are becoming better known and accepted, and given its favorable safety profile, a large number of countries globally have now legalized the use of CBD for medicinal purposes [6].

Studies suggest that CBD's molecular activities are via the human endocannabinoid system (ECS), which includes two main cannabinoid receptors (CB1 and CB2) and endogenous ligands called endocannabinoids known to modulate CB receptor activities [7–9]. CB1 receptors are predominantly found in the central nervous system (CNS) and are highly expressed in regions such as the cerebral cortex, basal ganglia, hippocampus, and cerebellum. CB1 receptors are also present in peripheral tissues like the heart, liver, pancreas, muscles, adipose tissue, and the reproductive system. CB2 receptors are mainly expressed in cells related to the immune system, such as leukocytes, and are also found in the spleen, thymus, bone marrow, and other tissues related to immune functions. Although the therapeutic benefits of CBD are mainly generated from CBD's role in the ECS, CBD

does not directly activate the cannabinoid receptors instead, it has been shown to influence endocannabinoid balance [9]. There are two endocannabinoids, anandamide (AEA) and 2-arachidonoylglycerol (2-AG), that act as ligands for the cannabinoid receptors, and degradation of these endocannabinoids by fatty acid amide hydrolase (FAAH) and monoacylglycerol lipase (MAGL) enzymes has been shown to regulate CB receptor activities. CBD by inhibiting FAAH enzymatic activity has been shown to increase endogenous levels of AEA, which in turn has been shown to modulate the CB receptors, thereby indirectly exhibiting a wide range of pharmacological effects (for further details, see review [9]).

In addition, CBD also binds with varying affinity to a series of other receptors, including but not limited to transient receptor potential vanilloid (TRPV), peroxisome proliferator-activated receptor gamma (PPARγ), as well as G protein-coupled receptors like GPR55 and serotonin 1A receptor (5-HT1A). CBD has allosteric binding activity with these receptors, where CBD binds to CB1 as an inverse agonist/antagonist; its binding to CB2 and GPR55 sees it acting as an antagonist; and on TRPV receptors and 5-HT1A, it acts as a partial agonist, respectively. It is also an inhibitor of the FAAH enzyme, and inhibition of FAAH and its interaction with 5-HT1A and TRPV1 receptors were found to play a role in CBD's antipsychotic properties. The anti-depressive and anxiolytic activities of CBD were also attributed to its interaction with 5-HT1A. CBD has also shown high affinity for receptors and channels related to epilepsy, including TRPV receptors, T-type Ca^{2+} channels, serotine receptors, and GPR55. Studies have also shown that by inhibiting FAAH enzymes and GABA receptors, CBD is able to influence sleep. On the other hand, suppression of IFN-γ and TNF-α production and inhibition of T-cell proliferation by CBD were attributed to its role in diabetes. The affinity and action of the CBD-related receptors and the molecular mechanisms of action of the therapeutic effects of CBD within different disease contexts have been summarized in detail by Peng, J. et al., 2022 [9]. Furthermore, CBD has also been shown to exhibit antioxidant properties not by interacting with any receptors or enzymes but simply due to the presence of two hydroxyl groups in its chemical structure (Figure 1) that endow it with antioxidant activity [10].

To date, several CBD-based drugs have been approved by the United States Food and Drug Administration (FDA), the European Medicines Agency (EMA), the Australian Therapeutic Goods Administration (TGA), and other regulatory agencies worldwide [11]. Some examples of approved CBD-based drugs include Epidiolex, which is currently approved by the FDA as an oral solution and primarily prescribed for managing seizures associated with Lennox–Gastaut syndrome or Dravet syndrome in patients 2 years of age and older [12]. Arvisol is another patented oral tablet that contains pure, natural CBD and is recommended for the treatment of Rett syndrome, schizophrenia, and epilepsy. Several other CBD-based medications are also currently undergoing clinical or pre-clinical trials for their therapeutic application in conditions such as those mentioned above; for details, see the review by Stella, B. et al., 2021 [13]. In addition, due to its antioxidant capabilities, there are now more than a few CBD-based skincare products also marketed in the form of oils, gummies, capsules, and even creams [10].

Nevertheless, even though CBD is increasingly being successfully used as a therapeutic agent and for assisting in the management of several conditions, future CBD-based medications and clinical applications remain subject to a number of limitations and challenges. Low oral bioavailability of CBD remains one of, if not the most challenging, issues posing a hindrance to the further success of these compounds as therapeutic agents. This opinion piece therefore aims to highlight some of the challenges associated with the poor bioavailability of CBD molecules, with the objective of presenting some of the current strategies being explored to overcome these challenges. To compile a comprehensive opinion piece, an extensive search of the literature was conducted on relevant databases like PubMed, Scopus, Science Direct, and Web of Science. Only peer-reviewed journal articles and already patented formulations/methods claiming to improve the solubility and/or bioavailability of CBD were included. Also, articles not dating back to more than 5–10 years

were selected in order to highlight recent and relevant research. Older articles were only included if they were seminal or had biological significance.

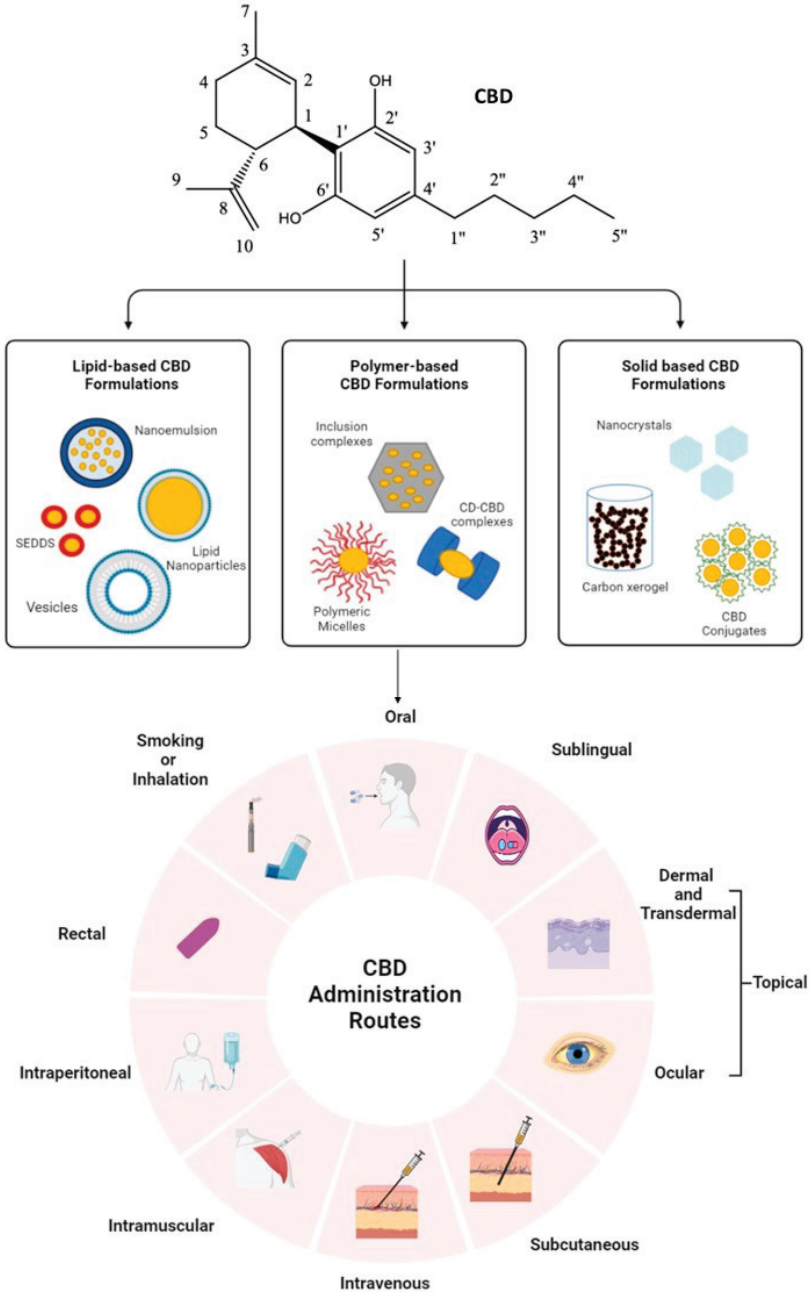

Figure 1. An illustration summarizing the range of different chemical modification or encapsulation approaches currently being examined in order to enhance CBD solubility, along with a variety of administration routes (Image created on Biorender.com).

2. CBD Chemical Structure, Absorption, and Bioavailability

CBD is a 21-carbon terpene phenolic compound, thus making it a relatively large molecule. Its chemical structure is composed of a long linear hydrocarbon chain with a benzene ring at one end, as shown in Figure 1. This structure gives it a large hydrophobic area, which contributes to its lipophilicity and hydrophobicity [14]. Thus, CBD's poor water solubility and high lipophilicity result in its relatively low and inconsistent bioavailability [15].

As a hydrophobic molecule, CBD is primarily absorbed through passive diffusion in the gastrointestinal tract. After oral administration, CBD interacts with bile salts and forms micelles, which facilitate its absorption by the small intestine [16]. The absorption of CBD can be influenced by factors such as formulation, food intake, and individual variations. In addition, evidence of its interaction and effects on the gastrointestinal microbiota is now emerging, which may also influence its absorption and activity (for further details, see the following review papers [17–19]). Once absorbed, CBD, being hydrophobic, binds to plasma carrier proteins, particularly lipoproteins and albumin, for transportation throughout the body. Although the search for intracellular transporters for phytocannabinoids is still being extensively researched, studies have shown fatty acid-binding proteins (FABPs) act as soluble intracellular carriers for the transportation of these hydrophobic compounds from the plasma membrane to the site of action [20]. FABPs are intracellular proteins that mediate AEA transport to its catabolic enzyme FAAH, primarily localized in the endoplasmic reticulum [21]. CBD has been shown to bind soluble FABPs for transportation to FAAH enzymes, and binding of CBD to FABPs has also been shown to inhibit transportation of AEA, resulting in reduced catabolism of AEA by FAAH [20,21]. Being lipophilic, CBD also tends to accumulate in lipophilic tissues such as adipose tissue, further contributing to its low bioavailability [22]. Despite these absorption obstacles and poor bioavailability, one of the advantages of CBD is that it can cross the blood–brain barrier and appears not to be a substrate for P-glycoprotein, thus making it an interesting drug for central nervous system applications [23]. Another advantage of CBD is that not only can it be structurally modified but also successfully formulated into various different dosage forms for administration via different routes, which presents a plethora of possibilities to overcome these obstacles. The following section highlights some of the factors affecting the bioavailability of these compounds and the delivery approaches being trialed in order to improve the bioavailability and solubility of CBD for enhanced therapeutic benefits.

3. Factors Affecting the Bioavailability of CBD

Physiochemical properties of CBD, like solubility and stability, along with its bioactivity, permeability, and metabolism, are some of the main elements that affect the bioavailability and absorption rates of CBD compounds, as well as variable pharmacokinetic profiles and possible polymorphisms. Studies have shown polymorphisms to significantly impact the behavior of the CBD molecule and, in turn, its potential therapeutic activity. CBD presents in two or more inherent crystalline forms that can affect its stability, which is a concern as this, in turn, influences CBD's absorption rate and thus its bioavailability [24]. CBD is also known to be sensitive to light [25], temperature [26] and auto-oxidation [10]. Mazzetti, et al. (2020) demonstrated that CBD samples stored in the dark showed less degradation compared to CBD samples exposed to light [25]. CBD is also sensitive to heat, where incubation of CBD compounds under high-temperature conditions for long periods of time can reduce CBD stability [26]. Furthermore, oxidation of CBD has been shown to contribute to its degradation, thus altering the pharmacological properties of CBD and reducing its potential therapeutic benefits, as most of it would be broken down before it reaches the bloodstream [10]. Although the greatest limitation in CBD drug development comes from the poor solubility of these compounds, another major factor that affects CBD's bioavailability is that it undergoes extensive first-pass metabolism when taken orally [27,28].

After oral administration, the portion of the CBD that is absorbed first travels to the liver via the hepatic portal system, where it undergoes extensive first-pass metabolism [27,28] primarily by cytochrome P450 (CYP) enzymes and specifically the CYP3A subfamily [29]. These enzymes convert CBD into various metabolites, the main ones being 7-carboxy-cannabidiol (7-COOH-CBD), 7-hydroxy-cannabidiol (7-OH-CBD), and a minor metabolite called 6-hydroxy-cannabidiol (6-OH-CBD). Among the identified major metabolites of CBD in humans, the most abundant metabolite, 7-COOH-CBD, was found to be inactive, which further impacts the bioavailability of these compounds [15]. The remainder is then transported in the blood to the site of action. Since the effectiveness of any CBD medication depends primarily on its successful delivery and uptake at the intended site of action, increasing efforts are being made to improve the bioavailability of cannabinoids. Hence, different routes of administration that can help bypass the first-pass hepatic metabolism are constantly being investigated in order to improve bioavailability [27,28].

4. Administration Routes of CBD

The choice of administration route can significantly impact the bioavailability, onset of action, and overall effectiveness of CBD. There are a variety of different administration routes, for example, oral, sublingual, dermal and transdermal, topical, subcutaneous, rectal, intramuscular, intraperitoneal, and smoking or inhalation, that have been implicated in improving CBD bioavailability.

Administration of CBD via the oral route is the most common and convenient for patients and involves the ingestion of CBD products such as capsules, edibles, or tinctures [30]. However, it is associated with several drawbacks. Firstly, CBD being hydrophobic results in low absorption of the drug, and what is absorbed is subjected to extensive first-pass metabolism, resulting in a low and variable reported oral bioavailability of approximately 9–13% [4,14]. Secondly, the oral route's onset of action is delayed compared to other routes, typically ranging from 30 min to 2 h [15]. To overcome this problem, studies have suggested oral consumption of CBD with food with high lipid content or in a lipid solution, which has been shown to enhance CBD bioavailability [3,4,31].

In addition, other routes of administration have also been investigated that have been shown to improve CBD bioavailability. One such route is the sublingual administration of CBD. This route allows CBD oil or extract to be absorbed directly into the bloodstream through the sublingual mucosa, which helps to bypass first-pass metabolism. Studies have shown CBD administered through the sublingual route results in a higher bioavailability of approximately 12% to 35% compared to the 9–13% observed for oral administration [32,33]. Currently, orally disintegrating tablets, or orodispersible (ODTs) CBD tablets, have also been developed by several different methods with varying formulations for sublingual administration, as these tablets are designed and formulated to disintegrate directly in the mouth for absorption [34–36]. ODTs also have the advantage of delivering large amounts of CBD that increase bioavailability, mainly due to the ease of manufacturing, where CBD can be compressed directly as solid or liquisolid powdered tablets [34–36]. In a study aimed at developing ODTs with CBD using varying formulations, an optimal formulation had a disintegration time of 27 s and 99.3 $\pm$ 6% of CBD released within 30 min [36]. Another study showed CBD–Ethanol liquisolid ODTs to exhibit a similarly high dissolution efficiency of 93.5 $\pm$ 2.6% [34].

However, the highest concentration of CBD in the blood was found using an intravenous injection method, followed closely by inhalation via smoking, which facilitated rapid delivery of CBD [3,4,37]. Inhalation of CBD involves vaporizing CBD oil or smoking CBD by using a vaporizer or traditional smoking methods, and these appear to offer some of the highest bioavailability among all administration routes, approximately 31–45%. However, studies have shown that vaporizing or smoking CBD has the effect of shortening the half-life of CBD in the blood [4,33]. In addition, a recent study showed that vaping CBD induces a potent inflammatory response with higher oxidative damage, leading to increased pathological changes associated with lung injury compared to vaping nicotine [38]. Hence,

there is a pressing need for further investigation and for alternative routes or strategies to improve CBD solubility and bioavailability.

Other routes that have also been investigated include dermal and transdermal administration. This route involves applying CBD-infused products, such as creams or lotions, directly to the skin, enabling CBD to penetrate through the skin layers and reach the systemic circulation. However, both dermal and transdermal routes offer limited bioavailability (1% to 10%) [33,39], and several studies reported the accumulation of CBD in the outermost layers of the epidermis without penetration to the deeper tissue layers (see review articles [4,11,14,40]). Another topical application involving the ocular administration of CBD, primarily for conditions such as glaucoma or inflammation, has also shown limited systemic absorption, with CBD predominantly acting locally within the eye [41]. Although topical administration routes target specific areas of the body, providing limited systemic absorption and localized relief, particularly for conditions such as inflammation, arthritis, and muscle pain, these routes are still associated with low bioavailability [37].

Evaluation of additional routes, such as the subcutaneous administration route where CBD was injected into the fatty tissue layer beneath the skin, has been shown to provide a slow and sustained release of CBD into the systemic circulation and bypass the liver first-pass metabolism [42,43]. Similar advantages were also provided by the intramuscular administration route, which involves injecting CBD directly into the muscle tissue [44]. However, these routes are associated with a delayed onset of action due to the slow release of the compound into the circulation. A current study aimed at investigating the intraperitoneal administration of CBD using nanoparticle delivery systems for ovarian cancer treatment showed rapid absorption of CBD into systemic circulation and provided high bioavailability [45], but this has the disadvantage of being an invasive procedure. Recently, rectal administration of CBD, in the form of suppositories or enemas, has been shown to be a very promising route, as it not only bypasses first-pass metabolism but also offers higher bioavailability in the range of 13% to 50% in comparison to oral administration [4,38]. Yet, there remains a lack of detailed studies, clinical trials, or preclinical trials examining the pharmacokinetics of CBD when administered rectally, and one cannot ignore the discomfort associated with rectal administration.

Despite several drawbacks, pharmaceutical-grade, regulated cannabinoid-based medicinal products are increasingly becoming readily available for prescription worldwide, either as an oily or alcoholic formulation, in soft-gel capsules, liquid solutions, sublingual drops or tablets, or as oromucosal sprays [11]. However, they still only offer limited bioavailability and are associated with poor solubility and stability. These present major difficulties in designing and systemically delivering cannabinoid-based formulations for most therapeutic applications. As such, a variety of studies aimed at developing new CBD formulations to overcome the physicochemical limitations of the molecule by delivering it through different routes remain ongoing [13,46]. In the meantime, alternate approaches are emerging, which are now aiming to improve and modulate drug solubility by using advanced carriers. Some of these strategies and approaches are highlighted and discussed below.

5. Approaches to Improve CBD Solubility and Bioavailability

Several techniques have been utilized to improve the drug's dissolution profile, reduce its degradation, and promote and control its site-specific release, all in order to improve CBD bioavailability. One such approach involves the incorporation or complexing of CBD with advanced carriers in order to formulate amorphous solid dispersions, polymer-based CBD inclusion complexes, lipid-based formulations, and/or nanoformulations administered via different routes [13]. These CBD formulations have been shown to exhibit enhanced solubility profiles, which in turn facilitate CBD absorption, resulting in improved bioavailability. Figure 1 illustrates the different approaches currently being tried to enhance CBD solubility, including via a variety of administration routes.

6. Lipid-Based CBD Formulations

Increasingly, investigations are turning to the use of lipid-based formulations, which tend to enhance the solubility and delivery of various lipophilic drug molecules. There are now numerous studies of CBD lipid-based formulations where CBD has been encapsulated in macro- or nano-structured lipid carriers like lipid nanocapsules, liposomes, vesicles, or loaded into self-emulsifying drug delivery systems (SEDDS) as nanoemulsions and/or as microemulsions to increase water solubility [11,47]. Distinct lipid nanocapsules with CBD located either in the oily core or at the surface have shown a 3.4-fold increase in solubility and permeability across the blood–brain barrier in comparison to CBD alone, due to their small particle size (20–55 nm), and have been implicated in treating gliomas in the brain [47–49]. Studies using vesicular CBD delivery systems also showed enhanced solubility and bioavailability. A vesicular lipid–CBD system termed ethosome, composed mainly of phospholipids, ethanol, and water, showed enhanced permeability through the skin, resulting in a 40% CBD plasma concentration after transdermal application in comparison to the 1–10% general seen from transdermal or dermal application of CBD [50]. Additionally, cardanol (a compound that acts as a co-surfactant when combined with cholesterol), when used as a solvent for CBD, has been shown to produce self-assembled nano-vesicular systems with enhanced aqueous solubility [51].

Other lipid-based methods to increase oral CBD bioavailability include self-emulsifying drug delivery systems (SEDDS). These are isotropic mixtures of oils, surfactants, and co-solvents that tend to emulsify into macro- or nanodroplets in an aqueous medium, such as in the gut, thereby providing in situ drug solubilization. The small nature of the droplets increases the surface area available for drugs to be dissolved and absorbed, thereby increasing both the solubility and bioavailability of cannabinoids [14,52–54]. For example, a patented oral CBD-based formulation named PTL101, manufactured using proprietary gelatin matrix pellets, demonstrated greater bioavailability of about 31–34% compared to a reference oromucosal spray in humans [55–57]. VESIsorb® (Baar, Switzerland) is another novel lipid-based delivery system that self-assembles into a colloidal delivery system on contact with water, resulting in a 4.4-fold increase in CBD plasma concentration [58]. Echo Pharmaceuticals and Ananda Scientific are also investigating formulations using their patented lipophilic compound delivery technology to increase CBD's water solubility. Currently, both compounds are in preclinical or clinical development phases [14]. Several other types of CBD nano- and microemulsions have also been developed using different oily mediums like soybean oil, sesame oil, and triglycerides with/without stabilizers, resulting in a high CBD load observed for all the emulsions in comparison to CBD alone [40,47,59].

7. Polymer-Based CBD Inclusion Complexes

Polymer-based CBD inclusion complexes, especially those produced using biodegradable polymers, have attracted attention as promising advanced drug carriers to enhance CBD solubility, bioavailability, stability, and different drug release profiles.

CBD inclusion complexes formed using two different biodegradable polymers, (poly-lactic-co-glycolic acid) (PLGA) and poly-ε-caprolactone (PCL) showed significantly different particle sizes and release profiles. Each polymer interacted differently with the release medium, leading to different degradation routes and rates, which further resulted in different drug diffusion times and profiles [45,47,60–62]. Hernán Pérez de la Ossa et al. (2012) developed spherical CBD-loaded poly-ε-caprolactone microparticles with a size range of 20–50 nm and high CBD entrapment efficiency to improve bioavailability by allowing slow release of the drug over a period of 10 days [62]. PLGA–CBD inclusion nanocomplexes coated with chitosan were also developed that showed significantly higher absorption after 2 and 6 h of incubation, resulting in higher bioavailability [40,63]. Rao et al. (2022) showed encapsulation of CBD in Poloxamer 407 (P407), which is a triblock copolymer composed of (poly)ethylene oxide and (poly)propylene oxide sections, results in the formation of self-assembled nanomicelles with improved bioavailability [64]. In a further study, zein/whey protein nanoparticles loaded with CBD showed a significantly

increased solubility of ca. 196 μg/mL in comparison to 12.6 μg/mL observed for CBD. The zein/whey protein–CBD nanoparticles also showed protection from CBD degradation by heat and UV light, thereby providing excellent storage stability [65].

Another approach to increasing solubility includes the use of cyclodextrins (CD) to carry lipophilic molecules by means of complexation methods [47,66,67]. Cyclodextrins can accommodate small organic molecules like CBD within their lipophilic central cavity, resulting in water-soluble CBD inclusion complexes with an apparent solubility of up to 5000 μg/mL. Several studies have also investigated the efficacy of different isoforms of cyclodextrin, such as α-CDs, β-CDs, and γ-CDs [47,66–72]. The water solubility of CD–cannabinoid complexes can be further improved by chemically derivatizing β-CD. AOP Orphan Pharmaceuticals significantly increased the aqueous solubility and bioavailability of the drug by using randomly methylated β-CD and hydroxypropyl-β-CD in a patented technology [11,73]. Medexus pharmaceuticals and Vireo Health LLC have developed two proprietary formulations of CBD and cyclodextrins with improved CBD solubility and bioavailability and are currently undertaking clinical trials [14]. Another patent application has been filed for the complexation of cannabinoids with sulfo-alkyl-β-CD in the presence of Cremophor EL (polyoxyl-35 castor oil) to promote cannabinoid solubility [74]. Furthermore, CBD–cyclodextrin complexes have the advantages of being cost-effective, easy to produce, and can be delivered in a solid-state dosage form with improved stability and shelf-life [47].

8. Solid-Based CBD Formulations

CBD nanocrystals, CBD on carbon xerogel microspheres, and CBD conjugates are examples of other approaches currently being explored to improve CBD solubility. CBD nanocrystals were developed to improve the stability, bioavailability, and therapeutic effects of CBD. A patent by Dickman D and Levin D (2017) describes a novel CBD crystalline form with increased aqueous solubility due to its lower melting point temperature [75]. Furthermore, solid CBD nanocrystals can help improve the bioavailability of the compounds as they can allow 100% of the drug to reach the gastrointestinal tract. BeneCeed™, a 200 mg CBD tablet by Columbia Care, is now being assessed under a UK clinical trial [11]. A randomized, open-label crossover trial is underway in Australia for two patent applications, filed by AusCann Group Holdings Ltd., Perth, Australia, for solid compositions containing either a single or a blend of CBD, medium-chain triglycerides, surfactants, and colloidal anhydrous silica [76,77]. Axim Biotech Inc., New York, NY, USA, has developed a controlled-release chewing gum containing a 1:1 combination of CBD and THC to treat patients with multiple sclerosis-related pain and spasticity, Parkinson's disease, dementia, restless leg syndrome, and post-herpetic neuralgia [78,79]. A patent by GW pharmaceuticals lists solid-state CBD as a potential clinical consideration in the treatment of inflammatory bowel disease [14,80]. Echo Pharmaceuticals has also developed a CBD pill formulation (Arvisol®, Leiden, The Netherlands) with improved bioavailability to treat neurological conditions, including Rett syndrome, schizophrenia, and epilepsy [81,82]. Furthermore, a dry, compressed cannabis inhalable formulation developed by Tetra Bio-Pharma, Orleans, ON, USA, is currently being tested in clinical trials in Canada and the USA [11].

Carbon xerogel microspheres are also claimed to provide an excellent carrier system for CBD due to their high purity, multiple controlled forms with well-developed and fitted porosity, and excellent surface chemistry [83,84]. A number of CBD gel formulations by Botanix pharmaceuticals are in early clinical development for transdermal applications to treat acne, psoriasis, and dermatitis [85–87]. Formulations based on CBD–carbon xerogel microspheres showed enhanced bioavailability when implemented for both oral and intranasal applications [14]. Zynerba Pharmaceuticals has also developed a permeation-enhanced CBD gel, "Zygel", for transdermal applications that is now in phase II clinical trials [88].

CBD conjugation is another useful method for overcoming problematic properties of the drug by increasing the bioavailability, solubility, dissolution rate, physical form, melting point, tableting, stability, or permeability of CBD complexes [11,14,47]. For example, TurboCBD^{TM} capsules developed by Lexaria Bioscience Corp. (Columbia, CA, USA) showed that association of CBD with long-chain fatty acids allowed higher concentrations of CBD to enter the circulatory system, resulting in a plasma concentration of 80–85% by 90 min [89]. Harris et al. (2019) showed conjugation of CBD with poly(2-oxazoline) connected via releasable linkages, resulting in a significantly slower hydrolytic release of the cannabidiol than the corresponding PEG–CBD and dextran–CBD conjugates [90]. Artelo Biosciences has developed a CBD–tetramethylpyrazine conjugate, ART12.11, that is currently in the nonclinical phase of pharmaceutical development targeted towards post-traumatic stress disorder (PTSD), inflammatory bowel disease (IBD), stroke, and rare diseases. This CBD–tetramethylpyrazine conjugate offered increased efficacy and bioavailability by acting synergistically and changing the physiochemical properties that are associated with ineffective absorption [14]. Claritas Pharmaceuticals, Seattle, WA, USA, is developing an oral CBD/naproxen combination drug that targets the spinal cord to treat acute and chronic pain. They are also working on an intravenous (IV) formulation of the CBD/naproxen drug [11]. Preclinical trials using CBD conjugates pioneered by Diverse Biotech Inc. (Orlando, FL, USA) are also currently underway for the treatment of cancer [91]. In addition to these approaches, water-soluble CDB derivatives like L-valine-ester or bisulphate CBD derivatives have also been developed by Kalytera for different routes of administration [92]. It is important to note, however, that many of the approaches to enhancing CBD bioavailability highlighted above still require consideration of the mode of administration, CBD extraction process, manufacturing techniques, product formulations, pharmacokinetic profiles, and ultimately the targeted therapeutic application.

9. General Discussion

Over the past several decades, numerous strategies and CBD formulations have been explored, such as route of administration, medium of administration, conjugation, and structural modifications of CBD itself, in order to overcome the challenges of low bioavailability. Several of these strategies and formulations have been highlighted in this opinion piece. We have seen how different encapsulation approaches, such as micro/nanoemulsions, dendrimers, liposomes, micelles, biodegradable polymer particles, and nano-structured lipid carriers, both at the nano- and micro-scale platforms, have been formulated using various strategies to improve the solubility and bioavailability of CBD to varying degrees. The use of long-chain triglycerides such as sesame oil, cocoa butter, tricaprin, or lipids from food has also been shown to improve CBD bioavailability, particularly by contributing to the lymphatic absorption of these cannabidiols [11]. Previously, the use of lipids has proven valuable for increasing the bioavailability of lipophilic drugs, such as cannabinoids. This, however, is greatly dependent on the type and length of the lipid chain, degree of saturation, and digestibility of the oily excipients, which may all influence the oral absorption and bioavailability of CBD, resulting in variable outcomes [93]. The use of several different adjuvants, like surfactants, solubilizers, cosolvency, hydrotrophy, and novel excipients, alone or in combination, has also been shown to improve solubility [11]. The use of nonionic surfactants like macrogolglycerol hydroxystearate to form CBD micelles demonstrated a two-fold increase in CBD bioavailability. But potential drawbacks of using adjuvants include the need to use significant amounts of these compounds, which might lead to irritation within the gastrointestinal tract. There is also the possibility of drug leakage from capsules and stability concerns, including the potential migration of co-solvents and drug precipitation during storage [93]. Polymeric encapsulation of CBD in PLGA and surface modification using coating agents like vitamin E, lecithin, chitosan, and PEG–chitosan increased encapsulation efficiency [45,60]. Despite their potential, there are certain drawbacks associated with the utilization of polymeric nanoparticles. These drawbacks pertain to their constrained shapes, chemical composition, broad size distribu-

tion, tendency to aggregate, and electromagnetic characteristics, all of which can result in issues such as limited absorption when taken orally, instability within the bloodstream, and insufficient dispersion in tissues. While most polymeric nanoparticles tend to be spherical in shape, their synthesis can yield a diverse array of sizes, resulting in batch-by-batch inconsistency at the industrial scale [94].

Apart from different formulations, the use of diverse strategies for CBD delivery has also been implemented. For example, several nanoparticle-based CBD delivery systems consisting of nanoconjugated cannabidoils in a multifunctional metallic nanocarrier, either classified as inorganic, organic, or hybrid nanosystems, depending upon the specific requirements and administration route, are currently in preclinical or clinical development [11,13,74]. Furthermore, lipid-based CBD nanoformulations are also a promising strategy; however, self-emulsifying CBD delivery systems (SEDDS) have become a more lucrative technique to improve CBD bioavailability. A study showed that the addition of natural absorption enhancers like curcumin, resveratrol, and piperine to SEDDS can further increase CBD oral bioavailability in vivo, with piperine having the maximum effect [76]. Despite the implementation of several new and novel approaches, its lipophilic nature, low bioavailability, and excessive first-pass metabolism still remain as challenges that largely impact access to CBD-based therapeutics.

In recent years, structural modification or complexation of CBD with cyclodextrins or carbohydrates has also shown promising results, where further structural and chemical modification of the cyclodextrins can greatly increase CBD solubility and hence bioavailability. Structural modification of several other lipophilic drugs by complexation with cyclodextrins or modified carbohydrates to enhance solubility has been successfully utilized and is now marketed worldwide for their therapeutic effects (for details, see reviews [95–98]). These complexes also have the ability to be formulated for delivery through various routes of administration, thus giving them an added advantage over other techniques [95–98]. Complexation does have definite advantages; however, proof that complexation does not alter the physiochemical and therapeutic characteristics of the drug remains to be confirmed and warrants further investigation.

10. Conclusions and Future Perspectives

CBD has gained significant attention for its potential therapeutic and medical benefits. Poor bioavailability, however, remains one of the significant obstacles to CBD's development and application for these purposes. Increasing bioavailability by improving CBD solubilization in the aqueous phase appears to be the main current focus. Utilizing technologies like nanoemulsion and liposomal delivery, co-administering with healthy fats, exploring sublingual administration, and considering inhalation or solubility enhancement methods, along with structural modification and/or complexation of the compounds, have all been shown to significantly improve their bioavailability. Future research will no doubt focus on further optimizing CBD formulations in order to overcome their physiochemical limitations. These include exploring new carriers, understanding the impact of different administration routes on bioavailability, and conducting thorough pharmacokinetics studies. In addition, long-term safety studies and clinical trials are needed to evaluate the efficacy and safety of CBD formulations with improved bioavailability across a variety of medical conditions. Although the field of CBD research is moving rapidly, it remains to be seen which of these various approaches will provide the best outcomes for the delivery of CBD and its positive short- and long-term effects and efficacy.

Author Contributions: Literature review and data curation done by K.R.H. and A.A.; writing, review and editing by K.R.H., A.A. and S.M.V. All authors have read and agreed to the published version of the manuscript.

Funding: This research was funded by Bod Science Ltd. (ACN 601225441).

Institutional Review Board Statement: Not applicable.

Informed Consent Statement: Not applicable.

Data Availability Statement: Not applicable.

Conflicts of Interest: The authors declare no conflict of interest.

List of Abbreviations

CBD: Cannabidiol; THC, delta-9-tetrahydrocannabinol; ECS, endocannabinoid system; CB, cannabinoid receptors; CNS, central nervous system; AEA, anandamide; 2-AG, 2-arachidonoylglycerol; FAAH, fatty acid amide hydrolase; MAGL, monoacylglycerol lipase; TRPV, transient receptor potential vanilloid; PPARγ, peroxisome proliferator-activated receptor gamma; 5-HT1A, serotonin 1A receptor; FDA, United States Food and Drug Administration; EMA, European Medicines Agency; TGA, Australian Therapeutic Goods Administration; FABPs, fatty acid-binding proteins; ODTs, orally disintegrating or orodispersible tablets; SEDDS, self-emulsifying drug delivery systems; PGLA, poly-(lactic-co-glycolic acid); PCL, poly-ε-caprolactone; P407, Poloxamer 407; CD, Cyclodextrins.

References

1. Marinotti, O.; Sarill, M. Differentiating Full-Spectrum Hemp Extracts from CBD Isolates: Implications for Policy, Safety and Science. *J. Diet. Suppl.* **2020**, *17*, 517–526. [CrossRef] [PubMed]
2. Russo, E.; Marcu, J. Cannabis Pharmacology: The Usual Suspects and a Few Promising Leads. *Adv. Pharmacol.* **2017**, *80*, 67–134. [CrossRef] [PubMed]
3. Britch, S.; Babalonis, S.; Walsh, S. Cannabidiol: Pharmacology and therapeutic targets. *Psychopharmacology* **2021**, *238*, 9–28. [CrossRef] [PubMed]
4. Millar, S.A.; Stone, N.L.; Yates, A.S.; O'Sullivan, S.E. A Systematic Review on the Pharmacokinetics of Cannabidiol in Humans. *Front. Pharmacol.* **2018**, *9*, 1365. [CrossRef] [PubMed]
5. Pisanti, S.; Malfitano, A.; Ciaglia, E.; Lamberti, A.; Ranieri, R.; Cuomo, G.; Abate, M.; Faggiana, G.; Proto, M.; Fiore, D.; et al. Cannabidiol: State of the art and new challenges for therapeutic applications. *Pharmacol. Ther.* **2017**, *175*, 133–150. [CrossRef] [PubMed]
6. Bridgeman, M.; Abazia, D. Medicinal cannabis: History, pharmacology, and implications for the acute care setting. *Pharm. Ther.* **2017**, *42*, 180.
7. Balachandran, P.; Elsohly, M.; Hill, K. Cannabidiol interactions with medications, illicit substances, and alcohol: A comprehensive review. *J. Gen. Intern. Med.* **2021**, *36*, 2074–2084. [CrossRef]
8. Micale, V.; Di Marzo, V.; Sulcova, A.; Wotjak, C.; Drago, F. Endocannabinoid system and mood disorders: Priming a target for new therapies. *Pharmacol. Ther.* **2013**, *138*, 18–37. [CrossRef]
9. Peng, J.; Fan, M.; An, C.; Ni, F.; Huang, W.; Luo, J. A narrative review of molecular mechanism and therapeutic effect of cannabidiol (CBD). *Basic Clin. Pharmacol. Toxicol.* **2022**, *130*, 439–456. [CrossRef]
10. Atalay, S.; Jarocka-Karpowicz, I.; Skrzydlewska, E. Antioxidative and Anti-Inflammatory Properties of Cannabidiol. *Antioxidants* **2019**, *9*, 21. [CrossRef]
11. Palrasu, M.; Wright, L.; Patel, M.; Leech, L.; Branch, S.; Harrelson, S.; Khan, S. Perspectives on Challenges in Cannabis Drug Delivery Systems: Where Are We? *Med. Cannabis Cannabinoids* **2022**, *5*, 102–119. [CrossRef] [PubMed]
12. Laux, L.; Bebin, E.; Checketts, D.; Chez, M.; Flamini, R.; Marsh, E.; Miller, I.; Nichol, K.; Park, Y.; Segal, E. Long-term safety and efficacy of cannabidiol in children and adults with treatment resistant Lennox-Gastaut syndrome or Dravet syndrome: Expanded access program results. *Epilepsy Res.* **2019**, *154*, 13–20. [CrossRef] [PubMed]
13. Stella, B.; Baratta, F.; Della Pepa, C.; Arpicco, S.; Gastaldi, D.; Dosio, F. Cannabinoid formulations and delivery systems: Current and future options to treat pain. *Drugs* **2021**, *81*, 1513–1557. [CrossRef] [PubMed]
14. Millar, S.; Maguire, R.; Yates, A.; O'Sullivan, S. Towards Better Delivery of Cannabidiol (CBD). *Pharmaceuticals* **2020**, *13*, 219. [CrossRef]
15. Baban, B.; Khodadadi, H.; Salles, É.; Costigliola, V.; Morgan, J.; Hess, D.; Vaibhav, K.; Dhandapani, K.; Jack, C. Inflammaging and cannabinoids. *Ageing Res. Rev.* **2021**, *72*, 101487. [CrossRef]
16. Takano, R.; Furumoto, K.; Shiraki, K.; Takata, N.; Hayashi, Y.; Aso, Y.; Yamashita, S. Rate-limiting steps of oral absorption for poorly water-soluble drugs in dogs; prediction from a miniscale dissolution test and a physiologically-based computer simulation. *Pharm. Res.* **2008**, *25*, 2334–2344. [CrossRef]
17. He, M.; Liu, A.; Shi, J.; Xu, Y.; Liu, Y. Multi-Omics Reveals the Effects of Cannabidiol on Gut Microbiota and Metabolic Phenotypes. *Cannabis Cannabinoid Res.* 2023; *ahead of print*. [CrossRef]
18. Ibrahim, I.; Syamala, S.; Ayariga, J.; Xu, J.; Robertson, B.; Meenakshisundaram, S.; Ajayi, O. Modulatory Effect of Gut Microbiota on the Gut-Brain, Gut-Bone Axes, and the Impact of Cannabinoids. *Metabolites* **2022**, *12*, 1247. [CrossRef]

19. Karoly, H.; Mueller, R.; Bidwell, L.; Hutchison, K. Cannabinoids and the Microbiota-Gut-Brain Axis: Emerging Effects of Cannabidiol and Potential Applications to Alcohol Use Disorders. *Alcohol Clin. Exp. Res.* **2020**, *44*, 340–353. [CrossRef]
20. Elmes, M.; Kaczocha, M.; Berger, W.; Leung, K.; Ralph, B.; Wang, L.; Sweeney, J.; Miyauchi, J.; Tsirka, S.; Ojima, I.; et al. Fatty acid-binding proteins (FABPs) are intracellular carriers for Δ9-tetrahydrocannabinol (THC) and cannabidiol (CBD). *J. Biol. Chem.* **2015**, *290*, 8711–8721. [CrossRef]
21. Kaczocha, M.; Glaser, S.; Deutsch, D. Identification of intracellular carriers for the endocannabinoid anandamide. *Proc. Natl. Acad. Sci. USA* **2009**, *106*, 6375–6380. [CrossRef]
22. Duggan, P. The chemistry of cannabis and cannabinoids. *Aust. J. Chem.* **2021**, *74*, 369–387. [CrossRef]
23. Hagan, K.; Varelas, P.; Zheng, H. Endocannabinoid System of the Blood–Brain Barrier: Current Understandings and Therapeutic Potentials. *Cannabis Cannabinoid Res.* **2022**, *7*, 561–568. [CrossRef] [PubMed]
24. Filer, C. Cannabinoid crystal polymorphism. *J. Cannabis Res.* **2022**, *4*, 23. [CrossRef]
25. Mazzetti, C.; Ferri, E.; Pozzi, M.; Labra, M. Quantification of the content of cannabinol in commercially available e-liquids and studies on their thermal and photo-stability. *Sci. Rep.* **2020**, *10*, 3697. [CrossRef] [PubMed]
26. Kosović, E.; Sýkora, D.; Kuchař, M. Stability Study of Cannabidiol in the Form of Solid Powder and Sunflower Oil Solution. *Pharmaceutics* **2021**, *13*, 412. [CrossRef]
27. Gonçalves, J.; Rosado, T.; Soares, S.; Simão, A.; Caramelo, D.; Luís, Â.; Fernández, N.; Barroso, M.; Gallardo, E.; Duarte, A. Cannabis and Its Secondary Metabolites: Their Use as Therapeutic Drugs, Toxicological Aspects, and Analytical Determination. *Medicines* **2019**, *6*, 31. [CrossRef]
28. Kicman, A.; Toczek, M. The Effects of Cannabidiol, a Non-Intoxicating Compound of Cannabis, on the Cardiovascular System in Health and Disease. *Int. J. Mol. Sci.* **2020**, *21*, 6740. [CrossRef] [PubMed]
29. Zendulka, O.; Dovrtelova, G.; Nosková, K.; Turjap, M.; Sulcova, A.; Hanus, L.; Jurica, J. Cannabinoids and cytochrome P450 interactions. *Curr. Drug Metab.* **2016**, *17*, 206–226. [CrossRef]
30. Chen, P.; Rogers, M. Opportunities and challenges in developing orally administered cannabis edibles. *Curr. Opin. Food Sci.* **2019**, *28*, 7–13. [CrossRef]
31. Perucca, E.; Bialer, M. Critical Aspects Affecting Cannabidiol Oral Bioavailability and Metabolic Elimination, and Related Clinical Implications. *CNS Drugs* **2020**, *34*, 795–800. [CrossRef]
32. Itin, C.; Barasch, D.; Domb, A.; Hoffman, A. Prolonged oral transmucosal delivery of highly lipophilic drug cannabidiol. *Int. J. Pharm.* **2020**, *581*, 119276. [CrossRef] [PubMed]
33. Rabgay, K.; Waranuch, N.; Chaiyakunapruk, N.; Sawangjit, R.; Ingkaninan, K.; Dilokthornsakul, P. The effects of cannabis, cannabinoids, and their administration routes on pain control efficacy and safety: A systematic review and network meta-analysis. *J. Am. Pharm. Assoc.* **2020**, *60*, 225–234.e226. [CrossRef] [PubMed]
34. Limpongsa, E.; Tabboon, P.; Pongjanyakul, T.; Jaipakdee, N. Preparation and Evaluation of Directly Compressible Orally Disintegrating Tablets of Cannabidiol Formulated Using Liquisolid Technique. *Pharmaceutics* **2022**, *14*, 2407. [CrossRef] [PubMed]
35. Vlad, R.; Antonoaea, P.; Todoran, N.; Muntean, D.; Rédai, E.; Silași, O.; Tătaru, A.; Bîrsan, M.; Imre, S.; Ciurba, A. Pharmacotechnical and analytical preformulation studies for cannabidiol orodispersible tablets. *Saudi Pharm. J.* **2021**, *29*, 1029–1042. [CrossRef] [PubMed]
36. Vlad, R.; Antonoaea, P.; Todoran, N.; Rédai, E.; Bîrsan, M.; Muntean, D.; Imre, S.; Hancu, G.; Farczádi, L.; Ciurba, A. Development and Evaluation of Cannabidiol Orodispersible Tablets Using a 23-Factorial Design. *Pharmaceutics* **2022**, *14*, 1467. [CrossRef]
37. Chan, J.; Duncan, R. Regulatory Effects of Cannabidiol on Mitochondrial Functions: A Review. *Cells* **2021**, *10*, 1251. [CrossRef]
38. Bhat, T.A.; Kalathil, S.G.; Goniewicz, M.L.; Hutson, A.; Thanavala, Y. Not All Vaping Is the Same: Differential Pulmonary Effects of Vaping Cannabidiol Versus Nicotine. *Thorax* **2023**, *2022*, thoraxjnl.
39. Tijani, A.; Thakur, D.; Mishra, D.; Frempong, D.; Chukwunyere, U.; Puri, A. Delivering therapeutic cannabinoids via skin: Current state and future perspectives. *J. Control Release* **2021**, *334*, 427–451. [CrossRef]
40. Grifoni, L.; Vanti, G.; Donato, R.; Sacco, C.; Bilia, A. Promising Nanocarriers to Enhance Solubility and Bioavailability of Cannabidiol for a Plethora of Therapeutic Opportunities. *Molecules* **2022**, *27*, 6070. [CrossRef]
41. Rebibo, L.; Frušić-Zlotkin, M.; Ofri, R.; Nassar, T.; Benita, S. The dose-dependent effect of a stabilized cannabidiol nanoemulsion on ocular surface inflammation and intraocular pressure. *Int. J. Pharm.* **2022**, *617*, 121627. [CrossRef]
42. Shilo-Benjamini, Y.; Cern, A.; Zilbersheid, D.; Hod, A.; Lavy, E.; Barasch, D.; Barenholz, Y. A case report of subcutaneously injected liposomal cannabidiol formulation used as a compassion therapy for pain management in a dog. *Front. Vet. Sci.* **2022**, *550*, 892306. [CrossRef]
43. Hložek, T.; Uttl, L.; Kadeřábek, L.; Balíková, M.; Lhotková, E.; Horsley, R.; Nováková, P.; Šíchová, K.; Štefková, K.; Tylš, F. Pharmacokinetic and behavioural profile of THC, CBD, and THC+ CBD combination after pulmonary, oral, and subcutaneous administration in rats and confirmation of conversion in vivo of CBD to THC. *Eur. Neuropsychopharmacol.* **2017**, *27*, 1223–1237. [CrossRef] [PubMed]
44. Fu, X.; Xu, S.; Li, Z.; Chen, K.; Fan, H.; Wang, Y.; Xie, Z.; Kou, L.; Zhang, S. Enhanced intramuscular bioavailability of cannabidiol using nanocrystals: Formulation, in vitro appraisal, and pharmacokinetics. *AAPS Pharm. Sci. Tech.* **2022**, *23*, 85. [CrossRef] [PubMed]

45. Fraguas-Sánchez, A.I.; Torres-Suárez, A.I.; Cohen, M.; Delie, F.; Bastida-Ruiz, D.; Yart, L.; Martin-Sabroso, C.; Fernández-Carballido, A. PLGA nanoparticles for the intraperitoneal administration of CBD in the treatment of ovarian cancer: In Vitro and In Ovo assessment. *Pharmaceutics* **2020**, *12*, 439. [CrossRef] [PubMed]
46. Bruni, N.; Della Pepa, C.; Oliaro-Bosso, S.; Pessione, E.; Gastaldi, D.; Dosio, F. Cannabinoid Delivery Systems for Pain and Inflammation Treatment. *Molecules* **2018**, *23*, 2478. [CrossRef]
47. Ramalho, Í.; Pereira, D.; Galvão, G.; Freire, D.; Amaral-Machado, L.; Alencar, É.; Egito, E. Current trends on cannabidiol delivery systems: Where are we and where are we going? *Expert Opin. Drug Deliv.* **2021**, *18*, 1577–1587. [CrossRef]
48. Aparicio-Blanco, J.; Romero, I.; Male, D.; Slowing, K.; García-García, L.; Torres-Suárez, A. Cannabidiol Enhances the Passage of Lipid Nanocapsules across the Blood-Brain Barrier Both in Vitro and in Vivo. *Mol. Pharm.* **2019**, *16*, 1999–2010. [CrossRef]
49. Aparicio-Blanco, J.; Sebastián, V.; Benoit, J.; Torres-Suárez, A. Lipid nanocapsules decorated and loaded with cannabidiol as targeted prolonged release carriers for glioma therapy: In vitro screening of critical parameters. *Eur. J. Pharm. Biopharm.* **2019**, *134*, 126–137. [CrossRef]
50. Lodzki, M.; Godin, B.; Rakou, L.; Mechoulam, R.; Gallily, R.; Touitou, E. Cannabidiol-transdermal delivery and anti-inflammatory effect in a murine model. *J. Control Release* **2003**, *93*, 377–387. [CrossRef]
51. Di Bello, M.; Bloise, E.; Mazzetto, S.; Giuseppe, M. Formulation and chemical stability in aqueous media of cannabidiol embedded in cardanol-based nanovesicles. *ACS Sustain. Chem. Eng.* **2017**, *5*, 8870–8875. [CrossRef]
52. Cherniakov, I.; Izgelov, D.; Barasch, D.; Davidson, E.; Domb, A.; Hoffman, A. Piperine-pro-nanolipospheres as a novel oral delivery system of cannabinoids: Pharmacokinetic evaluation in healthy volunteers in comparison to buccal spray administration. *J. Control Release* **2017**, *266*, 1–7. [CrossRef]
53. Cherniakov, I.; Izgelov, D.; Domb, A.; Hoffman, A. The effect of Pro NanoLipospheres (PNL) formulation containing natural absorption enhancers on the oral bioavailability of delta-9-tetrahydrocannabinol (THC) and cannabidiol (CBD) in a rat model. *Eur. J. Pharm. Sci.* **2017**, *109*, 21–30. [CrossRef]
54. Rani, S.; Rana, R.; Saraogi, G.; Kumar, V.; Gupta, U. Self-Emulsifying Oral Lipid Drug Delivery Systems: Advances and Challenges. *AAPS PharmSciTech* **2019**, *20*, 129. [CrossRef]
55. Atsmon, J.; Cherniakov, I.; Izgelov, D.; Hoffman, A.; Domb, A.; Deutsch, L.; Deutsch, F.; Heffetz, D.; Sacks, H. PTL401, a New Formulation Based on Pro-Nano Dispersion Technology, Improves Oral Cannabinoids Bioavailability in Healthy Volunteers. *J. Pharm. Sci.* **2018**, *107*, 1423–1429. [CrossRef]
56. Atsmon, J.; Heffetz, D.; Deutsch, L.; Deutsch, F.; Sacks, H. Single-Dose Pharmacokinetics of Oral Cannabidiol Following Administration of PTL101: A New Formulation Based on Gelatin Matrix Pellets Technology. *Clin. Pharmacol. Drug Dev.* **2018**, *7*, 751–758. [CrossRef]
57. Mitelpunkt, A.; Kramer, U.; Hausman Kedem, M.; Zilbershot Fink, E.; Orbach, R.; Chernuha, V.; Fattal-Valevski, A.; Deutsch, L.; Heffetz, D.; Sacks, H. The safety, tolerability, and effectiveness of PTL-101, an oral cannabidiol formulation, in pediatric intractable epilepsy: A phase II, open-label, single-center study. *Epilepsy Behav.* **2019**, *987*, 233–237. [CrossRef]
58. Knaub, K.; Sartorius, T.; Dharsono, T.; Wacker, R.; Wilhelm, M.; Schön, C. A Novel Self-Emulsifying Drug Delivery System (SEDDS) Based on VESIsorb®Formulation Technology Improving the Oral Bioavailability of Cannabidiol in Healthy Subjects. *Molecules* **2019**, *24*, 2967. [CrossRef]
59. Francke, N.; Schneider, F.; Baumann, K.; Bunjes, H. Formulation of Cannabidiol in Colloidal Lipid Carriers. *Molecules* **2021**, *26*, 1469. [CrossRef]
60. Ding, D.; Zhu, Q. Recent advances of PLGA micro/nanoparticles for the delivery of biomacromolecular therapeutics. *Mater. Sci. Eng. C Mater. Biol. Appl.* **2018**, *92*, 1041–1060. [CrossRef]
61. Fraguas-Sánchez, A.; Fernández-Carballido, A.; Simancas-Herbada, R.; Martin-Sabroso, C.; Torres-Suárez, A. CBD loaded microparticles as a potential formulation to improve paclitaxel and doxorubicin-based chemotherapy in breast cancer. *Int. J. Pharm.* **2020**, *574*, 118916. [CrossRef]
62. Hernán Pérez de la Ossa, D.; Ligresti, A.; Gil-Alegre, M.; Aberturas, M.; Molpeceres, J.; Di Marzo, V.; Torres Suárez, A. Poly-ε-caprolactone microspheres as a drug delivery system for cannabinoid administration: Development, characterization and in vitro evaluation of their antitumoral efficacy. *J. Control Release* **2012**, *161*, 927–932. [CrossRef]
63. Sosnik, A.; Shabo, R.; Halamish, H. Cannabidiol-Loaded Mixed Polymeric Micelles of Chitosan/Poly(Vinyl Alcohol) and Poly(Methyl Methacrylate) for Trans-Corneal Delivery. *Pharmaceutics* **2021**, *13*, 2142. [CrossRef]
64. Rao, Y.; Li, R.; Liu, S.; Meng, L.; Wu, Q.; Yuan, Q.; Liang, H.; Qin, M. Enhanced bioavailability and biosafety of cannabidiol nanomicelles for effective anti-inflammatory therapy. *Particuology* **2022**, *69*, 1–9. [CrossRef]
65. Wang, C.; Wang, J.; Sun, Y.; Freeman, K.; Mchenry, M.; Wang, C.; Guo, M. Enhanced Stability and Oral Bioavailability of Cannabidiol in Zein and Whey Protein Composite Nanoparticles by a Modified Anti-Solvent Approach. *Foods* **2022**, *11*, 376. [CrossRef]
66. Jansook, P.; Ogawa, N.; Loftsson, T. Cyclodextrins: Structure, physicochemical properties and pharmaceutical applications. *Int. J. Pharm.* **2018**, *35*, 272–284. [CrossRef]
67. Miranda, J.; Martins, T.; Veiga, F.; Ferraz, H. Cyclodextrins and ternary complexes: Technology to improve solubility of poorly soluble drugs. *Braz. J. Pharm. Sci.* **2011**, *47*, 665–681. [CrossRef]

68. Hatziagapiou, K.; Bethanis, K.; Koniari, E.; Christoforides, E.; Nikola, O.; Andreou, A.; Mantzou, A.; Chrousos, G.; Kanaka-Gantenbein, C.; Lambrou, G. Biophysical Studies and In Vitro Effects of Tumor Cell Lines of Cannabidiol and Its Cyclodextrin Inclusion Complexes. *Pharmaceutics* **2022**, *14*, 706. [CrossRef] [PubMed]
69. Lv, P.; Zhang, D.; Guo, M.; Lui, J.; Chen, X.; Guo, R.; Xu, Y.; Zhang, Q.; Liu, Y.; Guo, H.; et al. Structural analysis and cytotoxicity of host-guest inclusion complexes of cannabidiol with three native cyclodextrins. *J. Drug Deliv. Sci. Technol.* **2019**, *51*, 337–344. [CrossRef]
70. Mannila, J.; Järvinen, T.; Järvinen, K.; Jarho, P. Precipitation complexation method produces cannabidiol/beta-cyclodextrin inclusion complex suitable for sublingual administration of cannabidiol. *J. Pharm. Sci.* **2007**, *96*, 312–319. [CrossRef] [PubMed]
71. Mannila, J.; Järvinen, T.; Järvinen, K.; Tarvainen, M.; Jarho, P. Effects of RM-beta-CD on sublingual bioavailability of Delta9-tetrahydrocannabinol in rabbits. *Eur. J. Pharm. Sci.* **2005**, *26*, 71–77. [CrossRef] [PubMed]
72. Zhu, P.; Lv, P.; Zhang, Y.; Liao, R.; Liu, J.; Guo, R.; Chen, X.; Liao, X.; Gao, C.; Zhang, K.; et al. Self-Assembly System Based on Cyclodextrin for Targeted Delivery of Cannabidiol. *Front. Chem.* **2021**, *9*, 754832. [CrossRef] [PubMed]
73. Viernstein, H.; Toegel, S.; Schueller, R. Fast Disintegrating Compositions Comprising Nabilone and Randomly Methylated β-Cyclodextrin. U.S. Patent 13/989,540, 31 May 2012.
74. Kingsley, K.; Lee, S.; Greenbaum, E. Cannabinoid Formulations with Improved Solubility. U.S. Patent 2019003017, 31 January 2019.
75. Dickman, D.; Levin, D. Crystalline Form of Cannabidiol. U.S. Patent 20170349518, 7 December 2017.
76. MacLeman, P.; Mavlianov, M. Solid Self-Emulsifying Pharmaceutical Compositions Comprising Cannabinoids. WO2020024009, 6 February 2020.
77. MacLeman, P.; Mavlianov, M. Free-Flowing Powder Compositions for Oral Solid Dosages Containing Cannabinoids. WO2020024011, 6 February 2020.
78. Anastassov, G.; Changoer, L. Chewing Gum Composition Comprising Cannabinoids and Opioid Agonists and/or Antagonists. U.S. Patent 20180110730, 26 April 2018.
79. Changoer, L.; Anastassov, G. Chewing Gum Composition Comprising Cannabinoids and Nicotine. U.S. Patent 10842786, 24 November 2017.
80. Robson, P.; Guy, G.; Pertwee, R.; Jamontt, J. Use of Tetrahydrocannabinol and/or Cannabidiol for the Treatment of Inflammatory Bowel Disease. U.S. Patent 20100286098, 11 November 2007.
81. De Vries, J.A.; Fernandez Cid, M.V.; Lopez, A.M.H. Granulate Containing Cannabinoid, Method for Its Manufacture and Oral Dosage Unit Comprising Such Granulate. U.S. Patent 20150132400, 14 May 2015.
82. De Vries, J.; Fernandez Cid, M.; Heredia Lopez, A.; Eiroa Martinez, C. Compressed Tablet Containing Cannabidiol, Method for Its Manufacture and Use of Such Tablet in Oral Treatment of Psychosis or Anxiety Disorders. WO2015065179, 7 May 2015.
83. Abdul Khalil, H.; Yahya, E.; Tajarudin, H.; Balakrishnan, V.; Nasution, H. Insights into the Role of Biopolymer-Based Xerogels in Biomedical Applications. *Gels* **2022**, *8*, 334. [CrossRef] [PubMed]
84. Cortés, F.; Zapata, K.; Rojano, B.; Carrasco-Marín, F.; Gallego, J.; Hernández, M.; Franco, C. Dual-Purpose Materials Based on Carbon Xerogel Microspheres (CXMs) for Delayed Release of Cannabidiol (CBD) and Subsequent Aflatoxin Removal. *Molecules* **2019**, *24*, 3398. [CrossRef] [PubMed]
85. Cooper, E.; Callahan, M. Formulations of Cannabinoids for the Treatment of Acne. CA3053503, 23 August 2018.
86. Cooper, E.; Callahan, M. Formulations of Cannabinoids for the Treatment of Psoriasis. WO2018148787, 23 August 2018.
87. Cooper, E.; Callahan, M. Formulations of Cannabinoids for the Treatment of Dermatitis and Inflammatory Skin Diseases. WO2018148785, 23 August 2018.
88. Heussler, H.; Cohen, J.; Silove, N.; Tich, N.; Bonn-Miller, M.; Du, W.; O'Neill, C.; Sebree, T. A phase 1/2, open-label assessment of the safety, tolerability, and efficacy of transdermal cannabidiol (ZYN002) for the treatment of pediatric fragile X syndrome. *J. Neurodev. Disord.* **2019**, *11*, 16. [CrossRef]
89. Patrician, A.; Versic-Bratincevic, M.; Mijacika, T.; Banic, I.; Marendic, M.; Sutlović, D.; Dujić, Ž.; Ainslie, P. Examination of a New Delivery Approach for Oral Cannabidiol in Healthy Subjects: A Randomized, Double-Blinded, Placebo-Controlled Pharmacokinetics Study. *Adv. Ther.* **2019**, *36*, 3196–3210. [CrossRef]
90. Harris, J.; Bentley, M.; Moreadith, R.; Viegas, T.; Fang, Z.; Yoon, K.; Weimer, R.; Dizman, B.; Nordstierna, L. Tuning drug release from polyoxazoline-drug conjugates. *Eur. Polym. J.* **2019**, *120*, 109241. [CrossRef]
91. Hershberger, P.; Arlen, P. Cannabinoid Conjugate Molecules. WO2020263893, 30 December 2020.
92. Salzman, A.; Flower, K.; Garner, C.; Jagtap, P.; Musa, S. Cbd Prodrugs, Compositions, and Methods of Administering cbd and cbd Prodrugs. WO2018096504, 31 May 2018.
93. De Prá, M.; Vardanega, R.; Loss, C. Lipid-based formulations to increase cannabidiol bioavailability: In vitro digestion tests, pre-clinical assessment and clinical trial. *Int. J. Pharm.* **2021**, *609*, 121159. [CrossRef]
94. Begines, B.; Ortiz, T.; Pérez-Aranda, M.; Martínez, G.; Merinero, M.; Argüelles-Arias, F.; Alcudia, A. Polymeric Nanoparticles for Drug Delivery: Recent Developments and Future Prospects. *Nanomaterials* **2020**, *10*, 1403. [CrossRef]
95. Carneiro, S.; Costa Duarte, F.; Heimfarth, L.; Siqueira Quintans, J.; Quintans-Júnior, L.; Veiga Júnior, V.; Neves de Lima, Á. Cyclodextrin-Drug Inclusion Complexes: In Vivo and In Vitro Approaches. *Int. J. Mol. Sci.* **2019**, *20*, 642. [CrossRef]
96. di Cagno, M. The Potential of Cyclodextrins as Novel Active Pharmaceutical Ingredients: A Short Overview. *Molecules* **2017**, *22*, 1. [CrossRef]

97. Hirlekar, R.; Sonawane, S.; Kadam, V. Studies on the effect of water-soluble polymers on drug-cyclodextrin complex solubility. *AAPS PharmSciTech* **2009**, *10*, 858–863. [CrossRef] [PubMed]
98. Kost, B.; Brzeziński, M.; Socka, M.; Baśko, M.; Biela, T. Biocompatible Polymers Combined with Cyclodextrins: Fascinating Materials for Drug Delivery Applications. *Molecules* **2020**, *25*, 3404. [CrossRef] [PubMed]

International Journal of
Molecular Sciences

MDPI

Article

Hydroxyl Group Acetylation of Quercetin Enhances Intracellular Absorption and Persistence to Upregulate Anticancer Activity in HepG2 Cells

Kozue Sakao [1,2], Hanako Saruwatari [2], Shohei Minami [2] and De-Xing Hou [1,2,*]

[1] The United Graduate School of Agricultural Sciences, Kagoshima University, Kagoshima 890-0065, Japan; sakaok24@agri.kagoshima-u.ac.jp
[2] Department of Food Science and Biotechnology, Faculty of Agriculture, Kagoshima University, Kagoshima 890-0065, Japan; k2372356@kadai.jp (H.S.); k5157734@kadai.jp (S.M.)
* Correspondence: hou@agri.kagoshima-u.ac.jp; Tel.: +81-99-285-8649

Abstract: Quercetin, a flavonoid compound widely distributed in many plants, is known to have potent antitumor effects on several cancer cells. Our previous study revealed that the acetylation of quercetin enhanced its antitumor effect. However, the mechanisms remain unknown. This study aimed to elucidate the bioavailability of acylated quercetin in the HepG2 cell model based on its antitumor effect. The positions of quercetin 3,7,3′,4′-OH were acetylated as 3,7,3′,4′-*O*-tetraacetylquercetin (4Ac-Q). The inhibitory effect of 4Ac-Q on HepG2 cell proliferation was assessed by measuring cell viability. The apoptosis was characterized by apoptotic proteins and mitochondrial membrane potential shifts, as well as mitochondrial reactive oxygen species (ROS) levels. The bioavailability of 4Ac-Q was analyzed by measuring the uptake and metabolites in HepG2 cells with high performance liquid chromatography (HPLC)—photodiode array detector (PDA) and—ultraviolet/visible detector (UV/Vis). The results revealed that 4Ac-Q enhanced the inhibitory effect on HepG2 cell proliferation and induced its apoptosis significantly higher than quercetin. Protein array analysis of apoptosis-related protein indicated that 4Ac-Q increased the activation or expression of pro-apoptotic proteins, including caspase-3, -9, as well as second mitochondria-derived activator of caspases (SMAC), and suppressed the expression of apoptosis inhibiting proteins such as cellular inhibitor of apoptosis (cIAP)-1, -2, Livin, Survivin, and X-linked inhibitor of apoptosis (XIAP). Furthermore, 4Ac-Q stimulated mitochondrial cytochrome *c* release into the cytosol by enhancing ROS level and depolarizing the mitochondrial membrane. Finally, the analysis of uptake and metabolites of 4Ac-Q in HepG2 cells with HPLC-PDA and -UV/Vis revealed that 4Ac-Q was metabolized to quercetin and several different acetylated quercetins which caused 2.5-fold higher quercetin present in HepG2 cells than parent quercetin. These data demonstrated that acetylation of the quercetin hydroxyl group significantly increased its intracellular absorption. Taken together, our findings provide the first evidence that acetyl modification of quercetin not only substantially augments the intracellular absorption of quercetin but also bolsters its metabolic stability to elongate its intracellular persistence. Therefore, acetylation could serve as a strategic approach to enhance the ability of quercetin and analogous flavonoids to suppress cancer cell proliferation.

Keywords: quercetin; acylation; bioavailability; apoptosis; metabolites

Citation: Sakao, K.; Saruwatari, H.; Minami, S.; Hou, D.-X. Hydroxyl Group Acetylation of Quercetin Enhances Intracellular Absorption and Persistence to Upregulate Anticancer Activity in HepG2 Cells. *Int. J. Mol. Sci.* **2023**, *24*, 16652. https://doi.org/10.3390/ijms242316652

Academic Editor: Gabriella Calviello

Received: 12 October 2023
Revised: 19 November 2023
Accepted: 20 November 2023
Published: 23 November 2023

1. Introduction

Quercetin, known as a flavonol-type flavonoid, is a widespread polyphenol found in many vegetables, fruits, and tea. The pharmacological effects of quercetin, including antioxidant, anti-inflammatory, anti-atherosclerotic, anti-tumor, antihypertensive, and prevention of cerebrovascular diseases, have been reported [1]. Consuming large amounts of quercetin is considered to decrease the risk of lung cancer [2], stomach cancer [3], and colon cancer [4,5]. Partial data indicated that quercetin could inhibit hepatocellular carcinoma cell

growth by inducing apoptosis/cell death and cell cycle arrest. The combination of cancer therapy of fluorouracil (5-FU) with quercetin showed an additive or synergistic inhibitory effect on hepatocellular carcinoma cell growth [6]. Quercetin could also enhance the anticancer effects of doxorubicin chemotherapy on hepatocellular carcinoma cells, companying with the protection of normal hepatocytes [7].

Therefore, quercetin is considered a promising chemopreventive compound for potential chronic disease-preventive effects. On the other hand, quercetin has low bioavailability due to poor absorption [8,9] and rapid metabolism. Those properties limit the potential application of quercetin. Recent studies have attempted to improve its bioavailability and bioactivity by modifying quercetin structure with various chemical methods [10–12]. Acylation is one such modification, especially the *O*-acylation of quercetin, which has been reported to improve various biological activities, such as anticancer, antivirus, antiplatelet, and cytoprotection effects [13–16]. In our previous studies, we replaced the hydroxy groups of quercetin with methyl, benzyl, and acetyl groups to evaluate the changes in their bioactivity [17,18]. Of which, 3,7,3′,4′-*O*-tetraacetylquercetin (4Ac-Q), which was acylated at the 3,7,3′,4′-OH positions of quercetin revealed a higher ability of apoptosis induction in myeloid human leukemia cancer cells (HL-60 cell). However, the molecular regulators of the higher apoptotic response are not fully understood, and the effects of 4Ac-Q on intracellular absorption, metabolism, and bioavailability remain unknown. This study aimed to elucidate the bioavailability of 4Ac-Q by the HepG2 cell model based on its antitumor effect. The inhibitory effect of 4Ac-Q on HepG2 cell proliferation was assessed by measuring cell viability. The apoptosis was characterized by proteomic analysis of 35 human apoptosis-related proteins and mitochondrial membrane potential shifts, as well as mitochondrial reactive oxygen species (ROS) levels. To finally obtain an understanding of how quercetin bioavailability is altered by acetylation, the cellular uptake and metabolism of 4Ac-Q and parent quercetin in HepG2 cells were evaluated by measuring their metabolites with HPLC-PDA and -UV/Vis. Our study will clarify the effects of the *O*-acylation of the quercetin hydroxyl group on its bioavailability and antitumor activity.

2. Results

2.1. 4Ac-Q Enhances the Inhibitory Effect on HepG2 Cell Proliferation

In a previous study, the cell growth inhibitory effects of quercetin on HepG2 cells revealed a concentration- and time-dependent manner in an 3-(4,5-dimethyl-2-thiazolyl)-2,5-diphenyltetrazolium bromide (MTT) assay. A significant inhibition of cell growth was observed after 48 h treatment with an IC_{50} value of 76.1 μM [19]. Therefore, in this study, to compare the inhibitory effect of quercetin and 4Ac-Q on HepG2 cell proliferation, both dose- and time-course dependence were investigated via MTT assay. As shown in Figure 1C, 4Ac-Q significantly enhanced the inhibitory effect on HepG2 cell proliferation at 72 h in both 40 μM and 80 μM than quercetin, although both quercetin and 4Ac-Q inhibited HepG2 cell proliferation in a dose- and time-dependent manner.

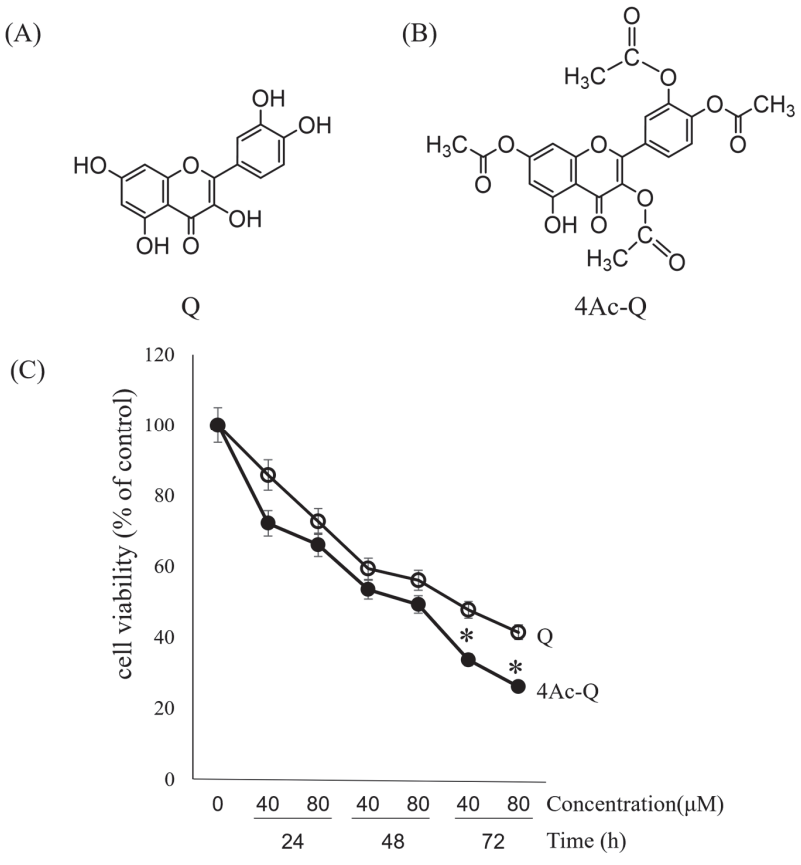

Figure 1. Chemical structure of quercetin (Q) (**A**) and 4Ac-Q (**B**), and the viability of HepG2 cells treated with Q or 4Ac-Q in the indicated times and doses (**C**). Cells were treated with 40 μM and 80 μM of Q or 4Ac-Q for 24, 48, and 72 h, respectively. Cell viability was determined via MTT assay. Data from at least three independent triplicated experiments were presented as mean ± SD, n = 9, and * mark denoted significant differences (* $p < 0.05$) between Q and 4Ac-Q.

2.2. 4Ac-Q Enhances Cell Death via Both Apoptosis and Necrosis

Next, we evaluated whether the proliferation inhibition of HepG2 cells by 4Ac-Q was due to apoptosis induction. After staining cells with Annexin V- fluorescein isothiocyanate (FITC) and propidium iodide (PI), 25,000 cells were counted by flow cytometry and sorted into apoptotic fraction (early (FITC+/PI−) + late (FITC+/PI+) and necrotic fraction (FITC−/PI+). Cell death was induced for 24–72 h with 80 μM of Q or 4Ac-Q. As shown in Figure 2, 4Ac-Q induced significantly higher apoptosis than quercetin at 24 h (Figure 2A) and 48 h (Figure 2B). Interestingly, 4Ac-Q induced significantly higher necrosis than quercetin at 72 h with a similar apoptosis as quercetin (Figure 2C). Consistent with the cell viability data (Figure 1C), 4Ac-Q enhanced inhibitory effectiveness on cell proliferation inhibition via increasing both apoptosis and necrosis at 24–48 h, and mainly via increasing necrosis after 72 h, compared with parent quercetin.

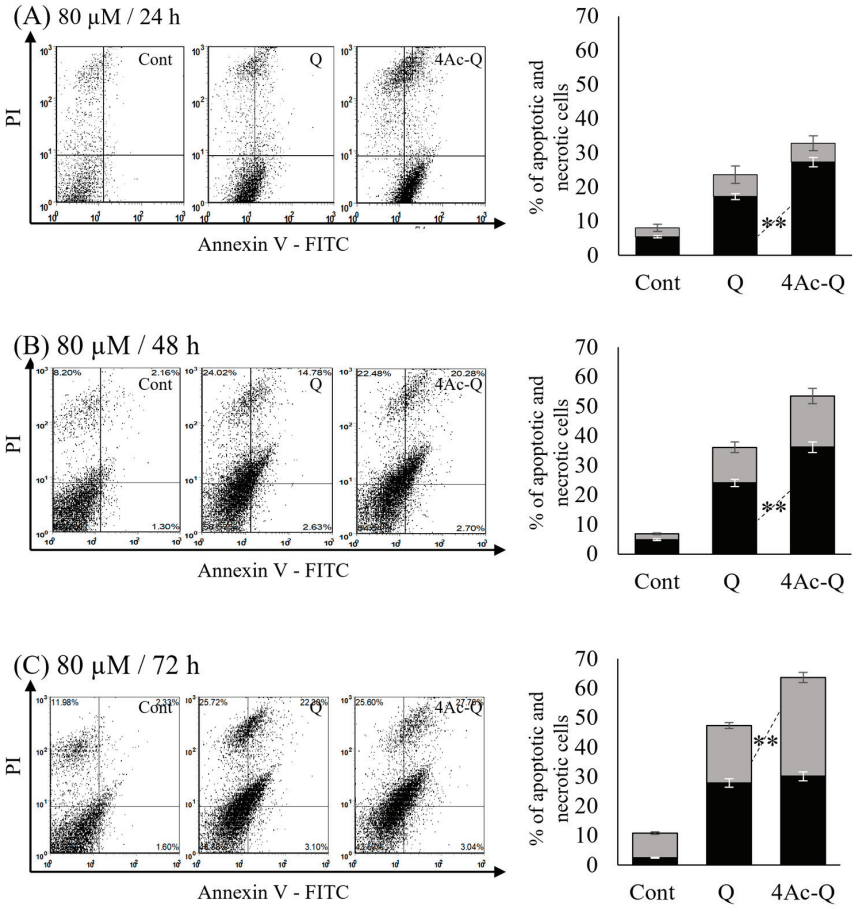

Figure 2. 4Ac-Q and quercetin (Q)-induced apoptosis and necrosis in HepG2 cells. HepG2 cells were treated with 80 μM 4Ac-Q or Q for (**A**) 24 h, (**B**) 48 h, and (**C**) 72 h, respectively. Left panels indicated the flow cytometry pattern of Annexin V-FITC/PI fluorescence intensity, and right panels showed the quantitative graph of apoptotic (black column) and necrotic (gray column) cell fractions. Results are expressed as the percentage of cell death of HepG2 cells treated with 0.1% dimethyl sulfoxide (DMSO) (Cont) or 4Ac-Q or Q (mean ± SD, n = 3) and statistically analyzed using one-way ANOVA followed by Tukey's test. Data from at least three independent triplicated experiments are presented as mean ± SD, n = 9, and * mark denoted significant differences (** $p < 0.01$) between Q and 4Ac-Q.

2.3. 4Ac-Q Significantly Regulates the Level of Apoptosis-Related Proteins Than Quercetin

To fully understand the mechanisms of 4Ac-Q-induced cell death, we first used protein array analysis of 35 apoptosis-related proteins (Figure 3A) to compare the expression level of each protein between Q and 4Ac-Q treatment (Figure 3B). As shown in Figure 3C, cleavage of caspase-3 and reduction in procaspase-3 were significantly detected in the 24 h treatment with 80 μM of Q and 4Ac-Q (Figure 3C). On the other hand, 4Ac-Q significantly suppressed the expression of apoptosis inhibitor proteins, including cellular inhibitor of apoptosis (cIAP-1), -2, Livin, Survivin, and X-linked inhibitor of apoptosis (XIAP) (Figure 3D). Furthermore, the expression level of the mitochondrial pro-apoptotic protein second mitochondria-derived activator of caspase/direct inhibitor of apoptosis-binding protein with low pI (SMAC/Diablo), which is involved in the execution of apoptosis by inhibiting the IAP family [20], was found to be significantly higher in 4Ac-Q treatment than

that in quercetin treatment (Figure 3E). Meanwhile, there was no change in the expression of high temperature requirement A2 (HtrA2)/Omi, which inhibits the function of IAP, as well as SMAC/Diablo.

(A)

Reference spots											Reference spots
Bad	Bax	Bcl-2	Bcl-x	**Pro-caspase-3**	**Cleaved caspase-3**	Catalase	**cIAP-1**	**cIAP-2**	Claspin	Clusterin	Cyto-chromeC
TRAIL R1/ DR4	TRAIL R2/ DR5	FADD	Fas/ TNFRSF6 /CD95	HIF-1α	HO-1/ HMOX1/ HSP32	HO-2/ HMOX2	HSP27	HSP60	HSP70	HTRA/ Omi	**Livin**
PON2	P21/CIP1/ CDKN1A	P27/Kip1	Phospho-p53 (Ser15)	Phospho-p53 (Ser46)	Phospho-p53 (Ser392)	Phospho-Rad17 (S635)	**SMAC/ Diablo**	**Survivin**	TNF R1/ TNF RSF1A	**XIAP**	PBS (Negative Control)
Reference spots											

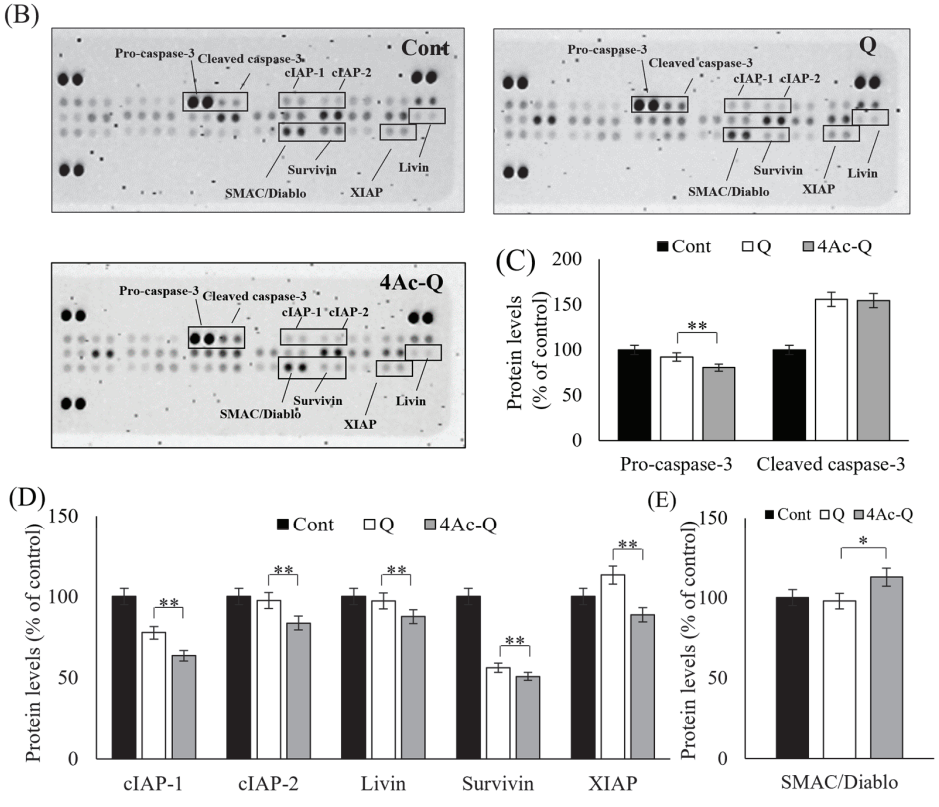

Figure 3. Protein array analysis of 35 apoptosis-related proteins in HepG2 cells treated with quercetin (Q) and 4Ac-Q. (**A**) The location of each apoptosis-related protein on the human apoptosis antibody array membrane. Of which, the protein with significant change was labeled in the black boxes. (**B**) Representative array images indicating the protein levels of various apoptosis-related proteins in HepG2 cells treated with 0.1% DMSO (Cont), 80 μM Q, or 4Ac-Q for 24 h. (**C**) The mean pixel density of pro-caspase-3 and cleaved caspase-3 in the Q or 4Ac-Q-treated group relative to the non-treated group (Cont). (**D**) The mean pixel density of IAP family proteins including cIAP-1 and -2, Livin, Survivin, and XIAP. (**E**) The mean pixel density of IAP antagonist SMAC/Diablo. * $p < 0.05$, ** $p < 0.01$, significant differences between quercetin and 4Ac-Q.

Furthermore, to check the accuracy of protein array analysis results, some important factors in the regulation of apoptosis, such as SMAC/Diablo, procaspase-9, XIAP, and Poly (ADP-ribose) polymerase (PARP), were reconfirmed via Western blotting (Figure 4). Almost all of them showed a similar expression pattern as protein array analysis data. In comparison with quercetin, 4Ac-Q significantly increased the protein expression of SMAC/Diablo (Figure 4A) and significantly reduced the protein expression of XIAP (Figure 4B), procaspase-9 (Figure 4C), as well as full PARP (Figure 4D).

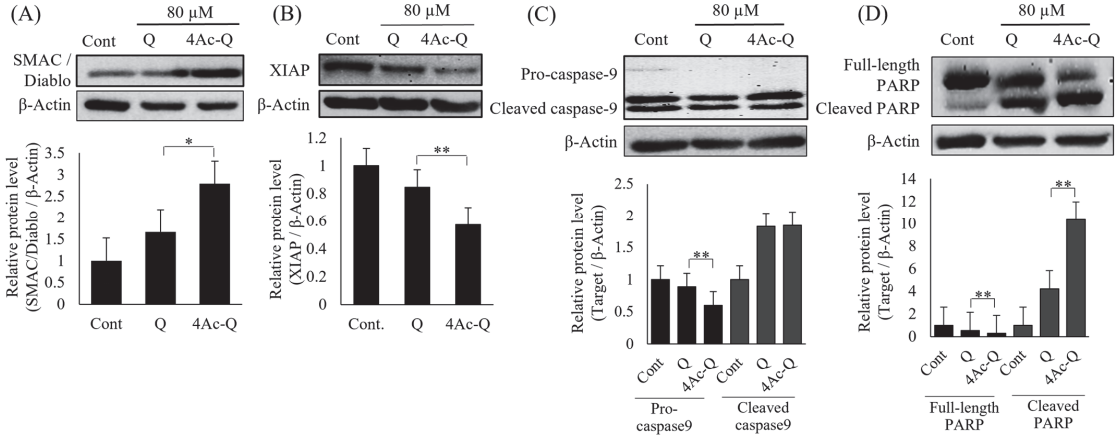

Figure 4. The typic expressions of some apoptosis factors were confirmed by Western blotting. HepG2 cells were treated with 80 μM of quercetin (Q) or 4Ac-Q for 24 h or with 0.1% DMSO (Cont). Protein levels of SMAC/Diablo (**A**), XIAP (**B**), Caspase-9 (**C**), and PARP (**D**) in HepG2 cells were detected by Western blotting. Quantification data were normalized by β-Actin level, and each value represents mean ± SD of 3 repeated experiments. * $p < 0.05$, ** $p < 0.01$, significant differences between quercetin and 4Ac-Q.

2.4. Mitochondrial Dysfunctions Are Involved in 4Ac-Induced Apoptosis

Mitochondria have been reported to play a key role in the regulation of apoptosis [21]. Especially, extra ROS production triggers mitochondrial dysfunctions, including the loss of mitochondrial membrane potential and the release of cytochrome c from the mitochondrion. Thus, we first measured the ROS levels with MitoSOX Red, a chemical probe that selectively reacts with superoxide in the mitochondrion. As shown in Figure 5A, 4Ac-Q produced significantly higher ROS level than quercetin, although both quercetin and 4Ac-Q caused a significant increase in mitochondrial ROS levels at 6 h compared to control. Next, we measured membrane potential loss by JC-1 staining, a membrane-permeable fluorescent probe that can measure mitochondrial membrane potential. As shown in Figure 5B, 4Ac-Q decreased significantly mitochondrial membrane potential more than quercetin, although both quercetin and 4Ac-Q caused a significant decrease in mitochondrial membrane potential at 6 h compared to control. Furthermore, we separated cytoplasmic and mitochondrial fractions from HepG2 cells treated with quercetin (Q) or 4Ac-Q or 0.1% DMSO (Cont) and then detected the protein levels by Western blotting (5A). Both quercetin and 4Ac-Q significantly increased cytoplasmic cytochrome *c* levels and significantly reduced mitochondrial cytochrome *c* levels compared to control. 4Ac-Q showed significantly stronger actions than quercetin. These data demonstrated that 4Ac-Q induced apoptosis by ROS-mediated mitochondrial dysfunction pathway.

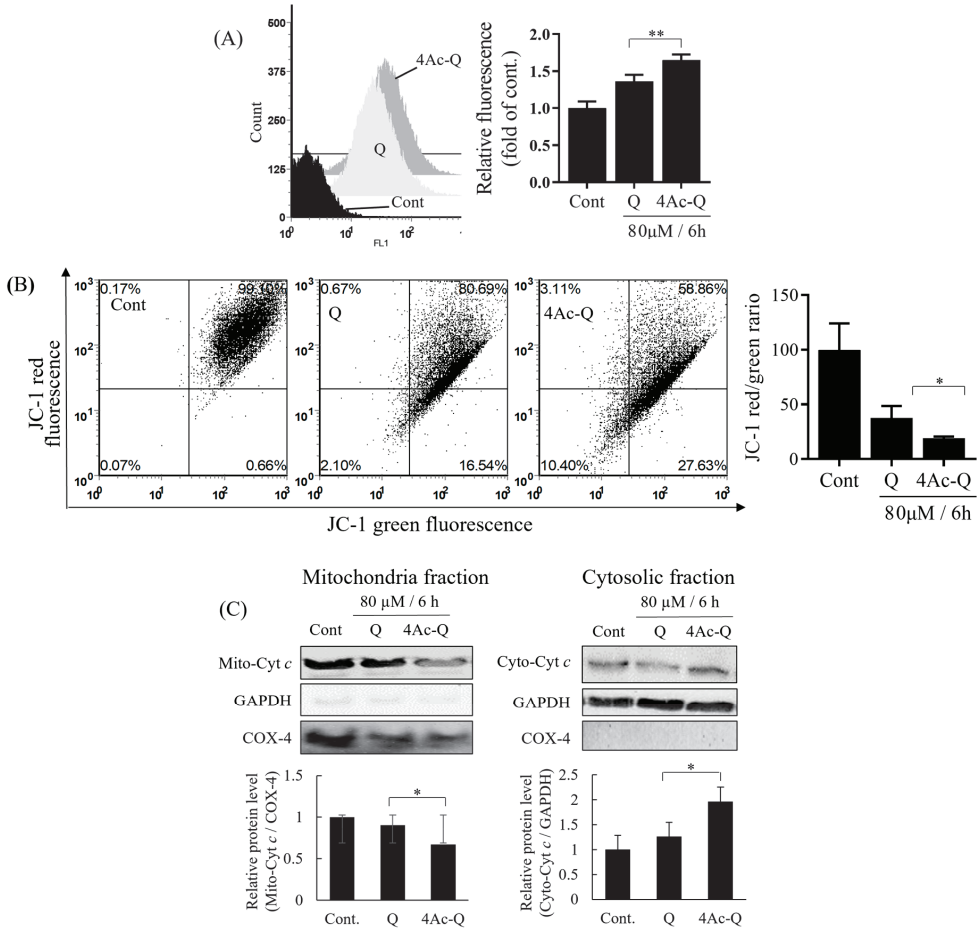

Figure 5. Mitochondrial dysfunctions by quercetin (Q) and 4Ac-Q. (**A**) Mitochondrial ROS generation was monitored by MitoSOX Red mitochondrial superoxide chemical probe. ROS level was expressed as relative fold to control HepG2 cells (Cont) treated with 0.1%DMSO. (**B**) Alterations in mitochondrial membrane potential (Ψm) were measured by flow cytometry using the JC-1 staining method, and the ratio of red/green fluorescence intensity was presented asΨm). (**C**) Cytochrome *c* release. Mitochondrial (Mito-Cyt *c*) and cytosolic fractions (Cyto-Cyt *c*) were fractionated, and cytochrome *c* release was detected by Western blotting. The amount of cytochrome *c* in the cytosolic or mitochondrial fractions was normalized, respectively, by compartment-specific glyceraldehyde-3-phosphate dehydrogenase (GAPDH) or mitochondrial cytochrome c oxidase subunit 4 (COX-4) protein levels. Data from at least three independent triplicated experiments are presented as mean ± SD, and * mark denoted significant differences (* $p < 0.05$, ** $p < 0.01$, between quercetin and 4Ac-Q).

2.5. 4Ac-Q Enhances the Cellular Uptake in HepG2 Cells

The above data indicated that 4Ac-Q induced HepG2 cell apoptosis in a similar apoptotic pathway as quercetin, but with stronger ability. It caused us to speculate that the acetylation of the hydroxyl group of quercetin may affect the absorption and/or metabolism of quercetin to improve its bioactivity. To clarify this speculation, we first determined the amounts of quercetin and 4Ac-Q taken up in HepG2 cells by HPLC-PDA and -UV/Vis detector with selectable wavelengths ranging from UV to visible light.

Figure 6A shows a three-dimensional chromatogram of quercetin-added HepG2 cells via HPLC-PDA detection. One major peak (retention time 32.82 min) and two smaller peaks were observed. The retention time of the major peak was consistent with the dominant peak in the chromatogram shown in Figure 6C, which was monitored at 370 nm, a characteristic wavelength of quercetin, and was assumed to be quercetin. On the other hand, the three-dimensional chromatogram of 4Ac-Q-added HepG2 cells showed several peaks. Of which, the retention time of the major peak was consistent with the dominant peak in the chromatogram shown by Figure 6F, which was monitored at 320 nm, a characteristic wavelength of 4Ac-Q, and was assumed to be 4Ac-Q. Besides this, the peak at a retention time of 32.74 min was consistent with that of quercetin, shown in Figure 6D. Other peaks are unknown metabolites. In comparison of quercetin levels obtained from Figure 6C,D, approximately 2.5-fold higher quercetin was observed in 4Ac-Q-added HepG2 cells than by quercetin addition. It is worth noting that the total peak area of the chromatograms in the 4Ac-Q treatment was quite larger than that of quercetin. This suggests that acetylation of the hydroxyl group of quercetin significantly increased its intracellular absorption.

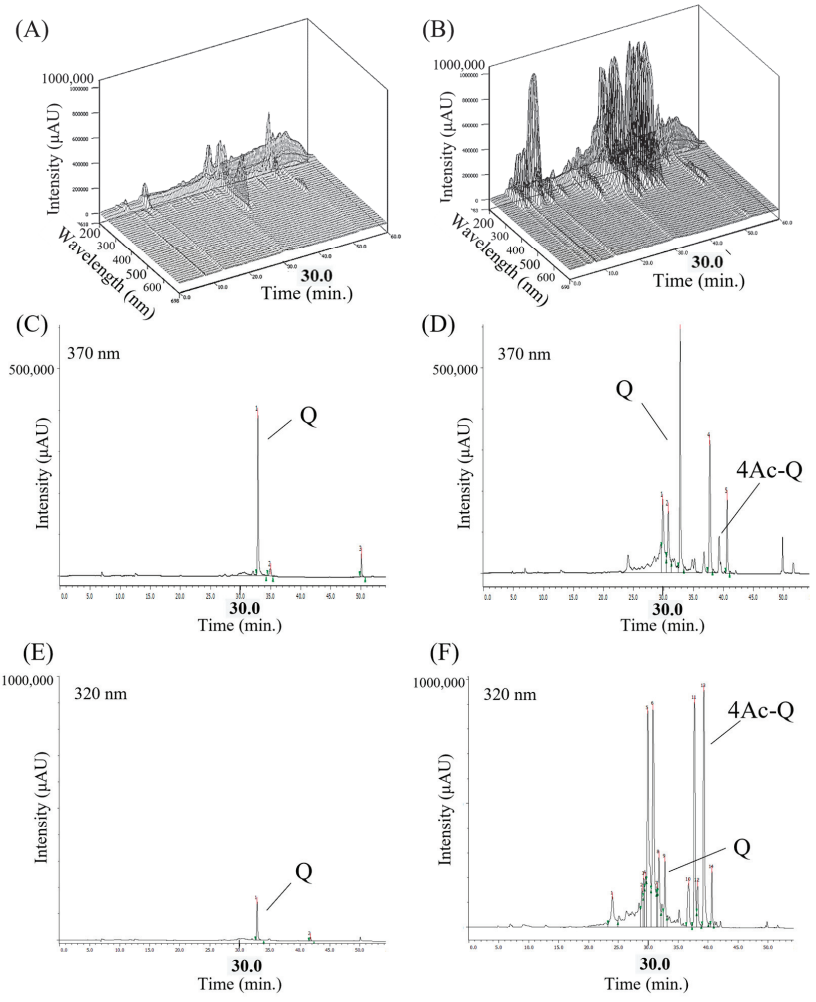

Figure 6. Chemical profile of HepG2 intracellular extract analyzed by HPLC-PDA and -UV/VIS. (**A**,**B**) Three-dimensional chromatograms of intracellular extracts from quercetin or 4Ac-Q-added

HepG2 cells for 3 h detected by HPLC-PDA (wavelength: 210–700 nm). Three-dimensional HPLC was represented by a 3D chromatogram with the retention time, absorption wavelength, and peak intensity of the components as the three axes. (**C**,**D**) HPLC-UV/Vis chromatograms of quercetin at maximum absorption wavelength (370 nm). (**E**,**F**) HPLC-UV/Vis chromatograms of 4Ac-Q at maximum absorption wavelength (320 nm).

2.6. 4Ac-Q Bolsters the Metabolic Stability to Elongate Its Intracellular Persistence

To clarify the unknown metabolites in quercetin and 4Ac-Q-added HepG2 cells, we next investigated these metabolites by liquid chromatography–mass spectrometry (LC-MS) analysis based on HPLC-UV/Vis profiling.

HPLC-UV/Vis profiling of quercetin detected two major metabolites (M1 and M3), excluding quercetin itself. Similarly, HPLC-UV/Vis profiling of 4Ac-Q detected five major metabolites (M1–M5), excluding both quercetin and 4Ac-Q. These HPLC profiling peaks were identified via electrospray ionization mass spectrometry (ESI-MS) analysis. In particular, the peaks corresponding to quercetin and 4Ac-Q were identified by co-elution with standard substances. The mass spectrum of quercetin metabolites showed that the $[M+H]^+$ ions of M1 and its fragment ions were detected at *m/z* 383.0 and *m/z* 303.0, respectively, and the $[M+H]^+$ ions of M3 were detected at m/z 317.0, suggesting that M1 and M3 may be quercetin-3′-sulfate and isorhamnetin, respectively (Figure 7B). The mass spectrum of 4Ac-Q metabolites showed that the $[M+H]^+$ ions of M1, M2, M3, M4, and M5 were detected at *m/z* 383.0, 345.0, 317.0, 387.0, and 429.0, respectively. These data suggested that M1, M2, M3, M4, and M5 would be Q-3′-*O*-sulfate, Mono-acetyl quercetin (1Ac-Q), isorhamnetin, di-acetyl-quercetin (2Ac-Q), and tri-acetyl-quercetin (3Ac-Q), respectively (Figure 7C). Additionally, there were no detectable quercetin-glucuronides or glucuronide conjugates of 3′-methylquercetin from LC–MS data.

Furthermore, the time courses of the metabolite formation of quercetin and 4Ac-Q were shown in Figure 7D,E. The HepG2 cells were incubated with either quercetin or 4Ac-Q for 0, 3, 6, 12, or 24 h. The graph of quercetin metabolic rates showed that quercetin decreased in a time-dependent manner; conversely, metabolite M1 increased significantly over time. The quercetin metabolite M3 decreased after 6 h. On the other hand, 4Ac-Q decreased in a time-dependent manner and disappeared at 12 h. Quercetin, as one of the metabolites of 4Ac-Q, peaked at 3 h and decreased over time, and metabolite M1 increased in a time-dependent manner. However, compared to quercetin metabolism in Figure 7D, the percentage of metabolic conversion to M1 was found to be low. Interestingly, the metabolite M3 showed different patterns between quercetin and 4Ac-Q metabolism. M3 peaked at 6 h and then reduced during quercetin metabolism, while M3 peaked at 12 h and then reduced during 4Ac-Q metabolism. These data indicated that a portion of 4Ac-Q is transformed into quercetin, as well as several different acetylated quercetins during its metabolism. This partial deacetylation may have caused a delay in the metabolism of quercetin.

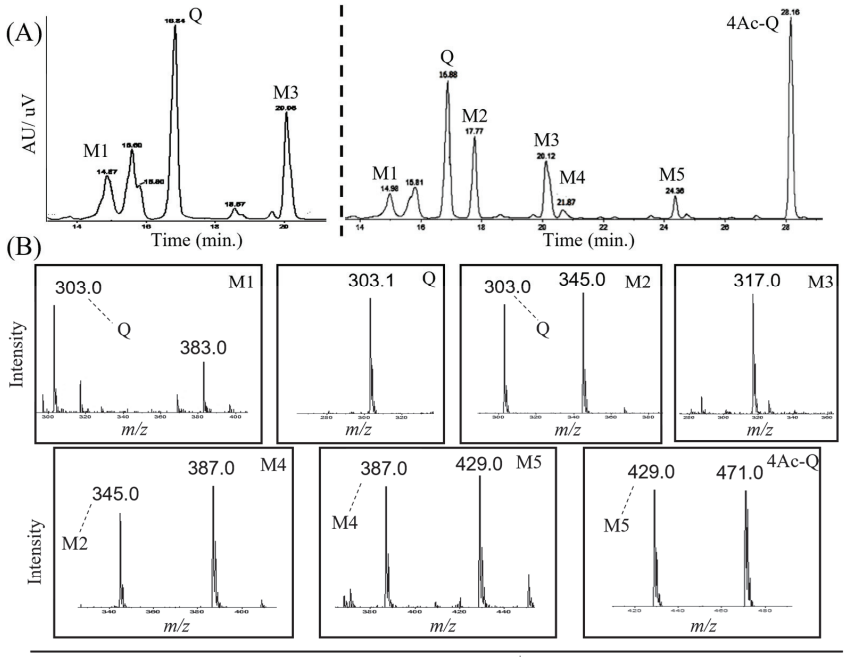

(C)

	Label	t_R (min)	Peak area ratio (%)	$[M+H]^+$ *m/z*	Parent or metabolites
Q	M1	14.9	13	383.0	Q-3'-*O*-sulfate
	Q	16.8	35	303.1	Quercetin
	M3	20.1	25	317.0	Isorhamnetin
4Ac-Q	M1	14.9	11	383.0	Q-3'-*O*-sulfate
	Q	16.8	17	303.1	Quercetin
	M2	17.7	7	345.0	Mono-acetyl quercetin (1Ac-Q)
	M3	20.1	12	317.0	Isorhamnetin
	M4	21.8	1	387.0	Di-acetyl quercetin (2Ac-Q)
	M5	24.8	2	429.0	Tri-acetyl quercetin (3Ac-Q)
	4Ac-Q	28.1	21	471.0	Tetra-acetyl quercetin (4Ac-Q)

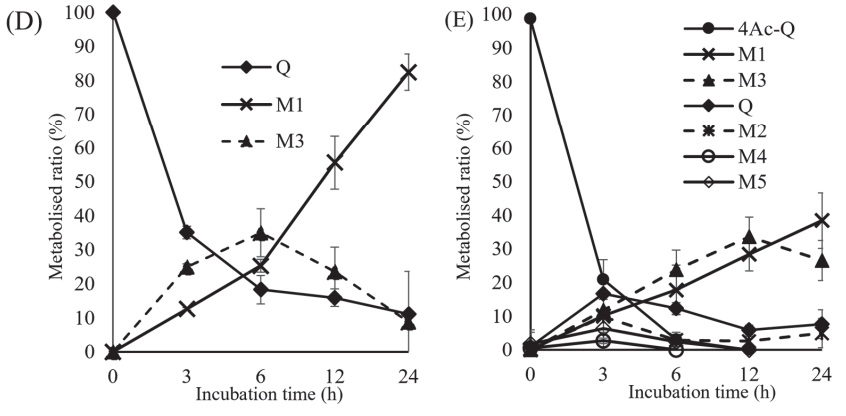

Figure 7. LC-MS analysis of HepG2 cell culture medium after treatment with quercetin(Q) and 4Ac-Q for the indicated times. (**A**) HPLC chromatograms of metabolites of quercetin (**left** side) and 4Ac-Q

(**right** side). (**B**) Extracted ion chromatograms corresponding to different *m/z* values for the peaks of the HPLC chromatograms. (**C**) List of metabolites predicted based on the results of LC-MS analysis. Time-course changes in metabolites of quercetin (**D**) and 4Ac-Q (**E**) in HepG2 cells. Each graph was derived from the average of three independent measurements, respectively.

3. Discussion

Acylated polyphenols from natural plant sources are often modified in glycosidic sugar chains and have been reported to stabilize pigment and structure [22,23] and to enhance cytoprotective, antioxidant, and anti-inflammatory effects [24–26]. In contrast, there are few reports of acylation of aglycones in nature and few information on *O*-acylated flavonoids [10,12]. Thus, we synthesized 4Ac-Q via acetylation of its hydroxyl group. The structural confirmation was carried out via nuclear magnetic resonance (NMR) spectral analysis. It has been reported that a new chemical shift (δ) in the signal, indicative of the acetyl group around δ = 2.3 ppm, is a distinctive feature of 4Ac-Q resulting from the acetylation of hydroxyl groups at the 3,7,3′,4′-positions [18,27]. The four new signal peaks in our synthesized 4Ac-Q were observed to be attributed to the acetyl group, appearing at δ = 2.34 ppm and 2.37 ppm, which confirmed the synthesis was successful. The signal attributions and integration ratios aligned perfectly with previous reports [18,27], further substantiating the acetyl modification of the hydroxyl group.

In this study, 4Ac-Q exhibited significantly stronger inhibition of cell proliferation compared to quercetin. Our previous experiments with HL-60 cells revealed that the IC_{50} value of 4Ac-Q and quercetin was 19 μM and 58 μM, respectively, which resulted in a 3.05-fold higher inhibitory effect on cell proliferation for 4Ac-Q compared to quercetin. These data suggested that 4Ac-Q also exhibits higher inhibitory activity than quercetin, even in adherent cells. Moreover, quercetin with all hydroxyl groups acetylated also showed 2.59 times stronger inhibition of cell growth than quercetin in MCF-7 breast cancer cells [13]. Although the cell types and the number of acetyl modifications differ, acetylation may enhance the anticancer activity of quercetin. It is necessary for further evaluation of the effects of changes in the number and position of acetyl groups on physiological activity and cellular characteristics. On the other hand, Rubio et al. reported that quercetin 3-methyl ether tetraacetate induced apoptosis in HL-60 cells via the activation of caspases with cytochrome *c* release [28]. Thus, the activation pathways of the apoptosis-inducing proteins are possibly not determined by the acetylation site. In future studies, it is also required to investigate relative enzyme activity inhibition as part of quercetin acetylation's anticancer efficacy. Quercetin is known to target various molecular kinase enzymes including Raf-1, MEK1 [29], ERK1/2, SEK1, JNK1/2, RSK2, and PI3K [30]. Silico analysis using a molecular docking model has reported that quercetin is bound to the same ATP-binding region as the specific PI3K inhibitor LY294002, which is considered a promising target for cancer therapy. Moreover, the slight differences in the mode of binding to the target protein can alter the inhibitory effect on PI3K [31]. It is interesting that a methylated derivative of quercetin effectively inhibited matrix metalloproteinase-1 (MMP-1), an enzyme involved in cancer invasion and metastasis, with a more potent effect than quercetin itself [32]. Methylated quercetin was reported to inhibit MMP-1 by binding near its active center, the metal ion, suggesting the position of the methyl group and the type of substituent may vary based on the specific protein. Therefore, future studies should examine the acetylation and other substituent modifications of hydroxyl groups, their positions and numbers, and the bioactivity of specific target proteins.

As an important aspect of this study, our data revealed that 4Ac-Q was taken up into the cell in larger amounts in a shorter time than parent quercetin and metabolized slowly (Figures 6 and 7). The hydroxyl group of quercetin has been reported to be a target for glucuronidation and sulfate conjugation in phase II metabolism in the liver [33]. The hydroxyl groups of 4Ac-Q are replaced by the acetyl group, which may be prevented from these metabolic processes. Methylated flavonoids have been reported to prolong the

metabolic stability [34]. In this study, more than 80% of quercetin was converted to sulfate conjugate in 24 h treatment in HepG2 cells (Figure 7D). On the other hand, only 40% of 4Ac-Q was converted to sulfate conjugate in 24 h treatment. Interestingly, 4Ac-Q itself disappeared after 12 h of incubation, while the monoacetylated quercetin was produced and remained in unmetabolized form after 24 h (Figure 7E). These data indicated that 4Ac-Q was more resistant to metabolism than quercetin.

Acetylation of (-)-epigallocatechin-3-*O*-gallate (EGCG) is reported to enhance a 30-fold cellular uptake and a 2.2-fold half-life in plasma elimination compared to EGCG [35]. Similarly, the conversion of the methyl group to an acetyl group at the C5 position of tangerine, a polymethoxyflavonoid, increased cellular uptake and prolonged its elimination half-life in mouse plasma [36]. Mono-acylated luteolin derivatives are considered to protect luteolin from metabolic activity [37]. These studies suggest that acetylation of the hydroxyl group of flavonoids may improve cellular uptake and avoid rapid metabolism, which is largely in agreement with the 4Ac-Q results in this study.

The increase in cellular uptake of quercetin acetyl derivatives was thought to be due in part to the change in polarity resulting from the substitution of the hydroxyl group with an acetyl group, thereby increasing bioaccessibility. Carrasco-Sandoval reported that the bioaccessibility of various phenolic compounds depended mostly on the chemical properties, especially their polarity [38]. Additionally, aglycones of flavonoids tend to form aggregates due to hydrophobic interactions among aromatic moieties and the hydrogen bonding of hydroxyl groups. This phenomenon is considered a key factor that reduces their solubility and restricts their bioavailability [39,40]. Based on our data combined with other reports, it can be inferred that the *O*-acetylation of quercetin may mitigate this aggregation by obstructing the formation of hydrogen bonds between hydroxyl groups and altering the compound's polarity. Indeed, the crystal packing diagram of our single-crystal X-ray structure analysis of pentaacetyl quercetin shows that hydrogen bonding is inhibited by the presence of acetyl groups [41]. These observations align with the previous chemical and physicochemical findings [38], [39], and [40], supporting the hypothesis that acetylation plays a significant role in altering the behavior of phenolic compounds. On the other hand, deacetylation of 4Ac-Q in the metabolic process was thought to occur via hydrolysis by human-carboxylesterase 1 (hCE1) and human-carboxylesterase 2 (hCE2) present in HepG2 cells [42–44]. hCE2 especially prefers substrates with small acyl groups and large alcohol groups [45]; for example, it hydrolyzes benzoyl ester and the acetyl group of aspirin [46,47]. Thus, we considered that the deacetylation of 4Ac-Q in this study may also involve hCE2 reaction. It is necessary to confirm the active state of hCE2 in the metabolic process of 4Ac-Q in the next study.

In summary, our findings provide the first evidence that acetyl modification of quercetin not only substantially augments the intracellular absorption but also bolsters its metabolic stability, thereby prolonging its intracellular persistence. This implies that acetylation could serve as a strategic approach to enhance the bioactivity efficacy of quercetin and analogous flavonoids. Investigations on the structure–activity relationships of the acetylation of flavonoids remain a critical area for future exploration.

4. Materials and Methods

4.1. Chemicals and Antibodies

Quercetin was purchased from Sigma-Aldrich (St. Louis, MO, USA). Stock solution of sample was prepared in DMSO and diluted with complete culture media immediately before use. An equal volume of DMSO was added to controls. MTT and β-Actin antibody were purchased from Sigma-Aldrich LLC (St. Louis, MO, USA). The antibodies against caspase-3, caspase-9, PARP, cytochrome *c*, COX-4, and GAPDH were from Cell Signaling Technology (Danvers, MA, USA), whereas the antibodies against XIAP were from Abcam (Cambridge, MA, USA). SMAC/Diablo antibody was from Proteintech (Tokyo, Japan).

4.2. Synthesis of 4Ac-Q

4Ac-Q was prepared using the chemical synthesis method as described previously [18]. In brief, acetic anhydride (4 equiv.) was added to a quercetin solution (5 mmol) in dry pyridine at room temperature. After stirring the mixture for 10 min, it was quenched in ice-cold water. The resulting precipitate was collected by filtration and subsequently washed with ice-cold water. The compound was then recrystallized from methanol. The chemical structures of the acetylated quercetin were characterized by ^{1}H-NMR. Spectra were recorded on a JEOL ECA-600 spectrometer (600 MHz for ^{1}H, JEOL, Tokyo, Japan) using [D6]CDCl3 as the solvent and tetramethylsilane (TMS) as the internal standard. The purity was confirmed to be >97% by HPLC.

4.3. Cell Culture

Human hepatocellular carcinoma cell lines HepG2 were obtained from RIKEN Cell Bank (RCB1648) (Ibaraki, JP). The cells were cultured at 37 °C in a 5% CO_2 atmosphere in Dulbecco's-Modified Eagle Medium (DMEM) containing 10% fetal bovine serum and 1% of penicillin–streptomycin glutamine for 24 h and then treated by samples in indicated times and doses.

4.4. Cell Viability Assay

Cell viability was determined by an MTT assay, as described previously [48]. In brief, HepG2 (9.35×10^4/well) cells were plated into each well of 12-well plates. The cells were treated with 40 or 80 μM of samples for 48 h. MTT solution was then added to each well and incubated for another 4 h. The resulting MTT–formazan product was dissolved by the addition of DMSO. The amount of formazan was determined by measuring the absorbance at 550 nm with Multiskan TM FC (Thermo Scientific™, Waltham, MA, USA). The cell viability was expressed as the optical density ratio of the treatment to control.

4.5. Apoptosis Detection by Annexin V-FITC/Propidium Iodide Flow Cytometry

Apoptosis induction was quantitatively assessed via flow cytometry using the FITC Annexin V Apoptosis Detection Kit I (BD Biosciences, San Diego, CA, USA) according to the manufacturer's manual [48]. In brief, HepG2 (2.4×10^5/Well) was plated into each well of 6-well plates. After treatment with 80 μM of samples for 24, 48, or 72 h, HepG2 cells were suspended in 100 μL of binding buffer and then incubated with FITC Annexin V and PI staining solution for 15 min. The cells were analyzed at FL1 (530 nm) and FL3 (630 nm) with the flow cytometry (CyFlow®, Sysmex Partec GmbH, Görlitz, Germany).

4.6. Protein Array Analysis of Apoptosis-Related Proteins

Proteome profiling of apoptosis-related protein was assessed with proteome profiler human apoptosis array kit (R&D Systems, Milpitas, CA, USA) according to the manufacturer's manual. Briefly, HepG2 cells were treated with DMSO control, 80 μM of quercetin or 4Ac-Q, then cultured for 24 h, and each cell lysate was prepared in the array kit lysis buffer. Cell lysates are diluted and incubated overnight at 4 °C with nitrocellulose membranes containing various duplicates of 35 different apoptotic antibodies to detect proteins. The membranes were washed to remove unbound proteins, followed by incubation with a cocktail of biotinylated detection antibodies. Then, the levels of apoptosis-related proteins were assessed using an HRP-conjugated antibody followed via chemiluminescence, and each array membrane was scanned using LumiVision Analyzer140 .exe (TAITEC, Saitama, Japan).

4.7. Western Blot Analysis

HepG2 cells were treated with DMSO (control), Quercetin, or 4Ac-Q for defined times and then collected by centrifugation at 1700× *g* for 10 min. After the cells were lysed as described previously [48], equal amounts of lysate protein were run on sodium dodecyl sulfate polyacrylamide gel electrophoresis (SDS-PAGE) and electrophoretically transferred onto

polyvinylidene difluoride (PVDF) membrane (GE Healthcare UK, Amersham, England). Immunoblotting was performed following our previous method [48]. Bound antibodies were detected using the enhanced chemiluminescence (ECL) system, and relative amounts of proteins associated with specific antibodies were quantified using LumiVision Analyzer (TAITEC, Saitama, Japan).

4.8. Subcellular Fractionation for Cytochrome c Detection

Mitochondria were prepared as described in our previous study [48] using the mitochondria/cytosol fractionation kit (BioVision, Milpitas, CA, USA). The harvested cells were suspended in a cytosol extraction buffer. After incubation on ice for 10 min, cells were homogenized and centrifuged at 700× *g* for 10 min. The supernatant was further centrifuged at 10,000× *g* for 30 min., and the cytosol and mitochondrial fractions were isolated. The supernatant was designated as the cytosol fraction. The pellet was dissolved in mitochondria extraction buffer and used as the mitochondrial fraction.

4.9. Determination of Mitochondrial Membrane Potential ($\Delta\Psi m$)

Mitochondrial membrane potential in HepG2 cells was determined by flow cytometry as described previously [49] using the JC-1 MitoMP Detection Kit (Dojindo Molecular Technologies, Kumamoto, Japan). HepG2 cells (2.4×10^5/well) were seeded in a 6-well plate and treated with DMSO, 80 μM quercetin, or 4Ac-Q for 0.5 h. Afterward, the cells were incubated for 30 min with JC-1 (2 μg/mL) in the dark. After incubation, the cells were washed twice with hanks' balanced salt solution (HBSS), suspended in a total volume of 200 μL of imaging buffer solution, and analyzed using a flow cytometer.

4.10. Determination of ROS Production

ROS production was measured via flow cytometry using MitoSOX^{TM} Red mitochondrial superoxide indicator (Invitrogen-Life Technologies, Carlsbad, CA, USA) as described previously [49]. For flow cytometric analysis, HepG2 (2.4×10^5/well) cells were plated into each well of 6-well plates. After treatment with 80 μM of samples for 30 min, HepG2 cells were incubated with 50 μM MitoSOX Red for 10 min. The cells were collected by centrifugation at 1700× *g* for 10 min and washed with phosphate-buffered saline (PBS). The fluorescence was detected using the flow cytometer.

4.11. Uptake of Quercetin and Acylated Quercetin into HepG2 Cells

The uptake of quercetin and 4Ac-Q into HepG2 cells was measured by the method of Wong et al. [50]. The cells were culturedto 80% confluent, and the medium was changed every 2 days. Uptake experiments were performed by adding 80 μM quercetin or 4Ac-Q to a serum-free medium. After 3 h of sample treatment, the supernatant was removed, and the pellet was washed two times with ice-cold PBS containing 0.2% bovine serum albumin (BSA) and one time with ice-cold PBS without BSA. The cells were collected with 50% methanol and stored at −80 °C for at least 24 h. Extraction was performed by sonication for 10 min, followed by the addition of ice-cold acetone to twice the volume of 50% methanol. The samples were placed in a −20 °C freezer for 1h and centrifuged at 17,000× *g* for 5 min. The supernatant was collected and evaporated for dryness in vacuo at 30 °C and stored at −20 °C until HPLC analysis.

4.12. HPLC Analysis

Cellular uptake of samples was analyzed via HPLC unit (LC-2000Plus series; JASCO Corporation, Tokyo, Japan) using COSMOSIL(R) πNAP packed column 4.6 mm I.D. × 250 mm (Nacalai Tesque, Kyoto, Japan). The solvent system was a mixture of water (A) and acetonitrile (B) with a flow rate of 1.0 mL/min and a gradient of 100% B for 0–25 min and 20% B for 25–30 min, starting with an A/B ratio of 80:20, returning to the initial condition for 10 min. A photodiode array (PDA) detector was used for scanning, accumulating spectral data for

all peaks in the absorption wavelength range 200–700 nm and recording chromatograms at 280, 320, and 370 nm, respectively.

4.13. Preparation of Metabolites of Quercetin and Acylated Quercetin in HepG2 Cells

Metabolites in HepG2 cells were measured based on the method of O'Leary et al. [51] with a few modifications. The cells were seeded in 58 cm^2 dishes at a density of around 1.12×10^5 cells/cm^2 and allowed to adhere overnight. Cells were cultured to 80% confluent, and the medium was changed every 2 days. On the day of the experiment, cells were washed twice with PBS, and a fresh medium was added. The cells were further incubated with 80 μM of quercetin or 4Ac-Q for 0, 3, 6, 12, or 24 h, respectively. At each time, the supernatant medium was collected and immediately cooled on ice. The medium was processed for HPLC analysis as follows: cold methanol containing 1 mM ascorbic acid was added 1.5 times as much as the collected medium. Samples were centrifuged at 13,500× *g* for 10 min at 4 °C. The pellet was dried by rotary evaporation and resuspended in 1 mL of 50% acetonitrile. Samples were filtered through a 0.22 μm filter prior to analysis by HPLC and LC-MS.

4.14. Liquid Chromatography–Mass Spectrometry (LC-MS) Characterization of Metabolites

For LC/MS analysis, a QTRAP® liquid chromatography-electrospray ionization-tandem mass spectrometry (LC-ESI-MS/MS) 3200 system (1.7 with HotFix 2, AB Sciex Pte. Ltd., Framingham, MA, USA) was connected to the LC20 HPLC instrument (Shimadzu Corporation, Kyoto, Japan) via an ESI interface. The analytical column was a phase C18 (octadecyl) (TSKgel ODS-100V, L × I.D. 150 mm × 3.0 mm, 3 μm particle size; Tosoh Corporation, Tokyo, Japan) equipped with a UV detector (280 nm) at a flow rate of 0.4 mL/min and with an injection volume of 10 μL. The mobile phase was solvent A (99.9% water + 0.1% formic acid) and solvent B (99.9% acetonitrile + 0.1% formic acid), starting with 10% solvent B at 0 min and gradient to 100% solvent B for 45 min. The mass spectrometer was monitored in the positive mode. The optimized detection parameters were as follows: scan type, electrospray ionization (ESI), ionization mode: positive mode, curtain gas: 20 psi, collision gas: High, ion spray voltage: 5.5 kV, temperature: 600 °C, ion source gas1: 50 psi, ion source gas2: 80 psi, and interface heater: ON.

4.15. Statistical Analysis

Statistical analysis of data was determined by one-way analysis of variance (ANOVA) followed by Tukey's multiple comparison test, using SPSS v26 and GraphPad Prism 9 software. Data are expressed as the mean ± standard deviation (SD). All experiments were conducted in biological triplicates (n = 3) with at least three individual replicates, and uptake and metabolism experiments generated at least three biological replicates. The significance level was set as p-values less than 0.05.

5. Conclusions

Hydroxyl group acetylation of quercetin enhances its intracellular absorption and metabolic stability, which strengthen the anticancer activity, including cell growth inhibition and apoptosis induction of cancer cells. This innovative approach will provide a novel strategy against cancer cell growth, not only for quercetin but also for related flavonoids.

Author Contributions: Conceptualization, D.-X.H. and K.S.; methodology, K.S.; validation, K.S. and D.-X.H.; formal analysis, H.S. and S.M.; investigation, K.S., H.S. and S.M.; data curation, K.S.; writing—original draft preparation, K.S. and H.S.; writing—review and editing, D.-X.H.; supervision, D.-X.H. and K.S.; project administration, K.S. and D.-X.H.; funding acquisition, K.S. and D.-X.H. All authors have read and agreed to the published version of the manuscript.

Funding: This work was supported by JSPS KAKENHI Grant Number JP26850084 and JP16K1870, as well as by the fund of Scholar Research of Kagoshima University (70030117).

Institutional Review Board Statement: Not applicable.

Informed Consent Statement: Not applicable.

Data Availability Statement: The data used to support the findings of this study are available from the corresponding author upon request.

Conflicts of Interest: The authors declare no conflict of interest.

References

1. Pérez-Vizcaíno, F.; Ibarra, M.; Cogolludo, A.L.; Duarte, J.; Zaragozá-Arnáez, F.; Moreno, L.; López-López, G.; Tamargo, J. Endothelium-independent vasodilator effects of the flavonoid quercetin and its methylated metabolites in rat conductance and resistance arteries. *J. Pharmacol. Exp. Ther.* **2002**, *302*, 66–72. [CrossRef] [PubMed]
2. Neuhouser, M.L. Dietary flavonoids and cancer risk: Evidence from human population studies. *Nutr. Cancer* **2004**, *50*, 1–7. [CrossRef] [PubMed]
3. Ekstrom, A.M.; Serafini, M.; Nyren, O.; Wolk, A.; Bosetti, C.; Bellocco, R. Dietary quercetin intake and risk of gastric cancer: Results from a population-based study in Sweden. *Ann. Oncol.* **2011**, *22*, 438–443. [CrossRef] [PubMed]
4. Djuric, Z.; Severson, R.K.; Kato, I. Association of dietary quercetin with reduced risk of proximal colon cancer. *Nutr. Cancer* **2012**, *64*, 351–360. [CrossRef]
5. Kyle, J.A.; Sharp, L.; Little, J.; Duthie, G.G.; McNeill, G. Dietary flavonoid intake and colorectal cancer: A case-control study. *Br. J. Nutr.* **2010**, *103*, 429–436. [CrossRef]
6. Hisaka, T.; Sakai, H.; Sato, T.; Goto, Y.; Nomura, Y.; Fukutomi, S.; Fujita, F.; Mizobe, T.; Nakashima, O.; Tanigawa, M.; et al. Quercetin Suppresses Proliferation of Liver Cancer Cell Lines In Vitro. *Anticancer Res.* **2020**, *40*, 4695–4700. [CrossRef]
7. Wang, G.; Zhang, J.; Liu, L.; Sharma, S.; Dong, Q. Quercetin Potentiates Doxorubicin Mediated Antitumor Effects against Liver Cancer through p53/Bcl-xl. *PLoS ONE* **2012**, *7*, e51764. [CrossRef]
8. Cai, X.; Fang, Z.; Dou, J.; Yu, A.; Zhai, G. Bioavailability of quercetin: Problems and promises. *Curr. Med. Chem.* **2013**, *20*, 2572–2582. [CrossRef]
9. Manach, C.; Morand, C.; Demigné, C.; Texier, O.; Régérat, F.; Rémésy, C. Bioavailability of rutin and quercetin in rats. *FEBS Lett.* **1997**, *409*, 12–16. [CrossRef]
10. Chen, L.; Teng, H.; Xie, Z.; Cao, H.; Cheang, W.S.; Skalicka-Woniak, K.; Georgiev, M.I.; Xiao, J. Modifications of dietary flavonoids towards improved bioactivity: An update on structure-activity relationship. *Crit. Rev. Food Sci. Nutr.* **2018**, *58*, 513–527. [CrossRef]
11. de Araujo, M.E.; Franco, Y.E.; Messias, M.C.; Longato, G.B.; Pamphile, J.A.; Carvalho, P.O. Biocatalytic Synthesis of Flavonoid Esters by Lipases and Their Biological Benefits. *Planta Med.* **2017**, *83*, 7–22. [CrossRef] [PubMed]
12. Sakao, K.; Hou, D.-X. Effects and Mechanisms of Acylated Flavonoid on Cancer Chemopreventive Activity. *Curr. Pharmacol. Rep.* **2020**, *6*, 286–305. [CrossRef]
13. Hoang, T.K.; Huynh, T.K.; Nguyen, T.D. Synthesis, characterization, anti-inflammatory and anti-proliferative activity against MCF-7 cells of O-alkyl and O-acyl flavonoid derivatives. *Bioorganic Chem.* **2015**, *63*, 45–52. [CrossRef] [PubMed]
14. Lopes, B.R.P.; da Costa, M.F.; Genova Ribeiro, A.; da Silva, T.F.; Lima, C.S.; Caruso, I.P.; de Araujo, G.C.; Kubo, L.H.; Iacovelli, F.; Falconi, M.; et al. Quercetin pentaacetate inhibits in vitro human respiratory syncytial virus adhesion. *Virus Res.* **2020**, *276*, 197805. [CrossRef] [PubMed]
15. Duan, Y.; Sun, N.; Xue, M.; Wang, X.; Yang, H. Synthesis of regioselectively acylated quercetin analogues with improved antiplatelet activity. *Mol. Med. Rep.* **2017**, *16*, 9735–9740. [CrossRef] [PubMed]
16. Warnakulasuriya, S.N.; Ziaullah; Rupasinghe, H.P. Long Chain Fatty Acid Esters of Quercetin-3-O-glucoside Attenuate H_2O_2-induced Acute Cytotoxicity in Human Lung Fibroblasts and Primary Hepatocytes. *Molecules* **2016**, *21*, 452. [CrossRef] [PubMed]
17. Sakao, K.; Fujii, M.; Hou, D.X. Clarification of the role of quercetin hydroxyl groups in superoxide generation and cell apoptosis by chemical modification. *Biosci. Biotechnol. Biochem.* **2009**, *73*, 2048–2053. [CrossRef] [PubMed]
18. Sakao, K.; Fujii, M.; Hou, D.X. Acetyl derivate of quercetin increases the sensitivity of human leukemia cells toward apoptosis. *Biofactors* **2009**, *35*, 399–405. [CrossRef]
19. Tanigawa, S.; Fujii, M.; Hou, D.X. Stabilization of p53 is involved in quercetin-induced cell cycle arrest and apoptosis in HepG2 cells. *Biosci. Biotechnol. Biochem.* **2008**, *72*, 797–804. [CrossRef]
20. Kroemer, G.; Galluzzi, L.; Brenner, C. Mitochondrial membrane permeabilization in cell death. *Physiol. Rev.* **2007**, *87*, 99–163. [CrossRef]
21. Tait, S.W.; Green, D.R. Mitochondrial regulation of cell death. *Cold Spring Harb. Perspect. Biol.* **2013**, *5*, a008706. [CrossRef] [PubMed]
22. Fossen, T.; Cabrita, L.; Andersen, O.M. Colour and stability of pure anthocyanins influenced by pH including the alkaline region. *Food Chem.* **1998**, *63*, 435–440. [CrossRef]
23. Torskangerpoll, K.; Andersen, Ø.M. Colour stability of anthocyanins in aqueous solutions at various pH values. *Food Chem.* **2005**, *89*, 427–440. [CrossRef]
24. Liu, X.; Shi, Y.; Hu, H.; Li, J.; Li, C.; Yang, L.; Wang, Z. Three new C-glycosyflavones with acetyl substitutions from Swertia mileensis. *J. Nat. Med.* **2018**, *72*, 922–928. [CrossRef] [PubMed]

25. Li, X.; Tian, Y.; Wang, T.; Lin, Q.; Feng, X.; Jiang, Q.; Liu, Y.; Chen, D. Role of the p-Coumaroyl Moiety in the Antioxidant and Cytoprotective Effects of Flavonoid Glycosides: Comparison of Astragalin and Tiliroside. *Molecules* **2017**, *22*, 1165. [CrossRef] [PubMed]
26. Le, J.; Lu, W.; Xiong, X.; Wu, Z.; Chen, W. Anti-Inflammatory Constituents from *Bidens frondosa*. *Molecules* **2015**, *20*, 18496–18510. [CrossRef] [PubMed]
27. Mattarei, A.; Biasutto, L.; Rastrelli, F.; Garbisa, S.; Marotta, E.; Zoratti, M.; Paradisi, C. Regioselective O-Derivatization of Quercetin via Ester Intermediates. An Improved Synthesis of Rhamnetin and Development of a New Mitochondriotropic Derivative. *Molecules* **2010**, *15*, 4722–4736. [CrossRef] [PubMed]
28. Rubio, S.; Quintana, J.; Eiroa, J.L.; Triana, J.; Estévez, F. Acetyl derivative of quercetin 3-methyl ether-induced cell death in human leukemia cells is amplified by the inhibition of ERK. *Carcinogenesis* **2007**, *28*, 2105–2113. [CrossRef]
29. Lee, K.W.; Kang, N.J.; Heo, Y.S.; Rogozin, E.A.; Pugliese, A.; Hwang, M.K.; Bowden, G.T.; Bode, A.M.; Lee, H.J.; Dong, Z. Raf and MEK protein kinases are direct molecular targets for the chemopreventive effect of quercetin, a major flavonol in red wine. *Cancer Res.* **2008**, *68*, 946–955. [CrossRef]
30. Russo, M.; Milito, A.; Spagnuolo, C.; Carbone, V.; Rosén, A.; Minasi, P.; Lauria, F.; Russo, G.L. CK2 and PI3K are direct molecular targets of quercetin in chronic lymphocytic leukaemia. *Oncotarget* **2017**, *8*, 42571–42587. [CrossRef]
31. Walker, E.H.; Pacold, M.E.; Perisic, O.; Stephens, L.; Hawkins, P.T.; Wymann, M.P.; Williams, R.L. Structural determinants of phosphoinositide 3-kinase inhibition by wortmannin, LY294002, quercetin, myricetin, and staurosporine. *Mol. Cell* **2000**, *6*, 909–919. [CrossRef] [PubMed]
32. Tsuchiya, A.; Kobayashi, M.; Kamatari, Y.O.; Mitsunaga, T.; Yamauchi, K. Development of flavonoid probes and the binding mode of the target protein and quercetin derivatives. *Bioorganic Med. Chem.* **2022**, *68*, 116854. [CrossRef] [PubMed]
33. Otake, Y.; Hsieh, F.; Walle, T. Glucuronidation versus oxidation of the flavonoid galangin by human liver microsomes and hepatocytes. *Drug Metab. Dispos. Biol. Fate Chem.* **2002**, *30*, 576–581. [CrossRef] [PubMed]
34. Wen, X.; Walle, T. Methylated flavonoids have greatly improved intestinal absorption and metabolic stability. *Drug Metab. Dispos. Biol. Fate Chem.* **2006**, *34*, 1786–1792. [CrossRef] [PubMed]
35. Lambert, J.D.; Sang, S.; Hong, J.; Kwon, S.J.; Lee, M.J.; Ho, C.T.; Yang, C.S. Peracetylation as a means of enhancing in vitro bioactivity and bioavailability of epigallocatechin-3-gallate. *Drug Metab. Dispos. Biol. Fate Chem.* **2006**, *34*, 2111–2116. [CrossRef] [PubMed]
36. Tsai, H.Y.; Yang, J.F.; Chen, Y.B.; Guo, J.L.; Li, S.; Wei, G.J.; Ho, C.T.; Hsu, J.L.; Chang, C.I.; Liang, Y.S.; et al. Acetylation Enhances the Anticancer Activity and Oral Bioavailability of 5-Demethyltangeretin. *Int. J. Mol. Sci.* **2022**, *23*, 13284. [CrossRef]
37. Lo, S.; Leung, E.; Fedrizzi, B.; Barker, D. Syntheses of mono-acylated luteolin derivatives, evaluation of their antiproliferative and radical scavenging activities and implications on their oral bioavailability. *Sci. Rep.* **2021**, *11*, 12595. [CrossRef]
38. Carrasco-Sandoval, J.; Aranda-Bustos, M.; Henríquez-Aedo, K.; López-Rubio, A.; Fabra, M.J. Bioaccessibility of different types of phenolic compounds co-encapsulated in alginate/chitosan-coated zein nanoparticles. *LWT* **2021**, *149*, 112024. [CrossRef]
39. Pohjala, L.; Tammela, P. Aggregating behavior of phenolic compounds--a source of false bioassay results? *Molecules* **2012**, *17*, 10774–10790. [CrossRef]
40. Biasutto, L.; Zoratti, M. Prodrugs of quercetin and resveratrol: A strategy under development. *Curr. Drug Metab.* **2014**, *15*, 77–95. [CrossRef]
41. Moriguchi, T.; Sakao, K.; Hou, D.-X.; Yoza, K.J.I. 3,5,7-Triacetoxy-2-(3,4-diacetoxyphenyl)-4H-1-benzopyran-4-one. *IUCrData* **2016**, *1*, x160028. [CrossRef]
42. Satoh, T.; Hosokawa, M. The mammalian carboxylesterases: From molecules to functions. *Annu. Rev. Pharmacol. Toxicol.* **1998**, *38*, 257–288. [CrossRef] [PubMed]
43. Hosokawa, M. Structure and catalytic properties of carboxylesterase isozymes involved in metabolic activation of prodrugs. *Molecules* **2008**, *13*, 412–431. [CrossRef] [PubMed]
44. Taketani, M.; Shii, M.; Ohura, K.; Ninomiya, S.; Imai, T. Carboxylesterase in the liver and small intestine of experimental animals and human. *Life Sci.* **2007**, *81*, 924–932. [CrossRef] [PubMed]
45. Williams, E.T.; Jones, K.O.; Ponsler, G.D.; Lowery, S.M.; Perkins, E.J.; Wrighton, S.A.; Ruterbories, K.J.; Kazui, M.; Farid, N.A. The biotransformation of prasugrel, a new thienopyridine prodrug, by the human carboxylesterases 1 and 2. *Drug Metab. Dispos. Biol. Fate Chem.* **2008**, *36*, 1227–1232. [CrossRef]
46. Yang, D.; Pearce, R.E.; Wang, X.; Gaedigk, R.; Wan, Y.J.; Yan, B. Human carboxylesterases HCE1 and HCE2: Ontogenic expression, inter-individual variability and differential hydrolysis of oseltamivir, aspirin, deltamethrin and permethrin. *Biochem. Pharmacol.* **2009**, *77*, 238–247. [CrossRef]
47. Takai, S.; Matsuda, A.; Usami, Y.; Adachi, T.; Sugiyama, T.; Katagiri, Y.; Tatematsu, M.; Hirano, K. Hydrolytic Profile for Ester- or Amide-linkage by Carboxylesterases pI 5.3 and 4.5 from Human Liver. *Biol. Pharm. Bull.* **1997**, *20*, 869–873. [CrossRef]
48. Yano, S.; Wu, S.; Sakao, K.; Hou, D.X. Wasabi 6-(methylsulfinyl)hexyl isothiocyanate induces apoptosis in human colorectal cancer cells through p53-independent mitochondrial dysfunction pathway. *Biofactors* **2018**, *44*, 361–368. [CrossRef]
49. Sakao, K.; Singh, S.V. D,L-sulforaphane-induced apoptosis in human breast cancer cells is regulated by the adapter protein p66Shc. *J. Cell Biochem.* **2012**, *113*, 599–610. [CrossRef]

50. Wong, C.C.; Williamson, G. Inhibition of hydroxycinnamic acid sulfation by flavonoids and their conjugated metabolites. *Biofactors* **2013**, *39*, 644–651. [CrossRef]
51. O'Leary, K.A.; Day, A.J.; Needs, P.W.; Mellon, F.A.; O'Brien, N.M.; Williamson, G. Metabolism of quercetin-7- and quercetin-3-glucuronides by an in vitro hepatic model: The role of human β-glucuronidase, sulfotransferase, catechol-O-methyltransferase and multi-resistant protein 2 (MRP2) in flavonoid metabolism. *Biochem. Pharmacol.* **2003**, *65*, 479–491. [CrossRef] [PubMed]

International Journal of
Molecular Sciences

MDPI

Article

Impact of Sinapic Acid on Bovine Serum Albumin Thermal Stability

Aurica Precupas and Vlad Tudor Popa *

"Ilie Murgulescu" Institute of Physical Chemistry, Romanian Academy, Splaiul Independentei 202, 060021 Bucharest, Romania; aprecupas@icf.ro
* Correspondence: vtpopa@icf.ro

Abstract: The thermal stability of bovine serum albumin (BSA) in Tris buffer, as well as the effect of sinapic acid (SA) on protein conformation were investigated via calorimetric (differential scanning microcalorimetry—μDSC), spectroscopic (dynamic light scattering—DLS; circular dichroism—CD), and molecular docking approaches. μDSC data revealed both the denaturation (endotherm) and aggregation (exotherm) of the protein, demonstrating the dual effect of SA on protein thermal stability. With an increase in ligand concentration, (i) protein denaturation shifts to a higher temperature (indicating native form stabilization), while (ii) the aggregation process shifts to a lower temperature (indicating enhanced reactivity of the denatured form). The stabilization effect of SA on the native structure of the protein was supported by CD results. High temperature (338 K) incubation induced protein unfolding and aggregation, and increasing the concentration of SA altered the size distribution of the protein population, as DLS measurements demonstrated. Complementary information offered by molecular docking allowed for the assessment of the ligand binding within the Sudlow's site I of the protein. The deeper insight into the SA–BSA interaction offered by the present study may serve in the clarification of ligand pharmacokinetics and pharmacodynamics, thus opening paths for future research and therapeutic applications.

Keywords: sinapic acid; serum albumin; thermal stability; denaturation; aggregation

Citation: Precupas, A.; Popa, V.T. Impact of Sinapic Acid on Bovine Serum Albumin Thermal Stability. *Int. J. Mol. Sci.* **2024**, *25*, 936. https://doi.org/10.3390/ijms25020936

Academic Editor: Antonio González-Sarrías

Received: 15 December 2023
Revised: 9 January 2024
Accepted: 10 January 2024
Published: 11 January 2024

1. Introduction

Thermal denaturation of proteins is a key factor in biotechnological processes and pharmaceutical applications. The complex influence of various ligands on the proteins unfolding is far from being elucidated. The interaction of proteins with polyphenols may result in various changes in the physicochemical and functional features for both sides. Additional information concerning the effect of phenolic compounds on protein thermal stability is needed to control the functional properties of proteins.

Sinapic acid (SA, 3,5-dimethoxy-4-hydroxycinnamic acid) is a naturally occurring hydroxycinnamic acid, found in plants, fruits, vegetables, several cereals, and oil crops [1–4] with potential use in food processing, cosmetics, and in the pharmaceutical industry. SA acts as an anti-inflammatory [5], antidiabetic [6], anticancer agent [7] with antioxidant [8], antibacterial [9], chemopreventive [10], neuroprotective [11], and antihypertensive [12] effects. At pH 7.4, SA is present as an anion (Figure 1), the COOH group (pKa = 4.47) being dissociated [13].

Bovine serum albumin (BSA) is a globular protein that binds and transports a wide range of endogenous and exogenous ligands, playing a significant role in the pharmacokinetic behavior of a variety of drugs [14]. Its structural and functional similarities with the human serum albumin (HSA) made it a model protein for research purposes.

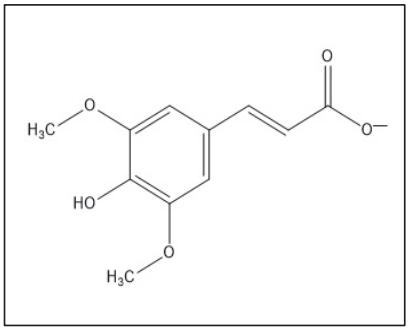

Figure 1. Chemical structure of carboxylate form of sinapic acid (SA).

BSA presents two important binding sites for the ligands: Sudlow's site I, located in subdomain IIA, and Sudlow's site II, located in subdomain IIIA [15]. The native structure of BSA is the key to its biological function, but at high temperatures the protein loses its activity [16]. As a result, the thermal stability of protein is an active field of fundamental research, and the use of polyphenols to modulate aggregate formation seems very promising. The effect of SA on thermally driven denaturation and aggregation of serum albumin above its melting temperature is of great theoretical and practical importance since protein aggregation is associated with various diseases, such as Alzheimer's and systemic amyloidosis [17]. The quest for new aggregation inhibitors for amyloid-forming proteins is crucial in the progress of novel therapeutics. Moreover, recent results pointed to thermal denaturation and aggregation as a threat to global distribution of biologics and research-use-only (RUO) proteins in a relatively high temperature environment [18]. Calorimetric [19], spectroscopic [20], and molecular docking [21,22] approaches are extensively used to study and analyze the interaction of different ligands with proteins and their applications in various research domains.

In our previous papers we evaluated the influence of different polyphenolic compounds on protein (BSA, hemoglobin) thermal stability. Furthermore, the aim of this study is to provide a better understanding of the impact of SA on heat-induced denaturation and aggregation of BSA. A previous study [23] using fluorescence measurements resulted in a binding constant of 4.5×10^5 M^{-1} for SA to BSA at 298 K with a stoichiometry of 1.26. The site-marker competitive experiment indicated subdomain IIA of the protein as the binding site of SA. Accordingly, two concentrations of SA were used to evidence the impact of free (excess) and bound ligands on protein thermal stability. Also, the present study reveals the influence of Tris buffer on the protein aggregation process that could be calorimetrically evidenced.

2. Results and Discussions

2.1. Evaluation of Protein Thermal Stability by Differential Scanning Microcalorimetry (μDSC)

Previous calorimetric studies [24] concerning BSA thermal stability in phosphate buffer evidenced only the endothermal denaturation process. That was confirmed by our previous contributions [25–27]. In other words, the phosphate buffer covers the exothermal calorimetric signature of the aggregation process; although, the later takes place in the temperature range investigated. This is the reason for using complementary techniques to investigate the aggregation process in phosphate buffer: dynamic light scattering, asymmetric flow field-flow fractionation, and analytical ultracentrifugation [28]. Detection of both processes within the same DSC run was demonstrated by Barone et al. [24] in acetate buffer. The present study demonstrates the possibility of obtaining the DSC thermal signatures of protein denaturation and aggregation processes in Tris buffer. It also evidenced changes of these signatures produced by the presence of sinapic acid. Protein aggregation in Tris buffer is caused by the interaction of Tris buffer molecules with the exposed hydrophobic

groups of denatured protein [29]. Tris buffer exhibits a pKa dependence with temperature [30]. However, pH measurements performed in the temperature range used for the μDSC method indicated that the results of this study were not significantly affected by the pH change with increasing temperature (Figure S1 from Supplementary Material).

Ligand binding on protein modifies the protein thermal stability, and this effect could be estimated by μDSC measurements [31]. Figure 2 presents the μDSC sigmoid baseline subtracted thermograms of the protein, in the absence and presence of SA, allowing for the evaluation of the ligand concentration influence on BSA thermal stability.

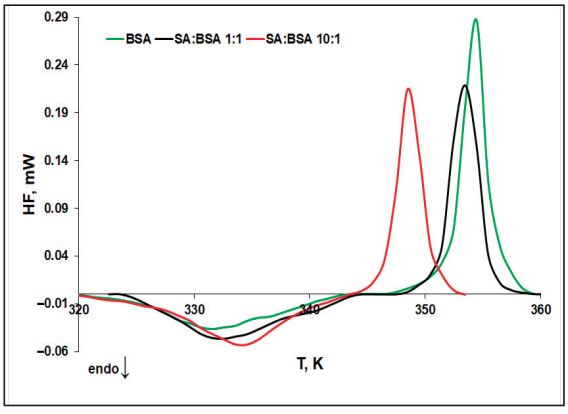

Figure 2. μDSC sigmoid baseline subtracted thermograms of BSA and BSA-SA systems.

Two signals could be noticed in the μDSC scans: (i) an endothermic one corresponding to the denaturation process of BSA, and (ii) an exothermic peak occurring at higher temperatures, related to the aggregation process of protein induced by the exposure of the hydrophobic residues. The thermodynamic parameters corresponding to the denaturation and aggregation processes of protein, in the absence and presence of increasing concentrations of SA, were calculated and are presented in Figure 3.

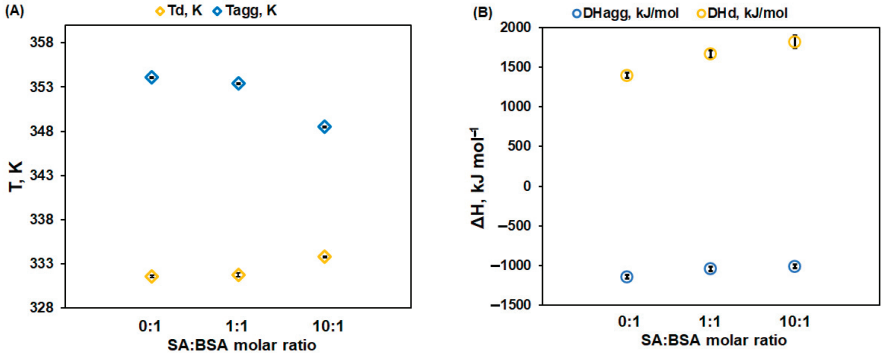

Figure 3. Thermodynamic parameters (**A**) temperatures and (**B**) enthalpies of BSA thermal denaturation and aggregation processes as a function of SA:BSA molar ratio. Standard deviations are presented as error bars.

SA exerts a dual effect on BSA thermal stability in dynamic scanning conditions:

1. The denaturation temperature (T_d) of protein increases with the SA concentration, pointing to a stabilization effect of SA on the protein native structure. Moreover, Figure 3 displays an increase in the denaturation enthalpy change (ΔH_d) with an

increasing in the ligand concentration. This may be ascribed to a lower exposure to the solvent molecules of the native protein's buried hydrophobic regions, during the unfolding process in the presence of SA [32].

2. The aggregation temperature (T_{agg}) and the absolute value of the enthalpy change ($|\Delta H_{agg}|$) decrease with SA concentrations: the ligand binding weakens the unfolded structure of protein. For a 10:1 SA:BSA molar ratio, the denaturation process and the aggregation one slightly overlap, producing a supplementary decrease in the calculated $|\Delta H_{agg}|$ value.

SA binding to the native form of the protein delays the protein denaturation, manifesting as an increase in T_d. A significant impact was observed for a 10:1 SA:BSA molar ratio, pointing to the stabilization effect of the excess free ligand. A similar influence was obtained for morin, a polyphenol that belongs to the flavanol class of flavonoids, in interaction with BSA [25]. The stabilization of protein structure could be generated by the electrostatic attraction between the negatively charged SA and the positively charged amino acid residues from the protein binding site, as observed by our group for the caffeic acid interaction with BSA [26].

The exposure of the hydrophobic core of the protein to the solvent molecules during unfolding is reduced in the presence of SA, the protein structure becomes more compact, and the ΔH_d value increases, as reported for the gallic acid effect on the BSA structure [27]. SA stabilizes the protein structure against thermal denaturation, in good agreement with data obtained by our group that report the enhancement of serum albumin thermal stability in the presence of various polyphenols (morin, caffeic acid, gallic acid, quercetin). The stabilization of the human serum albumin by the methotrexate drug [33], warfarin, and benoxaprofen [34] was also reported.

With increasing temperature, the hydrogen bonds that stabilize the native protein structure weaken, easing the exposure of hydrophobic protein groups to the solvent. As previously presented in the literature [29], a possible mechanism for the aggregation of BSA in Tris buffer is related to the favorable (exothermic) interaction of the hydrophobic groups of the unfolded protein with the buffer molecules. This favorable effect is added to the favorable protein–protein interaction and the result (the thermal fingerprint) is a well evidenced exothermic peak. As ligand binding to the unfolded/partially folded BSA decreases the T_{agg} and $|\Delta H_{agg}|$ of the protein, SA acts as promoter of aggregation above the denaturation temperature. Also, the adsorption of free polyphenol on the protein surface could cause conformational changes in the protein structure that further promote aggregation [35]. A similar action was reported for morin binding on bovine serum albumin.

2.2. Circular Dichroism (CD) Spectra

The conformational change in the protein's secondary structure in static conditions (isothermal incubation) was monitored by CD. The influence of SA concentration on the BSA secondary structure after incubation at 277 K and 338 K is presented in Figure 4.

At 298 K, the protein secondary structure is predominantly α-helix, and SA presence induces an increase in the negative mean residue ellipticity (MRE) value, as a result of the ligand–protein interaction. The stabilization effect on the secondary structure of the protein, observed for both 1:1 and 10:1 SA:BSA molar ratios, could be correlated with μDSC data, where T_d increases in the presence of the ligand. Similar results were obtained for the interaction of morin [25], caffeic acid [26], and caffeoylquinic acids [36] with BSA.

After protein incubation at 338 K for 20 and 48 h, the CD spectra of BSA in the presence and absence of SA show a significant decrease in MRE values at 208 and 222 nm assigned to the α-helix structure, thereby indicating the thermal denaturation of the protein. Increasing the concentration of SA induces an increase in the CD signal even after incubation at 338 K. This is more evident after 48 h for a 10:1 SA:BSA molar ratio, pointing to the stabilization effect of the ligand on the protein structure. Both the bound ligand (1:1 SA:BSA molar

ratio) and the free ligand (10:1 SA:BSA molar ratio) cause conformational changes in the protein structure.

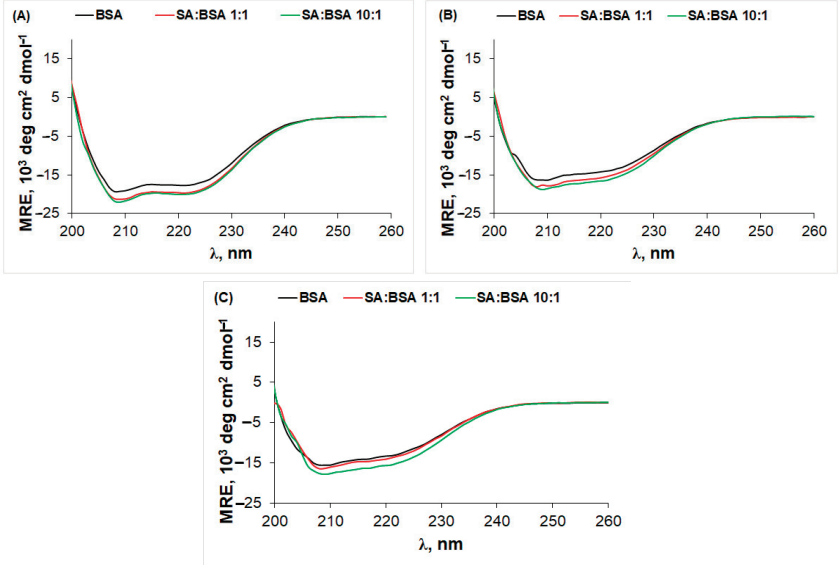

Figure 4. CD spectra of BSA in the absence and presence of different concentrations of SA after incubation at (**A**) 24 h 277 K, (**B**) 20 h at 338 K, and (**C**) 48 h at 338 K.

The protein secondary structure content obtained by Dichroweb (Figure 5) displays an increase in the α-helix structure with a simultaneous strand decrease for BSA in the presence of SA; this may be interpreted as complementary structural proof for the stabilization effect of SA evidenced in μDSC measurements.

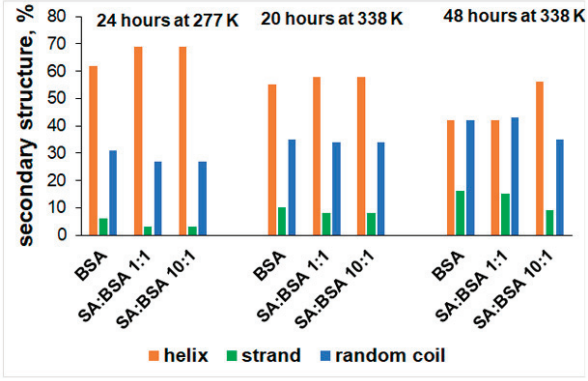

Figure 5. The secondary structure content of BSA and BSA–SA systems after incubation at 277 K and 338 K.

After incubation at 338 K for 20 h, the α-helix content of BSA decreases, while the β and unordered structure increase, indicating the protein thermal denaturation. Increasing the concentration of SA stabilizes the protein structure, the α-helix content increases, and the strand and random coil contents slightly decrease. After 48 h at 338 K, the denaturation of protein is more evident, the native structure of the protein is disrupted along with a concomitant increase in the strand and random coil contents [37]. SA acts as a stabilizer

only at high concentrations, enhancing the α-helix content, while the strand and random coil contents decrease.

2.3. Changes in the Hydrodynamic Dimeter of BSA Aggregates Investigated by Dynamic Light Scattering (DLS)

DLS measurements were carried out to determine the sizes of aggregates formed after incubating the protein samples in the absence and presence of SA. The intensity and number size distributions (Figures S2 and S3 from Supplementary Material) of the BSA solution at 277 K show a single population with the hydrodynamic diameter (D_h) value of 6.62 nm, corresponding to the native protein structure (monomeric form) which is in good agreement with the size of BSA reported in the literature [38]. In the presence of increasing concentrations of SA, no significant change in the D_h and polydispersity index (PDI) values could be observed (Figure 6).

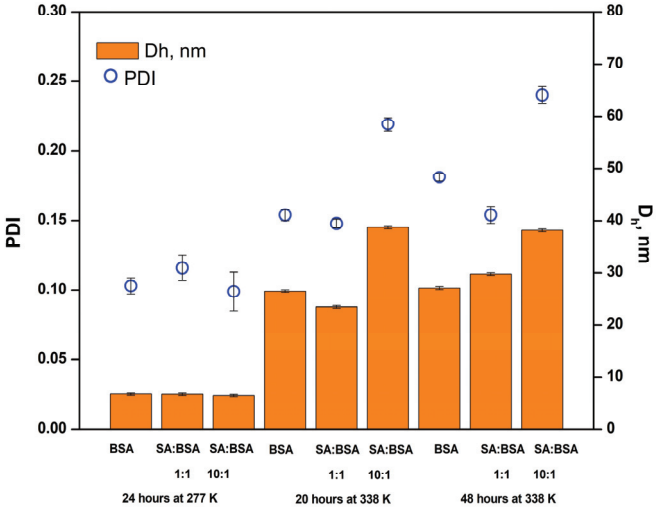

Figure 6. Hydrodynamic diameter and PDI of BSA population as a function of SA:BSA molar ratio. Standard deviations are presented as error bars.

After sample incubation for 20 h at 338 K, the DLS analysis still indicates a monomodal size distribution for the protein in the absence and presence of SA, with increasing particle size and PDI values as a consequence of denaturation and concomitant aggregation [39]. A high concentration of SA (10:1 SA:BSA molar ratio) induces a significant enhancement of PDI and D_h values, demonstrating the free ligand impact on protein aggregation at high temperatures. For a low concentration of SA, the aggregation effect is reduced compared to free BSA. In time, at 338 K, the size distributions of BSA and BSA–SA systems slightly change, so that after 48 h, a single population corresponding to larger aggregates is evidenced by DLS measurements. With increasing the incubating time at 338 K, the PDI values increase, suggesting the presence of a larger size species as result of the aggregation effect of the ligand. The influence of SA on the size distribution of the protein population at high temperature is manifested in two ways: At a low concentration (90.9 μM), after 20 h at 338 K, SA binding stabilizes the protein structure, in agreement with the CD results; after a longer incubating time (48 h), the ligand binding causes an opposite effect, promoting aggregation. At a high concentration (909 μM), SA promotes protein aggregation after 20 h at 338 K and the effect is maintained in time at 48 h incubation, with the same intensity, in good agreement with the CD results.

2.4. Molecular Docking

Molecular docking of SA with BSA (Figure 7) was used to identify the most favorable binding site of the ligand within the native structure of the macromolecule and to find the amino acid residues involved in the interaction.

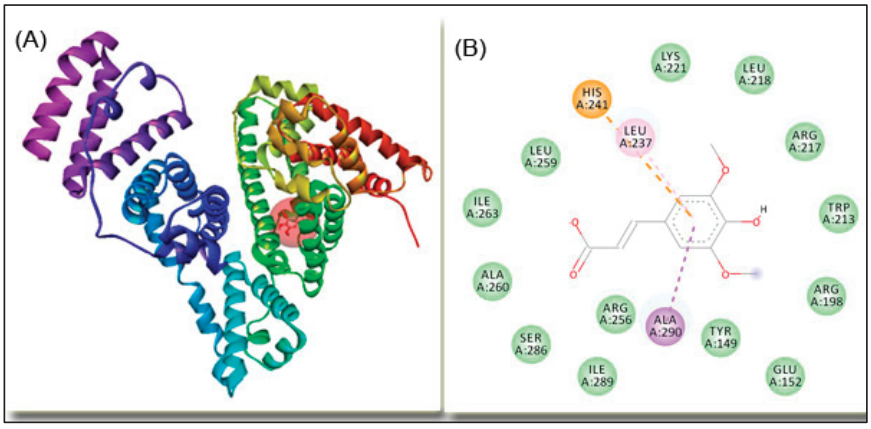

Figure 7. Molecular docking of SA and BSA; (**A**) SA is presented as stick and balls and the protein as solid ribbon. (**B**) The 2D representation of SA–BSA complex; the close amino acid residues are presented in green, dashed lines represent intermolecular interactions of different origin (electrostatic—orange line; π-alkyl—pink lines; π-σ—purple lines; π-π T-shaped—magenta lines; van der Waals interactions—light green lines).

SA binds to subdomain IIA (Sudlow's site I) of BSA with a binding affinity of −6.2 kcal/mol, corresponding to a binding constant of 3.52×10^4 M^{-1}, and the interaction is mainly driven by hydrophobic forces and electrostatic interaction, as shown in Table 1.

Table 1. Molecular interactions between SA and the amino acid residues in BSA binding site obtained by molecular docking.

Amino acid Residue	Distance, Å	Type of Interaction
HIS241	4.75	electrostatic
ALA290	3.69	hydrophobic
HIS241	5.50	hydrophobic
LEU237	4.80	hydrophobic

The present findings are consistent with the outcomes of previous investigations that indicated the binding of other polyphenols in the vicinity of TRP 213 of BSA [40,41].

3. Materials and Methods

3.1. Materials

BSA (A7030, lyophilized powder, purity ≥ 98%, CAS: 9048-46-8, Sigma-Aldrich, Saint Louis, MI, USA) and SA (D7927, purity 98.0%, CAS: 530-59-6, Sigma-Aldrich, Bangalore, India) were used with no further purification. Solutions of the protein and ligand were prepared in 25 mM Tris buffer (Trizma base, Honeywell Fluka, Charlotte, NC, USA, purity 99%) at pH 7.4. For μDSC, the samples of BSA (90.9 μM) in the absence and presence of SA were allowed to equilibrate for 24 h at 277 K and brought to room temperature before measurements. Similarly, for CD and DLS measurements, the protein samples (75 μM) in 25 mM Tris buffer, pH 7.4, were incubated at 277 K for 24 h in the absence and presence of ligand in various concentrations (SA:BSA molar ratio 1:1, 10:1). After this, the BSA samples

were further used in different ways: (i) diluted to the working concentration (50 μM for CD and 37.8 μM for DLS measurements) and measured at 298 K, or (ii) kept at 338 K in an incubator without stirring. At certain time intervals (20 h and 48 h), aliquots were taken from solution, cooled to room temperature, diluted to the working concentration (50 μM for CD and 37.8 μM for DLS measurements), and used for measurements at 298 K.

3.2. Methods

3.2.1. Differential Scanning Microcalorimetry (μDSC)

The thermal stability of BSA in the absence and presence of different concentrations of SA was studied in Tris buffer 25 mM, pH 7.4, using μDSC7 evo calorimeter (Setaram, Caluire, France) in the temperature range of 298 K–368 K, at 1 K min^{-1} heating rate. The thermodynamic parameters (enthalpy change and temperature) of denaturation and aggregation processes were determined by Calisto v.1077 software using a tangential sigmoid baseline. The per mol quantities were calculated from the absolute values (Joules), taking into account the sample volume and the protein concentration.

3.2.2. Circular Dichroism (CD)

The secondary structure of protein and the effect of SA binding at 277 K and after incubation at 338 K were evaluated using CD measurements by a JASCO J-815 spectropolarimeter (Jasco, Japan), equipped with a Peltier-type temperature controller. Far-UV CD spectra of BSA were obtained with three accumulations for each measurement, using a 1 cm quartz cuvette. The protein concentration (0.5 μM) was maintained constant. The time constant, scan speed, resolution, and sensitivity were set at 1 s, 100 nm min^{-1}, 1.0 nm, and 100 mdeg, respectively. The CD spectra of the samples were baseline-subtracted by using the spectrum of 25 mM Tris buffer, pH 7.4. The CD results were expressed in terms of mean residue ellipticity (MRE) in deg cm^2 $dmol^{-1}$ [36]. The secondary structure content of protein in the absence and presence of SA was evaluated using the K2D analysis algorithm [42] from the Dichroweb website [43] between 200 and 260 nm in order to remove the effect of chloride ions absorption below 200 nm [44]. Normalized root-mean square deviations (NRMSD) lower than 0.2 (the acceptable upper limit) were obtained for all fits of CD spectra [45,46] and are presented in Table S1 in Supplementary Material.

3.2.3. Dynamic Light Scattering (DLS)

The hydrodynamic diameter (D_h) of BSA (37.8 μM) and BSA–SA systems was determined by DLS measurements using a Nano ZS (Malvern Instruments, Worcestershire, UK) instrument with laser incident beam at λ = 633 nm and a fixed scattering angle of 173° equipped with a temperature-controlled system. A 0.22 μm pore-sized microfilter was used to filter all of the solutions. The analysis of intensity fluctuations enables the determination of the diffusion coefficients of particles, which are converted into a size distribution. Scattering data were collected as an average of 5 measurements [47], and the mean D_h value in the intensity distribution and the polydispersity index (PDI) were presented.

3.2.4. Molecular Docking

Molecular docking study of SA binding with BSA was performed for predicting the binding site, the interaction forces, and the binding affinity. The protein structure (PDB ID: 4F5S) [48] was obtained from the RSCB Protein Data Bank [49]. The geometry of the SA anion was optimized by DFT/B3LYP/6-311G++ level of theory using the Gaussian 03 software [50], as previously described [51]. The molecular docking was performed using the Autodock Vina 1.1.2 software [52]. Autodock tools [53] were used for protein and ligand file preparation to add all hydrogen atoms, to assign the Gasteiger charges, to detect and assign the rotatable bonds of SA. The Lamarckian genetic algorithm was applied to determine the optimum binding site of the SA anion to BSA, set as rigid. The grid box which covers the amino acid residues of Sudlow's site I and Sudlow's site II

was set up with 40 points in each of the X, Y, and Z dimensions centered on x, y, and z coordinates of 1 × 19 × 109, with a grid point spacing of 1 Å. The exhaustiveness of the global search was set to 8. The maximum number of binding modes was 9. The maximum energy difference between modes was 3 kcal/mol. The best docking mode in Autodock Vina was the minimum energy conformation of the ligand–protein complex (the largest ligand binding affinity). One possible (best) binding site was identified as Sudlow's site I. The conformer with the lowest binding energy was selected for analysis. The type of interaction was evaluated using the BIOVIA Discovery studio 2019 [54].

4. Conclusions

The results of this study provide significant insight into polyphenol–protein interaction and its impact on protein thermal stability. The thermal stability of BSA and the impact of SA concentration were evaluated using calorimetric and spectroscopic approaches. μDSC data pointed to the dual action of SA on BSA thermal stability. On the one hand, SA binding to the native form of the protein increases its thermal stability, and on the other hand, SA promotes protein aggregation above the denaturation temperature. At a low concentration, bound SA interacts directly with BSA in a site-specific manner: the native structure of protein is stabilized, resulting in a reduced exposure of the partially unfolded protein surface upon heating. At higher concentrations, non-bound (free) SA present in excess may interact with the protein surface, with displacement of the solvent molecules and thereby screening the solvent–protein interaction and enhancing the thermal stability of the later [55]. Presented CD data revealed both conformational changes induced by SA binding that stabilizes the protein structure, and the protein partial unfolding after incubation at higher temperature. After heating above the denaturation temperature, aggregation of the partially unfolded molecules is possible. As evidenced by DLS measurements, the BSA aggregates increased in size with the increasing concentration of SA. Sudlow's site I in subdomain IIA of BSA was identified as the binding site for the SA using molecular docking.

Supplementary Materials: The following supporting information can be downloaded at: https://www.mdpi.com/article/10.3390/ijms25020936/s1.

Author Contributions: Conceptualization, A.P. and V.T.P.; methodology, A.P.; formal analysis, A.P.; investigation, A.P.; writing—original draft preparation, A.P. and V.T.P.; writing—review and editing, V.T.P.; supervision, V.T.P. All authors have read and agreed to the published version of the manuscript.

Funding: This research received no external funding.

Institutional Review Board Statement: Not applicable.

Informed Consent Statement: Not applicable.

Data Availability Statement: Data are contained within the article and the Supplementary Material.

Acknowledgments: This research was carried out within the research project "Nonuniform biobinding" of "Ilie Murgulescu" Institute of Physical Chemistry of the Romanian Academy.

Conflicts of Interest: The authors declare no conflicts of interest.

References

1. Moreno, D.A.; Pérez-Balibrea, S.; Ferreres, F.; Gil-Izquierdo, A.; García-Viguera, C. Acylated anthocyanins in broccoli sprouts. *J. Food Chem.* **2010**, *123*, 358–363. [CrossRef]
2. Andreasen, M.F.; Landbo, A.-K.; Christensen, L.P.; Hansen, A.; Meyer, A.S. Antioxidant effects of phenolic rye (*Secale cereale* L.) extracts, monomeric hydroxycinnamates, and ferulic acid dehydrodimers on human low-density lipoproteins. *J. Agric. Food Chem.* **2001**, *49*, 4090–4096. [CrossRef]
3. Niciforovic, N.; Abramovic, H. Sinapic acid and its derivatives: Natural sources and bioactivity. *Compr. Rev. Food Sci. Food Saf.* **2014**, *13*, 34–51. [CrossRef] [PubMed]
4. Engels, C.; Schieber, A.; Gänzle, M.G. Sinapic acid derivatives in defatted oriental mustard (*Brassica juncea* L.) seed meal extracts using UHPLC-DADESI-MSn and identification of compounds with antibacterial activity. *Eur. Food Res. Technol.* **2012**, *234*, 535–542. [CrossRef]

5. Yun, K.J.; Koh, D.J.; Kim, S.H.; Park, S.J.; Ryu, J.H.; Kim, D.G.; Lee, J.Y.; Lee, K.T. Anti-inflammatory effects of sinapic acid through the suppression of inducible nitric oxide synthase, cyclooxygase-2, and proinflammatory cytokines expressions via nuclear factor-kappaB inactivation. *J. Agric. Food Chem.* **2008**, *56*, 10265–10272. [CrossRef] [PubMed]
6. Cherng, Y.G.; Tsai, C.C.; Chung, H.H.; Lai, Y.W.; Kuo, S.C.; Cheng, J.T. Antihyperglycemic action of sinapic acid in diabetic rats. *J. Agric. Food Chem.* **2013**, *61*, 12053–12059. [CrossRef] [PubMed]
7. Hudson, E.A.; Dinh, P.A.; Kokubun, T.; Simmonds, M.S.J.; Gescher, A. Characterization of potentially hemopreventive phenols in extracts of brown rice that inhibit the growth of human breast and colon cancer cells. *Cancer Epidemiol. Biomark. Prev.* **2000**, *9*, 1163–1170.
8. Kikuzaki, H.; Hisamoto, M.; Hirose, K.; Akiyama, K.; Taniguchi, H. Antioxidant properties of ferulic acid and its related compounds. *J. Agric. Food Chem.* **2002**, *50*, 2161–2168. [CrossRef]
9. Maddox, C.E.; Laur, L.M.; Tian, L. Antibacterial activity of phenolic compounds against the phytopathogen Xylella fastidiosa. *Curr. Microbiol.* **2010**, *60*, 53–58. [CrossRef]
10. Ansari, M.A.; Raish, M.; Ahmad, A.; Ahmad, S.F.; Mudassar, S.; Mohsin, K.; Shakeel, F.; Korashy, H.M.; Bakheet, S.A. Sinapic acid mitigates gentamicin-induced nephrotoxicity and associated oxidative/nitrosative stress, apoptosis, and inflammation in rats. *Life Sci.* **2016**, *165*, 1–8. [CrossRef]
11. Sun, X.L.; Ito, H.; Masuoka, T.; Kamei, C.; Hatano, T. Effect of Polygala tenuifolia root extract on scopolamine-induced impairment of rat spatial cognition in an eight-arm radial maze task. *Biol. Pharm. Bull.* **2007**, *30*, 1727–1731. [CrossRef] [PubMed]
12. Raish, M.; Ahmad, A.; Ansari, M.A.; Alkharfy, K.M.; Ahad, A.; Khan, A.; Aljenobi, F.I.; Ali, N.; Al-Mohizea, A.M. Effect of sinapic acid on aripiprazole pharmacokinetics in rats: Possible food drug interaction. *J. Food Drug Anal.* **2019**, *27*, 332–338. [CrossRef]
13. Smyk, B. Fluorescence study of sinapic acid interaction with bovine serum albumin and egg albumin. *J. Fluoresc.* **2003**, *13*, 349–356. [CrossRef]
14. Otagiri, M.A. Molecular functional study on the interactions of drugs with plasma proteins. *Drug Metabol. Pharmacokinet.* **2005**, *20*, 309–323. [CrossRef] [PubMed]
15. Sudlow, G.; Birkett, D.J.; Wade, D.N. The Characterization of Two Specific Drug Binding Sites on Human Serum Albumin. *Mol. Pharmacol.* **1975**, *11*, 824–832.
16. Nnyigide, O.S.; Hyun, K. The protection of bovine serum albumin against thermal denaturation and gelation by sodium dodecyl sulfate studied by rheology and molecular dynamics simulation. *Food Hydrocoll.* **2020**, *103*, 105656. [CrossRef]
17. Tipping, K.W.; van Oosten-Hawle, P.; Hewitt, E.W.; Radford, S.E. Amyloid fibres: Inert end-stage aggregates or key players in disease? *Trends Biochem. Sci.* **2015**, *40*, 719–727. [CrossRef] [PubMed]
18. Sridhar, B.V.; Janczy, J.R.; Hatlevik, Ø.; Wolfson, G.; Anseth, K.S.; Tibbitt, M.W. Thermal stabilization of biologics with photoresponsive hydrogels. *Biomacromolecules* **2018**, *19*, 740–747. [CrossRef]
19. Aricov, L.; Precupas, A.; Tudose, M.; Baltag, D.; Trică, B.; Sandu, R.; Leonties, A.R. Trametes versicolor laccase activity modulated by the interaction with gold nanoparticles. *Environ. Res.* **2023**, *237*, 116920. [CrossRef]
20. Banu, A.; Khan, R.H.; Qashqoosh, M.T.A.; Manea, Y.K.; Furkan, M.; Naqvi, S. Multispectroscopic and computational studies of interaction of bovine serum albumin, human serum albumin and bovine hemoglobin with bisacodyl. *J. Mol. Struct.* **2022**, *1249*, 131550. [CrossRef]
21. Dombi, G.; Horváth, P.; Fiser, B.; Mirzahosseini, A.; Dobó, M.; Szabó, Z.-I.; Tóth, G. Enantioselective Human Serum Albumin Binding of Apremilast: Liquid Chromatographic, Fluorescence and Molecular Docking Study. *Int. J. Mol. Sci.* **2023**, *24*, 2168. [CrossRef] [PubMed]
22. Toma, C.-M.; Imre, S.; Farczadi, L.; Ion, V.; Marc, G. Enantioselective binding of carvedilol to human serum albumin and alpha-1-acid glycoprotein. *Chirality* **2023**, *35*, 779–792. [CrossRef]
23. Sengupta, P.; Pal, U.; Mondal, P.; Bose, A. Multi-spectroscopic and computational evaluation on the binding of sinapic acid and its Cu(II) complex with bovine serum albumin. *Food Chem.* **2019**, *301*, 125254. [CrossRef]
24. Barone, G.; Giancola, C.; Verdoliva, A. DSC studies on the denaturation and aggregation of serum albumins. *Thermochim. Acta* **1992**, *199*, 197–205. [CrossRef]
25. Precupas, A.; Sandu, R.; Neculae, A.V.F.; Neacsu, A.; Popa, V.T. Calorimetric, spectroscopic and computational investigation of morin binding effect on bovine serum albumin stability. *J. Mol. Liq.* **2021**, *333*, 115953. [CrossRef]
26. Precupas, A.; Sandu, R.; Leonties, A.R.; Anghel, D.F.; Popa, V.T. Complex interaction of caffeic acid with bovine serum albumin: Calorimetric, spectroscopic and molecular docking evidence. *New J. Chem.* **2017**, *41*, 15003–15015. [CrossRef]
27. Precupas, A.; Leonties, A.R.; Neacsu, A.; Sandu, R.; Popa, V.T. Gallic acid influence on bovine serum albumin thermal stability. *New J. Chem.* **2019**, *43*, 3891–3898. [CrossRef]
28. Borzova, V.A.; Markossian, K.A.; Chebotareva, N.A.; Kleymenov, S.Y.; Poliansky, N.B.; Muranov, K.O.; Stein-Margolina, V.A.; Shubin, V.V.; Markov, D.I.; Kurganov, B.I. Kinetics of Thermal Denaturation and Aggregation of Bovine Serum Albumin. *PLoS ONE* **2016**, *11*, e0153495. [CrossRef]
29. Satish, L.; Millan, S.; Das, S.; Jena, S.; Sahoo, H. Thermal Aggregation of Bovine Serum Albumin in Conventional Buffers: An Insight into Molecular Level Interactions. *J. Solution Chem.* **2017**, *46*, 831–848. [CrossRef]
30. Samuelsen, L.; Holm, R.; Lathuile, A.; Schönbeck. Buffer solutions in drug formulation and processing: How pKa values depend on temperature, pressure and ionic strength. *Int. J. Pharm.* **2019**, *560*, 357–364. [CrossRef]

31. Shrake, A.; Ross, P.D. Origins and consequences of ligand induced multiphasic thermal protein denaturation. *Biopolymers* **1992**, *32*, 925–940. [CrossRef] [PubMed]
32. Yamasaki, K.; Nishi, K.; Anraku, M.; Taguchi, K.; Maruyama, T.; Otagiri, M. Metal-catalyzed oxidation of human serum albumin does not alter the interactive binding to the two principal drug binding sites. *Biochem. Biophys. Rep.* **2018**, *14*, 155–160. [CrossRef]
33. Preisz, Z.; Kunsági-Máté, S. Effect of methotrexate and its photodegradation products on the temperature induced denaturation of human serum albumin. *Spectrochim. Acta A* **2021**, *245*, 118905. [CrossRef] [PubMed]
34. Lohner, K.; Sen, A.C.; Prankerd, R.; Esser, A.F.; Perrin, J.H. Effects of drug-binding on the thermal denaturation of human serum albumin. *J. Pharm. Biomed. Anal.* **1994**, *12*, 1501–1505. [CrossRef] [PubMed]
35. Labieniec, M.; Gabryelak, T. Interactions of tannic acid and its derivatives (ellagic and gallic acid) with calf thymus DNA and bovine serum albumin using spectroscopic method. *J. Photochem. Photobiol. B* **2006**, *82*, 72–78. [CrossRef]
36. Qishu, J.; Wei, Z.; Yanyan, J.; Lijuan, J.; Xiangyang, C.; Bin, L. Study on the interactions between caffeoylquinic acids with Bovine Serum Albumin: Spectroscopy, antioxidant activity, LC-MSn, and molecular docking approach. *Front. Chem.* **2019**, *7*, 840. [CrossRef]
37. Basu, A.; Bhayye, S.; Kundu, S.; Dasa, A.; Mukherjee, A. Andrographolide inhibits human serum albumin fibril formations through site-specific molecular interactions. *RSC Adv.* **2018**, *8*, 30717. [CrossRef]
38. Jachimska, B.; Wasilewska, M.; Adamczyk, Z. Characterization of globular protein solutions by Dynamic Light Scattering, electrophoretic mobility, and viscosity measurements. *Langmuir* **2008**, *24*, 6866–6872. [CrossRef]
39. Khan, J.M.; Chaturvedi, S.K.; Rahman, S.K.; Ishtikhar, M.; Qadeer, A.; Ahmad, E.; Khan, R.H. Protonation favors aggregation of lysozyme with SDS. *Soft Matt.* **2014**, *10*, 2591–2599. [CrossRef]
40. Jin, X.L.; Wei, X.; Qi, F.-M.; Yu, S.-S.; Zhou, B.; Bai, S. Characterization of hydroxycinnamic acid derivatives binding to bovine serum albumin. *Org. Biomol. Chem.* **2012**, *10*, 3424–3431. [CrossRef]
41. Skrt, M.; Benedik, E.; Podlipnik, C.; Poklar Ulrih, N. Interactions of different polyphenols with bovine serum albumin using fluorescence quenching and molecular docking. *Food Chem.* **2012**, *135*, 2418–2424. [CrossRef] [PubMed]
42. Andrade, M.A.; Chacón, P.; Merelo, J.J.; Morán, F. Evaluation of secondary structure of proteins from UV circular dichroism using an unsupervised learning neural network. *Prot. Eng.* **1993**, *6*, 383–390. [CrossRef] [PubMed]
43. Whitmore, L.; Wallace, B.A. Protein secondary structure analyses from circular dichroism spectroscopy: Methods and Reference Databases. *Biopolymers* **2008**, *89*, 392–400. [CrossRef]
44. Kelly, S.M.; Jess, T.J.; Price, N.C. How to study proteins by circular dichroism. *Biochim. Biophys. Acta* **2005**, *1751*, 119–139. [CrossRef]
45. Mao, D.; Wachter, E.; Wallace, B.A. Folding of the mitochondrial proton adenosine triphosphatase proteolipid channel in phospholipid vesicles. *Biochemistry* **1982**, *21*, 4960–4968. [CrossRef] [PubMed]
46. Whitmore, L.; Wallace, B.A. Methods of Analysis for Circular Dichroism Spectroscopy of Proteins and the DichroWeb Server. In *Advances in Biomedical Spectroscopy, Vol. 1, Modern Techniques for Circular Dichroism and Synchrotron Radiation Circular Dichroism Spectroscopy*; Wallace, B.A., Janes, R.W., Eds.; IOS Press: Amsterdam, The Netherlands, 2009; pp. 165–182.
47. Precupas, A.; Leonties, A.R.; Neacsu, A.; Angelescu, D.G.; Popa, V.T. Bovine hemoglobin thermal stability in the presence of naringenin: Calorimetric, spectroscopic and molecular modeling studies. *J. Mol. Liq.* **2022**, *361*, 119617. [CrossRef]
48. Bujacz, A. Structures of bovine, equine and leporine serum albumin. *Acta Crystallogr. Sect. D Biol. Crystallogr.* **2012**, *D68*, 1278–1289. [CrossRef]
49. RSCB Protein Data Bank. Available online: https://www.rcsb.org/pdb (accessed on 15 March 2023).
50. Frisch, M.J.; Trucks, G.W.; Schlegel, H.B.; Scuseria, G.E.; Robb, M.A.; Cheeseman, J.R.; Montgomery, J.A., Jr.; Vreven, T.; Kudin, K.N.; Burant, J.C.; et al. *Gaussian 03, Revision C.01*; Gaussian, Inc.: Wallingford, CT, USA, 2004.
51. Varlan, A.; Hillebrand, M. Exploring the capabilities of TDDFT calculations to explain the induced chirality upon a binding process: A simple case, 3-carboxycoumarin. *J. Mol. Struct.* **2013**, *1036*, 341–349. [CrossRef]
52. Trott, O.; Olson, A.J. AutoDock Vina: Improving the speed and accuracy of docking with a new scoring function, efficient optimization, and multithreading. *J. Comput. Chem.* **2010**, *31*, 45–461. [CrossRef]
53. Morris, G.M.; Huey, R.; Lindstrom, W.; Sanner, M.F.; Belew, R.K.; Goodsell, D.S.; Olson, A.J. AutoDock4 and AutoDockTools4: Automated docking with selective receptor flexibility. *J. Comput. Chem.* **2009**, *16*, 2785–2791. [CrossRef]
54. Dassault Systemes BIOVIA, Discovery Studio Modeling Environment, Release 2019, San Diego, Dassault Systemes. Available online: http://accelrys.com/products/discovery-studio (accessed on 20 March 2023).
55. Chong, X.; Sun, L.; Sun, Y.; Chang, L.; Chang, A.K.; Lu, X.; Zhou, X.; Liu, J.; Zhang, B.; Jones, G.W.; et al. Insights into the mechanism of how Morin suppresses amyloid fibrillation of hen egg white lysozyme. *Int. J. Biol. Macromol.* **2017**, *101*, 321–325. [CrossRef] [PubMed]

International Journal of
Molecular Sciences

MDPI

Article

The Potential of Plum Seed Residue: Unraveling the Effect of Processing on Phytochemical Composition and Bioactive Properties

Sandra Rodríguez-Blázquez [1,2], Laura Pedrera-Cajas [1], Esther Gómez-Mejía [1], David Vicente-Zurdo [1,3], Noelia Rosales-Conrado [1], María Eugenia León-González [1,*], Juan José Rodríguez-Bencomo [1] and Ruben Miranda [2]

[1] Department of Analytical Chemistry, Faculty of Chemistry, Complutense University of Madrid, Avda. Complutense s/n, 28040 Madrid, Spain; sandro08@ucm.es (S.R.-B.); laurpedr@ucm.es (L.P.-C.); egomez03@ucm.es (E.G.-M.); davidvic@ucm.es (D.V.-Z.); nrosales@ucm.es (N.R.-C.); juanjr10@ucm.es (J.J.R.-B.)
[2] Department of Chemical Engineering and Materials, Faculty of Chemistry, Complutense University of Madrid, Avda. Complutense s/n, 28040 Madrid, Spain; rmiranda@ucm.es
[3] Centre for Metabolomics and Bioanalysis (CEMBIO), Department of Chemistry and Biochemistry, Pharmacy Faculty, San Pablo-CEU University, Boadilla del Monte, 28660 Madrid, Spain
* Correspondence: leongon@ucm.es

Abstract: Bioactive compounds extracted from plum seeds were identified and quantified, aiming to establish how the brandy manufacturing process affects the properties and possible cascade valorization of seed residues. Extraction with *n*-hexane using Soxhlet has provided oils rich in unsaturated fatty acids (92.24–92.51%), mainly oleic acid (72–75.56%), which is characterized by its heart-healthy properties. The fat extracts also contain tocopherols with antioxidant and anti-inflammatory properties. All the ethanol–water extracts of the defatted seeds contain neochlorogenic acid (90–368 $\mu g \cdot g^{-1}$), chlorogenic acid (36.1–117 $\mu g \cdot g^{-1}$), and protocatechuate (31.8–100 $\mu g \cdot g^{-1}$) that have an impact on bioactive properties such as antimicrobial and antioxidant. Anti-amyloidogenic activity (25 $mg \cdot mL^{-1}$) was observed in the after both fermentation and distillation extract, which may be related to high levels of caffeic acid (64 $\pm$ 10 $\mu g \cdot g^{-1}$). The principal component analysis showed that all plum seed oils could have potential applications in the food industry as edible oils or in the cosmetic industry as an active ingredient in anti-aging and anti-stain cosmetics, among others. Furthermore, defatted seeds, after both fermentation and distillation, showed the greatest applicability in the food and nutraceutical industry as a food supplement or as an additive in the design of active packaging.

Keywords: bioactive compounds; *Prunus domestica* L. seed; cascade valorization; oils; brandy processing; oxidative stability; antioxidant activity; antimicrobial activity; anti-amyloidogenic activity; nutraceutical application

Citation: Rodríguez-Blázquez, S.; Pedrera-Cajas, L.; Gómez-Mejía, E.; Vicente-Zurdo, D.; Rosales-Conrado, N.; León-González, M.E.; Rodríguez-Bencomo, J.J.; Miranda, R. The Potential of Plum Seed Residue: Unraveling the Effect of Processing on Phytochemical Composition and Bioactive Properties. *Int. J. Mol. Sci.* **2024**, *25*, 1236. https://doi.org/10.3390/ijms25021236

Academic Editor: Arnaud Bianchi

Received: 20 December 2023
Revised: 12 January 2024
Accepted: 17 January 2024
Published: 19 January 2024

1. Introduction

Currently, there is a growing interest in the agri-food industries for the development of healthier and more nutritious foods, enhancing the emerge of so-called "bioactive compounds". They are known to be natural extra-food components with biological and functional activities, such as antioxidant, anti-inflammatory, anti-diabetic, anti-cancer, anti-viral, and anti-tumor activities, which protect the human body from high levels of free radicals and reactive oxygen species (ROS) related to cell damage [1]. Some of the main bioactive compounds that have aroused the interest of the scientific community are polyphenols, unsaturated fatty acids, and tocopherols, among others [2].

One of the richest sources of bioactive compounds that are poorly studied is *Prunus domestica* L. seed residues [3]. During the production of plum brandy, large quantities of intact plum stone residues are generated, and although they provide flavor and aromas in

the brandy, plum seeds are one of the main by-products that are discarded (15–30 wt.% of the entire stone). This practice, which is usually carried out with plum fruits that are out of specification and cannot be marketed, consists of crushing the plum fruit with a crusher whilst keeping the stone intact, and a subsequent fermentation process in fermentation tanks for 25–30 days to obtain plum brandy with a low alcohol content. Afterwards, it is subjected to a distillation process to separate the alcohol from the aromas and is left to age in stainless steel vessels for a year. Then, the alcohol content is lowered to 42° with water, thus obtaining the plum brandy that ready to be marketed [4]. Bibliographic data indicate that plum seeds undergo changes in their composition during processing to obtain brandy [5]. Therefore, understanding the impact of each stage of plum brandy processing on the remaining seeds, both in terms of the composition of bioactive compounds and their bioactivities, will allow for the designing of efficient valorization, focused on the utter exploitation of the resulting extracts.

According to the nutritional composition, the principal component of these seed by-products from plum brandy processing are oils, which are commonly recovered via Soxhlet extraction with *n*-hexane used as a solvent [6]. Particularly, plum seed oils stand out for their high content of unsaturated fatty acids (UFA), mainly oleic acid (C18:1n9c) (60–73%) and linoleic acid (C18:2n6c) (16–31%) [6–8]. These fatty acids positively contribute to the healthy lipid indexes of the oils (desirable fatty acid (DFA), hypocholesterolemic/hypercholesterolemic (H/H) ratio, atherogenicity (AI), and thrombogenicity (TI)). Moreover, these compounds have an important role in the prevention of cardiovascular diseases, decreasing the concentration of low-density lipoproteins (LDL) that are deposited in the blood vessels, reducing arrhythmia, mortality from coronary heart diseases, and the rate of atherosclerosis, as well as blood pressure [6,9]. Other bioactive components present in the oils are tocopherols, also known as Vitamin E precursors. The predominant tocopherol in plum seed oils is γ-tocopherol (15.5–16.2 $mg \cdot kg^{-1}$). Notwithstanding, the active form with the greatest functionality in the body is α-tocopherol (12.3–3.55 $mg \cdot kg^{-1}$) since it can reduce blood cholesterol levels, as well as coronary mortality or cardiovascular diseases. On the other hand, β-tocopherol (9.2–11.2 $mg \cdot kg^{-1}$) and δ-tocopherol (2.7–4 $mg \cdot kg^{-1}$) could display anti-inflammatory and antioxidant activities against oxidative stress [10]. Besides tocopherols, fatty acids are also crucial to increase the oxidative stability of oils, thus avoiding the formation of toxic degradation products that reduce their nutritional quality [11].

Nevertheless, after the oil extraction process, a second-generation biowaste is generated, namely defatted plum seeds, which may contain compounds with positive biological activities for the human organism such as phenolic compounds [12]. Among the phenolic compounds found in defatted plum seeds, the main ones were rutin (64–5670 $\mu g \cdot g^{-1}$), 2,3-dihydroxybenzoic acid (400–3780 $\mu g \cdot g^{-1}$), gallic acid (143–1890 $\mu g \cdot g^{-1}$), catechin and epicatechin (1070 and 9.5 $\mu g \cdot g^{-1}$, respectively), syringic acid (8.7–900 $\mu g \cdot g^{-1}$), chlorogenic acid (250–300 $\mu g \cdot g^{-1}$), and caffeic acid (3–300 $\mu g \cdot g^{-1}$) [13,14]. It has been reported that the presence of these phenolic compounds in defatted plum seed extracts exhibited high antioxidant and neuroprotective activities that inhibit β-amyloid (Aβ) aggregation as well as antimicrobial activities against the growth of pathogens (*Escherichia coli* and *Staphylococcus aureus* among others). This highlights the impetus for the use of these residues as natural functional and nutritional ingredients [3,15–17]. However, *Prunus* seeds, especially those that have been subjected to high temperatures, may present amygdalin, a cyanogenic glucoside recognized by the European Food Safety Authority (EFSA) as an anti-nutritional and toxic compound for the body [18]. Therefore, it is essential to determine the presence of this contaminant, which will also define the potential use of the extracts. And in those extracts that contain this contaminant, it is necessary to apply detoxification processes to ensure its reduction or even its elimination [19].

The high content of bioactive compounds in *P. domestica* L. seeds, with well-known benefits for human health, makes the search for new industrial applications feasible [3]. In contrast, the enrichment of antioxidants in plum seed oils makes them interesting for

their use in the food industry as promising substitutes for olive and grape oils. In recent years, plum kernels have gained attention as potential edible cooking oils due to their high oil content [20]. In addition, its outstanding oxidative stability, as well as its antioxidant activity, allows for new applications in the cosmetic industry as an active ingredient in the production of anti-aging, anti-stain, and other potential cosmetics [21]. Not to mention its remarkable heart-healthy indexes, which open new ways for application in the nutraceutical industry for the elaboration of functional foods [22]. On the other hand, phenolic extracts of defatted plum seeds could be of interest to the food and nutraceutical industries as additives in active packaging formulation that protects food from external oxidants, as well as in the pharmaceutical industry as an active ingredient in the elaboration of drugs against neurodegenerative diseases, diabetes, and other important diseases [23–26]. Hence, the antioxidant activity that polyphenols are associated with could justify their use in the cosmetic industry to formulate anti-aging, anti-stain, and sunscreen cosmetics, to name but a few [25,27].

In this line, the present work aims to develop a cascade valorization process of plum seed waste generated in the different stages of plum brandy manufacturing (before fermentation (PBF), after fermentation (PAF), and after both fermentation and distillation (PAFD)) for the obtention of bioactive compounds of special interest such as unsaturated fatty acids, tocopherols, and phenolic compounds. Likewise, the effect of processing on the profile and composition of those compounds in the obtained extracts was evaluated. For this purpose, conventional Soxhlet extraction was used to separate the oils from the defatted seed residues. The resulting oils were characterized in terms of fatty acid profile and their respective heart-healthy indexes, the composition of tocopherols, as well as the evaluation of their antioxidant activities, and the determination of their oxidative stability against lipid degradation. Following this, phenolic compounds were extracted from defatted plum seeds using a matrix solid-phase dispersion (MSPD) methodology, being thereafter characterized in terms of individual and total polyphenol content, antioxidant, anti-amyloidogenic, and antimicrobial activities to explore their potential application in nutraceutical, cosmetic and/or pharmaceutical industries.

2. Results and Discussion

2.1. Determination of Soxhlet Extraction Yields of Plum Seeds

The oil content of plum seeds (PBF, PAF, and PAFD) obtained during the different stages of plum brandy production was determined using the Soxhlet extraction procedure with *n*-hexane as a solvent [28]. There were considerable differences in the appearance of the oils related to the manufacturing step they proceeded from (Figure S1), with a yellowish tone observed in the PBF and PAF seed oils, contrasting with a dark orange in the PAFD seed oil along with a stronger and more intense aroma. Similarly, significant differences were observed in the weight percentages of plum seed oils and defatted plum seeds. These percentages by weight are shown in Table 1.

Table 1. Oils and defatted seeds percentages from plum seed waste.

Sample	Seed Oil (%, *w*)	Defatted Seed (%, *w*)
PBF	$(37.6 \pm 0.4)^{a}$	$(62 \pm 1)^{a}$
PAF	$(45.2 \pm 0.1)^{b}$	$(47 \pm 4)^{b}$
PAFD	$(68 \pm 1)^{c}$	$(30 \pm 2)^{c}$

Values are expressed as mean ± standard deviation (n = 3) in dry weight. Values followed by a different superscript in a column differ significantly (p-value < 0.05), according to one-way analysis of variance (ANOVA) and Fisher's Least significant difference (LSD) test. All data were expressed on a dry basis. Moisture content of initial seeds: plum before fermentation (PBF) (4.5 ± 0.7%), plum after fermentation (PAF) (2.6 ± 0.1%), and plum after both fermentation and distillation (PAFD) (1.9 ± 0.2%). Moisture content of defatted seeds: PBF (4.45 ± 0.07%), PAF (2.4 ± 0.1%), and PAFD (1.82 ± 0.06%).

According to the results in Table 1, significant differences (p-value < 0.05) were observed in the contents of each industrial step oil and defatted seed by-products. Regarding the oil content, PBF seed presented the lowest value, withal it was observed that the oil yield increased in the other samples (PAF and PAFD), indicating a direct correlation between the industrial procedure and the extraction itself. However, the opposite behavior was observed when it came to the percentages of defatted plum seeds, the by-products generated in the Soxhlet extraction process. Accordingly, the highest value was achieved in the PBF seed, decreasing during processing and reaching the lowest value in the PAFD kernel. This is attributed to the potential extraction of other hydrophilic components of the seeds during Soxhlet extraction, which enriches the content of defatted seeds. That being so, the lower content of defatted seed in PAFD may be related to its lower content of hydrophilic compounds, such as proteins, sugars, and even polyphenols [12].

Furthermore, these results are in line with data found in the literature. The fat content of plum seeds of the variety *P. domestica* L. extracted by Soxhlet using *n*-hexane as a solvent usually varies between 30 and 38.7%, *w* [6,12]. Concerning the effect of processing on oil content, Rodríguez-Blázquez et al. [12] demonstrated that defatted *P. avium* L. seed residues decreased their content during brandy processing, thereby increasing their oil content.

In this context, both the oil extracted from the seeds and the by-product of defatted seeds could present numerous bioactive compounds with excellent properties or activities, such as polyphenols, tocopherols, and unsaturated fatty acids, among others [6,12,27]. Hence, exploring their nutritional value and potential content has become an emerging requirement for the scientific community.

2.2. Evaluation of the Lipid Profile of Plum Seed Oils

2.2.1. Fatty Acid Composition

As previously reported, plum kernel oils are well known for their desirable lipid profile composed mostly of oleic and linoleic acid, with multiple benefits for human health [6,8,17].

In the present work, the fatty acid content of different oils obtained from three plum seed residues (PBF, PAF, and PAFD) was determined to study the effect of processing on the lipid content. The resulting lipid profiles of the plum seed oils are shown in Table 2.

Table 2. Fatty acid composition of plum seed oils.

Fatty Acids	PBF Oil (%)	PAF Oil (%)	PAFD Oil (%)
Palmitic acid (C16:0)	(5.60 ± 0.05) ^{a}	(5.52 ± 0.01) ^{a}	(5.15 ± 0.01) ^{b}
Palmitoleic acid (C16:1n7)	(0.765 ± 0.004) ^{a}	(0.586 ± 0.006) ^{b}	(0.59 ± 0.03) ^{b}
Margaric acid (C17:0)	(0.0439 ± 0.0008) ^{a}	(0.04 ± 0.01) ^{a}	(0.048 ± 0.002) ^{a}
Cis-10-heptadecenoic acid (C17:1n10c)	(0.082 ± 0.004) ^{a}	(0.092 ± 0.001) ^{b}	(0.0879 ± 0.0009) ^{b}
Stearic acid (C18:0)	(1.9 ± 0.1) ^{a,b}	(1.85 ± 0.06) ^{a}	(2.13 ± 0.04) ^{b}
Oleic acid (C18:1n9c)	(75.56 ± 0.04) ^{a}	(74 ± 1) ^{a,b}	(72 ± 1) ^{b}
Linoleic acid (C18:2n6c)	(15.83 ± 0.02) ^{a}	(18.1 ± 0.9) ^{a,b}	(20 ± 1) ^{b}
Arachidic acid (C20:0)	(0.176 ± 0.001) ^{a}	(0.174 ± 0.001) ^{a,b}	(0.157 ± 0.003) ^{b}
∑SFA	(7.76 ± 0.07) ^{a}	(7.58 ± 0.09) ^{b}	(7.49 ± 0.06) ^{b}
∑UFA	(92.24 ± 0.07) ^{a}	(92.42 ± 0.09) ^{b}	(92.51 ± 0.06) ^{b}
∑MUFA	(76.40 ± 0.05) ^{a}	(74 ± 1) ^{a,b}	(72 ± 1) ^{b}
∑PUFA	(15.83 ± 0.02) ^{a}	(18.0 ± 0.9) ^{a,b}	(20 ± 1) ^{b}
PUFA/SFA ratio	(2.04 ± 0.02) ^{a}	(2.38 ± 0.09) ^{a}	(2.7 ± 0.2) ^{b}

Results are represented in percentages with estimates of standard deviation (n = 2). Values on the same row with different letters denote significant differences (p-value < 0.05) among samples according to ANOVA and Fisher's LSD test. SFA: saturated fatty acids. UFA: unsaturated fatty acids. MUFA: monounsaturated fatty acids. PUFA: polyunsaturated fatty acids (unsaturation ≥ 2). PUFA/SFA: ratio between polyunsaturated and saturated fatty acids.

A total of eight fatty acids were identified in the PBF, PAF, and PAFD seed oil samples (Table 2). Plum seed oils, independent of which stage the seeds were collected from during the brandy manufacturing process, were found to be a good source of UFA, mainly

C18:1n9c and, to a lesser extent, C18:2n6c. In addition, considerable amounts of C16:0 and C18:0 were also identified. The remaining four fatty acids were found in small amounts in all samples. These results are comparable with those shown in the literature for plum seeds of the variety *P. domestica* L. Specifically, Rodríguez-Blázquez et al. [6] found that plum seed oil, which was extracted by Soxhlet using *n*-hexane, mainly contain C18:1n9c (72.7 ± 0.2%) and C18:2n6c (16.4 ± 0.2%) and, in smaller amounts, C16:0 (5.71 ± 0.03%) and C18:0 (2.86 ± 0.05%). Górnás et al. [29] extracted plum seed oils of the same variety with an ultrasound probe using *n*-hexane and reported a composition of C18:1n9c (60.2 ± 7.4%), C18:2n6c (31.8 ± 6.9%), C16:0 (5.2 ± 0.7%), and C18:0 (1.5 ± 0.4%). Finally, Vladić et al. [8] determined that the lipid profile of *P. domestica* L. seed oils, extracted via supercritical CO_2 and cold pressing, was also predominantly C18:1n9c (65–68%), C18:2n6c (22–25%), C16:0 (5.79–5.80%), and C18:0 (1.62–1.92%).

To study the effect of plum seed processing on the lipid content of the seed oil, a one-factor ANOVA statistical study and Fisher's LSD test were carried out (Table 2). PAFD seed oil showed significant differences (p-value < 0.05) in all fatty acids, except C17:0 and C18:0, in comparison with PBF seed oil. Moreover, it is noteworthy that C17:0 was the only one that did not present significant differences (p-value ≥ 0.05) within the process. In addition, several studies affirm that the lipid profile of oils, as well as their bioactive compounds, can be modified with the processing that seeds undergo [5,30]. On one hand, Rabrenović et al. [5] studied the effect of processing that plum seeds of the "Čačanska rodna" variety underwent in obtaining plum brandy and demonstrated that C16:0 content in the obtained cold-pressed oils suffered a significant modification after the distillation procedure in slivovitz brandy manufacturing. The same was observed with the content of SFA, UFA, and MUFA. However, the PUFA content does not differ significantly (p-value < 0.05) between the different processed seed residues. Curiously, they found that after distillation, trans-fatty acids begin to appear, such as elaidic acid (C18:1n9t) or linoelaidic acid (C18:2n6t), although in small amounts. It may be related to the isomerization process that C18:1n9c and C18:2n6c undergo with the temperature applied in the distillation process, although the presence of these trans fats heavily reduces the nutritional quality of the oils. On the other hand, Bjelica et al. [30] demonstrated that wine processing of grape seed residues was a significant factor to consider in the lipid content of grape seed residue oils. In this case, they did not observe the appearance of trans-fatty acids and confirmed that the content of C18:1n9c, C18:2n6c, MUFA, and PUFA was modified during the different processing stages.

The presence of high amounts of unsaturated fatty acids, mainly C18:1n9c and C18:2n6c, in all plum seed oils studied means that they can be considered healthy for humans [31]. C18:1n9c is the main MUFA found in the circulatory system and is well known for its many benefits to human health [32]. It is known to be the key energy molecule in the maintenance and development of cell membranes. One of its most characteristic effects is its antioxidant character, as it can regulate both the synthesis and the activities of antioxidant enzymes, even reducing oxidative stress, one of the main hypotheses of Alzheimer's disease [33]. Along with its ability to decrease the expression of proteins related to cholesterol transport, thus reducing cholesterol absorption and oxidation of LDL and preventing atherosclerosis. This fatty acid also has potential anti-cancer activities as it can inhibit the overexpression of oncogenes and their apoptotic effects [32–34]. Regarding C18:2n6c, a major constituent of the dietary PUFA ratio and omega-6 essential fatty acid, it has been highlighted in the scientific community for its many positive activities on human health. Data available in the literature suggest that circulating concentrations of C18:2n6c can reduce the risk of cardiovascular disease not only due to its cholesterol-lowering effect but also its beneficial effect on glucose metabolism. In addition to C18:1n9c, several studies suggest that it may have a beneficial effect on inflammatory parameters, causally correlated with the development of many degenerative diseases, and may also reduce the concentration of LDL, which cause dysrhythmia, coronary heart disease mortality, and blood pressure [35–37]. In addition, the presence of a higher MUFA content compared to PUFA in plum seed oils is potentially interesting as monounsaturated fatty acids are characterized

by increased stability of oils against lipid oxidation, as well as higher anti-inflammatory activities that help to reduce the risk of developing coronary heart disease [6]. In tandem with the high PUFA/SFA ratio of the plum seed oils, which allows for the reduction in cholesterol levels in the blood. Thus, the levels were higher than the recommendations of the UK Department of Health [38], which established the PUFA/SFA ratio in the human diet above 0.45 to present outstanding benefits for the prevention or treatment of cardiovascular diseases.

All things considered, the lipid profile of the plum seed residue oils suggests that these oils may have an interesting value-added potential that needs to be explored; therefore, the determination of healthy quality indexes is necessary to evaluate their possible bioactivities for human health.

2.2.2. Heart-Healthy Lipid Quality Indexes

The determination of heart-healthy indexes of oils is an important factor in ensuring their lipid quality [9]. Healthy lipid indexes determined for PBF, PAF, and PAFD seed oils are shown in Table 3.

Table 3. Heart-healthy lipid indexes of plum seed oils.

Lipid Indexes	PBF Oil	PAF Oil	PAFD Oil
Desirable fatty acid (DFA) (%)	(94.18 ± 0.05) [a]	(94.27 ± 0.03) [a]	(94.64 ± 0.01) [c]
Atherogenicity (AI)	(0.0607 ± 0.0005) [a]	(0.0597 ± 0.0002) [b]	(0.0557 ± 0.0002) [c]
Hypocholesterolemic/Hypercholesterolemic (H/H)	(16.3 ± 0.1) [a]	(16.62 ± 0.05) [b]	(17.8 ± 0.1) [c]
Oleic acid/linoleic acid ratio (O/L)	(4.772 ± 0.002) [a]	(4.1 ± 0.3) [a,b]	(3.6 ± 0.3) [b]

Values are represented as mean ± standard deviation (n = 2). Values with different letters in the same row denote significant differences (p-value < 0.05) among samples according to ANOVA and Fisher's LSD test.

According to the DFA index, the formation of two homogeneous groups (p-value < 0.05) was observed (one group was formed between PBF and PAF seed oils, and the other group was formed via PAFD seed oil). High values were found in all seed oils (Table 3), evidencing their high hypocholesterolemic properties, and their capacity to reduce blood cholesterol levels in humans. In addition, the H/H ratio is positively correlated with the DFA index and measures the bioactive properties of oils. The values of H/H obtained for plum seed oils were statistically different (p-value < 0.05), indicating that this oil quality parameter was modified via processing, and in all studied cases, they were characterized by high values, which confirms that the seed oils studied could reduce the risk of suffering from cardiovascular diseases and could even have bioactive properties such as anti-inflammatory, even managing to reduce the risk of suffering from diabetes [9,39]. Considering the values of the AI index, significant differences (p-value < 0.05) were observed in all oils. Furthermore, according to data found in the literature [9], the low levels obtained for this index in all oils could be suitable for the prevention of coronary heart disease. Thus, the lower this value, the healthier the food, indicating the promising potential of these plum seed oils. Finally, the oleic acid/linoleic acid (O/L) ratio was calculated, which is positively correlated with the oxidative stability of the oils [40]. Higher ratios of O/L are associated with a longer shelf life because C18:2n6c (which has two double bonds) is more susceptible to the degradation process than C18:1n9c (which only has one double bond). The oils from plum seed residues obtained in the different stages of plum brandy manufacturing presented high values of the ratio (O/L), and the PAFD seed oil presented statistically significant differences (p-value < 0.05) with the PBF seed oil. Therefore, the variation in the O/L ratio in PAFD seed oil may indicate that it is more exposed to oxidative degradation processes [41]. Overall, the lipid indexes and, therefore, the fatty acid content of the plum seed oils were modified during brandy processing. Although PAFD seed oil showed the most suitable heart-healthy indices, namely lower AI and higher DFA and H/H values, its lowest O/L ratio could favor oil degradation and hence the formation of toxic compounds that could drastically

reduce their nutritional quality. In this line, all the studied oils showed heart-healthy lipid indexes that may be of interest as an active ingredient in the food or nutraceutical industry for the prevention of cardiovascular diseases [42]. While PBF and PAF seed oils would be suggested as a potential use in the elaboration of cosmetics against anti-aging or atopic dermatitis, as they present high ratios of O/L, which increase their oxidative stability [40,41].

2.3. Determination of Tocopherols Content of Plum Seed Oils

Tocopherols are paramount bioactive constituents of vegetable oils. These compounds are known to be associated with a lower risk of coronary heart disease and cancer. In addition, these compounds prevent lipids and lipid-containing foods from oxidizing during storage, prolonging their stability and shelf life, which is essential when it comes to food production and marketing [43].

The content of tocopherols in plum seed oils before fermentation, after fermentation, and after both fermentation and distillation was determined using a high-performance liquid chromatographic coupled to a photodiode array detector (HPLC/PDA). While the target was the determination of all four vitamin E isoforms (α-, β-, γ-, and δ-tocopherol), this separation was not achieved. Based upon bibliographic research, a stationary phase such as pentafluorophenylsilica (PFPS) was supposedly selective between these slightly different analytes [44], albeit none of them were even retained. Further research landed upon using C18 columns, highlighting the fact that such a stationary phase would never allow the separation between β- and γ-tocopherol due to their similarities in their chemical structures [45]. Abidi et al. [46] suggested the possibility of increasing the separation by using 2-propanol as the organic modifier of the mobile phase, given its lower dissociating effect toward analytes. Nonetheless, the resolution between β- and γ-tocopherol peaks was not acceptable with the mobile phase propanol–water 70:30 (*v*/*v*), only allowing the detection of high β-tocopherol concentration (which was not expected in plum samples). This fact, together with the broadening of the other chromatographic peaks, which decreased the sensitivity of the method, led to the selection of only methanol as the optimal mobile phase.

Table 4 includes the main analytical characteristics of the chromatographic method developed for the determination of tocopherols. Accordingly, the method was proved to be linear ($R^2 > 0.9990$) in two concentration ranges for all three analytes, other than the β-tocopherol, given its coelution with γ-tocopherol. As far as reproducibility is concerned, it appears that the method developed meets the requirements, particularly for the reproduction of peak areas. The coefficient of variation is less than 5% in all cases. Regarding the retention factor, given the nature of liquid chromatography itself, it is also reproducible, although its coefficient of variation is higher than the former.

Table 4. Calibration curve for α-, γ-, and δ-tocopherol.

Compound	LOD/LOQ (mg·L^{-1})	Linear Range (mg·L^{-1})	Calibration Curve			CV (%) Intraday (n = 3)		CV (%) Interday (N = 9)	
			a	b (L·mg^{-1})	R^2	k	Area	k	Area
α	0.17 */0.5 **	0.5–20 *; 20–100 **	$(0 \pm 2)\cdot10^3$ *; $(0 \pm 5)\cdot10^4$ **	$(115 \pm 2)\cdot10^2$ *; $(132 \pm 7)\cdot10^2$ **	0.9990 *; 0.9942 **	1.39 *; 2.10 ** 0.56 *; 1.20 ** 1.75 *; 2.12 **	4.3 *; 2.3 ** 3.7 *; 2.4 ** 3.8 *; 2.5 **	6.4 *; 3.9 **	3.7 *; 2.6 **
γ	0.17 */0.5 **	0.5–20 *; 20–100 **	$(3 \pm 4)\cdot10^3$ *; $(0 \pm 5)\cdot10^4$ **	$(129 \pm 4)\cdot10^2$ *; $(146 \pm 7)\cdot10^2$ **	0.9975 *; 0.9957 **	1.30 *; 1.79 ** 0.58 *; 1.24 ** 2.42 *; 2.22 **	5.2 *; 2.0 ** 3.6 *; 3.2 ** 2.9 *; 2.7 **	6.9 *; 4.0 **	4.3 *; 2.9 **
δ	0.10 */0.3 **	0.3–20 *; 20–100 **	$(7 \pm 5)\cdot10^3$ *; $(0 \pm 1)\cdot10^4$ **	$(88 \pm 4)\cdot10^2$ *; $(117 \pm 2)\cdot10^2$ **	0.9923 *; 0.9996 **	1.02 *; 1.94 ** 0.50 *; 1.37 ** 2.93 *; 2.45 **	3.5 *; 1.9 ** 4.5 *; 3.1 ** 3.3 *; 2.2 **	6.7 *; 4.1 **	4.1 *; 2.6 **

* Analytical parameter for α-tocopherol: 10 mg·L^{-1}, γ-tocopherol: 5 mg·L^{-1}, and δ-tocopherol: 2 mg·L^{-1}. ** Analytical parameter for α-tocopherol: 100 mg·L^{-1}, γ-tocopherol: 50 mg·L^{-1}, and δ-tocopherol: 50 mg·L^{-1}. Limits of detection (LOD) and quantification (LOQ) calculated as 3.3 and 10 times the background noise signal, respectively. All measures were taken at a wavelength of 292 nm.

According to what other authors have stated, the main tocopherol source in plum oil is the γ- homolog [47,48], which, in this study, varied between 5.7 and 11.2 mg·kg^{-1}, whereas α- and δ-tocopherol ranged from 2.02 to 2.5 mg·kg^{-1} and 1.48 to 2.2 mg·kg^{-1}, respectively. These results are in accordance with those obtained by Popa et al. [47]; in addition, the values are only comparable to a certain extent, considering the scarce information available in the literature about composition changes provoked by processing. The multifactorial ANOVA test performed with the obtained values confirmed that there are significant differences (p-value <0.05) between all the analytes in every sample, especially for the γ- homolog, experiencing a great decrease during the fermentation and a noticeable increase after distillation. The α- and δ- homologs present an alike behavior, increasing the concentration during the fermentation process and then maintaining it in the distillation. As can be observed in Figure S2, after fermenting, the appearance of two new peaks within the 5 and 6 min mark is visible. Those two peaks are only present in PAF and PAFD, indicating that during the said procedure, a change is induced in the samples, in addition to the drastic variety in the γ-tocopherol concentration.

As far as the total tocopherol content goes (Figure 1), a decrease in tocopherol content with fermentation can be easily observed, and then, during the distillation process, it increases yet again. Hubert et al. [49] suggested that this may be attributed to the incubation temperature during the fermentation step or the presence of O_2 that oxidizes the substrate via Ultraviolet-Visible or heat exposure. Notwithstanding, Winkler-Moser et al. [50] claimed that the total tocopherol content was higher in the post-fermentation samples, despite it being lower in tocopherol content, due to a possible transformation of tocopherols into tocotrienols and vice versa. Not only do tocopherols participate in those antioxidant reactions, but also in "side reactions" that are not fully unraveled yet, in tandem with an interconversion [50]. Bruscatto et al. [51] stated that the accelerated degradation of α-tocopherol resulted in secondary reactions of the tocoferoxil radical with hydroperoxides of fatty acids, which were not oxidized, to form new radicals. However, it may have also reacted with hydroperoxides, forming peroxil radicals and increasing lipid oxidation reactions. The oxidative degradation tocopherols experience is greatly influenced by the oxidation of unsaturated fatty acids, which increases with lipid oxidation, high oxygen concentration and the presence of radicals. It is not possible to only correlate the variation in the concentration to the oxidation reactions, considering it does not explain the increase in γ-tocopherol. Although there is no information concerning how the procedure directly affects the seed, previously, it has been discussed how the presence of alcohol enhances the porosity of the seed, and therefore, it makes it easier for the tocopherols to migrate to the must, which would explain why the concentration of the γ-homolog experiences a great decrease. As the process continues throughout the distillation, the alcohol evaporation has a detrimental effect on the migration, in contrast with the preconcentrating effect for the tocopherols in the seed.

As previously reported, concerning the properties of each homolog, Hensley et al. [52] stated that higher levels of α-tocopherol may induce a decrease in γ, undesirably, due to the capacity of γ-tocopherol to prevent myocardial diseases as well as be less prone to cancer induction than the former. Aksoz et al. [10] indicated that α- and γ-tocopherol have antagonist effects, and a high γ/α concentration ratio implies a higher risk of obesity. In this study, as the β homolog is minoritarian in comparison to γ, it was overruled. Hence, the obtained ratios were (5.0 ± 0.2), (2.27 ± 0.02), and (4.5 ± 0.1) for PBF, PAF, and PAFD, respectively, which implies that the oil with the lower risk is the one obtained from seeds after fermentation, albeit α-tocopherol is observed to reduce the mortality of a heart stroke in contrast with what was observed with γ-tocopherol. Likewise, Seppanen et al. [53] contrasted in a thorough review what other authors have prior observed, landing upon the conclusion that the α-tocopherol is more susceptible to suffer oxidation because of donating its hydroxyl radical than the γ homolog. Therefore, this tocopherol is believed to have higher antioxidant activity, at the very least, at a proven concentration of 40 mg·L^{-1}, in contrast with the γ-tocopherol, which requires between 100 and 200 mg·L^{-1} to equate

its capacity. Jung et al. [53] demonstrated that at concentrations higher than 100, 250, and 500 mg·L^{-1} of α-, γ-, and δ-tocopherol, respectively, they acted as pro-oxidants during lipid oxidation, resulting in an increase in the levels of hydroxyperoxide and conjugated dienes. Furthermore, they hypothesized that the higher the concentrations of tocopherols in lipids, the greater the amounts of radical intermediates formed from the oxidation of tocopherols during storage.

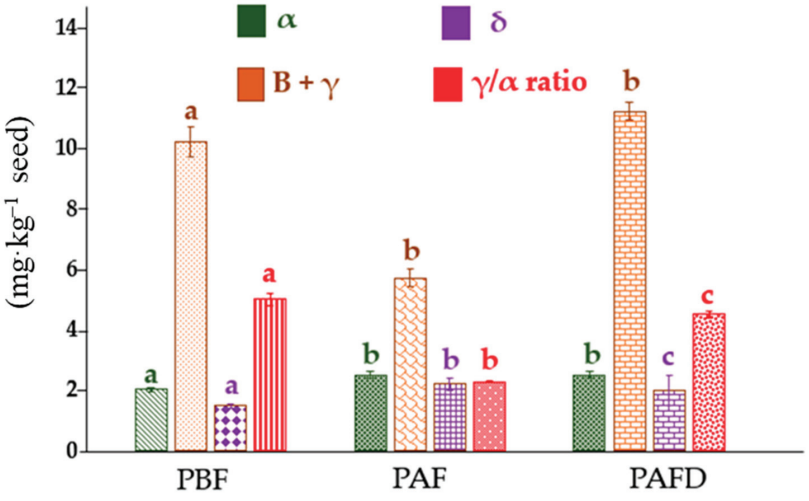

Figure 1. Tocopherol content in three plum seed oils. Values are expressed as mean ± standard deviation (n = 4). Different colors represent each tocopherol, in addition to a different pattern and a different letter denote significant differences in their content at a $p < 0.05$ value according to ANOVA and Fisher´s LSD test. PBF: plum before fermentation, PAF: plum after fermentation, and PAFD: plum after both fermentation and distillation. All data are expressed as mean ± standard deviation (n = 4) mg per kg of dry plum initial seed (moisture content of PBF (4.5 ± 0.7%), PAF (2.6 ± 0.1%), and PAFD (1.9 ± 0.2%).

2.4. Determination of Total Phenolic Content and Individual Polyphenols of Defatted Plum Seeds

The consumption of phenolic compounds has been shown to have positive health effects, such as preventing a variety of chronic degenerative diseases and delaying the aging process [14]. In this case, seeds obtained from plum kernels that do not meet market specifications were submitted to the correlation analysis between total phenolic content (TPC) and total flavonoid content (TFC) and the effect of plum brandy manufacturing. The TPC and TFC values from phenolic extracts are shown in Figure 2.

According to the TPC results represented in Figure 2, two homogeneous groups (p-value < 0.05) were observed. On one hand, PBF seed phenolic extract with PAF extract formed the first group, and on the other hand, PAFD phenolic extract. A statistically significant (p-value < 0.05) increase in TPC was observed in PAFD extract ((2.4 ± 0.5) mg GAE·g^{-1} defatted seed) contrasting with the phenolic extracts PBF ((0.63 ± 0.06) mg GAE·g^{-1} defatted seed) and PAF ((0.57 ± 0.08) mg GAE·g^{-1} defatted seed). Accordingly, Sheikh et al. [14] demonstrated that the TPC of *P. domestica* L. seeds subjected to various thermal processes ranged from 0.912 to 0.685 mg GAE·g^{-1}. Furthermore, Mehta et al. [16] determined that the TPC of dried *P. domestica* L. seeds were 1.05 mg GAE·g^{-1}. The highest TPC (p-value < 0.05) was observed in the defatted seed after fermentation and distillation, with respect to the other two defatted seeds, PBF and PAF. This increase may be attributed to the high temperatures to which the plum pits were subjected during the distillation process and could be the result of a simple phenolic compounds reaction, which could lead

to the formation of browning products favored at high temperatures and an increase in polyphenolic content when released [14].

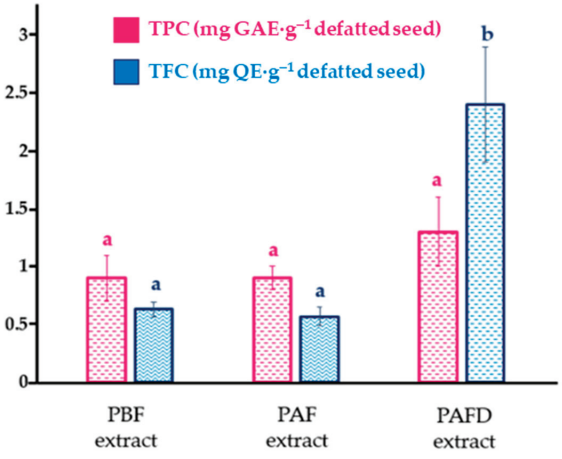

Figure 2. Total phenolic content (TPC) (mg GAE·g^{-1} defatted seed) and total flavonoid content (TFC) (mg QE·g^{-1} defatted seed) of plum seed extracts obtained under optimal MSPD extraction conditions. GAE: gallic acid equivalent; QE: quercetin equivalent. All data are expressed on a dry basis (moisture content of PBF defatted seed (4.45 ± 0.07%), PAF defatted seed (2.4 ± 0.1%), and PAFD defatted seed (1.82 ± 0.06%), as mean ± standard deviation (n = 3). Standard calibration curves of TPC: (y = (4.7 ± 0.5)·10^3x + (1.7 ± 0.7)·10^{-3}, R^2 = 0.9992) and of TFC: (y = (3.50 ± 0.0.08)·10^3x + (14 ± 2)·10^{-3}, R^2 = 0.9845). Mean values with different letters and with different patterns denote significant differences with *p*-value < 0.05, according to ANOVA and Fisher´s LSD test.

Considering the total flavonoid content, values between 0.9 and 1.3 mg QE·g^{-1} defatted seeds were obtained (Figure 2), which were slightly higher than those found in other studies performed on plum seeds of the European variety (<0.58 mg QE·g^{-1}) [16,54]. Likewise, no statistically significant differences (*p*-value < 0.05) were observed between the different plum samples; hence, plum brandy processing does not seem to affect the TFC content.

For the identification and quantification of individual phenolic compounds from three defatted plum seed samples, a non-targeted high-performance liquid chromatography coupled to a quadrupole time-of-flight mass spectrometer (HPLC-ESI-QTOF-MS) methodology was employed. Table S1 shows the retention time obtained for each polyphenol, its respective molecular formula, its molecular pseudo-peak, and its identified fragments. In all cases, a minimum of three fragments were obtained, which allowed for the unequivocal identification of each polyphenol present in the samples. The fragment used for quantification, which corresponded to the most intense fragment in all cases, is indicated in bold. A total of seventeen phenolic compounds were identified. Accordingly, ten phenolic acids, including five hydroxybenzoic acids, were identified as follows: gallic acid (peak 1, RT = 2.7 min), 2,3-dihydroxybenzoic acid (peak 2, RT = 4.9 min), vanillic acid (peak 7, RT = 9.2 min), syringic acid (peak 10, RT = 9.7 min), and protocatechuate (peak 4, RT = 5.0 min), as well as five hydroxycinnamic acids including the following: neochlorogenic acid (peak 3, RT = 4.9 min), chlorogenic acid (peak 6, RT = 7.8 min), caffeic acid (peak 9, RT = 9.6 min), *p*-coumaric acid (peak 11, RT = 11.8 min), and *trans*-ferulic acid (peak 12, RT = 15.2 min). Finally, seven low-molecular-weight flavonoids were identified, including two flavanols: catechin (peak 5, RT = 7.5 min) and its isomer, epicatechin (peak 8, RT = 9.8 min), a flavanone hesperidin (peak 15, RT = 18.4 min), and four flavanols: kaempferol (peak 17, RT = 32.6 min), kaempferol-3-rutinoside (peak 13, RT = 17.7 min), isorhamnetin-3-rutinoside (peak 14, RT = 17.9 min), and quercetin (peak 16, RT = 27.0 min).

The phenolic compounds identified in defatted plum seed extracts are in line with those reported in other studies. As such, Sheikh et al. [14] identified eleven phenolic compounds in plum seeds: gallic acid, chlorogenic acid, catechin, syringic acid, caffeic acid, *trans*-ferulic acid, 2,3-dihydroxy benzoic acid, quercetin, and three new phenolic compounds: rutin trihydrate, ellagic acid, and tannic acid. Savic et al. [13] found rutin, epigallocatechin, gallic acid, *trans*-ferulic acid, syringic acid, epicatechin, caffeic acid, and *p*-coumaric acid. Furthermore, a non-phenolic compound was detected in phenolic extracts from PBF and PAF seeds but not in PAFD. The peak occurred at 6.8 min, with a precursor [M-H] ion at m/z 456.151211 and MS/MS fragments at m/z 391.2956, 323.0798, 263.0537, 221.0551, 161.0341, and 119.0294, resulting in the molecular formula $C_{20}H_{27}NO_{11}$. According to the literature [55], the fragment at m/z 323 was produced because of the neutral loss of a disaccharide [M-H-133], which allowed for the unequivocal identification of this substance known as amygdalin. Amygdalin, a cyanogenic diglucoside compound (D-mandelonitrile-β-D-gentiobioside; syn: D-mandelonitrile-β-D-glucosido-6-β-glucoside), is responsible for the bitterness as well as the toxicity of seeds of the *Prunus* family, including plum seeds [56]. Amygdalin itself is not considered toxic, but its complete hydrolysis generates, in the presence of the enzyme *β*-glucosidases or α-hydroxynitrilolyases, hydrogen cyanide (HCN), a highly toxic and anti-nutritive compound, and glucose and benzaldehyde [18,56]. Several studies [14] reported that HCN undergoes a degradation process at high temperatures, and accordingly, it has not been found in the defatted plum seed after both fermentation and distillation due to the high temperatures applied during the distillation and subsequent defatting process. Nowadays, it is well known that amygdalin is supposed to be harmful to the human body when levels are exceeded in oral, intramuscular, or intravenous administration [18,56]. The permitted limits set by the European Commission (EU) Regulation (2017/123712) have been particularly a maximum HCN level of 5 $mg \cdot kg^{-1}$ in canned stoned fruits and 35.5 $mg \cdot kg^{-1}$ in alcoholic beverages [57]. In humans, the lethal dose of HCN is considered 50 mg, which is equivalent to 0.8 $mg \cdot kg^{-1}$ body weight. A blood cyanide level of 0.5 $mg \cdot L^{-1}$ is cited in the literature as the threshold for toxicity in humans. Makovi et al. [58] used a similar equipment (HPLC-QTOF-MS) and established the limit of detection (LOD) of amygdalin as 0.015 $mg \cdot mL^{-1}$; thus, as in PAFD seed was not detected, it means that it may contain amygdalin concentrations below that value. Despite the toxicity with which amygdalin is correlated, there is currently a scientific gap, given that several in vitro studies have proven that amygdalin could induce the apoptosis of cancer cells, as well as inhibit their proliferation, which could be potentially interesting in the treatment of neurodegenerative diseases and cancer [59,60]. Be that as it may, amygdalin has even been shown to have potential anti-inflammatory, antinociceptive, and neurotrophic effects [18,55,61,62]. Although its potential benefits are not known with absolute certainty, hence in vivo and clinical studies and safety measures are needed to assess its effects on human health. Nevertheless, it is important to point out that there are still no studies indicating its dermal toxicity levels, and it has been shown that it could have a valuable topical application; therefore, in this line, Gago et al. [63] have shown that an amygdalin analog could reduce the proliferative capacity of psoriasis-stimulated keratinocytes and their inflammatory response in vivo and in vitro. In view of the above, and considering the toxicity of HCN, it would be necessary, firstly, to quantify the former in the extracts obtained from the seed residues before fermentation and after fermentation to ultimately define their suitability as nutraceuticals or agri-food ingredients. Likewise, the application of methodologies to reduce amygdalin levels to minimum values, such as the detoxification processes [14], could be of interest for guaranteeing secure exploitation and applicability of those phenolic seed extracts.

The results corresponding to the phenolic quantification of the three defatted plum seeds evaluated (PBF, PAF, and PAFD) are shown in Table 5. Neochlorogenic acid, chlorogenic acid, protocatechuate, 2,3-dihydroxybenzoic acid, caffeic acid, and quercetin were the main polyphenols found in the three types of samples. Savic et al. [13] reported *trans*-ferulic acid (143 $\mu g \cdot g^{-1}$), *p*-coumaric acid (118 $\mu g \cdot g^{-1}$), rutin (64 $\mu g \cdot g^{-1}$), epigallocatechin

(19 μg·g^{-1}), epicatechin (9.5 μg·g^{-1}), syringic acid (8.7 μg·g^{-1}), gallic acid (6.4 μg·g^{-1}), and caffeic acid (3 μg·g^{-1}) as major phytochemicals in *P. domestica* L. seeds. Meanwhile, Sheikh et al. [14] found that rutin (5670 μg·g^{-1}), 2,3-dihyroxybenzoic acid (3780 μg·g^{-1}), gallic acid (1890 μg·g^{-1}), catechin (1070 μg·g^{-1}), syringic acid (900 μg·g^{-1}), caffeic acid (300 μg·g^{-1}), and chlorogenic acid (250 μg·g^{-1}) were the main polyphenols present in plum seeds. In relation to the latter study, the presence of lower quantities of phenolic compounds in the PBF, PAF, and PAFD seeds of this present study may be due to the plum brandy manufacturing process itself, as well as the subsequent defatting to which they have been subjected, which may favor the degradation or loss of labile phenolic compounds [4,64].

Table 5. Quantification of phenolic compounds by HPLC-ESI-QTOF-MS in defatted plum seed extracts.

Compound	PBF (μg·g^{-1})	PAF (μg·g^{-1})	PAFD (μg·g^{-1})
2,3-Dihydroxybenzoic acid ^{A}	27.3 ± 0.1 ^{a}	86 ± 4 ^{b}	35 ± 2 ^{c}
Neochlorogenic acid ^{B}	217 ± 1 ^{ab}	368 ± 98 ^{b}	90 ± 3 ^{a}
Chlorogenic acid ^{B}	36.1 ± 0.7 ^{a}	117 ± 22 ^{b}	51 ± 14 ^{a}
Vanillic acid ^{A}	*n.q.*	0.9 ± 0.1 ^{a}	*n.q.*
Caffeic acid ^{B}	3.6 ± 0.3 ^{a}	14 ± 2 ^{a}	64 ± 10 ^{b}
Syringic acid ^{A}	*n.q.*	*n.d.*	*n.q.*
p-Coumaric acid ^{C}	2.3 ± 0.9 ^{a}	2.301 ± 0.009 ^{a}	6.1 ± 0.3 ^{b}
trans-Ferulic acid ^{D}	18.5 ± 0.6 ^{a}	*n.d.*	3.4 ± 0.2 ^{b}
Kaempferol 3-rutinoside ^{E}	*n.q.*	*n.d.*	*n.q.*
Isorhamnetin 3-rutinoside ^{F}	1.86 ± 0.08 ^{a}	*n.q.*	*n.q.*
Quercetin ^{F}	15.1 ± 0.7 ^{a}	28 ± 2 ^{a}	15 ± 8 ^{a}
Kaempferol ^{E}	1.38 ± 0.02 ^{a}	0.9 ± 0.3 ^{a}	19 ± 12 ^{a}
Gallic acid ^{G}	8.9 ± 0.1 ^{a}	34 ± 2 ^{b}	*n.q.*
Hesperidin ^{H}	*n.d.*	*n.q.*	*n.q.*
Catechin ^{I}	*n.d.*	*n.d.*	*n.q.*
Epicatechin ^{J}	*n.d.*	*n.d.*	*n.q.*
Protocatechuate ^{A}	31.80 ± 0.08 ^{a}	100 ± 11 ^{b}	39 ± 7 ^{a}
Total phenolic acids	346 ± 1 ^{a}	722 ± 123 ^{b}	289 ± 12 ^{a}
Total flavonoids	18.4 ± 0.7 ^{a}	29 ± 2 ^{a}	34 ± 19 ^{a}
Total phenolics	364.2 ± 0.7 ^{a}	752 ± 121 ^{b}	324 ± 0.7 ^{a}

Upper-case letters indicate which calibration curve is applied. Standard calibration curves: A—2,3-dyhydroxibenzoic acid (y = (1.7 ± 0.1)·10^{7}x + (1.0 ± 0.1)·10^{6}, R^2 = 0.9962, LOD = 1.1 μg·L^{-1} and LOQ = 3.7 μg·L^{-1}); B—caffeic acid (y = (2.98 ± 0.07)·10^{7} x + (8.0 ± 0.7)·10^{5}, R^2 = 0.9990, LOD = 2.5 μg·L^{-1} and LOQ = 8.3 μg·L^{-1}); C—*p*-coumaric acid (y = (1.7 ± 0.1)·10^{7}x + (8.0 ± 0.7)·10^{5}, R^2 = 0.9964, LOD = 1.1 μg·L^{-1} and LOQ = 3.7 μg·L^{-1}); D—*trans*-ferulic acid (y = (5.4 ± 0.1)·10^{6}x + (1.0 ± 0.1)·10^{5}, R^2 = 0.9993, LOD = 1.7 μg·L^{-1} and LOQ = 5.7 μg·L^{-1}); E—kaempferol (y = (3.6 ± 0.1)·10^{7} x + (1.0 ± 0.1)·10^{6}, R^2 = 0.9962, LOD = 1.4 μg·L^{-1} and LOQ = 4.7 μg·L^{-1}); F—quercetin (y = (3.6 ± 0.1)·10^{7} x + (3 ± 1)·10^{6}, R^2 = 0.9965, LOD = 1.4 μg·L^{-1}, and LOQ = 4.7 μg·L^{-1}); G—gallic acid (y = (2.0 ± 0.1)·10^{7} x + (1.0 ± 0.1)·10^{6}, R^2 = 0.9962, LOD = 8.6 μg·L^{-1}, and LOQ = 28.7 μg·L^{-1}); H—hesperidin (y = (1.37 ± 0.02)·10^{7} x + (3 ± 1)·10^{5}, R^2 = 0.9997, LOD = 0.3 μg·L^{-1}, and LOQ = 0.1 μg·L^{-1}); I—catechin (y = (1.61 ± 0.01)·10^{7} x + (9 ± 1)·10^{4}, R^2 = 0.9998, LOD = 0.9 μg·L^{-1}, and LOQ = 3.0 μg·L^{-1}); J—epicatechin (y = (1.31 ± 0.02)·10^{7} x + (2 ± 1)·10^{5}, R^2 = 0.9996, LOD = 0.8 μg·L^{-1}, and LOQ = 2.7 μg·L^{-1}); *n.d.* = not detected; *n.q.* = not quantified. All data are expressed on a dry basis (moisture content of PBF defatted seed (4.45 ± 0.07%), PAF defatted seed (2.4 ± 0.1%), and PAFD defatted seed (1.82 ± 0.06%), as mean ± standard deviation (n = 3). Mean values with different lower-case letters denote significant differences with *p*-value < 0.05, according to ANOVA and Fisher´s LSD test.w

According to the functionalities, the main phenolic compounds determined in the seeds studied were neochlorogenic, chlorogenic, and protocatechuate acids, which are

known to be phenolic compounds with neuroprotective, antibacterial, anti-inflammatory, anti-cancer, anti-diabetic, and hypoallergenic activities [65–68]. 2,3-dihydroxybenzoic acid is attributed to present antibacterial properties against the growth of pathogens such as *Escherichia coli*, *Listeria motocytogenes*, or *Staphylococcus aureus* among others; thus, it is widely used against antibiotic resistance [69]. Caffeic acid, one of the main compounds coming only from the defatted PAFD seed, stands out not only for its effect against oxidative stress but also for its photoprotective effect against ultraviolet radiation, therefore reducing inflammation, genetic mutation, and immunosuppression in human skin cells [70]. In addition, it is key to preventing lipid oxidation and increasing the shelf life of food [71].

Regarding the effect of processing on the phenolic profile of defatted plum seed extracts, three different trends in the variation in phenolic composition with seed processing were observed (Table 5). Firstly, 2,3-dihydroxybenzoic acid, neochlorogenic acid, chlorogenic acid, gallic acid, vanillic acid, protocatechuate, and quercetin showed an increase in their content after the fermentation process (PAF phenolic extract). This could be explained by the fact that during the fermentation process, the appearance of alcohol could increase the porosity of the seeds, allowing the release of these phenolic compounds that, previously to the process, could be found bound to sugars or other biomolecules [72,73]. Other than quercetin, the increase in the content of these phenolic compounds in PAF phenolic extract was statistically significant (p-value < 0.05) compared to PBF extract. In addition, once the seeds were subjected to a subsequent distillation process (PAFD), a significant decrease (p-value < 0.05) in all the above was observed except for quercetin. According to the literature [74], the high temperatures used in the distillation process favor the degradation of phenolic compounds. Further to this, caffeic acid and *p*-coumaric acid showed a separate behavior, in which their content increased, although not in a statistically significant (p-value $\geq$ 0.05) way after the fermentation process. Nevertheless, after the subsequent distillation process, a statistically significant increase (p-value < 0.05) was observed in both cases. As indicated by Bjelica et al. [30], after the distillation process, the porosity of the seeds also increases even more, which could favor the separation of both compounds from the oil and enrichment therefore in the defatted seeds, along with an increase in the content of caffeic acid in PAFD phenolic extract, which could be explained by the fact that high temperatures favor the oxidative degradation process of vanillic acid into caffeic acid [75]. Hence, the content of vanillic acid decreases simultaneously as the content of caffeic acid increases in PAFD extract [72]. Regarding *trans*-ferulic acid and kaempferol, a different trend from those mentioned above was observed. PAF defatted seed extract presents a decrease in the content of both with respect to the initial seed extract (PBF). As indicated by Jericó-Santos et al. [72], this could be explained due to the fact that during the alcoholic fermentation process, a membrane diffusion mechanism of phenolic compounds from the plum seed to the plum must generates a concentration gradient observed by the loss of phenolic compounds in the plum seed and, at the same time, an increase in the content of phenolic compounds in the plum must. Therefore, the decrease in the content of these flavonoids in defatted plum seeds during the brandy production process could be attributed to the migration of phenolic compounds from the seed toward the pulp or other by-products, enriching the brandy obtained in phenolic compounds. Subsequently, after having undergone a later distillation process, a statistically significant (p-value < 0.05) increase was observed in both cases and could be correlated with the fact that these phenolic compounds probably were attached to previously glycosylated units and after being subjected to high temperatures they were released, thus heavily increasing their content.

Regarding the total phenolic acids (Table 5), a significant increase (p-value < 0.05) was observed in PAF phenolic extract with respect to the initial PBF. After the distillation process, PAFD extract significantly decreased (p-value < 0.05) its concentration with respect to PAF phenolic extract. In accordance with other studies that claimed alcohol capacity to increase the porosity of the seed in the fermentation process, which favors the release of phenolic compounds that could be bound to glycosylated units, and after the distillation, the degradation of phenolic compounds is favored [72,74]. This behavior differs from that

observed in the Folin–Ciocalteu spectrophotometric method to determine total polyphenol content. In the latter (Figure 2), it was observed that after both fermentation and distillation processes, the total polyphenol content increased, albeit, considering the low selectivity of the Folin–Ciocalteu reagent, it is likely that it is also reacting with the sugars released in the fermentation process and, therefore, interfering with the measurement [76]. In addition, Folin–Ciocalteu reagent can also react with other interferences, such as aromatic amino acids, proteins, or dehydroascorbic acid, which can affect the precision of the assay. Thus, high temperatures could also favor the formation and condensation of polymeric structures, such as sugars, which can react with the Folin–Ciocalteu reagent [77]. With respect to the total flavonoid content (Table 5), no significant differences (p-value ≥ 0.05) were observed between the three processes, although an increase is noteworthy, which correlates with that observed with the TFC aluminum complexation colorimetry method.

Overall, it is not only important to determine the phenolic composition of defatted plum seeds, but it is also necessary to evaluate their antioxidant activities to investigate their quality and their possible industrial applications.

2.5. Evaluation of Bioactive Properties of Plum Seed Oils and Defatted Plum Seeds

2.5.1. Antioxidant Activity

- Plum seed oils

The determination of the antioxidant capacity of oils is a crucial quality factor as it depends on the composition of bioactive compounds such as unsaturated fatty acids, tocopherols, and others [30]. One of the most popular methods for testing the antioxidant activity of oils is the 2,2-diphenil-1-picrylhydrazil (DPPH) radical scavenging assay [31]. Therefore, this method was used to determine the antioxidant capacity of plum seed oils (PBF, PAF, and PAFD). The antioxidant activity expressed as the concentration of oil required to scavenge 50% of DPPH free radical was represented in Table 6. Trolox was used as standard and its IC_{50} was $((2.5 \pm 0.1) \times 10^{-3}$ mg·mL$^{-1})$. The IC_{50} values of the three oils studied ranged from 20 to 36 mg·mL^{-1}. In addition, two statistically homogeneous groups were observed where PAFD seed oil showed significant differences (p-value < 0.05) with PBF and PAF oils. The increase in the IC_{50} value and, thus, the decrease in the antioxidant capacity of plum seed oil that has undergone fermentation and subsequent distillation may be due to the high temperatures used in the distillation process, which favor the degradation of bioactive compounds with potential antioxidant capacity [74]. Furthermore, these results could be attributed to the significant decrease in C16:0 content in PAFD seed oil (Table 2), which has been described as a potent antioxidant [78]. Regarding tocopherol content, the only significant difference observed in PAFD oil, with respect to the others, was the increase in β- + γ-tocopherol, given a higher content of the ratio of these tocopherols against the α homolog, which is known to be the active form with high antioxidant properties, could considerably reduce its antioxidant activity.

Table 6. Antioxidant activity determined after 24 h storage of plum seed oils.

Plum Seed Oils	DPPH IC_{50} (mg·mL^{-1} of Oil)
PBF	$(20 \pm 3)^{a}$
PAF	$(21 \pm 1)^{a}$
PAFD	$(36 \pm 2)^{b}$

Values are expressed as mean ± standard deviation (n = 2). Values with different letters denote significant differences (p-value < 0.05) among samples according to ANOVA and Fisher's LSD test. IC_{50} values represent the concentration of oil required to scavenge 50% of DPPH free radical.

Notwithstanding, another quality parameter for oils is their stability against lipid oxidation. Hence, the oxidative stability of plum seed oils was measured over a period of 1–22 days using the DPPH free-radical scavenging method. The results obtained are represented in Figure 3. The trend adopted by the IC_{50} data in the studied plum seed oils

(PBF, PAF, and PAFD) was non-linear and fitted adequately to a logarithmic model (with correlation coefficients (R^2) between 0.8205 and 0.9727). As a result, a logarithmic model of the first-order degradation kinetic reaction was used to follow the change in antioxidant capacity during storage time. A constant trend was observed in the kinetic curves of PBF and PAF seed oils, which indicated their high stability against lipid oxidation.

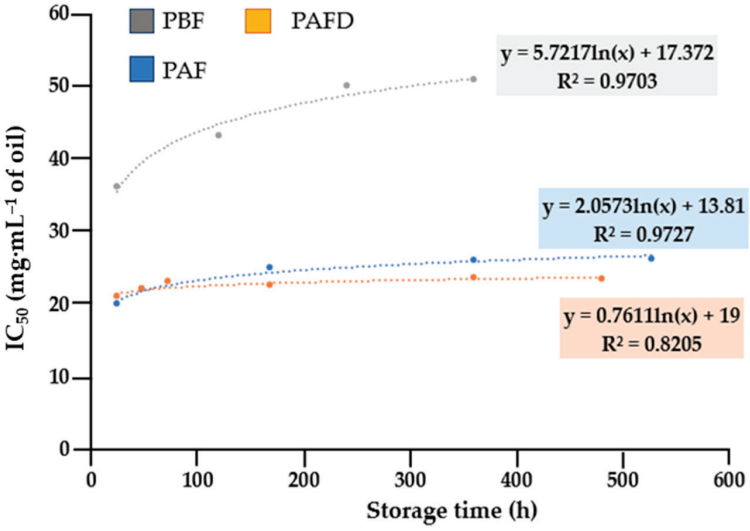

Figure 3. Kinetic curves of logarithmic model of IC_{50} values versus storage time of PBF, PAF and PAFD oils. IC_{50} values represents the concentration of oil required to scavenge 50% of DPPH free radical.

However, a different trend was observed in PAFD seed oil, where a progressive increase in IC_{50} could be observed with storage time, which showed that this oil was more susceptible to lipid oxidation.

On the other hand, the half-life time ($t_{1/2}$) was calculated for each oil following the procedure indicated by Rodríguez-Blázquez et al. [6]. The parameters corresponding to the linear fit (intercept, slope, and correlation coefficient (R^2)) are represented in Table 7.

Table 7. Kinetics parameters corresponding to the linear fit (intercept, slope, and correlation coefficient (R^2)) of $ln_{c.antioxidants}$ versus storage time of plum kernel oils.

Plum Seed Oils	Intercept ($mg \cdot mL^{-1}$)	Slope (h^{-1})	$t_{1/2}$ (h)	R^2
PBF	$(-4.2 \pm 0.1) \times 10^{-3}$	(4.05 ± 0.04)	1732 (72 days)	0.78
PAF	$(-2.0 \pm 0.5) \times 10^{-4}$	(4.03 ± 0.01)	3465 (144 days)	0.64
PAFD	$(-9 \pm 3) \times 10^{-3}$	(3.7 ± 0.2)	81 (3 days)	0.86

A linear trend in the data was observed in all plum seed (PBF, PAF, and PAFD) oils. The slope refers to the first-order constant (k) and the intercept to the logarithm of the initial concentration of antioxidant compounds (ln_{C0}).

According to the results indicated in Table 7, it was observed that all plum seed oils conformed to first-order kinetics with a high correlation factor (R^2) ranging from 0.64 to 0.86. The half-life time ($t_{1/2}$) in which the oils are considered stable was different for each of them. The longest shelf life was observed for PAF seed oil. PBF seed oil presented a high half-life of 1732 h (72 days); however, a drastic decrease in this parameter was observed in PAFD seed oil. Hence, the results obtained may indicate that the oil composition significantly affects their antioxidant activity and, thus, the oxidative stability [41]. A crucial factor in the oxidative stability of oils is the O/L ratio [79]. That being so, PAFD seed oil had the

lowest proportion of oleic acid with respect to linoleic acid (3.6 ± 0.3), which could explain its lower stability against lipid oxidation since linoleic acid (which has two double bonds) is more susceptible to degradation than oleic acid (which only has one double bond). In addition to the fatty acid content of the oils, other bioactive compounds that influence oxidative stability are tocopherols. According to the tocopherol content shown in Figure 1, PAFD seed oil differed from the others in the significant increase in the content of β- + γ-tocopherol, so a greater proportion of these tocopherols compared to the α homolog could result in a detrimental effect on oxidative stability [80].

According to the results obtained, it seems that the fatty acid content was the main variability factor in the oxidative stability of the oils, yet it is necessary to further study the possible correlations of tocopherols and fatty acids in the lipid fraction to fully prove it. Overall, PBF and PAF oils, due to their high stability against lipid degradation and their relevant antioxidant activity, could present potential applications in the cosmetic industry as an active ingredient in the production of anti-aging or other potential cosmetics [81]. However, in the case of PAFD oil, because of the low oxidative stability compared to PBF and PAF oils, the implementation of natural stabilizing agents is required to increase their stability [82].

- Defatted seed phenolic extracts:

Concerning PBF, PAF, and PAFD phenolic extracts, the antioxidant capacity was measured using two different methods: the DPPH -assay and the in vitro thiobarbituric acid reactive substances (TBARS) tissue-based assay, using the porcine brain as a biological substrate to evaluate the inhibition of lipid peroxidation. This assay was developed to estimate the oxidative damage caused to lipid membranes by oxidizing agents via the degradation product, malondialdehyde (MDA), which reacts with thiobarbituric acid (TBA) to form MDA-TBA_2 adducts [77]. The results obtained for the antioxidant activity of defatted plum seeds are shown in Table 8.

Table 8. Antioxidant capacity (DPPH free-radical scavenging assay and TBARS assay) of defatted plum seed phenolic extracts.

Defatted Seed Phenolic Extracts	DPPH IC_{50} ($mg \cdot g^{-1}$)	TBARS IC_{50} ($mg \cdot g^{-1}$)
PBF	$(1.0 \pm 0.2)^{a}$	$(2.1 \pm 0.1)^{b}$
PAF	$(0.9 \pm 0.2)^{a}$	$(5.0 \pm 0.6)^{b}$
PAFD	$(1.9 \pm 0.1)^{b}$	$(1.3 \pm 0.1)^{a}$

Values are represented as mean ± standard deviation (n = 3) on a dry basis (moisture content of PBF defatted seed (4.45 ± 0.07%), PAF defatted seed (2.4 ± 0.1%), and PAFD defatted seed (1.82 ± 0.06%). Values with different letters denote significant differences (p-value < 0.05) among samples according to ANOVA and Fisher's LSD test. IC_{50} values represent the concentration of defatted phenolic extracts sample required to scavenge 50% of DPPH free radical.

All the defatted seed phenolic extracts studied (Table 8) presented adequate antioxidant activity (DPPH IC_{50} of 0.9–1.9 $mg \cdot g^{-1}$ and TBARS IC_{50} of 1.3–5.0 $mg \cdot g^{-1}$). The positive control, Trolox, presented a value of IC_{50} = 2.5 ± 0.1 $mg \cdot mL^{-1}$ for the DPPH antioxidant activity assay and a value of IC_{50} = 11.6 ± 0.2 $mg \cdot mL^{-1}$ for the TBARS assay. In addition, the Trolox positive control showed a low coefficient of variation for DPPH (4%) and TBARS assays (2%), showing a high reproducibility in the applied methods. In the DPPH and TBARS assays, two statistically homogeneous groups (p-value < 0.05) were obtained. In the DPPH trial, PBF and PAF phenolic extracts showed significant differences (p-value < 0.05) with PAFD phenolic extracts, while in the TBARS assay, PAF phenolic extract showed statistically significant differences (p-value < 0.05) with respect to the other two phenolic extracts. Considering both assays, two different trends were observed. In the case of the DPPH free-radical scavenging assay, the antioxidant capacity in PAF extract increased, which resulted in a lower IC_{50} value, contrary to what was obtained after the consecutive distillation process (PAFD), where the antioxidant capacity decreased with respect

to PBF phenolic extract. Furthermore, according to the results shown in Table 5, this radical antioxidant capacity may be influenced by variations in the content of 2,3-dihydroxybenzoic acid, neochlorogenic acid, chlorogenic acid, gallic acid, vanillic acid, protocatechuic acid and quercetin in the defatted seed extracts under study. The TBARS anti-lipid peroxidation assay showed that after fermentation, the antioxidant capacity decreased, contrasting with an increment that occurred after distillation, compared to the PBF extract. Considering the phenolic content results shown in Table 5, TBARS antioxidant activity could be influenced by the variations in the phenolic content: caffeic acid, *p*-coumaric acid, and kaempferol.

In accordance with the antioxidant results presented in Table 8, all plum seed phenolic extracts presented outstanding lipid peroxidation inhibition activity, being useful as active ingredients in the development of active packaging to protect foods from external oxidizing agents and, thus, prolonging their shelf life [25]. In addition, all phenolic extracts showed high DPPH antiradical activity, which may be useful in the cosmetic industry as active ingredients in the development of anti-aging cosmetics, anti-stain, or even sunscreens [27]. Yet, the presence of amygdalin in PBF and PAF defatted seeds limits their application, requiring an amygdalin detoxification process to reduce its levels and, subsequently, security trials to ensure their applicability in the industrial sectors [18].

2.5.2. Neuroprotective Activity

Another bioactivity to consider is the neuroprotective one. Several studies [83,84] demonstrated that polyphenols can interact with Aβ peptides and form the polyphenol-protein Aβ interaction that blocks the self-association of $A\beta_{42}$ monomers to produce low-molecular-weight oligomers. $A\beta_{42}$ plaques are known as the main neuropathology of Alzheimer´s disease, being the keystone of the "amyloid cascade hypothesis".

Therefore, neuroprotection offered by defatted plum seed phenolic extracts after both fermentation and distillation was evaluated as the ability to inhibit $A\beta_{42}$ induced aggregation. This specific extract was chosen because it was the only one in which the presence of amygdalin had not been detected. Under normal conditions, in the absence of this neurodegenerative disease, $A\beta_{42}$ protein fibrils remained disaggregated, as shown in Figure 4a. However, in metal-induced Alzheimer´s disease, $A\beta_{42}$ fibrils formed aggregates often called amyloid plaques. This increase in amyloid aggregation can be observed in Figure 4b, where co-incubation with Fe(II) induced fibrils to form a dense tangle. Curcumin, used as a negative control due to its well-known anti-amyloidogenic properties, inhibited amyloid aggregation induced by Fe(II) (Figure 4c). Likewise, to evaluate the neuroprotective effect of PAFD phenolic extract, two different concentrations were tested (25 and 50 $mg{\cdot}L^{-1}$). In the absence of metal, no increase in amyloid aggregation was observed, making PAFD seed extract non-neurotoxic under these conditions (as shown for 25 $mg{\cdot}L^{-1}$ in Figure 4d). However, the highest concentration (50 $mg{\cdot}L^{-1}$) was not able to totally inhibit metal-induced aggregation (Figure 4f), although a slight improvement was observed in comparison to Fe(II)-induced aggregation. On the other hand, the lowest plum extract concentration (25 $mg{\cdot}L^{-1}$) could totally inhibit $A\beta_{42}$ aggregation (Figure 4e), providing a similar pattern to the obtained with curcumin, therefore being the most effective concentration for the treatment of this condition. The optimum concentration of phenolic extract that allowed maximum inhibition of metal-induced and $A\beta_{42}$ aggregation was comparable to that obtained by Gómez-Mejía et al. [85] for grape (*Vitis vinifera* L.) seed extracts, where they observed a similar effect at concentrations of 15 and 29 $mg{\cdot}L^{-1}$ phenolic extract.

Regarding fibril morphology, in normal conditions, the average width was (9 ± 2) nm, which slightly reduced in the presence of plum extract to (6.5 ± 0.6) nm (for 25 $mg{\cdot}L^{-1}$) and (6 ± 1) nm (for 50 $mg{\cdot}L^{-1}$). However, an increase up to (13 ± 2) nm was measured in the presence of Fe(II), which could be reduced to (6 ± 1) nm via co-incubation with curcumin. Similar measures were observed in the case of Fe(II) with plum extract at 25 $mg{\cdot}L^{-1}$ ((6.1 ± 0.6) nm), while the negative effect of 50 $mg{\cdot}L^{-1}$ extract was also confirmed under this parameter, achieving widths of (11 ± 2) nm, statistically similar to Fe(II) ones.

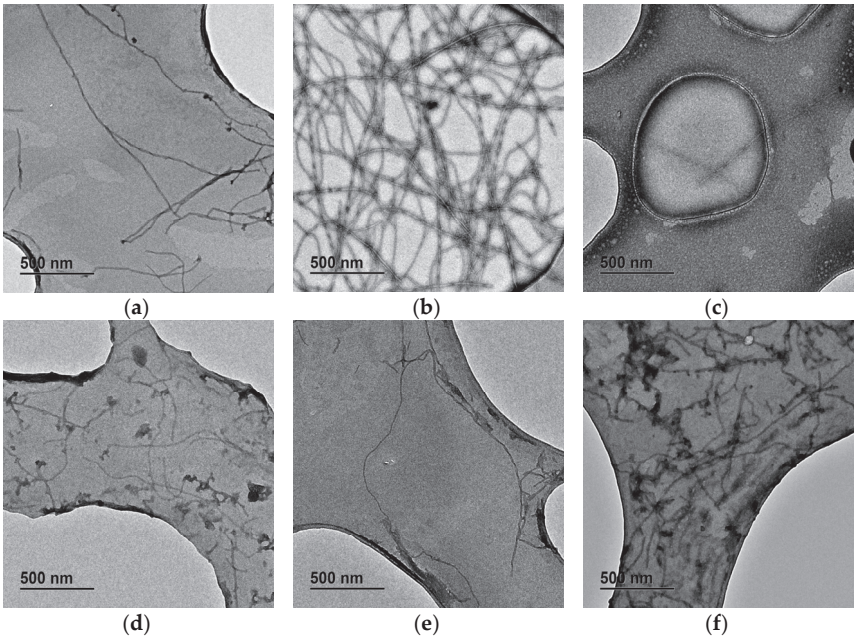

Figure 4. Transmission electron microscopy micrographs of $A\beta_{42}$ fibers under the effect of plum extract at different concentrations. (**a**) $A\beta_{42}$ alone, (**b**) $A\beta_{42}$ + Fe(II), (**c**) $A\beta_{42}$ + Fe(II) + curcumin, (**d**) $A\beta_{42}$ + 25 mg·L^{-1} of extract, (**e**) $A\beta_{42}$ + Fe(II) + 25 mg·L^{-1} of extract, (**f**) $A\beta_{42}$ + Fe(II) + 50 mg·L^{-1} of extract. Concentration of: $A\beta_{42}$= 50 μM; Fe(II)= 50 μM; Curcumin = 50 μM.

As a whole, it can be clearly stated that PAFD phenolic extract inhibited $A\beta_{42}$ protein aggregation and minimized the fibrils width, including that induced by metals, which is highly enhanced, highlighting its potential as a nutraceutical ingredient with neuroprotective properties [85].

2.5.3. Antimicrobial Activity

Antimicrobial activity is considered another interesting bioactive property of phenolic compounds in the development of food packaging applications or agri-food ingredients [25]. The results of the antimicrobial activity against two ubiquitous foodborne pathogens are presented in Table 9. As such, the lowest minimal inhibitory concentration values against *Escherichia coli* Gram-negative bacteria were observed for PAF and PAFD phenolic extracts (minimal inhibitory concentrations (MIC) = 20 mg·mL^{-1}). However, PBF phenolic extract required concentrations above 20 mg·mL^{-1} to inhibit bacterial growth. With respect to the positive control streptomycin, the MIC against *E. coli* was obtained for a concentration of 20 mg·mL^{-1}, which showed the appropriate antimicrobial activity of the extracts. Regarding the *Staphylococcus aureus* Gram-positive bacteria, only PAFD phenolic extract displayed antimicrobial potential, with a MIC value of 20 mg·mL^{-1}. A more effective concentration was achieved with streptomycin standard (2.5 mg·mL^{-1}), which showed its effectiveness in inhibiting bacterial growth. The differences in the antimicrobial activities of each of the phenolic extracts may be correlated with the difference in phenolic composition, hence the necessity to study their correlations via more advanced studies. In addition, the antimicrobial activities obtained for plum seed phenolic extracts agree with those reported by Alam et al. [15]. Thus, according to the antimicrobial results of the defatted plum seed extracts shown in Table 9, PAFD phenolic extract could be applicable as an added ingredient in the design of active packaging to prevent the growth of *Staphylococcus aureus* in food [25]. Similarly, PAF and PAFD phenolic extracts could have the same applicability

in inhibiting the proliferation of *Escherichia coli* bacteria in food. Once again, in the case of PAF phenolic extract, it is crucial to apply detoxification methods as well as carry out safety tests to ensure its unhazardousness.

Table 9. Antimicrobial activity of plum seed phenolic extracts.

Phenolic Extracts	Gram-Negative Bacteria *Escherichia coli* MIC (mg·mL^{-1})	Gram-Positive Bacteria *Staphylococcus aureus* MIC (mg·mL^{-1})
PBF	>20	>20
PAF	20	>20
PAFD	20	20
Streptomycin antibiotic-positive standard	20	2.5

Values are represented as mean ± standard deviation (n = 3). MIC means minimal inhibitory concentration.

2.6. Multivariate Statistical Analysis

With the aim to correlate the composition of plum seed oils and defatted seed phenolic extracts with their bioactive activities, a multivariate statistical analysis by principal component analysis (PCA) was carried out.

For plum seed oils, correlations between total fat content, fatty acid, and tocopherol content with DPPH free-radical scavenging activity and oil oxidative stability were studied. In addition, the processing effect upon the plum seeds was investigated. The resulting PCA has allowed the reduction in fourteen studied experimental factors to two principal components (PC) that explained 100% of the total data variability (Figure 5). PBF seed oil was characterized by the highest C16:1n7 content, while PAFD oil was characterized by the highest C18:0 content. PAF oil was depicted by the maximum C17:1n7c content and the greatest stability against lipid oxidation. With respect to the oil antioxidant activity, a positive correlation was observed between DPPH antioxidant capacity (low level of IC_{50}) and C16:0, as well as C20:0 content, and to a lesser extent, with C18:1n9c content. This correlates with what was observed by Rodríguez-Blázquez et al. [6] for *Prunus* seed oils. A high negative correlation was established between the oxidative stability and C18:0 content, in tandem with a negative correlation between β- + γ-tocopherol content and oxidative stability. All this indicated that PAFD oil had the lowest oxidative stability due to a higher content of β- + γ-tocopherol and C18:0.

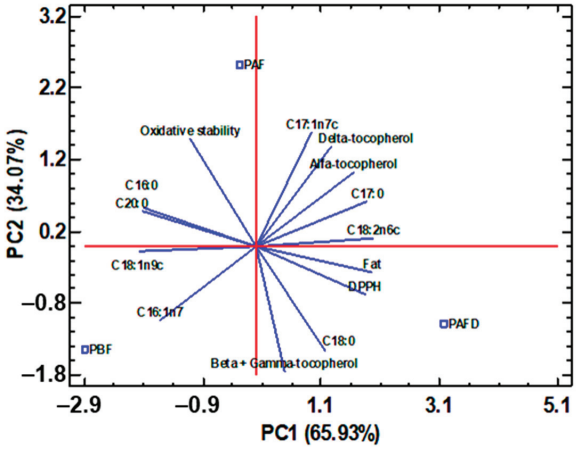

Figure 5. Two-dimensional principal component analysis plot of scores (PBF, PAF, and PAFD seed oils) and loadings (fat content, fatty acid content, tocopherol composition, antioxidant activity (IC_{50} value), and oxidative stability of plum seed oils).

Considering everything mentioned above, the PAF seed oil with the highest content of C17:1n7c could have potential applicability as an active ingredient in the preparation of drugs against cardiovascular diseases since this MUFA can reduce total and LDL cholesterol levels. In relation to carbohydrates, they increase high-density lipoprotein (HDL) cholesterol levels and thus decrease plasma triglyceride levels [86]. Not only its greater oxidative stability but also its high antioxidant activity allows its use in the production of anti-aging cosmetics, among others. PBF seed oil could also be of interest in the production of cosmetics as well as in the pharmaceutical industry as a treatment against cardiovascular diseases due to the high levels of C18:1n9c and C16:1n7 found [6,81]. Both PBF and PAF seed oils are the most interesting for their applicability in the nutraceutical, cosmetic, and food industries since PAFD oil is the one with the least oxidative stability, requiring natural stabilizers that increase its useful life. Moreover, its high content of C18:0, a saturated fatty acid, is known for increasing blood cholesterol levels with negative effects on health.

On the other hand, for plum seed phenolic extracts, correlations between individual polyphenols, TPC, and TFC, as well as the different bioactive properties (antioxidant and antimicrobial activities), were considered in the PCA plot in Figure 6. Vanillic acid, syringic acid, kaempferol-3-rutinoside, isoharmentin-3-rutinoside, hesperidin, catechin, and epicatechin were not included in the PCA study due to their low concentration in the samples, close to the limit of detection and the limit quantification of the method, which makes its contribution to the multivariate study irrelevant or minimal.

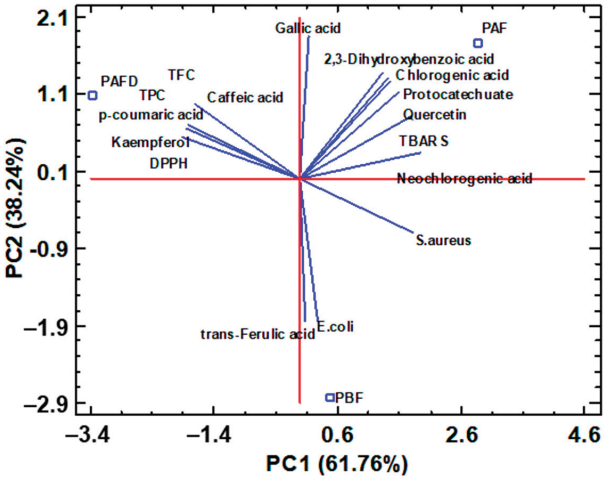

Figure 6. Principal component analysis biplot of scores (PBF, PAF and PAFD plum seed phenolic extracts) and loadings (individual polyphenols, TPC, TFC, thiobarbituric acid reactive substances (TBARS) and DPPH antioxidant assays and antimicrobial activities against *Escherichia coli* and *Staphylococcus aureus*).

According to the PCA biplot represented in Figure 6, It was observed that PBF defatted seed phenolic extract was characterized by the highest content of *trans*-ferulic acid, while PAF extract presented high levels of 2,3-dihydroxybenzoic acid, neochlorogenic acid, chlorogenic acid, gallic acid, vanillic acid, protocatechuate, and quercetin. In addition, these kinds of polyphenols were correlated by the greater antioxidant capacity DPPH (lower IC_{50}). For its part, PAFD phenolic extract was characterized by high levels of *p*-coumaric acid, kaempferol, which contributes to the TFC, as well as high content of caffeic acid, which seems to have the greatest effect on TPC. In addition, the latter extract presented the highest antioxidant capacity, TBARS, so these polyphenols contribute to increasing the shelf life of foods [25]. This residue was also positively correlated with the greatest antimicrobial activity with respect to *Staphylococcus aureus* (lowest MIC) and, to a lesser extent, with

Escherichia coli. Regarding the phenolic profile involved in antimicrobial activity, it was observed that gallic acid had the highest activity against the growth of *Escherichia coli*, while caffeic acid had the highest activity against the growth of *Staphylococcus aureus*. According to literature data, gallic acid is well known to have outstanding activity against the growth of the *Escherichia coli* pathogen, so much so that a high content of this polyphenol in phenolic extracts could be of interest [87]. Not to mention caffeic acid, which is also recognized for its inhibitory work on the growth of *Staphylococcus aureus*, hence has potential application in the design of active packaging against the growth of this pathogen in food, thus increasing its shelf life [25,88].

To summarize everything that has been already mentioned, PAFD phenolic extract would be the most interesting to be applied in the food and nutraceutical industry since it is the only one where amygdalin was not detected and thus could be included as an active ingredient in the production of active packaging against *Escherichia coli* and *Staphylococcus aureus* [25]. Furthermore, the presence of *p*-coumaric acid with kaempferol could highlight its applicability as a dietary supplement against cardiovascular diseases or even in the cosmetic industry in the production of cosmetics that reduce the development of erythema and skin pigmentation due to exposure to ultraviolet radiation [89,90]. Withal, the other two defatted seed extracts cannot be left behind since PAF and PBF phenolic extracts presented the greatest DPPH antioxidant activity and high levels of trans-ferulic acid, which may increase the protection against oxidative stress, respectively. Thus, a possible applicability for these extracts may be the nutraceutical industry once the amygdalin is removed [27,91].

3. Materials and Methods

3.1. Reagents, Standards, Bacterial Strains, and Solvents

Analytical grade reagents were required in the experimental procedures: *n*-Hexane (96%), methanol (MeOH, ≥99%), and ethanol absolute (EtOH, ≥99.8) for HPLC gradient quality; acetonitrile (ACN) and formic acid (FA) of MS quality. Hydrochloric acid (HCl, 37%) and sulfuric acid (H_2SO_4, 95–97%) were supplied by Scharlab (Barcelona, Spain). Dimethyl sulfoxide (DMSO, ≥99.9%), 2N Folin–Ciocalteu reagent, 2,2-diphenyl-1-picrylhydrazyl (DPPH, ≥99.9%), sodium methoxide (95%), trichloroacetic acid (TCA, 99%), thiobarbituric acid (≥98%), sanitary ethanol (96%), 1,1,1,3,3,3-hexafluoro-2-propanol (HFIP), curcumin (>65%), and LB broth with agar and Tryptic Soy Broth (TSB) were all supplied by Sigma-Aldrich (St. Louis, MO, USA). Curcumin was stored at −20 °C prior to analysis. Amyloid β protein fragment 1–42 ($A\beta_{1-42}$) (A9810, CAS: 107761-42-2, MW 4514.04 g mol^{-1}) was also obtained from Sigma-Aldrich (St. Louis, MO, USA) for incubation assays and stored at −80 °C until analysis. The standard Trolox (≥97%) was provided by Sigma-Aldrich (Burghasen, Germany). 2-Propanol for HPLC gradient (C_3H_8O, PrOH), Aluminum chloride 6-hydrate (99%), sodium carbonate anhydrous, sodium hydroxide (NaOH, 98%), *p*-iodonitrotetrazolium chloride (INT, 98%), ferrous-sulfate heptahydrate ($FeSO_4 \cdot 7H_2O$, 98%), and sodium nitrite (≥98%) were obtained from Panreac (Barcelona, Spain). Silica was purchased from Fisher Scientific (Pittsburgh, PA, USA).

Fatty acid standards FAME 37 component SUPELCO Ref CRM47885, tridecanoic acid (C13:0, ≥99%), and ethyl nonanoate (>98%) were purchased from Sigma-Aldrich (Barcelona, Spain).

α-tocopherol (≥96%), γ-tocopherol (≥96%), and δ-tocopherol (≥90%) standards were purchased from Sigma-Aldrich (St. Louis, MO, USA). β-tocopherol stock solution was supplied by Sigma-Aldrich (St. Louis, MO, USA) and was already dissolved in methanol, and the remaining stock solutions of 1000 mg·L^{-1} were prepared, dissolving the adequate quantity of analyte in methanol as well. Those solutions were later further diluted for the purpose of a calibration curve into solutions of 0.3, 0.5, 2.0, 5.0, 10.0, 20.0, 50.0, 75.0, and 100 mg·L^{-1}. Stock solution stability was also considered, and it was established in three months, at the very least, via conservation in darkness in the freezer at −20 °C.

Phenolic standards gallic acid monohydrate (≥98.0%), chlorogenic acid (≥95.0%), dihydroxybenzoic acid (≥97.0%), caffeic acid (≥98.0%), catechin (≥98.0%), *p*-coumaric

acid (≥98.0%), epicatechin (≥98.0%), rutin trihydrate (≥95.0%), *trans*-ferulic acid (98%), myricetin (≥96.0%), resveratrol (≥99.0%), quercetin (≥95.0%), kaempferol (≥97.0%), and naringin (≥95.0%) were obtained from Sigma-Aldrich (St. Louis, MO, USA). Hesperidin (≥98.0%) was provided by European Pharmacopoeia. Phenolic stock solutions (200 mg·L^{-1}) were prepared in MeOH, an ethanol–water mixture 80:20 (*v*/*v*) (quercetin), or a 5% (*v*/*v*) DMSO aqueous solution (hesperidin). They were stored in the dark at 4 °C or at −80 °C (hesperidin, *trans*-ferulic, myricetin, and caffeic acid) for up to one month. Fresh working standard solutions were prepared daily by diluting stock solutions as required. Nylon membrane filters with 0.22 μm pore size (Teknokroma, Barcelona, Spain) were used for mobile phase filtration before chromatographic analysis.

The antimicrobial activity of the extracts was evaluated against Gram-positive bacteria *Staphylococcus aureus* (ATCC 29213) and Gram-negative bacteria *Escherichia coli* (ATCC 25922). Streptomycin sulfate salt was used as a positive standard and was provided by Sigma-Aldrich (St. Louis, MO, USA).

3.2. Raw Materials

Plum stones of the family *P. domestica* L. and the variety of "Queen Claudia" before fermentation (PBF), as well as those obtained after different stages of plum brandy production, in particular stones after fermentation (PAF) and after both fermentation and distillation (PAFD) were provided by The Jerte Valley Cooperatives Group (Cáceres, Spain, 2022 campaign). The plum used to obtain plum brandy was crushed with rubber rollers, keeping the stone intact. The resulting intact stones, together with the pulp, were subjected to a biological must fermentation phase at a controlled temperature (18–20 °C) for 25–30 days. Subsequently, it was subjected to a distillation process using indirect heat in batch-loaded stills.

For the pretreatment of the plum pits, the experimental procedure proposed by Rodríguez-Blázquez et al. [6] was followed. Plum stones were air-dried at 40 °C (Digitheat oven, J.P Selecta®, Abrera, Barcelona, Spain) for 24 h and manually separated into their two components: shell and seed, using a hammer. The seeds were then crushed in an ultracentrifuge crusher (Retsh™ ZM200, Haan, Germany), and the particle size was reduced and homogenized to below 1 mm with a stainless-steel sieve.

3.3. Moisture Content of Seed Samples

Plum seeds moisture content was determined according to the standard procedure AOAC 925.10 [92], with some modifications. Approximately 2 g of seed sample was weighed on a dried crucible and introduced in an oven at 105 °C for 2 h and 30 min until a constant weight was obtained. After cooling, the crucible was weighed again, and the free water content was calculated as sample weight loss and expressed as a percentage in weight (mean ± standard deviation, n = 3).

3.4. Soxhlet Extraction of Plum Seeds

Oil extraction from plum seeds was performed following standard Soxhlet extraction [28] and the after-treatment described by Rodríguez-Blázquez et al. [6,12]. Approximately 15 g of plum seed with a particle size of less than 1 mm were extracted with 150 mL of *n*-hexane (seed-solvent ratio (1:10)) under reflux at 69 °C for 6 h (6–8 cycles per hour). Then, the solvent was evaporated using a rotary evaporator (Buchi™ Rotavapor™ R-100, Fisher Scientific, Hampton, VA, USA) at 69 °C. The collecting flask with the resulting plum oil and the by-product defatted plum seed contained in the cellulose cartridge were dried and placed in a vacuum oven (Vaciotem-TV, digital, J.P Selecta®, Abrera, Barcelona, Spain) at 40 °C for 24 h. This procedure was carried out in triplicate for each plum seed. Plum seed oils were stored in airtight, amber-colored glass bottles and kept at −20 °C, whereas the defatted plum seeds were stored in a clear plastic zip-lock bag until analysis. The percentages in weight (*w*, %) of plum seed oils and defatted plum seed by-products were expressed as mean ± standard deviation both on a dry basis.

3.5. Phenolic Extraction of Defatted Plum Seeds

With the aim of extracting phenolic compounds from defatted plum seed by-products, a sustainable MSPD method was used.

For this purpose, the optimized MSPD extraction previously developed was applied [12]. Briefly, 0.1000 g of defatted plum seeds and 0.1000 g of silica dispersant were mixed for 2 min to obtain a homogeneous powder and they were transferred to a 5 mL plastic tube. Then, 3 mL of EtOH-water (80:20 (v/v)) were added, and the mixture was stirred for 10 min at 402.48× g, using a vortex. A clear supernatant was collected after centrifugation for 30 min at 1528× g (centrifuge 5804, Eppendorf, Hamburg, Germany). Samples were prepared in triplicate.

3.6. Characterization of the Lipid Profile and Evaluation of the Health Lipid Indexes of Plum Seed Oils

The determination of fatty acid profile in the extracted plum seed oils was carried out using a gas chromatography (Agilent 6890) coupled to a Mass Spectrometer (Agilent 5973) following the internal derivatization procedure to fatty acid methyl esters (FAME). Prior to the chromatography analysis, the methyl esters of fatty acids were formed by methylation with sodium methoxide and esterification in an acid medium according to the usual methods described in the bibliography [93,94] with some modifications. In a 12 mL screw-capped tube, approximately 20 mg of seed oil were added with 0.6 mL of a methanolic internal standard solution (tridecanoic acid; 1730 mg·L^{-1}) and 1.4 mL of a methanolic sodium methoxide solution (4.3%, w/v). After stirring, the tube was kept for 10 min in an oven (Digitheat oven, J.P Selecta®, Abrera, Barcelona, Spain) at 60 °C. Then, 2 mL of a solution of sulfuric acid (4%, v/v) in methanol were added and again kept at 60 °C in an oven (Digitheat oven, J.P Selecta®, Abrera, Barcelona, Spain) for 20 min. For methyl esters extraction, 1 mL of distilled water and 1.5 mL of *n*-hexane were added. After shaking and centrifugation, 960 µL of *n*-hexane were recovered and placed in a 2 mL chromatography vial, followed by the addition of 40 µL of a solution of ethyl nonanoate (6400 mg·L^{-1}) in *n*-hexane, which was used as an internal standard. Finally, 1 µL was then injected into the gas chromatography system.

The chromatographic separation was carried out in a capillary chromatographic column (30 m length × 0.25 mm of internal dimeter × 0.25 µm film thickness) (DB-WAX-UI, J&W Scientific, Folsom, CA, USA). The column oven program was: 80 °C (5min), 8 °C/min from 80 °C to 145 °C, isothermal at 145 °C for 27 min, 4 °C /min up to 230 °C, and isothermal at 230 °C for 20 min. The injector temperature was 240 °C, and the injection was in split mode (1:40). The column flow was 1 mL·min^{-1}.

The mass spectrometer was operated in the electronic impact ionization mode (70 eV) and in SCAN (m/z range: 35–400) and SIM (m/z = 74, 87, 348, and 382) combined acquisition mode. Compound identification was carried out via a comparison of retention times and mass spectra of the reference compounds (commercial FAME mix and ethyl nonanoate) with those reported in the mass spectrum library NIST 2.0. The chromatogram of the FAME 37 SUPELCO standard mixture was registered and included in Figure S3. Moreover, the chromatograms of PBF, PAF, and PAFD seed oils are represented in Figure S4, Figure S5, and Figure S6, respectively. In addition, for quantification purposes, tridecanoic acid was used as an internal standard. Methyl esters integration peaks were carried out by using SIM chromatograms, and for ethyl nonanoate, m/z = 88 of the SCAN chromatograms. For obtaining the response factors (RF) of the methyl esters, the commercial mix was injected at three different concentrations (not diluted and diluted $\frac{1}{2}$ and $\frac{1}{4}$), obtaining an average RF. That average RF was used to establish the percentage of each methyl ester in samples, and the results corresponding to the average RF with their respective standard deviation are shown in Table S2. It presented a variation among samples lower than 3.8%, thus indicating the correct derivatization process. The limit of detection (LOD) and quantification (LOQ) was determinate considering 3.3 times the background noise signal for the former and 10 times for the latter. Analyses were

performed in duplicate, and the composition of the plum seed oils was expressed as a percentage (%) considering the RF obtained for each fatty acid standard using Equation (1).

$$\frac{C_i{}^m}{C_t{}^m}\ (\%) = \frac{\frac{A_i{}^m}{R_{fi}}}{\sum_{i=1}^{n}\frac{A_i{}^m}{R_{fi}}} \times 100 \quad (1)$$

where $C_i{}^m$ is the concentration of each FAME in the sample, $C_t{}^m$ is the total concentration of FAMEs in the sample, $A_i{}^m$ is the individual area for each FAME, and R_{fi} is the response factor obtained for each standard FAME.

According to the fatty acid profile obtained for each plum seed oil, the respective healthy nutritional value of each of them was determined. For this purpose, the total content of SFA, UFA, MUFA, and PUFA was determined, as well as the AI index, TI index, H/H ratio, and DFA index, as defined by Rodríguez-Blázquez et al. [6]. The following equations were used:

$$\sum \text{SFA} = \text{C16:0} + \text{C17:0} + \text{C18:0} + \text{C20:0} + \text{C22:0} + \text{C24:0} \quad (2)$$

$$\sum \text{UFA} = \sum \text{MUFA} + \sum \text{PUFA} \quad (3)$$

$$\sum \text{MUFA} = \text{C16:1n7} + \text{C18:1n7c} + \text{C18:1n9c} \quad (4)$$

$$\sum \text{PUFA} = \text{C18:2n6c} + \text{C18:3n3} + \text{C20:1n9} \quad (5)$$

$$\text{DFA} = \sum \text{MUFA} + \sum \text{PUFA} + \text{C18:0} \quad (6)$$

$$\text{AI} = \frac{\text{C12:0} + 4(\text{C14:0}) + \text{C16:0}}{\sum \text{MUFA} + \sum \text{PUFA}} \quad (7)$$

$$\text{H/H} = \frac{\text{C18:1} + \sum \text{PUFA}}{\text{C14:0} + \text{C16:0}} \quad (8)$$

where C12:0 is dodecanoic acid, C14:0 is myristic acid, C16:0 corresponds to palmitic acid, C16:1n7 is palmitoleic acid, C17:0 is margaric acid, C18:0 is stearic acid, C18:1n7c is cis-vaccenic acid, C18:1n9c is oleic acid, C18:2n6c is linoleic acid, C18:3n3 is α-linolenic acid, C20:0 is arachidic acid, C20:1n9 is 11-eicosenoic acid, C22:0 is behenic acid, and C24:0 is lignoceric acid.

Finally, the O/L ratio was determined as another widely used parameter to establish the quality of plum seed oils [79].

3.7. Characterization of Tocopherols in Plum Seed Oils

The analysis of α-, β-, γ-, and δ-tocopherol was carried out via HPLC-PDA, following the procedure previously described by Aksoz et al. [10]. The equipment consisted of a Jasco LC-NetII/ADC degasser, a Jasco PU-2089 Plus quaternary gradient pump, and a Jasco Md-2018 Photodiode Array Detector. A Luna C18 column (5 µm 150 × 4.6 mm 100 Å, Phenomenex, Torrance, CA, USA) was capable of separating three out of four analytes, other than the β and γ homologs, using pure methanol as the mobile phase. The flow rate was set at 1 mL·min^{-1}, and the UV-vis detection was performed at both 292 and 305 nm. The identification of tocopherols was based on the comparison of retention time and spectral characteristics with those of the standards. Quantitative analyses were performed at 292 nm, given the higher signal sensitivity, using two external calibration curves, one at low concentrations (n = 5) between 0.5 and 20.0 mg·L^{-1} for γ- and α-tocopherol and 0.3–20.0 mg·L^{-1} for δ-tocopherol; and the other for high concentrations (n = 4), between 20.0 and 100 mg·L^{-1}. The estimation of the LOD and LOQ was achieved considering 3.3 times the background noise signal for

the former and 10 times for the latter. The robustness of the method was studied at 10 and 100 mg·L^{-1} for α, 5 and 50 mg·L^{-1} for γ, and 2 and 50 mg·L^{-1} for δ, via the injection of the same standard solution for each of the two calibration curves thrice (n = 3) during three consecutive days (N = 9). The precision results were calculated as an analysis of the peak area and the retention factor (Table 4).

Finally, for the analysis of plum seed oils, samples were filtered through a 0.45 μm nylon filter beforehand and diluted in a 1:3 ratio using 2-propanol as a solvent, following the protocol developed by Aksoz et al. [10]. Samples were analyzed in quadruplicate, and the results were expressed as mean ± standard deviation in mg per kg of dry plum seed sample. For illustrative purposes, Figure S2 represents the corresponding chromatogram for each sample, as well as the standard mixture used for reference.

3.8. Determination of Phenolic Compounds from Defatted Plum Seed Extracts

3.8.1. Spectrophotometric Methods

The total phenolic content of defatted plum seed extracts was determined using the Folin–Ciocalteu method [12]. After combining 750 μL of defatted plum seed extracts with 70 μL of the Folin–Ciocalteu reagent, 60 μL of 7.5 (*w*/*v*) of Na_2CO_3, and Milli-Q water to a final volume of 10 mL, the absorbance of the solution was measured at 720 nm (Thermo Scientific Multiskan spectrophotometer, Agilent Technologies, Santa Clara, CA, USA) and the obtained results were displayed in terms of mg of gallic acid equivalent per gram of defatted seed dried sample (mg GAE·g^{-1} defatted seed), using gallic acid as standard (0–40 μM). The assay was performed in triplicate.

The total flavonoid content of defatted plum seed extracts was measured by the aluminum complexation colorimetry method [12]. Briefly, 750 μL of defatted plum seed extracts were combined with 2 mL of Milli-Q water and 150 μL of 5% (*w*/*v*) $NaNO_2$ for 5 min. Then, 150 μL of 10% (*w*/*v*) of $AlCl_3$ were added to the mixture and left for 5 min. After that, 1 mL of 1 M NaOH was added to stop the reaction solution and left for 15 min, which was then diluted to a volume of 10 mL with Milli-Q water. The absorbance of the flavonoid-Al (III) complex was measured at 415 nm, and the results were represented as mg of quercetin equivalent per gram of defatted seed dried sample (mg QE·g^{-1} defatted seed) using quercetin as standard (0–45 μM).

3.8.2. Chromatographic Method

The individual polyphenol determination of the plum seed phenolic extract at the different stages of brandy processing was performed by HPLC-ESI-QTOF-MS, following the procedure previously described by Rodríguez-Blázquez et al. [12].

Agilent liquid chromatography system (Mod. 1200) was used consisting of a quaternary pump (G1311A), a coupled degasser (G1322A), an automatic injector with thermostat (G1367B), a column module with thermostat (G1316A), and a QTOF mass spectrometer (G1316A), with electrospray ionization (ESI) source at atmospheric pressure and JetStream technology, operating in negative mode and scanning (SCAN) mode in the range *m*/*z* 100–1000. A capillary voltage of 4 kV and a pressure of 45 psi were employed in the chromatographic analyses. Nitrogen was used as the fogging and drying gas (10.0 L·min^{-1}, 325 °C), and the data treatment was performed using Masshunter Data Acquisition B.05.00, Masshunter Qualitative Analysis B.07.00, and Massprofinder Professional B.08.00.

The chromatographic separation was carried out using a Synergi™ C18 Fusion-RP 80 Å (150 mm, 3 mm I.D., 4 m, Phenomenex, Torrance, CA, USA), maintained at 30 °C. The flow rate was set to 0.5 mL·min^{-1} and the injection volume to 20 μL. Moreover, a mobile phase consisting of 0.1% (*v*/*v*) formic acid (FA) aqueous solution (solvent A) and acetonitrile (solvent B) was used, operating in gradient elution as follows: 10% of solvent B was held for 0.1 min, it then increased linearly to 35% in 30 min, and achieved 70% in 5 min. This state was maintained for 2 min, after which a final linear increase to 90% B was obtained in 3 min and maintained for 5 min. Finally, the gradient was re-equilibrated. The identification and quantification of phenolic compounds present in defatted plum

seed extracts were focused on high-resolution mass data collected from commercial standards and databases (FooDB and Mass Bank), and 5-level external calibration curves were obtained for the phenolic standards. When phenolic standards were not available, a semi-quantification was performed using the most similar standard available. In addition, the LOD and LOQ were determined considering the former is 3.3 times the background noise signal and 10 for the latter. Finally, the results were represented in mg per gram of defatted dried seed. Figures S7–S23 represent the standard solution mass spectrum of gallic acid, 2,3-dihydroxibenzoic acid, *p*-coumaric acid, quercetin, kaempferol, caffeic acid, *trans*-ferulic acid, hesperidin, catechin, epicatechin, chlorogenic acid, kaempferol 3-rutinoside, neochlorogenic acid, vanillic acid, protocatechuate, syringic acid, amygdalin, and isorhamnetin 3-rutinoside. Figure S24 represents the corresponding chromatograms obtained for PBF, PAF, and PAFD samples.

3.9. Evaluation of Bioactive Properties of Plum Seed Oils and Defatted Plum Seed Extracts

3.9.1. Antioxidant Activity

Free-radical scavenging assay: The scavenging ability of plum seed oils and defatted seed by-products was evaluated against the DPPH.

On one hand, for the evaluation of the antioxidant capacity of plum seed oils, the method proposed by Rodríguez-Blázquez et al. [6] was followed. Briefly, in a 96-well microplate, 30 µL of eight methanolic working solutions (0–30 µL) made by diluting oil solutions in DMSO (448–850 $mg \cdot mL^{-1}$) were combined with 270 µL of a $6 \cdot 10^{-5}$ M DPPH methanolic solution, following incubation for 60 min in the dark. Finally, the absorbance was measured at 515 nm. The results were represented as IC_{50} values ($mg \cdot mL^{-1}$ of oil), e.g., the concentration of sample needed to inhibit 50% of the original DPPH concentration, after the oil concentrations were plotted against the remaining DPPH percentages. Trolox was employed as a positive control. The experiment was run in duplicate, up for 22 days, to evaluate the oxidative stability of plum seed oils during storage. For this purpose, the data were fitted to first-order kinetics, and from this logarithmic calibration, the half-time was determined for each of the plum seed oils.

On the other hand, the antioxidant activity of the phenolic extracts was determined as described by Rodríguez-Blázquez et al. [6]. Concisely, 10–100 µL of sample aliquots and 100 µL of 0.28 mM DPPH solution in MeOH were combined to prepare a working solution in a 96-well microplate, with a total volume of 200 µL. Furthermore, a DPPH control and a blind control (defatted plum seeds mixed with pure MeOH) were prepared. Trolox served as a reference substance. The absorbance was measured at 515 nm after a 60 min incubation in the dark. Lastly, the IC_{50} value was calculated and reported as milligrams of extract per gram of defatted dried seed. The assay was performed in three independent experiments.

Lipid peroxidation assay: The antioxidant activity of the phenolic extract of defatted plum seeds estimated as the capability to inhibit lipid peroxidation was evaluated via the in vitro TBARS method. The TBARS assay was conducted with porcine brain cell homogenates and sample extract at concentrations of 4.0–0.125 $mg \cdot mL^{-1}$, in accordance with the protocol outlined by Gómez-Mejía et al. [77]. The inhibition ratio was calculated as the remaining percentage and represented in mg $extract \cdot g^{-1}$ of defatted dried seed at the IC_{50} value after the solutions' absorbance was measured at 532 nm. Every sample underwent three independent examinations. Furthermore, Trolox was employed as a positive control.

3.9.2. Anti-Amyloidogenic Activity

The anti-amyloidogenic effect was evaluated in the phenolic extract of PAFD defatted seed re-dissolved in HCl on pre-treated $A\beta_{42}$ monomer, employing Transmission electron microscopy (TEM) according to the procedure previously described by Vicente-Zurdo et al. [95], with slight modifications. Briefly, properly pre-treated $A\beta_{42}$ monomer was daily dissolved to obtain a final $A\beta_{42}$ working solution of 200 µM. In the aggregation experiments, a daily preparation of a 200 µM Fe(II) metal solution was conducted. Working

solutions were prepared by diluting stock solutions in 10 mM HCl, including $A\beta_{42}$ alone, $A\beta_{42}$ + Fe(II), $A\beta_{42}$ + PAFD phenolic extract, and $A\beta_{42}$ + Fe(II) + PAFD phenolic extract. PAFD phenolic extracts were prepared and tested at concentrations of 25 and 50 mg·L^{-1}, while $A\beta_{42}$ and Fe(II) were added at 50 μM. To evaluate amyloid inhibition capacity, all working solutions were incubated at 37 °C for 48 h and subsequently analyzed using TEM. Curcumin (50 μM) served as a negative control due to its recognized anti-amyloidogenic properties [96].

For TEM analysis, 1.5% (*w*/*v*) phosphotungstic acid was employed for negative staining of $A\beta_{42}$ fibrils. After removing the excess staining solution, the prepared grids were transferred and examined using a JEOL JEM 1400 Plus transmission electron microscope operating at 120 kV. TEM images were captured at different magnification powers. A comparative analysis was conducted to observe differences in the aggregation effect and the width of fibrils among the obtained images from the protein alone, in the presence of metal, in the presence of the target plum extracts, and in the presence of both. The fibril measurements were performed using the ImageJ software (https://imagej.net/ij/download.html) (n = 200).

3.9.3. Antibacterial Activity

The antibacterial activity of defatted plum seed phenolic extracts re-dissolved in water (0.156–20 mg·mL^{-1}) was tested against a Gram-negative bacteria (*Escherichia coli*) and a Gram-positive bacteria (*Staphylococcus aureus*) by the microdilution method combined with the *p*-iodonitrotetrazolium chloride (INT) rapid colorimetric assay proposed by Gómez-Mejía et al. [77]. Briefly, 100 μL of each diluted defatted plum seed extract (0.156–20 mg·mL^{-1}) were mixed with 100 μL Tryptic Soy Broth (TSB) and 10 μL of bacteria suspension in sterile water at 5.2 × 10^8 CFU·mL^{-1}. For each inoculum, Streptomycin (0.625–20 mg·L^{-1}) was used as a positive control in the TSB medium. In addition, three more controls were added: TSB medium inoculated with bacterial suspension, defatted seed phenolic extracts in TSB medium, and non-inoculated TSB medium. After incubation at 37 °C for 1 h, inhibition of bacterial growth was visually verified by color change after the addition of INT dye (50 μL at 0.2 mg·mL^{-1}). Antibacterial activity results were expressed as MIC; mg·mL^{-1}.

3.10. Statistical Analysis

Data were statically analyzed by LSD multiple comparison test, ANOVA, multifactorial ANOVA, and PCA using the software package Statgraphics 19 (Statgraphics Technologies, Inc., Rockville, MD, USA).

4. Conclusions

In this work, formerly low-interest residues of plum seed employed in the plum brandy manufacturing process were explored, revealing a cascade valorization process to obtain high-value bioactive added compounds such as polyphenols, tocopherols, and unsaturated fatty acids. To establish the effect of processing in the seed samples and therefore, in the obtained compounds, a Soxhlet extraction using *n*-hexane as a solvent was effectively performed to separate antioxidant oils from defatted seed by-products. A sustainable and reliable MSPD extraction procedure was also employed to obtain phenolic extracts with bioactive potential.

As far as results go, it has not been observed that any of the brandy processing stages (before fermentation, after fermentation, and after both fermentation and distillation) positively affect the properties of the plum seeds, which showed that depending on the applicability that is sought, it may be of most interest to use the oil or the defatted seed. Considering the lipid fraction, in which the main components were C18:1n9c (72–75.56%) and C18:2n6c fatty acids (15.83–20%) with outstanding heart-healthy lipid indexes, particularly, PBF and PAF seed oils presented the greatest applicability in the nutraceutical, pharmaceutical and cosmetic industries, characterized by a high content of UFA, specifically

C16:1n7 (0.765 ± 0.004%) and C17:1n7c (0.092 ± 0.001%), respectively. Both fatty acids contributed positively to the excellent oxidative stability (72–144 days for PBF and PAF seed oils, respectively) and to the antioxidant activity (IC_{50} = 20–21 mg·mL^{-1}). Chiefly, PAF presented the lowest γ/α ratio (2.27 ± 0.02).

Regarding the hydrophilic fraction of the seeds, all defatted plum seed phenolic extracts (PBF, PAF, and PAFD) showed high antiradical activity (IC_{50} = 0.9–1.9 mg·g^{-1}) and anti-lipid peroxidation activity (IC_{50} = 1.3–5.0 mg·g^{-1}) with potential applicability in the nutraceutical, pharmaceutical or cosmetic industries. Albeit, in PBF and PAF phenolic extracts, it is necessary to remove amygdalin since it negatively affects their nutritional value. This stage is not necessary for the PAFD phenolic extract since amygdalin was not detected, which makes this extract stand out considerably from the others. In addition, it was the one that presented the greatest inhibition against *Escherichia coli* and *Staphylococcus aureus* growth (MIC = 20 mg·mL^{-1}), Aβ_{42} aggregation (25 mg·mL^{-1}), and lipid peroxidation (1.3 mg·g^{-1}), with potential use in the nutraceutical industry or as an active ingredient in the manufacturing of food packaging.

Supplementary Materials: The following supporting information can be downloaded at https://www.mdpi.com/article/10.3390/ijms25021236/s1.

Author Contributions: Conceptualization, S.R.-B., L.P.-C., E.G.-M., D.V.-Z., N.R.-C., M.E.L.-G., J.J.R.-B. and R.M.; methodology, S.R.-B., L.P.-C., E.G.-M., D.V.-Z., N.R.-C., M.E.L.-G., J.J.R.-B. and R.M.; software, S.R.-B., L.P.-C., E.G.-M., D.V.-Z., N.R.-C., M.E.L.-G. and J.J.R.-B.; validation, S.R.-B., L.P.-C., E.G.-M., D.V.-Z., N.R.-C., M.E.L.-G., J.J.R.-B. and R.M.; formal analysis, S.R.-B., L.P.-C., E.G.-M., D.V.-Z. and J.J.R.-B.; investigation, S.R.-B., L.P.-C., E.G.-M., D.V.-Z., N.R.-C., M.E.L.-G., J.J.R.-B. and R.M.; resources, E.G.-M., N.R.-C., M.E.L.-G. and R.M.; data curation, S.R.-B., L.P.-C., E.G.-M., D.V.-Z. and J.J.R.-B.; writing—original draft preparation, S.R.-B., L.P.-C., D.V.-Z. and J.J.R.-B.; writing—review and editing, S.R.-B., L.P.-C., E.G.-M., D.V.-Z., N.R.-C., M.E.L.-G., J.J.R.-B. and R.M.; visualization, S.R.-B., L.P.-C., E.G.-M., D.V.-Z., N.R.-C., M.E.L.-G., J.J.R.-B. and R.M.; supervision, S.R.-B., L.P.-C., E.G.-M., D.V.-Z., N.R.-C., M.E.L.-G., J.J.R.-B. and R.M.; project administration, E.G.-M., N.R.-C., M.E.L.-G. and R.M.; funding acquisition, R.M. All authors have read and agreed to the published version of the manuscript.

Funding: This research has been funded by the Ministry of Science and Innovation, the state research agency, and by the European Union NextGenerationEU/ PRTR [project TED2021-129917B-I00]. Moreover, this work was supported and the Ministry of Science, Innovation and Universities [project PID 2020-114714RB-I00].

Institutional Review Board Statement: Not applicable.

Informed Consent Statement: Not applicable.

Data Availability Statement: The data presented in this study are available on request from the corresponding author.

Acknowledgments: The authors are grateful to the Analysis Service Unit facilities of ICTAN for the analysis of Liquid Chromatography and Mass Spectrometry and the sample providers, "The Jerte Valley Cooperatives Group". This work was supported by the Complutense University through a research staff contract in the "Investigo programme" (CT36/22-30-UCM-INV) and by the Ministry of Science and Innovation through a staff contract research support (PAII10/23-3/2023-05).

Conflicts of Interest: The authors declare no conflicts of interest.

References

1. Bonilla, J.; Vargas, F.C.; de Oliveira, T.G.; da Aparecida Makishi, G.L.; do Amaral Sobral, P.J. Recent Patents on the Application of Bioactive Compounds in Food: A Short Review. *Curr. Opin. Food Sci.* **2015**, *5*, 1–7. [CrossRef]
2. Câmara, J.S.; Albuquerque, B.R.; Aguiar, J.; Corrêa, R.C.G.; Gonçalves, J.L.; Granato, D.; Pereira, J.A.M.; Barros, L.; Ferreira, I.C.F.R. Food Bioactive Compounds and Emerging Techniques for Their Extraction: Polyphenols as a Case Study. *Foods* **2021**, *10*, 37. [CrossRef] [PubMed]
3. Farag, M.A.; Bahaa Eldin, A.; Khalifa, I. Valorization and Extraction Optimization of Prunus Seeds for Food and Functional Food Applications: A Review with Further Perspectives. *Food Chem.* **2022**, *388*, 132955. [CrossRef] [PubMed]

4. Kumar Joshi, V.; Sharma, R.; Shyam Abrol, G. 5 Stone Fruit: Wine and Brandy. In *Handbook of Plant-Based Fermented Food and Beverage Technology*; CRC: Boca Raton, FL, USA, 2011.
5. Rabrenović, B.B.; Demin, M.A.; Basić, M.G.; Pezo, L.L.; Paunović, D.M.; Sovtić, F.S. Impact of Plum Processing on the Quality and Oxidative Stability of Cold-Pressed Kernel Oil. *Grasas Aceites* **2021**, *72*, e395. [CrossRef]
6. Rodríguez-Blázquez, S.; Gómez-Mejía, E.; Rosales-Conrado, N.; León-González, M.E.; García-Sánchez, B.; Miranda, R. Valorization of Prunus Seed Oils: Fatty Acids Composition and Oxidative Stability. *Molecules* **2023**, *28*, 7045. [CrossRef] [PubMed]
7. Górnaś, P.; Rudzińska, M.; Soliven, A. Industrial By-Products of Plum *Prunus domestica* L. and *Prunus cerasifera* Ehrh. as Potential Biodiesel Feedstock: Impact of Variety. *Ind. Crops Prod.* **2017**, *100*, 77–84. [CrossRef]
8. Vladić, J.; Gavarić, A.; Jokić, S.; Pavlović, N.; Moslavac, T.; Popović, L.; Matias, A.; Agostinho, A.; Banožić, M.; Vidović, S. Alternative to Conventional Edible Oil Sources: Cold Pressing and Supercritical CO2 Extraction of Plum (*Prunus domestica* L.) Kernel Seed. *Acta Chim. Slov.* **2020**, *67*, 778–784. [CrossRef]
9. Ahmad, N.; Ahmad, N.; Manzoor, M.F.; Shabbir, U.; Ahmed, S.; Ismail, T.; Saeed, F.; Nisa, M.; Anjum, F.M.; Hussain, S. Health Lipid Indices and Physicochemical Properties of Dual Fortified Yogurt with Extruded Flaxseed Omega Fatty Acids and Fibers for Hypercholesterolemic Subjects. *Food Sci. Nutr.* **2020**, *8*, 273–280. [CrossRef]
10. Aksoz, E.; Korkut, O.; Aksit, D.; Gokbulut, C. Vitamin E (α-, β + γ- and δ-Tocopherol) Levels in Plant Oils. *Flavour. Fragr. J.* **2020**, *35*, 504–510. [CrossRef]
11. Barouh, N.; Bourlieu-Lacanal, C.; Figueroa-Espinoza, M.C.; Durand, E.; Villeneuve, P. Tocopherols as Antioxidants in Lipid-Based Systems: The Combination of Chemical and Physicochemical Interactions Determines Their Efficiency. *Compr. Rev. Food Sci. Food Saf.* **2022**, *21*, 642–688. [CrossRef]
12. Rodríguez-Blázquez, S.; Fernández-Ávila, L.; Gómez-Mejía, E.; Rosales-Conrado, N.; León-González, M.E.; Miranda, R. Valorization of Defatted Cherry Seed Residues from Liquor Processing by Matrix Solid-Phase Dispersion Extraction: A Sustainable Strategy for Production of Phenolic-Rich Extracts with Antioxidant Potential. *Antioxidants* **2023**, *12*, 2041. [CrossRef]
13. Savic, I.M.; Savic Gajic, I.M. Optimization Study on Extraction of Antioxidants from Plum Seeds (*Prunus domestica* L.). *Optim. Eng.* **2021**, *22*, 141–158. [CrossRef]
14. Sheikh, M.A.; Saini, C.S.; Sharma, H.K. Synergistic Effect of Microwave Heating and Hydrothermal Treatment on Cyanogenic Glycosides and Bioactive Compounds of Plum (*Prunus domestica* L.) Kernels: An Analytical Approach. *Curr. Res. Food Sci.* **2022**, *5*, 65–72. [CrossRef] [PubMed]
15. Jahangir Alam, M.; Barua Agriculture, R.; Food Canada, A. In Vitro Regeneration and Antibacterial Activity of *Prunus domestica* L. *J. BioSci. Biotechnol.* **2015**, *4*, 9–15.
16. Mehta, S.; Soni, N.; Satpathy, G.; Gupta, R.K. Evaluation of Nutritional, Phytochemical, Antioxidant and Antibacterial Activity of Dried Plum (*Prunus domestica*). *J. Pharmacogn. Phytochem.* **2014**, *3*, 166–171.
17. Shukla, R.K.; Kishan; Shukla, A.; Singh, R. Evaluation of Nutritive Value, Phytochemical Screening, Total Phenolic Content and in-Vitro Antioxidant Activity of the Seed of *Prunus domestica* L. *Plant Sci. Today* **2021**, *8*, 830–835. [CrossRef]
18. Barakat, H.; Aljutaily, T.; Almujaydil, M.S.; Algheshairy, R.M.; Alhomaid, R.M.; Almutairi, A.S.; Alshimali, S.I.; Abdellatif, A.A.H. Amygdalin: A Review on Its Characteristics, Antioxidant Potential, Gastrointestinal Microbiota Intervention, Anticancer Therapeutic and Mechanisms, Toxicity, and Encapsulation. *Biomolecules* **2022**, *12*, 1514. [CrossRef]
19. Kashyap, P.; Singh Riar, C.; Jindal, N. Detoxification of Meghalayan Cherry (*Prunus nepalensis*) Kernel and Its Effect on Structural and Thermal Properties of Proteins. *Food Res. Int.* **2023**, *164*, 112437. [CrossRef]
20. Özcan, M.M.; Ünver, A.; Arslan, D. A Research on Evaluation of Some Fruit Kernels and/or Seeds as a Raw Material of Vegetable Oil Industry. *Qual. Assur. Saf. Crops Foods* **2015**, *7*, 187–191. [CrossRef]
21. Prescha, A.; Grajzer, M.; Dedyk, M.; Grajeta, H. The Antioxidant Activity and Oxidative Stability of Cold-Pressed Oils. *JAOCS J. Am. Oil Chem. Soc.* **2014**, *91*, 1291–1301. [CrossRef]
22. Tura, M.; Mandrioli, M.; Valli, E.; Gallina Toschi, T. Quality Indexes and Composition of 13 Commercial Hemp Seed Oils. *J. Food Compos. Anal.* **2023**, *117*, 105112. [CrossRef]
23. Afonso, S.; Oliveira, I.V.; Meyer, A.S.; Aires, A.; Saavedra, M.J.; Gonçalves, B. Phenolic Profile and Bioactive Potential of Stems and Seed Kernels of Sweet Cherry Fruit. *Antioxidants* **2020**, *9*, 1295. [CrossRef] [PubMed]
24. Mohamed, D.A.; Hamed, I.M.; Mohammed, S.E. Utilization of Grape and Apricot Fruits By-Products as Cheap Source for Biologically Active Compounds for Health Promotion. *Egypt. J. Chem.* **2021**, *64*, 2037–2045. [CrossRef]
25. Bouarab Chibane, L.; Degraeve, P.; Ferhout, H.; Bouajila, J.; Oulahal, N. Plant Antimicrobial Polyphenols as Potential Natural Food Preservatives. *J. Sci. Food Agric.* **2019**, *99*, 1457–1474. [CrossRef] [PubMed]
26. Kelley, D.S.; Adkins, Y.; Laugero, K.D. A Review of the Health Benefits of Cherries. *Nutrients* **2018**, *10*, 368. [CrossRef] [PubMed]
27. de Lima Cherubim, D.J.; Buzanello Martins, C.V.; Oliveira Fariña, L.; da Silva de Lucca, R.A. Polyphenols as Natural Antioxidants in Cosmetics Applications. *J. Cosmet. Dermatol.* **2020**, *19*, 33–37. [CrossRef]
28. Association of Official Analytical Chemists (AOAC). *Method 960.39*, 17th ed.; AOAC International: Gaithersburg, MD, USA, 2000.
29. Górnaś, P.; Rudzińska, M.; Raczyk, M.; Mišina, I.; Segliņa, D. Impact of Cultivar on Profile and Concentration of Lipophilic Bioactive Compounds in Kernel Oils Recovered from Sweet Cherry (*Prunus avium* L.) by-Products. *Plant Foods Hum. Nutr.* **2016**, *71*, 158–164. [CrossRef]
30. Bjelica, M.; Vujasinović, V.; Rabrenović, B.; Dimić, S. Some Chemical Characteristics and Oxidative Stability of Cold Pressed Grape Seed Oils Obtained from Different Winery Waste. *Eur. J. Lipid Sci. Technol.* **2019**, *121*, 1800416. [CrossRef]

31. Fratianni, F.; d'Acierno, A.; Ombra, M.N.; Amato, G.; De Feo, V.; Ayala-Zavala, J.F.; Coppola, R.; Nazzaro, F. Fatty Acid Composition, Antioxidant, and in vitro Anti-Inflammatory Activity of Five Cold-Pressed Prunus Seed Oils, and Their Anti-Biofilm Effect Against Pathogenic Bacteria. *Front. Nutr.* **2021**, *8*, 775751. [CrossRef]
32. Sales-Campos, H.; Reis de Souza, P.; Crema Peghini, B.; Santana da Silva, J.; Ribeiro Cardoso, C. An Overview of the Modulatory Effects of Oleic Acid in Health and Disease. *Mini-Rev. Med. Chem.* **2013**, *13*, 201–210. [CrossRef]
33. Song, J.; Kim, Y.S.; Lee, D.H.; Lee, S.H.; Park, H.J.; Lee, D.; Kim, H. Neuroprotective Effects of Oleic Acid in Rodent Models of Cerebral Ischaemia. *Sci. Rep.* **2019**, *9*, 10732. [CrossRef] [PubMed]
34. Santa-María, C.; López-Enríquez, S.; Montserrat-de la Paz, S.; Geniz, I.; Reyes-Quiroz, M.E.; Moreno, M.; Palomares, F.; Sobrino, F.; Alba, G. Update on Anti-Inflammatory Molecular Mechanisms Induced by Oleic Acid. *Nutrients* **2023**, *15*, 224. [CrossRef]
35. Patterson, E.; Wall, R.; Fitzgerald, G.F.; Ross, R.P.; Stanton, C. Health Implications of High Dietary Omega-6 Polyunsaturated Fatty Acids. *J. Nutr. Metab.* **2012**, *2012*, 539426. [CrossRef] [PubMed]
36. Marangoni, F.; Agostoni, C.; Borghi, C.; Catapano, A.L.; Cena, H.; Ghiselli, A.; La Vecchia, C.; Lercker, G.; Manzato, E.; Pirillo, A.; et al. Dietary Linoleic Acid and Human Health: Focus on Cardiovascular and Cardiometabolic Effects. *Atherosclerosis* **2020**, *292*, 90–98. [CrossRef] [PubMed]
37. Calder, P.C. Functional Roles of Fatty Acids and Their Effects on Human Health. *J. Parenter. Enter. Nutr.* **2015**, *39*, 18S–32S. [CrossRef]
38. Karsli, B. Comparative Analysis of the Fatty Acid Composition of Commercially Available Fish Oil Supplements in Turkey: Public Health Risks and Benefits. *J. Food Compos. Anal.* **2021**, *103*, 104105. [CrossRef]
39. Hashempour-Baltork, F.; Torbati, M.; Azadmard-Damirchi, S.; Savage, G.P. Chemical, Rheological and Nutritional Characteristics of Sesame and Olive Oils Blended with Linseed Oil. *Adv. Pharm. Bull.* **2018**, *8*, 107–113. [CrossRef]
40. Davis, J.P.; Raleigh, A.; Price, K.; Lisa Dean, M.L.; Sweigart Jane Cottonaro Timothy H Sanders, D.S.; Davis, J.P.; Price, K.; Dean, L.; Sweigart, D.; Cottonaro, J.; et al. Peanut Oil Stability and Physical Properties Across a Range of Industrially Relevant Oleic Acid/Linoleic Acid Ratios. *Peanut Sci.* **2016**, *43*, 1–11. [CrossRef]
41. Maszewska, M.; Florowska, A.; Dłużewska, E.; Wroniak, M.; Marciniak-Lukasiak, K.; Zbikowska, A. Oxidative Stability of Selected Edible Oils. *Molecules* **2018**, *23*, 1746. [CrossRef]
42. Lamine, M.; Mliki, A.; Mlikia, A. Genetic Diversity and Salt Tolerance in Barley Germplasm: Physiological, Biochemical & Molecular Characterization View Project Citrus Waste Valorization View Project Nutritional Quality Perceptions through Fatty Acid Profiling, Health Lipid Indices and Antioxidant Potentialities. *Open J. Nutr. Food Sci.* **2021**, *3*, 1015.
43. Gliszczyńska-Świgło, A.; Sikorska, E.; Khmelinskii, I.; Sikorski, M. Tocopherol Content in Edible Plant Oils. *Pol. J. Food Nutr. Sci.* **2007**, *57*, 157–161.
44. Bakir, D.S.; Yalcin, G.; Cucu, A.K. Isolation and Determination of Tocopherols and Tocotrienols from the Seed of Capparis Ovata Grown in Turkey by Reversed-Phase High-Performance Liquid Chromatography. *Chromatographia* **2020**, *83*, 77–86. [CrossRef]
45. Gliszczyńska-Świgło, A.; Sikorska, E. Simple Reversed-Phase Liquid Chromatography Method for Determination of Tocopherols in Edible Plant Oils. *J. Chromatogr. A* **2004**, *1048*, 195–198. [CrossRef] [PubMed]
46. Abidi, S.L.; Mounts, T.L. Reversed-Phase High-Performance Liquid Chromatographic Separations of Tocopherols. *J. Chromatogr. A* **1997**, *782*, 25–32. [CrossRef]
47. Popa, V.M.; Bele, C.; Poiana, M.A.; Dumbrava, D.; Raba, D.N.; Jianu, C. Evaluation of Bioactive Compounds and of Antioxidant Properties in Some Oils Obtained from Food Industry By-Products. *Rom. Biotechnol. Lett.* **2011**, *16*, 6234–6241.
48. Górnaś, P.; Mišina, I.; Grāvīte, I.; Lācis, G.; Radenkovs, V.; Olšteine, A.; Segliņa, D.; Kaufmane, E.; Rubauskis, E. Composition of Tocochromanols in the Kernels Recovered from Plum Pits: The Impact of the Varieties and Species on the Potential Utility Value for Industrial Application. *Eur. Food Res. Technol.* **2015**, *241*, 513–520. [CrossRef]
49. Hubert, J.; Berger, M.; Nepveu, F.; Paul, F.; Daydé, J. Effects of Fermentation on the Phytochemical Composition and Antioxidant Properties of Soy Germ. *Food Chem.* **2008**, *109*, 709–721. [CrossRef]
50. Winkler-Moser, J.K.; Breyer, L. Composition and Oxidative Stability of Crude Oil Extracts of Corn Germ and Distillers Grains. *Ind. Crops Prod.* **2011**, *33*, 572–578. [CrossRef]
51. Bruscatto, M.H.; Pestana-Bauer, V.R.; Otero, D.M.; Zambiazi, R.C. Effects of Heating Temperature on the Tocopherol Contents of Chemically and Physically Refined Rice Bran Oil. *Grasas Aceites* **2019**, *70*, 294. [CrossRef]
52. Hensley, K.; Benaksas, E.J.; Bolli, R.; Comp, P.; Grammas, P.; Hamdheydari, L.; Mou, S.; Pye, Q.N.; Stoddard, M.F.; Wallis, G.; et al. New Perspectives on Vitamin E: γ-Tocopherol and Carboxyethylhydroxychroman Metabolites in Biology and Medicine. *Free. Radic. Biol. Med.* **2004**, *36*, 1–15. [CrossRef]
53. Seppanen, C.M.; Song, Q.; Saari Csallany, A. The Antioxidant Functions of Tocopherol and Tocotrienol Homologues in Oils, Fats, and Food Systems. *JAOCS J. Am. Oil Chem. Soc.* **2010**, *87*, 469–481. [CrossRef]
54. Soares Mateus, A.R.; Pena, A.; Sendón, R.; Almeida, C.; Nieto, G.A.; Khwaldia, K.; Sanches Silva, A. By-Products of Dates, Cherries, Plums and Artichokes: A Source of Valuable Bioactive Compounds. *Trends Food Sci. Technol.* **2023**, *131*, 220–243. [CrossRef]
55. Badr, J.; Tawfik, M.K.; Badr, J.M. Analytical and Pharmacological Investigation of Amygdalin in *Prunus armeniaca* L. Kernels. *J. Pharm. Res.* **2010**, *3*, 2134–2137.
56. Blaheta, R.A.; Nelson, K.; Haferkamp, A.; Juengel, E. Amygdalin, Quackery or Cure? *Phytomedicine* **2016**, *23*, 367–376. [CrossRef] [PubMed]

57. Schrenk, D.; Bignami, M.; Bodin, L.; Chipman, J.K.; del Mazo, J.; Grasl-Kraupp, B.; Hogstrand, C.; Hoogenboom, L.; Leblanc, J.C.; Nebbia, C.S.; et al. Risk to Human Health Related to the Presence of Perfluoroalkyl Substances in Food. *EFSA J.* **2020**, *18*, e06223. [CrossRef] [PubMed]
58. Makovi, C.M.; Parker, C.H.; Zhang, K. Determination of Amygdalin in Apricot Kernels and Almonds Using LC-MS/MS. *J. AOAC Int.* **2023**, *106*, 457–463. [CrossRef]
59. Song, Z.; Xu, X. Advanced Research on Anti-Tumor Effects of Amygdalin. *J. Cancer Res. Ther.* **2014**, *10*, C3–C7. [CrossRef]
60. Salama, R.H.; Ramadan, A.E.R.G.; Alsanory, T.A.; Herdan, M.O.; Fathallah, O.M.; Alsanory, A.A. Experimental and Therapeutic Trials of Amygdalin. *Int. J. Biochem. Pharmacol.* **2019**, *1*, 21–26. [CrossRef]
61. Jasar, D.; Filipovski, V.; Kubelka -Sabit, K.; Curcic-Trajkovska, B. Potential Benefits and Controversies Related to Use Amygdalin (Vitamin B17). *J. Eng. Des.* **2008**, *23*, 57–63.
62. Tsaur, I.; Thomas, A.; Monecke, M.; Zugelder, M.; Rutz, J.; Grein, T.; Maxeiner, S.; Xie, H.; Chun, F.K.H.; Rothweiler, F.; et al. Amygdalin Exerts Antitumor Activity in Taxane-Resistant Prostate Cancer Cells. *Cancers* **2022**, *14*, 3111. [CrossRef]
63. Gago-López, N.; Lagunas Arnal, C.; Perez, J.J.; Wagner, E.F. Topical Application of an Amygdalin Analogue Reduces Inflammation and Keratinocyte Proliferation in a Psoriasis Mouse Model. *Exp. Dermatol.* **2021**, *30*, 1662–1674. [CrossRef] [PubMed]
64. Gutiérrez-Escobar, R.; Aliaño-González, M.J.; Cantos-Villar, E. Wine Polyphenol Content and Its Influence on Wine Quality and Properties: A Review. *Molecules* **2021**, *26*, 718. [CrossRef] [PubMed]
65. Yu, M.H.; Hung, T.W.; Wang, C.C.; Wu, S.W.; Yang, T.W.; Yang, C.Y.; Tseng, T.H.; Wang, C.J. Neochlorogenic Acid Attenuates Hepatic Lipid Accumulation and Inflammation via Regulating Mir-34a in Vitro. *Int. J. Mol. Sci.* **2021**, *22*, 13163. [CrossRef] [PubMed]
66. Karthikesan, K.; Pari, L.; Menon, V.P. Antihyperlipidemic Effect of Chlorogenic Acid and Tetrahydrocurcumin in Rats Subjected to Diabetogenic Agents. *Chem. Biol. Interact.* **2010**, *188*, 643–650. [CrossRef] [PubMed]
67. Tajik, N.; Tajik, M.; Mack, I.; Enck, P. The Potential Effects of Chlorogenic Acid, the Main Phenolic Components in Coffee, on Health: A Comprehensive Review of the Literature. *Eur. J. Nutr.* **2017**, *56*, 2215–2244. [CrossRef]
68. Silva, R.; Losada-Barreiro, S.; Paiva-Martins, F.; Bravo-Díaz, C. Partitioning and Antioxidative Effect of Protocatechuates in Soybean Oil Emulsions: Relevance of Emulsifier Concentration. *Eur. J. Lipid Sci. Technol.* **2017**, *119*, 1600274. [CrossRef]
69. Littlefield, D.; Zhu, T.; Buckholt, M. Effects of 2,3-Dihydroxybenzoate on Growth and Antibiotic Resistance in *E. coli*. Ph.D. Thesis, Worcester Polytechnic Institute, Worcester, MA, USA, 2023.
70. Prasad, N.R.; Jeyanthimala, K.; Ramachandran, S. Caffeic Acid Modulates Ultraviolet Radiation-B Induced Oxidative Damage in Human Blood Lymphocytes. *J. Photochem. Photobiol. B* **2009**, *95*, 196–203. [CrossRef]
71. Khan, F.A.; Maalik, A.; Murtaza, G. Inhibitory Mechanism against Oxidative Stress of Caffeic Acid. *J. Food Drug Anal.* **2016**, *24*, 695–702. [CrossRef]
72. Jericó Santos, T.R.; Santos Vasconcelos, A.G.; Lins de Aquino Santana, L.C.; Gualberto, N.C.; Buarque Feitosa, P.R.; Pires de Siqueira, A.C. Solid-State Fermentation as a Tool to Enhance the Polyphenolic Compound Contents of Acidic Tamarindus Indica by-Products. *Biocatal. Agric. Biotechnol.* **2020**, *30*, 101851. [CrossRef]
73. Bhanja Dey, T.; Chakraborty, S.; Jain, K.K.; Sharma, A.; Kuhad, R.C. Antioxidant Phenolics and Their Microbial Production by Submerged and Solid State Fermentation Process: A Review. *Trends Food Sci. Technol.* **2016**, *53*, 60–74. [CrossRef]
74. Cisneros-Yupanqui, M.; Rizzi, C.; Mihaylova, D.; Lante, A. Effect of the Distillation Process on Polyphenols Content of Grape Pomace. *Eur. Food Res. Technol.* **2022**, *248*, 929–935. [CrossRef]
75. Marinova, E.M.; Yanishlieva, N. V Antioxidant Activity and Mechanism of Action of Some Phenolic Acids at Ambient and High Temperatures. *Food Chem.* **2003**, *81*, 189–197. [CrossRef]
76. Maier, T.; Schieber, A.; Kammerer, D.R.; Carle, R. Residues of Grape (*Vitis vinifera* L.) Seed Oil Production as a Valuable Source of Phenolic Antioxidants. *Food Chem.* **2009**, *112*, 551–559. [CrossRef]
77. Gómez-Mejía, E.; Roriz, C.L.; Heleno, S.A.; Calhelha, R.; Dias, M.I.; Pinela, J.; Rosales-Conrado, N.; León-González, M.E.; Ferreira, I.C.F.R.; Barros, L. Valorisation of Black Mulberry and Grape Seeds: Chemical Characterization and Bioactive Potential. *Food Chem.* **2021**, *337*, 127998. [CrossRef]
78. Akbari, S.; Abdurahman, N.H.; Yunus, R.M.; Alara, O.R.; Abayomi, O.O. Extraction, Characterization and Antioxidant Activity of Fenugreek (Trigonella-Foenum Graecum) Seed Oil. *Mater. Sci. Energy Technol.* **2019**, *2*, 349–355. [CrossRef]
79. Chamberlin, K.D.; Melouk, H.A.; Madden, R.; Dillwith, J.W.; Bannore, Y.; El Rassi, Z.; Payton, M. Determining the Oleic/Linoleic Acid Ratio in a Single Peanut Seed: A Comparison of Two Methods. *Peanut Sci.* **2011**, *38*, 78–84. [CrossRef]
80. Nimse, S.B.; Pal, D. Free Radicals, Natural Antioxidants, and Their Reaction Mechanisms. *RSC Adv.* **2015**, *5*, 27986–28006. [CrossRef]
81. Natić, M.; Zagorac, D.D.; Ćirić, I.; Meland, M.; Rabrenović, B.; Akšić, M.F. Cold Pressed Oils from Genus Prunus. In *Cold Pressed Oils: Green Technology, Bioactive Compounds, Functionality, and Applications*; Elsevier: Amsterdam, The Netherlands, 2020; pp. 637–658. [CrossRef]
82. Grosshagauer, S.; Steinschaden, R.; Pignitter, M. Strategies to Increase the Oxidative Stability of Cold Pressed Oils. *LWT* **2019**, *106*, 72–77. [CrossRef]
83. Ibrahim Fouad, G.; Zaki Rizk, M. Possible Neuromodulating Role of Different Grape (*Vitis vinifera* L.) Derived Polyphenols against Alzheimer's Dementia: Treatment and Mechanisms. *Bull. Natl. Res. Cent.* **2019**, *43*, 108. [CrossRef]

84. Vahedi-Mazdabadi, Y.; Karimpour-Razkenari, E.; Akbarzadeh, T.; Lotfian, H.; Toushih, M.; Roshanravan, N.; Saeedi, M.; Ostadrahimi, A. Anti-Cholinesterase and Neuroprotective Activities of Sweet and Bitter Apricot Kernels (*Prunus armeniaca* L.). *Iran. J. Pharm. Res.* **2020**, *19*, 216–224. [CrossRef]
85. Gómez-Mejía, E.; Vicente-Zurdo, D.; Rosales-Conrado, N.; León-González, M.E.; Madrid, Y. Screening the Extraction Process of Phenolic Compounds from Pressed Grape Seed Residue: Towards an Integrated and Sustainable Management of Viticultural Waste. *LWT* **2022**, *169*, 113988. [CrossRef]
86. Dhellot, J.R.; Matouba, E.; Maloumbi, M.G.; Nzikou, J.M.; Ngoma, D.G.S.; Linder, M.; Desobry, S.; Parmentier, M. Extraction, Chemical Composition and Nutrional Characterization of Vegetable Oils: Case of Amaranthus Hybridus (Var 1 and 2) of Congo Brazzaville. *Afr. J. Biotechnol.* **2006**, *5*, 1095–1101.
87. Muir, R.M.; Ibáñez, A.M.; Uratsu, S.L.; Ingham, E.S.; Leslie, C.A.; McGranahan, G.H.; Batra, N.; Goyal, S.; Joseph, J.; Jemmis, E.D.; et al. Mechanism of Gallic Acid Biosynthesis in Bacteria (*Escherichia coli*) and Walnut (*Juglans regia*). *Plant Mol. Biol.* **2011**, *75*, 555–565. [CrossRef] [PubMed]
88. Kępa, M.; Miklasińska-Majdanik, M.; Wojtyczka, R.D.; Idzik, D.; Korzeniowski, K.; Smoleń-Dzirba, J.; Wasik, T.J. Antimicrobial Potential of Caffeic Acid against Staphylococcus Aureus Clinical Strains. *BioMed Res. Int.* **2018**, *2018*, 7413504. [CrossRef] [PubMed]
89. Boo, Y.C. P-Coumaric Acid as an Active Ingredient in Cosmetics: A Review Focusing on Its Antimelanogenic Effects. *Antioxidants* **2019**, *8*, 275. [CrossRef] [PubMed]
90. Pei, K.; Ou, J.; Huang, J.; Ou, S. P-Coumaric Acid and Its Conjugates: Dietary Sources, Pharmacokinetic Properties and Biological Activities. *J. Sci. Food Agric.* **2016**, *96*, 2952–2962. [CrossRef]
91. Ogbuta, A.A.; Given, O.T.; Ebinistei, P.; Alexis, E.O.; Wellington, E.O.; Teke, E.C.; Manda, A.E. Protective Effects of Trans-Ferulic Acid on Tamoxifen Induced Heptatic and Renal Oxidative Stress in Male Wister Albino Rat. *J. Appl. Sci. Environ. Manag.* **2023**, *27*, 1727–1732. [CrossRef]
92. Association of Official Analytical Chemists (AOAC). *AOAC Method 925.10 (Air Oven Method) for Moisture in Flour*, 17th ed.; AOAC International: Gaithersburg, MD, USA, 2000.
93. The Comission of the European Communities. *Commission Regulation (EC) No 796/2002 of 6 May 2002 Amending Regulation (EEC) No 2568/91 on the Characteristics of Olive Oil and Olive-Pomace Oil and on the Relevant Methods of Analysis and the Additional Notes in the Annex to Council Regulation (EEC) No 2658/87 on the Tariff and Statistical Nomenclature and on the Common Customs Tariff*; The Comission of the European Communities: Brussels, Belgium, 2002.
94. García-González, A.; Velasco, J.; Velasco, L.; Ruiz-Méndez, M.V. An Analytical Simplification for Faster Determination of Fatty Acid Composition and Phytosterols in Seed Oils. *Food Anal. Methods* **2018**, *11*, 1234–1242. [CrossRef]
95. Vicente-Zurdo, D.; Romero-Sánchez, I.; Rosales-Conrado, N.; León-González, M.E.; Madrid, Y. Ability of Selenium Species to Inhibit Metal-Induced Aβ Aggregation Involved in the Development of Alzheimer's Disease. *Anal. Bioanal. Chem.* **2020**, *412*, 6485–6497. [CrossRef]
96. Tang, M.; Taghibiglou, C.; Liu, J. The Mechanisms of Action of Curcumin in Alzheimer's Disease. *J. Alzheimer's Dis.* **2017**, *58*, 1003–1016. [CrossRef]

International Journal of
Molecular Sciences

MDPI

Review

Sirtuins as Players in the Signal Transduction of *Citrus* Flavonoids

Giovanni Enrico Lombardo [1], Caterina Russo [1], Alessandro Maugeri [2,*] and Michele Navarra [1]

[1] Department of Chemical, Biological, Pharmaceutical and Environmental Sciences, University of Messina, 98166 Messina, Italy; gelombardo@unime.it (G.E.L.); carusso@unime.it (C.R.); mnavarra@unime.it (M.N.)
[2] Department of Veterinary Sciences, University of Messina, 98168 Messina, Italy
* Correspondence: amaugeri@unime.it

Abstract: Sirtuins (SIRTs) belong to the family of nicotine adenine dinucleotide (NAD^+)-dependent class III histone deacetylases, which come into play in the regulation of epigenetic processes through the deacetylation of histones and other substrates. The human genome encodes for seven homologs (SIRT1-7), which are localized into the nucleus, cytoplasm, and mitochondria, with different enzymatic activities and regulatory mechanisms. Indeed, SIRTs are involved in different physio-pathological processes responsible for the onset of several human illnesses, such as cardiovascular and neurodegenerative diseases, obesity and diabetes, age-related disorders, and cancer. Nowadays, it is well-known that *Citrus* fruits, typical of the Mediterranean diet, are an important source of bioactive compounds, such as polyphenols. Among these, flavonoids are recognized as potential agents endowed with a wide range of beneficial properties, including antioxidant, anti-inflammatory, hypolipidemic, and antitumoral ones. On these bases, we offer a comprehensive overview on biological effects exerted by *Citrus* flavonoids via targeting SIRTs, which acted as modulator of several signaling pathways. According to the reported studies, *Citrus* flavonoids appear to be promising SIRT modulators in many different pathologies, a role which might be potentially evaluated in future therapies, along with encouraging the study of those SIRT members which still lack proper evidence on their support.

Keywords: SIRT1; SIRT2; SIRT3; SIRT4; SIRT5; SIRT6; SIRT7; polyphenols; flavonoids; *Citrus* fruits

Citation: Lombardo, G.E.; Russo, C.; Maugeri, A.; Navarra, M. Sirtuins as Players in the Signal Transduction of *Citrus* Flavonoids. *Int. J. Mol. Sci.* **2024**, *25*, 1956. https://doi.org/10.3390/ijms25041956

Academic Editor: Juan Antonio Giménez-Bastida

Received: 29 December 2023
Revised: 2 February 2024
Accepted: 3 February 2024
Published: 6 February 2024

1. Introduction

Sirtuins, known as silent information regulator proteins (SIRTs), are nicotine adenine dinucleotide (NAD^+)-dependent class III histone deacetylases, able to regulate epigenetic processes by removing the acetylated groups from histones and other substrates [1,2]. Indeed, in recent decades, SIRTs emerged for their capability to also target transcription factors and metabolic enzymes, playing a pivotal role in the regulation of cellular homeostasis [3]. The chemical reaction promoted by SIRTs consists initially of the cleavage of the *N*-glycosidic bond of NAD^+, forming an imidate intermediate, which can either combine with nicotinamide, regenerating NAD^+, or proceed forward until deacetylation. The latter is favored by the formation of a bicyclic intermediate through the nucleophilic bond between the imidate and the 2′-OH group. Finally, the collapse of the bicyclic intermediate leads to the deacetylated lysine product (Figure 1) [4].

Interestingly, SIRTs are found in all living organisms, phylogenetically conserved in eubacteria, archaea, and eukaryotes [5,6]. In this regard, the first member of this family was the silent information regulator 2 (Sir2p), originally known as mating type regulator 1 protein (MAR1), discovered more than 40 years ago by Karl and collaborators in the budding of *Saccharomyces cerevisiae* [7]. The human genome encodes for seven homologs (SIRT1-7) with different enzymatic activities, regulatory mechanisms, subcellular localizations, and targets [8]. In particular, SIRT1 is localized in the nucleus, where it interacts with several transcription regulator factors, while SIRT2 is predominant in the cytosol, although it can also translocate into the nucleus [5,9]. SIRT3, SIRT4, and SIRT5 are mitochondrial enzymes

and play a key role in a wide range of mitochondrial metabolic processes, whereas SIRT6 and SIRT7 are located in the nucleus and nucleolus, respectively [10]. From a structural point of view, human SIRTs are characterized by a common core of about 250 amino acids with N- and C-terminal regions of different length acquiring diverse conformational states, which permit bonds with multiple substrates exerting different features in the cells [11].

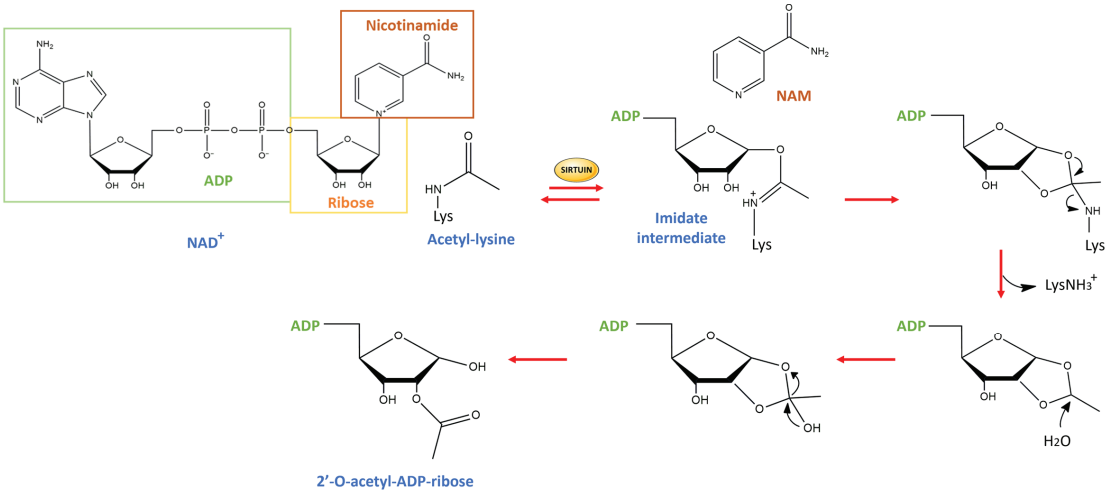

Figure 1. The chemical reaction catalyzed by SIRTs consists of forming an imidate intermediate, which can either combine with nicotinamide, regenerating NAD^+, or proceed forward until deacetylation of acetyl-lysine residues.

The SIRT family plays a biological role in the human organism as well as in specific disease cases. Physiologically, SIRTs are implied in several processes which take place within the cell, such as energy metabolism, through regulation of mitochondrial (i.e., SIRT1, SIRT3) and ribosome (SIRT7) biogenesis and maintaining lipid (i.e., SIRT1, SIRT5, and SIRT6), glucose (i.e., SIRT4 and SIRT6), and protein (i.e., SIRT5) homeostasis. Growth, differentiation, and cell death are also subjected to the control of SIRTs, through regulation of the cell cycle (i.e., SIRT2) and chromatin formation (i.e., SIRT1). SIRTs are also able to guarantee genomic stability, to monitor biological processes such as those of DNA transcription and repair, and microtubule organization (i.e., SIRT6) [12]. In addition, mechanisms of neurogenesis and protective effects against oxidative (i.e., SIRT3) and inflammatory (i.e., SIRT6) events depend on SIRT activity as well [13]. On these bases, SIRTs act as "cellular sensors" since, in response to stress phenomena caused by metabolic deficits or oxidative damage, they counteract aging by contributing to cell survival [14] (Figure 2). Consistent with this, changes in SIRT expression and activity are associated with pathological conditions, ranging from insulin resistance and type 2 diabetes (T2D) [15], to oxidative stress and kidney damage [16], cardiovascular and gynecological diseases [2,17,18], rheumatoid arthritis [19], neuro-inflammation [20,21], and various types of cancer [22–24]. In this light, a regulation of SIRT activity might support the treatment of the above-mentioned diseases.

Nowadays, we are observing an ever-increasing interest in phytochemicals from several plant sources. This is due mainly to their beneficial effects in counteracting a wide plethora of illnesses such as obesity and its related comorbidities [25,26], inflammation [27,28], cancer [29,30] and neurodegeneration [31,32]. Phytochemicals are organic metabolites produced by plants and fungi and can be classified in two groups according to their functions. The first group includes primary metabolites involved in plant growth, development, reproduction, and metabolism, while the second one consists of secondary metabolites, which are able to protect plants from injury and diseases [33]. Among the

latter, flavonoids are largely studied for their capability to protect and mitigate several diseases, exerting many different biological effects such as cardio-protective [34], anti-cancer [35,36], neuroprotective [37], antioxidant [38], and anti-obesity effects, as well as their role in the management of insulin resistance [39,40]. Interestingly, several scientific reports highlighted the beneficial effects of flavonoids contained in both *Citrus* fruits and their juices that, together with their byproducts [41], represent a real treasure for human health [42,43], for their capability to target multiple molecular targets [44–47].

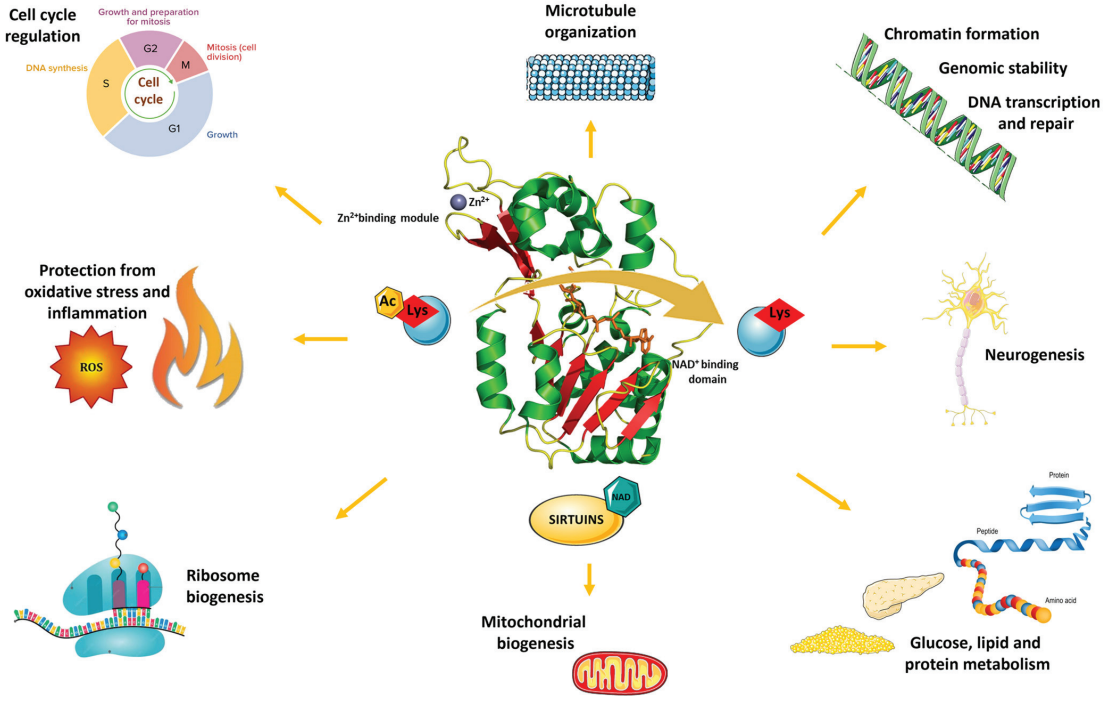

Figure 2. Biological effects mediated by the deacetylase activity of SIRTs.

This review collects the most relevant evidence on the potential of *Citrus* flavonoids to target and modulate human SIRTs, thus shedding light on the key role of these proteins in several physio-pathological processes for eventual future therapeutic approaches.

2. *Citrus* Fruits and their Flavonoids

Citrus fruits are typical of the Mediterranean diet and represent one of the pillars of many other dietary patterns. According to several studies, *Citrus* derivatives play a pivotal role in the prevention and/or management of different diseases [48–50]. The actors of these effects are acknowledged to be the flavonoids present in *Citrus* fruits. The biosynthesis of these compounds arises from the oxidative deamination of the aromatic amino acid phenylalanine and tyrosine in plants. The originated coumaroyl derivative can either undergo oxidation to give molecules such as caffeic and ferulic acids, or condensate with hydroxybenzyl derivatives (i.e., gallic acid), coming from the shikimate pathway, to give chalcones. The cyclization of these latter compounds creates the backbone of flavonoids, which is a benzo-pyrone moiety. Depending on the presence of unsaturation in the pyrone ring, flavonoids may be divided into flavones and flavanones [38]. In addition, the presence of a hydroxy group in the pyrone ring characterizes two other subclasses, namely flavonols (3-hydroxyflavones) and flavanonols (3-hydroxyflavanone). The most representative ones in *Citrus* fruits are flavones, flavanones, and flavonols (Figure 3). This basic structure can

be variously substituted with both hydroxy and methoxy groups. In particular, in *Citrus* fruits, polyhydroxy flavonoids are generally present in juice and pulp, while polymethoxy flavonoids are present in the peel, and hence in the essential oils [51]. The aglycones can be also linked to sugar residues, which are commonly D-glucose and L-rhamnose in *Citrus* fruits, via the hydroxy groups (O-glycosides) or, less commonly for *Citrus* fruits, via the carbons of the benzopyrone moiety (C-glycosides).

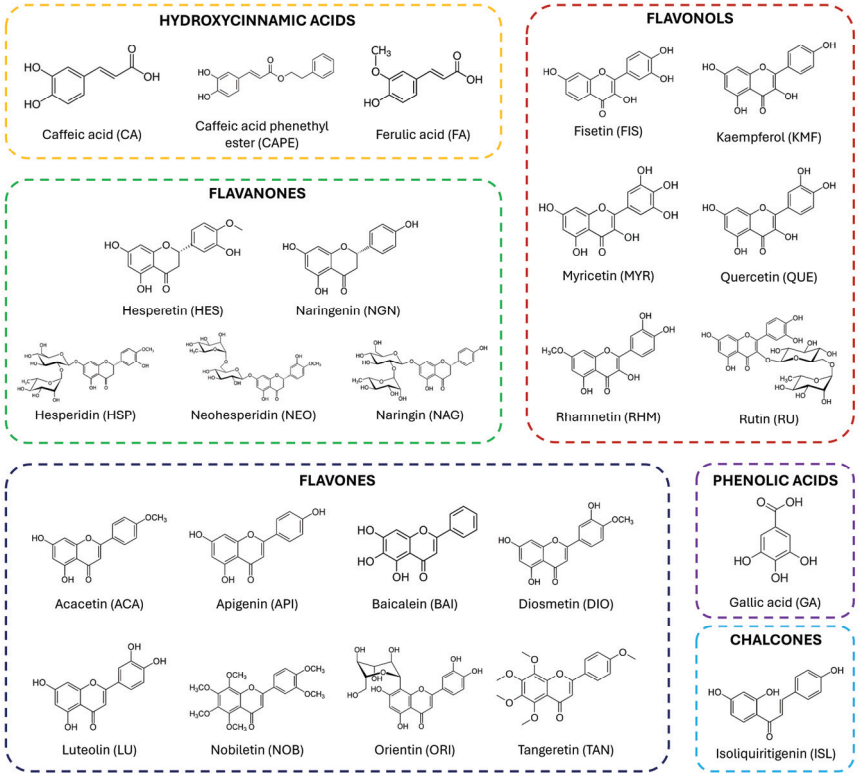

Figure 3. Molecular structures of the main flavonoids and polyphenolic precursors present in *Citrus* fruits and investigated for their role in the various SIRTs.

Among the *Citrus* species mainly cultivated, *Citrus sinensis* (orange) represents the most relevant fruit crop worldwide. An interesting anti-anxiety property has been ascribed to the essential oil of this fruit [52]. It has been reported that orange juice intake improves lipid metabolism by reducing triglycerides and cholesterol levels in obese and insulin-resistant subjects [53]. Interestingly, it is the flavonoid content in orange juice that is crucial in its effects. Indeed, several studies reported that the flavonoid-rich extract from orange juice (OJe) exerts, among other things, anti-inflammatory [54] and anti-convulsant [55] effects.

Citrus limon (lemon) is the other uncontested member of the *Citrus* genus and several studies report its beneficial effects on human health [56]. Indeed, it has been shown that in lemon juice nanovesicles, plenty of flavonoids hampered the proliferation of different tumor cell lines by activating TRAIL-mediated apoptotic cell death [57]. These flavonoid-rich nanovesicles have been also shown to inhibit redox imbalance in H_2O_2-stressed human dermal fibroblasts, via the AhR/nuclear transcription factor 2 (Nrf2) signaling pathway, as well as in LPS-stressed zebrafish [58].

Other scientific reports investigated the beneficial effects of *Citrus reticulata* (mandarin) juice (MJ) in both in vitro and in vivo experimental models. In particular, Testai and collaborators highlighted MJ capability to counteract metabolic syndrome, improving mitochondrial membrane potential in high-fat diet-fed rats [59]. On the other hand, it has been found that MJ is able to restore mitochondrial membrane potential, exerting antioxidant effects [60], as well as to hamper the proliferation and migration of anaplastic thyroid cancer cells [61].

Citrus bergamia Risso (bergamot) is cultivated to retrieve its essential oil (BEO), mainly employed in the perfume industry and aromatherapy [62]. Moreover, it has been found that BEO is able to exert anti-inflammatory and analgesic properties [63], while its coumarin fraction at low concentration hinders cancer cell proliferation [64]. Bergamot juice (BJ), which was considered as an industrial byproduct until the last decade, has been recently considered together with its flavonoid-rich extract (BJe), for its anti-inflammatory [65], anticancer [66,67], and anti-infective [68,69] properties, and in association with resveratrol and curcumin, it was shown to be able to mitigate cadmium-induced kidney damage [70]. Furthermore, recent studies highlighted that bergamot flavonoid fraction can be employed in the management of metabolic syndrome and against non-alcoholic fatty liver diseases (NAFLDs) [71,72].

3. SIRT1

SIRT1 is found in the cellular nucleus, and it is encoded by the *SIRT1* gene located on chromosome 10q22.1. It is characterized by a catalytic core containing a fold with a larger NAD^+ binding sub-domain of Rossman and a smaller subdomain containing a Zn^{2+} binding site [73] (Figure 4). Moreover, SIRT1 is able to deacetylate histones (H1, H3, and H4) and transcriptional factors such as p53 and NF-κB by employing NAD^+. This mechanism permits the attachment of ADP-ribose with the acetylic moiety of the substrate, releasing nicotinamide (NAM) and 2′-O-acetyl-adenosine diphosphate-ribose [74].

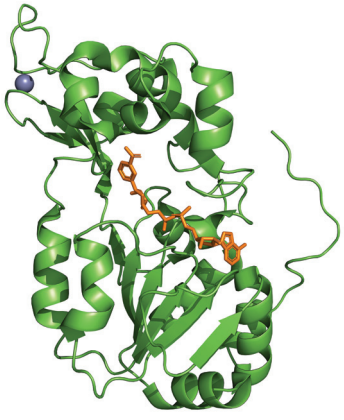

Figure 4. Crystal structure of the SIRT1 catalytic domain (in green) bound to NAD (in orange) and zinc (in violet; PDB: 4I5I).

Several studies reported the involvement of SIRT1 in the pathogenesis, development, and treatment of different illnesses, including inflammation [75], cancer [74], and neurological and metabolic diseases [76–78]. The modulation of SIRT1 is one of the multiple mechanisms by which *Citrus* flavonoids exert their biological properties.

In the context of oxidative pathogenesis, flavonoids were shown to exert a positive modulation on SIRT1. Indeed, in oxidative stress conditions such as those caused by exposure to environmental contaminants, Helmy and co-workers demonstrated that hesperidin (HES) exerts antioxidant effects through SIRT1 activation. This counteracted the aberration

of miR-126-3p and miR-181a observed in testicular damage and promoted their expression [79]. In addition, the flavonoid fisetin (FIS) was able to improve the quality of sperm in Wistar rats, by counteracting oxidative toxicity induced by glutamate at the testicular level [80], via an increase in SIRT1 and p-AMPK. Similarly, a common *Citrus* flavonoid, naringenin (NGN), was able to activate the AMPKα/SIRT1 axis, thus restoring mitochondrial Ca^{2+} balance and lowering radical oxygen species (ROS) levels in in vitro and in vivo models of ROS-induced endothelial damage [81]. Consistently, the same flavonoid protected against pain sensitivity caused by chronically disturbed sleep, through the activation of SIRT1, hampering both oxidative stress and inflammation [82].

Given the well-known link between inflammation and oxidative stress, it has been reported that FIS and the quercetin (QUE) glycoside, rutin (RU), mitigated both inflammation and oxidative stress in nucleus pulposus of mesenchymal stem cells (NPMSCs) and in chondrocytes, respectively, by activating SIRT1 [83,84]. Along the same line, an increase in SIRT1 deacetylase activity mediated by myricetin (MYR) was associated with NF-κB inhibition in A549 cells according to an in vitro model of chronic obstructive pulmonary diseases and asthma [85]. This flavonoid has been largely studied for its antioxidant, antifungal [86], antiviral [87], neuroprotective [88], and anticancer [89] properties. Interestingly, Wang and colleagues proved that HES was capable of counteracting both inflammation and oxidative stress, via SIRT1/peroxisome proliferator-activated receptor-gamma coactivator 1-alpha (PGC-1α)/NF-κB signaling pathways [90]. Remarkably, through the same mechanism of action, NGN was able to regulate ovarian function in polycystic ovary syndrome [91]. Another molecular mechanism underlying the anti-inflammatory and antioxidant effects of *Citrus* flavonoids leading to SIRT1 upregulation was investigated by Abo El-Magd. In this study, HES was able to hamper both inflammation and oxidative stress through the activation of the FOXO/SIRT1 axis in a murine model of hepatic encephalopathy [92]. Interestingly, the flavone luteolin (LU), largely found in *Citrus* fruits, revealed its capability to hamper renal fibrosis acting on the same SIRT1/FOXO3 pathway [93].

Several studies supported the involvement of the AMPK/SIRT1 axis in the anti-inflammatory effects observed for flavonoids. Remarkably, Risitano and co-workers reported that BJe was able to mitigate the inflammatory response in LPS-stimulated THP-1 cells, through SIRT1-mediated NF-κB inhibition [94]. Interestingly, molecular mechanisms underlying the anti-inflammatory effect of Bje were deeply investigated by Maugeri and colleagues. This study reported that this extract and its single flavonoids are direct activators of SIRT1 in both cell-free and in silico experimental models, and it was able to increase SIRT1 deacetylase activity by a mechanism implying 5′ adenosine monophosphate-activated protein kinase (AMPK) activation in vitro [95].

This mechanism was common to the other two in vitro studies. Indeed, naringin (NAR) and hesperetin (HSP) exerted their anti-inflammatory effects in human nucleus pulposus cells (NPCs) [96] and hepatocellular carcinoma (HepG2) cell lines [97], via activation of the SIRT1/AMPK axis. Again, this activation was favored by other *Citrus* flavonoids, including LU, orientin (ORI), and tangeretin (TAN). In this way, LU prevented atherosclerosis in LDL receptor-deficient mice by reducing macrophage inflammation [98], while ORI was able to mitigate mitochondrial dysfunction in rat NPCs [99]. Finally, TAN showed both anti-inflammatory and antioxidant properties in an in vitro model of neuroprotection, promoting both the upregulation of SIRT1 and the phosphorylation of AMPK, which hindered NF-κB activation [100]. Similarly, caffeic acid (CA) and its phenethyl ester (CAPE), activating the AMPK/SIRT1 axis, showed neuroprotective effects against Cd-induced neurotoxicity, by attenuating neuronal apoptosis and neuro-inflammation [101,102]. Therefore, the activation of AMPKα/SIRT1 pathways can be considered as one of the most important mechanisms by which *Citrus* flavonoids exert their biological effects.

At a central level, other mechanisms involving SIRT1 accounted for the protective effects of flavonoids, mainly related to their antioxidant and anti-inflammatory properties. This is the case of NGN, well-known for its different biological effects [42], some of which are related to SIRT1 modulation. Indeed, a recent study, carried out both in vitro and

in vivo, revealed that NGN protected from both brain function decline and dry age-related macular degeneration, by exerting SIRT1-mediated antioxidant effects [103,104]. Furthermore, the activation of SIRT1 by HES promoted the inhibition of NADPH oxidase-4 (NOX4) expression and protection against oxidative and inflammatory damage characterizing an in vivo model of neuropathy [105]. Remarkably, neurological dysfunctions also represent one of the most relevant age-related disorders. In this regard, Ahmad and co-workers observed that FIS was able to mitigate both inflammation and oxidative stress by modulating SIRT1/Nrf2 signaling pathways and suppressing the activated c-Jun N-terminal kinase (p-JNK)/NF-κB pathways in an in vivo model of age-related neurological disorders [106]. Finally, flavanone NAR might be considered as a therapeutic tool in the management of age-related disorders for its capability to counteract mitochondrial dysfunction in mice, through the activation of SIRT1 [107].

Interesting SIRT1-mediated anti-inflammatory mechanisms also concern the metabolic context. Several studies collected in a narrative review highlighted the beneficial effects of polyphenols on metabolic disease linked to their anti-inflammatory properties [40]. Indeed, the flavonoid nobiletin (NOB) was able to reduce liver inflammation and fibrosis through the suppression of the NOD-like receptor thermal protein domain-associated protein 3 (NLRP3) inflammasome in a SIRT1-dependent manner [108]. Liver inflammation was also mitigated by HSP, another relevant flavonoid found in *Citrus* fruits, exerting, similar to HES, antioxidant, anti-inflammatory, and anticancer properties, and also counteracting lung disorders [109–111]. In particular, HSP acted as a SIRT1 activator, which in turn led to the suppression of RelA/p65 acetylation, hampering NF-κB activation [112]. In the same context, Hua and co-workers proposed NGN as an activator of SIRT1 in the liver, leading to the improvement of non-alcoholic steatohepatitis (NASH). As a SIRT1 activator, NGN hindered hepatic inflammation and oxidative stress by promoting the deacetylation of liver kinase B1 (LKB1), PGC-1α, and NF-κB [113]. Interestingly, the same flavonoid was also able to prevent the pathogenesis of fibrotic disorders in vivo and in vitro through the regulation of signaling molecules, such as SIRT1, NF-κB, and ROS [114].

Moreover, it was recently reported that treatment with diosmin (DIO) against colitis counteracted colon oxidative damage and inflammation, through the upregulation of SIRT1 circular RNA (Circ-SIRT1) [115]. Also noteworthy is a study in which the association of HES and QUE increased SIRT1 levels in the liver and kidneys of diabetic rats, mitigating oxidative damage and hampering NF-κB activation [116]. Along this line, considering that one of the most validated methods to evaluate liver and kidney damage is the employment of lipopolysaccharides (LPSs), Rostami and collaborators demonstrated through this method the modulatory effect of MYR on SIRT1. Indeed, MYR reduced the serum levels of hepatic parameters, as well as the oxidative and inflammatory factors, through a mechanism characterized by the upregulation of hepatic SIRT1 [117]. Similarly, endotoxemic kidney injury was mitigated by RU in C57BL/6 mice by suppressing both oxidative and inflammatory processes via the activation of SIRT1 [118].

SIRT1-mediated antioxidant and anti-inflammatory activities were also responsible for cardio-protective effects induced by flavonoids in both in vitro and in vivo models. Along this line, LU as well as RU counteracted hypoxia/reoxygenation (H/R) in an in vitro model of myocardial injury [119] as well as in vivo myocardial ischemia/reperfusion (I/R) injury via activation of the SIRT1/NLRP3/NF-κB pathway [120]. Thanks to its antioxidant and anti-inflammatory properties, HSP and FIS showed cardio-protective effects by activating the SIRT1/Nrf2 signaling pathway [121,122].

In addition to the widely discussed antioxidant and anti-inflammatory effects, *Citrus* flavonoids were shown to play a relevant role by also hampering metabolic disorders through several other mechanisms, involving SIRT1 modulation. Overweight and obesity are becoming one of the major public health problems worldwide. Among the main comorbidities related to obesity are insulin resistance and type-2 diabetes (T2D), hypertension and cardiovascular disease (CVD), dyslipidemia, NAFLD, and renal dysfunctions [25]. A recent meta-analysis highlighted the beneficial effects of polyphenol supplementation on NAFLD [123]. Indeed,

regarding disorders related to lipid metabolism, it has been demonstrated that NOB is capable of restoring the expression of SIRT1, blocked by high levels of free fatty acids in hepatocytes, thus reprogramming the altered circadian clock [124], as well as counteracting lipotoxicity in vitro [108]. On the other hand, NEO showed its therapeutic potential in the regulation of lipid metabolism by hampering lipogenesis in the liver and activating fatty acid oxidation thanks to the activation of SIRT1 [125]. The increase in SIRT1 mRNA expression was also observed in the brown adipose tissue of Swiss male mice treated with gallic acid (GA), leading to the improvement of body metabolism and glucose homeostasis [126]. In this latter context, Kaempferol 3-O-rutinoside (KOR) caused the overexpression of SIRT1, which in turn led to the upregulation of insulin-dependent phospho-insulin receptor substrate (p-IRS), protein kinase B (AKT), and AMPK signaling pathways, stimulating GLUT4 activation in vitro [127]. On the contrary, as regards liver dysfunction due to fat accumulation, Li and collaborators proposed kaempferol (KMF) as an activator of AMPK/SIRT1, in order to mitigate NAFLD [128]. Therefore, it appears that the activation of SIRT1 plays a pivotal role in the management of hepatic illnesses. Interestingly, Sayed and co-workers performed molecular docking simulations, suggesting that flavonoids are able to modulate SIRT1, eliciting pharmacologic activities in different hepatic diseases [129]. In this regard, both in vitro and in vivo studies promoted NAR as a modulator of SIRT1 activation, hindering pro-inflammatory, pro-oxidant, and pro-apoptotic signaling pathways [130].

Other biological effects of *Citrus* flavonoids mediated by SIRT1 modulation are exerted on endothelial dysfunction and cardiovascular aging [131]. In this context, NOB protected from myocardial I/R injury through the downregulation of miRNA-433 (miR-433), which favors SIRT1 upregulation [132], and it also protected against hepatic I/R injury by SIRT1/forkhead box O3a (FOXO3a) activation [133]. Again, the flavonoid NAR, isolated from immature dry fruits of *Citrus wilsonii*, was able to exert anti-apoptotic, anti-inflammatory, and antioxidant effects, attenuating the severity of myocardial I/R injury through SIRT1 activation [134]. The myocardial degenerative processes are often associated with senescence, and in this context, Testai and colleagues reported that NGN was able to target SIRT1, thus protecting against the myocardial degradative processes associated with senescence [135].

Finally, SIRT1 can be implied in tumorigenesis. In this process, an upregulation of SIRT1 was associated with the antiproliferative effect of NOB. Indeed, this flavone reduced the proliferation of nasopharyngeal carcinoma C666-1 cells, inducing apoptosis through the upregulation of the Poly ADP ribose polymerase (PARP-2)/SIRT1/AMPK axis [136]. Another interesting anticancer mechanism proposed for the employment of GA was the activation of the SIRT1/Nrf2 signaling pathways, which in turn led to the upregulation of the telomerase reverse transcriptase (*hTERT*) gene expression in HepG2 cells [137].

In Table 1, the evidence regarding the effects of flavonoids present in *Citrus* fruits through SIRT1 modulation is reported.

Table 1. Effects of *Citrus* flavonoids elicited via the modulation of SIRT1 in cells or animal models.

Experimental Models	*Citrus* Flavonoid	Effect	Reference
Wistar rats	HES	Antioxidant effect by activating miR-126-3p/miR-181a-SIRT1 network	[79]
Wistar albino rats	FIS	Reduction in testicular toxicity via SIRT1 activation	[80]
SD rats HUVEC cells	NGN	Antioxidant effect against endothelial damage by activating AMPKα/SIRT1	[81]
Swiss albino mice	NGN	Amelioration of chronic sleep deprivation-induced pain via SIRT1 activation	[82]
Primary rat NPMSCs	FIS	Anti-inflammatory and antioxidant effects mitigating intervertebral disc degeneration through the activation of SIRT1 pathway	[83]

Table 1. *Cont.*

Experimental Models	*Citrus* Flavonoid	Effect	Reference
Rat chondrocytes	RU	Mitigation of osteoarthritis pathogenesis through the activation of SIRT1	[84]
A549 cells	MYR	Anti-inflammatory effect via SIRT1/NF-κB pathway	[85]
C57BL/6 mice	HES	Anti-inflammatory and antioxidant effects by the upregulation of SIRT1/NF-κB	[90]
SD rats	NGN	Mitigation of polycystic ovary syndrome by upregulating the gut microbiota and SIRT-1/PGC-1α	[91]
SD rats	HES	Antioxidant and anti-inflammatory effects via SIRT1/FOXO activation in hepatic encephalopathy	[92]
NRK49F cells/in vivo	LU	Attenuation of renal anemia caused by renal fibrosis through the SIRT1/FOXO3 pathway	[93]
THP-1 cells	NGN, NAR, HSP, NEO	Anti-inflammatory effect through the modulation of AMPK/SIRT1 axis	[94,95]
Human NPCs	NGN	Anti-inflammatory effect through the activation of AMPK/SIRT1 axis	[96]
HepG2 cells	HSP	Anti-inflammatory effect by activating SIRT1-AMPK pathway	[97]
THP-1 cells/LDLR$^{-/-}$ knockout mice	LU	Counteraction of atherosclerosis via the AMPK/SIRT1 signaling pathway	[98]
Rat NPCs	ORI	Antioxidant effect against mitochondrial dysfunction through AMPK/SIRT1 axis	[99]
BV2 cells/primary microglia	TAN	Anti-inflammatory effect via upregulation of SIRT1 in microglia	[100]
Kunming mice	CA	Neuroprotective effect via the activation of AMPK/SIRT1	[101]
PC12 cells	CAPE	Neuroprotective effect via the activation of AMPK/SIRT1	[102]
SD rats	QUE/NGN	Anti-inflammaging effect by increasing SIRT1 level in hippocampus	[103]
Kunming mice ARPE-19 cells	NGN	Antioxidant effect by upregulation of SIRT1	[104]
SD rats Rat glial C6 cells	HES	Antioxidant and anti-inflammatory effects by SIRT1/NOX4 activation	[105]
C57BL/6N mice	FIS	Protection from neuroinflammation by activation of SIRT1/Nrf2 axis	[106]
Swiss mice	NAR	Protection from mitochondrial dysfunction in lung by activation of SIRT1	[107]
AML-12 cells	NOB	Suppression of NLRP3 inflammasome by activating SIRT1	[108]
RAW264.7/AML-12—BALB/C mice	HSP	Protection from hepatic inflammation via AMPK/CREB through SIRT1 activation	[112]
ApoE$^{-/-}$ mice AML-12 cells	NGN	Anti-inflammatory, antioxidant, antifibrotic effects in NAFLD/NASH by activating hepatic SIRT1	[113]

Table 1. *Cont.*

Experimental Models	*Citrus* Flavonoid	Effect	Reference
C57BL/6 mice/Caco-2 and IEC-6 cells	DIO	Amelioration of colon inflammation and oxidative stress via the circ-SIRT1/SIRT1 axis	[115]
Wistar rats	HES/QUE	Antioxidant effect by upregulating SIRT1, hampering NF-κB activation	[116]
C57BL/6 mice	MYR	Antioxidant and anti-inflammatory effects through the upregulation of hepatic SIRT1	[117]
C57BL/6 mice	RU	Alleviation of acute endotoxemic kidney injury by upregulating SIRT1	[118]
H9c2 cells	RU	Mitigation of H/R in myocardial injury increasing SIRT1 expression	[119]
SD rats	LU	Mitigation of myocardial ischemia reperfusion injury via SIRT1/NLRP3/NF-κB	[120]
Kunming mice	HSP	Antioxidant, anti-inflammatory effects in myocardial ischemia by activation of SIRT1/Nrf2	[121]
HepG2 cells/Primary hepatocytes from C57BL/6	NOB	Mitigation of lipid metabolism by upregulating SIRT1 in hepatocytes and circadian rhythms	[124]
HepG 2 cells/ Homozygous C57BL/6 (C57) mice	NEO	Reduction in lipid metabolism through AMPK/SIRT1/PGC-1α axis	[125]
L6 cells	KOR	Stimulation of glucose uptake through SIRT1 induction	[127]
HepG2 cells/db/db mice	KMF	Counteraction of NAFLD through the activation of SIRT1/AMPK axis	[128]
AML-12 cells	NAR	Protection from liver damage by upregulation of SIRT1	[130]
H9c2 myocardial cells	NOB	Protection against myocardial I/R injury via the modulation of the miR-433/SIRT1 axis	[132]
C57BL/6 mice	NOB	Protection against hepatic I/R via SIRT1/FOXO3a activation	[133]
SD rats	NAR	Attenuation of myocardial I/R by reducing oxidative stress and inflammation, through SIRT1 activation	[134]
Enzymatic assay, computational study, C57BL/6J, H9c2 cells	NGN	Anti-senescence effect by reducing inflammation and ROS enhancing the expression of SIRT1	[135]
C666-1 nasopharyngeal carcinoma cells	NOB	Antiproliferative effect by the upregulation of PARP-2/SIRT1/AMPK pathways	[136]

Caffeic acid (CA), caffeic acid phenethyl ester (CAPE), diosmetin (DIO), fisetin (FIS), gallic acid (GA), hesperetin (HSP), hesperidin (HES), human nucleous polposus cell (HNPc), human umbilical vein endothelial cell (HUVEC), kaempferol (KMF), kaempferol 3-O-rutinoside (KOR), luteolin (LU), myricetin (MYR), naringenin (NGN), naringin (NAR), neohesperidin (NEO), nobiletin (NOB), nucleous polposus cells (NPCs), orientin (ORI), quercetin (QUE), rutin (RU), Sprague-Dawley (SD), tangeretin (TAN).

4. SIRT2

SIRT2 possesses a catalytic core of 304 amino acids and an N-terminal helical extension of 19 residues. The catalytic core is composed of an elongated pattern with two domains; the larger can be found in many different NAD(H)/NADP(H) binding enzymes, and the smaller domain contains a structural zinc atom. These two domains are separated by a large lipophilic area containing an active site for deacetylation of substrates [138] (Figure 5).

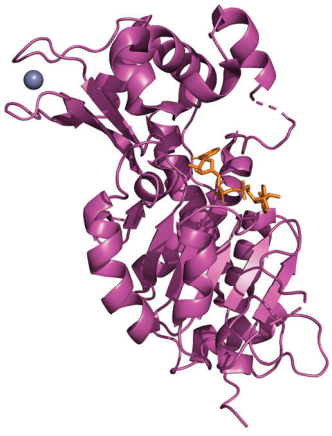

Figure 5. Human SIRT2 (in magenta) in complex with zinc (in violet) and NAD (in orange; PDB: 4RMG).

Given the multiple roles played by SIRT2 in regulating physiological and pathological signal transduction, it can be considered as a key target for the treatment of different illnesses [139], including neuroinflammation and Parkinson's disease [140,141], as well as cancer [142] and CVD [143]. Interestingly, a QUE analogue derivative, 2-Chloro-1,4-naphtoquinone-quercetin, was able to hamper SIRT2 enzymatic activity by docking the substrate in the binding site [144], thus suggesting SIRT2 inhibition as a potential mechanism through which *Citrus* flavonoids exert biological effects.

It is well-known that neurodegenerative diseases, such as Parkinson's, are associated with oxidative stress. In this regard, FIS was employed as a neuroprotective agent in a model of neuronal aging induced by oxidative stress and inflammation in rat brain. In particular, FIS exerted its neuroprotective effect by reducing pro-oxidant species and apoptotic cell death as well as ameliorating mitochondrial membrane depolarization in aging rat brain. The mechanism by which FIS exerted its effect is based on the upregulation of autophagy genes (*ATG3* and *BECN1*) and the downregulation of the *SIRT2* gene in aging brain [145]. In the same field, a recent study reported that treatment with ferulic acid (FA) causes the blocking of oxidative stress through ERK1/2-mediated activation of the Nrf2 and SIRT2 inhibition in an in vitro model of Parkinson's disease [146].

In the context of tumorigenesis, Maugeri and colleagues reported the anticancer effect of BJe against hematologic malignancies, employing THP-1 monocytes as a model of acute myeloid leukemia. Indeed, BJe exerted its anticancer effect, resulting in a reduction in cell proliferation, blockage of the cell cycle in S-phase, and induction of apoptosis. This occurred because BJe inhibited SIRT2 activity and its gene expression, thus increasing the acetylation and then activity of p53. Finally, the reduced phosphorylation of AKT resulted in the link between SIRT2 and p53, suggesting the involvement of the SIRT2/AKT/p53 pathway underlying the anti-leukemic effects mediated by Bje [147]. More in depth, it was revealed that the flavanones present in Bje, namely NAR, HSP, NGN, and NEO, can block SIRT2 activity on the isolated recombinant enzyme, and the association of both NAG and HSP reduces THP-1 cell proliferation. Moreover, as observed in docking studies, these two flavanones bind the SIRT2 inhibitory site, acting as anti-leukemic agents [148].

It is noteworthy that, in contrast to other studies, Deng and co-workers revealed that limonin (LIM), a furanolactone belonging to the limonoid family, was able to exert protective effects against doxorubicin-induced cardiotoxicity through the activation of Nrf2 and SIRT2 signaling pathways [149].

Table 2 gathers the studies dealing with the role of *Citrus* flavonoid in modulating SIRT2.

Table 2. Effects of *Citrus* flavonoids after modulation of SIRT2 in cells or animal models.

Experimental Models	*Citrus* Flavonoid	Effect	Reference
Enzymatic assay	2-Chloro-1,4-naphtoquinone-quercetin	Potent inhibition of SIRT2 enzymatic activity	[144]
Wistar rat Primary neuronal cells	FIS	Neuroprotective effect against aging-induced oxidative stress by the downregulation of *SIRT2* gene	[145]
Enzymatic assay SH-SY5Y cells	FA	Antioxidant effect via the inhibition of SIRT2 activity	[146]
THP-1 cells	NGN/HSP	Anti-leukemic effect via reduction in SIRT2 activity	[148]

Ferulic acid (FA), fisetin (FIS), hesperetin (HSP), naringenin (NGN).

5. SIRT3

SIRT3 is a NAD^+-dependent deacetylase found mainly in mitochondria. SIRT3 is the only sirtuin affecting human lifespan, playing a key role in several mitochondrial metabolic processes such as oxidative stress and energy metabolism [150] (Figure 6).

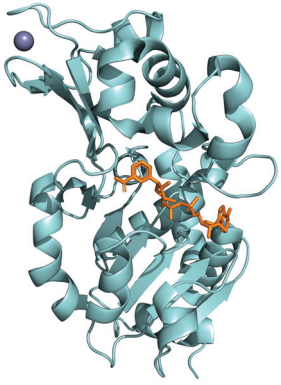

Figure 6. Crystal structure of SIRT3 (in cyan) in complex with zinc (in violet) and NAD (in orange; PDB: 4BV3).

Several studies highlighted the involvement of SIRT3 in neurodegenerative disorders [151], ischemic stroke, traumatic brain injury, intracerebral hemorrhage, neuroinflammation along with heart failure, oxidative stress, autophagy, and apoptosis [152–154]. The beneficial effects of *Citrus* flavonoids on human health have been deeply investigated, representing important ingredients for nutraceuticals and functional foods [155].

Although it is well-known that obesity-related insulin resistance may be mitigated by shifting from a high-fat diet to a normo-caloric one [156], the supplementation of *Citrus* flavonoids such as MYR to the diet could be employed as a therapeutic tool against obesity, since it was demonstrated to favor the upregulation of SIRT3 expression in adipose tissue, improving mitochondrial metabolism in C57BL6/J mice [157]. Under hyperglycemic conditions, HSP, the aglycone form of HES present in peels of *Citrus* fruits, was shown to exert protective effects by counteracting LPS-induced secretion of pro-inflammatory cytokines in THP-1 macrophages. The mechanism underlying this anti-inflammatory effect included the blocking of TLR2/4, MyD88, and NF-κB phosphorylation through the upregulation of both SIRT3 and SIRT6 [158]. Furthermore, considering that hyperglycemic conditions lead to an increase in ROS production, an interesting study revealed that FIS and LU are able to hinder ROS production in high-glucose-treated THP-1 monocytes through the activation of SIRT1, SIRT3, SIRT6, and FOXO3a [159]. Remaining in the field of diabetic pathology, it has been reported that apigenin (API) improves renal injuries in both

male Zucker lean (fa/+) rats (ZLRs) and male Zucker diabetic fatty (fa/fa) rats (ZDFRs) through the downregulation of NAD^+-degrading enzyme CD38 and the increase in both intracellular NAD^+/NADH ratio and SIRT3 [160].

At the hepatic level, Li and collaborators documented, in both in vitro and in vivo models, the anti-fibrotic effect of a monomer compound derived from HSP through the activation of AMPK/SIRT3, thus suggesting its employment as a hepatoprotective agent [161]. Similarly, this also occurred at the lung level, where baicalein (BAI) exerted its protective effect against fibrosis, regulating lung fibroblasts through an increase in SIRT3 expression [162].

However, oxidative stress and inflammation represent the main etiological causes of several pathologic conditions. Along this line, the antioxidant properties of *Citrus* flavonoids, even exerted through a modulation of SIRTs, led to beneficial effects in different ailments and oxidative disorders. NAR was able to fight mitochondrial oxidative stress in myocardial I/R-induced cardiomyocyte apoptosis through a mechanism involving the upregulation of the AMPK-SIRT3 axis [163]. Again, API exerted neuroprotective effects by increasing SIRT3 mitochondrial activity, reducing the accumulation of injured mitochondria, and promoting mitophagy [164]. Another two *Citrus* flavonoids, acacetin (ACA) and LU, were able to target SIRT3, promoting its upregulation, which in turn reduced the mitogen-activated protein kinase (MAPKs, p-38 and p-JNK) activation, by mitigating the oxidative damage and the skin photoaging caused by UVA and UVB, respectively, in both in vitro and in vivo experimental models [165,166].

Interestingly, SIRT3 was negatively associated with cancer. Consistently, Wang and colleagues reported that MYR-loaded nanoliposomes are able to inhibit cell survival in glioblastoma cells, through the downregulation of both SIRT3 and phosphorylated p53 [167].

In Table 3, the studies reporting the effects of *Citrus* flavonoids on SIRT3 are listed.

Table 3. Effects of *Citrus* flavonoids due to the modulation of SIRT3 in cells or animal models.

Experimental Models	*Citrus* Flavonoid	Effect	Reference
C3H10T1/2 cells/C57BL6/J mice	MYR	Anti-obesity effect through the upregulation of SIRT3 ex-pression in adipose tissue	[157]
THP-1 cells	HSP	Suppression of inflammation in diabetes via TLR/MyD88/NF-κB increasing SIRT3	[158]
THP-1 cells	FIS/LU	Suppression of oxidative stress in hyperglycemic condition through the upregulation of SIRT1, SIRT3, SIRT6	[159]
ZLRs and ZDFRs rats	API	Mitigates mitochondrial oxidative stress through the upregulation of SIRT3	[160]
LX-2 cells/C57BL/6J mice	HSP	Hepatoprotective effect by activating the AMPK/SIRT3 pathway	[161]
Mice	BAI	Counteraction of lung fibrosis by restoring SIRT3 expression	[162]
SD rats/H9c2 cells	NAG	Antioxidant effect in myocardial I/R through the activation of AMPK/SIRT3 axis	[163]
Swiss albino mice	API	Attenuation of neurotoxicity via promoting mitochondrial homeostasis by activating SIRT3	[164]
SD rats/Human dermal fibroblasts cells	LU	Protection from skin photoaging by upregulating the SIRT3/MAPKs axis	[165]
SD rats	ACA	Protection from skin photoaging by upregulating the SIRT3/MAPKs axis	[166]
DBTRG-05MG cells	MYR	Antiproliferative effects in glioblastoma cells by reducing SIRT3 levels	[167]

Acacetin (ACA), apigenin (API), baicalein (BAI), fisetin (FIS), hesperetin (HSP), luteolin (LU), myricetin (MYR), naringin (NAG).

6. SIRT4

Among the three mitochondrial SIRTs, SIRT4 has received the least focus from the scientific community [168]. Nevertheless, its key roles in both lipid and glutamine metabolism, as well as other possible enzymatic activities, have been reported [169]. The lack of studies is also reflected in the fact that the crystal structure of human SIRT4 is still missing, even though those of *Xenopus tropicalis* and *Danio rerio* possess a sequence similarity of the catalytic core of 67% and 65%, respectively [170] (Figure 7).

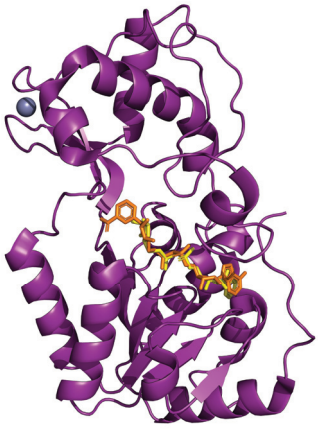

Figure 7. Crystal structure of SIRT4 (in purple) from *Xenopus tropicalis* in complex with ADP-ribose (in yellow) superimposed to NAD (in orange) and zinc (in violet; PDB: 5OJN).

Along this line, the evidence on the role of natural molecules in SIRT4 is very limited. However, it has been reported that rhamnetin (RHM), one of the most abundant methyl esters in *Citrus* fruits, protected cardiomyoblasts against H_2O_2-induced cell death, also enhancing cell protection against redox imbalance. These effects were ascribed to a modulation of mitogen-activated protein kinases (MAPKs), which were upstream influenced by an induction of both SIRT3 and SIRT4 expression, thus supporting RHM cardio-protection (Table 4) [171].

Table 4. Effects of rhamnetin in modulating SIRT4 activity.

Experimental Models	*Citrus* Flavonoid	Effect	Reference
H9c2 cardiomyoblast cells	RHM	Cardioprotective and antioxidant effects due to an increase in both SIRT3 and SIRT4 expression	[171]

Rhamnetin (RHM).

7. SIRT5

SIRT5 is a NAD^+-dependent deacetylase, containing both positively charged tyrosine and arginine in the active site, which are able to remove the acyl groups negatively charged from proteins [172]. SIRT5 consists of two domains; the larger one is a typical NAD^+ binding site containing six parallel beta-strands (β1–3 and β7–9) forming a central sheet surrounded by several alpha-helices (α1, α2, α7, α10–13), while the smaller one is characterized by structural zinc ions and five α-helices (α3–5, α8–9) and three antiparallel β-sheets (β4–6) [173] (Figure 8).

SIRT5 is mainly localized into the mitochondrial matrix, playing a key role in the detoxification of ROS and in the regulation of protein substrates in fatty acid metabolism [174]. In this regard, recent studies revealed that SIRT5 is involved in metabolic diseases, particularly in hepatic steatosis [175], in cancer, and in SARS-CoV-2 infection [176]. Emerging evidence supports the capability of QUE to modulate SIRT5 expression, promoting the mitigation

of several illnesses. In this frame, Chang and collaborators investigated the mechanism by which QUE counteracts myocardial fibrosis, improving cardiac function through an increase in SIRT5 expression, which in turn hampered oxidative stress and inflammatory response [177]. Furthermore, a recent study reported the capability of QUE to block DNA damage through the upregulation of SIRT5, which leads to the inhibition of PI3K/AKT phosphorylation, thus promoting apoptosis in an in vitro model of lung cancer [178]. In Table 5, the evidence on the effects of *Citrus* flavonoids on SIRT5 is reported.

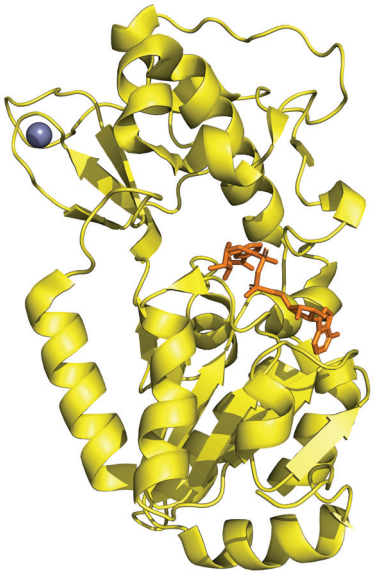

Figure 8. Crystal structure of SIRT5 (in yellow) in complex with zinc (in violet) and NAD (in orange; PDB: 3RIY).

Table 5. Effects of *Citrus* flavonoids due to the modulation of SIRT5 in cells or animal models.

Experimental Models	Citrus Flavonoid	Effect	Reference
HL-1 cells/C57BL/6J mice	QUE	Antioxidant and anti-inflammatory effects increasing SIRT5 expression	[177]
BEAS-2B, Human NSCLC, A559 and H1299 cells	QUE	Inhibition of DNA damage and induction of apoptosis via the direct binding and upregulation of SIRT5, along with the modulation of PI3K/AKT pathway	[178]

Quercetin (QUE).

8. SIRT6

SIRT6 is a nuclear member of SIRT family formed by 355 amino acids, characterized by the typical core of about 250 amino acids, plus N-terminal extension, enzymatic core domain residues, and C-terminal extension [179]. In detail, SIRT6 is characterized by two domains. The large domain contains the nucleotide binding element as well as the Rossmann fold, which is elected for NAD^+ binding. As regards the small domain, it is unique for SIRT6, containing Zn^{2+} binding loop able to stabilize the enzyme structure as well as the integrity of the catalytic domain [180] (Figure 9).

SIRT6 is able to promote long-chain fatty acid group deacetylation, as well as to catalyze the reaction of mono-ADP-ribosylation in chromatin silencing of the DNA repair proteins [181]. Moreover, SIRT6 acts as a signaling regulator of several illnesses, including

cardiovascular diseases and diabetes mellitus, and it plays a pivotal role in the regulation of brain mitochondrial processes and in cancer [17,182–185]. Interestingly, through the employment of a screening method for the identification of novel SIRT modulators from plant extract, it has been observed that QUE is a candidate able to target SIRT6 [186].

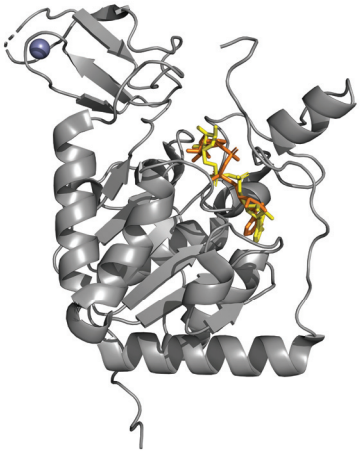

Figure 9. Crystal structure of SIRT6 (in gray) in complex with ADP-ribose (in yellow) superimposed to NAD (in orange) and zinc (in violet; PDB: 6QCD).

Structurally, You and colleagues reported that QUE-based compounds activate as well as inhibit SIRT6 through the isoform-specific binding site for pyrrolo[1,2-a]quinoxalines, which can be considered as a versatile allosteric site for the modulation of SIRT6 [187]. Biologically, the activation of SIRT6 was associated with several beneficial effects. A very recent study investigated chalcone isoliquiritigenin (ISL), present in grapefruits, highlighting its capability to upregulate SIRT6, attenuating vascular endothelial cell pyroptosis mediated by NLRP3 [188].

Since SIRT6 plays a pivotal role in glucose and lipid metabolism, several studies focused on its modulation. In particular, it has been reported that HES is able to target and increase SIRT6 expression in THP-1 cells, mitigating diabetic inflammation, through the modulation of TLR/MyD88/NF-κB signaling pathways [158]. Interestingly, in the same in vitro model, Kim and co-workers suggested that LU and FIS inhibit high glucose-induced ROS production through the activation of SIRT1, SIRT3, SIRT6, and FOXO3a [159].

Therefore, the capability of *Citrus* flavonoids to counteract inflammatory processes was observed to occur through a modulation of SIRT6. Along this line, LU suppressed in vitro TNF-α-induced inflammatory injury and senescence via the SIRT6/NF-κB [189]. To support the well-known anti-inflammatory effects of HSP, Jing and co-workers suggested that it counteracts neuro-inflammation in vivo, by mitigating oxidative stress via SIRT6/NLRP3 in mice [190]. In the same field, the CAPE appeared to play a key role in neurological complication after anesthesia and surgery though a mechanism involving SIRT6/Nrf2 activation, reducing oxidative stress and favoring microglia-protective polarization [191].

On the contrary, the downregulation of hippocampal SIRT6 induced by FA counteracted depression-like behaviors by increasing the activity of AKT/collapsin response mediator protein 2 (CRMP2) signaling in mice [192].

Table 6 lists the studies which investigated the role of SIRT6 and *Citrus* flavonoids.

Table 6. Effects of *Citrus* flavonoids due to the modulation of SIRT6 in cells or animal models.

Experimental Models	*Citrus* Flavonoid	Effect	Reference
THP-1 cells	HSP	Mitigation of diabetic inflammation through the modulation of TLR/MyD88/NF-κB signaling pathways, increasing SIRT6 expression	[158]
THP-1 cells	LU/FIS	Inhibition of ROS production through the elevation of SIRT6 and FOXO3a expression	[159]
Enzymatic assay/U2OS cells	QUE, LU	Modulation of SIRT6 activity	[187]
HUVEC cells	ISL	Decrease in vascular endothelial cell pyroptosis via the upregulation of SIRT6	[188]
HNPC cells	LU	Anti-inflammatory effect by upregulating SIRT6 and hindering the downstream activation of NF-κB pathway	[189]
C57BL/6J mice	HSP	Counteraction of neuroinflammation and oxidative stress by increasing SIRT6 levels	[190]
C57BL/6J mice/BV2 cells	CAPE	Mitigation of post-operative cognitive dysfunction, hindering oxidative stress by enhancing the SIRT6/Nrf2 pathway	[191]
C57BL/6 mice/Human HEK-293T and mouse HT-22 cells	FA	Reduction in depression-like behaviors by suppressing AKT/CRMP2 and acting as downregulator of SIRT6	[192]

Caffeic acid phenethyl ester (CAPE), ferulic acid (FA), fisetin (FIS), hesperetin (HSP), isoliquiritigenin (ISL), luteolin (LU), quercetin (QUE).

9. SIRT7

SIRT7 is a NAD^+-dependent histone deacetylase composed of 400 amino acids, showing deacetylase, desuccinylase, and deglutarylase activities [193]. SIRT7 contains a conserved catalytic core with long flanking N- and C-terminal extensions [194], and it has been reported that SIRT7 can be found in a chromatin-enriched fraction [195], despite the fact that a full crystal structure is still lacking (Figure 10).

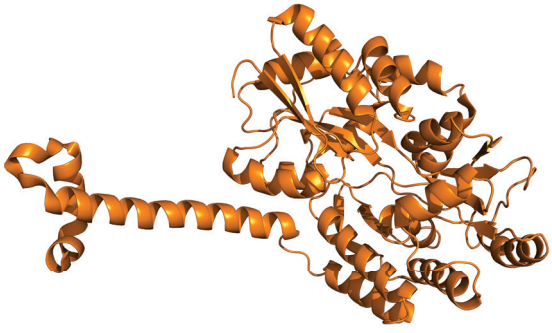

Figure 10. Crystal structure of N-terminal domain of human SIRT7 (PDB: 5IQZ).

It has been reported that SIRT7 plays a key role in the regulation of chronic inflammation [196], as well as in different kinds of cancer, including breast cancer [197], melanoma [198], and ovarian cancer [199]. As with the other SIRTs, *Citrus* flavonoids have been investigated for their effects on SIRT7. In this regard, it has been reported that HSP was able to target SIRT7, exerting a protective effect against calcific aortic valve disease both in vitro and in vivo. This effect was due to HSP's capability to directly bind SIRT7, hampering the release of pro-inflammatory cytokines and ROS production, mitigating dysfunctional mitochondria, via the upregulation of Nrf2 [200].

Another study reported that FA, at low concentration, exerted neuroprotective effects and prevented neuronal apoptosis in H_2O_2-stressed PC12 cells. This is due to the stabilization and degradation of p53 through an increase in both *SIRT1* and *SIRT7* gene expression in vitro [201]. In Table 7, the studies reporting the effects of *Citrus* flavonoids on SIRT7 are reported.

Table 7. Effects of *Citrus* flavonoids on the modulation of SIRT7 in cells or animal models.

Experimental Models	*Citrus* Flavonoid	Effect	Reference
C57BL/6 mice/ Docking studies/Human VICs	HSP	Protective effect in the aortic valve, increasing the SIRT7-mediated activation of the Nrf2–ARE axis	[200]
PC12 cells	FA	Neuroprotective effect through the upregulation of SIRT1 and SIRT7	[201]

Hesperetin (HSP), ferulic acid (FA).

10. Conclusions

SIRTs are NAD^+-dependent deacetylases able to maintain cellular homeostasis by silencing genes and modulating the activity of different factors, thus unleashing cascades of numerous events when in action. Given also their widespread localization within cells (i.e., nucleus, cytoplasm, and mitochondria), it is not surprising that SIRTs are involved in several physio-pathological conditions. During recent decades, this has captured the interest of the scientific community, which has put forth great effort to unravel the true significance of SIRT regulation in cells. The multi-target capacity of natural products perfectly accords with the essence of SIRTs. Indeed, in this review, we highlighted the fact that *Citrus* flavonoids are able to elicit a wide plethora of biological effects via modulating the activity of SIRTs, acting as crossroads. Antioxidant, anti-inflammatory, hypolipidemic, and neuroprotective effects were exhibited by flavonoids through the activation of SIRT1, SIRT3, and SIRT6. On the contrary, the inhibition of SIRT2 was mainly associated with antiproliferative and neuroprotective effects. Beneficial effects, such as cardioprotective effects, were preliminarily observed from SIRT4 activation, and anti-inflammatory and anticancer effects were related to SIRT5 activity, while neuroprotective effects were mediated by SIRT7 (Figure 11).

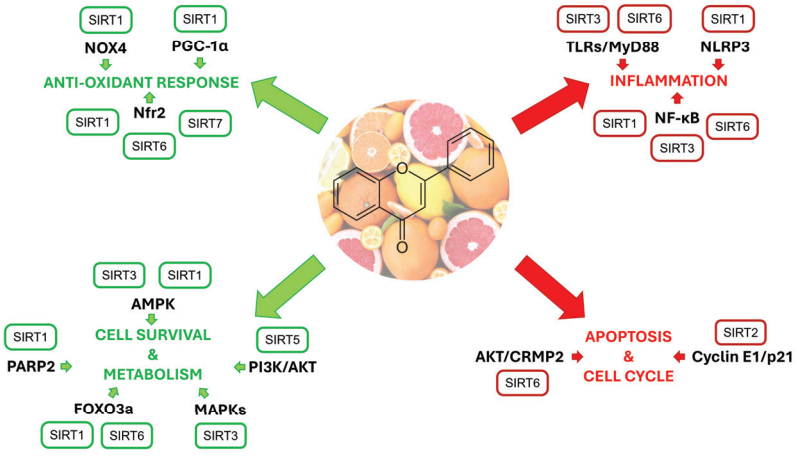

Figure 11. Pathways influenced by *Citrus* flavonoids via the modulation of SIRTs. Green arrows indicate activation, while red ones indicate inhibition.

Notably, the evidence of some members of the SIRT family is rich and robust, whereas others are still lacking studies to precisely define their role and hence investigate compounds able to target them. Considering that SIRTs belong to a family of multi-functional enzymes, a deepening of the current knowledge on the neglected SIRT members would be highly encouraged among scientists. Again, potential interactions on SIRTs or on more than one SIRT simultaneously should be considered, in order to fully define the mechanism of action and the selectivity rate of natural allies, such as *Citrus* flavonoids. Consequently, this could help to better establish their place in the management of several human illnesses.

To date, epigenetic inhibitors, such as histone deacetylase and DNA methyltransferase inhibitors, appear to represent an emerging scenario over conventional therapies, in different clinical settings. However, the impact of SIRT modulation on human health remains an open challenge among researchers. Adequate and well-established findings are essential for the development of effective therapies based on SIRTs. In this context, future investigations could pave the way towards combination therapies including natural and synthetic drugs or, even better, represent the starting point for the development of potent scaffolds targeting SIRTs.

Overall, this review helps in outlining a direction for further studies, thus suggesting *Citrus* flavonoids as holding potential promise in the development of novel effective drugs acting on the SIRT family.

Author Contributions: G.E.L. performed the literature review and drafted the paper; C.R. helped in the literature review; A.M. critically revised the paper; M.N. conceived the study and provided funding. All authors have read and agreed to the published version of the manuscript.

Funding: This research received no external funding.

Institutional Review Board Statement: Not applicable.

Informed Consent Statement: Not applicable.

Data Availability Statement: Not applicable.

Acknowledgments: A PON Industrial PhD fellowship from the Italian Minister of Instruction, University and Research (MIUR) to Caterina Russo (CUP: J11B21008430007) is gratefully acknowledged.

Conflicts of Interest: The authors declare no conflicts of interest.

References

1. Wang, Y.; He, J.; Liao, M.; Hu, M.; Li, W.; Ouyang, H.; Wang, X.; Ye, T.; Zhang, Y.; Ouyang, L. An overview of Sirtuins as potential therapeutic target: Structure, function and modulators. *Eur. J. Med. Chem.* **2019**, *161*, 48–77. [CrossRef]
2. Kratz, E.M.; Kokot, I.; Dymicka-Piekarska, V.; Piwowar, A. Sirtuins-The New Important Players in Women's Gynecological Health. *Antioxidants* **2021**, *10*, 84. [CrossRef]
3. Curry, A.M.; White, D.S.; Donu, D.; Cen, Y. Human Sirtuin Regulators: The "Success" Stories. *Front. Physiol.* **2021**, *12*, 752117. [CrossRef] [PubMed]
4. Sharma, C.; Donu, D.; Curry, A.M.; Barton, E.; Cen, Y. Multifunctional activity-based chemical probes for sirtuins. *RSC Adv.* **2023**, *13*, 11771–11781. [CrossRef] [PubMed]
5. Shoba, B.; Lwin, Z.M.; Ling, L.S.; Bay, B.H.; Yip, G.W.; Kumar, S.D. Function of sirtuins in biological tissues. *Anat. Rec.* **2009**, *292*, 536–543. [CrossRef] [PubMed]
6. Anderson, K.A.; Hirschey, M.D. Mitochondrial protein acetylation regulates metabolism. *Essays Biochem.* **2012**, *52*, 23–35. [CrossRef] [PubMed]
7. Klar, A.J.; Fogel, S.; Macleod, K. MAR1-a Regulator of the HMa and HMalpha Loci in SACCHAROMYCES CEREVISIAE. *Genetics* **1979**, *93*, 37–50. [CrossRef] [PubMed]
8. Hong, J.Y.; Lin, H. Sirtuin Modulators in Cellular and Animal Models of Human Diseases. *Front. Pharmacol.* **2021**, *12*, 735044. [CrossRef] [PubMed]
9. Kupis, W.; Palyga, J.; Tomal, E.; Niewiadomska, E. The role of sirtuins in cellular homeostasis. *J. Physiol. Biochem.* **2016**, *72*, 371–380. [CrossRef]
10. Zhang, H.N.; Dai, Y.; Zhang, C.H.; Omondi, A.M.; Ghosh, A.; Khanra, I.; Chakraborty, M.; Yu, X.B.; Liang, J. Sirtuins family as a target in endothelial cell dysfunction: Implications for vascular ageing. *Biogerontology* **2020**, *21*, 495–516. [CrossRef]
11. Sacconnay, L.; Carrupt, P.A.; Nurisso, A. Human sirtuins: Structures and flexibility. *J. Struct. Biol.* **2016**, *196*, 534–542. [CrossRef]

12. Fiorentino, F.; Mai, A.; Rotili, D. The role of structural biology in the design of sirtuin activators. *Curr. Opin. Struct. Biol.* **2023**, *82*, 102666. [CrossRef]
13. Kratz, E.M.; Solkiewicz, K.; Kubis-Kubiak, A.; Piwowar, A. Sirtuins as Important Factors in Pathological States and the Role of Their Molecular Activity Modulators. *Int. J. Mol. Sci.* **2021**, *22*, 630. [CrossRef]
14. Zietara, P.; Dziewiecka, M.; Augustyniak, M. Why Is Longevity Still a Scientific Mystery? Sirtuins-Past, Present and Future. *Int. J. Mol. Sci.* **2022**, *24*, 728. [CrossRef]
15. Kitada, M.; Ogura, Y.; Monno, I.; Koya, D. Sirtuins and Type 2 Diabetes: Role in Inflammation, Oxidative Stress, and Mitochondrial Function. *Front. Endocrinol.* **2019**, *10*, 187. [CrossRef]
16. Ogura, Y.; Kitada, M.; Koya, D. Sirtuins and Renal Oxidative Stress. *Antioxidants* **2021**, *10*, 1198. [CrossRef]
17. Saiyang, X.; Deng, W.; Qizhu, T. Sirtuin 6: A potential therapeutic target for cardiovascular diseases. *Pharmacol. Res.* **2021**, *163*, 105214. [CrossRef]
18. Velpuri, P.; Rai, V.; Agrawal, D.K. Role of sirtuins in attenuating plaque vulnerability in atherosclerosis. *Mol. Cell Biochem.* **2023**, *479*, 51–62. [CrossRef]
19. Poniewierska-Baran, A.; Bochniak, O.; Warias, P.; Pawlik, A. Role of Sirtuins in the Pathogenesis of Rheumatoid Arthritis. *Int. J. Mol. Sci.* **2023**, *24*, 1532. [CrossRef]
20. Zhang, Y.; Anoopkumar-Dukie, S.; Mallik, S.B.; Davey, A.K. SIRT1 and SIRT2 modulators reduce LPS-induced inflammation in HAPI microglial cells and protect SH-SY5Y neuronal cells in vitro. *J. Neural Transm.* **2021**, *128*, 631–644. [CrossRef]
21. Lin, J.; Xiong, Z.; Gu, J.; Sun, Z.; Jiang, S.; Fan, D.; Li, W. Sirtuins: Potential Therapeutic Targets for Defense against Oxidative Stress in Spinal Cord Injury. *Oxid. Med. Cell Longev.* **2021**, *2021*, 7207692. [CrossRef]
22. Palmirotta, R.; Cives, M.; Della-Morte, D.; Capuani, B.; Lauro, D.; Guadagni, F.; Silvestris, F. Sirtuins and Cancer: Role in the Epithelial-Mesenchymal Transition. *Oxid. Med. Cell Longev.* **2016**, *2016*, 3031459. [CrossRef]
23. Poniewierska-Baran, A.; Warias, P.; Zgutka, K. Sirtuins (SIRTs) As a Novel Target in Gastric Cancer. *Int. J. Mol. Sci.* **2022**, *23*, 15119. [CrossRef]
24. Onyiba, C.I.; Scarlett, C.J.; Weidenhofer, J. The Mechanistic Roles of Sirtuins in Breast and Prostate Cancer. *Cancers* **2022**, *14*, 5118. [CrossRef]
25. Cremonini, E.; Iglesias, D.E.; Kang, J.; Lombardo, G.E.; Mostofinejad, Z.; Wang, Z.; Zhu, W.; Oteiza, P.I. (−)-Epicatechin and the comorbidities of obesity. *Arch. Biochem. Biophys.* **2020**, *690*, 108505. [CrossRef]
26. Montalbano, G.; Maugeri, A.; Guerrera, M.C.; Miceli, N.; Navarra, M.; Barreca, D.; Cirmi, S.; Germana, A. A White Grape Juice Extract Reduces Fat Accumulation through the Modulation of Ghrelin and Leptin Expression in an In Vivo Model of Overfed Zebrafish. *Molecules* **2021**, *26*, 1119. [CrossRef]
27. Cirmi, S.; Maugeri, A.; Russo, C.; Musumeci, L.; Navarra, M.; Lombardo, G.E. Oleacein Attenuates Lipopolysaccharide-Induced Inflammation in THP-1-Derived Macrophages by the Inhibition of TLR4/MyD88/NF-kappaB Pathway. *Int. J. Mol. Sci.* **2022**, *23*, 1206. [CrossRef]
28. Maugeri, A.; Lombardo, G.E.; Cirmi, S.; Suntar, I.; Barreca, D.; Lagana, G.; Navarra, M. Pharmacology and toxicology of tannins. *Arch. Toxicol.* **2022**, *96*, 1257–1277. [CrossRef]
29. Imran, M.; Insaf, A.; Hasan, N.; Sugandhi, V.V.; Shrestha, D.; Paudel, K.R.; Jha, S.K.; Hansbro, P.M.; Dua, K.; Devkota, H.P.; et al. Exploring the Remarkable Chemotherapeutic Potential of Polyphenolic Antioxidants in Battling Various Forms of Cancer. *Molecules* **2023**, *28*, 3475. [CrossRef]
30. Darwiche, L.; Mesmar, J.; Baydoun, E.; El Kayal, W. In Vitro Evaluation of Biological and Anticancer Activities Exhibited by Five Varieties of *Vitis vinifera* L. *Int. J. Mol. Sci.* **2023**, *24*, 13440. [CrossRef]
31. El Gaamouch, F.; Chen, F.; Ho, L.; Lin, H.Y.; Yuan, C.; Wong, J.; Wang, J. Benefits of dietary polyphenols in Alzheimer's disease. *Front. Aging Neurosci.* **2022**, *14*, 1019942. [CrossRef]
32. Marino, A.; Battaglini, M.; Moles, N.; Ciofani, G. Natural Antioxidant Compounds as Potential Pharmaceutical Tools against Neurodegenerative Diseases. *ACS Omega* **2022**, *7*, 25974–25990. [CrossRef]
33. Wicinski, M.; Erdmann, J.; Nowacka, A.; Kuzminski, O.; Michalak, K.; Janowski, K.; Ohla, J.; Biernaciak, A.; Szambelan, M.; Zabrzynski, J. Natural Phytochemicals as SIRT Activators-Focus on Potential Biochemical Mechanisms. *Nutrients* **2023**, *15*, 3578. [CrossRef]
34. Wei, X.Y.; Zeng, Y.F.; Guo, Q.H.; Liu, J.J.; Yin, N.; Liu, Y.; Zeng, W.J. Cardioprotective effect of epigallocatechin gallate in myocardial ischemia/reperfusion injury and myocardial infarction: A meta-analysis in preclinical animal studies. *Sci. Rep.* **2023**, *13*, 14050. [CrossRef] [PubMed]
35. Gupta, M.; Ahmad, J.; Ahamad, J.; Kundu, S.; Goel, A.; Mishra, A. Flavonoids as promising anticancer therapeutics: Contemporary research, nanoantioxidant potential, and future scope. *Phytother. Res.* **2023**, *37*, 5159–5192. [CrossRef]
36. Maugeri, A.; Calderaro, A.; Patane, G.T.; Navarra, M.; Barreca, D.; Cirmi, S.; Felice, M.R. Targets Involved in the Anti-Cancer Activity of Quercetin in Breast, Colorectal and Liver Neoplasms. *Int. J. Mol. Sci.* **2023**, *24*, 2952. [CrossRef]
37. Siracusa, R.; Paterniti, I.; Impellizzeri, D.; Cordaro, M.; Crupi, R.; Navarra, M.; Cuzzocrea, S.; Esposito, E. The Association of Palmitoylethanolamide with Luteolin Decreases Neuroinflammation and Stimulates Autophagy in Parkinson's Disease Model. *CNS Neurol. Disord. Drug Targets* **2015**, *14*, 1350–1365. [CrossRef]
38. Abbate, F.; Maugeri, A.; Laura, R.; Levanti, M.; Navarra, M.; Cirmi, S.; Germana, A. Zebrafish as a Useful Model to Study Oxidative Stress-Linked Disorders: Focus on Flavonoids. *Antioxidants* **2021**, *10*, 668. [CrossRef]

39. Li, J.; Zhao, R.; Miao, P.; Xu, F.; Chen, J.; Jiang, X.; Hui, Z.; Wang, L.; Bai, R. Discovery of anti-inflammatory natural flavonoids: Diverse scaffolds and promising leads for drug discovery. *Eur. J. Med. Chem.* **2023**, *260*, 115791. [CrossRef]
40. Russo, C.; Maugeri, A.; Musumeci, L.; De Sarro, G.; Cirmi, S.; Navarra, M. Inflammation and Obesity: The Pharmacological Role of Flavonoids in the Zebrafish Model. *Int. J. Mol. Sci.* **2023**, *24*, 2899. [CrossRef]
41. Russo, C.; Maugeri, A.; Lombardo, G.E.; Musumeci, L.; Barreca, D.; Rapisarda, A.; Cirmi, S.; Navarra, M. The Second Life of Citrus Fruit Waste: A Valuable Source of Bioactive Compounds. *Molecules* **2021**, *26*, 5991. [CrossRef]
42. Alam, F.; Mohammadin, K.; Shafique, Z.; Amjad, S.T.; Asad, M. Citrus flavonoids as potential therapeutic agents: A review. *Phytother. Res.* **2022**, *36*, 1417–1441. [CrossRef]
43. Qiu, M.; Wei, W.; Zhang, J.; Wang, H.; Bai, Y.; Guo, D.A. A Scientometric Study to a Critical Review on Promising Anticancer and Neuroprotective Compounds: Citrus Flavonoids. *Antioxidants* **2023**, *12*, 669. [CrossRef]
44. Atoki, A.V.; Aja, P.M.; Shinkafi, T.S.; Ondari, E.N.; Awuchi, C.G. Naringenin: Its chemistry and roles in neuroprotection. *Nutr. Neurosci.* **2023**, 1–30. [CrossRef] [PubMed]
45. Hasan, A.K.; Babaei, E.; Al-Khafaji, A.S.K. Hesperetin effect on MLH1 and MSH2 expression on breast cancer cells BT-549. *J. Adv. Pharm. Technol. Res.* **2023**, *14*, 241–247. [CrossRef] [PubMed]
46. Tang, H.; Kuang, Y.; Wu, W.; Peng, B.; Fu, Q. Quercetin inhibits the metabolism of arachidonic acid by inhibiting the activity of CYP3A4, thereby inhibiting the progression of breast cancer. *Mol. Med.* **2023**, *29*, 127. [CrossRef] [PubMed]
47. Yao, C.; Dai, S.; Wang, C.; Fu, K.; Wu, R.; Zhao, X.; Yao, Y.; Li, Y. Luteolin as a potential hepatoprotective drug: Molecular mechanisms and treatment strategies. *Biomed. Pharmacother.* **2023**, *167*, 115464. [CrossRef] [PubMed]
48. Cirmi, S.; Navarra, M.; Woodside, J.V.; Cantwell, M.M. Citrus fruits intake and oral cancer risk: A systematic review and meta-analysis. *Pharmacol. Res.* **2018**, *133*, 187–194. [CrossRef] [PubMed]
49. Maugeri, A.; Cirmi, S.; Minciullo, P.L.; Gangemi, S.; Calapai, G.; Mollace, V.; Navarra, M. Citrus fruits and inflammaging: A systematic review. *Phytochem. Rev.* **2019**, *18*, 1025–1049. [CrossRef]
50. Musumeci, L.; Maugeri, A.; Russo, C.; Lombardo, G.E.; Cirmi, S.; Navarra, M. Citrus Flavonoids and Autoimmune Diseases: A Systematic Review of Clinical Studies. *Curr. Med. Chem.* **2023**, *30*, 2191–2204. [CrossRef] [PubMed]
51. Gattuso, G.; Barreca, D.; Gargiulli, C.; Leuzzi, U.; Caristi, C. Flavonoid composition of Citrus juices. *Molecules* **2007**, *12*, 1641–1673. [CrossRef] [PubMed]
52. Mannucci, C.; Calapai, F.; Cardia, L.; Inferrera, G.; D'Arena, G.; Di Pietro, M.; Navarra, M.; Gangemi, S.; Ventura Spagnolo, E.; Calapai, G. Clinical Pharmacology of Citrus aurantium and Citrus sinensis for the Treatment of Anxiety. *Evid. Based Complement. Alternat Med.* **2018**, *2018*, 3624094. [CrossRef]
53. Santos, K.G.D.; Yoshinaga, M.Y.; Glezer, I.; Chaves-Filho, A.B.; Santana, A.A.; Kovacs, C.; Magnoni, C.D.; Lajolo, F.M.; Miyamoto, S.; Aymoto Hassimotto, N.M. Orange juice intake by obese and insulin-resistant subjects lowers specific plasma triglycerides: A randomized clinical trial. *Clin. Nutr. ESPEN* **2022**, *51*, 336–344. [CrossRef] [PubMed]
54. Cirmi, S.; Randazzo, B.; Russo, C.; Musumeci, L.; Maugeri, A.; Montalbano, G.; Guerrera, M.C.; Lombardo, G.E.; Levanti, M. Anti-inflammatory effect of a flavonoid-rich extract of orange juice in adult zebrafish subjected to Vibrio anguillarum-induced enteritis. *Nat. Prod. Res.* **2021**, *35*, 5350–5353. [CrossRef]
55. Citraro, R.; Navarra, M.; Leo, A.; Donato Di Paola, E.; Santangelo, E.; Lippiello, P.; Aiello, R.; Russo, E.; De Sarro, G. The Anticonvulsant Activity of a Flavonoid-Rich Extract from Orange Juice Involves both NMDA and GABA-Benzodiazepine Receptor Complexes. *Molecules* **2016**, *21*, 1261. [CrossRef] [PubMed]
56. Klimek-Szczykutowicz, M.; Szopa, A.; Ekiert, H. Citrus limon (Lemon) Phenomenon-A Review of the Chemistry, Pharmacological Properties, Applications in the Modern Pharmaceutical, Food, and Cosmetics Industries, and Biotechnological Studies. *Plants* **2020**, *9*, 119. [CrossRef] [PubMed]
57. Raimondo, S.; Naselli, F.; Fontana, S.; Monteleone, F.; Lo Dico, A.; Saieva, L.; Zito, G.; Flugy, A.; Manno, M.; Di Bella, M.A.; et al. Citrus limon-derived nanovesicles inhibit cancer cell proliferation and suppress CML xenograft growth by inducing TRAIL-mediated cell death. *Oncotarget* **2015**, *6*, 19514–19527. [CrossRef]
58. Urzi, O.; Cafora, M.; Ganji, N.R.; Tinnirello, V.; Gasparro, R.; Raccosta, S.; Manno, M.; Corsale, A.M.; Conigliaro, A.; Pistocchi, A.; et al. Lemon-derived nanovesicles achieve antioxidant and anti-inflammatory effects activating the AhR/Nrf2 signaling pathway. *iScience* **2023**, *26*, 107041. [CrossRef]
59. Testai, L.; De Leo, M.; Flori, L.; Polini, B.; Braca, A.; Nieri, P.; Pistelli, L.; Calderone, V. Contribution of irisin pathway in protective effects of mandarin juice (*Citrus reticulata* Blanco) on metabolic syndrome in rats fed with high fat diet. *Phytother. Res.* **2021**, *35*, 4324–4333. [CrossRef]
60. Cilla, A.; Rodrigo, M.J.; De Ancos, B.; Sanchez-Moreno, C.; Cano, M.P.; Zacarias, L.; Barbera, R.; Alegria, A. Impact of high-pressure processing on the stability and bioaccessibility of bioactive compounds in Clementine mandarin juice and its cytoprotective effect on Caco-2 cells. *Food Funct.* **2020**, *11*, 8951–8962. [CrossRef]
61. Celano, M.; Maggisano, V.; De Rose, R.F.; Bulotta, S.; Maiuolo, J.; Navarra, M.; Russo, D. Flavonoid Fraction of *Citrus reticulata* Juice Reduces Proliferation and Migration of Anaplastic Thyroid Carcinoma Cells. *Nutr. Cancer* **2015**, *67*, 1183–1190. [CrossRef]
62. Chen, M.L.; Chen, Y.E.; Lee, H.F. The Effect of Bergamot Essential Oil Aromatherapy on Improving Depressive Mood and Sleep Quality in Postpartum Women: A Randomized Controlled Trial. *J. Nurs. Res.* **2022**, *30*, e201. [CrossRef]

63. Lombardo, G.E.; Cirmi, S.; Musumeci, L.; Pergolizzi, S.; Maugeri, A.; Russo, C.; Mannucci, C.; Calapai, G.; Navarra, M. Mechanisms Underlying the Anti-Inflammatory Activity of Bergamot Essential Oil and Its Antinociceptive Effects. *Plants* **2020**, *9*, 704. [CrossRef]
64. Maugeri, A.; Lombardo, G.E.; Musumeci, L.; Russo, C.; Gangemi, S.; Calapai, G.; Cirmi, S.; Navarra, M. Bergamottin and 5-Geranyloxy-7-methoxycoumarin Cooperate in the Cytotoxic Effect of Citrus bergamia (Bergamot) Essential Oil in Human Neuroblastoma SH-SY5Y Cell Line. *Toxins* **2021**, *13*, 275. [CrossRef] [PubMed]
65. Gugliandolo, E.; Fusco, R.; D'Amico, R.; Peditto, M.; Oteri, G.; Di Paola, R.; Cuzzocrea, S.; Navarra, M. Treatment With a Flavonoid-Rich Fraction of Bergamot Juice Improved Lipopolysaccharide-Induced Periodontitis in Rats. *Front. Pharmacol.* **2018**, *9*, 1563. [CrossRef]
66. Ferlazzo, N.; Cirmi, S.; Russo, M.; Trapasso, E.; Ursino, M.R.; Lombardo, G.E.; Gangemi, S.; Calapai, G.; Navarra, M. NF-kappaB mediates the antiproliferative and proapoptotic effects of bergamot juice in HepG2 cells. *Life Sci.* **2016**, *146*, 81–91. [CrossRef]
67. Navarra, M.; Femia, A.P.; Romagnoli, A.; Tortora, K.; Luceri, C.; Cirmi, S.; Ferlazzo, N.; Caderni, G. A flavonoid-rich extract from bergamot juice prevents carcinogenesis in a genetic model of colorectal cancer, the Pirc rat (F344/NTac-Apc(am1137)). *Eur. J. Nutr.* **2020**, *59*, 885–894. [CrossRef]
68. Filocamo, A.; Bisignano, C.; Ferlazzo, N.; Cirmi, S.; Mandalari, G.; Navarra, M. In vitro effect of bergamot (*Citrus bergamia*) juice against cagA-positive and-negative clinical isolates of Helicobacter pylori. *BMC Complement. Altern. Med.* **2015**, *15*, 256. [CrossRef]
69. Cirmi, S.; Bisignano, C.; Mandalari, G.; Navarra, M. Anti-infective potential of Citrus bergamia Risso et Poiteau (bergamot) derivatives: A systematic review. *Phytother. Res.* **2016**, *30*, 1404–1411. [CrossRef] [PubMed]
70. Cirmi, S.; Maugeri, A.; Micali, A.; Marini, H.R.; Puzzolo, D.; Santoro, G.; Freni, J.; Squadrito, F.; Irrera, N.; Pallio, G.; et al. Cadmium-Induced Kidney Injury in Mice Is Counteracted by a Flavonoid-Rich Extract of Bergamot Juice, Alone or in Association with Curcumin and Resveratrol, via the Enhancement of Different Defense Mechanisms. *Biomedicines* **2021**, *9*, 1797. [CrossRef] [PubMed]
71. Carresi, C.; Gliozzi, M.; Musolino, V.; Scicchitano, M.; Scarano, F.; Bosco, F.; Nucera, S.; Maiuolo, J.; Macri, R.; Ruga, S.; et al. The Effect of Natural Antioxidants in the Development of Metabolic Syndrome: Focus on Bergamot Polyphenolic Fraction. *Nutrients* **2020**, *12*, 1504. [CrossRef]
72. Musolino, V.; Gliozzi, M.; Scarano, F.; Bosco, F.; Scicchitano, M.; Nucera, S.; Carresi, C.; Ruga, S.; Zito, M.C.; Maiuolo, J.; et al. Bergamot Polyphenols Improve Dyslipidemia and Pathophysiological Features in a Mouse Model of Non-Alcoholic Fatty Liver Disease. *Sci. Rep.* **2020**, *10*, 2565. [CrossRef]
73. Nandave, M.; Acharjee, R.; Bhaduri, K.; Upadhyay, J.; Rupanagunta, G.P.; Ansari, M.N. A pharmacological review on SIRT 1 and SIRT 2 proteins, activators, and inhibitors: Call for further research. *Int. J. Biol. Macromol.* **2023**, *242*, 124581. [CrossRef]
74. Chen, J.; Chen, H.; Pan, L. SIRT1 and gynecological malignancies (Review). *Oncol. Rep.* **2021**, *45*, 43. [CrossRef]
75. Alqrad, M.A.I.; El-Agamy, D.S.; Ibrahim, S.R.M.; Sirwi, A.; Abdallah, H.M.; Abdel-Sattar, E.; El-Halawany, A.M.; Elsaed, W.M.; Mohamed, G.A. SIRT1/Nrf2/NF-kappaB Signaling Mediates Anti-Inflammatory and Anti-Apoptotic Activities of Oleanolic Acid in a Mouse Model of Acute Hepatorenal Damage. *Medicina* **2023**, *59*, 1351. [CrossRef] [PubMed]
76. Arab, H.H.; Eid, A.H.; Alsufyani, S.E.; Ashour, A.M.; El-Sheikh, A.A.K.; Darwish, H.W.; Georgy, G.S. Neuroprotective Impact of Linagliptin against Cadmium-Induced Cognitive Impairment and Neuropathological Aberrations: Targeting SIRT1/Nrf2 Axis, Apoptosis, and Autophagy. *Pharmaceuticals* **2023**, *16*, 1065. [CrossRef] [PubMed]
77. Chen, Y.; Peng, F.; Yang, C.; Hou, H.; Xing, Z.; Chen, J.; Liu, L.; Peng, C.; Li, D. SIRT1 activation by 2,3,5,6-tetramethylpyrazine alleviates neuroinflammation via inhibiting M1 microglia polarization. *Front. Immunol.* **2023**, *14*, 1206513. [CrossRef]
78. Yin, X.; Liu, Z.; Wang, J. Tetrahydropalmatine ameliorates hepatic steatosis in nonalcoholic fatty liver disease by switching lipid metabolism via AMPK-SREBP-1c-Sirt1 signaling axis. *Phytomedicine* **2023**, *119*, 155005. [CrossRef] [PubMed]
79. Helmy, H.S.; Senousy, M.A.; El-Sahar, A.E.; Sayed, R.H.; Saad, M.A.; Elbaz, E.M. Aberrations of miR-126-3p, miR-181a and sirtuin1 network mediate Di-(2-ethylhexyl) phthalate-induced testicular damage in rats: The protective role of hesperidin. *Toxicology* **2020**, *433–434*, 152406. [CrossRef] [PubMed]
80. Rizk, F.H.; Soliman, N.A.; Abo-Elnasr, S.E.; Mahmoud, H.A.; Abdel Ghafar, M.T.; Elkholy, R.A.; OA, E.L.; Mariah, R.A.; Amin Mashal, S.S.; El Saadany, A.A. Fisetin ameliorates oxidative glutamate testicular toxicity in rats via central and peripheral mechanisms involving SIRT1 activation. *Redox Rep.* **2022**, *27*, 177–185. [CrossRef] [PubMed]
81. Li, H.; Liu, L.; Cao, Z.; Li, W.; Liu, R.; Chen, Y.; Li, C.; Song, Y.; Liu, G.; Hu, J.; et al. Naringenin ameliorates homocysteine induced endothelial damage via the AMPKalpha/Sirt1 pathway. *J. Adv. Res.* **2021**, *34*, 137–147. [CrossRef]
82. Arora, S.; Venugopalan, A.; Dharavath, R.N.; Bishnoi, M.; Kondepudi, K.K.; Chopra, K. Naringenin Ameliorates Chronic Sleep Deprivation-Induced Pain via Sirtuin1 Inhibition. *Neurochem. Res.* **2021**, *46*, 1177–1187. [CrossRef] [PubMed]
83. Zhou, Q.; Zhu, C.; Xuan, A.; Zhang, J.; Zhu, Z.; Tang, L.; Ruan, D. Fisetin regulates the biological effects of rat nucleus pulposus mesenchymal stem cells under oxidative stress by sirtuin-1 pathway. *Immun. Inflamm. Dis.* **2023**, *11*, e865. [CrossRef] [PubMed]
84. Na, J.Y.; Song, K.; Kim, S.; Kwon, J. Rutin protects rat articular chondrocytes against oxidative stress induced by hydrogen peroxide through SIRT1 activation. *Biochem. Biophys. Res. Commun.* **2016**, *473*, 1301–1308. [CrossRef]
85. Chen, M.; Chen, Z.; Huang, D.; Sun, C.; Xie, J.; Chen, T.; Zhao, X.; Huang, Y.; Li, D.; Wu, B.; et al. Myricetin inhibits TNF-alpha-induced inflammation in A549 cells via the SIRT1/NF-kappaB pathway. *Pulm. Pharmacol. Ther.* **2020**, *65*, 102000. [CrossRef]

86. Wang, F.; Huang, Y.; Wu, W.; Zhu, C.; Zhang, R.; Chen, J.; Zeng, J. Metabolomics Analysis of the Peels of Different Colored Citrus Fruits (*Citrus reticulata* cv. 'Shatangju') During the Maturation Period Based on UHPLC-QQQ-MS. *Molecules* **2020**, *25*, 396. [CrossRef]
87. Munoz, A.L.; Cuellar, A.F.; Arevalo, G.; Santamaria, B.D.; Rodriguez, A.K.; Buendia-Atencio, C.; Reyes Chaparro, A.; Tenorio Barajas, A.Y.; Segura, N.A.; Bello, F.; et al. Antiviral activity of myricetin glycosylated compounds isolated from Marcetia taxifolia against chikungunya virus. *EXCLI J.* **2023**, *22*, 716–731. [CrossRef]
88. Kumar Sethiya, N.; Ghiloria, N.; Srivastav, A.; Bisht, D.; Kumar Chaudhary, S.; Walia, V.; Sabir Alam, M. Therapeutic Potential of Myricetin in the Treatment of Neurological, Neuropsychiatric, and Neurodegenerative Disorders. *CNS Neurol. Disord. Drug Targets* **2023**. [CrossRef]
89. Felice, M.R.; Maugeri, A.; De Sarro, G.; Navarra, M.; Barreca, D. Molecular Pathways Involved in the Anti-Cancer Activity of Flavonols: A Focus on Myricetin and Kaempferol. *Int. J. Mol. Sci.* **2022**, *23*, 4411. [CrossRef]
90. Wang, S.; He, N.; Xing, H.; Sun, Y.; Ding, J.; Liu, L. Function of hesperidin alleviating inflammation and oxidative stress responses in COPD mice might be related to SIRT1/PGC-1alpha/NF-kappaB signaling axis. *J. Recept. Signal Transduct. Res.* **2020**, *40*, 388–394. [CrossRef]
91. Wu, Y.X.; Yang, X.Y.; Han, B.S.; Hu, Y.Y.; An, T.; Lv, B.H.; Lian, J.; Wang, T.Y.; Bao, X.L.; Gao, L.; et al. Naringenin regulates gut microbiota and SIRT1/ PGC-1a signaling pathway in rats with letrozole-induced polycystic ovary syndrome. *Biomed. Pharmacother.* **2022**, *153*, 113286. [CrossRef] [PubMed]
92. Abo El-Magd, N.F.; El-Kashef, D.H.; El-Sherbiny, M.; Eraky, S.M. Hepatoprotective and cognitive-enhancing effects of hesperidin against thioacetamide-induced hepatic encephalopathy in rats. *Life Sci.* **2023**, *313*, 121280. [CrossRef] [PubMed]
93. Li, F.; Wei, R.; Huang, M.; Chen, J.; Li, P.; Ma, Y.; Chen, X. Luteolin can ameliorate renal interstitial fibrosis-induced renal anaemia through the SIRT1/FOXO3 pathway. *Food Funct.* **2022**, *13*, 11896–11914. [CrossRef] [PubMed]
94. Risitano, R.; Curro, M.; Cirmi, S.; Ferlazzo, N.; Campiglia, P.; Caccamo, D.; Ientile, R.; Navarra, M. Flavonoid fraction of Bergamot juice reduces LPS-induced inflammatory response through SIRT1-mediated NF-kappaB inhibition in THP-1 monocytes. *PLoS ONE* **2014**, *9*, e107431. [CrossRef] [PubMed]
95. Maugeri, A.; Ferlazzo, N.; De Luca, L.; Gitto, R.; Navarra, M. The link between the AMPK/SIRT1 axis and a flavonoid-rich extract of Citrus bergamia juice: A cell-free, in silico, and in vitro study. *Phytother. Res.* **2019**, *33*, 1805–1814. [CrossRef] [PubMed]
96. Chen, R.; Gao, S.; Guan, H.; Zhang, X.; Gao, Y.; Su, Y.; Song, Y.; Jiang, Y.; Li, N. Naringin protects human nucleus pulposus cells against TNF-alpha-induced inflammation, oxidative stress, and loss of cellular homeostasis by enhancing autophagic flux via AMPK/SIRT1 activation. *Oxid. Med. Cell Longev.* **2022**, *2022*, 7655142. [CrossRef]
97. Shokri Afra, H.; Zangooei, M.; Meshkani, R.; Ghahremani, M.H.; Ilbeigi, D.; Khedri, A.; Shahmohamadnejad, S.; Khaghani, S.; Nourbakhsh, M. Hesperetin is a potent bioactivator that activates SIRT1-AMPK signaling pathway in HepG2 cells. *J. Physiol. Biochem.* **2019**, *75*, 125–133. [CrossRef]
98. Li, J.; Dong, J.Z.; Ren, Y.L.; Zhu, J.J.; Cao, J.N.; Zhang, J.; Pan, L.L. Luteolin decreases atherosclerosis in LDL receptor-deficient mice via a mechanism including decreasing AMPK-SIRT1 signaling in macrophages. *Exp. Ther. Med.* **2018**, *16*, 2593–2599. [CrossRef]
99. Zhang, Z.; Wu, J.; Teng, C.; Wang, J.; Yu, J.; Jin, C.; Wang, L.; Wu, L.; Lin, Z.; Yu, Z.; et al. Orientin downregulating oxidative stress-mediated endoplasmic reticulum stress and mitochondrial dysfunction through AMPK/SIRT1 pathway in rat nucleus pulposus cells in vitro and attenuated intervertebral disc degeneration in vivo. *Apoptosis* **2022**, *27*, 1031–1048. [CrossRef]
100. Lee, Y.Y.; Lee, E.J.; Park, J.S.; Jang, S.E.; Kim, D.H.; Kim, H.S. Anti-Inflammatory and Antioxidant Mechanism of Tangeretin in Activated Microglia. *J. Neuroimmune Pharmacol.* **2016**, *11*, 294–305. [CrossRef]
101. Hao, R.; Song, X.; Li, F.; Tan, X.; Sun-Waterhouse, D.; Li, D. Caffeic acid phenethyl ester reversed cadmium-induced cell death in hippocampus and cortex and subsequent cognitive disorders in mice: Involvements of AMPK/SIRT1 pathway and amyloid-tau-neuroinflammation axis. *Food Chem. Toxicol.* **2020**, *144*, 111636. [CrossRef] [PubMed]
102. Ferreira, R.S.; Dos Santos, N.A.G.; Bernardes, C.P.; Sisti, F.M.; Amaral, L.; Fontana, A.C.K.; Dos Santos, A.C. Caffeic Acid Phenethyl Ester (CAPE) Protects PC12 Cells Against Cisplatin-Induced Neurotoxicity by Activating the AMPK/SIRT1, MAPK/Erk, and PI3k/Akt Signaling Pathways. *Neurotox. Res.* **2019**, *36*, 175–192. [CrossRef] [PubMed]
103. Sarubbo, F.; Ramis, M.R.; Kienzer, C.; Aparicio, S.; Esteban, S.; Miralles, A.; Moranta, D. Chronic Silymarin, Quercetin and Naringenin Treatments Increase Monoamines Synthesis and Hippocampal Sirt1 Levels Improving Cognition in Aged Rats. *J. Neuroimmune Pharmacol.* **2018**, *13*, 24–38. [CrossRef] [PubMed]
104. Chen, W.; Lin, B.; Xie, S.; Yang, W.; Lin, J.; Li, Z.; Zhan, Y.; Gui, S.; Lin, B. Naringenin protects RPE cells from $NaIO_3$-induced oxidative damage in vivo and in vitro through up-regulation of SIRT1. *Phytomedicine* **2021**, *80*, 153375. [CrossRef] [PubMed]
105. Syed, A.A.; Reza, M.I.; Yadav, H.; Gayen, J.R. Hesperidin inhibits NOX4 mediated oxidative stress and inflammation by upregulating SIRT1 in experimental diabetic neuropathy. *Exp. Gerontol.* **2023**, *172*, 112064. [CrossRef] [PubMed]
106. Ahmad, S.; Khan, A.; Ali, W.; Jo, M.H.; Park, J.; Ikram, M.; Kim, M.O. Fisetin Rescues the Mice Brains Against D-Galactose-Induced Oxidative Stress, Neuroinflammation and Memory Impairment. *Front. Pharmacol.* **2021**, *12*, 612078. [CrossRef] [PubMed]
107. Salama, A.A.A.; Yassen, N.N.; Mansour, H.M. Naringin protects mice from D-galactose-induced lung aging and mitochondrial dysfunction: Implication of SIRT1 pathways. *Life Sci.* **2023**, *324*, 121471. [CrossRef]
108. Peng, Z.; Li, X.; Xing, D.; Du, X.; Wang, Z.; Liu, G.; Li, X. Nobiletin alleviates palmitic acid-induced NLRP3 inflammasome activation in a sirtuin 1-dependent manner in AML-12 cells. *Mol. Med. Rep.* **2018**, *18*, 5815–5822. [CrossRef]

109. Hosawi, S. Current Update on Role of Hesperidin in Inflammatory Lung Diseases: Chemistry, Pharmacology, and Drug Delivery Approaches. *Life* **2023**, *13*, 937. [CrossRef]
110. Li, S.; Shao, L.; Fang, J.; Zhang, J.; Chen, Y.; Yeo, A.J.; Lavin, M.F.; Yu, G.; Shao, H. Hesperetin attenuates silica-induced lung injury by reducing oxidative damage and inflammatory response. *Exp. Ther. Med.* **2021**, *21*, 297. [CrossRef]
111. Yang, A.Y.; Choi, H.J.; Kim, K.; Leem, J. Antioxidant, Antiapoptotic, and Anti-Inflammatory Effects of Hesperetin in a Mouse Model of Lipopolysaccharide-Induced Acute Kidney Injury. *Molecules* **2023**, *28*, 2759. [CrossRef]
112. Wang, S.W.; Wang, W.; Sheng, H.; Bai, Y.F.; Weng, Y.Y.; Fan, X.Y.; Zheng, F.; Zhu, X.T.; Xu, Z.C.; Zhang, F. Hesperetin, a SIRT1 activator, inhibits hepatic inflammation via AMPK/CREB pathway. *Int. Immunopharmacol.* **2020**, *89*, 107036. [CrossRef]
113. Hua, Y.Q.; Zeng, Y.; Xu, J.; Xu, X.L. Naringenin alleviates nonalcoholic steatohepatitis in middle-aged Apoe$^{-/-}$mice: Role of SIRT1. *Phytomedicine* **2021**, *81*, 153412. [CrossRef]
114. Du, Y.; Ma, J.; Fan, Y.; Wang, X.; Zheng, S.; Feng, J.; Li, J.; Fan, Z.; Li, G.; Ye, Q. Naringenin: A Promising Therapeutic Agent against Organ Fibrosis. *Oxid. Med. Cell Longev.* **2021**, *2021*, 1210675. [CrossRef]
115. Li, H.L.; Wei, Y.Y.; Li, X.H.; Zhang, S.S.; Zhang, R.T.; Li, J.H.; Ma, B.W.; Shao, S.B.; Lv, Z.W.; Ruan, H.; et al. Diosmetin has therapeutic efficacy in colitis regulating gut microbiota, inflammation, and oxidative stress via the circ-Sirt1/Sirt1 axis. *Acta Pharmacol. Sin.* **2022**, *43*, 919–932. [CrossRef]
116. Iskender, H.; Dokumacioglu, E.; Sen, T.M.; Ince, I.; Kanbay, Y.; Saral, S. The effect of hesperidin and quercetin on oxidative stress, NF-kappaB and SIRT1 levels in a STZ-induced experimental diabetes model. *Biomed. Pharmacother.* **2017**, *90*, 500–508. [CrossRef]
117. Rostami, A.; Baluchnejadmojarad, T.; Roghani, M. Hepatoprotective Effect of Myricetin following Lipopolysaccharide/DGalactosamine: Involvement of Autophagy and Sirtuin 1. *Curr. Mol. Pharmacol.* **2023**, *16*, 419–433. [CrossRef]
118. Khajevand-Khazaei, M.R.; Mohseni-Moghaddam, P.; Hosseini, M.; Gholami, L.; Baluchnejadmojarad, T.; Roghani, M. Rutin, a quercetin glycoside, alleviates acute endotoxemic kidney injury in C57BL/6 mice via suppression of inflammation and up-regulation of antioxidants and SIRT1. *Eur. J. Pharmacol.* **2018**, *833*, 307–313. [CrossRef]
119. Yang, H.; Wang, C.; Zhang, L.; Lv, J.; Ni, H. Rutin alleviates hypoxia/reoxygenation-induced injury in myocardial cells by up-regulating SIRT1 expression. *Chem. Biol. Interact.* **2019**, *297*, 44–49. [CrossRef]
120. Zhao, L.; Zhou, Z.; Zhu, C.; Fu, Z.; Yu, D. Luteolin alleviates myocardial ischemia reperfusion injury in rats via Siti1/NLRP3/NF-kappaB pathway. *Int. Immunopharmacol.* **2020**, *85*, 106680. [CrossRef]
121. Liu, P.; Li, J.; Liu, M.; Zhang, M.; Xue, Y.; Zhang, Y.; Han, X.; Jing, X.; Chu, L. Hesperetin modulates the Sirt1/Nrf2 signaling pathway in counteracting myocardial ischemia through suppression of oxidative stress, inflammation, and apoptosis. *Biomed. Pharmacother.* **2021**, *139*, 111552. [CrossRef]
122. Li, D.; Liu, X.; Pi, W.; Zhang, Y.; Yu, L.; Xu, C.; Sun, Z.; Jiang, J. Fisetin Attenuates Doxorubicin-Induced Cardiomyopathy In Vivo and In Vitro by Inhibiting Ferroptosis Through SIRT1/Nrf2 Signaling Pathway Activation. *Front. Pharmacol.* **2021**, *12*, 808480. [CrossRef]
123. Yang, K.; Chen, J.; Zhang, T.; Yuan, X.; Ge, A.; Wang, S.; Xu, H.; Zeng, L.; Ge, J. Efficacy and safety of dietary polyphenol supplementation in the treatment of non-alcoholic fatty liver disease: A systematic review and meta-analysis. *Front. Immunol.* **2022**, *13*, 949746. [CrossRef]
124. Qi, G.; Guo, R.; Tian, H.; Li, L.; Liu, H.; Mi, Y.; Liu, X. Nobiletin protects against insulin resistance and disorders of lipid metabolism by reprogramming of circadian clock in hepatocytes. *Biochim. Biophys. Acta Mol. Cell Biol. Lipids* **2018**, *1863*, 549–562. [CrossRef]
125. Wu, H.; Liu, Y.; Chen, X.; Zhu, D.; Ma, J.; Yan, Y.; Si, M.; Li, X.; Sun, C.; Yang, B.; et al. Neohesperidin Exerts Lipid-Regulating Effects in vitro and in vivo via Fibroblast Growth Factor 21 and AMP-Activated Protein Kinase/Sirtuin Type 1/Peroxisome Proliferator-Activated Receptor Gamma Coactivator 1alpha Signaling Axis. *Pharmacology* **2017**, *100*, 115–126. [CrossRef]
126. Paraiso, A.F.; Sousa, J.N.; Andrade, J.M.O.; Mangabeira, E.S.; Lelis, D.F.; de Paula, A.M.B.; Martins, A.; Lima, W.J.N.; Guimaraes, A.L.S.; Melo, G.A.; et al. Oral gallic acid improves metabolic profile by modulating SIRT1 expression in obese mice brown adipose tissue: A molecular and bioinformatic approach. *Life Sci.* **2019**, *237*, 116914. [CrossRef]
127. Kashyap, B.; Saikia, K.; Samanta, S.K.; Thakur, D.; Banerjee, S.K.; Borah, J.C.; Talukdar, N.C. Kaempferol 3-O-rutinoside from Antidesma acidum Retz. Stimulates glucose uptake through SIRT1 induction followed by GLUT4 translocation in skeletal muscle L6 cells. *J. Ethnopharmacol.* **2023**, *301*, 115788. [CrossRef]
128. Li, N.; Yin, L.; Shang, J.; Liang, M.; Liu, Z.; Yang, H.; Qiang, G.; Du, G.; Yang, X. Kaempferol attenuates nonalcoholic fatty liver disease in type 2 diabetic mice via the Sirt1/AMPK signaling pathway. *Biomed. Pharmacother.* **2023**, *165*, 115113. [CrossRef]
129. Sayed, A.M.; Hassanein, E.H.M.; Salem, S.H.; Hussein, O.E.; Mahmoud, A.M. Flavonoids-mediated SIRT1 signaling activation in hepatic disorders. *Life Sci.* **2020**, *259*, 118173. [CrossRef]
130. Xi, Y.; Chi, Z.; Tao, X.; Zhai, X.; Zhao, Z.; Ren, J.; Yang, S.; Dong, D. Naringin against doxorubicin-induced hepatotoxicity in mice through reducing oxidative stress, inflammation, and apoptosis via the up-regulation of SIRT1. *Environ. Toxicol.* **2023**, *38*, 1153–1161. [CrossRef]
131. Ministrini, S.; Puspitasari, Y.M.; Beer, G.; Liberale, L.; Montecucco, F.; Camici, G.G. Sirtuin 1 in Endothelial Dysfunction and Cardiovascular Aging. *Front. Physiol.* **2021**, *12*, 733696. [CrossRef]
132. Chen, S.; Sun, T.; Li, X. Nobiletin alleviates the hypoxia/reoxygenation-induced damage in myocardial cells by modulating the miR-433/SIRT1 axis. *J. Food Biochem.* **2021**, *45*, e13844. [CrossRef]

133. Dusabimana, T.; Kim, S.R.; Kim, H.J.; Park, S.W.; Kim, H. Nobiletin ameliorates hepatic ischemia and reperfusion injury through the activation of SIRT-1/FOXO3a-mediated autophagy and mitochondrial biogenesis. *Exp. Mol. Med.* **2019**, *51*, 1–16. [CrossRef]
134. Liu, W.; Cheng, L.; Li, X.; Zhao, L.; Hu, X.; Ma, Z. Short-term pretreatment of naringin isolated from Citrus wilsonii Tanaka attenuates rat myocardial ischemia/reperfusion injury. *Naunyn Schmiedebergs Arch. Pharmacol.* **2022**, *395*, 1047–1059. [CrossRef]
135. Testai, L.; Piragine, E.; Piano, I.; Flori, L.; Da Pozzo, E.; Miragliotta, V.; Pirone, A.; Citi, V.; Di Cesare Mannelli, L.; Brogi, S.; et al. The Citrus Flavonoid Naringenin Protects the Myocardium from Ageing-Dependent Dysfunction: Potential Role of SIRT1. *Oxid. Med. Cell Longev.* **2020**, *2020*, 4650207. [CrossRef]
136. Zheng, G.D.; Hu, P.J.; Chao, Y.X.; Zhou, Y.; Yang, X.J.; Chen, B.Z.; Yu, X.Y.; Cai, Y. Nobiletin induces growth inhibition and apoptosis in human nasopharyngeal carcinoma C666-1 cells through regulating PARP-2/SIRT1/AMPK signaling pathway. *Food Sci. Nutr.* **2019**, *7*, 1104–1112. [CrossRef]
137. Moghadam, D.; Zarei, R.; Vakili, S.; Ghojoghi, R.; Zarezade, V.; Veisi, A.; Sabaghan, M.; Azadbakht, O.; Behrouj, H. The effect of natural polyphenols Resveratrol, Gallic acid, and Kuromanin chloride on human telomerase reverse transcriptase (hTERT) expression in HepG2 hepatocellular carcinoma: Role of SIRT1/Nrf2 signaling pathway and oxidative stress. *Mol. Biol. Rep.* **2023**, *50*, 77–84. [CrossRef]
138. Finnin, M.S.; Donigian, J.R.; Pavletich, N.P. Structure of the histone deacetylase SIRT2. *Nat. Struct. Biol.* **2001**, *8*, 621–625. [CrossRef]
139. Zhu, C.; Dong, X.; Wang, X.; Zheng, Y.; Qiu, J.; Peng, Y.; Xu, J.; Chai, Z.; Liu, C. Multiple Roles of SIRT2 in Regulating Physiological and Pathological Signal Transduction. *Genet. Res.* **2022**, *2022*, 9282484. [CrossRef]
140. Lu, W.; Ji, H.; Wu, D. SIRT2 plays complex roles in neuroinflammation neuroimmunology-associated disorders. *Front. Immunol.* **2023**, *14*, 1174180. [CrossRef]
141. Liu, Y.; Zhang, Y.; Zhu, K.; Chi, S.; Wang, C.; Xie, A. Emerging Role of Sirtuin 2 in Parkinson's Disease. *Front. Aging Neurosci.* **2019**, *11*, 372. [CrossRef] [PubMed]
142. Chen, G.; Huang, P.; Hu, C. The role of SIRT2 in cancer: A novel therapeutic target. *Int. J. Cancer* **2020**, *147*, 3297–3304. [CrossRef]
143. Taneja, A.; Ravi, V.; Hong, J.Y.; Lin, H.; Sundaresan, N.R. Emerging roles of Sirtuin 2 in cardiovascular diseases. *FASEB J.* **2021**, *35*, e21841. [CrossRef]
144. Heger, V.; Tyni, J.; Hunyadi, A.; Horakova, L.; Lahtela-Kakkonen, M.; Rahnasto-Rilla, M. Quercetin based derivatives as sirtuin inhibitors. *Biomed. Pharmacother.* **2019**, *111*, 1326–1333. [CrossRef]
145. Singh, S.; Singh, A.K.; Garg, G.; Rizvi, S.I. Fisetin as a caloric restriction mimetic protects rat brain against aging induced oxidative stress, apoptosis and neurodegeneration. *Life Sci.* **2018**, *193*, 171–179. [CrossRef]
146. Li, X.; Zhang, J.; Rong, H.; Zhang, X.; Dong, M. Ferulic Acid Ameliorates MPP^+/MPTP-Induced Oxidative Stress via ERK1/2-Dependent Nrf2 Activation: Translational Implications for Parkinson Disease Treatment. *Mol. Neurobiol.* **2020**, *57*, 2981–2995. [CrossRef]
147. Maugeri, A.; Russo, C.; Musumeci, L.; Lombardo, G.E.; De Sarro, G.; Barreca, D.; Cirmi, S.; Navarra, M. The Anticancer Effect of a Flavonoid-Rich Extract of Bergamot Juice in THP-1 Cells Engages the SIRT2/AKT/p53 Pathway. *Pharmaceutics* **2022**, *14*, 2168. [CrossRef]
148. Russo, C.; Maugeri, A.; De Luca, L.; Gitto, R.; Lombardo, G.E.; Musumeci, L.; De Sarro, G.; Cirmi, S.; Navarra, M. The SIRT2 Pathway Is Involved in the Antiproliferative Effect of Flavanones in Human Leukemia Monocytic THP-1 Cells. *Biomedicines* **2022**, *10*, 2383. [CrossRef]
149. Deng, J.; Huang, M.; Wu, H. Protective effect of limonin against doxorubicin-induced cardiotoxicity via activating nuclear factor—Like 2 and Sirtuin 2 signaling pathways. *Bioengineered* **2021**, *12*, 7975–7984. [CrossRef]
150. Zhou, L.; Pinho, R.; Gu, Y.; Radak, Z. The Role of SIRT3 in Exercise and Aging. *Cells* **2022**, *11*, 2596. [CrossRef] [PubMed]
151. Zhang, H.; Dai, S.; Yang, Y.; Wei, J.; Li, X.; Luo, P.; Jiang, X. Role of Sirtuin 3 in Degenerative Diseases of the Central Nervous System. *Biomolecules* **2023**, *13*, 735. [CrossRef]
152. Yang, H.; Zhou, Z.; Liu, Z.; Chen, J.; Wang, Y. Sirtuin-3: A potential target for treating several types of brain injury. *Front. Cell Dev. Biol.* **2023**, *11*, 1154831. [CrossRef] [PubMed]
153. Chen, J.; Chen, S.; Zhang, B.; Liu, J. SIRT3 as a potential therapeutic target for heart failure. *Pharmacol. Res.* **2021**, *165*, 105432. [CrossRef]
154. Yapryntseva, M.A.; Maximchik, P.V.; Zhivotovsky, B.; Gogvadze, V. Mitochondrial sirtuin 3 and various cell death modalities. *Front. Cell Dev. Biol.* **2022**, *10*, 947357. [CrossRef]
155. Zhao, C.; Wang, F.; Lian, Y.; Xiao, H.; Zheng, J. Biosynthesis of citrus flavonoids and their health effects. *Crit. Rev. Food Sci. Nutr.* **2020**, *60*, 566–583. [CrossRef] [PubMed]
156. Lombardo, G.E.; Arcidiacono, B.; De Rose, R.F.; Lepore, S.M.; Costa, N.; Montalcini, T.; Brunetti, A.; Russo, D.; De Sarro, G.; Celano, M. Normocaloric Diet Restores Weight Gain and Insulin Sensitivity in Obese Mice. *Front. Endocrinol.* **2016**, *7*, 49. [CrossRef]
157. Akindehin, S.; Jung, Y.S.; Kim, S.N.; Son, Y.H.; Lee, I.; Seong, J.K.; Jeong, H.W.; Lee, Y.H. Myricetin Exerts Anti-Obesity Effects through Upregulation of SIRT3 in Adipose Tissue. *Nutrients* **2018**, *10*, 1962. [CrossRef]
158. Lee, A.; Gu, H.; Gwon, M.H.; Yun, J.M. Hesperetin suppresses LPS/high glucose-induced inflammatory responses via TLR/MyD88/NF-kappaB signaling pathways in THP-1 cells. *Nutr. Res. Pract.* **2021**, *15*, 591–603. [CrossRef]

159. Kim, A.; Lee, W.; Yun, J.M. Luteolin and fisetin suppress oxidative stress by modulating sirtuins and forkhead box O3a expression under in vitro diabetic conditions. *Nutr. Res. Pract.* **2017**, *11*, 430–434. [CrossRef] [PubMed]
160. Ogura, Y.; Kitada, M.; Xu, J.; Monno, I.; Koya, D. CD38 inhibition by apigenin ameliorates mitochondrial oxidative stress through restoration of the intracellular NAD^+/NADH ratio and Sirt3 activity in renal tubular cells in diabetic rats. *Aging* **2020**, *12*, 11325–11336. [CrossRef]
161. Li, J.J.; Jiang, H.C.; Wang, A.; Bu, F.T.; Jia, P.C.; Zhu, S.; Zhu, L.; Huang, C.; Li, J. Hesperetin derivative-16 attenuates CCl_4-induced inflammation and liver fibrosis by activating AMPK/SIRT3 pathway. *Eur. J. Pharmacol.* **2022**, *915*, 174530. [CrossRef] [PubMed]
162. Ji-Hong, Y.; Yu, M.; Ling-Hong, Y.; Jing-Jing, G.; Ling-Li, X.; Lv, W.; Yong-Mei, J. Baicalein attenuates bleomycin-induced lung fibroblast senescence and lung fibrosis through restoration of Sirt3 expression. *Pharm. Biol.* **2023**, *61*, 288–297. [CrossRef] [PubMed]
163. Yu, L.M.; Dong, X.; Xue, X.D.; Zhang, J.; Li, Z.; Wu, H.J.; Yang, Z.L.; Yang, Y.; Wang, H.S. Naringenin improves mitochondrial function and reduces cardiac damage following ischemia-reperfusion injury: The role of the AMPK-SIRT3 signaling pathway. *Food Funct.* **2019**, *10*, 2752–2765. [CrossRef]
164. Ahmedy, O.A.; Abdelghany, T.M.; El-Shamarka, M.E.A.; Khattab, M.A.; El-Tanbouly, D.M. Apigenin attenuates LPS-induced neurotoxicity and cognitive impairment in mice via promoting mitochondrial fusion/mitophagy: Role of SIRT3/PINK1/Parkin pathway. *Psychopharmacology* **2022**, *239*, 3903–3917. [CrossRef]
165. Mu, J.; Ma, H.; Chen, H.; Zhang, X.; Ye, M. Luteolin Prevents UVB-Induced Skin Photoaging Damage by Modulating SIRT3/ROS/MAPK Signaling: An in vitro and in vivo Studies. *Front. Pharmacol.* **2021**, *12*, 728261. [CrossRef]
166. Mu, J.; Chen, H.; Ye, M.; Zhang, X.; Ma, H. Acacetin resists UVA photoaging by mediating the SIRT3/ROS/MAPKs pathway. *J. Cell Mol. Med.* **2022**, *26*, 4624–4628. [CrossRef] [PubMed]
167. Wang, G.; Wang, J.J.; Wang, Y.Z.; Feng, S.; Jing, G.; Fu, X.L. Myricetin nanoliposomes induced SIRT3-mediated glycolytic metabolism leading to glioblastoma cell death. *Artif. Cells Nanomed. Biotechnol.* **2018**, *46*, S180–S191. [CrossRef]
168. Li, Y.; Zhou, Y.; Wang, F.; Chen, X.; Wang, C.; Wang, J.; Liu, T.; Li, Y.; He, B. SIRT4 is the last puzzle of mitochondrial sirtuins. *Bioorg Med. Chem.* **2018**, *26*, 3861–3865. [CrossRef]
169. Tomaselli, D.; Steegborn, C.; Mai, A.; Rotili, D. Sirt4: A Multifaceted Enzyme at the Crossroads of Mitochondrial Metabolism and Cancer. *Front. Oncol.* **2020**, *10*, 474. [CrossRef]
170. Pannek, M.; Simic, Z.; Fuszard, M.; Meleshin, M.; Rotili, D.; Mai, A.; Schutkowski, M.; Steegborn, C. Crystal structures of the mitochondrial deacylase Sirtuin 4 reveal isoform-specific acyl recognition and regulation features. *Nat. Commun.* **2017**, *8*, 1513. [CrossRef]
171. Park, E.S.; Kang, J.C.; Jang, Y.C.; Park, J.S.; Jang, S.Y.; Kim, D.E.; Kim, B.; Shin, H.S. Cardioprotective effects of rhamnetin in H9c2 cardiomyoblast cells under H_2O_2-induced apoptosis. *J. Ethnopharmacol.* **2014**, *153*, 552–560. [CrossRef]
172. Osborne, B.; Bentley, N.L.; Montgomery, M.K.; Turner, N. The role of mitochondrial sirtuins in health and disease. *Free Radic. Biol. Med.* **2016**, *100*, 164–174. [CrossRef]
173. Wang, Y.; Chen, H.; Zha, X. Overview of SIRT5 as a potential therapeutic target: Structure, function and inhibitors. *Eur. J. Med. Chem.* **2022**, *236*, 114363. [CrossRef] [PubMed]
174. Curry, A.M.; Rymarchyk, S.; Herrington, N.B.; Donu, D.; Kellogg, G.E.; Cen, Y. Nicotinamide riboside activates SIRT5 deacetylation. *FEBS J.* **2023**, *290*, 4762–4776. [CrossRef] [PubMed]
175. Du, Y.; Hu, H.; Qu, S.; Wang, J.; Hua, C.; Zhang, J.; Wei, P.; He, X.; Hao, J.; Liu, P.; et al. SIRT5 deacylates metabolism-related proteins and attenuates hepatic steatosis in ob/ob mice. *EBioMedicine* **2018**, *36*, 347–357. [CrossRef] [PubMed]
176. Fabbrizi, E.; Fiorentino, F.; Carafa, V.; Altucci, L.; Mai, A.; Rotili, D. Emerging Roles of SIRT5 in Metabolism, Cancer, and SARS-CoV-2 Infection. *Cells* **2023**, *12*, 852. [CrossRef] [PubMed]
177. Chang, X.; Zhang, T.; Wang, J.; Liu, Y.; Yan, P.; Meng, Q.; Yin, Y.; Wang, S. SIRT5-Related Desuccinylation Modification Contributes to Quercetin-Induced Protection against Heart Failure and High-Glucose-Prompted Cardiomyocytes Injured through Regulation of Mitochondrial Quality Surveillance. *Oxid. Med. Cell Longev.* **2021**, *2021*, 5876841. [CrossRef] [PubMed]
178. Zhou, B.; Yang, Y.; Pang, X.; Shi, J.; Jiang, T.; Zheng, X. Quercetin inhibits DNA damage responses to induce apoptosis via SIRT5/PI3K/AKT pathway in non-small cell lung cancer. *Biomed. Pharmacother.* **2023**, *165*, 115071. [CrossRef]
179. Liu, G.; Chen, H.; Liu, H.; Zhang, W.; Zhou, J. Emerging roles of SIRT6 in human diseases and its modulators. *Med. Res. Rev.* **2021**, *41*, 1089–1137. [CrossRef] [PubMed]
180. Gertler, A.A.; Cohen, H.Y. SIRT6, a protein with many faces. *Biogerontology* **2013**, *14*, 629–639. [CrossRef]
181. Fiorentino, F.; Mai, A.; Rotili, D. Emerging Therapeutic Potential of SIRT6 Modulators. *J. Med. Chem.* **2021**, *64*, 9732–9758. [CrossRef]
182. D'Onofrio, N.; Servillo, L.; Balestrieri, M.L. SIRT1 and SIRT6 Signaling Pathways in Cardiovascular Disease Protection. *Antioxid. Redox Signal* **2018**, *28*, 711–732. [CrossRef]
183. Wu, K.; Wang, Y.; Liu, R.; Wang, H.; Rui, T. The role of mammalian Sirtuin 6 in cardiovascular diseases and diabetes mellitus. *Front. Physiol.* **2023**, *14*, 1207133. [CrossRef]
184. Smirnov, D.; Eremenko, E.; Stein, D.; Kaluski, S.; Jasinska, W.; Cosentino, C.; Martinez-Pastor, B.; Brotman, Y.; Mostoslavsky, R.; Khrameeva, E.; et al. SIRT6 is a key regulator of mitochondrial function in the brain. *Cell Death Dis.* **2023**, *14*, 35. [CrossRef]
185. Li, D.; Cao, C. The correlation of serum sirt6 with clinical outcome and prognosis in patients with gastric cancer. *Medicine* **2022**, *101*, e31568. [CrossRef] [PubMed]

186. Yasuda, M.; Wilson, D.R.; Fugmann, S.D.; Moaddel, R. Synthesis and characterization of SIRT6 protein coated magnetic beads: Identification of a novel inhibitor of SIRT6 deacetylase from medicinal plant extracts. *Anal. Chem.* **2011**, *83*, 7400–7407. [CrossRef] [PubMed]
187. You, W.; Zheng, W.; Weiss, S.; Chua, K.F.; Steegborn, C. Structural basis for the activation and inhibition of Sirtuin 6 by quercetin and its derivatives. *Sci. Rep.* **2019**, *9*, 19176. [CrossRef] [PubMed]
188. He, J.; Deng, Y.; Ren, L.; Jin, Z.; Yang, J.; Yao, F.; Liu, Y.; Zheng, Z.; Chen, D.; Wang, B.; et al. Isoliquiritigenin from licorice flavonoids attenuates NLRP3-mediated pyroptosis by SIRT6 in vascular endothelial cells. *J. Ethnopharmacol.* **2023**, *303*, 115952. [CrossRef] [PubMed]
189. Xie, T.; Yuan, J.; Mei, L.; Li, P.; Pan, R. Luteolin suppresses TNF-alpha-induced inflammatory injury and senescence of nucleus pulposus cells via the Sirt6/NF-kappaB pathway. *Exp. Ther. Med.* **2022**, *24*, 469. [CrossRef] [PubMed]
190. Jing, S.; Wang, X.; Zhang, Z.; Cao, D.; Huang, K.; Wang, Y.; Liu, Z.; Su, S.; Wang, Q. Hesperetin attenuates cognitive dysfunction via SIRT6/NLRP3 pathway in scopolamine-induced mice. *Metab. Brain Dis.* **2023**, *38*, 2443–2456. [CrossRef] [PubMed]
191. Wang, Y.; Cai, Z.; Zhan, G.; Li, X.; Li, S.; Wang, X.; Li, S.; Luo, A. Caffeic Acid Phenethyl Ester Suppresses Oxidative Stress and Regulates M1/M2 Microglia Polarization via Sirt6/Nrf2 Pathway to Mitigate Cognitive Impairment in Aged Mice following Anesthesia and Surgery. *Antioxidants* **2023**, *12*, 714. [CrossRef]
192. Li, W.; Liu, X.; Qiao, H. Downregulation of hippocampal SIRT6 activates AKT/CRMP2 signaling and ameliorates chronic stress-induced depression-like behavior in mice. *Acta Pharmacol. Sin.* **2020**, *41*, 1557–1567. [CrossRef]
193. Tang, M.; Tang, H.; Tu, B.; Zhu, W.G. SIRT7: A sentinel of genome stability. *Open Biol.* **2021**, *11*, 210047. [CrossRef]
194. Mitra, N.; Dey, S. Biochemical characterization of mono ADP ribosyl transferase activity of human sirtuin SIRT7 and its regulation. *Arch. Biochem. Biophys.* **2020**, *680*, 108226. [CrossRef]
195. Barber, M.F.; Michishita-Kioi, E.; Xi, Y.; Tasselli, L.; Kioi, M.; Moqtaderi, Z.; Tennen, R.I.; Paredes, S.; Young, N.L.; Chen, K.; et al. SIRT7 links H3K18 deacetylation to maintenance of oncogenic transformation. *Nature* **2012**, *487*, 114–118. [CrossRef]
196. Mendes, K.L.; Lelis, D.F.; Santos, S.H.S. Nuclear sirtuins and inflammatory signaling pathways. *Cytokine Growth Factor. Rev.* **2017**, *38*, 98–105. [CrossRef]
197. Huo, Q.; Chen, S.; Zhuang, J.; Quan, C.; Wang, Y.; Xie, N. SIRT7 Downregulation Promotes Breast Cancer Metastasis Via LAP2alpha-Induced Chromosomal Instability. *Int. J. Biol. Sci.* **2023**, *19*, 1528–1542. [CrossRef] [PubMed]
198. Yi, X.; Wang, H.; Yang, Y.; Wang, H.; Zhang, H.; Guo, S.; Chen, J.; Du, J.; Tian, Y.; Ma, J.; et al. SIRT7 orchestrates melanoma progression by simultaneously promoting cell survival and immune evasion via UPR activation. *Signal Transduct. Target. Ther.* **2023**, *8*, 107. [CrossRef]
199. Li, G.; Xu, W.; Li, X.; Chen, M.; Shi, Y.; Wei, M.; Peng, D. Oncogenic SIRT7 inhibits GATA4 transcriptional activity and activates the Wnt signaling pathway in ovarian cancer. *Gynecol. Oncol.* **2023**, *171*, 39–48. [CrossRef] [PubMed]
200. Zhao, H.; Xian, G.; Zeng, J.; Zhong, G.; An, D.; Peng, Y.; Hu, D.; Lin, Y.; Li, J.; Su, S.; et al. Hesperetin, a Promising Dietary Supplement for Preventing the Development of Calcific Aortic Valve Disease. *Antioxidants* **2022**, *11*, 2093. [CrossRef] [PubMed]
201. Moghadam, F.H.; Mesbah-Ardakani, M.; Nasr-Esfahani, M.H. Ferulic Acid exerts concentration-dependent anti-apoptotic and neuronal differentiation-inducing effects in PC12 and mouse neural stem cells. *Eur. J. Pharmacol.* **2018**, *841*, 104–112. [CrossRef] [PubMed]

International Journal of
Molecular Sciences

MDPI

Article

Biological Activity and Chemical Composition of Propolis Extracts with Potential Use in Vulvovaginal Candidiasis Management

Ana Margarida Silva [1], Beatriz Rocha [1], Manuela M. Moreira [1], Cristina Delerue-Matos [1], José das Neves [2,3,4,*] and Francisca Rodrigues [1,*]

[1] REQUIMTE/LAQV, ISEP, Polytechnic of Porto, Rua Dr. António Bernardino de Almeida, 4249-015 Porto, Portugal; ana.silva@graq.isep.ipp.pt (A.M.S.); beasrocha@hotmail.com (B.R.); manuela.moreira@graq.isep.ipp.pt (M.M.M.); cmm@isep.ipp.pt (C.D.-M.)
[2] i3S—Institute for Research and Innovation in Health, University of Porto, Rua Alfredo Allen, 208, 4200-135 Porto, Portugal
[3] INEB—Institute of Biomedical Engineering, University of Porto, Rua Alfredo Allen, 208, 4200-135 Porto, Portugal
[4] CESPU—Institute for Research and Advanced Training in Health Sciences and Technologies, Rua Central de Gandra 1317, 4585-116 Gandra, Portugal
* Correspondence: j.dasneves@i3s.up.pt (J.d.N.); francisca.rodrigues@graq.isep.ipp.pt (F.R.)

Abstract: Environmental sustainability is an increasing challenge in the pharmaceutical field, leading to the search for eco-friendly active ingredients. Among natural ingredients, propolis arises as an excellent alternative, being a complex substance with pharmacological properties. This work aims to explore the potential of propolis as a new pharmaceutical ingredient for the replacement of conventional vulvovaginal antifungals. Propolis extracts were obtained by Ultrasound-Assisted Extraction using different solvents (water, water/ethanol (50:50, *v*/*v*), and ethanol). Afterwards, the extracts were characterized regarding total phenolic content (TPC), antioxidant/antiradical activities, radical scavenging capacity, antifungal activity against strains of Candida species, and viability effect on two female genital cell lines. The aqueous extract achieved the best TPC result as well as the highest antioxidant/antiradical activities and ability to capture reactive oxygen species. A total of 38 phenolic compounds were identified and quantified by HPLC, among which ferulic acid, phloridzin and myricetin predominated. Regarding the anti-*Candida* spp. activity, the aqueous and the hydroalcoholic extracts achieved the best outcomes (with MIC values ranging between 128 and 512 μg/mL). The cell viability assays confirmed that the aqueous extract presented mild selectivity, while the hydroalcoholic and alcoholic extracts showed higher toxicities. These results attest that propolis has a deep potential for vulvovaginal candidiasis management, supporting its economic valorization.

Keywords: antioxidant activity; natural products; phenolic compounds; ultrasound-assisted extraction; vulvovaginal candidiasis

Citation: Silva, A.M.; Rocha, B.; Moreira, M.M.; Delerue-Matos, C.; das Neves, J.; Rodrigues, F. Biological Activity and Chemical Composition of Propolis Extracts with Potential Use in Vulvovaginal Candidiasis Management. *Int. J. Mol. Sci.* **2024**, *25*, 2478. https://doi.org/10.3390/ijms25052478

Academic Editor: Fabio Altieri

Received: 24 January 2024
Revised: 12 February 2024
Accepted: 19 February 2024
Published: 20 February 2024

1. Introduction

The global population continues growing, being estimated to reach totals near 8.5 billion people by 2030 and 10.9 billion by 2100 [1]. A 30% increase in food supplies will be needed in comparison to the present, while major challenges are also expected to emerge in food security and agricultural practices [2]. Therefore, the search for sustainable development has generated an attempt to use natural matrices and products that are readily available, adding value to local resources and generating profits for small producers. At the same time, the use of plant and animal extracts in traditional medicine is one of the oldest human practices, particularly in developing countries where modern medicines are not always available or affordable [3]. Fruits and vegetables have long been described as excellent

sources of polyphenols with demonstrated benefits for human health, such as antioxidant and cytoprotective activities [4]. Honey and related products, including propolis, are no exception [5]. Propolis is a natural adhesive resinous material produced by honeybees that results from the mixture of collected exudates of leaves, branches, and buds around the beehive with bee salivary secretions and beeswax. This complex matrix is used to build and seal cracks in the hive, protecting it from pathogens [6,7]. Propolis has a typically dark brown color, being solid and brittle at lower temperatures and becoming softer and stickier above 20 °C due to its resinous nature. Low toxicity and multiple functionalities also justify the traditional use of propolis for medical purposes [6]. Indeed, more than 300 constituents have been identified as bioactive [6,8]. Generally, propolis has been described as a rich source of benzoic acids and derivatives, cinnamic alcohol, cinnamic acid and respective derivatives, sesquiterpenes and triterpene hydrocarbons, benzaldehyde derivatives, alcohols, ketones, and heteroaromatic compounds, terpenes and sesquiterpene alcohols and their derivatives, aliphatic hydrocarbons, minerals, sterols and steroidal hydrocarbons, sugars, and amino acids [6,8,9]. Most important, the different combinations of these compounds are responsible for the antibacterial [10–12], antifungal [13,14], antiviral [15], anticancer [16,17], anti-inflammatory [18] and antioxidant [19–21] activities of propolis.

In particular, the ability of propolis to inhibit the growth of Candida species involved in vulvovaginal candidiasis (VVC) has recently attracted the attention of researchers [22–26]. VVC is typically caused by *Candida albicans* (around 90%), although cases of non-albicans VVC also occur and are usually more challenging to manage. Indeed, the failure of pharmacological treatments has increased due to intrinsic or acquired fungal resistance and can lead to cases of recurrent VVC (RVVC) [27]. This last condition affects 4% of women worldwide, causing genitourinary discomfort and inflammatory symptoms, and interfering with quality of life [28]. Hence, new alternative treatments are greatly required. Despite several previous reports on the potential application of propolis for the management of VVC [22–26], the use of the crude residue lacks the potential to yield products that could be used in the preparation of reproducible or even safe pharmaceutical products. Ultrasound-assisted extraction (UAE) arises as a green alternative extraction method, its main advantages being low-cost equipment and better extraction time as well as lower energy requirements [29]. This technique is based on cavitation, a phenomenon generated by the propagation of strong ultrasound waves in liquids [30] that cause the collapse of cavitation bubbles, leading to cell disruption and promoting a good penetration of the solvent into the cells and, consequently, to a better extraction of bioactive compounds [31]. Additionally, the probe system is more powerful than the ultrasound bath, producing additional energy and faster chemical reactions [30]. Therefore, the extraction of propolis bioactive compounds to manage vulvovaginal candidiasis could benefit from this sustainable technique that can be easily scaled up, constituting a more economical and eco-friendly alternative for industrial application [30]. To the best of our knowledge, this is the first study that employs UAE to obtain active ingredients from propolis crude residue.

In this work, eco-friendly UAE is employed to prepare different extracts of propolis obtained from the Natural Park of Montesinho, an area with protected designation of origin in northeast Portugal (Trás-os-Montes region). Extracts were screened and characterized in terms of phenolic composition, radical scavenging activity, antioxidant/antiradical properties, toxicity towards human genital cell lines, and biological activity against Candida species, aiming to select the best one to be used against VVC.

2. Results and Discussion

2.1. TPC and Antioxidant/Antiradical Activities

TPC is a spectrophotometric method widely used to evaluate the antioxidant activity of extracts from herbs, fruits, or cereals, among others [32–35]. The TPC results and antioxidant/antiradical activities of propolis extracts are summarized in Table 1.

Table 1. Total phenolic content (TPC) and antioxidant/antiradical activities of propolis extracts based on their abilities to reduce ferric iron (Fe^{3+}) to ferrous iron (Fe^{2+}) and to sequester the ABTS radical. Results are expressed as mean ± standard deviation (n = 3). Different letters (a, b, c) in the same column indicate significant differences between mean values ($p < 0.05$).

Propolis Extracts	TPC mg GAE/g dw	FRAP IC_{50} (μg/mL)	ABTS IC_{50} (μg/mL)
Aqueous	217.7 ± 5.1 [a]	77.2 ± 2.1 [a]	202.8 ± 14.9 [a]
Hydroalcoholic	119.0 ± 5.3 [b]	169.8 ± 4.4 [b]	463.1 ± 39.6 [b]
Alcoholic	79.7 ± 3.8 [c]	284.3 ± 6.7 [c]	469.7 ± 33.9 [b]

The aqueous extract achieved the best result, followed by the hydroalcoholic and the alcoholic ones (217.7, 119.0, and 79.7 mg GAE/g dw, respectively). Significant differences were observed among all extracts ($p < 0.01$). According to Silva et al. [36], the TPC of propolis from Trás-os-Montes region ranged between 72.2 mg GAE/g dw and 277.2 mg GAE/g dw. Interestingly, a lower concentration was observed for the aqueous extract (72.2 mg GAE/g dw) in contrast to the present study (217.7 mg GAE/g dw). This difference may be due to the extraction method employed by the authors, which consisted of palynological processing using water, methanol, or 80% ethanol/water (1/10, v/v) as solvents [36]. In another study, Campo et al. [20] reported that the phenolic content was influenced by the sample's origin, achieving a lower value in propolis obtained from the northern part of Portugal, probably due to the different apicultural practices implemented by beekeepers [36].

The antioxidant activity of propolis extracts was assessed by the FRAP assay, while the antiradical activity was screened via the ABTS method (Table 1). The aqueous extract presented the highest antioxidant activity, achieving an IC_{50} value of 77.2 μg/mL, while the hydroalcoholic and the alcoholic extracts obtained IC_{50} values of 169.8 μg/mL and 284.3 μg/mL, respectively, with significant differences being observed between all extracts ($p < 0.05$). Similarly, Lagouri et al. [37] studied the antioxidant activity of propolis collected from the Greek mainland (West Macedonia) and Rhodes (Greece), being both extracted with methanol, methanol 80% (v/v), and water, through conventional extraction procedures. The extract from West Macedonia prepared with methanol 80% obtained an IC_{50} value of 0.0065 mg/mL, while the aqueous extract from Rhodes reached an IC_{50} value of 0.1690 mg/mL [37], results considerably worse than the ones achieved in the present study.

Regarding antiradical activity, IC_{50} values ranged between 202.8 μg/mL and 469.7 μg/mL for the aqueous and alcoholic extracts, respectively (Table 1). Once again, significant differences were observed between the aqueous extract and the other extracts ($p < 0.05$), in contrast to the alcoholic and hydroalcoholic extracts ($p = 0.349$). Vongsak et al. [38] also analyzed the antiradical activity of propolis from three stingless bee species, *Lepidotrigona ventralis* Smith, *L. terminata* Smith, and *Tetragonula pagdeni* Schwarz, collected in Thailand. The extracts were prepared by sonication, with 80% of ethanol at 40 °C for 30 min, and, subsequently, with hexane at 40 °C for 20 min [38]. The ABTS assay led to IC_{50} values that varied between 59.5 and 605.4 μg/mL for *T. pagdeni* and *L. terminata*, respectively [38]. These results were in line with the ones obtained in the present study. As can be observed in Table 1, the aqueous extract presented the best results, followed by the hydroalcoholic and alcoholic extracts, which can be explained by the high polarity and affinity of water to the polar compounds. It should also be highlighted that the extraction yields for the aqueous, hydroalcoholic and alcoholic extracts were, respectively, 14.41 ± 0.71%, 24.63 ± 1.23%, and 48.66 ± 2.43%.

2.2. Identification and Quantification of the Phenolic Profile

The identification of the phenolic compounds of the different extracts may justify the antioxidant and antiradical activities observed. A total of 38 compounds were identified in the extracts (Table 2). Figure 1 summarizes the chromatograms attained for the polyphenol's

standard mixture, as well as the aqueous, hydroalcoholic, and alcoholic extracts. In line with the results achieved for the spectrophotometric methods (Section 3.1), the aqueous extract showed the highest phenolic content.

Table 2. Phenolic compounds identified and quantified in propolis extracts through HPLC-DAD analysis (n = 3). Results are expressed as mean ± standard deviations (mg of phenolic compound/100 g dw).

Phenolic Compound	Aqueous (mg/100 g dw)	Hydroalcoholic (mg/100 g dw)	Alcoholic (mg/100 g dw)
Phenolic acids			
Gallic acid	34.1 ± 1.7	26.6 ± 1.3	13.9 ± 0.7
Protocatechuic acid	74.0 ± 3.7	17.1 ± 0.9	<LOD
Neochlorogenic acid	49.1 ± 2.5	<LOD	6.1 ± 0.3
Caftaric acid	26.3 ± 1.3	27.1 ± 1.4	9.5 ± 0.5
Chlorogenic acid	168 ± 8	27.6 ± 1.4	22.0 ± 1.1
4-*O*-caffeyolquinic acid	293 ± 15	112 ± 6	44.4 ± 2.2
Vanillic acid	2638 ± 132	29.4 ± 1.5	7.1 ± 0.4
Caffeic acid	<LOQ	12.2 ± 0.6	6.4 ± 0.3
Syringic acid	26.6 ± 1.3	29.0 ± 1.4	14.4 ± 0.7
p-coumaric acid	767 ± 38	585 ± 29	256 ± 13
Ferulic acid	2833 ± 142	2193 ± 110	1081 ± 54
Sinapic acid	<LOQ	ND	ND
3,5-di-caffeoylquinic acid	507 ± 25	241 ± 12	113 ± 6
Ellagic acid	<LOD	60.9 ± 3.0	32.9 ± 1.6
3,4-di-*O*-caffeoylquinic acid	20.9 ± 1.0	<LOQ	18.8 ± 0.9
Cinnamic acid	215 ± 11	ND	ND
Σ Phenolic acids	7652.0 ± 382.5	3360.9 ± 168.5	1625.5 ± 81.7
Flavanols			
(+)-Catechin	95.0 ± 4.7	72.4 ± 3.6	19.6 ± 1.0
(−)-Epicatechin	<LOQ	16.6 ± 0.8	ND
Σ Flavanols	95.0 ± 4.7	89.0 ± 4.4	19.6 ± 1.0
Flavanones			
Naringin	35.7 ± 1.8	529 ± 26	249 ± 12
Naringenin	9.0 ± 0.5	<LOQ	<LOD
Σ Flavanones	44.7 ± 2.3	529.0 ± 26.0	249.0 ± 12.0
Flavonols			
Quercetin-3-*O*-galactoside	17.3 ± 0.9	ND	ND
Quercetin-3-*O*-glucopyranoside	<LOQ	ND	ND
Rutin	<LOD	ND	ND
Myricetin	1783 ± 89	2839 ± 142	1444 ± 72
Kaempferol-3-*O*-glucoside	63.5 ± 3.2	39.5 ± 2.0	3.2 ± 0.2
Kaempferol-3-*O*-rutinoside	58.0 ± 2.9	22.2 ± 1.1	<LOD
Isorhamnetin-3-*O*-rutinoside	<LOD	40.1 ± 2.0	22.6 ± 1.1
Isorhamnetin-3-*O*-glucoside	ND	ND	ND
Quercetin	<LOQ	20.1 ± 1.0	17.2 ± 0.9
Quercitrin	ND	ND	ND
Tiliroside	55.4 ± 2.8	12.2 ± 0.6	3.0 ± 0.2
Kaempferol	24.6 ± 1.2	17.5 ± 0.9	13.0 ± 0.6
Σ Flavonols	2001.8 ± 100.0	2990.06 ± 149.6	1503.0 ± 75.0
Flavones			
Apigenin	<LOD	<LOQ	7.6 ± 0.4
Chrysin	10.9 ± 0.5	5.0 ± 0.3	2.9 ± 0.1
Σ Flavones	10.9 ± 0.5	5.0 ± 0.3	10.5 ± 0.5
Others			
Caffeine	75.9 ± 3.8	75.5 ± 3.8	12.3 ± 0.6
trans-polydatin	163 ± 8	54.0 ± 2.7	48.3 ± 2.4
Resveratrol	<LOQ	<LOQ	ND
Phloridzin	2036 ± 102	1834 ± 92	996 ± 50
Phloretin	24.6 ± 1.2	44.7 ± 2.2	20.0 ± 1.0
trans-epsilon viniferin	<LOD	<LOQ	ND
Σ Others	2299.5 ± 115.0	2008.2 ± 100.7	1076.6 ± 54.0

ND: not detected; LOD: limit of detection; LOQ: limit of quantification.

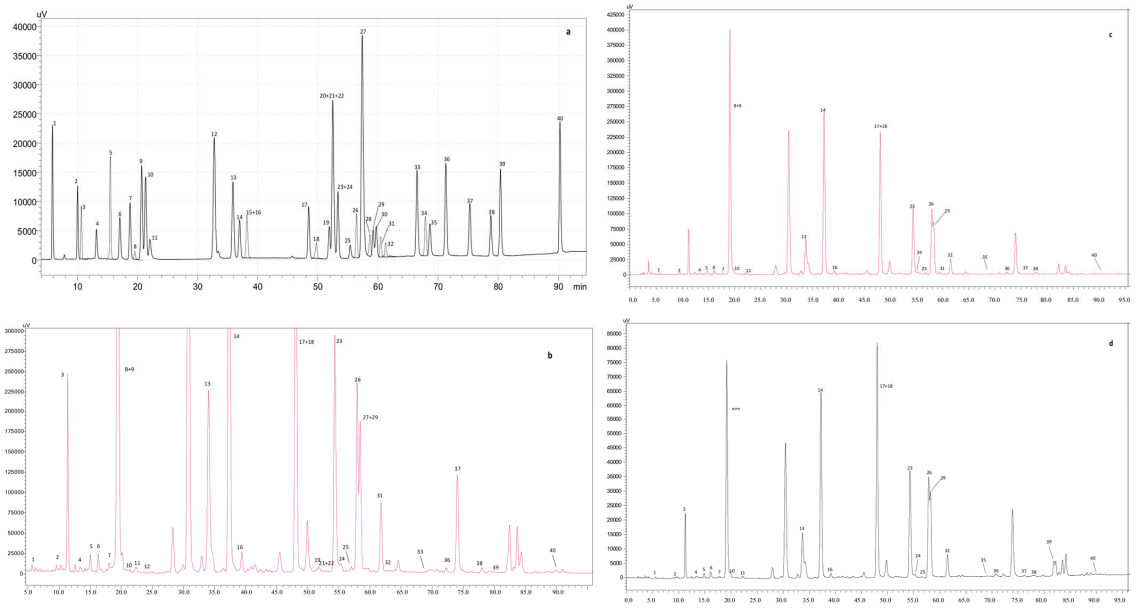

Figure 1. HPLC-DAD chromatograms at 280 nm for (**a**) polyphenols standard mixture of 5 mg/L, (**b**) propolis aqueous extract, (**c**) propolis hydroalcoholic (50:50; *v*/*v*) extract and (**d**) propolis alcoholic extract. Peak identification: (1) gallic acid, (2) protocatechuic acid, (3) neochlorogenic acid, (4) (+)-catechin, (5) caftaric acid, (6) caffeine, (7) chlorogenic acid, (8) 4-*O*-caffeoylquinic acid, (9) vanillic acid, (10) caffeic acid, (11) syringic acid, (12) (−)-epicatechin, (13) *p*-coumaric acid, (14) ferulic acid, (15) sinapic acid, (16) trans-polydatin, (17) naringin, (18) 3,5-di-caffeoylquinic acid, (19) quercetin-3-*O*-galactoside, (20) resveratrol, (21) quercetin-3-*O*-glucopyranoside, (22) rutin, (23) phloridzin, (24) ellagic acid, (25) 3,4-di-*O*-caffeoylquinic acid, (26) myricetin, (27) cinnamic acid, (28) quercitrin, (29) kaempferol-3-*O*-glucoside, (30) isorhamnetin-3-*O*-glucoside, (31) kaempferol-3-*O*-rutinoside, (32) isorhamnetin-3-*O*-rutinoside, (33) naringenin, (34) trans-epsilon viniferin, (35) quercetin, (36) phloretin, (37) tiliroside, (38) kaempferol, (39) apigenin, and (40) chrysin.

The main compounds present in the three extracts were phenolic acids, mostly ferulic acid. Vanillic and *p*-coumaric acid were also quantified in considerable amounts in the aqueous extract, while *p*-coumaric acid and 3,5-di-caffeoylquinic acid were the most representative phenolics (after ferulic acid) in the hydroalcoholic and alcoholic extracts. Flavonols were the second major class of compounds present in hydroalcoholic and alcoholic extracts, representing 33.30% and 33.51%, respectively. Myricetin was the main flavonol quantified in all extracts, followed by phloridzin. Catechin was identified in all extracts, although epicatechin was only identified in the hydroalcoholic extract. Additionally, apigenin, a well-known flavone, was only identified in the alcoholic extract, while chrysin was present in all extracts.

The different extracts revealed high levels of flavonoids, in accordance with a previous report for European samples of propolis [39]. Ozkok et al. [40] evaluated the phenolic composition of propolis collected from different Turkish regions and reported the presence of six phenolic acids, namely caffeic acid, *p*-coumaric acid, trans-ferulic acid, protocatechuic acid, trans-cinnamic acid, and caffeic acid phenethyl ester. The authors also quantified flavonoids, such as quercetin (1.12–4.14 mg/g), galangin (0.72–40.79 mg/g), apigenin (1.07–17.35 mg/g), and pinocembrin (1.32–39.92 mg/g), although some of these compounds were not evaluated in this study. Lagouri et al. [37] analyzed the phenolic composition of Greek propolis and reported the presence of caffeic acid (0.64–4.17 mg/g), ferulic acid (0.53–1.41 mg/g), *p*-coumaric acid (0.83–3.00 mg/g), apigenin (0.48–2.74 mg/g), and

galangin (1.32–8.55). Once again, the Portuguese propolis used in the present work seems to be richer in phenolic compounds when compared to the Greek propolis. These works demonstrate the richness of propolis in phenolic compounds and, most importantly, the influence of geographic conditions and the different extraction procedures on the bioactive composition of this complex matrix.

As expected, the phenolic profile results corroborate the antioxidant/antiradical results. The main phenolic compound quantified was ferulic acid, which is associated with antioxidant, antimicrobial, anti-inflammatory, anti-thrombosis, and anti-cancer properties [41]. In addition, the aqueous extract showed high amounts of vanillic acid when compared to the other extracts (2638 mg/100 g dw), which may justify the higher antiradical activity observed, being in line with previous authors [42]. Moreover, myricetin was also found in high quantities, acting as an antifungal against *C. albicans,* and reducing biofilm formation [43,44]. Catechin is another excellent antioxidant identified in the extracts. When used in combination with lower doses of antimycotics, catechin significantly inhibits the growth of fluconazole-resistant *C. albicans* [45]. These results highlight the antioxidant and anti-candidiasis effects of the phenolic compounds present in the propolis extracts prepared.

2.3. In Vitro Scavenging Capacity against ROS

ROS production is a consequence of normal metabolism, performing various physiological functions [46]. Although the role of moderately increased ROS levels in activating antifungal activity of neutrophils and macrophages may be beneficial for host response to vulvovaginal infection [47,48], the excessive production of these reactive species can exacerbate the inflammatory state associated with VVC [49]. The ROS scavenging capacities of the different extracts are summarized in Table 3.

Table 3. $O_2^{\bullet-}$ and HOCl scavenging capacities of propolis extracts. Values are expressed as mean ± standard deviation (n = 3). Different letters (a, b) in the same column indicate significant differences between mean values ($p < 0.05$).

	ROS	
	$O_2^{\bullet-}$	HOCl
	IC_{50} (μg/mL)	
Propolis extracts		
Aqueous	67.3 ± 1.0 [a]	7.5 ± 1.2 [a]
Hydroalcoholic	651.4 ± 11.2 [b]	11.3 ± 0.8 [a]
Alcoholic	>1000	38.1 ± 3.9 [b]
Positive Controls		
Gallic acid	24.6 ± 1.5	0.7 ± 0.1
Catechin	84.4 ± 4.6	0.1 ± 0.01

Regarding the $O_2^{\bullet-}$ uptake capacity, an IC_{50} value of 67.3 μg/mL was obtained for the aqueous extract, while a significantly higher value (651.4 μg/mL) was determined for the hydroalcoholic extract ($p < 0.01$). The scavenging capacity of the alcoholic extract was mild (inhibition percentage up to around 20%) at the highest tested concentration (1000 μg/mL). Furthermore, the aqueous extract attested a superior capacity to scavenge this oxygen species than the positive control catechin (IC_{50} = 84.4 μg/mL), supporting the excellent capacity of this extract.

Regarding the HOCl scavenging potential, the aqueous extract also achieved the highest activity (IC_{50} = 7.5 μg/mL), followed by the hydroalcoholic (IC_{50} = 11.3 μg/mL) and alcoholic extracts (IC_{50} = 38.1 μg/mL). Significant differences were observed ($p < 0.05$) for the alcoholic extract when compared to the other two, but not between the aqueous and the hydroalcoholic extracts (p = 0.130). Francisco et al. [50] registered IC_{50} values of 226.8 μg/mL and 13.3 μg/mL, respectively, for the scavenging activity against $O_2^{\bullet-}$ and HOCl of the Brazilian propolis, highlighting the promising results for the extracts proposed in the

present study. Additionally, the results are in line with the in vitro antioxidant/antiradical activities reported in the previous sections as well as the phenolic composition described. The higher scavenging efficacy of the aqueous propolis extract may be due to its superior content in phenolic compounds, particularly ferulic acid, well-known for its capacity to neutralize free radicals and act on the reduction of xanthine oxidase and cyclooxygenase activity [51]. Phloridzin is the main flavone found in propolis extracts and may inhibit the formation of $O_2^{\bullet -}$ as well as lipid peroxides [52]. Flavonols, such as kaempferol, quercetin, and myricetin, have huge potential as ROS scavengers due to the number of hydroxyl groups on the B-ring [53,54]. Overall, the scavenging capacity of the aqueous and hydroalcoholic propolis extracts may be beneficial for the purpose of VVC management.

2.4. Antifungal Activity

The activity of the different extracts against six standard ATCC *Candida* spp. strains was determined according to the clinically relevant CLSI M27-A4 method (Table 4).

Table 4. Anti-Candida activity of propolis extracts. Results are presented as MIC and MFC values against ATCC strains and vaginal isolates of Candida species. Results are presented singly or as range values (n = 3). Sensitivity of each strain to fluconazole is presented for reference purposes.

Strains	Fluconazole Susceptibility	Aqueous		Hydroalcoholic		Alcoholic	
		MIC (μg/mL)	MIC (μg/mL)	MFC (μg/mL)	MFC (μg/mL)	MIC (μg/mL)	MFC (μg/mL)
C. albicans ATCC 90028	S	256	128–256	>512	>512	512	>512
C. albicans ATCC 64550	R	128–256	128–512	>512	>512	512	>512
C. glabrata ATCC 2001	S-DD	≈512	≈512	>512	>512	≈512	>512
C. parapsilosis ATCC 22019	S	256	128	512	>512	512	>512
C. krusei ATCC 6258	S-DD	512	256–512	>512	>512	≈512	>512
C. tropicalis ATCC 750	S	≈512	256–512	>512	>512	≈512	>512

S: susceptible; S-DD: susceptible (dose-dependent); R: resistant.

All extracts presented fungistatic activity, with MIC values varying from 128 to 512 μg/mL, with mild differences between extracts. The higher activity of the aqueous and hydroalcoholic extracts when compared to the alcoholic one may be related to their superior polyphenol content. Touzani et al. [55] also suggested that the antifungal activity of propolis is related to the presence of this type of compound. Values of MFC higher than 512 μg/mL for nearly all strains further reinforce the fungistatic nature of the tested extracts. Importantly, anti-Candida activity appeared to be maintained for strains resistant or featuring dose-dependent susceptibility to fluconazole, suggesting that the extracts could be useful in cases of azole-resistant VVC, particularly those with scarce availability of alternative treatment options [56]. According to Tobaldini-Valerio et al. [57], propolis extracts with MIC values < 800 μg/mL are potentially useful inhibitors of Candida spp. and considered suitable for topical therapy. Additionally, Duarte et al. [58] proposed a broader classification for plant products, stating that MIC values around 0.5 mg/mL indicate strong antifungal inhibitory activity. According to these authors, MIC values up to 2 mg/mL are still indicative of suitable activity for medical use. Thus, all tested extracts seem to be suitable as promising antifungal candidates for managing candidiasis.

2.5. Cytotoxicity Activity

The effect of propolis extracts on the viability of two relevant human cell lines of genital origin, viz. HEC-1-A and Ca Ski [59,60], was tested after 4 h of incubation. The relatively short time of exposure was selected to better mimic the typically brief residence time of drug products in the vagina [61]. The results are summarized in Table 5.

Table 5. Effects of propolis extract exposure on the viability (%) of HEC-1-A and Ca Ski cell lines at different concentrations, as measured by the resazurin assay. Values are expressed as mean ± standard deviation (n = 3). Different letters (a, b, c, d) in the same line indicate significant differences between mean values ($p < 0.05$).

Sample	Concentration (μg/mL)				
	128	256	512	1024	2048
			HEC-1-A		
Aqueous extract	102.70 ± 5.14 ^{a}	102.50 ± 6.01 ^{a}	59.30 ± 2.97 ^{b}	56.60 ± 5.83 ^{b}	66.11 ± 8.06 ^{b}
Hydroalcoholic extract	91.80 ± 4.00 ^{a}	90.70 ± 6.80 ^{a}	60.40 ± 7.80 ^{b}	33.60 ± 1.70 ^{c}	36.60 ± 1.80 ^{c}
Alcoholic extract	121.80 ± 5.14 ^{a}	78.50 ± 6.01 ^{b}	69.90 ± 2.97 ^{b}	34.80 ± 5.83 ^{c}	7.30 ± 0.20 ^{d}
Positive control			99.55 ± 4.09		
Negative control			0.00 ± 0.45		
			Ca Ski		
Aqueousextract	127.80 ± 5.14 ^{a}	123.90 ± 6.01 ^{a}	90.00 ± 2.97 ^{b}	87.00 ± 5.83 ^{b}	85.60 ± 8.06 ^{b}
Hydroalcoholic extract	111.70 ± 6.63 ^{a}	104.50 ± 6.05 ^{a}	74.10 ± 2.20 ^{b}	54.80 ± 0.10 ^{c}	16.00 ± 0.81 ^{d}
Alcoholic extract	112.60 ± 6.62 ^{a}	114.10 ± 5.72 ^{a}	108.50 ± 5.43 ^{a}	59.50 ± 2.97 ^{b}	26.60 ± 1.60 ^{c}
Positive control			101.60 ± 6.08		
Negative control			0.00 ± 0.56		

The mean CC_{50} values for the aqueous extract were above the maximum tested concentration (2048 μg/mL) in both cell lines and at least four times higher than the MIC values. These results suggest, at least, mild selectivity of the aqueous extract between host and pathogen cells. Moreover, the toxicity was higher for the hydroalcoholic and alcoholic extracts, with CC_{50} values of 896 μg/mL and 813 μg/mL in HEC-1-A cells and 1264 μg/mL and above 2048 μg/mL in Ca Ski cells, respectively.

Generally, lower CC_{50} values were reported by other authors for propolis extracts. For example, Banskota et al. [62] stated values from 51 μg/mL to over 100 μg/mL for different extracts of Brazilian propolis after 4 days of incubation with HT-1080 fibrosarcoma and murine colon 26-L5 cells. Bonamigo et al. [63] established CC_{50} values around 0.4–0.5 mg/mL for ethanolic extracts of propolis from *Apis mellifera* when tested in peripheral blood mononuclear cells and an erythroleukemia cell line upon 24 h of contact. Recently, Campoccia et al. [64] reported CC_{50} values for various poplar-type propolis extracts ranging from 70 to 85 μg/mL for MG63 osteosarcoma cells and lower than 40 μg/mL for L929 fibroblasts after overnight incubation. Therefore, the extracts prepared in the present study seem to be suitable for vaginal application, presenting low toxicity for both cell lines.

3. Materials and Methods

3.1. Chemicals

Gallic acid, sodium carbonate (Na_2CO_3), catechin, nitrotetrazolium blue chloride (NBT), ascorbic acid, 2,2′-azinobis-3-ethylbenzothiozoline-6-sulfonic (ABTS), potassium persulfate ($K_2S_2O_8$), dihydrorodamine (DHR), and sodium hypochlorite (NaOCl) were purchased from Sigma-Aldrich, Taufkirchen, Germany. Ferric chloride ($FeCl_3$), sodium hydroxide (NaOH), dimethylformamide (DMF), disodium (Na_2HPO_4), monopotassium phosphate (KH_2PO_4) phenol reagent appropriate for Folin-Ciocalteu (Folin) and Sabouraud dextrose broth (SDA) were obtained from Merck, Darmstadt, Germany. 2,4,6-Tris(2-pyridyl)-s-triazine (TPTZ), ferrous sulfate, β-nicotinamide adenine dinucleotide (NADH), and phenazine methosulfate (PMS) were purchased from Sigma-Aldrich, Buchs (Switzerland), Anekal Taluk (India), and Burlington, VT, (USA), respectively. Sodium acetate, RPMI 1640 and morpholinopropanesulfonic acid (MOPS) was sourced from Sigma Chemical Co., Burlington, VT, USA, acetic acid from Chem-Lab NV, Zedelgem, Belgium, and anhydrous absolute ethanol from Carlo Erba Reagents, Val-de-Reuil, France. Ultra-pure water was

obtained in-house using a Milli-Q water purification system (TGI Pure Water Systems, San Diego, CA, USA). All other chemicals were of analytical grade or equivalent.

3.2. Propolis Samples and Extraction

Propolis was collected from *Apis mellifera* L. bee hives in apiaries located in the Natural Park of Montesinho (41°53′49″ N, 6°51′58″ W) in September 2021. The crude extracts were packed in sealed plastic bags and stored at −18 °C until further use. The propolis extraction was conducted by UAE using ethanol, water, or an hydroalcoholic mixture (50:50, *v*/*v*) as solvent, according to the procedure described by Cavalaro et al. [65]. Briefly, the extracts were obtained using an ultrasonic processor (Sonics Vibra-cell™, VCX 500/VCX 750, Lutterworth, UK) with a frequency of 20 KHz and a probe (630–0220) with 13 mm diameter. For extraction, 0.86 g of sample was added to 30 mL of solvent for 20 min, at 25 °C and with 30% sonication amplitude. The samples were subsequently centrifuged at 4700× *g* for 15 min at 25 °C and filtered using Whatman no. 2 filters. The aqueous extracts were frozen at −80 °C until lyophilization (Telstar LyoQuest, Barcelona, Spain), while the alcoholic and hydroalcoholic extracts were kept under refrigeration at 4 °C until evaporation in a rotary evaporator (Vacuum Controller V-800, Büchi, Aesch, Switzerland) at 40 °C. The yield was calculated using the dry weight of the extract and soaked samples.

3.3. Determination of Total Phenolic Content

The total phenolic content (TPC) was calculated spectrophotometrically, based on a complex redox reaction, as described by Pinto et al. [66]. The reaction mixture occurred in each well of a 96-well microplate and consisted of a mixture of sample, Folin-Ciocalteu reagent, and Na_2CO_3 solution (7.5%, *w*/*v*). Samples were in a concentration of 500 μg/mL. The absorbance was read at 765 nm using a Synergy HT Microplate Reader (BioTek Instruments, Winooski, VT, USA). Gallic acid was used as standard (linearity range = 5–100 μg/mL; R^2 = 0.9992). The results were expressed as milligrams of gallic acid equivalents (GAE) per gram of dry weight (dw) (mg GAE/g dw).

3.4. Determination of In Vitro Antioxidant/Antiradical Activities

3.4.1. Ferric Reducing Antioxidant Power

The ferric ion reduction antioxidant capacity (FRAP) was calculated based on the reduction of a ferric 2,4,6-trypyridyl-s-triazine complex (Fe^{2+}-TPTZ) to the ferrous form (Fe^{3+}-TPTZ), as described by Benzie and Strain [67], with minor modifications. The assay was performed directly in a 96-well microplate, adding sample and FRAP reagent to each well. The reaction mixture was incubated at 37 °C for 30 min and the absorbance was read at 595 nm in a Synergy HT Microplate Reader. Ferrous sulfate 1 mM ($FeSO_4 \cdot 7H_2O$) was used as standard (linearity range: 25–500 μM; R^2 = 0.9997). The results were presented as half-maximal inhibitory concentration (IC_{50}) values.

3.4.2. ABTS Radical Scavenging Assay

The evaluation of the ABTS radical sequestration capacity was performed according to the methodology described by Re et al. [68], with minor modifications. The assay was performed directly in a 96-well microplate by adding ABTS solution and sample to each well. Ascorbic acid was used as standard (linearity range: 5–100 μg/ mL; R^2 > 0.9922). The results were expressed as IC_{50} values.

3.5. Phenolic Profile Analysis

Propolis extracts were analyzed by high performance liquid chromatography with a diode-array detector (HPLC-DAD), as described by Moreira et al. [69]. The chromatographic separation was carried out on a reversed-phase Phenomenex Gemini C18 column (250 × 4.6 mm, 5 μm particle size) at 25 °C. The mobile phase comprised methanol and water, both with 0.1% of formic acid, and a gradient program was used. The chromatograms were acquired at a wavelength of 280 nm by a photodiode array detector (Merck® Hitachi

Diode Array Detector L-2455, Kent, UK). The results were expressed as mg of each phenolic compound per 100 g of extract on dw (mg/100 g dw).

3.6. Assessment of Reactive Oxygen Species Scavenging Capacity

3.6.1. Superoxide Radical Scavenging Assay

The superoxide anion radical ($O_2^{\bullet -}$) scavenging capacity was determined spectrophotometrically, as described by Gomes et al. [70]. Absorbance was read at 560 nm for 6 min at 37 °C in a Synergy HT Microplate Reader. The results were expressed as IC_{50} values of the reduction of NBT to a purple-colored diformazan upon reaction with O_2.

3.6.2. Hypochlorous Acid Scavenging Assay

The uptake capacity of hypochlorous acid (HOCl) was determined by monitoring the effect of propolis on the HOCl-induced oxidation of DHR to rhodamine, according to Gomes et al. [70]. The fluorescence was read at 37 °C for 5 min, at wavelengths of 485 ± 20 nm and 528 ± 20 nm. The results were expressed as the inhibition (IC_{50} values) of HOCl-induced DHR oxidation.

3.7. Determination of Antifungal Activity

The activity of propolis extracts against *Candida* spp. was determined using the CLSI M27-A4 broth microdilution method [71]. Six reference strains from the American Type Culture Collection (ATCC, Manassas, VA, USA) were used, namely *C. albicans* (ATCC 90028 and ATCC 64550), *C. glabrata* (ATCC 2001), *C. parapsilosis* (ATCC 22019), *C. krusei* (ATCC 6258) and *C. tropicalis* (ATCC 750). In brief, isolates were subcultured on Sabouraud Dextrose Broth (SDA) for 24 h at 37 °C before being dispersed in RPMI 1640 medium supplemented with MOPS (pH = 7.0) to a final concentration of 0.5–2.5 × 10^3 cells/mL. The assay was performed in 96-well microplates by mixing 100 µL of *Candida* spp. dispersions with 100 µL of extracts dispersed in the same medium. Final concentration of propolis extracts ranged from 4 to 512 µg/mL. The minimum inhibitory concentration (MIC; defined as the lowest concentration without growth) was determined after 48 h of incubation at 37 °C by visual inspection. Experiments were performed in triplicate. Additionally, the minimal fungicidal concentration (MFC) was assessed by collecting 20 µL of the content of wells at MIC and higher concentrations and plating it onto SDA in duplicate for 24 h at 37 °C. MFC values were defined as the lowest concentration at which no apparent growth was observable.

3.8. Cell Viability Assays

The toxicity of propolis extracts to human cell lines of female genital tract origin, namely HEC-1-A endometrial cells and Ca Ski cervical cells (ATCC), was determined through the resazurin reduction assay [72]. These cell lines were selected since they are representative in vitro models of the female genital epithelia and have been used in the past for screening the toxicity of drugs, excipients and formulations intended for vaginal use [73,74]. HEC-1-A cells and Ca Ski cells were maintained in McCoy's 5A medium and RPMI 1640 medium, respectively, in both cases supplemented with 10% (*v*/*v*) fetal bovine serum, 100 U/mL penicillin and 100 µg/mL streptomycin, and kept at 37 °C, 95% relative humidity (RH), and 5% CO_2. Cells were seeded at a density of 5000/well in 96-well plates and incubated for 24 h, after which propolis extracts were added at different concentrations (128–2048 µg/mL) and cells incubated for an additional 4 h. Cells incubated with plain culture medium and 1% (*w*/*v*) Triton X-100 were also used as controls. Resazurin was then added at a concentration of 10 µg/mL and cells left to incubate for 3 h. Finally, supernatants (100 µL) were transferred to an opaque 96-well plate and the fluorescence was measured at 590/530 nm using a Synergy HT Multi-Mode plate reader (BioTek). Experiments were performed in triplicate and cell viability was used to calculate half-maximal cytotoxic concentration (CC_{50}) values by log-logistic regression using Prism 8 (Graph-Pad, La Jolla, CA, USA).

3.9. Statistical Analysis

The results are presented as mean ± standard deviation (n = 3). Microsoft Office Excel 2020 and SPSS Statistics 28.0 software were used for data analysis. One-way ANOVA test, followed by HSD Tukey's post-hoc test, was applied to assess differences between trials. A paired sample Student's t-test was also performed to compare the means of the variables with each other. Values of $p < 0.05$ were considered as statistically significant.

4. Conclusions

The present work reported for the first time the assessment of propolis from the Natural Park of Montesinho, a protected Portuguese region, as a potential new antifungal ingredient for pharmaceutical applications. The green extraction methodology employed, coupled with the sustainable solvents used, allowed us to obtain extracts rich in bioactive compounds, with considerable antioxidant and antiradical activities. The aqueous extract achieved the best outcomes in the spectrophotometric tests employed, exhibiting a phenolic profile mainly characterized by the presence of ferulic acid, vanillic acid, *p*-coumaric acid, and myricetin. Also, this extract was shown to be effective against the tested Candida species. The cell viability assay attested the low toxicity of the aqueous extract in both cell lines used (Ca Ski and HEC-1-A). Therefore, the aqueous extract was revealed to be the most promising, presenting antioxidant and anti-candidiasis effects commonly involved in VVC. In the future, complementary studies, such as in vitro permeability assays, should be performed to ensure the safety and efficacy of this extract against VVC. Moreover, to complement the anti-fungal activity, the antimicrobial capacity should be analyzed.

Author Contributions: Conceptualization, J.d.N. and F.R.; methodology, A.M.S., B.R., M.M.M., J.d.N. and F.R.; software, A.M.S., B.R., M.M.M., J.d.N. and F.R.; validation, J.d.N. and F.R.; formal analysis, A.M.S., B.R., M.M.M., J.d.N. and F.R.; investigation, A.M.S., B.R., M.M.M., J.d.N. and F.R.; resources, C.D.-M., J.d.N. and F.R.; writing—original draft preparation, A.M.S. and B.R.; writing—review and editing, M.M.M., J.d.N. and F.R.; supervision, J.d.N. and F.R.; project administration, J.d.N. and F.R.; funding acquisition, C.D.-M., J.d.N. and F.R. All authors have read and agreed to the published version of the manuscript.

Funding: This work was funded by the project MTS/SAS/0077/2020—Honey+—New reasons to care honey from the Natural Park of Montesinho: A bioindicator of environmental quality & its therapeutic potential. This work also received financial support from projects LA/P/0008/2020 (DOI 10.54499/LA/P/0008/2020), UIDP/50006/2020 (DOI 10.54499/UIDP/50006/2020) and UIDB/50006/2020 (DOI 10.54499/UIDB/50006/2020).

Institutional Review Board Statement: Not applicable.

Informed Consent Statement: Not applicable.

Data Availability Statement: Data contained within the article.

Acknowledgments: The authors are grateful to Associação de Apicultores do Parque Natural de Montesinho for the samples. Ana Margarida Silva is grateful for her Ph.D. grant (SFRH/BD/144994/2019) financed by POPH-QREN and subsidized by the European Science Foundation and Ministério da Ciência, Tecnologia e Ensino Superior. Manuela M. Moreira (CEECIND/02702/2017), José das Neves (CEECIND/01280/2018) and Francisca Rodrigues (CEECIND/01886/2020) are grateful for their contracts financed by FCT/MCTES-CEEC Individual Program Contract. The authors also acknowledge the support of the Biointerfaces and Nanotechnology i3S Scientific Platform.

Conflicts of Interest: The authors declare no conflicts of interest.

References

1. United Nations, Department of Economic and Social Affairs, Population Division. *World Population Prospects 2019: Highlights*; United Nations: New York, NY, USA, 2019.
2. Wezel, A.; Casagrande, M.; Celette, F.; Jean-François, V.; Ferrer, A.; Peigné, J. Agroecological practices for sustainable agriculture. A review. *Agron. Sustain. Dev.* **2014**, *34*, 1–20. [CrossRef]

3. Peter, C.; Waller, S.; Picoli, T.; da Gama Osório, L.; Zani, J.L.; Meireles, M.; Faria, R.O.; Mello, J.; Hubner, S.; Lima, M.; et al. Chemical and cytotoxic analyses of three varieties of Brazilian propolis (green propolis, jataí propolis and brown propolis) and its anti-Sporothrix brasiliensis in vitro activity. *Arq. Bras. Med. Vet.* **2019**, *71*, 819–827. [CrossRef]
4. Kabir, F.; Tow, W.W.; Hamauzu, Y.; Katayama, S.; Tanaka, S.; Nakamura, S. Antioxidant and cytoprotective activities of extracts prepared from fruit and vegetable wastes and by-products. *Food Chem.* **2015**, *167*, 358–362. [CrossRef] [PubMed]
5. FAO. Available online: https://www.fao.org/fsnforum/consultation/beekeeping (accessed on 1 October 2023).
6. Damodaran, T. Chapter 46—Propolis. In *Nutraceuticals*, 2nd ed.; Gupta, R.C., Lall, R., Srivastava, A., Eds.; Academic Press: Cambridge, MA, USA, 2021; pp. 795–812.
7. Burdock, G.A. Review of the biological properties and toxicity of bee propolis (propolis). *Food Chem. Toxicol.* **1998**, *36*, 347–363. [CrossRef] [PubMed]
8. Cauich-Kumul, R.; Segura Campos, M.R. Chapter 12—Bee Propolis: Properties, Chemical Composition, Applications, and Potential Health Effects. In *Bioactive Compounds*; Campos, M.R.S., Ed.; Woodhead Publishing: Sawston, UK, 2019; pp. 227–243.
9. Anjum, S.I.; Ullah, A.; Khan, K.A.; Attaullah, M.; Khan, H.; Ali, H.; Bashir, M.A.; Tahir, M.; Ansari, M.J.; Ghramh, H.A.; et al. Composition and functional properties of propolis (bee glue): A review. *Saudi J. Biol. Sci.* **2019**, *26*, 1695–1703. [CrossRef] [PubMed]
10. Okińczyc, P.; Paluch, E.; Franiczek, R.; Widelski, J.; Wojtanowski, K.K.; Mroczek, T.; Krzyżanowska, B.; Skalicka-Woźniak, K.; Sroka, Z. Antimicrobial activity of *Apis mellifera* L. and *Trigona* sp. propolis from Nepal and its phytochemical analysis. *Biomed. Pharmacother.* **2020**, *129*, 110435. [CrossRef] [PubMed]
11. Lu, L.C.; Chen, Y.W.; Chou, C.C. Antibacterial activity of propolis against Staphylococcus aureus. *Int. J. Food Microbiol.* **2005**, *102*, 213–220. [CrossRef]
12. Marcucci, M.C.; Ferreres, F.; García-Viguera, C.; Bankova, V.S.; De Castro, S.L.; Dantas, A.P.; Valente, P.H.; Paulino, N. Phenolic compounds from Brazilian propolis with pharmacological activities. *J. Ethnopharmacol.* **2001**, *74*, 105–112. [CrossRef]
13. Ożarowski, M.; Karpiński, T.M.; Alam, R.; Łochyńska, M. Antifungal Properties of Chemically Defined Propolis from Various Geographical Regions. *Microorganisms* **2022**, *10*, 364. [CrossRef]
14. Koç, A.; Silici, S.; Kasap, F.; Hörmet-Oz, H.; Mavus-Buldu, H.; Ercal, B. Antifungal Activity of the Honeybee Products against *Candida* spp. and *Trichosporon* spp. *J. Med. Food* **2011**, *14*, 128–134. [CrossRef]
15. Mazia, R.S.; de Araújo Pereira, R.R.; de Francisco, L.M.B.; Natali, M.R.M.; Dias Filho, B.P.; Nakamura, C.V.; Bruschi, M.L.; Ueda-Nakamura, T. Formulation and Evaluation of a Mucoadhesive Thermoresponsive System Containing Brazilian Green Propolis for the Treatment of Lesions Caused by Herpes Simplex Type I. *J. Pharm. Sci.* **2016**, *105*, 113–121. [CrossRef] [PubMed]
16. Banskota, A.H.; Nagaoka, T.; Sumioka, L.Y.; Tezuka, Y.; Awale, S.; Midorikawa, K.; Matsushige, K.; Kadota, S. Antiproliferative activity of the Netherlands propolis and its active principles in cancer cell lines. *J. Ethnopharmacol.* **2002**, *80*, 67–73. [CrossRef] [PubMed]
17. Orsolić, N.; Knezević, A.H.; Sver, L.; Terzić, S.; Basić, I. Immunomodulatory and antimetastatic action of propolis and related polyphenolic compounds. *J. Ethnopharmacol.* **2004**, *94*, 307–315. [CrossRef] [PubMed]
18. Machado, J.L.; Assunção, A.K.; da Silva, M.C.; Dos Reis, A.S.; Costa, G.C.; Arruda Dde, S.; Rocha, B.A.; Vaz, M.M.; Paes, A.M.; Guerra, R.N.; et al. Brazilian green propolis: Anti-inflammatory property by an immunomodulatory activity. *Evid. Based Complement. Alternat Med.* **2012**, *2012*, 157652. [CrossRef]
19. Miguel, M.G.; Nunes, S.; Dandlen, S.A.; Cavaco, A.M.; Antunes, M.D. Phenols and antioxidant activity of hydro-alcoholic extracts of propolis from Algarve, South of Portugal. *Food Chem. Toxicol.* **2010**, *48*, 3418–3423. [CrossRef] [PubMed]
20. Isla, M.I.; Nieva Moreno, M.I.; Sampietro, A.R.; Vattuone, M.A. Antioxidant activity of Argentine propolis extracts. *J. Ethnopharmacol.* **2001**, *76*, 165–170. [CrossRef] [PubMed]
21. Sulaiman, G.M.; Sammarrae, K.W.A.; Ad'hiah, A.H.; Zucchetti, M.; Frapolli, R.; Bello, E.; Erba, E.; D'Incalci, M.; Bagnati, R. Chemical characterization of Iraqi propolis samples and assessing their antioxidant potentials. *Food Chem. Toxicol.* **2011**, *49*, 2415–2421. [CrossRef]
22. De Araújo Pereira, R.R.; Godoy, J.S.R.; Svidzinski, T.I.S.; Bruschi, M.L. Preparation and Characterization of Mucoadhesive Thermoresponsive Systems Containing Propolis for the Treatment of Vulvovaginal Candidiasis. *J. Pharm. Sci.* **2013**, *102*, 1222–1234. [CrossRef]
23. Bruschi, M.; Dota, K.; Consolaro, M.; Svidzinski, T. Antifungal Activity of Brazilian Propolis Microparticles against Yeasts Isolated from Vulvovaginal Candidiasis. *Evid. Based Complement. Alternat Med.* **2011**, *2011*, 201953.
24. Bonfim, A.P.; Sakita, K.M.; Faria, D.R.; Arita, G.S.; Vendramini, F.; Capoci, I.R.G.; Braga, A.G.; Dos Santos, R.S.; Bruschi, M.L.; Becker, T.C.A.; et al. Preclinical approaches in vulvovaginal candidiasis treatment with mucoadhesive thermoresponsive systems containing propolis. *PLoS ONE* **2020**, *15*, e0243197. [CrossRef]
25. Imhof, M.; Lipovac, M.; Kurz, C.; Barta, J.; Verhoeven, H.C.; Huber, J.C. Propolis solution for the treatment of chronic vaginitis. *Int. J. Gynaecol. Obstet.* **2005**, *89*, 127–132. [CrossRef] [PubMed]
26. Pairazaman, A.T.E.; Pinto, J.D.C.; Chávez, B.A.; Apac, G.L.; Sandoval, C.B.H.; Quispe, F.M.M.; Meza, V.A.J.C.; Fretell, W.G.I.; Loyola, G.A.R. Antifungal activity of propolis extract against *Candida albicans* in patients with vulvovaginal candidiasis. *F1000Research* **2022**, *11*, 1185. [CrossRef]
27. Sobel, J.D. Recurrent vulvovaginal candidiasis. *Am. J. Obstet. Gynecol.* **2016**, *214*, 15–21. [CrossRef]

28. Denning, D.W.; Kneale, M.; Sobel, J.D.; Rautemaa-Richardson, R. Global burden of recurrent vulvovaginal candidiasis: A systematic review. *Lancet Infect. Dis.* **2018**, *18*, e339–e347. [CrossRef] [PubMed]
29. Nie, J.; Chen, D.; Ye, J.; Lu, Y.; Dai, Z. Optimization and kinetic modeling of ultrasonic-assisted extraction of fucoxanthin from edible brown algae *Sargassum fusiforme* using green solvents. *Ultrason. Sonochem.* **2021**, *77*, 105671. [CrossRef] [PubMed]
30. Wen, C.; Zhang, J.; Zhang, H.; Dzah, C.S.; Zandile, M.; Duan, Y.; Ma, H.; Luo, X. Advances in ultrasound assisted extraction of bioactive compounds from cash crops—A review. *Ultrason. Sonochem.* **2018**, *48*, 538–549. [CrossRef]
31. Toma, M.; Vinatoru, M.; Paniwnyk, L.; Mason, T.J. Investigation of the effects of ultrasound on vegetal tissues during solvent extraction. *Ultrason. Sonochem.* **2001**, *8*, 137–142. [CrossRef]
32. Shahidi, F.; Zhong, Y. Measurement of antioxidant activity. *J. Funct. Foods* **2015**, *18*, 757–781. [CrossRef]
33. Rodrigues, F.; Palmeira-de-Oliveira, A.; das Neves, J.; Sarmento, B.; Amaral, M.H.; Oliveira, M.B. *Medicago* spp. extracts as promising ingredients for skin care products. *Ind. Crops Prod.* **2013**, *49*, 634–644. [CrossRef]
34. Krisch, J.; Ördögh, L.; Galgóczy, L.; Papp, T.; Vágvölgyi, C. Anticandidal effect of berry juices and extracts from Ribes species. *Open Life Sci.* **2009**, *4*, 86–89. [CrossRef]
35. Gallucci, M.N.; Carezzano, M.E.; Oliva, M.; Demo, M.S.; Pizzolitto, R.P.; Zunino, M.P.; Zygadlo, J.A.; Dambolena, J.S. In vitro activity of natural phenolic compounds against fluconazole-resistant Candida species: A quantitative structure–activity relationship analysis. *J. Appl. Microbiol.* **2014**, *116*, 795–804. [CrossRef] [PubMed]
36. Silva, J.C.; Rodrigues, S.; Feás, X.; Estevinho, L.M. Antimicrobial activity, phenolic profile and role in the inflammation of propolis. *Food Chem. Toxicol.* **2012**, *50*, 1790–1795. [CrossRef] [PubMed]
37. Lagouri, V.; Prasianaki, D.; Krysta, F. Antioxidant properties and phenolic composition of Greek propolis extracts. *Int. J. Food Prop.* **2014**, *17*, 511–522. [CrossRef]
38. Vongsak, B.; Kongkiatpaiboon, S.; Jaisamut, S.; Machana, S.; Pattarapanich, C. In vitro alpha glucosidase inhibition and free-radical scavenging activity of propolis from Thai stingless bees in mangosteen orchard. *Rev. Bras. Farmacogn.* **2015**, *25*, 445–450. [CrossRef]
39. Choi, S.J.; Shimomura, K.; Kumazawa, S.; Ahn, M.-R. Antioxidant properties and phenolic composition of propolis from diverse geographic regions in Korea. *Food Sci. Technol. Res.* **2013**, *19*, 211–222. [CrossRef]
40. Özkök, A.; Keskin, M.; Tanuğur Samancı, A.E.; Yorulmaz Önder, E.; Takma, Ç. Determination of antioxidant activity and phenolic compounds for basic standardization of Turkish propolis. *Appl. Biol. Chem.* **2021**, *64*, 37. [CrossRef] [PubMed]
41. Ou, S.; Kwok, K.C. Ferulic acid: Pharmaceutical functions, preparation and applications in foods. *J. Sci. Food Agric.* **2004**, *84*, 1261–1269. [CrossRef]
42. Tai, A.; Sawano, T.; Ito, H. Antioxidative properties of vanillic acid esters in multiple antioxidant assays. *Biosci. Biotechnol. Biochem.* **2012**, *76*, 314–318. [CrossRef]
43. Mo, F.; Zhang, P.; Li, Q.; Yang, X.; Ma, J.; Zhang, J. Development and Evaluation of a Film Forming System Containing Myricetin and Miconazole Nitrate for Preventing Candida albicans Catheter-Related Infection. *Microb. Drug Resist.* **2022**, *28*, 468–483. [CrossRef]
44. Lee, H.-S.; Kim, Y. Myricetin disturbs the cell wall integrity and increases the membrane permeability of *Candida albicans*. *J. Microbiol. Biotechnol.* **2022**, *32*, 37–45. [CrossRef]
45. Hirasawa, M.; Takada, K. Multiple effects of green tea catechin on the antifungal activity of antimycotics against *Candida albicans*. *J. Antimicrob. Chemother.* **2004**, *53*, 225–229. [CrossRef] [PubMed]
46. Almeida, D.; Pinto, D.; Santos, J.; Vinha, A.F.; Palmeira, J.; Ferreira, H.N.; Rodrigues, F.; Oliveira, M.B.P.P. Hardy kiwifruit leaves (*Actinidia arguta*): An extraordinary source of value-added compounds for food industry. *Food Chem.* **2018**, *259*, 113–121. [CrossRef] [PubMed]
47. Bonfim-Mendonca Pde, S.; Ratti, B.A.; Godoy Jda, S.; Negri, M.; Lima, N.C.; Fiorini, A.; Hatanaka, E.; Consolaro, M.E.; de Oliveira Silva, S.; Svidzinski, T.I. beta-Glucan induces reactive oxygen species production in human neutrophils to improve the killing of Candida albicans and Candida glabrata isolates from vulvovaginal candidiasis. *PLoS ONE* **2014**, *9*, e107805.
48. Dantas Ada, S.; Day, A.; Ikeh, M.; Kos, I.; Achan, B.; Quinn, J. Oxidative stress responses in the human fungal pathogen, Candida albicans. *Biomolecules* **2015**, *5*, 142–165. [CrossRef] [PubMed]
49. Chen, L.; Wang, F.; Qu, S.; He, X.; Zhu, Y.; Zhou, Y.; Yang, K.; Li, Y.X.; Liu, M.; Peng, X.; et al. Therapeutic potential of perillaldehyde in ameliorating vulvovaginal candidiasis by reducing vaginal oxidative stress and apoptosis. *Antioxidants* **2022**, *11*, 178. [CrossRef]
50. de Francisco, L.; Pinto, D.; Rosseto, H.; Toledo, L.; Santos, R.; Tobaldini-Valério, F.; Svidzinski, T.; Bruschi, M.; Sarmento, B.; Oliveira, M.B.P.P.; et al. Evaluation of radical scavenging activity, intestinal cell viability and antifungal activity of Brazilian propolis by-product. *Food Res. Int.* **2018**, *105*, 537–547. [CrossRef] [PubMed]
51. Zduńska, K.; Dana, A.; Kolodziejczak, A.; Rotsztejn, H. Antioxidant properties of ferulic acid and its possible application. *Skin. Pharmacol. Physiol.* **2018**, *31*, 332–336. [CrossRef] [PubMed]
52. Yan-Chun, Z.; Rong-Liang, Z. Phenolic compounds and an analog as superoxide anion scavengers and anti oxidants. *Biochem. Pharmacol.* **1991**, *42*, 1177–1179. [CrossRef]
53. Majer, P.; Neugart, S.; Krumbein, A.; Schreiner, M.; Hideg, É. Singlet oxygen scavenging by leaf flavonoids contributes to sunlight acclimation in Tilia platyphyllos. *Environ. Exp. Bot.* **2014**, *100*, 1–9. [CrossRef]

54. Hu, J.; Calomme, M.; Lasure, A.; De Bruyne, T.; Pieters, L.; Vlietinck, A.; Vanden Berghe, D. Structure-activity relationship of flavonoids with superoxide scavenging activity. *Biol. Trace Elem. Res.* **1995**, *47*, 327–331. [CrossRef]
55. Touzani, S.; Imtara, H.; Katekhaye, S.; Mechchate, H.; Ouassou, H.; Alqahtani, A.S.; Noman, O.M.; Nasr, F.A.; Fearnley, H.; Fearnley, J. Determination of phenolic compounds in various propolis samples collected from an African and an Asian region and their impact on antioxidant and antibacterial activities. *Molecules* **2021**, *26*, 4589. [CrossRef]
56. Sobel, J.D.; Sobel, R. Current treatment options for vulvovaginal candidiasis caused by azole-resistant Candida species. *Expert. Opin. Pharmacother.* **2018**, *19*, 971–977. [CrossRef]
57. Tobaldini-Valerio, F.K.; Bonfim-Mendonça, P.S.; Rosseto, H.C.; Bruschi, M.L.; Henriques, M.; Negri, M.; Silva, S.; Svidzinski, T.I. Propolis: A potential natural product to fight Candida species infections. *Future Microbiol.* **2016**, *11*, 1035–1046. [CrossRef] [PubMed]
58. Duarte, M.C.T.; Figueira, G.M.; Sartoratto, A.; Rehder, V.L.G.; Delarmelina, C. Anti-Candida activity of Brazilian medicinal plants. *J. Ethnopharmacol.* **2005**, *97*, 305–311. [CrossRef] [PubMed]
59. Facchinatto, W.M.; Galante, J.; Mesquita, L.; Silva, D.S.; dos Santos, D.M.; Moraes, T.B.; Campana-Filho, S.P.; Colnago, L.A.; Sarmento, B.; das Neves, J. Clotrimazole-loaded N-(2-hydroxy)-propyl-3-trimethylammonium, O-palmitoyl chitosan nanoparticles for topical treatment of vulvovaginal candidiasis. *Acta Biomater.* **2021**, *125*, 312–321. [CrossRef] [PubMed]
60. das Neves, J.; Sarmento, B. Precise engineering of dapivirine-loaded nanoparticles for the development of anti-HIV vaginal microbicides. *Acta Biomater.* **2015**, *18*, 77–87. [CrossRef] [PubMed]
61. das Neves, J.; Notario-Pérez, F.; Sarmento, B. Women-specific routes of administration for drugs: A critical overview. *Adv. Drug Deliv. Rev.* **2021**, *176*, 113865. [CrossRef] [PubMed]
62. Banskota, A.H.; Tezuka, Y.; Prasain, J.K.; Matsushige, K.; Saiki, I.; Kadota, S. Chemical constituents of Brazilian propolis and their cytotoxic activities. *J. Nat. Prod.* **1998**, *61*, 896–900. [CrossRef] [PubMed]
63. Bonamigo, T.; Campos, J.F.; Oliveira, A.S.; Torquato, H.F.V.; Balestieri, J.B.P.; Cardoso, C.A.L.; Paredes-Gamero, E.J.; de Picoli Souza, K.; Dos Santos, E.L. Antioxidant and cytotoxic activity of propolis of *Plebeia droryana* and *Apis mellifera* (Hymenoptera, Apidae) from the Brazilian Cerrado biome. *PLoS ONE* **2017**, *12*, e0183983. [CrossRef]
64. Campoccia, D.; Ravaioli, S.; Santi, S.; Mariani, V.; Santarcangelo, C.; De Filippis, A.; Montanaro, L.; Arciola, C.R.; Daglia, M. Exploring the anticancer effects of standardized extracts of poplar-type propolis: In vitro cytotoxicity toward cancer and normal cell lines. *Biomed. Pharmacother.* **2021**, *141*, 111895. [CrossRef]
65. Cavalaro, R.I.; da Cruz, R.G.; Dupont, S.; de Moura Bell, J.M.L.N.; Vieira, T.M.F.d.S. In vitro and in vivo antioxidant properties of bioactive compounds from green propolis obtained by ultrasound-assisted extraction. *Food Chem. X* **2019**, *4*, 100054. [CrossRef] [PubMed]
66. Pinto, D.; Braga, N.; Rodrigues, F.; Oliveira, M.B. Castanea sativa Bur: An Undervalued By-Product but a Promising Cosmetic Ingredient. *Cosmetics* **2017**, *4*, 50. [CrossRef]
67. Benzie, I.F.F.; Strain, J.J. Ferric reducing/antioxidant power assay: Direct measure of total antioxidant activity of biological fluids and modified version for simultaneous measurement of total antioxidant power and ascorbic acid concentration. In *Methods in Enzymology*; Academic Press: Cambridge, MA, USA, 1999; Volume 299, pp. 15–27.
68. Re, R.; Pellegrini, N.; Proteggente, A.; Pannala, A.; Yang, M.; Rice-Evans, C. Antioxidant activity applying an improved ABTS radical cation decolorization assay. *Free Radic. Biol. Med.* **1999**, *26*, 1231–1237. [CrossRef] [PubMed]
69. Moreira, M.M.; Barroso, M.F.; Boeykens, A.; Withouck, H.; Morais, S.; Delerue-Matos, C. Valorization of apple tree wood residues by polyphenols extraction: Comparison between conventional and microwave-assisted extraction. *Ind. Crops Prod.* **2017**, *104*, 210–220. [CrossRef]
70. Gomes, A.; Fernandes, E.; Silva, A.M.S.; Santos, C.M.M.; Pinto, D.C.G.A.; Cavaleiro, J.A.S.; Lima, J.L.F.C. 2-Styrylchromones: Novel strong scavengers of reactive oxygen and nitrogen species. *Bioorg Med. Chem.* **2007**, *15*, 6027–6036. [CrossRef] [PubMed]
71. Reference CLSI, Method for broth dilution antifungal susceptibility testing of yeasts. In *CLSI Standard M27*, 4th ed.; Clinical and Laboratory Standards Institute: Wayne, PA, USA, 2017.
72. Präbst, K.; Engelhardt, H.; Ringgeler, S.; Hübner, H. Basic colorimetric proliferation assays: MTT, WST, and resazurin. *Methods Mol. Biol.* **2017**, *1601*, 1–17. [PubMed]
73. Faria, M.J.; Machado, R.; Ribeiro, A.; Gonçalves, H.; Real Oliveira, M.E.C.D.; Viseu, T.; das Neves, J.; Lúcio, M. Rational Development of Liposomal Hydrogels: A Strategy for Topical Vaginal Antiretroviral Drug Delivery in the Context of HIV Prevention. *Pharmaceutics* **2019**, *11*, 485. [CrossRef] [PubMed]
74. Notario-Pérez, F.; Galante, J.; Martín-Illana, A.; Cazorla-Luna, R.; Sarmento, B.; Ruiz-Caro, R.; das Neves, J.; Veiga, M.-D. Development of pH-sensitive vaginal films based on methacrylate copolymers for topical HIV-1 pre-exposure prophylaxis. *Acta Biomat.* **2021**, *121*, 316–327. [CrossRef]

International Journal of
Molecular Sciences

MDPI

Article

The Biological Active Substances of *Taraxacum officinale* and *Arctium lappa* from the Siberian Federal District

Anna S. Frolova [1], Anna D. Fokina [1], Irina S. Milentyeva [1], Lyudmila K. Asyakina [2,*], Larisa A. Proskuryakova [3] and Alexander Y. Prosekov [4]

[1] Laboratory of Biotesting of Natural Nutraceuticals of Scientific and Innovative Management, Kemerovo State University, 6, Krasnaya St., Kemerovo 650000, Russia; frolova.anna.s@mail.ru (A.S.F.); fadan-2001@mail.ru (A.D.F.); irazumnikova@mail.ru (I.S.M.)
[2] Laboratory of Phytoremediation of Technogenically Disturbed Ecosystems, Kemerovo State University, 6, Krasnaya St., Kemerovo 650000, Russia
[3] Scientific and Innovative Management Department, Kemerovo State University, 6, Krasnaya St., Kemerovo 650000, Russia; lora-al@yandex.ru
[4] Department of Bionanotechnology, Kemerovo State University, 6, Krasnaya St., Kemerovo 650000, Russia; rector@kemsu.ru
* Correspondence: alk_kem@mail.ru

Abstract: Currently, scientists are increasingly focusing on utilizing the natural flora of the planet to search for and isolate individual bioactive substances that prevent various diseases, contribute to increased life expectancy, and affect all major life-supporting systems in the human body. This study describes the examination of the composition of plant raw materials from the Siberian Federal District. The research focuses on plant specimens from the root parts of *Taraxacum officinale* and *Arctium lappa*, collected in the Kemerovo region. The study determines the contents of the water-soluble vitamins B and C in the research subjects. The investigation includes assessing antioxidant properties, antimicrobial activity, and flavonoid content in extracts based on plant raw materials. All samples show a high percentage of antioxidant activity, with the highest antioxidant activity for *T. officinale* at 85.51 and that for *A. lappa* at 88.97. The results indicate low antimicrobial activity against *Escherichia coli* (growth inhibition zone up to 15.5 mm). Plant extracts contain significant amounts of B-group vitamins, with pyridoxine in *T. officinale* (156.40 μg/mL) and thiamine (46.20 μg/mL) and pyridoxine (357.10 μg/mL) in *Arctium lappa*. Flavonoids (rutin and quercetin) are identified in *T. officinale* and *A. lappa* extracts based on the study results.

Keywords: dandelion root; burdock root; raw material; antioxidants; flavonoids; bioactive substances; vitamins; *Escherichia coli*

Citation: Frolova, A.S.; Fokina, A.D.; Milentyeva, I.S.; Asyakina, L.K.; Proskuryakova, L.A.; Prosekov, A.Y. The Biological Active Substances of *Taraxacum officinale* and *Arctium lappa* from the Siberian Federal District. *Int. J. Mol. Sci.* **2024**, *25*, 3263. https://doi.org/10.3390/ijms25063263

Academic Editor: David Arráez-Román

Received: 2 February 2024
Revised: 1 March 2024
Accepted: 6 March 2024
Published: 13 March 2024

1. Introduction

The resources that our planet is rich in are dwindling, such as valuable minerals, forests, and naturally sourced food products. Climate conditions are becoming increasingly unpredictable each year. Population density and growth are on the rise.

According to United Nations projections, the world's population will reach 8.5 billion people by 2030, 9.7 billion by 2050, and 10.4 billion by 2100 [1]. Consequently, humanity faces pressing questions about finding new sources of food, achieving self-sufficiency in providing necessary food products, and strengthening population immunity against infections and pathogens using Russian foods, medicines, and functional additives to the basic human diet.

The Siberian Federal District offers a rich diversity of plant materials with varied phytochemical compositions and properties [2]. Currently, the study of individual bioactive substances (BAS) is a relevant field in biotechnology science [3]. Bioactive substances are chemical compounds obtained through microbiological or chemical synthesis that exhibit high physiological activity at low concentrations [4].

In recent years, biotechnologists have been closely focused on studying individual bioactive substances (BAS) in plant raw materials to develop functional preparations and dietary supplements containing antioxidants of natural or synthetic origin [5–7].

The human body is initially saturated with antioxidant substances in the early years of life, but over time, their contents decrease, and their natural effectiveness weakens [8,9]. There is a need to replenish antioxidant substances through food and additional sources, such as various antioxidant dietary supplements [10].

Antioxidants can protect cells through various mechanisms, such as:

1. Transforming reactive oxygen species (ROS) into non-radical forms (dependent on the involved antioxidant);
2. Interrupting the auto-oxidative chain reaction initiated by ROS;
3. Reducing localized oxygen concentrations [11].

Synthetic antioxidants include pharmaceuticals, functional food products, and dietary supplements that do not contain plant components. Synthetic antioxidants are used instead of natural ones because they provide higher stability and efficiency, lower cost, and widespread availability. The most frequently mentioned synthetic antioxidants in the food industry are butylated hydroxyanisole, butylated hydroxytoluene, propyl gallate, and tert-butylhydroquinone [12].

While synthetic antioxidants are widely used, safety concerns arise over time. Several published studies have suggested a link between prolonged intake of synthetic antioxidants and certain health issues [13]. High doses of synthetic antioxidants can cause DNA damage and premature aging [14]. Hence, the trend toward replacing synthetic antioxidants with natural ones is growing stronger.

Antioxidants derived from plant raw materials can react with reactive oxygen species, thereby protecting cellular structures from free-radical damage and contributing to the reduction of oxidative stress [15]. Substances such as vitamins, macro- and microelements, phenolic compounds, alkaloids, carotenoids, minerals, and enzymes found in fruits, vegetables, berries, and plants fall into the category of natural antioxidants.

Alkaloids are nitrogen-containing natural organic compounds that accumulate in all plant organs [16]. They have a positive impact on the cardiovascular, central nervous, and endocrine systems [17]. Notable alkaloids include caffeine, atropine, theobromine, and theophylline.

Carotenoids are plant pigments that impart bright yellow, orange, or red hues to plant materials. They possess antioxidant activity and immunomodulatory effects [18].

Phenolic acids represent aromatic secondary metabolites of plant origin. Phenolic acids have a protective function when consuming plant raw materials in the diet, especially in cardiovascular diseases and oncology. Examples of phenolic acid compounds include salicylic and gallic acids, as well as coumarins, catechins, quercetin, flavonoids, tannins, and others [19].

Considerable importance should be given to natural polyphenolic compounds, such as flavonoids, which exhibit pronounced biological properties. It has been established that flavonoids possess antibacterial and antiviral activity, anti-inflammatory, antiangiogenic, analgesic, and antiallergic effects, and hepatoprotective, cytostatic, apoptotic, estrogenic, and antiestrogenic properties [20]. They are characterized by capillary-strengthening, cardiotonic, spasmolytic, hypotensive, diuretic, choleretic, hepatoprotective, hemostatic, and anti-inflammatory actions [21].

Vitamins A, C, and E are important antioxidants that can reduce the body's susceptibility to oxidative damage [22]. Some of these compounds are particularly crucial for human health, such as vitamins C and E, which act as antioxidants and perform essential functions in our bodies. They are not synthesized by the human body, so they must be obtained through food [23]. Vitamin E counters oxidative stress, preventing age-related diseases [24]. Vitamin C is a water-soluble antioxidant necessary for collagen synthesis, iron absorption, and epigenetic regulation. Vitamin C promotes proper immune system

function, reduces inflammation, and prevents the occurrence and progression of various chronic and acute diseases [25].

Vitamin B_1 is an essential component of nutrition, and a deficiency in this micronutrient underlies various diseases, especially nervous system disorders [26]. Vitamin B_1 enhances plant resistance to environmental stress. Supplementary thiamine significantly increases the vitamin C content and the overall content of phenolic compounds in turnip varieties under drought conditions [27]. Vitamin B_6 exhibits free-radical-scavenging activity and antioxidant effects [28]. Riboflavin (vitamin B_2) is often referred to as the growth vitamin, controlling the protective antioxidant system in plants [29].

The common dandelion (*Taraxacum officinale*) is a perennial herbaceous plant of the Asteraceae family. It is a herbaceous plant that grows in North America, Europe, and Asia [30]. The dandelion was originally imported to America as a food crop and then spread to North America, New Zealand, Australia, South Africa, and India. It grows along roadsides, banks, lawns, pastures, and in areas with moist soils [31]. Owing to its wide range of nutrients, such as vitamins, minerals, polyphenols, flavonoids, and fatty acids, dandelion and its extracts exhibit anti-inflammatory and antioxidant effects. Additionally, they demonstrate anti-tumor and antimicrobial activity [32]. Dandelion alleviates inflammatory reactions in the intestine by restoring the balance of gut flora, suggesting that its anti-inflammatory effects are mediated by regulating gut microbial imbalance [33]. Traditionally, dandelion has been used to treat kidney, spleen, and liver diseases, as well as cardiovascular diseases, diabetes, and bacterial infections, and as an anti-inflammatory and diuretic agent [34].

Extracts from *T. officinale* are widely recognized as safe, and dandelion is considered a renewable resource, further enhancing its appeal as a natural food or medicinal product. Consequently, the popularity and usage of dandelion, its extracts, and key components are expected to continue growing. Recent articles report that flavonoids extracted from dandelion leaves and roots can be used as a functional supplement to starch to reduce the glycemic index [35]. Moreover, polysaccharides isolated from the entire dandelion plant during flowering exhibited prebiotic potential associated with microbiota composition modulation [36].

Greater Burdock (*Arctium lappa*) is a medicinal and edible homologous plant commonly known as burdock, belonging to the Asteraceae family [37]. Burdock is widespread in Europe [38], North America [39], China [40], Africa [41], and Asia [42], having both nutritional and medicinal value [43]. It is a globally cultivated medicinal and edible plant with predominantly phytochemical compounds and polysaccharides, possessing both nutritional and therapeutic properties [44]. The plant contains flavonoids and lignans, which are beneficial for treating high blood pressure, gout, thrombosis, hepatitis, and inflammatory diseases. Various biological properties, including antimutagenic, anticancer, and rejuvenating properties, are also attributed to its phenolic components [45]. Modern research reveals that *A. lappa* contains organic acids, flavonoids, terpenoids, lignans, and other components [46].

The roots, leaves, and fruits of burdock have varying therapeutic values and are widely used in some European and Asian countries. The fruits contain lignans and essential oils with anticancer and anti-inflammatory activity. The chemopreventive action of burdock fruits is linked to lignans such as arctiin and arctigenin [47]. *A. lappa* leaves exhibit high antioxidant activity and contain phenolic compounds, including phenolic acids, quercetin, quercitrin, and luteolin [48]. The main active ingredients extracted from burdock leaves are arctigenin, arctiin, coffee, and chlorogenic acids [49]. *A. lappa* roots contain a broad spectrum of bioactive substances such as polysaccharides, polyphenols, flavonoids, and volatile oils, contributing to their anti-inflammatory, antioxidant, antibacterial, antiviral, and other biological activities [50]. Phenolic acids (caffeic acid, chlorogenic acid, and cynarin), arctin, luteolin, and quercetin are found in burdock roots. The root possesses protective, anti-inflammatory, and free-radical-blocking activities that are attributed to chlorogenic acid derivatives. Burdock root contains inulin, essential oil, tannins, resins,

carbohydrates, iron, calcium, and vitamin C, with its bitter taste resulting from linoleic and oleic acids [51].

A more in-depth and comprehensive study of local plants is required to extract bioactive substances used in the food industry. The aim of the research was to assess the content of water-soluble vitamins and flavonoids, radical-scavenging activity by ABTS, and antimicrobial activity of plant material from the Siberian Federal District, specifically *T. officinale* and *A. lappa*.

2. Results

2.1. Obtaining Extracts with High Contents of BAS

Extracts, depending on the solvent (extractant) used, can be alcoholic, aqueous, aqueous–alcoholic, essential, and CO_2 extracts. Each method has its advantages and disadvantages. The optimal extractant for the extraction of BAS in order to obtain dietary supplements is an aqueous alcohol solvent. The parameters of extraction of plant raw materials were selected experimentally: temperature, solvent concentration, and incubation duration, as well as the hydromodule (ratio of raw materials to extractant). The results were evaluated using the antioxidant activity of the obtained extracts. The results are shown in Table 1.

Table 1. Results of antioxidant activity.

Sample	Antioxidant Activity (Mean ± SD), %	Sample	Antioxidant Activity (Mean ± SD), %
Water	0	Vitamin C (1000 mmol/L)	50.13 ± 1.03
1	69.62 ± 1.43 * Tst = 11.06 p = 0.001	37	87.21 ± 1.82 * Tst = 17.73 p = 0.0004
2	64.06 ± 1.32 * Tst = 8.32 p = 0.004	38	85.13 ± 1.75 * Tst = 17.24 p = 0.0004
3	61.15 ± 1.26 * Tst = 6.77 p = 0.01	39	83.72 ± 1.72 * Tst = 16.75 p = 0.0005
4	83.30 ± 1.76 * Tst = 16.27 p = 0.001	40	81.11 ± 1.67 * Tst = 15.79 p = 0.001
5	81.15 ± 1.67 * Tst = 15.81 p = 0.001	41	80.56 ± 1.66 * Tst = 15.58 p = 0.001
6	78.97 ± 1.63 * Tst = 14.96 p = 0.001	42	76.20 ± 1.57 * Tst = 13.88 p = 0.001
7	63.59 ± 1.31 * Tst = 8.08 p = 0.004	43	53.59 ± 1.10 Tst = 1.63 p = 0.20
8	62.39 ± 1.29 * Tst = 7.43 p = 0.01	44	49.66 ± 1.02
9	59.44 ± 1.22 * Tst = 5.83 p = 0.01	45	47.91 ± 0.99
10	66.07 ± 1.36 * Tst = 9.34 p = 0.003	46	77.26 ± 1.59 * Tst = 14.32 p = 0.001
11	63.42 ± 1.31 * Tst = 7.98 p = 0.004	47	76.32 ± 1.57 * Tst = 13.95 p = 0.001
12	62.18 ± 1.28 * Tst = 7.33 p = 0.01	48	74.57 ± 1.54 * Tst = 13.19 p = 0.001
13	49.36 ± 1.02	49	35.17 ± 0.72
14	47.91 ± 0.99	50	32.44 ± 0.67
15	47.05 ± 0.97	51	31.37 ± 0.65
16	48.55 ± 1.00	52	39.53 ± 0.81
17	46.67 ± 0.96	53	36.84 ± 0.76
18	46.03 ± 0.95	54	32.78 ± 0.68
19	63.42 ± 1.31 * Tst = 63.42 p = 0.004	55	72.22 ± 1.49 * Tst = 12.20 p = 0.001

Table 1. *Cont.*

Sample	Antioxidant Activity (Mean ± SD), %	Sample	Antioxidant Activity (Mean ± SD), %
20	60.90 ± 1.25 * Tst = 6.65 p = 0.01	56	70.90 ± 1.46 * Tst = 11.62 p = 0.001
21	56.84 ± 1.17 * Tst = 4.30 p = 0.02	57	68.76 ± 1.42 * Tst = 10.62 p = 0.002
22	67.05 ± 1.38 * Tst = 9.83 p = 0.002	58	88.97 ± 1.83 * Tst = 18.50 p = 0.0003
23	51.11 ± 1.05 Tst = 0.47 p = 0.67	59	87.56 ± 1.80 * Tst = 18.05 p = 0.0004
24	48.29 ± 0.99	60	85.85 ± 1.77 * Tst = 17.44 p = 0.0004
25	58.33 ± 1.20 * Tst = 5.19 p = 0.01	61	82.56 ± 1.70 * Tst = 17.82 p = 0.0004
26	49.15 ± 1.01	62	79.10 ± 1.63 * Tst = 15.02 p = 0.001
27	44.74 ± 0.92	63	74.96 ± 1.54 * Tst = 13.40 p = 0.001
28	85.51 ± 1.76 * Tst = 17.35 p = 0.0004	64	67.74 ± 1.40 * Tst = 10.13 p = 0.002
29	82.22 ± 1.69 * Tst = 16.21 p = 0.001	65	65.94 ± 1.36 * Tst = 9.27 p = 0.003
30	80.38 ± 1.66 * Tst = 15.48 p = 0.001	66	62.35 ± 1.28 * Tst = 7.44 p = 0.01
31	62.05 ± 1.28 * Tst = 7.26 p = 0.01	67	32.69 ± 0.67
32	59.87 ± 1.23 * Tst = 6.07 p = 0.01	68	28.93 ± 0.60
33	55.77 ± 1.15 * Tst = 3.65 p = 0.04	69	28.42 ± 0.59
34	63.42 ± 1.31 * Tst = 7.98 p = 0.004	70	54.49 ± 1.12 Tst = 2.04 p = 0.13
35	50.68 ± 1.04 Tst = 0.26 p = 0.81	71	47.22 ± 0.97
36	48.33 ± 1.00	72	44.19 ± 0.91

SD—standard deviation; *—Statistically significant results. The observed differences are statistically significant (significance level $p < 0.05$); Tst—Student's t-test value when comparing the studied treatment option with the control vitamin C (1000 mmol/L).

By analyzing the results of the determination of antioxidant activity, it can be argued that the choice of an extractant should be carried out individually for each type of raw material. Within the framework of the conducted research, according to our own observations, a pattern was tracked during the experiment: the lighter the extract, the higher its antioxidant activity; the lower the alcohol concentration, the higher the concentrations of extracts of biologically active substances.

According to the results of this study, a high percentage of antioxidant activity was noted in all samples. The highest antioxidant activity in *Taraxacum officinale* was 85.51, and that for *Arctium lappa* was 88.97.

2.2. Study of Extracts for Antimicrobial Activity

Antimicrobial activity was studied for extracts based on plant raw materials with maximum antioxidant yield. The disc diffusion method was used. The results are presented in Table 2.

Table 2. The results of the analysis of the antimicrobial activity of plant extracts against the test pathogen *E. coli*. Disc size = 6 mm; S = low susceptibility (7.0–10.0 mm); S+ = susceptibility (10.5–15.0 mm); S++ = high susceptibility (15.5–18.0 mm); R = resistant (0 mm).

Sample	Inhibition Zone (Mean ± SD), mm	Response	Sample	Inhibition Zone (Mean ± SD), mm	Response
Water	0	R	Tetracycline (10 µg)	13.0 ± 0.3	S+
1	11.0 ± 0.2	S+	37	12.0 ± 0.3	S+
2	10.0 ± 0.2	S	38	12.0 ± 0.3	S+
3	10.0 ± 0.2	S	39	11.5 ± 0.2	S+
4	13.0 ± 0.3	S+	40	13.5 ± 0.3 Tst = 1.18 p = 0.32	S+
5	11.0 ± 0.2	S+	41	13.0 ± 0.3	S+
6	11.0 ± 0.2	S+	42	11.5 ± 0.2	S+
7	10.0 ± 0.2	S	43	10.0 ± 0.2	S
8	10.0 ± 0.2	S	44	9.5 ± 0.2	S
9	10.0 ± 0.2	S	45	8.5 ± 0.2	S
10	9.5 ± 0.2	S	46	12.0 ± 0.3	S+
11	9.0 ± 0.2	S	47	12.0 ± 0.3	S+
12	9.0 ± 0.2	S	48	11.5 ± 0.2	S+
13	9.0 ± 0.2	S	49	9.0 ± 0.2	S
14	8.5 ± 0.2	S	50	6.5 ± 0.1	S
15	9.0 ± 0.2	S	51	0	R
16	8.0 ± 0.2	S	52	7.5 ± 0.2	S
17	7.0 ± 0.1	S	53	7.5 ± 0.2	S
18	0	R	54	6.5 ± 0.1	S
19	10.0 ± 0.2	S	55	11.5 ± 0.2	S+
20	10.0 ± 0.2	S	56	12.5 ± 0.3	S+
21	9.0 ± 0.2	S	57	12.5 ± 0.3	S+
22	9.5 ± 0.2	S	58	15.5 ± 0.4 * Tst = 5.89 p = 0.01	S++
23	9.0 ± 0.2	S	59	13.0 ± 0.3	S+
24	8.5 ± 0.2	S	60	11.5 ± 0.2	S+
25	9.0 ± 0.2	S	61	11.5 ± 0.2	S+
26	8.5 ± 0.2	S	62	10.5 ± 0.2	S+
27	0	R	63	11.5 ± 0.2	S+
28	13.5 ± 0.3 Tst = 1.18 p = 0.32	S+	64	10.5 ± 0.2	S+
29	11.5 ± 0.2	S+	65	9.5 ± 0.2	S
30	10.5 ± 0.2	S+	66	9.5 ± 0.2	S
31	10.0 ± 0.2	S	67	6.5 ± 0.1	S
32	9.5 ± 0.2	S	68	0	R
33	9.0 ± 0.2	S	69	0	R
34	10.0 ± 0.2	S	70	9.5 ± 0.2	S
35	9.0 ± 0.2	S	71	9.0 ± 0.2	S
36	8.0 ± 0.2	S	72	7.5 ± 0.2	S

SD—standard deviation; *—Statistically significant results compared with positive control (tetracycline). The observed differences are statistically significant (significance level $p < 0.05$); Tst—Student's t-test value when comparing the studied treatment option with the control tetracycline (10 µg).

The water–alcohol extracts of the plant materials *Taraxacum officinale* and *Arctium lappa* demonstrated high antimicrobial activity against *Escherichia coli*. The disc diffusion method showed growth inhibition zones ranging from 10.5 to 13.5 mm for samples: 1, 4–6, and 28–30, which were extracts from dandelion roots. Inhibition zones of 10.5 to 15.5 mm were observed for samples: 37–42, 46–48, and 55–64, which were extracts from burdock roots.

The maximum diameter of the growth inhibition zone for dandelion was 13.5 mm (sample 28), while for burdock it was 15.5 mm (sample 58). Thus, the investigated plant materials *T. officinale* and *A. lappa* represent promising sources of bioactive substances (BAS) with antibacterial properties.

For the extraction of plant material from *A. lappa* and *T. officinale* with the highest possible content of BAS and a high antioxidant activity index, the optimal parameters are an incubation duration of 4 h, extraction temperature of 60 °C, and a plant material to solvent ratio of 1:10, respectively. The concentration of the extractant (ethyl alcohol) was 70% for *T. officinale* (sample 28), and the concentration of ethyl alcohol for *A. lappa* extraction was 40% (sample 58).

2.3. The Content of Water-Soluble Vitamins in Extracts with High Contents of Biologically Active Substances (BAS)

The results of the analysis of the determination of the qualitative and quantitative composition of water-soluble vitamins of groups B and C by high-efficiency liquid chromatography (HPLC) are shown in Figure 1, Table 3.

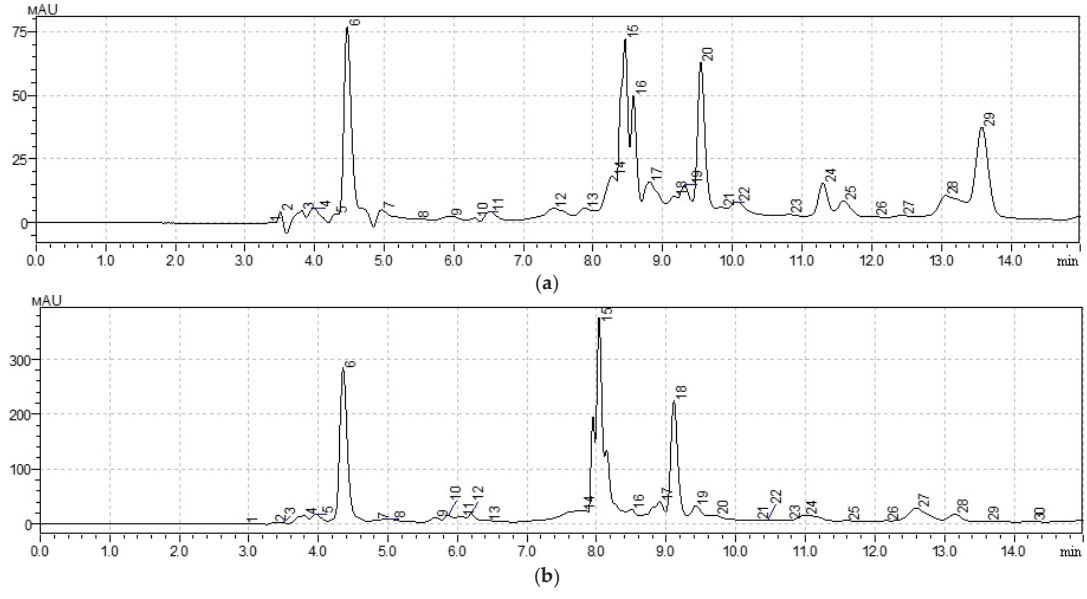

Figure 1. Chromatogram of HPLC analysis of plant extracts: (**a**) *Taraxacum officinale*: peak 6—vitamin C; peak 15, 16—vitamin B_1; peak 20—vitamin B_3; peak 24—vitamin B_6; (**b**) *Arctium lappa*: peak 6—vitamin C; peak 15, 16—vitamin B_1; peak 20—vitamin B_3; peak 24—vitamin B_6.

In the *Taraxacum officinale* sample, the study revealed a high content of pyridoxine (Vitamin B_6) at 156.40 μg/mL. The presence of thiamine and niacin (vitamins B_1 and B_3), as well as vitamin C, was also noted. The *Arctium lappa* sample exhibited a significant concentration of B-vitamins, particularly thiamine (46.20 μg/mL) and pyridoxine (357.10 μg/mL). Additionally, niacin, pantothenic acid (Vitamin B_5), and vitamin C were detected. It is noteworthy that sample 58 contains, on average, 13.02 times more B and C group vitamins than sample 28.

Table 3. The quantitative contents of water-soluble vitamins according to HPLC analysis.

Name of the Vitamin	Amount of Substance, ug/mL of Extract	
	Sample 28 (*Taraxacum officinale*)	**Sample 58 (*Arctium lappa*)**
Vitamin B_1	10.19	46.20
Vitamin B_2	–	–
Vitamin B_3	7.42	23.70
Vitamin B_5	–	7.57
Vitamin B_6	156.40	357.10
Vitamin C	0.46	21.87

2.4. The Contents of Flavonoids in the Studied Extracts

The results of the detection of flavonoids (rutin and quercetin) in an extract based on the plant raw materials *Taraxacum officinale* and *Arctium lappa* by TLC are presented in accordance with Figure 2, Table 4.

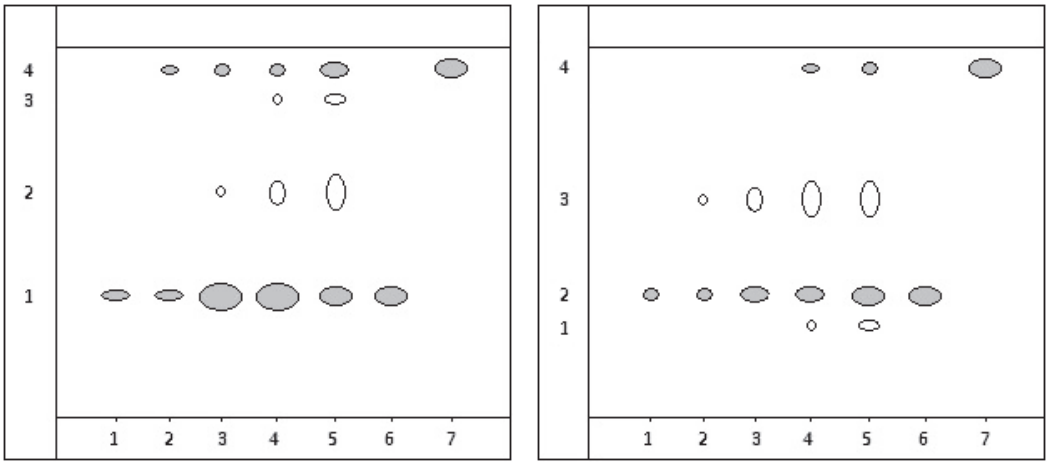

(**a**) (**b**)

Figure 2. Chromatogram diagram of extraction from the root: (**a**) *Taraxacum officinale*, (**b**) *Arctium lappa*: on the start line of point 1—2 µL of extraction; point 2—3 µL; point 3—5 µL; 4—7 µL; point 5—10 µL; point 6—3 µL 0.1% standard rutin solution; point 7—3 µL 0.1% standard quercetin solution.

Table 4. Parameters of chromatographic zone separation on the chromatogram of extraction from the root of *Taraxacum officinale* and *Arctium lappa*.

Taraxacum officinale			*Arctium lappa*		
Spot No.	**R*f* ± 0.02**	**Corresponding Compound**	**Spot No.**	**R*f* ± 0.02**	**Corresponding Compound**
1	0.54	Rutin	1	0.34	n/i
2	0.73	n/i	2	0.51	Rutin
3	0.91	n/i	3	0.71	n/i
4	0.96	Quercetin	4	0.99	Quercetin

n/i—not identified.

On the chromatogram of the extraction from the *Taraxacum officinale* root, when applying 2 µL, one spot was observed, which, based on the Rf value and the spot's position,

matched the rutin standard (Figure 2a, points 1, 6). When applying 3 μL of the extraction, two chromatographic zones appeared, identified as rutin and quercetin. Examining 5 μL of the extraction revealed 3 spots, with two being identified as rutin and quercetin. The unidentified compound is presumed to belong to flavonoids owing to its characteristic yellow–orange staining typical of flavones. Applying 7 and 10 μL of the extraction showed 4 chromatographic zones, with two being identified as rutin and quercetin (Table 4).

On the chromatogram of the extraction from the *Arctium lappa* root, applying 2 μL revealed one chromatographic zone identified as rutin, matching the standard solution (Figure 2b, points 1, 6). Applying 3 and 5 μL of the extraction showed 2 spots, with one being identified as rutin. The unidentified compound exhibited characteristic fluorescence under UV light after treating the plates with a 5% solution of aluminum chloride, indicating its flavonoid nature. Examining 7 and 10 μL of the extraction (Figure 2, points 4, 5) revealed 4 spots, with three being assigned to rutin, quercetin, and an unidentified flavonoid (Table 4).

3. Discussion

Plant material serves as a source of biologically active substances capable of preventing various diseases, including cardiovascular issues and cancer, and influencing the processes of skin aging and overall aging. This study focuses on two extracts based on the roots of *Taraxacum officinale* and *Arctium lappa*, examining their contents of BAS, specifically water-soluble vitamins and flavonoids. The investigated plant material also possesses antimicrobial activity and natural antioxidant compounds.

The conducted research demonstrates that extracts from dandelion and burdock roots exhibit low antimicrobial activity against *E. coli*, confirming the findings in the existing literature. In O. Kenny's [52] study, a dandelion root extract showed antimicrobial activity against *Bacillus cereus* and *Staphylococcus aureus*, with no inhibition observed for *E. coli*. Research on water–alcohol extracts of burdock (*A. lappa*) and dandelion (*T. officinale*) by D. Ionescu and colleagues [53] identified antimicrobial activity against *Staphylococcus aureus*, *Escherichia coli*, and *Salmonella abony enterica*.

The results indicate a decrease in antioxidant activity with an increase in extract concentration, aligning with findings in N.P. Tiguntseva's [54] study on extracting BAS from *Taraxacum officinale* using the water–alcohol extraction method. As alcohol concentration rises, the yield of biologically active compounds decreases to 9.6% for above-ground parts and 12.8% for roots. Minimal concentration leads to a 4% increase in the yield of extracted substances. The antioxidant activity under optimal extraction parameters was 85.51% for dandelion roots and 88.97% for burdock roots. In this study, a spectrophotometry method was used to measure the antioxidant capacity of plant extracts by capturing radicals using ABTS. Many scientists employ this method. Floegel A. and others [55] evaluated two of the most common radical-scavenging assays using the radicals 2,2′-azino-bis-3-ethylbenzthiazoline-6-sulphonic acid (ABTS) and 1,1-diphenyl-2-picrylhydrazyl (DPPH). The results showed that the ABTS assay better reflected the antioxidant content in various food products than the DPPH assay.

Our research reveals that extracts from *T. officinale* and *A. lappa* contain vitamins of the B and C groups. According to the obtained results, the dandelion root extract contains 10.19 mg/100 g of raw material of vitamin B_1, 7.42 mg/100 g of vitamin B_3, 156.40 mg/100 g of vitamin B_6, and 0.46 mg/100 g of vitamin C. The burdock root extract contains 46.20 mg/100 g of raw material of vitamin B_1, 23.70 mg/100 g of vitamin B_2, 7.57 mg/100 g of vitamin B_5, 357.10 mg/100 g of vitamin B_6, and 21.87 mg/100 g of vitamin C. These findings align with the existing literature. For instance, in the study by W. Biel and colleagues [56], dandelion leaves were found to be rich in vitamin C (156.6 mg/100 g^{-1}), thiamine (1.5 mg/100 g^{-1}), riboflavin (3.0 mg/100 g^{-1}), and niacin (11.8 mg/100 g^{-1}). Another study by M. Martinez and others [57] determined that dried dandelion leaves, in addition to having high levels of carbohydrates, protein, fat, crude fiber, etc., also contain a significant amount of phenols, flavonoids, ascorbic acid (34.70 mg/100 g), β-carotene,

chlorophyll, and antioxidants. In research conducted by Zakharov V.L. and team [58] on the content of biologically active substances (BAS) in the roots of medicinal herbaceous plants, traces of β-carotene, ascorbic acid (26.4 mg%), anthocyanins, carotenoids, flavanols (91.4 mg%), catechins, tannins, and coloring substances were found in *Taraxacum officinale*. The main active compounds identified in *A. lappa* include tannins, polyphenols, dietary fibers like inulin and lignans, and vitamins from groups B, C, K, and E, along with minerals (e.g., Na, Ca, Fe, Cu, Mg, P, K, and Zn). A study by X. Zhang and colleagues [59] confirms the presence of phenols, flavonoids (0.07–43.65 mg/g), carotenoids, vitamin C (0.18–13.02 mg/g), and in vitro antioxidant activity in burdock root.

In a study on the antioxidant activity of water-soluble vitamins, researcher Gliszczynska-Swigło A. [60] found that the vitamins thiamine (vitamin B_1), folic acid (vitamin B_9), pyridoxine, pyridoxal, and pyridoxamine (vitamin B_6) are capable of scavenging the cation-radical ABTS+, although they reacted with it relatively slowly. The highest radical-scavenging activity was observed with thiamine, followed by forms of folic acid and vitamin B_6.

According to the literature, flavonoids are also known to contribute to health improvement, partly owing to their antioxidant properties, as demonstrated in many in vitro studies [61]. In extracts from *T. officinale* and *A. lappa*, the presence of the medically significant anti-diabetic flavonoid quercetin was identified. In the study by T.M.A. Moro and colleagues [62], cynarin, chlorogenic acid, caffeic acid, and quercetin were identified as the main metabolites present in extracts from *A. lappa* roots. When investigating the hydroethanolic extract of *Arctium lappa* root, Predes F.S. and co-authors [63] identified the presence of compounds such as arctigenin, quercetin, chlorogenic acid, and caffeic acid. In a study by K. Schütz and others [64], phenolic acids and flavonoids were extracted from dandelion roots and leaves (*Taraxacum officinale* WEB. ex WIGG.). The extracts contained mainly chicoric acid, and glycosides of quercetin were also detected.

Rutin belongs to the flavonoid family. It is a molecule of quercetin with the addition of a disaccharide (rutinose and glucose). Thanks to its anti-inflammatory and antioxidant effects, it has gained significant importance in the pharmaceutical industry, and many drugs registered worldwide contain rutin [65,66]. Rutin is quite commonly found in plant material, and notably, ethanol extracts are used for its commercial purification [67]. In the work by de Souza A.R.C. and others [68], high contents of chlorogenic acid (1.84%) and rutin (1.46%) were found in the ethanol extract of *Arctium lappa* leaves, as well as significant concentrations of phytol, lupeol, and amyrin. When studying the antioxidant potential of Taraxacum officinale tincture, Epure A. and others [69] identified chicoric acid in the highest quantity in the polyphenolic composition, but other phenolic acids (protocatechuic, vanillic, syringic, and ferulic acids) were also present, along with flavonoids (rutin, quercitrin, luteolin, and apigenin).

Based on the results of our study, it can be inferred that quercetin and vitamin C play active roles in demonstrating antioxidant activity. Researchers Rusmana D. and others [70] conducted an antioxidant analysis of Phyllanthus niruri extract, as well as rutin and quercetin compounds, which are flavonoids with therapeutic properties. They found that the P. niruri extract and quercetin exhibited significant activity in reducing ABTS, with quercetin showing higher antioxidant activity than the extract. It was also found that rutin was not effective in reducing the ABTS radical. In the work by Duenas M. and co-authors [71], high antioxidant activity of metabolites was detected in the ABTS analysis, suggesting that quercetin derivatives may act as potential radical scavengers under physiological conditions. In this study, a solution of vitamin C was used as a control for determining the antioxidant activity of plant extracts, as it has demonstrated antioxidant activity [72,73]. In the study by Kim D.-O. and others [74], the antioxidant potential of phenolic compounds was assessed using vitamin C as a control. The authors also found that in the ABTS analysis, the antioxidant capacity of phenolic compounds was ranked as follows: gallic acid > quercetin > epicatechin > catechin > vitamin C > rutin > chlorogenic acid > trolox.

4. Materials and Methods

The objects of research were plant raw materials of the root part of *Taraxacum officinale Arctium lappa*, collected in the Kemerovo region. The general appearance of the objects is shown in Figure 3.

(**a**) (**b**)

Figure 3. The appearance of the objects of study: (**a**) *T. officinale*; (**b**) *A. lappa*.

Extraction of plant components. The roots of *Taraxacum officinale* and *Arctium lappa* were crushed to a size with a square side equal to 5 mm and then ground in a porcelain mortar with a pestle. An aqueous alcohol solvent was determined to be the optimal extractant for the extraction of bioactive substances (BAS). Ethanol concentrations of 40%, 70%, and 96% were utilized for extraction. According to the literature, optimal recovery conditions for tannins suggest the use of 40% ethanol as an extractant [75,76], while maximum extraction of flavonoids is achieved with 70% ethanol [77,78]. Additionally, 96% ethanol is employed for extracting major secondary metabolites such as alkaloids, tannins, flavonoids, saponins, steroids, and phlobatannins [79,80]. Hydromodule (ratio of vegetable raw materials–solvent)—1:10; 1:20; 1:30. Extraction temperature: 30 and 60 °C. The extraction time varied from 0.5 h to 4 h. Then, the resulting mixture was passed through desalted filters [81]. The extraction parameters are presented in Table 5.

Table 5. Extraction parameters of plant extracts.

Sample №	Incubation Duration, h	Alcohol Concentration, %	Temperature, °C	Hydromodule, Raw Material:Alcohol
		Taraxacum officinale root		
1	0.5	40	30	1:10
2	0.5	40	30	1:20
3	0.5	40	30	1:30
4	0.5	40	60	1:10
5	0.5	40	60	1:20
6	0.5	40	60	1:30
7	0.5	70	30	1:10
8	0.5	70	30	1:20
9	0.5	70	30	1:30
10	0.5	70	60	1:10
11	0.5	70	60	1:20
12	0.5	70	60	1:30
13	0.5	96	30	1:10
14	0.5	96	30	1:20
15	0.5	96	30	1:30
16	0.5	96	60	1:10

Table 5. *Cont.*

Sample №	Incubation Duration, h	Alcohol Concentration, %	Temperature, °C	Hydromodule, Raw Material:Alcohol
17	0.5	96	60	1:20
18	0.5	96	60	1:30
19	4.0	40	30	1:10
20	4.0	40	30	1:20
21	4.0	40	30	1:30
22	4.0	40	60	1:10
23	4.0	40	60	1:20
24	4.0	40	60	1:30
25	4.0	70	30	1:10
26	4.0	70	30	1:20
27	4.0	70	30	1:30
28	4.0	70	60	1:10
29	4.0	70	60	1:20
30	4.0	70	60	1:30
31	4.0	96	30	1:10
32	4.0	96	30	1:20
33	4.0	96	30	1:30
34	4.0	96	60	1:10
35	4.0	96	60	1:20
36	4.0	96	60	1:30
		Arctium lappa root		
37	0.5	40	30	1:10
38	0.5	40	30	1:20
39	0.5	40	30	1:30
40	0.5	40	60	1:10
41	0.5	40	60	1:20
42	0.5	40	60	1:30
43	0.5	70	30	1:10
44	0.5	70	30	1:20
45	0.5	70	30	1:30
46	0.5	70	60	1:10
47	0.5	70	60	1:20
48	0.5	70	60	1:30
49	0.5	96	30	1:10
50	0.5	96	30	1:20
51	0.5	96	30	1:30
52	0.5	96	60	1:10
53	0.5	96	60	1:20
54	0.5	96	60	1:30
55	4.0	40	30	1:10
56	4.0	40	30	1:20
57	4.0	40	30	1:30
58	4.0	40	60	1:10
59	4.0	40	60	1:20

Table 5. *Cont.*

Sample №	Incubation Duration, h	Alcohol Concentration, %	Temperature, °C	Hydromodule, Raw Material:Alcohol
60	4.0	40	60	1:30
61	4.0	70	30	1:10
62	4.0	70	30	1:20
63	4.0	70	30	1:30
64	4.0	70	60	1:10
65	4.0	70	60	1:20
66	4.0	70	60	1:30
67	4.0	96	30	1:10
68	4.0	96	30	1:20
69	4.0	96	30	1:30
70	4.0	96	60	1:10
71	4.0	96	60	1:20
72	4.0	96	60	1:30

The determination of antioxidant activity was conducted using a spectrophotometer with an original solution of 2,2′-azino-bis-[3-ethylbenzthiazoline sulfonate] (ABTS). Initial solutions of ABTS (7 mmol × L^{-1}) and potassium persulfate (140 mmol × L^{-1}) were prepared. The reaction mixture was prepared by combining these two initial solutions in equal volumes and leaving them for 16 h at room temperature in the dark. The final solution was diluted by mixing 5 mL of ABTS with 88 μm methanol to achieve an optical density of 0.70 ± 0.10 at 734 nm. In test tubes, 3 mL of ABTS solution and 1 mL of plant extract were added. After 8 min of incubation at 21 °C, the mixture was transferred to a quartz cuvette, and the optical density was measured at a wavelength of 734 nm [82]. Distilled water was used as a negative control. Vitamin C solution was performed as a positive control. For this purpose, a solution with a substance concentration of 1000 mmol/L was prepared.

The radical-scavenging activity for the samples was expressed as the percentage of $ABTS^+$ radical scavenging according to Formula (1):

$$X = \frac{(A_0 - A_1)}{A_0} \cdot 100\%, \quad (1)$$

where: X—percentage of $ABTS^+$ radical capture, %;

A_0—optical density of the control tube;

A_1—optical density of the samples.

For the investigation of antimicrobial activity in plant-based extracts, disc diffusion following the CLSI guidelines [83] was employed. To initiate the assay, the model microorganism *Escherichia coli* (B-8208, All-Russian State Collection of Microorganism Strains) was cultured overnight from a single colony in meat-peptone agar (MPA; Lenreaktiv, Russia) at 37 °C and 200 rpm. A suspension of the E. coli was then prepared in sterile 0.9% NaCl solution (Lenreaktiv, Russia) to an optical density of 0.5 on the McFarland scale (1.5×10^8 Colony Forming Units CFU/mL), utilizing a densitometer (Densichek plus, Sendle, Russia). The culture was subsequently spread-plated on Muller Hinton agar (Himedia, Mumbai, India). Processed extract disks with a diameter of 6 mm were placed on the agar surface. Each dish contained 5 disks with a single extract to minimize variations in the size of the inoculum, environment, and incubation conditions [84]. The dishes were then incubated at 37 °C for 24 h, and the results were interpreted by measuring the diameter of the inhibition zone with millimeter precision. Distilled water served as the negative control, while a tetracycline antibiotic solution (Himedia, Mumbai, India) served as the positive control, with an antibiotic concentration of 10 μg.

Determination of Vitamin Content: Qualitative and quantitative analysis of water-soluble (B and C groups) vitamins was performed using high-performance liquid chromatography (HPLC) [85]. The study was conducted on an LC-20 Prominence chromatograph with a diode array detector Shimadzu SPD20MA, a fluorescence detector RF-20Axs, and an integrated post-column derivatization system Phenomenex Gemini C-18 250 × 4.6 mm (Kyoto, Japan, Shimadzu).

Conditions for the qualitative and quantitative composition of water-soluble vitamins:

- Column thermostat temperature: 25 °C.
- Flow rate of the mobile phase: 800 mm/min.
- Sample injection volume: 20 mm.
- Gradient elution mode was used for separation (mobile phase A—a solution of potassium dihydrogen phosphate at a molar concentration of 0.05 mol/dm^3 and pH 3, mobile phase B—acetonitrile).

The determination of flavonoid contents in extracts based on the plant raw materials *Taraxacum officinale* and *Arctium lappa* was determined using the standard method of thin-layer chromatography (TLC) [86]. The analysis was carried out using TLC plates and a solution of n-butanol with glacial acetic acid and the addition of distilled water (in a ratio of 4:1:5). Volumes of 2, 3, 5, 7, 10 μL of the studied extract and 3 μL of 0.1% solutions of standard samples of rutin and quercitin were simultaneously applied to the plastic. To obtain standard solutions of rutin and quercetin, stock solutions of dimethyl sulfoxide (Lenreaktiv, St Petersburg, Russia) were prepared and diluted with distilled water [15]. After TLC analysis, the spots were exposed under a lamp with ultraviolet light at 254 nm. The value of the relative velocity of movement of flavonoids (R*f*) was determined using Formula (2):

$$R_f = \frac{x}{L} \quad (2)$$

where: x—the distance covered by the substance, cm;

L—the distance covered by the eluent.

Statistical analysis was conducted using Student's *t*-test for paired values to determine significant deviations from control values. Differences were considered statistically significant at $p < 0.05$. The tables and figures show the arithmetic mean values of the indicators under study. All the experiments were carried out in triplicate.

The equipment for the study was provided by the Instrumental Methods of Analysis in Applied Biotechnology Center at Kemerovo State University.

The work was carried out within the framework of the RNF project "Fundamentals of obtaining bioactive substances from medicinal plants of the Siberian region and creating phytogenic feed additives of immunomodulatory action on their basis", No. 23-16-00113, dated 15 May 2023.

Author Contributions: Conceptualization, L.A.P. and A.S.F.; methodology, A.D.F.; software, L.A.P. and L.K.A.; validation, I.S.M.; formal analysis, L.K.A.; investigation, A.D.F.; resources, A.Y.P.; data curation, I.S.M.; writing—original draft preparation, A.D.F.; writing—review and editing, A.S.F.; visualization, L.K.A.; supervision, I.S.M.; project administration, L.K.A.; funding acquisition, A.Y.P. All authors have read and agreed to the published version of the manuscript.

Funding: This research was funded by Russian Science Foundation grant number 23-16-00113.

Institutional Review Board Statement: Not applicable.

Informed Consent Statement: Not applicable.

Data Availability Statement: Data are contained within the article.

Acknowledgments: The study was performed using the equipment of the resource sharing center "Instrumental methods of analysis in the field of applied biotechnology" on the basis of KemSU.

Conflicts of Interest: The authors declare no conflict of interest.

References

1. Dewan, S.; Bamola, S.; Lakhani, A. Addressing ozone pollution to promote United Nations sustainable development goal 2: Ensuring global food security. *Chemosphere* **2024**, *347*, 140693. [CrossRef]
2. Fotina, N.V.; Emelianenko, V.P.; Vorob'eva, E.E.; Burova, N.V.; Ostapova, E.V. Contemporary Biological Methods of Mine Reclamation in the Kemerovo Region—Kuzbass. *Food Process. Tech. Technol.* **2021**, *51*, 869–882. [CrossRef]
3. Le, V.; Sukhikh, A.; Larichev, T.; Ivanova, S.; Prosekov, A.; Dmitrieva, A. Isolation of the main biologically active substances and phytochemical analysis of *Ginkgo biloba* callus culture extracts. *Molecules* **2023**, *28*, 1560. [CrossRef]
4. Golinskaya, L.V.; Vasilevskaya, Y.D.; Pavlova, A.A. Juices are a source of biologically active substances. *Alm. Young Sci.* **2013**, *4*, 6–8.
5. Khizrieva, S.S.; Borisenko, S.N.; Maksimenko, E.V.; Zharkova, G.V.; Borisenko, N.I.; Minkin, V.I. Evaluation of the Polyphenol Composition and Acetylcholinesterase Inhibitory Activity of *Ginkgo biloba* Leaf Extracts Produced in Subcritical Water. *Russ. J. Phys. Chem. B* **2020**, *16*, 1294–1300. [CrossRef]
6. Plumb, J.; Pigat, S.; Bompola, F.; Cushen, M.; Pinchen, H.; Nørby, E.; Astley, S.; Lyons, J.; Kiely, M.; Finglas, P. eBASIS (Bioactive Substances in Food Information Systems) and Bioactive Intakes: Major Updates of the Bioactive Compound Composition and Beneficial Bioeffects Database and the Development of a Probabilistic Model to Assess Intakes in Europe. *Nutrients* **2017**, *9*, 320. [CrossRef] [PubMed]
7. Musilova, J.; Lidikova, J.; Vollmannova, A.; Frankova, H.; Urminska, D.; Bojnanska, T.; Toth, T. Influence of Heat Treatments on the Content of Bioactive Substances and Antioxidant Properties of Sweet Potato (*Ipomoea batatas* L.) Tubers. *Bioact. Food Compon. Their Chronic Dis. Prev. Eff.* **2020**, *2020*, 8856260. [CrossRef]
8. Krishnaiah, D.; Sarbatly, R.; Nithyanandam, R. A review of the antioxidant potential of medicinal plant species. *Food Bioprod. Process.* **2011**, *89*, 217–233. [CrossRef]
9. Fusco, D.; Colloca, G.; Monaco, M.R.L.; Cesari, M. Effects of antioxidant supplementation on the aging process. *Clin. Interv. Aging* **2007**, *2*, 377–387. [PubMed]
10. Stojiljkovic, D.; Arsic, I.; Tadic, V. Extracts of wild apple fruit (*Malus sylvestris* (L.) Mill., Rosaceae) as a source of antioxidant substances for use in production of nutraceuticals and cosmeceuticals. *Ind. Crops Prod.* **2016**, *80*, 165–176. [CrossRef]
11. Oroian, M.; Escriche, I. Antioxidants: Characterization, natural sources, extraction and analysis. *Food Res. Int.* **2015**, *74*, 10–36. [CrossRef]
12. Chen, Y.; Li, W.; Liu, Y.; Lou, Y.; Chen, J.; Xu, X.; Shi, X.; Ma, L.; Yang, Y.; Chen, D. Eco-friendly miniaturized kapok-fiber supported liquid-phase extraction coupled with gas chromatography-flame ionization detector for high-throughput edible oil preparation and low-cost determination of synthetic antioxidants. *J. Food Compos. Anal.* **2024**, *126*, 105926. [CrossRef]
13. Engin, A.B.; Bukan, N.; Kurukahvecioglu, O.; Memis, L.; Engin, A. Effect of butylated hydroxytoluene (E321) pretreatment versus L-arginine on liver injury after sub-lethal dose of endotoxin administration. *Environ. Toxicol. Pharmacol.* **2011**, *32*, 457–464. [CrossRef]
14. Kornienko, J.S.; Smirnova, I.S.; Pugovkina, N.A.; Ivanova, J.S.; Shilina, M.A.; Grinchuk, T.M.; Shatrova, A.N.; Aksenov, N.D.; Zenin, V.V.; Nikolsky, N.N.; et al. High doses of synthetic antioxidants induce premature senescence in cultivated mesenchymal stem cells. *Sci. Rep.* **2019**, *9*, 1296. [CrossRef]
15. Milentyeva, I.S.; Vesnina, A.D.; Fedorova, A.M.; Ostapova, E.V.; Larichev, T.A. Chlorogenic acid and biohanin A from *Trifolium pratense* L. callus culture extract: Functional activity in vivo. *Food Process. Tech. Technol.* **2023**, *53*, 754–765. [CrossRef]
16. Verma, A.K.; Dubey, S.; Srivastava, S.K. Identification of alkaloid compounds as potent inhibitors of *Mycobacterium tuberculosis* NadD using computational strategies. *Comput. Biol. Med.* **2023**, *158*, 106863. [CrossRef] [PubMed]
17. Medvedeva, Y.D.; Medvedev, V.O. Modern biotechnological methods of alkaloid isolation. *Mod. Res. Dev.* **2018**, *6*, 470–474.
18. Siger, A.; Michalak, M.; Bąkowska, E.; Dwiecki, K.; Nogala-Kałucka, M.; Grześ, B.; Piasecka-Kwiatkowska, D. The effect of the genotype-environment interaction on the concentration of carotenoids, tocochromanol, and phenolic compounds in seeds of *Lupinus angustifolius* breeding lines. *J. Food Compos. Anal.* **2023**, *123*, 105511. [CrossRef]
19. da Silva, V.R.F.; Kempka, A.P. *Campomanesia xanthocarpa* (Mart.) O. Berg: Therapeutic potential through a comprehensive review of biological activities and phenolic compound interactions. *Biocatal. Agric. Biotechnol.* **2023**, *54*, 102927. [CrossRef]
20. Hodek, P.; Trefil, P.; Stiborová, M. Flavonoids-potent and versatile biologically active compounds interacting with cytochromes P450. *Chem. Biol. Interact.* **2002**, *139*, 1–21. [CrossRef] [PubMed]
21. Sinyutina, S.E.; Romantsova, S.V.; Savelyeva, V.Y. Extraction of flavonoids from plant raw materials and study of their antioxidant properties. *Tambov Univ. Rep.* **2011**, *16*, 345–347.
22. Ghezzi, P. Environmental risk factors and their footprints in vivo—A proposal for the classification of oxidative stress biomarkers. *Redox Biol.* **2020**, *34*, 101442. [CrossRef] [PubMed]
23. Granger, M.; Eck, P. Dietary Vitamin C in Human Health. *Adv. Food Nutr. Res.* **2018**, *83*, 281–310. [CrossRef]
24. Fatima, Z.; Quinto, M.; Zhou, J.L.; Li, D. Active substances of fat-soluble vitamins: Advances in extraction and analysis approaches. *Trends Anal. Chem.* **2023**, *167*, 117276. [CrossRef]
25. Paciolla, C.; Fortunato, S.; Dipierro, N.; Paradiso, A.; De Leonardis, S.; Mastropasqua, L.; de Pinto, M.C. Vitamin C in Plants: From Functions to Biofortification. *Antioxidants* **2019**, *8*, 519. [CrossRef]
26. Fitzpatrick, T.B.; Chapman, L.M. The importance of thiamine (vitamin B_1) in plant health: From crop yield to biofortification. *JBC Rev.* **2020**, *295*, 12002–12013. [CrossRef]

27. Jabeen, M.; Akram, N.A.; Ashraf, M.; Alyemeni, M.N.; Ahmad, P. Thiamin stimulates growth and secondary metabolites in turnip (*Brassica rapa* L.) leaf and root under drought stress. *Physiol. Plant* **2020**, *172*, 1399–1411. [CrossRef]
28. Skorna, P.; Rimarcik, J.; Poliak, P.; Lukes, V.; Klein, E. Thermodynamic study of vitamin B_6 antioxidant potential. *Comput. Theor. Chem.* **2016**, *1077*, 32–38. [CrossRef]
29. Nizar, M.; Shaukat, K.; Samad, A.; Zahra, N.; Saleem, I.; Raza, A. Impact of exogenous salicylic acid and hydrogen peroxide on vitamins, essential nutrients and silymarin content of milk thistle grown at two different altitudes of balochistan under cadmium stress. *J. Agric. Food Res.* **2023**, *13*, 100643. [CrossRef]
30. Napoli, A.D.; Zucchetti, P. A comprehensive review of the benefits of *Taraxacum officinale* on human health. *Bull. Natl. Res. Cent.* **2021**, *45*, 110. [CrossRef]
31. Escudero, N.; De Arellano, M.L.; Fernández, S.; Albarracín, G.; Mucciarelli, S. Taraxacum officinale as a food source. *Plant Foods Human. Nutr.* **2003**, *58*, 1–10. [CrossRef]
32. Yang, F.; Ye, X.; Chen, M.; Li, H.; Wang, Y.; Zhong, M.; Zhong, C.; Zeng, B.; Xu, L.; He, X.; et al. Inhibition of NLRP3 inflammasome activation and pyroptosis in macrophages by taraxasterol is associated with its regulation on mTOR signaling. *Front. Immunol.* **2021**, *12*, 632606. [CrossRef] [PubMed]
33. Chen, W.; Fan, H.; Liang, R.; Zhang, R.; Zhang, J.; Zhu, J. *Taraxacum officinale* extract ameliorates dextran sodium sulphate-induced colitis by regulating fatty acid degradation and microbial dysbiosis. *J. Cell Mol. Med.* **2019**, *23*, 8161–8172. [CrossRef] [PubMed]
34. Kania-Dobrowolska, M.; Baraniak, J. Dandelion (*Taraxacum officinale* L.) as a Source of Biologically Active Compounds Supporting the Therapy of Co-Existing Diseases in Metabolic Syndrome. *Foods* **2022**, *11*, 2858. [CrossRef]
35. Huang, Y.; Wu, P.; Chen, X.D. Mechanistic insights into the influence of flavonoids from dandelion on physicochemical properties and in vitro digestibility of cooked potato starch. *Food Hydrocoll.* **2022**, *130*, 107714. [CrossRef]
36. Cao, Z.; Ding, Y.; Liu, Z.; Liu, M.; Wu, H.; Zhao, J.; Dong, X.; Shang, H. Extraction condition optimization and prebiotic potential of dandelion (*Taraxacum mongolicum* Hand-Mazz.) polysaccharides. *Industrial Crop. Prod.* **2023**, *194*, 116318. [CrossRef]
37. Yosri, N.; Alsharif, S.M.; Xiao, J.; Musharraf, S.G.; Zhao, C.; Saeed, A.; Gao, R.; Said, N.S.; Minno, A.D.; Daglia, M.; et al. *Arctium lappa* (Burdock): Insights from ethnopharmacology potential, chemical constituents, clinical studies, pharmacological utility and nanomedicine. *Biomed. Pharmacother.* **2023**, *158*, 114104. [CrossRef]
38. Su, J.-Y.; Chen, Y.; Yang, C.-Y. Impact of nutrient from aqueous extract of burdock roots and ultrasonic stress on the growth and β-glucosidase activity of *Lactiplantibacillus plantarum* FEL112. *LWT* **2023**, *175*, 114495. [CrossRef]
39. Li, L.; Qiu, Z.; Dong, H.; Ma, C.; Qiao, Y.; Zheng, Z. Structural characterization and antioxidant activities of one neutral polysaccharide and three acid polysaccharides from the roots of *Arctium lappa* L.: A comparison. *Int. J. Biol. Macromol.* **2021**, *182*, 187–196. [CrossRef] [PubMed]
40. Chen, M.; Xu, J.; Wang, Y.; Wang, Z.; Guo, L.; Li, X.; Huang, L. *Arctium lappa* L. polysaccharide can regulate lipid metabolism in type 2 diabetic rats through the SREBP-1/SCD-1 axis. *Carbohydr. Res.* **2020**, *494*, 108055. [CrossRef] [PubMed]
41. Kola-Mustapha, A.T.; Abdulrahman, M.O.; Ishola, I.O. *Arctium lappa* root extract based emulgels attenuate inducible cytokines and prostaglandins formation: Potential in the management of chronic inflammatory disorders. *Sci. Afr.* **2023**, *22*, e01942. [CrossRef]
42. Don, R.A.S.G.; Yap, M.K.K. *Arctium lappa* L. root extract induces cell death via mitochondrial-mediated caspase-dependent apoptosis in Jurkat human leukemic T cells. *Biomed. Pharmacother.* **2019**, *110*, 918–929. [CrossRef]
43. Chan, Y.-S.; Cheng, L.-N.; Wu, J.-H.; Chan, E.; Kwan, Y.-W.; Lee, S.M.-Y.; Leung, G.P.-H.; Yu, P.H.-F.; Chan, S.-W. A review of the pharmacological effects of *Arctium lappa* (burdock). *Inflammopharmacol* **2011**, *19*, 245–254. [CrossRef] [PubMed]
44. de Marins, A.R.; Ribeiro, S.T.C.; de Oliveira, M.C.; Filho, L.C.; de Oliveira, A.J.B.; Gonçalves, R.A.C.; Gomes, R.G.; Feihrmann, A.C. Effect of extraction methods on the chemical, structural, and rheological attributes of fructan derived from *Arctium lappa* L. roots. *Carbohydr. Polym.* **2024**, *324*, 121525. [CrossRef] [PubMed]
45. Jin, X.; Liu, S.; Chen, S.; Wang, L.; Cui, Y.; He, J.; Fang, S.; Li, J.; Chang, Y. A systematic review on botany, ethnopharmacology, quality control, phytochemistry, pharmacology and toxicity of *Arctium lappa* L. fruit. *J. Ethnopharmacol.* **2023**, *308*, 116223. [CrossRef] [PubMed]
46. Han, J.H.; Kim, M.T.; Myung, C.S. Cytokine-induced Apoptosis Inhibitor 1 (CIAPIN1): Can It Be Eligible to Be a Novel Target for the Treatment of Atherosclerosis? *Cardiometab Syndr. J.* **2022**, *2*, 139–141. [CrossRef]
47. Ferracane, R.; Graziani, G.; Gallo, M.; Fogliano, V.; Ritieni, A. Metabolic profile of the bioactive compounds of burdock (*Arctium lappa*) seeds, roots and leaves. *J. Pharm. Biomed. Anal.* **2010**, *51*, 399–404. [CrossRef] [PubMed]
48. Lee, C.J.; Park, S.K.; Kang, J.Y.; Kim, J.M.; Yoo, S.K.; Han, H.J.; Kim, D.-O.; Heo, H.J. Melanogenesis regulatory activity of the ethyl acetate fraction from *Arctium lappa* L. leaf on α-MSH–induced B16/F10 melanoma cells. *Ind. Crop. Prod.* **2019**, *138*, 111581. [CrossRef]
49. Aguirre, M.J.; Chen, Y.Y.; Isaacs, M.; Matsuhiro, B.; Mendoza, L.; Torres, S. Electrochemical behaviour and antioxidant capacity of anthocyanins from Chilean red wine, grape and raspberry. *Food Chem.* **2010**, *121*, 44–48. [CrossRef]
50. Zeng, F.; Li, Y.; Zhang, X.; Shen, L.; Zhao, X.; Beta, T.; Li, B.; Chen, R.; Huang, W. Immune regulation and inflammation inhibition of *Arctium lappa* L. polysaccharides by TLR4/NF-κB signaling pathway in cells. *Int. J. Biol. Macromol.* **2024**, *254*, 127700. [CrossRef]
51. Nikoomanesh, N.; Zandi, M.; Ganjloo, A. Development of eco-friendly cellulose acetate films incorporated with Burdock (*Arctium lappa* L.) root extract. *Prog. Org. Coat.* **2024**, *186*, 108009. [CrossRef]

52. Kenny, O.; Brunton, N.P.; Walsh, D.; Hewage, C.M.; McLoughlin, P.; Smyth, T.J. Characterisation of Antimicrobial Extracts from Dandelion Root (*Taraxacum officinale*) Using LC-SPE-NMR. *Phytother. Res.* **2015**, *29*, 526–532. [CrossRef]
53. Ionescu, D.; Predan, G.; Rizea, G.D.; Mihele, D.; Dune, A.; Ivopol, G.; Ionita, C. Antimicrobial activity of some hydroalcoholic extracts of artichoke («*Cynara scolymus*»), burdock («*Arctium lappa*») and dandelion («*Taraxacum officinale*»). *Bull. Transilv. Univ. Bras.* **2013**, *6*, 113–120.
54. Tiguntseva, N.P. Methods and Composition of Biologically Active Dandelion *Taraxacum officinale* Wigg. Ph.D. Thesis, St. Petersburg State Technological Institute (Technical University), St. Petersburg, Russia, 4 March 2015.
55. Floegel, A.; Kim, D.-O.; Chung, S.-J.; Koo, S.I.; Chun, O.K. Comparison of ABTS/DPPH assays to measure antioxidant capacity in popular antioxidant-rich US foods. *J. Food Compost. Anal.* **2011**, *24*, 1043–1048. [CrossRef]
56. Biel, W.; Jaroszewska, A.; Lyson, E.; Telesinski, A. The chemical composition and antioxidant properties of common dandelion leaves compared to sea buckthorn. *Can. J. Plant Sci.* **2017**, *97*, 1165–1174. [CrossRef]
57. Martinez, M.; Poirrier, P.; Chamy, R.; Prüfer, D.; Schulze-Gronover, C.; Jorquera, L.; Ruiz, G. *Taraxacum officinale* and related species—An ethnopharmacological review and its potential as a commercial medicinal plant. *J. Ethnopharmacol.* **2015**, *169*, 244–262. [CrossRef] [PubMed]
58. Zakharov, V.L.; Kudashkina, T.A.; Zhikhoreva, V.I. Content of biologically active substances in the roots of medicinal plants. *Agro-Ind. Technol. Cent. Russ.* **2018**, *3*, 8–15. [CrossRef]
59. Zhang, X.; Herrera-Balandrano, D.D.; Huang, W.; Chai, Z.; Beta, T.; Wang, J.; Feng, J.; Li, Y. Comparison of Nutritional and Nutraceutical Properties of Burdock Roots Cultivated in Fengxian and Peixian of China. *Foods* **2021**, *10*, 2095. [CrossRef]
60. Gliszczyńska-Świgło, A. Antioxidant activity of water soluble vitamins in the TEAC (trolox equivalent antioxidant capacity) and the FRAP (ferric reducing antioxidant power) assays. *Food Chem.* **2006**, *96*, 131–136. [CrossRef]
61. Sampson, L.; Rimm, E.; Hollman, P.C.H.; de Vries, J.H.M.; Katan, M.B. Flavonol and Flavone Intakes in US Health Professionals. *J. Am. Diet. Assoc.* **2002**, *102*, 1414–1420. [CrossRef]
62. Moro, T.M.A.; Pereira, A.P.A.; Lopes, A.S.; Pastore, G.M.; Clerici, M.T.P.S. Retention of bioactive compounds and bifidogenic activity of burdock roots subjected to different processes. *Int. J. Gastron. Food Sci.* **2022**, *27*, 100448. [CrossRef]
63. Predes, F.S.; Ruiz, A.L.; Carvalho, J.E.; Foglio, M.A.; Dolder, H. Antioxidative and in vitro antiproliferative activity of *Arctium lappa* root extracts. *BMC Complement. Altern. Med.* **2011**, *11*, 25. [CrossRef]
64. Schütz, K.; Kammerer, D.R.; Carle, R.; Schieber, A. Characterization of phenolic acids and flavonoids in dandelion (*Taraxacum officinale* WEB. ex WIGG.) root and herb by high-performance liquid chromatography/electrospray ionization mass spectrometry. *Rapid Commun. Mass. Spectrom.* **2004**, *19*, 179–186. [CrossRef]
65. Abarikwu, S.O.; Olufemi, P.D.; Lawrence, C.J.; Wekere, F.C.; Ochulor, A.C.; Barikuma, A.M. Rutin, an antioxidant flavonoid, induces glutathione and glutathione peroxidase activities to protect against ethanol effects in cadmium-induced oxidative stress in the testis of adult rats. *Andrologia* **2017**, *49*, e12696. [CrossRef]
66. Ghorbani, A. Mechanisms of antidiabetic effects of flavonoid rutin. *Biomed. Pharmacother.* **2017**, *96*, 305–312. [CrossRef]
67. Meinhart, A.D.; Damin, F.M.; Caldeirão, L.; Teixeira-Filho, J.; Godoy, H.T. Rutin in herbs and infusions: Screening of new sources and consumption estimation. *Food Sci. Technol.* **2020**, *40*, 113–120. [CrossRef]
68. de Souza, A.R.C.; Stefanov, S.; Bombardelli, M.C.M.; Corazza, M.L.; Stateva, R.P. Assessment of composition and biological activity of Arctium lappa leaves extracts obtained with pressurized liquid and supercritical CO_2 extraction. *J. Supercrit. Fluids* **2019**, *152*, 104573. [CrossRef]
69. Epure, A.; Pârvu, A.E.; Vlase, L.; Benedec, D.; Hanganu, D.; Oniga, O.; Vlase, A.-M.; Ielciu, I.; Toiu, A.; Oniga, I. New Approaches on the Anti-Inflammatory and Cardioprotective Properties of Taraxacum officinale Tincture. *Pharmaceuticals* **2023**, *16*, 358. [CrossRef] [PubMed]
70. Rusmana, D.; Wahyudianingsih, R.; Elisabeth, M.; Balqis, B.; Maesaroh, M.; Widowati, W. Antioxidant Activity of *Phyllanthus niruri* Extract, Rutin and Quercetin. *Indones. Biomed. J.* **2017**, *9*, 84–90. [CrossRef]
71. Dueñas, M.; Surco-Laos, F.; González-Manzano, S.; González-Paramás, A.M.; Santos-Buelga, C. Antioxidant properties of major metabolites of quercetin. *Eur. Food Res. Technol.* **2011**, *232*, 103–111. [CrossRef]
72. Padayatty, S.J.; Katz, A.; Wang, Y.; Eck, P.; Kwon, O.; Lee, J.-H.; Chen, S.; Corpe, C.; Dutta, A.; Dutta, S.K.; et al. Vitamin C as an Antioxidant: Evaluation of Its Role in Disease Prevention. *J. Am. Coll. Nutr.* **2003**, *22*, 18–35. [CrossRef]
73. Njus, D.; Kelley, P.M.; Tu, Y.-J.; Schlegel, H.B. Ascorbic acid: The chemistry underlying its antioxidant properties. *Free Radic. Biol. Med.* **2020**, *159*, 37–43. [CrossRef]
74. Kim, D.-O.; Lee, K.W.; Lee, H.J.; Lee, C.Y. Vitamin C Equivalent Antioxidant Capacity (VCEAC) of Phenolic Phytochemicals. *J. Agric. Food Chem.* **2002**, *50*, 3713–3717. [CrossRef] [PubMed]
75. Sowbhagya, H.B.; Chitra, V.N. Enzyme-assisted extraction of flavorings and colorants from plant materials. *Crit. Rev. Food Sci. Nutr.* **2010**, *50*, 146–161. [CrossRef] [PubMed]
76. Popov, I.V.; Andreeva, I.N.; Gavrilin, M.V. Determination of tannin in raw materials and preparations of burnet officinalis using HPLC methods. *Chem. Pharm. J.* **2003**, *37*, 24–26. [CrossRef]
77. Ebrahimi, P.; Mihaylova, D.; Lante, A. Comparison of green technologies for valorizing sugar beet (*Beta vulgaris* L.) leaves. *Food Sci. Appl. Biotechnol.* **2022**, *5*, 119–130. [CrossRef]
78. Kovaleva, N.A.; Trineeva, O.V.; Nosova, D.K.; Kolotneva, A.I. Determination of extractives in the leaves of sea buckthorn. *Bull. Voronezh State Univ.* **2022**, *1*, 105–109.

79. Mulatu, G. Antibacterial Activities of *Calpurnia aurea* against Selected Animal Pathogenic Bacterial Strains. *Adv. Pharmacol. Pharm. Sci.* **2020**, *2020*, 8840468. [CrossRef] [PubMed]
80. Sorokin, V.V.; Weinstein, V.A.; Kaukhova, I.E.; Chibilyaev, T.K. Study of the extracting ability of one- and two-phase systems of extractants for the extraction of flavonoids from red clover herb. *Chem. Pharm. J.* **2008**, *42*, 23–25.
81. Orcho, A.M.; Badessa, T.S.; Tura, A.M.; Dirko, T.D. Shelf-life improvement of raw milk using ethanolic extracts of selected medicinal plants (*Moringa stenopetale*, *Artemesia anua* and *Mentha Spicata*). *Heliyon* **2023**, *9*, e17659. [CrossRef]
82. Re, R.; Pellegrini, N.; Proteggente, A.; Pannala, A.; Yang, M.; Rice-Evans, C. Antioxidant activity applying an improved ABTS radical cation decolorization assay. *Free Radic. Biol. Med.* **1999**, *26*, 1231–1237. [CrossRef] [PubMed]
83. CLSI. *Performance for Antimicrobial Susceptibility Testing*; Clinical and Laboratory Standards Institute: Wayne, PA, USA, 2013.
84. Diallo, D.; Yaméogo, B.G.J.; Nikiema, O.; Belem, M.; Goumbri, W.B.; Bassavé, B.M.; Ouédraogo, A.-S.; Kabré, E.; Semdé, R. Evaluation of the physicochemical quality and antimicrobial performance of amoxicillin and amoxicillin+clavulanic acid discs used in Burkina Faso. *Results Chem.* **2023**, *6*, 101020. [CrossRef]
85. de Assis, R.C.; Soares, R.L.G.; Siqueira, A.C.P.; de Rosso, V.V.; de Sousa, P.H.M.; Mendes, A.E.P.; Costa, E.A.; Carneiro, A.P.G.; Maia, C.S.C. Determination of water-soluble vitamins and carotenoids in Brazilian tropical fruits by High Performance Liquid Chromatography. *Heliyon* **2020**, *6*, e05307. [CrossRef] [PubMed]
86. Sharma, V.; Janmeda, P. Extraction, isolation and identification of flavonoid from *Euphorbia neriifolia* leaves. *Arab. J. Chem.* **2017**, *10*, 509–514. [CrossRef]

MDPI
St. Alban-Anlage 66
4052 Basel
Switzerland
www.mdpi.com

International Journal of Molecular Sciences Editorial Office
E-mail: ijms@mdpi.com
www.mdpi.com/journal/ijms

Academic Open
Access Publishing

mdpi.com

ISBN 978-3-7258-1002-4